



Hazus Hurricane Model Technical Manual

Hazus 5.1

July 2022



FEMA

If you require assistance interpreting any of the technical information contained in this report, assistance is available via the Hazus Help Desk by email at: FEMA-Hazus-Support@fema.dhs.gov (preferred) or by phone at 1-877-FEMA-MAP (1-877-336-2627).

Table of Contents

Table of Contents.....	i
List of Figures.....	ix
List of Tables.....	xix
Acronyms and Abbreviations.....	xxvi
Section 1. Introduction to the FEMA Hazus Loss Estimation Methodology	1-1
1.1 Background	1-1
1.2 Hazus Uses and Applications	1-1
1.3 Assumed User Expertise.....	1-3
1.4 When to Seek Help.....	1-3
1.5 Technical Support.....	1-4
1.6 Uncertainties in Loss Estimates	1-4
Section 2. Introduction to Hurricane Loss Estimation Methodology.....	2-2
2.1 Hurricane Hazards Considered in the Methodology.....	2-4
2.2 Definitions of Structures.....	2-5
2.3 Levels of Analysis.....	2-6
2.3.1 Analysis Based on Default Information.....	2-7
2.3.2 Analysis with User-Supplied Inventory	2-7
Section 3. Inventory.....	3-1
Section 4. Hurricane Wind and Surge Hazards	4-1
4.1 Hurricane Wind Field Model	4-1
4.1.1 Mean Wind Field Model	4-2
4.1.2 Surface Level Winds	4-2
4.1.2.1 Hurricane Boundary Layer Model.....	4-3
4.1.2.1.1 Empirical Model for the Marine Hurricane Boundary Layer.....	4-9
4.1.2.1.2 Hurricane Boundary Layer Height.....	4-11
4.1.2.1.3 Marine Boundary Layer Model Verification.....	4-13
4.1.2.1.4 Sea Land Transition.....	4-15
4.1.2.2 Model Verification	4-18
4.1.3 Summary.....	4-29
4.2 Hurricane Simulation Methodology.....	4-30
4.2.1 Storm Track Modeling.....	4-30
4.2.2 Modeling of Radius to Maximum Winds	4-32
4.2.3 Pressure Profile Parameter (B)	4-33
4.2.4 Filling Models.....	4-39

4.2.5	Track and Central Pressure Model Evaluation.....	4-40
4.2.6	Landfalling Hurricanes.....	4-42
4.2.7	Predicted Wind Speeds versus Return Period	4-55
4.2.8	Summary.....	4-56
4.3	Hurricane Rainfall Rate Model	4-57
4.3.1	Data and Prior Studies.....	4-57
4.3.2	Model Development.....	4-59
4.3.3	Hurricane Rainfall Rate Model Implementation and Calibration.....	4-63
4.4	Surface Roughness Modeling.....	4-69
4.4.1	MRLC-NLCD Database	4-72
4.4.1.1	Calibration of NLCD Land Cover Classifications against Aerial Photos.....	4-73
4.4.1.1.1	North Carolina.....	4-77
4.4.1.1.2	Texas.....	4-85
4.4.2	Mapping NLCD Land Cover Codes to Roughness Lengths	4-89
4.4.3	LULC codes 21 and 22 and MRLC-NLCD Data	4-92
4.4.4	Census Tract-and Census Block Averaged Roughness Length.....	4-93
4.4.5	Comparisons of z_0 Values Computed from NLCD Data on Rectangular Grids with Empirically Assigned z_0 Values.....	4-97
4.4.6	Example of Roughness Length (z_0) Calculation Using Lettau's Formula.....	4-105
4.4.7	Effect of Surface Roughness on Near Ground Gust Wind Speeds	4-110
4.5	Tree Blowdown	4-117
4.5.1	Related Research.....	4-118
4.5.2	Wind Throw Model	4-119
4.5.2.1	Wind Load Response and Breakage Model	4-119
4.5.2.2	Wind Modeling for Simple Terrains	4-126
4.5.2.3	Example Tree Response - Ponderosa Pine	4-129
4.5.2.4	Wind Modeling in Forested Areas.....	4-132
4.5.2.5	Canopy Modeling.....	4-135
4.5.2.6	Effective Wind Speeds in Forested Areas	4-137
4.5.2.7	Simulation Methodology.....	4-139
4.5.3	Blowdown Results.....	4-140
4.5.3.1	Tree Blowdown Curves	4-140
4.5.3.2	Tree Blowdown Validation	4-141
4.5.4	Tree Inventory Data by County.....	4-146
4.5.4.1	Forest Inventory Analysis (FIA) Program and Database	4-146
4.5.4.2	Average Tree Density and Tree Height Distribution at County Level.....	4-146
4.5.5	Hazus Tree Coverage Database.....	4-147
4.5.5.1	MRLC National Land Cover Data.....	4-147

4.5.5.2	Tree Density, Tree Height, and Predominant Tree Type by Census Tract and Census Block.....	4-147
4.6	Coastal Storm Surge.....	4-150
4.6.1	Integration of Storm Surge Models.....	4-152
4.6.1.1	Coupling of SLOSH and SWAN	4-153
4.6.2	Coastal Surge Analysis for Study Regions Spanning Multiple SLOSH Basins.....	4-156
4.6.3	Integration with Coastal Flood Model	4-159
4.6.3.1	Wave Exposure.....	4-160
4.6.3.2	Coastal Flood Outputs.....	4-161
Section 5.	Physical Damage Modeling.....	5-1
5.1	Wind Loads.....	5-3
5.1.1	Wall Pressures – Low-Rise Buildings.....	5-4
5.1.1.1	Effect of Wind Direction.....	5-6
5.1.1.2	Comparison of ASCE 7 Wall Pressures to Wind Tunnel Tests.....	5-10
5.1.2	Roof Pressures – Low-Rise Buildings.....	5-12
5.1.2.1	Effect of Wind Direction.....	5-17
5.1.2.2	Effect of Terrain.....	5-18
5.1.2.3	Comparison of ASCE 7 Roof Pressure Loads to Wind Tunnel Tests.....	5-19
5.1.3	Wind Loads on Low-Rise Buildings – Effect of Nearby Buildings.....	5-21
5.1.4	Integrated (Overall) Wind Loads on Low-Rise Buildings	5-21
5.1.4.1	Roof Uplift Loads.....	5-23
5.1.4.2	Integrated Roof and Wall Loads on Low-Rise Buildings with Flat Roofs.....	5-24
5.1.4.3	Overall Loads on Manufactured Homes.....	5-27
5.1.4.4	Wind Loads on Long Span Roof Elements	5-29
5.1.5	Wind Loads on High-Rise Buildings	5-36
5.2	Windborne Missile Models	5-49
5.2.1	Windborne Debris – Residential Missile Model.....	5-49
5.2.1.1	Windborne Debris Simulation and Analysis	5-49
5.2.1.2	Implementation of the Windborne Debris Model.....	5-53
5.2.2	Windborne Debris – Commercial Missile Model.....	5-55
5.2.2.1	Windborne Gravel Debris Simulation and Case Studies.....	5-56
5.2.2.1.1	Scope of the Simulation.....	5-56
5.2.2.1.2	Missile Generation from Roof Gravel.....	5-56
5.2.2.1.3	Missile Transport in the Wind Field.....	5-58
5.2.2.1.4	Missile Impact on Building Envelopes	5-59
5.2.2.2	Probability of Damage to Building Envelopes by Windborne Gravel Debris.....	5-76
5.2.2.2.1	Analytical Formulation for Probability of Impact Damage.....	5-76

- 5.2.2.2.2 Physical Modeling to Obtain the Number of Impacts and Momentum Distribution 5-76
- 5.2.2.2.3 Analysis of Modeled Results5-79
- 5.3 Tree Blowdown Damage to Buildings5-87
 - 5.3.1 Tree Drop Tests5-88
 - 5.3.2 Relationship Between Damage Severity and Impact Energy5-91
- 5.4 Resistance Models5-92
 - 5.4.1 Residential Buildings5-92
 - 5.4.2 Roof Sheathing in Wood Frame Construction5-93
 - 5.4.3 Air Permeable Roof Cover Systems5-94
 - 5.4.4 Windows and Sliding Glass Doors5-95
 - 5.4.5 Roof-Wall Connections5-96
 - 5.4.6 Masonry Walls5-96
 - 5.4.6.1 Failure Modes and Crack Patterns5-98
 - 5.4.6.2 Ultimate Failure Pressures 5-101
 - 5.4.6.3 Effects of Variable Material and Workmanship 5-102
 - 5.4.6.4 Estimation of Wall Failure Probability 5-106
 - 5.4.7 Wood Frame Walls 5-108
 - 5.4.7.1 Simplified Structural Model 5-108
 - 5.4.7.2 Lateral Failure Load for Nail Connections 5-118
 - 5.4.7.3 Variability and Effects of Workmanship 5-121
 - 5.4.7.4 Probability of Wall Failure5-122
 - 5.4.8 Manufactured Homes 5-125
 - 5.4.8.1 Main Wind Force Resistance Modeling 5-127
 - 5.4.8.2 Foundation and Tie Down Modeling 5-127
 - 5.4.8.3 Summary of Failure Modes Considered for Manufactured Homes5-129
 - 5.4.9 Roof Covers on Flat Roofs 5-130
 - 5.4.10 Open-Web Steel Joist Roof System 5-132
 - 5.4.10.1 Uplift Resistance 5-133
 - 5.4.10.2 Steel Joist and Steel Bearing Plate 5-134
 - 5.4.10.3 Resistance of the Weld Metal 5-134
 - 5.4.10.4 Resistance of the Plate Base Metal 5-134
 - 5.4.10.5 Resistance of the Steel Joist Base Metal 5-135
 - 5.4.10.6 Example Minimum Uplift Capacity5-135
 - 5.4.10.7 Steel Bearing Plate/Steel Joist and the Wall Anchorage. 5-135
 - 5.4.10.8 Bending Resistance 5-136
 - 5.4.10.9 Prediction of Joist Failures 5-136
 - 5.4.10.10 Example OWSJ Failure Probabilities5-137
 - 5.4.11 Metal Deck on Open-Web Steel Joists 5-140

5.4.11.1	An Overview of Metal Decking.....	5-141
5.4.11.2	Screwed Decks.....	5-141
5.4.11.3	Welded Decks	5-143
5.4.11.4	Probabilistic Finite Element Analyses.....	5-146
5.4.11.5	Finite Element Method (FEM) Results.....	5-150
5.4.12	Metal Building Wall System	5-152
5.4.12.1	Finite Element Mode	5-153
5.4.12.2	Simulation Results	5-156
5.4.13	Metal Building Roof System.....	5-158
5.5	Damage Model Validation	5-160
5.5.1	Residential Buildings	5-160
5.5.1.1	Roof Cover and Roof Deck Damage.....	5-161
5.5.1.1.1	Hurricane Andrew (1992	5-161
5.5.1.1.2	Hurricane Erin (1995).....	5-172
5.5.1.1.3	Hurricane Fran (1996).....	5-173
5.5.1.2	Window Damage	5-174
5.5.1.3	Whole Roof Failures	5-174
5.5.2	Manufactured Homes	5-178
5.5.2.1	Comparisons of Wind Speed versus Damage Predictions to the Vann and McDonald Model and the Vasquez Model	5-179
5.5.2.2	Hurricane Bertha Validation.....	5-180
5.5.2.3	Hurricane Andrew Validation.....	5-181
5.5.2.4	Hurricane Elena.....	5-184
5.5.3	Roof Covers on Flat Roofs.....	5-185
5.5.3.1	Hurricane Andrew (1992) – Dixie Highway	5-186
5.5.3.2	Hurricane Andrew (1992) – Aerial Photograph 3.	5-187
5.6	Damage Model Results	5-188
5.6.1	Residential Buildings	5-188
5.6.1.1	Effect of Mitigation on Residential Building Damage.....	5-203
5.6.2	Manufactured Homes	5-209
5.6.3	Marginally- or Non-Engineered Hotel/Motel and Multi-Family Residential Buildings ..	5-212
5.6.4	Low-Rise Masonry Strip Mall Buildings.....	5-222
5.6.5	Pre-Engineered Metal Buildings.....	5-242
5.6.6	Engineered Residential and Commercial Buildings.....	5-246
5.6.7	Damage Model Results for Industrial Buildings.....	5-256
5.6.8	Essential Facilities	5-259
5.6.8.1	Fire Stations	5-262
5.6.8.2	Elementary Schools.....	5-265

5.6.8.3 High Schools..... 5-268

5.6.8.4 Hospitals 5-272

Section 6. Induced Damage Methods – Building and Tree Debris..... 6-1

6.1 Description of Building Debris Generation Methodology..... 6-2

6.1.1 Component Unit Weight..... 6-4

6.1.2 Default Component Construction Types for Commercial Buildings..... 6-11

6.2 Building Debris Validation Studies 6-19

6.3 Description of Tree Debris Methodology 6-21

6.3.1 Total Weight and Volume of Downed Trees 6-21

6.3.2 Tree Debris Collection Model..... 6-24

6.3.3 Implementing into Hazus 6-27

6.3.4 Comparison of Modeled and Reported Tree Debris 6-29

6.3.4.1 Example Tree Collection Data – Hurricane Isabel, North Carolina..... 6-29

6.3.4.2 Example Tree Collection Data – Hurricane Isabel, Virginia 6-31

6.3.4.3 Comparison to Other Collection Data..... 6-35

Section 7. Direct Social Losses – Displaced Households and Short-Term Shelter Needs..... 7-1

7.1 Scope..... 7-1

7.2 Displaced Household..... 7-1

7.2.1 Input Requirements 7-2

7.2.2 Description of Methodology 7-2

7.3 Short-term Shelter Needs..... 7-10

7.3.1 Input Requirements 7-10

7.3.2 Description of Methodology 7-11

7.4 Guidance for Estimates Using Advanced Data and Models 7-14

7.4.1 Changes to Shelter Weighting and Modification Factors..... 7-14

7.4.2 Guidance for Estimating Long-Term Housing Recovery 7-14

Section 8. Direct Economic Losses 8-1

8.1 Methodology 8-1

8.1.1 Residential Input Parameters 8-1

8.1.2 Residential Subassembly Costs..... 8-3

8.1.2.1 Default Residence 8-4

8.1.2.2 Subassembly Cost Ratios..... 8-5

8.1.3 Explicit Costing of Residential Losses..... 8-7

8.1.4 Modeling of Residential Interior and Content Losses and Loss of Use 8-9

8.1.4.1 Economic Damage to Building Interior..... 8-9

8.1.4.2 Economic Damage to Contents..... 8-12

8.1.4.3 Loss of Use for Residential Buildings..... 8-14

8.1.5	Residential Loss Model Validation Examples	8-14
8.1.6	Manufactured Home Loss Module.....	8-17
8.1.6.1	Losses Associated with Exterior Damage.....	8-17
8.1.6.2	Losses Associated with Frame Damage or Foundation Failure	8-17
8.1.6.3	Interior and Content Losses	8-18
8.1.7	Economic Loss Module for Commercial Buildings and Essential Facilities.....	8-18
8.1.7.1	Subassembly Cost Ratios.....	8-18
8.1.7.1.1	Cost Ratio Adjustment – Number of Stories.....	8-18
8.1.7.1.2	Cost Ratio Adjustment – Door, Window, and Glazed Wall Areas.....	8-20
8.1.7.2	Building Loss Model	8-22
8.1.7.3	Content Loss Model	8-27
8.1.8	Business Interruption Model.....	8-28
8.1.8.1	Loss of Function for Essential Facilities.....	8-30
8.1.8.2	Loss of Function for Fire Stations.....	8-30
8.1.8.3	Loss of Function for Schools	8-31
8.1.8.4	Loss of Function for Hospitals.....	8-32
8.2	Average Annual Losses.....	8-34
8.2.1	Residential Buildings	8-34
8.2.1.1	Mitigation	8-35
8.2.2	Manufactured Homes	8-37
8.2.3	Marginally Engineered or Non-Engineered Hotel/Motel and Multi-Family Residential Buildings.....	8-38
8.2.4	Low-Rise Masonry Strip Mall Buildings.....	8-44
8.2.5	Pre-Engineered Metal Buildings.....	8-47
8.2.6	Engineered Residential and Commercial Buildings.....	8-51
8.2.7	Industrial Buildings	8-61
8.2.8	Essential Facilities	8-64
8.2.8.1	Loss Model Results for Fire Stations.....	8-71
8.2.8.2	Loss Model Results for Elementary Schools.....	8-72
8.2.8.3	Loss Model Results for High Schools.....	8-73
8.2.8.4	Loss Model Results for Hospitals.....	8-74
8.3	Additional Losses to Single-Family Homes Due to Tree Blowdown	8-75
8.3.1	Cost Estimation Assumptions and Data.....	8-75
8.3.2	Additional Assumptions for One-Story.....	8-78
8.3.3	Additional Assumptions for Two-Story.....	8-78
8.3.4	Losses Due to Tree Blowdown	8-82
8.3.5	Loss Function for a Specific Building Type in Given Census Tract.....	8-88
8.4	Combined Wind and Flood Losses for Coastal Storm Surge	8-89

8.4.1 Building Subassembly Approach.....8-91

8.4.2 Development of Subassembly Replacement Cost Tables8-95

 8.4.2.1 Development of Subassembly Loss Tables for Wind Losses8-98

 8.4.2.1.1 Computing Subassembly Wind Losses at the Specific Occupancy Level 8-100

 8.4.2.1.2 Computing Subassembly losses at GBT Level 8-102

 8.4.2.1.3 Final Wind Subassembly Loss Tables..... 8-102

 8.4.2.2 Development of Subassembly Loss Tables for Flood Losses 8-103

8.4.3 Combined Building Contents and Inventory Approach 8-106

Section 9. References.....9-1

List of Figures

Figure 2-1 Hazus Hurricane Model Methodology Schematic.....	2-3
Figure 2-2 Levels of Hazus Analysis.....	2-6
Figure 4-1 Mean Wind Profiles	4-4
Figure 4-2 Mean and Fitted Logarithmic Profiles for Drops Near the RMW for all MBL Cases	4-6
Figure 4-3 Variation of the Sea Surface Drag Coefficient with Mean Wind Speed at 10 meters, Near the RMW	4-7
Figure 4-4 Mean Wind Profiles and Fitted Logarithmic Profiles for Outside RMW Case	4-8
Figure 4-5 Variation of the Sea Surface Drag Coefficient with Mean Wind Speed at 10 meters, Outside RMW case.....	4-9
Figure 4-6 Observed and Modeled Velocity Profiles for the 10 – 30 Kilometers and 30 – 60 Kilometers RMW Cases.....	4-10
Figure 4-7 Comparison of Regression Model, Kepert (2001) Model and Observed Boundary Layer Heights.....	4-13
Figure 4-8 Observed and Modeled Velocity Profiles Near the RMW for the 10 to 30 kilometers and 30 to 60 kilometers RMW Cases	4-14
Figure 4-9 Mean Error in Modeled Wind Speeds versus Height for Dropsonde Data Taken Near RMW ..	4-14
Figure 4-10 Comparison of Modeled and Observed Ratios of Mean Wind Speed at 10 meters to Mean Wind Speeds at the Top of the Boundary Layer Near the RMW	4-16
Figure 4-11 Mean Error in Modeled Wind Speeds versus Height for Dropsonde Data Taken Outside RMW Region	4-16
Figure 4-12 Ratio of the Fully Transitioned Mean Wind Speed Over Land ($z_0=0.03$ meters) to the Mean Wind Speed Over Water ($z_0=0.0013$ meters) as a Function of Boundary Layer Height.....	4-18
Figure 4-13 ESDU and Modified ESDU Wind Speed Transition Functions	4-18
Figure 4-14 Jet Strength Computed Using the Slab Model for a Hurricane Moving Towards the Top of the Page.....	4-20
Figure 4-15 Example Plots Showing Modeled and Observed Wind Speeds, Surface Pressures and Wind Directions.....	4-22
Figure 4-16 Example Plots Showing Modeled and Observed Wind Speeds, Surface Pressures and Wind Directions (continued)	4-23
Figure 4-17 Example Plots Showing Modeled and Observed Wind Speeds, Surface Pressures and Wind Directions (continued)	4-24
Figure 4-18 Example Plots Showing Modeled and Observed Wind Speeds, Surface Pressures and Wind Directions (continued)	4-25
Figure 4-19 Example Plots Showing Modeled and Observed Wind Speeds, Surface Pressures and Wind Directions (concluded).....	4-26
Figure 4-20 Comparison of Modeled and Observed Maximum Peak Gust Wind Speeds for 15 Land Falling Hurricanes.....	4-28
Figure 4-21 Example Comparisons of Modeled and Predicted Maximum Surface Level Peak Gust Wind Speeds in Open Terrain from US Landfalling Hurricanes	4-29
Figure 4-22 Examples of the Eliminated Profiles.....	4-36
Figure 4-23 Examples of Surface Pressure Profiles for a Traverse Across a Given Hurricane.....	4-37

Figure 4-24 Geographical Distribution of all the Filtered Profiles.....4-38

Figure 4-25 Filling Constant, a , versus $\Delta p_{oc}/RMW$ for Gulf, Florida and Atlantic Coast and Versus Δp_{oc} for New England Coast4-40

Figure 4-26 Locations of Milepost Stations Along the U.S. Coastline.....4-41

Figure 4-27 Comparison of Simulated and Observed Key Hurricane Parameters vs. Milepost (Vickery et al., 2009b).....4-42

Figure 4-28 Building Repair Cost Estimates as Functions of Impact Energy.....4-44

Figure 4-29 Comparison of Number of Annual Landfalling Intense Hurricanes by Storm Category (IH defined by pressure).....4-51

Figure 4-30 Comparisons of Modeled and Observed4-53

Figure 4-31 Comparisons of Modeled and Observed Hurricane Landfall Rates as a Function of Storm Category (Continued)4-54

Figure 4-32 Comparison of Modeled and Observed Storm Central Pressure at Landfall versus Return Period for Various Geographic Regions (Vickery et al., 2009b).....4-55

Figure 4-33 Predicted 100 Year Return Period Wind Speed for U.S. Atlantic and Gulf Coast4-56

Figure 4-34 Average Rain Rate.....4-58

Figure 4-35 Rainfall Rate as Function of Normalized Radial Distance from the Eye (R_{max} is Assumed to be 30 Kilometers).....4-59

Figure 4-36 Plot Showing the Original Rainfall Rate with the Estimation from Equation 4-194-60

Figure 4-37 Ratio of Rainfall Rates for Hurricane Against Non-hurricane Tropical Cyclones as a Function of Normalized Radial Distance, Following Rogers et al. (1994)4-61

Figure 4-38 Observed and Estimated Rainfall Rates for Hurricane Florence (Flo, Pred-Flo), Hurricane Hugo in Developing Stages (Hugo1, Pred-Hu1), and in Developed Stages (Hugo2, Pred-Hu2)4-63

Figure 4-39 Relationship Between the Modification Factor and R/R_{max} 4-65

Figure 4-40 Comparison of Observed and Modeled Hurricane Rainfall Rates.....4-66

Figure 4-41 Comparison of Observed and Modeled Hurricane Rainfall Rates (Concluded)4-67

Figure 4-42 Example A of Overlaid NLCD Data Map and Street Layout (COMM 01: Dade County)4-74

Figure 4-43 Example B of Overlaid NLCD Data Map and Street Layout (INDU01: Dade County).....4-75

Figure 4-44 Color-Coded Land Cover Characteristics of the State of North Carolina as Derived from NLCD Database (1991)4-78

Figure 4-45 Color Scheme Used Throughout Remainder of this Section4-78

Figure 4-46 Metropolitan Raleigh, NC (upper: Aerial photograph; lower: NLCD 1991).....4-79

Figure 4-47 West Suburb of Raleigh, NC (upper: Aerial photograph; lower: NLCD 1991).....4-80

Figure 4-48 Close-Up Views of Two Areas in West Suburb of Raleigh, NC4-81

Figure 4-49 Downtown Wilmington, NC (upper: Aerial photograph; lower: NLCD)4-83

Figure 4-50 Close-Up of Downtown Wilmington, NC (upper: Aerial photograph; lower: NLCD)4-84

Figure 4-51 Galveston-Texas City-Santa Fe Area, TX (upper: Aerial photo; lower: NLCD).....4-86

Figure 4-52 Close-up of Santa Fe Area, TX (upper: Aerial photograph; lower: NLCD).....4-87

Figure 4-53 Northeast Suburb of Houston, TX (upper: Aerial photograph; lower: NLCD)4-88

Figure 4-54 Percent Tree Canopy for the State of Florida4-92

Figure 4-55 Census Tract-Averaged Roughness for New Hanover.....4-95

Figure 4-56 Census Tract-Averaged Roughness for Wake County4-96

Figure 4-57 Census Tract-Averaged Roughness Length Derived from NLCD Data, Texas4-96

Figure 4-58 z_0 Values Computed from NLCD Data and Assigned Empirically for Houston, TX4-97

Figure 4-59 z_0 Values Computed from NLCD Data and Assigned Empirically for Miami, FL, Including Downtown (Cell # 6-3)4-98

Figure 4-60 z_0 Values Computed from NLCD Data and Assigned Empirically for Raleigh, NC, Including Downtown (Cell # 10-4)..... 4-100

Figure 4-61 z_0 Values Computed from NLCD Data and Assigned Empirically for a Location in South Suburban of Providence, RI..... 4-102

Figure 4-62 Comparison Between z_0 Values Computed from NLCD Data and Assigned Empirically for a Location in East Suburban of Houston, TX..... 4-103

Figure 4-63 Comparison Between z_0 Values Computed from NLCD Data and Assigned Empirically for Miami, FL, Including Downtown Area..... 4-103

Figure 4-64 Comparison Between z_0 Values Computed from NLCD Data and Assigned Empirically for Raleigh, NC, Including Downtown Area..... 4-104

Figure 4-65 Comparison Between z_0 Values Computed from NLCD Data and Assigned Empirically for a Location in Southern Providence, RI 4-104

Figure 4-66 Comparison Between z_0 Values Computed from NLCD Data and Assigned Empirically for the Four Locations Studied..... 4-105

Figure 4-67 Medium Density Residential Area in Escambia County..... 4-107

Figure 4-68 Medium Density Residential Area in Lee County 4-107

Figure 4-69 Medium Density Residential Area in Dade County..... 4-108

Figure 4-70 Medium Density Residential Area in Palm Beach County..... 4-108

Figure 4-71 Medium Density Residential Area in Duval County 4-109

Figure 4-72 Wind Speed Ratios as a Function of Surface Roughness for Various Heights..... 4-112

Figure 4-73 Reduction in Wind Speed at a Height of 3 meters (Open Terrain to Suburban Terrain). 4-113

Figure 4-74 Reduction in Wind Speed at a Height of 10 meters (Open Terrain to Suburban Terrain)4-114

Figure 4-75 Reduction in Wind Speed at a Height of 50 meters (Open Terrain to Suburban Terrain)4-115

Figure 4-76 Reduction in Wind Speed at a Height of 10 meters (Open Terrain to Heavily Treed Terrain) 4-116

Figure 4-77 Examples of Peak Gust Velocity Profiles as a Function of z_0 4-117

Figure 4-78 Estimation of Tree Blowdown Debris and Damage to Buildings..... 4-118

Figure 4-79 Drag Function Parameters k_1 and k_2 versus σ for Green Wood (Broadleaf Trees)..... 4-122

Figure 4-80 Velocity Spectra and Base Moment Spectra for Ponderosa Pine (Suburban Exposure). 4-130

Figure 4-81 Mean, RMS, and Peak Base Bending Moment Versus Wind speed Showing Effect of Crown Weight on Tree Response..... 4-131

Figure 4-82 Mean and Peak Base Bending Moment Versus Peak Wind speed at Center of Pressure (Open and Suburban Terrains) 4-132

Figure 4-83 Measured Comparison of Modeled Mean and Turbulence Intensity Profiles in Forests 4-134

Figure 4-84 Mean and Turbulence Intensity Profiles for Various Values of C_dLAI 4-136

Figure 4-85 z_0/H and d/H Plotted versus C_dLAI for Three Different Values of Crown Fraction..... 4-137

Figure 4-86 Tree Blowdown Curves 4-141

Figure 4-87 Probability of Blowdown Curves with Treefall Data Collected Following Hurricane Isabel..... 4-145

Figure 4-88 Shifted Probability of Blowdown Curves for Coniferous Trees with Treefall Data Collected Following Hurricane Isabel 4-146

Figure 4-89 Hazus Tree Coverage Data for Wake County, NC..... 4-149

Figure 4-90 Map of Tree Density for Wake County, NC 4-150

Figure 4-91 Surge and Coastal Flood User Requirements 4-151

Figure 4-92 Hazus Storm Surge Options 4-153

Figure 4-93 Hazus Coastal Storm Surge and Wave Model Flow Chart..... 4-154

Figure 4-94 Hazus Coastal Storm Surge and Wave Model Software Components 4-155

Figure 4-95 Difference (feet) in Peak Modeled Storm Tide with and without Coupling of Surge and Wave Models for Hurricane Ike 4-156

Figure 4-96 SLOSH Basins..... 4-157

Figure 4-97 Modeled Controlling Wave Heights Produced by the Hazus Methodology for a Transect Extending Inland from the Coastline to the Location of SSS-TX-GAL-002 4-160

Figure 5-1 Approach Used to Simulate Damage to Buildings..... 5-2

Figure 5-2 Wall Pressure Zones as Defined in ASCE 7 (Left figure) and SBCCI and NBCC (Right figure) 5-6

Figure 5-3 Locations of Pressure Estimates on Rectangular Building as Presented in Table 5-5 and Table 5-6 (Plan View)..... 5-10

Figure 5-4 Comparison of Measured and Modeled Wall Pressure Coefficients on a Flat Roof Building in Open Terrain ($z_0 = 0.1$ meters)..... 5-11

Figure 5-5 Comparison of Measured and Modeled Wall Pressure Coefficients on a Flat Roof Building in Suburban Terrain ($z_0 = 0.3$ meters) 5-12

Figure 5-6 Zones used for Defining Pressure Coefficients for Gable and Hip Roofs for the SBCCI (Top Drawings), the NBCC (Middle Drawings) and ASCE 7-95 (Bottom Drawings)..... 5-15

Figure 5-7 Peak Pressure Coefficients on Hip and Gable Roofs in Open Terrain (taken from Meecham, 1988)..... 5-16

Figure 5-8 Pressure Coefficient Zones Used in the UK Wind Loading Code for Hip Roof Buildings..... 5-17

Figure 5-9 Comparison of Modeled and Measured Peak Roof Pressure Coefficients on a Flat Roof Low-Rise Building..... 5-20

Figure 5-10 Comparisons of Modeled (Integrated) Uplift Loads on Hip and Gable Roofs to those Obtained from Wind Tunnel Experiments..... 5-23

Figure 5-11 Integration Areas Used for Comparison of Overall Roof and Wall Loads 5-25

Figure 5-12 Comparison of Modeled and Measured Wall Forces on Rectangular Building in Suburban Terrain 5-25

Figure 5-13 Comparison of Modeled and Observed Measured Uplift Coefficients on a Rectangular Building in Open Terrain 5-26

Figure 5-14 Comparison of Modeled and Observed Measured Uplift Coefficients on a Rectangular Building in Suburban Terrain..... 5-26

Figure 5-15 Comparison of Modeled, Wind Tunnel Measured, Full Scale Measured and ASCE 7 Estimated Drag, Lift and Moment Coefficients on a Manufactured Home 5-28

Figure 5-16 Close-up View of Model of School Building Used in Wind Tunnel Tests..... 5-29

Figure 5-17 View of Model in Wind Tunnel Showing Upstream Terrain..... 5-30

Figure 5-18 Layout of OWSJs as Modeled in Wind Tunnel Tests..... 5-30

Figure 5-19 Plan View of School Showing Location of Truss Uplift Loads (North is towards top of page) 5-31

Figure 5-20 Plan View of School Showing Location of all Pressure Taps Used in the Wind Tunnel Tests (North is towards top of page) 5-31

Figure 5-21 Comparison of Wind Tunnel Measured (open squares) and Simulated (solid squares) Joist Uplift Coefficients as a Function of Wind Direction5-33

Figure 5-22 Comparison of Wind Tunnel Measured (open squares) and Simulated (solid squares) Joist Uplift Coefficients as a Function of Wind Direction (Continued)5-34

Figure 5-23 Comparison of Wind Tunnel Measured (open squares) and Simulated (solid squares) Joist Uplift Coefficients as a Function of Wind Direction (Concluded).....5-35

Figure 5-24 Location of Pressure Points for 2.5:1 High-Rise Building5-36

Figure 5-25 Location of Pressure Points for 1:1 High-Rise Building.....5-37

Figure 5-26 Maximum and Minimum Pressure Coefficients versus Wind Direction Used in Modeling of a Rectangular High-Rise Building Having a Length to Width Ratio of 2.5.....5-38

Figure 5-27 Maximum and Minimum Pressure Coefficients versus Wind Direction Used in Modeling of a Rectangular High-Rise Building Having a Length to Width Ratio of 2.5 (continued).....5-39

Figure 5-28 Maximum and Minimum Pressure Coefficients versus Wind Direction Used in Modeling of a Rectangular High-Rise Building Having a Length to Width Ratio of 2.5 (continued).....5-40

Figure 5-29 Maximum and Minimum Pressure Coefficients versus Wind Direction Used in Modeling of a Rectangular High-Rise Building Having a Length to Width Ratio of 2.5 (continued).....5-41

Figure 5-30 Maximum and Minimum Pressure Coefficients vs. Wind Direction Used in Modeling of a Rectangular High-Rise Building Having a Length to Width Ratio of 2.5 (continued).....5-42

Figure 5-31 Maximum and Minimum Pressure Coefficients versus. Wind Direction Used in Modeling of a Rectangular High-Rise Building Having a Length to Width Ratio of 2.5 (continued).....5-43

Figure 5-32 Maximum and Minimum Pressure Coefficients versus Wind Direction Used in Modeling of a Square High-Rise Building (concluded)5-44

Figure 5-33 Maximum and Minimum Pressure Coefficients versus Wind Direction Used in Modeling of a Square High-Rise Building.....5-45

Figure 5-34 Maximum and Minimum Pressure Coefficients versus Wind Direction Used in Modeling of a Square High-Rise Building (continued).....5-46

Figure 5-35 Maximum and Minimum Pressure Coefficients versus Wind Direction Used in Modeling of a Square High-Rise Building (continued).....5-47

Figure 5-36 Maximum and Minimum Pressure Coefficients versus Wind Direction Used in Modeling of a Square High-Rise Building (concluded)5-48

Figure 5-37 Example Model Subdivision Used in the Missile Risk Study.....5-50

Figure 5-38 Example Hurricane Wind Speed Traces Used for the 150 mph Case – Hurricane #15-51

Figure 5-39 Example Hurricane Wind Speed Traces Used for the 150 mph Case – Hurricane #25-52

Figure 5-40 Example Hurricane Wind Speed Traces Used for the 150 mph Case – Hurricane #35-52

Figure 5-41 Example Energy Reliability Curves Derived for a Subdivision Comprised of Single-Story Homes with Asphalt Shingle Roofs.....5-53

Figure 5-42 Comparison of Reliability Curves Derived from the Explicit Missile (lines) Simulation to Those Obtained from the Simplified Model (points only)5-55

Figure 5-43 Example of Computer-Modeled Surface Flow Pattern Compared with Wind Tunnel Observation5-57

Figure 5-44 Example of Gravel Scour Pattern Compared with Field and Experimental Observations ..5-58

Figure 5-45 Example of Gravel Missile Trajectory5-59

Figure 5-46 The Marriott-Datran Complex in Kendall, Florida.....5-60

Figure 5-47 Approximate Plan of the Marriott-Datran Complex5-61

Figure 5-48 Impacts on Walls with Momentum Exceeding the Threshold for Damage..... 5-62

Figure 5-49 Damage Scenarios for Datran Towers I and II Downstream of the Marriott Hotel..... 5-63

Figure 5-50 General View of the Houston Central Business District (Kareem and Stevens, 1985) 5-65

Figure 5-51 Aerial Perspective of Damaged High-Rise Buildings (Beason et al., 1984)..... 5-66

Figure 5-52 Plan View of Damaged High-Rise Building Towers (Beason et al., 1984)..... 5-67

Figure 5-53 Plan Geometry of the Modeled Buildings in the Houston Downtown Central Business District
..... 5-67

Figure 5-54 A General View of the School Complex..... 5-70

Figure 5-55 The Windward Face of the Main Missile Source Building (facing southwest)..... 5-70

Figure 5-56 Roof Gravel on the Upstream Building..... 5-71

Figure 5-57 Glass Damage on the Windward Face of the Downstream Building..... 5-72

Figure 5-58 Geometry of the Modeled Complex..... 5-73

Figure 5-59 Trees in Front of the Lower-Right Glazed Area of the Downstream Building 5-75

Figure 5-60 The Layout of Modeled Gravel Source Roof and Target Walls Relative to the Wind Directions
Modeled..... 5-79

Figure 5-61 Number of Impacts per m² hr on Walls Averaged Over the Lowest 30 meters, as Function of
Building Spacing..... 5-82

Figure 5-62 Number of Impacts per m² hr on Walls Averaged Over the Lowest 30 meters, as Function of
Building Spacing..... 5-83

Figure 5-63 Examples of Fitted Number of Impacts Varying with Peak Gust Speed for Selected Building
Spacing Cases in Comparison with Simulation Results 5-83

Figure 5-64 Height Factor for Number of Impacts for Various Cases with Building Spacing from 20 to
150 meters..... 5-84

Figure 5-65 Fitted Height Factor for Number of Impacts for Building Spacing from 20 to 150 meters..... 5-84

Figure 5-66 The Mean Trend of the 95th Percentile Impact Momentum with the Peak-Gust Speed, and
the Variability for which the One Standard Deviation Bounds are Shown by the Short Bars..... 5-86

Figure 5-67 Distribution of the Normalized Impact Momentum..... 5-86

Figure 5-68 Simulation Scheme for Tree Blow-Down Damage to Building..... 5-88

Figure 5-69 Small Pipe Impacting Wall Without Plywood Sheathing, 3,600 foot-pounds at Impact,
Breaking Top Plates and Half-Way Cutting Into Wall 5-89

Figure 5-70 Small Pipe Impacting Wall with Plywood Sheathing, 3,600 foot-pounds at Impact, Breaking
Top Plates and 1/4 Cutting Into Wall 5-89

Figure 5-71 Large Pipe Impacting Roof and Wall Without Plywood Sheathing, 7,600 foot-pound at
Impact, Breaking Roof, Top Plates and Entire Wall with Apparent Residual Energy Hitting Ground... 5-
90

Figure 5-72 Large Pipe Impacting Roof and Wall With Plywood Sheathing, 7,600 foot-pound at Impact,
Breaking Roof, Top Plates and 1/8 Wall 5-90

Figure 5-73 Wind-Induced Masonry Wall and Brick Veneer Damage..... 5-97

Figure 5-74 Typical Cracking Patterns for Various Wall Spans and Different Edge Support Conditions
(Drysdale and Essawy, 1988)..... 5-99

Figure 5-75 Typical Cracking Pattern for Top and Bottom Supported Prestressed Masonry Wall (Dawe
and Aridru, 1993) 5-100

Figure 5-76 Typical Crack Patterns for Masonry Walls of Small and Large Aspect Ratios, with and
without Top Supports..... 5-100

Figure 5-77 Comparison of Failure Pressure Variation with Wall Span..... 5-105

Figure 5-78 Effects of Workmanship on Actual Flexural Strength versus Nominal Value..... 5-106

Figure 5-79 Estimated Failure Probability as a Function of Pressure Load for Various Wall Spans with Roof Support..... 5-107

Figure 5-80 Estimated Failure Probability as a Function of Pressure Load for Various Wall Spans without Roof Support..... 5-108

Figure 5-81 Examples of Wind-Induced Damage to Residential Wood-Framed Wall System (Oklahoma Tornado Out-Break, May 1999)..... 5-110

Figure 5-82 Examples of Wind-Induced Damage to Residential Wood Framed System (Oklahoma Tornado Outbreak..... 5-111

Figure 5-83 Examples of Wind-Induced Damage to Residential Wood-Framed Wall System (Oklahoma Tornado Out-Break, May 1999)..... 5-112

Figure 5-84 Examples of Wind-Induced Damage to Residential Wood-Framed Wall System (FEMA, 1992, Hurricane Andrew, Florida) 5-113

Figure 5-85 Examples of Wind-Induced Damage to Residential Wood-Framed Wall System (FEMA, 1992, Hurricane Andrew, Florida) (concluded) 5-114

Figure 5-86 Examples of Wind-Induced Damage to Residential Wood-Framed Wall System (HUD, 1993, Hurricane Andrew, Florida) 5-115

Figure 5-87 Typical Wood Frame Walls for Residential Construction (CMHC, 1989)..... 5-116

Figure 5-88 Typical Nailing Patterns for Wood Frame Wall Structure of Residential Construction (AFPA/AWC, 1996) 5-117

Figure 5-89 Measured Ultimate Capacity (Mean \pm 1 Standard Deviation) of 8d Nail Connections for Lateral Loading in Comparison to the NDS Value for Various Rates of Loading..... 5-121

Figure 5-90 Estimated Failure Probability as a Function of Pressure Load for Various Wall Spans, Top Supported and Let-In Braced Wood Frame Walls..... 5-124

Figure 5-91 Estimated Failure Probability as a Function of Pressure Load for Various Wall Spans, Top Supported and Sheathed Wood Frame Walls 5-124

Figure 5-92 Estimated Failure Probability as a Function of Pressure Load for Various Wall Spans, Top Unsupported Wood Frame Walls, Let-In Braced or Sheathed5-125

Figure 5-93 OWSJ Roof Damage States for a 12' High Building in Suburban Terrain 5-139

Figure 5-94 OWSJ Roof Damage States for a 20' High Building in Suburban Terrain 5-140

Figure 5-95 Metal Deck Profile with Three Fasteners 5-146

Figure 5-96 Metal Deck Profile with Four Fasteners 5-146

Figure 5-97 Metal Deck Profile with Five Fasteners..... 5-146

Figure 5-98 Metal Deck Profile with Seven Fasteners..... 5-146

Figure 5-99 Finite Element Model of the 3' by 8' Panel 5-147

Figure 5-100 Flowchart of the Probabilistic Finite Element Analysis..... 5-149

Figure 5-101 CDFs of Metal Deck Failure Pressures (Screw Connections)..... 5-152

Figure 5-102 CDFs of Metal Deck Failure Pressures (Weld Connections) 5-152

Figure 5-103 Example of a Metal Wall System with Exposed Fasteners (Newman, 1997) 5-154

Figure 5-104 Metal Deck Profile for Wall and Roof Systems 5-154

Figure 5-105 Finite Element Mesh of the Wall Panels 5-155

Figure 5-106 Refined Mesh around the Fastener 5-156

Figure 5-107 Stress Distribution of Wall Panels with Superimposed Deformation..... 5-157

Figure 5-108 Cumulative Distribution Functions of Wall System Failure Pressures 5-158

Figure 5-109 Cumulative Distribution Functions of Metal Roof Failure Pressures 5-160

Figure 5-110 NAHB Site Locations 5-161

Figure 5-111 Wind Speed and Direction Traces (10 meters, Open Terrain) at Locations of Photographs
1, 2 3, and 4 (HUD Locations, F, E, D, and H) 5-163

Figure 5-112 Comparison of Observed Damage States for Single-Story Gable Homes Obtained from
Aerial Photography and HUD Damage Survey – Location of Photograph 1 (HUD Location F) 5-165

Figure 5-113 Comparison of Observed Damage States for Single-Story Gable Homes Obtained from
Aerial Photography and HUD Damage Survey – Location of Photograph 2 (HUD Location E) 5-165

Figure 5-114 Comparison of Observed Damage States for Single-Story Gable Homes Obtained from
Aerial Photography and HUD Damage Survey – Location of Photograph 3 (HUD Location D)..... 5-166

Figure 5-115 Comparison of Modeled and Observed Roof Damage States to Two-Story Gable Houses
(Photograph 1)..... 5-168

Figure 5-116 Comparison of Modeled and Observed Roof Damage States to Two-Story Gable Houses
(Photograph 2)..... 5-168

Figure 5-117 Comparison of Modeled and Observed Roof Damage States to Single-Story Gable Houses
(Photograph 2)..... 5-169

Figure 5-118 Comparison of Modeled and Observed Roof Damage States to Single-Story Gable Houses
(Photograph 3)..... 5-170

Figure 5-119 Comparison of Modeled and Observed Roof Damage States to Single-Story Hip Houses
(Photograph 2)..... 5-171

Figure 5-120 Comparison of Modeled and Observed Roof Damage States to Single-Story Hip Houses
(Photograph 3)..... 5-171

Figure 5-121 Comparison of Simulated and Observed Roof Covering Damage for Gable and Hip Roof
Houses..... 5-174

Figure 5-122 Comparison of Simulated and Observed Window Damage States for One and Two-Story
Houses, Hurricane Andrew (1992) 5-174

Figure 5-123 Examples of Whole Roof Failures Depicted in Photograph Number 3.....5-175

Figure 5-124 Modeled Failure Rates for Single-Story Gable Roof Homes with Strapped Roof-Wall
Connections and Toe Nailed Roof-Wall Connections 5-177

Figure 5-125 Modeled Failure Rates for Single-Story Hip Roof Homes with Strapped Roof-Wall
Connections and Toe Nailed Roof-Wall Connections 5-178

Figure 5-126 BUR Cover Damage for Hurricane Andrew - Dixie Highway..... 5-187

Figure 5-127 BUR Cover Damage for Hurricane Andrew - Aerial Photograph 3..... 5-188

Figure 5-128 Damage State 0 5-191

Figure 5-129 Damage State 1 5-192

Figure 5-130 Damage State 1 (concluded) 5-193

Figure 5-131 Damage State 2 5-194

Figure 5-132 Damage State 3 5-195

Figure 5-133 Damage State 4 5-196

Figure 5-134 Damage State (concluded) 5-197

Figure 5-135 Model House Geometries Used in Damage Simulation Study..... 5-198

Figure 5-136 Model Building Geometries Used in Building Simulation Study.....5-214

Figure 5-137 Model Building for One-Story Low-Rise Masonry Strip Mall Building with Roof Height = 12’ 5-224

Figure 5-138 Geometries of Small Metal Buildings Used in Study..... 5-242

Figure 5-139 Geometries of Medium Metal Buildings Used in Study..... 5-243

Figure 5-140 Geometries of Large Metal Buildings Used in Study..... 5-243

Figure 5-141 Modeled Two-Story Fully-Engineered Buildings 5-248

Figure 5-142 Modeled Five-Story Fully-Engineered Buildings. 5-248

Figure 5-143 Modeled Eight-Story Fully-Engineered Buildings..... 5-249

Figure 5-144 Model Building for Large Industrial Building – 200’x120’x20’ High..... 5-258

Figure 5-145 Water Damage to Interior Ceiling of a Fire Station in the Houston Area as a Result of Roof Damage (2008, Hurricane Ike)..... 5-260

Figure 5-146 Bent Bay Door Rollers for a Fire Station in the Houston Area (2008, Hurricane Ike)... 5-261

Figure 5-147 Torn Awning over Rear Entry Door for a Fire Station in the Houston Area (2008, Hurricane Ike)..... 5-261

Figure 5-148 Panel Damage to Bay Doors for a Fire Station in the Houston Area (2008, Hurricane Ike) 5-262

Figure 5-149 Fire Station Geometry Used in Study 5-263

Figure 5-150 Elementary School Geometry Used in Study..... 5-266

Figure 5-151 High School (Two-Story) Geometry Used in Study..... 5-269

Figure 5-152 Large High School (Three-Story) Geometry Used in Study 5-269

Figure 5-153 Small Hospital (<50 beds) Geometry Used in Study..... 5-273

Figure 5-154 Medium Hospital (50-150 beds) Geometry Used in Study 5-274

Figure 5-155 Large Hospital (>150 beds) Geometry Used in Study..... 5-274

Figure 6-1 Tree Debris Functions in Pounds per Acre6-23

Figure 6-2 Calculation of Perimeter Collection Area.....6-26

Figure 6-3 Equivalent Census Block Width versus Buildings per Acre for Hampton Roads Region of Virginia.....6-26

Figure 6-4 Addition of Tree Collection Factor to Tree Parameter Table in Hazus.....6-28

Figure 6-5 Hazus Debris Results Table.....6-28

Figure 6-6 Comparison of Modeled Total and Collected Tree Debris Weight with Collection Totals Reported by NC Department of Emergency Management by County in North Carolina for Hurricane Isabel.....6-31

Figure 6-7 Ratio of Modeled Tree Debris to Actual Debris Collected by County in Virginia for Hurricane Isabel.....6-33

Figure 6-8 Comparison of Modeled Tree Debris Collected to Reported Amounts for Various Locations and Various Hurricanes6-36

Figure 7-1 Modeled Probability Mass Function of Loss Ratios for Lower Peak Gust Wind Speeds (between 50 mph and 100 mph) 7-3

Figure 7-2 Modeled Probability Mass Function of Loss Ratios for Medium Peak Gust Wind Speeds (between 100 mph and 150 mph)..... 7-4

Figure 7-3 Modeled Probability Mass Function of Loss Ratios for High Peak Gust Wind Speeds (between 150 mph and 200 mph)..... 7-5

Figure 7-4 Building Stock Regions Used for the Loss Ratio Computation..... 7-6

Figure 7-5 Empirical Uninhabitability Function for Single-Family Buildings..... 7-7

Figure 7-6 Empirical Uninhabitability Function for Multi-Family Buildings 7-7

Figure 7-7 Example of Computed Percentage of Household Being Displaced as a Function of Peak Gust
Wind Speed at Site 7-8

Figure 7-8 Uninhabitability as a Function of Mean Building Loss for Single-Family Buildings 7-13

Figure 7-9 Uninhabitability as a Function of Mean Building Loss for Multi-Family Buildings 7-14

Figure 8-1 Schematic Representation of the Residential Damage-to-Loss Model 8-2

Figure 8-2 Implicit Loss Functions Associated with Damage to the Roof Cover 8-11

Figure 8-3 Content and Interior Losses Associated with Roof Sheathing Failure 8-12

Figure 8-4 Content Losses Due to Fenestration Breach 8-13

Figure 8-5 Predicted and Actual Losses 8-16

Figure 8-6 Plots of Influence Functions 8-26

Figure 8-7 Relationship between Open Terrain Gust Wind Speed and Building Loss Ratio for a Four-Story
Motel 8-26

Figure 8-8 Relationship between Building Loss Ratio and Content Loss Ratio for a Four-Story Motel. 8-28

Figure 8-9 Relationship between Building Loss, Loss of Use, and Business Interruption for a Motel .. 8-30

Figure 8-10 Relationship Between Modeled loss of Function and Actual Loss of Function for a Given Fire
Station 8-31

Figure 8-11 Relationship Between Modeled Loss of Function and Actual Loss of Function for an
Elementary School of Moderate Strength located in a Residential Area 8-32

Figure 8-12 Relationship Between Modeled Loss of Function and Actual Loss of Function for a Small
Hospital 8-33

Figure 8-13 Relationship Between Modeled Loss of Function and Actual Loss of Function for a Medium
Hospital 8-33

Figure 8-14 Relationship Between Model Loss of Function and Actual Loss of Function for a Large
Hospital 8-34

Figure 8-15 Example of Self-Adhering Waterproof Underlayment Used to Tape Plywood Joints, Ridges
and Eaves; Photo Depicts Use Around Fenestrations 8-36

Figure 8-16 Building Repair Cost Estimates as Functions of Impact Energy 8-80

Figure 8-17 Contents Repair Cost Estimates as Functions of Impact Energy 8-81

Figure 8-18 Total Repair Cost Estimates as Functions of Impact Energy 8-81

Figure 8-19 Dependence on Tree Density of Building (Upper) and Contents (Lower) Loss Functions.. 8-83

Figure 8-20 Dependence on Tree Height of Building (Upper) and Contents (Lower) Loss Functions ... 8-84

Figure 8-21 Dependence on Tree Type of Building (Upper) and Contents (Lower) Loss Functions 8-85

Figure 8-22 Dependence on Building Dimensions (ft) of Building (Upper) and Contents (Lower) Loss
Functions 8-86

Figure 8-23 Dependence on Wall Type of Building (Upper) and Contents (Lower) Loss Functions 8-87

Figure 8-24 Building and Contents Loss Comparison 8-88

Figure 8-25 Depth-Damage Curve in Hazus for One-Story, Single-Family Houses on Slab Foundations in
the Coastal Zone A 8-92

Figure 8-26 RES1 (Single-Family) Subassembly Losses for Flood as a Percentage of Subassembly
Replacement Cost 8-105

List of Tables

Table 4-1 Hurricane Boundary Layer Model Parameters Inside RMW	4-11
Table 4-2 Number of Wind Speed Records for Each Hurricane	4-26
Table 4-3 Saffir-Simpson Storm Categories.....	4-43
Table 4-4 Storm Category and Central Pressure at Landfall	4-45
Table 4-5 Comparison of HURDAT Hurricane Classification to Classifications Resulting from Detailed Studies Performed by NOAA/HRD	4-52
Table 4-6 Sector Values for Rainfall Rate Parameter, s	4-62
Table 4-7 24-Hour Total Rainfall Comparison	4-68
Table 4-8 Roughness Lengths of Homogeneous Surface Types (from Wieringa, 1993).....	4-70
Table 4-9 Roughness Lengths For Various Surface Types (from Simiu and Scanlan, 1996).....	4-71
Table 4-10 Roughness Lengths of Rather Homogeneously Built-up Areas (from Wieringa, 1993)	4-71
Table 4-11 NLCD 2011 Database Classification System	4-73
Table 4-12 NLCD 2001 Land Cover Classification Versus Surface Roughness Length.....	4-76
Table 4-13 Assignment of z_0 values to NLCD LULC Codes.....	4-89
Table 4-14 Assignment of z_0 values to NLCD LULC Codes (Continued)	4-90
Table 4-15 z Values Computed from NLCD Data and Assigned Empirically for Houston, TX.....	4-98
Table 4-16 z_0 Values Computed from NLCD Data and Assigned Empirically for Miami, FL, Including Downtown (Cell # 6-3).....	4-99
Table 4-17 z_0 Values Computed from NLCD Data and Assigned Empirically for Raleigh, NC, Including Downtown (Cell # 10-4).....	4-101
Table 4-18 z_0 Values Computed from NLCD Data and Assigned Empirically for a Location in South Suburban of Providence, RI.....	4-102
Table 4-19 Examples for Roughness Length Calculation Using Lettau's Formula.....	4-110
Table 4-20 Input Parameters for Modeling of Trees.....	4-125
Table 4-21 Characteristics of Key Parameters for Example Ponderosa Pine Tree Response Estimates..	4-129
Table 4-22 Summary of Tree Blowdown Data	4-142
Table 4-23 Summary of Number of Failed Trees by Height Class	4-142
Table 4-24 Hazus Tree Data Format.....	4-149
Table 4-25 SLOSH Basins Used in Hazus Coastal Surge Methodology.....	4-157
Table 4-26 Shoreline Wave Exposure Classification for Hazus Flood Model	4-161
Table 5-1 Comparison of Positive Wall Pressure Coefficients – Buildings with Roof Slopes Less than 10°	5-5
Table 5-2 Comparison of Positive Wall Pressure Coefficients – Buildings with Roof Slopes Greater than 10°	5-5
Table 5-3 Comparison of Negative Wall Pressure Coefficients – Buildings with Roof Slopes Less than 10°	5-5
Table 5-4 Comparison of Negative Wall Pressure Coefficients – Buildings with Roof Slopes Greater than 10°	5-5
Table 5-5 Positive Wall Pressure Coefficients Estimated for Buildings Shown in Figure 5-7 Given as a Function of Wind Direction.....	5-6

Table 5-6 Negative Wall Pressure Coefficients Estimated for Building Shown in Figure 5-7, Given as a Function of Wind Direction 5-8

Table 5-7 Comparison of Negative Pressure Coefficients on Flat Roofs 5-13

Table 5-8 Comparison of Negative Pressure Coefficients on Gable Roofs..... 5-13

Table 5-9 Comparison of Negative Pressure Coefficients on Hip Roofs..... 5-14

Table 5-10 Basic Inputs of Missile Sources (Roof Gravel) and Target Glazing Properties 5-68

Table 5-11 Number of Damaged Windows: Simulation versus Available Observations..... 5-68

Table 5-12 Basic Inputs of Missile Sources (Roof Gravel) and Target Glazing Properties 5-73

Table 5-13 Number of Damaged Windows: Simulation versus Available Observations..... 5-74

Table 5-14 Variables that Influence the Number of Impacts and Momentum Distribution 5-78

Table 5-15 Damage States in Relation to Impact Energy..... 5-91

Table 5-16 Uplift Resistances of 8-by-4 Roof Sheathing Panels from Laboratory Testing 5-93

Table 5-17 Failure Pressures (p_r) and Crack Pattern Parameters (x or z) Derived from Yield-Line Analysis 5-103

Table 5-18 Failure Pressures (p_r) and Crack Pattern Parameters (x or z) Derived from Yield-Line Analysis, with the Assumption of Discontinuity at Initial Horizontal Center Crack 5-104

Table 5-19 Estimated Resistance Capacity of Nail Connections within One Stud Spacing (Typically 16") 5-120

Table 5-20 Adjustment Factors Required by NDS of Nail Connections within One Stud Spacing (Typically 16") 5-120

Table 5-21 Results of Field Pull-Out Tests on Soil Anchors Installed and Loaded at Various Angles (Yokel et al., 1982)..... 5-128

Table 5-22 Results of Field Pull-Out Tests on Fully Embedded Soil Anchors: $\beta_1 = 90^\circ$, $\beta_2 = 90^\circ$ (Yokel et al., 1982)..... 5-128

Table 5-23 Results of Field Pull-Out Tests on Fully Embedded Soil Anchors: $\beta_1 = 45^\circ$, $\beta_2 = 105^\circ$ (Pearson et al., 1991) 5-129

Table 5-24 Roof Cover Damage Model - Normal Distribution Parameters..... 5-131

Table 5-25 Uplift Resistances of an Unreinforced Roof-Wall Anchor, 6' O.C..... 5-136

Table 5-26 Nominal Deck Information, from SDI (1992) 5-141

Table 5-27 Typical Screw Properties..... 5-142

Table 5-28 Design Wind Pressures Calculated Using ASCE 7-88 and SBCCI 1988..... 5-144

Table 5-29 Determined Case Studies for Screw Connections..... 5-145

Table 5-30 Determined Case Studies for Weld Connections 5-145

Table 5-31 Simulated Failure Loads for Different Designs..... 5-150

Table 5-32 Calculated Design Pressure Using MBMA and Simulated Failure Pressure Statistics from FEM Analysis 5-159

Table 5-33 Connection Layout for Example Metal Roofs 5-159

Table 5-34 Mapping Used to Match Aerial Photograph Estimated Damage States and HUD Damage States 5-163

Table 5-35 Surface Roughness Values used in Hurricane Erin Sheathing Damage Validation Study at Navarre Beach, Florida..... 5-172

Table 5-36 Comparison of Observed and Modeled Roof Sheathing Damage at Navarre Beach, Florida. 5-173

Table 5-37 Comparison of Observed and Modeled Whole Roof Failures at Locations of Aerial Photographs, Hurricane Andrew (1992) 5-176

Table 5-38 Comparison of Threshold Velocities for Various Manufactured Home Damage States... 5-179

Table 5-39 Comparison of Observed and Modeled Manufactured Home Damage States on Topsail Island Produced by Hurricane Bertha (1996) 5-181

Table 5-40 Damage Classes Described by Vann and McDonald and the Corresponding Damage States from the Damage Simulation Model5-182

Table 5-41 The Corresponding Damage States from the Damage Simulation Model 5-182

Table 5-42 Comparison of Modeled and Observed Manufactured Home Damage States Following Hurricane Andrew in South Florida..... 5-183

Table 5-43 Comparison of Simulated and Observed Manufactured Home Damage States Produced by Hurricane Elena..... 5-185

Table 5-44 Damage States for Residential Construction Classes..... 5-188

Table 5-45 Component Resistance Values Used to Model Residential Buildings..... 5-199

Table 5-46 Average Building Damage States 5-200

Table 5-47 Percent Increases in the Per Storm Average Building Damage State Due to Changes in Building Parameters (Minimum/Average/Maximum) - Residential Buildings..... 5-202

Table 5-48 Average Building Damage States – Install Shutters..... 5-204

Table 5-49 Average Building Damage States – Upgrade Roof..... 5-205

Table 5-50 Average Building Damage States – Install Shutters and Upgrade Roof..... 5-208

Table 5-51 Percent Decreases in the Per Storm Average Building Damage State Due to Mitigation (Minimum/Average/Maximum) - Residential Buildings5-209

Table 5-52 Damage Classes Described by Vann and McDonald 5-210

Table 5-53 The Corresponding Damage States from the Damage Simulation Model 5-211

Table 5-54 Resistance Parameters Used to Model Manufactured Homes 5-211

Table 5-55 Per Storm Average Damage States 5-212

Table 5-56 Component Resistance Values Used to Model Marginally-Engineered or Non-Engineered Hotel/Motel and Multi-Family Residential Buildings..... 5-215

Table 5-57 Average Building Damage States – Marginally- or Non-Engineered Hotel/Motel and Multi-Family Residential Buildings – Gable/Hip Roof with Shingles 5-216

Table 5-58 Average Building Damage States – Marginally- or Non-Engineered Hotel/Motel and Multi-Family Residential Buildings – Flat Roofs with BUR..... 5-218

Table 5-59 Average Building Damage States – Marginally- or Non-Engineered Hotel/Motel and Multi-Family Residential Buildings – Flat Roofs with EPDM..... 5-219

Table 5-60 Percent Increases in the Per Storm Average Building Damage State Due to Changes in Building Parameters (Minimum/Average/Maximum) - Marginally- or Non-Engineered Hotel/Motel and Multi-Family Residential Buildings5-221

Table 5-61 Damage States for Low-Rise Masonry Strip Mall Construction..... 5-223

Table 5-62 Description of Low-Rise Masonry Strip Mall Buildings 5-224

Table 5-63 Component Resistance Values Used for Strip-Mall Type Building 5-226

Table 5-64 Description of Missile Environments..... 5-228

Table 5-65 Average Damage States for Building A - Twelve Foot High Strip Mall Building with Six Units and Wood Deck with Two Foot Truss Spacing..... 5-228

Table 5-66 Average Damage States for Building B - Twenty Foot High Strip Mall Building with Six Units and Wood Deck with Two Foot Truss Spacing.....	5-230
Table 5-67 Average Damage States for Building A - Twelve Foot High Strip Mall Building with Six Units and Metal Deck with Four Foot Joist Spacing	5-232
Table 5-68 Average Damage States for Building B - Twenty Foot High Strip Mall Building with Six Units and Metal Deck with Four Foot Joist Spacing	5-234
Table 5-69 Average Damage States for Building C - Twenty Foot High Strip Mall Building with Six Units and Metal Deck with Six Foot Joist Spacin.....	5-236
Table 5-70 Average Damage States for Building D - Twenty Foot High Strip Mall Building with One Unit and Metal Deck with Six Foot Joist Spacing.....	5-238
Table 5-71 Percent Increases in the Per Storm Average Building Damage State due to Changes in Building Parameters (Minimum/Average/Maximum) - Strip Mall Building with Wood Roof System	5-241
Table 5-72 Percent Increases in the Per Storm Average Building Damage State due to Changes in Building Parameters (Minimum/Average/Maximum) - Strip Mall Building with Steel Roof System	5-241
Table 5-73 Percent Increases in the Per Storm Average Building Damage State Due to Changes in Building Configuration (Minimum/Average/Maximum)	5-242
Table 5-74 Damage States Metal Buildings	5-244
Table 5-75 Component Resistances for Pre-Engineered Metal Buildings.....	5-244
Table 5-76 Average Per Storm Damage States for Pre-Engineered Metal Buildings	5-246
Table 5-77 Percent Increases in the Per Storm Average Building Damage State Due to Changes in Building Parameters (Minimum/Average/Maximum) - Pre-Engineered Metal Buildings.....	5-246
Table 5-78 Damage State Definitions for Engineered Steel Buildings	5-247
Table 5-79 Failure Pressure Models for Metal Deck on Steel Joists.....	5-251
Table 5-80 Average Building Damage States – Two-Story Engineered Building	5-251
Table 5-81 Average Building Damage States – Five-Story Engineered Building	5-252
Table 5-82 Average Building Damage States – Eight-Story Engineered Building.....	5-254
Table 5-83 Percent Increases in the Per Storm Average Building Damage State Due to Changes in Building Parameters (Minimum/Average/Maximum) - Engineered Residential and Commercial Buildings.....	5-255
Table 5-84 Damage States for Industrial Buildings.....	5-256
Table 5-85 Component Resistance Values Used for Strip-Mall Type Building	5-258
Table 5-86 Per Storm Average Building Damage States – Industrial Building.....	5-259
Table 5-87 Average Damage States for the Fire Station Building	5-263
Table 5-88 Percent Increases in the Per Storm Average Building Damage State due to Changes in Building Parameters (Minimum/Average/Maximum) – Fire Station.....	5-265
Table 5-89 Average Damage States for the Elementary School Building.....	5-266
Table 5-90 Percent Increases in the Per Storm Average Building Damage State due to Changes in Building Parameters (Minimum/Average/Maximum) – Elementary School	5-268
Table 5-91 Average Damage States – Two-Story High School	5-270
Table 5-92 Average Damage States – Three-Story High School.....	5-271
Table 5-93 Percent Increases in the Per Storm Average Building Damage State due to Changes in Building Parameters (Minimum/Average/Maximum) – High School	5-272

Table 5-94 Average Damage States – Small Hospital.....	5-275
Table 5-95 Average Damage States – Medium Hospital.....	5-276
Table 5-96 Average Damage States – Large Hospital.....	5-277
Table 5-97 Percent Increases in the Per Storm Average Building Damage State due to Changes in Building Parameters (Minimum/Average/Maximum) – Hospital.....	5-278
Table 6-1 Component Unit Weights Used in the Debris Model.....	6-5
Table 6-2 Sustained Load Statistics.....	6-9
Table 6-3 Debris Distribution Matrix.....	6-9
Table 6-4 Default Building Component Construction Types.....	6-12
Table 6-5 Roof Frame Construction Types and Unit Weights.....	6-15
Table 6-6 Insulation Types and Unit Weights.....	6-16
Table 6-7 Partition Construction Types and Unit Weights.....	6-16
Table 6-8 Floor Finish Types and Unit Weights.....	6-16
Table 6-9 Floor Construction Types and Unit Weights.....	6-17
Table 6-10 Wall Finish Types and Unit Weights.....	6-18
Table 6-11 Ceiling Finish Types and Unit Weights.....	6-19
Table 6-12 Structural Debris Comparison for Hurricane Andrew.....	6-21
Table 6-13 Debris Comparison for Hurricanes Hugo and Andrew.....	6-21
Table 6-14 Tree Debris Related Bulking Factors from Various Sources.....	6-22
Table 6-15 Comparison of Modeled Tree Debris Generation and Collection Weight with Tree Parameters Compiled at the Census Tract and Census Block Levels.....	6-29
Table 6-16 North Carolina Tree Debris Collection Data for Hurricane Isabel (2003).....	6-30
Table 6-17 Virginia Debris Collection Data for Hurricane Isabel (2003).....	6-32
Table 6-18 Building Density and Average Tree Debris Collection Rate by County for North Carolina and Virginia.....	6-34
Table 6-19 Locations of Collected Tree Debris Estimates by Hurricane Name and Year.....	6-35
Table 7-1 Default Weights for Demographic Variables.....	7-12
Table 7-2 Default Fractions of Displaced Households Seeking Public Shelter.....	7-12
Table 8-1 Model Parameters - Building Characteristics.....	8-2
Table 8-2 Model Parameters - Damage State.....	8-3
Table 8-3 Roof Installed Materials Cost Modification Factors.....	8-3
Table 8-4 Residential Classification Based on Income Ratio.....	8-4
Table 8-5 Default Residential Subassembly Cost Ratios.....	8-5
Table 8-6 Subassembly Cost Ratios - Tiles versus Shingle.....	8-5
Table 8-7 Cost Ratio Comparison for Brick and Tile Modification.....	8-6
Table 8-8 Location Index Factor – Florida.....	8-8
Table 8-9 Predicted and Actual Losses.....	8-15
Table 8-10 Building and Content Losses Associated with Manufactured Home Frame Damage or Foundation Failure.....	8-17
Table 8-11 Cost Ratio – RSMeans Model Building and Hazus Model Building.....	8-21
Table 8-12 Influence Matrix for Explicit Building Loss.....	8-23
Table 8-13 Influence Matrix for Implicit Building Loss.....	8-24
Table 8-14 Influence Functions.....	8-25
Table 8-15 Business Interruption Timetable.....	8-29

Table 8-16 Percent Increases in the Average Annual Total Loss Due to Changes in Building Parameters
– Residential Buildings.....8-37

Table 8-17 Percent Decreases in the Average Annual Total Loss Due to Mitigation Parameters–
Residential Buildings.....8-37

Table 8-18 Annual Average Building Loss Ratios – Manufactured Homes.....8-38

Table 8-19 Annual Average Content Losses – Manufactured Homes.....8-38

Table 8-20 Subassembly Cost Distributions for One-Story Motels.....8-39

Table 8-21 Subassembly Cost Distributions for Two and Three-Story Motels.....8-40

Table 8-22 Subassembly Cost Distributions for Four to Seven-Story Hotels.....8-41

Table 8-23 Percent Increases in the Average Annual Total Loss Due to Changes in Building Parameters
– Marginally- or Non-Engineered Hotel/Motel and Multi-Family Residential Buildings.....8-43

Table 8-24 Subassembly Cost Distributions for Low-Rise Masonry Strip Mall8-45

Table 8-25 Percent Increases in the Average Annual Total Loss Due to Changes in Building Parameters
–Strip Mall Building with Wood Roof System8-46

Table 8-26 Percent Increases in the Average Annual Total Loss Due to Changes in Building Parameters
– Strip Mall Building with Steel Roof System8-47

Table 8-27 Percent Increases in the Average Annual Total Loss Due to Changes in Building
Configuration8-47

Table 8-28 Subassembly Cost Distributions for Pre-Engineered Metal Buildings.....8-48

Table 8-29 Average Annual Building Loss Normalized by Building Value for Pre-Engineered Metal
Buildings (Annual Loss Ratio).....8-50

Table 8-30 Average Annual Content Loss Normalized by Building Value for Pre-Engineered Metal
Buildings (Annual Loss Ratio).....8-50

Table 8-31 Percent Increases in the Average Annual Total Loss due to Changes in Building Parameters –
Pre-Engineered Metal Buildings8-50

Table 8-32 Subassembly Cost Distributions for Two-Story Apartments8-51

Table 8-33 Subassembly Cost Distributions for Five-Story Apartments8-52

Table 8-34 Subassembly Cost Distributions for Eight-Story Apartments.....8-54

Table 8-35 Subassembly Cost Distributions for Two-Story Office Buildings.....8-55

Table 8-36 Subassembly Cost Distributions for Five-Story Office Buildings.....8-56

Table 8-37 Subassembly Cost Distributions for Eight-Story Office Buildings8-58

Table 8-38 Percent Increases in the Average Annual Total Loss due to Changes in Building Parameters –
Engineered Residential and Commercial Buildings8-60

Table 8-39 Subassembly Cost Distributions for Industrial Buildings.....8-62

Table 8-40 Average Annual Building Loss Normalized by Building Value – Industrial Building8-63

Table 8-41 Average Annual Content Loss Normalized by Building Value – Industrial Building.....8-64

Table 8-42 Percent Increase in Average Annual Total Loss Due to Changes in Building Parameters –
Industrial Buildings.....8-64

Table 8-43 Subassembly Cost Distributions for Fire Stations8-64

Table 8-44 Subassembly Cost Distributions for Small Hospitals8-66

Table 8-45 Subassembly Cost Distributions for Medium and Large Hospitals8-67

Table 8-46 Subassembly Cost Distributions for Elementary Schools.....8-68

Table 8-47 Subassembly Cost Distributions for High Schools.....8-70

Table 8-48 Percent Increases in the Average Annual Total Loss due to Changes in Building Parameters – Fire Station8-71

Table 8-49 Percent Increases in the Average Annual Total Loss due to Changes in Building Parameters – Elementary School.....8-72

Table 8-50 Percent Increases in the Average Annual Total Loss due to Changes in Building Parameters – High Schools.....8-73

Table 8-51 Percent Increases in the Average Annual Total Loss Due to Changes in Building Parameters – Hospitals8-75

Table 8-52 Assumed Damage Areas Used in One-Story Cost Estimates.....8-76

Table 8-53 Assumed Damage Areas Used in Two-Story Cost Estimates.....8-77

Table 8-54 Estimated Building Repair Costs to Wood Buildings by Damage State.....8-79

Table 8-55 Estimated Building Repair Costs to Masonry Buildings by Damage State.....8-79

Table 8-56 Parameter Matrix for the 288 Cases Studied8-82

Table 8-57 Combined Wind and Flood Loss Matrix for the Idealized Case of Wind and Flood Losses.8-90

Table 8-58 Distribution of Flood Losses to Building Subassemblies as a Function of Still Water Height Above First Floor.....8-93

Table 8-59 Distribution of Flood Losses to Building Subassemblies as a Function of Depth of Flooding (Concluded)8-93

Table 8-60 Distribution of Flood Losses to Building Subassemblies as a Function of Flood-Only Building Loss8-93

Table 8-61 Distribution of Wind Losses to Subassemblies Relative to Building Value as a Function of Wind-Only Building Loss8-94

Table 8-62 Combined Wind and Flood Loss Matrix Assuming Wind and Flood Losses are each Uniformly Distributed within each of Five Building Subassemblies8-95

Table 8-63 Subassembly Replacement Cost by Specific Occupancy or General Building Type as a Percentage of Total Building Replacement Cost (Pre-FIRM)8-96

Table 8-64 Subassembly Replacement Costs by Specific Occupancy or General Building Type as a Percentage of Total Building Replacement Cost (Post-FIRM)8-97

Table 8-65 Sample Subassembly Losses Relative to Total Building Replacement Cost..... 8-100

Table 8-66 Sample Subassembly Losses Relative to Building Value for COM1..... 8-101

Table 8-67 Subassembly Losses Relative to Building Value for SBT SPMBs..... 8-102

Table 8-68 Sample Final Wind Subassembly Loss Relative to Subassembly Replacement Cost for RES1 (%), Pre-FIRM Construction..... 8-102

Table 8-69 Guidelines for Development of Flood Subassembly Loss Tables..... 8-103

Table 8-70 Sample Final Flood Subassembly Loss Relative to Subassembly Replacement Cost for RES1, Pre-FIRM, Zone A Construction..... 8-106

Acronyms and Abbreviations

Acronym/ Abbreviation	Definition
AAMA	American Architectural Manufacturers Association
ASCE	American Society of Civil Engineers
ARA	Applied Research Associates, Inc.
ASD	Allowable Stress Design
AOML-HRD	Atlantic Oceanographic and Meteorological Laboratories - Hurricane Research Division
AAL	Average Annualized Loss
BIA	Building Industry Association
BLOWTRAN	BLOWdown TRANSport
COV	Coefficient of Variation
DF	Douglas Fir
d_{min}	Distance of closest approach
EOC	Emergency Operations Center
ESDU	Engineering Sciences Data Unit
FD	Drag force
FEMA	Federal Emergency Management Agency
FIA	Forest Inventory Analysis
ft	Feet
ft ²	Square foot
GBT	General Building Type
GBS	General Building Stock
H _s	significant wave height
HTW	Hazardous or Toxic Waste
HUD	United States Department of Housing and Urban Development
HuRRDE	Hurricane Rainfall Rate and Distribution Estimator
IH	Intense Hurricane
lbf	Pound-force
lbs.	Pounds
ksi	Kips per square inch
LRFD	Load and Resistance Factor Design
LULC	Land Use and Land Cover
MBL	Mean Boundary Layer
MBMA	Metal Building Manufacturers Association
MRLC	Multi-Resolution Land Characteristics
NBCC	National Building Code of Canada
NCMA	National Contract Management Association
NLDC	National Land Cover Data

Acronym/ Abbreviation	Definition
NOAA	National Oceanic and Atmospheric Administration
NWS	National Weather Service
NWS/MDL	National Weather Service's Meteorological Development Laboratory
NSF	National Science Foundation
OSB	Oriented Strand Board
OWSJ	Open Web Steel Joists
PBL	Planetary Boundary Layer
pcf	per cubic foot
plf	pounds per linear foot
psf	per square foot
R_{max}	Radius to maximum winds
RMS	Root Mean Square
RMW	Radius of Maximum Wind
SBC	Standard Building Code
SBCCI	Southern Building Code Congress International
SFBC	South Florida Building Code
SG	Specific Gravities
SLOSH	Sea, Lake, and Overland Surges from Hurricanes
SLTT	State, Local, Tribal, and Territorial
SOCC	Specific Occupancy
SPF	Spruce-Pine-Fir
SYP	Southern Yellow Pine
SWAN	Simulating WAVes Nearshore
T_p	peak wave period
UBC	Uniform Building Codes
USACE	U.S. Army Corps of Engineers
USFS	US Forest Service
WHAFIS	Wave Height Analysis for Flood Insurance Studies

Section 1. Introduction to the FEMA Hazus Loss Estimation Methodology

1.1 Background

The Hazus Hurricane Loss Estimation Methodology provides state, local, tribal, and territorial (SLTT) officials with a decision support software for estimating potential losses from hurricane events. This loss estimation capability enables users to anticipate the consequences of hurricanes and develop plans and strategies for reducing risk. The Geographic Information Systems (GIS) based software can be applied to study geographic areas of varying scale with diverse population characteristics and can be implemented by users with a wide range of technical and subject matter expertise.

This Methodology has been developed, enhanced, and maintained by the Federal Emergency Management Agency (FEMA) to provide a tool for developing hurricane loss estimates for use in:

- Anticipating the possible nature and scope of the emergency response needed to cope with a hurricane-related disaster.
- Developing plans for recovery and reconstruction following a disaster.
- Mitigating the possible consequences of hurricanes.

The use of this standardized methodology provides nationally comparable estimates that allow the federal government to plan hurricane responses and guide the allocation of resources to stimulate risk mitigation efforts.

This *Hazus Hurricane Model Technical Manual* documents the methods used in calculating losses. There are two companion documents, the *Hazus Hurricane Model Technical Manual Appendices* (FEMA, 2021) and the *Hazus Inventory Technical Manual* (FEMA, 2022). The *Hazus Hurricane Model Technical Manual Appendices* provides detailed information on damage state functions, loss functions and subassembly loss tables, and validation studies. The *Hazus Inventory Technical Manual* (FEMA, 2022) provides a more detailed methodology and data descriptions for the inventory shared by each hazard model. Together, these documents provide a comprehensive overview of this nationally applicable loss estimation methodology.

The *Hazus Hurricane Model User Guidance* (FEMA, 2022) outlines the background and instructions for developing a Study Region and defining a scenario to complete a hurricane loss estimation analysis using Hazus. It also provides information on how to modify inventory, improve hazard data and analysis parameters for advanced applications, and guidance on calculating and interpreting loss results.

1.2 Hazus Uses and Applications

Hazus can be used by various types of users with a wide range of informational needs. A SLTT government official may be interested in the costs and benefits of specific mitigation strategies, and thus may want to know the expected losses if mitigation strategies have (or have not) been applied.

Health officials may want information regarding the demands on medical care facilities and may be interested in the number and severity of casualties for different hurricane scenarios. Emergency response teams may use the results of a loss study in planning and performing emergency response exercises. In particular, they might be interested in the operating capacity of emergency facilities such as fire stations, emergency operations centers, and police stations. Emergency planners may want estimates of temporary shelter requirements for different hurricane scenario events. Federal and state government agencies may use loss analysis to obtain quick estimates of impacts in the hours immediately following a hurricane, to best direct resources to the disaster area. Insurance companies may be interested in the estimated monetary losses so they can determine asset vulnerability.

Hurricane loss estimation analyses have a variety of uses for various departments, agencies, and community officials. As users become familiar with the loss estimation methodology, they are able to determine which Hazus Methodology is the most suitable for their needs, and how to appropriately interpret the study results.

The products of Hazus analyses have several pre- and post-hurricane applications in addition to estimating the scale and extent of damage and disruption. Examples of pre-hurricane applications of the outputs include:

- Development of hurricane hazard mitigation strategies that outline policies and programs for reducing hurricane losses and disruptions indicated in the initial loss estimation study. Strategies can involve rehabilitation of existing buildings (e.g., adding shutters), building code enforcement, development of appropriate zoning ordinances for land use planning in areas of surge inundation, and the adoption of advanced wind building codes.
- Development of preparedness (contingency) planning measures for hurricane preparedness and education seminars.
- Anticipation of the nature and extent of response and recovery efforts, including the identification of alternative housing, the location, availability and scope of required response services, and the establishment of a priority ranking for restoration of essential facilities.

Post-hurricane applications of the outputs include:

- Projection of immediate economic impact assessments for state and federal resource allocation and support, including support for state and/or federal disaster declarations by calculating direct economic impact on public and private resources, local governments, and the functionality of the area.
- Activation of immediate emergency recovery efforts, including search and rescue operations, provision of emergency housing shelters, and rapid repair and availability of essential facilities.
- Application of long-term reconstruction plans, including the identification of long-term reconstruction goals, implementation of appropriate wide-range economic development plans for the impacted area, allocation of permanent housing needs, and the application of land use planning principles and practices.

1.3 Assumed User Expertise

Users can be divided into two groups: those who perform the analysis and those who use the analysis's results. For some analyses, these two groups occasionally consist of the same people, but generally, this will not be the case. However, the more interaction that occurs between these two groups, the better the analysis will be. End users of the loss estimation analysis need to be involved from the beginning to make results more usable.

Any risk modeling effort can be complex and would benefit from input from an interdisciplinary group of experts. A hurricane loss analysis could be performed by a representative team consisting of the following:

- Meteorologists
- Wind engineers
- Structural engineers
- Architects
- GIS specialists
- Economists
- Social scientists
- Emergency planners
- Policy makers

The individuals needed to perform the study can provide valuable insight into the risk assessment process. In addition to subject matter expert involvement, at least one GIS specialist should participate on the team.

If a SLTT agency is performing the analysis, some of the expertise may be found in-house. Experts are generally found in several departments: building permits, public works, planning, public health, engineering, information technologies, finance, historical preservation, natural resources, and land records. Although internal expertise may be most readily available, the importance of the external participation of individuals from academic institutions, citizen organizations, and private industry cannot be underestimated.

1.4 When to Seek Help

The results of a loss estimation analysis should be interpreted with caution because baseline values have a great deal of uncertainty. Baseline inventory datasets are the datasets that are provided with Hazus. Further information on these can be found in the *Hazus Inventory Technical Manual* (FEMA, 2022). If the loss estimation team does not include individuals with expertise in the areas described

above, it is advisable to retain objective reviewers with subject matter expertise to evaluate and comment on the map and tabular data outputs.

If a meteorologist is not available to assist in the selection of hurricane track, intensity, and other parameters, the user should defer to available hurricane data provided by the National Hurricane Center (NHC). This will allow users to take advantage of NHC subject matter expertise when defining their historical and forecasted hurricane scenarios.

If the user intends to modify the baseline inventory data or default parameters, assistance from an individual with expertise in the subject would benefit the project. For example, if the user wishes to change default percentages of specific building types for the region, collaborating with a structural engineer with knowledge of regional design and construction practices will be helpful.

1.5 Technical Support

Technical Support contact information is provided in the Hazus application at **Help | Obtaining Technical Support**; technical assistance is available via the Hazus Help Desk by email at FEMA-Hazus-support@fema.dhs.gov (preferred) or by phone at 1-877-FEMA-MAP (1-877-336-2627). The [FEMA Hazus website](#) also provides answers to Frequently Asked Questions, and information on software updates and training opportunities.

FEMA-provided resources also include the [Hazus Virtual Training Library](#), a series of short videos arranged into playlists that cover various Hazus topics, from an introduction to Hazus Methodologies, to targeted tutorials on running Hazus analyses, to best practices when sharing results with decision makers. This easily-accessible learning material provides quick topic-refreshers, free troubleshooting resources, and engaging guides to further Hazus exploration.

The application's **Help** menu references the help files for ArcGIS. Since Hazus was built as an extension to ArcGIS functionality, knowing how to use ArcGIS and ArcGIS Help Desk will help Hazus users.

Technical support on any of the four hazards is available at the contacts shown via **Help | Obtaining Technical Support**.

1.6 Uncertainties in Loss Estimates

Although the Hazus software offers users the opportunity to prepare comprehensive loss estimates, it should be recognized that uncertainties are inherent in any estimation methodology, even with state-of-the-art techniques. Any region or city studied will have an enormous variety of buildings and facilities of different sizes, shapes, and structural systems that have been built over a range of years under different building codes and practices.

Due to this complexity, there is inherent uncertainty in modeling the structural resistance of most buildings and other facilities. Further, there are not sufficient data from past hurricanes or wind tunnel experiments to determine precise estimates of damage based on known wind speeds, even for specific buildings and other structures. To deal with this complexity and lack of data, buildings are grouped into categories based upon key characteristics. The relationships between key features of wind speeds and

average degree of damage with associated losses for each building category are based on current data and available theories.

The results of a hurricane loss analysis should not be looked upon as a prediction. Instead, they are only an estimate, as uncertainty inherent to the model will be influenced by the quality of inventory data and the hazard parameters. This is particularly true in areas where hurricane events are infrequent or where recorded data is scarce.

1.7 Modeling Hurricanes for U.S. Caribbean Territories

An adapted version of the Hazus Hurricane model is available for use in Puerto Rico and the U.S. Virgin Islands. The methodology described in this document was used as a basis for these areas, with adjustments made for localized terrain and tree cover, the addition of new building types based on regional construction practices, and refined methods for creating local building inventory. If users are modeling hurricanes in Puerto Rico or the U.S. Virgin Islands, it is strongly recommended they consult the technical documentation *Hazus Hurricane Wind for Puerto Rico and the U.S. Virgin Islands* (FEMA, 2021) for more information. No separate downloads or software patches are required to run Hazus for Caribbean territories – the appropriate data and model functionality are included in the Hazus software, and users can download Puerto Rico or U.S. Virgin Island datasets from the same MSC location as other state databases.

Section 2. Introduction to Hurricane Loss Estimation Methodology

This brief overview of the Hurricane Methodology is intended for SLTT officials contemplating a hurricane loss analysis.

The Hazus Methodologies will generate an estimate of the consequences to a city or region from a hurricane scenario or from a 100,000-year ensemble of probabilistic events. The resulting "loss estimate" will generally describe the scale and extent of damage and disruption that may result from the modeled hurricane event. The following information can be obtained:

- *Quantitative estimates of losses* in terms of direct costs for repair and replacement of damaged buildings, direct costs associated with loss of function (e.g., loss of business revenue, relocation costs), household displacements, shelter requirements, quantity of debris, and regional economic impacts.
- *Functionality losses* in terms of loss-of-function and restoration times for hospitals, police stations, fire stations, and emergency operations centers.

To generate this information, the Methodology includes:

- Classification systems used in assembling inventory and compiling information on the General Building Stock (GBS), the components of transportation and utility systems, and demographic and economic data.
- Vulnerability functions for estimating type and extent of damage and for summarizing losses.
- National and regional databases containing information for use as baseline (built-in) data useable in the calculation of losses if there is an absence of user-supplied data.

These systems, methods, and data have been combined in a user-friendly GIS software for this loss estimation application.

The Hazus software uses GIS technologies for performing analyses with inventory data and displaying losses and consequences on applicable tables and maps. The Methodology permits estimates to be made at several levels of complexity, based on the level of inventory data entered for the analysis (i.e., baseline data versus locally enhanced data). The more concise and complete the inventory information, the more accurate the results.

The following figure provides a graphic representation of the modules that the Hazus Hurricane Model Methodology is comprised of, and their interrelation in deriving estimates.

Hazus Hurricane Model Methodology

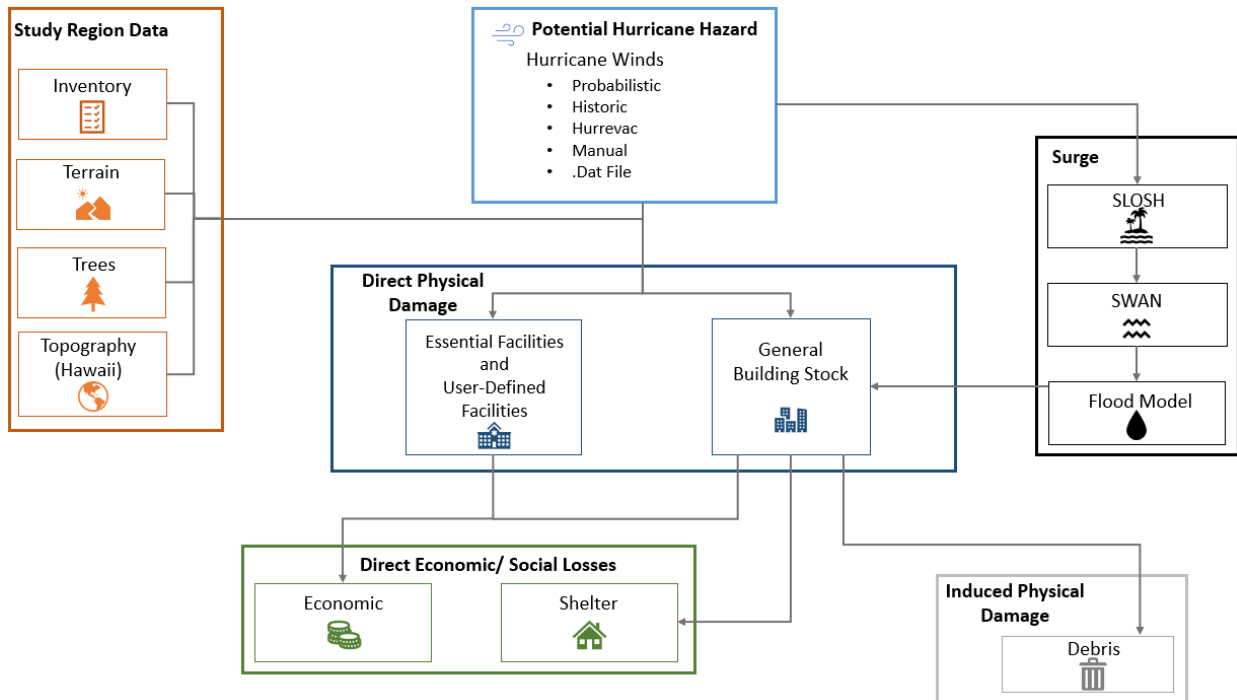


Figure 2-1 Hazus Hurricane Model Methodology Schematic

While Figure 2-1 shows the conceptual relationships, the steps used in the Hazus Hurricane Model are as follows:

- *Select the area to be studied.* The Hazus Study Region (the region of interest) is created based on Census block, Census tract, county, or state level aggregation of data. The area generally includes a city, county, or group of municipalities. It is generally desirable to select an area that is under the jurisdiction of an existing regional planning group.
- *Integrate local inventory data.* Include essential facilities, General Building Stock (GBS), or user-defined facilities.
- *Specify the hurricane hazard scenario.* In developing the scenario hurricane, consideration should be given to credible hurricane sources and potential hurricane tracks, wind speeds, and surge inundation areas using the NHC and Hazus datasets, or subject matter experts.
- *Update the tree and surface roughness parameters if improved data are locally available.* The tree database contains information on predominant tree type, density, and height categories.
- *Use the formulas embedded in Hazus.* Compute probability distributions for damage to different classes of buildings and facilities. Then, estimate the loss-of-function, displaced households, and short-term shelter requirements.
- *Compute estimates of direct economic loss.* Use a comprehensive set of economic loss functions which incorporate tree blowdown losses to single-family homes and manufactured housing.

- *Estimate the amount and type of debris.*
- *Calculate combined wind and storm surge hazard losses, if applicable.*

The user plays a significant role in selecting the scope and nature of the output of a loss estimation analysis. A variety of maps can be generated for visualizing the extent of the losses. Generated reports provide numerical results that may be examined at the level of the Census tract or aggregated by county or region. For study regions that have been created to model both wind and flood hazards, results are provided at the Census block level.

2.1 Hurricane Hazards Considered in the Methodology

The hurricane-related hazards considered by the Hazus Methodology in evaluating damage, resultant losses, and displaced population are introduced in this section. Additional details are provided in subsequent sections. Most damage and loss caused by a hurricane is directly or indirectly the result of wind and storm surge forces. Thus, Hazus evaluates the geographic distribution of wind speed and surge depth as a result of a specific hurricane scenario.

The following five features of hurricanes can have an adverse effect on structures and facilities and are assessed in Hazus:

- *Wind pressure:* It is important to understand how wind loads get applied to a building's walls and roof. This includes characterizing the hurricane itself in terms of wind speed and wind direction, as well as how the building is configured and built.
- *Windborne debris:* A significant amount of the damage to buildings and facilities associated with hurricane winds is produced by windborne debris impacting the buildings and damaging the building exterior, including roof covering, windows, doors, and other openings. Two windborne debris models are used in the model. The first applies to residential environments, and the second is a commercial building model for predicting the damage produced by windborne gravel.
- *Rainwater penetration:* A majority of the hurricane damage to the interior and contents of buildings results from rain entering the buildings through damage to the roof, fenestrations (i.e., windows and doors), or cladding. The effects of rainwater penetration are included in the development of the damage and loss functions used to predict the combined effects of wind pressure, windborne debris, and rainfall acting on a structure.
- *Tree blowdown:* Trees have both positive and negative effects in the presence of extreme winds. On the positive side, trees provide shelter to structures, reducing the likelihood of damage produced by the direct action of wind. On the negative side, the existence of many trees surrounding a building increases the likelihood of a tree striking and damaging the building. Using the hurricane characteristics and a tree database, Hazus uses tree blowdown probability curves and empirical damage models to determine additional residential damage and loss due to tree blowdown. The tree fall models are applied as an additive term for building and contents losses to small residential structures (i.e., single-family homes and manufactured housing).
- *Storm Surge:* Storm surge can have a major impact on structures along the coast that are impacted by wind and water. Hazus uses a customized version of the NOAA Sea, Lake and Overland Surges

from Hurricanes (SLOSH) model to estimate storm surge depths. Hazus also provides a methodology that combines the wind and flood losses so that they are not double counted.

A critical component in the modeling of wind effects, damage, and loss to buildings and facilities is the assessment of the surface roughness. As the ground surface becomes rougher, the wind speeds near the ground decrease while the upper-level wind speed remains the same. The wind loads experienced by buildings located in a typical suburban, treed, or urban environment are much lower than those experienced by buildings located in relatively unobstructed regions such as waterfront and open field locations. The wind loads experienced by one- and two-story structures located in forested areas may be as low as one half of those experienced by similar structures located in an open environment.

2.2 Definitions of Structures

There are differences between the terminology used to designate distinctions between types or categories of structures. The term “structure” refers to all constructions, such as a building, bridge, water tank, shed, carport, or other man-made things that are at least semi-permanent. A building is a structure with a roof and walls that is intended for use by people and/or inventory and contents, such as a house, school, office, or commercial storefront. A facility corresponds to a particular place, generally a building, with an intended purpose such as a school, hospital, electric power station, or water treatment facility. Some facilities are defined as ‘essential facilities’ meaning the facility is critical to maintaining services and functions vital to a community, especially during disaster events. The buildings, essential facilities, and transportation and utility systems considered by the methodology are as follows:

- *General building stock:* The key General Building Stock (GBS) databases in Hazus include square footage by occupancy and building type, building count by occupancy, and building type, building and content valuation by occupancy and building type, and general occupancy mapping. Most of the commercial, industrial, and residential buildings in a region are not considered individually when calculating losses. Buildings within each Census tract are aggregated and categorized. Building information, derived from Census and employment data, is used to form groups of 39 hurricane specific building types and 33 specific occupancy classes (additional information on the Hazus baseline GBS inventory data is provided in the *Hazus Inventory Technical Manual* (FEMA, 2022). The degree of damage and loss is computed for each grouped combination of specific building type and occupancy class. Wind and surge losses are provided individually and combined in the results.
- *Essential facilities:* Essential facilities are the facilities that are vital to emergency response and recovery following a disaster. These facilities can include, but are not limited to, medical care facilities, emergency operations centers, police stations, fire stations, and schools. For this class of structures, damage state probabilities and loss-of-function are evaluated on a building-by-building basis in the wind model. There may be significant uncertainties in each estimate. The flood (surge) model provides a damage percentage and loss. Hazus does not provide a combined wind and surge damage or loss for essential facilities.
- *Transportation systems:* Transportation systems, (including highways, railways, light rail, bus systems, ports, ferry systems, and airports) are classified into components such as bridges,

stretches of roadway or track, terminals, and port warehouses. Impacts to transportation systems are not included in the wind or surge models.

- *Utility systems:* Utility systems, including potable water, electric power, wastewater, communications, and liquid fuels (oil and gas), are treated in a manner similar to transportation systems. Impacts to utility systems are not included in the wind model. Damage, loss, and a functionality assessment can be modeled for potable water, wastewater, natural gas, and electric power facilities in the flood (surge) model.
- *High potential loss facilities:* In any region or community, there will be certain types of structures or facilities for which damage and losses will not be (reliably) evaluated without facility-specific supplemental studies. These facilities include dams and levees, nuclear power plants, and military installations. Impacts to high potential loss facilities are not included in the wind or surge models.

Site-specific data can be used to estimate potential damage states using the User-Defined Facilities (UDF) module, which is addressed in the *Hurricane Model User Guidance*. The UDF module does not consider the economic loss of the structure.

2.3 Levels of Analysis

Hazus is designed to support two general types of analysis (Basic and Advanced), split into three levels of data updates (Levels 1, 2, and 3). Figure 2-2 provides a graphic representation of the various levels of analysis.

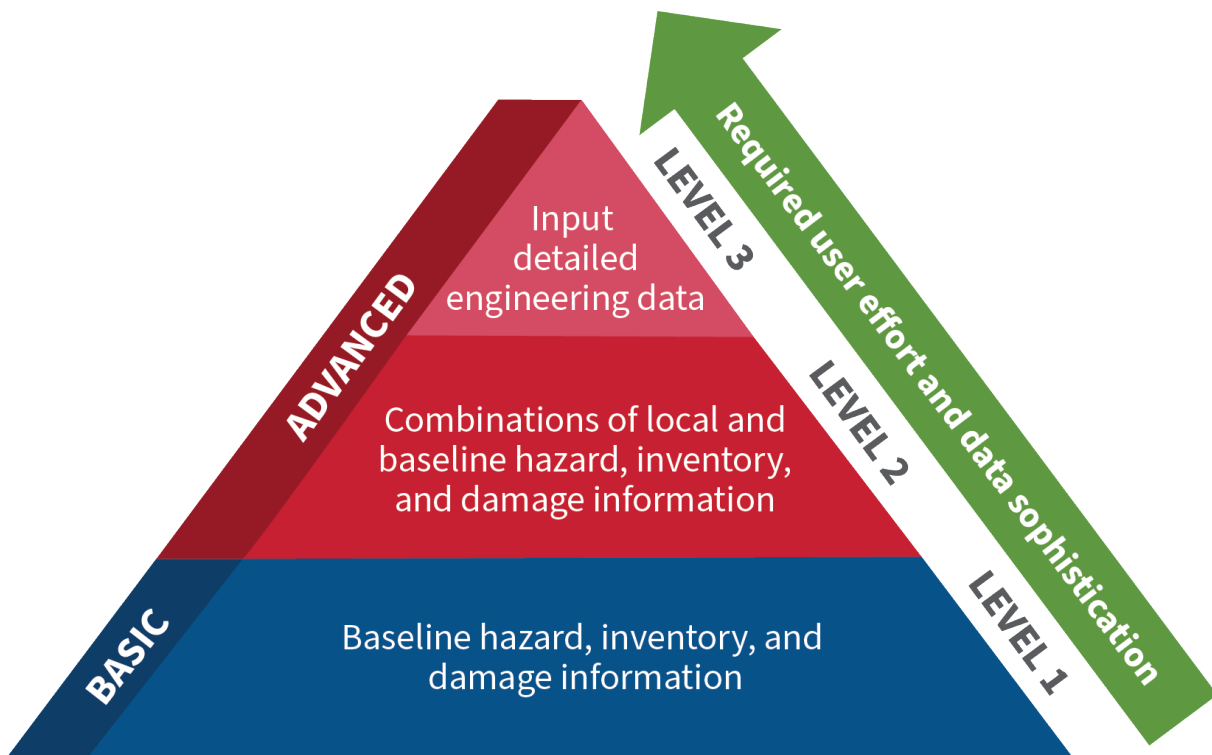


Figure 2-2 Levels of Hazus Analysis

2.3.1 Analysis Based on Default Information

The basic level of analysis uses only the baseline databases built into the Hazus software and Methodology for building square footage and value, population characteristics, costs of building repair, and certain basic economic data. This level of analysis is commonly referred to as a Level 1 analysis. In a Level 1 (Basic) analysis, the tree inventory and surface roughness databases are derived from national datasets. Direct economic and social losses associated with the GBS and essential facility damage state probabilities are computed.

Other than defining the Study Region, selecting the hurricane(s), and making decisions concerning the extent and format of the output, an analysis based on baseline data requires minimal effort from the user. As indicated, the estimates involve large uncertainties when inventories are limited to the baseline data. This level of analysis is suitable primarily for preliminary evaluations and crude comparisons among different Study Regions with a Census tract as the smallest regional unit. A Level 1 (Basic) analysis could be used for comparisons and preliminary evaluations to assist in identifying potential mitigation actions within a community, which could be useful if evaluating funding priorities for projects.

2.3.2 Analysis with User-Supplied Inventory

Results from an analysis using only baseline inventory data can be improved upon greatly with at least a minimum amount of locally developed input. Improved results are highly dependent on the quality and quantity of improved inventory data. The significance of the improved results also relies on the user's analysis priorities. This level of advanced analysis is commonly referred to as a Level 2/Level 3 (Advanced) analysis. The following inventory improvements impact the accuracy of Level 2/Level 3 (Advanced) Analysis results:

- Preparation of a detailed inventory of all essential facilities.
- Use of locally available data or estimates of the square footage of buildings in different occupancy classes.
- Use of locally available data concerning construction costs or other economic parameters.
- Use of local expertise to modify the mapping scheme databases that determine the percentages of specific building types associated with different occupancy classes and the wind characteristics of buildings.
- Development of maps of tree inventories and surface roughness. These maps, if available, are used for evaluating the effects of these local conditions on damage and losses.

Section 3. Inventory

The technical guidance related to inventory data associated with the Hazus Hurricane Methodology and software is detailed in the *Hazus Inventory Technical Manual* (FEMA, 2022). The *Hazus Inventory Technical Manual* (FEMA, 2022) describes the classification of different buildings and infrastructure systems, data and attributes required for performing damage and loss estimation, and the data supplied with the Hazus software.

Section 4. Hurricane Wind and Surge Hazards

Underfunding by the National Science Foundation (NSF), with additional support provided by the National Association of Homebuilders, as well as Applied Research Associates, Inc. (ARA), an advanced probabilistic hurricane model was developed by ARA during the period 1995-1997. This model was reviewed by the ASCE 7 Committee in 1998 and published as two journal papers (Vickery et al., 2000a, 2000b). Predicted hurricane wind speeds resulting from the ARA model were the basis of the national standard for wind load design provisions as defined in ASCE 7-98, ASCE 7-02, and ASCE 7-05. The ARA model was improved in 2006 using a new inland decay model (Vickery, 2005) and a significantly expanded set of flight level data to update the probability distributions for R_{max} and the Holland pressure profile parameter (Vickery and Wadhera, 2008). The resulting model was presented in two journal papers (Vickery et al., 2009a, 2009b). The updated ARA model became the basis for the design wind speed map in ASCE 7-10 and the current hurricane wind hazard model in Hazus.

The probabilistic model uses a life cycle simulation approach in which the full track of a hurricane or tropical storm is modeled, beginning with its initiation over the ocean and ending with its final dissipation. Using this approach, the central pressure is modeled as a function of sea surface temperature, and the storm heading, speed, etc., are updated at each six-hour point in the storm history. Linear interpolation is used between the six-hour points. The approach is validated by comparing the site-specific statistics of the key hurricane parameters of the simulated hurricane tracks with the statistics derived from the historical data. This model includes a numerical wind field model (Vickery et al., 2009a), which incorporates a full nonlinear solution to the equations of motion. Later, the probabilistic model methodology was expanded to include the other Hazus scenario types with the exception of the .dat scenario, which takes the output of other wind hazard models to incorporate into Hazus.

4.1 Hurricane Wind Field Model

A critical component in the simulation of hurricanes is a good representation of the hurricane wind field, given information regarding the storm intensity, size, and translation speed. The hurricane wind field model contains two components. The first component is the overall mean flow field describing the upper-level winds, and the second is the boundary layer model used to estimate wind speeds at the surface of the earth, given the upper-level wind speeds.

The mean flow field model (Vickery et al., 2009a) solves the full nonlinear equations of motion of a translating hurricane and then parameterizes these for use in fast running simulations. The use of a full numerical solution to the equations of motion for a hurricane allows the modeling of asymmetries in the storm that arises from the complex interaction of the frictional forces and the winds, which vary throughout the storm. They can produce very high wind speeds wrapping around the eyewall in some small and intense storms. The use of simple empirical models to define the hurricane will not reproduce these effects.

The current hurricane boundary layer model (Vickery et al., 2009a) was developed using a combination of velocity profiles computed using dropsonde (a weather reconnaissance device designed to be dropped from an aircraft at altitude over water to measure storm conditions) data and a linear

theoretical hurricane boundary layer model developed by Kepert (2001). The final hurricane boundary layer model incorporates a combined logarithmic-quadratic variation of the mean wind speed with height used to replicate the height of the low-level jet observed in the hurricane boundary layer. This allows for a more realistic representation of the wind speeds near the surface, and for better estimates of the effect of the sea-land interface in reducing wind speeds near the coast.

Numerous comparisons between modeled and observed hurricane wind speed records have been performed. These include both comparisons of the mean wind speeds and the peak gust wind speeds.

4.1.1 Mean Wind Field Model

The Hazus wind field model is based on a dynamic numerical model of the planetary boundary layer (PBL). The model considers the equation of horizontal motion, vertically averaged over the height of the PBL. A finite difference scheme is used to solve for the steady-state wind field over a set of nested rectangular grids. These wind fields are then fit using a Fourier fitting approach so that each wind field can be described using a relatively small number of parameters. The equations are solved for 1,560 combinations of central pressure, translation speed, and radius to maximum winds for hurricanes both over land and over water. Parameterizing the solved wind field models retains the more accurate modeling associated with the numerical modeling of the hurricane while increasing the speed of the computations. A similar approach for modeling hurricane wind fields resulting from a numerical solution to the equations of motion for a translating hurricane was first used by Georgiou (1985) and then by Vickery and Twisdale (1995a). In both studies, the numerical model results were obtained from Shapiro's (1983) model, where the solutions to the equations of motion were themselves solved using a spectral approach employing the first two terms of the expansion. The approach used in the Hazus Methodology has an advantage over the use of the Shapiro model, in that the full nonlinear equations are solved, and then the results are fit to a Fourier series using more than two terms, hence maintaining a more precise solution to the equations of motion.

4.1.2 Surface Level Winds

The hurricane boundary layer is frequently defined using empirical relationships between the upper-level winds and the surface (10 meters) level winds. The ratio of the surface level winds to the upper-level winds within these empirical models is very high (0.8-0.9) compared to typical values in extra-tropical storms (ratio of about 0.6 in open country terrain). The hurricane wind field model (Vickery et al., 2009a) described here uses a more theoretically based model of the hurricane boundary layer and is developed using a combination of velocity profiles computed using dropsonde data and a linear theoretical hurricane boundary layer model developed by Kepert (2001). The final hurricane boundary layer model incorporates a combined logarithmic-quadratic variation of the mean wind speed with height used to replicate the height of the low-level jet observed in the hurricane boundary layer. The empirical hurricane boundary layer model reproduced the shape of the hurricane boundary layer over the lower 1,000 meters. The analysis of the profiles from dropsonde data reproduces the observations noted in Powell et al. (2003) that the sea drag coefficient reaches a maximum value. The results also suggest that the magnitude of this maximum value decreases with decreasing storm Radius of Maximum Wind (RMW).

4.1.2.1 Hurricane Boundary Layer Model

Dropsondes are dropped from reconnaissance aircraft generally from heights between 1.5-3 kilometers and fall vertically downwards at a speed of about 10 meters per second measuring wind speed, temperature, humidity, etc. at every 0.5 seconds. Dropsondes hit the sea surface after several minutes from the time of drop, drifting 10-15 kilometers tangentially and hundreds of meters radially (Powell et al., 2003). Further dropsonde details are given in Hock and Franklin (1999) and Franklin et al. (2003). The dropsonde dataset used here was obtained from the Atlantic Oceanographic and Meteorological Laboratories -Hurricane Research Division (AOML-HRD) and consists of all profiles collected during the 1997-2003 hurricane seasons. Most of these profiles are from the Atlantic and Gulf of Mexico hurricanes, with a few coming from Pacific Ocean hurricanes. The dropsonde data has been previously subjected to a quality control criterion by AOML-HRD to remove any identifiable errors. All measurements have been smoothed by AOML-HRD using a 5-second low pass filter to remove noise due to switching of the satellites.

In the analysis of the dropsonde data, the drops were separated into those associated with profiles measured at or near the RMW and those associated with drops away from the RMW. The assignment of a particular profile to either the RMW region or the outer vortex region was determined using comments of the flight meteorologist, an examination of concurrent flight level radial wind profiles (if available), airborne radar reflectivity imagery, and H*Wind (Powell et al. 1996,1998) objective wind field analyses. Following the approach of Powell et al. (2003), the wind profiles were analyzed in a composite sense, as a function of the mean boundary layer (MBL) wind speed, defined as the mean wind speed averaged over a height range of 10 meters to 500 meters. The six different MBL groups correspond to mean MBL wind speeds of 20 – 29 meters per second, 30 – 39 meters per second, 40 – 49 meters per second, 50 – 59 meters per second, 60 – 69 meters per second, and 70-85 meters per second. Each group was divided vertically into height bins chosen to provide maximum resolution close to the sea surface. The mean wind speeds versus height were computed by taking the average of all wind speed measurements within height bins of 10 meters for heights less than 300 meters, 20 meters bins for heights ranging between 300 and 500 meters, 50 meters bins for heights between 500 meters and 1,000 meters, and 100 meters bins for heights greater than 1,000 meters. The single height value assigned to each bin is the mean value computed within the height bin.

Figure 4-1 shows the mean velocity profiles near the RMW for each of the six MBL wind speed groups: 20-29 meters per second, 30-39 meters per second, 40-49 meters per second, 50-59 meters per second, 60-69 meters per second, 70-85 meters per second. Qualitatively, Figure 4-1 indicates that in the lower few hundred meters of the boundary layer, the mean velocity profile is approximately logarithmic, and the height at which the maximum wind speed occurs decreases with increasing wind speed, ranging from a maximum height of about 700 meters for the 20 – 29 meters per second, MBL case, to a minimum of about 400 meters for the 60 – 69 meters per second, MBL case. The lowering of the height at which the maximum wind speed occurs is consistent with the analysis described in Kepert (2001) and Kepert and Wang (2001), where the existence of a lower level “jet” is discussed. The jet strength is defined as the ratio of the maximum wind speed divided by the gradient balance wind speed. Kepert considers the jet height to be equivalent to the boundary layer height, and that concept is carried through Hazus. Kepert (2001) demonstrates that both the magnitude and height of the jet are a function of the inertial stability, I , defined as:

Equation 4-1

$$I = \sqrt{\left(f + \frac{2V}{r}\right) \left(f + \frac{V}{r} + \frac{\partial V}{\partial r}\right)}$$

Where:

- V is the azimuthally averaged tangential gradient wind speed (as computed from the surface pressure field)
- f is the Coriolis parameter
- r is the radial distance from the center of the storm

As indicated in Equation 4-1, the inertial stability factor is a function of both wind speed and radius; therefore, the dropsonde data were further divided into bins having similar values of r. Two sets of radii groups were developed. The first group corresponded to drops performed at or near the radius to maximum winds, and the second group corresponded to drops performed outside of the RMW.

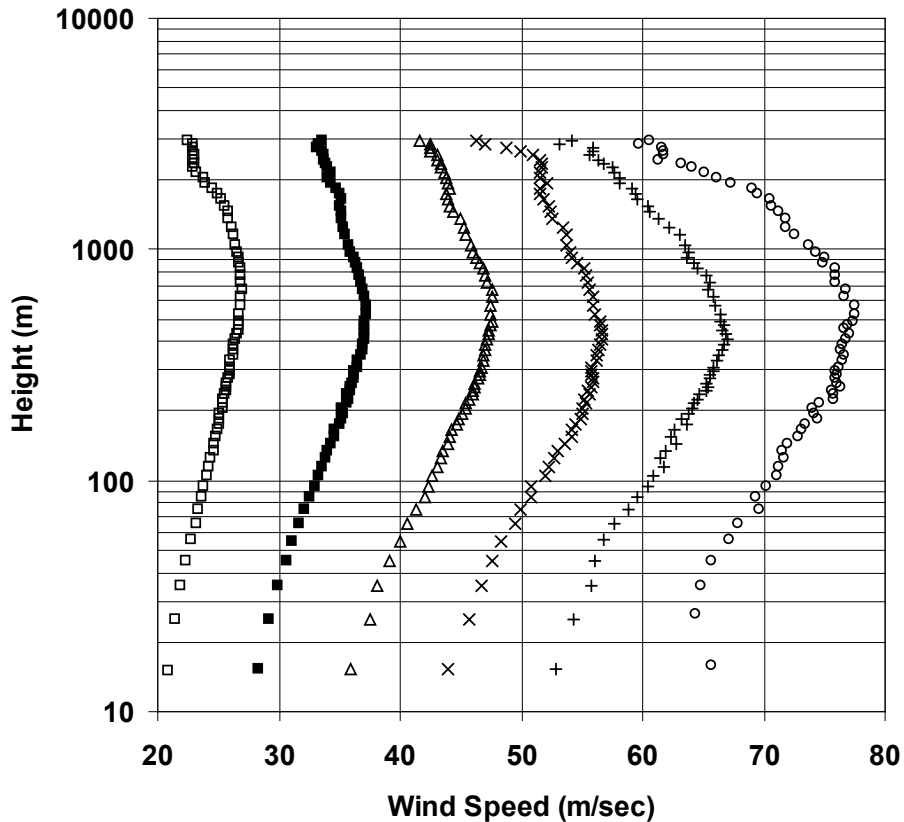


Figure 4-1 Mean Wind Profiles

For a neutrally stable boundary layer, the increase in the mean wind speed with height near the surface is given by:

Equation 4-2

$$U(z) = \frac{u_*}{k} \ln\left(\frac{z}{z_0}\right)$$

Where:

- k is the von-Karman coefficient having a value of 0.4
- u_* is the friction velocity
- z is the height above the surface
- z_0 is the surface roughness

The friction velocity is related to the surface shear stress (τ) as:

Equation 4-3

$$\tau = \rho u_*^2 = \rho C_d U_{10}^2$$

Where:

- ρ is the density
- C_d is the surface drag coefficient
- U_{10} is the mean wind speed (representative of the wind speed averaged over a period of 30 minutes to an hour) at a height of 10 meters

For each combination of r and MBL, an estimate of the surface roughness and sea surface drag coefficient was obtained using the least squares fit (in linear-logarithmic space) of the measured wind speeds over height ranges of 20 to 200 meters, 20 to 150 meters, and 20 to 100 meters (Figure 4-2). The velocity profiles given in Figure 4-2 show a trend for the height of the mean wind speed maxima to decrease as both the RMW decreases, and the wind speed increases, consistent with the analysis of Kepert (2001). Using the intercepts from the least square fits, estimates of the effective surface roughness, z_0 , and the associated uncertainty, were obtained for each profile. Given a value of z_0 , the surface drag coefficient is computed using Equation 4-2 and Equation 4-3. In Figure 4-2, horizontal error bars represent the 95th percentile error on the estimate of the mean wind speed. LSF fits are for the 20 – 200-meter case. (MBL cases correspond to 20-29 meters per second, 30-39 meters per second, 40-49 meters per second, 50-59 meters per second, 60-69 meters per second., and 70-85 meters per second.)

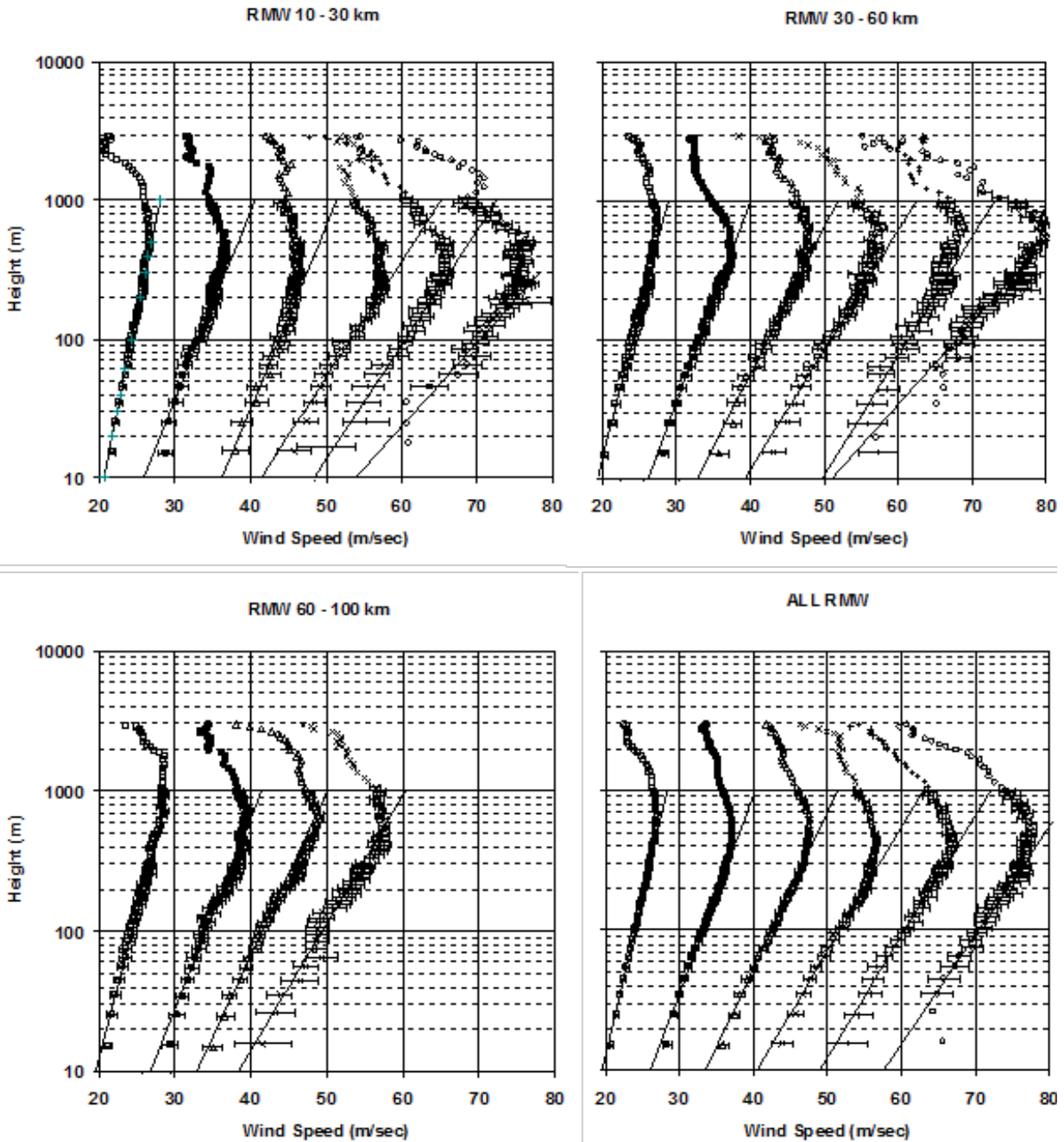


Figure 4-2 Mean and Fitted Logarithmic Profiles for Drops Near the RMW for all MBL Cases

Figure 4-3 presents the resulting C_d versus U_{10} data for the three height ranges. Results are given for the MBL data separated by RMW bins, and for the case with no separation by RMW (as in Powell et al., 2003). The 95% confidence bounds shown in Figure 4-3 represent a lower bound because the error in the intercept does not include any errors associated with the estimates of the dropsonde height, z , nor the errors in the estimates of the measured wind speed at each height. As seen in Figure 4-3, on average, the drag coefficient increases with increasing wind speed up to wind speeds of about 24-28 meters per second and then starts to level off or perhaps even decrease for higher wind speeds, consistent with the results of Powell et al. (2003). The data suggest that the magnitude of the maximum

value of C_d decreases with decreasing RMW. Also shown in Figure 4-3 is the Large and Pond (1981) drag coefficient model, modified to have a maximum value that varies with the RMW. The maximum (cap) values range from 0.0019 for the smallest storms up to 0.0024 for the largest storms.

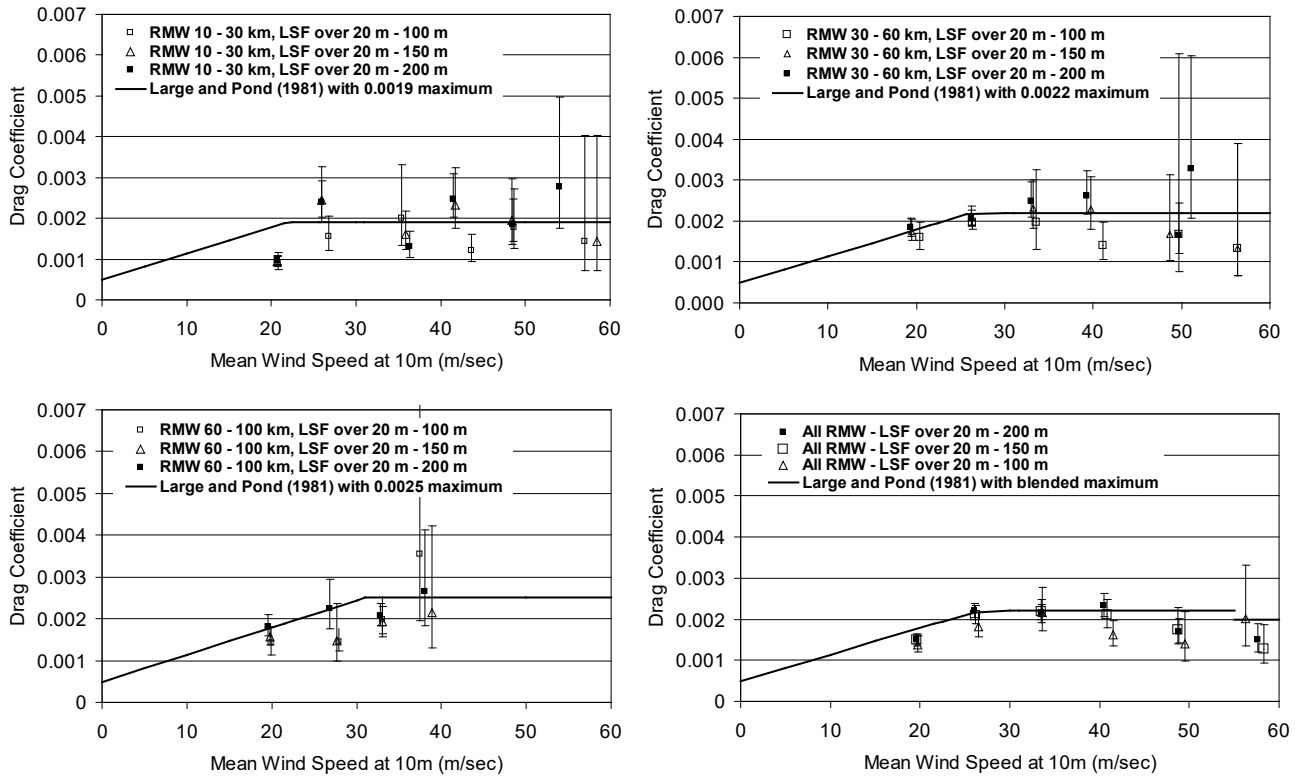


Figure 4-3 Variation of the Sea Surface Drag Coefficient with Mean Wind Speed at 10 meters, Near the RMW

The approach taken for examining the characteristics of the hurricane boundary layer near the RMW was repeated for dropsonde profiles measured outside the RMW. The radius groups chosen were determined based on the number of profiles associated within each MBL group. Figure 4-4 shows the resulting mean velocity profiles along with the logarithmic fits to the wind data, fit using the wind speed data for a surface layer of 20 - 200-meter range. The radius range used to compute the mean velocity profile is noted in the figure. MBL cases correspond to 20-29 meters per second, 30-39 meters per second, 40-49 meters per second, 50-59 meters per second, and 60-69 meters per second. As indicated in Figure 4-4, there is a trend for the height of the wind maxima to increase as the radius increases and decreases with an increase in wind speed, which is again consistent with the analysis described by Kepert (2001). Figure 4-5 shows a comparison of the estimated values of C_d and the error bounds corresponding to 95% confidence interval plotted versus U_{10} , ((a) Least square fit for a height range of 20 - 200 meters, (b) Least square fit for a height range of 20 - 150 meters, and (c) Least square fit for a height range of 20 meters). As seen in Figure 4-5, on average, the drag coefficient increases with increasing wind speed up to about 30 meters per second and then levels off, but the apparent decrease in C_d seen in the case of the near RMW observations is not evident here. To incorporate the effect of radius on the limiting value of C_d , the limiting value of C_d is modeled as a function of radius, r in the form:

Equation 4-4

$$C_{d_{max}} = (0.0881r + 17.66)10^{-3}; 0.0019 \leq C_{d_{max}} \leq 0.0025$$

Where:

r is the radial distance from the storm center (km), but is constrained to have a minimum value equal to the RMW

A possible explanation for this reduction in C_d as a function of radius is given in Makin (2005), where it is suggested that a limiting value of C_d is caused by the production of sea spray inhibiting the transfer of momentum from the wind to the sea surface. Makin suggests that most of the sea spray is produced by the mechanical tearing by the wind from steep short waves, and thus for storms with small RMW (and hence small wind fetches), more of the waves will be short as compared to the large RMW case.

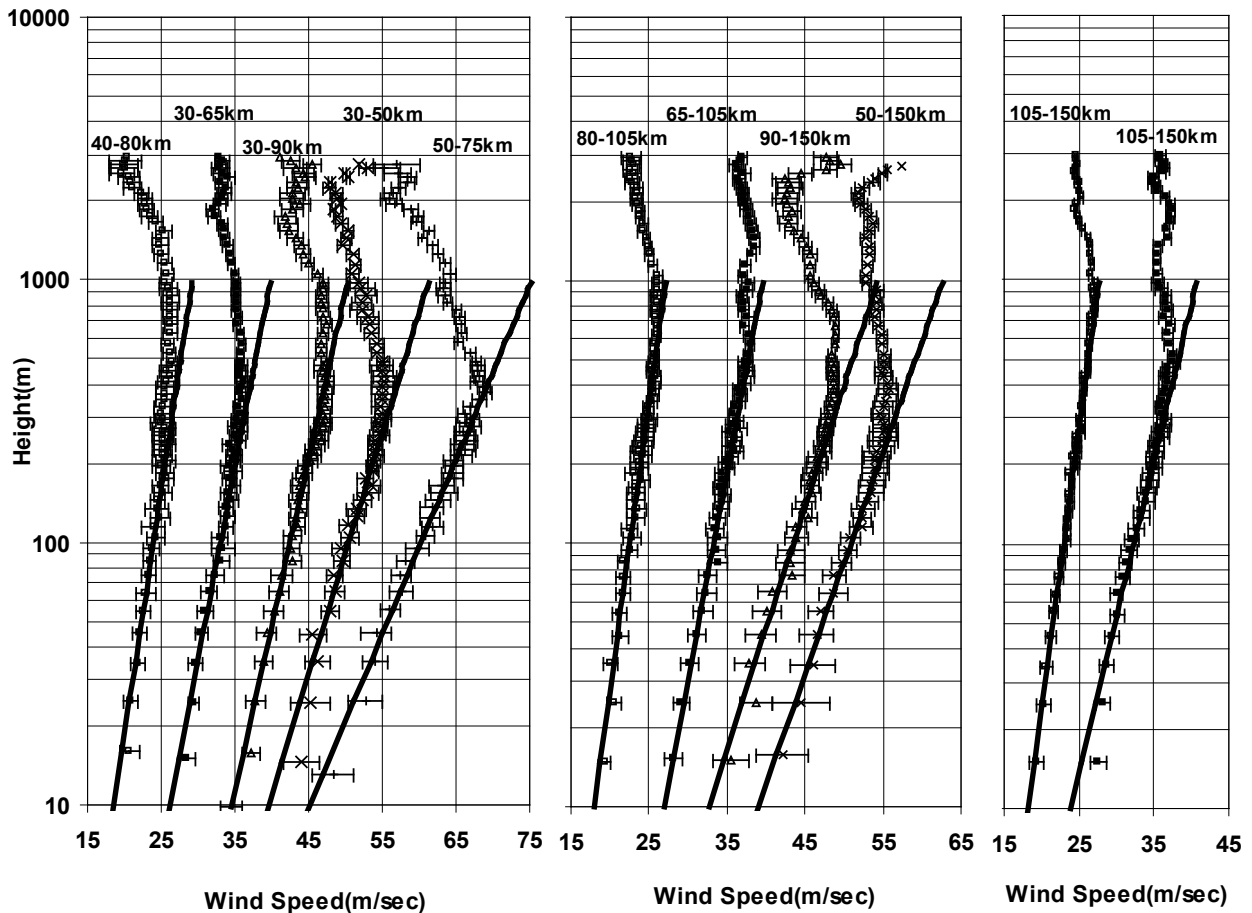


Figure 4-4 Mean Wind Profiles and Fitted Logarithmic Profiles for Outside RMW Case

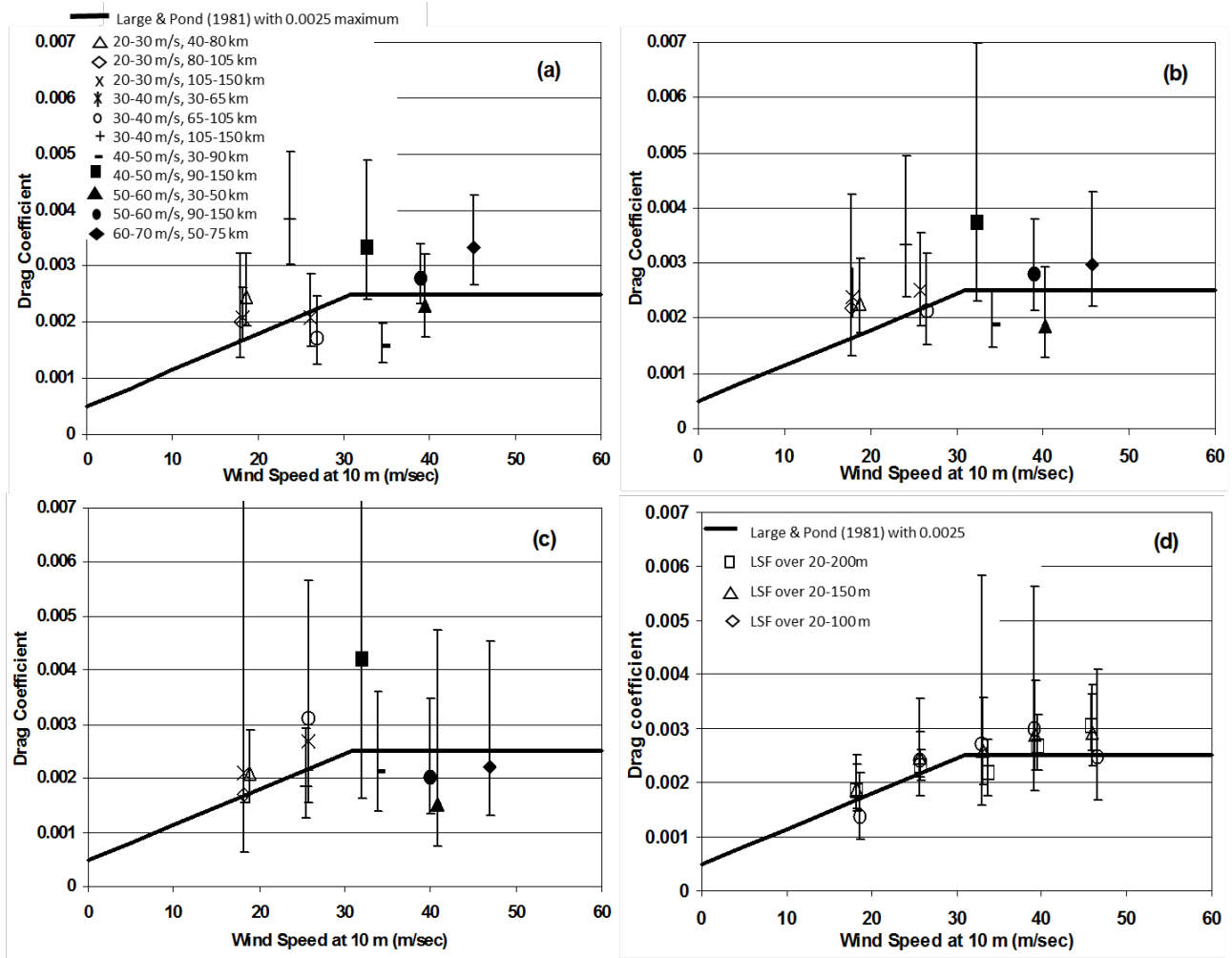


Figure 4-5 Variation of the Sea Surface Drag Coefficient with Mean Wind Speed at 10 meters, Outside RMW case

4.1.2.1.1 Empirical Model for the Marine Hurricane Boundary Layer

In the lower few hundred meters, the atmospheric boundary layer of the hurricane is adequately modeled using the logarithmic law, and the profiles shown in Figure 4-2 and Figure 4-4 clearly indicate that, in some cases, such a model can be used well beyond heights of about 300 meters. In most of the high wind speed cases, however, the logarithmic law breaks down, and the wind speeds begin to decrease with increasing height. The height at which the logarithmic law fails to describe the variation of the mean wind speed with height is strongly correlated with the height at which the mean wind speed reaches a maximum value (i.e., jet or boundary layer height). With this observation noted, the hurricane boundary layer was modeled in the form:

Equation 4-5

$$U(z) = \frac{u_*}{k} \left[\ln \left(\frac{z}{z_0} \right) - a \left(\frac{z}{H^*} \right)^n \right]$$

Each of the parameters, a and n , were treated as free parameters but were required to be constant for all values of r , and H^* is a boundary layer height parameter. The boundary layer or jet height was allowed to vary with each profile. To determine the appropriate parameters for use in Equation 4-5, two approaches were taken, namely:

- *Method 1:* The values of u_* and z_0 were computed from the regression analysis, and the values of u_* , a , n , and H^* were selected to minimize the error over the height range of 20 meters to 1,000 meters.
- *Method 2:* The values of z_0 were computed using the capped Large and Pond drag coefficient model in Figure 4-6, and the values of u_* , a , n , and H^* were selected to minimize the error over the height range of 20 meters to 1,000 meters.

Figure 4-6 presents the observed and modeled mean velocity profiles near the RMW for the 10 to 30 kilometers and 30 to 60 kilometers RMW cases. Table 4-1 presents the values of H^* , U_{10} , C_d , z_0 , and the resulting R^2 values computed over the 20 - 1,000-meter height range for all RMW ranges. In all cases, the best values a and n were 0.4 and 2.0, respectively. By setting the derivative of Equation 4-5 with respect to z equal to zero, it is seen that the boundary layer or jet height, H is equal to $1.12H^*$. In Figure 4-6, solid lines represent model data derived using least squares fit values of surface roughness and friction velocity using LSF over a 20 - 200-meter range. Dashed lines represent model results using C_d derived from truncated Large and Pond (1981) drag coefficient model.

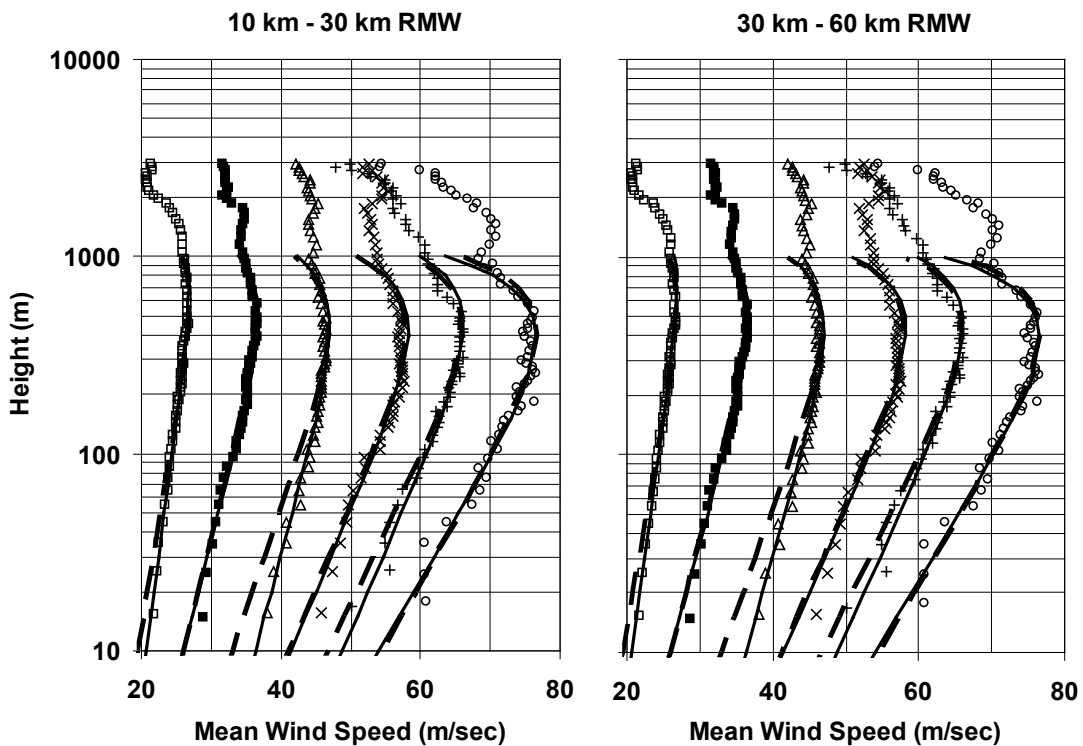


Figure 4-6 Observed and Modeled Velocity Profiles for the 10 – 30 Kilometers and 30 – 60 Kilometers RMW Cases

Table 4-1 Hurricane Boundary Layer Model Parameters Inside RMW

RMW (km)	MLB (m s ⁻¹)	Boundary Layer Model Parameters Obtained Using Method 1 (20 - 200- meter LSF Values)					Boundary Layer Model Parameters Obtained Using Method 2				
		U ₁₀ (m s ⁻¹)	C _d	Z ₀ (m)	H (m)	R ²	U ₁₀ (m s ⁻¹)	C _d	Z ₀ (m)	H (m)	R ²
10-30	20-29	20.7	0.0010	0.0000	650	0.98	19.5	0.0018	0.0007	520	0.93
10-30	30-39	25.9	0.0024	0.0029	440	0.97	26.5	0.0019	0.0010	460	0.98
10-30	40-49	48.9	0.0013	0.0002	380	0.92	34.5	0.0019	0.0010	400	0.83
10-30	50-59	41.5	0.0025	0.0032	380	0.91	42.5	0.0019	0.0010	375	0.93
10-30	60-69	48.9	0.0019	0.0009	400	0.93	48.7	0.0019	0.0010	390	0.94
10-30	70-85	54.1	0.0028	0.0049	350	0.90	56.0	0.0019	0.0010	320	0.92
30-60	20-29	19.5	0.0018	0.0009	650	0.98	19.5	0.0018	0.0007	675	0.98
30-60	30-39	26.2	0.0021	0.0016	600	0.96	26.4	0.0022	0.0020	480	0.99
30-60	40-49	32.9	0.0025	0.0033	550	0.99	33.5	0.0022	0.0020	510	0.98
30-60	50-59	39.3	0.0026	0.0041	550	0.97	40.8	0.0022	0.0020	480	0.95
30-60	60-69	49.7	0.0017	0.0005	550	0.96	48.0	0.0022	0.0020	500	0.94
30-60	70-85	51.0	0.0033	0.0093	700	0.89	55.0	0.0022	0.0020	550	0.95
60-100	20-29	19.5	0.0018	0.0009	1,000	0.98	19.7	0.0018	0.0007	1,000	0.98
60-100	30-39	26.8	0.0022	0.0021	750	0.95	27.0	0.0022	0.0022	750	0.97
60-100	40-49	32.9	0.0021	0.0015	900	0.95	33.0	0.0025	0.0034	700	0.97
60-100	50-59	38.0	0.0026	0.0042	800	0.95	38.9	0.0025	0.0034	675	0.96

4.1.2.1.2 Hurricane Boundary Layer Height

According to Kepert (2001), the jet height or boundary layer height is inversely proportional to the square root of the inertial stability parameter as given by:

Equation 4-6

(A)

$$H = \sqrt{\frac{2K}{I}} \tan^{-1} \left(-1 - \frac{2}{X} \right)$$

(B)

$$x = C_d V \sqrt{\frac{2}{KI}}$$

Where:

- K is the turbulent diffusivity of momentum
- I is the inertial stability
- C_d is the surface drag coefficient
- V is the gradient velocity

Here, the boundary layer height is also modeled as a function of I, where in the calculation of I, an average value of the radius within a radius bin is used to define r, and the maximum wind speed from mean velocity profile is used as a surrogate for the gradient velocity, V. Using the estimates of the boundary layer height, H* for r both near and outside the RMW, regression models for relating H* and I are given by:

Equation 4-7

(A)

$$H^* = 343.7 + 0.260/I \quad r^2 = 0.75, \quad \sigma_e = 99m$$

(B)

$$H^* = 186.6 + \frac{12.66}{\sqrt{I}} \quad r^2 = 0.70, \quad \sigma_H = 106m$$

The regression model for H*, modeled as a function of 1/I explains 75% of the variance associated with the underlying data, whereas when H* is modeled as a function of the model explains 70% of the variance. The boundary layer height model is in general agreement with Kepert's (2001) analysis, where the boundary layer height scaling parameter was shown to be inversely proportional to the square root of the inertial stability. Based on the observed values of H*, the model is capped using a lower bound of 300 meters and an upper bound of 1,200 meters. Figure 4-7 shows a comparison of the H* derived from the regression models, H derived using Equation 4-6 with K=75 square meters per second (Kepert, 2001) and the observed values of H*.

4.1.2.1.3 Marine Boundary Layer Model Verification

Using Equation 4-3 and Equation 4-5 to define the variation of the mean wind speed with height, coupled with Equation 4-7(A) to define the boundary layer height, the characteristics of the boundary layer were estimated given only U_{max} and r . In the verification process, the value of U_{max} is set equal to the maximum mean wind speed obtained by the dropsondes over the range of 20 to 1,000 meters, and r is equal to the mean value of r used to determine the RMW or r bin.

Figure 4-8 presents examples of the modeled and measured boundary layers for the 10 to 30 kilometers and 30 to 60 kilometers RMW cases. Solid lines represent model wind speeds computed given U_{max} , RMW, and f . Figure 4-9 shows the mean error plotted vs. height (with the errors computed over ranges of heights) where it is seen that in most cases the error is less than 5%, however; there is a weak trend evident where the underestimate of wind speeds near the surface increases as RMW decreases. The modeled and observed wind speeds were grouped into height bins of 10-50 meters, 50-100 meters, 100-200 meters, 200-300 meters, 300-400 meters, 400-500 meters, 500-700 meters, and 700-1,000 meters.

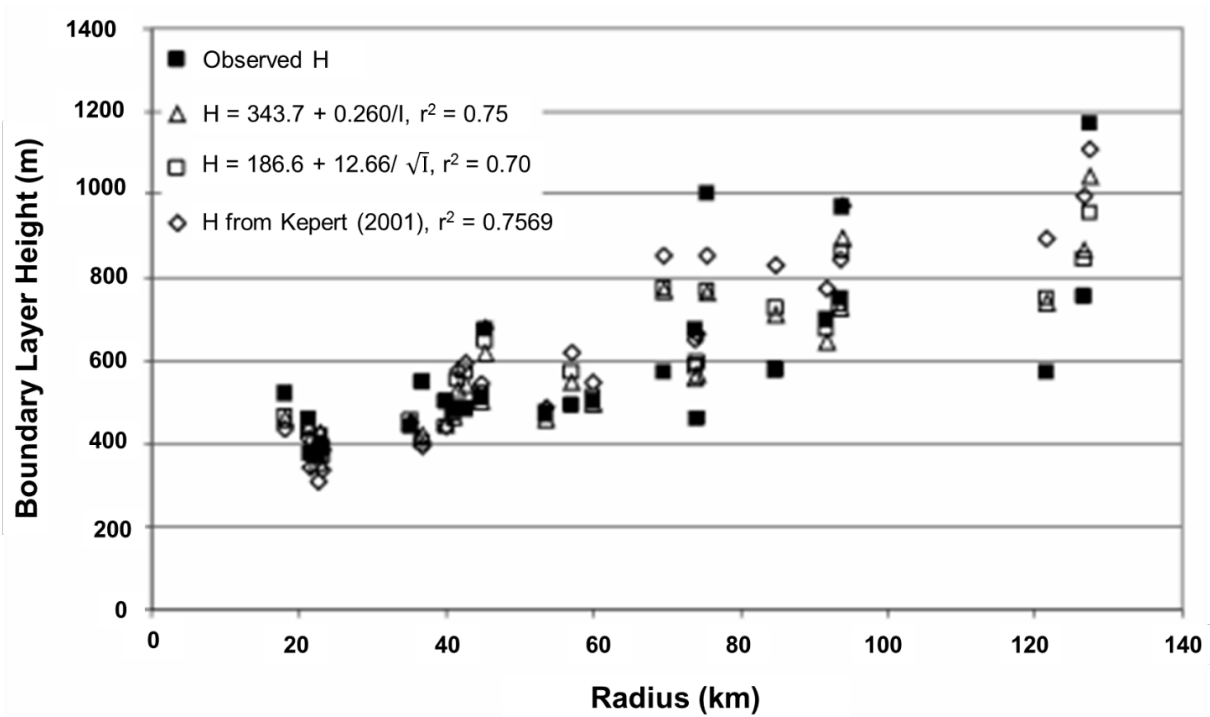


Figure 4-7 Comparison of Regression Model, Kepert (2001) Model and Observed Boundary Layer Heights

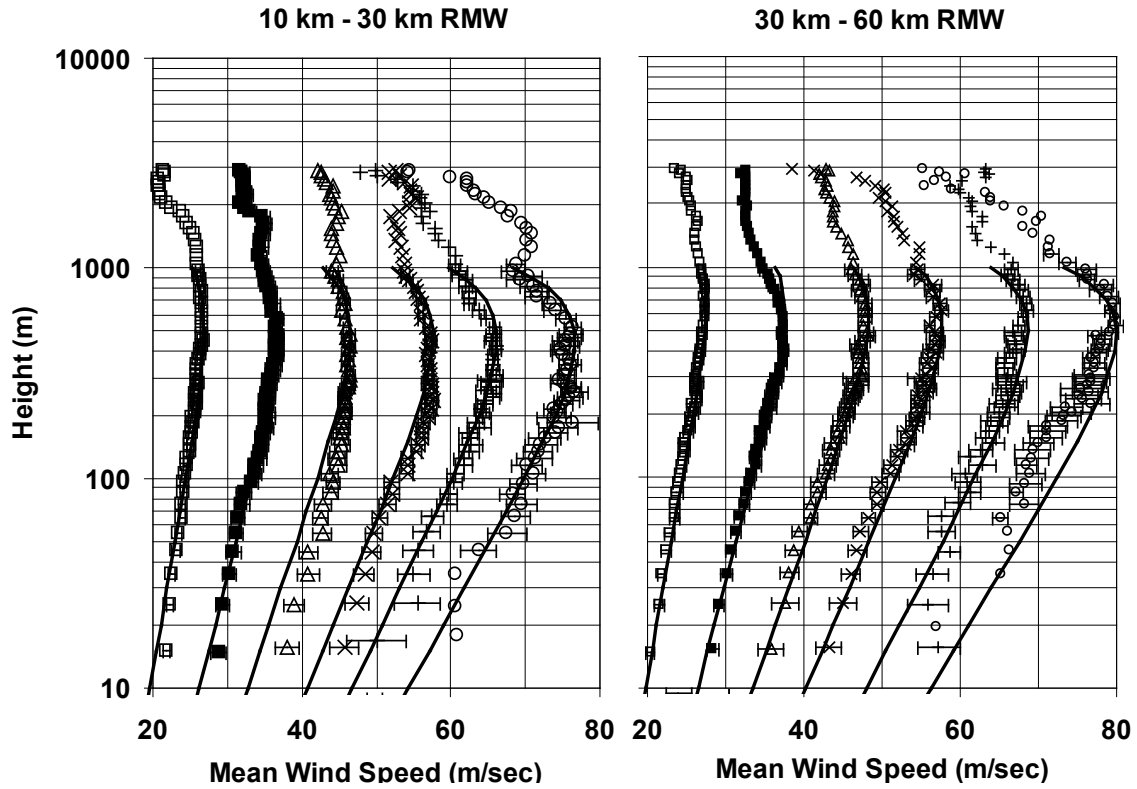


Figure 4-8 Observed and Modeled Velocity Profiles Near the RMW for the 10 to 30 kilometers and 30 to 60 kilometers RMW Cases

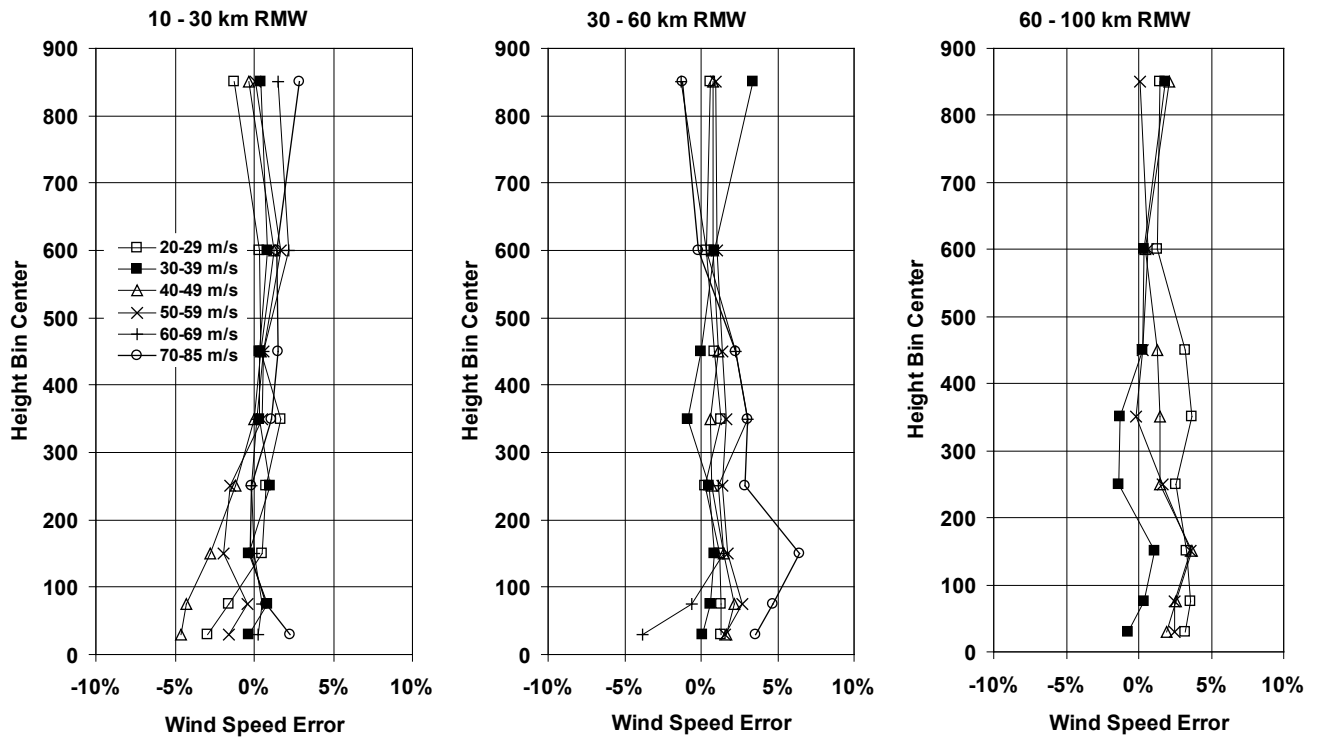


Figure 4-9 Mean Error in Modeled Wind Speeds versus Height for Drosonde Data Taken Near RMW

Figure 4-10 presents a comparison of the modeled and observed ratios of U_{10}/U_{max} plotted versus U_{max} for dropsonde data collected around the RMW. Observed values of U_{10}/U_{max} are obtained by extending the log-law velocity profiles to the 10 meters level using the LSF results over the three different height ranges discussed earlier. The mean value of U_{10}/U_{max} obtained from the model is 0.716. The mean values of computed U_{10}/U_{max} from the data using an LSF over height ranges of 20-200 meters, 20-150 meters, and 20-100 meters are 0.703, 0.713, and 0.719, respectively. The corresponding r^2 values are 0.32, 0.57, and 0.65, respectively. The mean modeled value of U_{10}/\bar{U}_{500} where \bar{U}_{500} is the wind speed averaged over the lower 500 meters of the boundary layer is 0.755, which is slightly lower than the value of 0.78 reported in Powell et al. (2003).

Figure 4-11 presents the variation of the mean error with height for the outside RMW cases. It is seen that in all the cases, the mean error is less than 5%. Outside of the RMW, the mean ratios of U_{10}/U_{max} for the observed and the modeled wind speeds are 0.698 and 0.686, respectively, implying a mean underestimate of the surface level wind speeds of about 2%. The empirical hurricane boundary layer model described here is shown to be able to reproduce the shape of the marine hurricane boundary layer reasonably well given only a wind speed at gradient or jet height, and a distance, r , from the center of the storm. The height of the jet is adequately described using a simple model where the jet height is inversely proportional to either, l or $1/\sqrt{l}$. Due to the limitation of the number of available mean velocity profiles, there was insufficient data to further separate the profiles by azimuth in addition to MBL and r bins, and as a result, any variation in the jet height as a function of azimuth (as is indicated by Kepert (2001) does in fact exist) is lost in the hurricane boundary layer model presented here. However, the magnitude of the jet strength and its variation with azimuth is modeled using the slab model representation of the hurricane wind field, as described in Section 4.1.2.2.

4.1.2.1.4 Sea Land Transition

The characteristics of the hurricane boundary layer described previously are representative of open water (marine) conditions and not for the over land case. There are virtually no dropsonde data to determine the characteristics of the over land hurricane boundary layer. The approach taken here to model the sea-land transition follows the classical approach (e.g., Deaves, 1981; Kao et al., 1974), where the wind speed at the top of the boundary layer is assumed to remain unchanged as the flow moves over a new roughness regime. The shape of the mean boundary layer over land is assumed to be adequately represented by Equation 4-5, and the methodology outlined in Kepert (2001) is used to estimate the increase in the boundary layer height associated with a change in surface roughness. The increase in the boundary layer height (H) is modeled using Equation 4-6, which requires an estimate of the increase in K as a function of the increase in C_d . For estimating the increase in the value of K as the wind moves from sea to land (open terrain), K is taken as:

Equation 4-8

$$K \approx C_d U^2 / \frac{\partial U}{\partial z} = u_*^2 / \frac{\partial U}{\partial z} \approx kz u_*$$

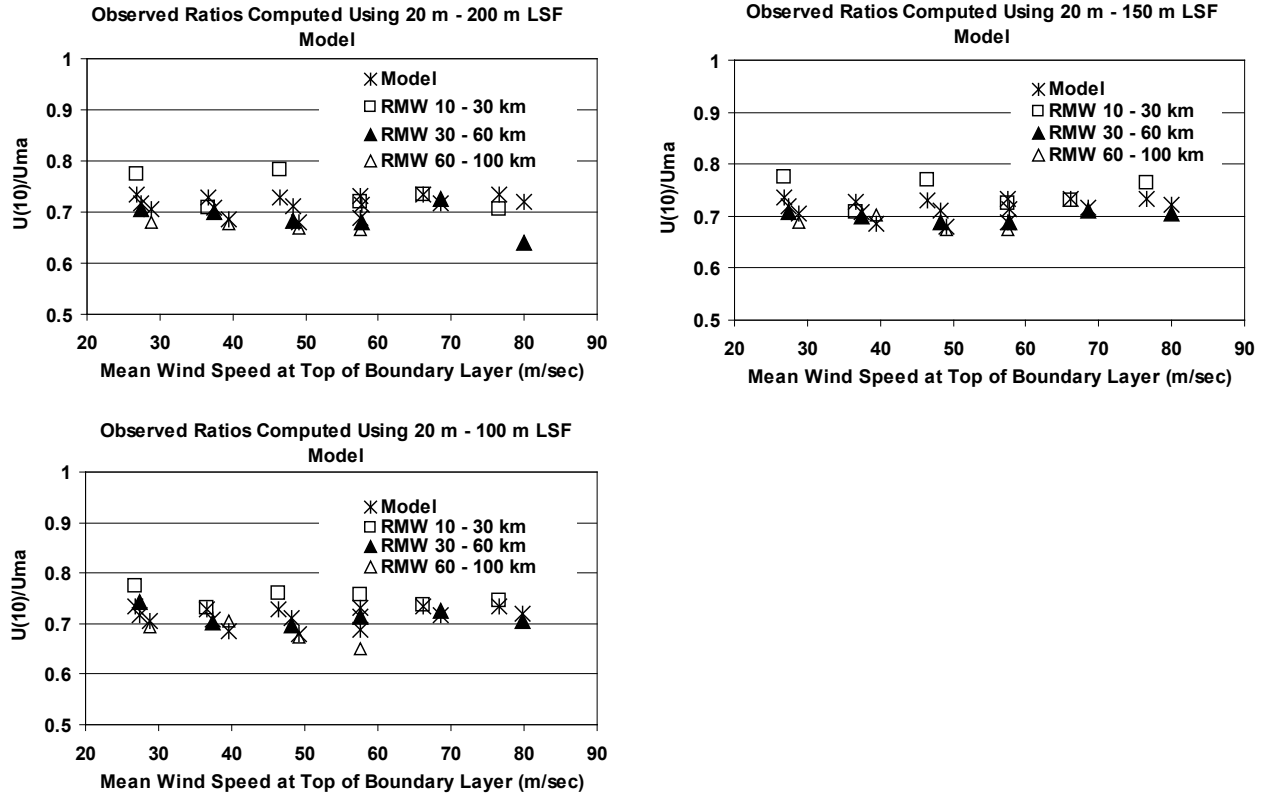


Figure 4-10 Comparison of Modeled and Observed Ratios of Mean Wind Speed at 10 meters to Mean Wind Speeds at the Top of the Boundary Layer Near the RMW

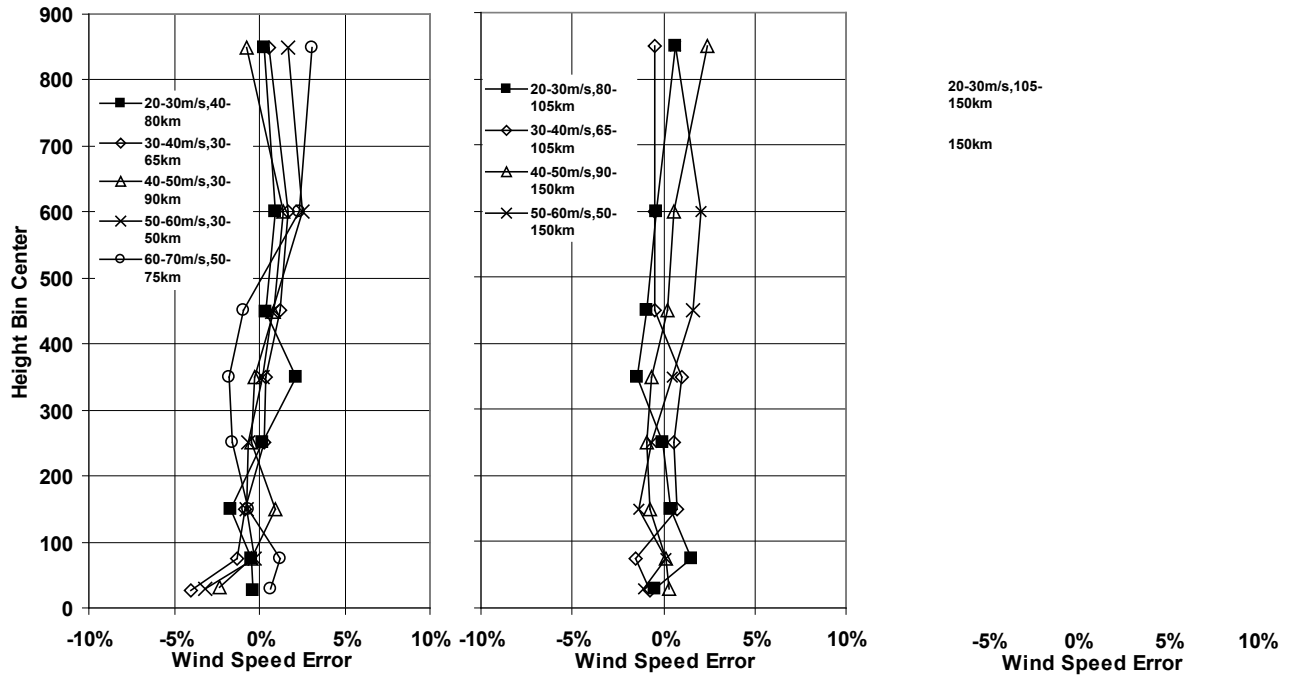


Figure 4-11 Mean Error in Modeled Wind Speeds versus Height for Dropsonde Data Taken Outside RMW Region

Equation 4-6 and Equation 4-8 are used to estimate the increase in H, yielding typical estimates of the increase in H ranging between 20% and 30% for land defined with $z_0=0.03$ meters, with the magnitude of the increase varying with both wind speed and radius. The value of H computed using Equation 4-6 and Equation 4-8 is dependent on the value of z used in Equation 4-8, but the ratio of the two boundary layer heights is, for practical purposes, independent of the value of z used in Equation 4-8.

Figure 4-12 presents the ratio of the mean wind speed over land ($z_0=0.03$ meters) to the mean wind speed over water ($z_0= 0.0013$ meters) as a function of the marine boundary layer height. Also shown in Figure 4-12 is the wind speed ratio computed using the Engineering Sciences Data Unit (ESDU) (1982) transition model. Figure 4-12 shows that the reduction of the mean wind speed as the wind moves from the sea to the land associated with a hurricane is less than that estimated using the ESDU model and that the wind speed reduction factor is dependent on H, and hence storm intensity and size. The wind speed reduction factors given in Figure 4-12 are larger than those predicted by ESDU for large H but match the model given in Simiu and Scanlan (1996) for large H. In the model implementation, the increase in the boundary layer height predicted using

Equation 4-6, and Equation 4-8 is further increased so that the resulting reduction in the wind speed associated with the sea land transition matches that given in ESDU (1982) for large H. Using this approach, for typical values of H (~600 meters) near the RMW, the predicted reduction in the mean wind speed matched that given by the model given in Simiu and Scanlan (1996). The wind speed reduction factors shown in Figure 4-12 are representative of a fully transitioned boundary layer.

As the wind moves from the sea to the land, the value of the maximum wind speed at a given height in the new rougher terrain approaches the fully transitioned value asymptotically over some fetch distance, F. Published estimates of the fetch length vary markedly, ranging from a few kilometers (e.g., Melbourne, 1992) to in excess of 100 kilometers (ESDU, 1982; Deaves, 1981). Powell et al. (1996) suggest that wind measurements at the height of 10 meters taken as far as 20 kilometers to 30 kilometers inland are still influenced by the upstream marine roughness. For modeling the transition from sea to land, the ESDU model is used, but the limiting fetch distance is reduced to 20 kilometers rather than the ~100 kilometers used in ESDU (1982). The use of the smaller fetch distance is consistent with the lower boundary layer heights associated with tropical cyclones (~600 meters) compared to much larger values (~3,000 meters) used in ESDU where H scales as u^*/f rather than $\sqrt{2K/l}$.

The ESDU transition model was chosen since it provides a means to transition the wind speeds associated with an arbitrary averaging time (i.e., hourly, 10-minute mean, peak gust, etc.). Figure 4-13 shows a comparison of the original and modified ESDU transition functions for the gust and hourly mean wind speeds. In either model, it is evident that at a distance of about 1 kilometer, approximately 60% of the transition (or wind speed reduction) has already occurred. An exact value of F is considered to be difficult, if not impossible to verify, and an inspection of Figure 4-13 indicates that the error in the predicted wind speed is not particularly sensitive to the value of F (for $F>10$ kilometers). For example, the difference between the model estimates of the degree to which the wind speed has reached equilibrium at 10 kilometers (approximately where the difference between the ESDU [$F\sim 100$ kilometers] and the modified ESDU [$F=20$ kilometers] function reaches a maximum) is about 10%. Referring to Figure 4-12, it is seen that the maximum reduction in the mean wind speed using the ESDU model is

about 17% thus, the magnitude of the wind speed error associated with the assumed fetch length is about 10% of 17%, or ~1.7%. The error in the estimate of the peak gust wind speed associated with the assumed fully transitioned fetch length is even less.

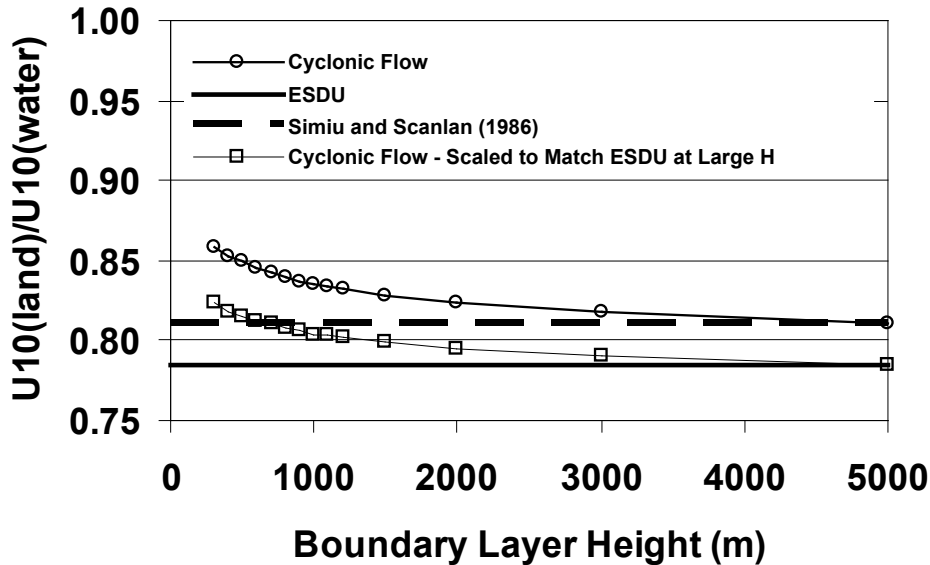


Figure 4-12 Ratio of the Fully Transitioned Mean Wind Speed Over Land ($z_0=0.03$ meters) to the Mean Wind Speed Over Water ($z_0=0.0013$ meters) as a Function of Boundary Layer Height

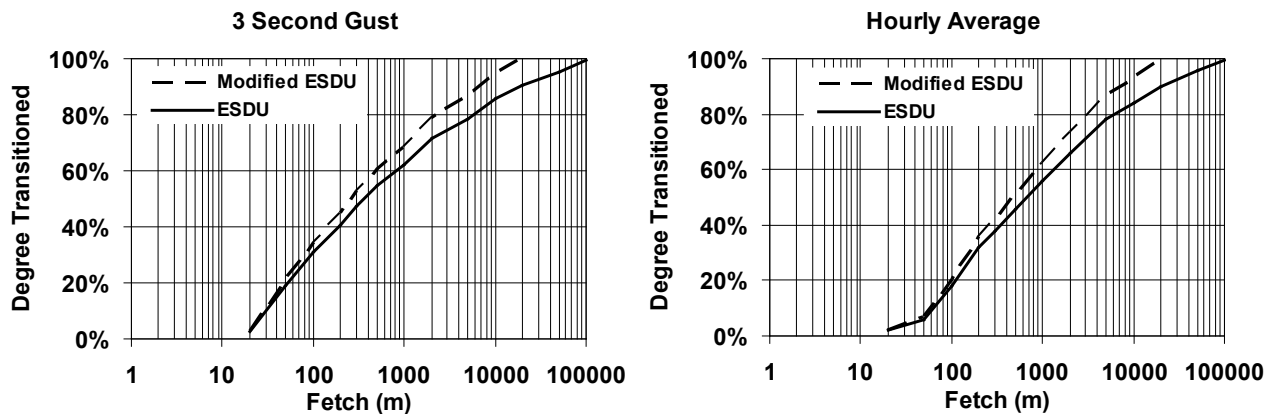


Figure 4-13 ESDU and Modified ESDU Wind Speed Transition Functions

4.1.2.2 Model Verification

Verification of the boundary layer model as a whole, with emphasis on the sea-land transition, is made difficult because of the paucity of measurements of both marine and near-by over land wind speeds in landfalling hurricanes. Furthermore, experimental verification of the results suggesting that the reduction in wind speed associated with the change in roughness from sea to land is less than what is expected in non-cyclonic winds, is complicated by the fact that the reduction in wind speed as a function of distance inland includes the combined effect of the transition model and the wind speed reduction model. The approach taken to verify the combined boundary layer-transition model uses comparisons of

time series of measured mean and gust wind speeds combined with model estimates of wind speeds. These model estimates are made using a slab representation of a hurricane coupled with the hurricane boundary layer model and terrain transition models. The mean wind speeds obtained from the HBL model are converted to gust or sustained (one minute) values using the ESDU gust factor models. The ESDU models have been shown by Vickery and Skerlj (2005) to be valid for hurricanes. Details of the slab model approach are given in Thompson and Cardone (1996) and Vickery et al. (2000a).

The slab model used here is a modification of the model described in Vickery et al. (2000a), where the drag coefficient used in Vickery et al. (2000a) has been replaced by the truncated Large and Pond (1981) model, and the number of nested grids has been increased from four to six. In the use of the slab model, the resulting integrated wind speed (mean value throughout the boundary layer) is adjusted to be representative of the maximum wind speed in the boundary layer. The difference between the maximum wind speed and the depth averaged wind speed is only a few percent and varies depending upon when the averaging is performed over the assumed 1,000 meters boundary layer height used in the slab model, or if the averaging height taken is the modeled boundary layer, or jet height. In the comparisons of modeled and observed marine and land wind speeds, an additional 2% increase in the modeled winds was required to eliminate a low overall bias in the comparisons. This minor increase is consistent with the underestimate of the surface winds discussed earlier in the case of small RMW storms, the underestimate for winds outside the eyewall and the difference between given in Powell et al. (2003) that is computed herein. The slab model approach to modeling the hurricane wind field brings out features of the wind field that are not reproduced in simple gradient U_{10}/\bar{U}_{500} balance vortex models or empirical models such as those described in the NOAA Technical Report NWS-23 (Schwerdt et al., 1979). For example, Figure 4-14 presents the distribution and magnitude of the jet determined (here defined as the depth average wind speed divided by the gradient balance wind speed) using the slab model. A comparison of the jet strength and its variation with azimuth resulting from the 2-D slab model with the results of a full 3-D model of a translating hurricane as presented in Kepert and Wang (2001) indicate that the 2-D numerical slab model is able to reproduce the horizontal variation and magnitude of the jet characteristics corresponding to a height of ~ 500 meters produced by a full 3-D numerical model. The variation of the jet height with azimuth is not maintained using the slab model.

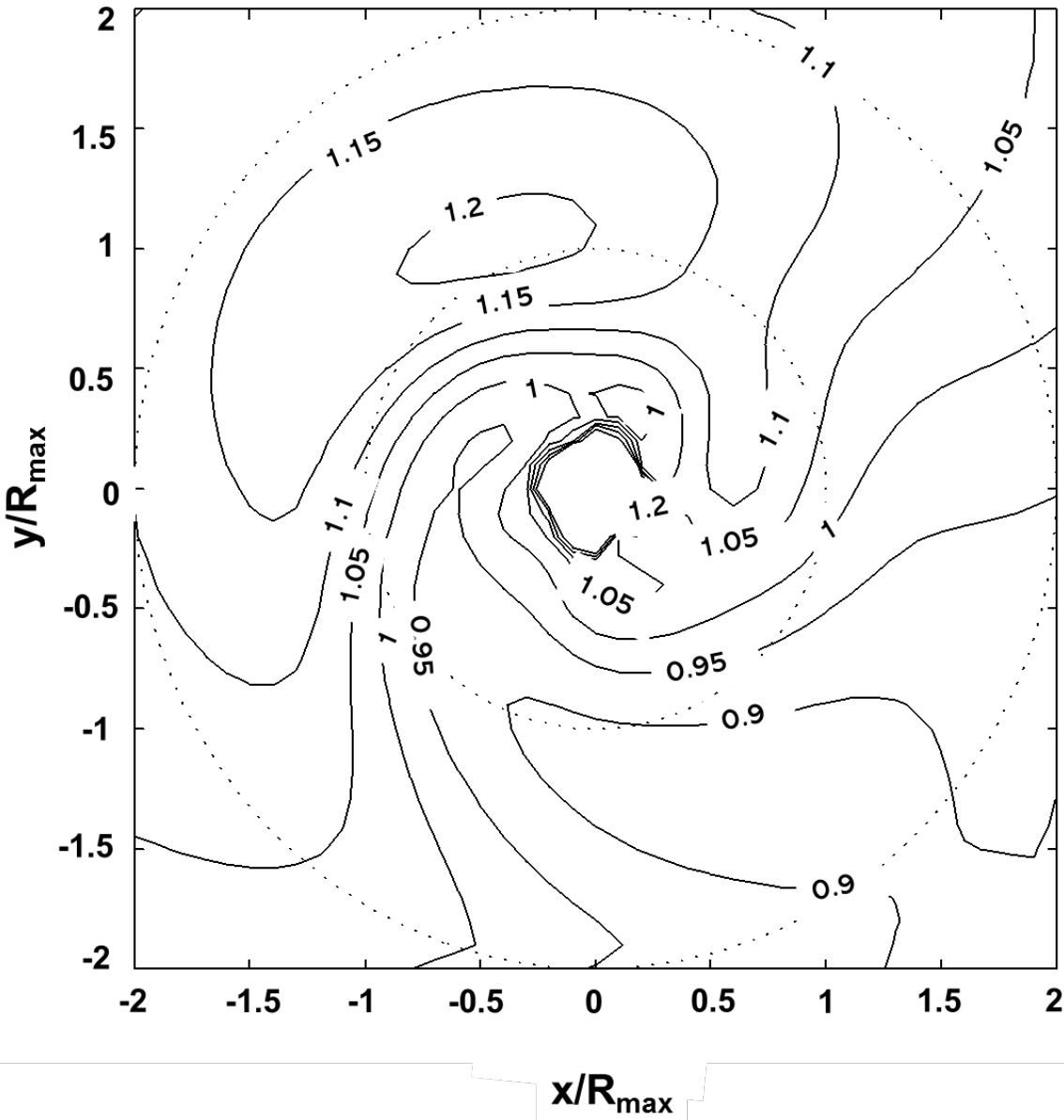


Figure 4-14 Jet Strength Computed Using the Slab Model for a Hurricane Moving Towards the Top of the Page

In the verification of the model with an emphasis on the sea-land transition, only hurricanes having continuous measurements of wind speeds both over land and over water near the landfall location are useful. Reasonably well documented storms that meet this criterion include Hurricanes Bertha and Fran (1996), Hurricane Bonnie (1999) near the North Carolina coast, and Hurricane Ivan (2004) along the Gulf Coast. The validation approach is indirect, with the process involving a comparison of modeled and observed maximum peak gust wind speeds produced by the hurricanes over both marine and land terrains. Conclusions as to the validity of the model are inferred by determining if there is a bias in the estimates of the modeled marine winds versus the modeled over land winds. All measured gust wind speeds have been adjusted to be representative of 3-second gust speeds at the height of 10 meters, in either open terrain ($z_0 = 0.03$ meters) or marine conditions. In the case of marine wind speed measurements obtained from 3 meters discus buoys, the measured wind speeds in high wind cases

have been increased by 10% to account for the underestimates in the measured wind speeds as described in Gilhousen (2006). Each hurricane is modeled using information on the hurricane track (position and central pressure) obtained from the National Hurricane Center, coupled with estimates of the RMW and the Holland B parameter. The modeled pressure field is axi-symmetric but varies with time. The initial estimate of the RMW is usually obtained from H*Wind snapshots of the hurricane wind field at or near the time of landfall. The final estimates of B and the RMW and their variation with time after landfall are obtained through an iterative approach by reproducing the overall shapes of the wind speed and direction traces and surface pressure traces obtained from as many ground stations as possible. Figure 4-15 through Figure 4-19 present examples of comparison of wind speed and pressure data obtained from stations located near the point of landfall for different hurricanes; Model results are represented by a solid line, observed values are represented by the open squares.

An extensive set of validation studies has been performed using the hurricane windfield/boundary layer model described herein through comparisons of modeled and observed wind speed and pressure data obtained for 19 landfalling hurricanes occurring since 1985. In each validation study, estimates of RMW and B, and their variation in time were obtained using the iterative approach described above. The number of anemometer stations with either complete continuous records of wind speeds, or records where the maximum wind speed during the storm was measured, is given in Table 4-2. Note that in many cases, additional incomplete records of wind speeds and pressures were used to assist in estimating the variation in both RMW and B.

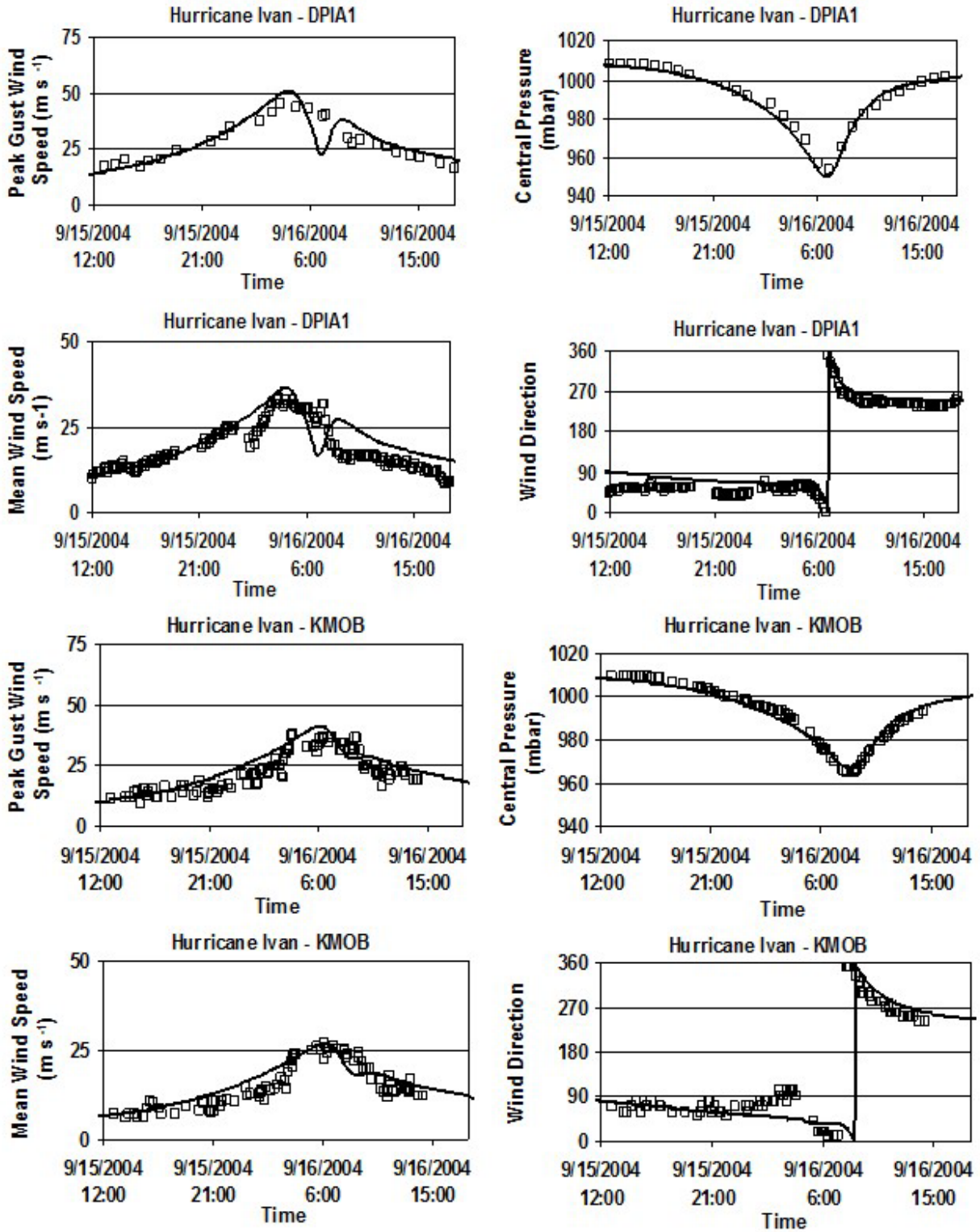


Figure 4-15 Example Plots Showing Modeled and Observed Wind Speeds, Surface Pressures and Wind Directions

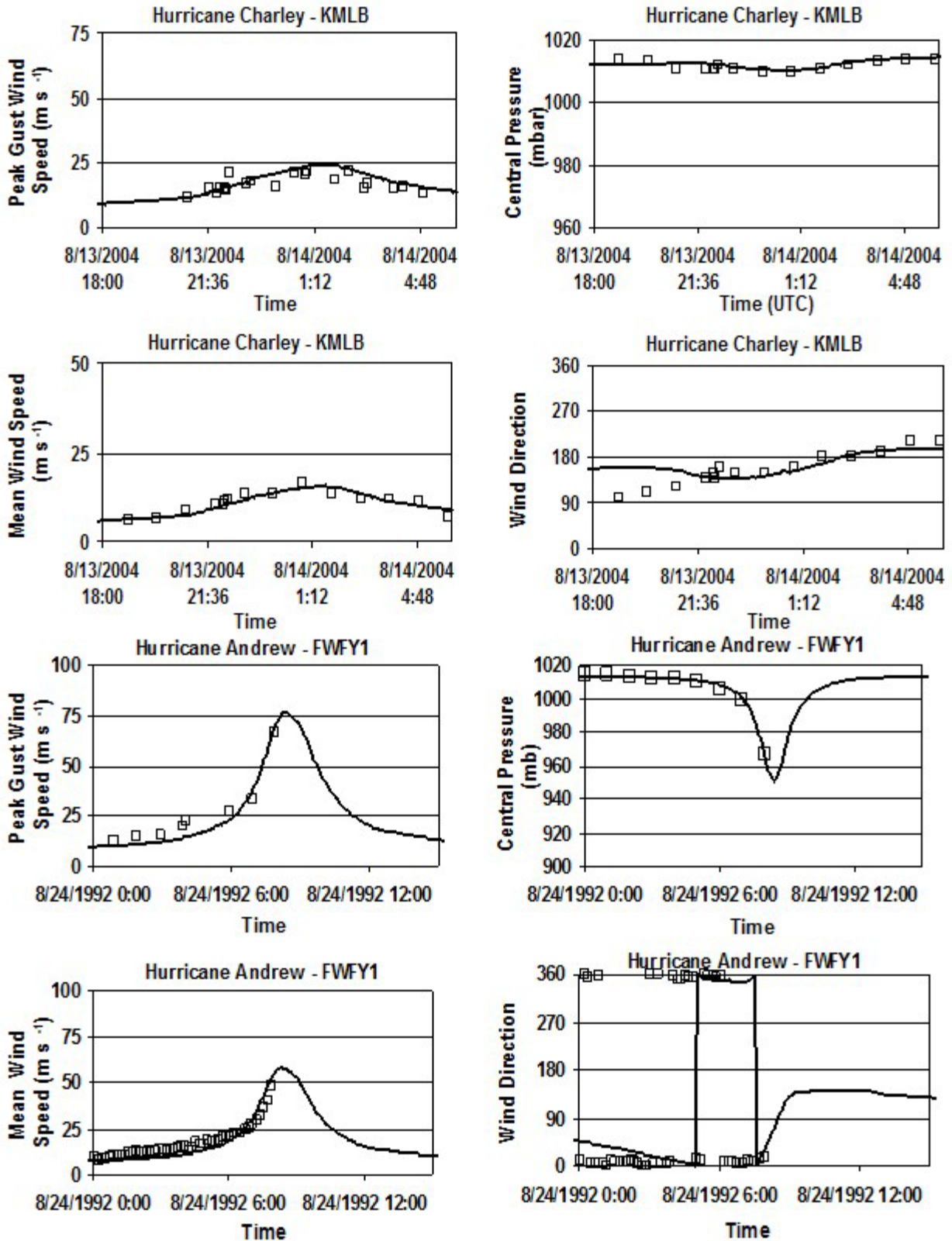


Figure 4-16 Example Plots Showing Modeled and Observed Wind Speeds, Surface Pressures and Wind Directions (continued)

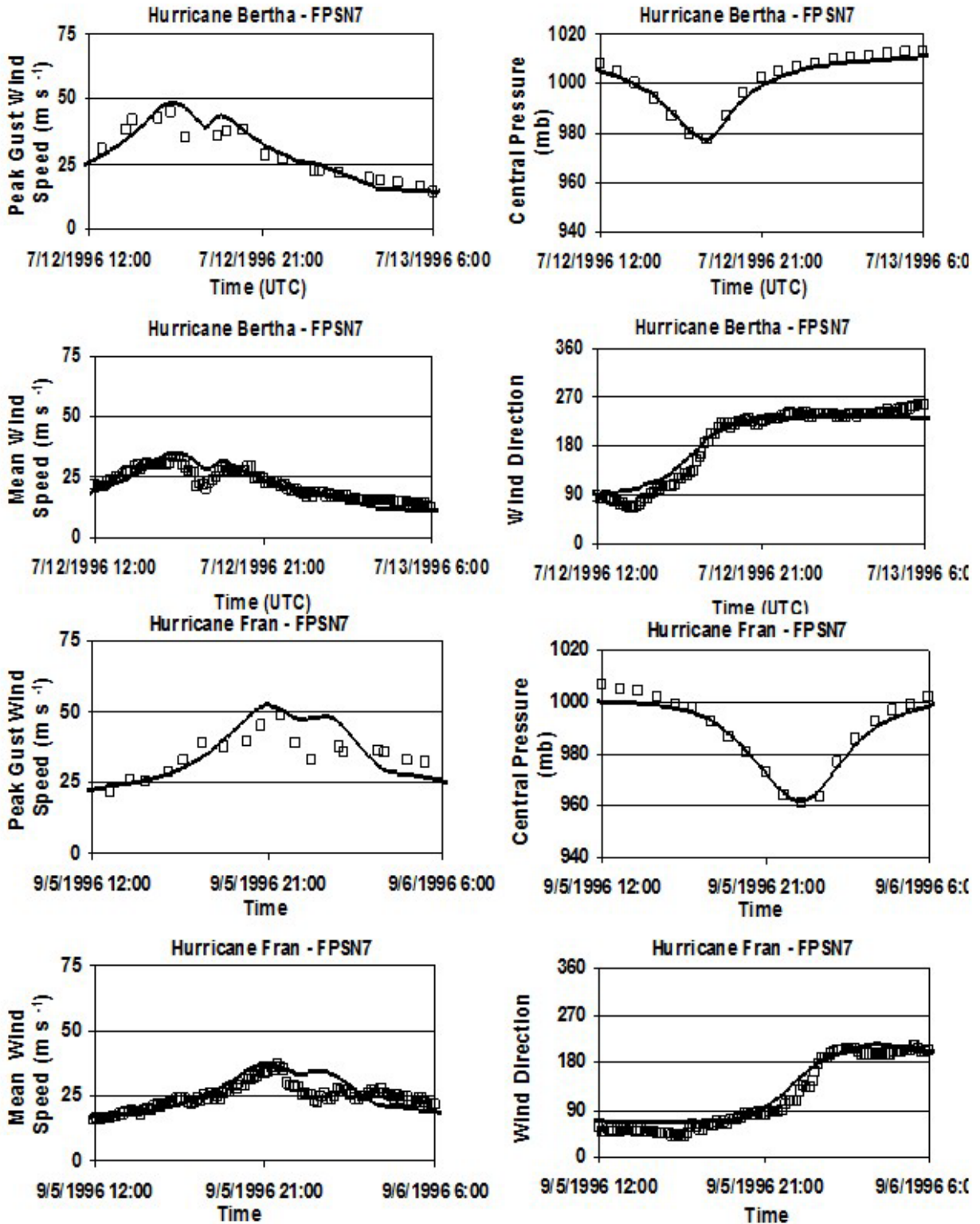


Figure 4-17 Example Plots Showing Modeled and Observed Wind Speeds, Surface Pressures and Wind Directions (continued)

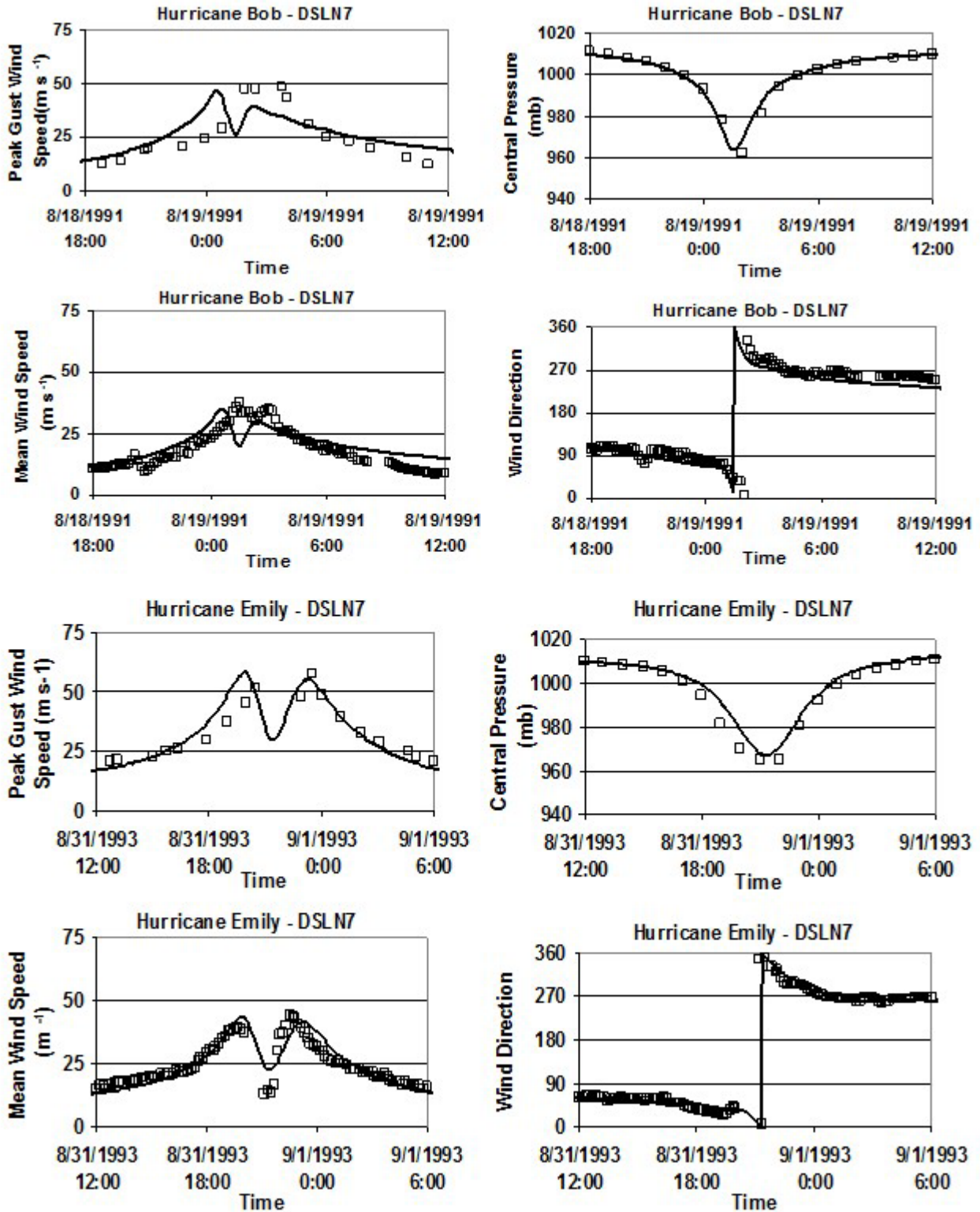


Figure 4-18 Example Plots Showing Modeled and Observed Wind Speeds, Surface Pressures and Wind Directions (continued)

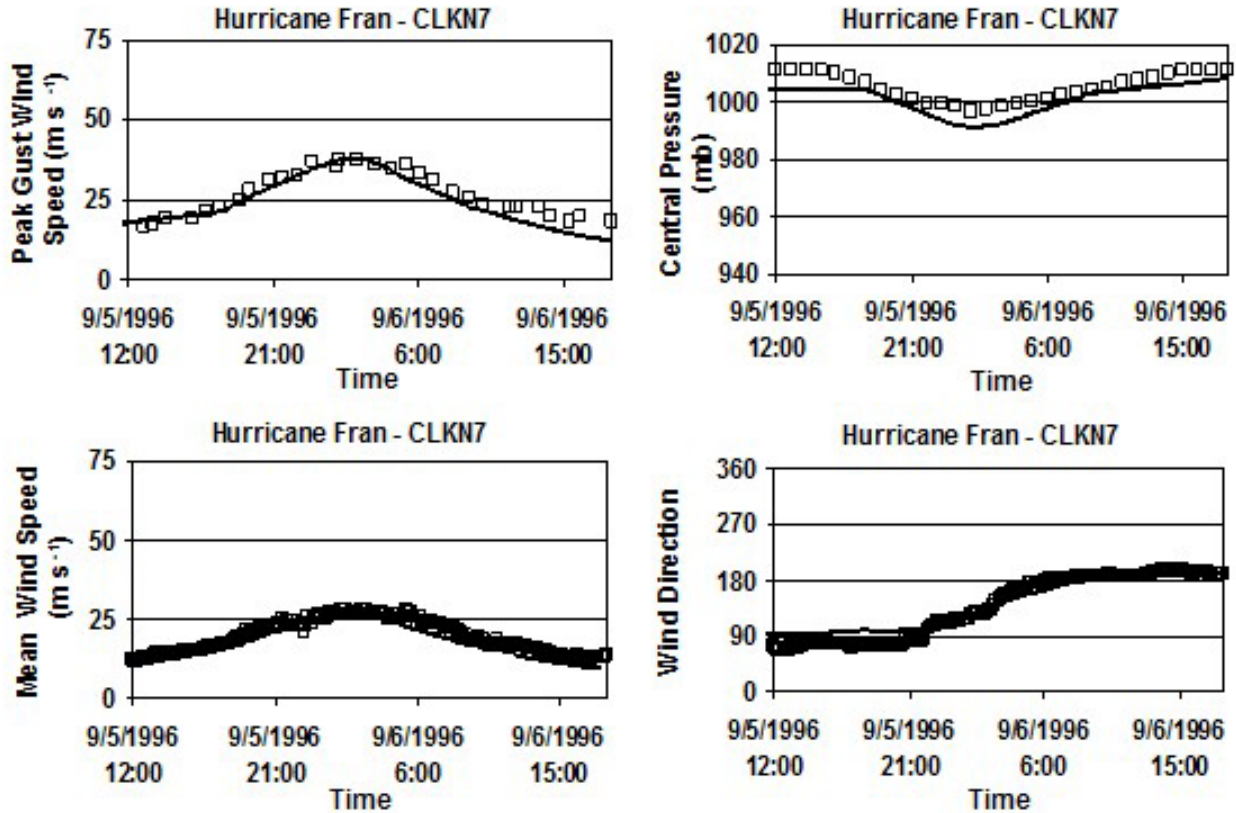


Figure 4-19 Example Plots Showing Modeled and Observed Wind Speeds, Surface Pressures and Wind Directions (concluded)

Table 4-2 Number of Wind Speed Records for Each Hurricane

Year	Name	Number of Complete Wind Speed Records		
		Land	Marine	Total
1979	Frederic	4		4
1985	Elena	3	2	5
1989	Hugo	6	1	7
1991	Bob	2	5	7
1992	Andrew	1	2	3
1993	Emily		9	9
1995	Erin	5	2	7
1996	Bertha	5	3	8
1996	Fran	9	3	12
1996	Opal	5	2	7
1998	Bonnie	2	4	6
1998	Georges	3	10	13

Year	Name	Number of Complete Wind Speed Records		
		Land	Marine	Total
1999	Floyd	2	4	6
1999	Irene	4	5	9
2003	Isabel	10	7	17
2004	Charlie	7		7
2004	Frances	13		13
2004	Ivan	13	6	19
2004	Jeanne	14	1	15
2005	Dennis	9	3	12
2005	Katrina	8	2	10
2005	Ophelia	5	7	12
2005	Rita	14		14
2005	Wilma	21	2	23
Total		165	80	245

Figure 4-20 presents scatter plots summarizing the comparisons of modeled and observed maximum peak gust wind speeds produced by the storms. In the figure, open squares represent land-based measurements; solid squares represent marine based measurements. All wind speeds are at the height of 10 meters in either open terrain or for marine conditions. In each plot, the slope and r^2 values are given resulting from a linear regression analysis where the regression line is forced to pass through the origin. In all cases, the regression slopes are within 3% of unity. Figure 4-21 presents a summary comparison of the maximum peak gust wind speeds computed using the wind field model described in Vickery et al. (2008), to observations for both marine and land-based anemometers. Wind speeds measured on land are given for open terrain and wind speeds measured over water are given for marine terrain. There are a total of 245 comparisons summarized in data presented in Figure 4-21 (165 land-based measurements and 80 marine based measurements). The agreement between the model and observed wind speeds is good, however, there are relatively few measured gust wind speeds greater than 100 mph (45 meters per second).

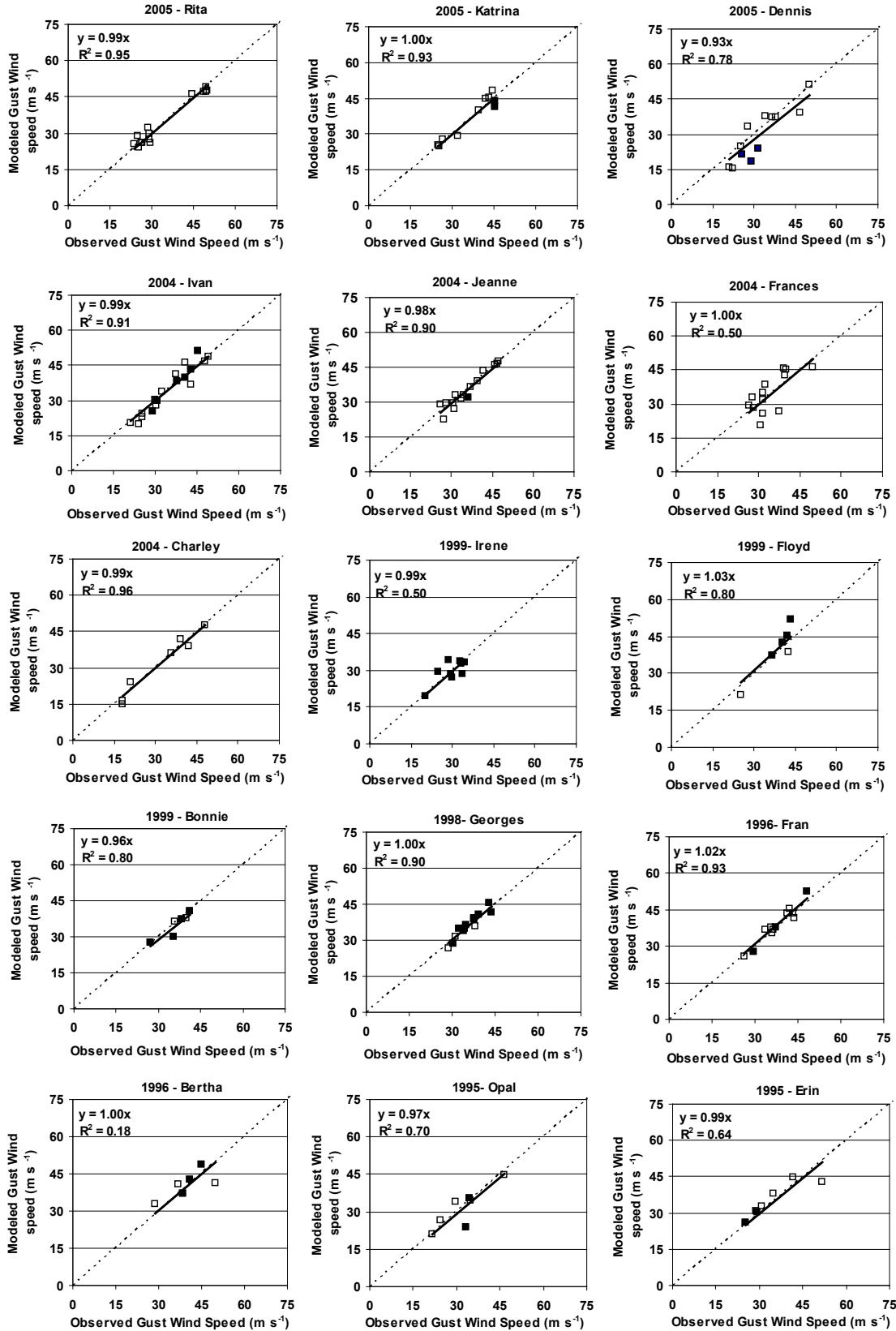


Figure 4-20 Comparison of Modeled and Observed Maximum Peak Gust Wind Speeds for 15 Land Falling Hurricanes

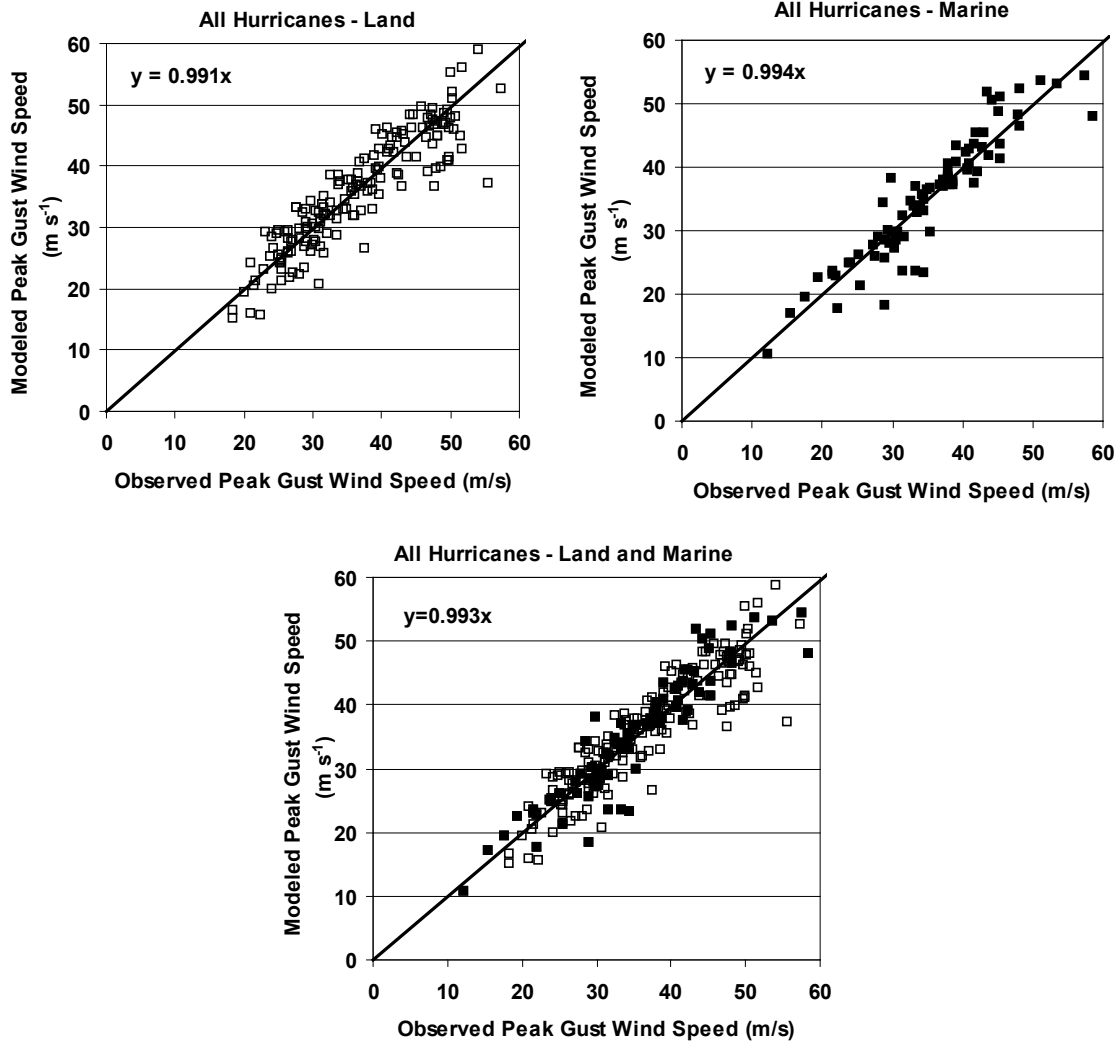


Figure 4-21 Example Comparisons of Modeled and Predicted Maximum Surface Level Peak Gust Wind Speeds in Open Terrain from US Landfalling Hurricanes

The largest observed gust wind speed is only 128 mph (57 meters per second). The differences between the modeled and observed wind speeds are caused by a combination of the inability of wind field model to be adequately described by a single value of B and RMW, errors in the modeled boundary layer, errors in height, terrain and averaging time adjustments applied to measured wind speeds (if required) as well as storm track position errors and errors in the estimated values of Δp , RMW, and B.

4.1.3 Summary

The boundary layer modeling has been improved over the models used in prior hurricane risk studies, by considering the dropsonde data, considering the theoretical model of Kepert (2001), and using a physically based gust factor model that properly models the variation in the gust factor with surface roughness.

The modeling of the hurricane wind field has also been improved in comparison to models used in previous studies. It employs the full nonlinear solution to the equations of motion of a hurricane rather than the spectral model used in Georgiou (1985) or Vickery and Twisdale (1995a), or the empirical models used in all other studies. Evaluation of the hurricane model through comparisons with real hurricane wind speed data shows that the model provides a good representation of the hurricane wind field. The hurricane wind field model relies, wherever possible, on physical models rather than empirical models to describe the wind speeds within the storm.

4.2 Hurricane Simulation Methodology

Mathematical simulation of probabilistic hurricanes is the most accepted approach for estimating wind speeds for the design of structures and assessment of hurricane risk. The basic approach in all previously published hurricane simulation studies is the same in that site-specific statistics of key hurricane parameters (including central pressure difference (Δp), Holland pressure profile parameter (B), radius to maximum winds (R_{max}), heading (θ), translation speed (c), and the coast crossing position or distance of closest approach (d_{min}) are first obtained. Given that the statistical distributions of these key hurricane parameters are known, a Monte Carlo approach is used to sample values from each of the aforementioned distributions and a mathematical representation of a hurricane is passed along the straight-line path, satisfying the sampled data, while the simulated wind speeds are recorded. The intensity of the hurricane is held constant until landfall is achieved, after which time the hurricane is decayed using filling rate models.

A probabilistic hurricane simulation approach has been developed where the full track of a hurricane or tropical storm is modeled, beginning with its initiation over the ocean and ending with its final dissipation (Vickery et al., 2000a). Using this approach, the central pressure is modeled as a function of sea surface temperature, and the storm heading, speed, etc., are updated at each six-hour point in the storm history. Linear interpolation is used between the six-hour points. The approach is validated by comparing the site-specific statistics of the key hurricane parameters of the simulated hurricane tracks with statistics derived from the historical data. When coupled with the wind field model, the model is able to reproduce the continually varying hurricane statistics along the U.S. coastline, and can treat multiple landfalling storms, by-passing storms, storm curvature, and re-intensification in cases where the storm re-enters the water before making a second or third landfall.

4.2.1 Storm Track Modeling

The storm track simulation model is initiated by randomly sampling a starting position, date, time, heading, and translation speed from one of the tropical storms given in the HURDAT database. The number of storms to be simulated in any one year is obtained by sampling from a negative binomial distribution having a mean value of 8.4 storms per year and a standard deviation of 3.56 storms per year. Given the initial storm heading, speed, and intensity, the simulation model estimates the new position and speed of the storm based on the changes in the translation speed, c , and direction (or heading) of the storm, θ , over the current six-hour period. The changes in the speed and direction between times i and $i+1$ are obtained from:

Equation 4-9

$$\Delta \ln c = a_1 + a_2 \psi + a_3 + a_4 \ln c_i + a_5 \theta_i + \varepsilon$$

Equation 4-10

$$\Delta \theta = b_2 + b_2 \psi + b_3 \lambda + b_4 c_i + b_5 \theta_i + b_6 \theta_{i-1} + \varepsilon$$

Where:

- $a_1, a_2, \text{ etc.}$ are constants
- ψ and λ are the storm latitude and longitude
- c_i is the storm translation speed at time step i
- θ_i is the storm heading at time step i
- θ_{i-1} is the heading of the storm at time step $i-1$
- ε is a random error term

The coefficients $a_1, a_2, \text{ etc.}$ have been developed using 5° by 5° grids over the entire Atlantic basin. A different set of coefficients for easterly and westerly headed storms is used. As the storm moves into a different 5° by 5° square, the coefficients are used to define the changes in heading and speed change accordingly. The maximum change in the direction of a simulated storm was truncated to ensure realistic limits on the maximum change in storm direction as a function of wind speed. The bounding value of the upper limit in the change of storm direction over a six-hour period is a function of storm translation speed.

The central pressure modeling method used in the approach eliminates the need to model the central pressure of the hurricane explicitly by using a relative intensity parameter, which is coupled to the sea surface temperature. This relative intensity approach is an improvement over traditional simulation techniques in that the central pressures derived are bounded by physical constraints, thus eliminating the need to artificially truncate the central pressure distribution. The method was first used in single point simulations by Darling (1991). The approach is validated by comparing the statistics of the observed and modeled hurricane central pressure statistics along the U.S. coastline.

During the hurricane simulation process, the values of the relative intensity, i , at each time step are obtained from:

Equation 4-11

$$\ln(I_{i+1}) = c_0 + c_1 \ln(I_i) + c_2 \ln(I_{i-1}) + c_3 \ln(I_{i-2}) + c_4 T_s + c_5 (T_{s_{i+1}} - T_{s_i}) + \varepsilon$$

Where:

- T_s is the sea surface temperature and the coefficients
- $c_0, c_1, \text{ etc.}$ vary with storm latitude, basin (Gulf of Mexico or Atlantic Ocean), and heading (i.e., Easterly or Westerly direction)

Near the U.S. coastline, where more continuous pressure data are available, finer, regionally specific values of these coefficients are developed. These regionally specific coefficients consider changes in the relationships between sea surface temperature and storm intensity that are influenced by subsurface water temperatures, as described in Cooper (1988). The maximum increase in storm intensity over a six-hour period was set equal to 40 millibars, (6.7 millibars per hour) which is greater than the largest average six hour change of about 25 millibars per 6 hours (4.2 millibars per hour) observed in Super Typhoon Forrest in the western Pacific in 1983, but less than the maximum rate of 7.14 millibars per hour also observed in Super Typhoon Forrest, but for a period of fewer than 3 hours. Once a simulated storm makes landfall, the change in central pressure with time is modeled using the filling models described in Vickery (2005). If a storm moves back over water, Equation 4-11 is again used to model the variation in central pressure with time. Using this modeling approach, the central pressure of the storm continuously changes with time, unlike traditional hurricane simulations, where a constant value of central pressure is assumed until landfall is achieved. As indicated by Equation 4-11, most Hazus storm tracks are modeled for the Gulf of Mexico or Atlantic coastlines. Track modeling for Hawaii/Pacific storms varies slightly and is described in the *Hazard Mitigation Study for the Hawaii Hurricane Relief Fund* (Applied Research Associates, Inc., 2001).

4.2.2 Modeling of Radius to Maximum Winds

In Vickery and Wadhera (2008), two models are given for the RMW (km), one for Gulf of Mexico hurricanes, and one for all hurricanes. Here, the storms' RMW model is applied to the Atlantic basin hurricanes, and the Gulf of Mexico RMW model is applied to storms in the Gulf of Mexico. The models for RMW used in the simulation are:

Equation 4-12

$$\ln(\text{RMW}_{\text{Atlantic}}) = 3.015 - 6.291 * 10^{-5} \Delta p^2 + 0.0337 \psi + \epsilon_{\text{Atlantic}}$$

$$r^2 = 0.297, \sigma_{\ln \text{RMW}} = 0.441$$

Equation 4-13

$$\ln(\text{RMW}_{\text{Gulf}}) = 3.859 - 7.700 * 10^{-5} \Delta p^2 + \epsilon_{\text{Gulf}}$$

$$r^2 = 0.290, \sigma_{\ln \text{RMW}} = 0.390$$

The two statistical models for the RMW (Gulf of Mexico and Atlantic Ocean) are combined to yield one RMW model for each simulated storm in the form:

Equation 4-14

$$RMW = a_1 RMW_{Atlantic} + (1 - a_1) RMW_{Gulf}$$

$$a_1 = \frac{\sum \Delta p_{Atlantic}}{\sum [\Delta p_{Atlantic} + \Delta p_{Gulf}]}$$

Where:

Δp is the central pressure difference and the summation is performed over all six hour time steps from storm origination to the current time

All simulated storm tracks containing the storm location (latitude and longitude), heading, central pressure, RMW, B, and translation speed are saved and later combined with the wind field model to compute wind speeds.

4.2.3 Pressure Profile Parameter (B)

Upper-level aircraft data from NOAA were used to estimate Holland’s pressure profile parameter (B) (Vickery and Wadhera, 2009). The upper-level aircraft dataset used here contains a total of 4546 radial profiles from 62 Atlantic storms. This data is the same as that used by Willoughby et al. (2006) in their analysis of B, with the main difference in the analysis methodology being that pressures are used here, and Willoughby et al. (2006) performed their analysis using wind speeds. For every storm, data has been organized based on the different flights that passed through the storm. For each flight, the airplane traversed through the hurricane several times in different directions. For every pass, the data was collected from the center of the storm to a certain radius (usually 150 kilometers). Available data were then organized according to their radial distance from the center of the storm. For each bin (based on the radius from the center of the storm), flight level pressure, flight altitude, dew point temperature, wind speed, and air temperature are available. Each profile from every flight and every storm is treated as an independent observation. Holland (1980) describes the radial distribution of surface pressure in a hurricane in the form:

Equation 4-15

$$p(r) = p_0 + \Delta p * \exp - \left[\frac{RMW}{r} \right]^B$$

Where:

- $p(r)$ is the surface pressure at a distance r from the storm center
- p_0 is the central pressure
- Δp is the central pressure difference
- B is the Holland’s pressure profile parameter

The surface pressure and radial distance are transformed to the form of Equation 4-15. The missing quantities in Equation 4-15 are RMW and B. First, an estimate of RMW is made from the recorded wind speed profile, i.e., RMW is the radius to the measured maximum wind speed. From here on, the radius corresponding to the maximum wind speed in a profile is referred to as RMW. To estimate the optimum values of B and RMW, RMW and B are varied over the range [0.5RMW, 1.5RMW] and [0.5, 2.5], respectively. The algorithm calculates an optimum B value by minimizing the mean of the square differences between the measured and the modeled surface pressure in a range of 0.5RMW to 1.5RMW for different B and RMW values. Mathematically, the mean square error between the measured and the modeled surface pressure can be written as:

Equation 4-16

$$\epsilon^2 = \sum_{i=0.5RMW}^{1.5RMW} (P_{obs_i} - P_{the o_i})^2 / n$$

Where:

- P_{obs_i} is the measured pressure
- $P_{the o_i}$ is the theoretical pressure calculated using Equation 4-15
- n is the number of data points in the range [0.5RMW, 1.5RMW]

The values of B and RMW are chosen to correspond to those yielding the minimum mean square error, ϵ^2 . The corresponding r^2 value for the fit is given by:

Equation 4-17

$$r^2 = 1 - \frac{\epsilon^2}{\sigma^2}$$

Where:

- σ is the standard deviation of the measured pressure data in the range of [0.5RMW, 1.5RMW]

A quality control criterion was used to filter out profiles. Each of the filtered profiles has at least one of the following characteristics associated with it:

1. Flight level pressure is less than 700 millibars (i.e., height greater than 3,000 meters)
2. Central pressure difference is less than 25 millibars
3. Radius to maximum winds is greater than two-thirds of the sampling domain
4. Distance of aircrafts closest approach to the center is greater than half of the radius to maximum winds

5. Data is available for less than one-third of the sampling range (i.e., less than 50 kilometers)
6. Visual inspection which involved eliminating profiles with a considerable amount of data missing in the range of interest [0.5RMW, 1.5RMW]

The rationale for using criteria (1) is that the higher the measurement height, the less representative measurements are of the surface observations. Criteria (2) results in the data associated with Category 1 or higher hurricanes only. The rationale for using criteria (3), (4), (5), and (6) is to ensure that there is a sufficient number of measurements on both sides of the radius to maximum winds to have a clear representation of the shape of the profile (Willoughby et al., 2006). The use of the quality control criteria eliminated a total of 2,291 profiles from a set of 4,556 profiles. Figure 4-22 presents a few examples of pressure profiles that were eliminated from the analysis. Both the measured pressure data and the corresponding fit to Holland's equation are shown. Each of the subplots in Figure 4-22 is compromised by at least one of the above-mentioned quality control criteria.

Figure 4-23 presents examples of pressure profiles that were retained for analysis. Each row in Figure 4-23 corresponds to a complete airplane traverse in one direction. The shaded regions in Figure 4-23 represent the error minimizing the range of 0.5RMW to 1.5RMW. The fit parameters (i.e., the B value), the central pressure difference, and the RMW are also provided in the title of every profile. For a given traverse through a hurricane, differences in the B values for two different profiles is due to the change in the radius to the maximum winds and the central pressure difference. The geographical distribution of the filtered profiles, based on the storm center, is shown in Figure 4-24. The filtered profiles have a wide geographical distribution and provide a wide domain of hurricane climatic characteristics. The filtered dataset has an average RMW of 46 kilometers (standard deviation of 22 kilometers), an average central pressure difference of 51 millibars (18 millibars) and an average location of 25.84° N (5.74° N) and 74.78° W (12.82° W). 71% of the fits yield r^2 values greater than 0.95, and 80% of the fits have a mean square error of less than 2.5 millibars. The maximum mean square error was 24.6 millibars, which occurred for one of Hurricane Opal's profiles, where Holland's equation overestimated the pressures at all points. The approach for analyzing the B data involved the estimation of RMW and B from each single pass of a flight through the storm.

The B values computed as discussed above were found to be correlated to the radius to maximum winds, central pressure difference, latitude, and sea surface temperature.

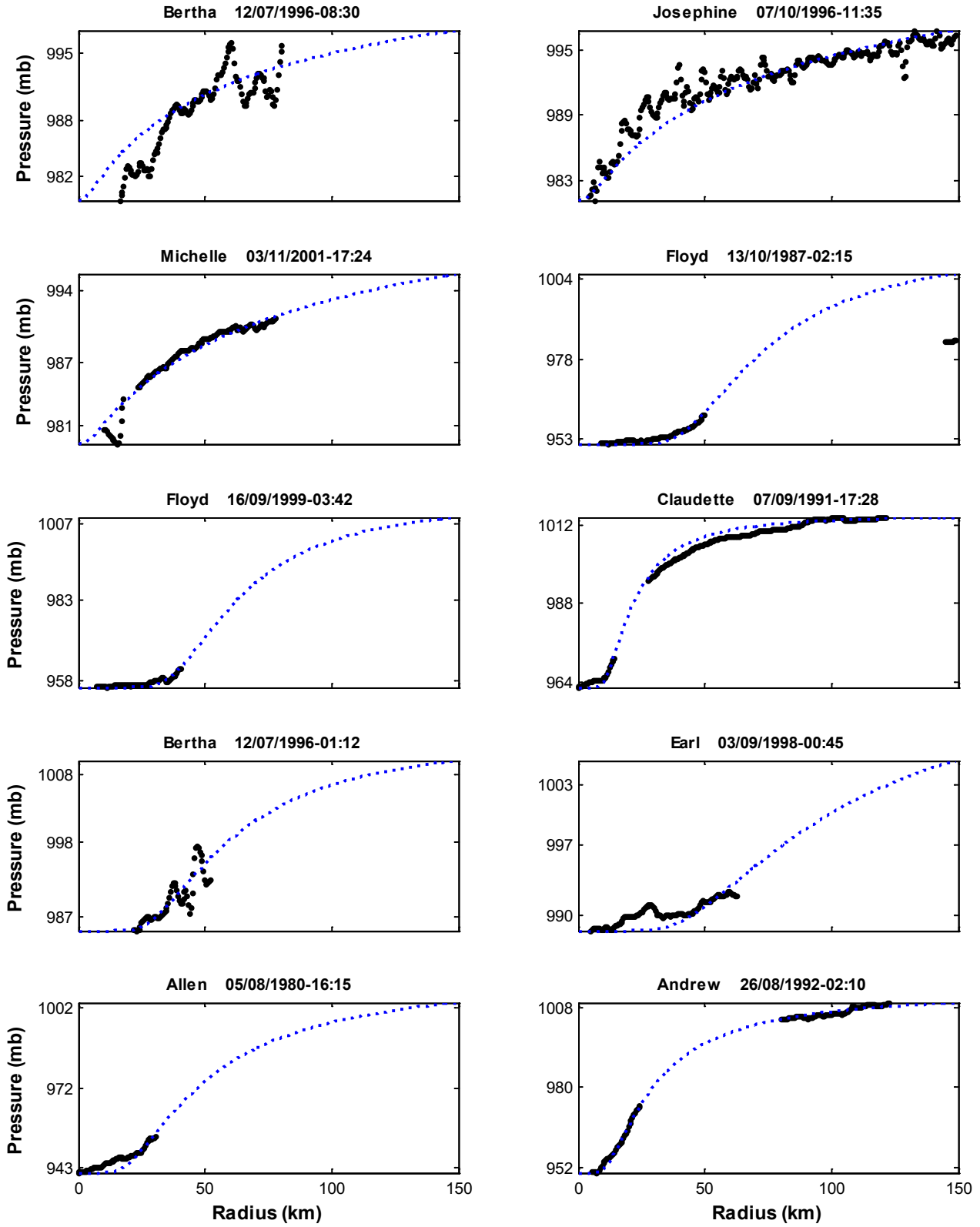


Figure 4-22 Examples of the Eliminated Profiles

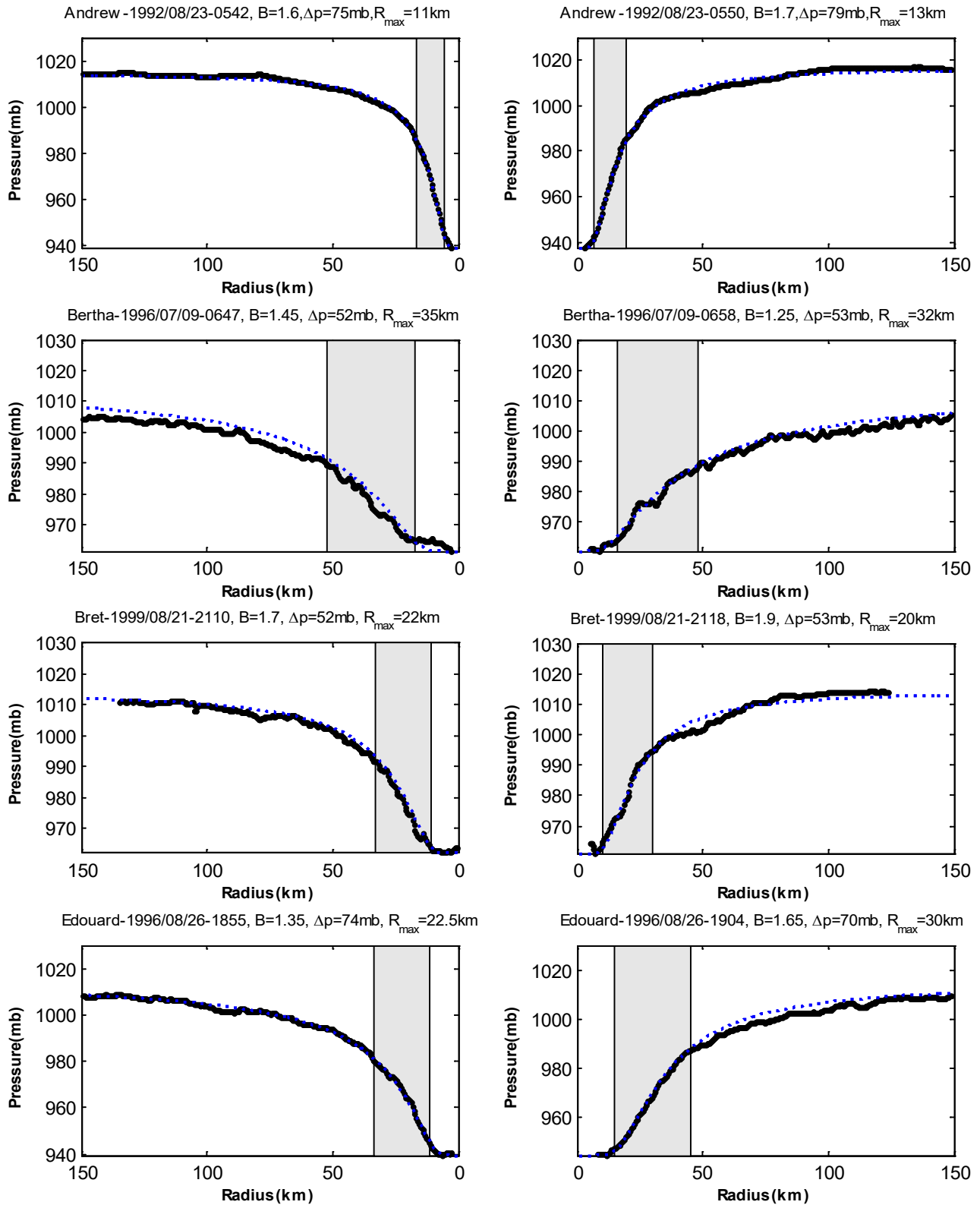


Figure 4-23 Examples of Surface Pressure Profiles for a Traverse Across a Given Hurricane

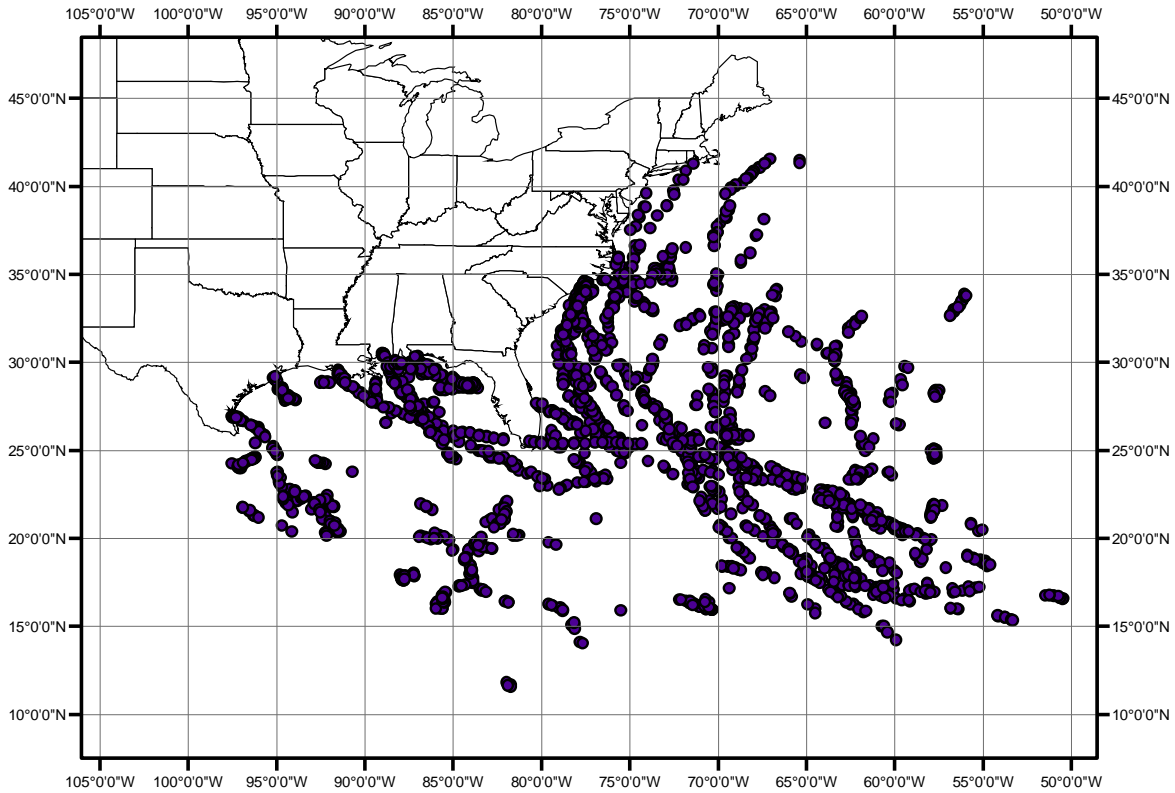


Figure 4-24 Geographical Distribution of all the Filtered Profiles

Only points associated with central pressures less than 980 millibars are included in the analysis. The resulting model of B is:

Equation 4-18

$$B = 1.76 - 1.21\sqrt{A} + \varepsilon, r^2 = 0.345, \text{ and } \sigma_B = 0.226A = \frac{RMW * f}{\sqrt{2R_d T_s * \ln \left(1 + \frac{\Delta p}{p_c * e}\right)}}$$

Where:

- ε is the random error term, sampled from a normal distribution with a mean of zero and standard deviation equal to σ_B
- RMW is the radius to maximum winds (m)
- f is the Coriolis parameter
- R_d is the gas constant for dry air
- T_s is the sea surface temperature in degrees C
- pc is the central pressure of the tropical cyclone; delta p is the difference (millibars) between the pc and the far field pressure, taken here as 1,013 millibars
- e is the base of natural logarithms

4.2.4 Filling Models

The filling models used in Hazus are described in Vickery (2005). The form of the filling models is an exponential decay function in the form:

Equation 4-19

$$\Delta p(t) = \Delta p_e \exp(-at)$$

Where:

$\Delta p(t)$ expressed in millibars, is the difference between the central pressure of the storm and the far field pressure (normally taken as the pressure associated with the outermost closed isobar), t hours after landfall

Δp_0 expressed in millibars, is the difference between the central pressure of the storm and the far field pressure at the time the storm makes landfall and a is the filling constant

The magnitude of the filling constant used in the exponential decay function is modeled as a function of readily defined characteristics of a tropical cyclone at the time of landfall. For storms making landfall along the Gulf Coast of the United States and the Florida peninsula, the reduction in the central pressure difference following landfall is modeled as a function of $\Delta p_{0c}/RMW$. Along the Mid-Atlantic coast, the reduction in the central pressure difference following landfall is adequately modeled either as a function of $\Delta p_{0c}/RMW$ or a function of Δp_0 alone. Along the New England coast, the reduction in central pressure difference following landfall is modeled with decay constant $\Delta p_{0c}/RMW$ modeled as a function of Δp_0 . Figure 4-25 shows the values of the decay constant versus for Gulf, Florida, and Mid Atlantic coast and versus Δp_0 for the New England coast. Solid line represents linear regression line. Thin dashed lines represent the mean error $\pm 2\sigma_\epsilon$. The models implemented in Hazus are as follows:

- Gulf Coast: $a = 0.0413 + 0.0018(\Delta p_{0c}/RMW)$; $\sigma_\epsilon=0.0169$
- Florida Peninsula Coast: $a = 0.0225 + 0.0017(\Delta p_{0c}/RMW)$; $\sigma_\epsilon=0.0158$
- Mid-Atlantic Coast: $a = 0.0364 + 0.0016(\Delta p_{0c}/RMW)$; $\sigma_\epsilon=0.0161$
- New England Coast: $a = 0.0034 + 0.0010\Delta p_0$; $\sigma_\epsilon=0.0114$

When implemented, the minimum allowable value of a sampled filling coefficient is set at 0.015, with the sampled error constrained to lie within $\pm 3\sigma_\epsilon$.

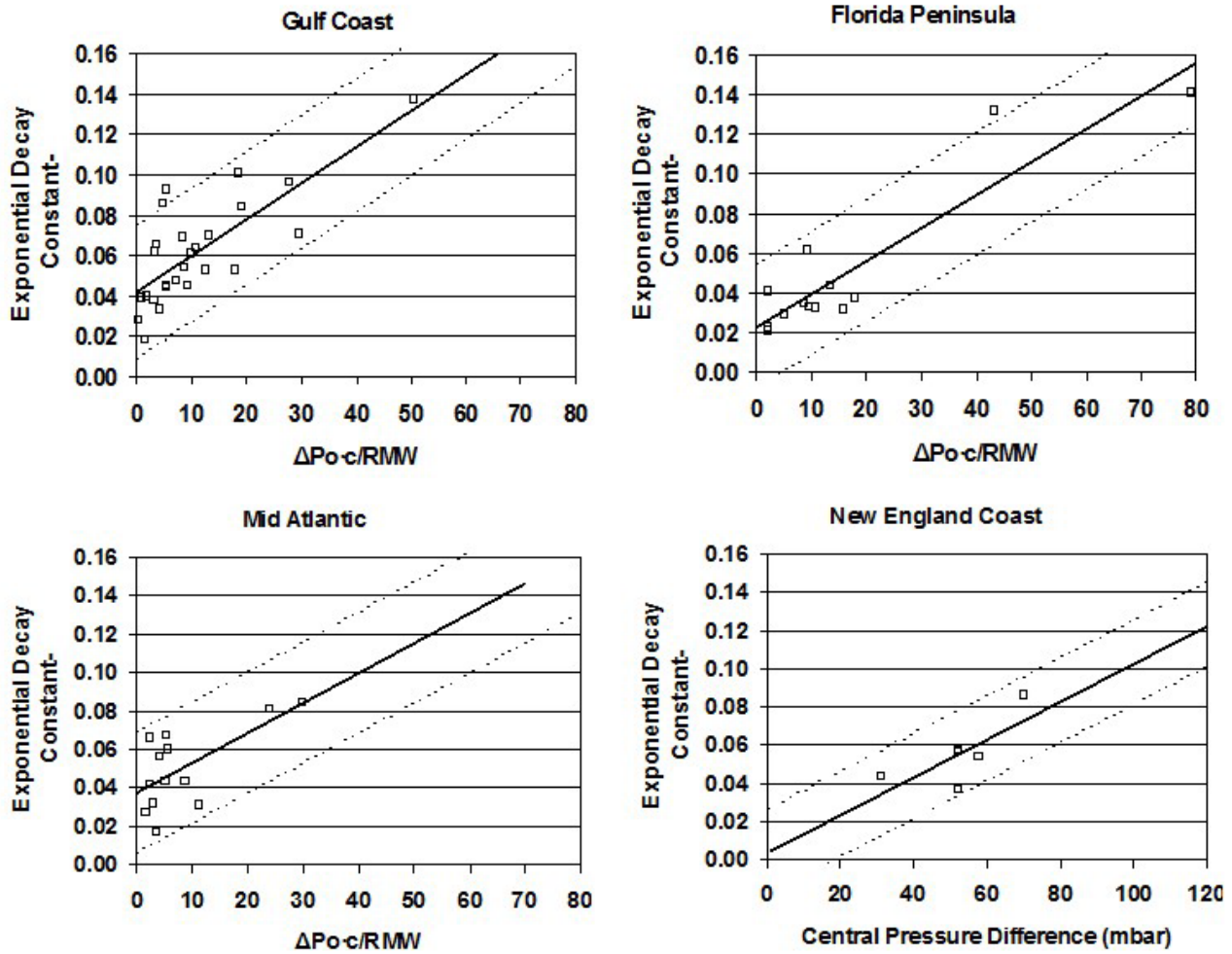


Figure 4-25 Filling Constant, a, versus $\Delta p_{oc}/RMW$ for Gulf, Florida and Atlantic Coast and Versus Δp_o for New England Coast

4.2.5 Track and Central Pressure Model Evaluation

The hurricane modeling methodology described above is evaluated through comparisons of observed and simulated hurricane statistics along the U.S. coastline. The simulated statistics are derived from a 100,000-year simulation of storms occurring in the Atlantic Basin. Comparisons are given for the statistics of simulated and real storms approaching within 250 kilometers of the coastal mileposts shown in Figure 4-26. The central pressure difference statistics are computed using the minimum values observed within the 250 kilometers radius sub-region. All other parameters are those computed or observed at the point of closest approach to the milepost. For modeling of Pacific basin storm tracks in Hawaii, see the *Hazard Mitigation Study for the Hawaii Hurricane Relief Fund* (Applied Research Associates, Inc., 2001).

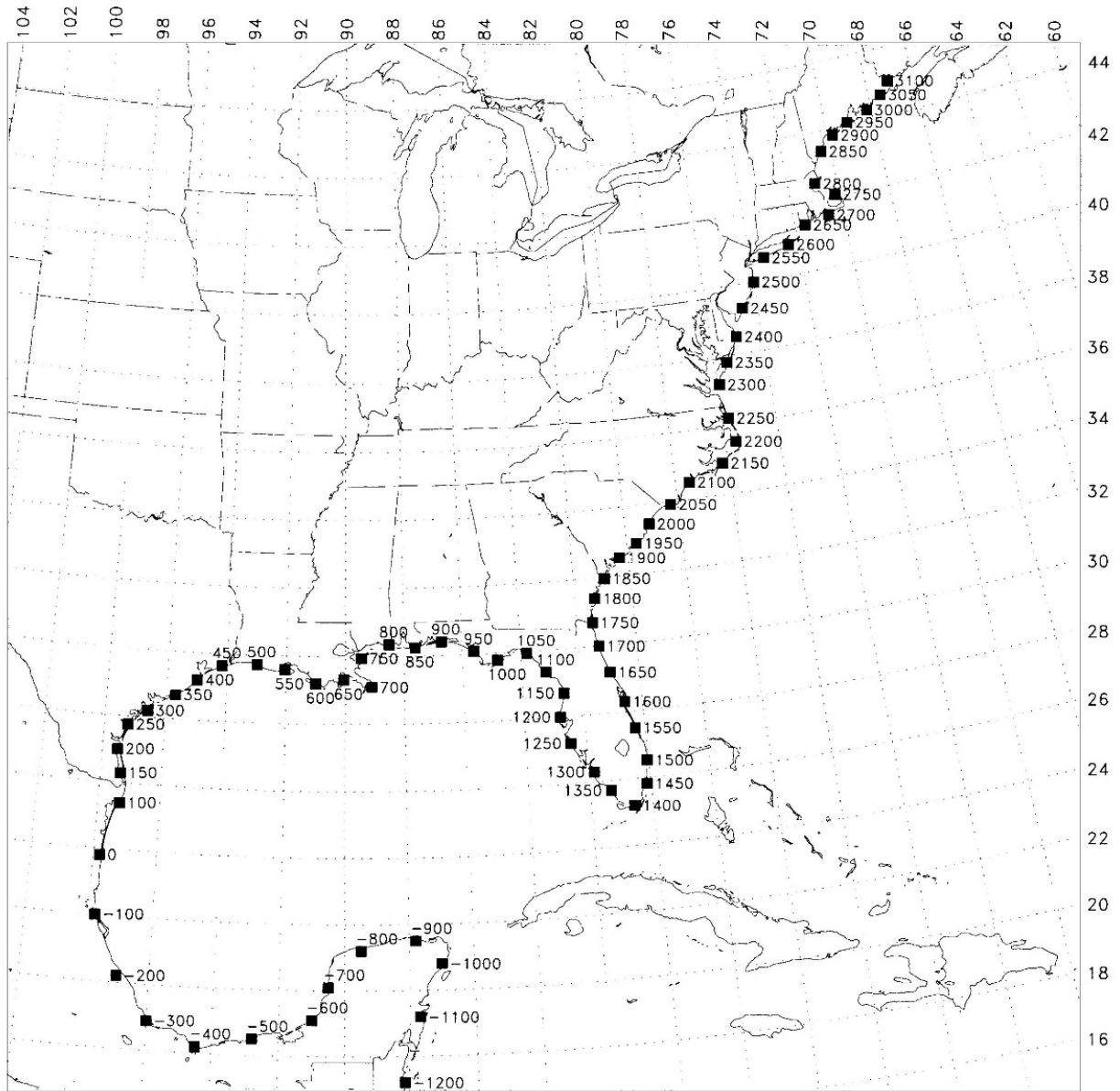


Figure 4-26 Locations of Milepost Stations Along the U.S. Coastline

Figure 4-27 shows comparisons of the mean and, in some cases, the standard deviation of the simulated and observed values of heading, translation speed, minimum approach distance (d_{min}), occurrence rate, and central pressure along the Mexican and U.S. coastlines at 50 nautical mile increments (~185 kilometers). The HURDAT statistics given in Figure 4-27 are derived for storms occurring during the period 1886-2001. The comparison of simulated and observed hurricane statistics shown in Figure 4-27 indicates that the modeling approach provides good estimates of the five key hurricane parameters at nearly all locations along the coastline. The empirical storm track modeling approach has been shown to successfully reproduce the statistics of the key hurricane parameters along the U.S. coastline. The approach is able to properly model the probabilities of a single storm passing near multiple sites (results not presented here). Using this simulation procedure, the storm intensities change with time, and the storms change both direction and speed as they pass by a site.

This approach more realistically models storm paths when compared to traditional hurricane simulation methods.

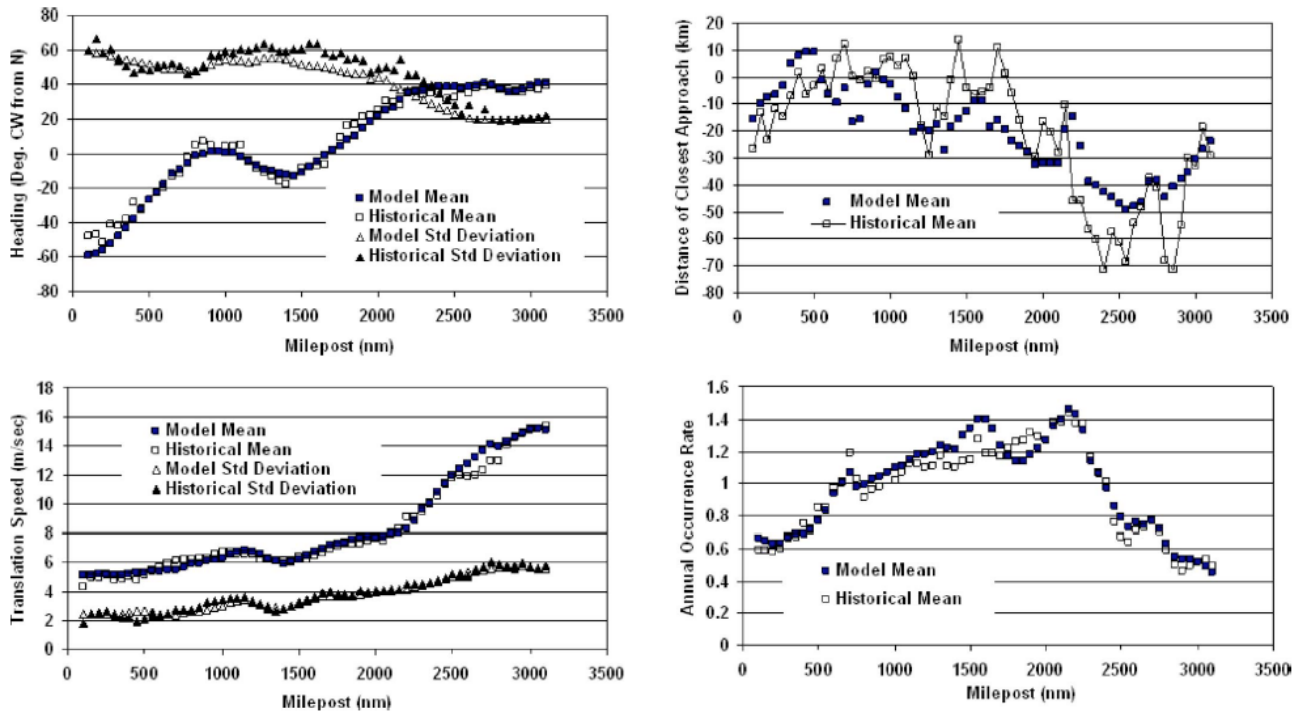


Figure 4-27 Comparison of Simulated and Observed Key Hurricane Parameters vs. Milepost (Vickery et al., 2009b)

4.2.6 Landfalling Hurricanes

The historical information on landfalling hurricanes along the coastline provides another means to evaluate the probabilistic hurricane simulation model. During the simulation process, when a simulated storm makes landfall, the central pressure, maximum sustained wind speed (one-minute average, over water), and landfall location are retained. Using the magnitude of the central pressure and wind speed at the time of landfall, the simulated storm is assigned a category as defined by Table 4-3. Historical information on the central pressure at the time of landfall is available for all intense hurricanes (IH) as defined by Saffir-Simpson Category 3 and higher storms, and for all other landfalling hurricanes occurring between 1964 and 2005. Between 1900 and 2019, there have been a total of 234 hurricane landfalls, 217 of which have central pressure data associated with the storm at the time of landfall. Note that in the counting of the 234 landfalls, each time a storm crosses land from the water, a landfall is considered to have occurred.

For example, Hurricane Andrew made two landfalls, once as a Category 4 storm in South Florida, and once as a Category 3 storm in Louisiana. The upgrade of Hurricane Andrew from a Category 4 to a Category 5 in South Florida occurred after the analysis presented in this section was completed. Thus, the definition of a landfalling storm used herein differs from that usually used by the NHC that scores only one landfall per storm when counting the total number of landfalls in the U.S. All of the 189 landfalls have a Saffir-Simpson Category, based on the estimated maximum sustained wind speed at

the time of landfall. The comparisons of landfalling storms that follow concentrate on comparing the modeled and observed landfall intensities based on central pressure rather than wind speed.

Figure 4-28 shows comparisons of the modeled and observed rates of intense hurricane landfalls, by region, for the Saffir-Simpson storm category defined by central pressure at the time of landfall. Table 4-3 presents the information used to categorize each landfalling storm, along with the category of the storm as defined by central pressure and the category of the storm as given in HURDAT. Central pressure data with sources are given, with the majority of the central pressure data obtained from the NOAA publication NWS 38 (Ho et al., 1987).

Table 4-3 Saffir-Simpson Storm Categories

Saffir-Simpson Category	Minimum Central Pressure	Maximum Sustained Wind Speed (Over Water)		Maximum Gust Speed (Over Water)		Maximum Gust Speed (Over Land, $z_0 = 0.03$ meters)	
	(millibar)	(meters per second)	(mph)	(meters per second)	(mph)	(meters per second)	(mph)
1	≥980	33.1-42.0	74-94	40.6-51.9	91-116	36.8-48.1	82-108
2	979-965	42.0-49.6	94-110	51.9-61.7	116-140	48.1-58.1	108-130
3	964-945	49.6-58.1	110-130	61.7-72.7	140-165	58.1-69.7	130-156
4	944-920	58.1-69.3	130-155	72.7-87.3	165-195	69.7-85.5	156-191
5	<920	>69.3	>155	87.3	>195	>85.5	>191

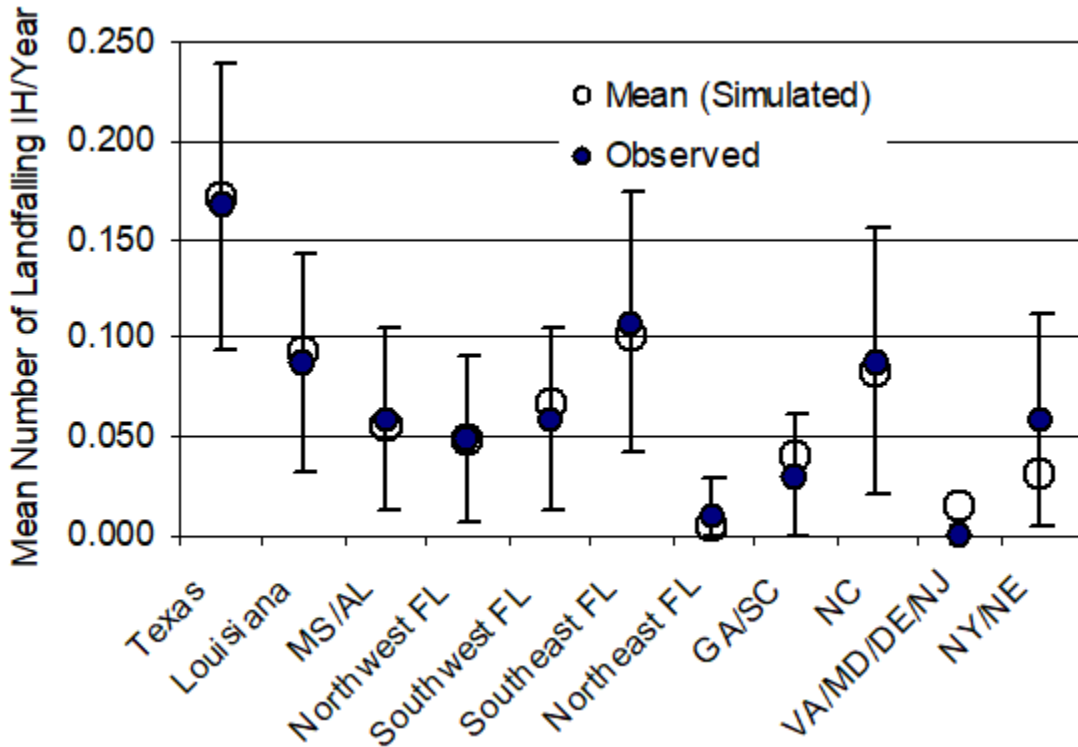


Figure 4-28 Building Repair Cost Estimates as Functions of Impact Energy

The simulated landfall rates given in Figure 4-29 have been derived from a 100,000-year simulation of storms in the Atlantic basin. The observed data are given as the mean value (i.e., the 95th ±1.96σ percentile confidence range) for observed IH storms categorized by central pressure. Modeled data are given as mean values only. Based on central pressure, the observed and simulated rates of landfalling intense hurricanes are seen to be nearly in agreement, with the variation of intense hurricane landfall rate with location along the coastline accurately reproduced. The simulation yields a landfall rate of 0.71 intense hurricanes per year versus an observed rate of 0.72 intense hurricanes per year.

Figure 4-29 presents similar data to that presented in Figure 4-28, except that the distribution of landfall intensity by storm category is presented without regard to the landfall region. In the case of Category 4 and higher storms, the simulation produces an average annual landfall rate, derived from central pressure, of about one Category 4 or 5 storm every five years. This landfall rate is slightly less than that given in Vickery et al. (2000b), where a rate of one Category 4 or 5 storm every four years was simulated.

The comparison of modeled and observed intense hurricanes, where the observed hurricane intensity is based on wind speed, suggests that the model underestimates the occurrence of intense hurricanes. The apparent underestimation of the landfall rate of intense hurricanes when defined by wind speed is discussed in Vickery et al. (2000b), where it is shown that many of the Category 3 storms (as defined in HURDAT) should have been Category 2 storms. Table 4-4 shows a comparison of the Saffir-Simpson rating of recent landfalling storms that have been followed by detailed studies of the wind field at the time of landfall. All of the reconstructed wind fields were produced by NOAA/HRD. The results of these

studies are given in Powell (1987); Powell, Dodge, and Black (1991); Powell and Houston (1996); Powell and Houston (1998); and Houston, Powell, and Dodge (1997).

Table 4-4 Storm Category and Central Pressure at Landfall

Year	Name	Land Fall State	Central Pressure	Pressure Category	Wind Speed Category	NHC Category
1900	1900-NOTNAMED-01	TX	936	4	4	4
1901	1901-NOTNAMED-03	NC	983	1	1	1
1901	1901-NOTNAMED-04	MS	973	2	1	1
1903	1903-NOTNAMED-03	FLA	977	2	1	1
1903	1903-NOTNAMED-03	FLC	976	2	1	1
1903	1903-NOTNAMED-04	NJ	990	1	1	1
1904	1904-NOTNAMED-02	SC	985	1	1	1
1904	1904-NOTNAMED-03	FLC	985	1	1	1
1906	1906-NOTNAMED-02	FLC	979	2	1	1
1906	1906-NOTNAMED-05	SC	977	2	1	1
1906	1906-NOTNAMED-06	MS	958	3	2	2
1906	1906-NOTNAMED-08	FLB	953	3	3	3
1908	1908-NOTNAMED-03	NC	985	1	1	1
1909	1909-NOTNAMED-02	TX	972	2	2	2
1909	1909-NOTNAMED-04	TX	959	3	3	3
1909	1909-NOTNAMED-08	LA	952	3	3	3
1909	1909-NOTNAMED-10	FLB	957	3	3	3
1910	1910-NOTNAMED-03	TX	965	2	2	2
1910	1910-NOTNAMED-05	FLB	955	3	2	2
1911	1911-NOTNAMED-02	FLA	985	1	1	1
1911	1911-NOTNAMED-03	SC	972	2	2	2
1912	1912-NOTNAMED-04	AL	988	1	1	1
1912	1912-NOTNAMED-06	TX	973	2	2	2
1913	1913-NOTNAMED-01	TX	988	1	1	1
1913	1913-NOTNAMED-04	NC	976	2	1	1
1913	1913-NOTNAMED-05	SC	989	1	1	1
1915	1915-NOTNAMED-01	FLD	990	1	1	1
1915	1915-NOTNAMED-02	TX	940	4	4	4
1915	1915-NOTNAMED-04	FLA	982	1	1	1
1915	1915-NOTNAMED-06	LA	944	4	3	3
1916	1916-NOTNAMED-02	MS	950	3	3	3
1916	1916-NOTNAMED-04	SC	960	3	2	2

Year	Name	Land Fall State	Central Pressure	Pressure Category	Wind Speed Category	NHC Category
1916	1916-NOTNAMED-06	TX	932	4	4	4
1916	1916-NOTNAMED-14	FLA	970	2	2	2
1917	1917-NOTNAMED-04	FLA	949	3	3	3
1918	1918-NOTNAMED-01	LA	955	3	3	3
1918	1918-NOTNAMED-03	NC	988	1	1	1
1919	1919-NOTNAMED-02	TX	950	3	3	3
1920	1920-NOTNAMED-02	LA	975	2	2	2
1921	1921-NOTNAMED-01	TX	980	1	1	1
1921	1921-NOTNAMED-06	FLB	952	3	3	3
1923	1923-NOTNAMED-03	LA	983	1	1	1
1924	1924-NOTNAMED-05	FLA	980	1	1	1
1924	1924-NOTNAMED-10	FLB	975	2	1	1
1925	1925-NOTNAMED-04	FLB	985	1	1	1
1926	1926-NOTNAMED-01	FLD	967	2	2	2
1926	1926-NOTNAMED-03	LA	955	3	3	3
1926	1926-NOTNAMED-07	MS	955	3	3	3
1926	1926-NOTNAMED-07	FLC	930	4	4	4
1926	1926-NOTNAMED-10	FLC	949	3	2	2
1928	1928-NOTNAMED-01	FLC	977	2	2	2
1928	1928-NOTNAMED-04	SC	976	2	1	1
1928	1928-NOTNAMED-04	FLC	929	4	4	4
1929	1929-NOTNAMED-01	TX	982	1	1	1
1929	1929-NOTNAMED-02	FLA	975	2	1	1
1929	1929-NOTNAMED-02	FLC	948	3	3	3
1932	1932-NOTNAMED-02	TX	935	4	4	4
1932	1932-NOTNAMED-03	AL	979	2	1	1
1933	1933-NOTNAMED-05	FLC	990	1	1	1
1933	1933-NOTNAMED-08	NC	963	3	1	1
1933	1933-NOTNAMED-11	TX	940	4	3	3
1933	1933-NOTNAMED-12	FLC	948	3	3	3
1933	1933-NOTNAMED-13	NC	952	3	2	2
1934	1934-NOTNAMED-02	LA	966	2	2	2
1934	1934-NOTNAMED-03	TX	979	2	1	1
1935	1935-NOTNAMED-02	FLA	985	1	1	1
1935	1935-NOTNAMED-02	FLB	892	5	5	5
1935	1935-NOTNAMED-06	FLC	965	2	2	2

Year	Name	Land Fall State	Central Pressure	Pressure Category	Wind Speed Category	NHC Category
1936	1936-NOTNAMED-03	TX	987	1	1	1
1936	1936-NOTNAMED-05	FLA	964	3	3	3
1938	1938-NOTNAMED-02	LA	985	1	1	1
1938	1938-NOTNAMED-04	NY	941	4	3	3
1939	1939-NOTNAMED-02	FLA	990	1	1	1
1939	1939-NOTNAMED-02	FLC	990	1	1	1
1940	1940-NOTNAMED-02	LA	972	2	2	2
1940	1940-NOTNAMED-03	SC	970	2	2	2
1941	1941-NOTNAMED-02	TX	958	3	3	3
1941	1941-NOTNAMED-05	FLA	981	1	2	2
1941	1941-NOTNAMED-05	FLC	937	4	2	2
1942	1942-NOTNAMED-01	TX	992	1	1	1
1942	1942-NOTNAMED-02	TX	951	3	3	3
1943	1943-NOTNAMED-01	TX	969	2	2	2
1944	1944-NOTNAMED-03	NC	990	1	1	1
1944	1944-NOTNAMED-07	NY	953	3	2	3
1944	1944-NOTNAMED-13	FLB	962	3	2	3
1945	1945-NOTNAMED-01	FLA	985	1	1	1
1945	1945-NOTNAMED-05	TX	963	3	2	2
1945	1945-NOTNAMED-09	FLC	949	3	4	3
1946	1946-NOTNAMED-06	FLB	980	1	1	1
1947	1947-NOTNAMED-03	TX	984	1	1	1
1947	1947-NOTNAMED-04	LA	964	3	2	3
1947	1947-NOTNAMED-04	FLC	945	3	4	4
1947	1947-NOTNAMED-09	SC	966	2	2	2
1948	1948-NOTNAMED-05	LA	985	1	1	1
1948	1948-NOTNAMED-08	FLB	940	4	4	3
1948	1948-NOTNAMED-09	FLC	963	3	2	2
1949	1949-NOTNAMED-02	FLC	954	3	4	3
1949	1949-NOTNAMED-11	TX	960	3	3	2
1950	1950-BAKER	AL	979	2	1	1
1950	1950-EASY	FLA	958	3	3	3
1950	1950-KING	FLC	955	3	3	3
1952	1952-ABLE	SC	980	1	2	1
1953	1953-BARBARA	NC	975	2	1	1
1953	1953-FLORENCE	FLA	975	2	1	1

Year	Name	Land Fall State	Central Pressure	Pressure Category	Wind Speed Category	NHC Category
1953	1953-HAZEL	FLB	987	1	1	1
1954	1954-CAROL	NY	955	3	3	3
1954	1954-EDNA	MA	948	3	3	3
1954	1954-HAZEL	NC	938	4	4	4
1955	1955-CONNIE	NC	962	3	3	3
1955	1955-DIANE	NC	987	1	1	1
1955	1955-IONE	NC	960	3	3	3
1956	1956-FLOSSY	LA	983	1	2	2
1956	1956-FLOSSY	FLA	974	2	1	1
1957	1957-AUDREY	LA	945	3	4	4
1958	1958-HELENE (BP)	NC	946	3	3	3
1959	1959-CINDY	SC	993	1	1	1
1959	1959-DEBRA	TX	984	1	1	1
1959	1959-GRACIE	SC	950	3	3	3
1960	1960-DONNA	NC	955	3	2	3
1960	1960-DONNA	NY	959	3	2	3
1960	1960-DONNA	FLB	930	4	4	4
1960	1960-ETHEL	MS	976	2	1	1
1961	1961-CARLA	TX	931	4	4	4
1963	1963-CINDY	TX	996	1	1	1
1964	1964-CLEO	FLC	968	2	2	2
1964	1964-DORA	FLD	961	3	2	2
1964	1964-HILDA	LA	959	3	3	3
1964	1964-ISBELL	FLB	969	2	2	2
1965	1965-BETSY	FLC	952	3	3	3
1965	1965-BETSY	LA	941	4	3	3
1966	1966-ALMA	FLA	982	1	2	2
1966	1966-INEZ	FLB	984	1	1	1
1967	1967-BEULAH	TX	950	3	3	3
1968	1968-GLADYS	FLA	977	2	2	2
1969	1969-CAMILLE	MS	909	5	5	5
1969	1969-GERDA	ME	980	1	1	1
1970	1970-CELIA	TX	945	3	3	3
1971	1971-EDITH	LA	978	2	2	2
1971	1971-FERN	TX	979	2	1	1
1971	1971-GINGER	NC	990	1	1	1

Year	Name	Land Fall State	Central Pressure	Pressure Category	Wind Speed Category	NHC Category
1972	1972-AGNES	FLA	980	1	1	1
1974	1974-CARMEN	LA	952	3	3	3
1975	1975-ELOISE	FLA	955	3	3	3
1976	1976-BELLE	NY	980	1	1	1
1977	1977-BABE	LA	995	1	1	1
1979	1979-BOB	LA	986	1	1	1
1979	1979-DAVID	FLC	968	2	2	2
1979	1979-DAVID	GA	968	2	2	2
1979	1979-FREDERIC	AL	946	3	3	3
1980	1980-ALLEN	TX	945	3	3	3
1983	1983-ALICIA	TX	962	3	3	3
1984	1984-DIANA	NC	979	2	3	3
1985	1985-BOB	SC	1003	1	1	1
1985	1985-DANNY	LA	987	1	1	1
1985	1985-ELENA	MS	959	3	3	3
1985	1985-GLORIA	NY	961	3	1	1
1985	1985-JUAN	LA	971	2	1	1
1985	1985-KATE	FLA	967	2	2	2
1986	1986-BONNIE	TX	990	1	1	1
1986	1986-CHARLEY	NC	992	1	1	1
1987	1987-FLOYD	FLB	993	1	1	1
1988	1988-FLORENCE	LA	984	1	1	1
1989	1989-CHANTAL	TX	986	1	1	1
1989	1989-HUGO	SC	934	4	4	4
1989	1989-JERRY	TX	983	1	1	1
1991	1991-BOB	RI	962	3	2	2
1992	1992-ANDREW	LA	956	3	3	3
1992	1992-ANDREW	FLC	922	4	5	5
1993	1993-EMILY (BP)	NC	960	3	3	3
1995	1995-ERIN	FLC	984	1	1	1
1995	1995-ERIN	FLA	973	2	2	2
1995	1995-OPAL	FLA	942	4	3	3
1996	1996-BERTHA	NC	974	2	2	2
1996	1996-FRAN	NC	954	3	3	3
1997	1997-DANNY	AL	984	1	1	1
1998	1998-BONNIE	NC	964	3	2	2

Year	Name	Land Fall State	Central Pressure	Pressure Category	Wind Speed Category	NHC Category
1998	1998-EARL	FLA	987	1	1	1
1998	1998-GEORGES	MS	964	3	2	2
1999	1999-BRET	TX	951	3	3	3
1999	1999_FLOYD	NC	956	3	2	2
1999	1999-IRENE	FLB	987	1	1	1
2002	2002-LILI	LA	963	3	1	1
2003	2003-CLAUDETTE	TX	979	2	1	1
2003	2003-ISABEL	NC	957	3	2	2
2004	2004-CHARLEY	SC	992	1	1	1
2004	2004-CHARLEY	FLB	941	4	4	4
2004	2004-FRANCES	FLC	960	3	2	2
2004	2004-GASTON	SC	985	1	1	1
2004	2004-IVAN	AL	946	3	3	3
2004	2004-JEANNE	FLC	950	3	3	3
2005	2005-CINDY	LA	991	1	1	1
2005	2005-DENNIS	FLA	946	3	3	3
2005	2005-KATRINA	FLC	984	1	1	1
2005	2005-KATRINA	LA	920	4	3	3
2005	2005-OPHELIA (BP)	NC	982	1	1	1
2005	2005-RITA	LA	937	4	3	3
2005	2005-WILMA	FLB	950	3	3	3

*FLA = Northwest Florida, FLB = Southwest Florida, FLC = Southeast Florida, FLD = Northeast Florida, and BP = By-Passing Hurricane

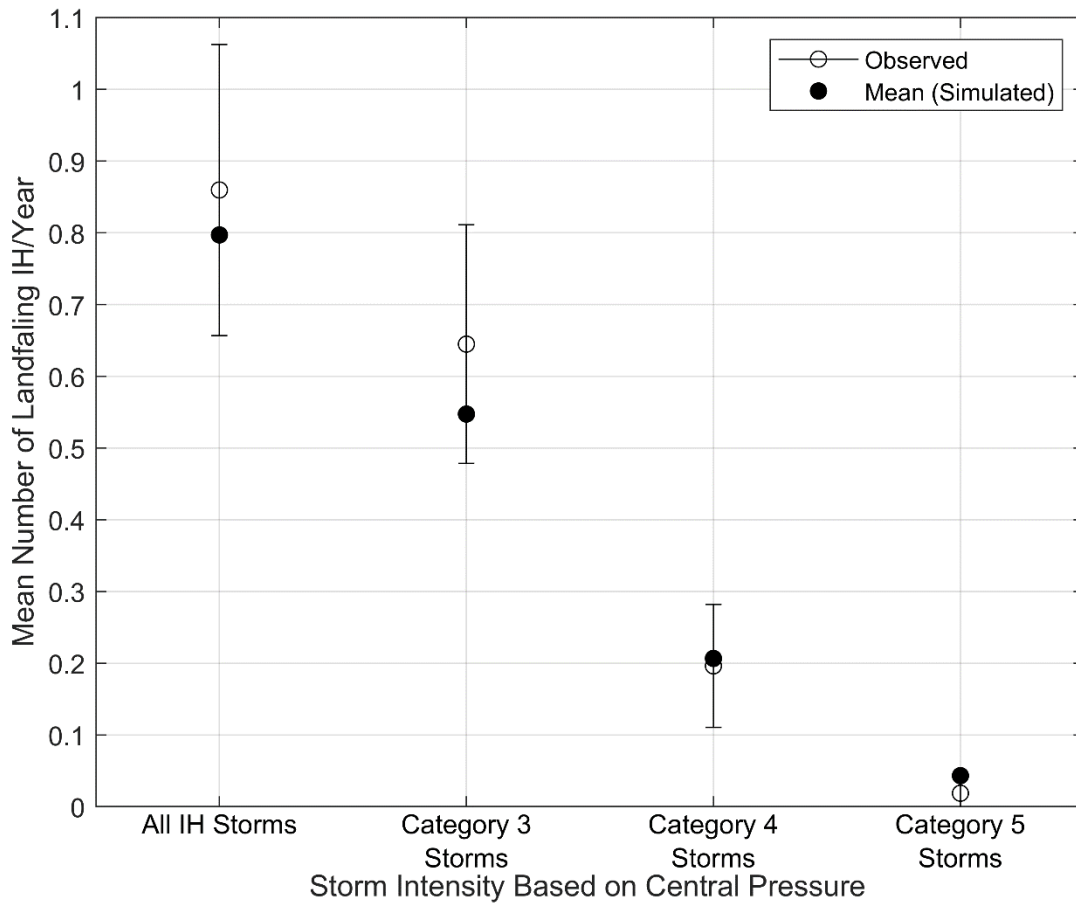


Figure 4-29 Comparison of Number of Annual Landfalling Intense Hurricanes by Storm Category (IH defined by pressure)

As indicated in Table 4-5, the official rating (defined by wind speed) given to many of the hurricanes is high. In Table 4-5, the shaded rows indicate storms where the official landfall category is higher than that indicated by the wind speed analysis performed and published by NOAA/HRD. Most of these over-ratings occur when Category 2 storms are scored as Category 3 storms. At least 50% of the Category 3 storms given in Table 4-5 are over-rated by one category. In the case of the Hurricane Alicia surface wind field analysis given in Powell (1987), the averaging time is not explicitly stated, although a sustained (or one-minute average) is implied. The maximum surface level wind speed is given in Powell (1987) for Alicia at landfall is 39 meters per second. If this wind speed is taken as a one-minute average, then the storm would be a Category 1 hurricane. If this 39 meters per second wind speed is taken to correspond to a mean hourly value, then the storm would be rated as a Category 2 storm; hence, a range of storm categories is given in Table 4-5.

Table 4-5 Comparison of HURDAT Hurricane Classification to Classifications Resulting from Detailed Studies Performed by NOAA/HRD

Hurricane	Year	HURDAT Category at Landfall	Category by Central Pressure at Landfall	Category by Maximum Wind Speeds at Landfall (NOAA/HRD)
Frederic	1979	3	3	3
Alicia*	1983	3	3	1-2
Hugo	1989	4	4	4
Andrew	1991	4	4	4
Emily	1993	3	3	3
Erin*	1995	2	2	1
Opal*	1995	3	4	2
Bertha	1996	2	2	2
Fran*	1996	3	3	2

* Shaded rows and hurricanes with an asterisk indicate storms where the official landfall category is higher than that indicated by the wind speed analysis performed and published by NOAA/HRD.

If the hurricanes given in Table 4-5 had been categorized by central pressure instead of the estimated maximum wind speed at the time of landfall, there would almost be a one-to-one correspondence between the scored category and the actual category, with only Hurricane Opal having a different category. Considering that the hurricane categories assigned to the storms by the National Hurricane Center (NHC) (given in Table 4-3) are based on upper level wind speeds measured by numerous aircraft, coupled with surface level wind speeds measured at data buoy and C-MAN stations, it is not unreasonable to assume that the errors in hurricane classification (as defined by the peak wind speed) in earlier years, when the quantity and quality of full scale data were not as high as today’s, were even more frequent. In general, it is much simpler to determine the minimum central pressure in a hurricane than it is to reconstruct the wind field, and only since Hurricane Hugo (1989) has a significant effort gone into post-storm hurricane wind field reconstruction. Errors associated with the measurements of wind speed are much greater than those associated with the measurements of central pressure. Figure 4-30 and Figure 4-31 show comparisons of landfall rates of all hurricanes as a function of location along the coastline and storm intensity (defined by central pressures). Note that for the landfalling storms that have no value of central pressure assigned to them, it has been assumed that the landfall category of the storm as given in HURDAT (Table 4-4) is consistent with the landfall category associated with the storm central pressure at the time of landfall. A simulated storm is categorized as a hurricane only if the modeled sustained wind speed at the time of landfall (one minute average over water) exceeds 74 mph, irrespective of the value of the central pressure. The model yields an average of 1.79 hurricane landfalls per year versus a historical average of 1.72 storms per year. The histograms of landfall rates shown in Figure 4-30 and Figure 4-31 are statistically equivalent, as indicated by an χ^2 test performed at a 5% significance level. Figure 4-32 shows a comparison of the modeled and observed central pressures at landfall plotted versus return period for storms making landfall along the Gulf coast (west of the FL-AL border), the Florida coastline, the Atlantic coastline north of Florida and for the entire Gulf and Atlantic U.S. coastline. Note that in the development of Figure 4-32, there is some uncertainty in the ranking of some of the storms having central pressures higher than Category 3 values

since central pressure data is not available for all Category 1 and 2 storms. The probability distributions of the historical data used to derive the central pressure versus return period plots given in Figure 4-32 have been developed assuming that all the storms having no central pressure data are weaker (i.e., have higher central pressures) than the strongest Category 2 storm which has central pressure data. Figure 4-32 shows excellent agreement between the modeled and observed central pressures as a function of the return period for the coastal U.S. as a whole and for the three individual regions.

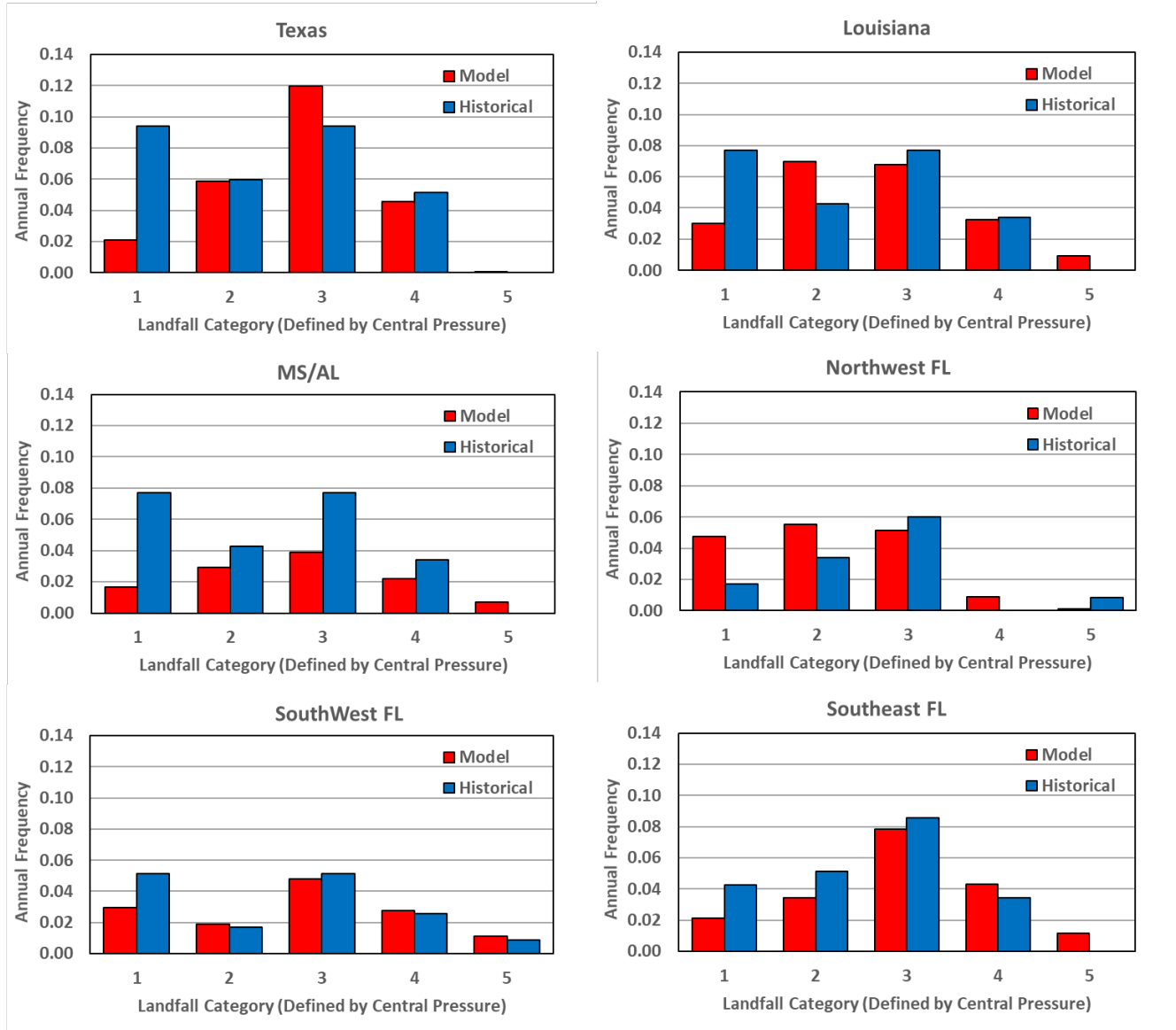


Figure 4-30 Comparisons of Modeled and Observed

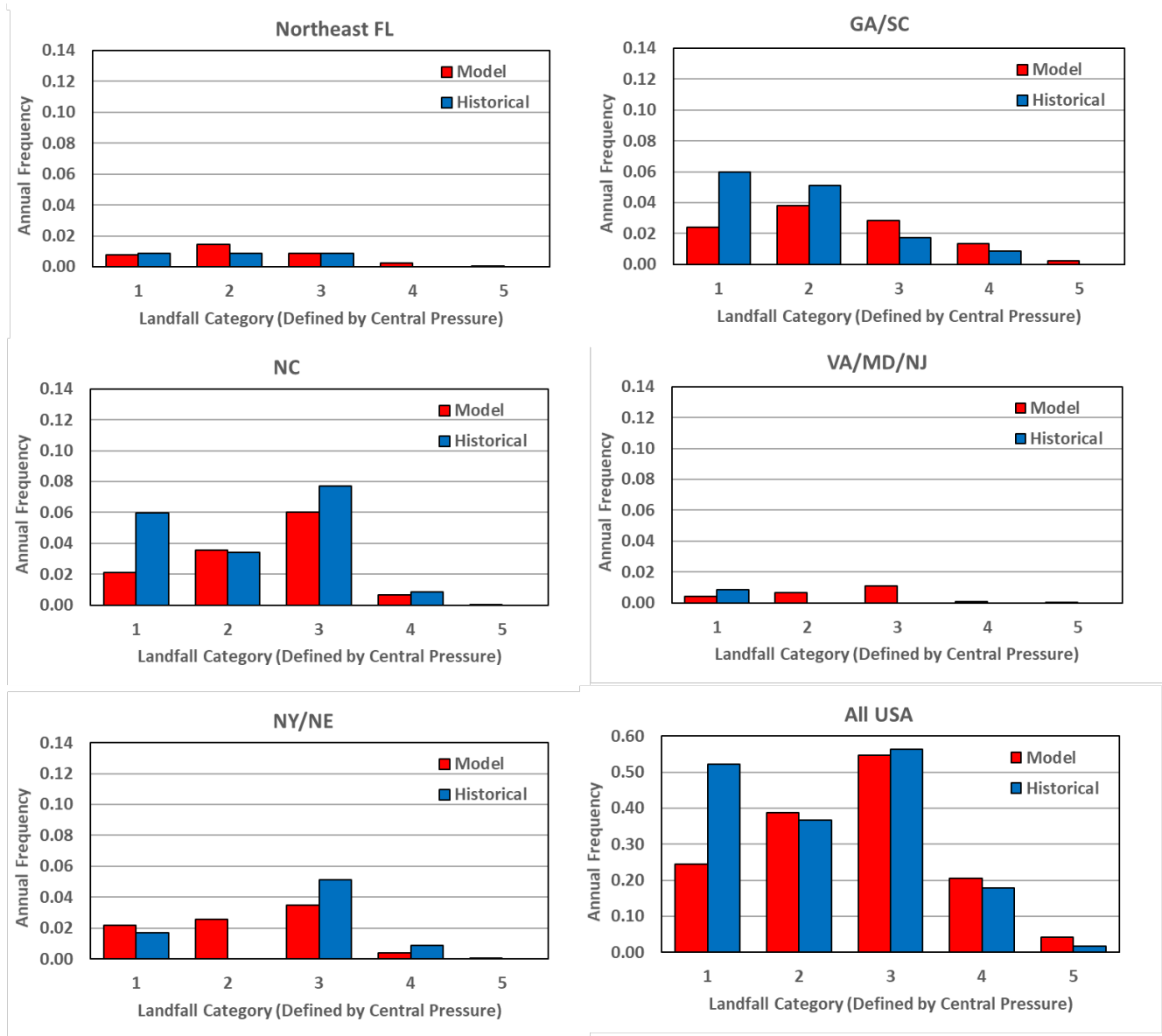


Figure 4-31 Comparisons of Modeled and Observed Hurricane Landfall Rates as a Function of Storm Category (Continued)

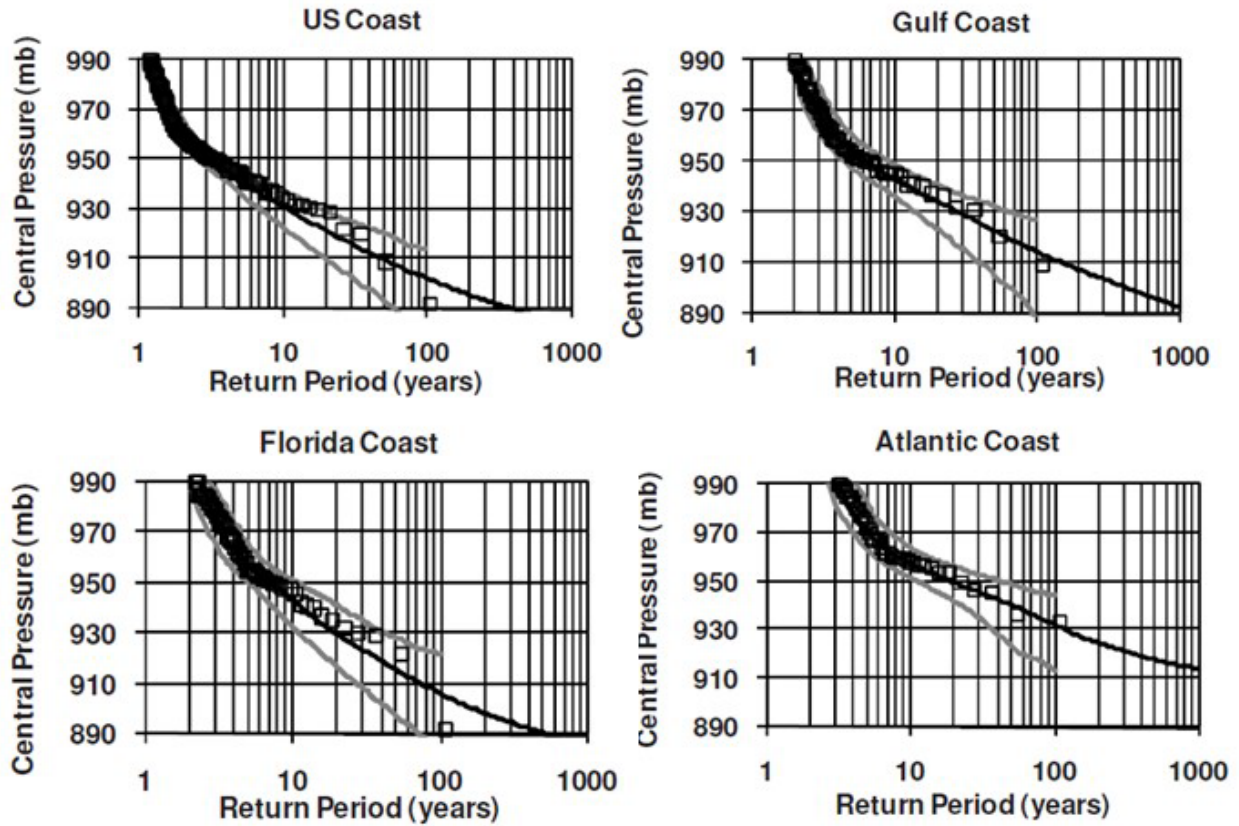


Figure 4-32 Comparison of Modeled and Observed Storm Central Pressure at Landfall versus Return Period for Various Geographic Regions (Vickery et al., 2009b)

4.2.7 Predicted Wind Speeds versus Return Period

Using the storm track simulation methodology combined with the wind field and gust factor models described in Vickery et al. (2009), 100,000 years of storms were simulated. When a simulated storm is within 250 kilometers of a milepost, the peak gust wind speeds are recorded at 15-minute intervals, with the largest wind speed in each of 16 directions and the largest overall being retained. Upon completion of a 100,000-year simulation, the wind speed data are rank ordered and then used to define the wind speed probability distribution conditional on a storm being within 250 kilometers of the site. The probability that the tropical cyclone wind speed (independent of direction) is exceeded during time period t is:

Equation 4-20

$$P_t(v > V) = 1 - \sum_{x=0}^{\infty} P(v < V | x) p_t(x)$$

Where:

$P(v < V|x)$ is the probability that velocity v is less than V given that x storms occur

$p_t(x)$ is the probability of x storms occurring during time period t

From Equation 4-20, with $p_t(x)$ defined as Poisson and setting t to one year, the annual probability of exceeding a given wind speed is

Equation 4-21

$$P_a(v > V) = 1 - \exp[-vP(v > V)]$$

Where:

v represents the average annual number of storms approaching with 250 kilometers of the site (i.e., the annual occurrence rate)

Figure 4-33 presents a plot of 100-year return period peak gust wind speeds along the Gulf and Atlantic coastlines derived from the updated hurricane simulation model used in Hazus. The wind speeds given in Figure 4-33 are peak gust wind speeds at a height of 10 meters above ground over open terrain.

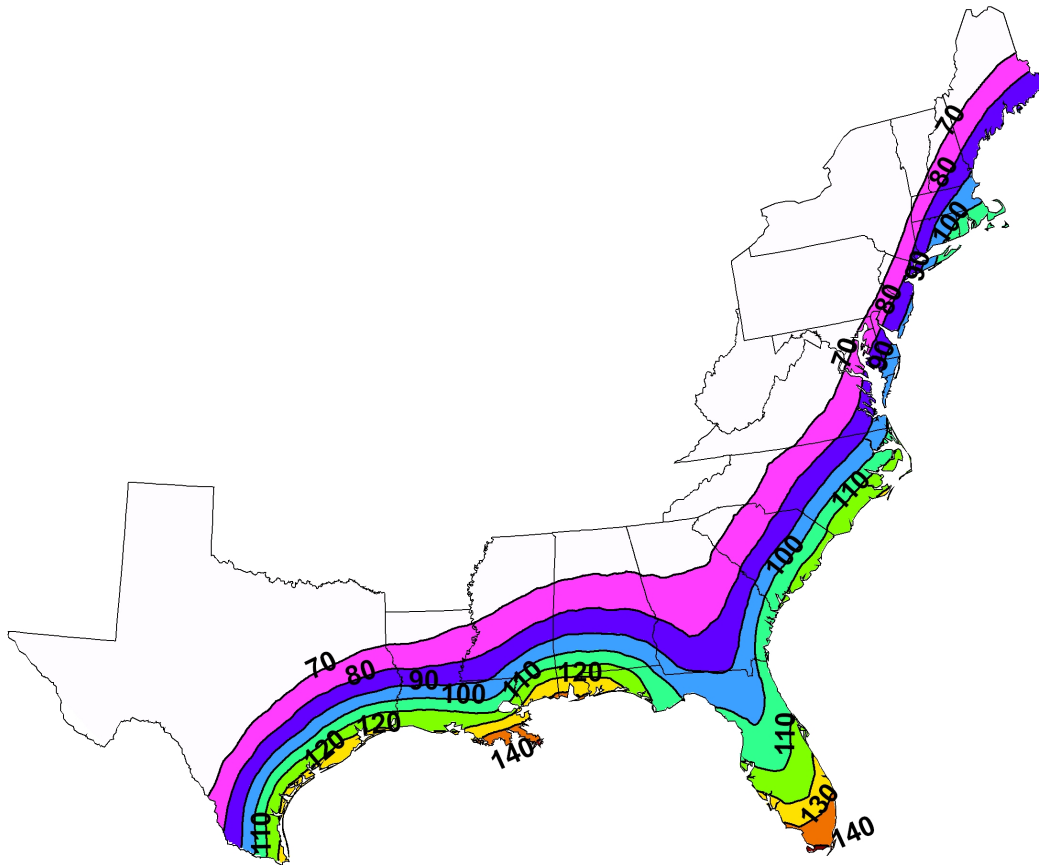


Figure 4-33 Predicted 100 Year Return Period Wind Speed for U.S. Atlantic and Gulf Coast

4.2.8 Summary

The hurricane simulation methodology models the entire track of a tropical storm in the Atlantic basin and has been validated through comparisons to historical data along the U.S. coastline. The modeling

approach allows the storms to curve, change speed, and intensify as they move and reproduce the continually varying statistics associated with central pressure, heading, etc., along the U.S. coastline. The model is an improvement over earlier hurricane simulation techniques since it eliminates the problems associated with the selection of a sub-region from which to derive the statistical distributions needed in traditional simulation models. In traditional models, the use of large areas to derive the hurricane statistics will smear any local climatological features that are inherently reproduced in this method. The prime advantage of this approach compared to the traditional approaches is the ability to properly model hurricane wind risk over large regions, within which the hurricane climatology can vary significantly. This improved prediction capability provides significant technical advantages for portfolio analyses, which encompass larger geographic areas than those of the previously published and accepted models such as those described by Batts et al. (1980), Georgiou (1985), Neumann (1991), and the NOAA publications NWS 23 and NWS 38.

4.3 Hurricane Rainfall Rate Model

Hurricane flow is a complex atmospheric system comprising of multiscale systems interacting in a nonlinear and varying degree of intensity. Some of the known environmental features affecting the hurricane dynamics include vertical wind shear, trough interactions, warm eddy core interactions, outflow patterns, eddy angular flow convergence, upper level cooling, dry air intrusions, eye wall cycles, low-level temperature advection, rain band downdrafts, and ocean currents (cf., Hong et al., 1998). For near-land cyclonic flows, additional interactions such as fronts, coastline shape, topography, and soil moisture availability play a significant role in the storm dynamics, particularly during the land falling stages (Reddy and Raman, 1997a, 1997b; Schneider, 1998).

Traditionally, one of the most difficult variables to model within an atmospheric system is rainfall. The variation of the rainfall amount within the hurricane system is a result of numerous nonlinear processes interacting simultaneously. Even the most comprehensive modeling systems, with very detailed physics, and numerical algorithms assimilating observational data, have limited success estimating the rainfall intensity and location associated with the hurricane (Elsberry, 1998).

However, rainfall rates and their locations are important variables to be considered for a risk management system. Even approximate estimates can provide vital information necessary for resource planning, flooding, erosion, as well as structural risk assessment. Hence, there is an ongoing requirement to adopt even heuristic approaches for estimating rainfall rates and distribution within the hurricane flow. To satisfy this need, an empirical approach (referred to as “HuRRDE”: Hurricane Rainfall Rate and Distribution Estimator), relating the sectorial rainfall rate with annular distance from the hurricane center, has been developed and implemented in the Hazus Hurricane Model.

4.3.1 Data and Prior Studies

There is a paucity of high resolution, continuous observations of rainfall rates within the hurricane flow. However, several efforts have been made to assimilate satellite information with surface and aircraft data (e.g., Shi et al., 1998). The present model focuses on published analyses of Special Sensor Microwave/Imagery (SSM/I) (see Alliss et al., 1992; Rodgers et al., 1994; Ferraro et al., 1996). The SSM/I analyses provide detailed radial rainfall rate information. Over 50 studies were evaluated for the purpose of obtaining relevant data.

The starting point for developing the model was the observational study by Rodgers et al., in which 103 SSM/I observations for 18 western North Atlantic tropical cyclones from 1987 to 1989 were used for documenting the precipitation characteristics. The tropical cyclones used in their study were:

- 1987 storms: Cindy, Dennis, Emily, and Floyd
- 1988 storms: Chris, Debby, Florence, Gilbert, Helene, Isacc, Joan, and Keith
- 1989 storms: Dean, Felix, Gabrielle, Hugo, Iris, and Jerry

Figure 4-34, adapted from Rodgers et al. (1994), summarizes the SSM/I derived azimuthally averaged rain rates for the eight 55 kilometers annuli (rings) around the center. The distribution is considered robust as it is averaged over 47 depressions ($P_{min} > 1,000$ millibars), 29 tropical storms ($P_{min} = 1,000-977$ millibars), and 27 hurricanes ($P_{min} < 977$ millibars). The radial distribution for the hurricane case is considered the first step in the model development. However, it should be noted that the Rodgers et al. (1994) data has a 55-kilometer resolution.

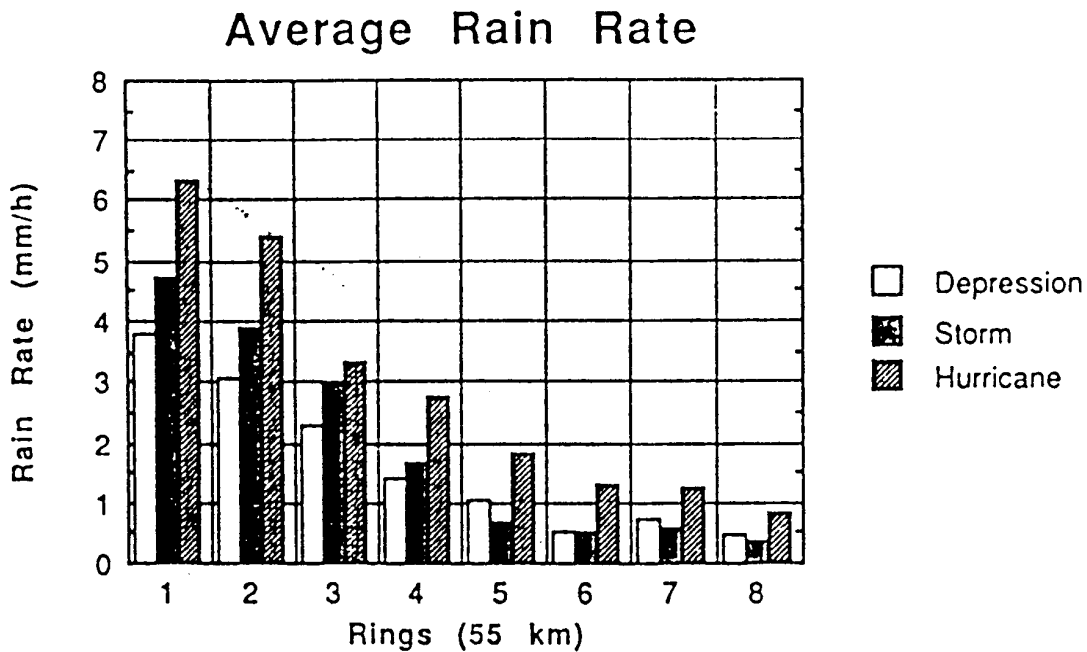


Figure 4-34 Average Rain Rate

Evidence from both observational studies (Alliss et al., 1993) and numerical studies (Drury and Evans, 1998) suggests there is even more intense precipitation at the inner-core than at the first 55 kilometers annular ring. Hence, in the next step of the model development, a sharp increase from the first ring to the inner core is assumed. The inner core is assumed to be at a distance of R_{max} from the eye. Though, typically R_{max} will vary for every hurricane at different stages of development, for the purpose of developing the simple rainfall rate model, R_{max} was initially assumed to be a constant close to landfall. Accordingly, R_{max} was considered to be 30 kilometers. Note that considering the overall uncertainty associated with the entire system, this first-order assumption is not expected to affect the results

significantly. Accordingly, Figure 4-35 shows the ‘observed’ or ‘analyzed’ radial rainfall distribution used for model development. The sharp increase in the rainfall rate from 1.83 R_{max} (55 kilometers) to R_{max} is apparent. It should be noted that the center ‘eye’ generally does not experience any significant precipitation and hence the $R = 0$ case is assigned to be rainfall free (see also Alliss et al., 1993, for Hurricane Florence case).

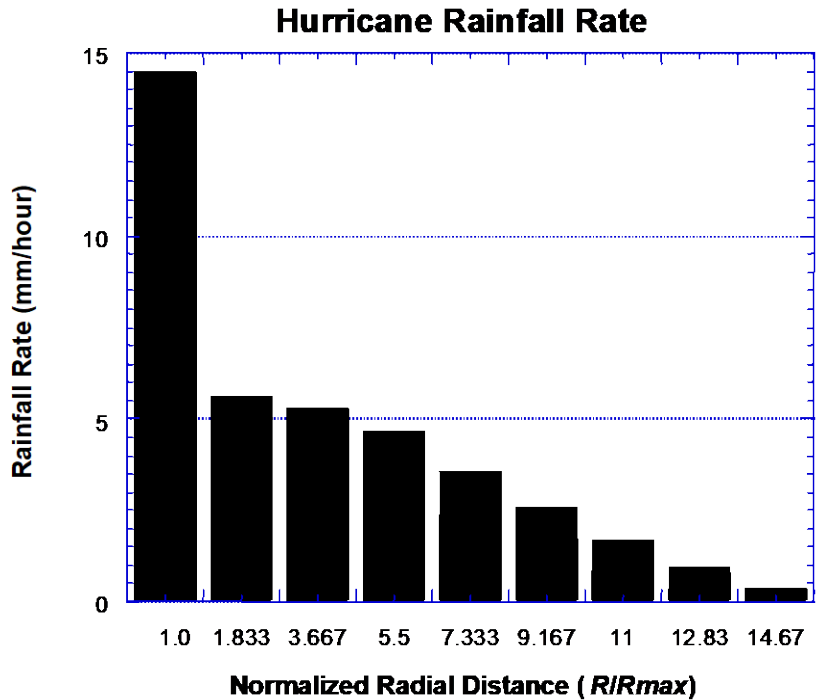


Figure 4-35 Rainfall Rate as Function of Normalized Radial Distance from the Eye (R_{max} is Assumed to be 30 Kilometers)

4.3.2 Model Development

To develop the relationship between the rainfall rate (RR) and radial distance, the first approach was to relate RR through a fifth-order polynomial to R/R_{max} . However, this approach has obvious serious stability considerations. The higher order (cubic and beyond) terms are linked with increasingly larger distances (R/R_{max} increases as R increases). Thus, a small error would amplify in the system several folds making the outcome extremely sensitive and unrealistic. To overcome this, a relationship between RR and the inverse of R/R_{max} (R_{max}/R) was developed. Accordingly, for the data shown in Figure 4-35, the relationship is of the form:

Equation 4-22

$$RR = -5.5 + 110(R_{max}/R) - 390(R_{max}/R)^2 + 550(R_{max}/R)^3 - 250(R_{max}/R)^4$$

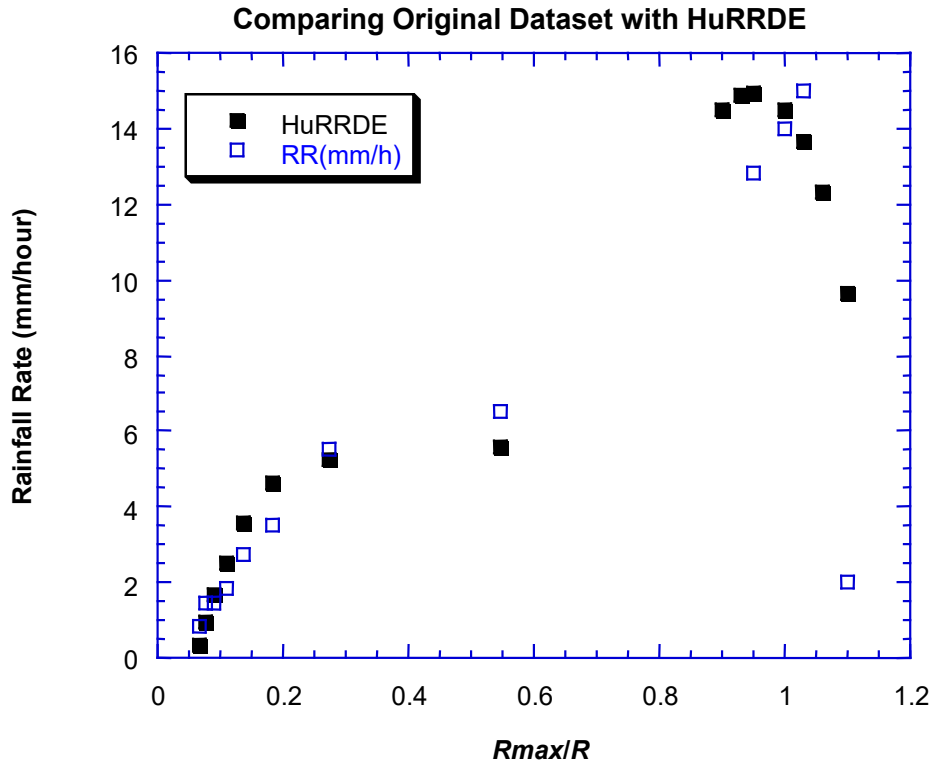


Figure 4-36 Plot Showing the Original Rainfall Rate with the Estimation from Equation 4-19

Figure 4-36 shows the rainfall rates from Figure 4-35 and the rainfall rates represented by Equation 4-22. Overall, there is a good agreement between the two ($r^2 = 0.92$). Some differences are also seen between the ‘analyzed’ data and the prediction using Equation 4-22, particularly in terms of the decreased precipitation from R_{max} to the eye. This ‘error’ exists due to the approximate estimation of R_{max} in this particular case. Also, caution was exercised so as not to ‘over fit’ the equation to the data set, which could cause loss in predictive skills. Within these constraints, Equation 4-22 provides a reasonable means of estimating the rainfall rate in the hurricane as a function of annular distance from the eye.

In order to make the empirical relation applicable to various hurricane intensities, corrections were made to Equation 4-22. Three corrections, as described in the following paragraphs, were considered, and two have been implemented.

The first correction involves the changes in the central pressure with time (dP/dt) (and, hence, the intensity of the hurricane). Note that Equation 4-22, due to the averaging involved, may best represent Category 1-2 type-hurricanes. Typically, as the central pressure drops, a storm becomes more intense, yielding larger rainfall rates. For Equation 4-22, this correction is inherent if R_{max} is calculated as a function of ΔP .

By adopting relations between R_{max} , ΔP , and latitude, ψ , similar to Equation 4-22, changes in the rainfall rate will occur with changes in ΔP . Figure 4-37 shows a summary of a review from Rogers et al. (1994) comparing hurricanes ($P_{min} < 977$ millibars), storms ($977 \text{ millibars} < P_{min} < 1,000$ millibars), and depressions ($P_{min} > 1,000$ millibars). As seen in Figure 4-37, the hurricane rainfall rate is about 30 to

40% more than the storm rainfall rate, and about 75% more than the depression rainfall rate. Extrapolating this, it is assumed that for every 20 millibar drop, a 35% higher effective rainfall rate can be expected for the tropical cyclone. Hence, RR can be corrected for the hurricane category as follows:

Equation 4-23

$$RR_e = k * RR$$

The mid-values of k for Category 1 through 4 hurricanes are assumed to be 1, 1.35, 1.85, and 2.5. A Category 5 hurricane making landfall will have rainfall rates that would be governed by very special forcing and cannot be estimated in any simple manner.

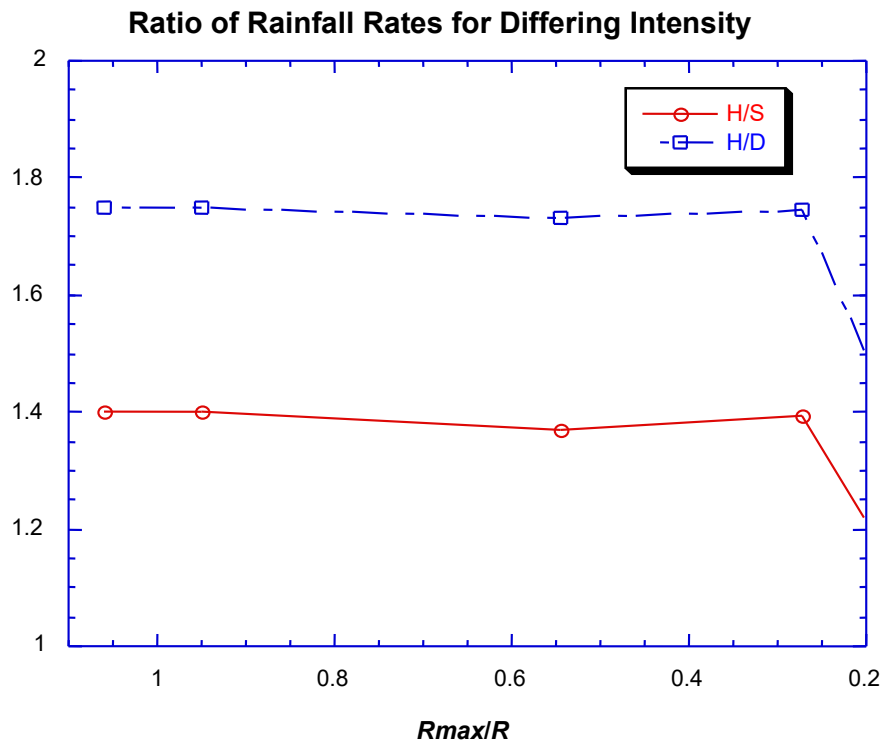


Figure 4-37 Ratio of Rainfall Rates for Hurricane Against Non-hurricane Tropical Cyclones as a Function of Normalized Radial Distance, Following Rogers et al. (1994)

Additionally, for a more dynamic change in the rainfall rate, due to the rate of change of central pressure (without change in the category), it is assumed that:

Equation 4-24

$$RR_p = RR_e [1 - (dP/dt)/100]$$

Thus, for example, a 10 millibar drop would lead to a change in the rainfall rate by a factor of 1.1, while a rise in the central pressure (positive dP/dt) by 5 millibars would effectively decrease the rainfall rate to 0.95 RR_e. Thus, following Equation 4-22 and Equation 4-24, an increase in the central pressure over time will lead to increased R_{max}, hence an indirect reduction in RR, and a direct decrease in the central pressure intensity corrected rainfall rate (RR_p).

The second correction is dependent on how fast the storm is moving. Studies suggest (see Jones, 1987; Baik, 1989, for instance) that there is an asymmetric rainfall distribution as a function of the storm motion. Once again, using the data from Rogers et al. (1994), sectorial rainfall rate corrections can be made for slow (<8 knots) and fast (>15 knots) moving tropical systems as follows:

Equation 4-25

$$RR_{sp} = s * RR_p$$

The value of the coefficient 's' is shown in Table 4-6.

Table 4-6 Sector Values for Rainfall Rate Parameter, s

Sector	s in slow storms	s in fast storms
0-45	1.45	1.15
46-90	1.05	1.15
91-135	0.55	1.35
16-180	0.65	1.15
181-225	0.85	0.85
226-270	0.95	0.65
271-335	1.15	0.8
336-359	1.35	0.95

A third potential correction is for the land falling component. Studies, particularly numerical simulations, suggest that in the first sector with the onshore winds (0-45 with zero angle corresponding to the coastline), the rainfall rate is increased by 25% (Chen, 2006). This correction is not implemented into the rainfall rate model.

Figure 4-38 shows an independent verification for data obtained for Hurricane Florence and Hurricane Hugo (in the developing as well as the developed stage). The observations are obtained from Alliss (1992). Note that there is a lack of rainfall rate observations at higher R_{max} . In this “off-line” comparison, there has been no correction for the storm speed or for the sector. Only the category change has been accounted for. Thus, for Hurricane Florence, a Category 2 was assumed. For Hurricane Hugo, it is initially assumed a storm correction (reducing the RR_e), and for the developed hurricane, a Category 4 correction was assumed. As can be observed, there is an encouraging agreement in the ‘observed’ and the estimated rainfall rates.

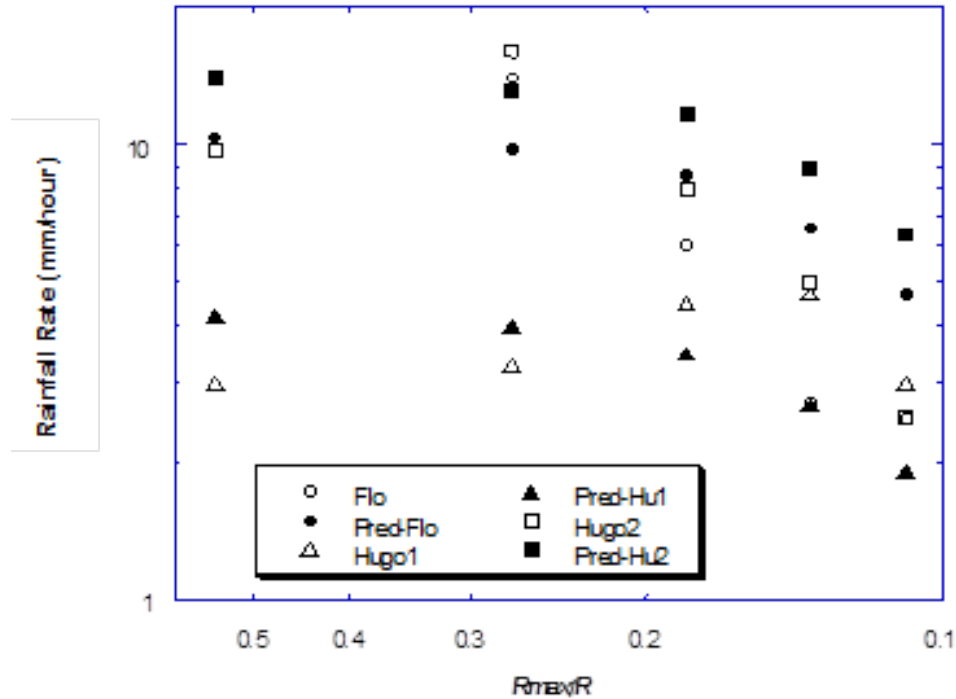


Figure 4-38 Observed and Estimated Rainfall Rates for Hurricane Florence (Flo, Pred-Flo), Hurricane Hugo in Developing Stages (Hugo1, Pred-Hu1), and in Developed Stages (Hugo2, Pred-Hu2)

4.3.3 Hurricane Rainfall Rate Model Implementation and Calibration

In the hurricane simulation model, Equation 4-22 is used to determine the base rainfall rate (RR) for R/R_{max} greater than or equal to one. For values of R/R_{max} between zero and one, a linear model is used where the RR is zero at R/R_{max} equal to zero and then increases linearly up to the value of RR determined by Equation 4-22 at R/R_{max} equal to one. The base rainfall rate is adjusted for the storm category. Instead of using distinct k factors for a given storm category (see Equation 4-22), k is determined using the following linear function of central pressure deficit (millibars):

Equation 4-26

$$k = 0.0319\Delta p - 0.0395, k \geq ak$$

This line was developed by plotting the factors given following Equation 4-22 at the middle of the range in central pressure deficit for the particular storm category and then fitting a line ($r^2 = 0.9933$).

The base rainfall rate is also adjusted for storm translation speed using the sector dependent factors given in Table 4-6.

Several Hurricanes, including Hugo (1989), Bertha (1996), Fran (1996), and Bonnie (1998), for which relatively high-quality rainfall measurements at a number of meteorological stations are available, were used to calibrate the rainfall rate model. By comparing the model predictions and the actual measurements, the rainfall rate model was found to provide reasonably accurate estimations of the peak rainfall rates for most of the stations investigated. However, the off-peak rainfall rates were significantly overestimated. A number of factors may contribute to the overestimation:

1. The drop of rainfall rate with the increase in R/R_{\max} may be much faster than that predicted using Equation 4-22
2. Rain gauges located on the ground often underpredict the rainfall during high winds due to the effects of the flow aerodynamics around the rain gauges
3. Other features, such as the hurricane's interaction with other weather systems, outflow patterns, and sea to land transitions may also contribute to the inconsistency between the measured rainfall rates and the predicted ones

To overcome this problem, a modification factor (MF), defined as the ratio of the actual measurement to the model prediction, was developed in order to provide the best estimation of the rainfall rate in a hurricane. Figure 4-39 shows the relationship between the modification factor and R/R_{\max} for the hurricanes investigated. The modification factor is seen to decrease with the increase of R/R_{\max} . To be used in the rainfall rate model, a relationship between the modification factor and R/R_{\max} was determined using least square regression, which is of the form:

Equation 4-27

$$MF = -0.7 * \ln(R/R_{\max}) + 1.0$$

Note that when MF is greater than 3.0, it is taken as 3.0 and when MF is less than 0.2, it is taken as 0.2. Note also that when R/R_{\max} is less than 1.0 (i.e., within the hurricane eye), the modification factor is greater than 1.0, which indicates the rainfall rate around the eyewall is relatively uniform (i.e., stable rainband). Accordingly, the linear model assumed previously may underestimate the rainfall rate for this region. Considering the modification factor, the final rainfall rate output from the simulation model is:

Equation 4-28

$$RR_{MFsp} = MF * RR_{sp}$$

Figure 4-40 and Figure 4-41 show the comparison between the model predictions and the actual measurements for Hurricanes Hugo (1989), Bertha (1996), Fran (1996), and Bonnie (1998). Most of the sites investigated for these four storms are ordinary commercial airports with open terrain except Kure Beach, NC, which is a private meteorological station located about 300 meters inland. All the data collected are continuous hourly rainfall rates. The model is seen to provide reasonably accurate predictions for most of the sites investigated. However, abnormalities still exist for several sites and will be addressed individually in the following paragraphs.

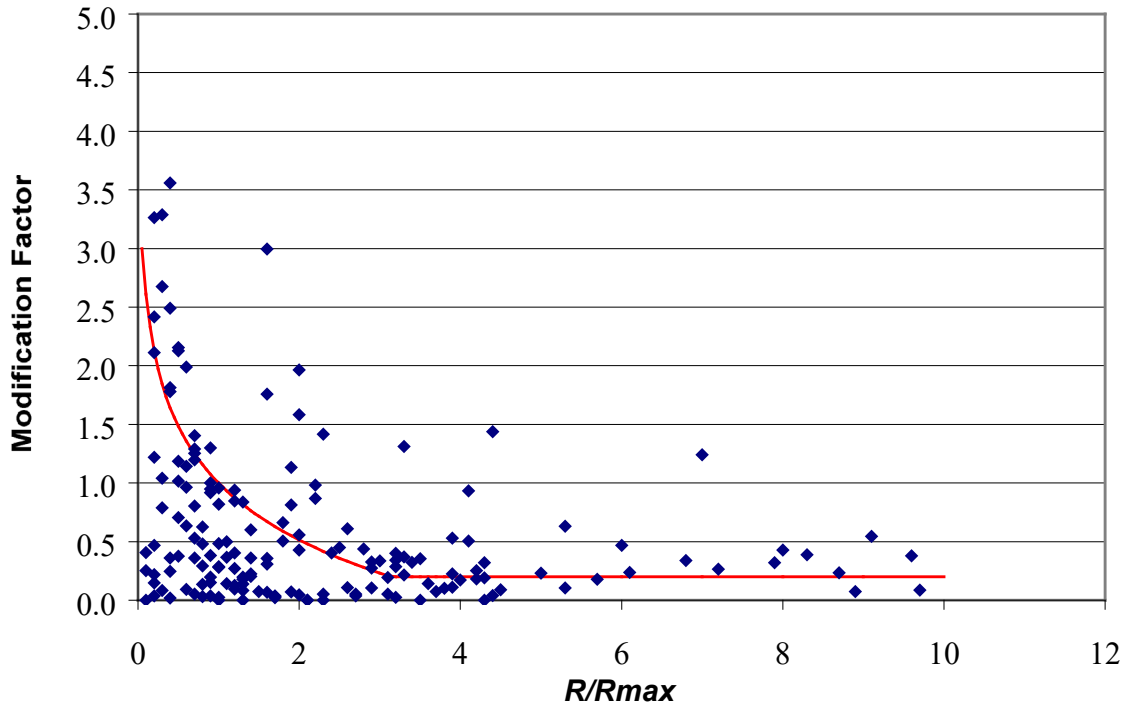
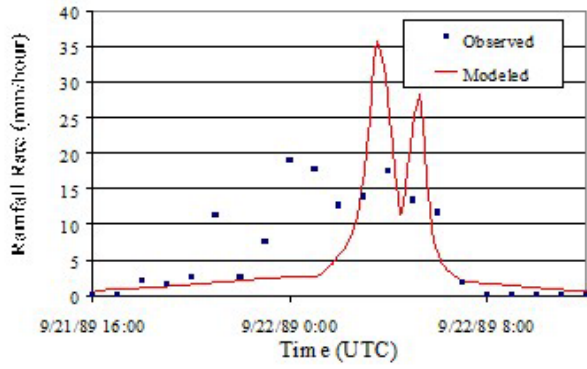


Figure 4-39 Relationship Between the Modification Factor and R/R_{max}

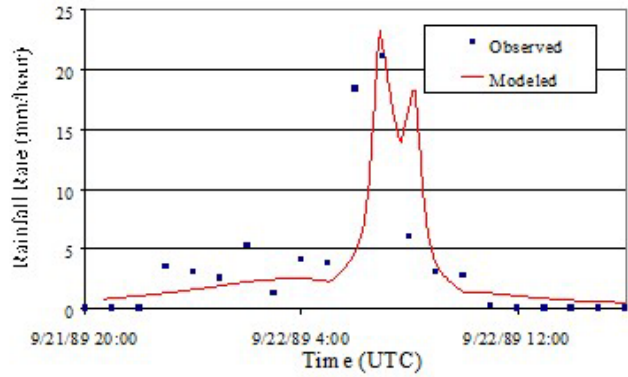
The eye of Hurricane Hugo passed over the coast of South Carolina near Charleston at approximately 04:00 UTC on September 22, 1989. The model is seen to underestimate the rainfall rate when Hurricane Hugo was approaching Charleston Airport. One possible explanation is that the rainfall might be intensified significantly within the onshore flow regime when Hurricane Hugo made landfall and this rainfall enhancement effect was not considered in the proposed model.

Considering rainfall intensification within the onshore flow regime for a landfalling hurricane is not currently implemented in the model but can be an area of future development. Besides the underestimation of the rainfall rate at the approaching stage of Hurricane Hugo, the peak rainfall rate at Charleston Airport was significantly overestimated by the model. The reason for the overestimation is unknown. The rainfall rate model predictions agree well with the actual measurements at Columbia Airport and Greenville/Spartanburg Airport, two inland sites located about 180 kilometers and 330 kilometers to the coast, respectively.

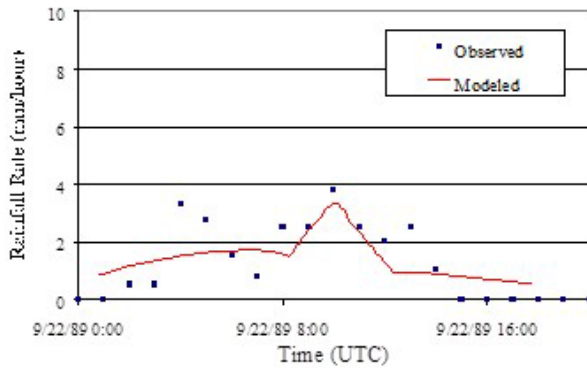
The rainfall model catches the general trend and the first peak of the rainfall rate at Wilmington Airport for Hurricane Bertha (1996). The model indicates a second peak when the backside of the storm moved across Wilmington Airport. However, this peak was not apparent on the actual records. A similar trend was also observed at Kure Beach. Moreover, at Kure Beach, one extremely high peak rainfall rate (compared to the value at Wilmington Airport, which is fairly close to Kure Beach) was recorded by the rain gauge, which is believed to be caused by rainband downdrafts. Note that the rainfall data obtained at Kure Beach in Hurricane Bertha was not used in the calibration. Therefore, the fairly good agreement between the model predictions and the actual measurements at this site validated the rainfall rate model.



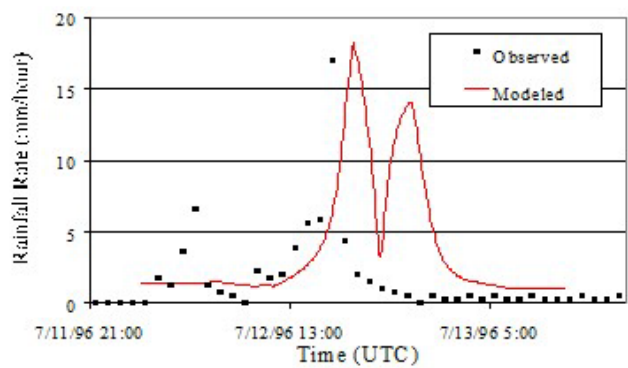
Charleston Airport, Hugo (1989)



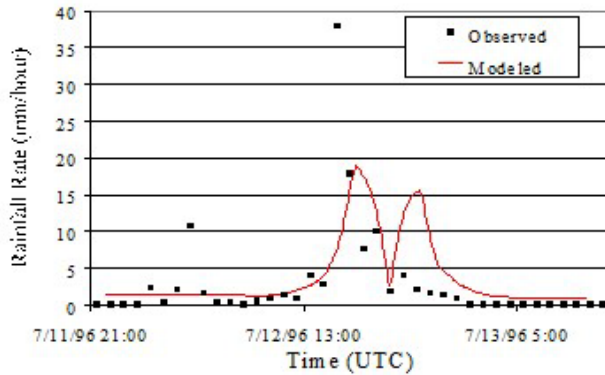
Columbia Airport, Hugo (1989)



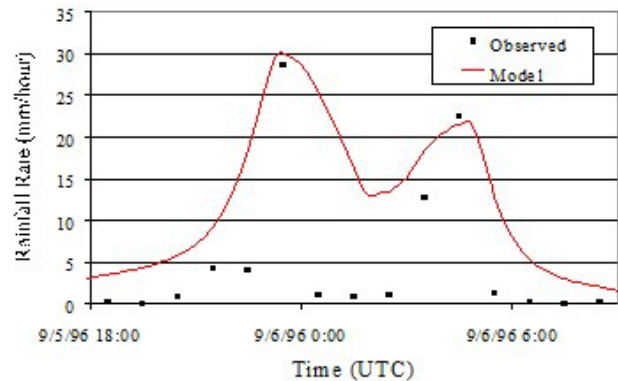
Greenville/Spartanburg Airport, Hugo (1989)



Wilmington Airport, Bertha (1996)



Kure Beach, Bertha (1996)



Wilmington Airport, Fran (1996)

Figure 4-40 Comparison of Observed and Modeled Hurricane Rainfall Rates

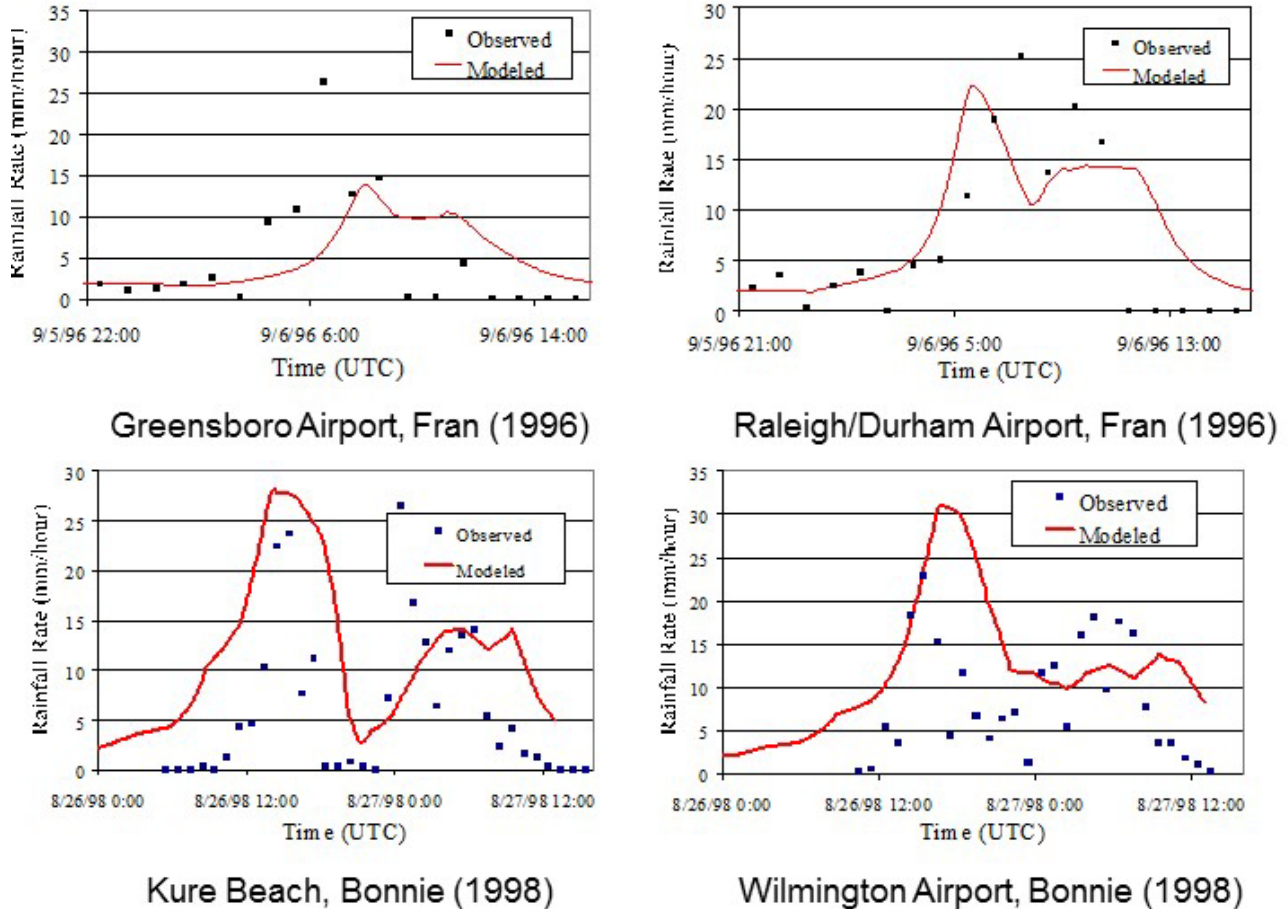


Figure 4-41 Comparison of Observed and Modeled Hurricane Rainfall Rates (Concluded)

Hurricane Fran was a Cape Verde hurricane that moved across the Atlantic during the peak of the 1996 hurricane season. It made landfall around 00:30 UTC on September 6, 1996, on the North Carolina coast. The model is seen to provide a very good estimation of the rainfall rate during the passage of Hurricane Fran at Wilmington Airport. However, the model overestimated the rainfall rate in the eye when virtually no rain was recorded by the rain gauge. The model underestimated the peak rainfall rate at Greensboro Airport. The rainband shifting to the north-west quadrant may have caused unusually high precipitation at Greensboro Airport. The model predictions at Raleigh/Durham Airport agree relatively well with the actual measurements.

Hurricane Bonnie (1998) made landfall at almost the same location as Hurricane Fran, but instead of moving straight inland, drifted along the North Carolina coast, causing difficulties in predicting its intensity and rainfall rate. From the last two charts in Figure 4-41, the model is seen to follow the general trend of the actual measurements at Kure Beach and Wilmington Airport. However, the correlation between the model predictions and the actual measurements is poor (compared with those in Hurricanes Hugo, Bertha, and Fran). When a hurricane is drifting along the coast, complex internal boundary layers and significant transverse eddies may be observed in the storm, resulting in unusually large fluctuations in the measured wind speeds and rainfall rates. Further efforts are required to model this complex situation.

Another feature of interest for risk management is the total rainfall at a particular location during the whole event. Therefore, total rainfall data collected from eight hurricanes, i.e., Frederic (1979), Elena (1985), Hugo (1989), Erin (1995), Opal (1995), Bertha (1996), Fran (1996), and Bonnie (1998), were used to validate the rainfall model. The comparisons between the model predictions and the actual measurements are shown in Table 4-7. The total rainfalls listed in the column, Full Scale 1, were calculated from continuous hourly rainfall data shown in Figure 4-40 and Figure 4-41. The values in the column, Full Scale 2, were obtained from the annual Atlantic hurricane season summary for the years of 1979, 1985, 1989, and 1996 (Hebert, 1980; Case, 1986; Case and Mayfield, 1990; Pasch and Avila, 1999). Preliminary reports by the National Hurricane Center for Hurricanes Erin and Opal were used to determine the total rainfall for these two storms (Rappaport, 1995; Mayfield, 1995). Since no information about the time span for the total rainfall was given in the annual Atlantic hurricane season summaries or the preliminary reports, a period of plus and minus 12 hours from the time when peak rainfall rate occurred was assumed in the model to calculate the total rainfall, which means a 24-hour cumulative rainfall given by the model. Accordingly, the model predictions are expected to be slightly lower than the values shown in the column denoted full scale 2. The mean and standard deviation of the ratios of the model predictions to the full-scale measurements are 0.96 and 0.50, respectively. Note that if the extremely high value (2.53) at Wilmington in Hurricane Fran is taken out from the data set, the mean and standard deviation drop to 0.91 and 0.41, respectively. Note also that when both continuous station records and total rainfall data for an event are available, the model predictions always lie in between these two values, i.e., full scale set 1 and full scale set 2.

Table 4-7 24-Hour Total Rainfall Comparison

Hurricane	Location	Full Scale 1* (mm)	Full Scale 2* (mm)	Model (mm)	Model/Full Scale **
Frederic (1979)	Pensacola FSS		83	59	0.71
	Dauphin Island		215	176	0.82
	Mobile		217	167	0.77
Elena (1985)	Pensacola NAS		63	37	0.58
	Pensacola Reg. Airport		65	34	0.52
	Tallahassee		84	24	0.28
	Mobile		60	31	0.52
	Dauphin Island		76	85	1.12
Hugo (1989)	Charleston Airport	135		101	0.75
	Columbia	75		67	0.90
	GSP Airport	27		26	0.98
	Myrtle Beach		58	41	0.71
Erin (1995)	Panama City Beach		137	50	0.36
	Pensacola NAS		56	96	1.72
	Mobile		65	95	1.46
Opal (1995)	Pensacola NAS		185	93	0.50

Hurricane	Location	Full Scale 1* (mm)	Full Scale 2* (mm)	Model (mm)	Model/Full Scale **
Opal (1995)	Pensacola NPA		176	93	0.53
	Mobile		190	48	0.25
Bertha (1996)	Wilmington	59	144	116	0.80
	Kure Beach	107		123	1.14
	Greenville		104	117	1.12
	New Bern		116	145	1.26
Fran (1996)	Wilmington	79		200	2.53
	Raleigh/Durham	128	224	161	0.72
	Greensboro	89	99	94	0.95
	Fort Bragg		119	139	1.16
	New River		179	190	1.06
	Pope AFB		171	136	0.80
	Rocky Mount		94	142	1.51
Bonnie (1998)	Kure Beach	207		351	1.70
	Wilmington	230		377	1.64

* Full scale 1 represents total rainfall calculated from continuous hourly rainfall data reported by individual stations. Full scale 2 represents total rainfall reported in annual Atlantic hurricane season summary included in Monthly Weather Review except for Hurricanes Erin and Opal, for which preliminary reports from the National Hurricane Center were used.

** In the case when both full-scale data are available, the total full-scale rainfall is taken as the value given in the column of full scale 2.

The rainfall rate model is capable of providing reasonable rainfall rate predictions in a hurricane. However, due to the complex nature of a hurricane, a significant degree of variability should be expected. Further development is needed to account for all possible aspects affecting the rainfall rate in a hurricane. Uncertainties associated with input parameters and physical models should also be addressed to provide more reliable predictions.

4.4 Surface Roughness Modeling

A critical component in modeling wind effects, damage, and loss to buildings and facilities is the assessment of the ground roughness. As the ground surface becomes rougher, the wind speeds near the ground decrease, although the upper-level wind speed remains the same. The wind loads experienced by structures located in a typical suburban, treed, or urban environment are much lower than those experienced by buildings located in relatively unobstructed regions such as waterfront and open field locations. The wind loads experienced by one- and two-story structures located in forested areas may be as low as one half of those experienced by similar structures located in an open environment.

The effect of surface roughness is treated in a simple fashion in building codes and standards using exposure categories. For example, open terrain and suburban terrain are designated as Exposures C and B, respectively, in ASCE 7. The approach taken in that standard, and most national and international standards, is to define a basic wind speed, which represents the wind speed at a height of 10 meters in open terrain. The effect of the actual local terrain is then considered by modifying that wind speed by a factor, which is dictated by the exposure category for the local terrain.

The ground surface roughness is defined using a characteristic roughness length, denoted as z_0 . This roughness length is a function of the height and spacing of the buildings, trees and other obstructions on the ground surface. As described earlier in Section 4, the hurricane model yields estimates of wind speed at any location for open terrain conditions. Hence, given information on the upstream fetch and the associated surface roughness length, the wind speed at any location and any height can be estimated.

Numerous studies have been performed over the last several decades attempting to categorize z_0 using surface exposure description. However, no consistent agreement has been reached among researchers. Wieringa (1992,1993) summarized most of the traceable studies on roughness lengths for various terrains performed in the last thirty years (including field projects, numerical modeling studies, and wind tunnel investigations) and gave a table showing best estimations. This table, included herein as Table 4-8, serves as a reasonable basis for determining appropriate roughness lengths for areas on the mainland. For comparison, roughness lengths given by one set of researchers, Simiu and Scanlan (1996), are shown in Table 4-9. Surface roughness lengths proposed by a number of researchers, emphasizing built-up areas, are presented in Table 4-10.

Table 4-8 Roughness Lengths of Homogeneous Surface Types (from Wieringa, 1993)

Surface Type	Roughness Length (meter)
Sea, loose sand and snow	» 0.0002 (wind speed dependent)
Concrete, flat desert, tidal flat	0.0002 – 0.0005
Flat snow field	0.0001 – 0.0007
Rough ice field	0.001 – 0.012
Fallow ground	0.001 – 0.004
Short grass and moss	0.008 – 0.03
Long grass and heather	0.02 – 0.06
Low mature agricultural crops	0.04 – 0.09
High mature crops (“grain”)	0.12 – 0.18
Continuous bushland	0.35 – 0.45
Mature pine forest	0.8 – 1.6
Tropical forest	1.7 – 2.3
Dense low buildings (“suburb”)	0.4 – 0.7
Regularly-built large town	0.7 – 1.5

Table 4-9 Roughness Lengths For Various Surface Types (from Simiu and Scanlan, 1996)

Type of Surface	z ₀ (meter)
Sand	0.0001-0.001
Snow Surface	0.001-0.006
Mown Grass (~0.01 meters)	0.001-0.01
Low Grass, Steppe	0.01-0.04
Fallow Field	0.02-0.03
High Grass	0.04-0.10
Palmetto	0.10-0.30
Pine Forest (mean height of trees: 15 meters; one tree per 10 square meters)	0.90-1.00
Sparsely Built-up suburbs	0.20-0.40
Densely Built-up suburbs and towns	0.80-1.20
Centers of large Cities	2.00-3.00

Table 4-10 Roughness Lengths of Rather Homogeneously Built-up Areas (from Wieringa, 1993)

Surface Type	z ₀ (meter)	Reference
Scattered low buildings	0.5±0.2	Shiotani (1962)
Low buildings and trees	»0.7	Duchêne-Marullaz (1979)
Regular dense low houses	0.5±0.1	Steyn (1982)
“Regular” city buildings	»1.3	Jensen (1958)
“Regular” city buildings	1.1±0.4	Brook (1972)
“Regular” city buildings	1.0±0.6	Karlsson (1986)
“Regular” city buildings	0.9±0.3	Yersel and Goble (1986)

Note that the data in these tables are for homogeneous terrain only, which means the wind must pass several kilometers of fetch of the same terrain before it reaches the area investigated. For areas on the mainland, due to relatively homogeneous land exposure, the transition layer in the vertical wind profile can be taken as fully adapted up to the standard height of 10 meters (even though local integration over an area of several square kilometers may be used to determine the effective value of heterogeneous roughness). However, this is not the case for barrier islands. Typically, the overland fetch is fairly short in this case. When a hurricane moves from the open water onto the barrier island, no obvious over-land boundary layer can be developed (i.e., not enough fetch distance). Therefore, the effective roughness length will be much smaller than that for areas on the mainland for the same land use category.

As an alternative to the information given in Table 4-8, Table 4-9, and Table 4-10, the effective roughness length over a particular local area can be estimated using a simple equation proposed by Lettau (1969):

Equation 4-29

$$z_0 \approx 0.5HS/A$$

Where:

- H average height within the area
- S total projected frontal area of the obstacles
- A surface area

Because the ground surface roughness has a major impact on the magnitude of the loads experienced by a structure, it is important to be able to estimate the local surface roughness. Currently, no direct databases exist describing the distribution of the surface roughness over regions within the U.S. Consequently, indirect methods are used to estimate the surface roughness distribution. The approach for estimating the surface roughness is to obtain information on land use and land cover (LULC), for which databases do exist, and then estimate the surface roughness for each LULC class. By assigning a value of the surface roughness associated with a given land use, a surface roughness map can be developed directly from a LULC map and the mean wind speeds and gustiness can be reasonably estimated at any surface location within a storm.

4.4.1 MRLC-NLCD Database

The most nationally consistent and up-to-date source of land use data is the National Land Cover Data (NLCD) compiled by the Multi-Resolution Land Characteristics (MRLC) Consortium. The MRLC is a partnership of federal agencies who generate consistent and relevant land cover information at the national scale for a wide variety of applications. The NLCD uses a modified version of the Anderson Land Cover Classification System (Anderson et al., 1976). The classification system is summarized in Table 4-11.

The primary data source is the nominally 2011 Landsat TM coverage. This data is augmented by NLCD with ancillary data sets to help resolve uncertainties and otherwise enhance the data set. All data sets are validated by NLCD prior to release. A three-tiered validation procedure is used and includes general data integrity screening, comparisons to existing data sets, and formal accuracy assessments. The release notes of MRLC-NLCD data provide detailed descriptions of these processes, including land characteristics for each land category, which is helpful in defining a z_0 value for a category.

Table 4-11 NLCD 2011 Database Classification System

Anderson Land Cover Classification System Description	NLCD Code	NLCD Description
Water	11	Open Water
	12	Perennial Ice/Snow
Developed	21	Developed, Open Space
	22	Developed, Low Intensity
	23	Developed, Medium Intensity
	24	Developed, High Intensity
Barren	31	Barren Land
	32	Unconsolidated Shore
Natural Forested Upland (non-wet)	41	Deciduous Forest
	42	Evergreen Forest
	43	Mixed Forest
Shrubland	52	Shrub/Scrub
Herbaceous	71	Grassland/Herbaceous
Planted/Cultivated	81	Pasture/Hay
	82	Cultivated Crops
Wetlands	90	Woody Wetlands
	95	Emergent Herbaceous Wetlands

4.4.1.1 Calibration of NLCD Land Cover Classifications against Aerial Photos

To ensure the overall correctness of the original, regional roughness lengths derived for Hazus from the NLCD 2001 database, the land cover classifications were verified and calibrated for representative roughness lengths against aerial photos. The z_0 values to be used for a land cover class were determined by the calibration results, with adjustments based on the detailed descriptions of the land cover characteristics provided by the NLCD 2001 release notes for each land cover class. Aerial photos of 12 regions in Southeast Florida ranging from 0.2 to 0.5 square miles in area were used, with 11 of them in Dade County and one in Broward County. The photos were taken as of early 1998 and most of them are for suburban locations. The calibration process is described below. Since the land cover characteristics were expected to be different across regions, the z_0 values were valid for Southeast Florida.

Examples of the MRLC-NLCD data maps for areas corresponding to the aerial photos are displayed using color codes, as shown in Figure 4-42 and Figure 4-43. Each small square block (pixel) represents a 30-meter by 30-meter area. The data maps are overlaid with street layout data from another source to help match locations to the aerial photos. The boundaries of the aerial photos are identified and indicated by the polygon shown in the center of the data map. Within the polygon, each small sub-region of roughly equal area and of similar land cover characteristics as shown by the aerial photos is assigned a representative roughness length (z_0 value) empirically, consistent with the criteria for z_0 assignment

used throughout this document. (Normally, the small sub-region coincides with an area represented by a cluster of 30 meters by 30 meters NLCD pixels with the same classification code.) The statistics of the z_0 values assigned to the small sub-regions having the same NLCD 2001 classification are listed in Table 4-12, along with the number of sub-region z_0 values used for computing these statistics for each NLCD class. These statistics are derived based on all twelve aerial photos.

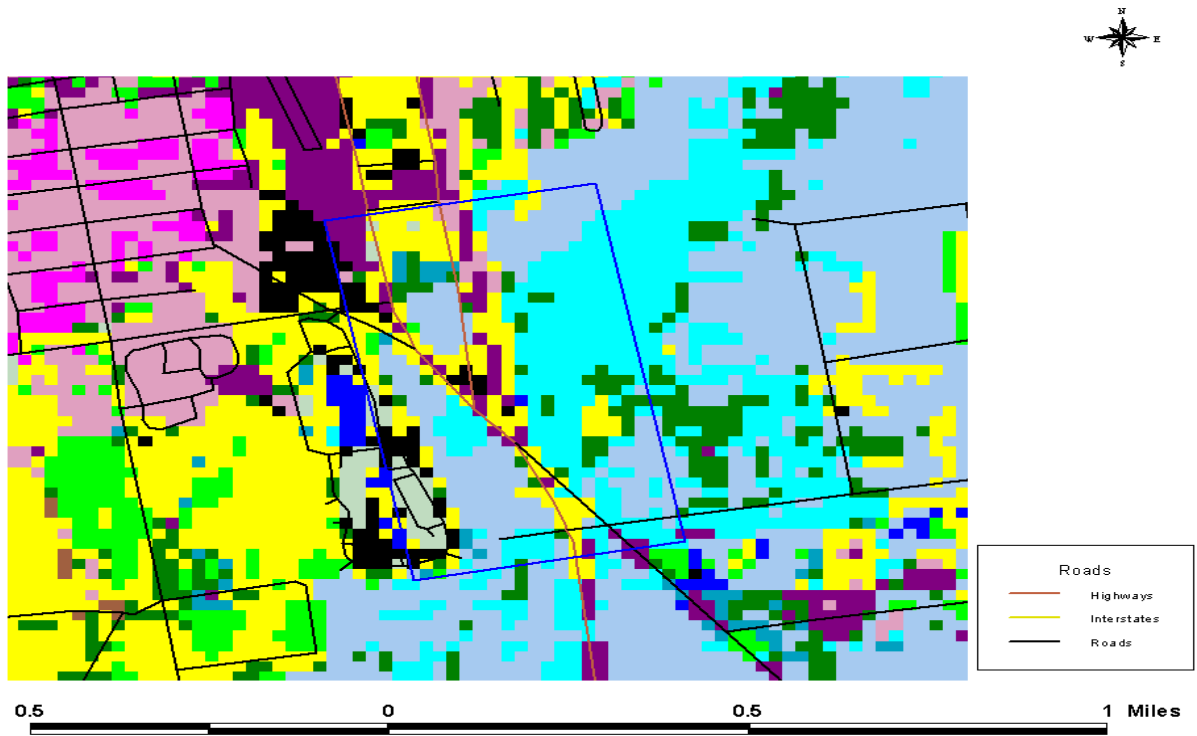


Figure 4-42 Example A of Overlaid NLCD Data Map and Street Layout (COMM 01: Dade County)

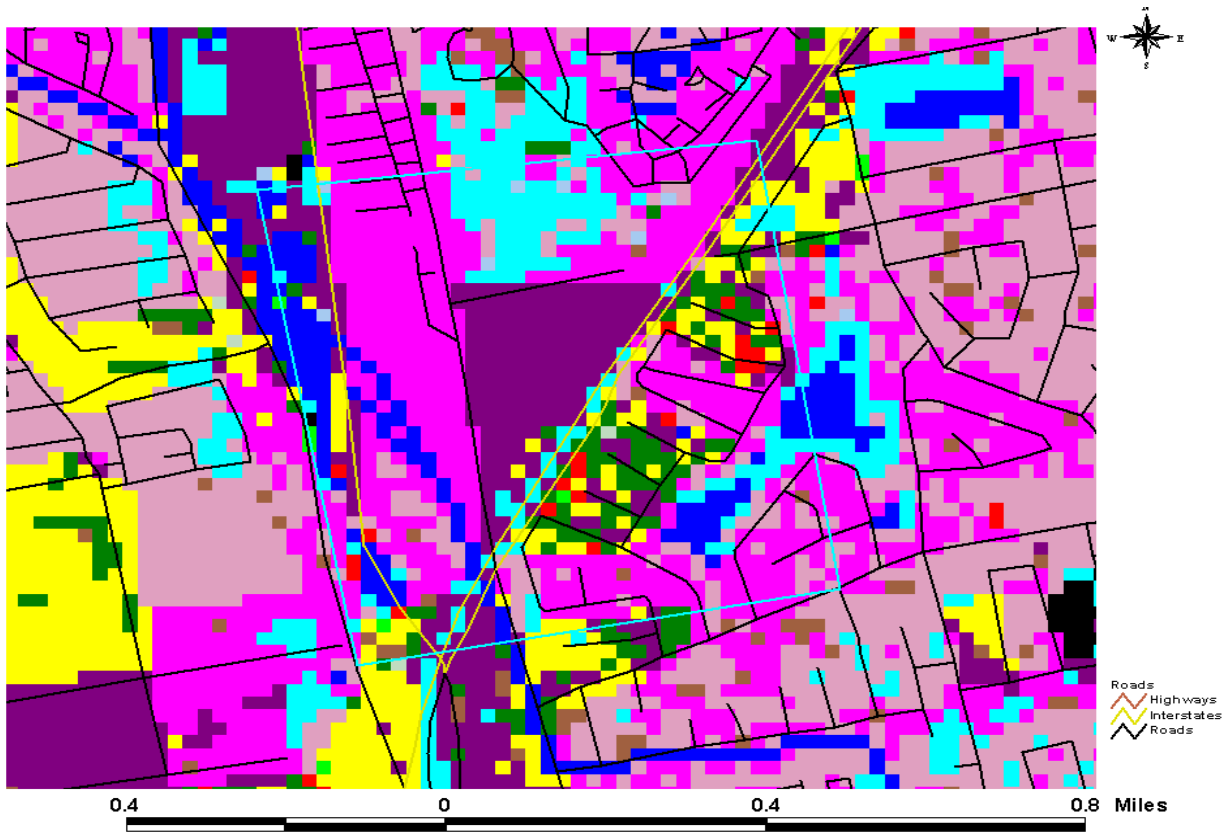


Figure 4-43 Example B of Overlaid NLCD Data Map and Street Layout (INDU01: Dade County)

It was found that the general pattern of NLCD 2001 data was consistent with the land cover/land use as shown by the aerial photos. However, two types of errors were observed during the verification and calibration process, which were acknowledged in the NLCD 2001 release notes. The first is a location mismatch, which is estimated to be up to about 120 meters from the comparison with the aerial photos and the street layout. The aerial photos and the street layout data generally correspond very well. The second type is misclassification of land cover. For example, areas shown as barren land in the NLCD map were actually residential areas in the aerial photos. This could be due to the fact that the aerial photos are more recent and showing new development not captured by NLCD data. There were also misclassifications across the three sub-classes (Low Intensity Residential, High Intensity Residential, and Commercial/Industrial/Transportation) under the Developed class. Less frequently, some areas that were shown to be undeveloped in the aerial photos were classified as Developed in the NLCD database. The latter two cases of errors were indications of inaccuracy in the NLCD data acquisition and processing instead of the results of new development.

Table 4-12 NLCD 2001 Land Cover Classification Versus Surface Roughness Length

NLCD 2001 Land Cover Classification and Numerical Coding	Land Surface Roughness Length, z ₀ (meters)					Number of Sub-Regions Used
	Used	Avg.	COV*	Max.	Min.	
Water						
11 Open Water	0.010	0.013	0.612	0.030	0.010	6
12 Perennial Ice/Snow	0.012					0
Developed						
21 Low Intensity Residential	0.350	0.307	0.496	0.600	0.010	51
22 High Intensity Residential	0.600	0.401	0.498	0.800	0.080	39
23 Commercial/Industrial/Transportation	0.350	0.265	0.605	0.600	0.030	28
Barren						
31 Bare Rock/Sand/Clay	0.200	0.300				1
32 Quarries/Strip Mines/Gravel Pits	0.400					0
33 Transitional	0.400	0.400	0.661	0.600	0.100	3
Forested Upland						
41 Deciduous Forest	0.600					0
42 Evergreen Forest	0.600	0.500				1
43 Mixed Forest	0.600					0
Shrubland						
51 Shrubland	0.060	0.040				1
Non-natural Woody						
61 Orchards/Vineyards/Other	0.210	0.213	0.777	0.400	0.050	4
Herbaceous Upland						
71 Grasslands/Herbaceous	0.150	0.193	0.662	0.300	0.050	4
Herbaceous Planted/Cultivated						
81 Pasture/Hay	0.150	0.160	1.301	0.400	0.030	3
82 Row Crops	0.100	0.100	0.913	0.300	0.030	8
83 Small Grains	0.030					0
84 Fallow	0.030					0
85 Urban/Recreational Grasses	0.150	0.155	0.514	0.250	0.030	6
Wetlands						
91 Woody Wetlands	0.300	0.545	0.594	1.100	0.300	10
92 Emergent Herbaceous Wetlands	0.030	0.188	0.959	0.600	0.050	10

*COV = Coefficient of Variation

Based on the calibration results and considering other factors such as possible bias towards suburban regions with the sample aerial photos used, a set of z_0 values corresponding to specific NLCD 2001 classifications was adopted for use in estimating regional representative roughness lengths for Southeast Florida, as included in Table 4-12. In principle, the adopted z_0 values are based on the average values from the calibration with mostly minor adjustments based on the detailed descriptions of the land cover characteristics provided by the NLCD release notes for each land cover class. However, two major adjustments from the calibrated averages, which are associated with the Developed and Wetlands classes, are worth mentioning. For the Developed class, since the aerial photos used contain only suburban developments, the z_0 values for all three subclasses of the Developed class were adjusted upwards to accommodate those areas closer to city centers that are rougher but have the same NLCD classifications, for example, areas with many multi-story residential and commercial buildings. For wetlands, the aerial photos do not include any everglade areas that have much lower z_0 values than those from the photos but are also classified as either Woody Wetlands or Emergent Herbaceous Wetlands. Thus, the z_0 values for Wetlands were adjusted downwards to accommodate such areas as the everglades that were not represented by the aerial photos.

To verify the accuracy of the NLCD land cover classification and map land cover codes to roughness lengths for different regions of the U.S., aerial photographs downloaded from Microsoft TerraServer were used to empirically determine the roughness lengths of selected areas with constant NLCD land cover codes. Some examples are presented below for North Carolina and Texas.

4.4.1.1.1 North Carolina

Figure 4-44 shows the land cover for the entire state of North Carolina, where the land cover codes (or pixel values) are represented with the color scheme shown in Figure 4-45, which approximately matches the natural color and will be used throughout this section. It is seen that the NLCD data used reflects the characteristics of the state's general landscape. Figure 4-46 shows the aerial photograph and the NLCD land cover data for the Raleigh area of North Carolina, which demonstrates that the patterns match reasonably well. By zooming into a smaller area, Figure 4-47 shows that the accuracy of the NLCD data seems to be satisfactorily representing the true land cover types shown by the 1993 aerial photograph. (The NLCD data were derived from satellite images taken between November 1990 and June 1993). Further review was conducted in areas where uncertainties existed. For example, areas A and B initially appeared to be developed areas in the aerial photograph (Figure 4-48), but they are classified by the NLCD data as herbaceous land (Pasture/Hay and Row Crop). However, zooming in on the aerial photograph confirms that areas A and B are herbaceous land, as shown in Figure 4-48.

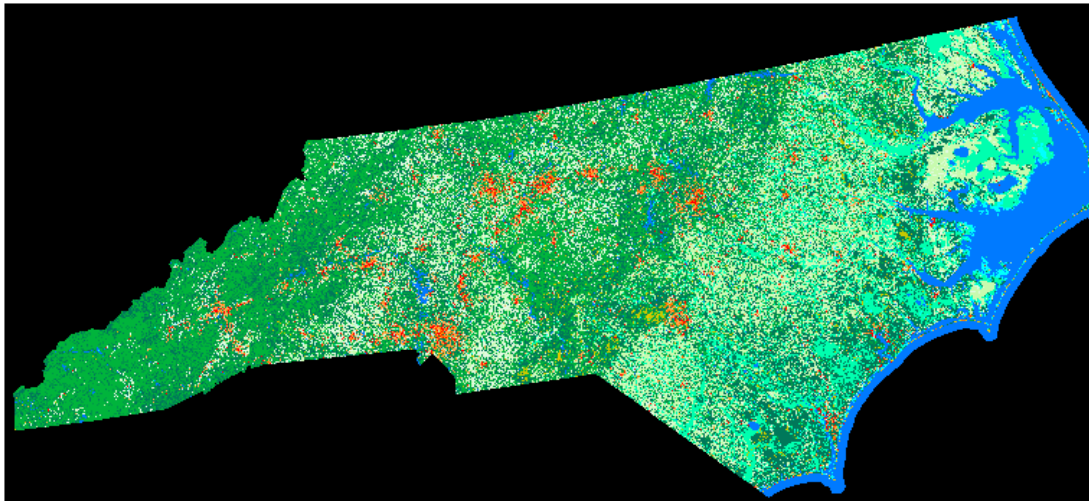


Figure 4-44 Color-Coded Land Cover Characteristics of the State of North Carolina as Derived from NLCD Database (1991)






Category Group	Class Code	Class Color	Class Name
<i>Water</i>	11		Water
	12		Ice / Snow
<i>Developed</i>	21		Low Intensity Residential
	22		High Intensity Residential
	23		Comm. / Ind. / Trans.
<i>Barren</i>	31		Rock / Sand / Clay
	32		Quarry / Strip Mine / Gravel Pit
	33		Transitional
<i>Forested Upland</i>	41		Deciduous Forest
	42		Evergreen Forest
	43		Mixed Forest
<i>Shrubland</i>	51		Shrubland
<i>Non-natural Woody</i>	61		Orchard / Vine yard / Other
<i>Herbaceous Upland</i>	71		Grassland / Herbaceous
<i>Herb. Planted / Cultivated</i>	81		Pasture / Hay
	82		Row Crop
	83		Small Grain
	84		Fallow
	85		Urban / Recreational Grass
<i>Wetland</i>	91		Woody Wetland
	92		Herbaceous Wetland

Figure 4-45 Color Scheme Used Throughout Remainder of this Section

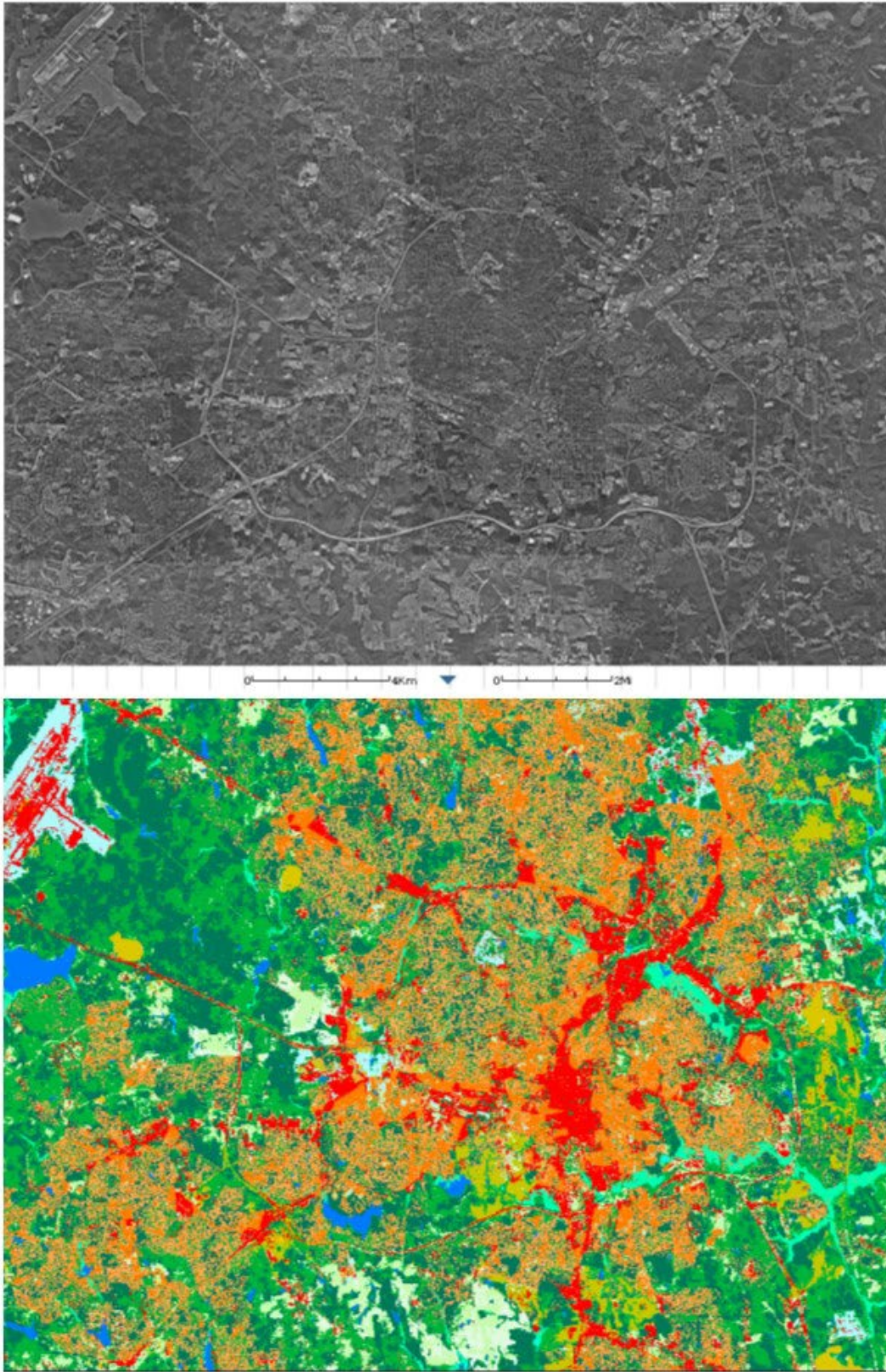


Figure 4-46 Metropolitan Raleigh, NC (upper: Aerial photograph; lower: NLCD 1991)

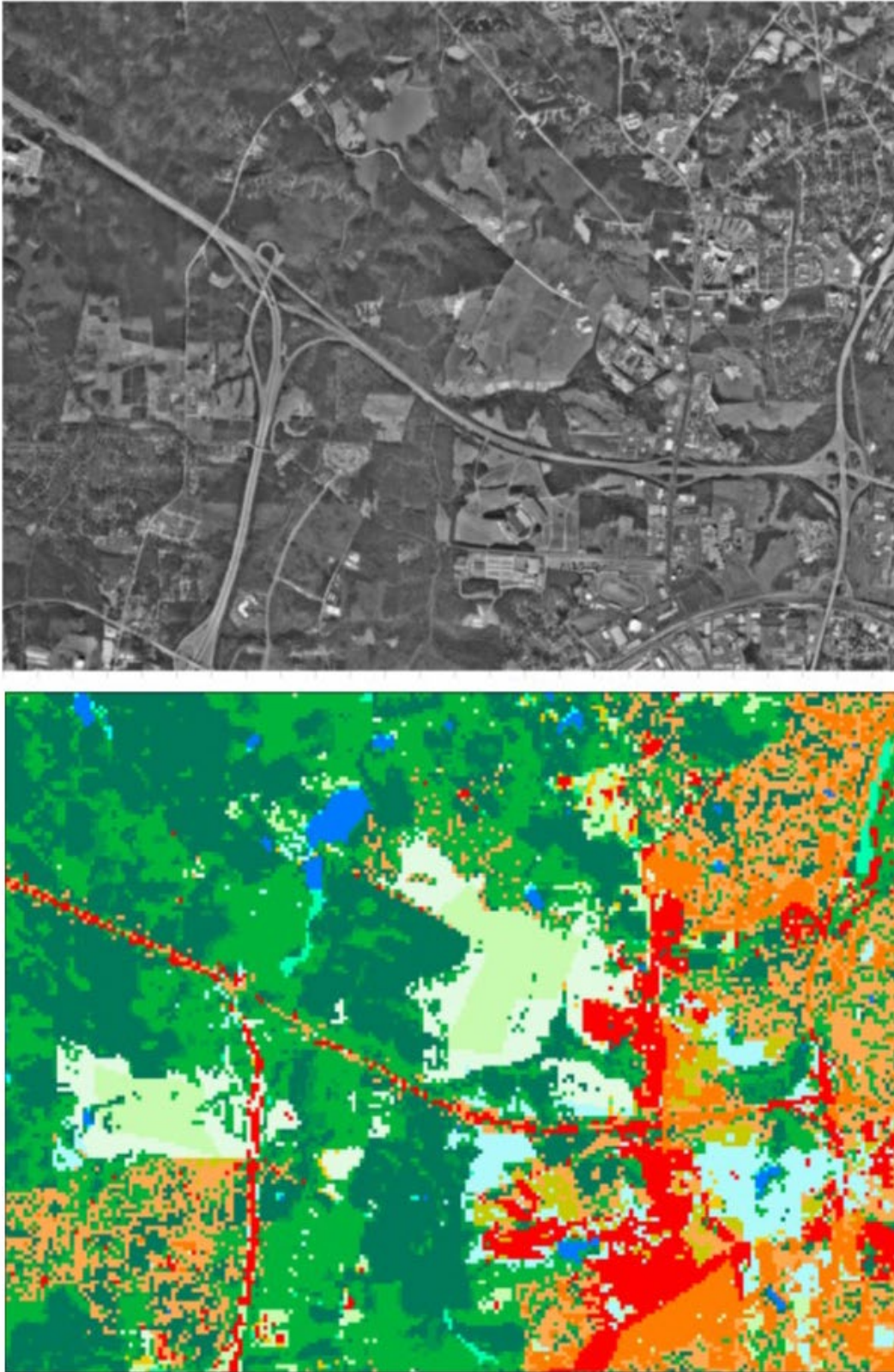


Figure 4-47 West Suburb of Raleigh, NC (upper: Aerial photograph; lower: NLCD 1991)



Area A



Area B

Figure 4-48 Close-Up Views of Two Areas in West Suburb of Raleigh, NC

As examples of the empirical assignment of roughness length, a roughness length of 0.05 was assigned to these two specific areas in Figure 4-48. For the developed areas next to them, roughness lengths of 0.25 to 0.3 were assigned, while roughnesses of 0.55 to 0.7 were estimated for the surrounding forest and other woody areas.

Figure 4-49 shows downtown Wilmington, North Carolina, and the predominantly herbaceous wetland across from the river. Consistent patterns are observed between the NLCD data and the aerial photograph. Close-ups near the USS North Carolina battleship museum are presented in Figure 4-50, where a roughness length of 0.65 was assigned to the downtown portion on the right, 0.01 for the water, 0.10 for the herbaceous wetland (reed marsh) and 0.7 for the woody wetland (treed). For the highways, which are classified as comm./industrial/trans. (Coded 23), a value of 0.1 was used.

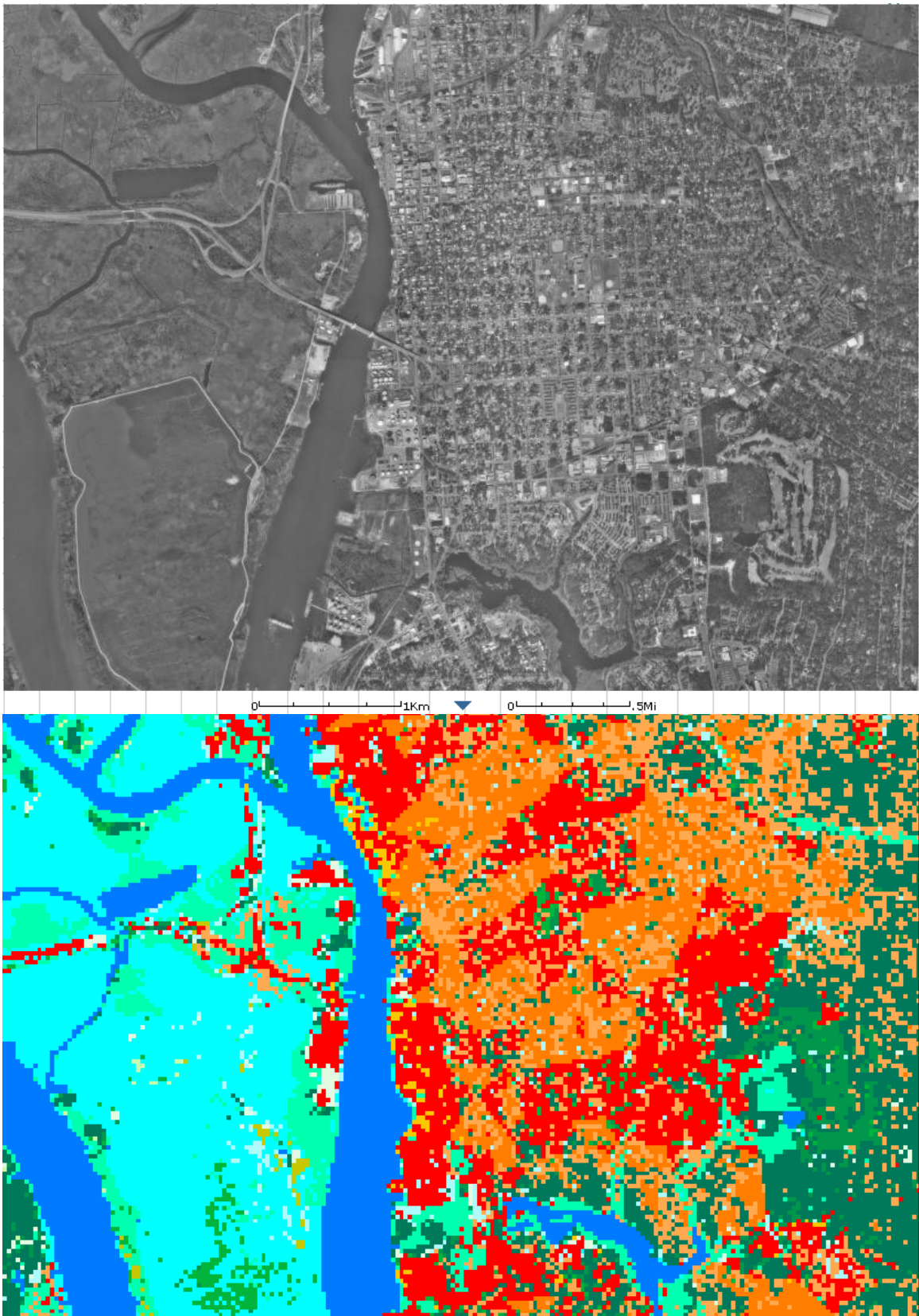


Figure 4-49 Downtown Wilmington, NC (upper: Aerial photograph; lower: NLCD)

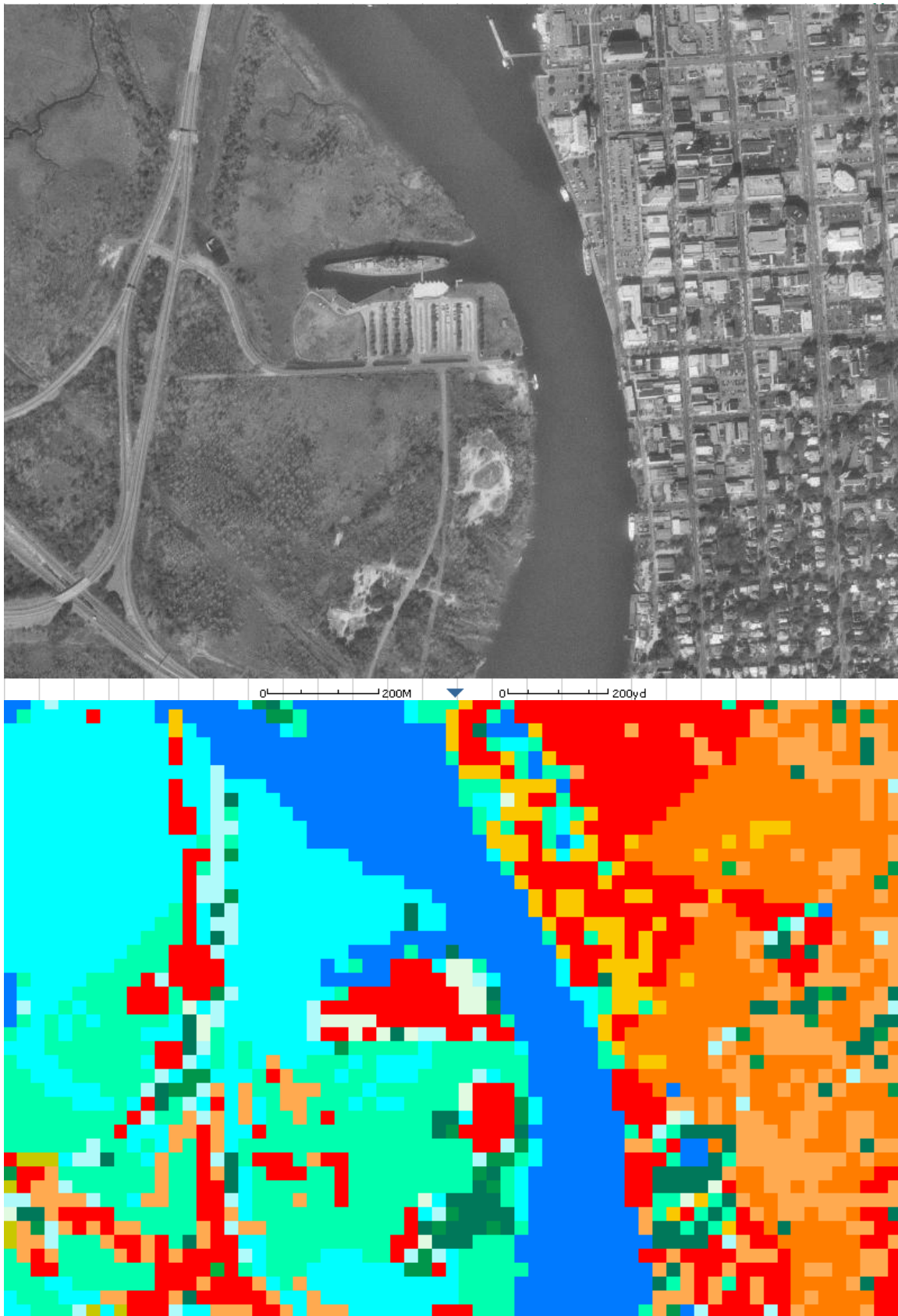


Figure 4-50 Close-Up of Downtown Wilmington, NC (upper: Aerial photograph; lower: NLCD)

4.4.1.1.2 Texas

The Galveston-Texas City-Santa Fe area of Texas is presented in Figure 4-51. Again, the general patterns and detailed land cover characteristics are consistent. By zooming into sampled areas on the aerial photograph, roughness lengths were assigned. As an example, a close-up of the region corresponding to area #1 of the NLCD data map reveals that it is predominantly a cluster of residential buildings, consistent with the NLCD data, as shown in Figure 4-52. The area next to it and between the two major highways is shown as being covered by a mixture of trees, farming and other features, also consistent with the NLCD data.

Another example for Texas is shown in Figure 4-53, which is a suburban area about 40km northeast of downtown Houston. The land cover characteristics represented by NLCD data and shown by the aerial photograph are remarkably consistent for this area of complicated land covers, as interlaced with residential, commercial/industrial, highways, recreational, waters, forests, wetlands and farms. Roughness lengths were assigned to various featured areas, respectively, by zooming into corresponding regions.

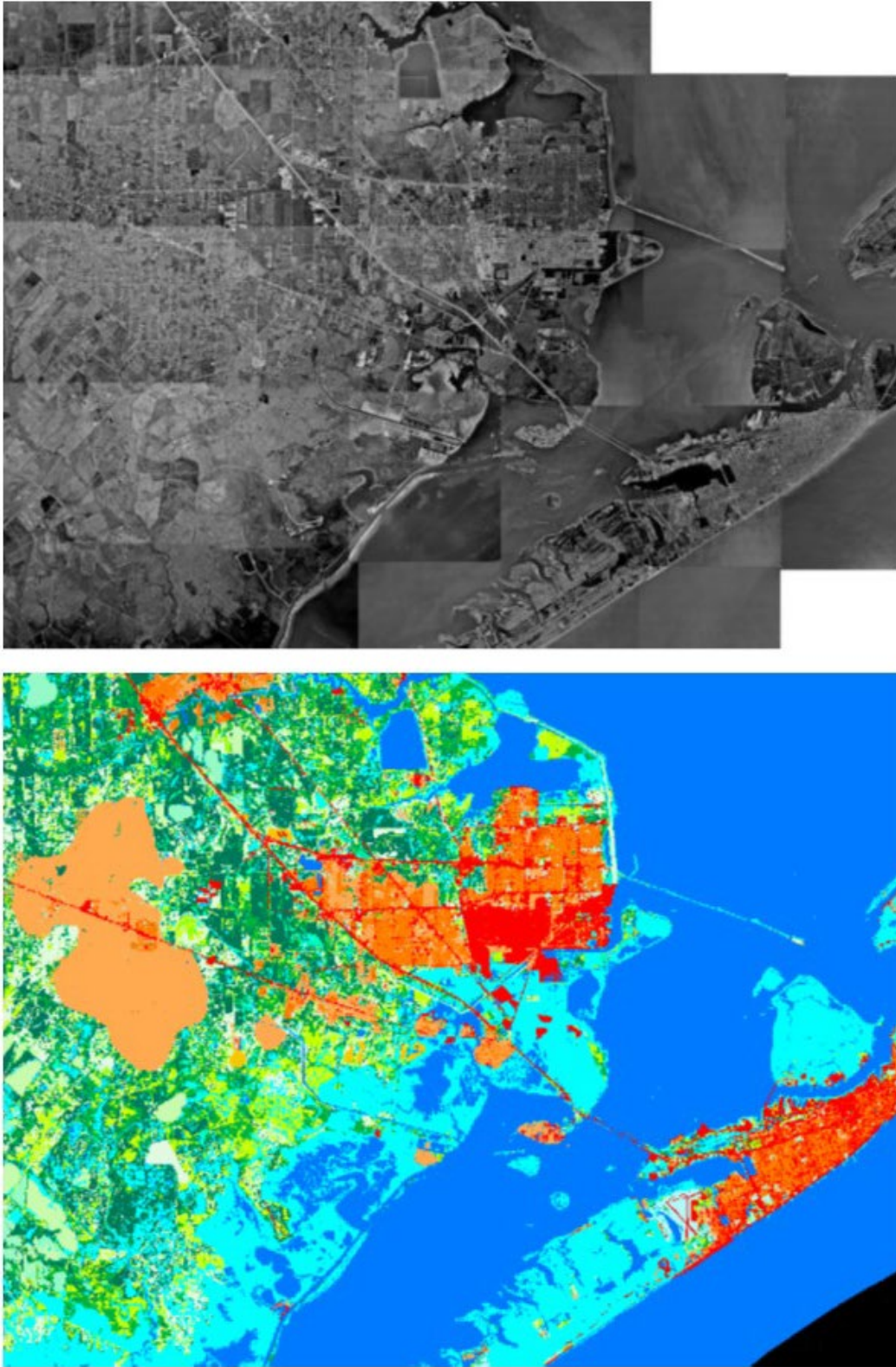


Figure 4-51 Galveston-Texas City-Santa Fe Area, TX (upper: Aerial photo; lower: NLCD)

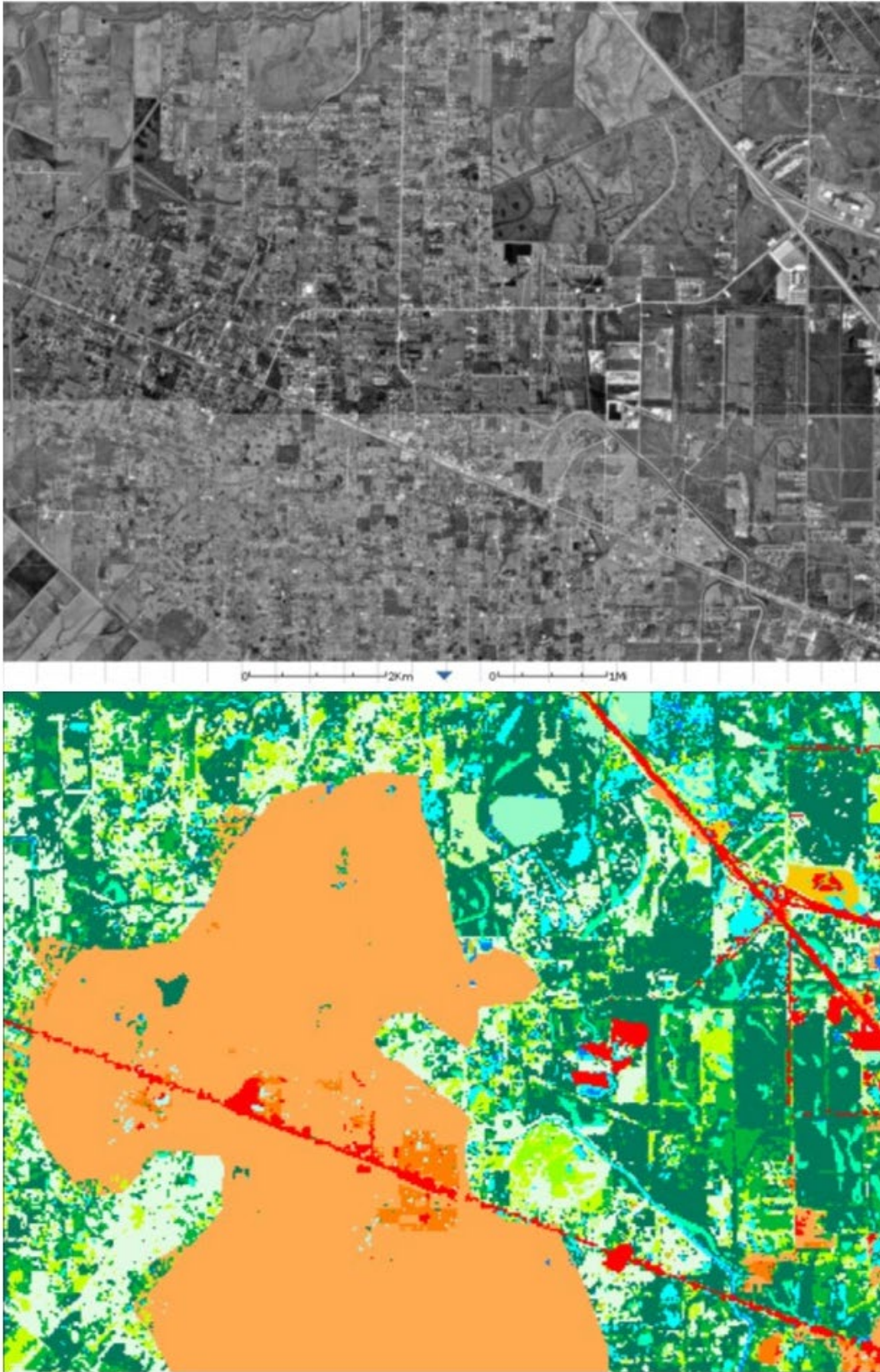


Figure 4-52 Close-up of Santa Fe Area, TX (upper: Aerial photograph; lower: NLCD)

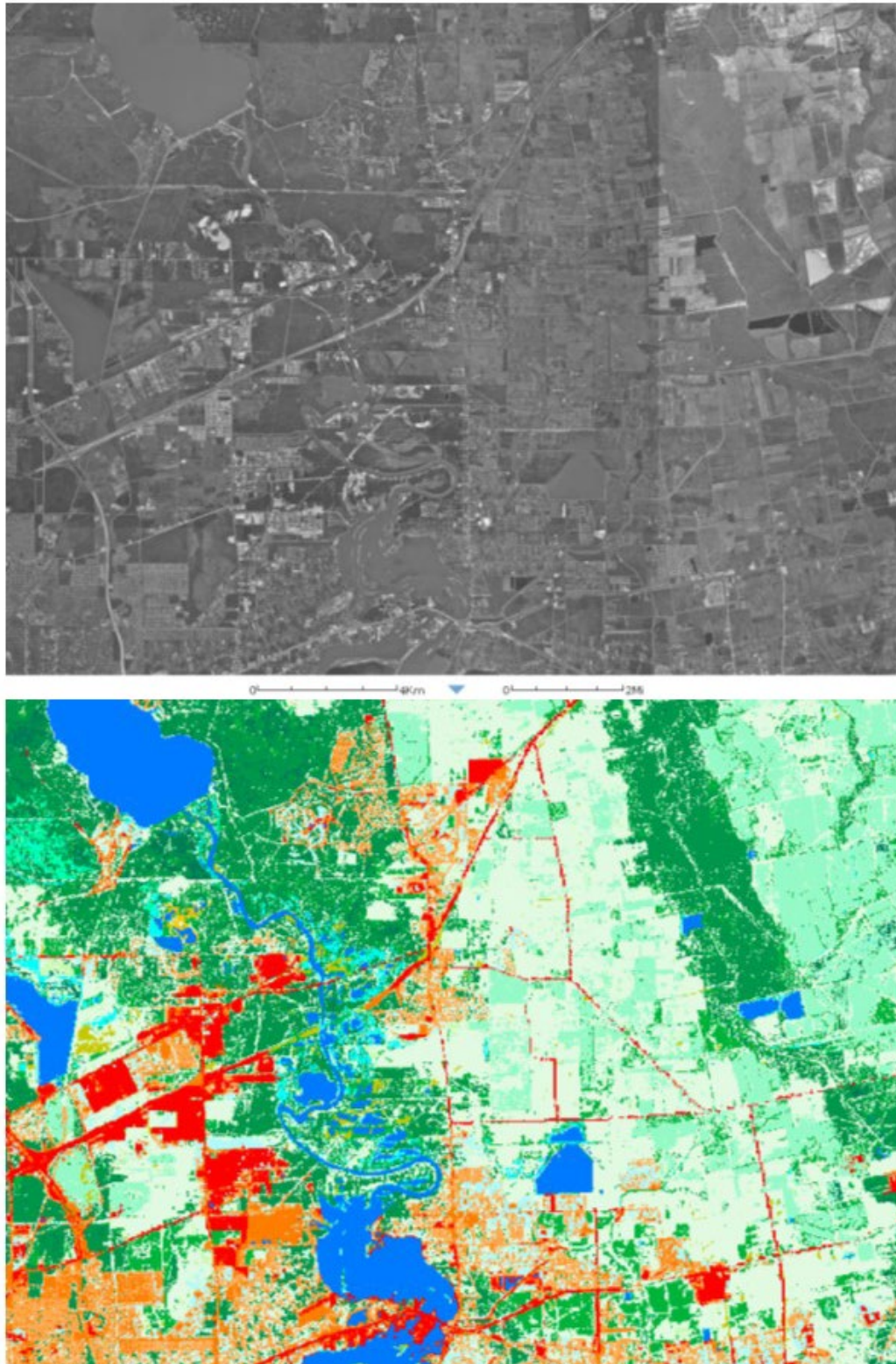


Figure 4-53 Northeast Suburb of Houston, TX (upper: Aerial photograph; lower: NLCD)

4.4.2 Mapping NLCD Land Cover Codes to Roughness Lengths

With the help of aerial photographs, and in addition to the NLCD classification descriptions, roughness lengths were empirically estimated for sampled individual areas, as illustrated in the above examples. Area-weighted averages of the assigned values yield the representative roughness length (z_0) for a specific land cover class. The averaged values of z_0 are shown in Table 4-13 and Table 4-14 for each Gulf and Atlantic coastal state or region. Florida has been partitioned into four sub-regions: panhandle, west, southeast and northeast, and New York has been partitioned into three subregions: Manhattan, Long Island, and the remainder of the state. Note that the roughness values are not uniform across states.

Table 4-13 Assignment of z_0 values to NLCD LULC Codes

LULC Class	Description	HI	TX	LA	MS	AL	Pan FL	W FL	SE FL	NE FL	GA	SC	NC
11	Open Water	0.003	0.003	0.003	0.003	0.003	0.003	0.003	0.003	0.003	0.003	0.003	0.003
12	Perennial Ice/Snow	0.012	0.012	0.012	0.012	0.012	0.012	0.012	0.012	0.012	0.012	0.012	0.012
21	Developed, Open Space	0.080	0.100	0.090	0.090	0.090	0.090	0.100	0.090	0.090	0.100	0.100	0.100
22	Developed, Low Intensity	0.500	0.350	0.330	0.330	0.330	0.330	0.340	0.340	0.330	0.350	0.360	0.350
23	Developed, Medium Intensity	0.530	0.550	0.500	0.530	0.530	0.530	0.540	0.570	0.540	0.570	0.570	0.550
24	Developed, High Intensity	0.550	0.440	0.390	0.350	0.350	0.350	0.390	0.380	0.340	0.350	0.340	0.330
31	Barren Land	0.020	0.100	0.090	0.090	0.090	0.090	0.100	0.090	0.090	0.100	0.100	0.100
32	Unconsolidated Shore*	0.090	0.100	0.090	0.090	0.90	0.090	0.090	0.090	0.090	0.100	0.100	0.100
41	Deciduous Forest	0.900	0.900	0.900	0.900	0.900	0.900	0.900	0.900	0.900	0.900	0.900	0.900
42	Evergreen Forest	0.900	0.900	0.900	0.900	0.900	0.900	0.900	0.900	0.900	0.900	0.900	0.900

LULC Class	Description	HI	TX	LA	MS	AL	Pan FL	W FL	SE FL	NE FL	GA	SC	NC
43	Mixed Forest	0.900	0.900	0.900	0.900	0.900	0.900	0.900	0.900	0.900	0.900	0.900	0.900
52	Shrubland	0.120	0.100	0.120	0.120	0.120	0.120	0.120	0.120	0.120	0.110	0.130	0.100
71	Grasslands / Herbaceous	0.085	0.040	0.040	0.040	0.040	0.040	0.040	0.040	0.040	0.050	0.040	0.040
81	Pasture / Hay	0.040	0.040	0.060	0.050	0.050	0.050	0.050	0.050	0.060	0.050	0.060	0.060
82	Cultivated Crops	0.030	0.060	0.060	0.050	0.050	0.050	0.060	0.060	0.060	0.060	0.060	0.060
90	Woody Wetlands	0.900	0.900	0.900	0.900	0.900	0.900	0.900	0.900	0.900	0.900	0.900	0.900
95	Emergent Herbaceous Wetlands	0.150	0.100	0.110	0.090	0.090	0.090	0.080	0.040	0.090	0.100	0.100	0.100

Table 4-14 Assignment of z₀ values to NLCD LULC Codes (Continued)

LULC Class	Description	VA	MD	DE	PA	NJ	NY	MAN	LONG IS	CT	RI	MA	NH	ME
11	Open Water	0.003	0.003	0.003	0.003	0.003	0.003	0.003	0.003	0.003	0.003	0.003	0.003	0.003
12	Perennial Ice/Snow	0.012	0.012	0.012	0.012	0.012	0.012	0.012	0.012	0.012	0.012	0.012	0.012	0.012
21	Developed, Open Space	0.100	0.100	0.100	0.140	0.080	0.090	0.090	0.090	0.100	0.100	0.120	0.120	0.120
22	Developed, Low Intensity	0.350	0.350	0.350	0.360	0.350	0.430	0.500	0.420	0.340	0.340	0.360	0.290	0.290
23	Developed, Medium Intensity	0.530	0.530	0.530	0.620	0.580	0.730	0.840	0.620	0.480	0.480	0.590	0.530	0.530
24	Developed, High Intensity	0.380	0.380	0.380	0.440	0.420	0.920	1.550	0.440	0.350	0.350	0.510	0.310	0.310
31	Barren Land	0.100	0.100	0.100	0.140	0.080	0.090	0.090	0.090	0.100	0.100	0.120	0.120	0.120

LULC Class	Description	VA	MD	DE	PA	NJ	NY	MAN	LONG IS	CT	RI	MA	NH	ME
32	Unconsolidated Shore*	0.100	0.100	0.100	0.140	0.080	0.090	0.090	0.090	0.100	0.100	0.120	0.120	0.120
41	Deciduous Forest	0.900	0.900	0.900	0.900	0.900	0.900	0.900	0.900	0.900	0.900	0.900	0.900	0.900
42	Evergreen Forest	0.900	0.900	0.900	0.900	0.900	0.900	0.900	0.900	0.900	0.900	0.900	0.900	0.900
43	Mixed Forest	0.900	0.900	0.900	0.900	0.900	0.900	0.900	0.900	0.900	0.900	0.900	0.900	0.900
52	Shrubland	0.120	0.120	0.120	0.140	0.130	0.130	0.130	0.130	0.110	0.110	0.130	0.110	0.110
71	Grasslands / Herbaceous	0.040	0.040	0.040	0.040	0.040	0.050	0.050	0.050	0.040	0.050	0.040	0.040	0.040
81	Pasture / Hay	0.050	0.050	0.050	0.050	0.060	0.050	0.050	0.050	0.050	0.050	0.050	0.060	0.060
82	Cultivated Crops	0.050	0.050	0.050	0.050	0.050	0.060	0.060	0.060	0.060	0.060	0.060	0.060	0.060
90	Woody Wetlands	0.900	0.900	0.900	0.900	0.900	0.900	0.900	0.900	0.900	0.900	0.900	0.900	0.900
95	Emergent Herbaceous Wetlands	0.100	0.100	0.100	0.100	0.080	0.100	0.100	0.100	0.090	0.090	0.090	0.090	0.090

4.4.3 LULC codes 21 and 22 and MRLC-NLCD Data

The NLCD Percent Tree Canopy layer is an independent, per-pixel estimate of tree canopy percentage derived from imagery and ancillary data. Figure 4-54 displays the tree canopy layer for Florida. The tree canopy layer is used in the following equations to account for increased surface roughness in developed, open spaces (LULC 21) and developed, low intensity (LULC 22) areas due to the presence of trees:

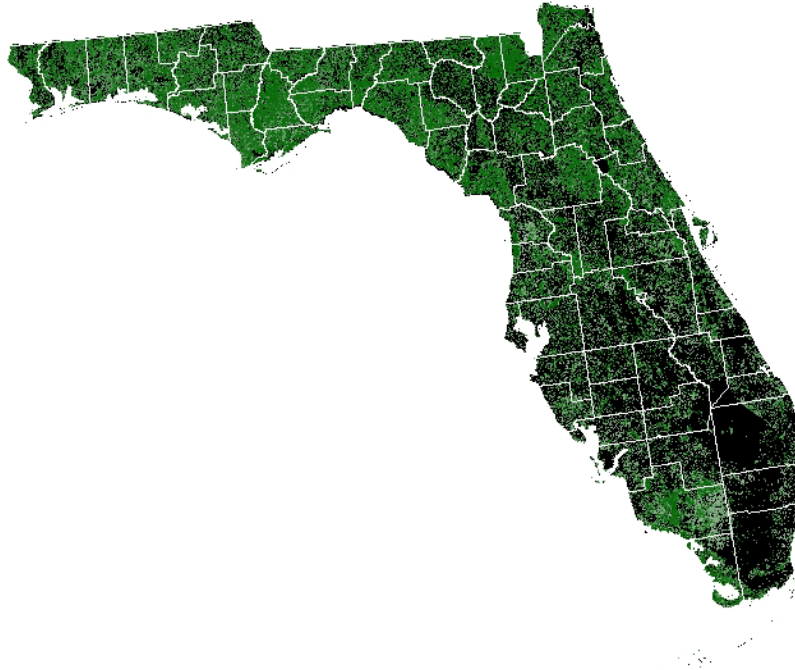


Figure 4-54 Percent Tree Canopy for the State of Florida

For Developed, Open Space (LULC 21):

Equation 4-30

$$z_{0dos} = \sqrt{z_{0brsc}^2 + (z_{0ef}^2 - z_{0brsc}^2) * \left(\frac{P_{Tdos}}{P_{Tef}}\right)^2}$$

Where:

- z_{0dos} z_0 for Developed, Open Space
- z_{0brsc} z_0 for Bare Rock/Sand/Clay (NLCD 2001)
- z_{0ef} z_0 for Evergreen Forest
- P_{Tdos} % tree canopy in Developed, Open Space (by county)
- P_{Tef} % tree canopy in Evergreen Forest (by county)

For Developed, Low Intensity (LULC 22):

Equation 4-31

$$z_{0dli} = \sqrt{z_{0lir}^2 + (z_{0ef}^2 - z_{0lir}^2) * \left(\frac{P_{Tdli}}{P_{Tef}}\right)^2}$$

Where:

z_{0dli}	z_0 for Developed, Low Intensity
z_{0lir}	z_0 for Low Intensity Residential (NLCD 2001)
z_{0ef}	z_0 for Evergreen Forest
P_{Tdli}	% tree canopy in Developed, Low Intensity (by county)
P_{Tef}	% tree canopy in Evergreen Forest (by county)

As noted in the equations above, the variation in z_0 mapping for these two particular LULC codes is implemented at the county level.

4.4.4 Census Tract-and Census Block Averaged Roughness Length

Using the roughness length-mapped NLCD data, average roughness lengths have been computed for the Year 2010 Census tracts and blocks.

At the Census block level, terrain roughness was computed by taking the average z_0 value assigned to LULC data that overlapped the Census block spatially. However, for those Census blocks that had less than approximately one square kilometer in area, the average z_0 value computed was based on a circular area one kilometer in diameter centered at the centroid of the Census block. This was done to obtain a minimum fetch of approximately 500 meters for small Census blocks.

At the Census tract level, z_0 values were computed by weighting Census block z_0 values with building square footage as per Equation 4-32.

Equation 4-32

$$Z_t = \sum_{i=1}^n Z_{ci} * \frac{S_{Ci}}{S_{Ti}}$$

Where:

Z_t	Terrain roughness at the tract level
Z_{ci}	Terrain roughness computed for Census block i
S_{ci}	Total building square footage for Census block i
S_T	Total building square footage for the Census tract
n	Number of Census blocks in the tract

This approach weights the Census tract surface roughness towards those Census blocks that have more buildings contained within them instead of simply taking an unweighted average of the Census block surface roughnesses.

Examples developed during the initial processing and data development using the 2010 census tract shapes are presented in Figure 4-55 and Figure 4-56 and Figure 4-57 for North Carolina and Texas, respectively, where two counties are shown for each state, one coastal county and another relatively inland. For North Carolina, New Hanover County is the coastal county and Wake County is the inland county. For Texas, two adjacent counties (Harris and Galveston) were arbitrarily selected along with part of a third county (Chambers). By comparing the land cover including the built-up areas in the counties to the surface roughness values, the results are reasonable.

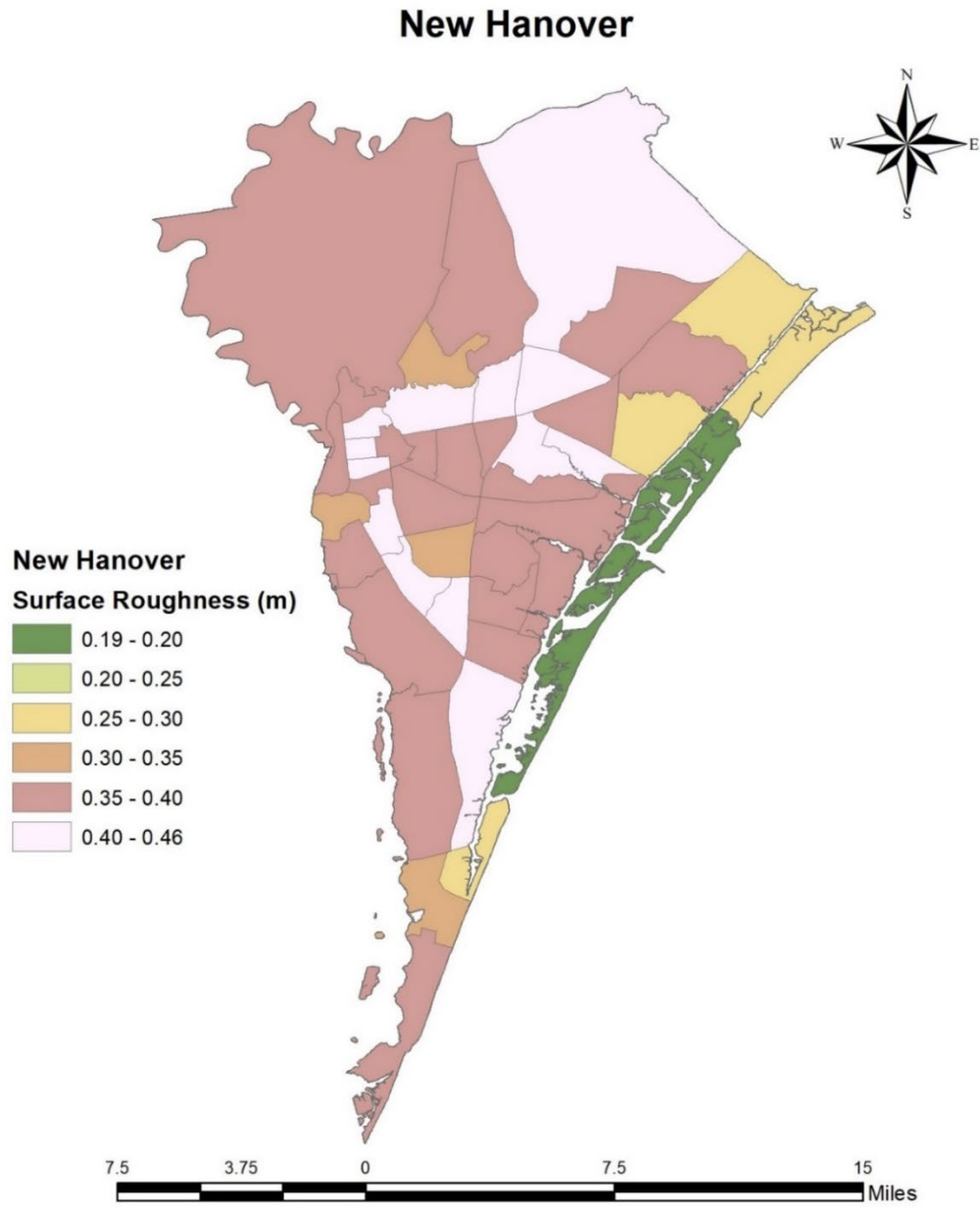


Figure 4-55 Census Tract-Averaged Roughness for New Hanover

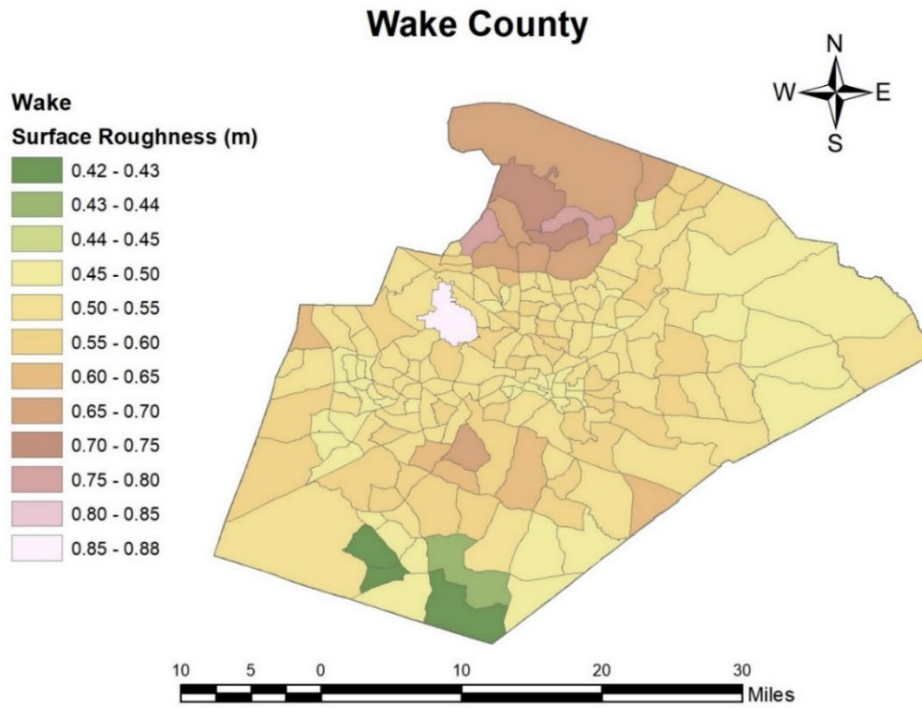


Figure 4-56 Census Tract-Averaged Roughness for Wake County

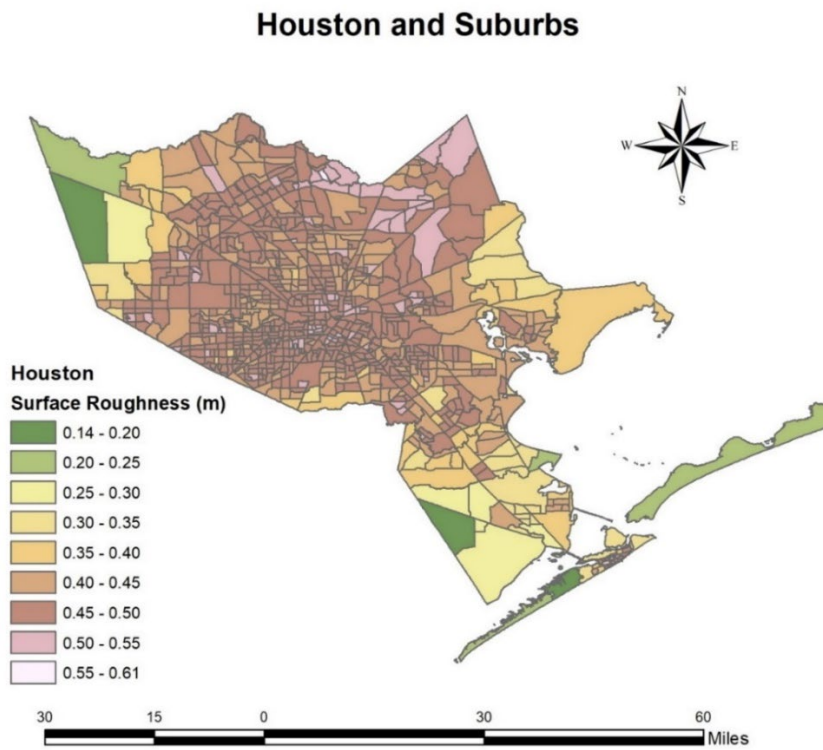


Figure 4-57 Census Tract-Averaged Roughness Length Derived from NLCD Data, Texas

4.4.5 Comparisons of z_0 Values Computed from NLCD Data on Rectangular Grids with Empirically Assigned z_0 Values

In the initial stages of the hurricane model development effort, averaged z_0 values were also computed from NLCD data on 1.8 kilometers by 1.2 kilometers rectangular grids and compared to empirically assigned z_0 values based on observations from aerial photographs. Examples of the comparison are presented in Figure 4-58 and Table 4-15, Figure 4-59 and Table 4-16, Figure 4-60 and Table 4-17, and Figure 4-61 and Table 4-18 for selected locations in Texas, Florida, North Carolina, and Rhode Island, respectively. The grid shown in the map correlates with the grid values in the corresponding table. The correlation between the two sets of z_0 values is shown in Figure 4-62, Figure 4-63, Figure 4-64, and Figure 4-65 for these four locations, respectively. The correlation coefficients are, respectively, 0.88, 0.93, 0.63, and 0.77 for the four locations. The results from all four locations are combined in Figure 4-66, for which the correlation coefficient is 0.926, which is higher than the average of the four individual correlation coefficients. This reflects that estimation of z_0 values using NLCD data provides better relative accuracy when involving a larger variety of land cover characteristics than for a smaller, localized land area. These comparisons serve as a check on the reasonableness of averaged z_0 values computed from NLCD data. It indicates that the degree of agreement is acceptable in general, except for a few grid cells that, in particular, involve commercial high-rise buildings in downtown areas, such as for the studied cases of Raleigh, NC, and Miami, FL.

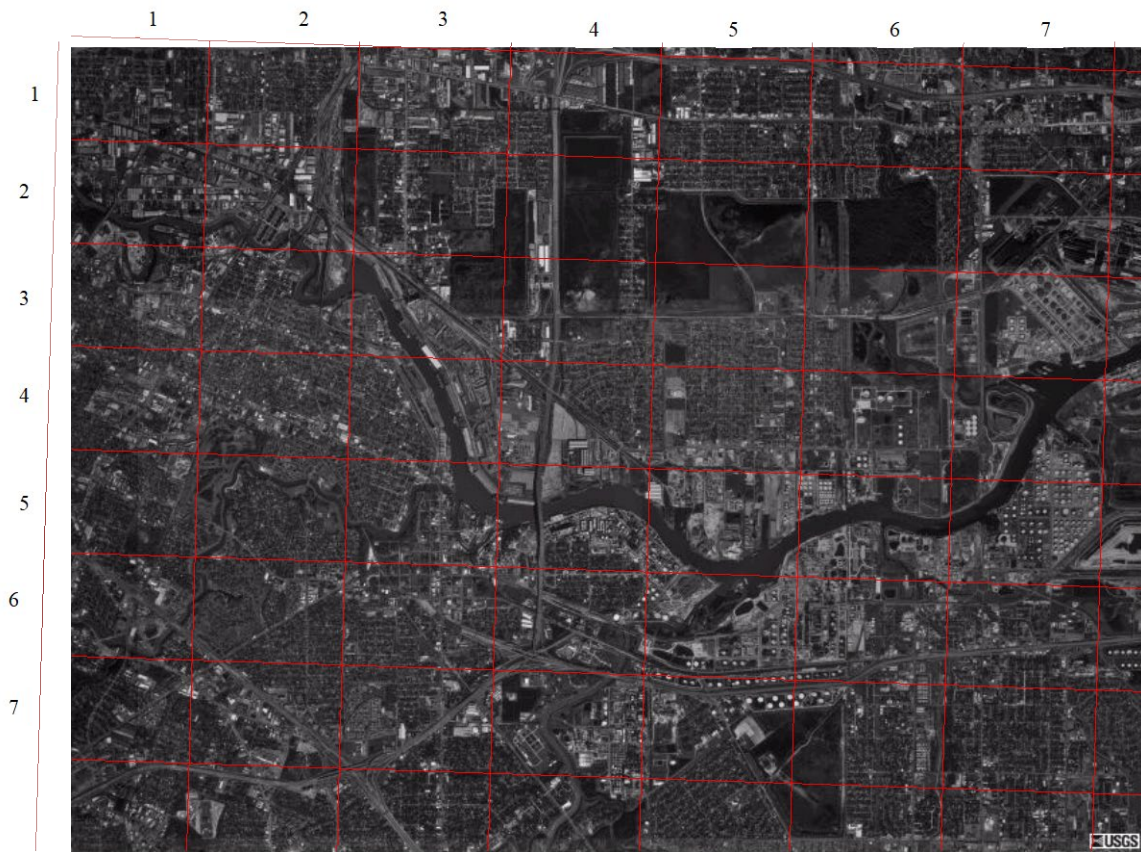


Figure 4-58 z_0 Values Computed from NLCD Data and Assigned Empirically for Houston, TX

Table 4-15 z Values Computed from NLCD Data and Assigned Empirically for Houston, TX

Assigned Z_0		Row Numbers (From Figure 4-58)						
		1	2	3	4	5	6	7
Column Numbers (From Figure 4-58)	1	0.45	0.45	0.45	0.40	0.40	0.40	0.40
	2	0.40	0.45	0.32	0.30	0.40	0.40	0.40
	3	0.45	0.48	0.40	0.32	0.33	0.30	0.35
	4	0.50	0.45	0.42	0.40	0.45	0.30	0.28
	5	0.42	0.30	0.40	0.35	0.32	0.32	0.35
	6	0.42	0.30	0.42	0.40	0.35	0.40	0.38
	7	0.40	0.45	0.48	0.32	0.32	0.40	0.42
Computed Z_0		1	2	3	4	5	6	7
Column Numbers (From Figure 4-58)	1	0.447	0.441	0.438	0.367	0.372	0.384	0.408
	2	0.418	0.428	0.372	0.320	0.414	0.341	0.414
	3	0.471	0.483	0.399	0.332	0.330	0.341	0.373
	4	0.491	0.468	0.429	0.403	0.421	0.339	0.305
	5	0.416	0.304	0.385	0.358	0.361	0.327	0.389
	6	0.448	0.319	0.409	0.410	0.397	0.429	0.418
	7	0.394	0.439	0.431	0.391	0.389	0.403	0.423



Figure 4-59 Z_0 Values Computed from NLCD Data and Assigned Empirically for Miami, FL, Including Downtown (Cell # 6-3)

Table 4-16 z_0 Values Computed from NLCD Data and Assigned Empirically for Miami, FL, Including Downtown (Cell # 6-3)

Assigned Z_0		Row Numbers (From Figure 4-59)					
		1	2	3	4	5	6
Column Numbers (From Figure 4-59)	1	0.45	0.43	0.20	0.01	0.10	0.30
	2	0.42	0.45	0.10	0.02	0.15	0.25
	3	0.45	0.50	0.15	0.01	0.20	0.30
	4	0.52	0.60	0.35	0.10	0.10	0.30
	5	0.55	0.50	0.40	0.15	0.10	0.25
	6	0.55	0.50	0.50	0.02	0.10	0.10
Computed Z_0		1	2	3	4	5	6
Column Numbers (From Figure 4-59)	1	0.472	0.470	0.192	0.014	0.113	0.300
	2	0.447	0.464	0.140	0.036	0.129	0.260
	3	0.494	0.463	0.178	0.017	0.160	0.290
	4	0.463	0.447	0.225	0.127	0.137	0.306
	5	0.423	0.426	0.255	0.196	0.093	0.266
	6	0.485	0.468	0.224	0.040	0.107	0.114

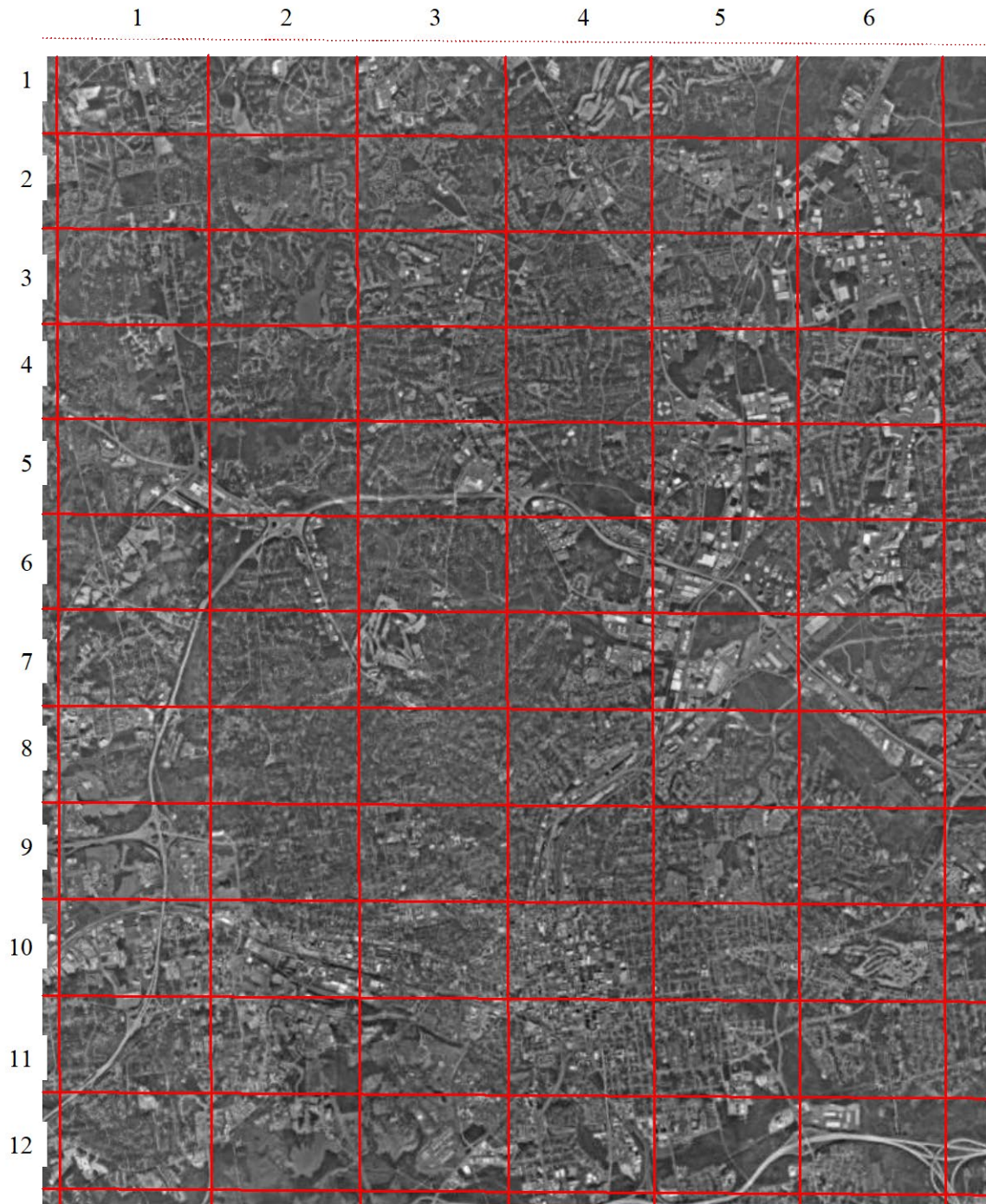


Figure 4-60 z_0 Values Computed from NLCD Data and Assigned Empirically for Raleigh, NC, Including Downtown (Cell # 10-4)

Table 4-17 z₀ Values Computed from NLCD Data and Assigned Empirically for Raleigh, NC, Including Downtown (Cell # 10-4)

Assigned Z ₀		Row Numbers (From Figure 4-60)					
		1	2	3	4	5	6
Column Numbers (From Figure 4-60)	1	0.60	0.60	0.55	0.45	0.50	0.55
	2	0.60	0.65	0.60	0.50	0.55	0.50
	3	0.60	0.55	0.52	0.55	0.55	0.48
	4	0.60	0.60	0.60	0.60	0.58	0.50
	5	0.50	0.58	0.50	0.55	0.55	0.55
	6	0.50	0.55	0.58	0.55	0.50	0.50
	7	0.55	0.55	0.45	0.50	0.45	0.50
	8	0.50	0.60	0.60	0.55	0.48	0.55
	9	0.35	0.55	0.50	0.48	0.50	0.55
	10	0.42	0.42	0.45	0.62	0.45	0.40
	11	0.45	0.40	0.35	0.62	0.45	0.45
	12	0.50	0.50	0.35	0.45	0.55	0.55
Computed Z ₀		1	2	3	4	5	6
Column Numbers (From Figure 4-60)	1	0.557	0.546	0.518	0.482	0.619	0.666
	2	0.567	0.562	0.604	0.498	0.512	0.491
	3	0.622	0.580	0.514	0.535	0.534	0.479
	4	0.607	0.597	0.542	0.533	0.525	0.520
	5	0.519	0.584	0.524	0.522	0.487	0.476
	6	0.537	0.528	0.542	0.490	0.448	0.500
	7	0.573	0.572	0.499	0.529	0.448	0.500
	8	0.491	0.552	0.535	0.487	0.449	0.536
	9	0.365	0.521	0.489	0.465	0.513	0.524
	10	0.418	0.430	0.451	0.399	0.495	0.462
	11	0.527	0.466	0.428	0.411	0.508	0.539
	12	0.554	0.522	0.375	0.430	0.532	0.524

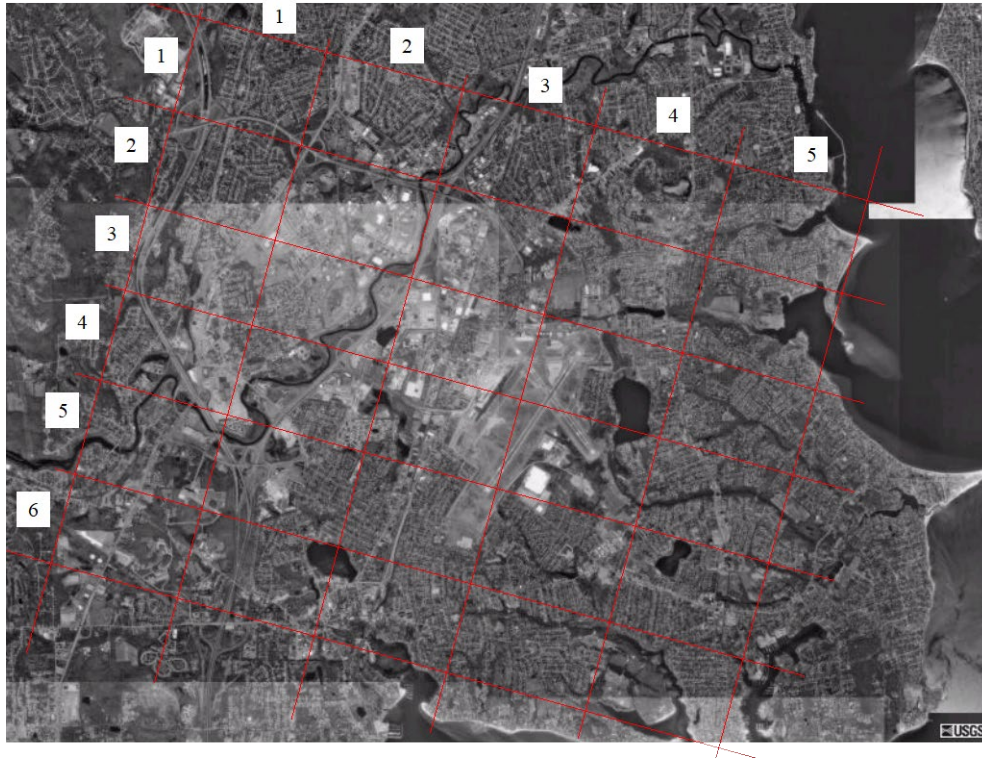


Figure 4-61 z_0 Values Computed from NLCD Data and Assigned Empirically for a Location in South Suburban of Providence, RI

Table 4-18 z_0 Values Computed from NLCD Data and Assigned Empirically for a Location in South Suburban of Providence, RI

Assigned Z_0		Row Numbers (From Figure 4-61)					
		1	2	3	4	5	6
Column Numbers (From Figure 4-61)	1	0.38	0.35	0.32	0.34	0.32	0.30
	2	0.40	0.32	0.35	0.40	0.30	0.25
	3	0.45	0.35	0.28	0.20	0.40	0.30
	4	0.40	0.40	0.32	0.35	0.40	0.30
	5	0.40	0.30	0.38	0.42	0.38	0.25
	6	0.45	0.40	0.38	0.45	0.32	0.10
Computed Z_0		1	2	3	4	5	6
Column Numbers (From Figure 4-61)	1	0.409	0.368	0.367	0.397	0.317	0.300
	2	0.382	0.346	0.357	0.388	0.324	0.260
	3	0.406	0.354	0.312	0.250	0.419	0.290
	4	0.394	0.364	0.305	0.349	0.389	0.306
	5	0.427	0.381	0.330	0.380	0.367	0.266
	6	0.507	0.447	0.328	0.405	0.351	0.114

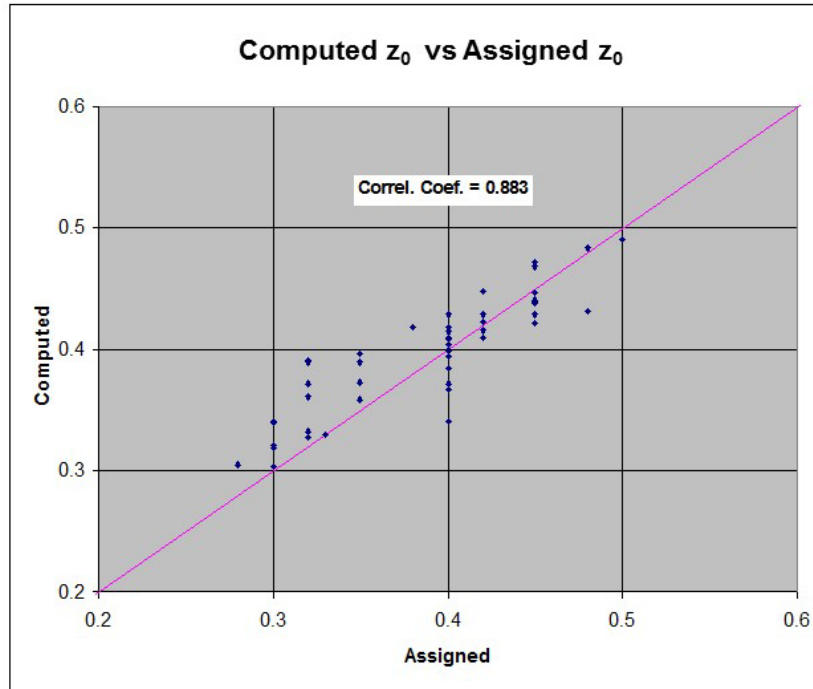


Figure 4-62 Comparison Between z_0 Values Computed from NLCD Data and Assigned Empirically for a Location in East Suburban of Houston, TX

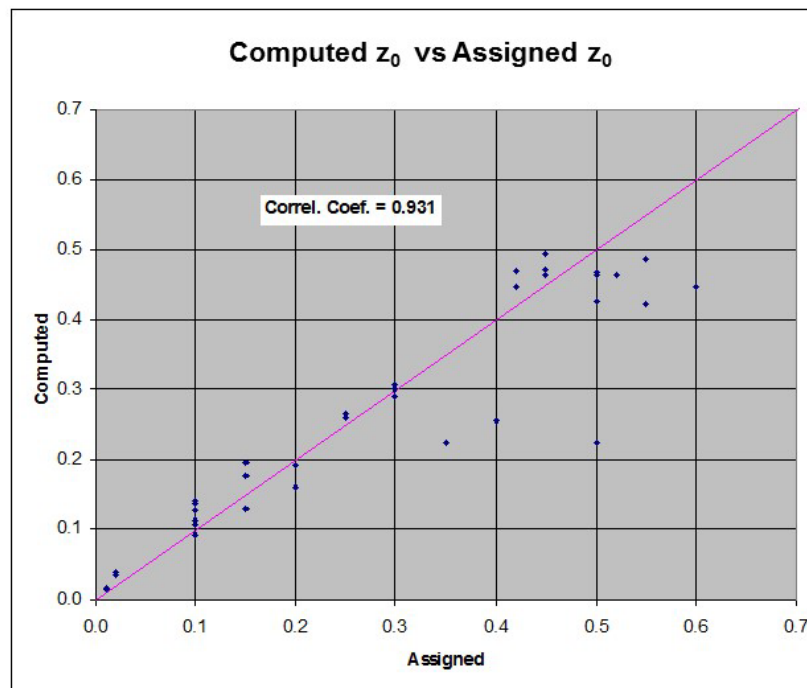


Figure 4-63 Comparison Between z_0 Values Computed from NLCD Data and Assigned Empirically for Miami, FL, Including Downtown Area

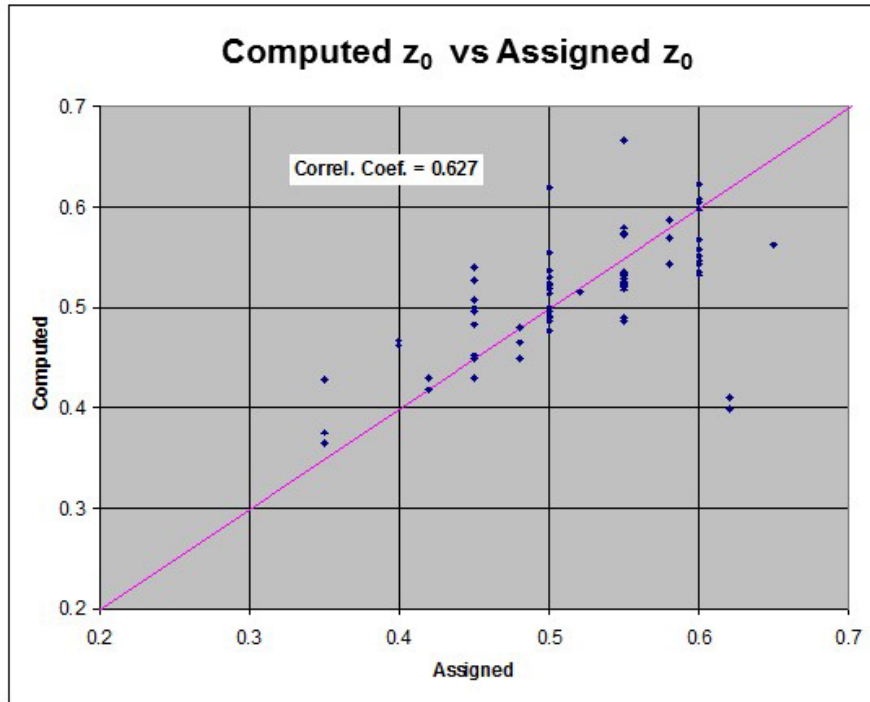


Figure 4-64 Comparison Between z_0 Values Computed from NLCD Data and Assigned Empirically for Raleigh, NC, Including Downtown Area

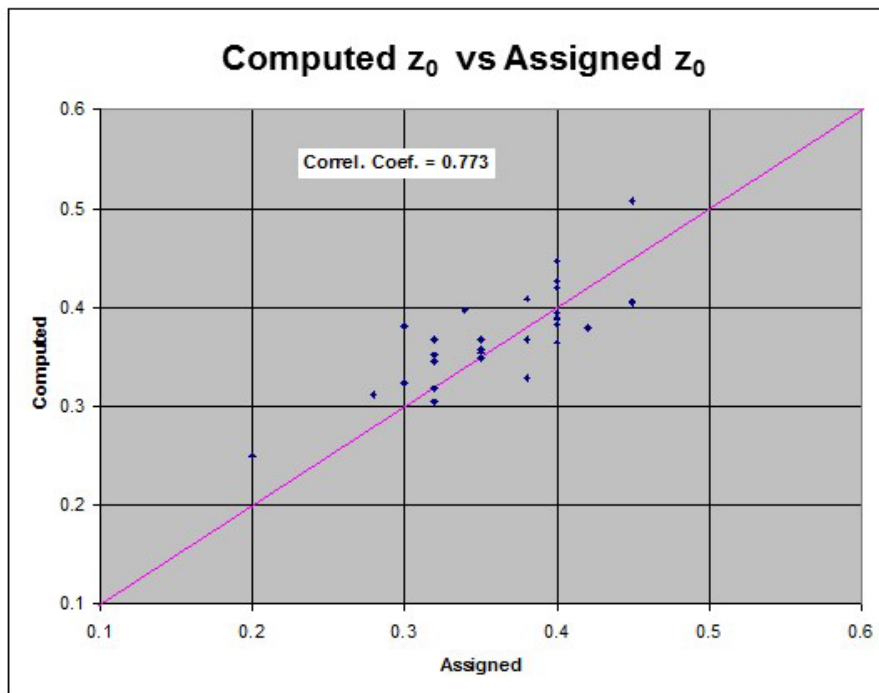


Figure 4-65 Comparison Between z_0 Values Computed from NLCD Data and Assigned Empirically for a Location in Southern Providence, RI

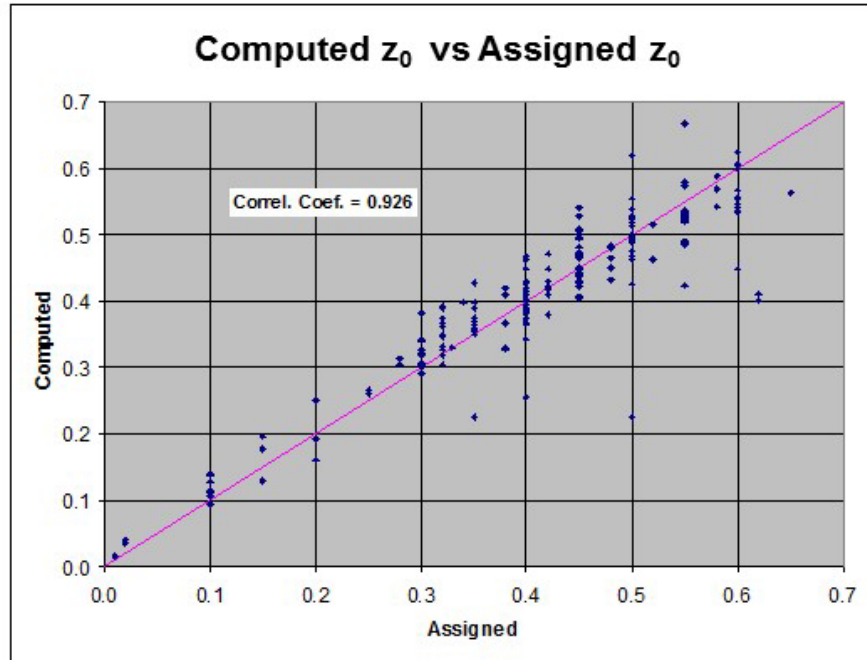


Figure 4-66 Comparison Between z_0 Values Computed from NLCD Data and Assigned Empirically for the Four Locations Studied

4.4.6 Example of Roughness Length (z_0) Calculation Using Lettau’s Formula

The empirical relationship between z_0 and the ground roughness physical dimensions proposed by Lettau (1969) forms the basis of the methodology given in ASCE 7-02 for the computation of the roughness length (z_0) for the purpose of determining if a building is located in Exposure B (defined as Suburban Terrain) or Exposure C (defined as Open Terrain). In ASCE 7-02, a building is considered to be located in a suburban terrain (Exposure B) if the value of z_0 computed using Lettau’s method is greater than or equal to 0.15 meters and less than 0.7 meters. The representative value of Exposure B in ASCE 7-02 is defined with a surface roughness of 0.3 meters.

Recall that Lettau’s formula for estimating the surface roughness length, z_0 , is:

Equation 4-33

$$z_0 \approx 0.5HS/A$$

Where:

- H is the average height of the obstacle in the upwind terrain
- S is the average projected frontal area per obstruction presented to the wind
- A is the average area of ground occupied by each obstruction (including the open area surrounding it)

When calculating an average value of z_0 over a region, S and A can be substituted by the total projected frontal area of all the obstacles upwind of a site and the total ground area these obstacles collectively occupy.

When trees or bushes are present, their contribution to the frontal area must also be considered. ASCE 7-02 suggests that for conifers and other evergreens no more than 50% of their gross frontal area can be taken to be effective in obstructing the wind. For deciduous trees and bushes ASCE 7-02 states that no more than 15% of the gross frontal area can be taken to be effective in obstructing the wind, however in hurricane prone regions, trees are generally still in full leaf during the time period hurricanes are likely to impact a region, thus an effective area of 50% is probably more appropriate. Recall, that the objective in estimating the surface roughness is to enable a realistic estimate of losses, and thus there should not be any tendency to choose a low value of frontal area in an attempt to obtain a conservative (low) value of z_0 as may be done in a building design situation.

The following is a step-by-step demonstration to show how to use the Digital Orthophoto Quarter Quads (DOQQs) to obtain the information required for Lettau's formula and the logic in defining the input parameters. For demonstration purpose, the DOQQs from one medium density residential area in each of five counties in Florida (Escambia, Lee, Dade, Palm Beach, and Duval, see Figure 4-67, Figure 4-68, Figure 4-69, Figure 4-70, and Figure 4-71) are used.

Medium density residential areas are selected because:

1. Building density is in such a range that the possibility of a building being shadowed by trees is small and ambiguity does not exist in distinguishing two separate buildings
2. Building heights for a residential area are relatively uniform and relatively easy to estimate, thus providing more reliable results.

It may be difficult to accurately determine an obstacle's height by looking at the DOQQs or aerial photography. Sometimes, the length of the sun shadow projected by an obstacle can help if any known reference object exists. Familiarity with a region will aid considerably in reducing errors associated with estimates of both building and tree heights.

Here, using Figure 4-67 as an example, the steps used to calculate the roughness length with Lettau's method are demonstrated. This is a medium density residential area in the Panhandle of Florida (Escambia County). The wind was assumed coming from the direction shown by the arrow in Figure 4-67. The study area defined by the polygon shown in Figure 4-67 has a total ground area of about 60,800 square meters. By counting all the buildings in the study area, a total frontal (perpendicular to the wind direction) length of about 630 meters was estimated. In this example, the homes are assumed to exist in a subdivision having a mixture of one- and two-story homes, with an assumed average roof height of about 6 meters. Therefore, the total frontal area from all the buildings is: 6 meters * 630 meters = 3,780 square meters.



Figure 4-67 Medium Density Residential Area in Escambia County



Figure 4-68 Medium Density Residential Area in Lee County



Figure 4-69 Medium Density Residential Area in Dade County



Figure 4-70 Medium Density Residential Area in Palm Beach County



Figure 4-71 Medium Density Residential Area in Duval County

In this demonstration, the trees were assumed to be about 15 meters tall. The gross tree frontal area is estimated to be roughly 1.5 times the building frontal area by looking at Figure 4-67. Therefore, the total effective tree frontal area is about $(1.5 * 3780) * 50\% = 2835$ square meters, given that the ratio of effective area to gross frontal area is assumed to be 50% for both deciduous and coniferous trees during hurricane seasons.

Then, by using Lettau's equation, the roughness length for this area is calculated from:

Equation 4-34

$$z_0 = 0.5 \frac{HS}{A} = 0.5 \frac{(HS)_{\text{bldg}} + (HS)_{\text{tree}}}{A} = 0.5 \frac{6 * 3780 + 15 * 2835}{60800} = 0.5 \frac{22680 + 42525}{60800} = 0.56\text{m}$$

Note that when the trees are the major obstacles in the areas being investigated (which is common), significant uncertainties may exist in the estimated tree heights, frontal areas, and relative densities but as seen in the example given above, trees account for about two-thirds of the surface roughness length computed using Lettau's approach.

Similar procedures have been applied to the other DOQQs included in this section. The parameter values determined at each step for the five examples are listed in Table 4-19. The assumed wind directions are shown for Escambia County, Lee County, Dade County, Palm Beach County, and Duval County as shown in Figure 4-67, Figure 4-68, Figure 4-69, Figure 4-70, and Figure 4-71, respectively. The computed roughness lengths all fall into the definition of Exposure B (as defined in ASCE 7), and all

roughness lengths fall within the roughness length ranges given in Table 4-15 and Table 4-17 for Medium Density Residential.

Table 4-19 Examples for Roughness Length Calculation Using Lettau’s Formula

Parameter	Escambia County	Lee County	Dade County	Palm Beach County	Duval County
Ground Area (square meters)	60,800	225,000	77,000	150,000	35,000
Estimated Mean Roof Height (meters)	6	5	4.5	4.5	6
Building Frontal Length (meters)	630	2,800	1,000	2,900	240
Building Frontal Area (square meters)	3,780	14,000	4,500	1,3050	1,440
Mean Tree Height (meters)	15	6	-	6	15
Tree/Building Area Ratio	1.50	0.15	0.00	0.10	3.00
Tree Frontal Area (square meters)	5,670	2,100	0	1,305	4,320
SH (building)	22,680	70,000	20,250	58,725	8,640
Effective SH (trees)	42,525	6,300	0	3,915	32,400
Roughness Length z_0 (meters)	0.56	0.17	0.13	0.21	0.59

Note that the calculated roughness length is wind-direction dependent. For uniform building orientations within a region, the difference in the computed roughness lengths for different wind directions can be significant. For instance, in the Palm Beach County example, if the wind direction changes $\pm 90^\circ$, the projected width of the buildings is in the range of 50% to 70% of that seen in the worked example, and thus the computed roughness length reduces to 50% to 70% of the original value. To remove the effect of directionality associated with building orientation, the frontal width of the building can be substituted with an effective width defined as the square root of the estimated plan area.

Although Lettau’s method provides a convenient and quantitative means to estimate roughness length from DOQQs, aerial photography, etc., it should be used with caution. Engineering judgment needs to be applied to the results through comparisons with estimates of z_0 given in the literature. Inevitably, some variations and uncertainties are associated with the estimation of the surface roughness length in any terrain, but as will be shown later, this parameter plays a very important role in the estimation of wind induced damage and loss.

4.4.7 Effect of Surface Roughness on Near Ground Gust Wind Speeds

In this section, the effects of z_0 on gust wind speeds (defined as a 3 second average) near the ground surface and on the hourly mean wind speed near the ground surface are shown. It is important to note that changes in wind speeds in areas of transitioning surface roughness are not treated in the default Hazus surface roughness model. However, a discussion of transition effects is provided in this section to assist the user in understanding their possible impact on damage and loss estimates. Transition effects are illustrated using the methodology described in ESDU (1983). The ESDU methodology forms

the basis of the fetch length requirements given in ASCE 7-02 to enable the user to determine what exposure category a building is in given information on the upstream fetch lengths.

Figure 4-72 shows the ratio of the wind speed, as normalized by the reference open terrain value, as a function of surface roughness and height above ground. Wind speed ratios are given for both the peak gust wind speed and the one hour mean wind speed. The data in Figure 4-72 clearly show that the effect of surface roughness is greatest near the ground ($z = 3$ meters and $z = 5$ meters), around the eave height of most single-story buildings. Figure 4-72, also shows that the change in wind speed (with respect to the reference terrain value) is less for the peak gust wind speed than for the mean wind speed. For example, at a height of 10 meters, a change in z_0 from 0.03 meters (open terrain) to 0.35 meters (typical suburban terrain), the peak gust wind speed reduces by about 18%, whereas the hourly average wind speed reduces by about 32%. The reduction in the wind speed associated with an averaging time of one minute is about 25%, falling almost exactly halfway between the reduction in gust wind speed and the reduction in the one hour mean wind speed. In Hazus, all damage and loss functions are given as a function of peak gust wind speed, not the one-minute wind speed.

The wind speed ratio data given in Figure 4-72 are for the case of a fully transitioned boundary layer (i.e., the wind has blown over a long enough fetch of new terrain that the flow characteristics are influenced only by the local terrain, and not the previous terrain). In reality, the wind at a given height does not change immediately to reflect the new terrain, but rather the flow gradually makes a transition, changing to reflect the characteristics associated with the new terrain. The distance over which this transition takes place varies with height, with the wind at lower heights changing more rapidly than wind at higher levels. Figure 4-73, Figure 4-74, and Figure 4-75 show examples of the rates of change of the mean and gust wind speeds as the terrain changes from an open terrain ($z_0 = 0.03$ meters) to an example suburban terrain ($z_0 = 0.3$ meters) for heights of 3 meters, 10 meters, and 50 meters, respectively. In each of the figures, the upper plot shows the wind speed ratio with respect to open terrain as a function of the distance into the new terrain, and the lower plot shows the percentage adjustment of the wind to the new terrain as a function of the distance. The lower plots suggest that the wind speed in the new terrain asymptotically approaches (but never reaches) the fully transitioned value. In ASCE 7-02, this problem was handled by defining the fetch required to assume a fully transitioned case as the distance over which the wind speed adjustment reaches about 80% of the fully transitioned value. Notice in the 3 meters height example, about 50% of the reduction occurs within the first 10 meters of the terrain change. Thus, homes located on the front row of a barrier island, or the front row in a subdivision facing open farmland, are actually situated within a transition zone. The effective wind speeds that these front row structures experience will be notably higher than those experienced by homes located even as close as one row back from these front-line homes.

Topographic effects on windspeed increases are treated differently for Hawaii and the U.S. Caribbean territories. For more information, see *Hazard Mitigation Study for the Hawaii Hurricane Relief Fund* (Applied Research Associates, Inc., 2001) and *Hazus Hurricane Wind for Puerto Rico and the U.S. Virgin Islands* (FEMA, 2021).

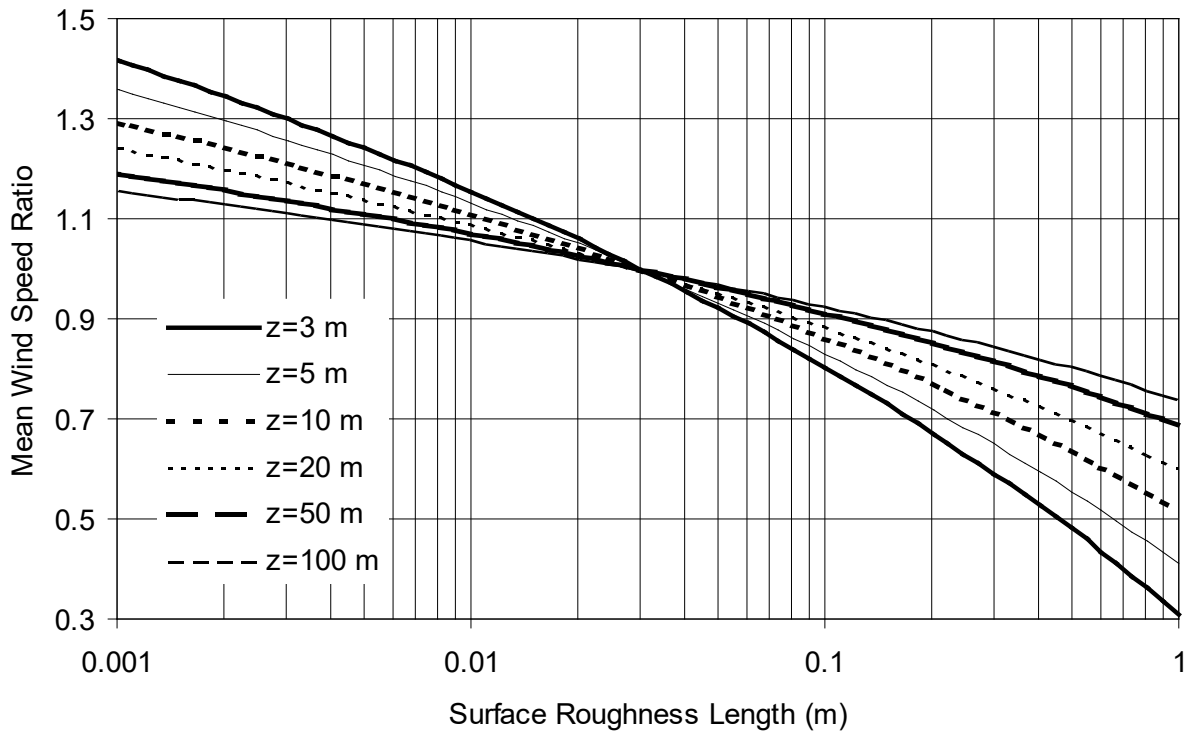
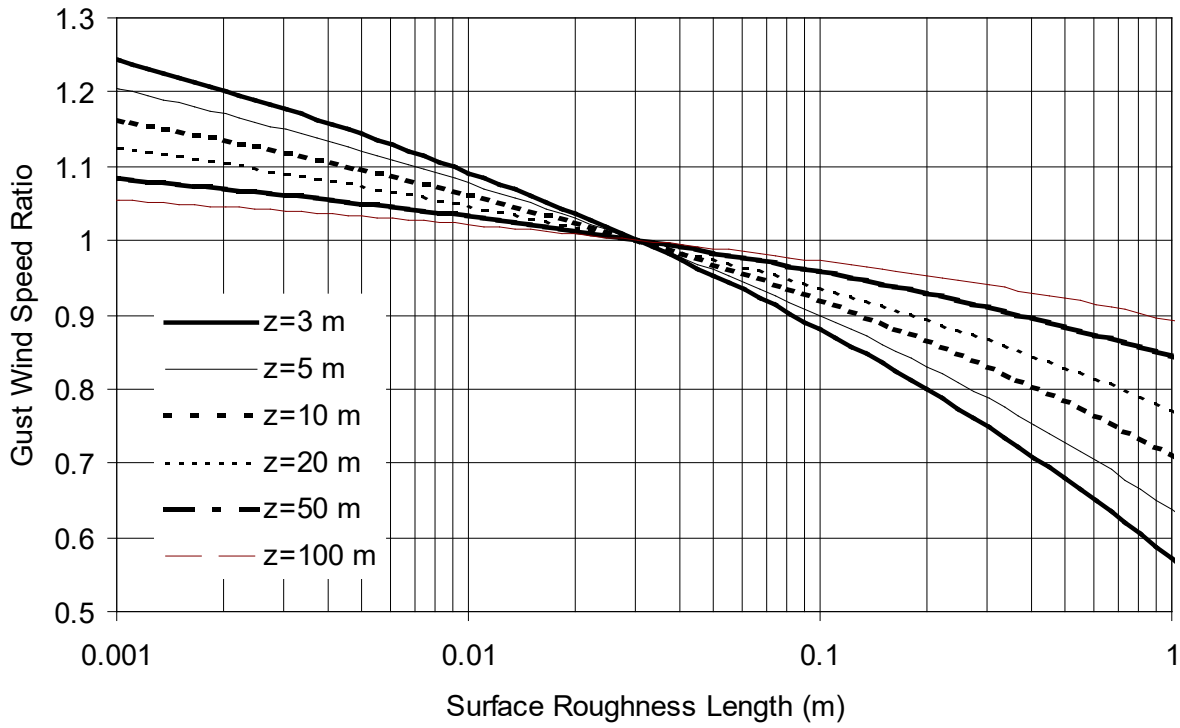


Figure 4-72 Wind Speed Ratios as a Function of Surface Roughness for Various Heights

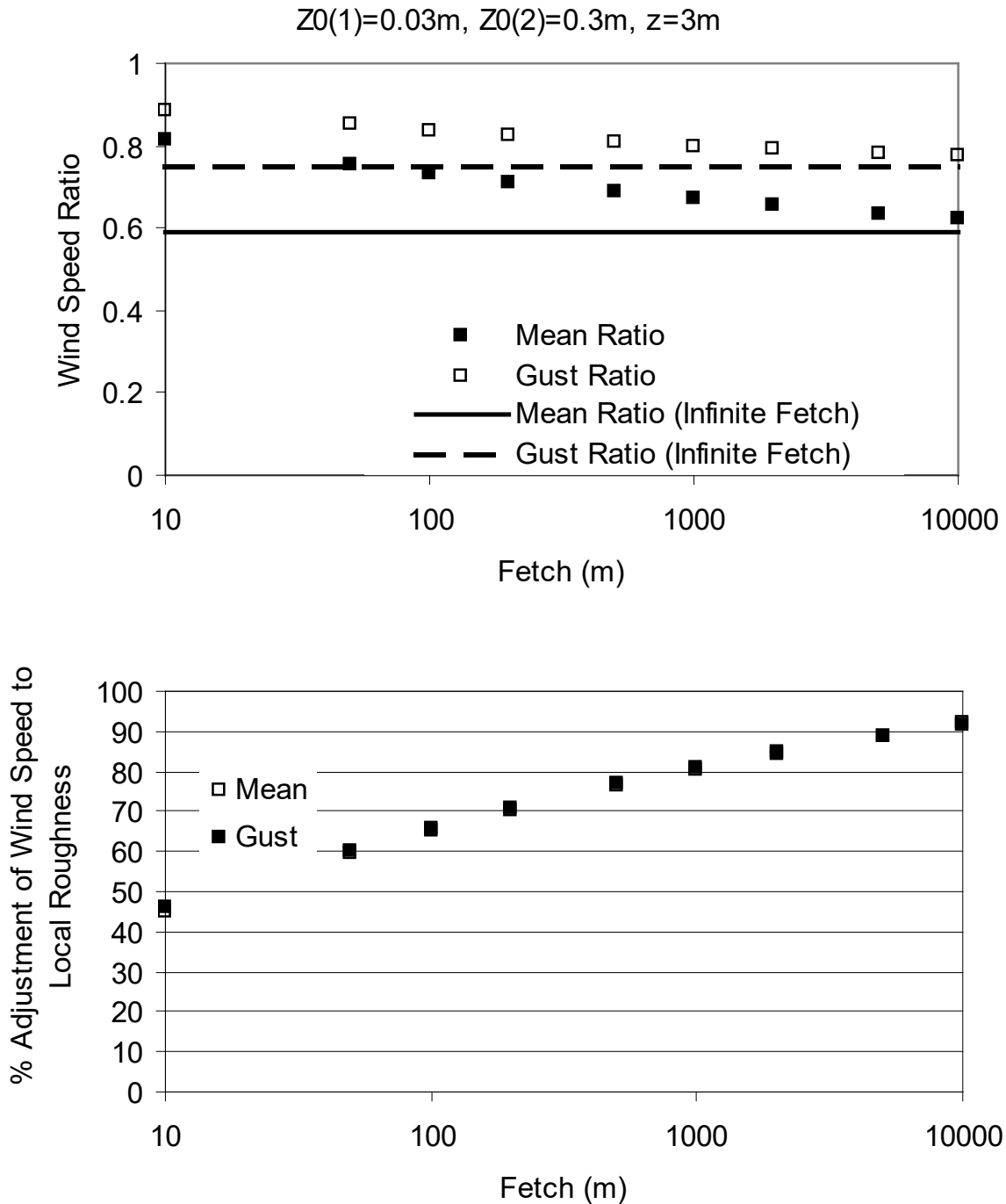


Figure 4-73 Reduction in Wind Speed at a Height of 3 meters (Open Terrain to Suburban Terrain)

In cases where loss studies are being performed in relatively small regions that encompass significant changes in terrain, it would be advisable to properly estimate the fraction of buildings that are likely to experience winds associated with terrains other than the default suburban values that would be appropriate for most of the building population.

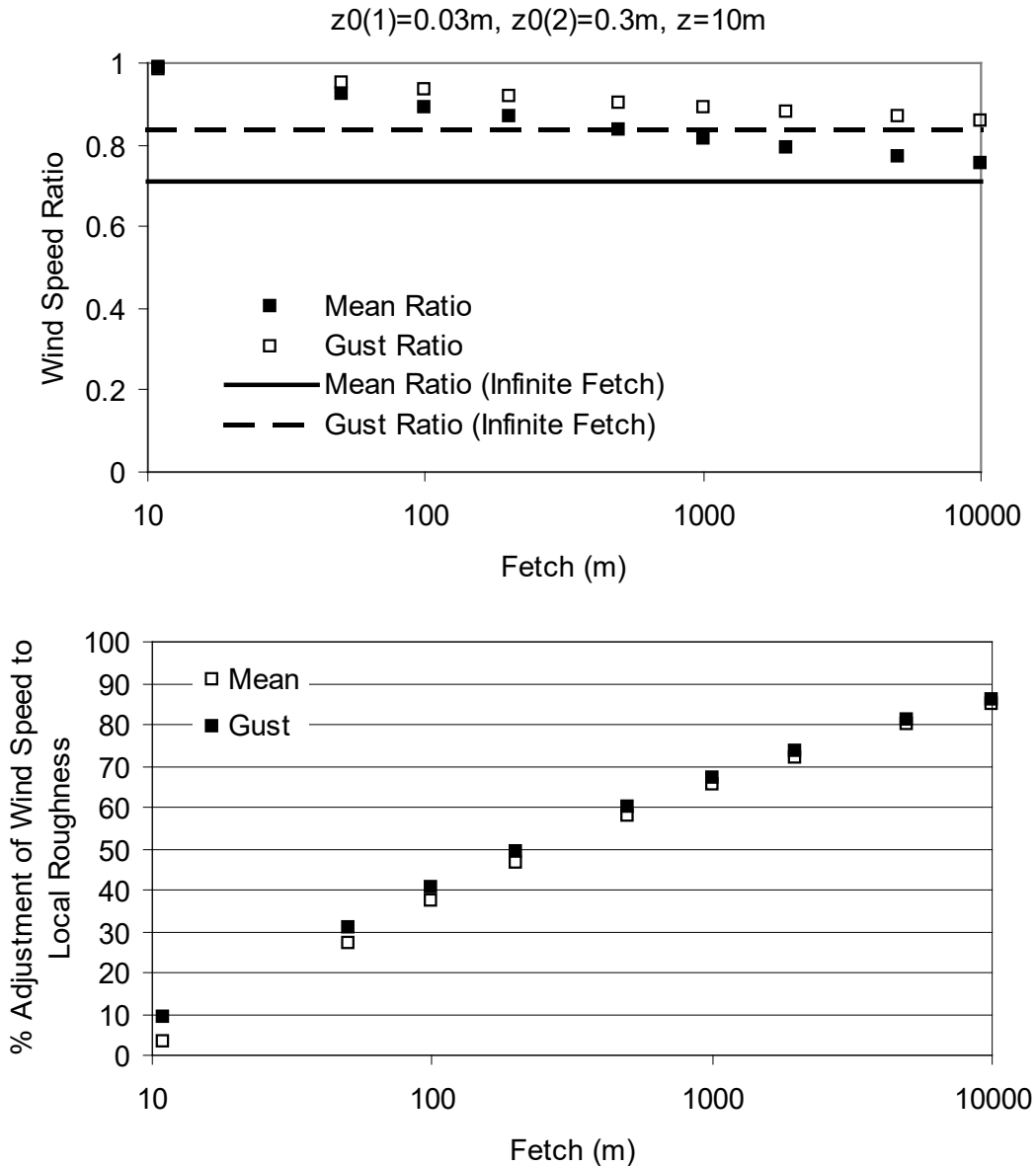


Figure 4-74 Reduction in Wind Speed at a Height of 10 meters (Open Terrain to Suburban Terrain)

In the case of the 50 meters height example (Figure 4-75), it is readily seen that even for a fetch distance of 1 kilometer, the wind speed has only undergone 30% of the full adjustment. This example indicates that for taller buildings relatively isolated or in front row, the appropriate terrain selection is governed by the terrain at distances of 1 kilometer or more away from the building rather than at the location of the building itself. It should also be recognized, that the taller the building, the less the effect of terrain on the wind speeds at roof height.

Figure 4-76 shows the rapid and significant reduction in wind speed at a height of 3 meters associated with a change in terrain from an open terrain to a heavily treed terrain. As shown in the upper graph, a 30% reduction in the peak gust wind speed (~70% reduction in wind load) occurs within the first 100

meters of the transition. This example clearly shows why significant reductions in observed damage are seen when comparing damage on barrier islands to that seen within forested regions of the mainland, even right at the coast.

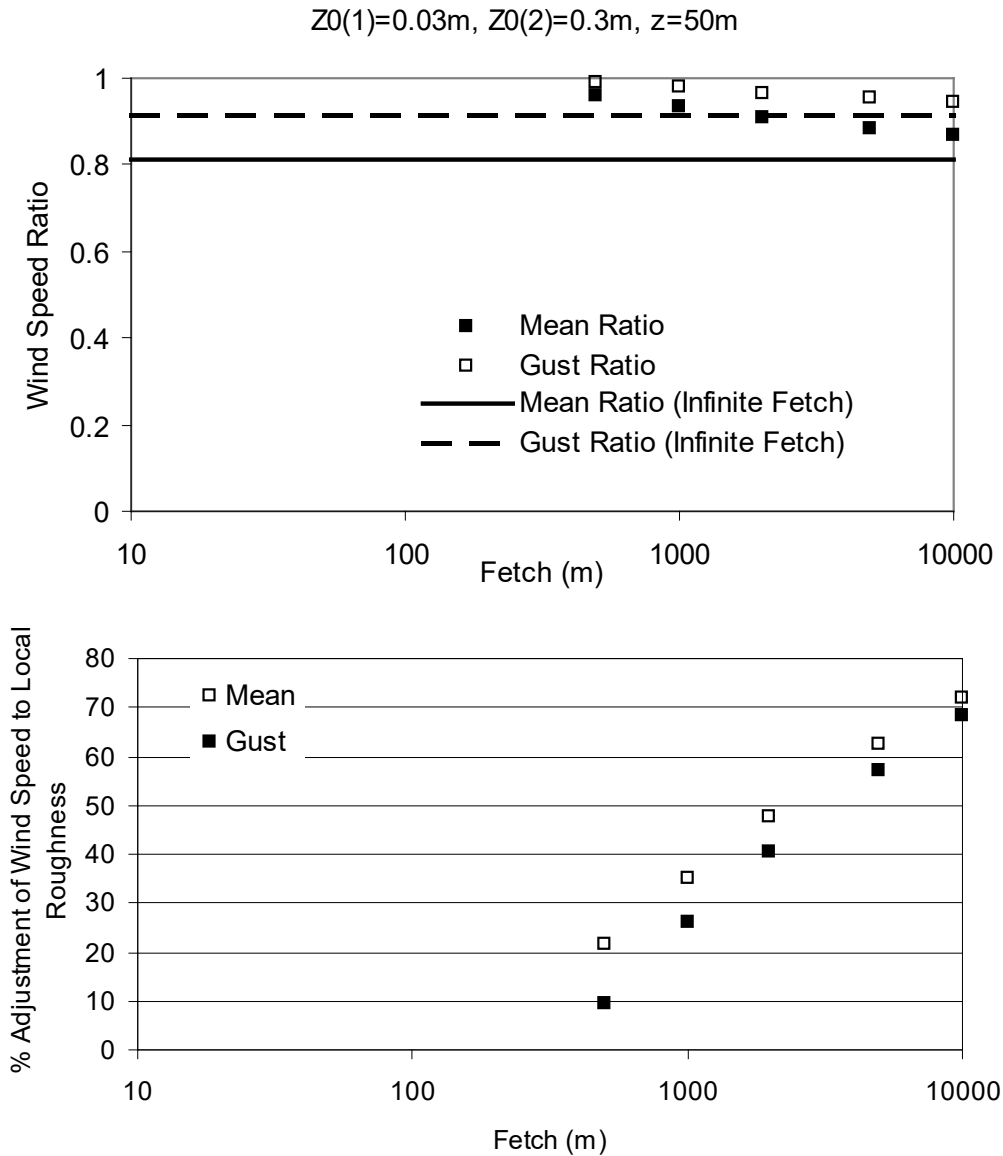


Figure 4-75 Reduction in Wind Speed at a Height of 50 meters (Open Terrain to Suburban Terrain)

Large changes in roughness associated with trees located very near the intra-coastal waterways are seen in many regions along the Gulf and Atlantic coasts.

Examples of fully transitioned peak gust profiles are shown in Figure 4-77 for a range of roughness lengths. These examples are given to show the impact of z_0 on the magnitude of the peak gust wind speed as a function of height. All gust profiles given in Figure 4-77 are referenced to the peak gust wind speed at a height of 10 meters in open terrain.

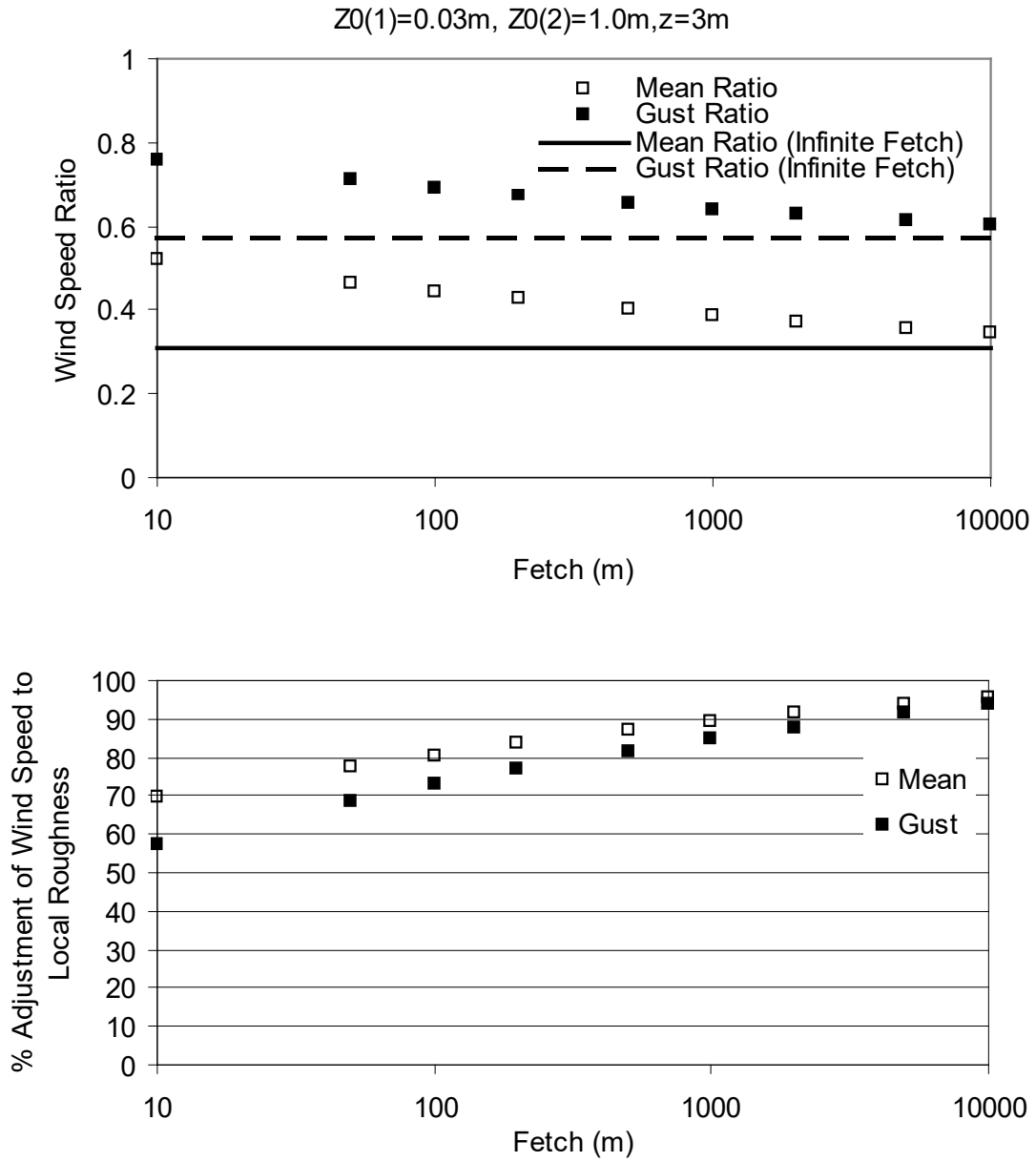


Figure 4-76 Reduction in Wind Speed at a Height of 10 meters (Open Terrain to Heavily Treed Terrain)

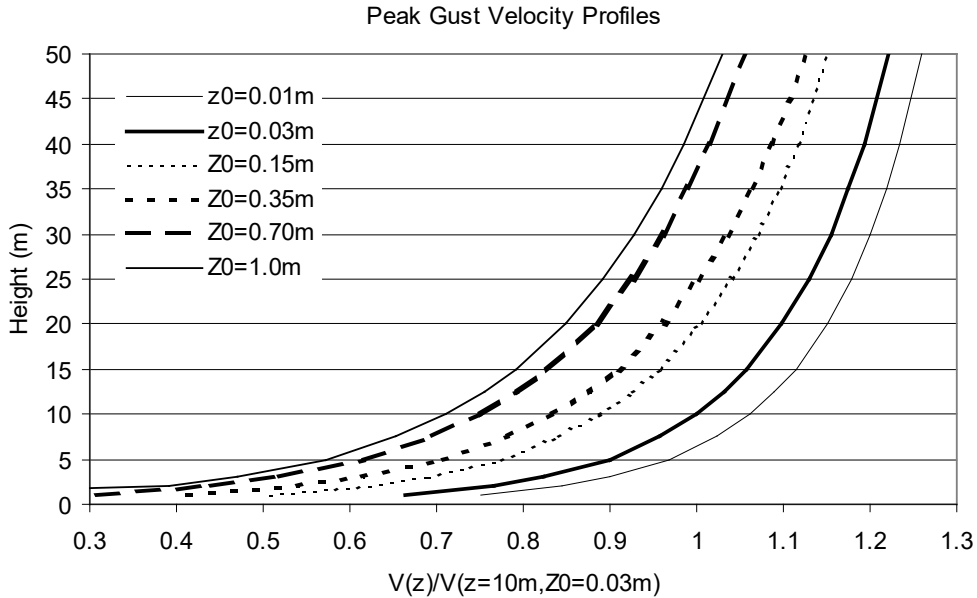


Figure 4-77 Examples of Peak Gust Velocity Profiles as a Function of z_0

4.5 Tree Blowdown

Damage to structures caused by windthrown trees is an ongoing problem in forested areas. During Hurricane Hugo for example, most of the damage to the electric power distribution system was caused not by the direct action of wind, but by trees falling on the distribution lines and breaking the lines (Cook, 1990). Tree debris produced by Hurricane Hugo also hampered emergency crews and delayed repairs to essential facilities (Cook, 1990). At Charleston Naval Base, windthrown trees broke buried water lines, disrupting the water supply (Strehmeyer, 1990).

Extreme winds associated with thunderstorms and extratropical storms also cause extensive tree-induced damage. For example, in May 1990, there were in excess of 300 separate reports of downed trees. Of the 150 reported downed power lines, approximately 30% were caused by trees falling across the lines. Of the 100 reports of damage to structures, approximately 40% were caused by downed trees, with one case producing a fatality.

Trees have both positive and negative effects in the presence of extreme winds. On the positive side, trees provide shelter to structures, reducing the likelihood of damage produced by the direct action of wind. On the negative side, the existence of many trees surrounding a structure increases the likelihood of a tree striking and damaging the structure.

This section describes the tree blowdown methodology implemented in Hazus and the two damage/loss models that use the results produced by the tree blowdown methodology. The first estimates the quantity of tree debris after a hurricane. The second estimates the additional economic loss to residential buildings and contents caused by fallen trees.

Figure 4-78 shows a high-level flow chart of the data and the models. The combination of tree data by census tract and a tree blowdown probability model provides the elements needed for estimating debris quantities, while the tree data, blowdown model, hit probability and damage model, along with a cost model, yield the estimation of damage and loss to residential buildings due to tree blowdown, given a defined hurricane climate.

Outside of Section 4, information on the damage and loss models for residential buildings and contents are presented in Section 5.3 and Section 8.3, and the tree debris methodology can be found in Section 6.3.

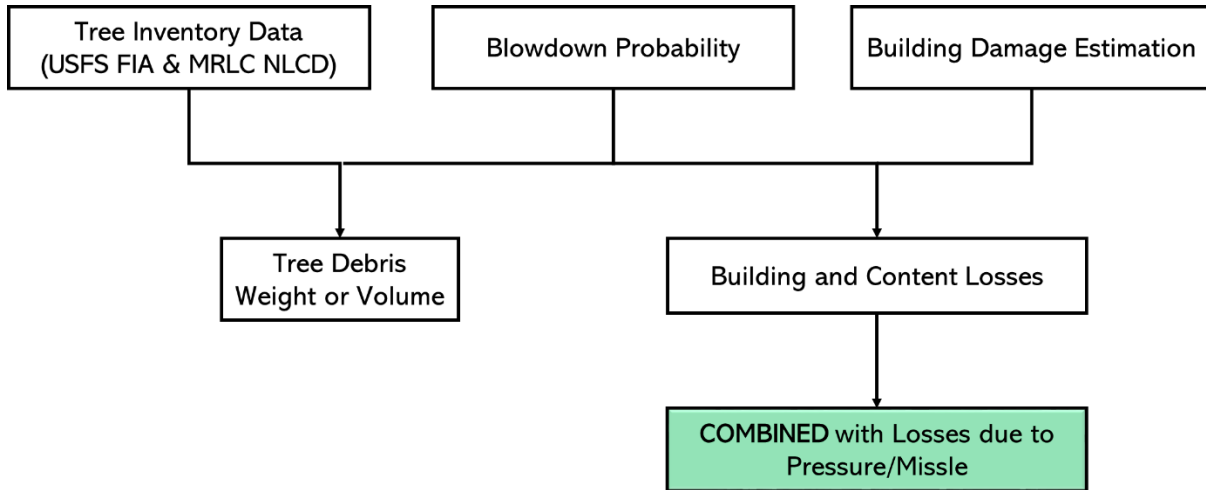


Figure 4-78 Estimation of Tree Blowdown Debris and Damage to Buildings

4.5.1 Related Research

Virtually all the research related to the natural blowdown of trees has been performed by the forestry industry. This research is prompted by large annual losses of harvestable wood in many countries. In New Zealand, the average annual losses of softwood trees due to catastrophic wind events ranges between 0.02% and 3.5% (depending on the forest) of the total stock. The extent of attritional damage associated with lesser winds varies between 0% and 1% of the growing stock per annum (Somerville, 1993). Over the period 1981-1990, more than 50% of the total yield in the Czech Republic had to be cut down due to injuries produced by windthrow or snowbreak (Slodicak, 1993).

The research performed by the forestry industry (predominately in the U.K. and Europe) includes full-scale measurement of tree response due to wind action, measurements of wind speeds within canopies, static pull down tests and relatively simple mathematical models to estimate the forest blowdown potential. The model described herein draws on work done by the forestry industry in the U.K. and Europe combined with research performed in the United States. Very little research in the U.S. has been directed toward assessing the risk of forest blowdown produced by natural wind; however, the most relevant research was directed toward assessing tree blowdown probabilities associated with the effects of nuclear weapons (Twisdale et al., 1984). The ten-year research program produced a computer simulation methodology termed BLOWTRAN (BLOWdown TRANSport) described in the section “Damage to Forests” in the EM-1 Nuclear Effects Manual. The BLOWTRAN model is adapted as described herein to obtain estimates of tree blowdown associated with natural wind.

4.5.2 Wind Throw Model

4.5.2.1 Wind Load Response and Breakage Model

The mathematical model used in BLOWTRAN to determine the drag loads acting on a tree is based on the model developed by the United States Forest Service (USFS) during the early 1950s. The drag force, F_D , acting on the tree crown is a function of the dynamic pressure acting on the tree crown combined with the effective surface area and the effective drag coefficient. Both the drag coefficient and the effective crown area of a tree subject to strong winds decrease due to streamlining of the leaves and branches, with the end result being that the wind force acting on the tree is nearly proportional to velocity.

To determine the effect of streamlining the tree-crown system, and to develop a model to define the wind loads, the USFS conducted full-scale drag tests on 13 coniferous trees (Sauer et al., 1951) and 18 broadleaf trees (Lai, 1955). More recent full-scale measurements on over 30 coniferous trees (Frank et al., 1987; Frank et al., 1989; Frank et al., 1991) supplement the USFS data. All of the full-scale test data used herein were carried out by mounting full-size trees on the rear of a tractor trailer and driving at a constant velocity. Base overturning moments and shear forces were measured for mean velocities ranging between 6 meters per second and 32 meters per second in the more recent tests, and 5 meters per second to 25 meters per second in the USFS tests.

The drag data from these full-scale tests are correlated as functional relationships of two dimensionless parameters that describe the variation in the drag force with the bending moment at the base of the crown, as a function of the wind force, and the tree crown and stem characteristics. The drag force, F_D , in the USFS model is expressed as:

Equation 4-35

$$\frac{F_D}{\frac{1}{2}\rho U^2} = \frac{d_c^3}{h} \frac{1}{W_{dbf}} \Psi_D$$

Where:

h	is the distance between the effective center of pressure and the base of the crown
d_c	is the diameter at the base of the crown
ρ	is the density of air
W_{dbf}	is the ratio of the weight of the dry branches to the weight of the dry foliage
Ψ_D	is a drag function

The wind velocity, U , in Equation 4-35 is the relative velocity (i.e., wind velocity minus the velocity of the tree) and, therefore, aerodynamic damping is inherently included in Equation 4-35. The drag function, Ψ_D , is given as:

Equation 4-36

$$\Psi_D = \frac{k_2 k_2 \left(\frac{R}{W_{dc}} \right)^{-1.5}}{k_1 + k_2 \left(\frac{R}{W_{dc}} \right)^{-1.5}}$$

Where:

- k_1 and k_2 are drag function parameters
- W_{dc} is the dry crown weight
- R is the restoring force in the stem at the base of the crown

In the static case, the restoring force, R , is equal to the drag force, FD . In Equation 4-36, the parameter k_1 is directly proportional to the drag coefficient for a perfectly rigid tree, and k_2 is the parameter responsible for reducing the effective drag force with increases in wind speed. Small values of k_2 describe a tree that streamlines readily; conversely, large values of k_2 describe a tree that does not readily streamline. The dry crown weight, W_{dc} , in Equation 4-36 does not need to be determined explicitly for each tree since it has been found to be strongly correlated with the height of the crown, H_c , and the stem diameter, d_c , at the base of the crown. Empirical relationships for the dry crown weight have been developed for a number of hardwood and coniferous tree species (Storey, Fons, and Sauer, 1955; Lai, 1955; Twisdale et al., 1989) in the form:

Equation 4-37

$$\ln(W_{dc} H_c) = a + b \ln d_c + \varepsilon$$

Where:

- H_c is the height of the crown
- a and b are regression constants
- ε is a normally distributed error term

The r^2 values for these species-dependent empirical relationships exceed 0.93 in all cases. Similar relationships for the parameter $W_{db/f}$ have also been developed.

Because the dry crown weight, W_{dc} , and the ratio of the weight of the dry branches to the weight of the dry foliage, $W_{db/f}$, are determined through empirical relationships, the basic inputs required for the drag (or loading) side of the model are:

- Tree height, H_{bh}
- Diameter at breast height, d_{bh} (1.3 meters above ground)

- Species Stem form parameters, a_s and c_s , which describe the taper in the stem
- Percent crown
- Drag parameters k_1 and k_2

The species-dependent variables, a_s , c_s , k_1 , and k_2 , are given for a variety of conifers and broadleaf trees in Twisdale et al. (1989) and Vickery et al. (1993).

Statistical distributions for the drag parameter, k_1 , have been developed for 12 species (three conifers and nine broadleaf trees) and a relationship between the modulus of rupture and k_1 was developed so that the value of k_1 can be estimated for species where direct measurements are not available. Figure 4-79 shows the drag parameters k_1 , and k_2 plotted versus the modulus of rupture, σ_r , for broadleaf trees where it is evident that trees having higher drag coefficients (as defined using k_1) are generally stronger. In the case of conifers, no trend of increasing k_1 with increasing σ_r was observed; however, a weak positive correlation between σ_r and k_2 was observed. For broadleaf trees, the drag parameter k_1 (as shown in Figure 4-79) is modeled as a lognormal distribution where:

Equation 4-38

$$m_{\ln k_1} = 7.777 + 0.04198\sigma_r$$
$$\sigma_{\ln k_2} = 0.679$$

are the logarithmic mean and standard deviation, respectively. The drag parameter k_2 is also lognormally distributed with the logarithmic mean and standard deviation given as:

Equation 4-39

$$m_{\ln k_1} = 12.98 + 0.0145\sigma_r$$
$$\sigma_{\ln k_2} = 0.679$$

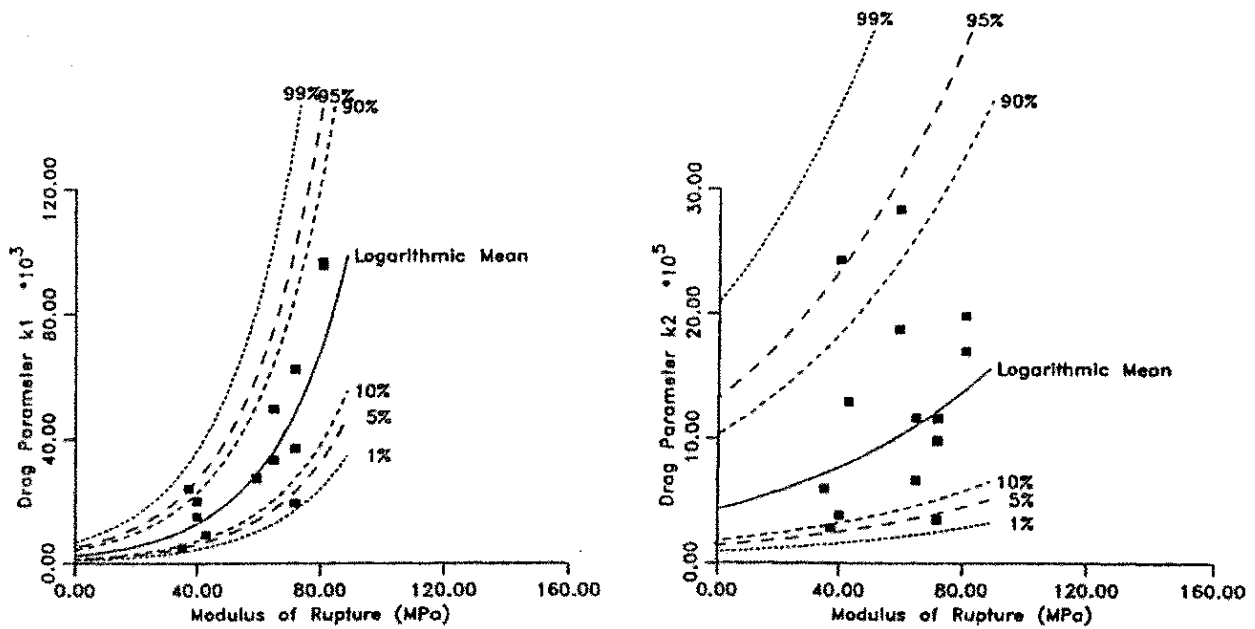


Figure 4-79 Drag Function Parameters k_1 and k_2 versus σ_r for Green Wood (Broadleaf Trees)

Tree response is modeled using a single degree of freedom model given as:

Equation 4-40

$$m_e \ddot{x} + c \dot{x} + kx = F_D(t)$$

Where:

m_e is an effective mass located at the center of pressure, is used to predict the dynamic response of the tree subjected to either a static or dynamic wind load

$F_D(t)$ is the drag force, and is assumed to function as a point load located at the center of pressure (in the crown at a height, H_{cp} above breast height)

The linear spring stiffness for the tree is derived from small deflection theory as:

Equation 4-41

$$K = \frac{3EI_{bh}}{H_{bh}^3} \bar{K}\psi(c_s, f_1)$$

Where:

I_{bh} is the moment of inertia at breast height

H_{bh} is the height of the tree above breast height

E is the species-dependent Young's modulus

\bar{K} is a stiffness modulus parameter which accounts for the natural variations in the stiffness from the reference (or theoretical value)

Statistical distributions of \bar{K} used herein have been determined from static pull-down tests on both conifers and broadleaf trees (Frank et al., 1987, 1989; Vickery et al., 1991). The shape function, $\Psi(c_s, f)$, accounts for the variable moment of inertia along the tree stem. The shape of the stem of a tree is hyperbolic in nature (Behre, 1927), such that the inside diameter, d , at any point along the stem is defined by:

Equation 4-42

$$d = d_{bh} \frac{f}{a_s(f + c_s)}$$

Where:

a_s and c_s are the species-dependent stem form parameters

f is the non-dimensional distance measured from the top of the tree

The $3EI/H^3$ term in Equation 4-42 is the stiffness of a uniform cantilever. The shape function modifies the stiffness to account for the shape of the stem.

The tree period and effective mass of the equivalent single degree of freedom system is determined using species-dependent empirical relationships for the tree period combined with the calculated spring constant, K . The tree period, T , is obtained from:

Equation 4-43

$$T = a_1 + b_1 \frac{H_{bh}^2}{d_{bh}} + \varepsilon$$

Where:

a_1 and b_1 are species-dependent regression constants

ε is a normally distributed error term

Bending stresses in the extreme fiber of the tree along the length of the stem prior to yielding are given by:

Equation 4-44

$$\sigma = \frac{Md}{2I}$$

$$I = \frac{\pi d^4}{64} \left[\frac{1}{a_s (f + c_s)} \right]^4$$

d is the inside diameter

M is the bending moment

The region of maximum stress, and hence the point at which the tree will likely fail, varies with the position of the applied load. In general, trees loaded near the top will tend to break in the crown, and as the effective load point moves closer to the ground, the location of maximum stress moves toward the base of the tree.

In order to determine whether or not failure occurs, a reference deflection, y_r , at the point of application of the load is determined from small deflection theory for a reference strain equal to σ_r/E , where σ_r is the modulus of rupture for green wood. The maximum linear spring resistance, R_m , is given as:

Equation 4-45

$$R_m = \bar{R}_b K_r y_r$$

Where:

\bar{R}_b is a random variable representing the variability in the strength of the tree stem

Statistical distributions for \bar{R}_b have been described in Frank et al. (1987; 1989) and Vickery et al. (1993) from the results of static pull-down tests for a number of broadleaf and coniferous trees.

In the case of conifers, \bar{R}_b was found to be negatively correlated with diameter at breast height for both root and stem failures (i. e., larger diameter trees are less likely to be able to develop the theoretical maximum resistance moment). This negative correlation was less pronounced in the case of broadleaf trees.

The breakage deflection, y_b , is obtained from:

Equation 4-46

$$y_b = \mu y_r$$

Where:

μ is the ductility and a random variable whose statistical parameters have been determined using the results of static tree pull-down experiments for a wide range of species

Once the breakage deflection has been reached, the tree is assumed to have failed. The height above ground at which a stem failure occurs is determined by sampling uniformly over the region where the stem bending stress exceeds 90% of the maximum calculated value.

Uprooting failures are treated similarly to stem breakage failures by replacing \bar{R}_b and μ with data derived from pull-down tests, where the failure occurred by uprooting. Given tree size and the modulus of rupture, σ_r , the single most important (and uncertain) parameter describing the overall resistance of the tree to blowdown is \bar{R}_b . Table 4-20 summarizes the basic parameters (and relationships between parameters) necessary for modeling the response of a tree to wind (or blast) loads. Information on the parameters a_s , c_s , T , μ , \bar{K} , \bar{R}_b , C_p , W_{dc} , $W_{db/f}$, and k_2 are species-dependent and are derived from experimental studies. The values of these parameters are given in Vickery, Frank, and Twisdale (1993) for several tree species. The information given in Vickery, Frank, and Twisdale summarizes data from a wide range of sources. In addition to species-dependent parameters, data is given for generic conifers and broadleaf trees. Information on tree height, H_{bh} , diameter, d_{bh} , and % crown, f_c , varies with species and location; however, information on typical values of H_{bh} , d_{bh} , and f_c is readily available in the forestry literature. Values of σ_r and E are given in the USDA Wood Handbook (USDA, 1974).

Table 4-20 Input Parameters for Modeling of Trees

Number	Variable	Description	Functional Relationship	Distribution
1	d_{bh}	Diameter at breast height	User supplied	Uniform
2	H_{bh}	Height above breast	User supplied	Truncated Normal
3	f_c	% Crown	User supplied	Truncated Normal
4	a_s	Stem form parameter	User supplied	Lognormal
5	c_s	Stem form parameter	$c_s = \frac{a}{a_s} - 1$ (1)	Normal Error Term
6	T	Fundamental period	$T = a + bH_{bh}^2/d_{bh}$ (1)	Normal Error Term
7	$\mu^{(2)}$	Ductility	User supplied ⁽¹⁾	Lognormal
8	$\bar{K}^{(2)}$	Stiffness parameter	User supplied ⁽¹⁾	Lognormal
9	$\bar{R}_b^{(2)}$	Strength parameter	$\ln \bar{R}_b = a + b \ln d_{bh}$ (1)	Normal Error Term
10	C_p	Center of pressure (tree in uniform flow)	User supplied ⁽¹⁾	Truncated Normal
11	W_{dc}	Weight of dry crown	$\ln(w_{dc} H_c) = a + b \ln d_{bh}$ (1)	Normal Error Term
12	$W_{db/f}$	Ratio of dry branches weight to dry foliage	$\ln(w_{dc}/f) = a + b \ln d_{bh}$ (1)	Normal Error Term
13	K_1, k_2	Drag function parameters	User supplied ⁽¹⁾	Normal Error Term
14	d_c	Diameter of base of crown	$d_c = \frac{d_{bh} f_c}{a_s (f_c + c_s)}$	NA
15	σ_r	Modulus of rupture for green wood	User supplied	NA ⁽³⁾

Number	Variable	Description	Functional Relationship	Distribution
16	E	Modulus of elasticity for green wood	User supplied	NA ⁽⁴⁾

(1) Species- (site-) dependent data derived from tests. Data available in Vickery, Frank, and Twisdale (1992).

(2) Separate distributions are given for stem failure and uprooting.

(3) Natural variation in σ is accounted for with \bar{R}_b distribution.

(4) Natural variation in E is accounted for with K distribution.

4.5.2.2 Wind Modeling for Simple Terrains

In the case of relatively open terrain, similar to open country or suburban exposures in most building codes, where the variation in wind speed with height can be adequately modeled using logarithmic or power law models, simulating the incident windfield is relatively straightforward. In these basic cases, a wind speed time history is simulated using:

Equation 4-47

$$U(t) = \bar{U} + \sum_{j=1}^N a_j \cos(2\pi\Delta f_j + \phi_j) t$$

Where:

- U(t) is the instantaneous wind speed at time (at the height of the center of pressure)
- \bar{U} is the mean wind speed at the height of the estimated center of pressure within the crown of the tree
- Δf is a frequency increment
- ϕ_j is a random phase angle sampled uniformly over the interval $0 \leq \phi \leq 2\pi$
- a_j is a frequency dependent amplitude.

The amplitude term, a_j , is given as:

Equation 4-48

$$a_j = [2S_u(f_j)\chi^2(f_j)]^{\frac{1}{2}}\Delta f$$

Where:

$S_u(f_j)$ is the value of the spectrum of longitudinal turbulence at frequency f_j

$\chi^2(f_j)$ is the magnitude of the aerodynamic admittance function at frequency f_j

The velocity spectrum, $S_u(f)$, used in this study is based on the ESDU (1975) formulation:

Equation 4-49

$$\frac{fS_u(f)}{\sigma_u^2} = \frac{4n}{(1 + 70.8n^2)^{\frac{5}{6}}}$$

Where:

Equation 4-50

$$n = xL_u f / \bar{U}$$

and the integral length scale xL_u is given as:

Equation 4-51

$$xL_u = \frac{25z^{0.35}}{z_0^{0.063}}$$

Where:

Z is the height above ground, and is equal to the height to the center of pressure of the crown

Z_0 is the aerodynamic surface roughness

The aerodynamic admittance function, $\chi^2(f)$, is determined using the coherence function for vertical separations given in Bowen, Flay, and Panofsky (1983), where the square of the coherence function is given as:

Equation 4-52

$$R_{uu}^2(z_1, z_2, f) = \exp \left[- \left(12 + \frac{11\Delta z}{z} \right) \frac{f\Delta z}{z} \right]$$

and:

Equation 4-53

$$\chi^2(f) = \iint_{H_c} R_{uu}(z_1, z_2, f) dz_1, dz_2$$

The integral in Equation 4-53 is solved numerically for various combinations of crown height, H_c , and H_b (height to base of the crown), with the solution approximated as:

Equation 4-54

$$\chi^2(f) = \frac{1.0}{1 + a_1 n + a_x n^2}$$

Where:

Equation 4-55

$$n = \frac{fH_c}{\bar{U}}$$

The coefficients a_1 and a_2 vary with H_c/H_b . They are evaluated for H_c/H_b ranging between 0.1 and 10 and stored for later use. Ignoring the displacement height, d , the mean and turbulence profiles for these “open” cases are given as (ESDU 1982):

Equation 4-56

$$\frac{\bar{U}(z)}{U_{ref}} = \frac{\ln\left(\frac{z}{z_0}\right)}{\ln\left(\frac{z_{ref}}{z_0}\right)}$$

and:

Equation 4-57

$$\frac{\sigma_u}{\bar{U}(z)} = \frac{7.5\eta \left[0.538 + 0.09 \ln\left(\frac{z}{z_0}\right)\right]^p}{1 + 0.156 \ln\left(\frac{u_*}{f_c z_0}\right)}$$

Where:

- z_{ref} is the reference height
- $\bar{U}(z)$ is the wind speed at height z
- $\sigma_u(z)$ is the RMS longitudinal wind speed at height z
- \bar{U}_{ref} is the mean wind speed at the reference height
- u_* is the friction velocity
- f_c is the Coriolis parameter

Equation 4-58

$$\eta = 1 - \frac{6f_c z}{u_*} \text{ and } p = \eta^{16}$$

4.5.2.3 Example Tree Response – Ponderosa Pine

The wind-induced response of a Ponderosa Pine tree characterized in Table 4-21 was examined in some detail, as described here. Figure 4-80 shows the input velocity spectrum at the center of pressure in conjunction with the resulting base bending moment spectrum for mean wind speeds ranging between 10 meters per second and 25 meters per second. The intensity of turbulence at the center of pressure is about 25%. A resonant peak is seen clearly in Figure 4-80; however, the importance of the resonant response diminishes with increasing wind speed due to increases in the aerodynamic damping. Sensitivity studies performed where the weight of the dry crown (W_{dc}) was both increased and decreased indicate that the resonant portion of the tree response decreases with increasing crown weight. For very large values of W_{dc} the tree response is nearly quasi-static.

Table 4-21 Characteristics of Key Parameters for Example Ponderosa Pine Tree Response Estimates

Parameter	Value
Height (meter)	16.4
Diameter at Breast Height (centimeter)	18
% Crown	56
Dry Crown Weight (N)	90
Drag Parameter k1	8,669
Drag Parameter k2	399,528
Period (seconds)	3.28

Figure 4-81 shows the mean, RMS, and maximum base bending moments plotted versus the mean wind speed 10 meters above ground, showing the effect of dry crown weight (W_{dc}) on tree response. The wind speed is increased to the point where the tree fails. The dry crown weight has little effect on the base bending moments at low wind speeds. In this example, for a mean wind speed of 10 meters per second, the peak base bending moment is proportional to W_{dc} raised to the power of 0.14, whereas for a mean wind speed of 25 meters per second, the peak base bending moment is proportional to W_{dc} raised to the power 0.4. In this example, the effect of crown weight is less important than the model of Mayhead et al. (1975), where the mass of the crown is included in the drag force model raised to the power of 0.67. It is noteworthy that the drag model proposed by Mayhead et al. (1975) for Sitka Spruce given in the form of Figure 4-65 yields a maximum drag force for a wind speed equal to 32 meters per second.

Equation 4-59

$$F_D = A_1 U^2 m_c^{0.67} \exp\{-0.0009779 U_2\}$$

Where:

m_c is the live branch weight

A_1 is a constant

Higher wind speeds result in a drag force, F_D , which decreases.

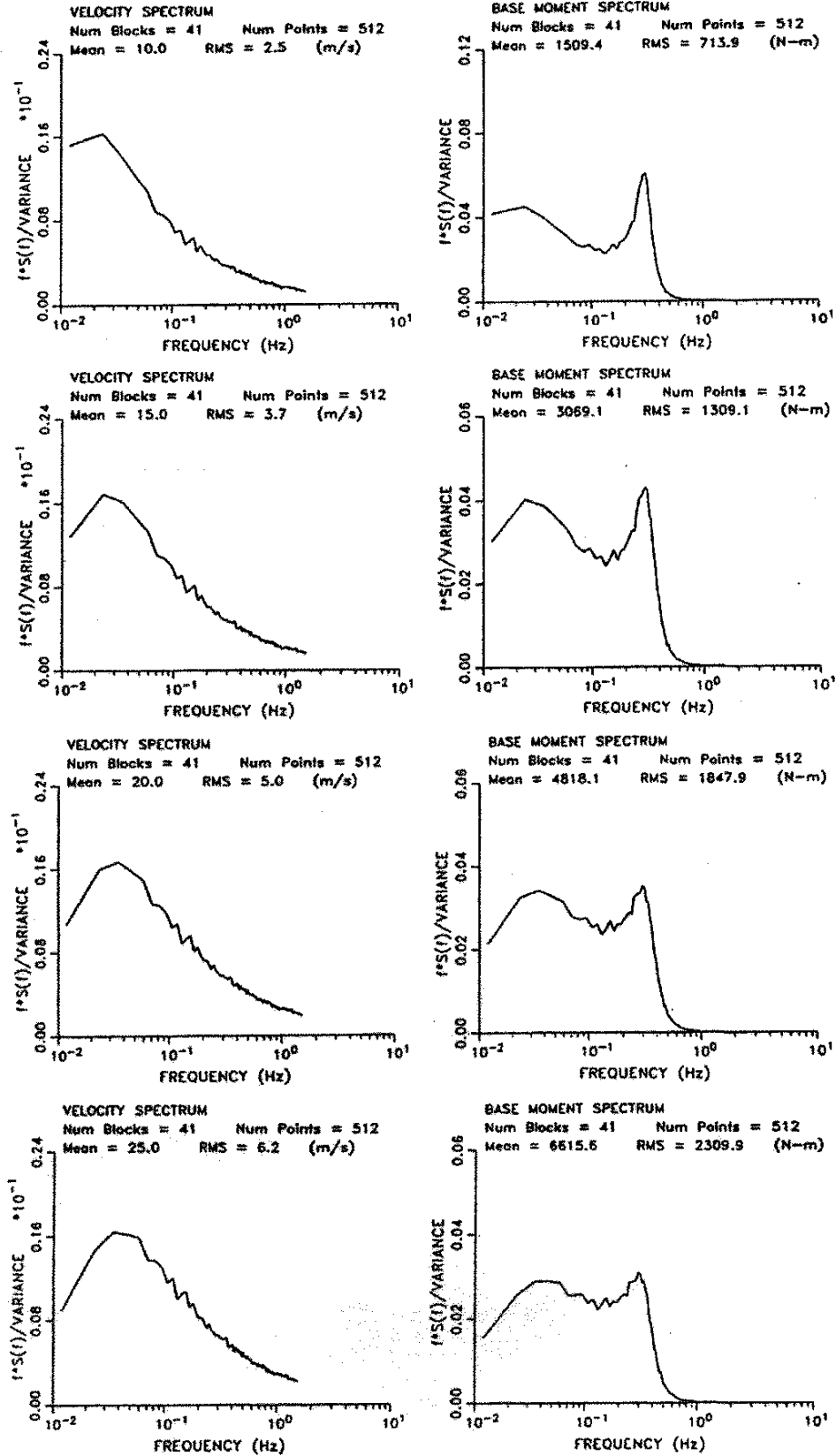


Figure 4-80 Velocity Spectra and Base Moment Spectra for Ponderosa Pine (Suburban Exposure)

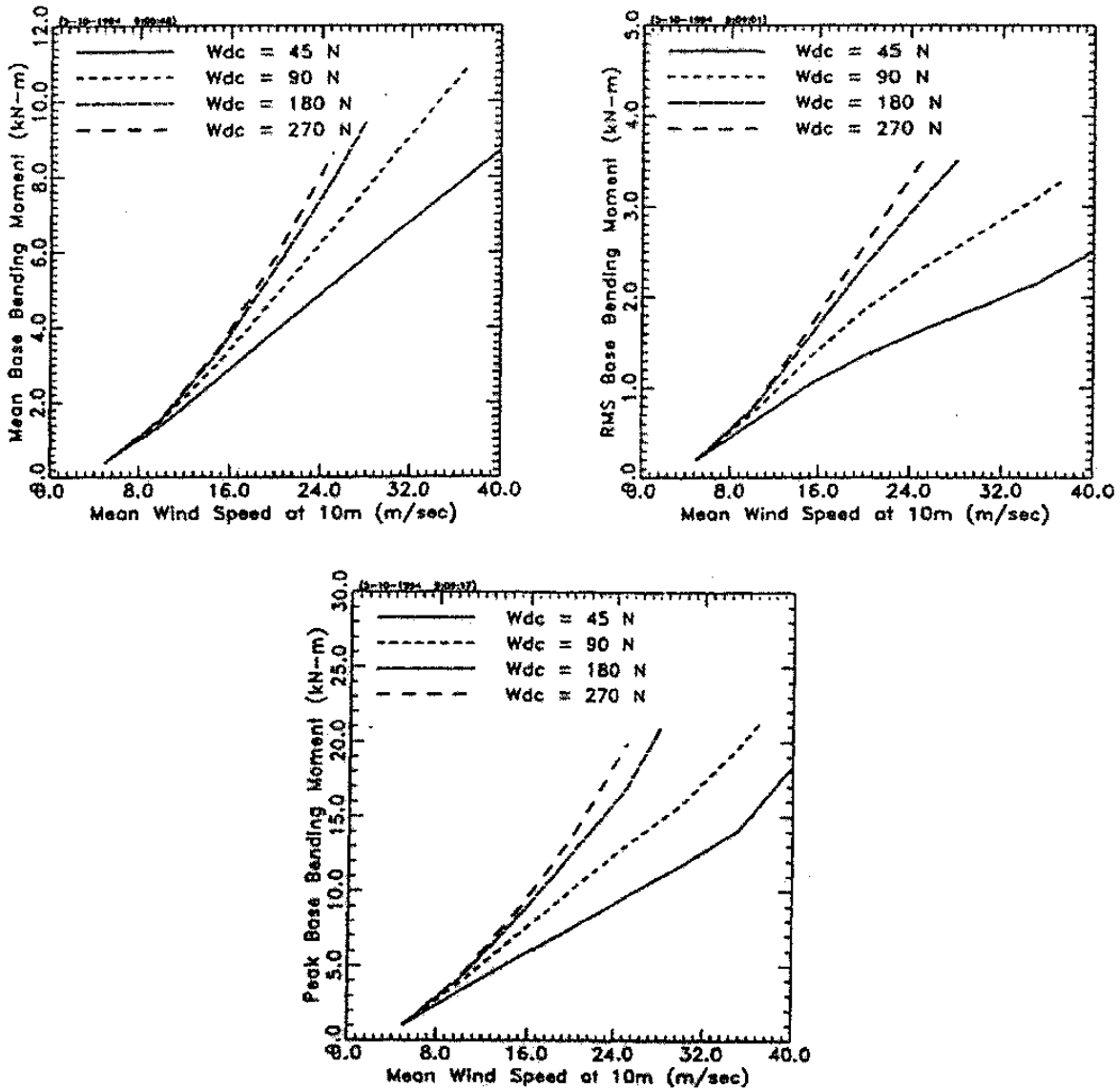


Figure 4-81 Mean, RMS, and Peak Base Bending Moment Versus Wind speed Showing Effect of Crown Weight on Tree Response

Figure 4-82 shows the peak base bending moment for the Ponderosa Pine tree characterized in Table 4-21, plotted versus both the mean wind speed at 10 meters and the peak wind speed at the center of the crown for typical open country ($z_0 = 0.03$ meters) and suburban ($z_0 = 0.3$ meters) windfields. The response of this example tree is clearly governed by the peak wind speed, and that the peak base bending moment increases approximately linearly with increases in the peak wind speed.

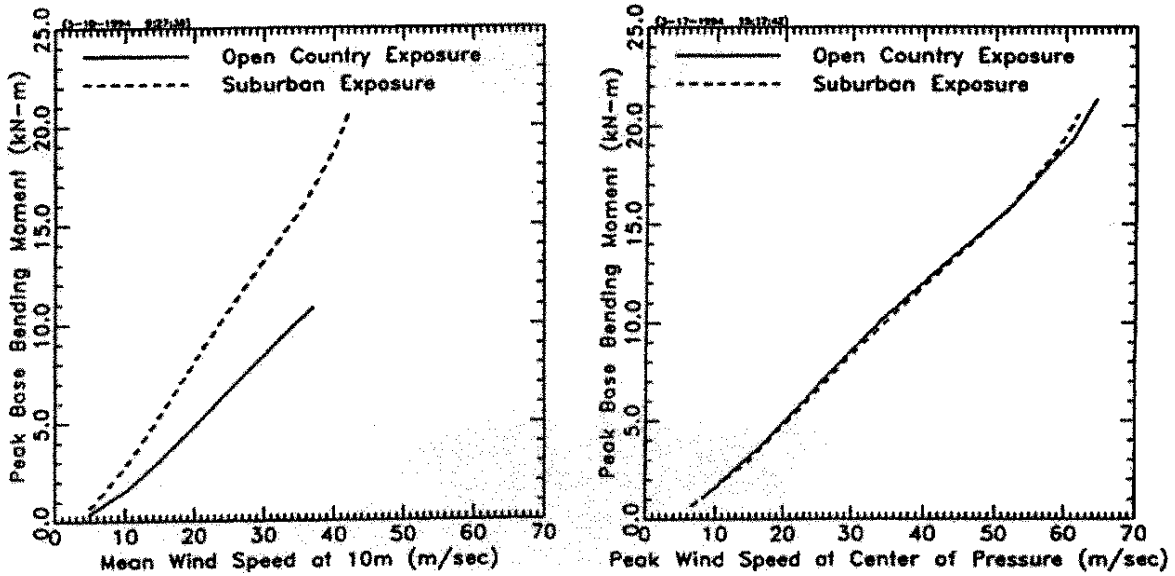


Figure 4-82 Mean and Peak Base Bending Moment Versus Peak Wind speed at Center of Pressure (Open and Suburban Terrains)

4.5.2.4 Wind Modeling in Forested Areas

Flow within and above plant canopies has been studied by numerous investigators. These studies include full-scale measurements, wind tunnel investigations, and mathematical modeling. In the case of forest flows, examples of full-scale measurements are given in Oliver and Mayhead (1974), Thompson (1979), and Bergstrom and Hogstrom (1989) for pine forests; Amiro and Davis (1988) for a Black Spruce forest; Amiro (1990a) for pine, spruce, and aspen forests; Baldocchi and Meyers (1988) for an Oak-Hickory forest; and Milne (1993) and Gardiner (1994) for a Sitka Spruce forest. Wind tunnel simulations range from simplistic models using arrays of rigid rods to model the vegetation (Seginer et al., 1976) to detailed aeroelastic modeling of forests (Stacey et al., 1994). Mathematical models used to model flow within and above plant canopies include first-order closure models (e.g., Li et al., 1985), second-order closure models (e.g., Meyers and Paw, 1986) and simplified empirical models (e.g., Cionco, 1972). A review of mathematical techniques used to model flow within canopies is given in Massman (1987). All of the full-scale studies noted above were conducted in relatively dense forests, so the results are not directly usable for estimating flow conditions in relatively lightly forested suburban areas, and no published measurements of wind flow conditions in lightly forested regions typical of suburban areas were found.

In the investigation described herein, the first-order closure model described in Li et al. (1985), Li et al. (1990), and Miller et al. (1991) was used to describe the flow structure within and above the “forest” canopy. D. R. Miller of the University of Connecticut provided the computer code. The main inputs to the model include a description of the Leaf Area Index (LAI) profile of the plant canopy, defined as the leaf area per unit area of soil, an effective drag coefficient for the vegetation, and two wind speeds. Mean wind speed and turbulence intensity profiles resulting from the model were compared to full-scale measurements in forests for cases where information on the LAI profile was also available.

Figure 4-83 shows profiles of LAI along with the measured and simulated mean, turbulence intensity, and peak wind speed profiles (peak wind speed is defined as the mean plus three standard deviations)

for data given in Gardiner (1994), Stacey et al. (1994), Baldocchi and Meyers (1988), and Amiro (1990). A drag coefficient of 0.16 (e.g., Meyers and Paw (1986) and Amiro (1990b)) was used in all cases. Figure 4-83 indicates that the first order closure model results reproduce the mean velocity profile reasonably well, through to the underside of the canopy where the secondary maxima produced by the model is greater than the maxima observed in the full-scale measurements. The RMS velocity, at height $\sigma_u(z)$, z , is estimated from:

Equation 4-60

$$\sigma_u(z) = 2u_* = 2l(z) \frac{\partial u}{\partial z}$$

Where:

$l(z)$ is the mixing length at height z above the ground surface

Details on the mixing length model are given in Miller et al. (1991). Equation 4-60 is valid above the displacement height, d , but not beneath $z = d$. Below $z = d$, the turbulence intensity is set equal to the value computed at the lowest level in the grid. As indicated in Equation 4-60, there is no inclination for modeled local turbulence intensities to consistently overestimate or underestimate the measured intensities within the canopy; however, the modeled intensities consistently underestimate the observed intensities beneath the canopy. Within the canopy, the modeled turbulence intensities agree surprisingly well with the measured intensities. The agreement is better than the agreement between observed and modeled intensities in a Maize canopy given in Meyers and Paw (1986) using a second order closure model.

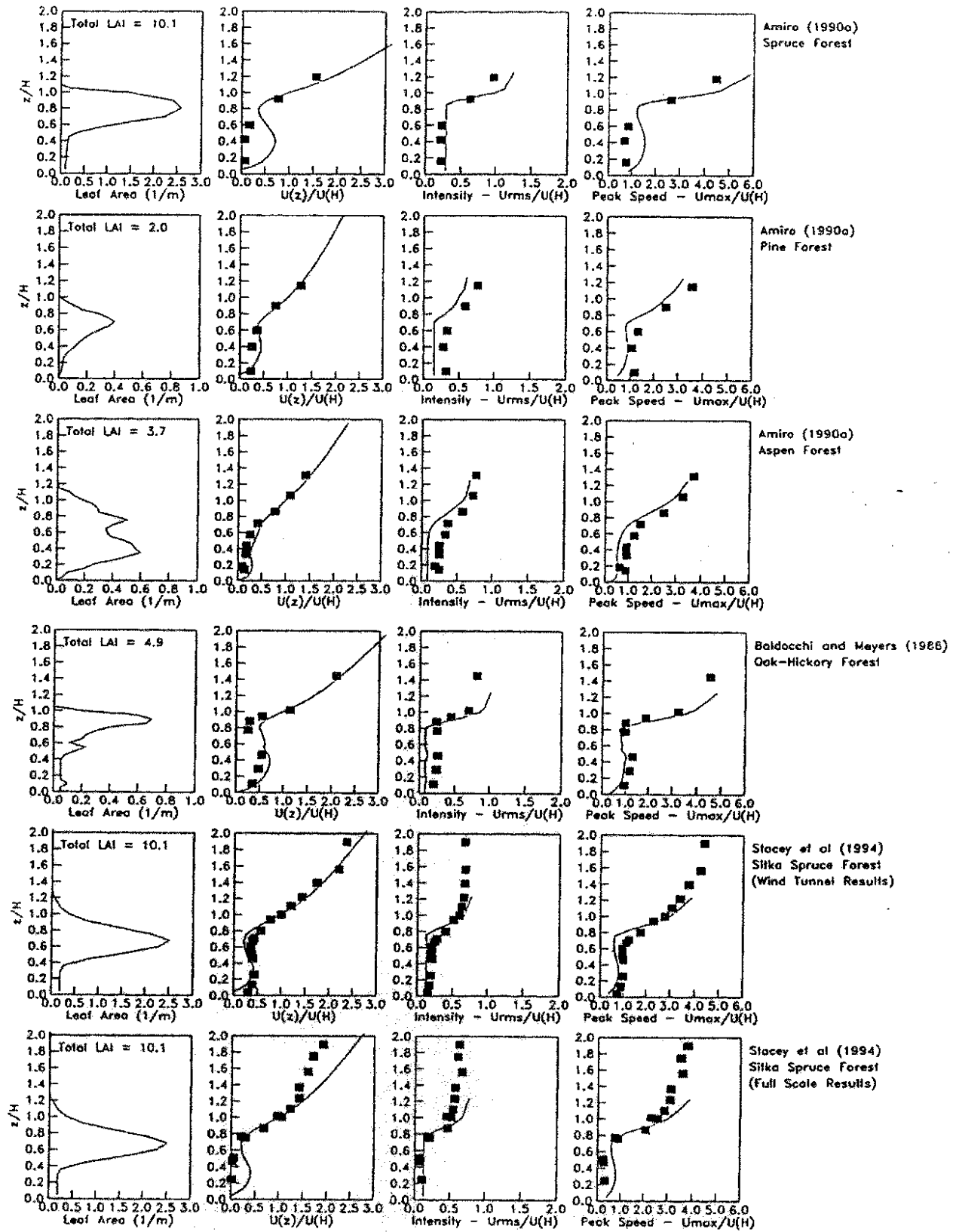


Figure 4-83 Measured Comparison of Modeled Mean and Turbulence Intensity Profiles in Forests

4.5.2.5 Canopy Modeling

The LAI distribution for a forested suburban region is modeled in the form:

Equation 4-61

$$LAI(z) = \frac{B}{\sqrt{2\pi S}} \left[-\frac{1}{2} \left[\frac{\xi - \bar{\xi}_p}{S} \right]^2 \right]$$

Where:

- S is 0.25
- $\bar{\xi}_p$ is the nondimensional distance to the center of pressure measured from the base of the crown
- B is a scale factor which is a function of LAI and $\bar{\xi}_p$

A model similar to Equation 4-61 was used by Milne and Brown (1990) to describe the LAI profile in a Sitka Spruce forest. Mean and turbulence intensity profiles were developed for values of C_dLAI ranging from 0.01 and 0.3 for forests having average percentage crowns of 30%, 40%, 50%, and 60%. The mean value is taken as $\bar{\xi}_p$ being equal to 0.5 (i.e., acting in the center of the crown).

Figure 4-84 shows the mean velocity and turbulence intensity profiles generated for some example C_dLAI profiles. Profiles are given for mean crown percentages within the forested area of 60%. Also shown in Figure 4-84 are the turbulence intensity and mean velocity profiles generated using the ESDU models for the atmospheric boundary layer. In developing the velocity profiles given in Figure 4-84, the displacement height, d and the surface roughness length, z_0 were obtained by plotting the mean wind speed profile in semi-logarithmic space with various assumed values of d/H and selecting the combination of the two values that best fit the wind speed profile resulting from the simulation. The resulting values of d/H and z_0/H are consistent with the information given in Shaw and Pereira (1982) and Massman (1987). The relationships between d/H and z_0/H are presented in Figure 4-85 as a function of C_dLAI . The comparison of the numerical model results with the ESDU model show remarkable agreement above the height of the canopy for both the mean velocity and the turbulence intensity.

Given the mean velocity and turbulence intensity profiles generated for the range of C_dLAI described above, the mean wind speed at a height of $(2H-d)$ coupled with the estimate of the local z_0 is used to estimate the open terrain wind speed using the methodology given in ESDU (1982). The velocity spectrum at the center of pressure is determined using Equation 4-51, with the height replaced by $z - d$, and is combined with the admittance function defined in Equation 4-54 to develop the effective wind spectrum for use in the response estimates. In the development of the velocity profiles used herein, the influence of buildings and structures on the flow field is ignored.

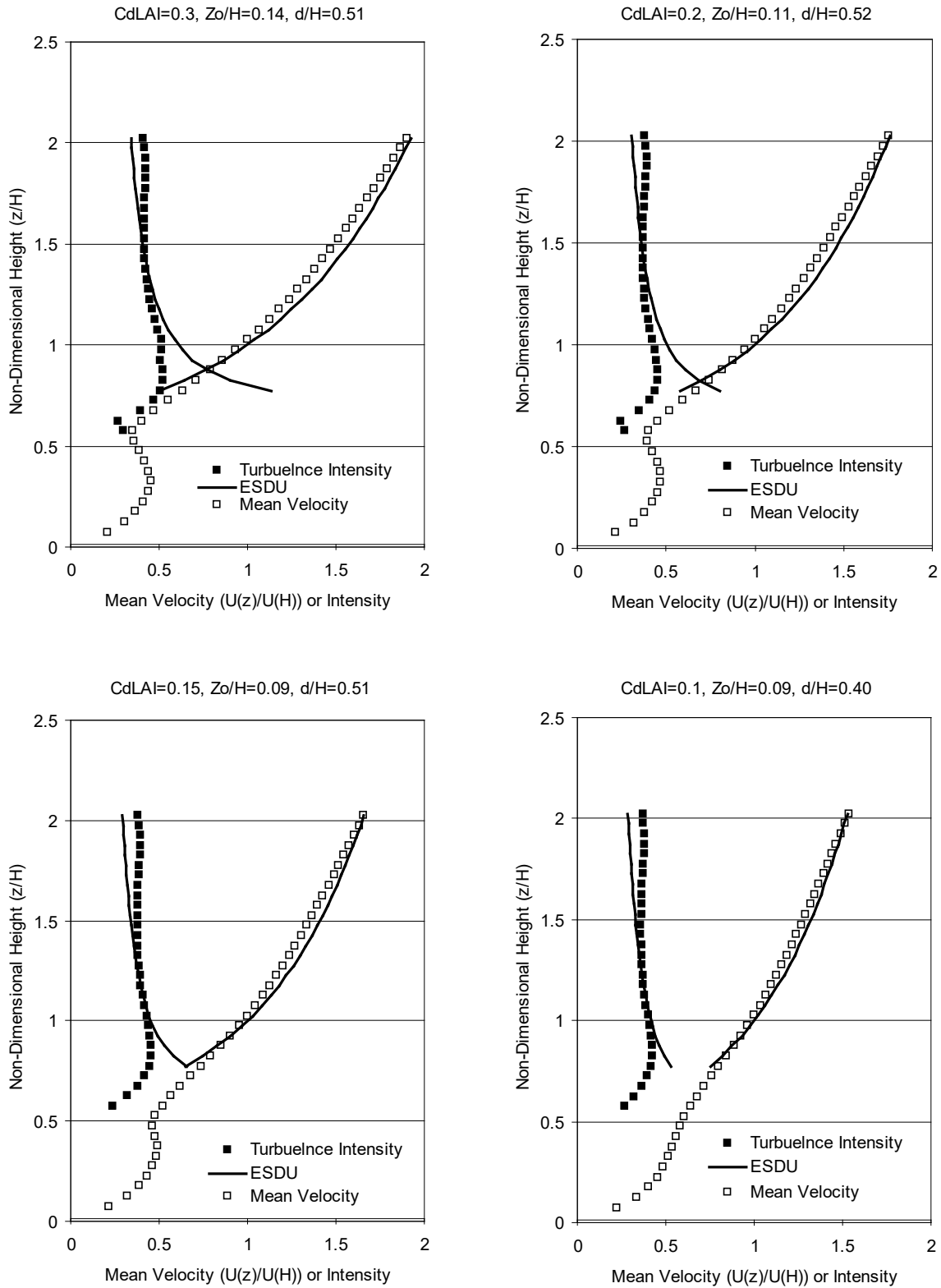


Figure 4-84 Mean and Turbulence Intensity Profiles for Various Values of C_dLAI

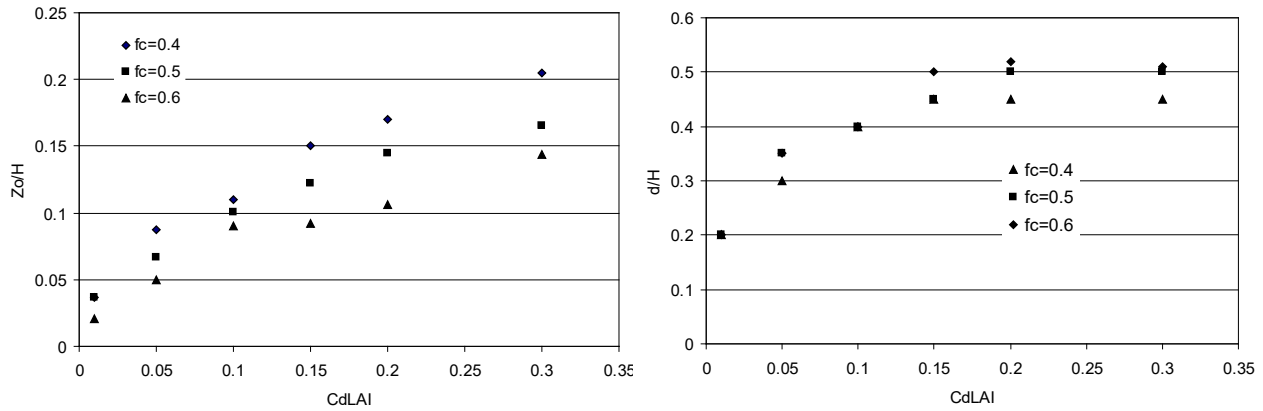


Figure 4-85 z_0/H and d/H Plotted versus C_dLAI for Three Different Values of Crown Fraction

4.5.2.6 Effective Wind Speeds in Forested Areas

Since the tree blowdown model requires the wind speed acting at the effective center of pressure to determine the wind-induced response, effective values of \bar{U} and σ_u acting at the center of pressure must be defined. These effective values are determined by integrating the product of the wind speed at height z and the frontal area at height z (assuming C_d is constant over the tree height) and equating this product with the product of an effective wind speed and the full-frontal area of the tree. Effective values of the mean wind speed and turbulence intensity acting at the center of pressure were computed using two different approaches, the first of which assumes that the drag force is linearly proportional to velocity, and a second approach where the drag force is assumed to be related to the local velocity squared.

Equation 4-62 demonstrates the drag force proportional to velocity. Effective values of the mean velocities acting at the center of pressure of a tree in a forested area are computed as:

Equation 4-62

$$\bar{U}_{\text{eff}} = U_H \frac{\int_0^H \xi(z) LAI(z) dz}{\int_0^H LAI(z) dz}$$

Where:

$\xi(z)$ equals $U(z)/U_H$ and is obtained from the first order closure model and $LAI(z)$ is the distribution of the leaf density over the height of the tree.

The effective RMS velocity is computed from:

Equation 4-63

$$\bar{U}_{\text{eff}} \left(1 + g \frac{\sigma_{u_{\text{eff}}}}{\bar{U}_{\text{eff}}} \right) = U_H \int LAI(z) \xi(z) (1 + gI_u(z)) dz$$

Where:

g is the peak factor and is taken as 3.0

$I_u(z)$ is the turbulence intensity profile obtained from the first order closure model

As noted earlier, the response of the tree is governed by the peak wind speed, not the mean wind speed, and as a result the effective location of the center of pressure is derived using the estimated peak wind profile.

The effective center of pressure is determined from:

Equation 4-64

$$H_{cp\text{eff}} = \frac{U_H \int_0^H \xi(z)(1 + gI_u(z))LAI(z)zdz}{\hat{U}_{\text{eff}} \int_0^H LAI(z)dz}$$

Where:

\hat{U}_{eff} is the effective peak velocity given in Equation 4-65

Equation 4-65

$$\hat{U}_{\text{eff}} = \bar{U}_{\text{eff}}(1 + g\sigma_{u\text{eff}})$$

Equation 4-66 demonstrates the drag force proportional to velocity squared. The effective value of the mean velocity, \bar{U}_{eff} , acting at the center of pressure is derived from:

Equation 4-66

$$\bar{U}_{\text{eff}}^2 = U_H^2 \frac{\int_0^H \xi^2(z)LAI(z)dz}{\int_0^H LAI(z)dz}$$

The effective turbulence intensity, defined as:

Equation 4-67

$$I_{u\text{eff}} = \frac{\sigma_{u\text{eff}}}{\bar{U}_{\text{eff}}}$$

and is derived from:

Equation 4-68

$$\bar{U}_{\text{eff}}^2 = \frac{U_H \int_0^H LAI(z)\xi^2(z)[1 + 2gI_u(z) + g^2I_u^2(z)]dz}{\int_0^H LAI(z)dz}$$

The effective peak velocity \bar{U}_{eff}^2 is given as:

Equation 4-69

$$\bar{U}_{eff}^2 = \bar{U}_{eff}^2 [1 + 2gI_{u_{eff}} + g^2I_{u_{eff}}^2]$$

Where:

g is the peak factor and is set equal to 3

The effective height at the center of pressure is determined from:

Equation 4-70

$$H_{cp\,eff} = \frac{U_H^2 \int_0^H \xi^2(z) [1 + 2g_i(z)]^2}{\hat{U}_{eff}^2 \int_0^H LAI(z) dz}$$

The effective values \bar{U}_{eff} , $\sigma_{u_{eff}}$, and $H_{cp\,eff}$ determined using the linear and quadratic dependencies on wind speed typically vary by less than 10%, with the average of the two approaches being used to compute the tree response.

4.5.2.7 Simulation Methodology

In the simulation process, values of the key tree parameters given in Table 4-20 are obtained from sampling from the appropriate distributions. Using the sampled value of the center of pressure, the crown shape parameters B and $\bar{\xi}_p$ are determined, after which the values of U_{eff}/U_H and σ_u/U_H and effective value of center of pressure taking into account the velocity profile are calculated as described in Section 4.5.2.5. Given the new value of the center of pressure, combined with the sampled values of \bar{R}_b , for root and stem failure, the failure mode (root failure or stem breakage) is determined. Given this information, time series of wind speeds (ten minutes in length) are generated, having a mean wind speed, U_H , and turbulence intensity, σ_r/U_H , and the response of the tree is calculated. Using an iterative interval halving technique, the minimum mean wind speed, U_H , required to fail the tree is determined, after which another tree is sampled and the process is repeated. The simulation process is repeated 100 times with the resulting failure wind speeds (converted to equivalent open country mean values) used to define the probability of failure distribution. Simulations for each tree examined are performed for a range of forest densities. Using the mean values of C_dA calculated for trees in a uniform wind, the average tree density, γ , (stems/Ha) necessary to provide the effective C_dLAI corresponding to the velocity and turbulence intensity profiles used can then be determined from:

Equation 4-71

$$\gamma = \frac{10^4 C_d LAI}{C_d A} \text{stems/Ha}$$

The information on failure wind speeds and tree density are used to determine the probabilities of trees failing and striking a typical residential structure as discussed in the following sections.

4.5.3 Blowdown Results

4.5.3.1 Tree Blowdown Curves

Simulations were performed for values of C_dLAI of 0.3, 0.2, 0.15, 0.10, 0.05, and 0.01. For each simulation, the forest canopy was approximately uniform in height (Coefficient of Variation (COV) = 8%) and the tree diameters varied by ± 1.25 centimeters about the mean value. Figure 4-86 shows example cumulative failure probability distribution for both homogenous deciduous and coniferous forests for three different mean values of height-diameter classes. Information on typical height and diameters and relationships between diameter and crown weight was taken from Storey and Pong (1957) for trees in a mixed hardwood forest in North Carolina. As noted in Figure 4-86 gust failure wind speed (in open country terrain) decreases with increasing forest density.

Damage curve values can be viewed in the Hazus SQL database tables. Losses are plotted by specific building type and can be viewed for all specific building types, including Manufactured Housing, in the “huTreeBlowdownLossFunctions” table within the syHazus database.

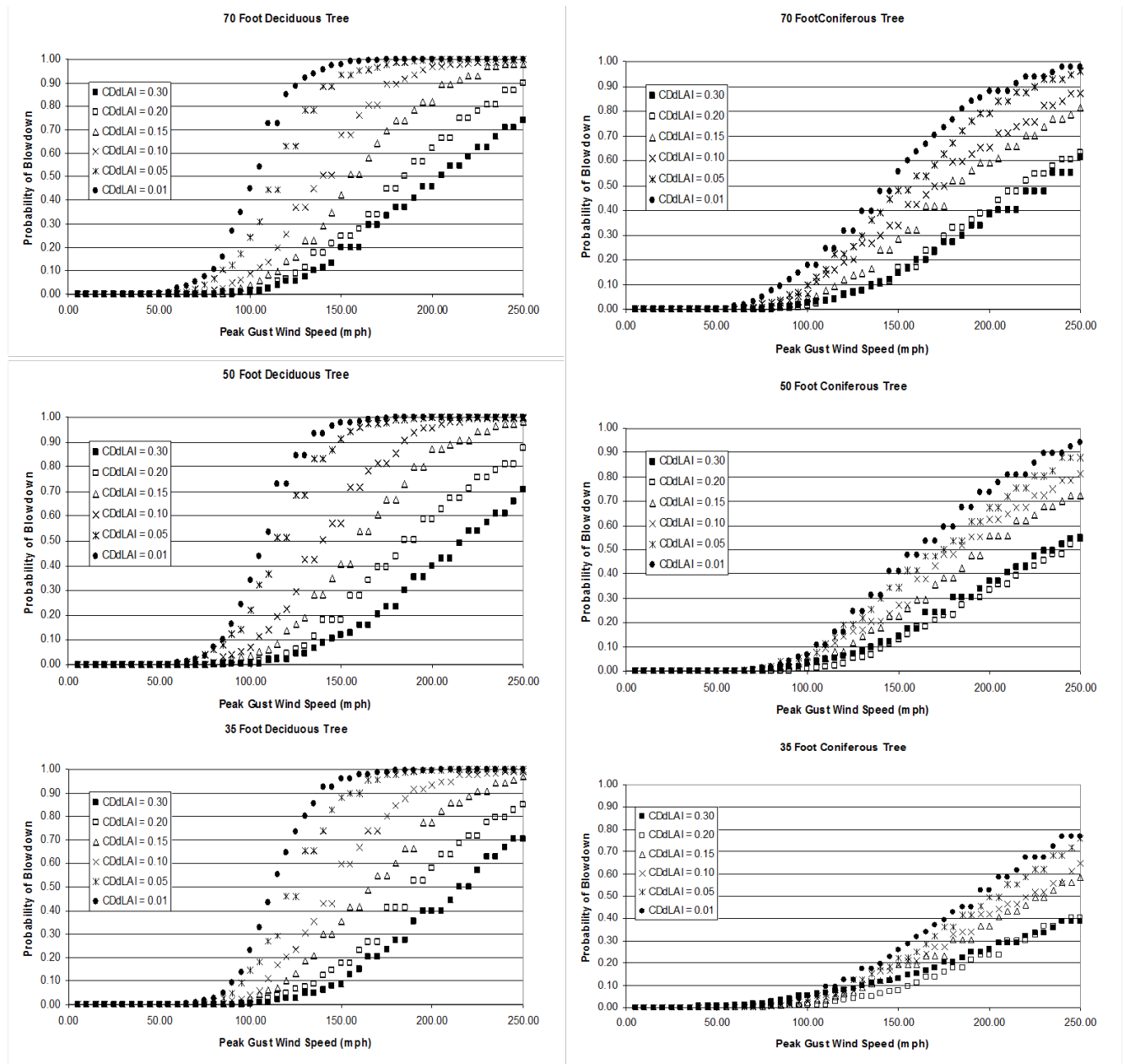


Figure 4-86 Tree Blowdown Curves

4.5.3.2 Tree Blowdown Validation

A validation study of the tree blowdown curves presented in Section 4.5.3.1 was undertaken in eight randomly selected subdivisions in eastern North Carolina immediately following Hurricane Isabel in 2003. In each of the selected residential subdivisions the survey teams counted the number of trees on each lot, counting the number of trees in each of three previously defined height ranges (consistent with the height ranges used in Hazus), the tree type (evergreen or deciduous) and the performance of the tree (uproot failure, stem failure or no failure). In one of the surveyed subdivisions (South Mills, NC) each tree height was estimated and the diameter at breast height was measured, and the dimensions of each lot was obtained. In all cases the address of the lot was recorded.

Table 4-22 presents a summary of the data collected at the eight sites, including the estimated peak gust wind speed, the number of lots surveyed, the total number of trees surveyed, the percent of trees blown down, and the total area surveyed. A total of 1,158 trees were surveyed, with the sample comprising 628 conifers and 530 deciduous trees.

Table 4-23 presents a more detailed summary presenting the number of trees in each height class as well as indicating the number of trees in each height class that fail by uprooting or through stem failure. Approximately 12% of the conifers were blown down and about 10% of the deciduous trees were blown down. The deciduous trees were more likely to fail from uprooting, whereas in the case of the conifers, stem and uprooting failures were approximately equally likely.

Table 4-22 Summary of Tree Blowdown Data

Location	Peak Gust Wind Speed (mph)	Number of Lots Surveyed	Total Number of Trees	% of Trees Blown Down
Ahoski 1	86	20	54	3.7%
Ahoski 2	86	28	113	5.3%
Elizabeth City 1	95	34	171	5.8%
Elizabeth City 2	95	45	217	8.8%
Manteo 1	92	9	178	18%
Manteo 2	92	32	150	11%
South Mills	92	27	150	19.3%
Windsor	84	28	125	8.8%
Total		223	1158	10.8%

Table 4-23 Summary of Number of Failed Trees by Height Class

Location		Conifers					Deciduous				
		Height Range (feet)					Height Range (feet)				
		<30	30-40	40-60	> 60	All	<30	30-40	40-60	> 60	All
Ahoski 1	# Trees	1	4	11	4	20	9	8	17	0	34
	# Uproot Failures	0	0	0	0	0	1	0	0	0	1
	# Stem Failures	0	1	0	0	1	0	0	0	0	0
	Total # Failures	0	1	0	0	1	1	0	0	0	1
Ahoski 2	# Trees	5	9	9	15	38	23	14	19	19	75
	# Uproot Failures	1	1	0	0	2	1	0	2	0	3
	# Stem Failures	0	0	0	1	1	0	0	0	0	0
	Total # Failures	1	1	0	1	3	1	0	2	0	3
Elizabeth City 1	# Trees	0	10	41	39	90	17	22	38	4	81
	# Uproot Failures	0	0	0	2	2	1	1	4	0	6
	# Stem Failures	0	1	0	0	1	0	0	1	0	1

Location		Conifers					Deciduous				
		Height Range (feet)					Height Range (feet)				
		<30	30-40	40-60	> 60	All	<30	30-40	40-60	> 60	All
	Total # Failures	0	1	0	2	3	1	1	5	0	7
Elizabeth City 2	# Trees	3	11	73	61	148	26	23	11	9	69
	# Uproot Failures	1	0	2	0	3	2	2	1	3	8
	# Stem Failures	0	0	2	3	5	2	0	1	0	3
	Total # Failures	1	0	4	3	8	4	2	2	3	11
Manteo 1	# Trees	2	4	91	0	97	26	45	10	0	81
	# Uproot Failures	0	1	6	0	7	4	3	0	0	7
	# Stem Failures	0	2	13	0	15	0	3	0	0	3
	Total # Failures	0	3	19	0	22	4	6	0	0	10
Manteo 2	# Trees	14	24	21	23	82	6	48	14	0	68
	# Uproot Failures	0	0	5	1	6	0	3	0	0	3
	# Stem Failures	0	1	3	2	6	0	1	0	0	1
	Total # Failures	0	1	8	3	12	0	4	0	0	4
Windsor	# Trees	3	6	23	23	55	25	23	12	10	70
	# Uproot Failures	0	0	1	1	2	1	1	0	0	2
	# Stem Failures	0	0	1	1	2	1	1	1	2	5
	Total # Failures	0	0	2	2	4	2	2	1	2	7
South Mills	# Trees	2	47	21	28	98	5	19	17	11	52
	# Uproot Failures	0	7	2	8	17	0	2	1	0	3
	# Stem Failures	0	1	1	1	3	0	2	2	2	6
	Total # Failures	0	8	3	9	20	0	4	3	2	9
Total	# Trees	30	115	290	193	628	137	202	138	53	530
	# Uproot Failures	2	9	16	12	39	10	12	8	3	33
	# Stem Failures	0	6	20	8	34	3	7	5	4	19
	Total # Failures	2	15	36	20	73	13	19	13	7	52

Within the Hazus tree blowdown model, each family of tree blowdown curves (probability of blowdown versus wind speed) is stored as a function for a range of tree densities (trees/acre) for three pre-defined height classes for the coniferous and deciduous tree types. The original tree blowdown curves were developed by computing the probability of blowdown as a function of the effective drag per unit land area within the modeled “forest” canopy, rather than the number of trees per acre. The effective drag per unit land area is defined using a parameter referred to as C_dLAI , where C_d is a drag coefficient and LAI is the Leaf Area Index. The value of C_dLAI for an area is often obtained using satellite imagery to estimate the LAI and multiplying by a typical drag coefficient but can also be estimated by dividing the effective total drag area in the forested region, C_dA , by the total land area covered by the trees.

The estimated values of C_dLAI at the eight sites range between 0.01 and 0.02. The lowest two values of C_dLAI used in the development of the tree blowdown curves used in Hazus are 0.01 and 0.05, and these curves are given in Figure 4-87 along with the observed blowdown data for each Study Region. Separate plots are given for each height class and tree type (deciduous or coniferous). The large diamond shaped point on each plot represents the weighted average probability of blowdown for all trees of the class at all sites surveyed.

From the plots, it is seen that the collected data from Hurricane Isabel agrees well with the probability of blowdown curves for deciduous trees. However, less agreement is seen when coniferous trees are considered. It appears that for this case, the curves underestimate the actual probability of blowdown. In light of this comparison, the tree blowdown probabilities for coniferous trees were shifted to better agree with the available validation data.

The blowdown functions have been shifted as follows:

- All functions for short (< 40') conifers were shifted by 30 mph
- All functions for medium (40' to 60') conifers were shifted by 15 mph
- All functions for tall (> 60') conifers were shifted by 10 mph

Figure 4-88 shows the resulting shifted functions for coniferous trees along with the validation data.

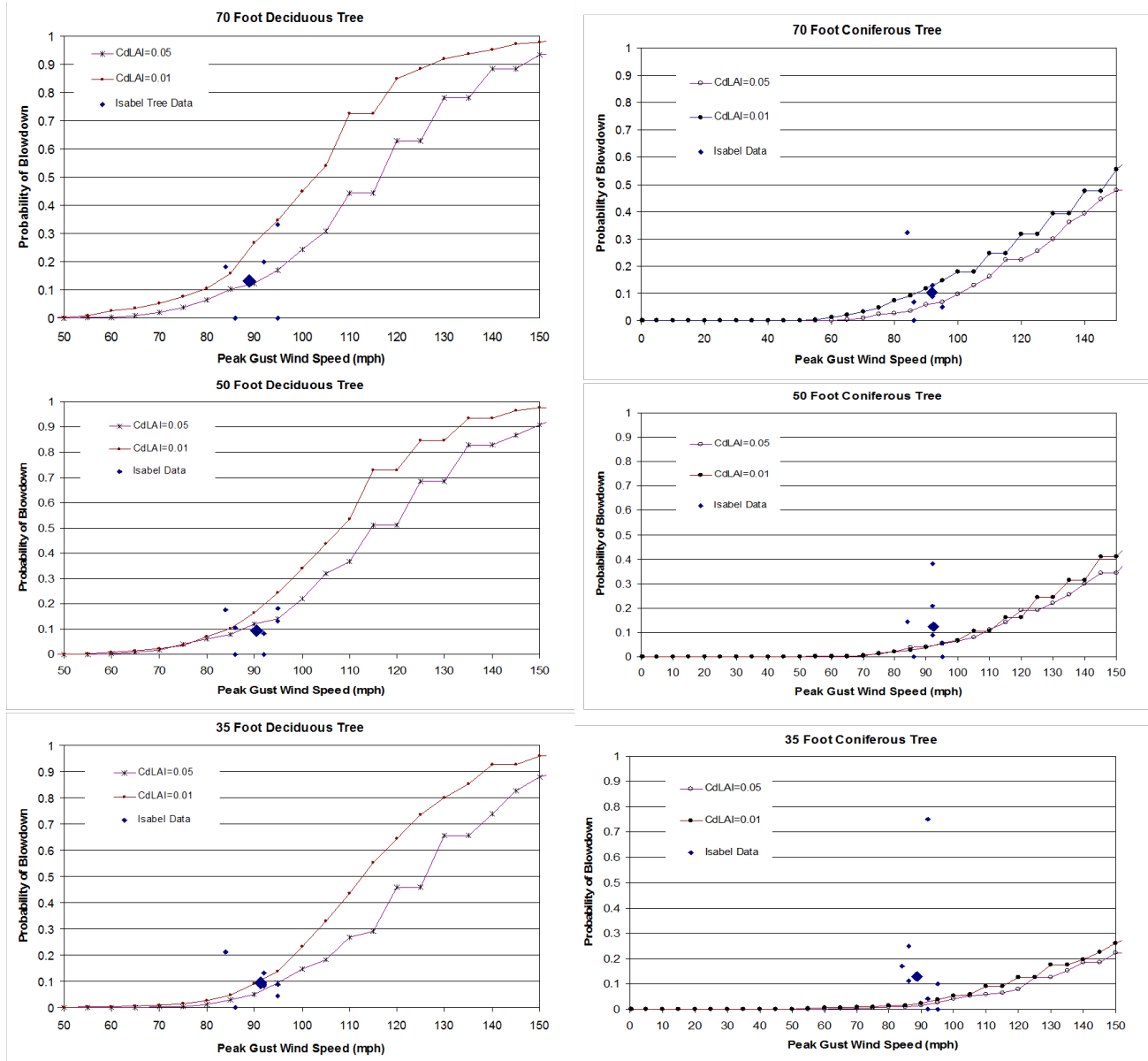


Figure 4-87 Probability of Blowdown Curves with Treefall Data Collected Following Hurricane Isabel

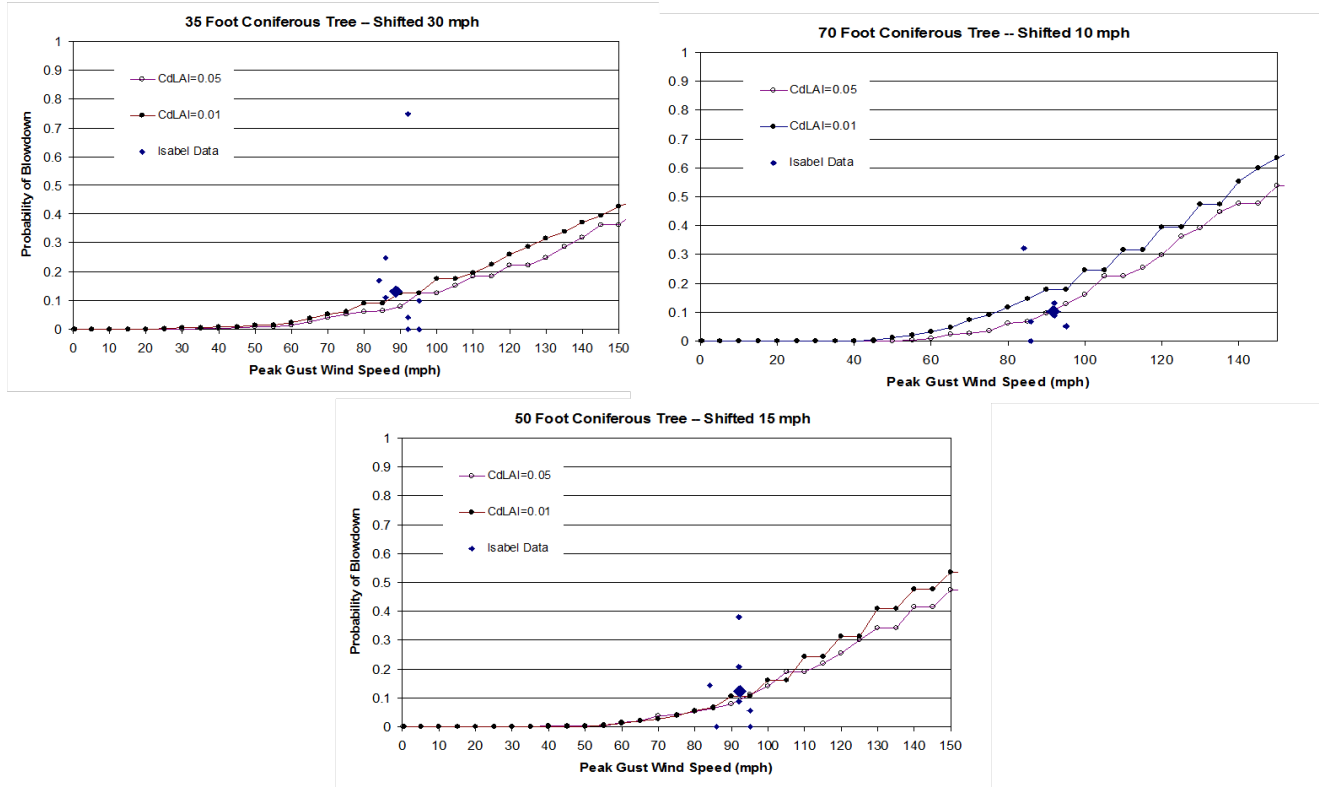


Figure 4-88 Shifted Probability of Blowdown Curves for Coniferous Trees with Treefall Data Collected Following Hurricane Isabel

4.5.4 Tree Inventory Data by County

4.5.4.1 Forest Inventory Analysis (FIA) Program and Database

The Forest Inventory Analysis (FIA) Program and Database of US Forest Service (USFS) is a nationwide tree inventory database updated on a 5-year cycle by states/regions. It is derived through a field survey and statistical analysis procedure. The database provides a spatial resolution down to the county level for the final product that is accessible in the public domain. It was initially designed for use by the lumber industry primarily; however, it contains data such as tree count and tree diameter distribution per species in every county that are useful for the analysis described in this section. It is recognized as an authoritative source of forest/tree data on a nationwide scale. The MRLC uses FIA data to verify the accuracy of satellite imagery analysis on forest cover.

4.5.4.2 Average Tree Density and Tree Height Distribution at County Level

The tree blowdown methodology utilizes FIA's tree count on forest land and tree height per species per county, downloaded from the USFS website. The data incorporated into Hazus 2.0 and later versions dates between 2006 and 2010 for all states (except Hawaii, which was not available during the tree inventory update) with the vast majority being from 2008-2009. Prior versions of Hazus relied upon diameter distributions to determine tree height, but tree height is now readily available for most of the 1279 counties in the 22 hurricane states and the District of Columbia via download from the FIA. For those counties that did not have tree height or tree density distribution information, data from

neighboring counties were used. In the case of Hawaii, data from American Samoa were used. The FIA data now includes Hawaii.

Using tree height information, tree height distributions were simplified into three groups (30-40 feet, 40-60 feet, and over 60 feet tall) and summarized over all species for each county.

For each county, the average tree density is derived by dividing the tree count on forest land by the total area of forest land of the county. The forest land area used was also downloaded from the FIA database.

It should be noted that the FIA field survey and resulting database includes only contiguous tree covered areas not less than 12 acres in area. For the purpose of the Hazus model, the average tree density and tree height distribution obtained as described above are applied to all tree covered areas in a county, including smaller patches and strips of tree covered areas embedded in residential subdivisions as identified by the MRLC land cover database.

4.5.5 Hazus Tree Coverage Database

The procedures conducted to derive a default tree database for Hazus from the MRLC land use database, and the FIA tree database are described in this section.

4.5.5.1 MRLC National Land Cover Data

As described in detail in Section 4.4, the MRLC (Multi-Resolution Land Characteristics consortium) land cover database, presented in 30 meters resolution grids, provides a relatively high spatial resolution of defined land cover types and percent tree canopy. Using the MRLC land cover database, combined with data derived from the FIA database, makes it possible to estimate the number of trees and predominant tree type at higher geographical resolutions than counties, including resolution at the Census block level as required for Hazus.

4.5.5.2 Tree Density, Tree Height, and Predominant Tree Type by Census Tract and Census Block

For the Hazus wind risk software product, a default tree database is developed that contains variables as outlined below for each Census tract.

The predominant tree type is defined in the MRLC land cover database as:

- *Coniferous*: if 75% or more of the tree covered area is identified as “Evergreen” type in the MRLC land cover database
- *Deciduous*: if 75% or more of the tree covered area is identified as “Deciduous” type in the MRLC land cover database
- *Mixed*: if neither of the above two criteria hold

Census blocks also hold to the same set of rules, however, if a Census block had no forested land according to the MRLC, then its predominate type defaults to the tract’s predominant type.

To determine tree density at the Census block level, the average tree density at the county level is first determined by dividing the tree count on forest land by the total area of forest land of the county. Second, the average canopy percentage in each county over areas determined to be evergreen forest, deciduous forest, mixed forest and woody wetlands was computed. Third, the stems per acre for 100% tree canopy for each county was computed assuming tree density and average canopy computed over forested areas are proportional. For example, if a county had 75 stems per acre with an average tree canopy of 50%, the stems per acre at 100% canopy was assumed to be 150 stems per acre. The maximum stems per acre was capped at 400. Finally, the average tree canopy over forested land of each Census block was multiplied by its county's corresponding stems per acre for 100% tree canopy.

Stems per acre at the tract level is calculated by weighting the stems per acre at the Census block level by area of the Census block, and aggregating up to the Census tract level as per Equation 4-72:

Equation 4-72

$$S_t = \sum_{i=1}^n S_i * \frac{A_{Ci}}{A_T}$$

Where:

- S_t is stems per acre at the tract level
- S_i is stems per acre at Census block i
- A_{Ci} is area of Census block i
- A_T is total area of Census tract
- N is the number of Census blocks in the tract

Trees less than 30 feet tall and less than 5 inches in diameter are not included in the variable of "Forest Land Tree Density of County" or in the subsequent analysis. Trees less than 30 feet tall normally have trunk diameters less than 5 inches and small crown weights. These trees are neglected in the debris volume and building damage models.

The tree height distribution represents the proportions of short (30-40 feet), medium (40-60 feet) and tall (>60 feet) trees. They sum up to 100%. In general, tree heights rarely exceed 100 feet, which represents the 99.9th percentile height for trees over 30 feet tall in the 22 states covered by the hurricane model. On a nationwide base, the average tree heights within the three bins are 35.0, 49.7, and 74.9 feet, respectively.

The format of the Hazus tree coverage database is summarized in Table 4-24. An example of the Hazus tree data is shown in Figure 4-89 for Wake County, NC at the Census tract level. A map of tree density is shown in Figure 4-90. The city of Raleigh, NC is in the lower density area in the center of the county.

Table 4-24 Hazus Tree Data Format

Census Tract	Predominant Tree Type	Stems per Acre of Land	Tree Height Distribution, %		
			30-40 feet	40-60 feet	>60 feet
xxxxxxxxxx	Coniferous, Deciduous, or Mixed	0-400	0-100	0-100	0-100

Table:

	Census Tract	Predominate Tree Type	Stems per Acre	Tree Height Less 40 ft	Tree Height 40 ft To 60 ft	Tree Height Greater than 60 ft	Tree Collection Factor
1	37183050100	Mixed	6	11	44	45	0.80
2	37183050300	Mixed	22	11	44	45	0.92
3	37183050400	Mixed	16	11	44	45	0.75
4	37183050500	Mixed	43	11	44	45	0.75
5	37183050600	Mixed	26	11	44	45	0.75
6	37183050700	Mixed	27	11	44	45	0.80
7	37183050800	Mixed	50	11	44	45	0.44
8	37183050900	Mixed	11	11	44	45	0.77
9	37183051000	Mixed	17	11	44	45	0.90
10	37183051100	Mixed	22	11	44	45	0.22
11	37183051200	Mixed	31	11	44	45	0.85
12	37183051400	Mixed	60	11	44	45	0.99
13	37183051501	Mixed	78	11	44	45	0.87
14	37183051502	Deciduous	82	11	44	45	0.92
15	37183051600	Mixed	66	11	44	45	0.98
16	37183051700	Mixed	79	11	44	45	0.77
17	37183051800	Mixed	38	11	44	45	0.80
18	37183051900	Mixed	70	11	44	45	0.82
19	37183052001	Mixed	44	11	44	45	0.46
20	37183052002	Mixed	60	11	44	45	0.93
21	37183052101	Mixed	67	11	44	45	0.65
22	37183052102	Mixed	62	11	44	45	0.41
23	37183052201	Mixed	33	11	44	45	0.55
24	37183052202	Mixed	49	11	44	45	0.41
25	37183052301	Mixed	91	11	44	45	0.51
26	37183052302	Mixed	58	11	44	45	0.39
27	37183052401	Mixed	59	11	44	45	0.18
28	37183052402	Mixed	51	11	44	45	0.75
29	37183052404	Coniferous	72	11	44	45	0.94
30	37183052405	Coniferous	34	11	44	45	0.81
31	37183052501	Mixed	68	11	44	45	0.79
32	37183052503	Mixed	75	11	44	45	0.56
33	37183052504	Mixed	53	11	44	45	0.66
34	37183052601	Mixed	75	11	44	45	0.96
35	37183052602	Mixed	64	11	44	45	0.95
36	37183052603	Mixed	76	11	44	45	0.79
37	37183052701	Mixed	38	11	44	45	0.62

Figure 4-89 Hazus Tree Coverage Data for Wake County, NC

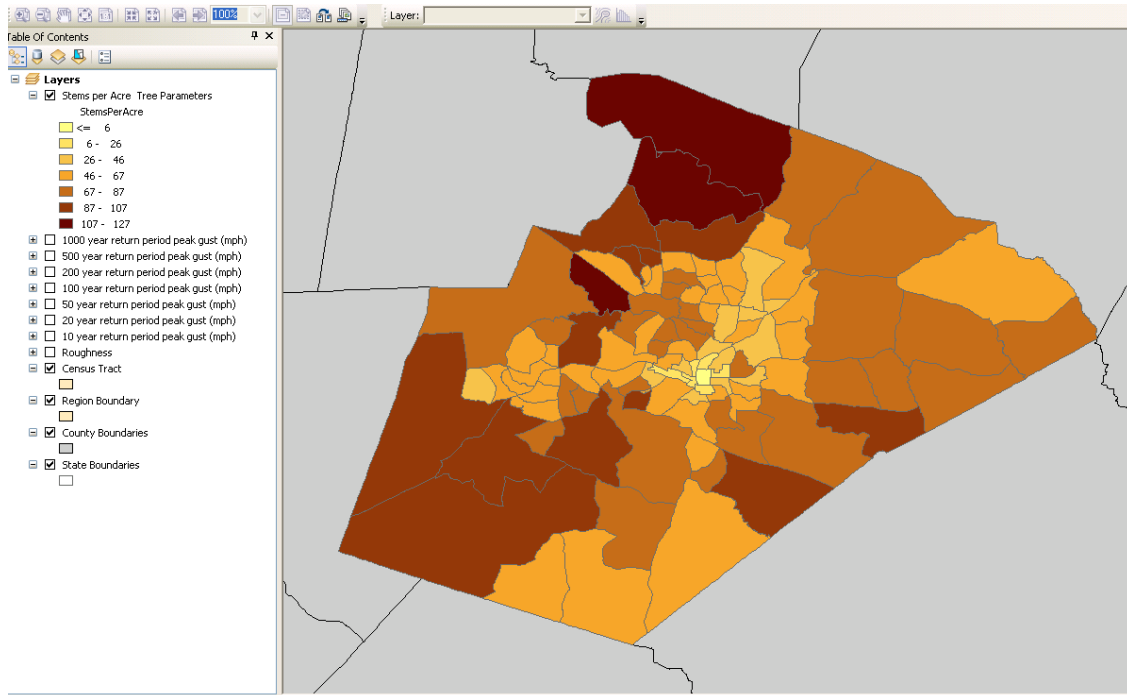


Figure 4-90 Map of Tree Density for Wake County, NC

4.6 Coastal Storm Surge

This section describes the development and validation of a hurricane storm surge and wave hazard modeling capability for Hazus. Due to the nature of surge modeling, this functionality can only be accessed through a combined wind and flood Study Region. Hazus draws on functionality in the wind and flood models to produce a hurricane storm surge risk assessment.

The process for generating a hurricane surge requires the Hazus Hurricane Model, which couples existing, publicly available hazard models to estimate the storm tide and coastal wave heights produced by a single hurricane event. The storm tide model is the SLOSH (Sea, Lake, and Overland Surges from Hurricanes) methodology described in NOAA Technical Report NWS 48 (Jelesnianski et al., 1992). The storm surge wave model is the SWAN (Simulating WAVes Nearshore) model, developed and distributed by Delft University of Technology (Delft University of Technology, 2020). The process of hurricane surge generation also requires the Hazus Flood Model, which includes the wave height model (a simplified version of the Wave Height Analysis for Flood Insurance Studies [WHAFIS]) (FEMA, 2015). Although the Hazus Coastal Flood Model is part of the surge generation process, the requirements to run a surge differ slightly than those needed to run a coastal flood. Additionally, Hazus also has the ability to import a user-supplied hurricane surge depth grid in the Hazus Flood Model. The import process may be found in the *Hazus Hurricane Model User Guidance* (FEMA, 2020). Figure 4-91 shows how the surge and coastal flood requirements differ from each other. Running a coastal flood in the Hazus Flood Model requires a user-provided DEM, stillwater elevation (SWEL) values, and shoreline breaks (location where the SWEL values change along the shoreline). Running a surge model in the Hazus Flood Model requires a user-provided DEM and wave exposure (fetch length). If a user is bringing in their own surge,

only the surge depth grid is required. The model differences between the analysis types are provided later in Figure 4-92.

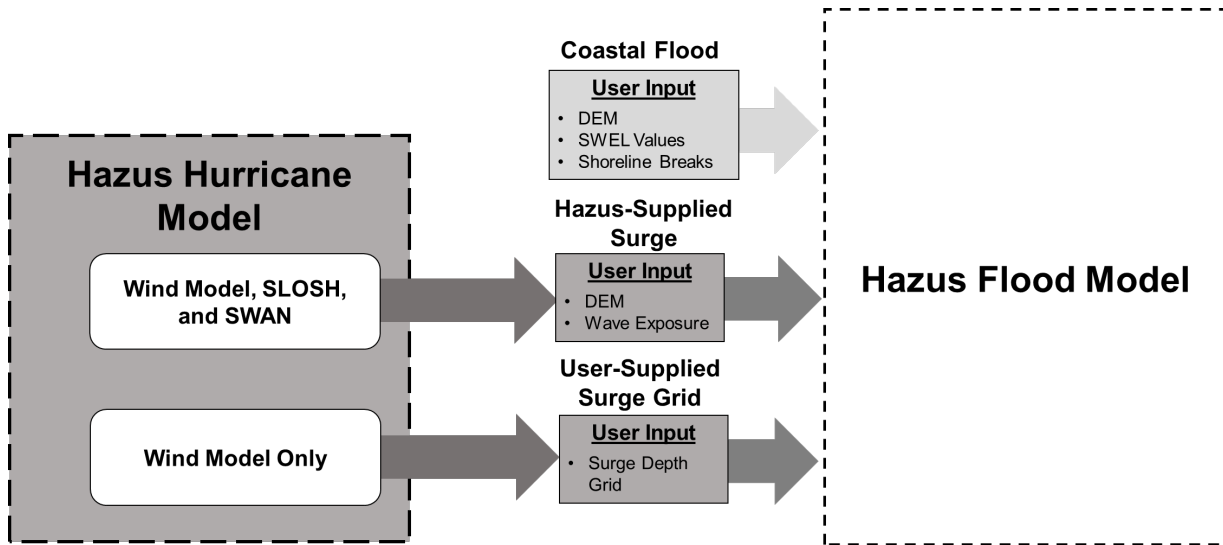


Figure 4-91 Surge and Coastal Flood User Requirements

In the Hazus Hurricane Model, the coupled surge and wave models have been modified to use the hurricane wind field model. The primary motivation for this decision was to use the same validated and peer reviewed wind field model for predicting both direct wind damage and coastal surge damage. In addition, the storm tide estimates obtained from SLOSH using the hurricane wind field model are more accurate, on average, than the storm tide estimate obtained from SLOSH using the default SLOSH wind field model. For more information on the validation studies for the surge models, please contact the Hazus Help Desk (see Section 1.5) for the *Hazus Hurricane Model Technical Manual Appendices* (FEMA, 2021).

The steps required to import a user-supplied surge depth grid created outside of Hazus are found in the *Hazus Model Flood User Guidance* (FEMA, 2022).

A methodology for combining wind and flood losses to buildings at the building subassembly level is presented in Section 8.4. The methodology is designed to avoid “double counting” of damage to building components due to wind and flood; however, the methodology does not attempt to determine the fraction of the combined loss that is attributable to wind or flood.

The coastal storm surge hazard and combined wind and flood loss methodologies have been implemented in Hazus to estimate direct, building-related economic losses to the General Building Stock due to a deterministic hurricane scenario.

The following hazard models have been integrated into the Hazus Hurricane and Hazus Flood Models.

1. *Hazus Hurricane Wind Field Model*: Executable code distributed with Hazus; source code developed and owned by ARA. The hurricane wind field model is described in Section 4.1 of this manual. Additional details and updates are provided in Vickery et al. (2000 and 2009).

2. *SLOSH*: The National Weather Service (NWS) developed the SLOSH model. It is a computerized numerical model to estimate storm surge heights resulting from historical, hypothetical, or predicted hurricanes. It considers the atmospheric pressure, size, forward speed, and track data. These parameters are used to create a model of the wind field, which drives the storm surge. FORTRAN and C source code for version 3.94 (2009) provided by National Weather Service's Meteorological Development Laboratory (NWS/MDL). The SLOSH methodology is described in NOAA Technical Report NWS 48 (Jelesnianski et al., 1992).
3. *SWAN*: SWAN is a third-generation spectra wave model capable of generating two-dimensional wave energy spectra under specified conditions of winds, currents, and bathymetry. It accounts for nearshore wave behavior such as wave breaking and wave setup and thus is suitable for shallow water computations of wave characteristics. This model was developed and distributed by Delft University of Technology. This software can be used freely under the terms of the GNU General Public License. See the [SWAN site](#) for more information. This is an optional model that will not be used if the no waves option is selected under the surge analysis described in Section 4.6.1.
4. *Simplified WHAFIS Model*: FEMA's WHAFIS model develops overland wave heights based on stillwater elevations, starting wave conditions, ground elevation, and obstructions in the inland area. More information can be found in FEMA's Coastal Overland Propagation Guidance from 2015 (FEMA, 2015).
5. *Hazus Coastal Flood Model*: The model is an executable code distributed with Hazus. The Coastal Flood Model creates transects used by the simplified WHAFIS model, contains a national shoreline and wave characteristics database, and generates damages and losses from the surge depths and coastal zones as well as a combined loss from wind and surge damage. The coastal flood model is described in the *Hazus Flood Model Technical Manual* (FEMA, 2022).

SLOSH and SWAN have been modified to use the hurricane wind field model in Hazus. For the purposes of this manual, the models will be referred to as "SLOSH" and "SWAN" throughout.

4.6.1 Integration of Storm Surge Models

For use in Hazus, the primary purpose of the wave hazard model is to predict hurricane-induced wave heights in developed areas inundated by hurricane storm surge. A secondary purpose is to estimate wave setup stresses for coupling back into SLOSH, which will result in higher stillwater elevation predictions.

There are three different storm surge modeling options available to a Hazus user, no waves, near shore waves, and deep water. Figure 4-92 shows the differences between the three options. As the model runtime increases, the accuracy of the model increases. All three models require SLOSH, but the no waves option does not require the SWAN model. Selecting this option speeds up the model's runtime but decreases the accuracy.

Figure 4-93 presents a flow chart of how a storm surge is generated in Hazus. The Hazus Wind Model and Hazus Flood Model are shown with their integrated models and processes.

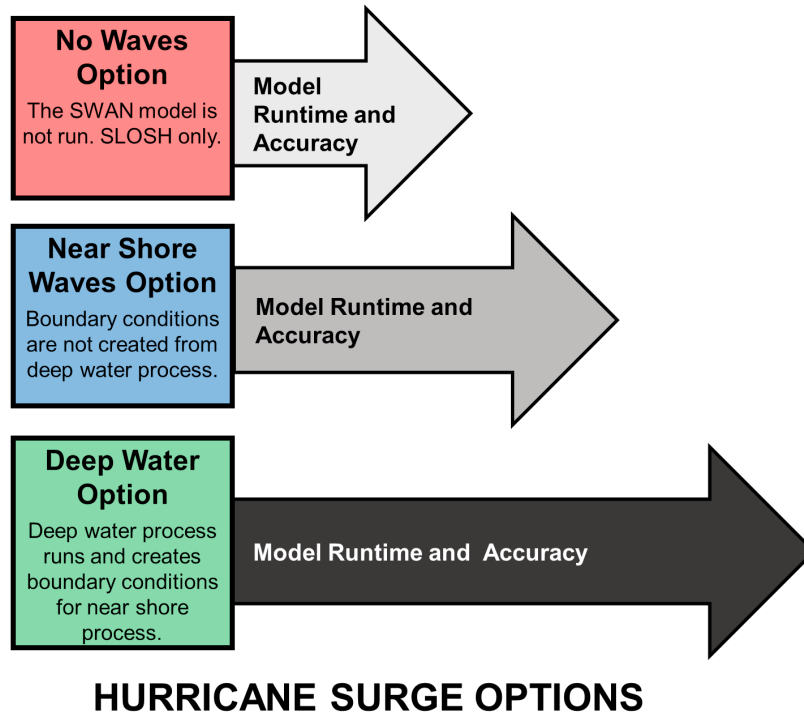


Figure 4-92 Hazus Storm Surge Options

4.6.1.1 Coupling of SLOSH and SWAN

Two-way coupling between the storm tide model and the nearshore wave model has been implemented for the Hazus Coastal Surge Methodology. The process is illustrated in Figure 4-93 and Figure 4-94. For a given hurricane event, the storm surge analysis is run for a fixed period of simulation time (i.e., 15 minutes) and then suspended. The new water levels from SLOSH are then passed to SWAN, and the wave model is advanced for the same fixed period of simulation time. The nearshore breaking wave stresses from SWAN are then passed back to SLOSH for the next time increment, and the simulation continues until the hurricane passes through and beyond the Study Region.

HAZUS HURRICANE MODEL

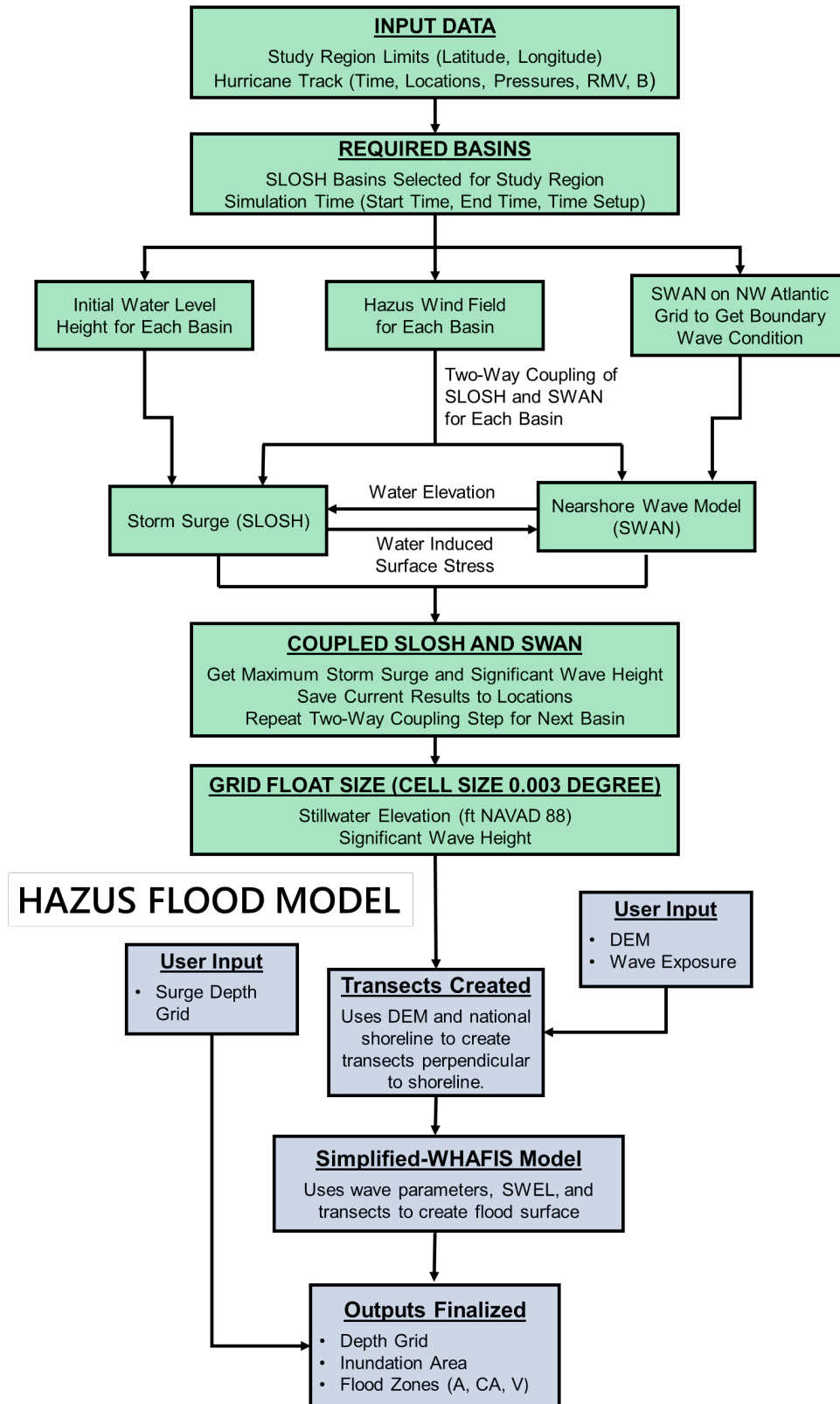


Figure 4-93 Hazus Coastal Storm Surge and Wave Model Flow Chart

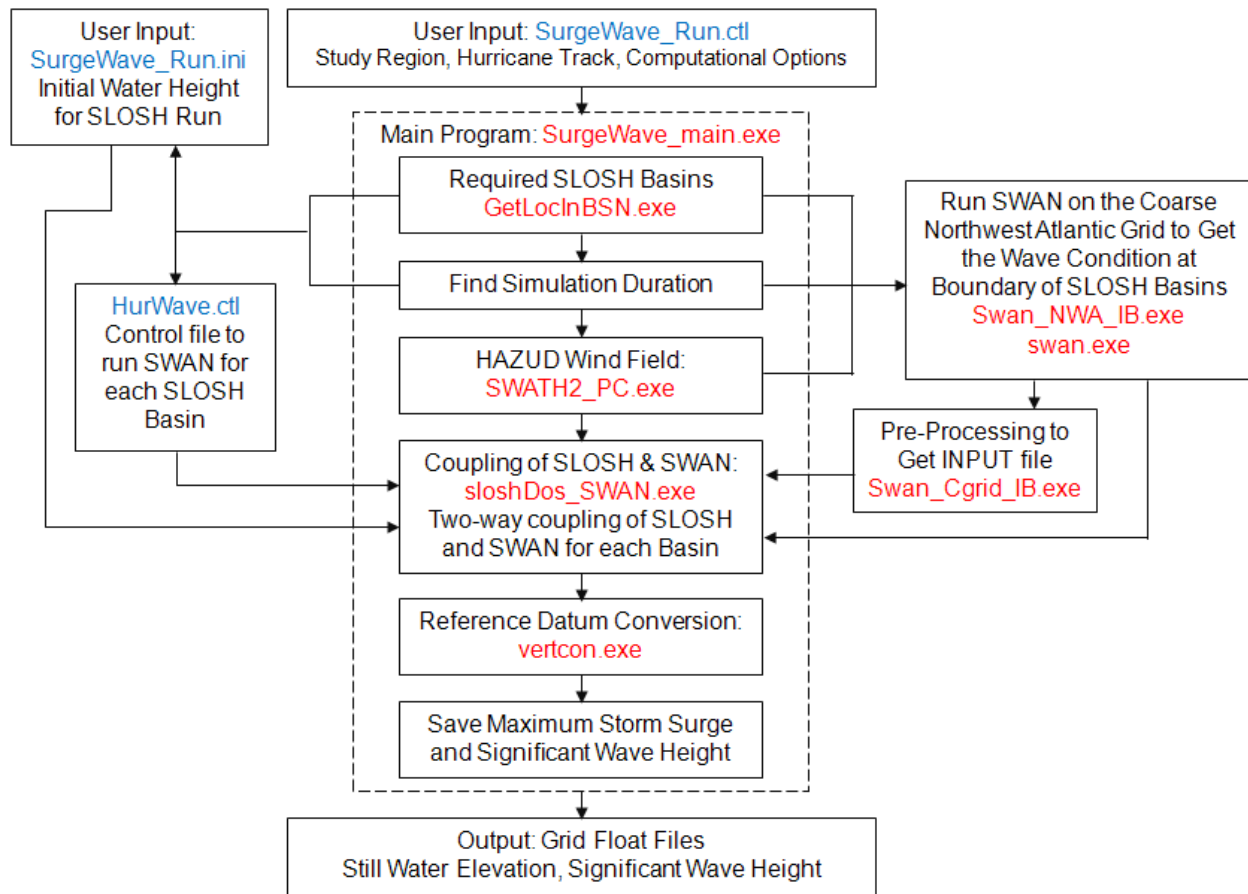


Figure 4-94 Hazus Coastal Storm Surge and Wave Model Software Components

The effect of the two-way coupling on the modeled storm surge elevation is illustrated for Hurricane Ike in Figure 4-95. In these plots, the increase in the peak modeled storm surge elevations due to the inclusion of wave stresses is shown for the Galveston Bay SLOSH Basin. For the flooded cells, the mean increase in surge elevation is 0.44 feet.

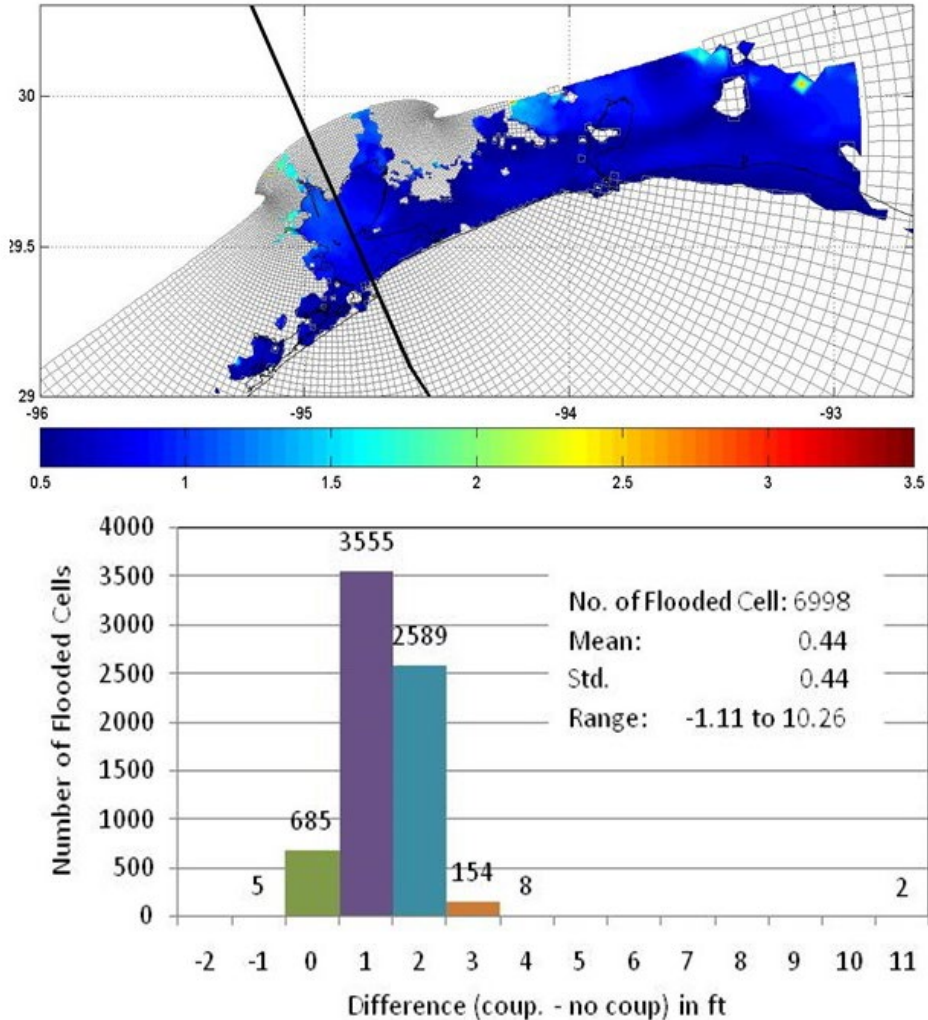


Figure 4-95 Difference (feet) in Peak Modeled Storm Tide with and without Coupling of Surge and Wave Models for Hurricane Ike

4.6.2 Coastal Surge Analysis for Study Regions Spanning Multiple SLOSH Basins

At present, there are 32 SLOSH basins along U.S. Atlantic and Gulf of Mexico coastlines, as shown in Figure 4-96 and listed in geographical order in Table 4-25. Eleven basins, highlighted in Table 4-25, were updated by NOAA in 2009 to incorporate the latest topography and bathymetric data and to provide higher grid size resolution and better representation of basin features. Given user-provided locations, priority for basin selection is governed by the grid resolution and the computer run time. Hazus model run times depend on simulated storm duration, basin size, and the number of basins. For a given Study Region, there is a significant increase in the run time as the number of selected basins increases.

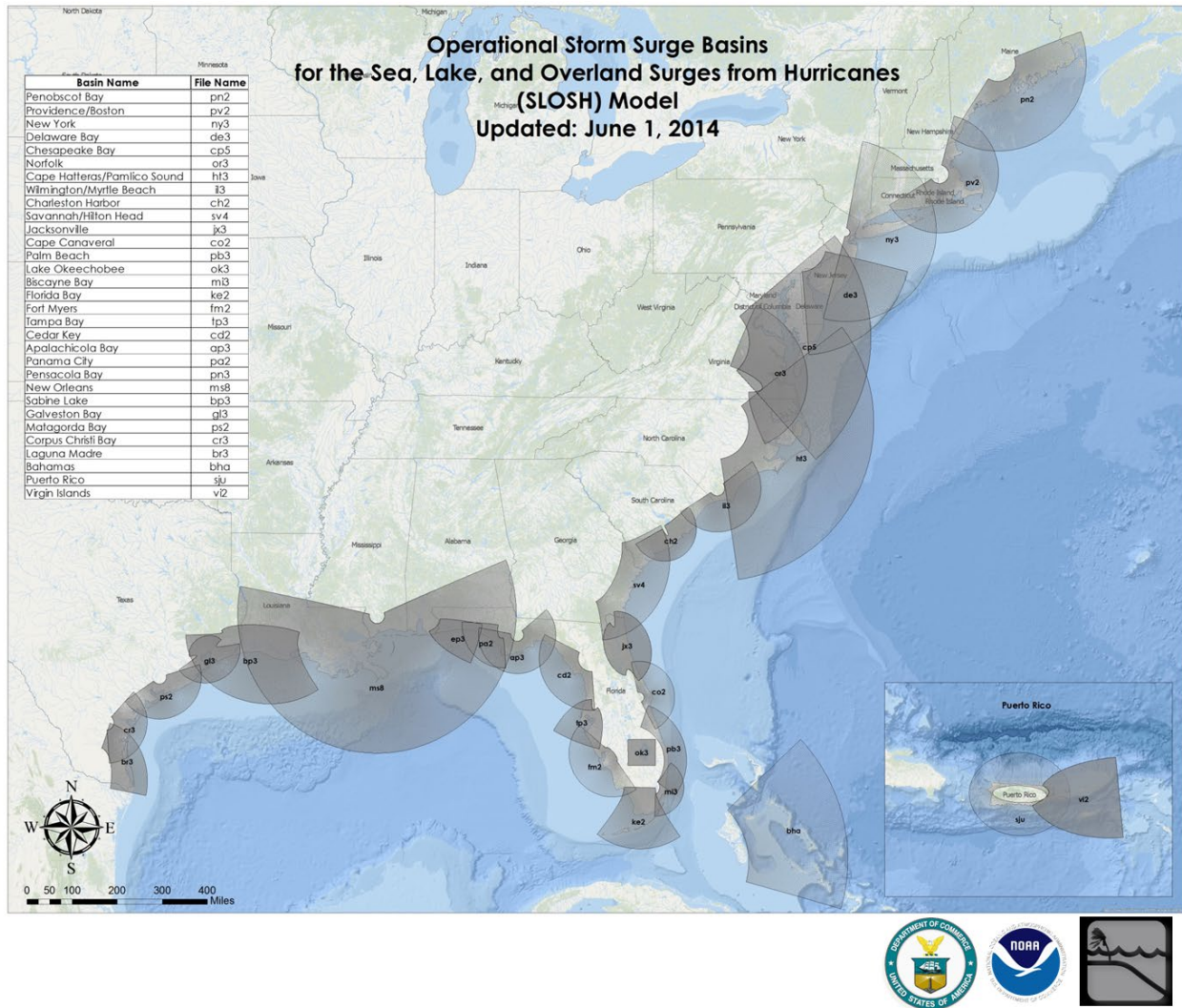


Figure 4-96 SLOSH Basins

Table 4-25 SLOSH Basins Used in Hazus Coastal Surge Methodology

IDBSN	Basin Name (bsnname)	Basin Code (bsncode)	Dimensions (miles)	Used in Hazus
1	Laguna-Madre	br2	85 x 108	✓
2	Corpus-Christi	cr2	67 x 75	✓
3	Matagorda- Bay	ps2	192 x 211	✓
4	Galveston- Bay	egl2	115 x 100	✓
5	Sabine-Lake	ebp3	224 x 350	✓
6	Vermilon-Bay	lft	128 x 156	
7	New-Orleans	ms4	175 x 189	✓
8	MS-GulfCoast	hbix	120 x 120	

IDBSN	Basin Name (bsnname)	Basin Code (bsncode)	Dimensions (miles)	Used in Hazus
9	<i>Mobile-Bay</i>	<i>emo2</i>	<i>229 x 135</i>	✓
10	<i>Pensacola-Bay</i>	<i>epn3</i>	<i>200 x 330</i>	✓
11	Panama-City	hpam	105 x 118	✓
12	Apalachicola-Bay	apc	71 x 93	✓
13	Cedar-Key	cdr	79 x 85	✓
14	<i>Tampa-Bay</i>	<i>etp3</i>	<i>188 x 215</i>	✓
15	Fort-Meyers	efmy	111 x 100	✓
16	Florida-Bay	ekey	170 x 200	✓
17	Biscayne-Bay	hmia	125 x 190	✓
18	<i>Okeechobee</i>	<i>eok2</i>	<i>129 x 136</i>	✓
19	Palm-Beach	pbi	71 x 153	✓
20	Cape-Canaveral	cof	69 x 89	✓
21	Jacksonville	ejax	84 x 96	✓
22	<i>HiltonHead</i>	<i>esv3</i>	<i>152 x 200</i>	✓
23	Charleston-Harbor	hchs	95 x 150	✓
24	<i>Wilmington-NC</i>	<i>il2</i>	<i>171 x 236</i>	✓
25	<i>Pamlico-Sound</i>	<i>eht2</i>	<i>180 x 130</i>	✓
26	Norfolk	eorf	100 x 110	
27	Chesapeake-Bay	cp2	79 x 84	✓
28	Ocean-City	oce	75 x 99	
29	Atlantic-City	acy	87 x 108	✓
30	New York	ny2	90 x 83	✓
31	<i>Buzzards-Bay</i>	<i>pv2</i>	<i>183 x 280</i>	✓
32	Penobscot-Bay	pnb	108 x 115	✓

* Shaded Italicized cells and basins with an asterisk represent the updated basins that also use the newer North American Vertical Datum of 1988 (NAVD 88) instead of the older National Geodetic Vertical Datum of 1929 (NGVD29).

The following criteria are used to determine which basins will be selected for a Hazus Study Region:

- Where multiple basins overlap for a given location, the one with the finer grid size resolution (usually the one with minimum distance from the basin origin to the location) will be used
- All of the 2009 versions of SLOSH basins are used because they better represent local features

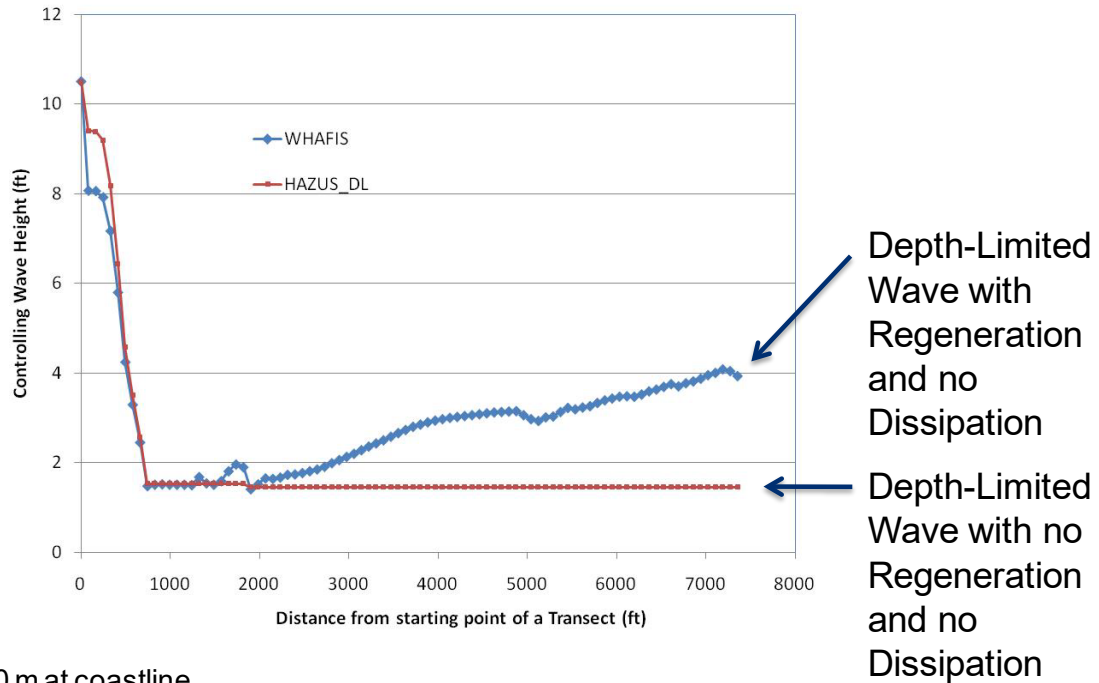
The advantage of this basin selection approach is that it offers good grid resolution in areas of greatest interest while conserving computer resources by minimizing the number of basins required to simulate the storm surge and wave levels in a Study Region.

4.6.3 Integration with Coastal Flood Model

The relatively rapid changes in ground elevation and the significant increase in wave dissipation effects over land cannot be accurately modeled with the SWAN model's course grid. To address this limitation, the methodology implemented in Hazus is to model waves over land using a simplified, WHAFIS-like transect analysis methodology documented in the *Hazus Flood Model User Guidance* (FEMA, 2022). The starting wave height used in the transect analysis is the modeled significant wave height from the first completely offshore cell in the analysis grid.

For the initial implementation of the overland wave model, both wave dissipation and wave regeneration effects are neglected. No allowance is made for modeling the effects of surface roughness, vegetation, or obstructions on wave height in the Hazus transect analysis methodology. Developing a robust dissipation procedure would be difficult given the minimal information required of hurricane surge model users and given the detail that would be required to accurately capture dissipation over upland areas.

The simplified WHAFIS model in Hazus and the regular WHAFIS model have some differences, including the simplified model neglecting wave dissipation and wave regeneration effects. Figure 4-97 shows the modeled controlling wave heights produced by the simplified WHAFIS model in Hazus using a depth-limited wave height analysis methodology along a transect extending inland from the coastline to the location of SSS-TX-GAL-002 (in red). Results are compared to a model that has incorporated wave generation and dissipation (in blue). The results without wave regeneration are in reasonable agreement with the actual wave heights observed at SSS-TX-GAL-001 and SSS-TX-GAL-002. More information on the limitations of the coastal flood model can be found in the *Hazus Flood Model Technical Manual* (FEMA, 2022).



- Hsig=2.0 m at coastline
- SWEL=12.0 ft (assumed to be 100-year RP)
- All of the results from HAZUS except first point are “instantaneous” depth limited waves

Figure 4-97 Modeled Controlling Wave Heights Produced by the Hazus Methodology for a Transect Extending Inland from the Coastline to the Location of SSS-TX-GAL-002

Although wave dissipation and regeneration effects are not included in the Hazus Coastal Flood Model, the wave exposure, significant wave height (H_s), and peak wave period (T_p) are required for a hurricane surge analysis. The significant wave height is defined as the average of the highest one-third (33%) of waves (measured from trough to crest) that occur in a given period. The peak wave period is the wave period with the highest energy.

4.6.3.1 Wave Exposure

Wave exposure is based on the classification of the severity of wave conditions that will accompany the hurricane surge event. It is the fetch length where the winds can act on the water without obstruction. Fetch is defined as the overwater distance across which winds blow, and waves develop or grow. Users should select a wave exposure that corresponds to its fetch under the hurricane surge conditions, not under normal conditions. For example, a mainland shoreline segment, landward of a low-lying island, may have a short fetch under normal conditions, but the island may be flooded, and the fetch may increase under more severe conditions. For the purposes of the Hazus Flood Model, the user classifies shoreline segments according to one of four exposures, from open coast (full exposure – the most severe wave conditions) to sheltered (waves can be ignored, and flooding will be approximated by stillwater flooding).

Calculations were made to estimate significant wave height, H_s , versus local stillwater depth, d_s , under a range of wind speed and water depth conditions, and the results are shown in Table 4-26. The H_s versus d_s relationships for Moderate and Minimal Exposure scenarios are approximate, given the

number of factors that come into play and the wide range in fetch distances included within the Moderate Exposure and Minimal Exposure categories. The relationships represent expected fetch-limited wave conditions (no depth or duration constraints) near the mid-point of the fetch range for each category.

Table 4-26 Shoreline Wave Exposure Classification for Hazus Flood Model

Wave Exposure at Shoreline	Wave Height at shoreline (feet)	Typical Peak Wave Period at shoreline (seconds)
Exposed, Open Coast	$H_s = 0.49$ times local stillwater depth, d_s	$T_p \approx 2-20$ sec (varies by coast and flood return period)
Moderate Exposure	$H_s \approx 0.40 d_s$	$T_p \approx 0.45$ to $0.70 T_p$ open coast (varies by coast)
Minimal Exposure	$H_s \approx 0.20 d_s$	$T_p \approx 0.25$ to $0.40 T_p$ open coast (varies by coast)
Sheltered	$H \approx 0$	$T \approx 0$

· Wave heights and periods will vary by region, degree of exposure and flood return period.

Location descriptions of wave shorelines (for Table 4-26) are listed below:

- *Open coast (full exposure):* Shorelines directly fronting Atlantic and Gulf of Mexico, (deepwater with fetches >50 miles)
- *Moderate exposure:* Large bays and water bodies, with fetches between 10 miles and 50 miles
- *Minimal exposure:* Small bays and water bodies, with fetches between 1 mile and 10 miles
- *Sheltered:* Water bodies, with fetches <1 mile

4.6.3.2 Coastal Flood Outputs

Given a known building (i.e., specific occupancy, foundation type, and building height grouping) at a known location, the Hazus Coastal Flood Model require two inputs to estimate the extent of coastal flooding damage as a percentage of building or contents replacement value:

- Wave height at the location
- Total water depth at the location (i.e., wave crest elevation subtracted by ground elevation)

The wave height is used to determine the flood hazard zone (Zone V, Coastal Zone A, or Zone A) and, hence, the depth-damage function, where the water depth (along with the foundation type) is used to determine where to enter into the depth-damage function. Depth-damage functions are currently only available in the Hazus Library for Zones V and A. When generating a depth grid, Hazus will use only Zone

V functions. If a user provides their own surge depth grid instead of using Hazus to generate it, Hazus identifies the entire inundated area as a Coastal Zone A.

The steps a user can take to run a combined analysis for computing combined hurricane and flood losses can be found in Section 11 of the *Hazus Flood Model User Guidance* (FEMA, 2020). The methodology describing the combined loss analysis can be found in Section 8.4.

Section 5. Physical Damage Modeling

The physical damage model predicts wind-induced pressure damage to windows, doors, wall cladding, roof cladding, and roof cover. The model also predicts glazing failure due to impacts from windborne debris. Wall failures due to inward and outward pressure loads are also modeled for masonry and wood frame walls. Failure of the connections between the roof frame and the perimeter walls are also modeled for both wood and steel roof framing systems. In addition to these failure mechanisms, the physical damage model predicts foundation failures (i.e., sliding, overturning, and uplift) for manufactured homes, and tree blowdown damage to single-family homes and manufactured homes.

The physical damage model predicts hurricane-induced building damage by comparing loads to resistances. For a given building, directionally dependent pressure coefficients are estimated (see Section 5.1) for all building components and cladding. In addition, loads acting on walls surfaces (for predicting wall failures), on roof surfaces (for predicting failure at roof/wall connections), and on the entire building (for predicting foundation failure) are computed by spatially integrating the pressure coefficients estimated at each point on a uniform grid covering the appropriate building surface. The resistance associated with each failure mechanism is defined by a probability distribution from which resistances are sampled for a given storm simulation.

Given the estimates of the loads and resistances associated with the modeled failure mechanisms, the approach used to predict building damage consists of monitoring the wind speed and direction at fifteen-minute intervals over the entire duration of the storm. At each time step, wind loads are compared to resistances to predict direct wind damage. At the same time, the number of missiles impacting the building walls is computed (using the fast-running missile impact model described in Section 5.2) to predict glazing damage as well as damage to the wall finish.

Internal pressurization of the building is also considered in the physical damage model. That is, the total pressure acting on a window, for example, is computed as the sum of the external suction acting on the outside of the window and the internal pressure acting on the inside of the window. The internal pressure is estimated based on the number and size of wall breaches due to failed windows, doors, and wall cladding. In a given time step, if additional envelope breaches occur, the internal pressure is re-computed, as are the net loads associated with each of the failure mechanisms, which again are compared to the resistance in the same time step to assess additional building damage. This modeling approach is shown schematically in Figure 5-1. Note that all resistances and modeling error statistics associated with the wind loads are sampled before the storm passes by the building and are held constant for the duration of the storm. To obtain statistics on the possible damage outcomes for each storm, the component resistances and loading error statistics are re-sampled and a new damage simulation is performed using the same storm. The possibility of additional damage to single-family homes and manufactured homes due to tree blowdown is modeled separately. Building and contents losses due to tree blowdown are combined with the wind pressure and windborne debris losses in a later step as described in Section 5.2.

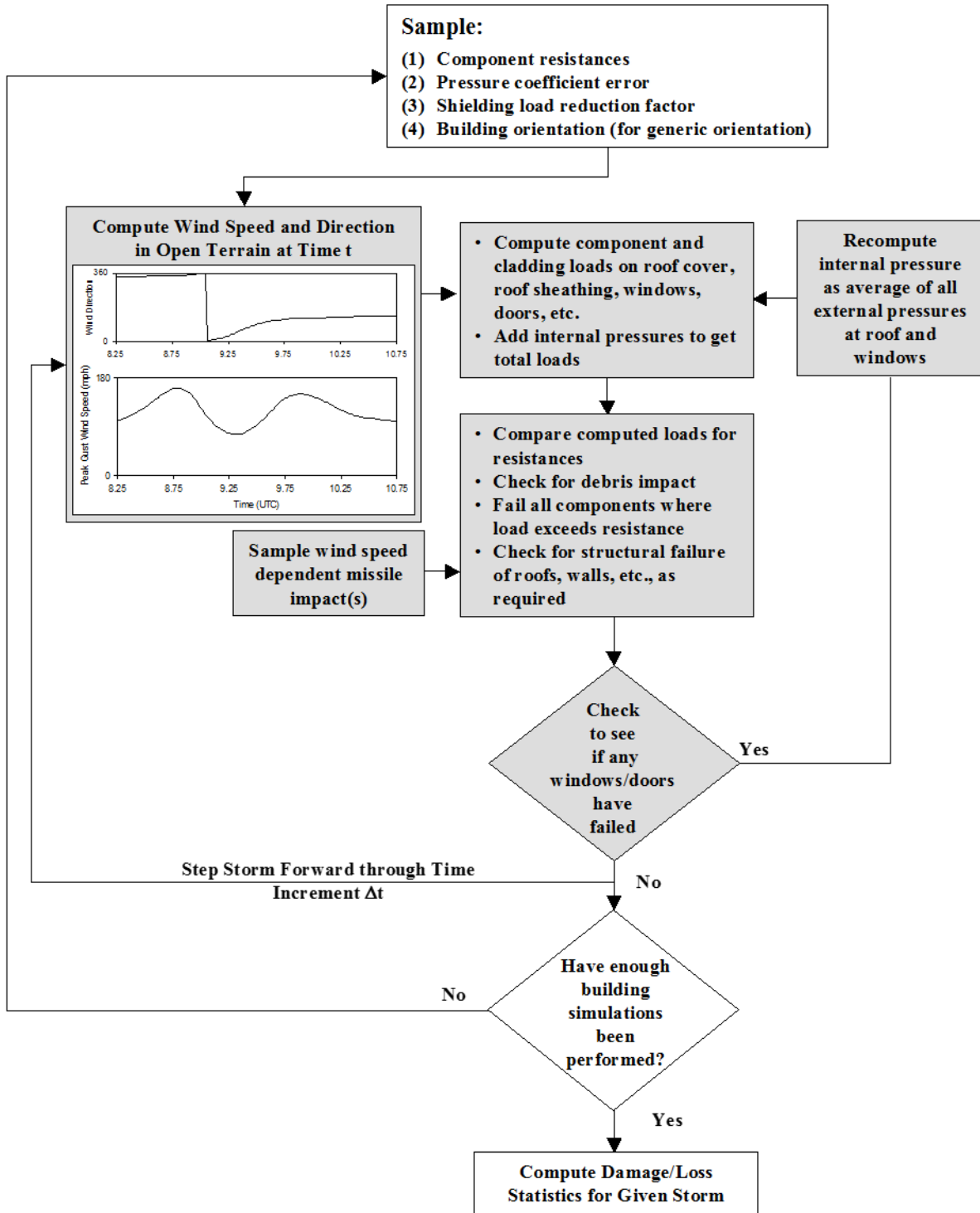


Figure 5-1 Approach Used to Simulate Damage to Buildings

This section describes and quantifies the wind pressure loads, the windborne debris loads, the tree blowdown loads, and the resistances of the various components used to model buildings and, where possible, presents examples of predicted and observed building damage states using data available at the time of initial development (1998-2001) to demonstrate the suitability of the load and resistance model for estimating wind induced damage.

After the loading models are described in Section 5.1, the following sections describe the resistances of components commonly found in residential buildings, and a validation of the load-resistance model for residential buildings. Next, the development of the manufactured home resistance and damage model is given, again followed by a validation study. Finally, descriptions of the models developed for modeling the failures of single ply membrane and built-up roofs, metal buildings, steel joists, and metal roof decks are given. The suitability of this model is tested through comparisons to the limited available full-scale damage data.

Single-wall construction practices can vary in island jurisdictions due to local conditions. For additional detail on single-wall dwellings in Hawaii and the U.S. Caribbean territories, see *Hazard Mitigation Study for the Hawaii Hurricane Relief Fund* (Applied Research Associates, Inc., 2001) and *Hazus Hurricane Wind for Puerto Rico and the U.S. Virgin Islands* (FEMA, 2021), respectively.

5.1 Wind Loads

Wind loads on buildings are usually estimated using either boundary layer wind tunnel tests performed for a specific building or using code-specified loads that have been developed by committees from boundary layer wind tunnel test data. If wind tunnel loads are used in the design of a building or its components, the wind loading coefficients are typically measured for 36 different wind directions, with the results combined with a statistical model of the wind climate for the location where the building is to be built. Using this approach, the design loads obtained for the building consider the effect of the variation of the wind loads with the direction of the approaching wind, and how these variations in load with direction align with the directional characteristics of the wind.

Essentially all low-rise buildings are designed using wind loads obtained from building codes. While the loading coefficients given in the codes have been developed using wind tunnel test data, the directional effects are not explicitly reproduced in North American building codes and standards. For simplicity and ease of use, the loads given in building codes represent an estimate of the maximum load acting on a portion of the building. Different values of the loading coefficients are given in the codes for various zones on the roofs and walls. The selection of the number and size of these zones is a compromise between the true spatial variability of the maximum wind loads and the use of as few zones as possible to simplify the design procedure. The greater the number of zones specified in a building code, the more accurate will be the final estimate of the distribution of the maximum loads acting on the building. The maximum values of the pressure coefficients given in the codes for each zone do not necessarily occur for winds approaching from the same wind direction, and therefore code-specified loads alone cannot be used to model wind loads on a building for wind approaching from a given direction.

Designers are able to take advantage of the variation of the wind loads with wind direction in both the UK and Australia, if they chose to use the detailed design procedures given in their respective building codes.

For predicting wind loads on buildings in the development of fast running damage and loss functions, it is necessary to model the variation in the wind loads acting on the building as a function of the location on the building and as a function of the direction and magnitude of the wind speed. The best approach is to use the results from wind tunnel tests directly and combine these results with the simulated

hurricane winds and directions to estimate the loads. Unfortunately, this approach is not viable since the detailed wind tunnel test data (if available) are limited by the number and locations of the pressure taps used in the models, the number of terrains in which the model buildings were tested, and the number of different geometries tested. Without the use of wind tunnel data, the next best method for developing wind loads as a function of direction is the development of an analytic or empirical model that is able to reasonably reproduce the variation of wind loads with direction, as well as the effects of aspect ratio, terrain, etc. The Australian and UK wind loading provisions represent simple examples of such an approach.

The methodology selected by the Hazus Wind Committee for developing damage and loss functions was to use code-specified loads as the basis for the model. To treat wind directionality for roof loads, tabulated values of the pressure coefficients as a function of direction are estimated using wind tunnel data, and the UK Building Code. In the case of wall loads, the pressure coefficients are modeled with cosine functions. Using this approach, the peak magnitudes of the loads correspond to the values specified in the building code adopted “standards.” The pressure coefficients developed using this approach are discussed in the following sections, and the results of the empirical direction model are compared to measurements of loads acting on buildings determined from wind tunnel tests. The wind loads derived using the hybrid code/directional model are applied to a number of simply shaped buildings. The shapes of the buildings considered are all either square or rectangular in plan and have either flat, hip, or gable shaped roofs.

5.1.1 Wall Pressures – Low-Rise Buildings

The magnitudes of the wall pressures used for modeling wind loads for the prediction of wind induced failures of components and cladding were derived considering the pressure coefficients given in North American wind loading standards and/or codes. The standards/codes considered in the development of the wind loads are the American Society of Civil Engineers (ASCE) 7-95, Southern Building Code Congress International (SBCCI) (1998 Edition), and the 1995 edition of the National Building Code of Canada (NBCC). In order to compare the magnitudes of the loading coefficients given in each standard/code, all coefficients were adjusted to be referenced to the mean hourly wind speed at roof height. In the case of both the NBCC and SBCCI pressure coefficients, the coefficients were divided by a value of 0.8 to remove the directionality factor that is explicitly included in the pressure coefficients given in the codes (Mehta, 1984). Additionally, in the case of the SBCCI coefficients, an internal pressure coefficient having a value of 0.2 was removed from the coefficients as given in the code before any comparisons were made. To convert the coefficients given in ASCE 7-95 from values which are normalized by the peak gust wind speed at roof height to the value, which is normalized by the mean hourly wind speed, a gust factor of 1.57 was used. The gust factor (1.57) used for converting the mean hourly wind speed to a 3-second gust was derived from the Engineering Sciences Data Unit (ESDU) (1982) gust factor models for open terrain conditions ($z_0 = 0.03$ meters) and a mean roof height of about 4 meters. In the case of the SBCCI coefficients, which are referenced to the fastest mile wind speed at roof height, a gust factor of 1.27 was used in the change of the reference dynamic pressure to a mean hourly value. The 1.27 gust factor was also computed using the ESDU (1982) gust factor model assuming open terrain conditions at the height of 4 meters and an averaging time of 32 seconds (i.e., 3600/110). Table 5-1, Table 5-2, Table 5-3, and Table 5-4 show the comparison of the peak

coefficients derived from the three sources for the edge and central regions of the walls (as shown in Figure 5-2) normalized by the mean hourly wind speed at the average roof height.

Table 5-1 Comparison of Positive Wall Pressure Coefficients – Buildings with Roof Slopes Less than 10°

Pressure Zone			Pressure Coefficient		
NBCC	SBCCI	ASCE 7-95	NBCC	SBCCI	ASCE 7-95
e	e	5	2.3	2.1	2.2
w	w	4	2.3	2.1	2.2

Table 5-2 Comparison of Positive Wall Pressure Coefficients – Buildings with Roof Slopes Greater than 10°

Pressure Zone			Pressure Coefficient		
NBCC	SBCCI	ASCE 7-95	NBCC	SBCCI	ASCE 7-95
e	e	5	2.3	2.3	2.5
w	w	4	2.3	2.3	2.5

Table 5-3 Comparison of Negative Wall Pressure Coefficients – Buildings with Roof Slopes Less than 10°

Pressure Zone			Pressure Coefficient		
NBCC	SBCCI	ASCE 7-95	NBCC	SBCCI	ASCE 7-95
e	e	5	-2.6	-2.5	-3.1
w	w	4	-2.3	-2.1	-2.5

Table 5-4 Comparison of Negative Wall Pressure Coefficients – Buildings with Roof Slopes Greater than 10°

Pressure Zone			Pressure Coefficient		
NBCC	SBCCI	ASCE 7-95	NBCC	SBCCI	ASCE 7-95
e	e	5	-2.6	-2.7	-3.5
w	w	4	-2.3	-2.5	-2.7

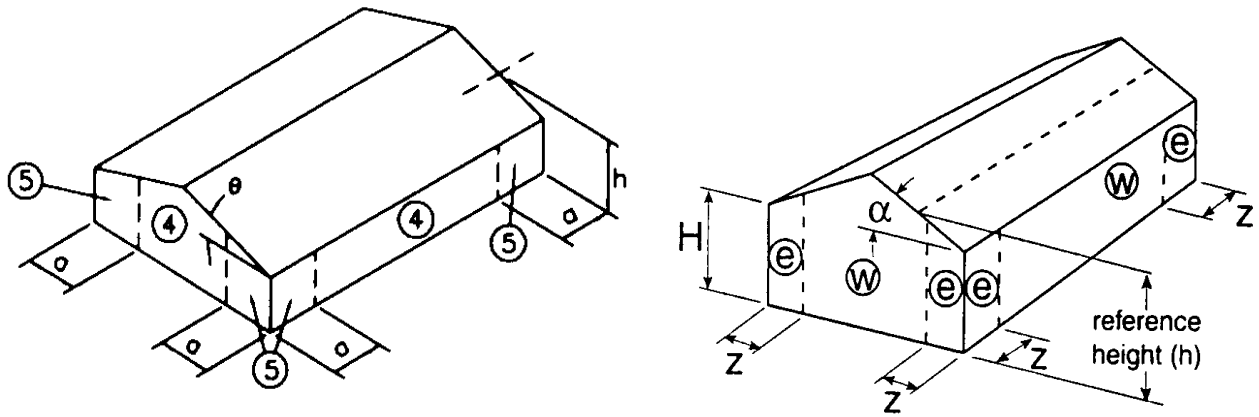


Figure 5-2 Wall Pressure Zones as Defined in ASCE 7 (Left figure) and SBCCI and NBCC (Right figure)

The coefficients given in the above tables represent the maximum (or minimum) values for design purposes and do not reflect the fact that the actual pressure coefficients vary as a function of wind direction.

5.1.1.1 Effect of Wind Direction

To consider the effect of wind direction, wind tunnel data obtained from various sources including, Ho (1992), Stathopoulos (1979) and Lin and Surry (1997), were used to determine the variation of the pressure coefficients with wind direction. Table 5-5 and Table 5-6 shows an example of positive and negative pressures acting on the walls of a rectangular building for wind directions in 30° increments. The locations where the pressure coefficients are computed are given in Figure 5-3. In the example given in Table 5-5 and Table 5-6, the magnitudes of the maximum (or minimum) pressures are defined using the ASCE 7-95 values for the sloped roof case.

Table 5-5 Positive Wall Pressure Coefficients Estimated for Buildings Shown in Figure 5-7 Given as a Function of Wind Direction

Location	Wind Direction (Clockwise from North)											
	0	30	60	90	120	150	180	210	240	270	300	330
1	0.1	0.1	0.1	0.1	1.2	2.2	2.5	2.2	1.2	0.1	0.1	0.1
2	0.1	0.1	0.1	0.1	1.2	2.2	2.5	2.2	1.2	0.1	0.1	0.1
3	0.1	0.1	0.1	0.1	1.2	2.2	2.5	2.2	1.2	0.1	0.1	0.1
4	0.1	0.1	0.1	0.1	1.2	2.2	2.5	2.2	1.2	0.1	0.1	0.1
5	0.1	0.1	0.1	0.1	1.2	2.2	2.5	2.2	1.2	0.1	0.1	0.1
6	0.1	0.1	0.1	0.1	1.2	2.2	2.5	2.2	1.2	0.1	0.1	0.1
7	0.1	0.1	0.1	0.1	1.2	2.2	2.5	2.2	1.2	0.1	0.1	0.1
8	0.1	0.1	0.1	0.1	1.2	2.2	2.5	2.2	1.2	0.1	0.1	0.1
9	0.1	0.1	0.1	0.1	1.2	2.2	2.5	2.2	1.2	0.1	0.1	0.1
10	0.1	0.1	0.1	0.1	1.2	2.2	2.5	2.2	1.2	0.1	0.1	0.1

Location	Wind Direction (Clockwise from North)											
	0	30	60	90	120	150	180	210	240	270	300	330
11	0.1	0.1	0.1	0.1	1.2	2.2	2.5	2.2	1.2	0.1	0.1	0.1
12	0.1	0.1	0.1	0.1	1.2	2.2	2.5	2.2	1.2	0.1	0.1	0.1
13	0.1	0.1	0.1	0.1	1.2	2.2	2.5	2.2	1.2	0.1	0.1	0.1
14	0.1	0.1	0.1	0.1	1.2	2.2	2.5	2.2	1.2	0.1	0.1	0.1
15	0.1	0.1	0.1	0.1	1.2	2.2	2.5	2.2	1.2	0.1	0.1	0.1
16	0.1	1.2	2.2	2.5	2.2	1.2	0.1	0.1	0.1	0.1	0.1	0.1
17	0.1	1.2	2.2	2.5	2.2	1.2	0.1	0.1	0.1	0.1	0.1	0.1
18	0.1	1.2	2.2	2.5	2.2	1.2	0.1	0.1	0.1	0.1	0.1	0.1
19	0.1	1.2	2.2	2.5	2.2	1.2	0.1	0.1	0.1	0.1	0.1	0.1
20	0.1	1.2	2.2	2.5	2.2	1.2	0.1	0.1	0.1	0.1	0.1	0.1
21	0.1	1.2	2.2	2.5	2.2	1.2	0.1	0.1	0.1	0.1	0.1	0.1
22	0.1	1.2	2.2	2.5	2.2	1.2	0.1	0.1	0.1	0.1	0.1	0.1
23	0.1	1.2	2.2	2.5	2.2	1.2	0.1	0.1	0.1	0.1	0.1	0.1
24	2.5	2.2	1.2	0.1	0.1	0.1	0.1	0.1	0.1	0.1	1.2	2.2
25	2.5	2.2	1.2	0.1	0.1	0.1	0.1	0.1	0.1	0.1	1.2	2.2
26	2.5	2.2	1.2	0.1	0.1	0.1	0.1	0.1	0.1	0.1	1.2	2.2
27	2.5	2.2	1.2	0.1	0.1	0.1	0.1	0.1	0.1	0.1	1.2	2.2
28	2.5	2.2	1.2	0.1	0.1	0.1	0.1	0.1	0.1	0.1	1.2	2.2
29	2.5	2.2	1.2	0.1	0.1	0.1	0.1	0.1	0.1	0.1	1.2	2.2
30	2.5	2.2	1.2	0.1	0.1	0.1	0.1	0.1	0.1	0.1	1.2	2.2
31	2.5	2.2	1.2	0.1	0.1	0.1	0.1	0.1	0.1	0.1	1.2	2.2
32	2.5	2.2	1.2	0.1	0.1	0.1	0.1	0.1	0.1	0.1	1.2	2.2
33	2.5	2.2	1.2	0.1	0.1	0.1	0.1	0.1	0.1	0.1	1.2	2.2
34	2.5	2.2	1.2	0.1	0.1	0.1	0.1	0.1	0.1	0.1	1.2	2.2
35	2.5	2.2	1.2	0.1	0.1	0.1	0.1	0.1	0.1	0.1	1.2	2.2
36	2.5	2.2	1.2	0.1	0.1	0.1	0.1	0.1	0.1	0.1	1.2	2.2
37	2.5	2.2	1.2	0.1	0.1	0.1	0.1	0.1	0.1	0.1	1.2	2.2
38	2.5	2.2	1.2	0.1	0.1	0.1	0.1	0.1	0.1	0.1	1.2	2.2
39	0.1	0.1	0.1	0.1	0.1	0.1	0.1	1.2	2.2	2.5	2.2	1.2
40	0.1	0.1	0.1	0.1	0.1	0.1	0.1	1.2	2.2	2.5	2.2	1.2
41	0.1	0.1	0.1	0.1	0.1	0.1	0.1	1.2	2.2	2.5	2.2	1.2
42	0.1	0.1	0.1	0.1	0.1	0.1	0.1	1.2	2.2	2.5	2.2	1.2
43	0.1	0.1	0.1	0.1	0.1	0.1	0.1	1.2	2.2	2.5	2.2	1.2
44	0.1	0.1	0.1	0.1	0.1	0.1	0.1	1.2	2.2	2.5	2.2	1.2
45	0.1	0.1	0.1	0.1	0.1	0.1	0.1	1.2	2.2	2.5	2.2	1.2

Location	Wind Direction (Clockwise from North)											
	0	30	60	90	120	150	180	210	240	270	300	330
46	0.1	0.1	0.1	0.1	0.1	0.1	0.1	1.2	2.2	2.5	2.2	1.2

Table 5-6 Negative Wall Pressure Coefficients Estimated for Building Shown in Figure 5-7, Given as a Function of Wind Direction

Location	Wind Direction (Clockwise from North)											
	0	30	60	90	120	150	180	210	240	270	300	330
1	-0.9	-0.8	-0.6	-1.1	-0.8	-0.3	-0.4	-0.2	-2.0	-3.5	-2.1	-2.1
2	-0.7	-0.6	-0.5	-0.9	-0.6	-0.2	-0.3	-0.2	-1.6	-2.7	-1.6	-1.3
3	-0.7	-0.6	-0.5	-0.9	-0.6	-0.2	-0.3	-0.2	-1.6	-2.7	-1.6	-1.0
4	-0.7	-0.6	-0.5	-0.9	-0.6	-0.2	-0.3	-0.3	-1.7	-2.7	-1.7	-0.8
5	-0.7	-0.6	-0.5	-0.9	-0.6	-0.2	-0.3	-0.3	-1.7	-2.7	-1.7	-0.7
6	-0.7	-0.6	-0.5	-0.9	-0.6	-0.2	-0.3	-0.4	-1.8	-2.7	-1.8	-0.6
7	-0.7	-0.6	-0.5	-0.9	-0.6	-0.2	-0.3	-0.4	-1.8	-2.7	-1.8	-0.6
8	-0.7	-0.6	-0.5	-0.9	-0.6	-0.2	-0.3	-0.5	-1.9	-2.7	-1.9	-0.6
9	-0.7	-0.6	-1.8	-2.7	-1.8	-0.4	-0.3	-0.2	-0.6	-0.9	-0.5	-0.6
10	-0.7	-0.6	-1.8	-2.7	-1.8	-0.4	-0.3	-0.2	-0.6	-0.9	-0.5	-0.6
11	-0.7	-0.7	-1.7	-2.7	-1.7	-0.3	-0.3	-0.2	-0.6	-0.9	-0.5	-0.6
12	-0.7	-0.8	-1.7	-2.7	-1.7	-0.3	-0.3	-0.2	-0.6	-0.9	-0.5	-0.6
13	-0.7	-1.0	-1.6	-2.7	-1.6	-0.2	-0.3	-0.2	-0.6	-0.9	-0.5	-0.6
14	-0.7	-1.3	-1.6	-2.7	-1.6	-0.2	-0.3	-0.2	-0.6	-0.9	-0.5	-0.6
15	-0.9	-2.1	-2.1	-3.5	-2.0	-0.2	-0.4	-0.3	-0.8	-1.1	-0.6	-0.8
16	-3.5	-2.0	-0.2	-0.4	-0.3	-0.8	-1.1	-0.5	-0.7	-0.7	-0.7	-2.0
17	-2.7	-1.6	-0.2	-0.3	-0.2	-0.6	-0.9	-0.4	-0.5	-0.6	-0.5	-1.6
18	-2.7	-1.6	-0.2	-0.3	-0.2	-0.6	-0.9	-0.4	-0.5	-0.6	-0.5	-1.6
19	-2.7	-1.7	-0.3	-0.3	-0.2	-0.6	-0.9	-0.4	-0.5	-0.6	-0.5	-1.7
20	-0.9	-0.6	-0.2	-0.3	-0.3	-1.6	-2.7	-1.6	-0.5	-0.6	-0.5	-0.4
21	-0.9	-0.6	-0.2	-0.3	-0.2	-1.6	-2.7	-1.6	-0.5	-0.6	-0.5	-0.4
22	-0.9	-0.6	-0.2	-0.3	-0.2	-1.5	-2.7	-1.5	-0.5	-0.6	-0.5	-0.4
23	-1.1	-0.8	-0.3	-0.4	-0.2	-2.0	-3.5	-2.0	-0.7	-0.7	-0.7	-0.5
24	-0.4	-0.3	-0.8	-1.1	-0.6	-0.8	-0.9	-2.1	-2.1	-3.5	-2.0	-0.2
25	-0.3	-0.2	-0.6	-0.9	-0.5	-0.6	-0.7	-1.3	-1.6	-2.7	-1.6	-0.2
26	-0.3	-0.2	-0.6	-0.9	-0.5	-0.6	-0.7	-1.0	-1.6	-2.7	-1.6	-0.2
27	-0.3	-0.2	-0.6	-0.9	-0.5	-0.6	-0.7	-0.8	-1.7	-2.7	-1.7	-0.3

Location	Wind Direction (Clockwise from North)											
	0	30	60	90	120	150	180	210	240	270	300	330
28	-.3	-.2	-.6	-.9	-.5	-.6	-.7	-.7	-1.7	-2.7	-1.7	-.3
29	-.3	-.2	-.6	-.9	-.5	-.6	-.7	-.6	-1.8	-2.7	-1.8	-.4
30	-.3	-.2	-.6	-.9	-.5	-.6	-.7	-.6	-1.8	-2.7	-1.8	-.4
31	-.3	-.2	-.6	-.9	-.5	-.6	-.7	-.6	-1.9	-2.7	-1.9	-.5
32	-.3	-.4	-1.8	-2.7	-1.8	-.6	-.7	-.6	-.5	-.9	-.6	-.2
33	-.3	-.4	-1.8	-2.7	-1.8	-.6	-.7	-.6	-.5	-.9	-.6	-.2
34	-.3	-.3	-1.7	-2.7	-1.7	-.7	-.7	-.6	-.5	-.9	-.6	-.2
35	-.3	-.3	-1.7	-2.7	-1.7	-.8	-.7	-.6	-.5	-.9	-.6	-.2
36	-.3	-.2	-1.6	-2.7	-1.6	-1.0	-.7	-.6	-.5	-.9	-.6	-.2
37	-.3	-.2	-1.6	-2.7	-1.6	-1.3	-.7	-.6	-.5	-.9	-.6	-.2
38	-.4	-.2	-2.0	-3.5	-2.1	-2.1	-.9	-.8	-.6	-1.1	-.8	-.3
39	-3.5	-2.0	-.7	-.7	-.7	-.5	-1.1	-.8	-.3	-.4	-.2	-2.0
40	-2.7	-1.6	-.5	-.6	-.5	-.4	-.9	-.6	-.2	-.3	-.2	-1.6
41	-2.7	-1.6	-.5	-.6	-.5	-.4	-.9	-.6	-.2	-.3	-.2	-1.6
42	-2.7	-1.7	-.5	-.6	-.5	-.4	-.9	-.6	-.2	-.3	-.3	-1.7
43	-.9	-.4	-.5	-.6	-.5	-1.6	-2.7	-1.6	-.3	-.3	-.2	-.6
44	-.9	-.4	-.5	-.6	-.5	-1.6	-2.7	-1.6	-.2	-.3	-.2	-.6
45	-.9	-.4	-.5	-.6	-.5	-1.5	-2.7	-1.5	-.2	-.3	-.2	-.6
46	-1.1	-.5	-.7	-.7	-.7	-2.0	-3.5	-2.0	-.2	-.4	-.3	-.8

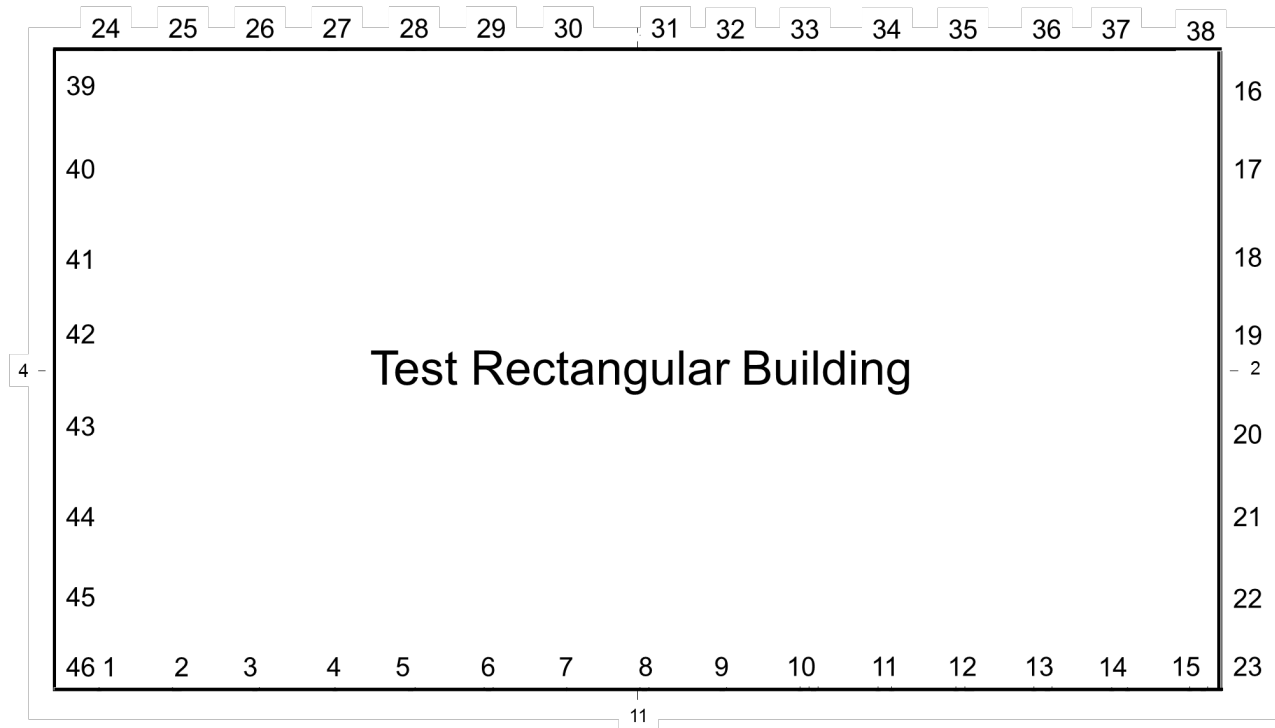


Figure 5-3 Locations of Pressure Estimates on Rectangular Building as Presented in Table 5-5 and Table 5-6 (Plan View)

5.1.1.2 Comparison of ASCE 7 Wall Pressures to Wind Tunnel Tests

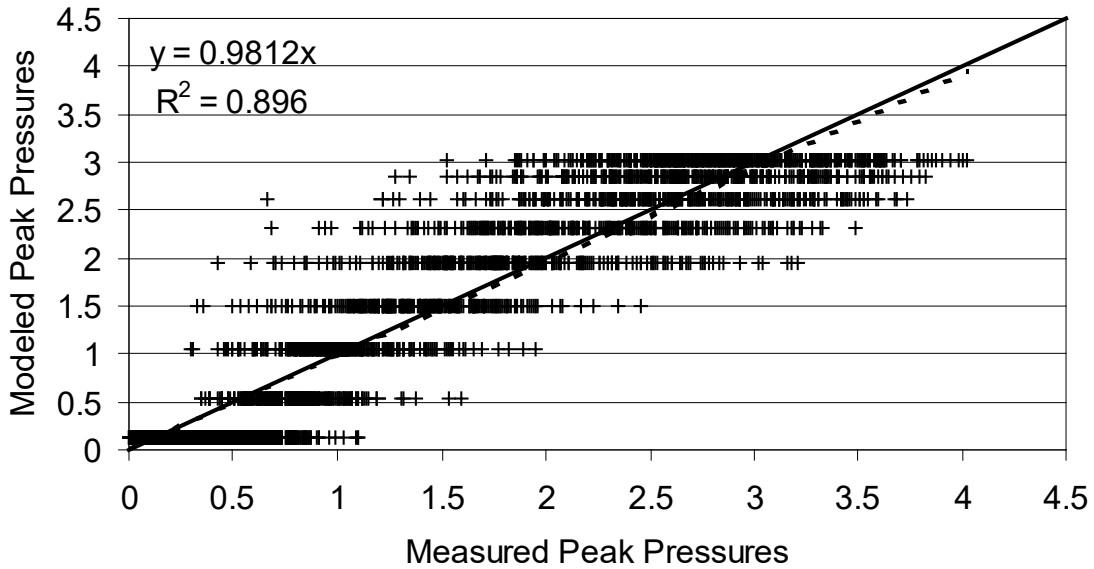
Figure 5-4 and Figure 5-5 show comparisons of wall pressures estimated using the ASCE 7 based model for roofs with slopes less than 10° to those obtained from boundary layer wind tunnel tests (Lin and Surry, 1997) in nominally open and suburban terrains. These plots compare pressure tap-by-pressure tap for a wind tunnel tested rectangular building, and show measured versus ASCE 7 based-model pressure coefficients. The plot includes comparisons over the full azimuth range in 10° increments. The model building, tested at scales of 1:100 and 1:200, has an eave height of 30’ and plan dimensions of 100’x200’. The model was instrumented so that the full azimuthal range of data was available for 145 wall taps and 112 roof taps. In the comparisons given in Figure 5-4 and Figure 5-5, the pressure coefficients are normalized by the mean hourly wind speed at roof height. Note that in the pressure modeling process, all pressure coefficients are based on the peak gust wind speed at roof height. The magnitudes of the coefficients, normalized by the mean wind speed at roof height, therefore increase with increasing surface roughness.

The banding evident in Figure 5-4 and Figure 5-5 arises primarily from the cosine functions used in the modeling of the code based pressures and suctions that limit the value a modeled pressure can have for any given wind direction. In contrast, the measured peak pressure data, while following a mean trend with azimuth, are scattered about the mean azimuthal trend curve.

The agreement between the ASCE 7 based positive pressures and the measured positive pressures is reasonable. In the case of the negative pressures, there is significantly more scatter evident in the comparisons since the ASCE 7 loads for the negative pressures in Zone 4 (interior zone) have a

minimum value of -2.1, whereas in reality, for long buildings, the minimum negative pressure will have a magnitude which is less than 2.1.

Rectangular Building - Suburban Terrain - ASCE-7 Based Positive Pressures



Rectangular Building - Suburban Terrain -ASCE-7 Based Negative Pressures

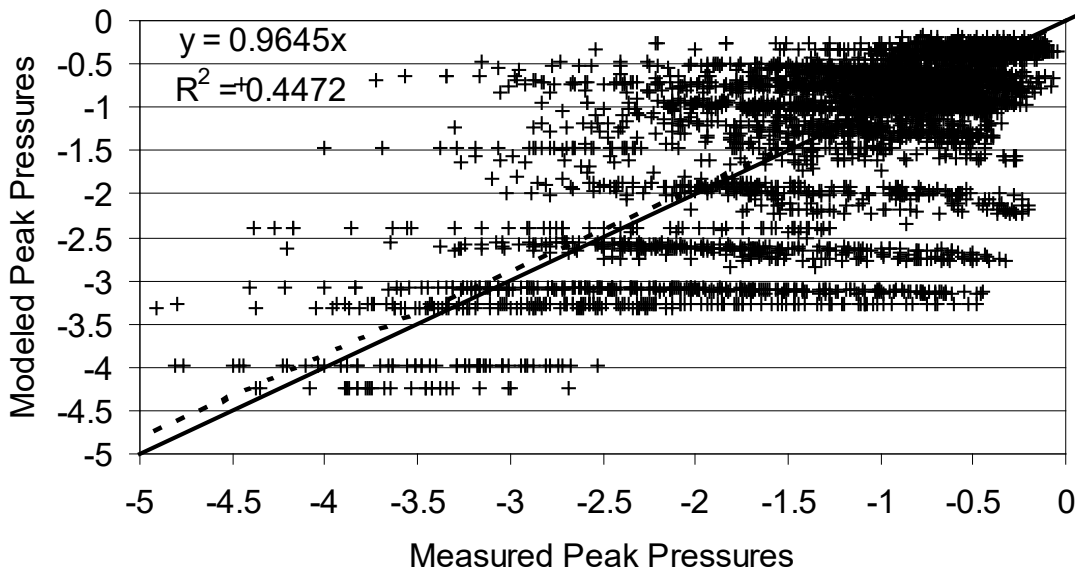
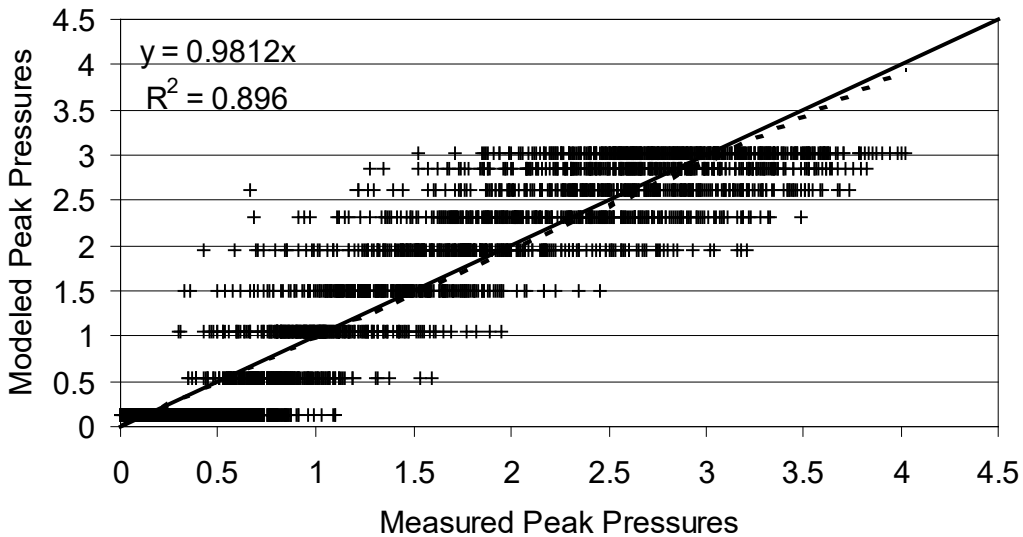


Figure 5-4 Comparison of Measured and Modeled Wall Pressure Coefficients on a Flat Roof Building in Open Terrain ($z_0 = 0.1$ meters)

Rectangular Building - Suburban Terrain - ASCE-7 Based
Positive Pressures



Rectangular Building - Suburban Terrain -ASCE-7 Based
Negative Pressures

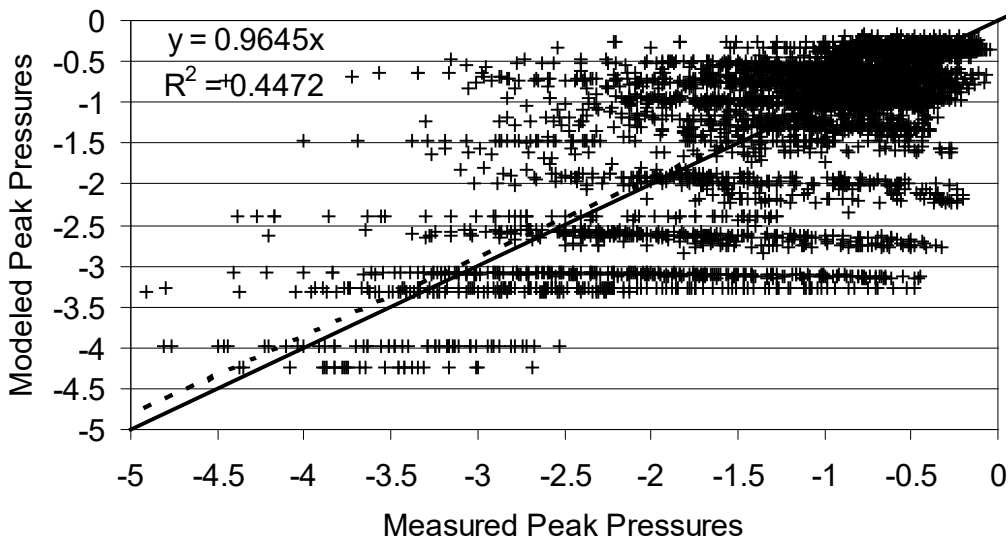


Figure 5-5 Comparison of Measured and Modeled Wall Pressure Coefficients on a Flat Roof Building in Suburban Terrain ($z_0 = 0.3$ meters)

5.1.2 Roof Pressures - Low-Rise Buildings

As in the case of the wall pressures, wind loads on the roofs of low-rise buildings used for the prediction of the failure of components and cladding were derived using North American based building codes and

standards. As in the case of the wall pressures, comparisons of the roof pressures specified by ASCE 7, SBCCI, and NBCC were performed with the coefficients referenced to the mean hourly wind speed at the mean roof height. Table 5-7, Table 5-8, and Table 5-9 present comparisons of the various coefficients. Again, as in the case of wall pressures, the effect of the directionality factor has been removed from the coefficients given in the SBCCI Code and the NBCC. The pressure zones associated with each of the codes and standards are given in Figure 5-6.

Comparisons of the peak coefficients prescribed in each of the above noted standards to those produced by Meecham (1988), shown in Figure 5-7, suggest that the coefficients prescribed in ASCE 7 are generally too high along the roof ridge and eaves, whereas those prescribed by the NBCC and the SBCCI tend to be low along the roof edge and eaves. All of the above noted codes/standards appear to underestimate the wind-induced loads at the ridge/gable end corner, and this underestimation of the loads in this region is also supported in the pressure coefficient data given in Case (1996). A comparison of the SBCCI loads and the ASCE loads for hip and gable roofs suggests that the average of the two sets of pressure coefficients would yield results that most closely reproduce those obtained from the wind tunnel (except at the gable ridge). For the estimation of wind loads and resulting damage, both the SBCCI loads and the ASCE loads are investigated in the damage/loss studies.

Table 5-7 Comparison of Negative Pressure Coefficients on Flat Roofs

Pressure Zone			Pressure Coefficient		
NBCC	SBCCI	ASCE 7-95	NBCC	SBCCI	ASCE 7-95
c	c	3	6.8	5.6	6.9
s	Si	2	3.1	3.1	4.5
r	re	1	2.3	2.3	2.5

Table 5-8 Comparison of Negative Pressure Coefficients on Gable Roofs

Pressure Zone			Pressure Coefficient		
NBCC	SBCCI	ASCE 7-95	NBCC	SBCCI	ASCE 7-95
c	c	3	5.1	5.2	5.2
s	Si	2	2.5	2.5	5.2
s'	Se	2	3.9	4.0	5.2
r	re	1	2.0	2.1	2.1

Table 5-9 Comparison of Negative Pressure Coefficients on Hip Roofs

Pressure Zone			Pressure Coefficient		
NBCC	SBCCI	ASCE 7-95	NBCC	SBCCI	ASCE 7-95
c	c	3	5.1	5.2	5.2
s	S _i	2	2.5	2.5	5.2
s'	S _e	2	2.5	4.0	5.2
r	r _e	1	2.0	2.1	2.1

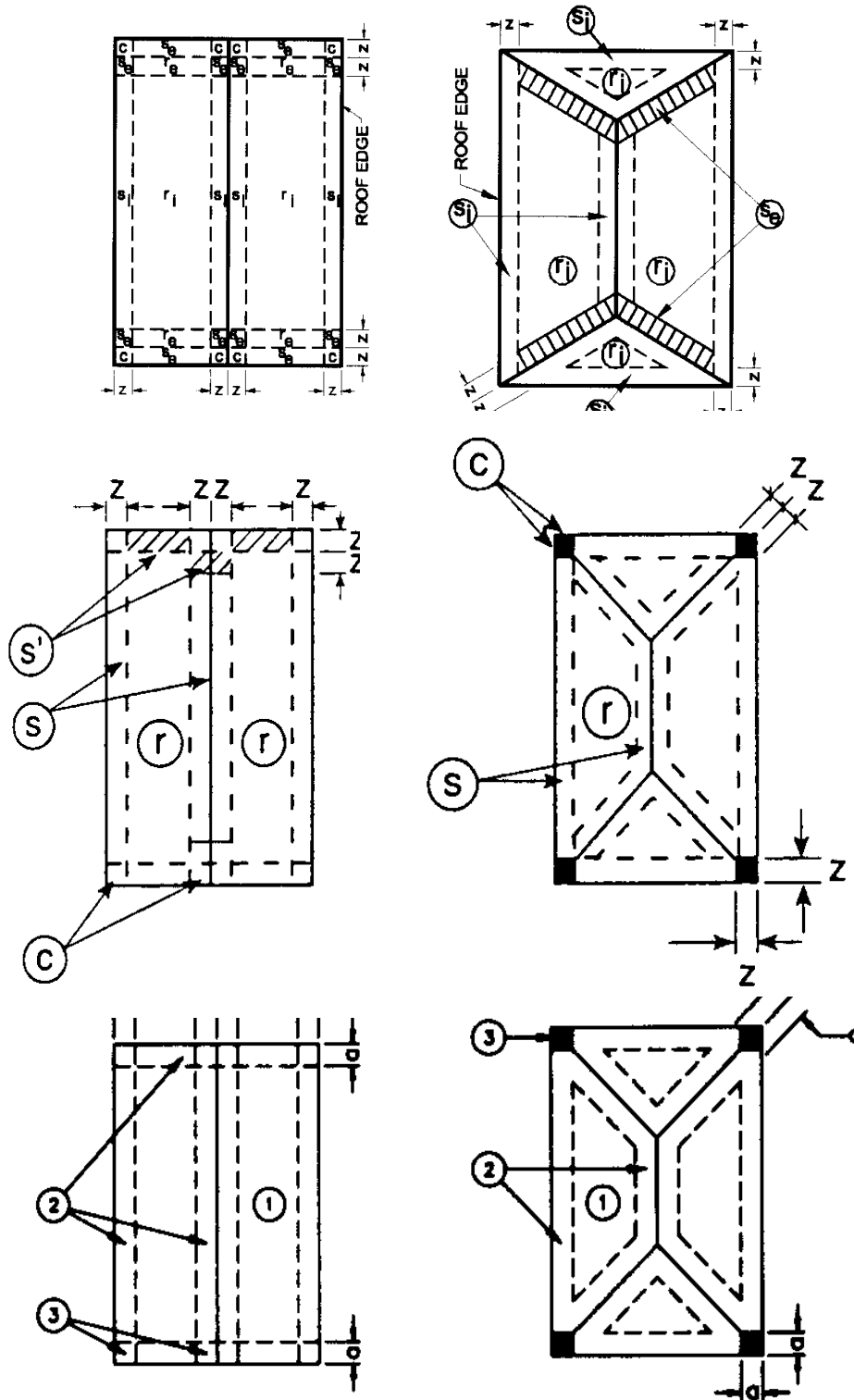
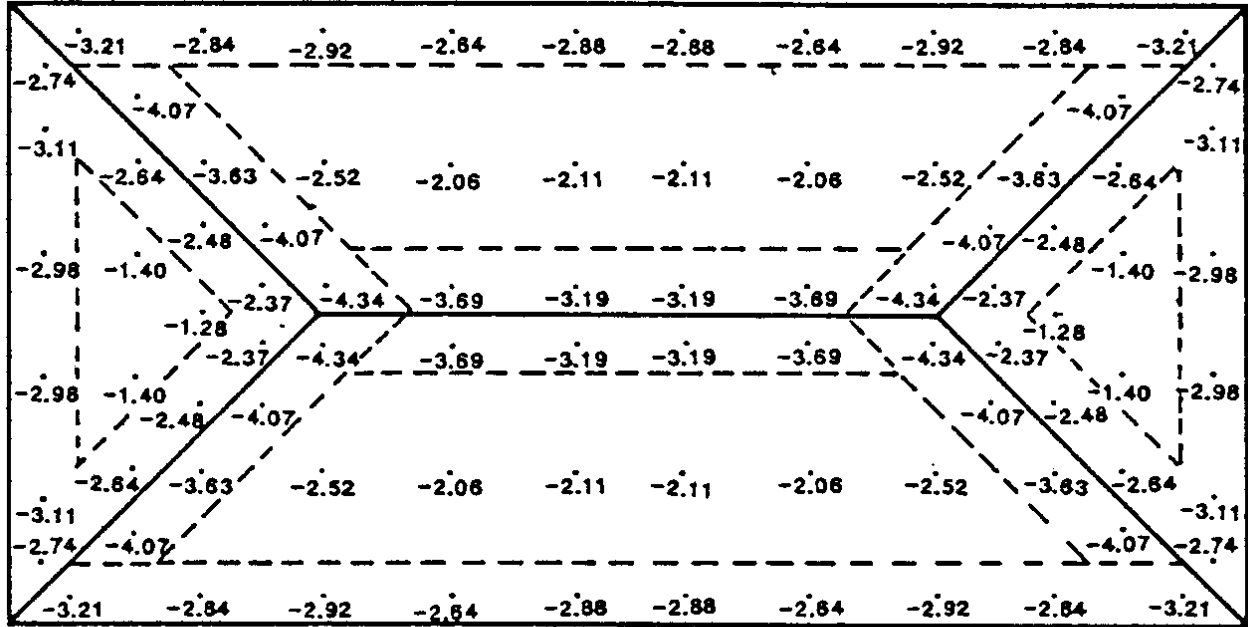


Figure 5-6 Zones used for Defining Pressure Coefficients for Gable and Hip Roofs for the SBCCI (Top Drawings), the NBCC (Middle Drawings) and ASCE 7-95 (Bottom Drawings)



Enveloped Experimental Peak Negative CpCg's

-5.51	-2.47	-2.29	-3.28	-2.39	-2.39	-3.28	-2.29	-2.47	-5.51
-4.08	-2.50	-1.92	-1.98	-2.27	-2.27	-1.98	-1.92	-2.50	-4.08
-6.63	-2.69	-3.17	-3.07	-3.07	-3.07	-3.07	-3.17	-2.69	-6.63
-6.63	-4.78	-4.34	-3.42	-3.26	-3.26	-3.42	-4.34	-4.78	-6.63
-6.63	-4.78	-4.34	-3.42	-3.26	-3.26	-3.42	-4.34	-4.78	-6.63
-6.63	-2.69	-3.17	-3.07	-3.07	-3.07	-3.07	-3.17	-2.69	-6.63
-4.08	-2.50	-1.92	-1.98	-2.27	-2.27	-1.98	-1.92	-2.50	-4.08
-5.51	-2.47	-2.29	-3.28	-2.39	-2.39	-3.28	-2.29	-2.47	-5.51

Enveloped Experimental Peak Negative CpCg's

Figure 5-7 Peak Pressure Coefficients on Hip and Gable Roofs in Open Terrain (taken from Meecham, 1988)

5.1.2.1 Effect of Wind Direction

The effect of wind direction on the estimated pressure coefficients on the roofs of low-rise buildings was determined independently of the building code/standard information using the results of wind tunnel test data given in Stathopolous (1979); Meecham (1988); Ho (1992); and Surry, Davenport, and Mikituk (1993). This wind tunnel information was supplemented by the directional pressure coefficient data given in the United Kingdom Building Code, CP3.

In the development of the wind loads as a function of direction, a zone-based approach was used for the hip and gable roofs using the data noted above. In the case of the gable roof, the zones are based on those given in the SBCCI where, because more zones exist here than in either the ASCE 7 provisions or the NBCCI provisions, the effect of wind directionality can be better modeled. For example, the largest loads on eave zone occur when the wind is blowing perpendicular to the eave or ridge), whereas the largest loads in the corner zones tend to occur when the wind is approaching from an oblique angle, and the largest loads in the center of the gable end occur when the wind is approaching in a direction which is approximately parallel to the ridge line.

In the case of the hip roof buildings, the zones (or sub-zones) used to incorporate the effect of directionality are based primarily on the UK wind loading code, Code of Practice 3 (CP3), as shown in Figure 5-8.

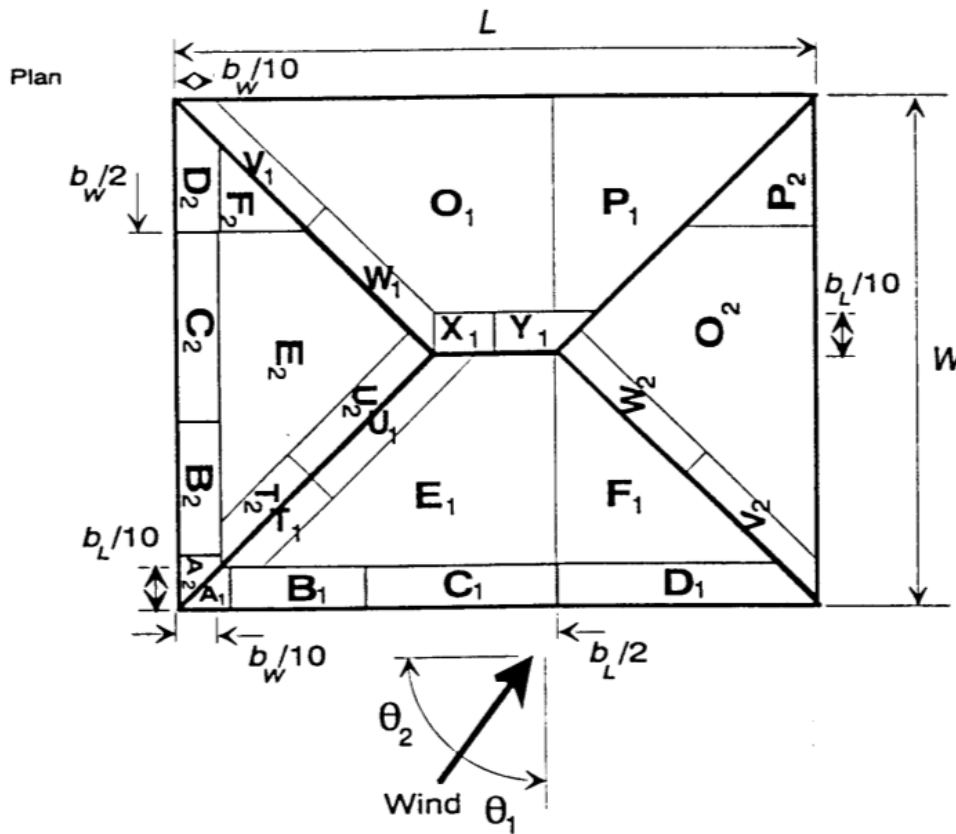


Figure 5-8 Pressure Coefficient Zones Used in the UK Wind Loading Code for Hip Roof Buildings

5.1.2.2 Effect of Terrain

A key assumption in the use of pressure coefficients for estimating wind loads, is that the pressure coefficients, normalized with respect to the peak gust wind speed at roof height, do not change with changes in the flow characteristics (e.g., turbulence intensity). This assumption is important because most pressure coefficient data derived from wind tunnel tests given in the literature are presented as coefficients normalized by the mean wind speed at roof height. To adjust these coefficients referenced to the mean wind speed to coefficients referenced to the peak gust speed, information on the flow characteristics used in the wind tunnel tests must be known. If the key flow parameters needed to convert the reference wind speed from mean hourly to peak gust are known (i.e., mean velocity and longitudinal turbulence intensity profiles), then the wind tunnel pressure coefficient data referenced to the mean dynamic pressure can be readily converted to a coefficient normalized to the peak gust velocity pressure. In instances when wind tunnel tests have been performed on the same building in different terrain conditions (e.g., typical open terrain and typical suburban terrain), one would expect the pressure coefficients normalized by the peak gust velocity pressure at roof height to collapse to the same value.

Using wind tunnel data given in Monroe (1996), Ho (1992), Meecham (1988), Case (1996), Stathopolous (1979), and Lin and Surry (1997), all of which present roof pressure coefficients normalized by the mean dynamic pressure at roof height for more than one terrain condition, the coefficients were adjusted to be normalized with respect to the peak gust velocity pressure at roof height. The degree to which the pressure coefficients normalized by the local gust velocity pressure (at mean roof height) collapsed to yield the same negative pressure coefficient varied from study to study and building to building. In general, it was found that the peak gust pressure coefficients in the rougher terrain (normalized to the local gust velocity pressure) were higher than those at the same location in the smoother terrain.

For example, Monroe (1996) measured roof suctions on a model building with a 1:12 roof slope having an eave height of 4.9 meters (full scale) in flow conditions having turbulence intensities at roof height of 12.5% and 19%. On average, the peak roof suction coefficients (normalized with respect to the mean velocity pressure at roof height) obtained in the rougher flow conditions were 75% higher than those obtained in the smoother flow conditions. By normalizing the pressures by the peak gust velocity pressure at roof height (defined as the mean wind speed plus three standard deviations of the fluctuating wind speed), the difference reduces so that the pressure coefficients in the rougher terrain are about 35% higher than those obtained in the smooth terrain. These higher coefficients suggest that using the peak gust velocity pressure to normalize the pressure coefficients is not sufficient to explain the differences in the measured pressure coefficients associated with changes in the flow characteristics.

In the case of Ho (1992), the negative pressures in the suburban terrain case do not collapse to a constant value, with the peak suction coefficients referenced to the peak gust velocity pressure being higher in suburban terrain than in open terrain. For example, converting a roof corner pressure in suburban terrain to be referenced to the peak gust velocity pressure yields a coefficient that is 15% higher than the open country value referenced to the local peak gust velocity pressure.

Similar observations were made using the Lin and Surry pressure data, the Case (1996) pressure data and a large portion of the Stathopolous (1979) data. The observation that the pressure coefficients in the rougher terrains, even when normalized with respect to the local peak gust wind, are larger (in magnitude) than those in open terrain is apparently recognized in ASCE 7-95, where the wind loads on buildings in suburban terrain (Exposure B) are limited to be no less than 85% of the value that would be computed if the building were in open terrain.

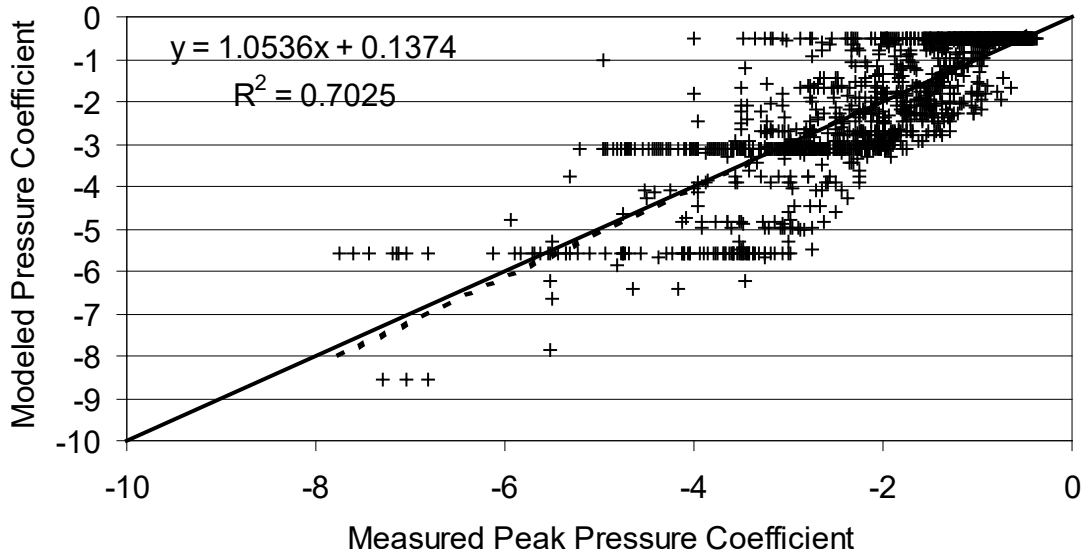
To consider this apparent increase in the peak pressure coefficients, the basic pressure coefficient referenced to the peak gust wind speed is increased by a factor equal to the square root of the ratio of the turbulence intensity at roof height in the local terrain to the turbulence at roof height in the reference open terrain. This empirical adjustment in the pressure coefficients helps collapse the pressure coefficient data noted above but is clearly a subject requiring more research. The use of this factor does yield estimates of pressures in low buildings in a standard suburban terrain ($z_0 = 0.3$ meters), which are much closer to those required by ASCE 7 than if the adjustment were not made. As an illustration of the effect of the turbulence intensity, consider the following example of a building located in suburban terrain having a mean roof height of 5 meters.

Using the ESDU representation of the gust velocity profile, the ratio of the 5 meters gust wind speed in suburban terrain to the 5 meters gust wind speed in open terrain is 0.787, implying a wind load equal to 62% of the open terrain wind load. The roof height turbulence intensities in the open and suburban terrains (from ESDU, 1992) are 18% and 29%, respectively, resulting in a 27% increase in the pressure coefficient (i.e., $100\sqrt{0.29/0.18}$). The net effect of the reduction in the peak gust velocity combined with the increase in the pressure coefficient associated with the turbulence intensity adjustment is a wind load equal to 79% of the open terrain wind load, which is comparable to the 85% factor given in ASCE 7-98.

5.1.2.3 Comparison of ASCE 7 Roof Pressure Loads to Wind Tunnel Tests

Figure 5-9 shows a comparison of the ASCE 7 based roof pressure loads to those obtained from wind tunnel tests for a relatively open terrain case and a suburban terrain case. Note that the surface roughness associated with the nominal open terrain case is described by a z_0 value of 0.1 meters, which is larger than the value of about 0.03 meters, which is typically associated with open terrain conditions. The suburban terrain case is characterized by a roughness length of about 0.30 m. The modeled pressures (based on the ASCE 7 loads) presented in Figure 5-9 were produced using the actual values of z_0 as derived from the wind tunnel tests.

Rectangular Building - Open Terrain ASCE-7 Based Pressures



Rectangular Building - Suburban Terrain - ASCE-7 Based Pressures

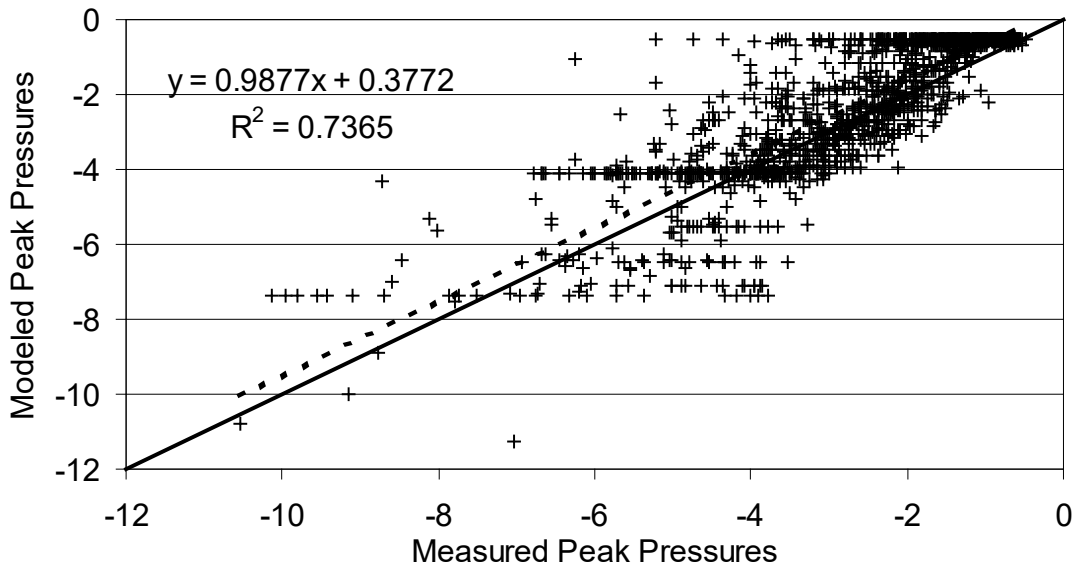


Figure 5-9 Comparison of Modeled and Measured Peak Roof Pressure Coefficients on a Flat Roof Low-Rise Building

The comparisons of the modeled and measured wind loads suggest that the ASCE 7 based loads with the directional models and the empirical turbulence intensity adjustment factors reproduce the wind tunnel results reasonably well.

A directional pressure coefficient model has been developed using code-based loads to define the maximum pressure coefficients. The roof slopes considered are in the range of 3:12 to 5:12. The effect of directionality is considered using available wind tunnel data, scaled (or truncated) to ensure the maximum values of the pressures are equivalent to the code specified values. The reduction in the roof loads associated with decreased wind speeds caused by increasing surface roughness is lessened through the use of a turbulence intensity adjustment factor, which yields a final reduction in wind loads comparable to that specified in ASCE 7-95.

5.1.3 Wind Loads on Low-Rise Buildings – Effect of Nearby Buildings

The preceding discussion of wind loads on the roofs and walls of low-rise buildings was applicable to isolated structures located within a homogeneous open or suburban terrain. In the case of buildings situated in environments surrounded by buildings of like size, on average there is a reduction in the loads experienced by these buildings. The reduction in load is a function of both the spacing and size of the nearby buildings as indicated in Holmes (1994). Comprehensive wind tunnel test data showing the effects of nearby buildings on the wind loads experienced by the test building is limited. The wind tunnel test results given in Ho (1992) are probably the most widely quoted results. In Ho (1992), low-rise, flat roofed buildings were tested in both open and suburban terrain conditions with and without the existence of nearby buildings. For the cases where nearby buildings were in place, a total of 16 different representations of surrounding buildings were modeled. The results of the Ho (1992) study indicate that the average reduction in the wind loads on the roofs is about 25% compared to the isolated building case, although the amount of the reduction varied with the location on the roof. The coefficient of variation of the reduction in wind loads was about 20%, but this value also varied with the location on the roof. The reduction in the wind loads on the walls of the test building was shown to be somewhat lower, ranging from about a minimum of a 10% reduction up to a maximum of a 25% reduction in load. The coefficient of variation was about 20%. Ho made no attempt to separately examine the effects of nearby buildings on the positive and negative pressures.

In Case (1996), models of a gable roof building with a 4:12 roof slope were tested as isolated buildings and then tested for three different representations of the building surrounded by other buildings. Case found that the reduction in the negative roof and wall loads was similar to that found by Ho (1992) (i.e., a 25% reduction), but found no mean reduction in the peak positive wall pressures. Case found that the positive roof pressures actually increased in the presence of nearby buildings.

In the simulation of wind loads on low-rise buildings for the prediction of damage and loss, the effects of nearby buildings are considered by reducing the peak negative pressures by a mean value of 25%. No decrease in the positive wall pressures is taken.

5.1.4 Integrated (Overall) Wind Loads on Low-Rise Buildings

The prime thrust of this effort with respect to wind-induced damage and loss estimation is directed towards the prediction of damage to the relatively small building envelope components. Overall (large area) loads are important for the prediction of overturning and uplifting of manufactured homes, whole roof failures on residential and small commercial buildings, and failures of structural systems such as those that exist in metal buildings, roof systems, etc. The estimates of the overall loads must consider the fact that the peak pressures which act on the exterior of buildings and other structures are not fully correlated, and as the area over which the pressures are averaged increases, the effective loading

coefficient decreases. This relationship of decreasing loading coefficient with the increasing area is reflected in the pressure coefficients given in wind loading codes and standards such as the SBCCI and ASCE 7, but not in the main wind force resisting calculations as defined in ASCE 7-95. The reduction in the effective pressures given in these codes/standards are based on limited wind tunnel test data. In the development of the overall loading model, a model for the prediction of the mean exterior pressures was developed using the code-based wind loading model developed for components and cladding as described earlier. This mean pressure model did not exist prior to the development of the overall load model as the loading and damage models were directed towards envelope component loads and failures only.

To estimate overall loads for the prediction of overturning moments, uplift forces, etc., the modeled local pressures described earlier for the hip and gable roof buildings were integrated over the area of interest with the lack of correlation considered using a correlation coefficient approach similar to that originally developed by Davenport (1961). The major differences between the approach developed by Davenport and the approach used herein are: (1) Davenport properly uses the mean and standard deviations of the fluctuating pressures, whereas the present approach uses the mean and peak values (since these are estimated using the empirical pressure model) and (2) Davenport’s approach was developed for line-like structures, whereas the present methodology is applied to three dimensional structures.

To estimate the peak integrated loads acting on a structure, the pressures are integrated using:

Equation 5-1

$$\hat{R} = \frac{1}{2} \rho V^2 \left[\iint_A I_i \hat{C}_{pi} I_j \hat{C}_{pj} \exp(-\Delta r/\lambda) dA_i dA_j \right]^{1/2}$$

Where:

- \hat{R} is a peak force, moment, or structural action
- ρ is the fluid density
- V is the fluid velocity
- \hat{C}_{pi} is the peak pressure coefficient (minus the mean value) at location i
- I_i is an influence coefficient converting the pressure at location i to a global force
- Δr is the distance between locations i and j
- λ is a length scale which can be considered a measure of the extent over which the fluctuating pressures are correlated
- A_i is the Area at location i

In the modeling approach used for negative pressures here, the length scale decreases with increasing magnitude of the negative pressures (i.e., the very high local negative pressures are correlated over relatively small areas), and the basic value of λ is a function of the building height.

5.1.4.1 Roof Uplift Loads

Using the integration methodology described above, the code based component and cladding loads were integrated over the roof surface of a hip roof and gable roof residence. The roof slopes in both cases are 4:12, the plan dimensions of the buildings are 30'x60' and the eave height is 9'.

As indicated in Figure 5-10, predictions of integrated loads for uplift have been compared to the results of Meecham (1988) for the uplift loads on hip and gable roofs with 4:12 roof slopes. Comparisons of the uplift load estimates to those obtained from Figure 6-3 of ASCE 7-95 are also given in Figure 5-10.

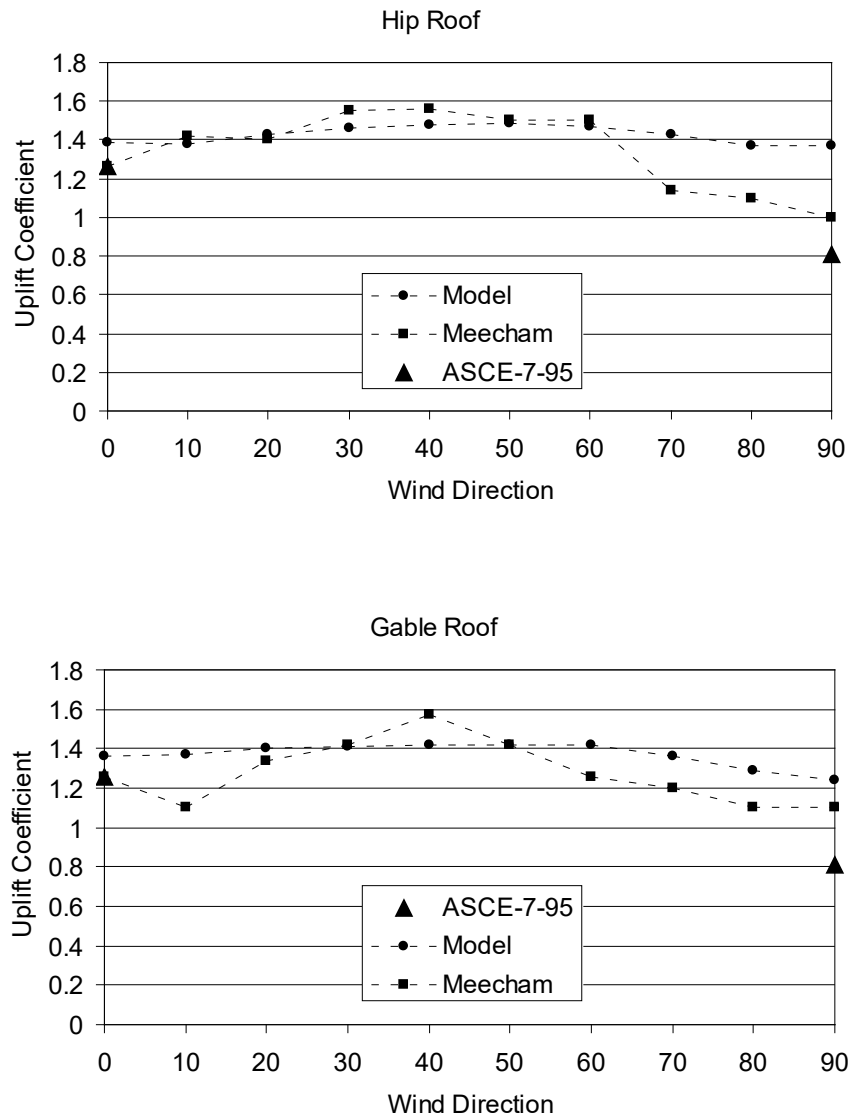


Figure 5-10 Comparisons of Modeled (Integrated) Uplift Loads on Hip and Gable Roofs to those Obtained from Wind Tunnel Experiments

The comparisons of the total uplift forces given in Figure 5-10 indicate that the modeled uplift loads are in general agreement with the results given in Meecham (1988), although the variation of the uplift coefficients with wind direction is less evident in the model results. The uplift coefficients are defined with respect to the mean dynamic pressure at roof height.

ASCE 7 allows for the computation of overall uplift for gable and flat roofs using Figure 6-3 of the standard. The methodology allows for the computation of the uplift loads for wind approaching normal to the roof ridge and parallel to the roof ridge only. The uplift loads computed for these two directions are shown in Figure 5-10, where it is seen that for winds approaching normal to the roof ridge, the ASCE 7 uplift loads obtained from Figure 6-3 of ASCE 7 agree well with the uplift loads computed by integrating the component and cladding loads discussed earlier. In the case of the hip roof, the ASCE 7 uplift loads presented in Figure 5-10 are the same as the gable values since ASCE 7 does not provide a means to compute uplift loads on roof shapes that are hip shaped. For winds approaching parallel to the roof ridge (90° as shown in Figure 5-10) the ASCE 7 uplift values are lower than either the Meecham data or the integrated uplift data.

For the prediction of roof uplift failure, the integrated loading approach is used since the methodology is based on code type loads, it produces values of uplift (for the 0° case) that are very similar to those predicted using ASCE 7. The approach allows the effect of directionality (however small in this case) to be incorporated in the damage model, consistent with the approach used in the Hazus model.

5.1.4.2 Integrated Roof and Wall Loads on Low-Rise Buildings with Flat Roofs

In order to further validate the pressure integration loading model, comparisons were made with integrated loads obtained directly from wind tunnel tests. The integrated wind tunnel loads were obtained by integrating the time series of wind induced pressures obtained from the wind tunnel tests of the 100' by 200' buildings described in Section 5.1.2. The individual measured pressures acting on the roof were integrated over a number of different areas, as indicated in Figure 5-10. Note that in the case of the integrated wall loads, panels 1, 2, and 3 are located on the back side of the building but are shown in Figure 5-11 as being on the front side for clarity. Comparisons of the modeled and measured force coefficients for the wall and roof sections are given in Figure 5-12, Figure 5-13, and Figure 5-14. All force coefficients are expressed as the total wind induced force acting on the element divided by the mean dynamic pressure at roof height times the area of the element.

The model results are seen to agree reasonably well with the measured results, reproducing both the reduction in the force coefficient with the increasing area, and the directional characteristics of the loads.

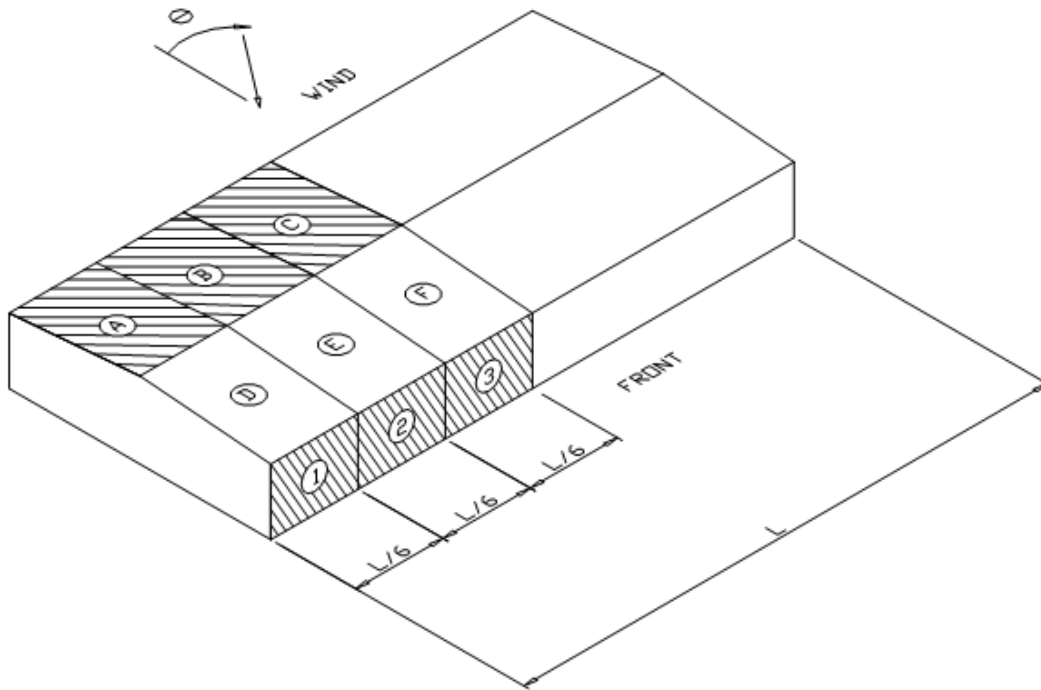


Figure 5-11 Integration Areas Used for Comparison of Overall Roof and Wall Loads

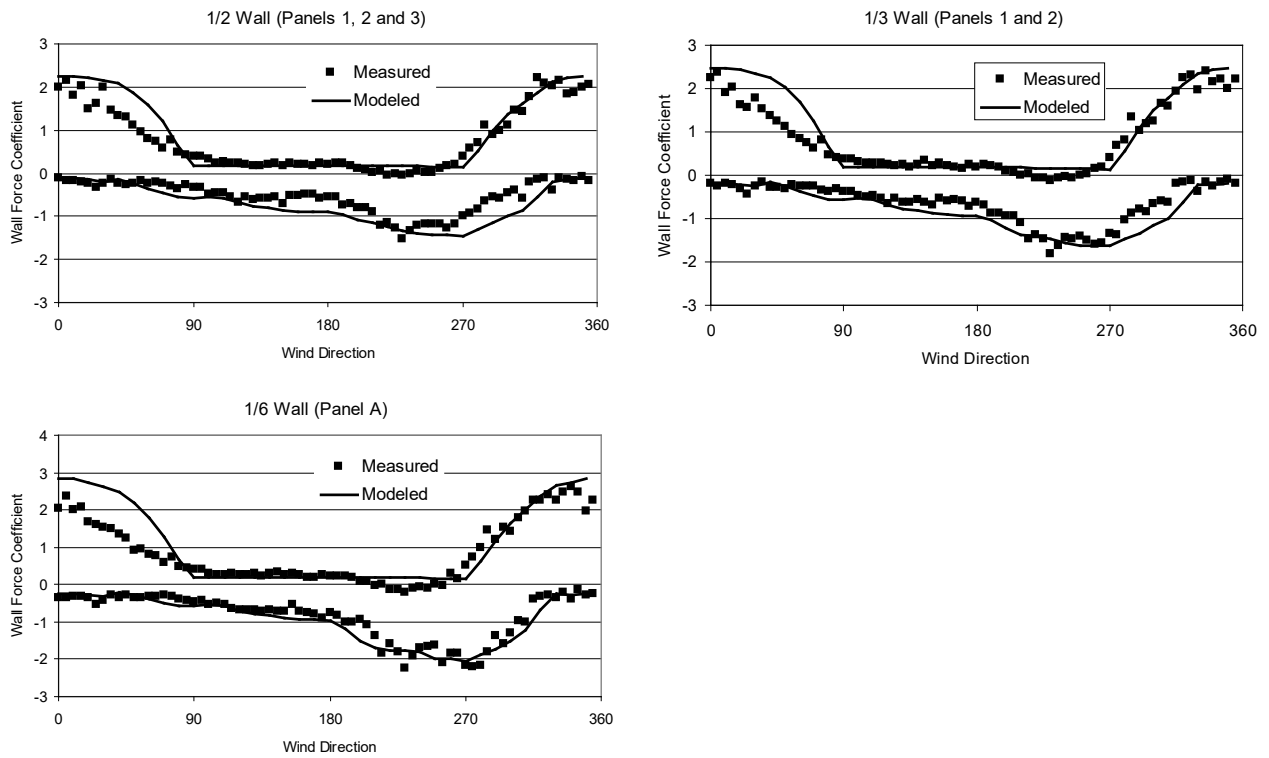


Figure 5-12 Comparison of Modeled and Measured Wall Forces on Rectangular Building in Suburban Terrain

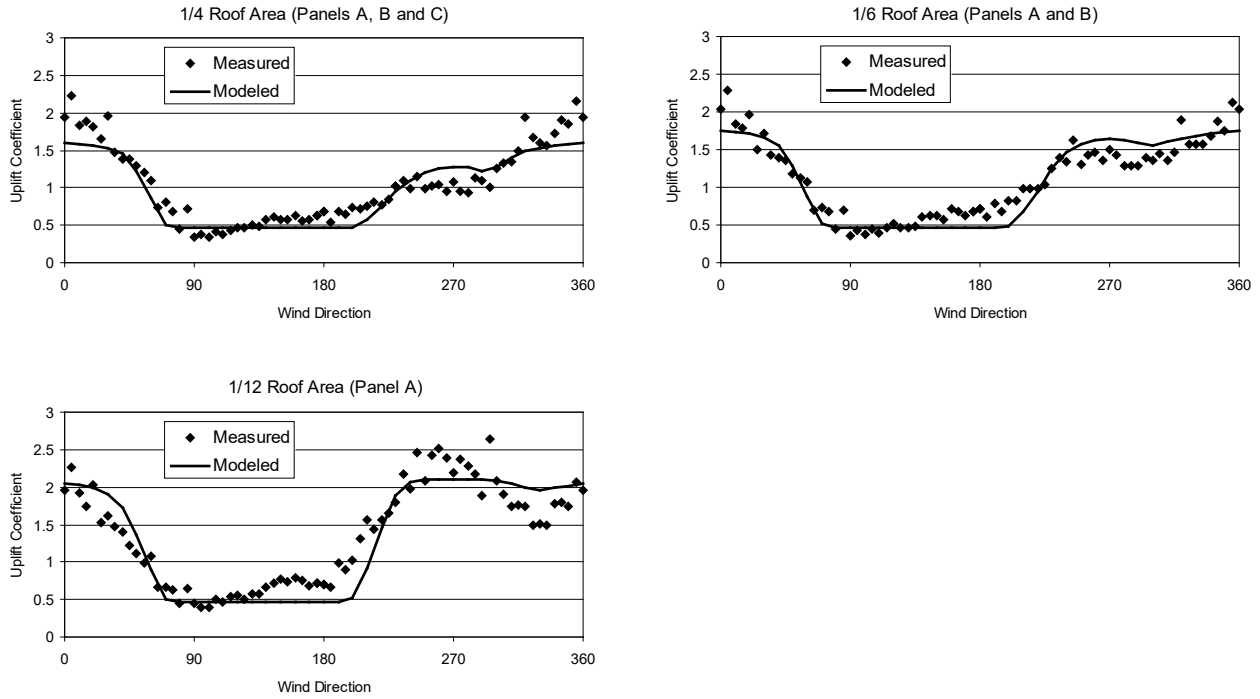


Figure 5-13 Comparison of Modeled and Observed Measured Uplift Coefficients on a Rectangular Building in Open Terrain

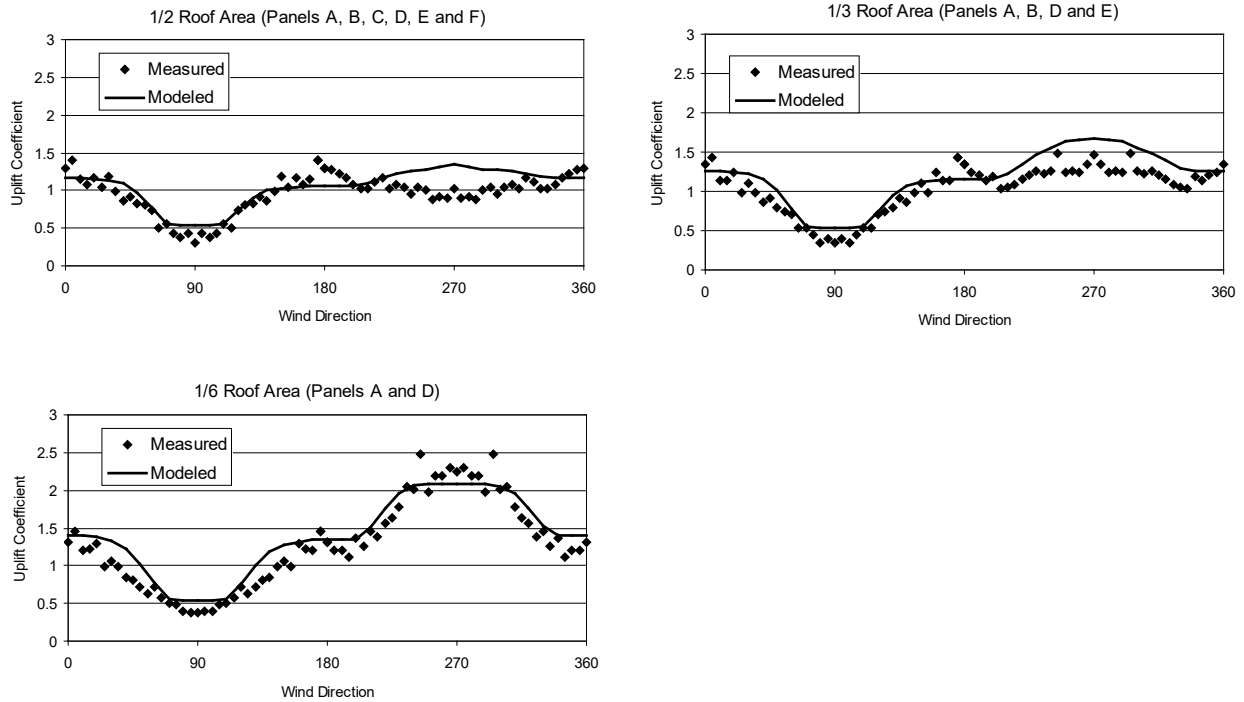


Figure 5-14 Comparison of Modeled and Observed Measured Uplift Coefficients on a Rectangular Building in Suburban Terrain

5.1.4.3 Overall Loads on Manufactured Homes

Using Equation 5-1, the code-based roof and wall loads were integrated over the surface of a manufactured home in order to evaluate the effectiveness of the approach in estimating the lift, drag, and overturning moments on manufactured homes. The results of the integration are compared to the full-scale measurements described in Marshall (1977) as well as Roy (1983) and the estimates of lift, drag, and overturning obtained from ASCE 7. Figure 5-15 presents the comparisons of lift, drag, and overturning coefficients.

The results given in Figure 5-15 show the modeled load estimates to be in general agreement with the limited full-scale lift and drag data, as well as the wind tunnel measured lift and moment data. The drag and moment coefficients for the zero wind direction case (winds approaching the long side of a manufactured home) obtained from the model are about 20% to 30% lower than the values estimated using ASCE 7. For use in damage prediction, the modeled lift and drag forces are increased by 10% for all wind directions examined, yielding loading estimates that have maxima closer to the values produced by ASCE 7 than indicated in Figure 5-15, but limiting the overestimate of the loads as compared to the bulk of the full scale and model scale data. This approach retains a reasonable representation of the effect of wind direction on the loads and strikes a balance between the ASCE 7-98 loads obtained using Figure 6-3 in ASCE 7 and the loads obtained from full scale and wind tunnel experiments.

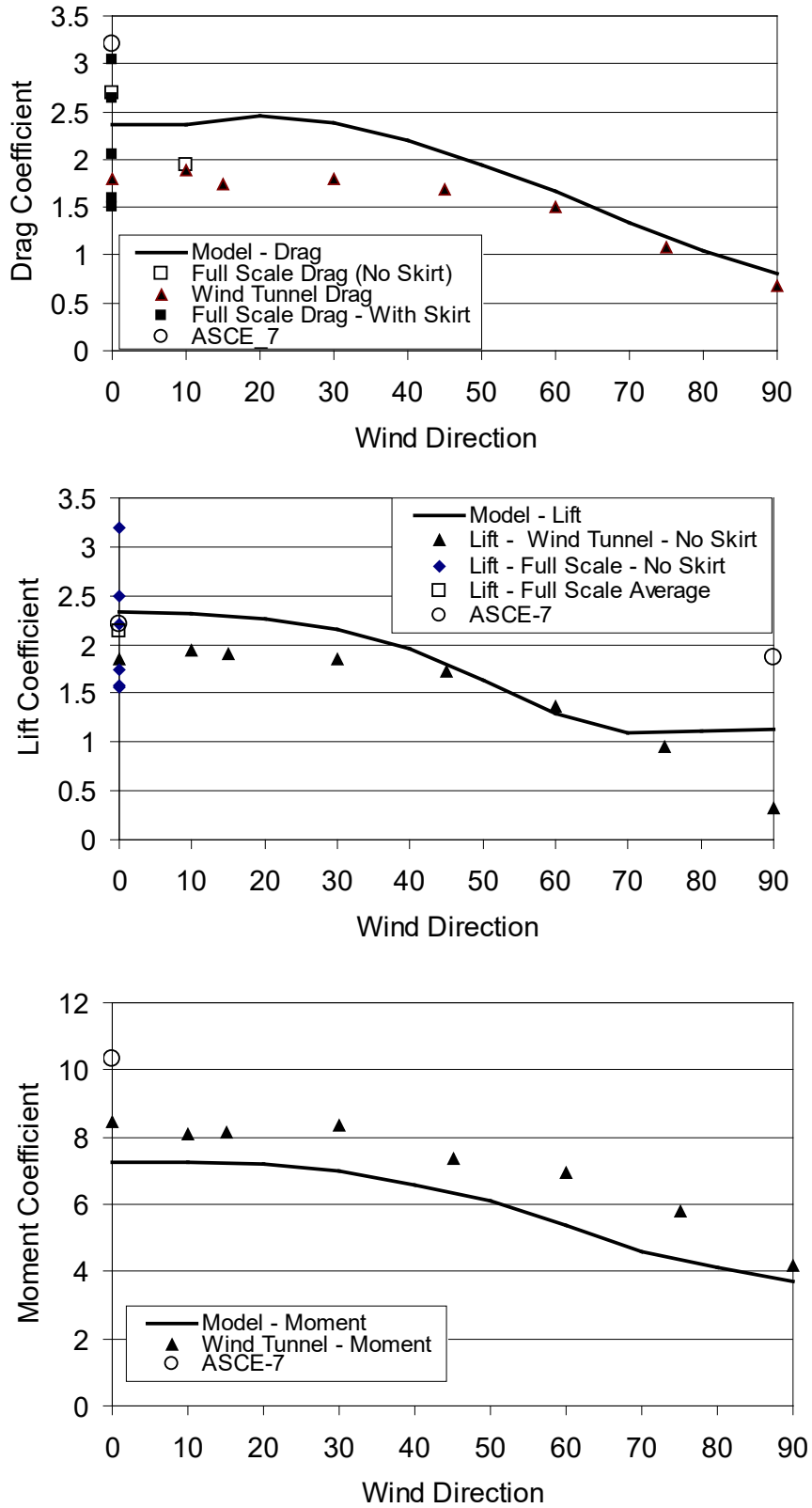


Figure 5-15 Comparison of Modeled, Wind Tunnel Measured, Full Scale Measured and ASCE 7 Estimated Drag, Lift and Moment Coefficients on a Manufactured Home

5.1.4.4 Wind Loads on Long Span Roof Elements

To compute the wind induced uplift loads and bending moments acting on long span roof elements (such as trusses, open web steel joists, pre-cast concrete tees, etc.), an influence line approach is used. Using this methodology, influence functions describing a specific structural action associated with the application of a load at a given point on the member, are used in conjunction with Equation 5-1 to produce estimates of the wind loads acting on the structural element. The influence function methodology was evaluated through comparisons of modeled and measured uplift coefficients for simply supported joists used as the primary roof system in a low-rise school building. The uplift loads at the joist supports were determined from wind tunnel tests performed at the University of Western Ontario using a 1:100 scale model of the building. Details of the wind tunnel tests and results are given in Young and Vickery (1994). Figure 5-16 and Figure 5-17 show photographs of the model in the wind tunnel.

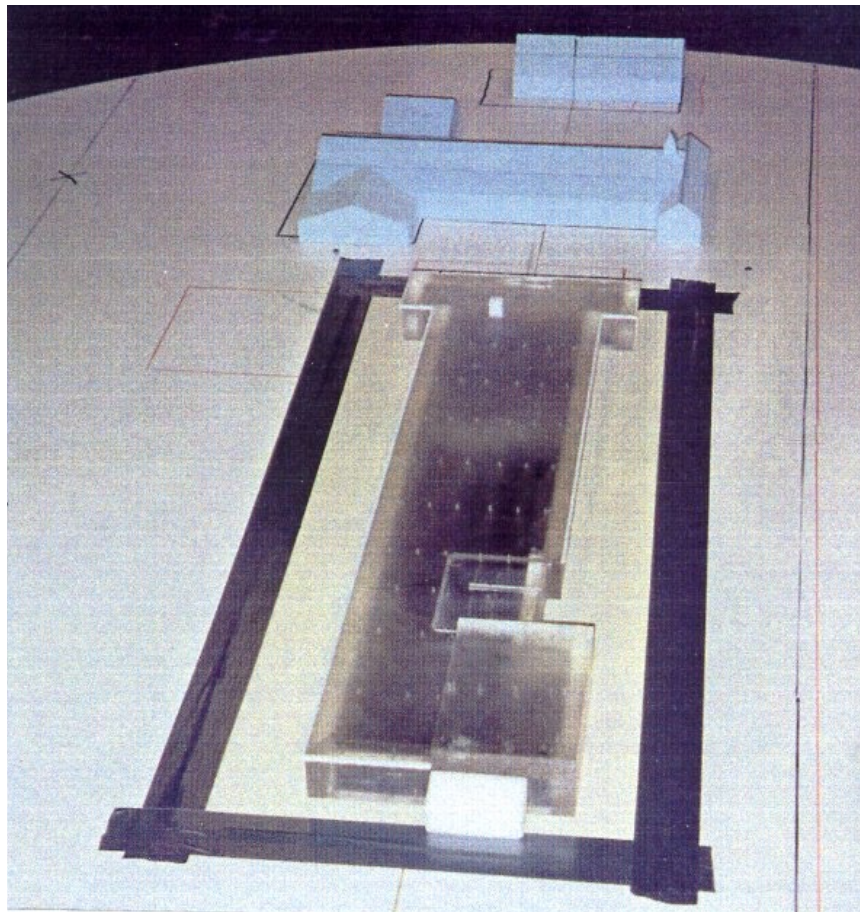


Figure 5-16 Close-up View of Model of School Building Used in Wind Tunnel Tests

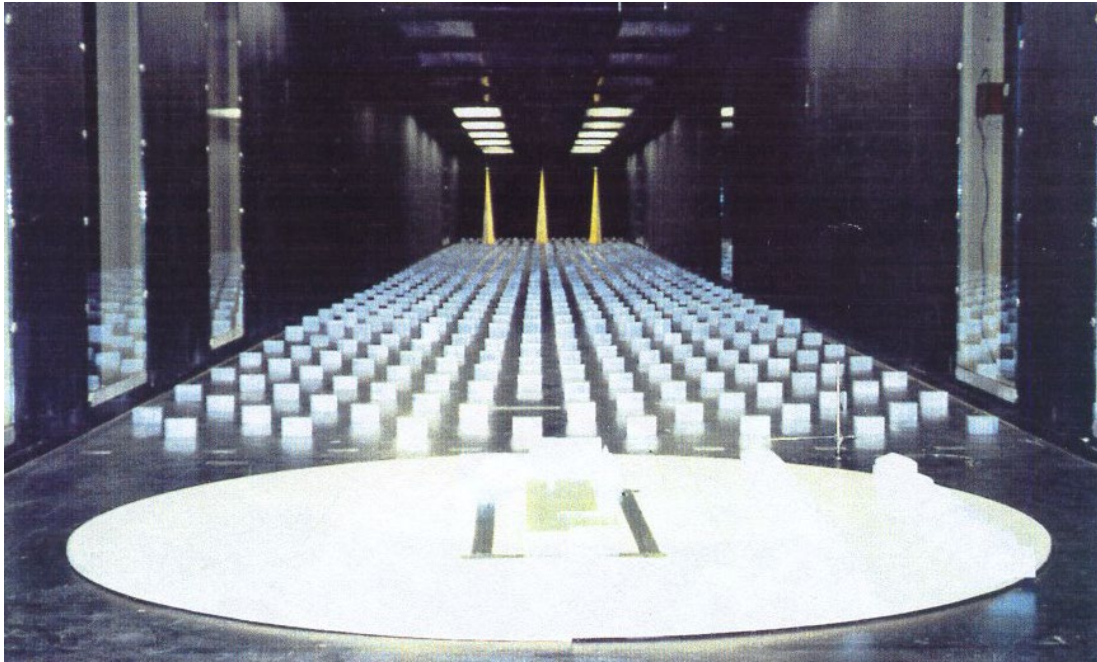


Figure 5-17 View of Model in Wind Tunnel Showing Upstream Terrain

The roof system of the structure is comprised of open web steel joists (OWSJ) spanning the school in the North-South direction. Three trusses are used in the complete span, each supported by a masonry wall. The two longest OWSJs, spanning the classrooms (span of 25'), are supported by the outer walls and the inner hallway walls, while one shorter OWSJ truss spans the hallway. The joist layout is shown in Figure 5-18.

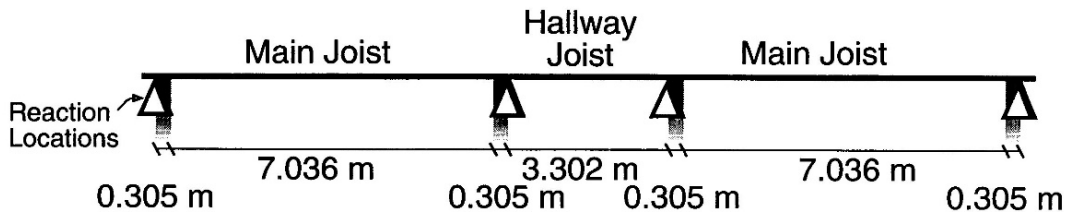


Figure 5-18 Layout of OWSJs as Modeled in Wind Tunnel Tests

The location of the supports as modeled in the wind tunnel are shown in Figure 5-19, and Figure 5-20 shows the locations of all pressure taps used in the modeling. Comparing the layout of pressure taps to the locations of the computed up-lift points, it is evident that a total of four pressure taps are positioned along each main joist. The pressures measured at the locations of the four individual pressure taps located along the line of each main joist were combined instantaneously with pre-computed influence coefficients to obtain estimates of the uplift loads acting at the ends of each OWSJ. The uplift loads were computed for winds approaching the building for the full 360° azimuth range at intervals of 10°.

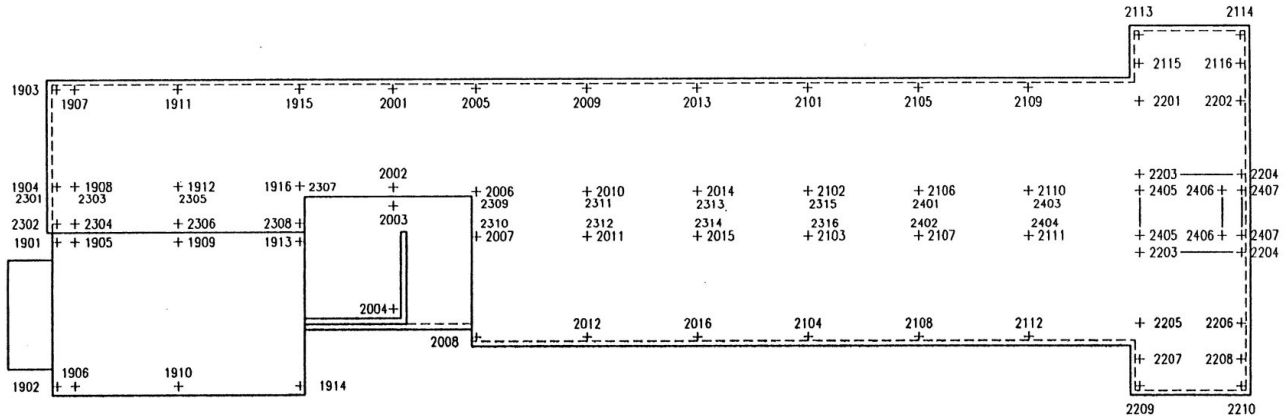


Figure 5-19 Plan View of School Showing Location of Truss Uplift Loads (North is towards top of page)

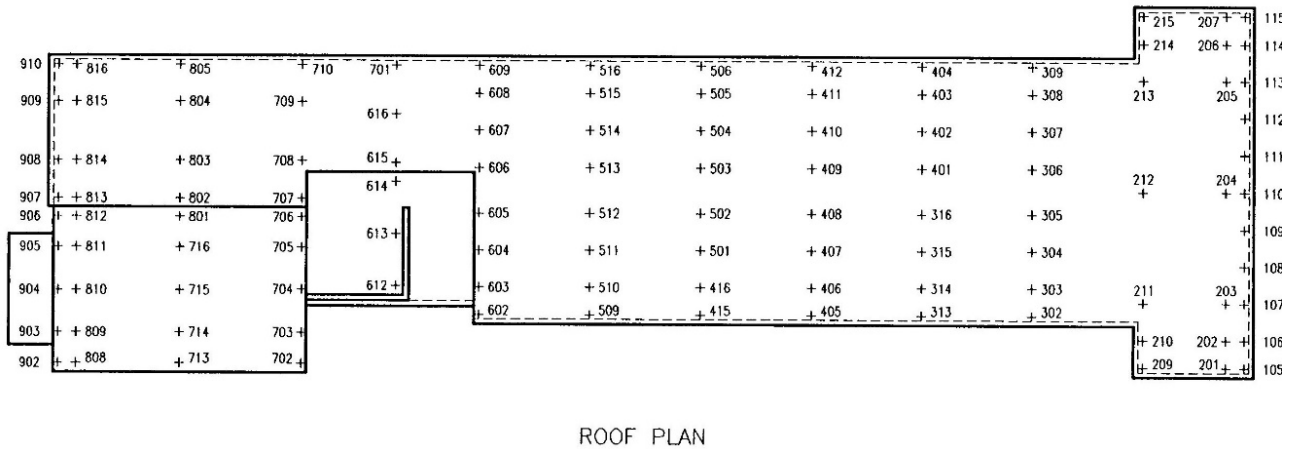


Figure 5-20 Plan View of School Showing Location of all Pressure Taps Used in the Wind Tunnel Tests (North is towards top of page)

To validate the model used to estimate OWSJ loads, comparisons of modeled and measured uplift loads were made for the uplift reactions at the points designated by the numbers 2007 through 2016, and 2101 through 2112. The measured uplift loads are compared to the modeled uplift (or reaction) loads in coefficient form, where both the wind tunnel and modeled coefficients are presented in the form:

Equation 5-2

$$C_R = \frac{R}{\frac{1}{2} \rho U_H^2 L}$$

Where:

L is the length (or span) of the joist

- R is the uplift load per unit width
- ρ is the density of air
- U_H is the mean wind speed at roof height

Figure 5-21 shows comparisons of the simulated and measured uplift coefficients as a function of wind direction for a total of 11 joists (22 reactions).

As indicated in the comparisons between modeled and measured uplift coefficients, the agreement between the two data sets is generally quite good, particularly for OWSJs located on the north side of the building, away from the corners. The model tends to overestimate the maximum uplift loads acting on the OWSJs located on the south side of the building (denoted as 2012, 2016, 2104, 2108, and 2112) by as much as 30% (see location 2012), but this overestimate varies from joist to joist, and considering the geometry of the building, it is expected that the peak loads experienced by these joists would be nominally the same suggesting that some of the differences can be attributed to experimental variability. In the case of the OWSJs located on the north side of the building, the agreement between the measured and modeled uplift coefficients is better than for those located on the south side of the building, with the model both slightly overestimating and underestimating the magnitudes of the peak uplift coefficients at the locations of the individual joists.

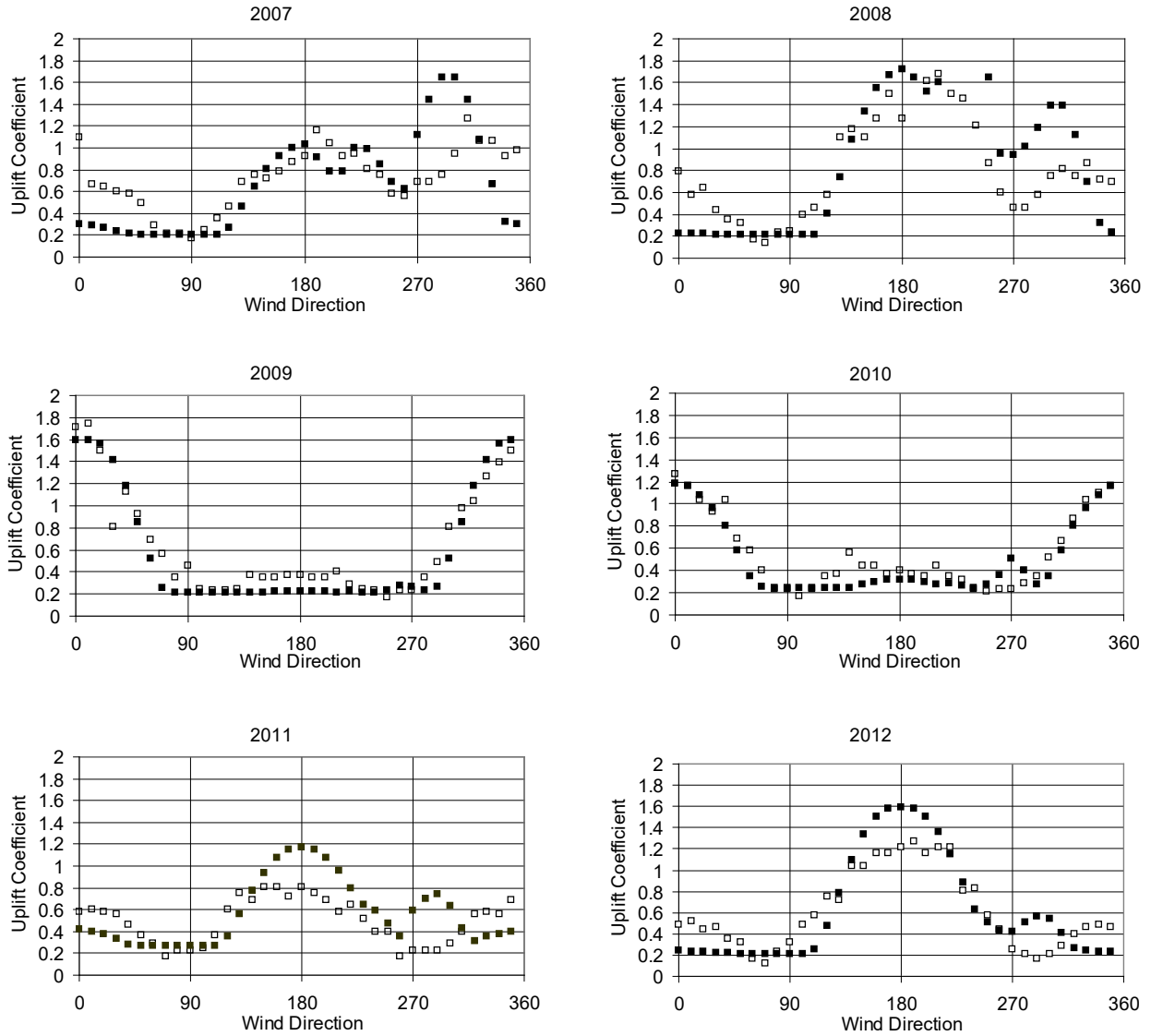


Figure 5-21 Comparison of Wind Tunnel Measured (open squares) and Simulated (solid squares) Joist Uplift Coefficients as a Function of Wind Direction

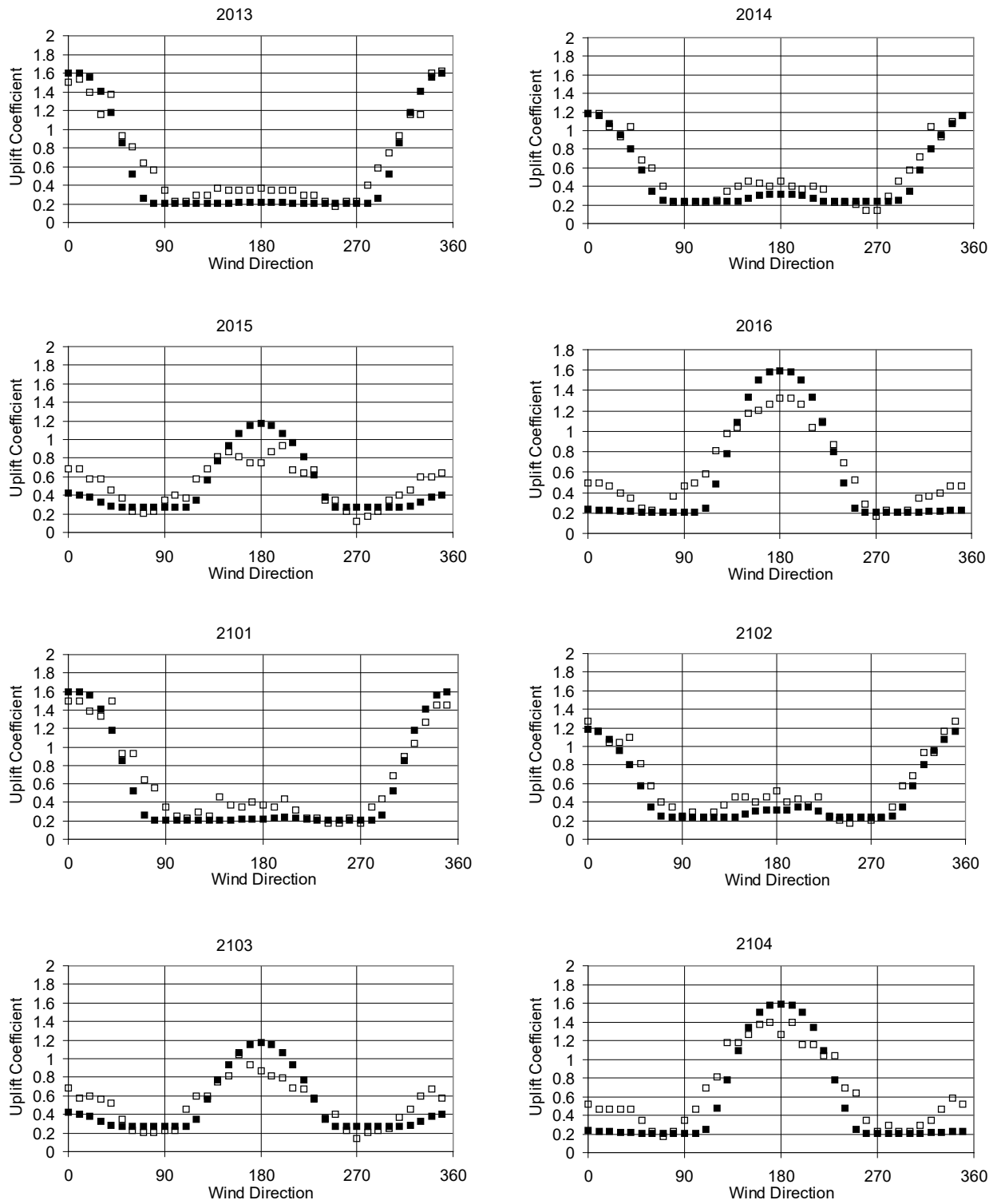


Figure 5-22 Comparison of Wind Tunnel Measured (open squares) and Simulated (solid squares) Joist Uplift Coefficients as a Function of Wind Direction (Continued)

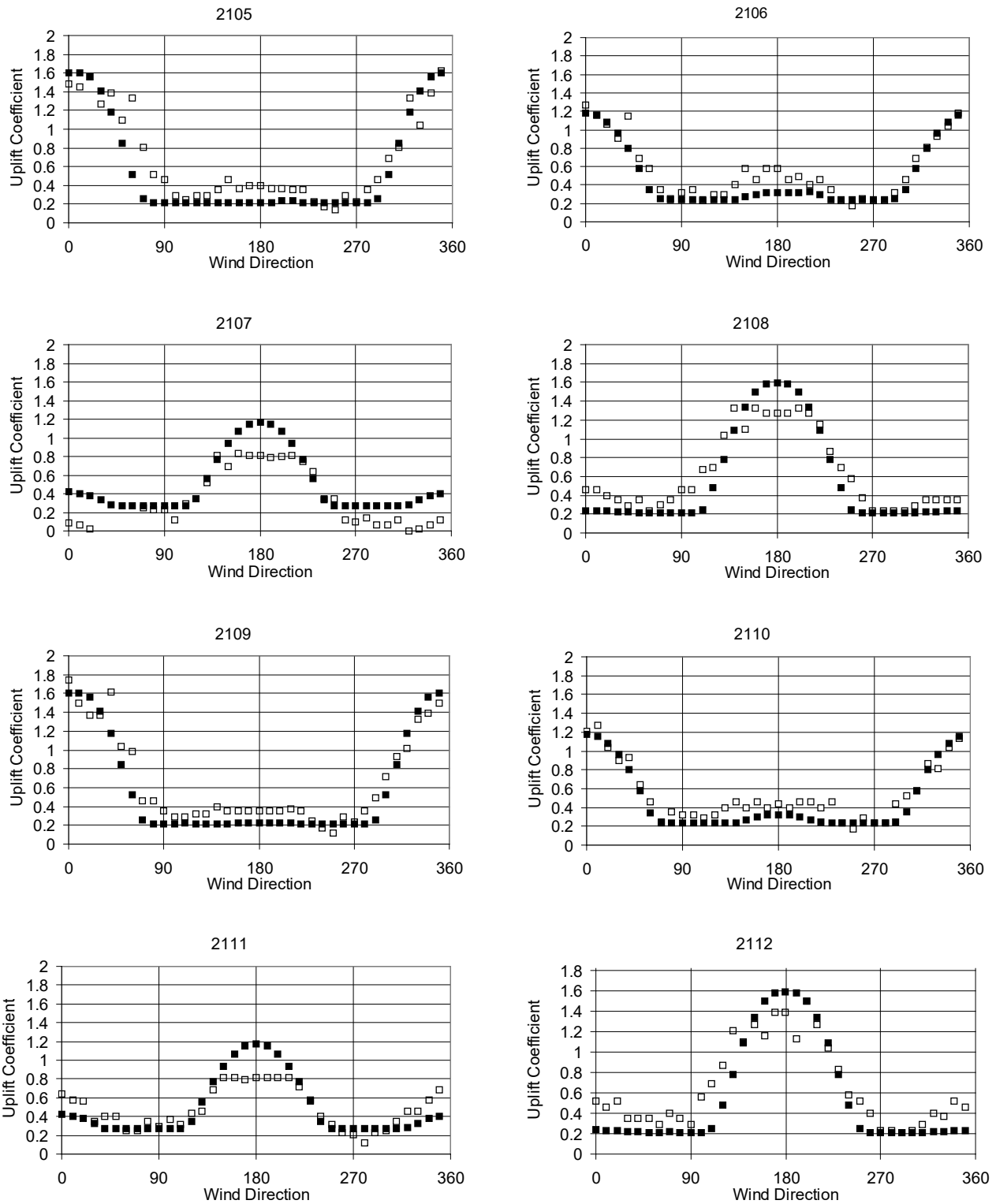


Figure 5-23 Comparison of Wind Tunnel Measured (open squares) and Simulated (solid squares) Joist Uplift Coefficients as a Function of Wind Direction (Concluded)

The overestimate of the wind uplift loads for joists located on the south side of the building is thought to be a result of the low buildings located to the south of the building, as indicated in Figure 5-13, interfering with the flow. The net reduction in wind loads produced by these upstream buildings is

consistent with the load reduction factor applied to buildings located in “real” environments as described earlier in Section 5.1.2.

5.1.5 Wind Loads on High-Rise Buildings

In the case of high-rise buildings, overall structural loads are not modeled. Wind induced damage to high-rise buildings is modeled as being associated with wind induced failure of components (i.e., windows) and damage to windows caused by windborne debris. The maximum magnitudes of the directionally dependent exterior cladding pressure load model are set equal to the peak values given in ASCE 7-02, and information on directionality was derived using data given in the 1995 version of the British Wind Loading Standard, CP3.

Example directional plots of modeled wind induced pressures and suctions have been developed for a rectangular and square building. The rectangular building has a length of 100 feet and a width of 40 feet, while the square building has a width of 40 feet. The exterior pressures are given along a ring around the building spaced 5 feet apart, with the first location positioned 2.5 feet from the edge. Figure 5-24 and Figure 5-25 indicate the locations on the model buildings for which the pressure coefficients apply.

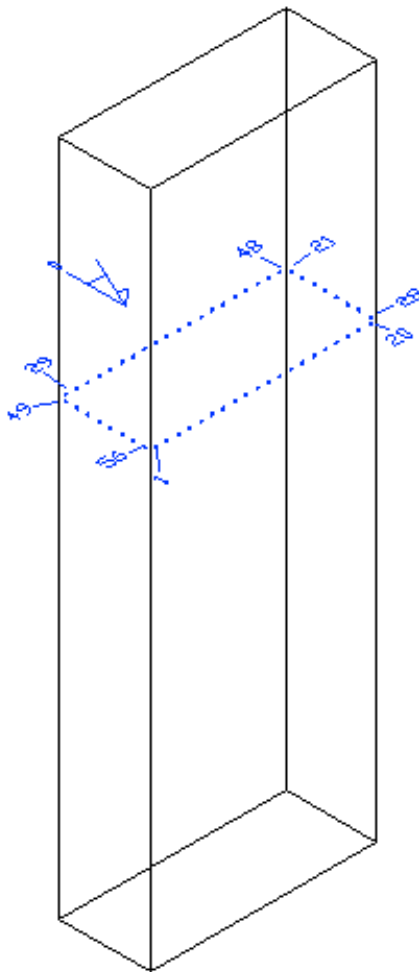


Figure 5-24 Location of Pressure Points for 2.5:1 High-Rise Building

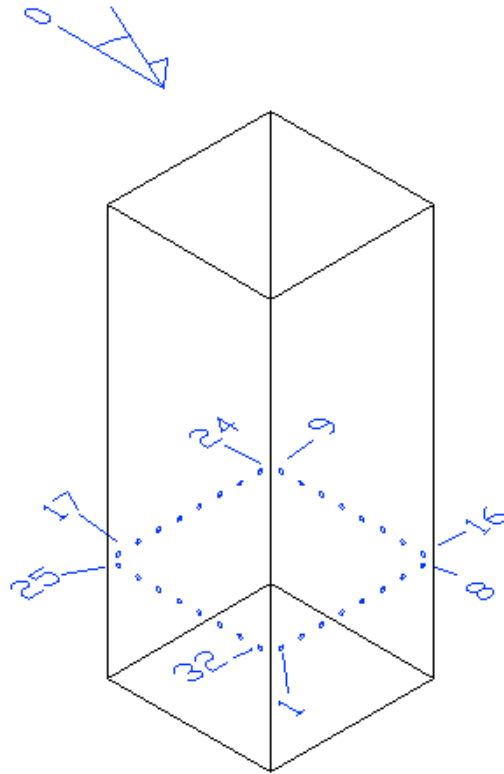


Figure 5-25 Location of Pressure Points for 1:1 High-Rise Building

Plots of the pressure coefficients as a function of wind direction are given in Figure 5-26 through Figure 5-32 and Figure 5-33 through Figure 5-36 for the buildings having length to width ratios of 2.5:1 (rectangular) and 1:1 (square), respectively. Note that in the case of the building having an aspect ratio of 2.5:1, locations on the short face experience large peak negative pressures for winds approaching from both 0° and 180°, reflecting the fact that the flow does not reattach to the short wall. In the case of winds approaching perpendicular to the short wall, the peak negative pressures on the long wall occur for one direction only, because the flow reattaches to the long wall.

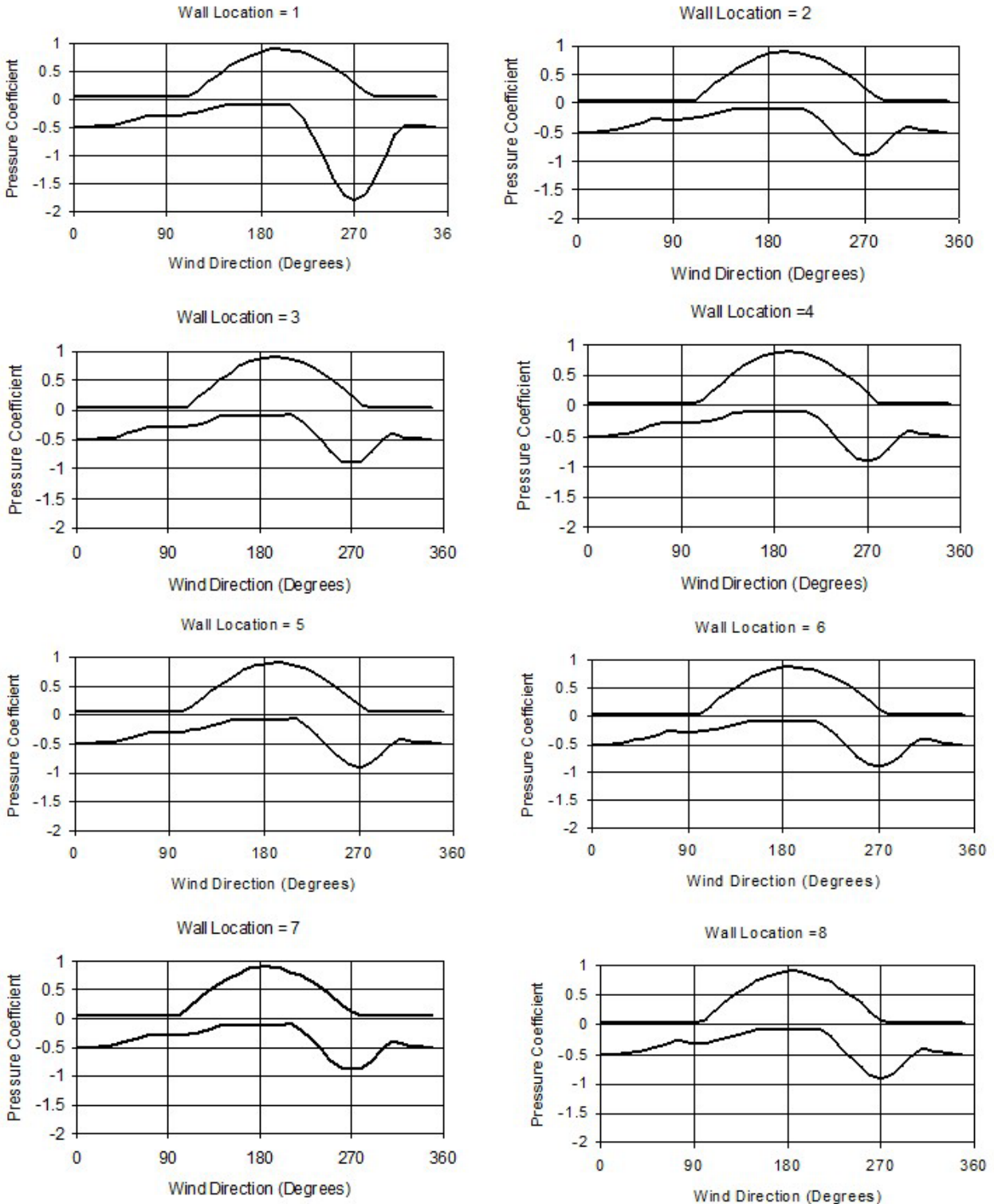


Figure 5-26 Maximum and Minimum Pressure Coefficients versus Wind Direction Used in Modeling of a Rectangular High-Rise Building Having a Length to Width Ratio of 2.5

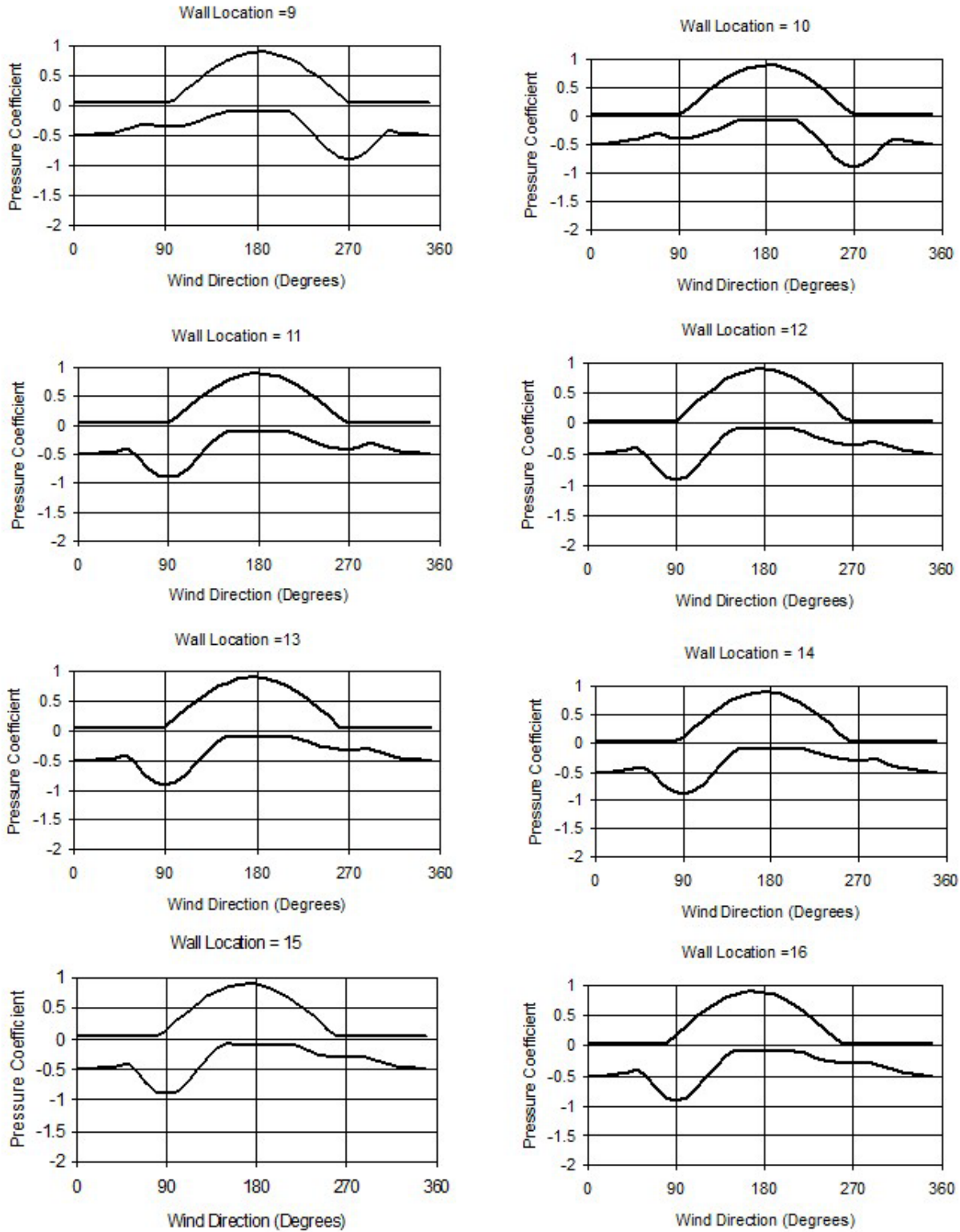


Figure 5-27 Maximum and Minimum Pressure Coefficients versus Wind Direction Used in Modeling of a Rectangular High-Rise Building Having a Length to Width Ratio of 2.5 (continued)

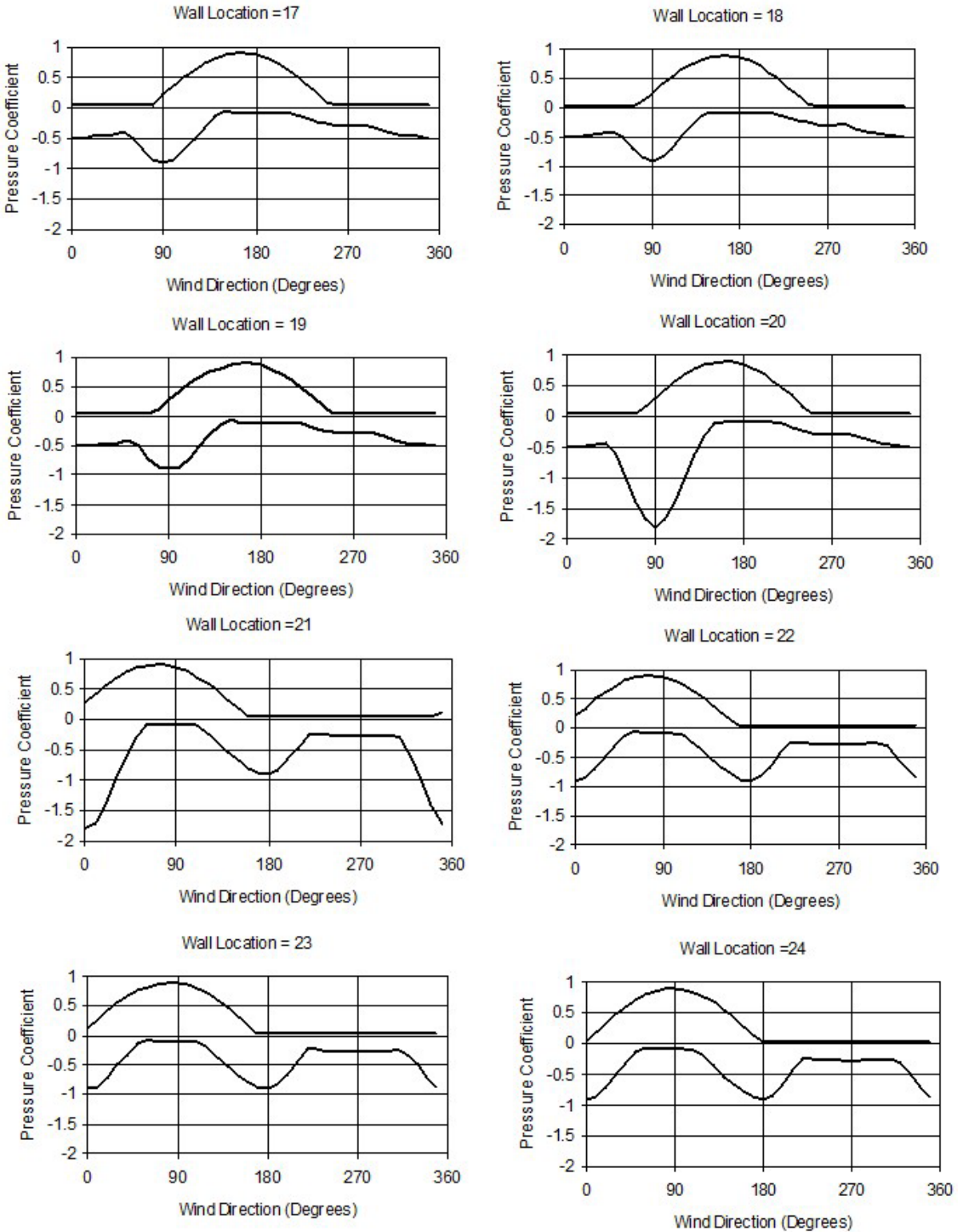


Figure 5-28 Maximum and Minimum Pressure Coefficients versus Wind Direction Used in Modeling of a Rectangular High-Rise Building Having a Length to Width Ratio of 2.5 (continued)

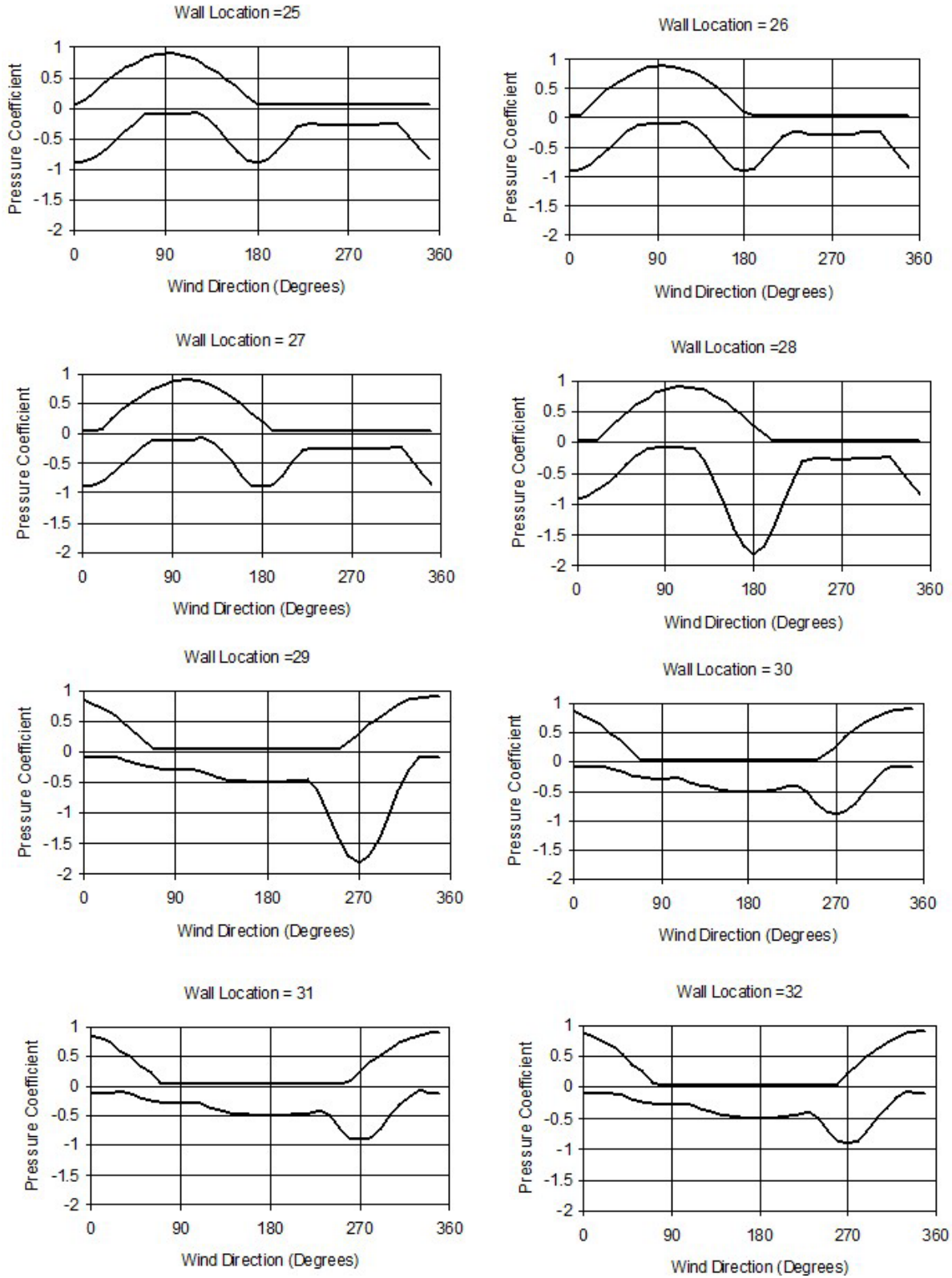


Figure 5-29 Maximum and Minimum Pressure Coefficients versus Wind Direction Used in Modeling of a Rectangular High-Rise Building Having a Length to Width Ratio of 2.5 (continued).

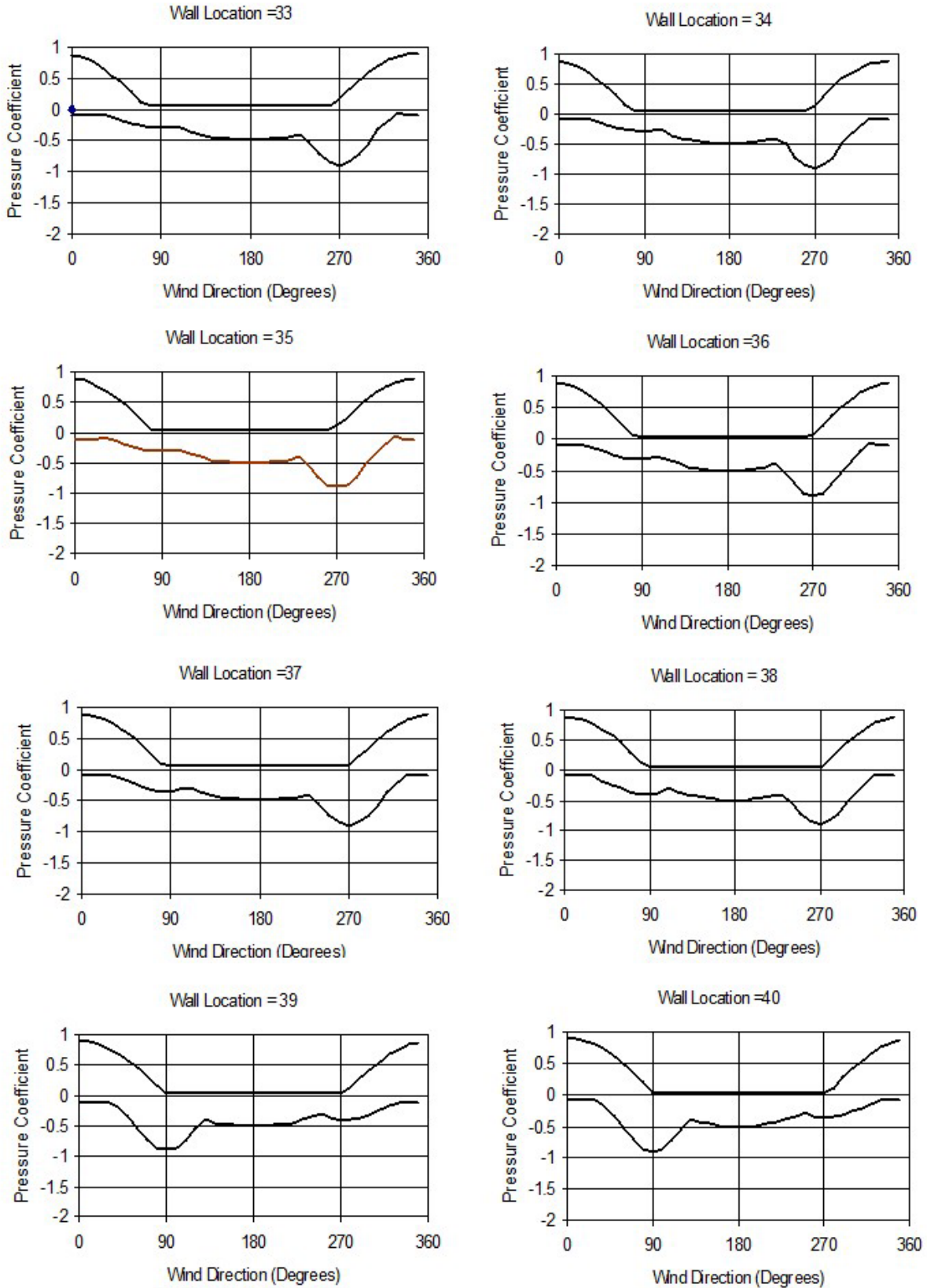


Figure 5-30 Maximum and Minimum Pressure Coefficients vs. Wind Direction Used in Modeling of a Rectangular High-Rise Building Having a Length to Width Ratio of 2.5 (continued)

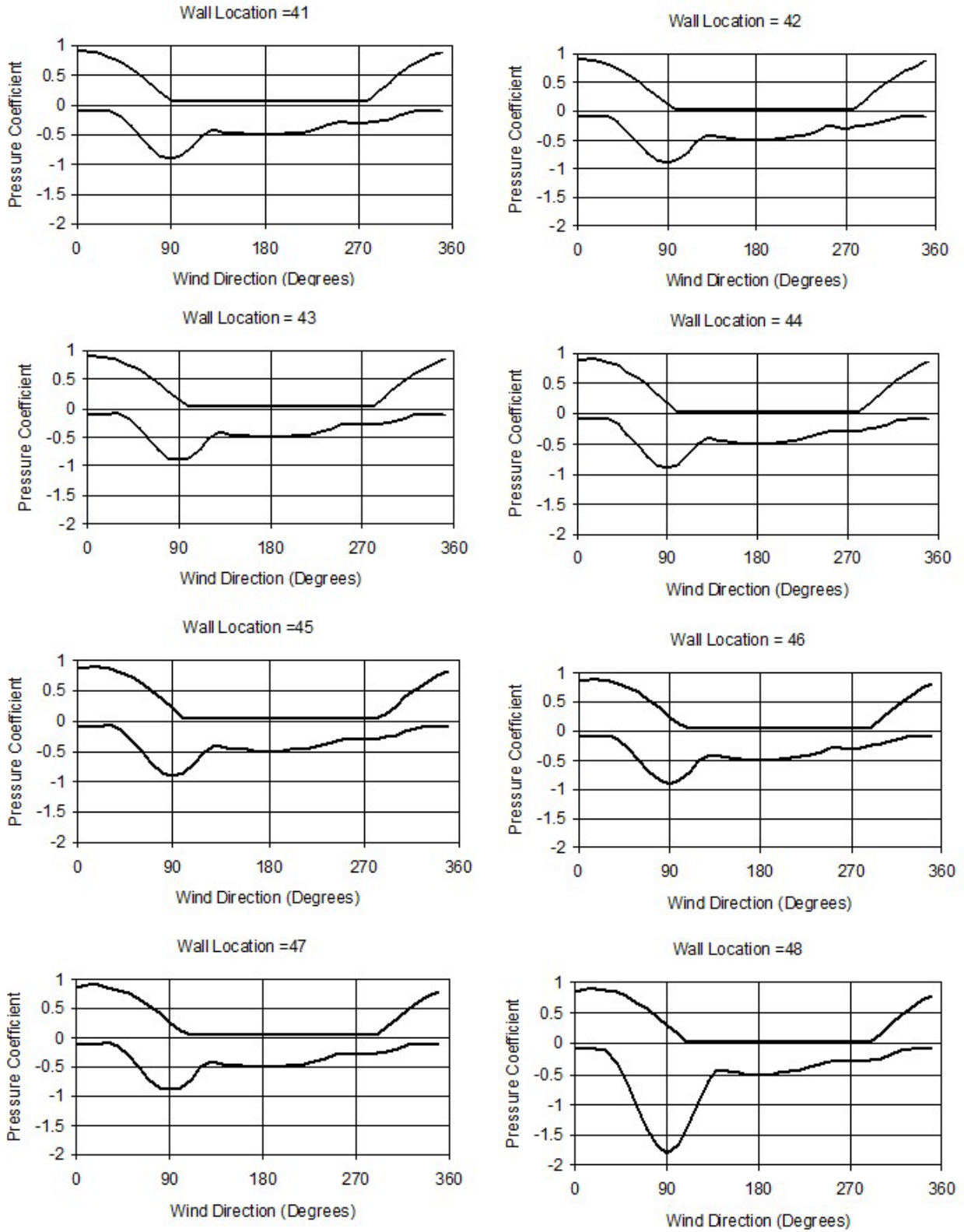


Figure 5-31 Maximum and Minimum Pressure Coefficients versus. Wind Direction Used in Modeling of a Rectangular High-Rise Building Having a Length to Width Ratio of 2.5 (continued)

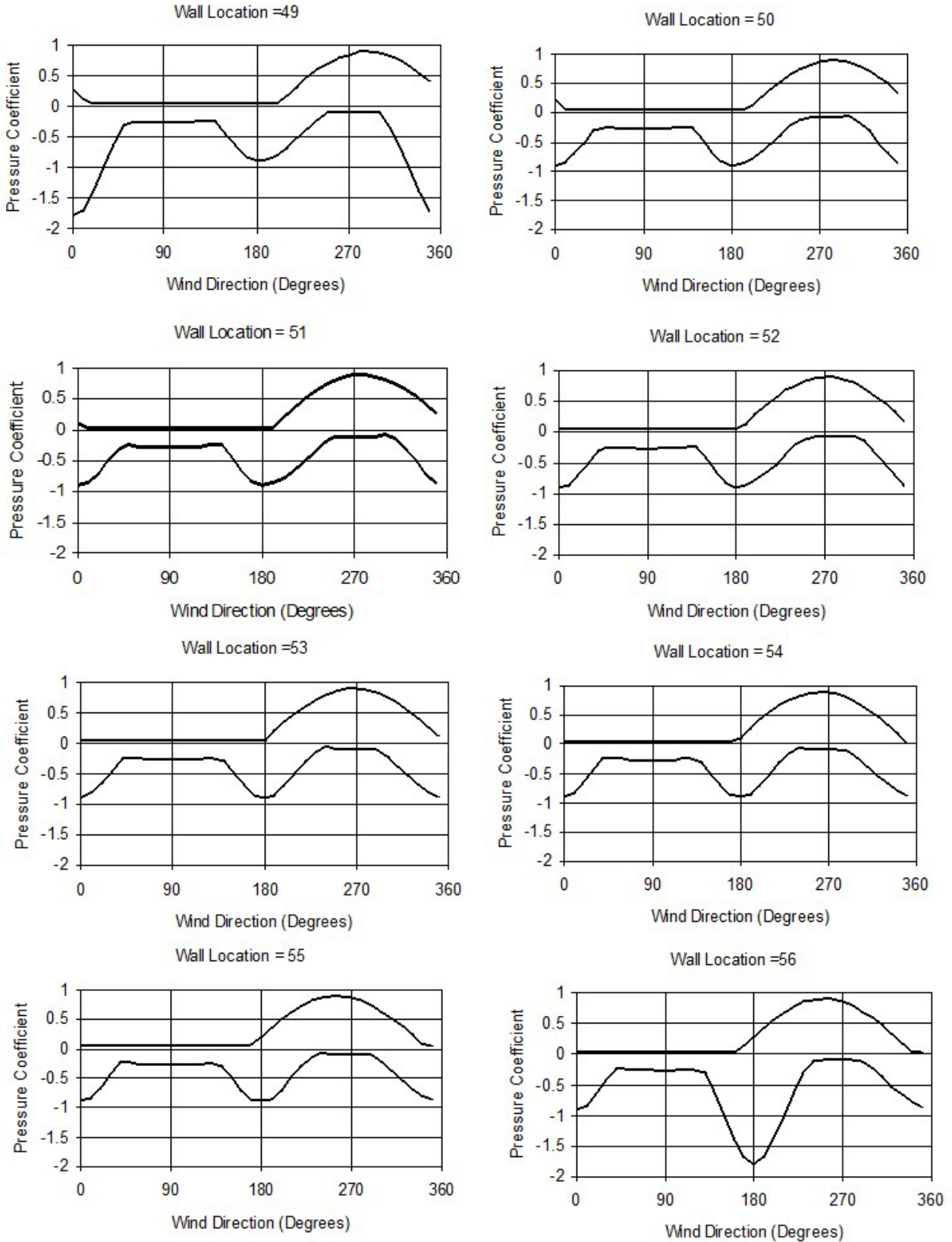


Figure 5-32 Maximum and Minimum Pressure Coefficients versus Wind Direction Used in Modeling of a Square High-Rise Building (concluded)

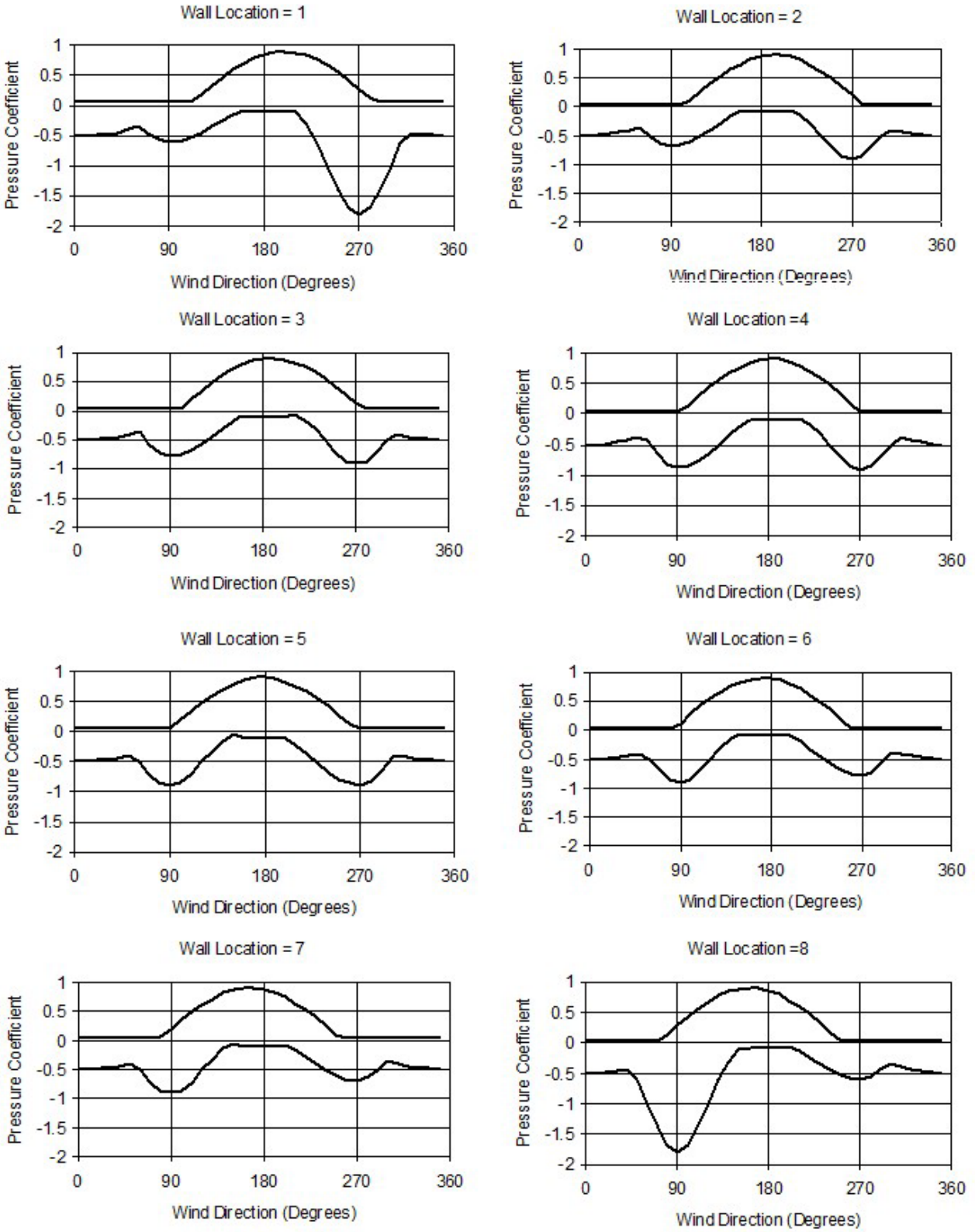


Figure 5-33 Maximum and Minimum Pressure Coefficients versus Wind Direction Used in Modeling of a Square High-Rise Building

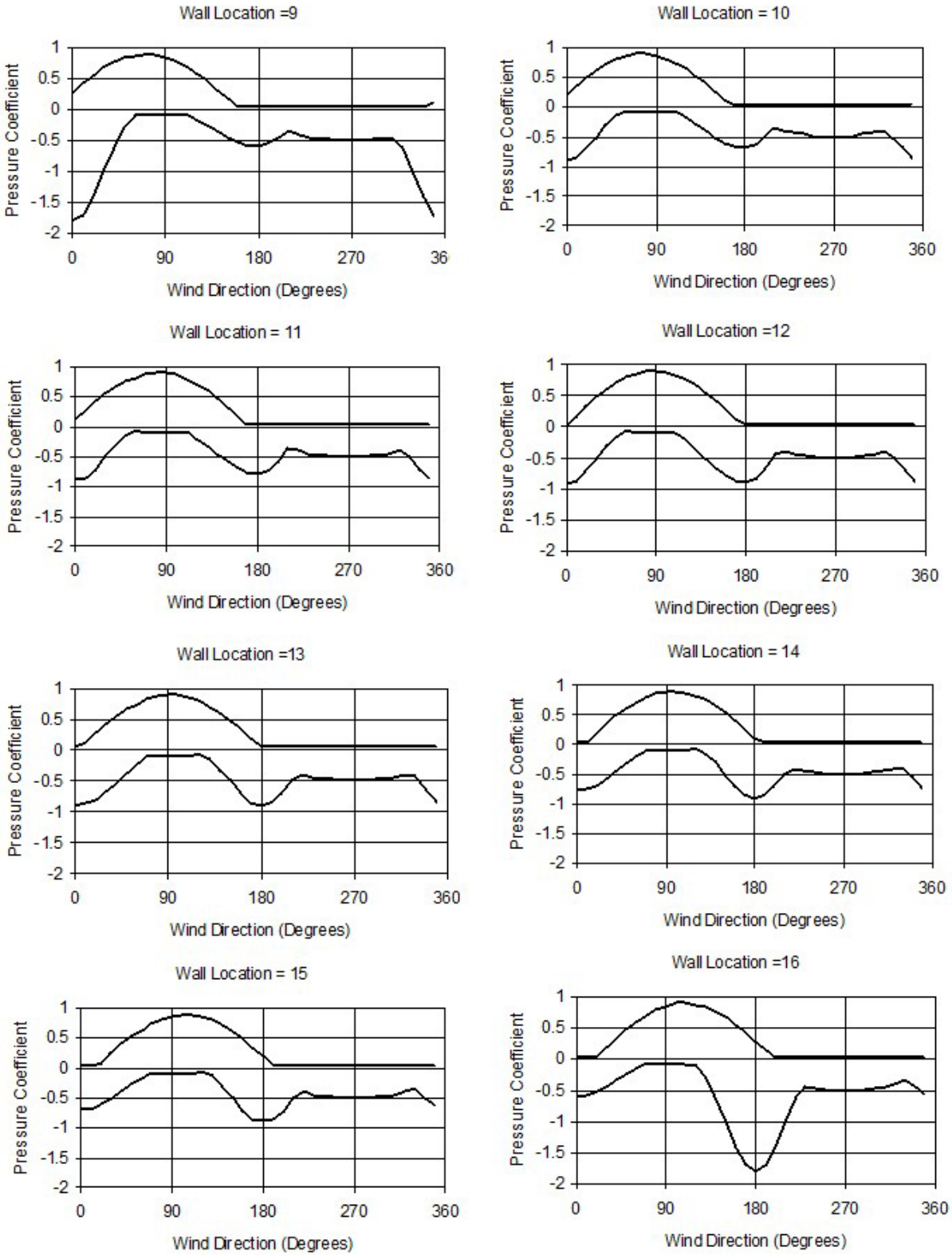


Figure 5-34 Maximum and Minimum Pressure Coefficients versus Wind Direction Used in Modeling of a Square High-Rise Building (continued)

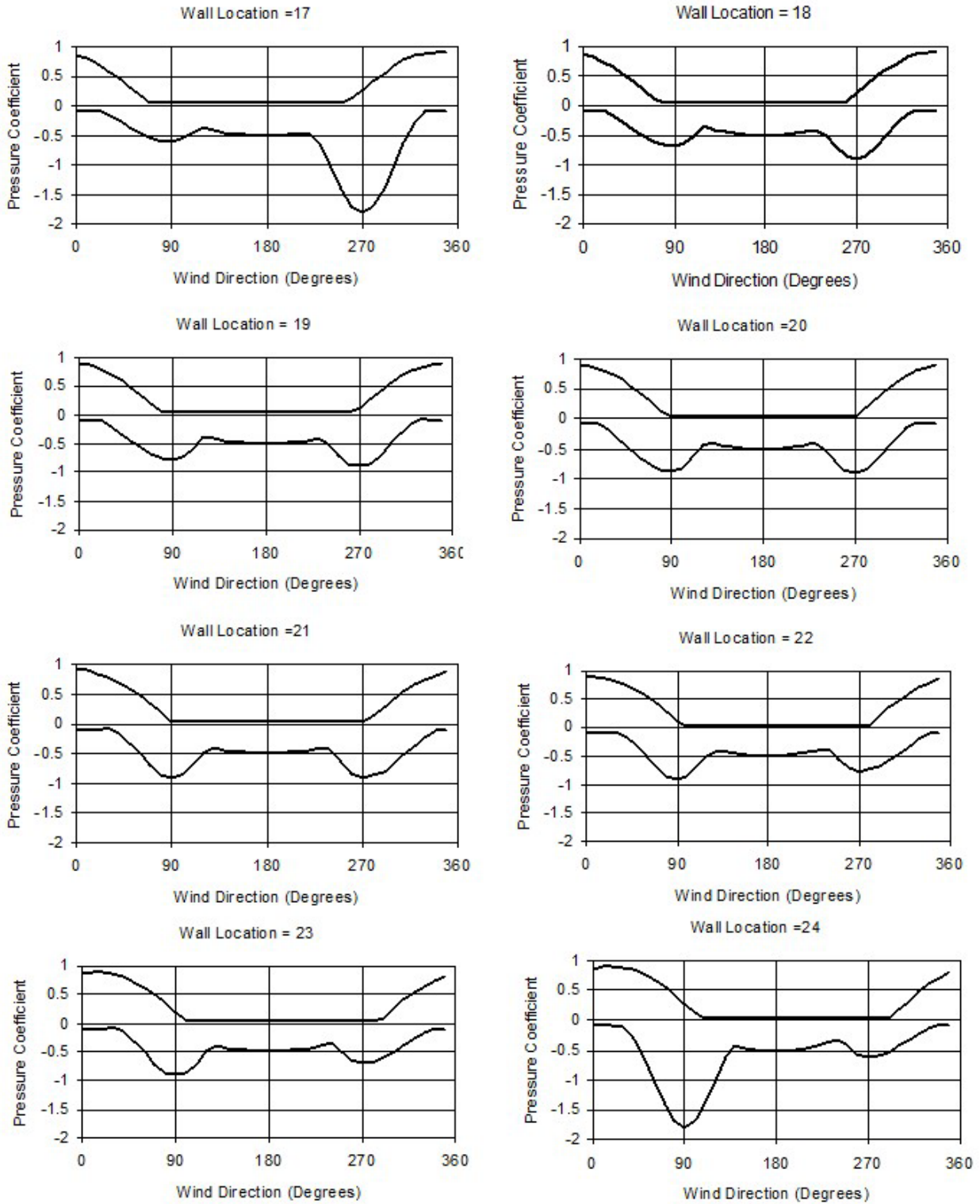


Figure 5-35 Maximum and Minimum Pressure Coefficients versus Wind Direction Used in Modeling of a Square High-Rise Building (continued)

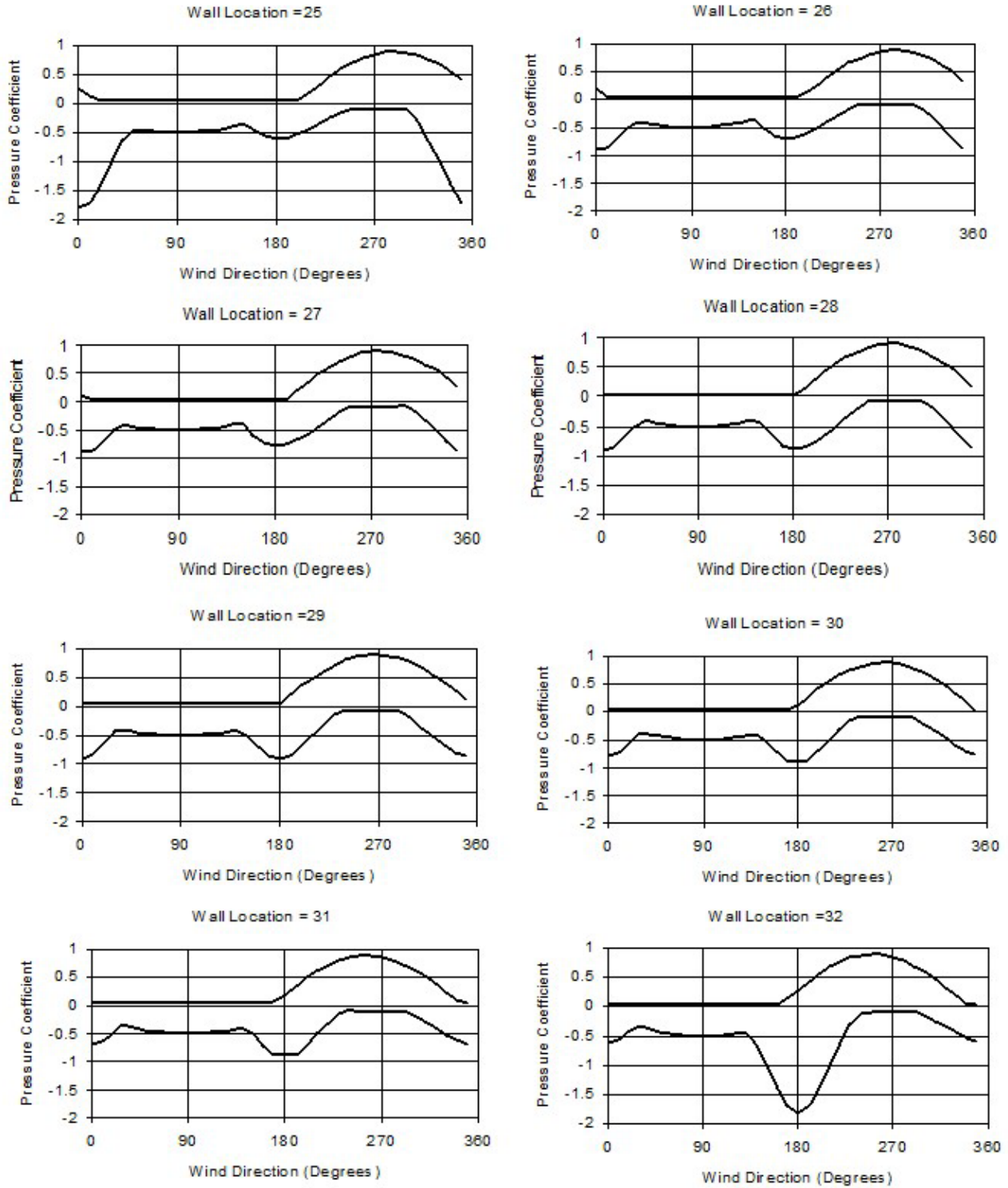


Figure 5-36 Maximum and Minimum Pressure Coefficients versus Wind Direction Used in Modeling of a Square High-Rise Building (concluded)

5.2 Windborne Missile Models

A significant amount of the damage to structures associated with hurricane winds is produced by windborne debris impacting the buildings and damaging the building exterior, including roof coverings, windows, doors, and other openings. Two windborne debris models are used in Hazus. The first applies to residential environments, and the second is a commercial building model for predicting the damage produced by windborne gravel. The windborne debris model used to estimate impact risk in residential environments is based on the model described in Twisdale et al. (2000a, 2000b). The residential windborne debris model uses an explicit damage and missile transport approach. A description of the residential windborne debris model and its simplified implementation in damage simulations is provided in Section 5.2.1. The gravel missile model, developed to predict the damage to buildings from roof gravel missiles, is described in Section 5.2.2.

5.2.1 Windborne Debris – Residential Missile Model

5.2.1.1 Windborne Debris Simulation and Analysis

The windborne debris model developed by Twisdale et al. (2000a, 2000b), is used to quantify the windborne debris risk in typical residential environments. The residential missile model focuses on debris produced from the roofs of residential structures. As observed in the field after severe wind events, most of the impact damage is caused by debris generated from the roofs of nearby buildings. The debris types modeled include roof tiles, shingles, sheathing panels, planks (structural members), and whole roofs. The model represents the first attempt to quantify, using physically-based models, the risk of impact damage to buildings in a residential environment.

The approach used in the residential model consists of modeling typical subdivisions, as shown for example in Figure 5-37, and impacting the buildings with debris generated from within the model subdivision. Through simulations of hurricane winds striking the subdivision, the roof components fail when the modeled wind loads exceed the component capacity. Once a component fails, it is released into the turbulent hurricane wind field, where the trajectory is computed until the component strikes either the ground or another structure. If a missile strikes the wall of another building, the impact velocity, energy, and momentum are recorded. In the trajectory model, the turbulence within the hurricane wind field is modeled using an approach in which both the longitudinal and vertical components of the turbulent wind field are simulated. The missile risk simulations were performed for the subdivisions located in three different surrounding terrain environments.

For each terrain case examined, a total of 36 hurricanes were simulated for four maximum peak gust speeds of 110 mph, 130 mph, 150 mph, and 170 mph. A total of nine different representative hurricane tracks relative to the subdivision site were simulated for each wind speed case. Typical terrain conditions representative of open, suburban, and treed terrain were modeled for the wind simulation.

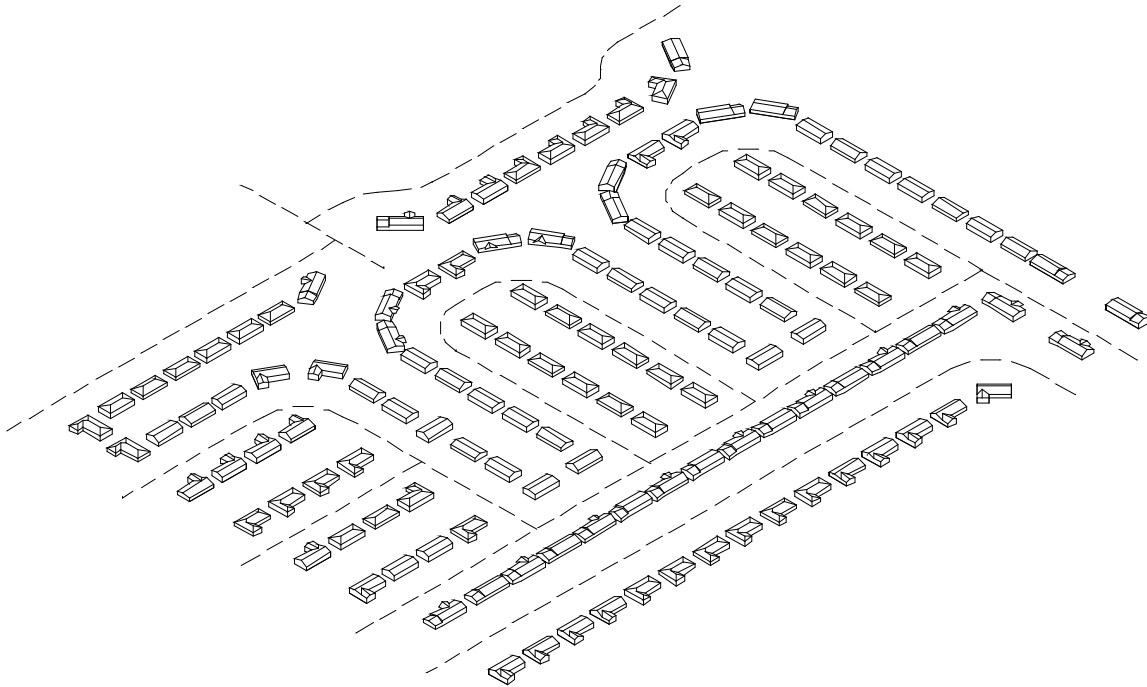


Figure 5-37 Example Model Subdivision Used in the Missile Risk Study

The open terrain case was representative of the wind conditions expected to be experienced on barrier islands. The suburban terrain (i.e., $z_0 = 0.3$ meters) is representative of a residential area with relatively few tall trees to reduce the wind speeds (such as South Florida), and the treed terrain (i.e., $z_0 = 1.0$ meters) is representative of a terrain with trees having heights greater than the heights of the buildings. This last terrain type is representative of many suburban locations along the U.S. hurricane coastline, away from barrier islands.

Examples of the turbulent wind traces generated for open country conditions at the height of 10 meters above ground are given in Figure 5-38 through Figure 5-40. Also shown, in Figure 5-38 through Figure 5-40, is the “gust speed envelope” represented by the solid line. This envelope is defined as the mean wind speed multiplied by the three-second gust factor. A comparison of the turbulent wind trace and the theoretical envelope shows that the peak gusts produced by the turbulent model equal or slightly exceed the envelope value about three to four times per hour.

Upon completing the wind speed simulations (i.e., nine hurricanes), information on the total number of hits and associated energy and momentum levels are available. Given the information on the expected number of missile impacts on the walls of a structure, the risk of damage to an opening, $P_v(D)$ for a given wind speed, V can be obtained from:

Equation 5-3

$$P_v(D) = 1 - \exp[-\lambda q(1 - P(\xi < \xi_d))]$$

Where:

ξ_d is the energy or momentum level assumed to produce damage

- q is the fraction of the building surface occupied by windows and glass doors
- λ represents the mean number of missile impacts per building
- $P(\xi < \xi_d)$ is the probability for the impact energy or momentum (ξ) to be less than the damage threshold value (ξ_d) given an impact

The probability of no damage, R is expressed in Equation 5-4:

Equation 5-4

$$R = 1 - P_v(D) = \exp[-\lambda q(1 - P(\xi < \xi_d))]$$

Using Equation 5-4, probability curves for R versus wind speed were developed, which indicate the energy or momentum level a window or door must be able to withstand in order to achieve a given probability level of no damage. Figure 5-38, Figure 5-39, and Figure 5-40 show an example of the reliability curves generated for one of the cases examined in the windborne debris risk study. The example in Figure 5-41, and presents reliability curves for several impact energies and a q value of 0.2.

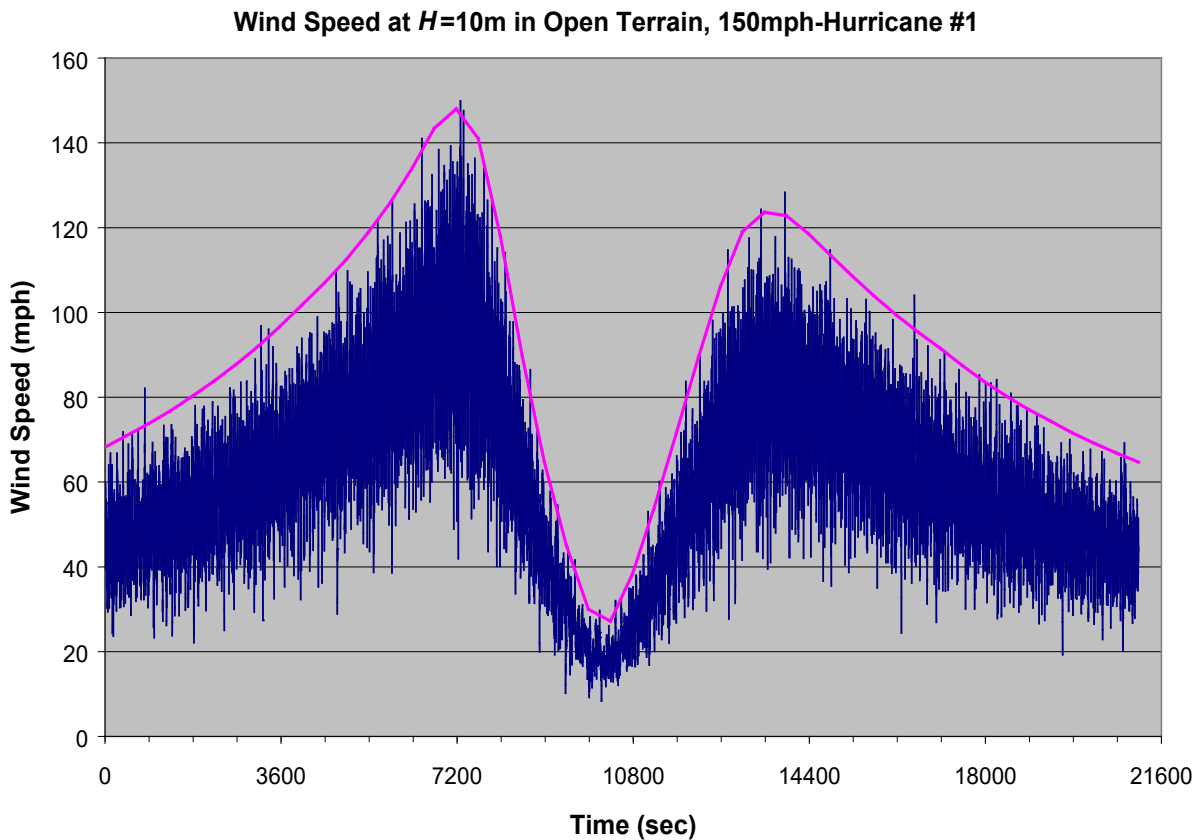


Figure 5-38 Example Hurricane Wind Speed Traces Used for the 150 mph Case – Hurricane #1

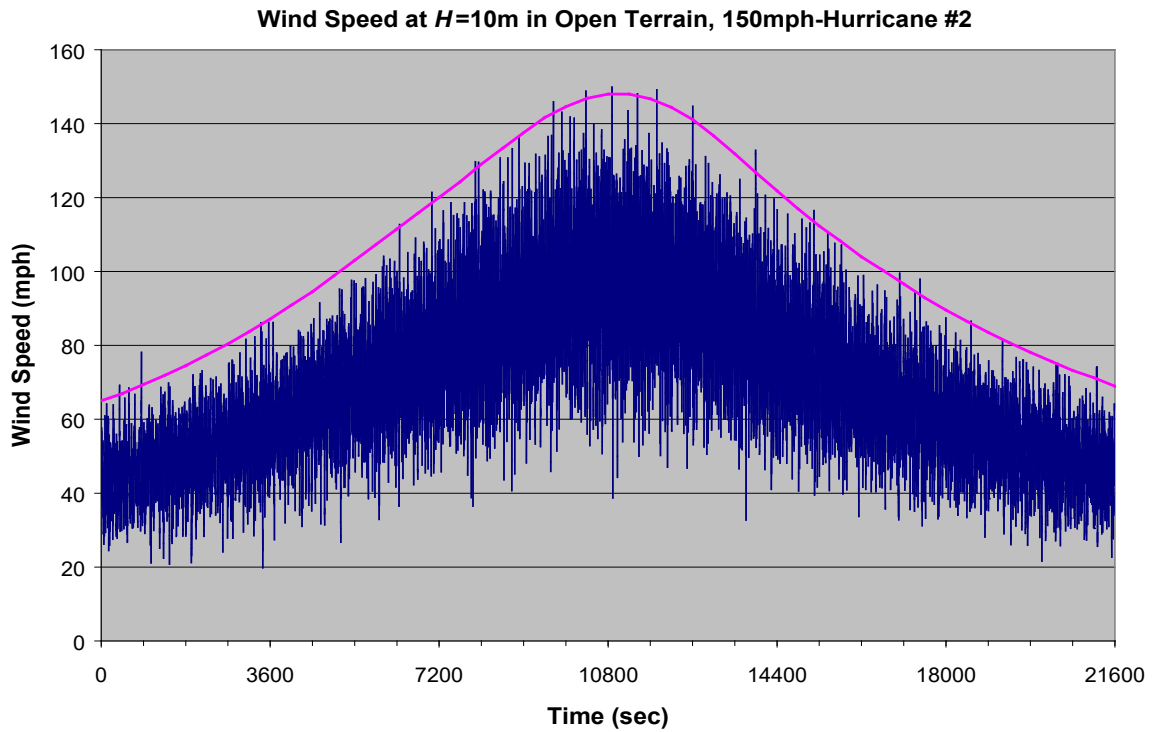


Figure 5-39 Example Hurricane Wind Speed Traces Used for the 150 mph Case – Hurricane #2

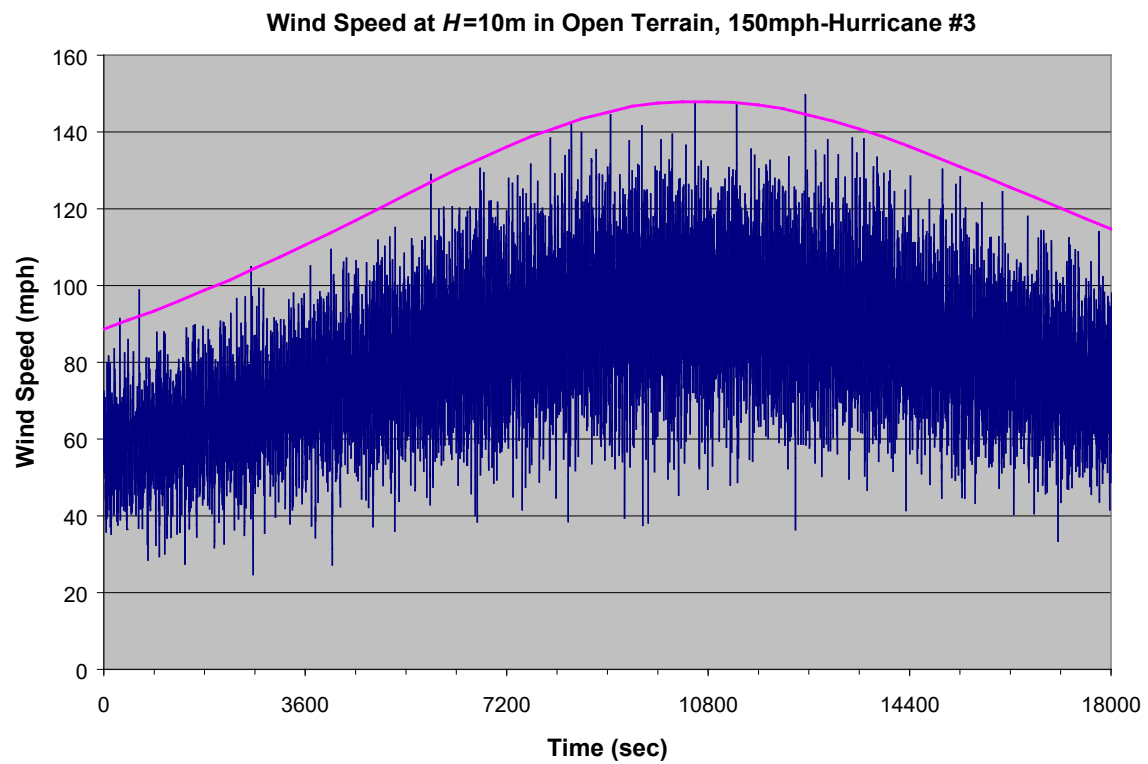


Figure 5-40 Example Hurricane Wind Speed Traces Used for the 150 mph Case – Hurricane #3

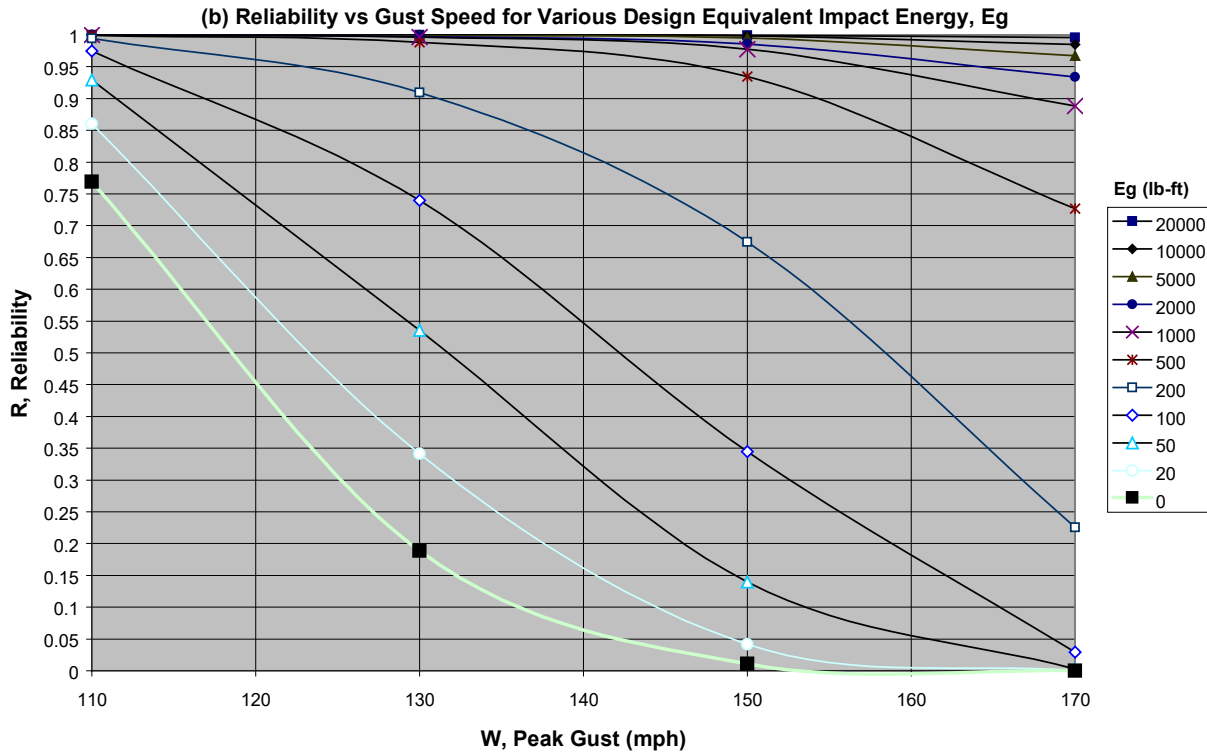


Figure 5-41 Example Energy Reliability Curves Derived for a Subdivision Comprised of Single-Story Homes with Asphalt Shingle Roofs

5.2.1.2 Implementation of the Windborne Debris Model

In the development of the damage and loss functions described herein, it is not possible to explicitly model the windborne debris on a storm-by-storm basis using the detailed first principles-based trajectory and impact model described above because of the computer run-time limitations. The simplified windborne debris model uses the results of the explicit study using an analytical model that yields results similar to those obtained from the explicit model.

Using the simplified debris modeling approach, at each time step in a hurricane simulation, the number of missiles impacting the wall is given as:

Equation 5-5

$$N_w = a\theta P_1(v)N_2(v)$$

Where:

- a is a constant
- θ is a constant representing the number, density and size of the missile source buildings in a 45° sector
- $P_1(v)$ is the fraction of missiles that hit the wall for the wind speed v

$N_2(v)$ represents the number of missiles generated at each time step

Using a value of θ equal to one for the eight 45° sectors represents a missile environment similar to that used in the explicit study. Increasing or decreasing θ has the effect of changing the density of the surrounding homes.

The function $P_1(v)$ is obtained directly from the explicit missile simulation. In contrast, the function $N_2(v)$ is obtained by performing roof damage simulations using the same damage model used in the missile study, but for a larger number of wind speeds. The fraction of missiles generated that impact another building is a linear function of wind speed, whereas the number of missiles generated at each time step increases more rapidly.

Given that the building is impacted by a missile at a given time step, the impact energy is determined by sampling from Weibull distribution in the form:

Equation 5-6

$$P_e(e < E) = 1 - \exp(-(E/C)^k)$$

The Weibull parameters C and k were determined by fitting the energy exceedance data derived from the physically-based debris model. Both of the Weibull parameters are functions of the peak gust wind speed.

Note that the building can only be impacted by missiles generated from within a 90° sector, centered on a vector normal to the wall surface, and the wind must be approaching from within this sector. These criteria ensure that walls can be impacted by missiles only when the wind is blowing towards the wall, and only when there are missile sources upwind of the structure.

Figure 5-42 shows a comparison of the reliability curves generated from the physically based model to those derived using the simplified model. In this figure, the points shown without lines connecting the data points represent those derived from the simplified model, whereas those shown with lines connecting the data points represent the original data as produced by the explicit missile simulation.

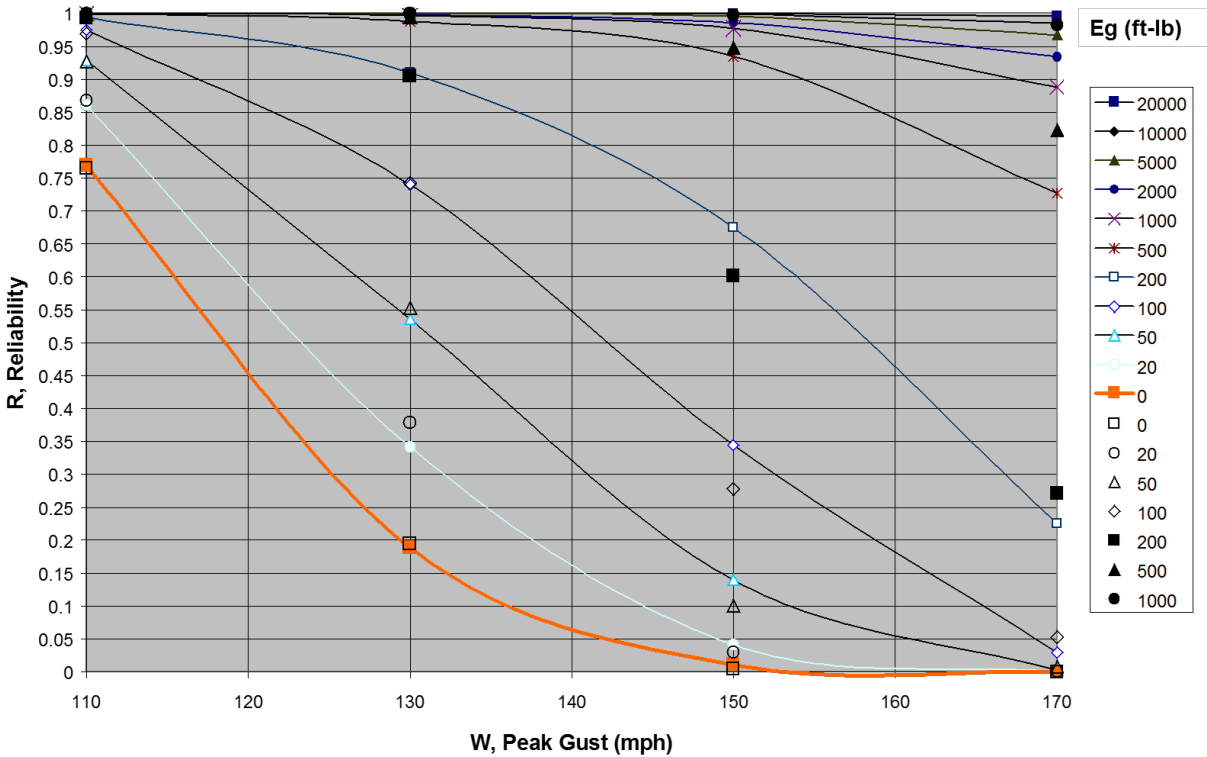


Figure 5-42 Comparison of Reliability Curves Derived from the Explicit Missile (lines) Simulation to Those Obtained from the Simplified Model (points only)

The comparisons of the two sets of reliability curves show reasonable agreement, for all impact energy levels for wind speeds less than 130 mph. In the 150-mph case, the simplified model tends to slightly underestimate the reliability (i.e., overestimate the probability of missile impact). At a wind speed of 170 mph, the reverse is true. In general, for missile impact energies less than 500 foot-pounds, the simplified model satisfactorily reproduces the results obtained from the explicit model. For very high impact energies (~1,000 foot-pounds), the simplified model underestimates the frequency of impact, as indicated by the overestimate in the computed reliability levels. This underestimation of the frequency of very high energy impacts is not of great concern since damage to window protection (discussed later) occurs at energies much lower than 1,000 foot-pounds.

In summary, a simplified, fast running missile impact model is used, which approximates the results derived with an explicit modeling approach. The simplified model, which yields reasonable estimates of the windborne debris risk, is used in the building damage model to develop the fast-running Hazus damage and loss functions.

5.2.2 Windborne Debris – Commercial Missile Model

The Hazus Methodology of the connection risk of damage to commercial buildings by windborne gravel debris consists of two components. The first component is a mathematical simulation of the debris generation, transport, and impact on building envelopes during a hurricane passage. This windborne gravel debris model simulates the characteristic layout of the gravel layers, the turbulent hurricane wind trace, local wind fields on the roof, wind action on gravel stones, gravel scour and transport, and the eventual interception of its trajectory with a building’s envelope (or with the ground). Throughout a

hurricane, the simulation provides detailed records of individual gravel missiles generated, their origin location, transport distance, impact location, and impact momentum, as well as the characteristic layout of the gravel remaining on the roof. The development of this model, along with its validation against three field-observed cases, is described in detail in Section 5.2.2.1. It is demonstrated that the model agrees with field observations reasonably well.

The second component of the Methodology aims at constructing a fast-running risk model to estimate the probability of damage to building envelope by windborne gravel debris given the impact resistance capacity of the target surfaces. The fast-running debris risk model estimates the expected number and location of fenestration elements breached by debris within each short time interval in order to interactively account for the rainwater penetration and internal pressure change in a building. The model utilizes the previous analytical formulation on debris risk (Twisdale et al., 2000a, 2000b) and the above physical modeling on generic configurations to provide inputs (for example, the expected number of impacts and impact momentum) required by the analytical risk formulation. The number of impacts per unit area within a time interval and the impact momentum distribution for a target surface element, such as a window, with specified location and orientation relative to the source are derived from the simulation record. The derived number of impacts and momentum distribution are functions of the reference wind speed, wind direction, terrain, height and area of gravel source roof, depth of the gravel ballast layer, and gravel size. Based on this information, a set of simplified expressions describing the relationships between the variables yields a fast-running debris module that is incorporated into the damage model. This second part of the model is described in Section 5.2.2.2.

5.2.2.1 Windborne Gravel Debris Simulation and Case Studies

Flat, built-up roofs and ballasted membrane roofs are commonly seen on high-rise and low-rise commercial buildings in urban and suburban areas. Gravel used on these roofs often becomes windborne missiles during high winds. This problem has been observed and reported by many field investigators (e.g., Minor et al., 1978; Minor, 1994; Minor and Behr, 1993a, 1993b; and Behr and Minor, 1994). This section describes the computer modeling of gravel missile generation (scour and blow-off), transport trajectory, and physical impact on surfaces. Three case studies are presented along with comparisons against field observations.

5.2.2.1.1 Scope of the Simulation

The problem of debris generation, transport, and impact involves many variables. The model includes the effects of the mean hurricane wind trace (speed and direction variation with time), correlated three-dimensional turbulence components, building geometry and street layout, roof gravel configuration (diameter distribution and thickness), as well as upstream terrain influences. Local wind velocity fields over the roof and in the wake behind the buildings are also approximated. The gravel scour pattern, trajectories, and impact statistics are used to compute the information required for model calibration and for risk prediction.

5.2.2.1.2 Missile Generation from Roof Gravel

Within an assembly of gravel stones of nearly spherical shape and variable diameters loosely lying on a flat bed, an individual stone on the top layer will be subject to a drag, an uplift, and an overturning moment caused by the wind blowing over the surface. Gravity and the constraint of other stones balance these wind forces; however, when the wind speed increases and exceeds some threshold

value, the wind forces overcome these constraints. At this point, the stone starts to intermittently rotate and shift horizontally. At another slightly higher threshold wind speed, the stone will be lifted and blown away. Both the first and second threshold wind speeds have been shown to be proportional to the square root of the stone diameter (Kind and Wardlaw, 1984). The model developed here considers the second threshold wind speed, since only at this higher wind speed is the stone released into the wind field.

In determining the local wind speeds on the roof surface, the flow separation and vortex induced velocity field is included in the model as a function of building geometry and the free stream wind speed and direction. An example of the horizontal component of the mean wind velocity on the roof surface of a cube-shaped building is shown in Figure 5-43 for an oblique on-coming wind. Figure 5-43 also shows a photograph of streamlines obtained from a flow visualization test given for comparison. The streamline patterns are in good agreement.

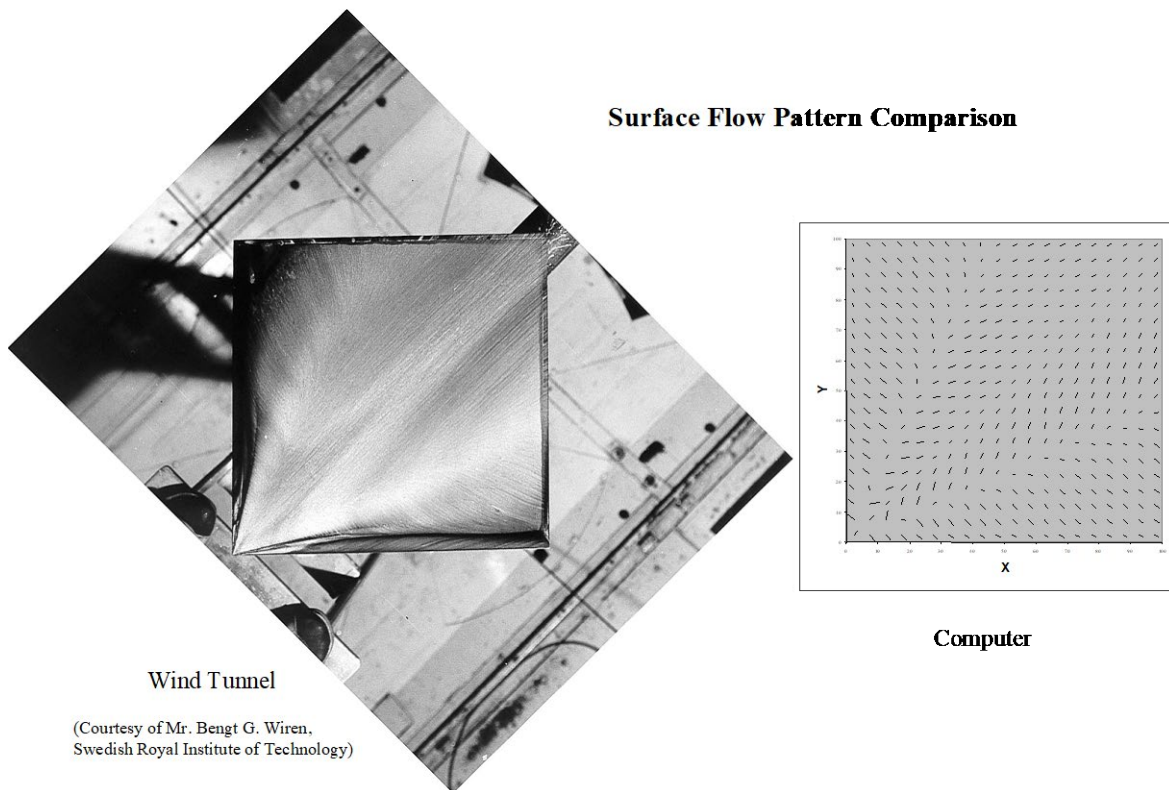


Figure 5-43 Example of Computer-Modeled Surface Flow Pattern Compared with Wind Tunnel Observation

The resulting scour pattern is illustrated in Figure 5-44 and compared with qualitative wind tunnel and field observations (Kind and Wardlaw, 1984). It is seen that the computer model reproduces the typical two-lobed scour pattern under oblique winds. Note that the wind tunnel model of Kind and Wardlaw has a low parapet so that the scour pattern shifts slightly downstream. Moreover, their model represents a low-rise building such that the high turbulence in the lower part of the simulated boundary layer flow reduces the sharpness of the two-lobed pattern compared to the field observation and the computer model results which are both for multi-story buildings (low turbulence intensity).

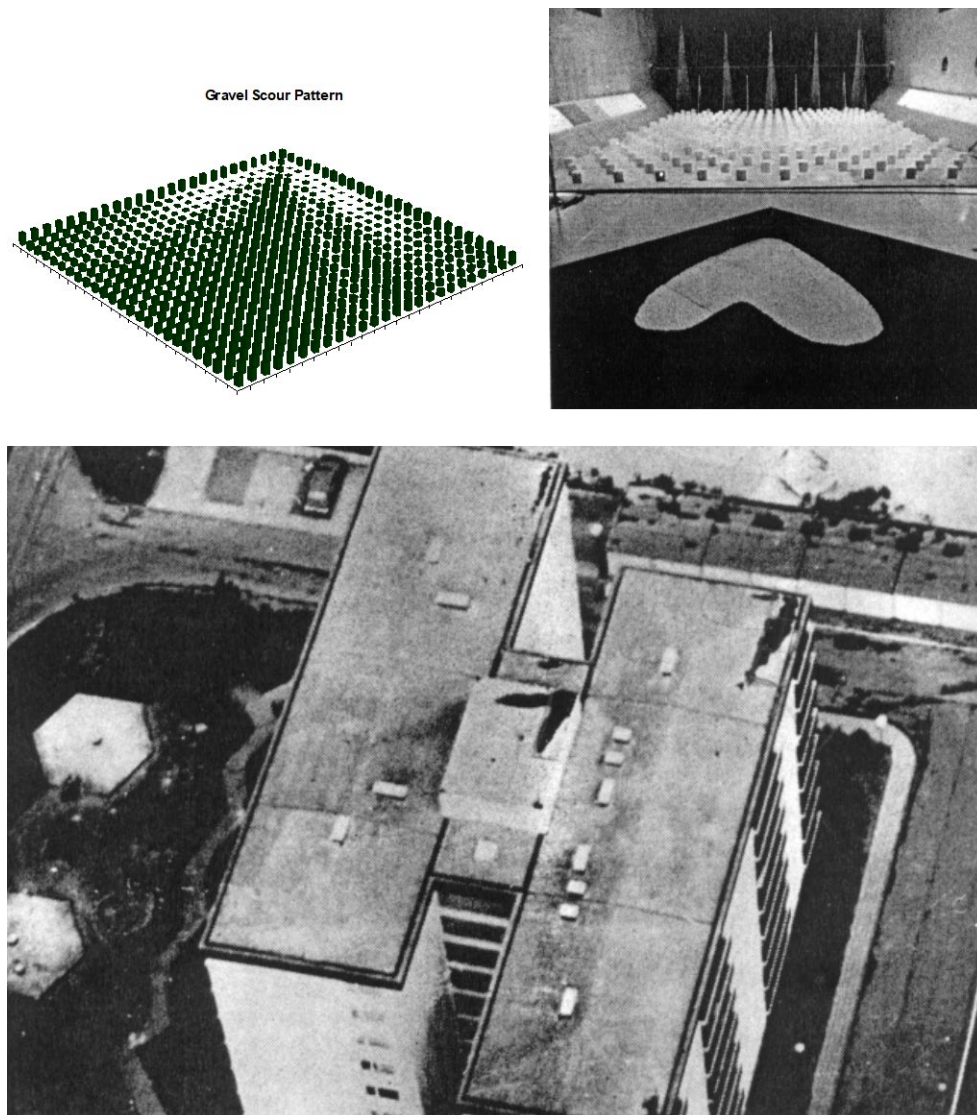


Figure 5-44 Example of Gravel Scour Pattern Compared with Field and Experimental Observations

5.2.2.1.3 *Missile Transport in the Wind Field*

When gravel is released into the three-dimensional wind field, it is transported by the turbulent wind. This is modeled by numerically solving the equation of motion for a particle of mass, with the wind force acting on the gravel updated as a function of location and time. The influence of the vortex flow over the rooftop and the wake flow downstream of the buildings are incorporated with the on-coming turbulent wind to obtain a resultant wind field.

As an example, the computed trajectory for a sample gravel missile generated from the roof of a cube-shaped building is illustrated in Figure 5-45 for a 45° oblique wind. The gravel missile is first moved sideways toward one of the upstream roof edges by the spiral vortex flow near the roof surface. Kind and Wardlaw's (1984) wind tunnel experiments on gravel scour and blow-off also indicate that gravel missiles generated from the front portion of the roof would leave the roof over the upstream edges. After it leaves the roof, the trajectory starts to gradually bend into the on-coming wind. The gravel

missiles generated from the downstream portion of the roof would have less curved trajectories since the spiral vortex flow will be weakened downstream.

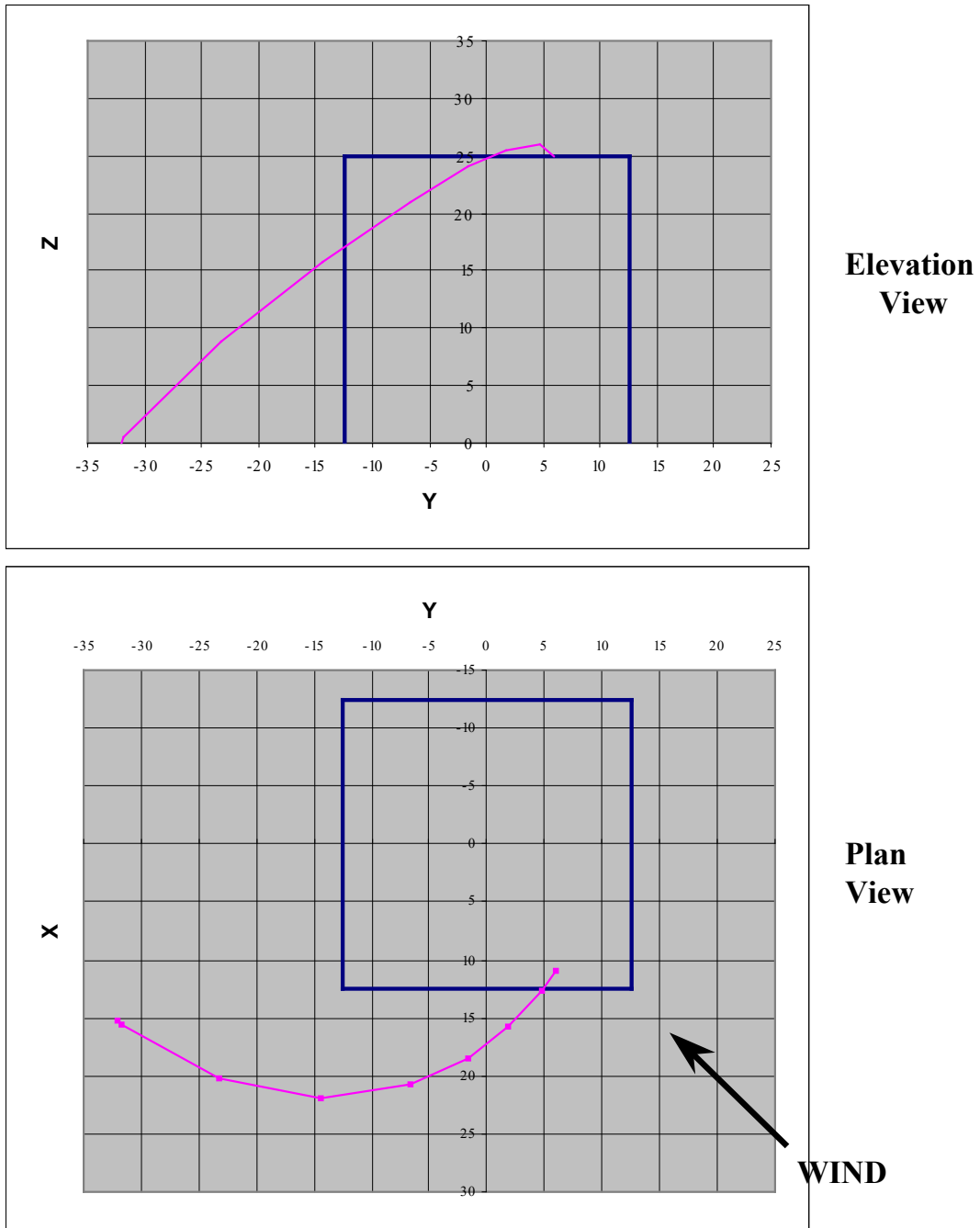


Figure 5-45 Example of Gravel Missile Trajectory

5.2.2.1.4 Missile Impact on Building Envelopes

The trajectory of the gravel missile will eventually intersect with a surface, either the ground or a building envelope, which are geometrically defined on a global coordinate frame. The impact location and velocity are recorded. The impact momentum and energy are then calculated for each gravel missile of a given mass. This information can be used to derive statistical distributions of the impact

location, momentum or energy, and the number of impacts on a specific area of the building envelope, which are subsequently used to predict the risk of building envelope breach during a storm. The recorded impact results for specific building complexes can also be used to perform model calibration and validation studies by comparing them with the field observed data for the same buildings and environments.

5.2.2.1.4.1 Case Study 1 – Kendall, Florida, Hurricane Andrew

During Hurricane Andrew, the downstream buildings in a high-rise complex in Kendall, Florida (Figure 5-46), suffered severe windborne debris impact damage to the windows, which has been investigated and documented by several researchers (e.g., Smith, 1999; Behr and Minor, 1994; and Minor, 1994). This case provides a basis for examining the results obtained with the windborne debris model.



Figure 5-46 The Marriott-Datran Complex in Kendall, Florida

The plan of the complex is shown in Figure 5-47. The missile source is the Marriott Hotel roof gravel ballast. The gravel missiles were generated from the two penthouse roofs only, since the other parts of the roof have tall parapets that prevented gravel from leaving the roof. For the case study, a Hurricane Andrew mean wind trace was recreated for the site using the hurricane model described in Section 4.1. The mean wind direction changed from northerly to southeasterly in a time period of about 2.5 hours, during which open terrain 10 meter-height peak gust winds are above 90 mph. The largest peak gusts reached 140 mph when the mean wind direction was approximately normal to the northeast walls of the buildings. Typical 3-dimensional turbulence components for a terrain roughness length of 0.5 meters (slightly rougher than standard suburban) were simulated. The mean diameter of the roof gravel was determined to be 12 millimeters from survey records reported in Behr and Minor (1994) and Smith (1999) with a distribution given in ASTM Standards, Designation D1863-93 (Reapproved 1996) for Size # 67A. The depth of the gravel ballast layer on the roof was 76 millimeters (Behr and Minor, 1994). The window glass on the downstream buildings is 6 millimeters thick, fully tempered monolithic glass (Behr

and Minor, 1994) that provides an estimated threshold average breakage momentum of 0.1 kilogram-meter per second (Minor, 1994).

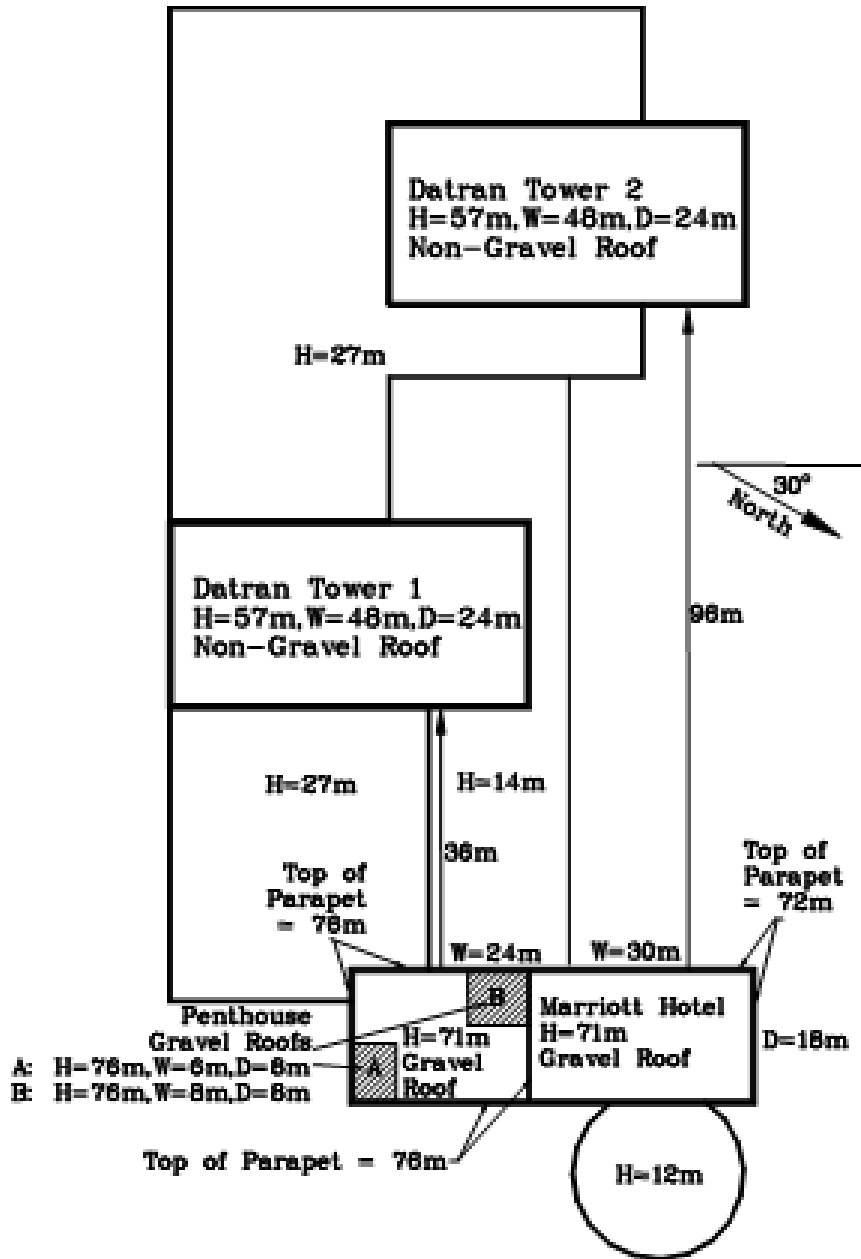


Figure 5-47 Approximate Plan of the Marriott-Datran Complex

The impact results obtained with the computer model are shown in Figure 5-48 for the northeast walls of the two downstream buildings, where each dot represents a damaging hit. A damaging hit is an impact by a gravel missile with its momentum's component normal to the wall being larger than the 0.1 kilogram-meters per second threshold. The coordinate grid approximately corresponds to the window grid, one cell containing one window. One or more damaging hits within a cell yield one count of

damaged window. Note that, for the case where windows occupy only a percentage of the wall area such as these buildings, only the corresponding percentage of generated gravel missiles that are randomly sampled is used for damage counts. The results shown in Figure 5-48 are these sampled hits. The photographs (Minor, 1994; Smith, 1999) documenting the window breaches are shown in Figure 5-49. For the northeast wall of Datran Tower I, the simulation yields a window failure rate of 96.7% for the upper 10 floors, in good agreement with the observed value of 97.4% as counted from Figure 5-49 (a) for the same part of the wall.

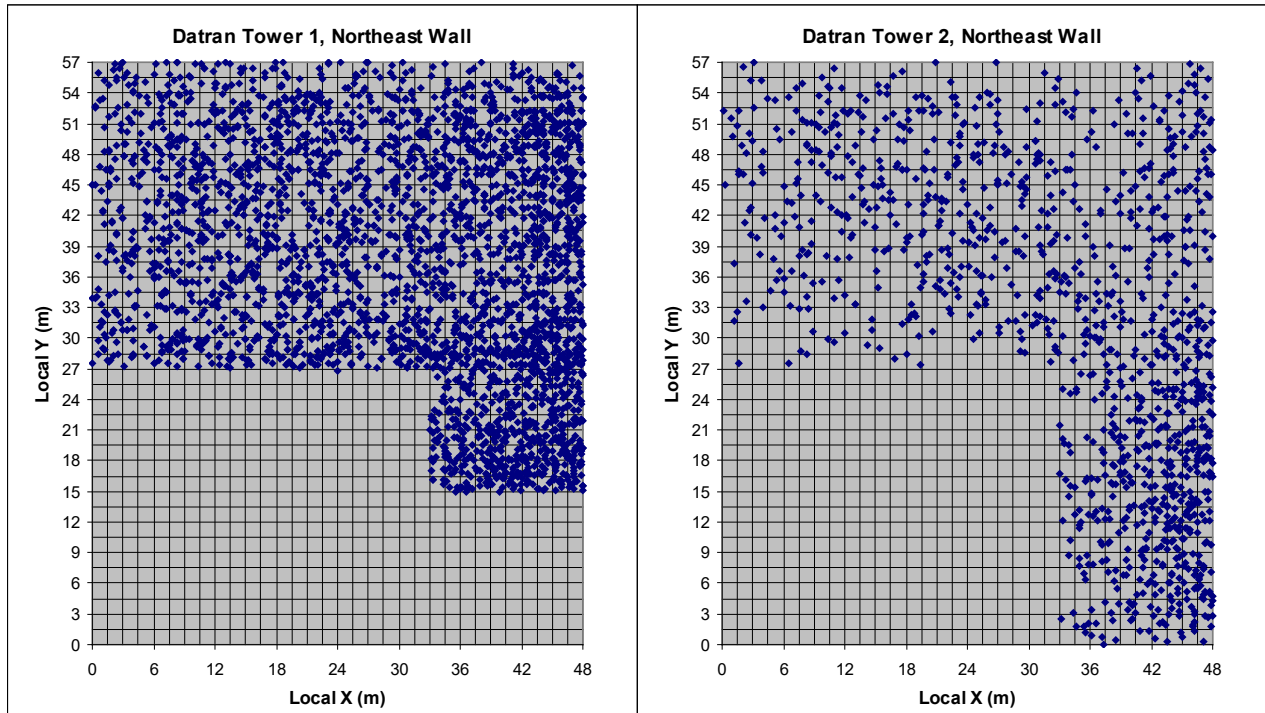


Figure 5-48 Impacts on Walls with Momentum Exceeding the Threshold for Damage



Datran Tower I, Plywood Boarding of Broken Windows Underway (Picture from Minor, 1994). Arrows indicate windows that were not damaged



Datran Towers I and II, Plywood Boarding of Broken Windows Complete Except for Lower Floors (Courtesy of TlSmith Consulting).

Figure 5-49 Damage Scenarios for Datran Towers I and II Downstream of the Marriott Hotel

Other photos were used to aid the counting for the upper left corner of the wall and to confirm the counts on other parts, while the lower few floors were omitted from the counting because the damage

state cannot be determined for this small area using any of the available photos or reports. For the northeast wall of Datran Tower II, the simulation shows a failure rate of 61.9% for the upper 10 stories. This is also consistent with the observed damage-state of 63.2% for the same part as determined from Figure 5-49 (b). Again, window breakage on the lower right corner of Datran Tower II cannot be clearly identified from the photos presented here, nor with other available photos and reports.

It is seen that the agreement between the modeled and observed damage states are remarkably good for this case.

5.2.2.1.4.2 Case Study 2 – Downtown Houston, Texas, Hurricane Alicia

For this case, only partial information is available on the details of the missile sources, target glazing properties, and damage states. Assumptions on some of the required information were thus made to facilitate the simulation. A qualitative comparison of simulated and observed glass damage is presented.

Figure 5-50, Figure 5-51, and Figure 5-52 show the area in downtown Houston for which the simulations were carried out and compared with available observations. The seven buildings bounded by McKinney and Polk Streets in the NE to SW direction and by Milam and Smith Streets in the SE to NW direction were simulated for missile source and/or impact damage. The plan geometry of these buildings was modeled as shown in Figure 5-53. The available information and the assumed values of required inputs are listed in Table 5-10.

The time-varying hurricane wind speed and direction trace at the site was re-created using the hurricane model described in Section 4.1. The site was modeled as an urban terrain with a roughness length of about 1 meter for all upstream directions. The strong winds were from a quadrant centered on the east. The peak gust wind speed was estimated to be about 56 meters per second (125 mph) at the roof height (110 meters) of the gravel missile source buildings.

The results of the simulation are presented in Table 5-11, in comparison with the available observations. The overall agreement between the simulated results and the observations is reasonable.



Figure 5-50 General View of the Houston Central Business District (Kareem and Stevens, 1985)

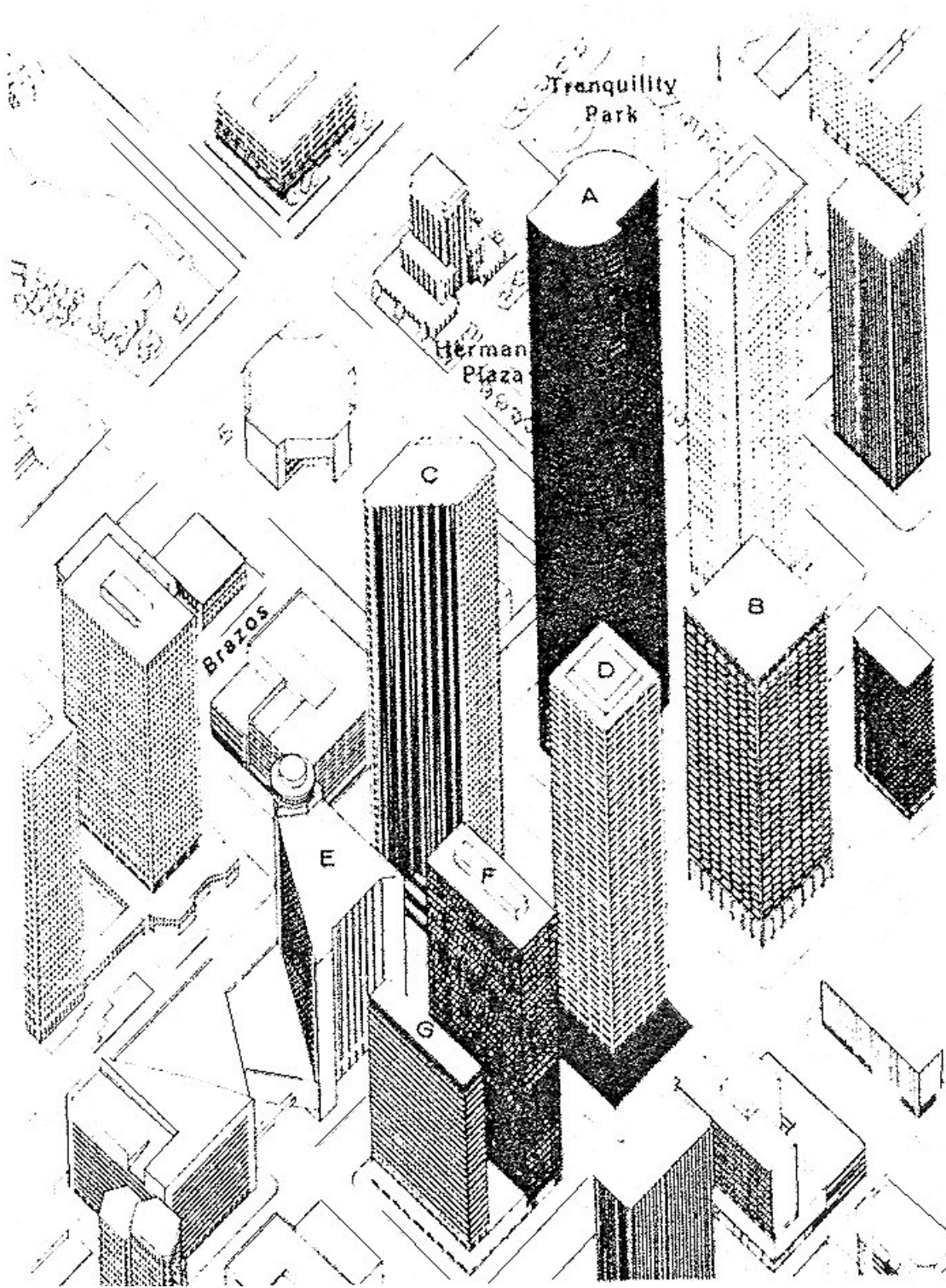


Figure 5-51 Aerial Perspective of Damaged High-Rise Buildings (Beason et al., 1984)

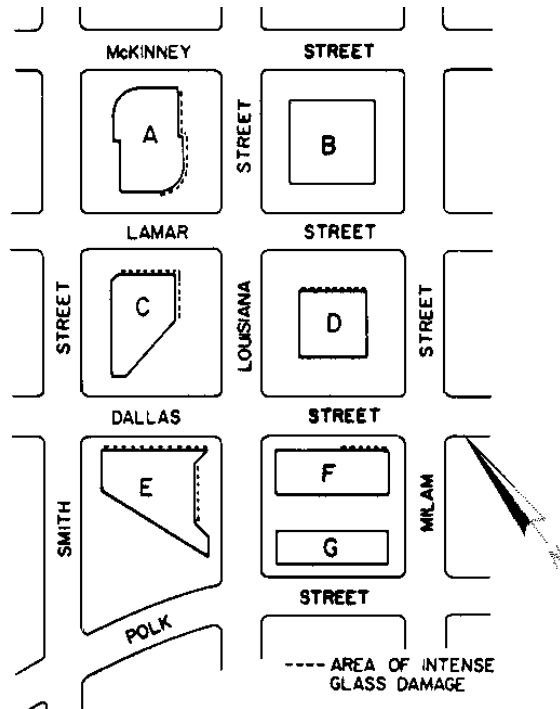


Figure 5-52 Plan View of Damaged High-Rise Building Towers (Beason et al., 1984)

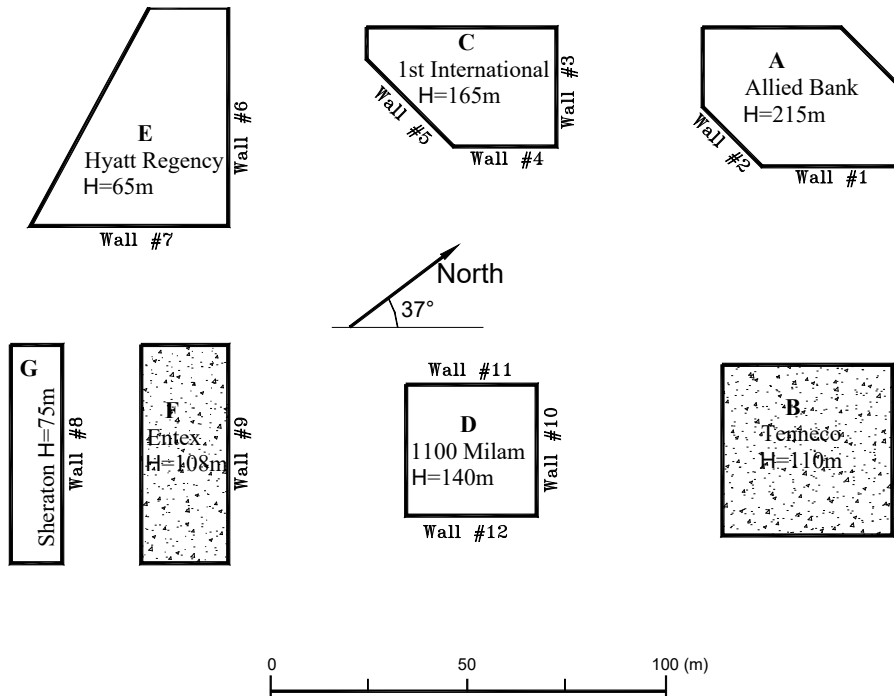


Figure 5-53 Plan Geometry of the Modeled Buildings in the Houston Downtown Central Business District

Table 5-10 Basic Inputs of Missile Sources (Roof Gravel) and Target Glazing Properties

Building	Roof Gravel		Glazing					Building Height (m)
	Mean Depth (cm)	Mean Diameter (cm)	Glaze/Wall (%)	Avg. Size (m x m)	Thickness Panes (cm x#)	Glass Treatment	Impact Resistance (kg-m/s)	
Allied Bank Plaza			100	1x1	0.6 x 2	T(2)	0.08	215
Tenneco Building	2*	1*						110
First International Plaza			40	2x1.5	0.6x2*	A	0.05	165
1100 Milam			60	1.8x1	0.6x2*	A*	0.05*	140
Hyatt Regency Hotel			45	2x2	0.6x2*	A*	0.05*	65
Entex Building	1*	1*	100	1.5x1	0.6x2*	A*	0.05*	108
Sheraton Houston Hotel			40	1.2x1	0.6x2*	A*	0.05*	75

(1) Shaded cells with an asterisk (*) indicate assumed values.

(2) T - Tempered, A - Annealed and H - Heat Strengthened.

Table 5-11 Number of Damaged Windows: Simulation versus Available Observations

Building	Wall No.	Wall Height (m)	Wall Width (m)	Resistance (kg-m/s)	Total No. Window Panes	Simulated No. Panes Damaged	Simulated % Damaged	Total No. Simulated Damaged Panes per Building	Observed No. Panes Damaged
Allied Bank Plaza	1	215	35	0.08	7,500	539	7.2		400~1,000
	2	215	21	0.08	4,500	258	5.7	707	(Kareem)
First Intern. Plaza	3	165	30	0.05	1,300	143	11.0		650
	4	165	25	0.05	1,100	200	18.2		(Kareem)
	5	165	32	0.05	1,400	0	0.0	491	
Hyatt-Regency	6	65	55	0.05	1,200	36	3.0		No Data
	7	65	50	0.05	1,100	29	2.6	65	
Sheraton Houston Hotel	8	75	55	0.05	1,400	34	2.4	34	No Data
Entex Building	9	108	55	0.05	4,000	98	2.5	98	143 (Minor)
1100 Milam Street Building	10	140	33	0.05	1,550	223	14.4	247	256 (Beason, Minor, Kareem)

Building	Wall No.	Wall Height (m)	Wall Width (m)	Resistance (kg-m/s)	Total No. Window Panes	Simulated No. Panes Damaged	Simulated % Damaged	Total No. Simulated Damaged Panes per Building	Observed No. Panes Damaged
	11	140	33	0.05	1,550	0	0.0		No Data
	12	140	33	0.05	1,550	24	1.5		32 (Beason, Minor, Kareem)

5.2.2.1.4.3 Case Study 3 – Williston School, Wilmington, NC, Hurricane Bonnie

The Williston School two-building complex represents a case of low-rise buildings. Information on the details of the missile sources, target glazing properties and damage states, was collected shortly after Hurricane Bonnie’s landfall at the North Carolina coast.

Figure 5-54 shows the complex (looking north). The taller portion of the building on the right (east) was the major source of gravel missiles that hit the windward face of the two-story building on the left (west). The three-story building located at the north end of the complex (the far end in the picture) was not a missile source, nor could it act as a shielding building, so it was not included in the simulation. Flow interference from this building was expected to be small and was neglected in the simulation. Figure 5-55 shows the windward face of the main missile source building in the complex (looking southwest), which was the upstream building during the high wind period of Hurricane Bonnie when it was hovered over the Wilmington area. Figure 5-56 indicates the sizes of the roof gravel on this building. The same type of roof gravel was also used on other buildings of the complex; however, the majority of the glass damage is believed to have been caused by gravel originating from the roof of the upstream building, as indicated by both the field observations and the simulation. Figure 5-57 shows the glass damage on the downstream building, in which part of the roof of the upstream building is also seen. The geometry of the modeled complex is shown in Figure 5-58. The input data for the simulation are listed in Table 5-12.



Figure 5-54 A General View of the School Complex



Figure 5-55 The Windward Face of the Main Missile Source Building (facing southwest)



Figure 5-56 Roof Gravel on the Upstream Building



A) Looking Southwest



B) Looking Northwest

Figure 5-57 Glass Damage on the Windward Face of the Downstream Building

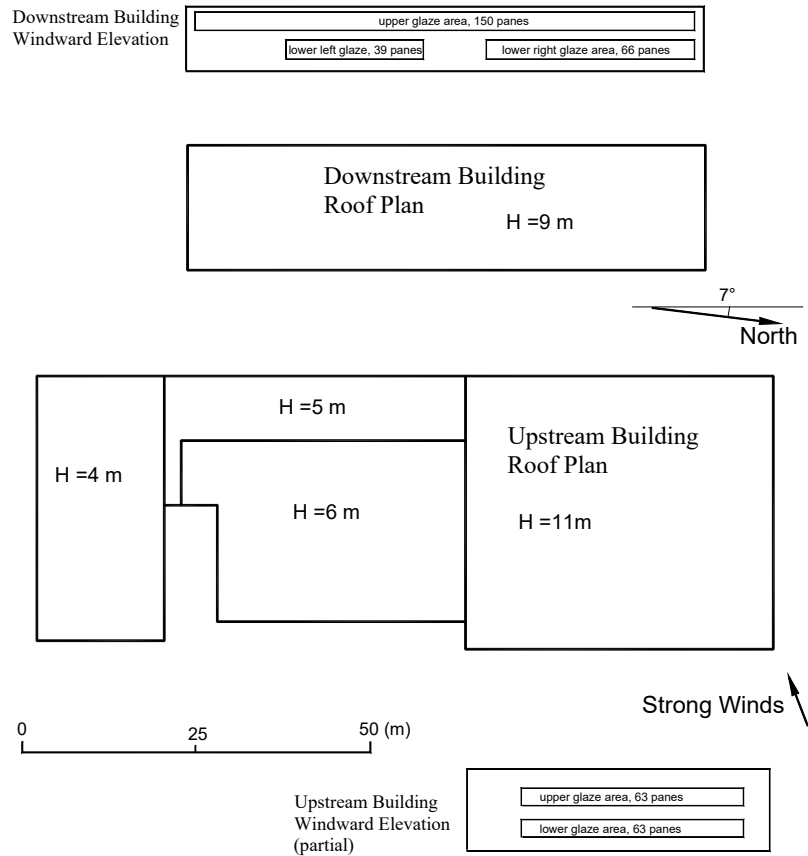


Figure 5-58 Geometry of the Modeled Complex

Table 5-12 Basic Inputs of Missile Sources (Roof Gravel) and Target Glazing Properties

Building	Roof Gravel		Glazing					Building Height (m)
	Mean Depth (cm)	Mean Diameter (cm)	Glaze/Wall (%)	Avg. Size (m×m)	Thickness × Panes (cm×#)	Glass Treatment	Impact Resistance (kg-m/s)	
Upstream Bldg	3	1.2	18	1.2×0.6	0.3×2	T*	0.03	11
Downstream Bldg	3	1.2	45	1.2×0.8	0.3×2	T	0.03	9

1) T – Tempered.

The time-varying hurricane wind trace at the site was re-created and used as the input wind speed and direction data for the missile simulation. The site was modeled as open terrain with a roughness length of 0.03 meters for the strong wind directions, which was within the NE quadrant. The maximum peak gust speed was estimated to be about 40 meters per second (90 mph) at roof height (11 meters).

The results of the simulation are presented in Table 5-13 and compared with the observations. The overall agreement between the simulated results and the observations is reasonable. One exception is

that the number of damaged window glass panes is significantly overestimated for the lower-right glazed area on the front wall of the downstream building. This may be attributed to the shielding effects provided by a row of trees in front of this glazed area, as shown in Figure 5-59, which was not modeled in the simulation.

Table 5-13 Number of Damaged Windows: Simulation versus Available Observations

Building	Glaze Area No. on Front Wall	Resistance (kg-m/s)	Total Number of Window Panes	Modeled			Observed		
				Number of Damaged Panes	Percent Damaged Panes	Number of Damaged Panes per Building	Number of Damaged Panes	Percent Damaged Panes	Number of Damaged Panes per Building
Down-Stream Building	Upper	0.03	150	94	63.0		89	60.0	
	Lower left	0.03	39	8	20.5	151	13	33.3	122
	Lower right	0.03	66	49	74.2		20	30.0	
Upstream Building	Upper	0.03	63	0	0.0		0	0.0	
	Lower	0.03	63	0	0.0	0	0	0.0	0



A) The Trees in Front of the Lower-Right Glazed Area



B) Significantly Less Windows Damaged on the Lower-Right Glazed Area than on the Upper Glazed Area

Figure 5-59 Trees in Front of the Lower-Right Glazed Area of the Downstream Building

A first principles-based model of windborne gravel debris generation and trajectory has been developed for commercial buildings in urban or suburban areas. Some qualitative comparisons with experimental and field observed data have been made for rooftop wind fields and roof gravel scour patterns. The three case studies carried out show, in general, good agreement with the field observed data for window glass breaches.

5.2.2.2 Probability of Damage to Building Envelopes by Windborne Gravel Debris

This section describes the development of a fast-running model for estimating damage to building envelopes caused by windborne gravel debris in Hazus. As a first step, the model was developed for low-rise buildings in suburban commercial areas. The model utilizes the analytical formulation for debris impact damage risk developed previously and the physical modeling methodology described above to obtain the information required by the analytical formulation (i.e., expected number of impacts and impact momentum distribution). The general scheme and the results are presented below.

5.2.2.2.1 Analytical Formulation for Probability of Impact Damage

Several analytical formulations have been derived to estimate the probability of impact damage as a function of the number of impacts and the impact momentum distribution (Twisdale et. al, 2000a and 2000b). It was found that the following simple model, which assumes mutually independent (i.e., noncontingent) impacts and uses a Poisson distribution for the number of impacts, provides a sufficiently good approximation to the results generated by the detailed model presented in Section 5.2.2.1. This simple model is adopted as the basic formulation for the impact damage risk and is modified to express the probability of impact damage during a hurricane for a given area of the target, A, and in a given time interval, T, as follows:

Equation 5-7

$$P_D = 1 - e^{-A \cdot T \cdot N \cdot (1 - P_M)}$$

Where:

- | | |
|----------------|--|
| N | is the expected number of impacts on the surface per unit area and per unit time interval |
| P _M | is the probability of an impact having its momentum (m) less than the impact momentum resistance capacity of the surface (m _d) |

Many variables influence the expected number of impacts and the momentum distribution, and thus the damage probability. These variables and their effects are discussed below.

5.2.2.2.2 Physical Modeling to Obtain the Number of Impacts and Momentum Distribution

As mentioned above, the number of impacts and the momentum distribution are functions of many variables. The functional relationships are implicit and physical modeling is required to provide “data” for quantifying these relationships. Table 5-14 lists the set of variables that the present model considers. Also shown in the table are the values that were used as inputs for the physical modeling to develop the fast-running module for estimating the risk of windborne debris damage in suburban commercial areas.

Within the overall damage model, into which the fast-running debris model is incorporated, the values of some of the variables, such as the peak gust speeds and the location, orientation, and size of the target fenestration elements, are explicitly known for each time increment. However, some variables, such as the detailed configuration of the gravel sources are not specifically known and can only be accounted for generically or statistically. Alternatively, within the detailed physical modeling, millions of gravel stones are modeled, and some critical records are stored for off-line analysis. Each simulation case will normally take several hours to a couple of days to complete. Hence, the number of values for each variable needs to be limited to avoid creating an unrealistically large case matrix.

Table 5-14 Variables that Influence the Number of Impacts and Momentum Distribution

Variable	Wind Parameters				Source Parameters (Roof Gravel)				Target Parameters (Wall Fenestration)					Shielding Effects
	Peak Gust	Mean Direction Relative to Source Building	Time Length for Sustained Mean Wind	Terrain	Source Roof Height	Source Roof Area	Gravel Mean Dia.	Depth of Gravel	Distance to Source	Lateral Location	Elevation above Ground	Orientation	Area (Size)	
Notation	V	τ	T	z0	Hs	S	Dg	Dp	d	l	h	β	A	
Units	m/s (mph)	deg	hr	m	m (ft)	m×m (ft×ft)	cm	cm	m	m	m	deg	m×m	Accounted for with Source Reduction Factor in General Model
Values Used for Simulation	40 (90)	0 to 45 in increments of 5	0.25	0.3	6 (20)	15×15 (50×50)	1.1	4	Detailed in Figure 5-60			Equation 5-7		
	60 (134)	0 to 45 in increments of 5	0.25	0.3	18 (60)	60×60 (197×197)	1.1	4	Detailed in Figure 5-60			Equation 5-7		
	75 (168)	0 to 45 in increments of 5	0.25	0.3	18 (60)	60×60 (197×197)	1.1	4	Detailed in Figure 5-60			Equation 5-7		

For each case, the detailed physical model was run for 15 minutes using a mean wind speed that would produce the specified open 10 meters peak gust speed when the turbulence trace is superimposed. This process was repeated for each mean wind direction relative to the upstream edge of the source building. The mean wind directions from 0 to 45° are considered the representative wind angles for a nearly square roof, due to symmetry. A roughness length for suburban terrain was modeled, which is typical for areas where low-rise commercial buildings are normally located. Two source roof heights and two source roof areas were modeled, which yield four roof height-area combinations. The modeled heights and roof areas were chosen to represent lower- and upper-end values for low-rise commercial buildings. Only one value of the mean gravel diameter was used; however, the model automatically assumes a dual-linear diameter distribution bounded by zero and twice the mean diameter. The assumed depth of gravel on the roof is 4 centimeters. This parameter mainly affects the supply of missiles within local regions on the roof, which were modeled as 1 meter by 1-meter cells.

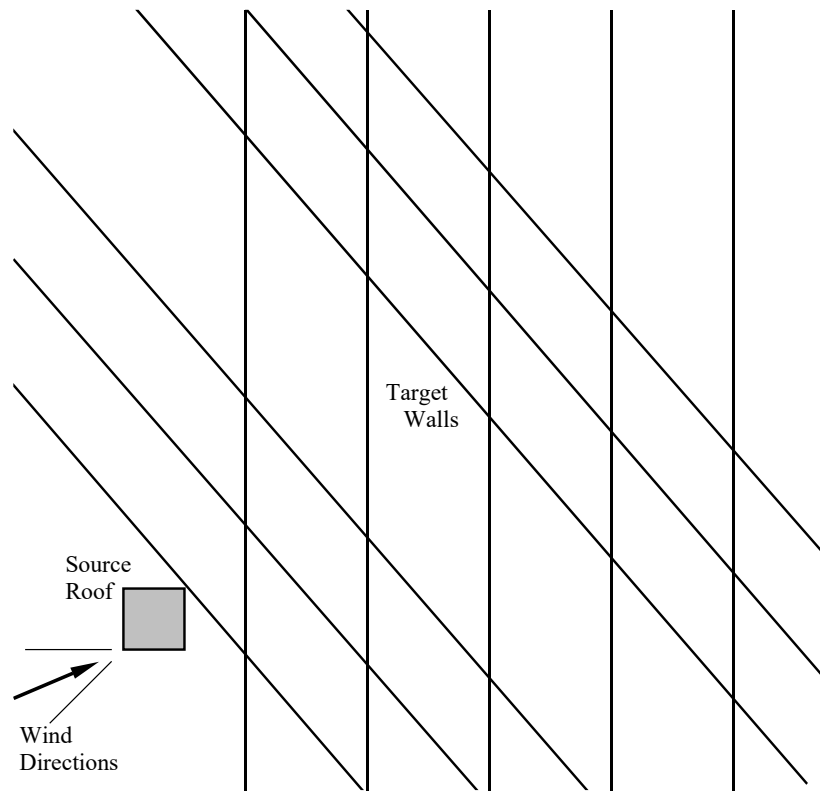


Figure 5-60 The Layout of Modeled Gravel Source Roof and Target Walls Relative to the Wind Directions Modeled

To model the targets, 12 vertical, semi-infinite planes were placed downstream of the source building, as illustrated in Figure 5-60. Five of the surfaces are spaced 30 meters apart to the right of the source building. The other seven surfaces are spaced 21 meters apart, at 45° to the source building. The normal vectors of these planes are all within $\pm 45^\circ$ to any of the wind directions modeled. Outside this relative wind quadrant, the general model assumes no risk of debris damage. This simplification approximates the actual case since both the number of impacts and the impact momentum (the normal component of the debris' terminal momentum) decrease with increasing wind angle relative to the surface normal on both sides, forming a bell shape. The number of impacts and the impact momentum, along with the lateral impact location and its height above ground, were recorded for each modeled surface for off-line analysis.

5.2.2.2.3 Analysis of Modeled Results

To be suitable for use by the damage model, the modeled results have been simplified into functional relationships as described below.

Within the damage model, the values of some variables may not be specifically known. Some others may only be generically specified. For example, the exact number of buildings having gravel roofs, their detailed layout, respective heights and plan areas, will not be specifically known, but may be reflected by reference to the geographical region, built environment or terrain type. For some of these variables, such as source building height, plan area and orientation, their effects are accounted for by averaging the results over all cases modeled. A source reduction factor is also already in place in the damage

model to roughly account for the percentage of buildings having gravel roofs. Its value is empirically defined to vary between one and zero, where the value of one is typical for areas having many gravel roofs and the value of zero is for areas having no gravel roof (e.g., open water upstream of the target building). For the areas having some gravel roofs and some non-gravel roofs, the non-gravel roofed buildings will not produce gravel missiles but are present as shielding for other buildings. In this case, the source reduction factor will be some value between zero and one, approximately equal to the percentage of gravel roofs in the area.

The stream-wise and lateral layout of the upstream source buildings is assumed to be homogeneous in the general model. Thus, the typical building spacing for the area becomes representative of the expected distance from the target building to the first building or the first row of buildings directly upstream, and the lateral distribution of impact locations on the target wall is treated as homogeneous. To obtain the number of impacts per unit area on the target surface as a function of wind speed, typical building spacing and the vertical location above ground, etc., the results were averaged laterally across the target wall over a defined width, which is the typical building spacing in this case. Results for different target wall orientations relative to the wind direction were also averaged within the $\pm 45^\circ$ quadrant in consistence with the treatment by the general model as described in the previous section.

As a result of the simplifications, the expected number of impacts per unit area and the impact momentum become a function of the open-10 meters peak gust speed (V), typical center-to-center spacing between buildings (d) and the vertical location above ground (h). The following expressions fit to the data represent the expected number of impacts on a target surface per square meter and per hour:

Equation 5-8

$$N = n(V, d) * f(d, h)$$

Where:

$n(V, d)$ is the average over the height from ground up to 30 meters, expressed in Equation 5-9

Equation 5-9

$$n(V, d) = 53 \frac{\left(1 + \tanh \frac{V^{1.11} - 80}{18}\right)}{(e^x + e^{-x})}, x = \frac{d - 15}{0.33V}$$

Where:

$f(d, h)$ is the height factor, expressed in Equation 5-10

Equation 5-10

$$f(d, h) = \frac{60}{h_0} \cos^2 \left(\frac{\pi h}{2 h_0} \right), h \leq h_0, = 0, h > h_0; h_0 = 30 - \frac{d}{10}$$

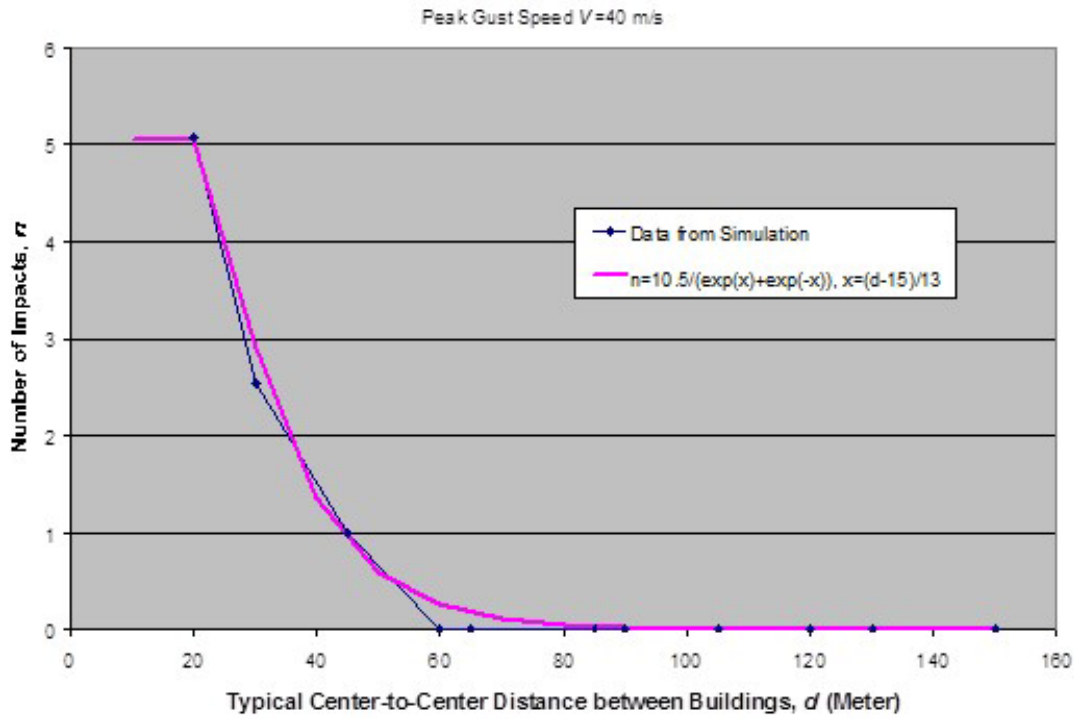
Where:

- V is the peak gust speed (m/s) in a short time interval T
- d represents the estimated typical center-to-center distance (m) of buildings for the area to be modeled
- h_o is the vertical location above ground (m) of the target surface element

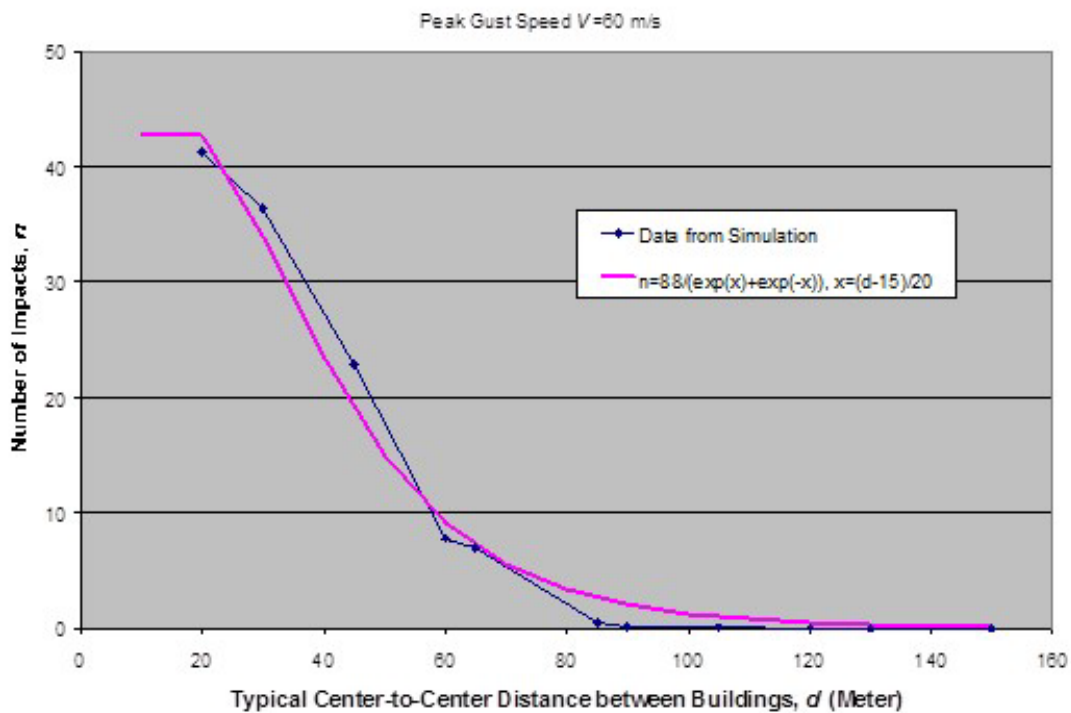
Equation 5-9 is illustrated in Figure 5-61 for peak gust speeds of 40, 60, and 75 meters per second, where the average number of impacts per square meter per hour on the wall from 0 to 30 meters is shown as the function of typical building spacing. The data derived from the physical model to which Equation 5-9 is fitted are also shown in these figures. The variation of the number of impacts with peak gust speed is illustrated in Figure 5-62, for selected center-to-center distances between buildings.

The height factors calculated from the simulated results are presented in Figure 5-63, while their empirical approximations as expressed by Equation 5-10 are shown in Figure 5-64.

The impact momentum, defined as the component of the terminal momentum perpendicular to the surface impacted, generally varies with many variables such as individual gravel diameter, terminal speed and incident angle of impact, etc. Some of these variables are in turn dependent on many other parameters, for example, wind speed, building spacing, vertical location, configuration of the source and target buildings, etc. The detailed relationships of its dependence on these parameters are rather complicated; however, as indicated by the simulation results, the statistical distributions of the impact momentum for various cases have similar shapes. When normalized by a given percentile, the distributions of the impact momentum for various cases tend to collapse. Figure 5-65 shows the averaged cumulative distribution function (CDF) of the impact momentum and the one standard deviation bounds over all cases, where the impact momentum is normalized by its 95th percentile.



A) For Peak Gust Speed of 40 m/s (90 mph)



B) For Peak Gust Speed of 60m/s (134mph)

Figure 5-61 Number of Impacts per m² hr on Walls Averaged Over the Lowest 30 meters, as Function of Building Spacing

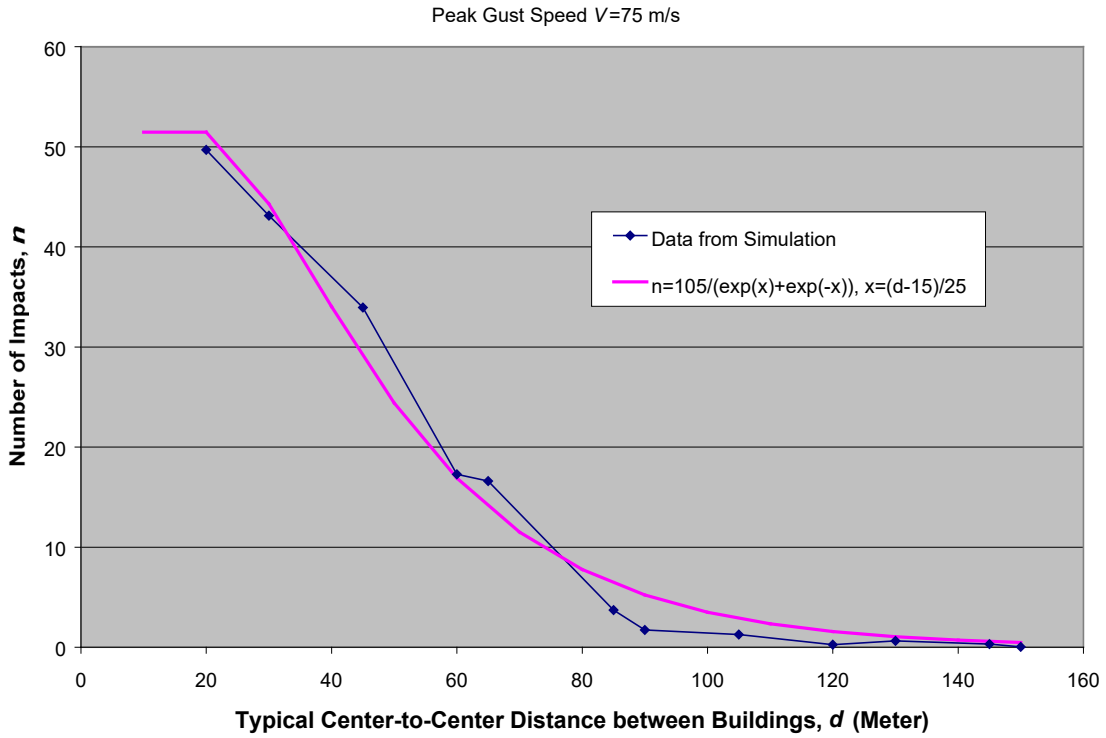


Figure 5-62 Number of Impacts per m² hr on Walls Averaged Over the Lowest 30 meters, as Function of Building Spacing

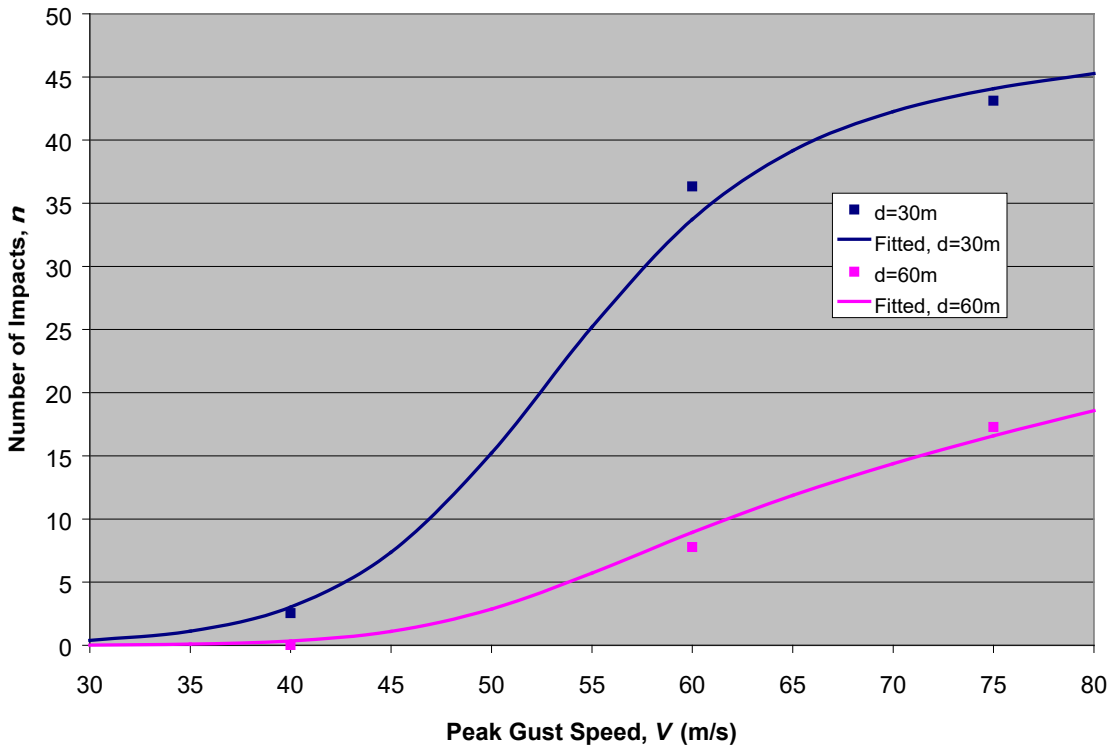


Figure 5-63 Examples of Fitted Number of Impacts Varying with Peak Gust Speed for Selected Building Spacing Cases in Comparison with Simulation Results

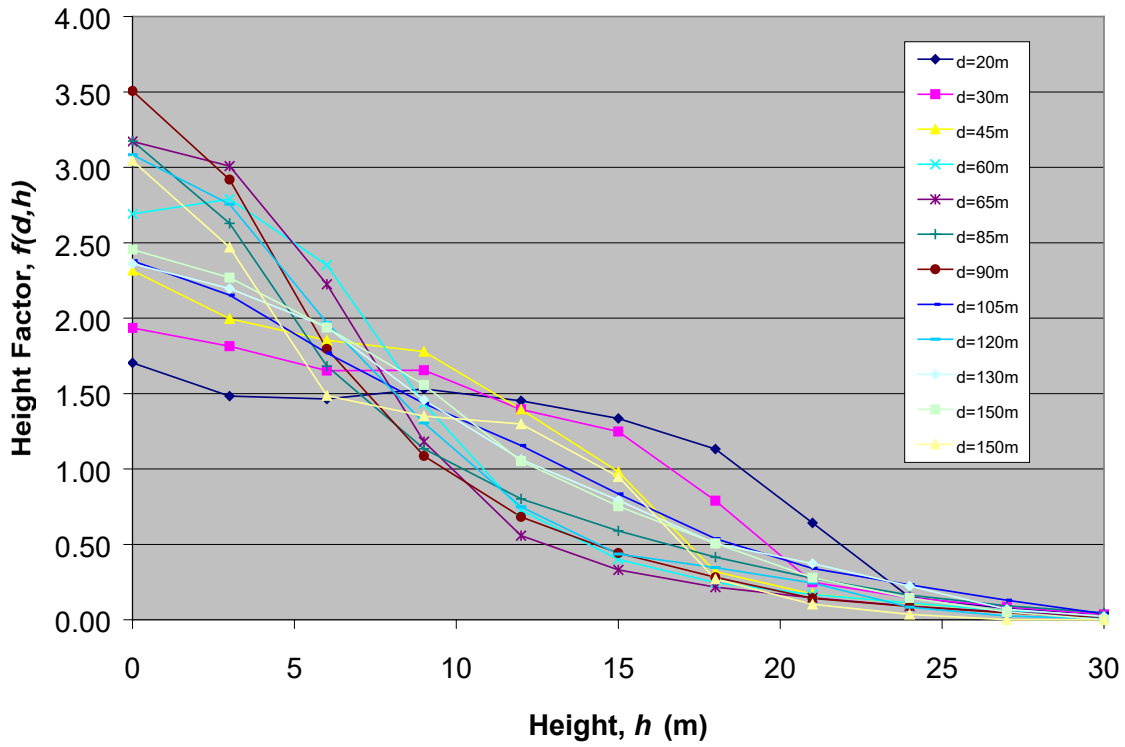


Figure 5-64 Height Factor for Number of Impacts for Various Cases with Building Spacing from 20 to 150 meters

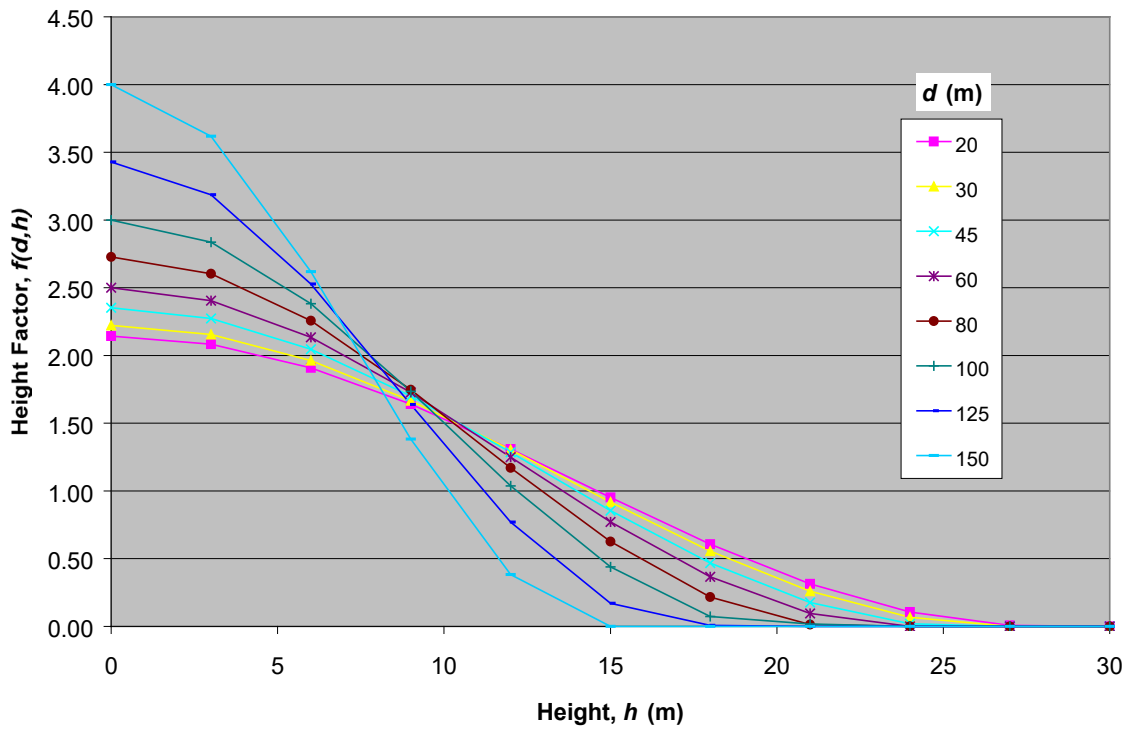


Figure 5-65 Fitted Height Factor for Number of Impacts for Building Spacing from 20 to 150 meters

Prior to the normalization, the distributions have been truncated at a momentum of 0.025 (kilogram-meter per second), below which gravel missiles are considered to have no damage effects on window glass products. The above results for the numbers of impacts have included only those that exceed the 0.025 kilogram-meters per second threshold.

The 95th percentile is empirically chosen as the normalizing factor mainly because it is a convenient number and for the many cases modeled, it represents a moderate value of momentum that is able to produce damage to window glass. As indicated by the results, the 95th percentile varies for different cases, dependent on various parameters mentioned above; however, there appears to be a trend of increase with wind speed, with certain variability at each wind speed. Figure 5-66 illustrates this trend and variability of the data, along with the empirical fit to their mean. Each data point plotted is derived from an individual impact momentum distribution obtained on every 25 square meters wall area that received at least 25 hits with impact momentum larger than 0.025 kilogram-meters per second. There are about 12,500 such data points for all cases modeled, which are all included in Figure 5-66.

Omitting the variability at each wind speed, the impact momentum distribution, simplified to be conditional on peak gust speed only, is expressed as:

Equation 5-11

$$P_m = P_m(M) = \text{CDF} \left(\frac{m - 0.025}{95\text{th percentile}} \right)$$

$$= \text{CDF} \left(\frac{M - 0.025}{2417 * 10^{-5}V^2 - 1.379 * 10^{-3}V + 6.200 * 10^{-2} - 0.025} \right)$$

Where:

V (m/s) is the peak gust speed in the time interval T

M (kg-m/s) represents the estimated resistance capacity for impact momentum

Equation 5-7, Equation 5-8, Equation 5-9, Equation 5-10, and Equation 5-11, along with the mean CDF function presented in Figure 5-67, constitute the fast-running windborne gravel debris module for low-rise commercial buildings in suburban areas. It is specifically designed for the general simulation model for hurricane damages and estimates the probability of impact damage (PD) caused by windborne gravel missiles to a vulnerable surface element of area A (square meters) during a short time interval T (hour).

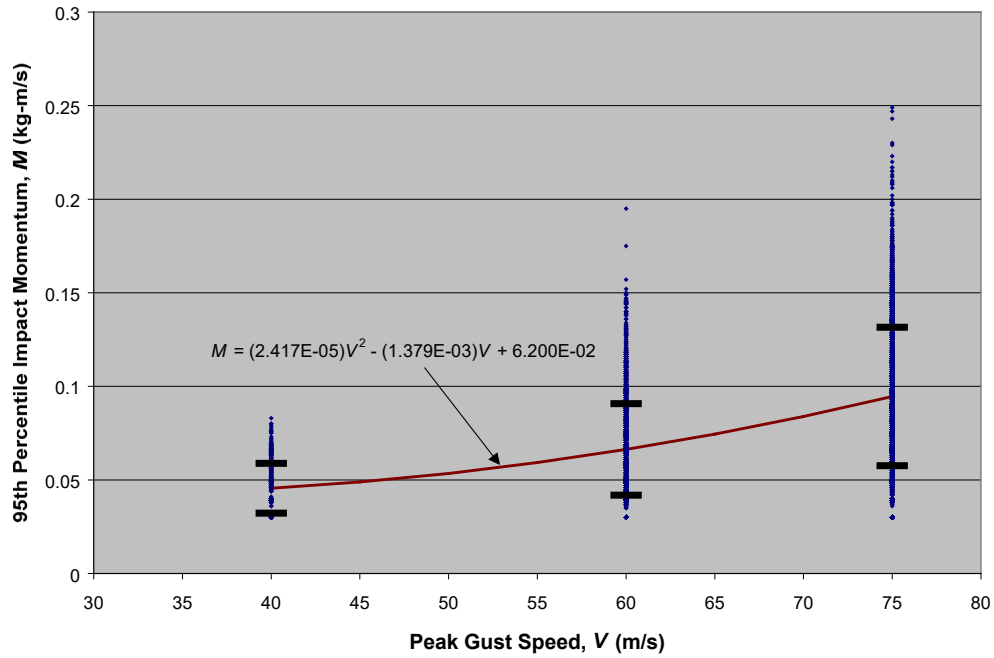


Figure 5-66 The Mean Trend of the 95th Percentile Impact Momentum with the Peak-Gust Speed, and the Variability for which the One Standard Deviation Bounds are Shown by the Short Bars

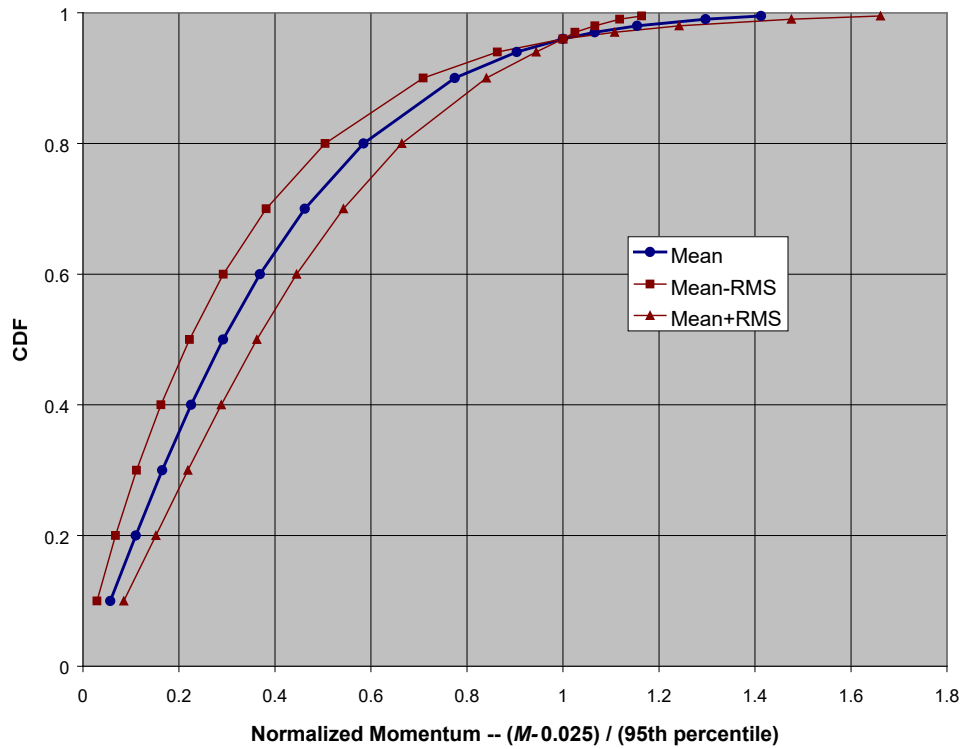


Figure 5-67 Distribution of the Normalized Impact Momentum

A fast-running model has been developed to estimate the risk of damage by windborne gravel debris to low-rise buildings in suburban commercial areas. The model utilizes a previously developed analytical

formulation for debris damage risk (Equation 5-7). A detailed physical modeling methodology is used to obtain the information required by the analytical formulation, including the expected number of impacts and impact momentum distribution. The detailed physical model simulates the effects of turbulent boundary layer winds, wind directionality, and the general layout of the gravel source buildings and target buildings. The output data from the detailed physical model were analyzed and simplified in accordance with the approach used in the general hurricane damage simulation model. The resulting fast-running model estimates the probability of impact damage (P_D) caused by windborne gravel missiles to a vulnerable surface element of area A during a short time interval T . Thus, it is readily integrated into the general model, which simulates the processes of a hurricane strike on a built area progressively in time and is required to estimate the number and location of fenestration elements breached by debris within each short time interval, in order to interactively account for the rainwater penetration and internal pressure change in a building.

In the development of the fast-running model, the effects of some variables, such as the detailed configurations and layout of upstream buildings, on the damage probability were averaged over an anticipated range of values since these variables are not specifically modeled in the general model. This approach provides averaged, approximate estimates of the damage probability as far as these variables are concerned. There exists propagated variability about the average resulting from such simplifications, which is undetermined at this time. The lack of analysis of this uncertainty remains to be a current model limitation.

5.3 Tree Blowdown Damage to Buildings

The building damage-to-loss model estimates expected loss as function of wind speed for two tree types, three tree height groups, six tree densities, four building geometries, and two wall construction types. These result in 288 normalized loss curves for tree blowdown damage to buildings, for building loss, and contents loss, respectively. The tree blowdown loss curves are combined with the fast-running normalized loss curves presented earlier in Section 4.5 to form loss curves in each Census tract that model wind, missile, and tree damage effects.

A Monte Carlo simulation approach is employed to derive the blowdown loss functions. A total of 10,000 simulations are performed to derive each function, which is taken to be the mean of the 10,000 simulated losses. Figure 5-68 illustrates the process for one simulation. The following sections describe the tree drop tests and the relationship between damage severity and impact energy.

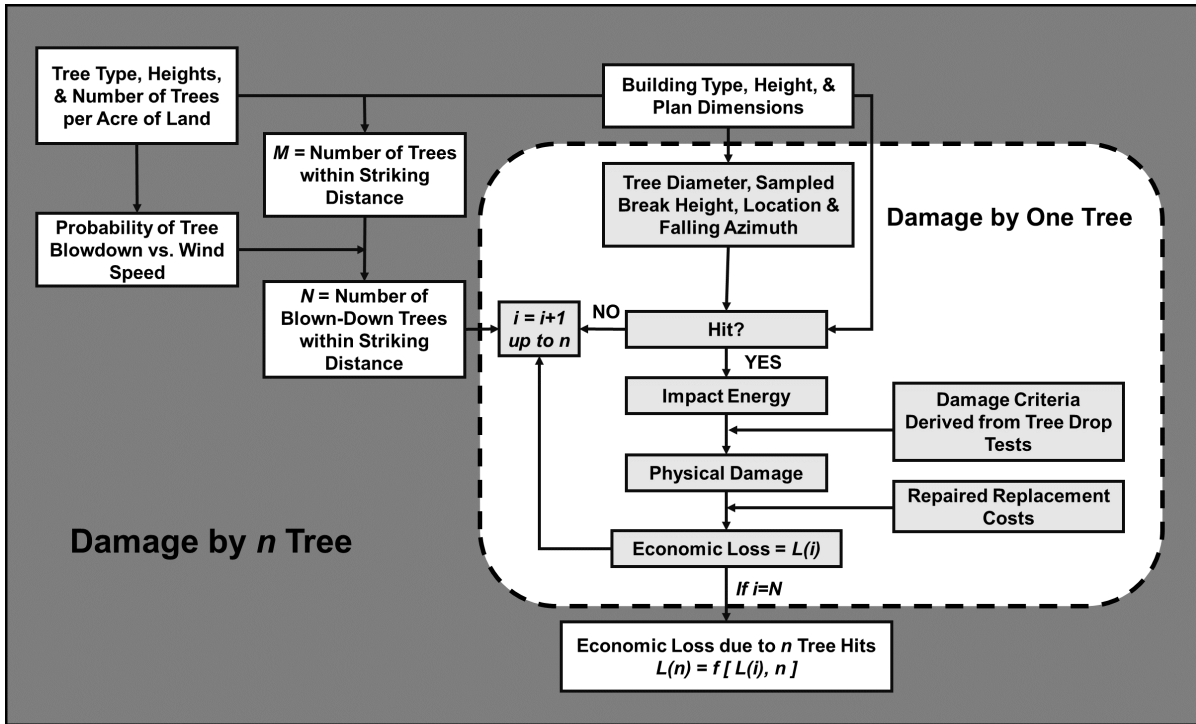


Figure 5-68 Simulation Scheme for Tree Blow-Down Damage to Building

5.3.1 Tree Drop Tests

The severity of tree damage to buildings is dependent on the tree impact energy and the structure’s impact resistance. In an effort to investigate tree impact damage on residential structures, the Wind Load Test Facility at Clemson University conducted tree drop tests on modeled partial house structures (Reinhold et al., 1996). To simulate the tree trunk, the Clemson tests used two steel pipes of different weights, namely 450 pounds and 950 pounds, both at a length of 20 feet. The pipes were released from standing position on a rig about 18 feet from the modeled structure and free-fell to the modeled house structure. The lighter pipe hits the eave with an impact energy of 3,600 foot-pounds, and the larger pipe hits with an impact energy of 7,600 foot-pounds.

Video recordings were taken during the fall and impact, and still pictures were also taken of the damage after impact. Figure 5-69, Figure 5-70, Figure 5-71, and Figure 5-72 show examples of the impact damage recorded from the tests on several modeled structures with different impact resistance capacities.



Figure 5-69 Small Pipe Impacting Wall Without Plywood Sheathing, 3,600 foot-pounds at Impact, Breaking Top Plates and Half-Way Cutting Into Wall



Figure 5-70 Small Pipe Impacting Wall with Plywood Sheathing, 3,600 foot-pounds at Impact, Breaking Top Plates and 1/4 Cutting Into Wall



Figure 5-71 Large Pipe Impacting Roof and Wall Without Plywood Sheathing, 7,600 foot-pounds at Impact, Breaking Roof, Top Plates and Entire Wall with Apparent Residual Energy Hitting Ground



Figure 5-72 Large Pipe Impacting Roof and Wall With Plywood Sheathing, 7,600 foot-pounds at Impact, Breaking Roof, Top Plates and 1/8 Wall

5.3.2 Relationship Between Damage Severity and Impact Energy

A quantitative relationship between physical damage state and the tree impact energy is essential to estimate tree blowdown damage and ensuing economic losses to buildings. The Clemson University tree drop test data aided in developing this relationship. The assumptions involved in establishing the damage state severity model include:

- A tree falls solely under the action of gravity. The actions of blowing wind and the remaining resistance from root-soil interaction (for uprooting) or the remaining resistance from wood fibers at breakpoint (for above ground breakage) are neglected.
- A tree trunk impact is required to cause damage.
- The tree trunk does not bounce after it hits the building.
- If it exceeds the impact resistance of the structure, an impacting tree trunk cuts into the building until all of its kinetic energy dissipates into the structure.
- A tree hit does not cause the complete collapse of a building.

Different building components will present different resistances to a tree trunk as it cuts through the structure. The resistance associated with a specific component of the building, such as the roof deck, top plate or bond-beam, wall sheathing, or an elevated floor, is assumed to be constant. Based on the limited number of tree drop damage states recorded by Clemson University and additional engineering inferences, an extended number of damage states are defined for the subsequent estimation of direct economic losses, in relation to impact energy, as shown in Table 5-15. Tree heights that will potentially produce the indicated impact energy and corresponding damage states are also presented for given stand-off distance, breaking point, and fall azimuth, etc., using pine trees as an example.

Table 5-15 Damage States in Relation to Impact Energy

Damage State #		1	2	3	4	5	6	7	8
One-Story Wood	Impact Energy (foot-pound) ⁽¹⁾	250	2,000	5,600	6,400	8,800			
	Example Tree Height ⁽²⁾ (feet)	30.0	46.9	57.5	59.0	62.6			
	Damage State Description	Surface damage	Roof deck crack	Top-plates rupture	One-Fourth Cut into wall	Cut through wall			
Two-Story Wood	Impact Energy (foot-pound)	250	2,000	5,600	6,400	8,800	14,400	15,200	17,600

Damage State #		1	2	3	4	5	6	7	8
	Example Tree Height (feet)	32.0	50.2	61.3	62.8	66.6	72.5	73.3	75.2
	Damage State Description	Surface damage	Roof deck crack	Top-plates rupture	One-Fourth Cut into upper wall	Cut through upper wall	Floor-plates rupture	One-Fourth Cut into lower wall	Cut through lower wall
One-Story Masonry	Impact Energy (foot-pound)	250	2,000	11,000	13,000	19,000			
	Example Tree Height (feet)	30.0	46.9	65.2	67.2	72.0			
	Damage State	Surface damage	Roof deck crack	Bond-beam rupture	¼ Cut into wall	Cut through wall			
Two-Story Masonry	Impact Energy (foot-pound)	250	2,000	11,000	13,000	19,000	30,000	32,000	38,000
	Example Tree Height (feet)	32.0	50.2	69.3	71.4	76.2	82.1	83.0	85.3
	Damage State Description	Surface damage	Roof deck crack	Bond-beam rupture	One-Fourth Cut into upper wall	Cut through upper wall	Floor-plates rupture	One-Fourth Cut into lower wall	Cut through lower wall

(1) Impact Energy is defined as the energy derived from the normal component of impact velocity with respect to the eave line.

(2) Assume a pine tree with stand-off distance of 30 feet, breaking at ground level and hitting eave perpendicularly.

5.4 Resistance Models

5.4.1 Residential Buildings

The direct wind-induced damage (wind pressures and windborne debris) to buildings modeled herein is directed towards the performance of components and cladding, including roof covering (shingles, tiles, membrane), roof sheathing (wood frame construction only), windows, and doors. Structural wall failures for masonry and wood frame walls and uplift of whole roof systems due to failure at the roof/wall connections are also modeled. Foundation failures (i.e., sliding, overturning, and uplift) are considered for manufactured homes (Section 5.5).

The wind and/or missile resistance of the various components noted above have been derived from laboratory test data, engineering analyses given in the literature, and judgment based on the performance of components observed during post-hurricane damage investigations. The empirical models based on judgment and experience are required in some cases since information on the loads and failure mechanisms for some systems are simply not known. Examples of such systems are

discussed later. The resistance of the cladding components used in the damage modeling is discussed in the following sections.

5.4.2 Roof Sheathing in Wood Frame Construction

The roof sheathing failure model is based primarily on the experimental uplift failure tests performed on 8'x4' sheets of plywood and Oriented Strand Board (OSB) reported by the American Plywood Association (Cunningham, 1993), and Clemson University (Mizzel, 1994; Shane, 1996; Rosowsky et al., 1999; Rosowsky and Schiff, 1997). Table 5-16 summarizes the relevant uplift resistance data from the various tests.

As indicated in Table 5-16, the variability of uplift capacities for a given nail size and spacing is significant. This variation is clouded by the fact that different species of wood having different specific gravities (SG) yield significantly different nail pullout resistances. The resistance of a nail to pullout varies with the specific gravity of the wood raised to the power of 2.5 (NDS-97), and the pullout capacity also varies with the moisture content of the wood.

The SG of the Douglas Fir (DF) used in the APA experiments had a reported mean value of 0.51 with a COV of 0.11. In the Clemson tests, the specific gravity of the wood is not reported, but the United States Department of Housing and Urban Development (HUD) 1999 suggests a value of 0.37 would be representative of the SG for the Spruce-Pine-Fir (SPF) wood used in the Clemson tests. HUD (1999) also notes that the Southern Yellow Pine (SYP) reported in Rosowsky and Schiff (1997) was in fact SPF. Thus, to compare the uplift capacities of the roof sheathing panels obtained from the Clemson tests to those obtained from the APA tests, the Clemson results should be increased by a factor of about 2.2.

Table 5-16 Uplift Resistances of 8-by-4 Roof Sheathing Panels from Laboratory Testing

Source	Nail Size	Nail Pattern	Species ¹	Mean (psf)	COV
Cunningham	6d	6/12	DF	60	0.12
Shane	6d	6/12	Unknown	71	0.12
Mizzel	6d	6/12	SPF	25	N/S
Cunningham	8d	6/12	DF	118	0.14
Shane	8d	6/12	Unknown	90	0.20
Rosowsky et al. (a)	8d	6/12	SPF	72	0.19
Rosowsky et al. (b)	8d	6/12	SPF	87	0.28
Mizzel	8d	6/12	SPF	61	N/S
Cunningham	8d	6/6	DF	218	N/A
Rosowsky and Schiff	8d	6/6	SYP	131	0.14
Mizzel (c)	8d	6/6	SPF	107	N/S
Mizzel (d)	8d	6/6	SPF	172	N/S
Mizzel (e)	8d	6/6	SPF	112	N/S

¹ DF = Douglas Fir; SPF = Spruce-Pine-Fir; SYP = Southern Yellow Pine

In the South Florida area, most homes are constructed with high density SYP lumber ($SG = 0.55$), and thus, the uplift resistance obtained from the APA tests are considered to be most representative of the uplift resistance of the 8'x4' panels. Thus, for modeling the resistance of well-applied roof sheathing, a mean of 61 psf and a COV of 11% are used for the 6d nail case and a mean of 114 psf and a COV of 11% are used for the 8d case. In the implementation of the damage model, the mean uplift capacities are reduced by 10% to account for the quality of installation ($\Phi = 0.9$).

5.4.3 Air Permeable Roof Cover Systems

Air permeable roof cover systems include such systems as shingles (asphalt, metal, etc.), tiles, wood shakes, and slate. The systems are referred to as air permeable since both the upper and lower faces of the system experience wind induced pressures. The net pressure load on the system is equal to the difference between the pressures acting on the top and bottom sides of the cover. The ability of the system (or components of the system) to resist wind loads is clearly a function of the hold capacity of the adhesive or mechanical attachment used to connect the roof cover to the deck. Prior to the early 1990's, no research had been performed to quantify the loads acting on an air permeable system in a windstorm or the requirements for attaching the system to the roof deck to resist these loads. The first research was performed by the Redland Roof Company in the United Kingdom (Cherry, 1991), where effective uplift and overturning coefficients on roof tiles were obtained. The effective uplift coefficients obtained in the Redland study have been incorporated in both the Standard Building Code (SBC) and the South Florida Building Code (SFBC) for use in the design of roof tile connections for both residential and commercial applications. The research program also addressed the resistance of roof tiles against blowing off the roof by measuring the moment resistance associated with different mechanical attachment techniques. The attachment techniques examined in the Redland Study included connecting the tiles to the roof deck using different nail connections, including one 10d nail, two 10d nails, one 8d nail, two 8d nails, one 2.5" screw, and two 2.5" screws.

For the prediction of the performance of tile roofs, the loading and damage model incorporates the Redland roofing company results for a typical tile. The nominal resistance chosen corresponds to that of the one nail case. While it is recognized that in most of South Florida, roof tiles are attached to the roof using mortar rather than mechanical connections, no data exists for a mortared connection. Thus, while the model does not properly reproduce the actual resistance of a mortared tile to be blown off in a storm, it does provide a method to enable reasonable predictions of the effective loads acting on the tiles; thus, a reasonable representation of the variation of these loads with both wind speed and location on the roof of a structure. The usefulness of the model in predicting the failure rates of tiles attached with mortar is evaluated through a calibration process.

The only available data on the effective loads acting on asphalt shingles are presented in Peterka et al. (1997). The study by Peterka et al., showed that, as in the case of roof tiles, the effective loads acting on shingles are reduced because negative pressures act on both the top and bottom sides of the shingle. The resistance of a shingle to the uplift pressures acting on the shingle tabs is provided by the adhesive strip on the underside of the shingle tab towards its leading edge. If the shingle tabs do lift, complete failure of the shingle occurs when the nails or staples tear from the roof or alternately, the shingle tears around the nails. To properly assess the uplift capacity of a shingle, the uplift capacity of the adhesive strip must be known, and at the time this model was being developed no public domain data are available to properly assess the uplift capacity of shingles. Thus, for the prediction of the

performance of shingle roofs, the same load-resistance model is used as for the tile roof case except that the nominal resistance of the shingles have been reduced by 10% over the basic tile case. While this modeling approach is empirical, the mechanism in which either the tiles or shingle are loaded is the same; thus, as in the case of roof tiles, the approach enables a reasonable means to model the variation of the loads with both wind speed and location on the roof. Again, the usefulness of the model is evaluated through comparisons of modeled and observed roofing performance.

5.4.4 Windows and Sliding Glass Doors

The wind pressure induced failure of both windows and sliding glass doors is produced by either a failure in the glass, a failure in the frame or a failure in the frame-wall connection. The wind resistance capabilities of the above noted components can vary enormously between manufacturers and the required design pressure. For this study, the assumed failure pressure is based on the minimum loads as specified in the SBC.

Prior to 1974, the design wind pressure specified in the Standard Building Code (SBC) for buildings located within 125 miles of the coast, having a mean roof height of 30' or less, was 25 psf. The American Architectural Manufacturers Association (AAMA) requirements for windows and doors states that the product must be able to resist loads of 1.5 times the design pressure; thus, most products installed in this time period should have a minimal wind load resistance of about 38 psf. When the product is tested to meet the R25 rating, a static pressure having a magnitude of 37.5 psf is applied to the product and if it does not fail, it meets the R25 specification and can be marketed as such. The ultimate capacity of the product is unknown and may be as low as 38 psf, but it could be higher.

For damage simulation purposes, it is assumed that the nominal pressure resistance of window and sliding glass door components installed in this period can be modeled using a mean resistance of 40 psf with a coefficient of variation of 0.2. The assumed distribution of the product capacity is taken as being normal. This assumption implies that about 80% of the products installed in low-rise buildings during that time period meet or exceed the minimum requirements as specified by the SBC. It is also assumed that during this time period, the same products used on low-rise buildings in Palm Beach County were installed on buildings in Dade and Broward Counties, even though the Building Code provisions were not the same.

From 1974 through to 1982, the basic design pressures in the South Florida area increased to 34 psf for buildings less than 30' in height. For the design of windows and doors, wind loading coefficients of +1.1 and -0.55 were used to compute the design pressures, implying the products should be able to resist inward acting loads of up to 56 psf ($34 \times 1.1 \times 1.5$) and negative pressures of 28 psf.

The revision of the SBC wind load provisions in 1982 provided more realistic estimates of the pressure coefficients than the preceding versions; however, the design wind pressures for typical fenestration products on typical low-rise buildings were in the range of 30 to 40 psf depending upon the height of the building, the location of the fenestration and the size of the fenestration. The implied resistances for fenestration products meeting these load criteria range between 45 psf and 60 psf.

Although the wind load criteria for the design of windows and doors increased somewhat between the 1950s and the early 1990s, the mean resistance of 40 psf with a COV of 20% is used for all single-family residential homes.

5.4.5 Roof-Wall Connections

Since the inception of the SFBC in the late 1950's, tie down straps have been required for the roof to wall connections in both Dade and Broward Counties. In Palm Beach County, roof-wall tie downs have been required on every truss-wall connection since the late 1970's but, prior to this time, strapped connections were required only on every other truss. The uplift capacity of hurricane straps or clips varies significantly with the type of wood used to manufacture the truss, the size (thickness and width) of the strap, number of nails, etc.

Conner et al. (1997) reported on the uplift capacity of various wood to wood connections obtained from laboratory tests using Douglas Fir wood members. For conventional toe-nail connections (three 8d nails), they reported a mean uplift capacity of 676 pounds with a COV of 8%. The strapped connection yielded a mean uplift capacity of 867 pounds with a COV of 18%. The straps used in the experiments were 0.5" wide (no thickness is given) with two 6d nails used for both the rafter and top plate connections. The clipped connection yielded a mean uplift capacity of 908 pounds with COV of 10%.

Reed et al. (1997) reported test results using SPF lumber. For a toenail connection using three 8d nails they report a mean uplift capacity of 430 pounds and for a small strap (five 8d nails in each of the rafter and top plate) they report a mean uplift capacity of 1,900 pounds.

Canfield et al. (1991) reported on the uplift capacity of a number of straps tested with SPF lumber. They reported a mean uplift capacity of 208 pounds for the three 8d toenail case, with strapped connections yielding mean uplift capacities ranging between about 500 pounds to 1,200 pounds, depending on the strap thickness and number of nails used in the connection. In the Canfield et al. (1991) tests, the strap most closely representing that typically used in the South Florida area yielded a mean uplift resistance of 1,000 pounds with a COV of 15%.

The true uplift capacity for a field installed strap connection depends on the quality of installation, number and size of nails, and the size of the strap. The South Florida Building Code requires a strap having a thickness of 0.125" with three 8d nails be used to attach the strap to the truss or rafter. Based on the above noted experimental results, the uplift capacity of a strapped or properly clipped roof-wall connection is modeled with a mean resistance of 1,200 pounds and a COV of 30%.

5.4.6 Masonry Walls

Wall failure models were developed as a step towards modeling catastrophic structural failures. Wall failure modeling includes failures due to both inward and outward uniform pressure loading. Two different circumstances have been considered: walls without roof support and walls with roof support. The former is for the case where the wind uplift force has already blown off the roof. The latter is for walls that are within an integrated structure. A wall within an integrated structure can become a weak link, particularly when mitigation measures have been taken to protect windows and doors, to improve roof-sheathing connections, and to strengthen roof to wall connections by using tie downs. Variability of

wall resistance capacity due to variable material and workmanship etc., is incorporated in the wall failure modeling.

For edge-supported (by roof, floor, and adjacent walls, etc.) unreinforced masonry walls under uniform lateral pressure loading, the major failure mechanism is associated with cracking due to flexural tensile stress. The cracking normally starts at and develops along the mortar joints (both horizontal bed joints and vertical head joints) between the concrete masonry units (CMU) owing to the failure of mortar-CMU bond as the weakest link in the wall system. Occasionally, in the vertical direction, the developing crack may proceed across a CMU from a mortar head joint to another mortar head joint. Examples of masonry wall or brick veneer damage are shown in Figure 5-73.



A) BRICK veneer (Hogan and Karwoski, 1990)



B) Collapse of masonry walls (Zollo, 1993): (top); A wall of 40' span Walls on a two-story building (bottom)



C) Collapse of masonry wall and steel frame roof system (NRC, 1991)



D) Collapse of masonry wall (HUD, 1993)

Figure 5-73 Wind-Induced Masonry Wall and Brick Veneer Damage

Structurally, a masonry wall can be considered as an orthotropic slab with different bending moment resistance capacities in horizontal and vertical directions. Yield line theory is used to derive a wall failure model applicable for various wall spans, wall heights, cross-sectional configurations, and material properties. This method has been adopted for masonry by a number of researchers (e.g., Drysdale and Essawy, 1988), as well as by the British code (BSI, 1978). While true yield-line behavior cannot be fully justified, a substantial body of data (Haseltine, 1975; Hendry and Kheir, 1976; West et al., 1973a, 1973b) and some recent tests tend to support the use of this analytical tool.

Given the edge support conditions, the accuracy of a yield-line analysis depends on the correctness of the assumed crack pattern. The resulting capacity will be the expected capacity if the assumed pattern is correct, or an upper bound value if the assumed pattern deviates from the correct one. The next section describes in detail the crack patterns observed by a number of researchers for a series of walls with varying dimensions and edge support conditions, followed by the yield-line analysis and results for the masonry wall model.

5.4.6.1 Failure Modes and Crack Patterns

Drysdale and Essawy (1988) carried out experimental investigations on the failure modes and crack patterns for a series of 9' tall, 8" thick, full-scale masonry walls of varying spans under uniform pressure loads. The walls were built by an experienced mason using type-S mortar and standard 8"x8"x16" two-cell concrete blocks that are most commonly used in masonry construction. The running bond pattern, curing time, and other parameters were all consistent with code requirements. The walls were investigated for different span to height ratios (i.e., aspect ratios) and various support conditions. Three repetitions for each combination of parameters were performed to provide a better statistical sample, primarily for a better measurement of the mean. The first-crack pressures and ultimate failure pressures were recorded.

The typical crack patterns observed by Drysdale and Essawy are presented in Figure 5-74 for various wall aspect ratios and support conditions. Figure 5-74(a) shows a cracking pattern for a small span wall (width $W = 11.2'$, aspect ratio = 1.21) simply supported along all four edges. It was observed that a vertical crack started near the middle of the wall, where a maximum flexural moment is expected. The crack split diagonally and extended to the four corners of the wall under higher pressures leading to its collapse. Figure 5-74(b) shows a wider wall ($W = 16.4'$, aspect ratio = 1.79) where the initial crack was a horizontal one that split at its two ends under higher pressures and extended at roughly 45° to the four wall corners shortly before collapse. Wider walls supported on all four sides also generally followed the same failure pattern described in Figure 5-74(b). The wider the wall, the longer the initial horizontal crack would be. Thus, for a wall of infinitely large span, hypothetically, one could only see the horizontal crack. This result agrees with Drysdale and Essawy's observations on walls with only top and bottom supports (equivalent to two-end supported beams), which resemble the middle section of a wall with an infinite span where little shear and moment load transfer would occur horizontally under uniform lateral loading. Drysdale and Essawy clearly described the horizontal crack for the top and bottom supported walls in their text although they did not reproduce the picture. Dawe and Aridru's work (1993) on prestressed masonry confirmed this cracking pattern (see Figure 5-75). It can be assumed that the side supports become insignificant to the crack pattern and failure pressure for long span masonry walls. These observations and measured failure pressures provide an important data point for verifying the wall failure model in terms of long span masonry walls.

Figure 5-74(c) exhibits a crack pattern of a wall without top support, for a specific horizontal wall span of 16.4' (aspect ratio = 1.79), where a vertical initial crack was joined by two diagonal cracks extending to the lower corners. It can be expected that, as the aspect ratio increases, the vertical crack will shorten and the junction of the two oblique cracks will move upwards; eventually the pattern will become one with only the two oblique cracks that extend to the top edge of the wall and disjoint from each other.

The cracking pattern for walls with only two sides supported was also investigated by Drysdale and Essawy, as reproduced in Figure 5-74(d), where a vertical crack ran through the height of the wall near the mid-span, alternately passing through head joints and blocks in a nearly straight line. This would also depict the crack pattern for a wall of infinitely large height or of infinitely small aspect ratio.

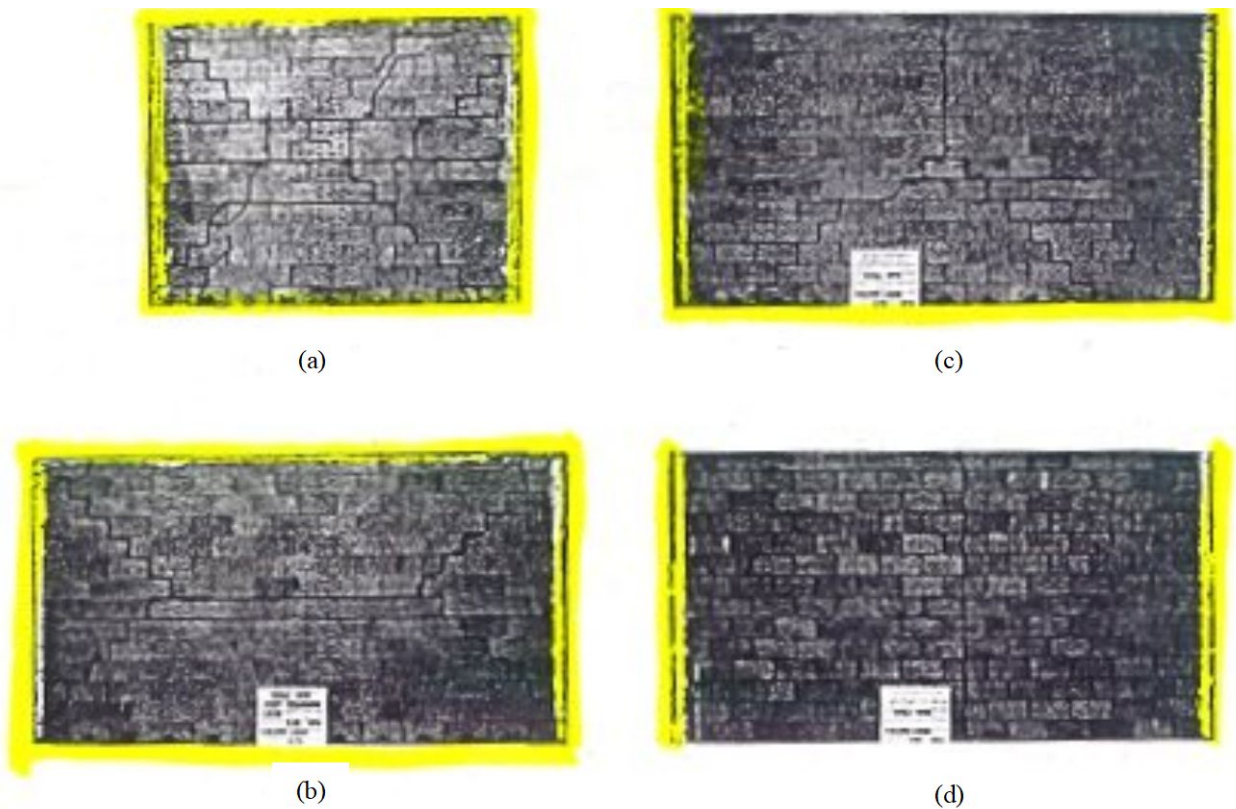


Figure 5-74 Typical Cracking Patterns for Various Wall Spans and Different Edge Support Conditions (Drysdale and Essawy, 1988)

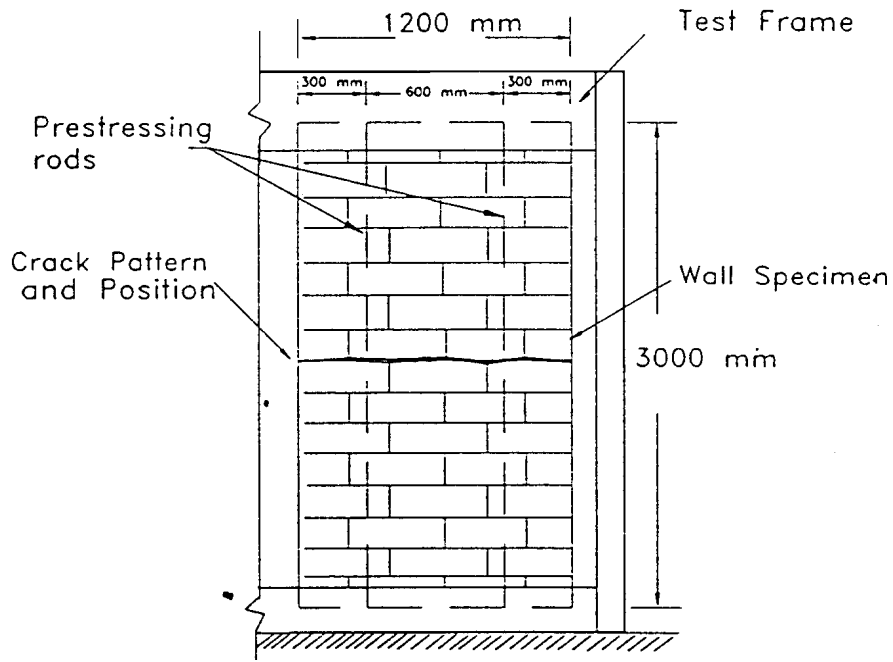


Figure 5-75 Typical Cracking Pattern for Top and Bottom Supported Prestressed Masonry Wall (Dawe and Aridru, 1993)

The cracking patterns are summarized in Figure 5-76 for various edge support conditions and aspect ratios, based on the above observations and theoretical inferences or assumptions. The yield line analysis will either confirm or reject an assumed pattern. The correct pattern should provide the minimum capacity, while the rest will all give higher values.

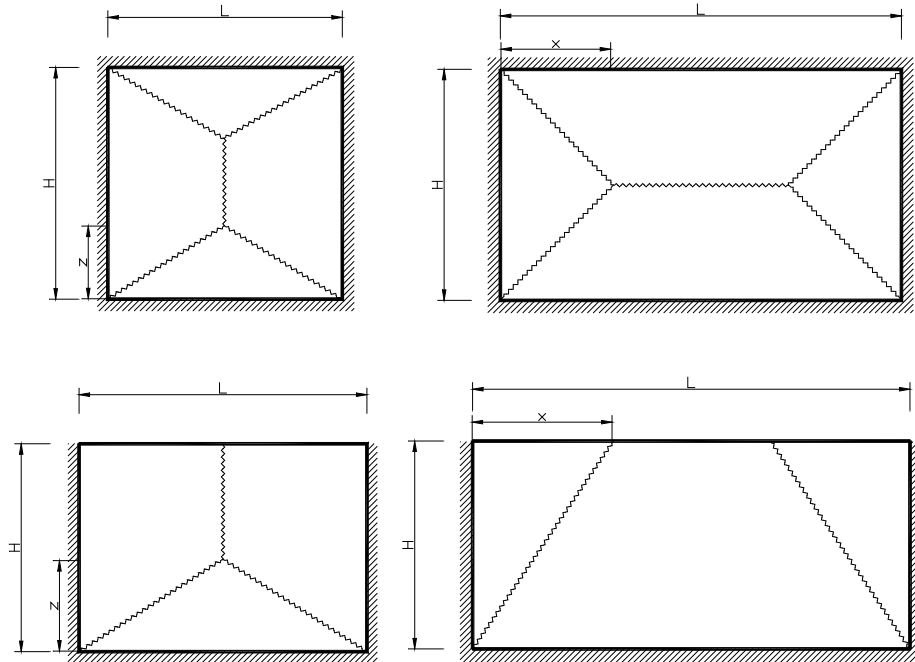


Figure 5-76 Typical Crack Patterns for Masonry Walls of Small and Large Aspect Ratios, with and without Top Supports

5.4.6.2 Ultimate Failure Pressures

The basic fundamentals and main assumptions for yield line theory are as follows (Ghali and Neville, 1989):

1. At fracture, the bending moment per unit length along all the fracture lines is constant and equal to the “yield” value.
2. The fractured slab parts rotate about axes along the supported edges.
3. Fractured slab parts are in the same plane, and therefore, they intersect in straight lines; in other words, the “yield lines” are straight.
4. The lines of fracture on the sides of two adjacent slab parts pass through the point of intersection of their axes of rotation.

Based on these assumptions and using the energy method, the solutions for the crack pattern parameters (x or z) and corresponding ultimate pressure loads (p_r) are obtained through a series of lengthy mathematical manipulations. The results are presented in Table 5-17, in normalized form, for the walls illustrated in Figure 5-76 and with ultimate flexural moment capacities of m and Φm for vertical and horizontal bending, respectively.

Drysdale and Essawy (1988) argued that, for walls with four simply-supported edges and moderate spans for which an initial horizontal crack occurs at mid-height and near the middle of the span at pressures significantly lower than the ultimate values, the initial horizontal crack should be treated as a free edge when estimating the ultimate failure load. This assumption results in the modified estimates of ultimate pressures shown in Table 5-18; however, the estimated failure pressures are not dramatically different than the unmodified results in Table 5-17.

For comparison, the ultimate failure pressures measured by Drysdale and Essawy are reproduced in Figure 5-77 for varying horizontal span, along with the estimated values obtained by applying the above theoretical results to their tested full-scale walls. The measured data shown are the average of three repetitions. The variation of measured failure pressures among the three repetitions is relatively small, with the coefficient of variation being in the order of 6%. The first set of data (see legend) is for walls with all four sides supported and without prestress. The three data points for spans between 11' and 19' are adopted directly from Drysdale and Essawy (1988). Good agreement is observed between the theoretical estimates and the measured data. The fourth point of this group, to the far end of the abscissa, is their result for walls with only top and bottom supports, hypothetically representing the case for all-side simply supported walls of infinite horizontal span. They re-tested this “extreme span” wall case using available extra specimens. The resulting average value of 47.2 psf nearly coincides with the theoretical extreme span asymptote or lower bound value. For these wall cases, the theoretical failure pressures do not significantly change for spans beyond 40' since they are sufficiently large spans such that the side supports no longer significantly influence the expected failure pressure.

The average failure pressure measured by Drysdale and Essawy for top unsupported walls with a horizontal span of 16.4' is also shown in Figure 5-77 in comparison with the theoretical estimate. Again, there is good agreement. This was, unfortunately, the only data they obtained for top unsupported walls.

5.4.6.3 Effects of Variable Material and Workmanship

It is recognized that relatively large variability of wall resistance capacity exists due to variable material and workmanship, versus laboratory-controlled conditions (variation of laboratory measured failure pressure were shown to be relatively small, as mentioned above). The effect of this variability is accounted for based on the data of Gross et al. (1969) as quoted by Grimm (1999), which is reproduced in Figure 5-78. The data was for clay brick masonry; however, it is assumed also to be typical for the strength variability of concrete block masonry since the bond strength of the mortar, which is used for both types of masonry walls, controls in large part the ultimate resistance capacity. The data are presented as the distribution of the flexural strength ratio between un-inspected workmanship and material and inspected or laboratory workmanship and material. Assuming a normal distribution for the resistance capacity, the mean and standard deviation of the flexural strength ratio are calculated based on the data to be about 0.8 and 0.2, respectively.

Table 5-17 Failure Pressures (p_r) and Crack Pattern Parameters (x or z) Derived from Yield-Line Analysis

Support	Support Type	Failure Pressure and Crack Parameter (z)	Failure Pressure and Crack Parameter (x)	Bounds
With Top Support	Modified Aspect Ratio $r_L = \frac{1}{r_H} = \frac{L}{\sqrt{\phi}H}$	≤ 1	≥ 1	$\rightarrow +\infty$
	Four Simple Edge Supports	$\frac{p_r HL}{m} = \frac{6\sqrt{\phi}}{r_H} \left(\frac{z}{H}\right)^{-2}$ $\frac{z}{H} = \frac{\sqrt{3r_H^2 + 1} - 1}{2r_H^2}$	$\frac{p_r HL}{m} = \frac{6\sqrt{\phi}}{r_L} \left(\frac{x}{L}\right)^{-2}$ $\frac{x}{L} = \frac{\sqrt{3r_L^2 + 1} - 1}{2r_L^2}$	$p_r \rightarrow \frac{8m}{H^2}$
	Modified Aspect Ratio $r_L = \frac{1}{r_H} = \frac{L}{\sqrt{\phi}H}$	≤ 1	≥ 1	$\rightarrow +\infty$
	Four Fixed Edge Supports	$\frac{p_r HL}{m} = \frac{12\sqrt{\phi}}{r_H} \left(\frac{z}{H}\right)^{-2}$ $\frac{z}{H} = \frac{\sqrt{3r_H^2 + 1} - 1}{2r_H^2}$	$\frac{p_r HL}{m} = \frac{12\sqrt{\phi}}{r_L} \left(\frac{x}{L}\right)^{-2}$ $\frac{x}{L} = \frac{\sqrt{3r_L^2 + 1} - 1}{2r_L^2}$	$p_r \rightarrow \frac{16m}{H^2}$
Without Top Support	Modified Aspect Ratio $r_L = \frac{1}{r_h} = \frac{L}{\sqrt{\phi}H}$	≤ 1.466	≥ 1.466	$\rightarrow +\infty$
	Three Simple Edge Supports	$\frac{p_r HL}{m} = \frac{8\sqrt{\phi}}{r_L} \left(\frac{x}{L}\right)^{-2}$ $\frac{x}{L} = \frac{\sqrt{9r_L^2 + 4} - 1}{3r_L^2}$	$\frac{p_r HL}{m} = \frac{8\sqrt{\phi}}{r_L} \left(\frac{x}{L}\right)^{-2}$ $\frac{x}{L} = \frac{\sqrt{9r_L^2 + 4} - 1}{3r_L^2}$	$(p_r \rightarrow 0)$
	Modified Aspect Ratio $r_L = \frac{1}{r_h} = \frac{L}{\sqrt{\phi}H}$	≤ 1.657	≥ 1.657	$\rightarrow +\infty$

Support	Support Type	Failure Pressure and Crack Parameter (z)	Failure Pressure and Crack Parameter (x)	Bounds
	Three Fixed Edge Supports	$\frac{p_r HL}{m} = \frac{12\sqrt{\phi}}{r_H} \left(\frac{z}{H}\right)^{-2}$ $\frac{z}{H} = \frac{\sqrt{12r_H^2 + 1} - 1}{4r_H^2}$	$\frac{p_r HL}{m} = \frac{2\sqrt{\phi}}{r_L} \left(\frac{x}{L}\right)^{-1}$ $* \left(\frac{x}{L} r_L^2 + 8\right)$ $\frac{x}{L} = \frac{\sqrt{6r_L^2 + 4} - 2}{2r_L^2}$	$p_r \rightarrow \frac{2m}{H^2}$

Table 5-18 Failure Pressures (pr) and Crack Pattern Parameters (x or z) Derived from Yield-Line Analysis, with the Assumption of Discontinuity at Initial Horizontal Center Crack

Support	Support Type	Failure Pressure and Crack Parameter (z)	Failure Pressure and Crack Parameter (x)	Bounds
With Top Support	Modified Aspect Ratio $r_L = \frac{1}{r_H} = \frac{L}{\sqrt{\phi}H}$	≤ 0.733	≥ 0.733	$\rightarrow +\infty$
	Four Simple Edge Supports	$\frac{p_r HL}{m} = \frac{6\sqrt{\phi}}{r_H} \left(\frac{z}{H}\right)^{-2}$ $\frac{z}{H} = \frac{\sqrt{12r_H^2 + 1} - 1}{2r_H^2}$	$\frac{p_r HL}{m} = \frac{8\sqrt{\phi}}{r_L} \left(\frac{x}{L}\right)^{-2}$ $\frac{x}{L} = \frac{\sqrt{9r_L^2 + 1} - 1}{6r_L^2}$	Lower-Bounded by $p_r = \frac{8m}{H^2}$

For Table 5-17 and Table 5-18, the equation variables are:

- p_r is the failure pressures
- x or z crack pattern parameters
- H is the wall depth
- L is the wall span
- r_L is the span to depth aspect ratio
- r_H is the depth to span to aspect ratio

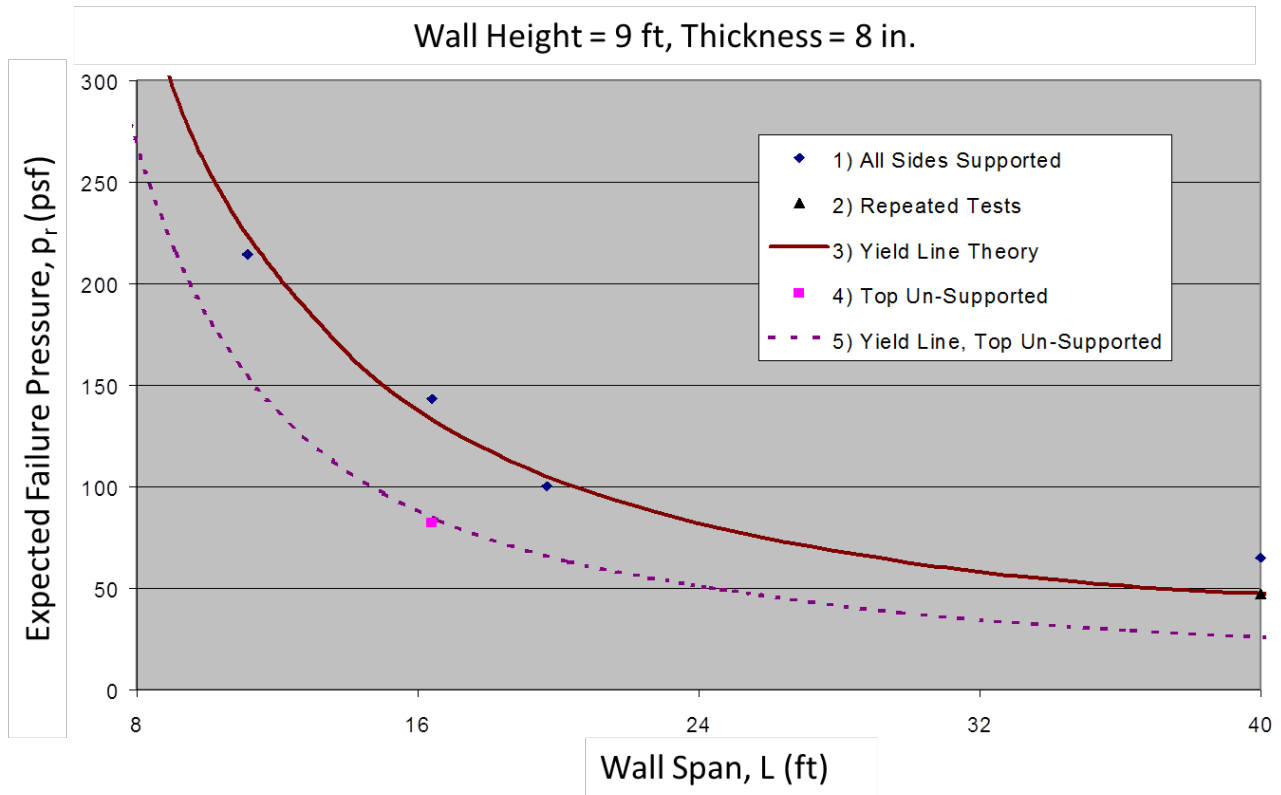


Figure 5-77 Comparison of Failure Pressure Variation with Wall Span

Fattal and Cattaneo (1977) discussed the effect of workmanship on masonry wall strength and recommended the use of reduction factors in estimating the strength of un-inspected masonry walls to account for variability in workmanship. They recommended a reduction factor of 0.67 to be multiplied to the mean strength obtained from laboratory or sources than directly measured from the wall under investigation. They also quoted code recommended workmanship reduction factors of 0.67 by Building Industry Association (BIA) to 0.5 by Uniform Building Codes (UBC) and National Contract Management Association (NCMA). All these reduction factors are used as a simple method to account for the overall effect of variable workmanship on wall strength, including the effects on both the mean and the dispersion. A value of 0.67 corresponds approximately to the 25th percentile of a normal distribution of $N(0.8, 0.2)$, and 0.5 roughly to the 5th percentile. These values provide further support to the use of a mean strength ratio of 0.8 and a standard deviation of 0.2, as derived from the data reproduced in Figure 5-78.

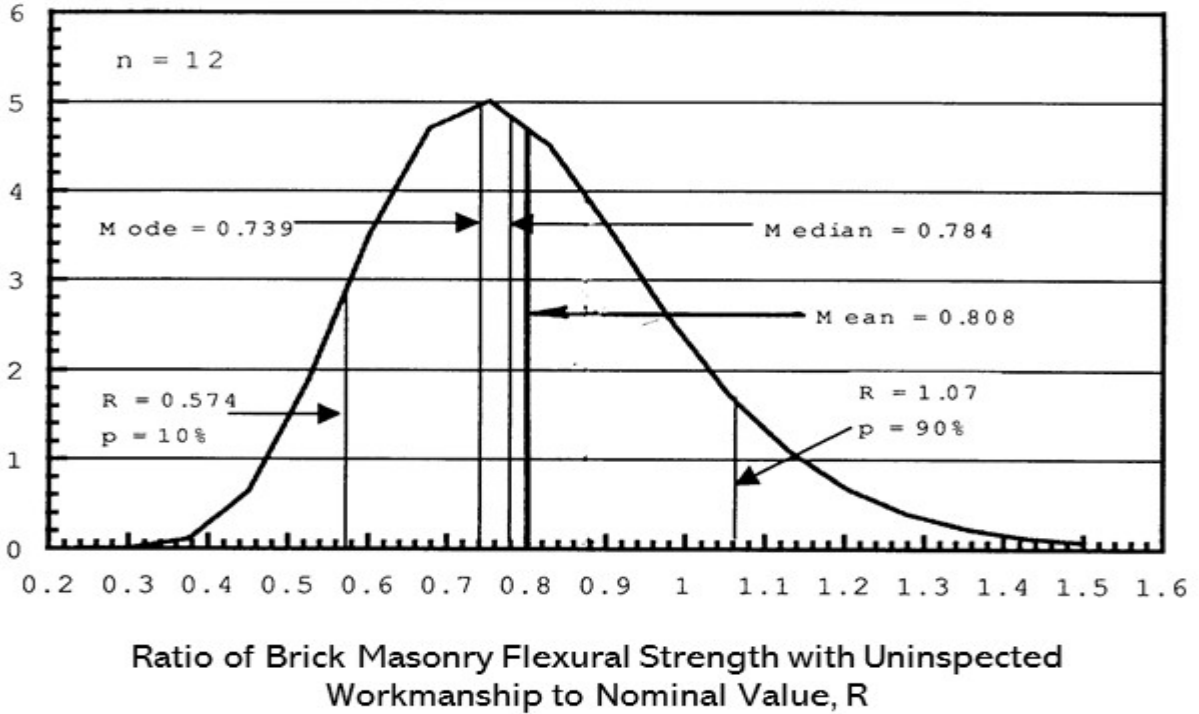


Figure 5-78 Effects of Workmanship on Actual Flexural Strength versus Nominal Value

5.4.6.4 Estimation of Wall Failure Probability

Based on the above discussions, the probability of failure, P_f , for a masonry wall of span L under uniform lateral pressure loading p is estimated as:

Equation 5-12

$$P_f = \Phi \left(\frac{p - 0.8p_r(L)}{0.2p_r(L)} \right)$$

Where:

- $\Phi(*)$ denotes the standard normal cumulative distribution function.
- $p_r(L)$ is the laboratory measured or nominal failure pressure as a function of wall span and heights, edge supports, and ultimate flexural moments (dependent on material and concrete masonry configuration), as represented by the theoretical results in Table 5-17 for walls with and without roof support

Examples of estimated probabilities of failure are shown in Figure 5-79 and Figure 5-80 for top supported and unsupported walls, respectively. Data are presented for simply supported, 9' high walls of various spans.

The model focuses on the most common failure mechanism of masonry walls that is associated with cracking of mortar joints and concrete blocks, assuming that the wall edge supports are perfect when they are present. Thus, it treats the failure probability for walls under outward resultant pressure load the same as for walls under inward resultant pressure load, ignoring potential differences in the resistance capacities of wall anchorage along the edges between inward and outward loads. Outward loading may cause pullout of the wall anchorage while inward loading is exerted against walls, presumably with edge supports closer to “perfect.” It is possible that the failure probability for outward loading will be somewhat higher than for inward loading. In addition, it is assumed that there are no openings on the wall, or the openings and their perimeter framing do not decrease nor increase the wall capacity in resisting pressure loads.

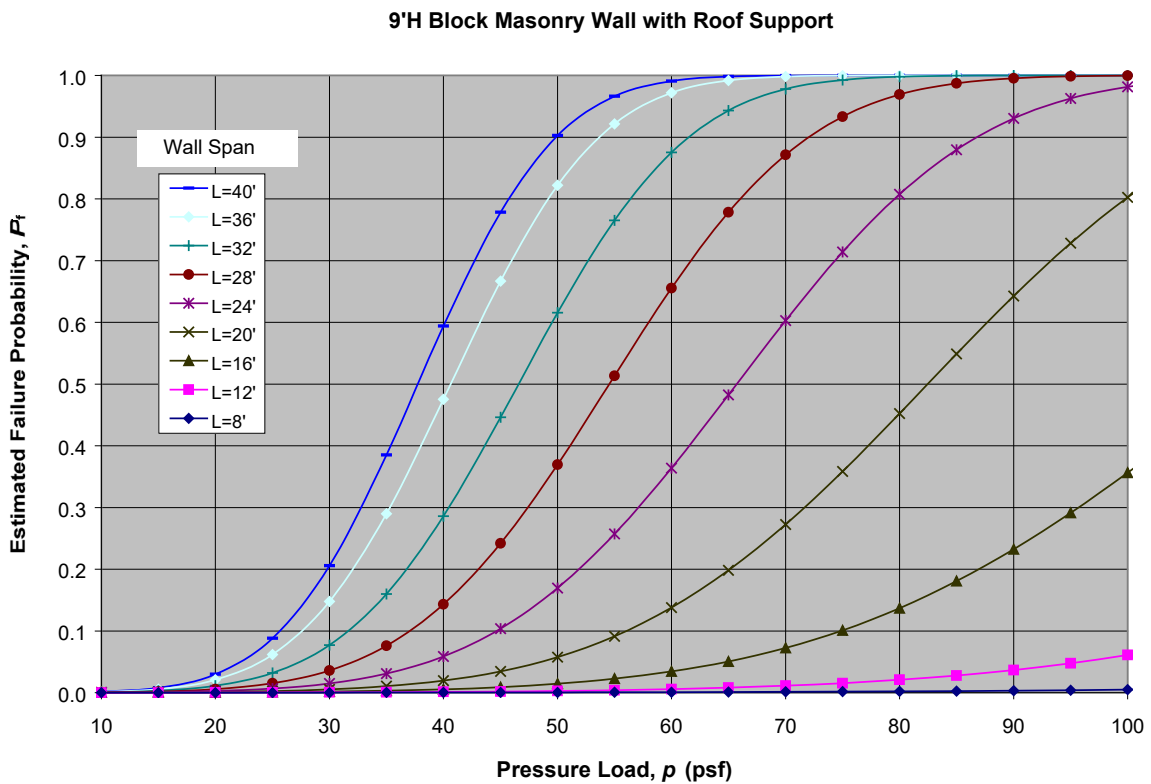


Figure 5-79 Estimated Failure Probability as a Function of Pressure Load for Various Wall Spans with Roof Support

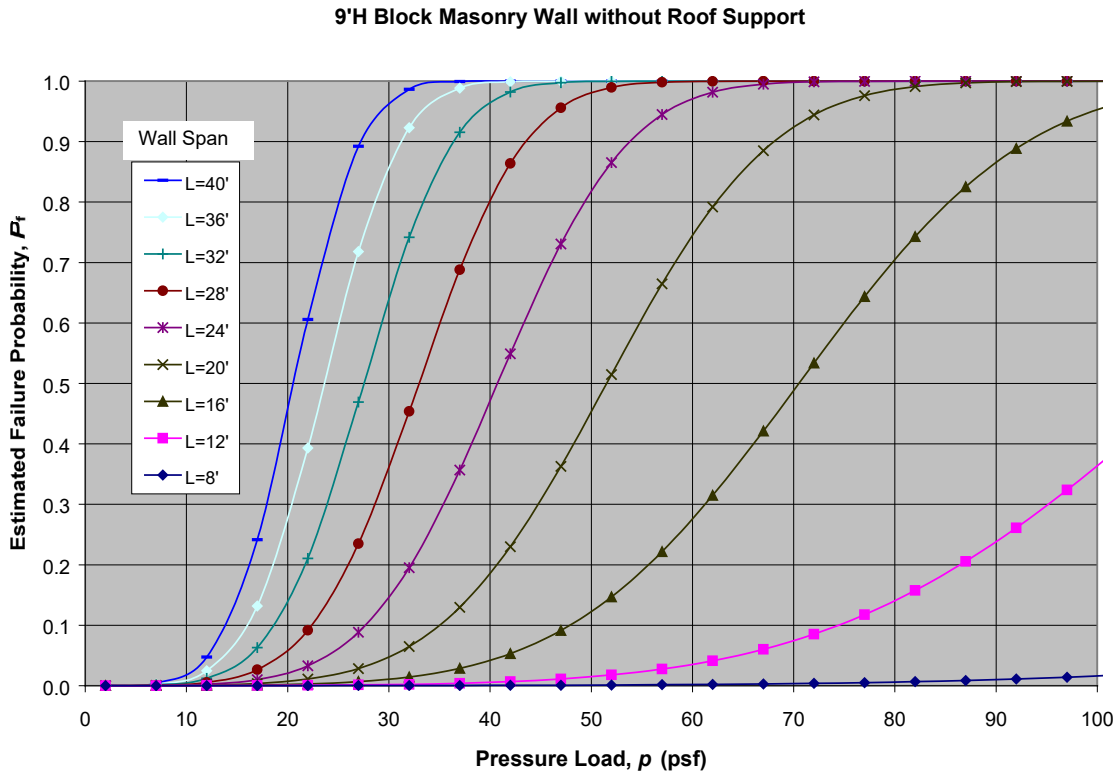


Figure 5-80 Estimated Failure Probability as a Function of Pressure Load for Various Wall Spans without Roof Support

Yield-line theory is used to assess the effects of wall dimensions, support conditions, and orthotropic ultimate moment capacities on the failure of masonry walls. The theoretical results agree well with experimental data. The theoretical results of expected or nominal failure pressure, along with the data on field variability of workmanship and material, provide a useful model for estimating failure probabilities of masonry walls.

5.4.7 Wood Frame Walls

For wood frame walls under lateral loads, post-storm surveys show that failures are nearly always associated with connection failures. Various examples are shown in Figure 5-81, Figure 5-82, Figure 5-83, Figure 5-84, Figure 5-85, and Figure 5-86. This situation is similar to the observation that failures of light-frame roof systems are nearly always a result of inadequate connections rather than the capacities of the elements themselves, as shown by studies and confirmed by anecdotal evidence from post-hurricane investigation (Sparks et al., 1994). Hence, at present, wall failure modeling for wood framed structures is focused on modeling the failure mechanism of the nail being bent and/or pulled out on wall edges that connect the wall to other parts of the structure and connect various components within the wall system.

5.4.7.1 Simplified Structural Model

The main structural components of the exterior walls include the bottom plate, studs, and the double top plates, as well as bracing or sheathing. Figure 5-87 illustrates a typical wall construction. The

present model deals with connections using nails only, which are typical for residential constructions. Figure 5-88 shows the most common nailing pattern as stipulated by the Wood Frame Construction Manual (1995 SBC High Wind Edition, AFPA/AWC, 1996), which is also required by many building codes. Wood frame walls are built by stories. For each story, the bottom plate of the wood frame wall is installed to the floor with two 16d face nails at each of the 16" spaced stations. The wood studs, typically also spaced at 16" on center, are either toe-nailed to the bottom plate with two 8d nails on each side of a stud, or end-nailed to the bottom plate using two 16d nails before it is installed onto the floor. The double top plates are end-nailed to the studs with two 16d nails on each stud. The upper and lower top plates are typically connected together with two 10d face nails at stations of 16" spacing. Ceiling joists or roof rafters are normally toe-nailed to the double top plates of the wood frame wall, with three 8d common nails at each of the 16" spaced stations along the top plate. At the exterior corners of the structure, and sometimes also at the intersections of exterior and interior (partition) walls, multiple studs are typically face-nailed together with 16d nails spaced at 24". The above nailing schedule is mainly based on the Standard Building Code. There are some variations, depending on the codes/manuals used; however, the resulting variation in combined resistance capacity is expected to be relatively insignificant and can be accounted for when needed.



A) Exterior wall fails in sections at connections to other parts of the structure



B) Wall failure at the other side of the same building shown in (a)

Figure 5-81 Examples of Wind-Induced Damage to Residential Wood-Framed Wall System (Oklahoma Tornado Out-Break, May 1999)



B) Wall failure while roof frame still in place



B) This photo reveals that the wall fails at nail connections to the roof and foundation

Figure 5-82 Examples of Wind-Induced Damage to Residential Wood Framed System (Oklahoma Tornado Outbreak



A) Garage wall fails at the connections to the foundation

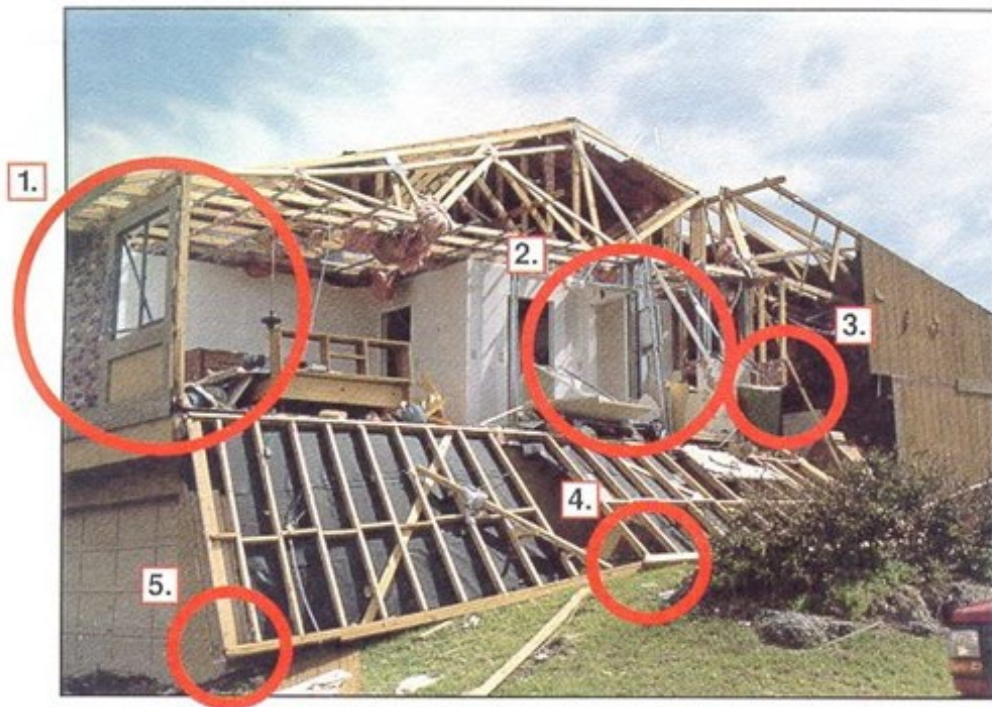


B) A wall section collapses

Figure 5-83 Examples of Wind-Induced Damage to Residential Wood-Framed Wall System (Oklahoma Tornado Out-Break, May 1999)



A) A let-in braced wall section collapses, while other sections also fail at connections to gable end truss



B) Several sections of a let-in braced wall collapse, failed at connections to gable end truss

Figure 5-84 Examples of Wind-Induced Damage to Residential Wood-Framed Wall System (FEMA, 1992, Hurricane Andrew, Florida)



C) End wall separated from end unit of a modular home



D) Another example of gable end wall connection problem

Figure 5-85 Examples of Wind-Induced Damage to Residential Wood-Framed Wall System (FEMA, 1992, Hurricane Andrew, Florida) (concluded)



A) Improper connection in a blown-out wall section



B) Complete failure of a wood framing system

Figure 5-86 Examples of Wind-Induced Damage to Residential Wood-Framed Wall System (HUD, 1993, Hurricane Andrew, Florida)

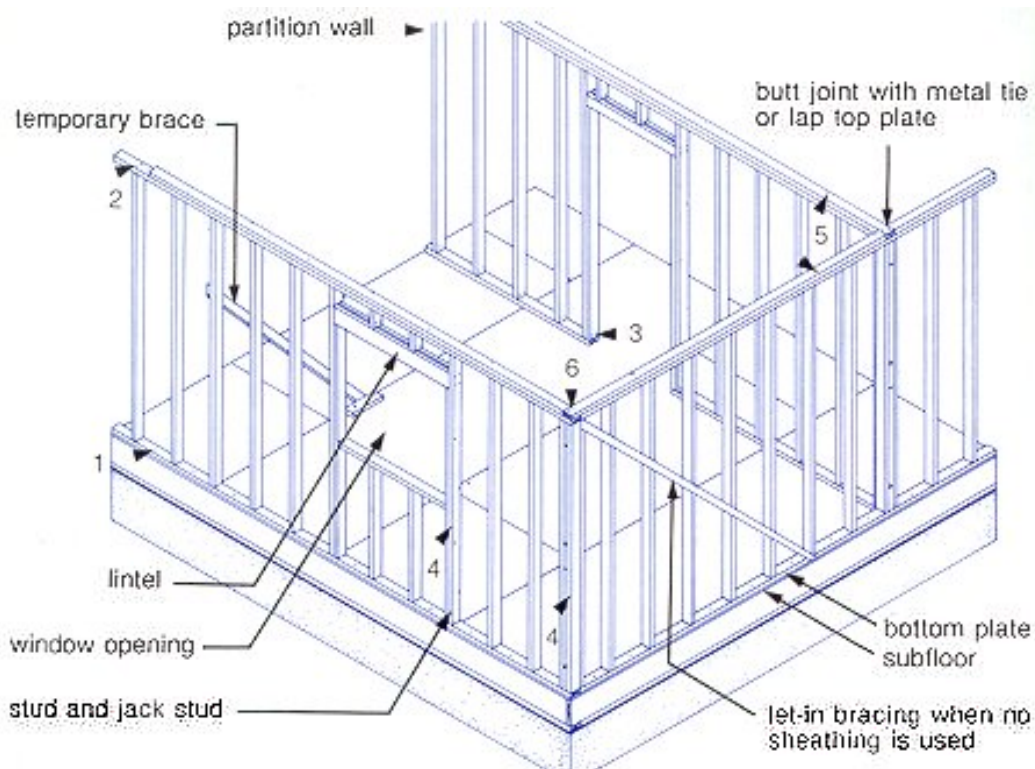


Figure 5-87 Typical Wood Frame Walls for Residential Construction (CMHC, 1989)

Wood frame walls are required to be let-in braced with 1"x4" wood strips at about 45° to plumb or be sheathed with 4'x8' plywood or other structural boards, at least at the corners of the structure. They are nailed to the lower top plate, studs, and bottom plate of a braced wall section. Although the bracing or sheathing is intended mainly to strengthen the wall's resistance capacity for in-plane loads, it also tends to bond the wall components within its span together to react as a unit and share the lateral loads.

The present simple model treats each wall section, which is braced or sheathed together, as a structural unit, and each unit is supported only by the floor(s) and/or roof to resist uniform lateral loading, independent of other similar units. This implies that there would be perfect load sharing horizontally within the unit and no load is transferred beyond a unit. This assumption is a close approximation of the behavior of the wall sections near the mid-span of the wall under uniform pressure loading. Corner units gain additional support from the adjacent wall; however, there normally exist higher suction loads near corners that are not accounted for by the model. These effects on the corner units tend to counteract each other. Thus, corner units are treated the same as interior units in the model. Additional support by interior partition walls is ignored for walls with top support, but it is considered when dealing with walls without top support. In addition, it is assumed that wall openings and their perimeter framing do not decrease nor increase the wall capacity in resisting pressure loads.

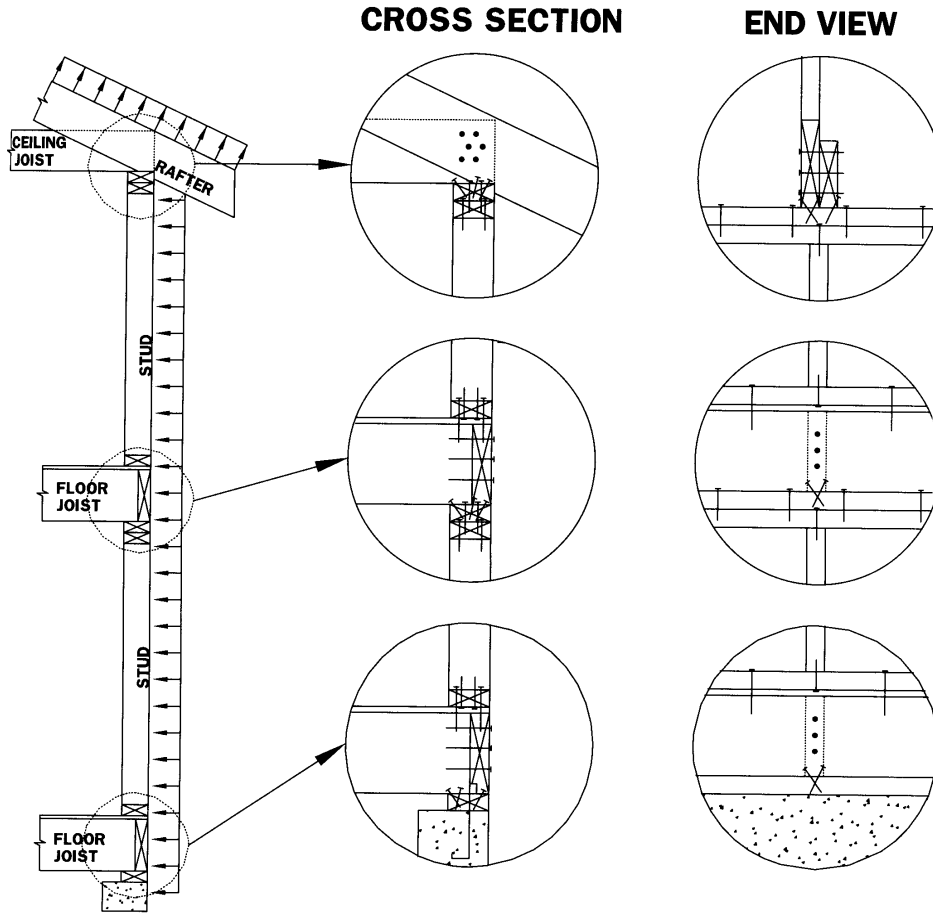


Figure 5-88 Typical Nailing Patterns for Wood Frame Wall Structure of Residential Construction (AFPA/AWC, 1996)

Such a simplified model depicts a span-wise semi-flexible wall structure, versus a completely rigid slab wall model or a completely flexible model (each individual stud reacts independently). It is deemed to be a reasonable representation of the actual system, but Hazus could be improved by properly incorporating the effects of adjacent and partitioning wall supports. The span width of a unit represents the span-wise influence width, by which a gradually varying influence function is approximated with a step function. Thus, the unit width is a critical parameter in the model and its effective value needs to be calibrated when data become available. At present, it is taken to be the bracing width for let-in braced walls, which equals the wall height (normally 8') when 45° bracing is used. For sheathed walls, the 4'x8' sheathing boards are used vertically and also horizontally on some occasions, which provide 4' and 8' bracing widths. Considering the fact that sheathing boards possess higher span-wise load transfer capability and adjacent boards are nailed to the same stud through the entire length of their edge, its effective unit width is also set to 8' in the present model.

Post-storm surveys have indicated that wood frame walls collapse typically in sections. This observation lends some confidence in the concept for the above sectional design of the wood frame wall model.

5.4.7.2 Lateral Failure Load for Nail Connections

A relatively simple way to estimate the resistance capacity of nail connections for various wood materials and products is to use the specified allowable design load data already compiled in the National Design Specification (AFPA/AWC, 1997) and adjust them to expected ultimate failure load with proper “safety factors.” This approach is a practical alternative to collecting and analyzing a large volume of laboratory data, which would be an expensive undertaking given the large number of wood materials and products as well as their widely varying properties for different humidity, temperature, and nailing application methods.

Several types of timber are more commonly used for residential constructions along the East Coast. These include Southern Pine (typical specific gravity, SG = 0.55), Douglas Fir-Larch (SG = 0.50), Northern Douglas Fir-Larch (SG = 0.49), Southern Douglas Fir (SG = 0.46), Spruce-Pine-Fir (SG = 0.42) and Southern Spruce-Pine-Fir (SG = 0.36). The basic lateral design loads for these timbers as compiled from NDS are listed in Table 5-19, along with the values of the applicable adjustment factors for the nailing schedule and applications described in the last section. Since the exact proportions of these timbers’ usage by the industry for residential constructions are not available, their average design value is used to estimate the anticipated ultimate load with proper safety factors. This is equivalent to assuming that the usage is equally distributed among these timbers. The associated root-mean-squared variations and the coefficients of variation due to varied timber usage are indicated in the table. The coefficients of variation range from 0.13 to 0.20.

To some extent, the design loads reflect the expected failure loads with some safety factors. The safety factors may vary from one situation to another since normally a percentile value, often the 5th percentile, derived from the available distribution data of failure loads, is used as the base for determining an allowable design load. The ratio of the mean failure load to this percentile value varies with the coefficient of variation in the data. After being combined with other factors, the final basic allowable design load varies greatly relative to the actual mean failure load. For simplicity, a representative safety factor is desired in estimating the mean or expected failure load from the published allowable design load. Rosowsky and Reinhold (1999) investigated the rate-of-load effects on nail connections for wood. They presented some test results that indicate the ratio of tested lateral failure loads to the NDS allowable design value is about 4, as shown in Figure 5-89. From 16 specimens, Reed et al. (1996) obtained an average withdrawal capacity of 350 pounds for a toe-nail connection using three 8d nails versus an NDS value of 96 pounds, indicating a factor of 3.6. Zaitz (1994) loosely suggested, by referring to the Wood Handbook (“Wood as an Engineering Material,” Forest Products Laboratory, DOA, 1987), that safety factors up to a value of 6 have been used to obtain the allowable loads listed in NDS. The relatively large values of safety factors used may stem from the inherently large variability with nail connections for wood, which is a biological material having highly variable properties and strength itself.

For this present study, a basic safety factor of 4.0 is used for estimating the ultimate loads from the NDS design loads. Some other values in a range from 4.0 to 5.0 are also used depending on specific situations. For example, the safety factors used to estimate the ultimate capacity of the nail connections between the studs and the top plate and those between the studs and the bottom plate are increased to 4.5 and 5.0 for let-in braced and sheathed walls, respectively. This is because the bracing and sheathing are expected to provide additional strength to the connection between these

components. The resulting ultimate lateral failure loads are shown in Table 5-19 and Table 5-20 for the typical nail connections on wood frame walls.

Table 5-19 Estimated Resistance Capacity of Nail Connections within One Stud Spacing (Typically 16”)

Connections	Penny Weight of Nail	Thickness of Side Member (inches)	Resistance of Nail Connections (lbs.)						Average (lbs.)	STD (lbs.)	COV
			Southern Pine (G=0.55)	Douglas Fir-Larch (G=0.50)	Northern Douglas Fir-Larch (G=0.49)	Southern Douglas Fir (G=0.46)	Spruce Pine Fir (G=0.42)	Southern Spruce Pine Fir (G=0.36)			
Joist to Top Plate	8d	0.75	104	90	87	80	70	58	81.5	16.1	0.198
Double Top Plates	10d	1.5	128	118	115	109	96	77	107.2	18.2	0.170
Top Plate to Stud	16d	1.5	154	141	138	131	120	104	131.3	17.5	0.133
Stud to Bottom Plate	8d	0.75	104	90	87	80	70	58	81.5	16.1	0.198
Bottom Plate to Floor	16d	1.5	154	141	138	131	120	104	131.3	17.5	0.133

Table 5-20 Adjustment Factors Required by NDS of Nail Connections within One Stud Spacing (Typically 16”)

Connections	Number of Nails per Connection	Adjustment Factors Required by NDS							Assumed Safety Factor	Reduction Factor for Workmanship	Estimated Ultimate Failure Load (lbs.)
		Duration of Load CD	Wet Service CM	Temp.Ct	Penetration Depth Cd	End Grain Ceg	Diaphragm Cdi	Toe-Nail Ctn			
Joist to Top Plate	3	1	0.85	1	1	1	1	0.83	4	0.75	517
Double Top Plates	2	1	0.85	1	0.84	1	1	1	4	0.8	490
Top Plate to Stud	2	1	0.85	1	1	0.67	1	1	4.5 *	0.8	539
Stud to Bottom Plate	4	1	0.85	1	1	1	1	0.83	4.5 *	0.75	776
Bottom Plate to Floor	2	1	0.85	1	1	1	1	1	4	0.8	714

* 4.5 for Walls with Let-In Braces, and 5.0 for Walls with Sheathing Boards

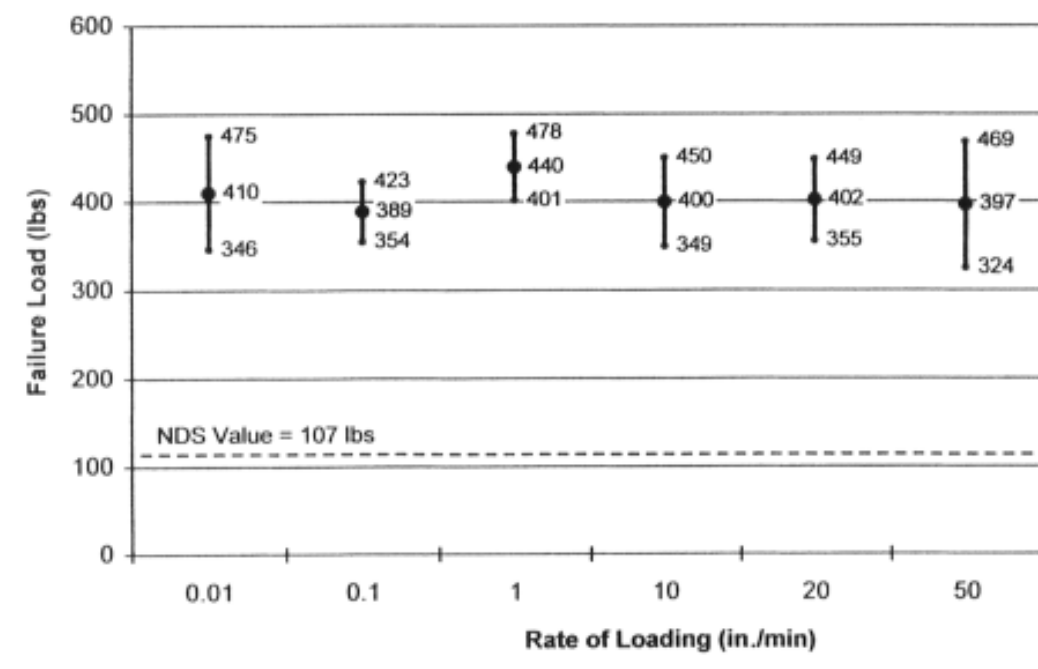


Figure 5-89 Measured Ultimate Capacity (Mean ± 1 Standard Deviation) of 8d Nail Connections for Lateral Loading in Comparison to the NDS Value for Various Rates of Loading

5.4.7.3 Variability and Effects of Workmanship

There exists relatively high variability in the failure load of nail connections for wood. The overall variability in the ultimate capacity of wood structures is associated with such factors as variable properties in similar species of wood, use of different timbers, deviation of installed component’s strength in a full-scale system from component test value, and variable workmanship, etc.

The variability in the strength of the same species of wood is reflected in the laboratory test result variations. For example, Rosowsky and Reinhold (1999) showed a COV of 0.13 for lateral failure load from 10 8d box nail test specimens, and 0.30 for withdrawal load from over 30 8d common nail test specimens. Reed et al. (1996) scored a COV of 0.23 for withdrawal load from 16 8d toenail specimens. The variability of strength among a number of commonly used timbers is represented by COVs ranging from 0.13 to 0.20 (with an average of 0.167) for the typical nailing applications shown in Table 5-19 and Table 5-20, assuming an equal utilization probability distribution for these timbers. Variation of the installed component’s strength in a full-scale system from the component’s test value will also be a significant contributing factor to the overall variability; unfortunately, it is not quantitatively known and it is difficult to estimate. Variable workmanship always plays a role in the reduction of the expected ultimate capacity and in the variability of the ultimate capacity of a structure. For example, missing nails are frequent in residential wood construction. There are no data available for workmanship variability for wood structures, but it may be comparable to that for masonry walls, represented by a COV of 0.25.

The combined strength variability for wood structural systems is difficult to estimate. The combined COV due to the above-identified factors could approximately be a root-sum-square value of the individual COV’s. This would have resulted in a combined COV somewhat larger than any individual COV, the largest of which would probably be that for variable workmanship. Alternatively, when components form a unit in

resisting loads, the components of similar function share the load. For example, within a wall structural unit, as described in the sectional wall model noted above, all nails connecting the bottom plate to the floor tend to share the lateral load simultaneously. Thus, their total capacity will be the sum of the individual capacities and the variability of the sum will be reduced by a factor equal to the square root of the number of nails performing the same function.

Given the above factors, a combined COV value of 0.20 is thought to be a reasonable compromise and is applied in the current version of the model.

5.4.7.4 Probability of Wall Failure

Based on the sectional wall model described above in Section 5.4.7.1, several assumptions are made in order to derive the probability of wall failure:

1. Within a span-wise section, all nail connections for a link between any two components, such as all those between the bottom plate and the floor, simultaneously resist the load passing through this link, in such a way that the total resistance is the sum of the individual capacities.
2. All the links, such as those from studs to bottom plate, from the bottom plate to floor, and from the top plate to ceiling joists or roof rafters etc., form a series system of the section so that the failure of any one of these links results in failure of the section.
3. All sections are identical and form a series system of the wall so that the failure of any one of the sections results in failure of the wall.

With the concept of a sectional wall and the above assumptions, the probability of wall failure, P_f , under uniform pressure load, p , can be formulated as:

Equation 5-13

$$P_f = 1 - \left[\left(1 - \Phi \left(\frac{p \frac{A}{2} - R_1}{0.2R_1} \right) \right) \left(1 - \Phi \left(\frac{p \frac{A}{2} - R_2}{0.2R_2} \right) \right) \dots \left(1 - \Phi \left(\frac{p \frac{A}{2} - R_5}{0.2R_5} \right) \right) \right]^{L/S}$$

Where:

- $\Phi(*)$ denotes the standard normal cumulative distribution function
- R_1, R_2, \dots are the estimated total ultimate capacity of all nail connections for links 1 to 5, respectively, within a section
- $A/2$ represents half of the area of the section since the uniform pressure load is equally divided by the upper and lower supports
- L is the wall span
- S represents the effective section span

Estimated ultimate capacities for the individual connections are given in Table 5-19, and the number of connections equals the effective section span (S) divided by stud spacing.

Examples of P_f versus p for various wall spans, calculated assuming an effective section span, S, of 8', are shown in Figure 5-90 and Figure 5-91 for let-in braced and sheathed walls, respectively.

These results are estimated ignoring the additional supports by adjacent and partition walls. This approximates the case of outward suction loads more appropriately than the case of inward pressure loads. Estimated failure probability for inward loading would be slightly lower than for outward loading of the same magnitude.

For top-unsupported walls, which models the case where the roof has been destroyed and the wall is still standing, the required supports will be transferred to the adjacent or partition walls, and the floor. Walls are normally joined through multiple studs, which are connected, typically, with 16d face nails spaced at 2' (SBCCI,1977). The probability of wall failure is controlled by the failure of the upper nail connections along the joining edge of the adjacent walls. Assuming linear reaction along the height of the supporting walls, the most vulnerable top three connections (i.e., 6 nails) together will approximately share 9/16 of the total pressure load on the wall section spanned between the supporting walls. The failure probability is then estimated by:

Equation 5-14

$$P_f = 1 - \left[1 - \Phi \frac{\frac{9}{16} p H W - R}{0.25 R} \right]^{(L/W)+1}$$

Where:

- H is the wall height (floor to eave)
- W is the typical distance between supporting walls
- L is the total wall span

The resistance capacity, R, is provided by six 16d face nails and is estimated to be 2,142 pounds. The coefficient of variation of 0.25 used here is empirically increased from the value of 0.20 for the case of walls with a top support, due to the uncertainty anticipated with the damage states of roofs and supporting walls.

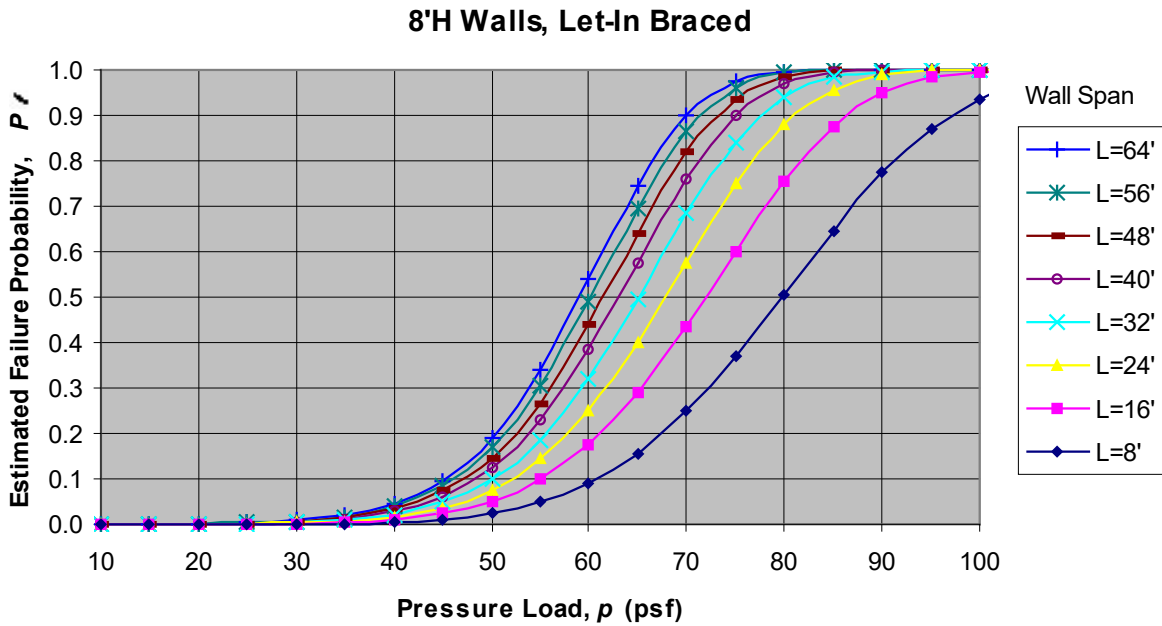


Figure 5-90 Estimated Failure Probability as a Function of Pressure Load for Various Wall Spans, Top Supported and Let-In Braced Wood Frame Walls

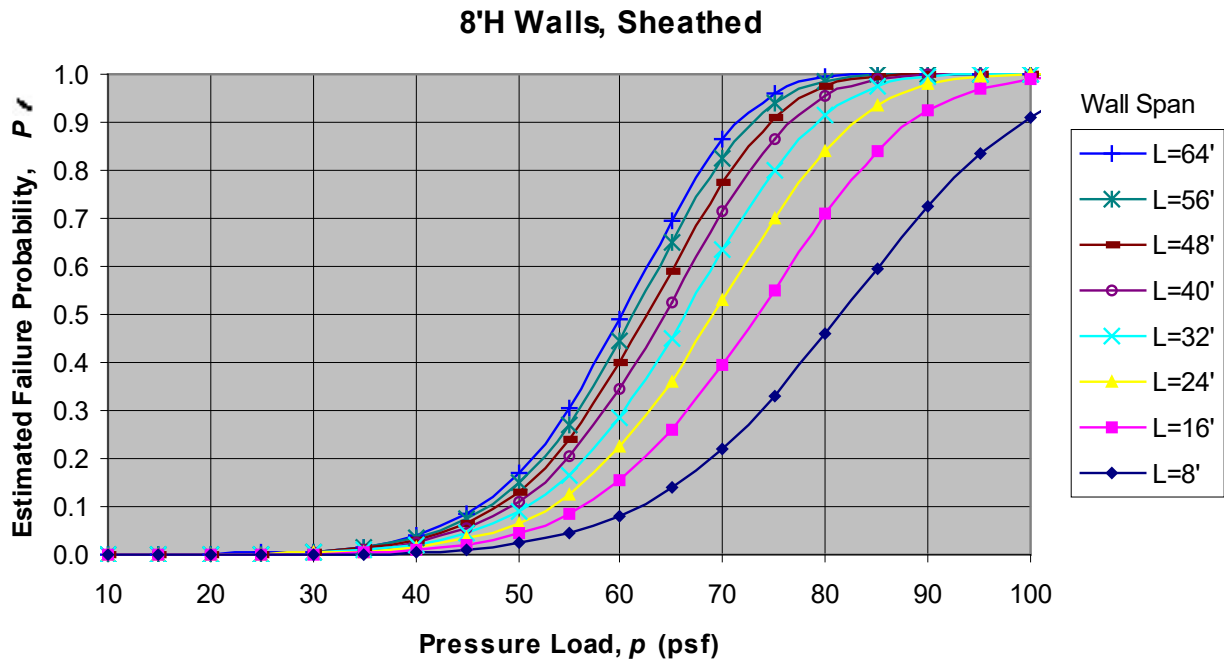


Figure 5-91 Estimated Failure Probability as a Function of Pressure Load for Various Wall Spans, Top Supported and Sheathed Wood Frame Walls

Examples of P_r versus p for various wall spans, calculated assuming a typical distance, W , of 12', are shown in Figure 5-92.

8'H Walls, without Roof Support

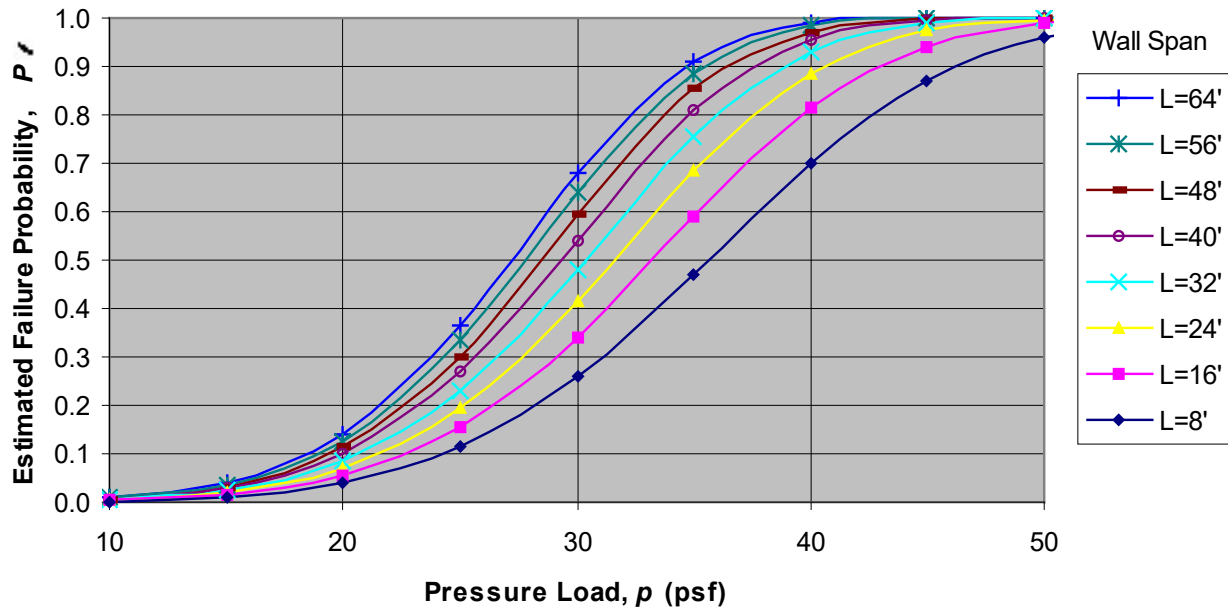


Figure 5-92 Estimated Failure Probability as a Function of Pressure Load for Various Wall Spans, Top Unsupported Wood Frame Walls, Let-In Braced or Sheathed

Based on post-storm observations and suggestions from published literature, wood frame wall failure probability is estimated based on the failure of nail connections between the wall’s double top plate and ceiling joists or roof rafters, and between the bottom plate and the floor, as well as the nail connections of the wood studs to these plates. A sectional wall model, along with the concept of an effective section span, is introduced. A probabilistic failure model has been derived, relating the wall failure probability for given pressure on the wall to the mean capacity and coefficient of variation of individual connections. The mean lateral capacity and coefficient of variation of the nail connections for wood are determined from the analysis of the data available in technical papers and design manuals. For data from design manuals, conversions from the specified allowable design value to the expected ultimate capacity are made using estimated safety factors. Variability of capacity due to various effects is also modeled.

Neither roof weight nor roof uplift is included in the present wall models. It is also recognized that these models ignore some failure modes. These include, for example, the interaction of a wall-roof structural failure in which the wall and roof act as an inter-linked structural system and support each other in resisting different load effects caused by wind, such as the uplift and the lateral forces on the roof, or the lateral forces on walls. The failure of one element may in some cases increase the likelihood of the failure of others.

5.4.8 Manufactured Homes

Manufactured homes are treated separately from single-family homes and engineered structures. The damage model developed for manufactured homes includes a stability failure mechanism (overturning and sliding off its foundations) that is not treated for other buildings. The model also allows for frame failure, which is currently not treated in the modeling of other building types (except roof uplift failures in the case of residential buildings). This section briefly reviews the history of the manufactured home

regulatory environment, which describes how the design criteria changed with time, as well as describing the failure model and presenting examples of predicted and observed manufactured home failures.

A manufactured home is defined as: "...a structure, transportable in one or more sections, which in the traveling mode, is eight body feet or more in width and forty body feet or more in length, or, when erected on site, is three hundred twenty or more square feet, and which is built on a permanent chassis and designed to be used as a dwelling with or without a permanent foundation when connected to the required utilities, ..." (MHCSS, 1992). A brief history of the development of manufactured housing in this country is provided in testimonies of industry leaders before congressional subcommittee hearings on raising standards (U.S. Congress, 1981).

The design and fabrication processes are governed by U.S. Department of Housing and Urban Development (HUD) regulations known as the "Manufactured Home Construction and Safety Standards (MHCSS)" 24 CFR, Part 3280. These standards went into effect in 1976. There were no national statutes covering manufactured homes. There was, however, a national standard entitled American National Standards Institute ANSI A119.1, "Standard for Manufactured Homes." Some states adopted this standard, but even in those states, enforcement was often lax. Homes built in 1976 or later are sometimes referred to as "HUD-code homes."

The original MHCSS wind load provisions were similar to those in ANSI A119.1-1973 (NFPA, 1973), defining two different wind zones (although the zone boundaries differed). Zone I was the standard zone, and Zone II was the Hurricane Zone, extending along the Gulf, Atlantic, and Alaskan coastlines. For structures located in Zone II, the wind loads given in the ANSI provisions required the unit to resist wind loads of 15 psf acting upwards on the roof surface and a wind load of 25 psf acting horizontally on one side wall. As noted above, the wind loads prescribed in the 1976 HUD code were the same as those given in ANSI A119.1-1973, the only difference between the pre- and post-1976 homes being the degree to which the provisions were enforced.

The wind loading requirements were not changed appreciably until 1994, when they were increased in response to years of excessive damage, and particularly in the wake of Hurricane Andrew (HUD, 1994). The 1994 requirements boosted wind loads to levels much closer to ASCE 7 loads, and redefined the wind zones, adding a more stringent Zone III located in southern Louisiana, southern Florida, coastal Alaska, and Hawaii.

Although home construction is regulated by HUD, installation is not. It is left to states and/or local governments. Several states have no tie-down requirements (Louisiana, for example). The manufacturer's responsibility is to provide a homeowner's manual with installation details for the specific model. The American National Standards Institute's Standard A225.1, "Manufactured Home Installations" (most recently A225.1-1994), is a consensus standard for the installation of manufactured homes and minimum construction requirements for manufactured home communities. Model building codes also address the issue of tie-down of manufactured homes (SBCCI, 1991).

The manufactured home damage and loss model is based primarily on the work of Vasquez (1994). The failure modes considered in the model include damage to components and cladding (roof cover, roof sheathing, windows, doors, and siding), stability failures (overturning and sliding), and failure of the main

wind force resisting system (roof uplift and failure of the wall-to-floor connections). For modeling windborne debris, the same model developed for residential buildings is used.

The roof membrane systems on manufactured homes vary considerably and may consist of metal skins attached directly to the roof trusses, or roof sheathing attached to the roof trusses where shingles provide the waterproof layer. The siding of the older manufactured homes typically was comprised of either wood, vinyl, or metal panels. The model manufactured home selected for the development of a first principles-based load-resistance damage model employs metal panel siding and either plywood or OSB roof sheathing.

5.4.8.1 Main Wind Force Resistance Modeling

The nominal resistance of the superstructure of the manufactured home is computed using the wind load criteria for manufactured homes located in Zone II, noted above. The factor of safety assumed in the development of the superstructure resistance functions is assigned a mean value of 1.5 and a coefficient of variation of 25%. If the load acting on the roof of the structure exceeds this nominal capacity, the roof-wall connection is considered to be damaged, but the roof does not fail. A complete roof failure is assumed to occur if the uplift forces on the roof exceed a value equal to 1.8 times the nominal resistance (i.e., 20% higher than the load used to define initial damage to the roof-wall connection). Using this approach, the mean capacity of the roof to resist uplift failure is defined as 15 psf multiplied by the safety factor.

In the estimation of the capacity of the floor-to-wall connections, a simple overturning computation was performed where the manufactured home is loaded with a vertical roof load of 15 psf and a horizontal wall load of 25 psf. The uplift forces at the floor-to-wall connections are determined using moment equilibrium. A nominal factor of safety of 1.6 (COV = 25%) is assumed to apply to the connection capacity for modeling the initial failure, and a 20% increase in this value is assumed to apply for the condition describing a complete failure of the floor-wall connection.

In cases where the roof fails, a wall is considered to fail if the load acting on the wall exceeds 12.5 psf (COV = 25%) (i.e., half the value of load used to design the manufactured home in shear). The above values all apply to post-HUD construction. In the case of pre-HUD code manufactured homes, the nominal resistances for the connections noted above are reduced by 20%.

5.4.8.2 Foundation and Tie Down Modeling

The primary method for anchoring manufactured homes against lateral and uplift loads is soil anchors. These systems have often proven to be unreliable and a major source of damage. Soil types and conditions, anchor types, installation practices, and maintenance all have a tremendous influence on the pullout capacity of the anchors. Kovacs and Yokel (1979) issued a report comparing pullout capacity of common anchors in various soil types with theoretical solutions based on the principles of soil mechanics. They concluded that the soil mechanics theories did not adequately predict pullout capacity. Given the failure of the theoretical approach, Yokel et al. (1982) performed a more systematic, empirical study. It was concluded that typical manufactured home installation practices did not yield anchor performance as required by the standards, and the capacity of the anchors varies significantly with the depth of the anchor, and of course, the soil type. Knowledge of the anchor pullout capacity, the quality of the installation of the anchors and the capacity and corrosion states of the hardware connecting the

anchor to the manufactured home unit is critical in the prediction of the performance of manufactured homes in severe windstorms.

The anchor capacity used here is derived from the Yokel et al. (1982) data as given in Vasquez (1994), where data are given for the pullout capacity of anchors in sandy soils, silty soils, and clay soils, for a range of penetration depths, and direction of the applied load. The results of the Yokel et al. (1982) study are summarized in Table 5-21, Table 5-22, and Table 5-23. As indicated in these three tables, there is significant variability in the ultimate pullout capacity. Note that in Table 5-21, Table 5-22, and Table 5-23 the angles, β , represent the angle of the direction of the pullout force, with 90° representing a vertical load. The selection of the representative resistance characteristics of the manufactured home anchor capacity, which may be expected to realistically model the in-service characteristics of the anchor system, requires significant judgment and cannot be edited in Hazus.

Table 5-21 Results of Field Pull-Out Tests on Soil Anchors Installed and Loaded at Various Angles (Yokel et al., 1982)

Soil Type	Angles β_1/β_2 (degrees)	Load at 102 mm (4") (lbf)		Ultimate Load (lbf)		Maximum Displacement (inches)	
		Mean	COV	Mean	COV	Mean	COV
Silt	60/90	2,967	0.29	7,565	0.15	10.07	0.35
Silt	45/90	1,350	0.19	7,933	0.02	13.85	0.09
Sand	40/90	2,583	0.20	6,187	0.05	9.08	0.07
Clay	40/90	767	0.15	3,267	0.21	18.60	0.20
Silt	60/135	433	0.13	3,387	0.13	25.15	0.04
Silt	45/135	413	0.08	4,243	0.03	33.80	0.04
Silt	15/135	433	0.07	4,775	0.14	54.00	0.05

* Each case based on three tests. All tests conducted under moist soil conditions.

Table 5-22 Results of Field Pull-Out Tests on Fully Embedded Soil Anchors: $\beta_1 = 90^\circ$, $\beta_2 = 90^\circ$ (Yokel et al., 1982)

Soil Type	No. of Tests	Load at 51 Millimeters (2") (lbf)		Ultimate Load (lbf)		Maximum Displacement (inches)	
		Mean	COV	Mean	COV	Mean	COV
Moist Silt	11	4,295	0.20	5,173	0.10	7.17	0.53
Wet Silt	5	2,320	0.40	3,640	0.17	11.04	0.35
Moist Sand	6	4,488	0.13	5,063	0.13	3.82	0.35
Wet Sand	3	5,100	0.17	5,953	0.18	4.35	0.25
Moist Clay	3	3,067	0.22	3,433	0.16	5.83	0.49

**Table 5-23 Results of Field Pull-Out Tests on Fully Embedded Soil Anchors:
 $\beta_1 = 45^\circ$, $\beta_2 = 105^\circ$ (Pearson et al., 1991)**

Stabilizer Plates	No. of Tests	Load at 102 mm (4") (lb _f)		Ultimate Load (lb _f)		Maximum Displacement (inches)			
		Mean	COV	Mean	COV	Horizontal		Vertical	
						Mean	COV	Mean	COV
No	5	662	0.18	2490	0.26	11.3	0.17	3.2	0.63
Yes	19	805	0.41	2578	0.22	16.1	0.26	5.1	0.57

The anchor tie down system used herein, is modeled with a mean capacity of 1,500 pounds/anchor with a coefficient of variation of 35%. No reduction in the foundation capacity is used to model the foundations for pre-HUD manufactured homes. The computation of the forces required to initiate sliding or overturning are made using a static equilibrium analysis following the approach described in Vasquez (1994) and Marshall (1994). A total of five anchors are assumed to be installed for a 60' long unit. In the stability analysis, the weight of the unit is modeled using a mean value of 25 psf (COV = 10%) and a value of 10 psf (COV = 20%) to define the weight of the contents. The combined unit weight of 35 psf is less than the 41 psf value assumed by Vasquez (1994), but higher than the 25 psf value assumed by Marshall (1993). The failure modes considered in the foundation failure analysis include sliding and overturning. Following the definition of manufactured home damage states suggested by Vann and McDonald (1978), the sliding mode of failure is broken into minor and major categories. Major sliding is considered to have occurred if the wind load required to initiate sliding exceeds 1.2 times the nominal sliding resistance.

The cladding components modeled include metal siding, windows, roof sheathing (plywood or OSB) and roof cover (shingles). The same shingle model used on single-family homes is used to model the shingles on manufactured homes. The metal siding is assumed to have a mean resistance of 25 psf (COV = 15%). Failure of the cladding is considered for the case of negative loads only. The nominal resistance of the windows is taken as 32 psf (COV = 18%) for both positive and negative loads. The mean uplift capacity of the roof sheathing is taken as 45 psf.

5.4.8.3 Summary of Failure Modes Considered for Manufactured Homes

The complete list of failure modes considered for manufactured homes is as follows:

1. Roof Cover Loss
2. Roof Sheathing Loss
3. Window Breakage (Pressure and Windborne Debris)
4. Siding Failure
5. Roof-Wall Connection Failure (Minor)
6. Roof-Wall Connection Failure (Major)

7. Wall Failure Following Roof Failure
8. Floor-Wall Connection Failure (Minor)
9. Floor-Wall Connection Failure (Major)
10. Foundation Failure (Minor Sliding)
11. Foundation Failure (Major Sliding)
12. Foundation Failure (Overturning)

5.4.9 Roof Covers on Flat Roofs

This section describes the model used to estimate wind-induced damage to roof covers on flat roofs. The two roof cover systems modeled are built-up roof covers and single-ply membrane covers. For both roof types, the failure of a roof cover system is initiated by the failure of the flashing.

- *Built-up Roof Covers:* Built-up roof (BUR) covers are composed of multiple plies of roofing felts adhered to each other and to the insulation substrate with a full mop of hot asphalt, coal tar or cold adhesive. The number of plies of roofing felt ranges from three to five. Roofing felts are commonly made of polyester, organic or glass-based materials. The surfacing on BUR covers is most often gravel or slag.
- *Single-ply Membrane Covers:* Single-ply membrane (SPM) covers are normally attached to the insulation substrate by adhesives (hot asphalt or cold applied materials) or by mechanical fasteners. Adhered SPM covers can be fully adhered or partially adhered. The adhesive in partially adhered SPM covers will typically have 50% coverage in the central portions of the roof and greater coverage at or near the edges and corners of the roof. Common membranes are thermoplastic membranes, thermoset membranes, modified bitumen membranes, and liquid applied membranes.

Most wind-induced failures of BUR and SPM covers are initiated by the failure of the perimeter flashing. When the flashing fails due to wind suctions, the wind can peel back the roof cover membrane at the newly exposed edge and, depending on how well the roof cover is attached to the substrate, the peeling failure can continue throughout the storm and result in large-scale damage to the roof cover system. Another failure mode is bubbling, where the roof cover is separated from the substrate by wind-induced suctions. If the bubbled area expands to an area where the roof cover is torn or missing, the airflow may “balloon” the bubbled area and the roofing membrane may tear, provided the resultant forces exceed the tearing strength of the membrane. Subsequent damage may then occur due to peeling at the newly exposed edges of the roof membrane. A bubbled section of the roof membrane may also become breached by impact from flying debris or by tearing at the perimeter of the bubble.

The capacity of the flashing varies significantly between manufacturers and mainly depends on the flashing shape and size, how the flashing is fastened to the roof (e.g., cleated versus uncleated), and the quality of the installation. The flashing on a properly designed roof system complying with the minimum Factory Mutual Research Corporation roof system uplift rating (i.e., FM 1-60), should have a horizontal

resistance equal to 45 psf. This equates to 22.5 plf (pounds per linear foot) for typical 6” wide flashing. For the purposes of modeling flashing failure, the resistance of the flashing to horizontal wind suction is taken as having a mean value of 22.5 plf and a coefficient of variation of 30%.

The roof cover damage model samples resistances from normal distributions with the means and standard deviations shown in Table 5-24. These roof cover resistances are based on a combination of engineering judgment and on data obtained from a survey on roof cover types conducted in Palm-Beach, Broward and Miami-Dade counties. The survey showed that the majority of the roof covers complied only with the minimum Factory Mutual Research Corporation roof system uplift rating. The minimum uplift rating (i.e., FM 1-60) corresponds to a static test pressure of 60 psf.

Table 5-24 Roof Cover Damage Model - Normal Distribution Parameters

Roof Cover System	Roof Cover Peeling Resistance		Roof Cover Bubbling Resistance		Flashing Resistance	
	Mean(psf)	COV(%)	Mean(psf)	COV(%)	Mean(psf)	COV(%)
BUR Cover	50	15	150	15	22.5	30
SPM Cover (adhesive)	40	15	60	15	22.5	30
SPM Cover (mech. fasteners)	40	15	60	15	22.5	30

The flashing resistance and roof cover resistances shown in Table 5-24 are used for “average” quality construction. Another result of the roof cover survey mentioned above is that approximately 50% of the existing roof covers in Miami-Dade, Broward and Palm Beach counties are classified as being of “poor” quality. Owing to the variability in the quality of materials and installation of existing roof cover systems, an additional resistance model was added to represent “poor” quality roof covers. The resistances associated with the “poor” quality roof cover system are 30% lower than those listed in Table 5-24. Also, an additional model was added to represent “good” quality roof cover systems, which are modeled with failure capacities 50% higher than those associated with “average” quality roof covers listed in Table 5-24. Note that this 50% increase is consistent with the increase in the test pressure associated with moving the Factory Mutual Research Corporation uplift rating from the minimum rating (FM 1-60) to the next discrete level (FM 1-90).

In the roof cover damage model, the roof area is divided into square elements of equal area (e.g., 4 square feet). The square elements are assigned directionally dependent loads according to the ASCE wind loading provisions. The loads assigned to the flashing are set according to the vertical suction loads assigned to the adjacent roof cover elements multiplied by a factor. The factor transforms the vertical suction acting upward on the roof near the edge to a horizontal suction acting outward on the wall near the same edge. A factor of one is chosen for all flashing, whether located at a corner or at edges away from the corners. The factor of unity is a simplified approximation based on full-scale measurements of flashing loads made at Texas Tech University (McDonald et al., 1997). In the full-scale flashing tests, the ratio of the horizontal force to the vertical force estimated near the roof edge varied significantly between different flashing styles.

The final estimate of both the effective loads and the resistance of the roof flashing is subject to significant uncertainties, but the limited comparisons of simulated and modeled roof damage states performed to date show the model yields reasonable results.

In the damage model, a failed roof cover element implies that it has been removed and the associated roof substrate area is exposed to rainwater. On the other hand, bubbled roof cover areas will not expose the underneath roof surface area to rainwater. The roof cover damage algorithm performs the following four checks at each time step within a storm simulation:

1. All non-failed flashing is checked for failure. When a piece of flashing fails, the adjacent roof cover elements also fail.
2. All non-damaged roof cover elements adjacent to failed roof cover elements are checked for peeling failure.
3. All non-damaged roof cover elements are checked for bubbling.
4. All bubbled areas that have migrated to a failed portion of the roof cover are failed.

The roof cover damage model yields failed roof cover only when the flashing fails. The only damage that results if the flashing remains intact is bubbling of the roof cover, which, as stated above, will not expose the roof substrate to rainwater. Upon further development of the roof cover damage model, bubbled roof cover areas will also be checked for tearing at the bubble perimeter and for membrane breaches caused by windborne debris impacts.

5.4.10 Open-Web Steel Joist Roof System

Light weight Open-Web Steel Joist (OWSJ) roof systems represent an efficient and inexpensive means to design and build a roof system to resist gravity loads. The joists consist of steel members that make up the top chord, bottom chord, and the web. The top and bottom chords are usually a set of two equal or unequal angle members. The web may either be angle or bar members, depending on the span and depth of the steel joist. Under normal loading, the steel joist is designed for compression in the top chord and tension in the bottom chord (Steel Joist Institute, 1998). The top compression member is often braced by the roof deck connected to the upper chord of the joist, preventing buckling of the top chord. If the uplift pressures are greater than the dead loads of the steel joist, then the joist members undergo a stress reversal. The bottom chord members, which were designed for tension, now reverse to compression. If the bracing of the bottom chord of the joist is inadequate, this stress reversal may cause the bottom chord to buckle, failing the steel joist. The buckling of the bottom chord of an OWSJ is one of the two more commonly observed wind-induced failure modes associated with OWSJ roof systems. The other is the failure of the roof-wall connection (uplift failure), which is often associated with inadequate anchoring.

Steel joists are commonly used in light weight commercial structures, such as shopping malls, storage facilities, schools, warehouses, etc., and are usually simply supported. The OWSJ roof system can be used in combination with all steel buildings as well as buildings where the joists are supported by reinforced or unreinforced masonry walls. Different types of roof-wall connections are used to anchor steel joists,

depending on the type of wall construction. The most common types of construction and anchorage are as follows:

- *Steel Frame Construction:* For steel frame buildings, the open-web joists are usually welded to the building frame at both ends of the joist. The welded connection is designed such that the uplift capacity of the connection exceeds the design uplift load, but in no cases shall the welded connection be less than two 1"x1/8" fillet welds. Open-web joists may also be bolted at each end using a minimum of two 1/2" bolts on each side of the joist. Steel bearing plates are not usually used in fastening steel joist to steel frame construction.
- *Reinforced Masonry Construction:* In buildings constructed with reinforced masonry walls, the open-web joists are anchored to a tie beam or bond beam. The anchorage consists of a minimum of 1/2" diameter anchor bolts or 1/2" (#4) reinforcing bars not spaced more than 6' on center. If the beam is at least 8" deep and has a minimum continuous reinforcement of 0.2 square inches at the top of the wall, then the anchorage is either welded to or hooked tightly around the longitudinal reinforcement in the beam. The bolts or reinforcing bars need to be extended into the wall a minimum of 6". To complete the roof-wall connection, either the joist is bolted to the anchor bolts or the reinforcing bars are bent over each side of the joist and then welded. Steel bearing plates are not usually used when connecting steel joists to reinforced masonry walls. If the tie beam or bond beam is less than 8" deep, then the masonry wall is considered unreinforced masonry.
- *Unreinforced Masonry:* In buildings constructed with unreinforced masonry walls, steel bearing plates are more common due to the fact that the bearing capacity of unreinforced masonry walls is less than that of either steel frame or reinforced masonry construction. The joist is usually anchored to the wall using J-bolts with a length of 6" or 1/2" bolts with a length of 15". A steel plate is attached to the head of the 15" bolt with a minimum surface area of 6 square inches which is fully embedded into the masonry. If bearing plates are used, the plates are welded to the joist and then anchored to the masonry wall using the 6" J-bolts or the 15" bolts. The welding of the joist to the steel plate follows the same requirements mentioned in steel frame construction.

The uplift capacity of OWSJ anchored to unreinforced masonry walls is much less than the resistance of the joists anchored to reinforced masonry walls since the walls do not contain bond beams or tie beams with reinforcement to which the anchorage can be welded to or wrapped around (NRC, 1991).

As discussed earlier, most steel joist failures occur due to inadequate roof-wall anchoring or from buckling of the bottom chord of the steel joist. The uplift damage model developed herein considers the failure of the roof-wall connection at the weld connecting the joist to either a steel bearing plate or a larger steel beam and the failure of unreinforced masonry walls at the mortar interface between blocks. In the case of reinforced masonry walls, the failure of the wall associated with the uplift loads acting on the joist is not considered (i.e., the welded connection will always fail before the wall fails).

5.4.10.1 Uplift Resistance

The possible failure modes modeled for the steel joist roof-wall connection are the failure of the welds between the steel joist and the steel bearing plate and the anchorage failure between the bearing plate

and the unreinforced masonry wall. If a bearing plate is not present, then the failure mode is between the steel joist and the unreinforced masonry wall.

5.4.10.2 Steel Joist and Steel Bearing Plate

The steel joist is welded to the steel bearing plate using a minimum of two 1"x1/8" fillet welds. Larger steel joists may require larger welds. The resistance of the joist/plate connection is based on the design strength of the welds using AISC Manual of Steel Construction (LRFD method) Second Edition Specifications (AISC, 1995).

The weld metal, the plate metal or the joist metal are the three possible failure modes for this type of connection. Each are calculated using the number of welds, the length of each weld and the size of the weld. The lesser of the following three resistances is used to calculate the combined resistance for this type of connection. All capacities are based on the design procedure as given in AISI 8-129.

5.4.10.3 Resistance of the Weld Metal

The nominal resistance of one weld is:

Equation 5-15

$$R_n = F_w * A_w$$

Where:

- F_w is the nominal tensile strength of the weld material ($F_w = 0.60 F_{EXX}$ in pounds per square inch)
- A_w is the effective area of the weld ($A_w = \text{Length} \times \text{Throat}$) in square inches
- F_{EXX} is the classification strength of the weld metal for an EXX electrode in pounds per square inch, Throat is the effective throat thickness ($\text{Throat} = 0.707 \times \text{Size}$) in inches, Size is the size of the fillet weld in inches

5.4.10.4 Resistance of the Plate Base Metal

The nominal resistance of the plate metal is:

Equation 5-16

$$R_n = F_{bm} * A_{bm}$$

Where:

- F_{bm} is the nominal tensile strength of the plate material in pounds per square inch
- A_{bm} is the effective cross-sectional area of the plate ($A_{bm} = \text{Effective Width of Base Metal} \times \text{Thickness}$) in square inches

5.4.10.5 Resistance of the Steel Joist Base Metal

The nominal resistance of the joist metal is:

Equation 5-17

$$R_n = F_{bm} * A_{bm}$$

Where:

F_{bm} is the nominal tensile strength of the joist material in pounds per square inch

A_{bm} is the effective cross-sectional area of the joist metal (A_{bm} = Effective Width of Base Metal x Thickness of Base Metal) in square inches

The steel bearing plate is usually A36 steel with a yield strength of 36,000 psi and the joist steel yield strength is 50,000 psi. The type of weld electrode commonly used with A36 steel is an E70 Electrode.

5.4.10.6 Example Minimum Uplift Capacity

A typical open-web steel joist with a span of 40' normally has a chord thickness equal to 3/16". The steel bearing plate has a thickness of 3/16". An E70 Electrode was used to produce 1/8" fillet welds with a total length of 2", 1" on each side of the joist. The resistances of each of the three cases are as follows:

- *Resistance of the Weld Metal: 7,424 pounds*
- *Resistance of the Plate Base Metal: 9,000 pounds*
- *Resistance of the Steel Joist Base Metal: 12,500 pounds*

In this example, the limiting failure mode is the failure of the weld metal at a nominal value of 7,424 pounds.

5.4.10.7 Steel Bearing Plate/Steel Joist and the Wall Anchorage.

The resistance of the wall anchorage for both the steel bearing plate and the steel joist without bearing plate are based on the same procedure. Experimental uplift failure tests have been performed at Clemson University (Leland, 1988) on anchors with embedment depths of 6" and 15" into walls 6' in length. The wall length of 6' was to simulate the Standard Building Code requirements for a maximum spacing not more than 6' on centers. The resistances of this type of connection are highly variable because it relies on the tensile bond strength between mortar and masonry units (Leland, 1988). Table 5-25 presents a summary of the uplift test results.

Table 5-25 Uplift Resistances of an Unreinforced Roof-Wall Anchor, 6' O.C.

Type of Roof-Wall Anchor	Mean	COV
6 ² embedment J-Bolt Anchors	3,312 lbs.	42%
15 ² embedment Anchor with 6 in ² endplate	4,868 lbs.	46%

5.4.10.8 Bending Resistance

In the case of bending failures, there is not enough information on member sizes, depth of the joist, etc., to permit a detailed engineering estimate of the capacity of the joist, which would require examining the various bending failure modes (i.e., bottom flange buckling, bottom chord yielding and web members yielding or buckling). The capacity of the OWSJ to resist moments associated with the wind induced loads are based on the maximum uplift moments computed using the Standard Building Code (SBC) wind load requirements on a simply supported steel joist. No information on the actual mode of bending failure is known, although buckling probably represents the actual limit state.

5.4.10.9 Prediction of Joist Failures

The premise behind the joist failure model is the same as the other failure models described herein, in that at each time step during a hurricane simulation, the loads acting on the joists are compared to the sampled resistances, and if the load exceeds the sampled resistance, the joist is assumed to fail. In the case of moment failures, if the computed wind induced bending moment exceeds the sampled moment resistance, the joist is assumed to have buckled and can carry no more load. The portion of the wind load acting on the joist that exceeds the buckling load is then distributed to the neighboring joists. Each joist is checked to determine if failure has occurred. If failure has occurred, the excess load is redistributed. After all joists have been checked for failure, the checking process is repeated, considering the redistributed loads. The load redistribution process continues until all redistributed loads have been proportioned to joists that have not failed, or all joists have failed. In the case of an uplift connection failure, the joist is not able to carry any load, and thus all of the wind loads acting on the joist must be distributed to the neighboring joists.

At any time during a damage simulation, the uplift reaction loads (R_A and R_B) at either end of the joist, and the bending moment (M) at the center, are computed from the following:

Equation 5-18

$$R_A = q_H C_{f_l} l w - (L + D) l w / 2 + p_i w l / 2$$

Equation 5-19

$$R_B = q_H C_{F_B} l w - (L + D) l w / 2 + p_i w l / 2$$

Equation 5-20

$$M = q_H C_M l^2 w - (L + D) w l^2 / 8 + P_i w l^2 / 8$$

Where:

q_H	is the dynamic pressure at roof height (based on the peak gust wind speed at roof height)
C_{FA} and C_{FB}	are the directionally dependent uplift coefficients for the reaction at each end of the joist
C_M	is the directionally dependent mid-point moment coefficient
l	is the span
w	is the distance between joists
L and D	are the live and dead loads
p_i	is the internal pressure

The uplift and moment coefficients are computed using the influence line approach described earlier.

5.4.10.10 Example OWSJ Failure Probabilities

No quantitative statistical studies examining the performance of buildings with OWSJ roofs in hurricane winds have been performed to enable the failure model to be quantitatively evaluated. Thus, the modeled results presented here are not compared to any full-scale performance data and are given only to show the reasonableness of the predicted failure rates.

In the examples given, two simple rectangular buildings were modeled. Each building has a length of 180' and a width of 40'. The 40' width is spanned by OWSJs spaced at 6' on center. One building has a roof height of 12', and the other building has a roof height of 20'. On the front side of the building, there are a total of twelve windows having dimensions of 6' high and 12' wide, and six glass entry doors, each of which is 6'8" tall and 3' wide. At the rear of the building, there are six non-glazed entry doors. The roof deck is assumed to be comprised of lightweight metal with a BUR cover. The roof system is designed to resist the wind loads as prescribed in the SBC Wind Load Provisions for a structure located in the 100 mph (fastest mile) wind zone. Joists designed to meet the loads applied in the more highly loaded end-zones are assumed to be used throughout the roof system. The dead and live loads used in the design of the joists are 6.25 and 25 psf, respectively. The buildings are assumed to be constructed in a terrain described by a typical suburban environment (i.e., $z_0 = 0.35$ meters), with the windborne debris environment represented with the residential model. In the damage simulation, if a window is breached, the internal pressures are assumed to act over the entire underside of the roof. The mean value of the bending resistance of the joist is taken as 1.3 times the design value. The COV is assumed to be equal to 20%. The resistance factor associated with the welded connection for uplift is assigned a mean value of 1.5 with a COV of 20%.

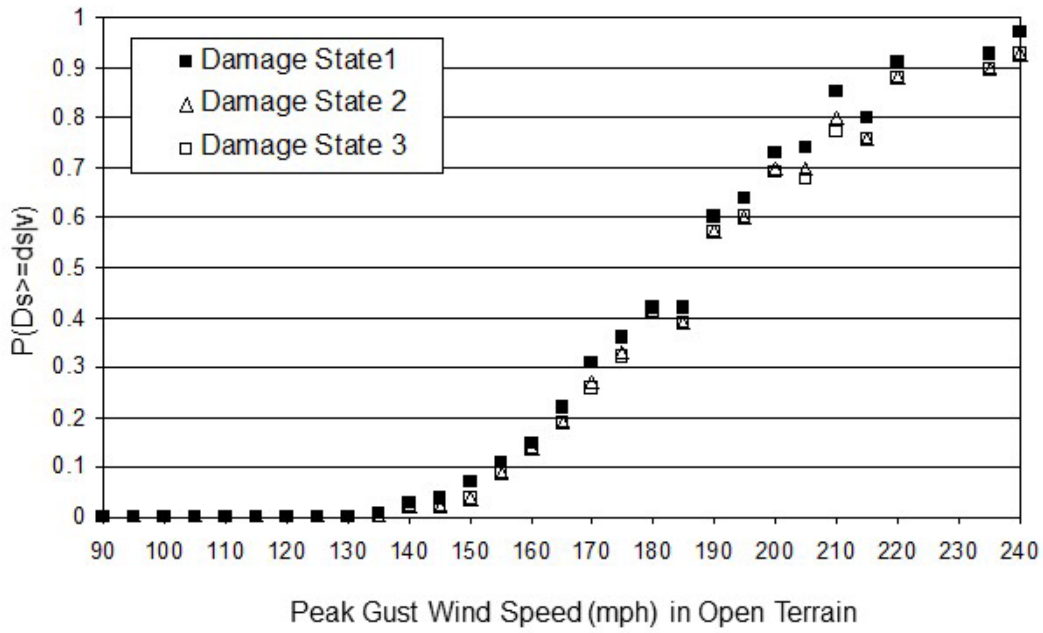
The probability of joist failure as a function of wind speed is developed by passing hurricane wind speed traces past the buildings. The hurricane wind speed traces used to develop the joist failure probabilities shown in Figure 5-93 and Figure 5-94 are the traces derived from a 20,000-year simulation of hurricanes

in the South Florida area. Results are given for both the reinforced and unreinforced masonry wall case. Note that for modeling purposes, the performance of joists on steel frame buildings is the same as the performance of joists on reinforced masonry buildings. In the damage simulation model, the number of failed joists and the peak wind speed produced by the storm is retained and used to develop the damage state curves given in Figure 5-93 and Figure 5-94. Damage states 1, 2, and 3, noted in Figure 5-93 and Figure 5-94, represent the following:

- *Damage State 1*: at least one failed joist, but less than 25% failed joists
- *Damage State 2*: at least 25% failed joists but less than 50% failed joists
- *Damage State 3*: more than 50% failed joists

Note that for a given building, the damage state curves, given in Figure 5-93 and Figure 5-94, are very close together, indicating that once a single joist has failed, the likelihood of other joists failing immediately afterwards is high, implying a system with little redundancy.

Unreinforced Masonry Walls, H = 12'



Reinforced Masonry Walls, H = 12'

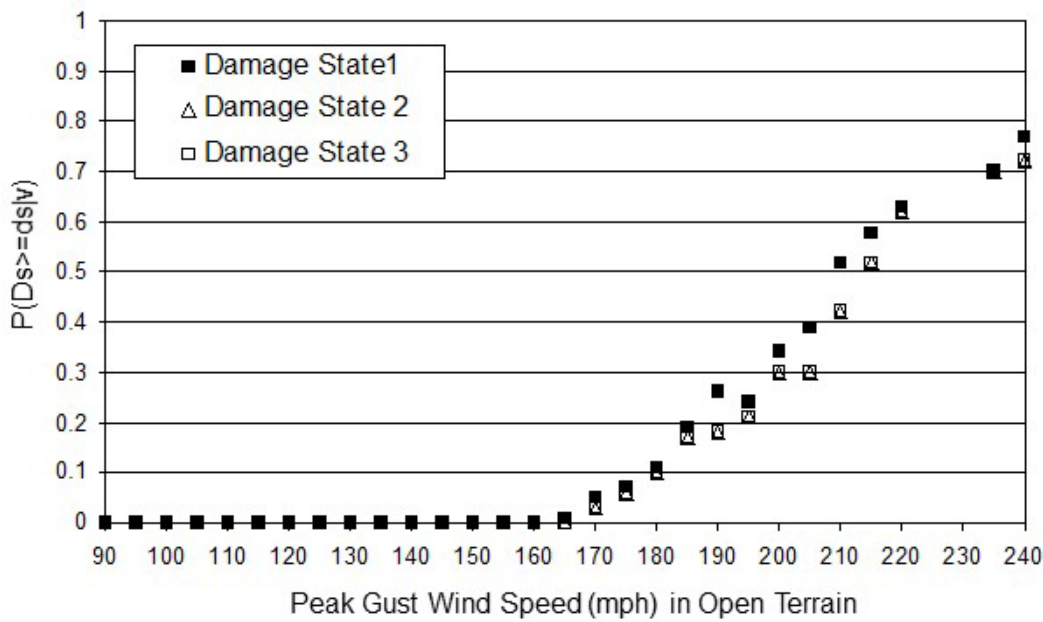


Figure 5-93 OWSJ Roof Damage States for a 12' High Building in Suburban Terrain

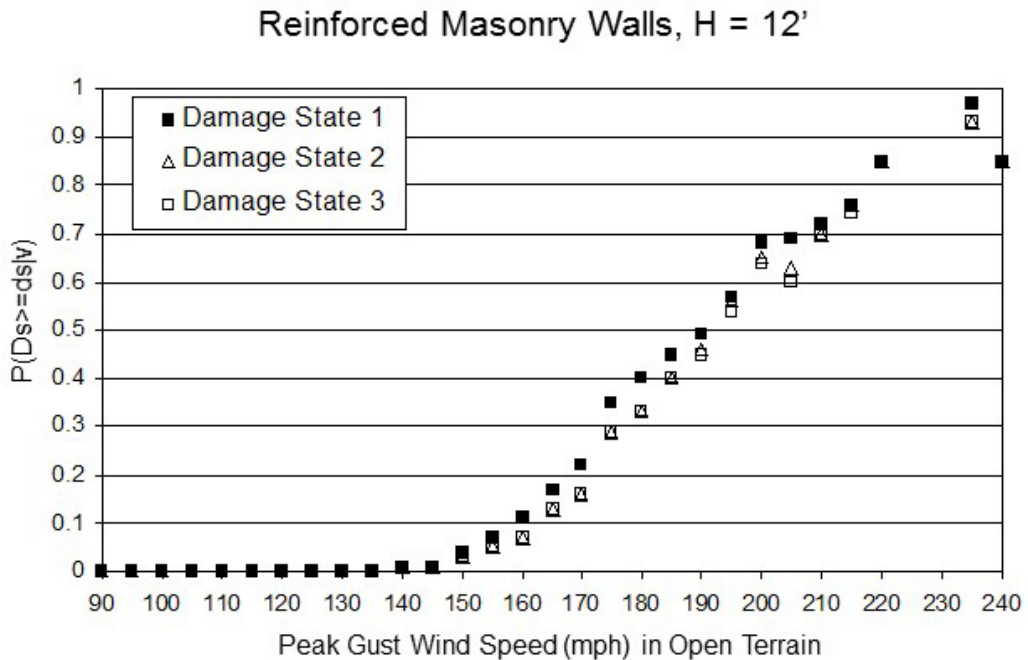
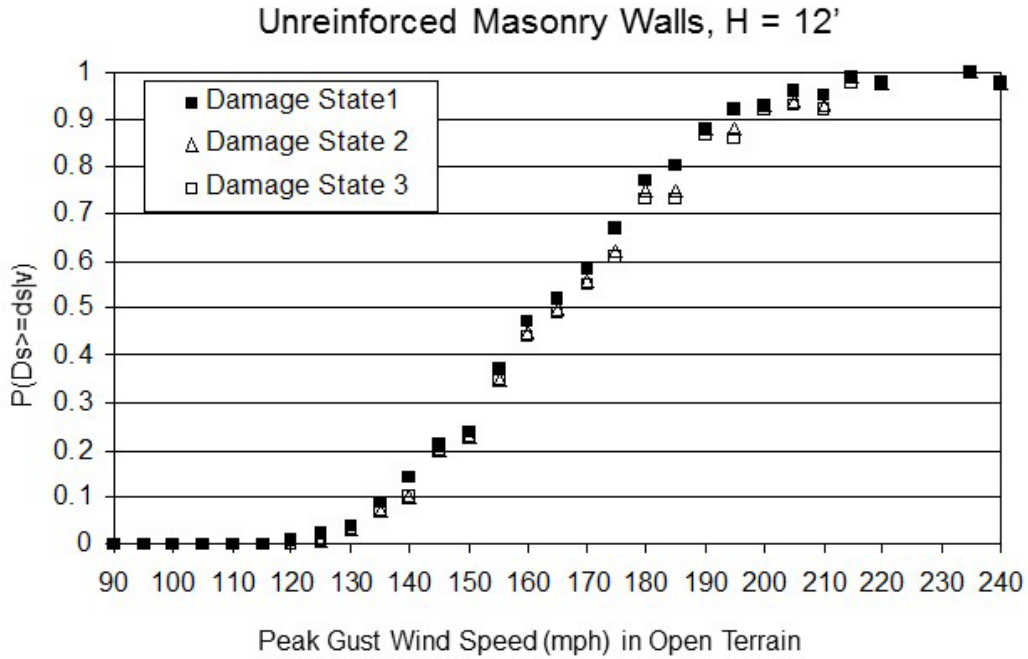


Figure 5-94 OWSJ Roof Damage States for a 20' High Building in Suburban Terrain

5.4.11 Metal Deck on Open-Web Steel Joists

Metal decks on steel joists are frequently used as the primary roof deck system for both steel buildings and concrete/masonry buildings. The performance of these metal decks in high wind events varies with deck size, thickness, attachment method, joist spacing, quality of installation and number of fasteners. The approach taken here to estimate the uplift capacity of a metal deck panel is to design some typical

systems using the requirements given in AISI (1996) and then perform a failure analysis using a finite element model.

The approach involves the selection of the fastener requirements to meet the design loads, coupled with a review of recent experimental studies examining the resistance of screwed and welded connections. Given these inputs, a stochastic finite element study is used to determine the failure loads.

This section describes the methodology used to estimate the uplift capacity for two example cases; however, the approach is general and can be applied to any configuration of metal deck roof systems.

5.4.11.1 An Overview of Metal Decking

The metal deck is made from cold formed structural grade sheet steel that conforms to ASTM Designations A611 Grade C, D, or E (for painted deck) or A653 Grade 33, 40, 50, or 80 (for galvanized deck) (USD, 1997). The minimum yield strength of the steel is 33 ksi. The metal deck can be categorized into four types (i.e., A, B, F, and N) according to different profiles of the ribs. Table 5-26 lists the profiles, nominal thickness ranges and weight ranges of these four deck types. Standard deck widths vary from 12" to 36" with an increment of 6" (the length will vary depending on the spacing of bar joists). Typical thicknesses of the metal deck are 16, 18, 20, and 22 gauges.

Table 5-26 Nominal Deck Information, from SDI (1992)

Deck Type	Name (profile)	Nominal Thickness Range	Weight Range
Type A	1-1/2"x6" Wide Rib (WR)	0.03" to 0.06"	2 psf to 4 psf
Type B	1-1/2"x6" Intermediate Rib (IR)	0.03" to 0.06"	2 psf to 4 psf
Type F	1-1/2"x6" Narrow Rib (NR)	0.03" to 0.06"	2 psf to 4 psf
Type N	3"x8" Deep Rib (WR)	0.03" to 0.06"	2 psf to 4 psf

The metal decks are attached to the building frame with arc puddle welds, self-drilling screws, or powder-actuated or pneumatically-driven pins. Sheet to sheet fastening is performed with screws, button punching (crimping) or welds. The deck is end-lapped a minimum of 2" with the overlapping occurring at the location of the supports. The minimum end bearing is 1-1/2". According to SDI (1992b), the common connection layout patterns are:

- 36" (width) deck: 36/9, 36/7, 36/5, 36/4 for 2" or 3" composite, and 36/3
- 30" (width) deck: 30/6, 30/4 and 30/3
- 24" (width) deck: 24/4

Where, for example, 36/N represents the number of fasteners, N, across the 36" width of the panel.

5.4.11.2 Screwed Decks

In determining the parameters for the case studies, two types of fasteners were considered: screws and welds. Screws are most often #12 or 1/4" diameter when fastening the roof deck to structural members. Sheet to sheet connections (also known as stitch connections) usually use self-drilling #8 or 1/4" diameter screws. Table 5-27 presents the properties of typical screws used to fasten the steel decks to

the underlying structural roof system. Screws can be installed either at the valley or at the crest of the metal deck with or without washers (in this investigation, all the screws are assumed to be valley-fixed).

Table 5-27 Typical Screw Properties

Screw Size	d, Diameter (in)	D _w , Nominal Head Diameter (in)	Avg. Tested Tensile Strength (kips)
10	0.190	0.415 or 0.400	2.56
12	0.210	0.430 or 0.400	3.62
1/4	0.250	0.480 or 0.520	4.81

For a screw-connected roof panel, post storm damage investigations following extreme wind events have shown that the two most common steel deck failure modes are: (1) a pull over failure, where the metal deck pulls over the fastener and (2) a pull-out failure where the screw pulls out from the structural steel member. The thin steel sheathing often pulls through (pulls over) the screw heads due to either the large stress concentration around the fastener holes or fatigue under wind fluctuations. Pull through failures can occur when very thin high-strength steel battens or purlins are used, and the screw fasteners can be pulled out of the steel battens or purlins. The American standard (AISI, 1996) provides two different formulas for these two failure modes:

The pull-over strength, P_{nov} (kips), is given as:

Equation 5-21

$$P_{nov} = 1.5t_1 d_w F_{ult}$$

Where:

- t₁ is the thickness of the deck (in)
- d_w is the diameter of the washer or head of screw (in)
- F_{ult} is the tensile strength of the deck metal (ksi)

The pull-out strength, P_{not} (kips), is given as:

Equation 5-22

$$P_{not} = 0.85t_c d F_{ult}$$

Where:

- t_c is the thickness of the support member (in)
- d is the diameter of the screw shaft (in)
- F_{ult} is the tensile strength of the support member (ksi)

A number of researchers have investigated pull-over and pull-out failures for a wide variety of base metal materials, deck profiles, load conditions, and test procedures (Ellifritt and Burnette, 1990; Pekoz, 1990; García, 1994; Smith, 1995; Mahendran, 1994,1997; Mahendran and Tang, 1998). In this investigation, the results summarized by Pekoz (1990) and Mahendran and Tang (1998) were used to derive the statistics of the mean to nominal ratios of the screw resistances computed using Equation 5-21 and Equation 5-22 for the pull-over failure and pull-out failures, respectively.

Pekoz (1990) investigated more than 360 pull-over failure cases and proposed a design formula (Equation 5-21) that has been adopted by the American standard (AISI, 1996). The reported mean-to-nominal and COV are 1.027 and 0.235, respectively.

Mahendran and Tang (1998) conducted a series of pull-out tests for a range of steel battens, purlins, girts, and screw fasteners commonly used in the building industry. The test results were compared with the predicted values based on the current design formula (Equation 5-22) using both the measured properties and the specified properties. It was found that the current design formula used with specified properties (nominal value) provides better agreement with the test results than those predicted using the measured properties. A mean-to-nominal ratio of 1.20 and a (COV) of 0.21 were determined using all 592 test cases. The mean-to-nominal values and COVs for pull-out and pull-over failure modes form the basis for sampling screw resistances in the stochastic finite element analysis described later.

5.4.11.3 Welded Decks

In this investigation, only arc spot weld connections were considered and modeled in the finite element analysis. The supporting members were assumed to be the top chords of open-web steel joists (however, the results are applicable to hot-rolled steel beams or girders). The study by LaBoube and Yu (1993) was used to determine the resistances of the weld connections. Based on more than 260 tension tests of arc spot weld connections with variations in steel thickness, tensile strength, weld process, loading condition, and geometry, LaBoube and Yu (1993) developed equations to predict the tension capacity of an arc spot weld connection. The following equations have been adopted in the current American standard (AISI, 1996):

When $F_u/E < 0.00187$:

Equation 5-23

$$P_n = \left[6.59 - 3150 \left(\frac{F_u}{E} \right) \right] t d_a F_u \leq 1.46 t d_a F_u$$

When $F_u/E \geq 0.00187$:

Equation 5-24

$$P_n = 0.70 t d_a F_u$$

Where:

- P_n is the nominal tension capacity
- F_u is the tensile strength of the sheet steel
- t is the sheet steel thickness
- d_a is the average weld diameter at mid-thickness of t , where $d_a = (d-t)$ for a single sheet and $(d-2t)$ for a double sheet
- E is Young's modulus of the sheet steel.

Based on concentric loading cases, LaBoube and Yu (1993) found the ratio of the failure load (P_u) to the predicted load (P_n) to have a mean value of 1.18 and a COV of 0.242.

At the perimeter of a steel deck roof system where there may be strong spatial gradients in the uplift loads, the arc spot welds may experience eccentric loading conditions, and the weld capacities in these cases can be significantly lower than those under concentric loads. Based on the 34 eccentric test results reported by LaBoube and Yu (1993), a mean-to-nominal value of 0.617 and a COV of 0.242 were determined, indicating a strength reduction of about 40% compared to the behavior of a concentrically loaded connection. In the finite element analysis, for welded connections, the relative location of the metal deck panel was considered, and the resistances were sampled from the eccentric load conditions for panels located at the edge of a roof system.

For the purpose of estimating the resistances of metal deck configurations used in engineering practice, the two most widely used building codes in southeastern United States (ASCE 7-88 and SBCCI 1988) were adopted to design the metal deck roofs of two baseline buildings (a one-story building and a two-story building). These two buildings were assumed to be located in hurricane-prone regions with design fastest mile wind speeds of 90 mph, 100 mph, and 110 mph. The mean roof heights for the flat-roof model buildings were 15' (one-story) and 25' (two-story). The metal roof system is comprised of 3' by 8' metal deck panels and supported by open-web steel joists spaced at 4'. Table 5-28 lists the calculated design wind pressures obtained from ASCE 7-88 and SBCCI 1988. Based on expert opinion, an importance factor of 1.05 was used to obtain the ASCE loads.

Table 5-28 Design Wind Pressures Calculated Using ASCE 7-88 and SBCCI 1988

Code	Number of Stories	Zone	Wind Pressure for Components & Cladding (psf)		
			90 mph	100 mph	110 mph
ASCE	One-Story	1	-28.71	-35.45	-42.89
		2	-44.26	-54.64	-66.12
		3	-59.44	-73.38	-88.79
	Two-Story	1	-33.38	-41.21	-49.86
		2	-51.45	-63.52	-76.86
		3	-69.10	-85.31	-103.22

Code	Number of Stories	Zone	Wind Pressure for Components & Cladding (psf)		
			90 mph	100 mph	110 mph
SBCCI	One-Story	r	-20.74	-25.62	-30.50
		s	-28.90	-35.70	-42.50
		z	-39.10	-48.30	-57.50
	Two-Story	r	-24.40	-29.59	-35.99
		s	-34.00	-41.23	-50.15
		z	-46.00	-55.78	-67.85

The variables considered in the design were fastener size, layout, steel deck gauge, steel deck strength, base metal thickness and base metal strength. The current American standard for cold-formed steel structures (AISI, 1996) was used to select appropriate designs for the calculated design loads. The deck resistances were calculated for six different layouts of fastener attachment schemes for both welded and screwed connections. Both load and resistance factor design (LRFD) and allowable stress design (ASD) were used to select the appropriate fastener layout. Table 5-29 and Table 5-30 lists the six different attachment layouts for the screw connections and for the welded connections, respectively.

Table 5-29 Determined Case Studies for Screw Connections

Case	Screw Size	Layout	Installation	Steel Deck			Base Metal		
				Gauge	F _y (ksi)	F _u (ksi)	Thickness (in.)	F _y (ksi)	F _u (ksi)
s1	#10	36/3	Valley-Fixed	22	40	55	0.125	33	45
s2	#10	36/4	Valley-Fixed	22	50	60	0.125	33	45
s3	#10	36/5	Valley-Fixed	22	50	60	0.125	33	45
s4	#12	36/5	Valley-Fixed	20	50	60	0.125	40	55
s5	#10	36/7	Valley-Fixed	20	50	60	0.125	40	55
s6	#12	36/7	Valley-Fixed	20	50	60	0.125	40	55

Table 5-30 Determined Case Studies for Weld Connections

Case	Weld Size	Layout	Installation	Steel Deck			Base Metal		
				Gauge	F _y (ksi)	F _u (ksi)	Thickness (in.)	F _y (ksi)	F _u (ksi)
w1	0.500	36/3	Valley-Fixed	22	40	55	0.125	33	45
w2	0.500	36/3	Valley-Fixed	22	50	60	0.125	33	45
w3	0.625	36/3	Valley-Fixed	22	50	60	0.125	33	45
w4	0.625	36/3	Valley-Fixed	20	50	60	0.125	40	55
w5	0.625	36/4	Valley-Fixed	20	50	60	0.125	40	55
w6	0.850	36/4	Valley-Fixed	20	50	60	0.125	40	55

A total of 12 cases were used in the finite element analysis (six screw connections and six weld connections). Recall the layout pattern of 36/N means N fasteners across the 36" width of the metal deck panel. Since a 3' by 8' panel covers two spans of the bar joists, there will be a total of $3N+4$ fasteners on the panel (four fasteners connecting adjacent roof panels at the middle of the span). The deck profile was assumed to be an intermediate rib type B and the deck gauge was selected from the manufacture's manual. Figure 5-95, Figure 5-96, Figure 5-97, and Figure 5-98 show the metal deck profile and the different fastener patterns (layouts) used in the case studies.

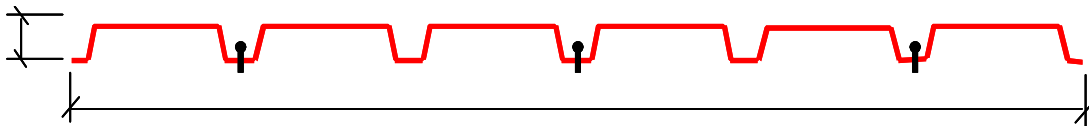


Figure 5-95 Metal Deck Profile with Three Fasteners



Figure 5-96 Metal Deck Profile with Four Fasteners



Figure 5-97 Metal Deck Profile with Five Fasteners



Figure 5-98 Metal Deck Profile with Seven Fasteners

5.4.11.4 Probabilistic Finite Element Analyses

Isoparametric shell elements were used to model the metal deck. The shell element was a four-node quadrilateral element with six degrees of freedom at each node. The 3'x8' metal deck panel was divided into 1,600 (32x50) shell elements, detailed enough to give accurate fastener forces and still allow the analysis to be run in a relatively short time period. Figure 5-99 shows the plan view of the mesh grids for the metal deck panel along with the fastener locations (denoted using stars) for a 36/4 fastener pattern. A previous study (Mahendran, 1994) suggested that despite the occasional local metal deck failure around the fasteners, the majority of the metal deck was still in elastic range when the fasteners failed, and thus the metal deck was modeled here as a linear elastic material with a Young's modulus of 29,000 ksi and a Poisson's ratio of 0.29.

The fasteners used to attach the deck panel to the bar joists were modeled as a fixed support with restrictions in the x, y, and z directions. No moment resistance was assumed for these fasteners. For the fasteners on the lap joints, the movements in the x and y directions were restrained, but the fasteners were allowed to move freely in the z direction.

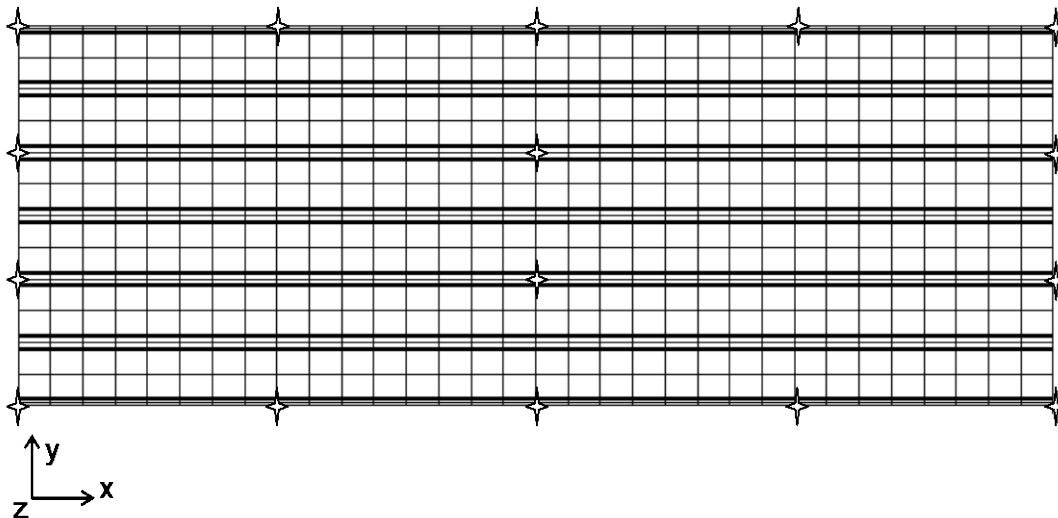


Figure 5-99 Finite Element Model of the 3' by 8' Panel

The metal deck was subjected to a uniform pressure with both the ultimate tensile strength and serviceability being considered in determining the failure of a panel. Failures caused by shear and local buckling were not modeled in the finite element analysis. If screws are used, both pull-out and pull-over strengths were sampled and the resistance was taken as the smaller of the two sampled strengths. Failure of a fastener occurs when the computed fastener load exceeds the sampled fastener resistance. For the complete failure of the whole panel, the failure criteria are:

1. Less than three fasteners remain on the panel (all the other fasteners have failed)
2. All the remaining fasteners align in a pattern such that the panel can rotate
3. The maximum deflection of the panel is greater than 2'

A Monte Carlo simulation was used to determine the statistics of the failure pressure for the metal deck (considering the randomness in the material properties and the fastener strengths).

Figure 5-100 shows the flowchart of the probabilistic finite element analysis. In the simulation, for each fastener, the nominal value (i.e., design value) was calculated first using the appropriate design formula. The statistics (i.e., mean and standard deviation) of the fastener resistance were obtained by multiplying the calculated design value by the mean-to-nominal ratio statistics. The resistance of each screw was then obtained by sampling from the resulting normally distributed resistance. For screw connections, both pull-out strength and pull-over strength were sampled, and the resistance was taken as the smaller of the two values. Similar procedures were also applied to the base metal properties of the metal deck (e.g., F_y and F_u). The finite element mesh, material properties, boundary conditions, fastener's strengths, and initial loads on the metal deck were generated automatically by a program written specifically for the Monte Carlo simulation. Then, a full finite element analysis was carried out to calculate the reaction in each fastener and the maximum deformation of the metal deck. Failure criteria were then checked against the calculated reactions and deformation. If the failure state was reached, the load (pressure) was then recorded as the failure load and a new simulation would start. Otherwise, failure of individual

fasteners were checked and any failed fasteners were removed from the analysis. The boundary conditions were then regenerated, and a new finite element analysis was carried on the modified sets of the fasteners while the pressure remained the same (i.e., considering progressive failure). If no more fasteners fail, the pressure was increased, and the procedure was repeated until failure of the metal deck panel was reached. The output from the finite element analysis was the initial failure pressure (i.e., the pressure at which any one of the fasteners fails) and the final failure pressure (i.e., the pressure at which the whole metal deck panel fails according to the failure criteria). After 100 simulations had been performed, the simulation results were used to characterize the statistics of the metal deck uplift capacity.

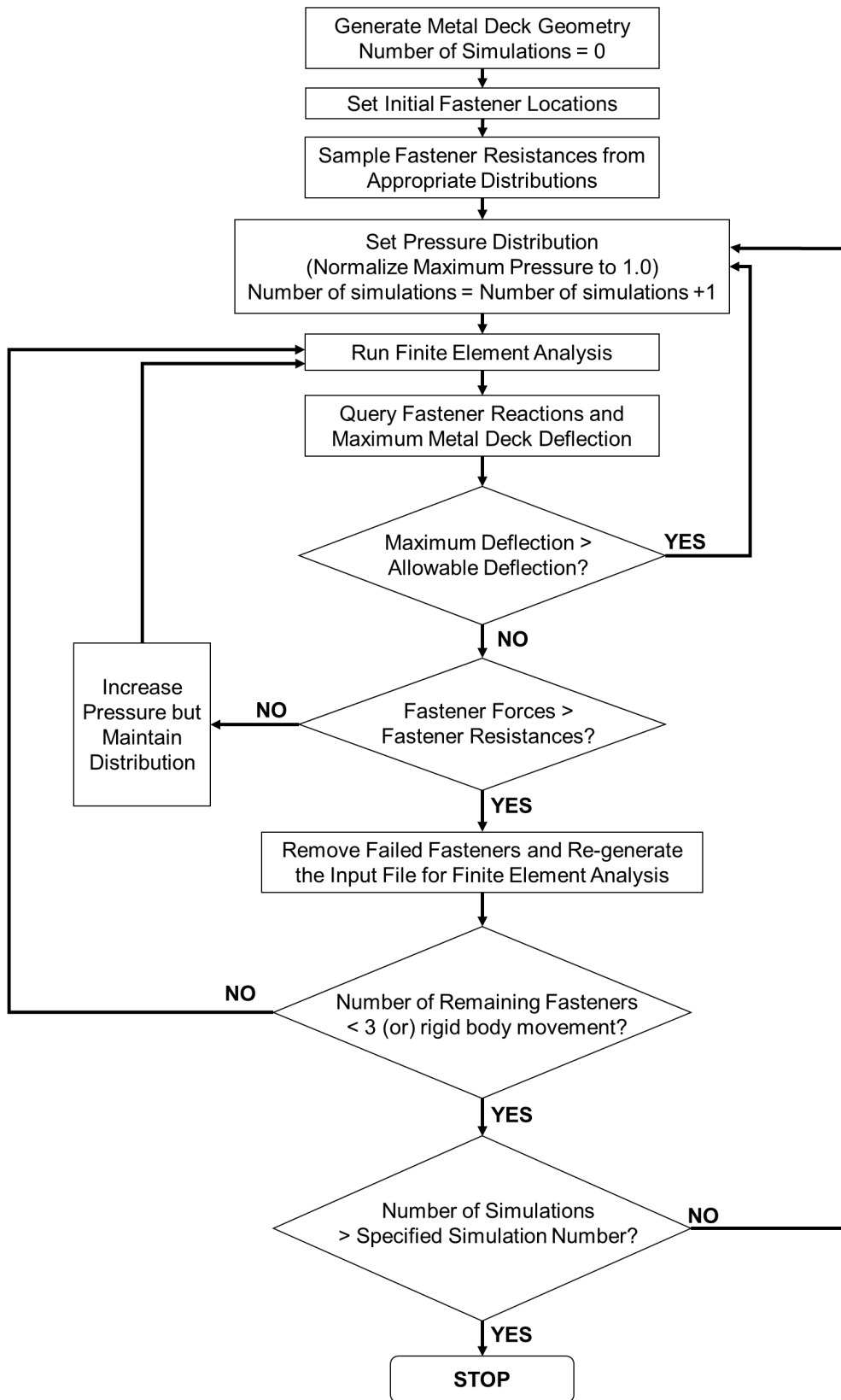


Figure 5-100 Flowchart of the Probabilistic Finite Element Analysis

5.4.11.5 Finite Element Method (FEM) Results

For each example, 100 finite element analyses were performed, from which the statistics of the failure pressure were computed. Table 5-29 lists the resulting means and standard deviations of the failure loads for selected case studies (associated with the design loads for different regions of the baseline model buildings). Note that the design pressures listed in Table 5-31 are different from the wind pressures calculated previously (see Table 5-28) because of the inclusion of dead load (for both ASD and LRFD) and the application of load factors (for LRFD only) in calculating the design pressures. In most cases, a lognormal distribution was found to provide the best fit to the failure pressures. Figure 5-101 and Figure 5-102 show the cumulative distribution function (CDFs) of the failure pressures for the metal deck with screw connections and welded connections, respectively. For screw connections, the increase in resistance with higher design values and stronger designs (in a sequence of case 1 to case 6) is clear. The coefficient of variation of the failure loads is seen to be relatively constant throughout the case studies (in a range of 10-15%).

However, for welded connections, the resistances do not increase monotonically with stronger designs, and cases 3 and 6 have larger variations than the other cases. Note that for welded connections, cases 1 and 2 are assumed to be in the middle of a roof system, cases 3 and 4 are assumed to be along one edge of a roof system, and cases 5 and 6 are assumed to be at the corner of a roof system. The welds along the edge of a roof system will experience eccentric loads that have lower resistances than the welds experiencing concentric loads. Therefore, the relative location of the roof deck panel has a significant impact on the panel uplift capacity.

Note that due to the relatively small coefficient of variation (less than 20%) of the simulated failure pressures, the potential sampling error of the estimated mean failure pressure will be less than 2% of the mean value (i.e., $20\%/\sqrt{n} = 20\%/\sqrt{100} = 2\%$). Therefore, 100 simulations provide sufficient accuracy.

A damage model for metal decks on open-web steel joists has been developed by combining a finite element analysis of a deck subject to a uniform pressure load, with the results of experimental data for fastener uplift resistance. Note that a number of parameters or factors that may contribute to the failure probability, such as fatigue, local buckling, membrane strength, workmanship, and deterioration were not explicitly considered. The potential impact of the reduction in deck capacity due to fatigue, corrosion, etc. is addressed in the building damage simulation results.

Table 5-31 Simulated Failure Loads for Different Designs

Code	No. of Story	Wind Speed (mph)	Zone	Design Pressure (psf)	Screw Design			Weld Design		
					Case	Mean (psf)	Std (psf)	Case	Mean (psf)	Std (psf)
ASCE 7-88	1	90	1	-34.6	s1	187.3	24.7	w1	168.8	22.3
			2	-54.8	s1	187.3	24.7	w1	168.8	22.3
			3	-74.6	s2	212.4	23.0	w1	168.8	22.3
		100	1	-43.4	s1	187.3	24.7	w1	168.8	22.3
			2	-68.3	s2	212.4	23.0	w1	168.8	22.3
			3	-92.7	s3	233.5	30.9	w1	168.8	22.3

Code	No. of Story	Wind Speed (mph)	Zone	Design Pressure (psf)	Screw Design			Weld Design		
					Case	Mean (psf)	Std (psf)	Case	Mean (psf)	Std (psf)
ASCE 7-88	2	110	1	-53.1	s1	187.3	24.7	w1	168.8	22.3
			2	-83.3	s3	233.5	30.9	w1	168.8	22.3
			3	-112.7	s4	299.0	37.1	w3	222.0	40.3
	2	90	1	-40.7	s1	187.3	24.7	w1	168.8	22.3
			2	-64.2	s2	212.4	23.0	w1	168.8	22.3
			3	-87.1	s3	233.5	30.9	w1	168.8	22.3
		100	1	-50.9	s1	187.3	24.7	w1	168.8	22.3
			2	-79.9	s3	233.5	30.9	w1	168.8	22.3
			3	-108.2	s4	299.0	37.1	w3	222.0	40.3
		110	1	-62.1	s2	212.4	23.0	w1	168.8	22.3
			2	-97.2	s4	299.0	37.1	w3	222.0	40.3
			3	-131.5	s5	435.8	42.0	w4	305.2	40.4
SBCCI	1	90	r	-17.7	s1	187.3	24.7	w1	168.8	22.3
			s	-25.9	s1	187.3	27.7	w1	168.8	22.3
			z	-36.1	s1	187.3	24.7	w1	168.8	22.3
		100	r	-22.6	s1	187.3	24.7	w1	168.8	22.3
			s	-32.7	s1	187.3	24.7	w1	168.8	22.3
			z	-45.3	s1	187.3	24.7	w1	168.8	22.3
		110	r	-27.5	s1	187.3	24.7	w1	168.8	22.3
			s	-39.5	s1	187.3	24.7	w1	168.8	22.3
			z	-54.5	s2	212.4	23.0	w1	168.8	22.3
	2	90	r	-21.4	s1	187.3	24.7	w1	168.8	22.3
			s	-31.0	s1	187.3	24.7	w1	168.8	22.3
			z	-43.0	s1	187.3	24.7	w1	168.8	22.3
		100	r	-26.6	s1	187.3	24.7	w1	168.8	22.3
			s	-38.2	s1	187.3	24.7	w1	168.8	22.3
			z	-52.8	s2	212.4	23.0	w1	168.8	22.3
		110	r	-33.0	s1	187.3	24.7	w1	168.8	22.3
			s	-47.2	s1	187.3	24.7	w1	168.8	22.3
			z	-64.9	s2	212.4	23.0	w1	168.8	22.3

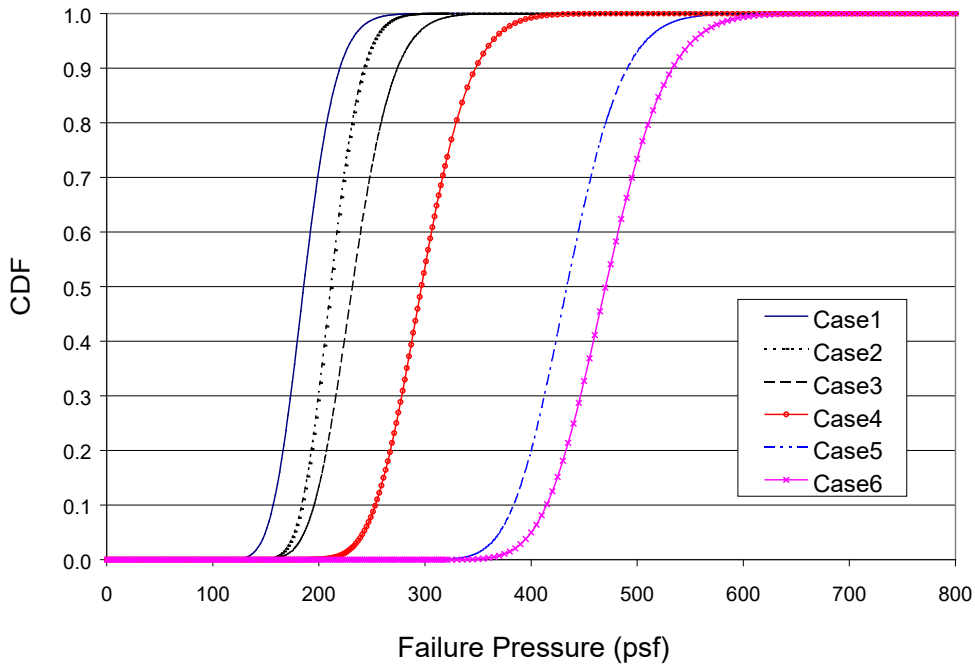


Figure 5-101 CDFs of Metal Deck Failure Pressures (Screw Connections)

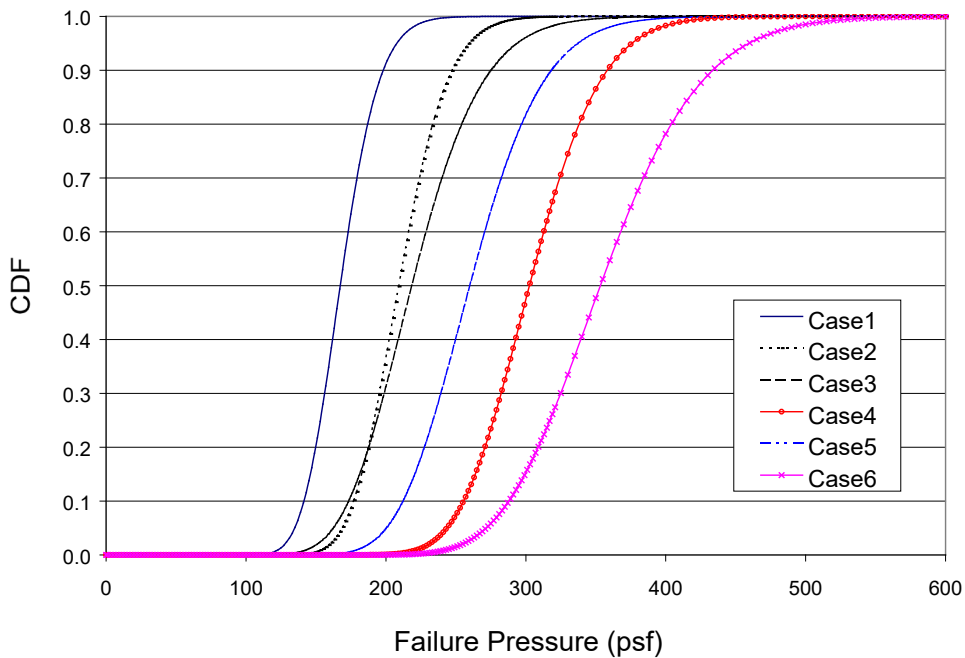


Figure 5-102 CDFs of Metal Deck Failure Pressures (Weld Connections)

5.4.12 Metal Building Wall System

Because of their fast construction, flexible expansion capability, and low maintenance, metal building systems dominate the low-rise non-residential market. For example, according to the Metal Building Manufacturers Association (MBMA), 65% of the new one and two-story buildings were built using metal building structures in 1995. Pre-engineered metal building systems are found in many applications,

including warehouses, small office buildings, garages, supermarkets, retail stores, industrial factories, schools, town halls, and even churches (Newman, 1997). A metal building system is typically comprised of primary frames (hot-rolled wide-flange beams and girders, hot-rolled steel rigid frame, or steel trusses), secondary frames (purlins and girts), endwall posts, a roof system, wall systems, a foundation, and bracing.

In this analysis, as in the low-rise residential building analysis, the physical damage modeling for metal buildings is limited to modeling the damage to components and cladding, specifically the metal wall system, the metal roof system, and the entry doors and overhead doors.

Wall panels on metal buildings are normally supported on cold-formed C or Z girts. The thickness of the galvanized-steel siding ranges from 18 to 29 gauge, with the midrange gauges being the most popular (Newman, 1997). Exposed-fastener wall panels behave similarly to through-fastened roofing and some products can be used for both wall and roof systems. Figure 5-103 shows one section of a typical exposed-fastener wall system. The wall panels are attached to the supporting members using self-drilling screws. Two adjacent panels are overlapped and joined together with side-lap fasteners, which are typically spaced at 24" O.C.

The development of the damage model for metal wall system follows a similar procedure to that used for the metal deck systems. That is, the model development entails case study selections, probabilistic finite element analyses, and evaluation of simulation results. Two case studies (both are one-story buildings) were selected for the metal wall system: one with a design pressure of 20 psf and the other with a design pressure of 40 psf. The wall section for these two case studies is composed of two over-lapped corrugated USD C36 panels with exposed fasteners (screw connections). Note that this kind of panel can be used for both wall systems and roof systems. Figure 5-104 shows the profile of the metal panel. Each panel is 3' wide by 10' tall with a supporting girt at 7' from the ground (see Figure 5-103). Each panel in case 1 has 3 size 10 screws (12" O.C.) at both ends and three size 10 screws (12" O.C.) on the girt. Each panel in case 2 has five size-10 screws (7.2" O.C.) at both ends and three size 10 screws (12" O.C.) on the girt. The panel steel conforms to ASTM A653 Grade 33 sheet steel ($F_y = 33$ ksi and $F_u = 50$ ksi) for case 1 and Grade 37 sheet steel ($F_y = 37$ ksi and $F_u = 58$ ksi) for case 2. The girt was assumed to be a gauge 16 (0.06" thickness) cold-formed Z section with a 10" depth. The ultimate strength of the base metal was slightly less than that of the panel. The two panels for the metal wall section are joined together using six lap-joint screws spaced at 24" O.C.

5.4.12.1 Finite Element Mode

A major concern regarding the finite element analysis of the wall system lies in how to model the lap joints. When subjected to a pressure load, the two panels of the wall section tend to move away from each other, resulting in significant tension forces at the lap joints. Because of the restraints provided by the lap-joint screws, the upper and bottom panels around the screw will move together until yield stress is reached. To simulate this phenomenon, a number of methods were investigated, including slave nodes, rigid beams, and rigid shell elements. The final modeling of the lap joint was accomplished by placing a small steel member with the same properties as those of the panel connecting the two separate panels. Figure 5-105 shows the finite element mesh of the wall section. Note that there is a gap between the two wall panels (i.e., no connection between the wall panels except at the lap joints). Mesh grid refinement was made at each fastener and at each lap joint. Figure 5-106 shows the refined mesh around one

fastener. Four nodes surrounding each fastener were fixed to model the boundary conditions (denoted as stars in Figure 5-106).

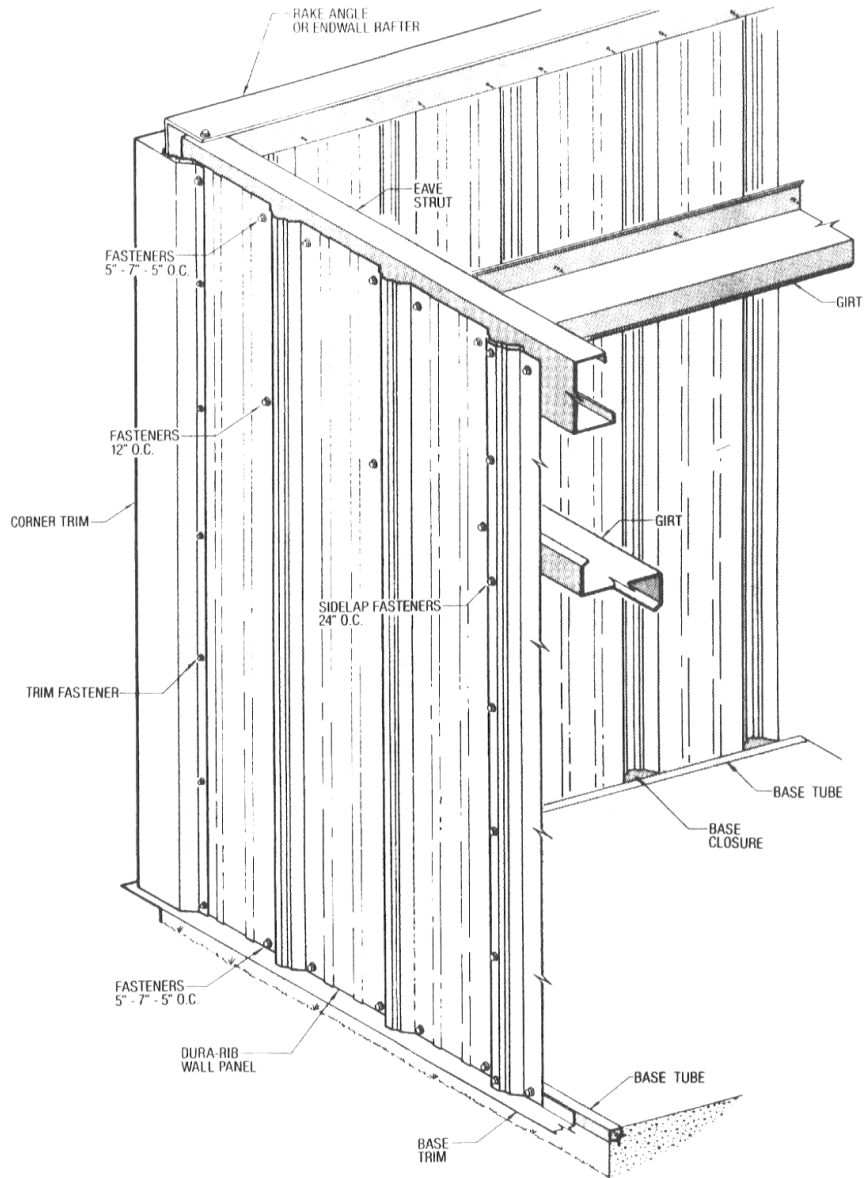


Figure 5-103 Example of a Metal Wall System with Exposed Fasteners (Newman, 1997)

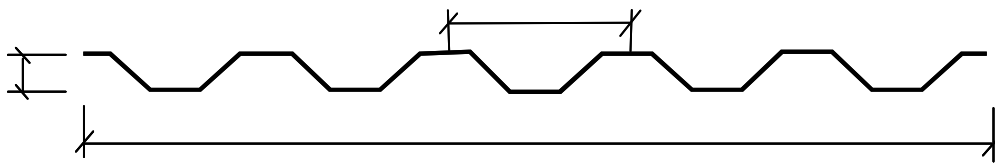


Figure 5-104 Metal Deck Profile for Wall and Roof Systems

In the FEM analysis, once an element reaches yield stress, its modulus of elasticity (E) is reduced to a certain percentage to simulate the plastic behavior of the element. If during the following runs that element reaches yield stress again, another percentage of reduction is applied until the whole wall section fails. However, for the lap joint elements that reach yield stress, the modulus of elasticity is dropped to near zero (to model the weak link between the two panels).

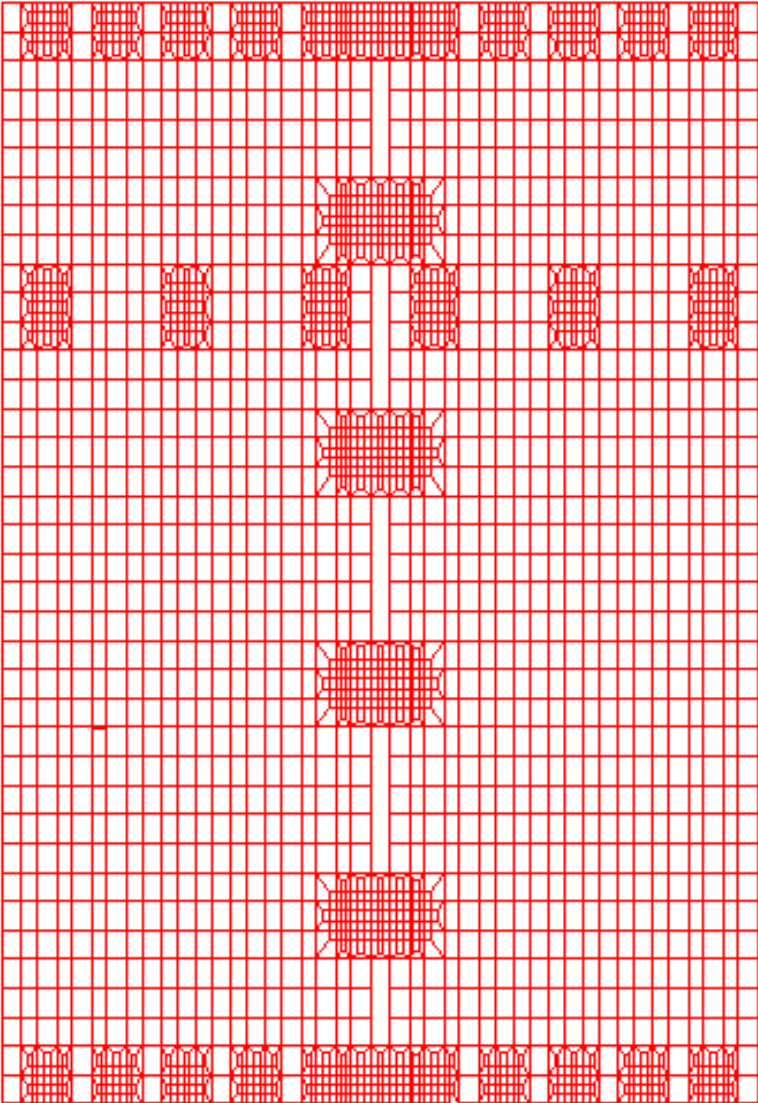


Figure 5-105 Finite Element Mesh of the Wall Panels

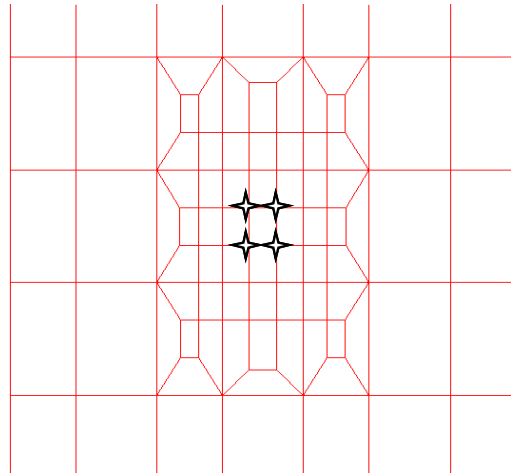


Figure 5-106 Refined Mesh around the Fastener

As in the FEM analysis of the metal deck on steel joists, the panel-to-support connection failure was modeled as a major failure mode. Both pull-over and pull-out strengths were considered and modeled as random variables with the resistance of the fastener taken as the smaller of the two sampled values. All the other properties, such as the steel strength and panel dimensions are assumed to be deterministic (due to their relatively small variation). Once again, a number of other parameters (such as workmanship, fatigue, and corrosion) that may produce significant effects on the pressure resistance of the panel, were not explicitly considered.

The wall section is considered to have failed once any of the following criteria are met:

1. Less than 3 fasteners remain on the panel (all the other fasteners have failed)
2. All the remaining fasteners align in a pattern such that the panel can rotate
3. The maximum vertical deflection (z direction) of the panel is greater than 1'
4. The maximum horizontal deflection (x direction) of the panel is greater than 0.5'

A more stringent restriction on the vertical deflection was applied to wall systems compared to the metal deck on steel joists. Horizontal deflection was added to the failure criteria for the consideration of internal pressurization if an opening develops between the wall panels.

5.4.12.2 Simulation Results

Following the procedures described in Section 5.4.11 and shown with the flowchart in Figure 5-100, probabilistic finite element analyses were performed for the two example cases. Figure 5-107 shows one example of the stress distribution computed in the wall panels under a uniform suction of 200 psf. The stress concentrations around the fasteners are obvious. Moderate stresses are also seen around one or two lap joints. Under this high pressure, a number of elements have reached their yield stress and most of the screws have already failed.

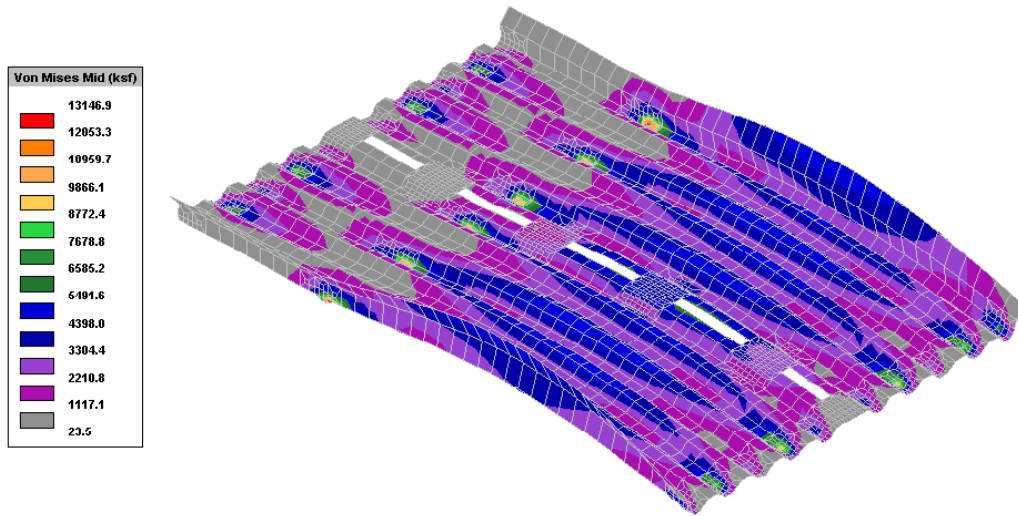


Figure 5-107 Stress Distribution of Wall Panels with Superimposed Deformation

A total of 50 simulations were performed for each case and the statistics of the wall panel failure pressures were determined from the simulation results. As expected, the load resistance capability of case 1 is smaller than that of case 2. The mean and the standard deviation of the computed failure pressure for case 1 are 84.0 psf and 7.5 psf, respectively. The mean and the standard deviation of the computed failure pressure for case 2 are 124.2 psf and 16.5 psf, respectively.

Figure 5-108 shows the CDFs of the failure pressures for these two case studies, which form the basis for the development of the damage model for metal wall systems.

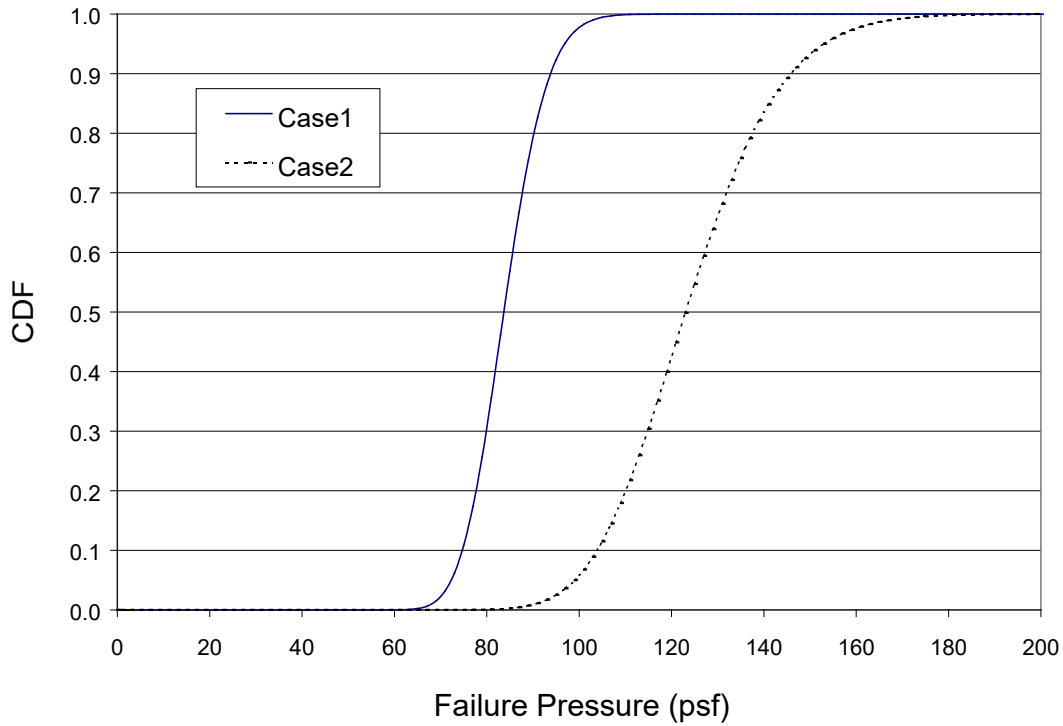


Figure 5-108 Cumulative Distribution Functions of Wall System Failure Pressures

5.4.13 Metal Building Roof System

The metal roofs investigated herein are similar to the metal decks on open-web steel joists except that the metal roof is fastened to C or Z purlins rather than steel joists. The 1996 Metal Building Manufacturers Association (MBMA) design manual was used to determine the design loads for two example buildings. The metal roof panel was assumed to be a USD C36 roof panel (USD, 1998) 3' wide and 10' long (covering 2 spans). Refer to Figure 5-104 for its profile. The purlin was assumed to be a cold-formed Z section with a 10" depth, a gauge of 14 (0.075" thickness), and spaced at 5' on the primary frame. As noted by Newman (1997), purlin spacing is controlled by the load-carrying capacity of the roof panels, with a 5' spacing being the most common. Table 5-32 shows the calculated design pressures for the two example buildings. The metal roof failure analysis followed the same procedure used to develop the model for decks on OWSJ, with the joist properties replaced by the purlin properties. The statistics of the metal roof failure pressures from 100 probabilistic finite element runs are given in Table 5-32. The CDFs of the failure pressures for the seven screw connection design cases (Table 5-33) used in the two example buildings are shown in Figure 5-109. Note that the failure pressures for cases 4 and 5 are almost identical since the only difference between case 4 and case 5 is the metal panel gauge.

Table 5-32 Calculated Design Pressure Using MBMA and Simulated Failure Pressure Statistics from FEM Analysis

Building Code	Roof Height (feet)	Wind Speed (mph)	Zone	Design Pressure (psf)	Screw Design ¹	Failure Pressure (psf)		
						Mean	Standard	
MBMA	15	90	r	-21.7	s1	88.5	9.7	
			s	-29.0	s1	88.5	9.7	
			c	-51.0	s2	104.4	11.6	
		100	r	-27.2	s1	88.5	9.7	
			s	-36.1	s1	88.5	9.7	
			c	-63.1	s3	119.8	14.3	
		110	r	-33.3	s1	88.5	9.7	
			s	-44.2	s1	88.5	9.7	
			c	-76.8	s4	151.4	16.1	
		30	90	r	-25.3	s1	88.5	9.7
				s	-33.7	s1	88.5	9.7
				c	-58.9	s3	119.8	14.3
	100		r	-31.0	s1	88.5	9.7	
			s	-41.2	s1	88.5	9.7	
			c	-71.7	s5	151.0	16.2	
	110		r	-38.9	s1	88.5	9.7	
			s	-51.5	s6	109.1	13.6	
			c	-89.2	s7	176.9	18.6	

¹See Table 5-33

Table 5-33 Connection Layout for Example Metal Roofs

Design Case	Screw Size	Layout	Installation	Roof Panel			Girt		
				Thickness	F _y (ksi)	F _u (ksi)	Thickness (in.)	F _y (ksi)	F _u (ksi)
s1	#10	36/3	Valley-Fixed	0.024 (gauge 24)	40	55	0.075	33	45
s2	#10	36/3	Valley-Fixed	0.024 (gauge 24)	50	60	0.075	40	55
s3	#12	36/3	Valley-Fixed	0.030 (gauge 22)	50	60	0.075	40	55
s4	#10	36/5	Valley-Fixed	0.036 (gauge 20)	40	55	0.075	33	45
s5	#10	36/5	Valley-Fixed	0.030 (gauge 22)	40	55	0.075	33	45
s6	#10	36/3	Valley-Fixed	0.030 (gauge 22)	50	60	0.075	40	55

Design Case	Screw Size	Layout	Installation	Roof Panel			Girt		
				Thickness	F _y (ksi)	F _u (ksi)	Thickness (in.)	F _y (ksi)	F _u (ksi)
s7	#10	36/5	Valley-Fixed	0.036 (gauge 20)	50	60	0.075	40	55

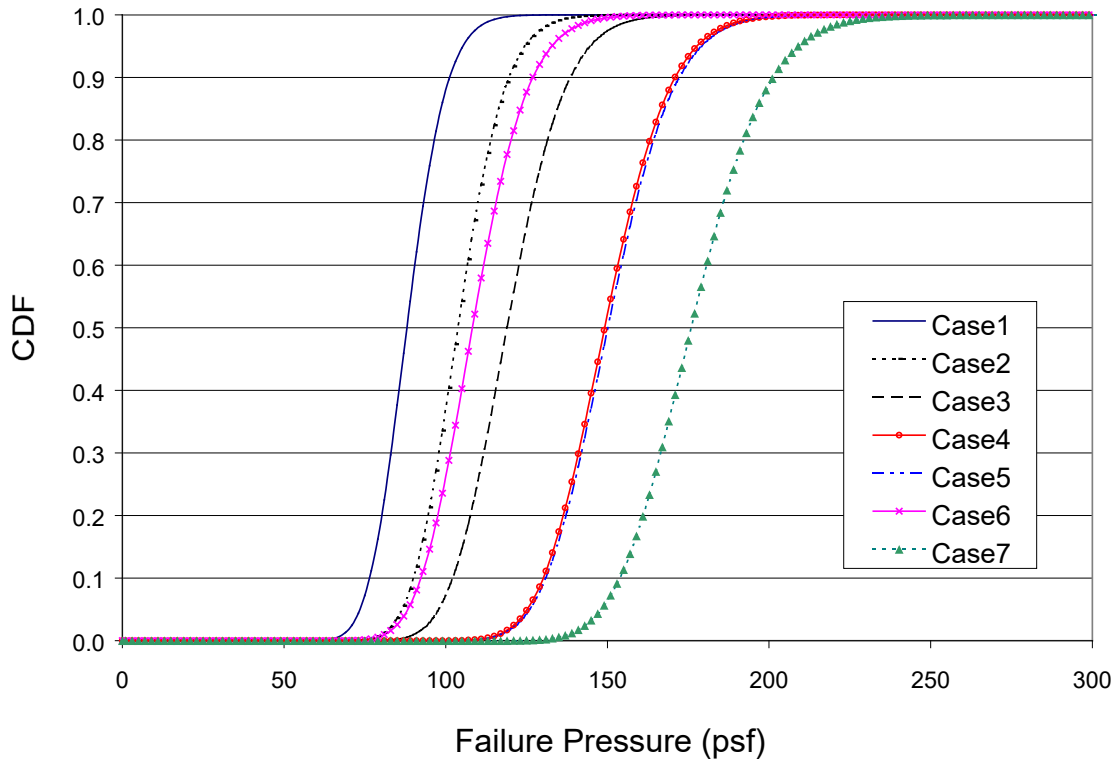


Figure 5-109 Cumulative Distribution Functions of Metal Roof Failure Pressures

5.5 Damage Model Validation

5.5.1 Residential Buildings

In order to validate the model’s ability to predict damage to buildings, comparisons of simulated and observed damage states are performed. The damage states examined here include roof cover damage, roof sheathing damage and damage to windows. Roof cover and roof sheathing damage states are simulated and compared to roof damages experienced during Hurricanes Andrew (1992), Erin (1995), and Fran (1996). In the case of window damage to residential buildings, the information collected by HUD, as described in Crandell et al. (1993), provides the only source of relatively unbiased statistics on window damage associated with Hurricane Andrew.

In all the comparisons, the observed damage states are compared to those obtained by modeling the wind loads experienced by the homes using the wind loading and damage models described earlier. To obtain estimates of the wind speeds at the sites of the observed damage, a full reproduction of the wind speed and direction time history at the site are obtained using the hurricane wind field model described in Section 4.1.

5.5.1.1 Roof Cover and Roof Deck Damage

5.5.1.1.1 Hurricane Andrew (1992)

The most comprehensive existing report on the performance of roof systems for residential buildings during Hurricane Andrew is given in HUD (1993). In the HUD (1993) study, the survey team randomly selected 466 homes located in the high damage areas and then proceeded to quantify the damage states for each structure. The homes were located in nine separate clusters (A through I) as shown in Figure 5-110.

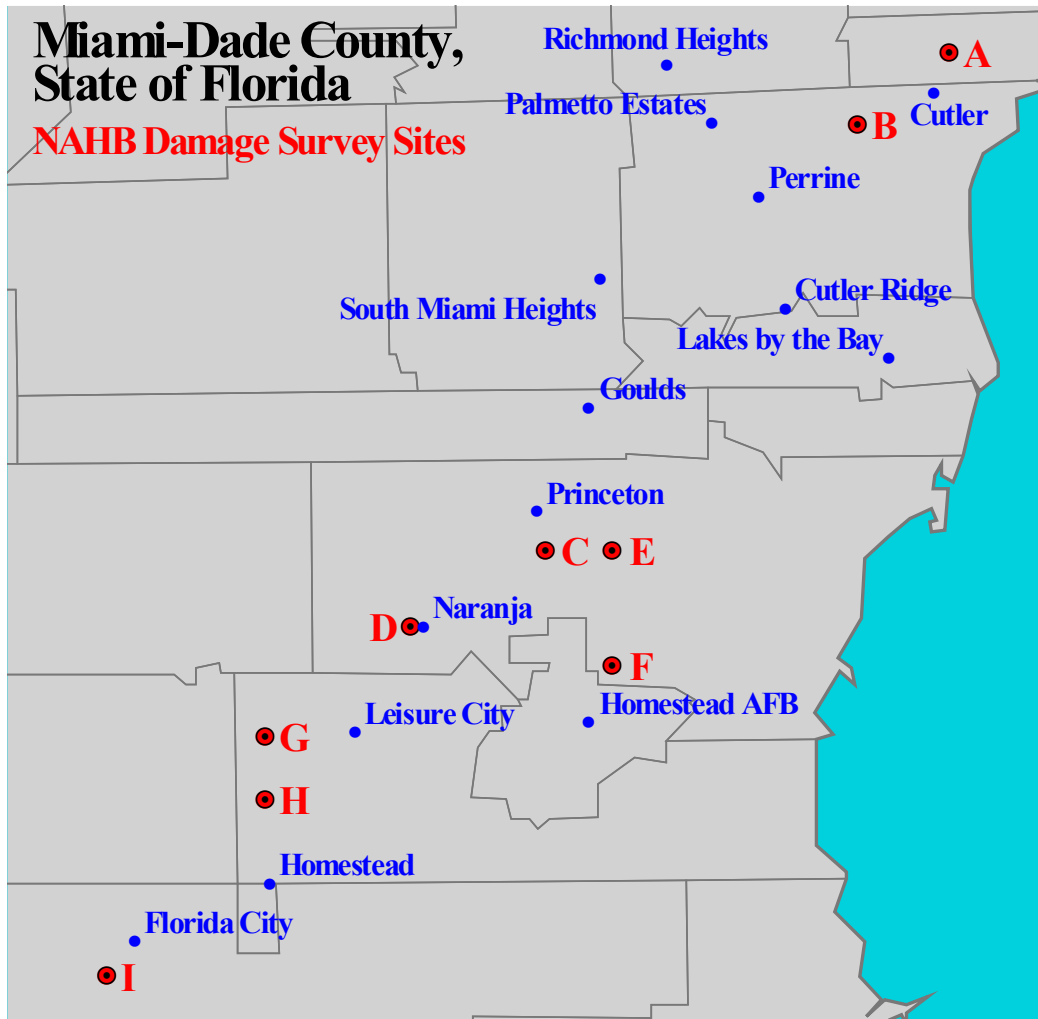


Figure 5-110 NAHB Site Locations

To expand on the HUD roof damage data, aerial photographs were obtained that correspond to four of the locations used in the HUD damage survey. The aerial photographs were produced at a scale of 1" = 100'. This scale provides enough resolution so that the damage to the roof cover and roof sheathing can be directly estimated. The exact location of the HUD study areas is determined by geocoding the addresses of the homes surveyed by the HUD team.

The wind speed traces at the locations of the four photographs determined from the simulation of Hurricane Andrew are given in Figure 5-111. As seen from Figure 5-111, the basic wind speeds experienced at each location are very similar.

The HUD building damage states were categorized into four distinct damage states defined as:

- *Damage State 0: No Damage*
- *Damage State 1: $0 < \text{Damage} \leq 33\%$*
- *Damage State 2: $33\% < \text{Damage} \leq 66\%$*
- *Damage State 3: $\text{Damage} > 66\%$*

The damage states recorded included roof cover damage, roof sheathing damage, roof-wall connection damage, gable end damage, and window damage.

Based on conversations with members of the HUD damage team, it has been assessed that the high damage states indicated in the HUD report overstate the total damage. Thus, the roof damage states used in the analysis of the damage evident in the aerial photography are as follows:

- *Damage State 0: No Damage*
- *Damage State 1: $0\% < \text{Damage} \leq 5\%$*
- *Damage State 2: $5\% < \text{Damage} \leq 10\%$*
- *Damage State 3: $10\% < \text{Damage} \leq 20\%$*
- *Damage State 4: $20\% < \text{Damage} \leq 50\%$*
- *Damage State 5: $50\% < \text{Damage} \leq 100\%$*
- *Damage State 6: $\text{Damage} = 100\%$*

When examining the photographs, if uncertainty exists as to the extent of damage, because the roof was covered with a tarp or plastic, the damage state is entered as unknown. Prior to performing comparisons of simulated and observed damage states, comparisons of the damage estimates obtained from the photographs to those reported by HUD were made. To perform these comparisons, Damage States 1, 2, and 3 observed from the aerial photographs were combined into one category, corresponding to HUD Damage State 1. The four distinct damage states represent no damage, minor damage, moderate damage, and major damage, as described in Table 5-34.

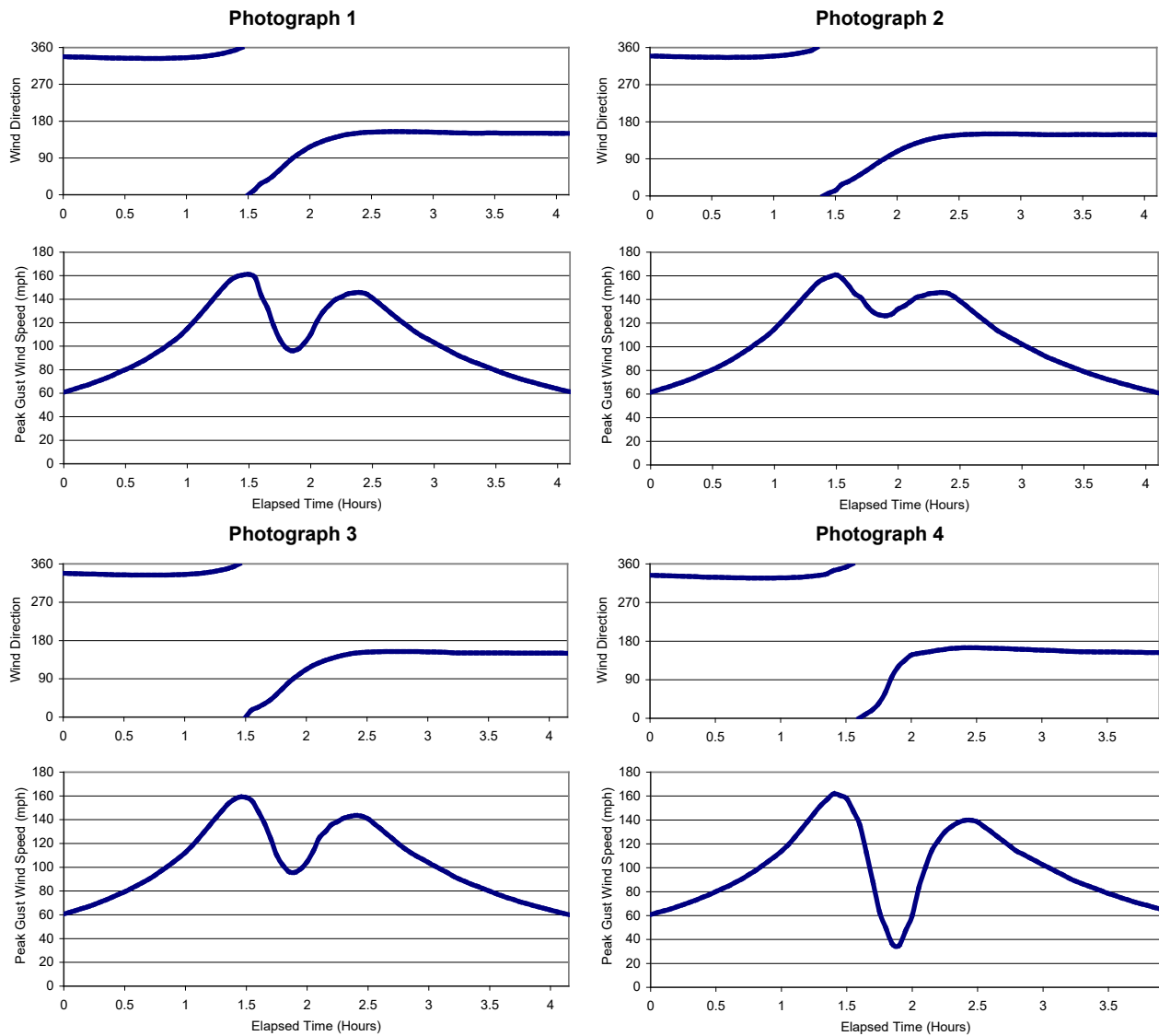


Figure 5-111 Wind Speed and Direction Traces (10 meters, Open Terrain) at Locations of Photographs 1, 2 3, and 4 (HUD Locations, F, E, D, and H)

Table 5-34 Mapping Used to Match Aerial Photograph Estimated Damage States and HUD Damage States

Damage State	Aerial Photograph Estimated Damage State	HUD Damage State
0	No Damage	No Damage
1	0-20%	0-33%
2	20%-50%	33%-66%
3	>50%	>66%

5.5.1.1.1 Photograph 1 (HUD Location F)

This subdivision was comprised of closely-spaced two-story homes. The estimated value of the surface roughness within the subdivision is about 0.6 meters. The surrounding terrain to the south and east of

the homes is open. In the damage simulation, the subdivision was modeled with a z_0 of 0.3 meters, representing a compromise between the low z_0 value around the buildings and the high z_0 value within the subdivision. Upon reviewing the aerial photography, it was obvious that the roofs of some of the homes had been repaired. All homes with repaired roofs were removed from the damage analysis. A total of 330 two-story gable homes are shown in the photograph. Of these 330 homes, 98 had obviously been repaired, leaving a total of 232 non-repaired homes. Of these 232 homes, ARA could identify the roof cover damage for 223 cases, and the roof sheathing damage in 213 cases. The HUD team surveyed 63 homes in this subdivision and were able to identify damage for 57 of the 63 cases.

The comparison of the observed damage states, shown in Figure 5-112, indicates that in the case of roof sheathing, the larger sample taken from the photograph suggests about 50% of the homes experienced the loss of a least one piece of roof sheathing whereas the HUD data suggests that about 60% of the homes experienced the loss of at least one piece of roof sheathing. The only other notable difference between the two damage state estimates is that the HUD data places a higher percentage of the homes experiencing the highest roof cover damage state than the data obtained from the photograph, even though the highest HUD damage state begins at a higher level of damage than the highest damage state used here.

5.5.1.1.1.2 Photograph 2 (HUD Location E)

In the case of Photograph 2, 438 homes appear in the photograph. The composition of these homes was made up of 308 single-story gable roof units, 97 single-story hip roof units and 30 two-story gable roof buildings. The roof shape of three units could not be identified. Of the 438 homes, 45 were re-roofed before the photograph was taken. Of the 393 homes that had not been re-roofed, damage states could be discerned for 239 single-story gable buildings (77% of those in the photograph), 70 single-story hip buildings (from 97 units), and 30 two-story gable buildings (from 30 units). The damage states associated with the remaining 54 homes could not be determined.

The houses within the subdivision were widely spaced. The estimated value of the surface roughness, based on the approach given by Latteu (1969), within the subdivision is about 0.15 meters.

The HUD team surveyed a total of 63 homes within the area encompassed by this photograph. These 63 homes were comprised of 59 single-story gable buildings, one two-story gable, and three single-story hip roof buildings. Of the 59 single-story gable roof buildings, sheathing damage could be estimated on 42 of these (71%) and roofing damage for 45 of the homes.

Figure 5-113 compares the damage states arising from the analysis of the aerial photograph to the HUD data. A comparison of the roof sheathing damage states clearly indicate that the HUD data overestimated the true level of sheathing damage. The HUD data suggests that 89% of the single-story gable buildings experienced the loss of at least one piece of sheathing, whereas examination of the aerial photography indicates the loss of at least one piece of roof sheathing for 62% of the homes.

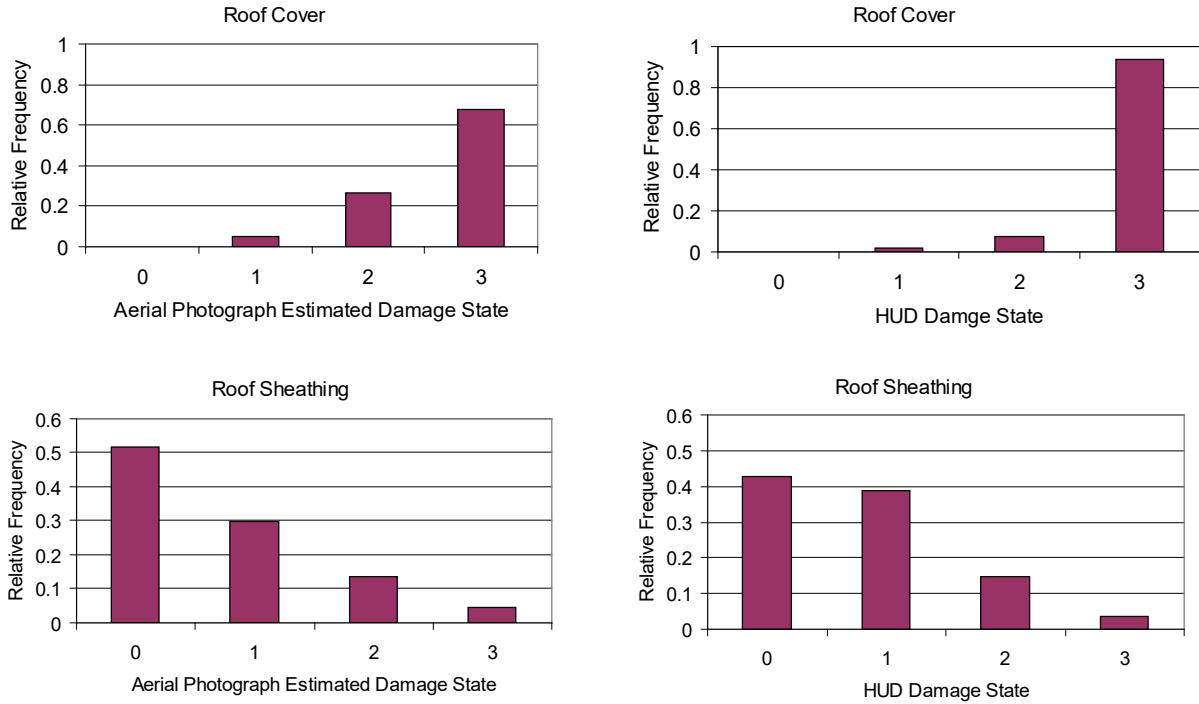


Figure 5-112 Comparison of Observed Damage States for Single-Story Gable Homes Obtained from Aerial Photography and HUD Damage Survey - Location of Photograph 1 (HUD Location F)

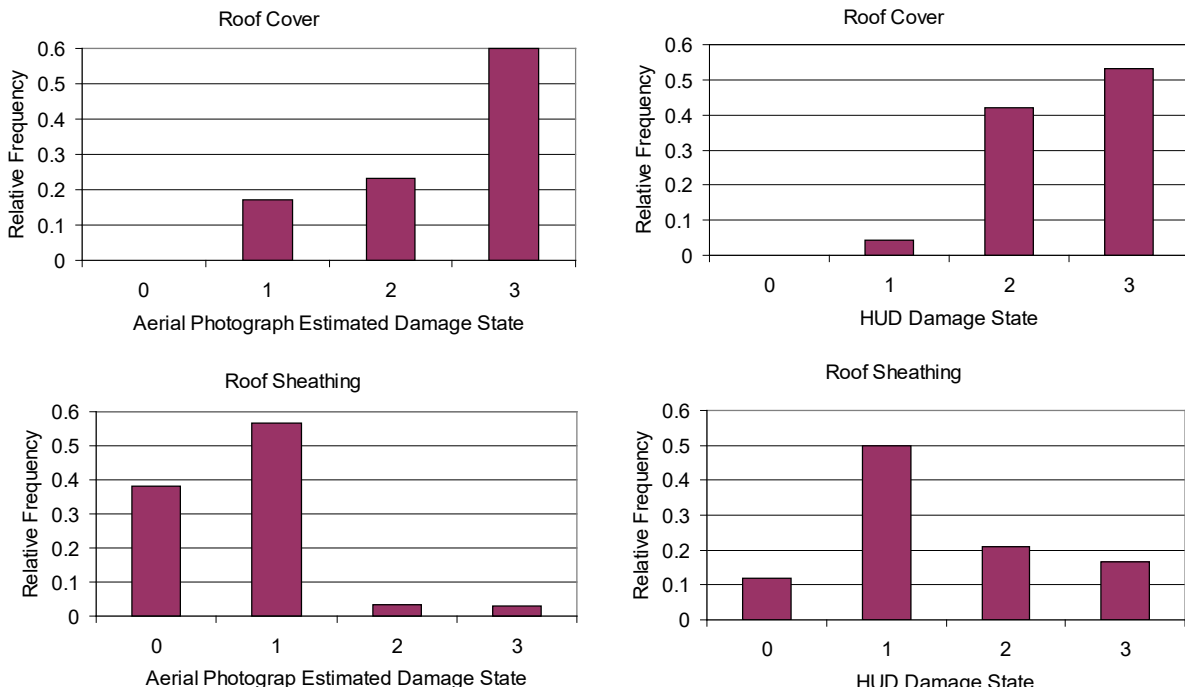


Figure 5-113 Comparison of Observed Damage States for Single-Story Gable Homes Obtained from Aerial Photography and HUD Damage Survey - Location of Photograph 2 (HUD Location E)

5.5.1.1.1.3 Photograph 3 (HUD Location D)

In Photograph 3, the single-family home population was comprised of 193 single-story gable homes and 42 single-story hip roof homes. Of the 193 gable roof homes, 145 units (75%) had not been re-roofed and the damage could be estimated. In the case of the hip roof homes, 28 units (67%) had not been re-roofed and the damage states could be estimated.

Like the homes examined in Photograph 2, the houses within the subdivision were widely spaced. Again, using the approach given in Latteu (1969), the estimated value of the surface roughness within the subdivision is 0.11 meters.

Figure 5-114 presents a comparison of the HUD damage states and the damage states determined from the aerial photography. The agreement between the results obtained from the two damage surveys is reasonable. In the case of roof sheathing, both the analysis of the photography and the ground survey performed by HUD indicates that about 70% of the single-story gable homes had at least one piece of roof sheathing fail. This 70% value agrees with the results from the analysis of the homes analyzed from Photograph 2, which was subjected to nearly identical hurricane winds during the storm.

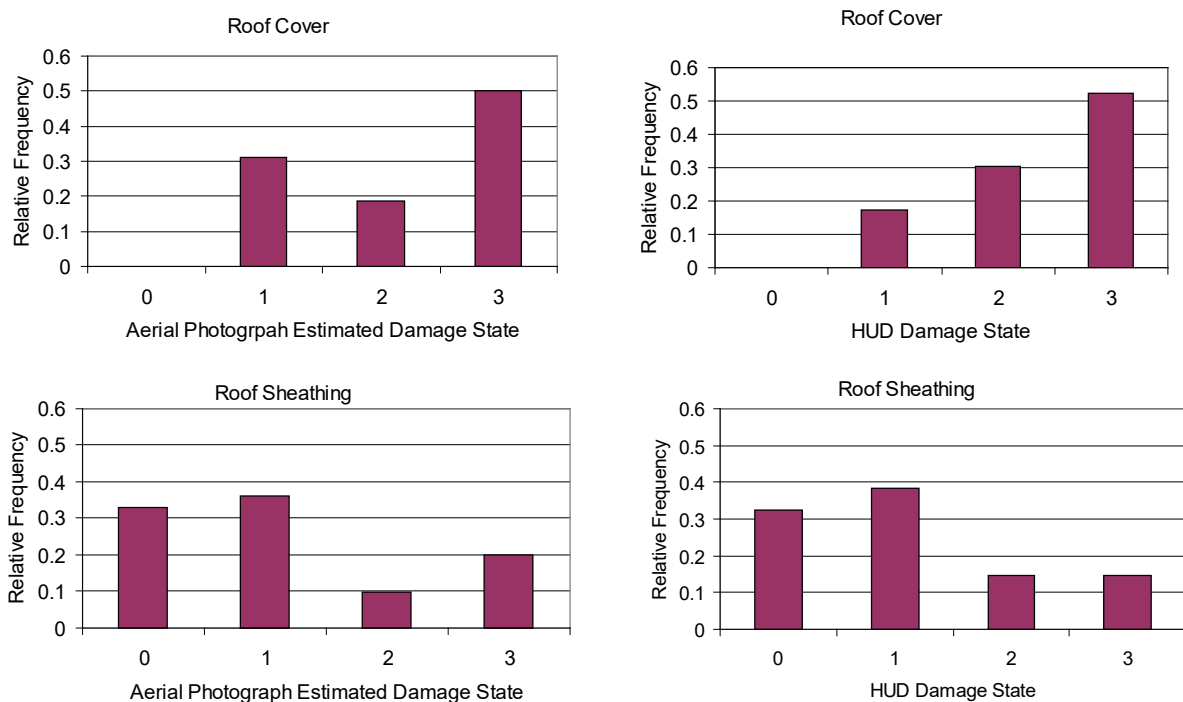


Figure 5-114 Comparison of Observed Damage States for Single-Story Gable Homes Obtained from Aerial Photography and HUD Damage Survey - Location of Photograph 3 (HUD Location D)

5.5.1.1.1.4 Photograph 4 (HUD Location H)

In the case of Photograph 4, too many of the homes had been repaired and thus estimates of roof damage could not be properly ascertained.

In the comparison of the simulated and observed roof damage states, a difficulty arises (particularly in the case of the roof sheathing) because the nail sizes used to attach the roof sheathing to the roof

trusses were not known. Prior to 1992, the South Florida Building Code required a minimum of 6d nails spaced at 6" on center at the edges and 12" on center in the field for sheathing less than 1/2" thick. For a sheathing thickness greater than 1/2", 8d nails were required using the same 6"/12" spacing. As previously discussed, the uplift resistance of a sheathing panel attached to the rafters using 8d nails is about twice the value that is obtained using 6d nails.

In the HUD damage survey, the nail size was recorded on only two of the 466 homes examined (both had 8d nails). Data collected as part of the Residential Construction Mitigation Program under the direction of the Florida Department of Community Affairs, suggests that approximately 60% of the homes are constructed using 8d nails to attach the roof sheathing to the roof trusses, with 6d nails used in the remaining 40% of the homes. The default for characterizing the building stock is taken as 40% of the homes constructed using the code minimum requirements with a sheathing thickness of less than 1/2" and the remaining 60% of the homes constructed using the code minimum requirements with sheathing roof panels having a thickness greater the 1/2".

In the comparisons of simulated and observed roof damage states that follow, the comparisons are given for all buildings modeled using 6d sheathing nails, all buildings modeled using 8d sheathing nails, and the default building stock (i.e., 40% of the buildings modeled with 6d nails and 60% with 8d nails). The simulated damage is derived using the wind loads specified in ASCE 7 and assuming that the buildings are randomly oriented.

5.5.1.1.1.5 Two-Story Gable Houses

Figure 5-115 and Figure 5-116 show comparisons of the simulated and observed damage states for the two-story gable roof homes. Figure 5-115 presents the comparisons with the data obtained from Photograph 1, whereas Figure 5-116 shows the comparisons for the damage states taken from Photograph 2. Using the default building stock (i.e., 40% of the buildings have roof decks attached with 6d nails and 60% with 8d nails) as being representative of the building stock associated with the observed damage, the comparisons given in Figure 5-115 and Figure 5-116 suggest that modeling the loads with the ASCE 7 based pressure coefficients overestimates the damage to the roof sheathing and roof covering for two-story given in Figure 5-115 and Figure 5-116 suggest that modeling the loads with the ASCE 7 based pressure gable houses.

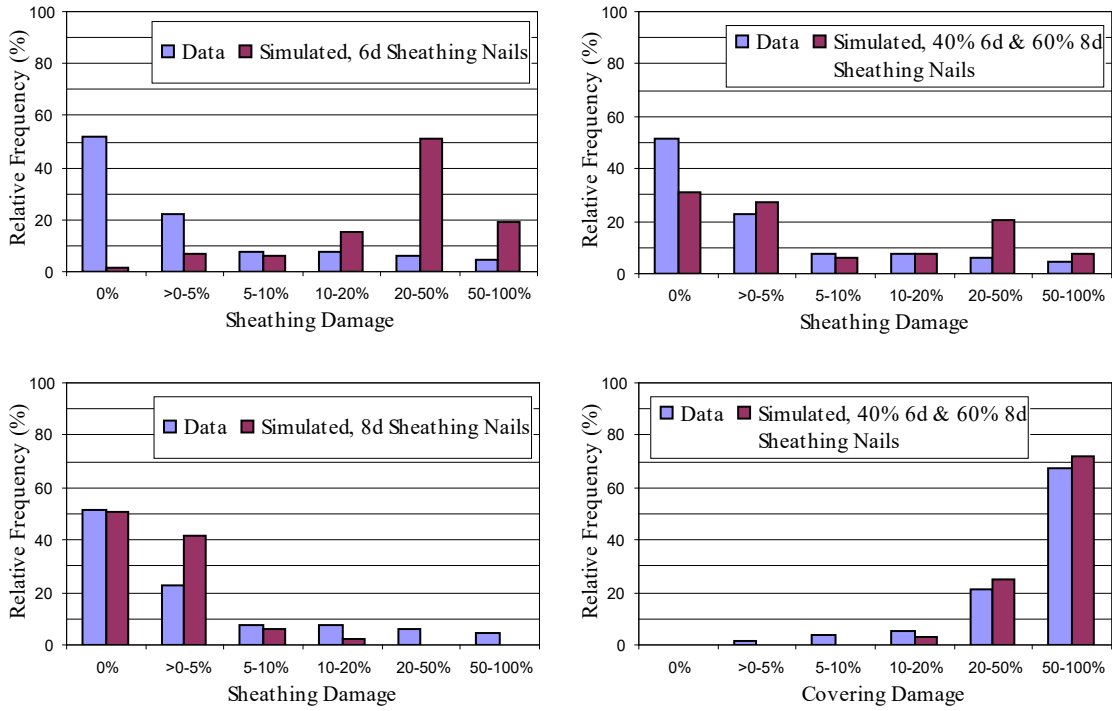


Figure 5-115 Comparison of Modeled and Observed Roof Damage States to Two-Story Gable Houses (Photograph 1)

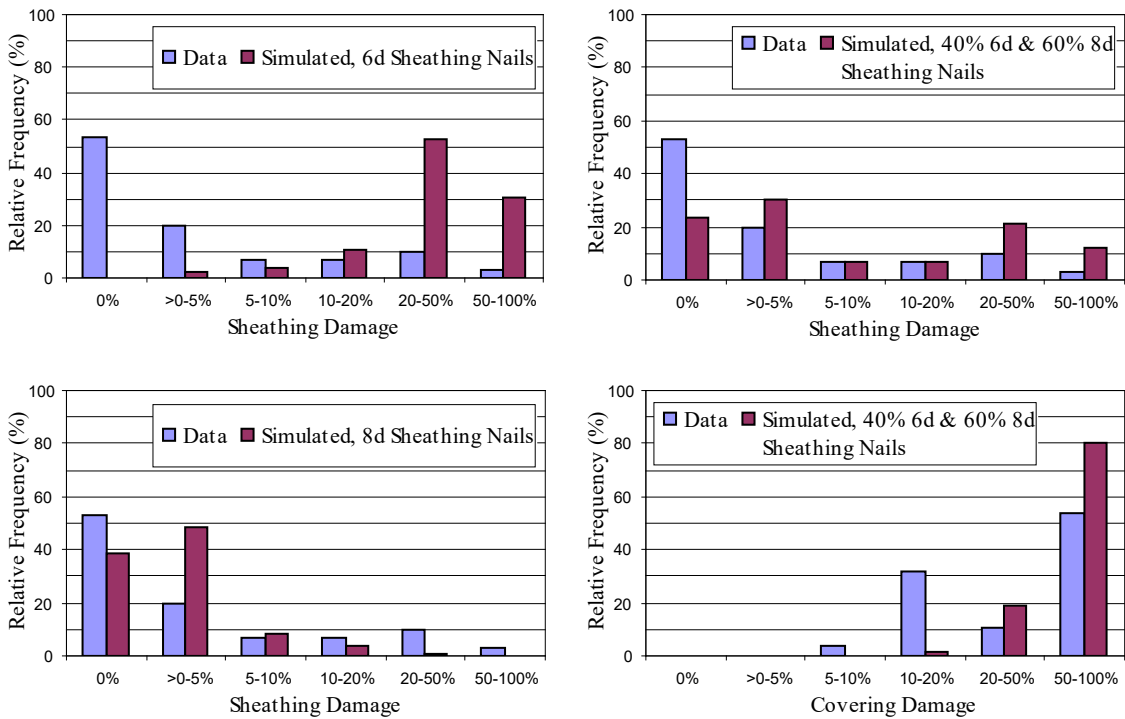


Figure 5-116 Comparison of Modeled and Observed Roof Damage States to Two-Story Gable Houses (Photograph 2)

5.5.1.1.1.6 Single-Story Gable Houses

Figure 5-117 and Figure 5-118 show comparisons of the simulated and observed roof damage states for the single-story gable roof homes. For the default building stock case, the modeled roof sheathing and roof covering damage states obtained using the ASCE 7 based loads agree reasonably well with the observed damage.

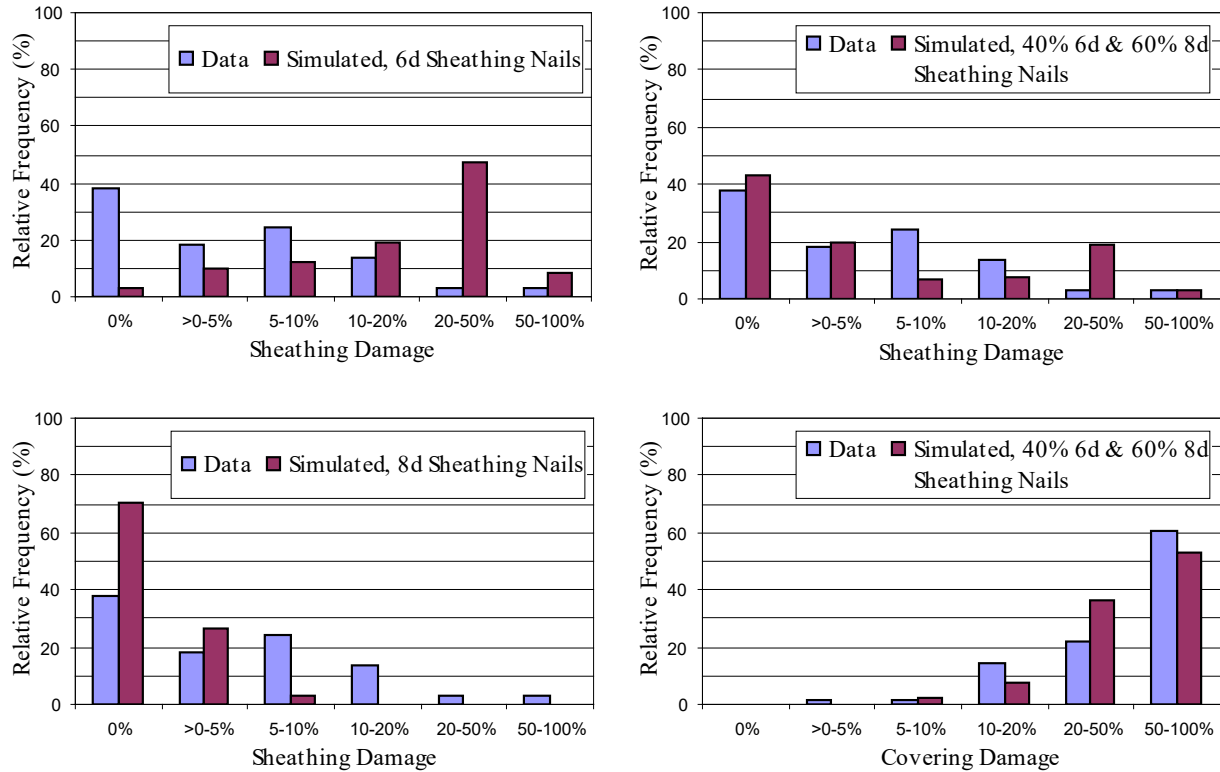


Figure 5-117 Comparison of Modeled and Observed Roof Damage States to Single-Story Gable Houses (Photograph 2)

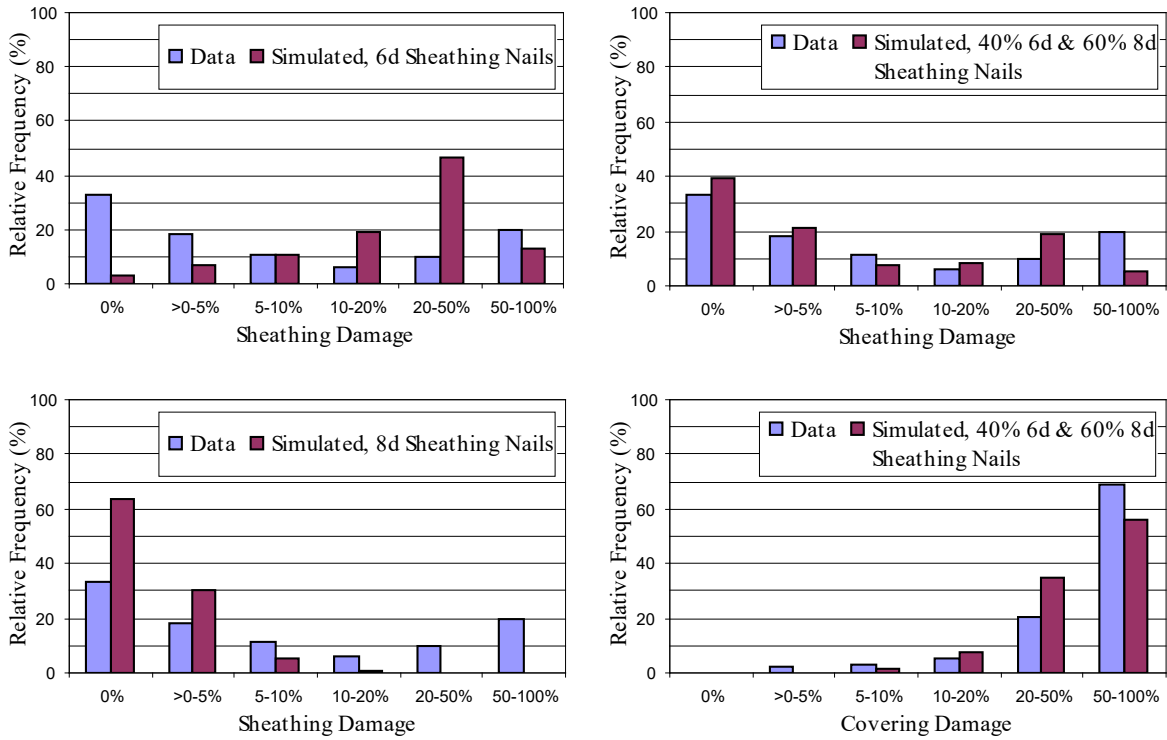


Figure 5-118 Comparison of Modeled and Observed Roof Damage States to Single-Story Gable Houses (Photograph 3)

Figure 5-119 and Figure 5-120 show the roof damage state comparisons for the single-story hip roof homes. The comparison of the roof damage states derived from the observations taken from Photograph 2 (Figure 5-119) show good agreement between the observed damage states and the predicted damage states using the ASCE 7 based loads for the default building stock. On the other hand, the comparisons of predicted and observed roof damage states for Photograph 3 (Figure 5-120) show the damage model to overestimate the roof damage to the single-story hip roof homes.

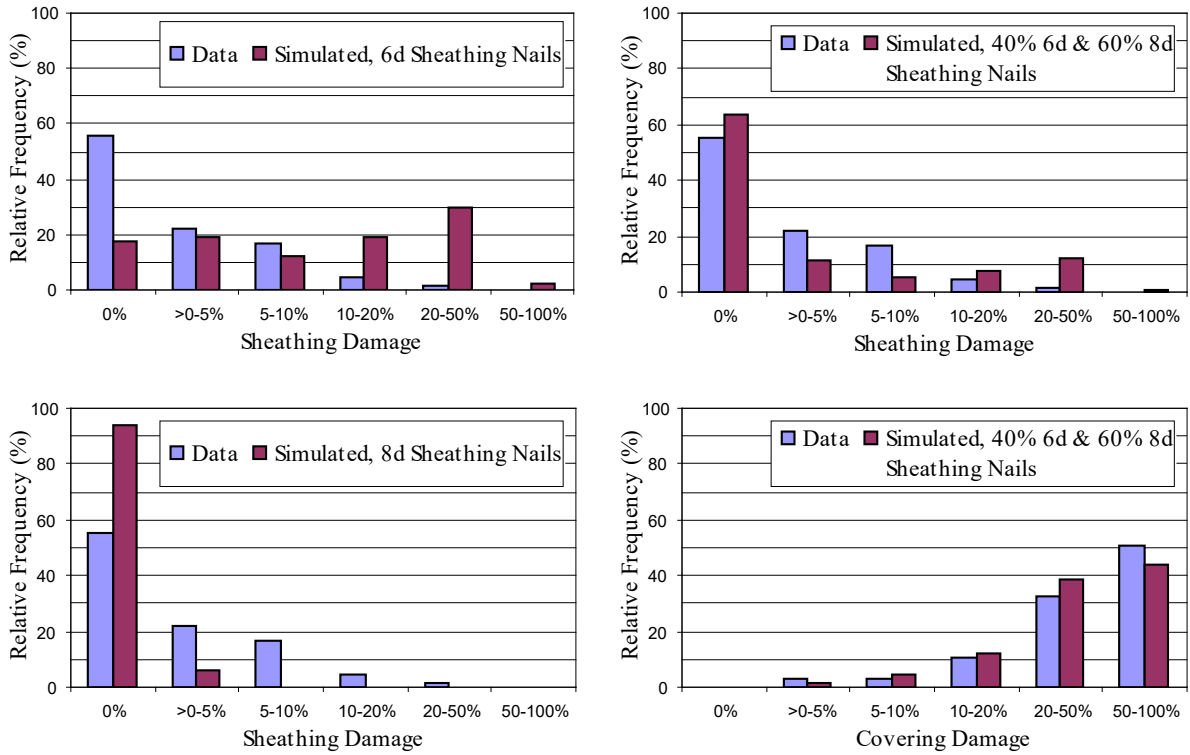


Figure 5-119 Comparison of Modeled and Observed Roof Damage States to Single-Story Hip Houses (Photograph 2)

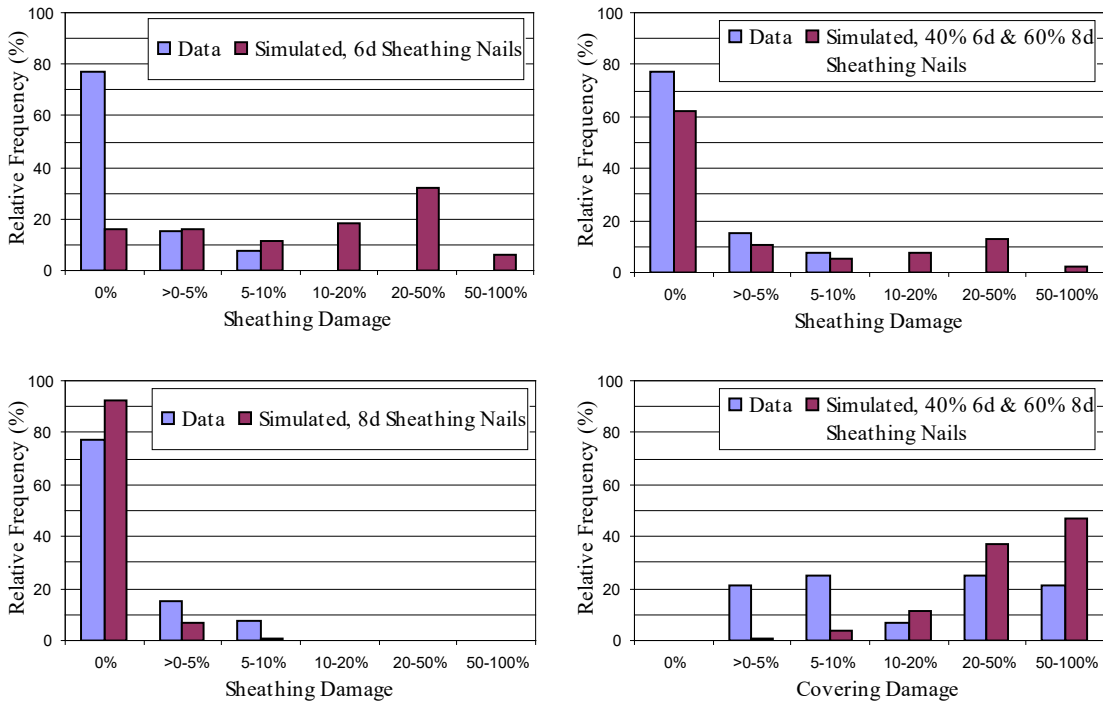


Figure 5-120 Comparison of Modeled and Observed Roof Damage States to Single-Story Hip Houses (Photograph 3)

In summary, given the assumption of the building stock with respect to the fraction of homes roofed with 6d and 8d sheathing nails, the predicted roof damage states obtained using the ASCE 7 based loads compare well with the observed roof damage states. In all cases examined, the simulated roof sheathing damage using 6d nails overestimated the observed damage and the simulated roof sheathing damage using 8d nails underestimated the observed damage – i.e., the observed data was contained within the two limiting simulations for all cases examined.

5.5.1.1.2 Hurricane Erin (1995)

The roof sheathing failure model is further validated through comparisons to damage sustained at Navarre Beach, Florida during Hurricane Erin. This area experienced peak gust wind speeds (open terrain at 10 meters above ground) in excess of 100 mph. The damage survey includes 161 wood frame residential structures. Table 5-35 shows the surface roughness values used in the simulation. Note that the shoreline at Navarre Beach runs east-west. The roof sheathing damage simulation is performed with 30% of the homes located along the first row adjacent to the shoreline and 70% of the homes located on inside rows. The building stock with respect to sheathing attachment is also taken here as 40% of the buildings roofed with 6d sheathing nails and 60% with 8d sheathing nails.

Table 5-35 Surface Roughness Values used in Hurricane Erin Sheathing Damage Validation Study at Navarre Beach, Florida

Wind Direction	Surface Roughness (m)	
	First Row of Homes Along Shoreline	Inside Rows
Onshore	0.03	0.1
Offshore	0.2	0.2
Along Shoreline ($\pm 15^\circ$)	0.1	0.15

Of the 161 structures surveyed, 91 have gable roofs and 43 have hip roofs. The gable roof homes are further divided into categories considering their orientation (i.e., gable ridge parallel to the shoreline and perpendicular to the shoreline) and their height. Comparisons of the observed roof sheathing damage and the simulated roof sheathing damage are shown in Table 5-36. Note that the modeled number of homes with sheathing damage is computed as the modeled percentage multiplied by the total number of homes in the survey rounded to the nearest integer.

As seen in Table 5 35, the comparison of the observed sheathing damage and modeled sheathing damage indicates that the damage model performs reasonably well, with a bias towards overestimating the damage levels for the two-story gable roof homes oriented perpendicular to the coast and underestimating the damage levels for the two-story gable roof homes oriented parallel to the shoreline. The sheathing damage for the hip roof homes is simulated considering an equal mix of single-story and two-story homes and an equal mix of homes with roof ridges parallel and perpendicular to the shoreline.

Table 5-36 Comparison of Observed and Modeled Roof Sheathing Damage at Navarre Beach, Florida

Case	Total Number of Structures in the Survey	Observed		Modeled	
		Number of Structures with Sheathing Damage	Percentage of Structures with Sheathing Damage	Number of Structures with Sheathing Damage	Percentage of Structures with Sheathing Damage
Single-Story Gable Roof Homes Oriented Parallel to Beach	10	0	0	0	0.60
Single-Story Gable Roof Homes Oriented Perpendicular to Beach	5	0	0	0	0.51
Two-Story Gable Roof Homes Oriented Parallel to Beach	56	12	21.4	3	4.7
Two-Story Gable Roof Homes Oriented Perpendicular to Beach	20	0	0	1	4.2
Hip Roof Homes	43	0	0	0	0.07

5.5.1.1.3 Hurricane Fran (1996)

Using aerial photography obtained from the American Association of Wind Engineers and an aerial video obtained from the North Carolina Department of Transportation, the performance of roof covering during Hurricane Fran on hip and gable roof residential structures was reviewed. A total of 49 gable roof homes and 112 hip roof homes were identified for the study. The structures are located in North Carolina at the north end of Wrightsville Beach and at the south end of Figure Eight Island. Note that this area was chosen since it received little or no damage during Hurricane Bertha, which preceded Hurricane Fran by about two months. The study area experienced peak gust speeds (open terrain at 10 meters above ground) between 105 and 110 mph during Hurricane Fran.

The shoreline at Wrightsville Beach and Figure Eight Island is oriented roughly northeast-southwest. The surface roughness values used in the simulation are the same as those used in the Hurricane Erin roof sheathing damage validation study (see Table 5-35). Consistent with observations from the aerial photography and video, the building stock used in the roof cover damage simulation for both the hip and gable roof homes comprised an equal mix of homes with roof ridges parallel and perpendicular to the shoreline, a three to one ratio of two-story homes versus single-story homes, and a seven to three ratio of homes located immediately adjacent to the ocean versus homes located at least one row away from the ocean. Also, a 40%/60% mix of structures with 6d and 8d sheathing nails were used in the damage simulation. The results of the analysis are shown in Figure 5-121.

As seen in Figure 5-121, the agreement between the observed and modeled damage states is quite good and the small difference in the performance of hip and gable roofs is seen in both the modeled and observed data.

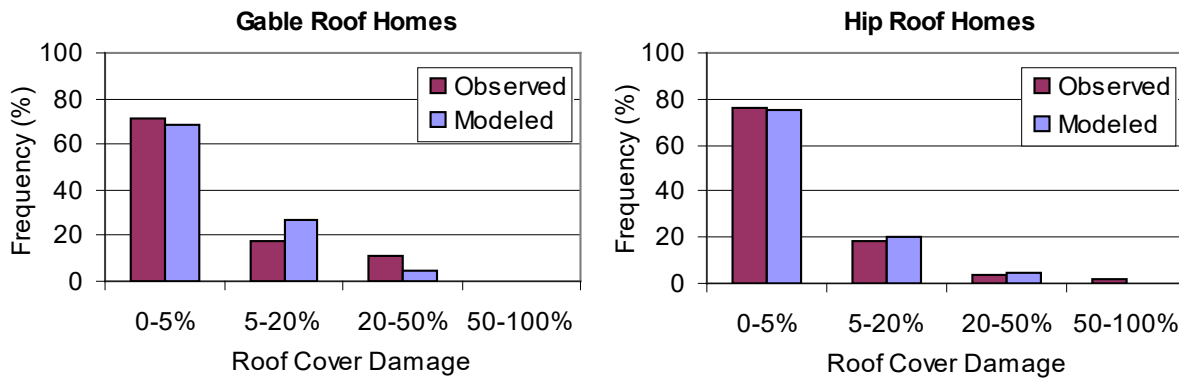


Figure 5-121 Comparison of Simulated and Observed Roof Covering Damage for Gable and Hip Roof Houses

5.5.1.2 Window Damage

Figure 5-122 shows a comparison of the window damage states resulting from the HUD damage survey following Hurricane Andrew and the damage simulation using ASCE 7 loads. The data given in Figure 5-122, both observed and modeled, are for the four locations used in the roof damage validation study. The comparison of the simulated and observed damage states are reasonable, but the model tends to overestimate the number of single-story homes that experience no window damage. In the case of two-story homes, both the simulation and the observations suggest that nearly all homes experienced the loss of at least one window. The damage simulation clearly reproduces the observation that two-story homes are likely to experience more window damage than one-story homes for the same wind event.

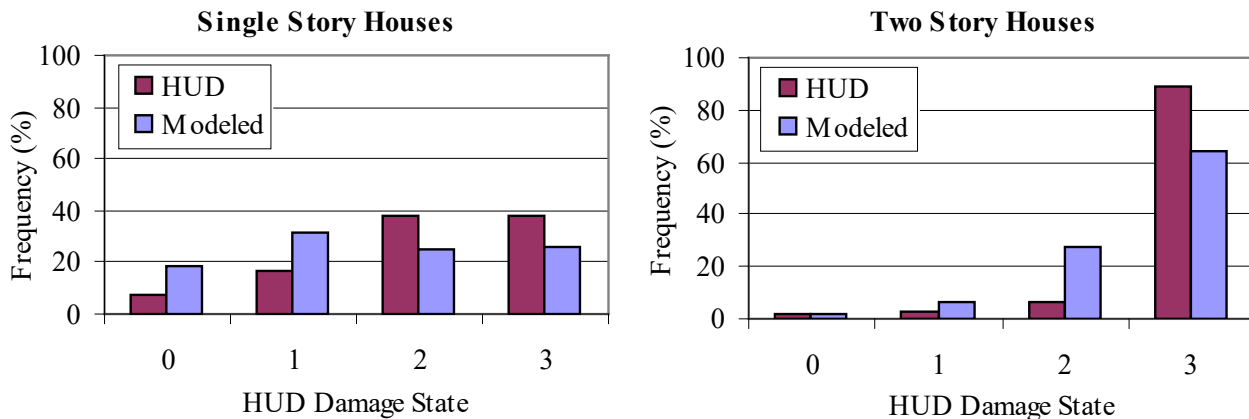


Figure 5-122 Comparison of Simulated and Observed Window Damage States for One and Two-Story Houses, Hurricane Andrew (1992)

5.5.1.3 Whole Roof Failures

The whole roof failure model is a relatively simple model, where the roof is considered to fail as a complete unit if the wind induced uplift loads (computed as a combination of the internal pressure effect and the external loads) exceed the total uplift capacity of the roof provided by the roof-wall connections and the self weight. In the case of gable roofs, roof trusses (or rafters) are assumed to be spaced at 24" on center along two walls of the building. In the case of hip roofs, a roof-wall connection is assumed to

exist at 24" intervals along the entire perimeter of the building (i.e., for a square building, the hip roof has twice as many roof-wall connections as the gable roof).

Using the data collected from the four aerial photographs of damage sustained during Hurricane Andrew discussed earlier, comparisons between the observed and modeled whole roof failure rates were performed. Observed whole roof failures from the aerial photography are assumed to be gable roofs and not hip roofs. Figure 5-123 shows a section from Photograph 3 depicting eight homes, three of which are seen to have experienced a complete (or near complete) roof failure.



Figure 5-123 Examples of Whole Roof Failures Depicted in Photograph Number 3

All roof-wall connections were modeled as a strapped connection having a mean resistance of 1,200 pounds and a coefficient of variation of 30%. Roof trusses are spaced at 24" on center. The statistics of the modeled failure rates are computed from 1,000 simulations of a randomly oriented house located at the position of the photograph. Note that these comparisons include a calibration factor of 0.8 applied to the uplift resistances. The calibration factor was developed by comparing the modeled values with the ground-truthed values and applied to make more accurate predictions. Shingle and tile roof coverings were both considered in the analysis. The self weight of the roof with shingles is estimated to be 10.4 psf and with tiles it is estimated to be 18.4 psf. The default building stock with respect to roof covers is taken as 70% with shingles and 30% with tiles after HUD (1993). Comparisons are given in Table 5-37. In the case of the observed failure rates, the fraction given in parentheses represent the number of failures over the number of buildings observed in the photograph. The comparisons given in Table 5-37 show good agreement between the modeled and observed failure rates for the default building stock for Photographs 3 and 4. The model overestimates the whole roof failure rate for Photograph 2.

Table 5-37 Comparison of Observed and Modeled Whole Roof Failures at Locations of Aerial Photographs, Hurricane Andrew (1992)

Photograph	Frequency of Whole Roof Failures □ Single-Story Gable Roof Homes			
	Observed	Modeled		
		Shingles	Tiles	70% Shingles/ 30% Tiles
1	-	-	-	-
2	0.65% (3/308)	8.0%	0.60%	5.8%
3	10.8% (21/193)	14.3%	1.4%	10.4%
4	0.32% (1/311)	0.50%	0.00%	0.35%
Average	3.1% (25/812)	6.6%	0.6%	4.8%

Figure 5-124 and Figure 5-125 show modeled failure rates for strapped and toe-nailed single-story hip and gable roof homes, for three different generic terrains (open terrain, defined with $z_0 = 0.03$ meters, standard suburban terrain, defined with $z_0 = 0.35$ meters and treed terrain, defined with $z_0 = 1.0$ meter) as a function of the peak gust wind speed at a height of 10 meters above ground in open terrain. The mean uplift capacity and coefficient of variation of an individual toe-nailed connection are 415 pounds and 25%, respectively. Note that the experimental values of the toe-nail connections discussed in Section 5.4.5 present results with mean capacities ranging between 208 pounds up to 676 pounds, and thus the 415 pounds value used herein is simply a representative value.

The failure rates were computed using a simulation of hurricanes in the South Florida area, where for each simulation, the number of homes experiencing a whole roof failure (using 30 simulations/storm) was saved along with the peak gust wind speed (10 meters in open terrain) experienced at the site. The results given in Figure 5-124 and Figure 5-125 clearly indicate the hip roofs are less susceptible to failure than the gable roofs (as has been well documented in the literature), and that the results are very strongly dependent on the assumed terrain.

The potential for detailed validation of the non-strapped results presented in Figure 5-124 and Figure 5-125 is limited, since there are no known systematic, statistically unbiased studies examining the performance of roofs in regions where the application of straps (or clips) at the roof-wall connections are not used. Thus the results given in Figure 5-124 and Figure 5-125 are given primarily to assess the reasonableness of the simple uplift failure model.

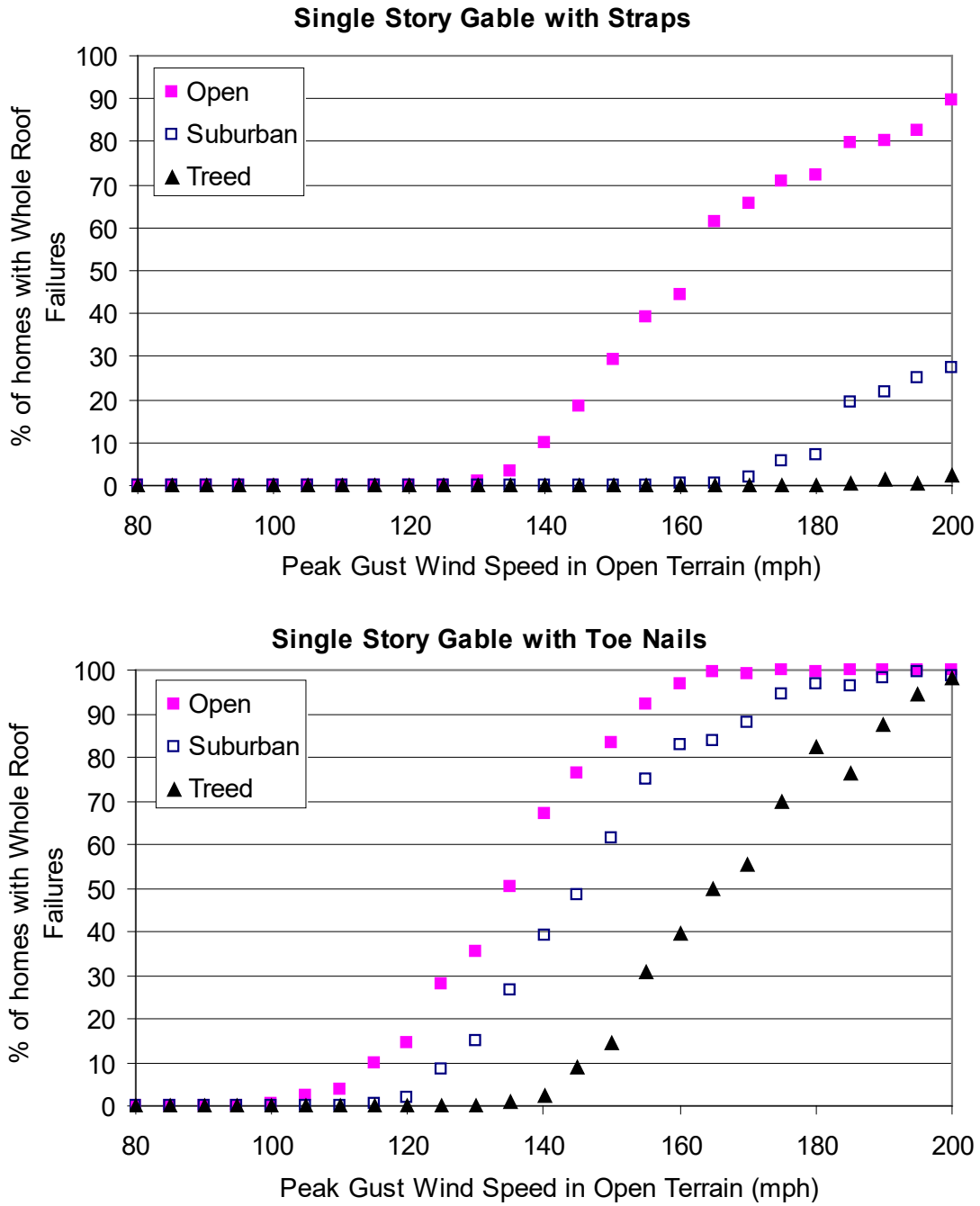


Figure 5-124 Modeled Failure Rates for Single-Story Gable Roof Homes with Strapped Roof-Wall Connections and Toe Nailed Roof-Wall Connections

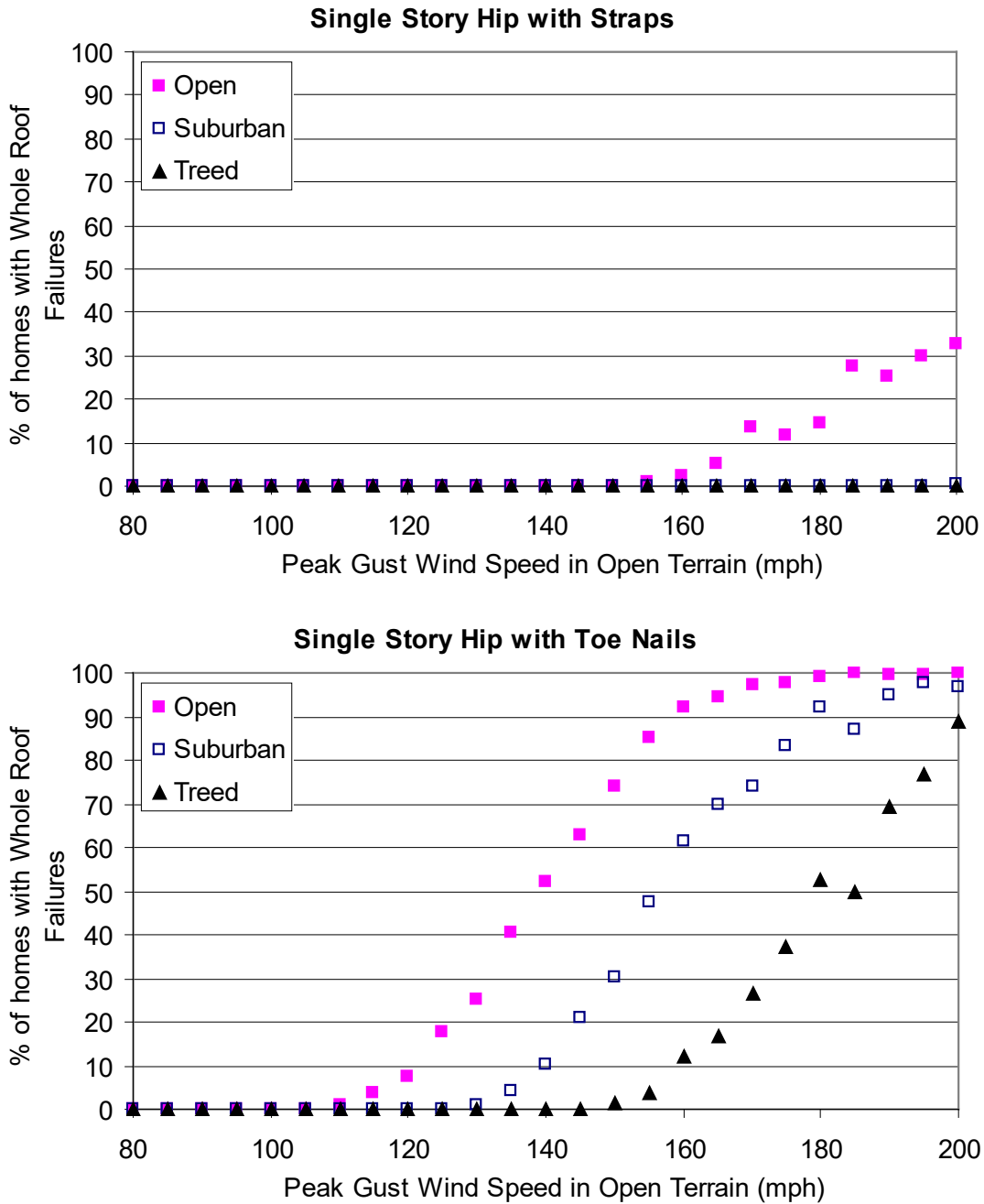


Figure 5-125 Modeled Failure Rates for Single-Story Hip Roof Homes with Strapped Roof-Wall Connections and Toe Nailed Roof-Wall Connections

5.5.2 Manufactured Homes

The manufactured home damage model has been validated through comparisons of damage states predicted from the above model to the damage states predicted from the models of Vann and McDonald (1978) and Vasquez (1994), as well as through comparisons of observed damage from Hurricane Bertha (1996) along the North Carolina coast, Hurricane Andrew (1992) in Dade County Florida, and Hurricane Elena (1986) along the Central Gulf Coast.

5.5.2.1 Comparisons of Wind Speed versus Damage Predictions to the Vann and McDonald Model and the Vasquez Model

Table 5-38 presents a comparison of the threshold wind speeds (peak gust, 10m open terrain) associated with various damage states obtained from the load and resistance model described herein, to those given by Vann and McDonald (1978) and Vasquez (1994). The damage states given in Table 5-38 are valid for units located in open terrain. The first column in Table 5-38 presents the damage identification codes given in Vasquez (1994). The Vann and McDonald damage states are applicable to pre-HUD units only, whereas the Vasquez data likely includes a mix of pre-HUD and HUD units. Both models have been derived from wind speed versus damage data collected from post-storm damage surveys. In the case of the modeled damages, the threshold wind speeds are defined as the wind speeds where approximately 5% of the modeled units experience the indicated damage.

Table 5-38 Comparison of Threshold Velocities for Various Manufactured Home Damage States

Damage Code	Damage Description	Vann and McDonald	Vasquez	ModelPre-HUD	ModelHUD
1.1A (MI)	Minor Sliding Damage - No Anchors	60-70	<85-100	90-100	90-100
1.1A (MA)	Major Sliding Damage - No Anchors	65-90	<100-115	115-125	115-125
1.1B (MA)	Major Vaulting Damage - No Anchors				
1.1B (DE)	Total Vaulting Damage - No Anchors				
1.1C (MA)	Major Overturning Damage - No Anchors	60-70	<85-100		
1.1C (DE)	Total Overturning Damage - No Anchors	90-125	<85-100	110-120	110-120
1.2A (MA)	Total Overturning Damage - Anchor Pull Out	120-130	<120-130	130-140	130-140
1.2B (DE)	Total Overturning Damage - Tie Failure	120-130	<120-130	130-140	130-140
2A (MI)	Roof to Wall Connection Failure - Minor	60-70		100-110	100-110
2A (MA)	Roof to Wall Connection Failure - Major	90-125	110-120	100-110	110-120
2A (DE)	Roof to Wall Connection Failure - Destruction	120-130	<120-130	100-110	120-130
2B (MA)	Floor to Wall Connection Failure - Major	120-130	100-110	95-105	100-110
2B (DE)	Floor to Wall Connection Failure - Destruction		<120-130		
2C (MA)	Structural Member Failure - Major	120-130			

Damage Code	Damage Description	Vann and McDonald	Vasquez	ModelPre-HUD	ModelHUD
2C (DE)	Structural Member Failure – Total		<120-130		
2D (MA)	Tree or Large Missile Impact – Major	120-130	110-110		
2D (DE)	Tree or Large Missile Impact – Total	120-130	<120-130		
3A (MI)	Window Damage – Minor		<110-120	100-110	100-110
3B (MI)	Door Damage – Minor		<120-130		
3C (MI)	Roof Covering Damage – Minor	65-90	85-95	70-80	70-80
3C (MA)	Roof Covering Damage – Major	120-130	85-95	120-130	120-130
3C (DE)	Roof Covering Damage – Total		<120-130	120-130	120-130
3D (MI)	Wall Panel Damage – Minor		85-95	90-100	90-100
3D (MI)	Wall Panel Damage – Major		85-95	120-130	120-130
3D (DE)	Wall Panel Damage – Total	120-130	<120-130		
3E (MI)	Small Debris Damage – Minor		100-110		
3E (MA)	Small Debris Damage – Major		<85-95		

The general observation that can be made by comparing the threshold wind speeds given in Table 5-38 is that the model developed here tends to yield higher threshold wind speeds for foundation failures, but lower threshold wind speeds for the initiation of the roof-wall connection failures. The threshold wind speeds associated with the initiation of wall-floor connection failures are comparable to those given in the Vasquez model, but lower than those suggested by the Vann and McDonald model. The wind speeds associated with the initiation of cladding failures are generally comparable between models, with the exception that the load-resistance model developed here yields higher estimates of the wind speeds required to initiate wall cladding loss.

5.5.2.2 Hurricane Bertha Validation

Following Hurricane Bertha (1996), ARA sent a team of engineers to perform a post-storm damage survey quantifying the wind induced damage to buildings along the North Carolina coast. During this damage survey, 114 manufactured home units around the Surf City area on Topsail Island were surveyed. All of the manufactured homes surveyed were tied down, and it was not determined what fraction of the homes were pre-HUD and HUD homes. The survey recorded the condition of the manufactured homes, noting damage to windows, siding and the roof system. The overall damage states of the 114 buildings are given in Table 5-39, along with the modeled damage produced by simulating the full time series of wind speed and direction produced by Hurricane Bertha at Surf City. The terrain around the manufactured home

parks was typically fairly open, and thus a surface roughness of 0.1 meters is used to model the basic terrain. The modeled damage states in Table 5-39 are given for both the HUD and pre-HUD model manufactured homes. The peak gust wind speed (open terrain, 10 meters) resulting from the Hurricane Bertha simulation was 103 mph.

Table 5-39 Comparison of Observed and Modeled Manufactured Home Damage States on Topsail Island Produced by Hurricane Bertha (1996)

Observed Damage State	Percent Observed	HUD Home Simulation	Pre-HUD Home Simulation
No Damage	85%	85%	85%
Loss of One Metal Siding Panel	7%	10%	10%
Partial Roof Deck Failure	2.6%	0.3%	0.3%
Whole Roof Failure	1.8%	2.2%	3.7%
One Broken Window	6%	2.4%	2.4%
More than One Broken Window	0.9%	2.2%	2.2%

The comparison of the simulated and observed damage states shown in Table 5-39 indicates reasonable agreement between the modeled and observed damage states, with the model tending to slightly overestimate the number of units with minor siding damage and the number of units with whole roof damage. The overestimate of the whole roof damage is somewhat offset by the underestimate of the number of units experiencing partial roof loss. The model tends to underestimate the number of units with window damage, but the prediction of the number of units expected to sustain no damage is correct.

5.5.2.3 Hurricane Andrew Validation

Following Hurricane Andrew, a report was prepared for the Manufacturing Housing Institute by Ferguson and Cardwell (1992) describing the intensity and type of damage experienced by manufactured home units located throughout the region impacted by the storm. The damage to the units in each of the surveyed parks was characterized using the damage classification system developed by Vann and McDonald (1978). To further validate the manufactured home damage model, comparisons of simulated and observed damage states in six of the parks surveyed by Ferguson and Caldwell are performed. In order to facilitate these comparisons, the damage states predicted by the damage model had to be mapped to correspond to the damage classification scheme developed by Vann and McDonald. Table 5-40 describes the damage states associated with each of the five damage classes suggested by Vann and McDonald and Table 5-41 describes the predicted using the load and resistance based manufactured home damage model for each class for each damage state. It is noteworthy that there is a fine line between the damage associated with Classes 3 and 4, and it is likely that in both the observations and the mapping between modeled damage to Class 3 and 4 damage, there will be a number of misclassifications.

Table 5-40 Damage Classes Described by Vann and McDonald and the Corresponding Damage States from the Damage Simulation Model

Damage Class	Description of Damage (Vann and McDonald, 1978)
0	<i>No Damage or Very Minor Damage</i> - Little or no visible damage from the outside. Slight shifting on the blocks that would suggest re-leveling, but not off the blocks. Some cracked windows, but no resulting water damage.
1	<i>Minor Damage</i> - Shifting off the blocks or so that blocks press up to the floor; re-leveling required. Walls, doors, etc., buckled slightly, but able to be corrected by re-leveling. Minor eave and upper wall damage, with slight water damage but roof not pulled all the way back. Minor pulling away of siding with slight water damage. Minor missile and/or tree damage. Slight window breakage and attendant water damage.
2	<i>Moderate Damage (Still Livable)</i> - Severe shifting off the blocks with some attendant floor and superstructure damage (punching, racking, etc.). Roof removed over a portion or all of the home but the joists remain intact, walls not collapsed. Missile and/or tree damage to a section of the wall or roof, including deep dents or punctures. Serious water damage from holes in roof, walls, windows, doors or floors.
3	<i>Severe Damage (Not Livable, but Repairable)</i> - Unit rolled onto side but frame intact. Extreme shifting causing severe racking and separations in the superstructure. Roof off, joists damaged or removed, walls damaged from lack of lateral support at top. Severe tree damage, including crushing of one wall or roof section. Superstructure partially separated from under frame.
4	<i>Destruction (Not Livable)</i> - Unit rolled onto top or rolled several times. Unit tossed or vaulted through the air. Superstructure separated from the underframe or collapsed to side of the underframe. Roof off, joists removed and walls collapsed. Destruction of a major section by a falling tree.

Table 5-41 The Corresponding Damage States from the Damage Simulation Model

Damage Class	Modeled Damage States*					
	Roof Cover Damage	Siding Damage	Window and Door Failures	Roof Sheathing Failures	Roof to Wall and/or Wall to Foundation Connection Failures	Foundation to Ground Anchor Failures
0	≤10%	≤1 Panel	None	None	None	None
1	>10% to ≤25%	>1 to ≤25%	1 or 2	None	None	Minor Sliding
2	>25%	>25%	>2 to ≤50%	>0% to ≤25%	Minor	Typically Minor Sliding
3	Typically >25%	Typically >25%	>50%	>25%	Typically Minor	Major Sliding
4	Typically >25%	Typically >25%	Typically >50%	Typically >25%	Major	Overturning or Uplift

The location of each manufactured home park surveyed by Ferguson and Caldwell was noted only approximately. For example, the location of the park referred to as University Lakes is given as “South side of U.S. 41, one mile west of the Florida Turnpike.” The locations given by Ferguson and Caldwell are accurate enough to place the parks for the purposes of performing a site-specific wind speed simulation, but not accurate enough to place the parks for the purposes of estimating a surface roughness length. Damage simulations have been performed for each location using surface roughness lengths of 0.1 meters and 0.3 meters. All damage simulations were performed using a site-specific simulation of the hurricane wind velocities, but the orientation of the units was taken as random, with a total of 1,000 damage simulations performed for each park.

Table 5-42 presents the results of the damage simulations, along with a comparison of the damage descriptions for each site given by Ferguson and Caldwell. Also given in Table 5-42 are the simulated maximum peak gust wind speeds (10 meters, open terrain) at each site obtained from the simulation of Hurricane Andrew.

Table 5-42 Comparison of Modeled and Observed Manufactured Home Damage States Following Hurricane Andrew in South Florida

Park Name and Number of Units	Description of Park and Damage Along with Estimated Peak Gust Wind Speed (10 m, Open Terrain)	Modeled Percent of Manufactured Homes Predicted in Each Damage Class										
		Unit Class	z ₀ = 0.10 m					z ₀ = 0.30 m				
			0	1	2	3	4	0	1	2	3	4
Courtly Manor (521 Spaces)	50% HUD-labeled; Some Class 0 and 1 damage; 1 pre-HUD Class 3 damage; Peak gust wind speed 104 mph	Pre-HUD	85	7	3	<1	5	95	3	1	<1	1
		HUD	88	7	2	<1	2	96	3	<1	<1	<1
University Lakes (1,100 spaces)	40% HUD-labeled; 20 Class 3 or 4 damage, all pre-HUD; HUD Class 0 or 1 damage; Peak gust wind speed 135 mph	Pre-HUD	11	15	8	6	60	41	16	12	5	27
		HUD	13	6	10	9	52	44	18	13	6	20
Un-named Park	Old Park, no HUD units; Class 3 and 4 damage; Peak Gust Wind Speed 156 mph	Pre-HUD	4	2	1	3	94	5	11	5	6	73
		HUD										
Dadeland (Estimate 200)	50% HUD-labeled; All class 2, 3, and 4 damage; Peak gust wind speed 159 mph	Pre-HUD	0	1	<1	1	98	11	6	3	4	86
		HUD	0	1	<1	2	97	11	7	4	8	80
Redlands (Estimate 90)	Older Park, mostly pre-HUD; 1 HUD Class 1 damage, else class 3 and 4 damage; Peak gust wind speed 162 mph	Pre-HUD	0	<1	<1	1	99	1	6	2	3	88
		HUD	0	<1	<1	2	97	1	7	3	6	84
Isla Gold	50% RV, 10-20% HUD; Mostly Class 4 damage; Some HUD Class 2 and 3 damage; 1 HUD Class 1 damage; Peak gust wind speed 162 mph	Pre-HUD	<1	1	1	2	95	2	7	4	4	83
		HUD	<1	1	2	4	92	2	9	7	8	74

The overall agreement between the observed and simulated damage states is generally good, except in the case of the homes located at University Lakes, where the model overestimated the number of HUD units experiencing Class 3 and 4 level damage, and the model underestimated the number of units experiencing the lower-level Class 0 and 1 damage states. In the low wind speed case (Courtly Manor), the predicted and observed percentage of units experiencing damage levels in Classes 0 and 1 is agreeable. In the high wind speed cases (Unnamed Park, Dadeland, Redlands and Isla Gold), the lack of knowledge of the true terrain at the sites clouds the comparisons, but generally the agreement is good.

5.5.2.4 Hurricane Elena

The damage data described in McDonald and Vann (1986) is used to validate the manufactured home damage model using the observed manufactured home damage surveyed following Hurricane Elena (1985) along the Central Gulf Coast. A total of ten parks were surveyed, but the location of only eight of the ten are given by the authors. The description of each of the sites, in terms of the surrounding terrain, is limited with the statement made that some communities were located in heavily wooded areas while others were sited on rolling hills that were free of trees and other obstructions to the wind. The authors go on to say that the site on Dauphin Island and the one located on the west shore of Mobile Bay were the most exposed to hurricane winds. In the damage simulations, a surface roughness of 0.3 meters was used for all parks, except the one located on Dauphin Island where a surface roughness of 0.1 meters was used.

In McDonald and Vann (1986), the fraction of anchored homes were noted for four of the eight parks. The fraction of homes in each damage state resulting from the damage simulation was presented as a weighted average of the anchored and non-anchored cases. At the remaining four sites, no information is given as to what fraction of the units were anchored. In these latter four cases, simulated damage states are given separately for anchored and non-anchored units. The survey of the anchor systems at the first four parks suggest that, on average, 70% of the units were properly anchored. Also, no information is given in McDonald and Vann (1986) as to what fraction of the units were HUD or pre-HUD units, although the authors do note that the HUD units performed better than the pre-HUD units. In the damage simulations, only non-HUD units are modeled, and thus the model results should yield a bias towards higher than observed damage.

The comparisons of the simulated and observed damage states are given in Table 5-43. As in the case of the Hurricane Andrew data, the observed unit damage classes are defined using the Vann and McDonald damage classification system. The peak gust wind speeds given in Table 5-43 are those resulting from the simulation of Hurricane Elena and are representative of the peak gust wind speed at a height of 10 meters in open terrain.

Table 5-43 Comparison of Simulated and Observed Manufactured Home Damage States Produced by Hurricane Elena

Manufactured Home Park	Observed Percentage of Units in Each Damage Class					Modeled Percentage of Units in Each Damage Class ¹				
	0	1	2	3	4	0	1	2	3	4
Trade Winds, Dauphin Island, AL (20)Peak Gust Wind Speed 126 mph	5	35	20	0	40	16	15	7	6	55
Trav Park, West Shore of Mobile Bay, AL (12)Peak Gust Wind Speed 109 mph	75	25				89	6	1	0	4
Old Fort Village, Gautier, MS (97)Peak Gust Wind Speed 122 mph	42	39	4	3	11	54	16	7	3	13
Isle of Pines North, Gautier, MS (102)Peak Gust Wind Speed 124	48	23	6	4	19	44	17	10	4	26
Isle of Pines South, Gautier, MS (86)Peak Gust Wind Speed 124 mph	55	22	5	2	16	40	19	9	1	31
Imperial Estates, North Biloxi, MS (87)Peak Gust Wind Speed 122 mph	89	3	1	3	3	68	17	1	0	14
Rolling Hills, North Biloxi, MS (175)Peak Gust Wind Speed 122 mph	87	10	1	1	1	61	17	1	0	21
Anchor, Gautier, MS (70)Peak Gust Wind Speed 126 mph	76	19	1	0	4	40	19	9	1	31

¹ Two rows of modeled data given at sites where the fraction of anchored units is not known. The upper line represents non-anchored units and the lower line represents anchored units. When a single row of modeled data is presented, results represent a weighted average of anchored and non-anchored damage states.

Considering the uncertainties associated with terrain, anchor systems and age of the units, the comparison of the simulated and observed damage states given above is encouraging. Furthermore, following the discussion given in McDonald and Vann (1986), comparisons of the damage states should be made through comparisons of the total fraction of units in Classes 0, 1 and 2 combined (minor damage) and those in Classes 3 and 4 combined (major damage). With this grouping of damage states, the overall level of agreement between the simulated and observed damage states from the three validation studies is seen to be good.

5.5.3 Roof Covers on Flat Roofs

Two detailed validation studies have been performed for Hurricane Andrew (1992).

5.5.3.1 Hurricane Andrew (1992) – Dixie Highway

The first validation study uses an aerial photograph taken after Hurricane Andrew in a commercial area located in Miami-Dade County in the vicinity of Dixie Highway and SW 184th Street. The photograph shows an area of approximately 1,600'×4,100'. The estimated peak gust wind speed for this area at a height of 10 meters above ground is 129 mph. This translates to about 163 mph at the same height in open country terrain. Twenty-seven buildings were identified with built-up roof (BUR) covers and the percent roof cover damage was estimated for each of them. It is likely that the roof cover materials and installation methods vary over the buildings used in this validation study. Of the 27 buildings identified, 13 are two-story commercial buildings and 14 are one-story residential structures. The majority of the two-story buildings are rectangular in plan with several of them being square or comprised of two or more rectangular elements (i.e., L-shaped). The one-story buildings are all rectangular in plan. The simulation is performed on a two-story rectangular building (aspect ratio of 2.25) and a one-story rectangular building (aspect ratio of 1.5). The aspect ratios are consistent with the those of the surveyed buildings. The building stock considered in the analysis was assumed to comprise 40% of the buildings with roof sheathing attached with 6d nails and 60% with 8d nails.

Figure 5-126 shows the histogram of observed BUR cover damage in comparison to that predicted by the model. The one-story residential buildings were modeled with “average” and “poor” quality roof cover systems, while the two-story commercial building was modeled with “average” and “good” quality roof cover systems. It can be seen in Figure 5-126 that the one-story residential buildings performed consistently to the predictions using the “poor” quality BUR cover model, and the two-story commercial buildings performed consistently to the predictions using the “good” quality BUR cover model.

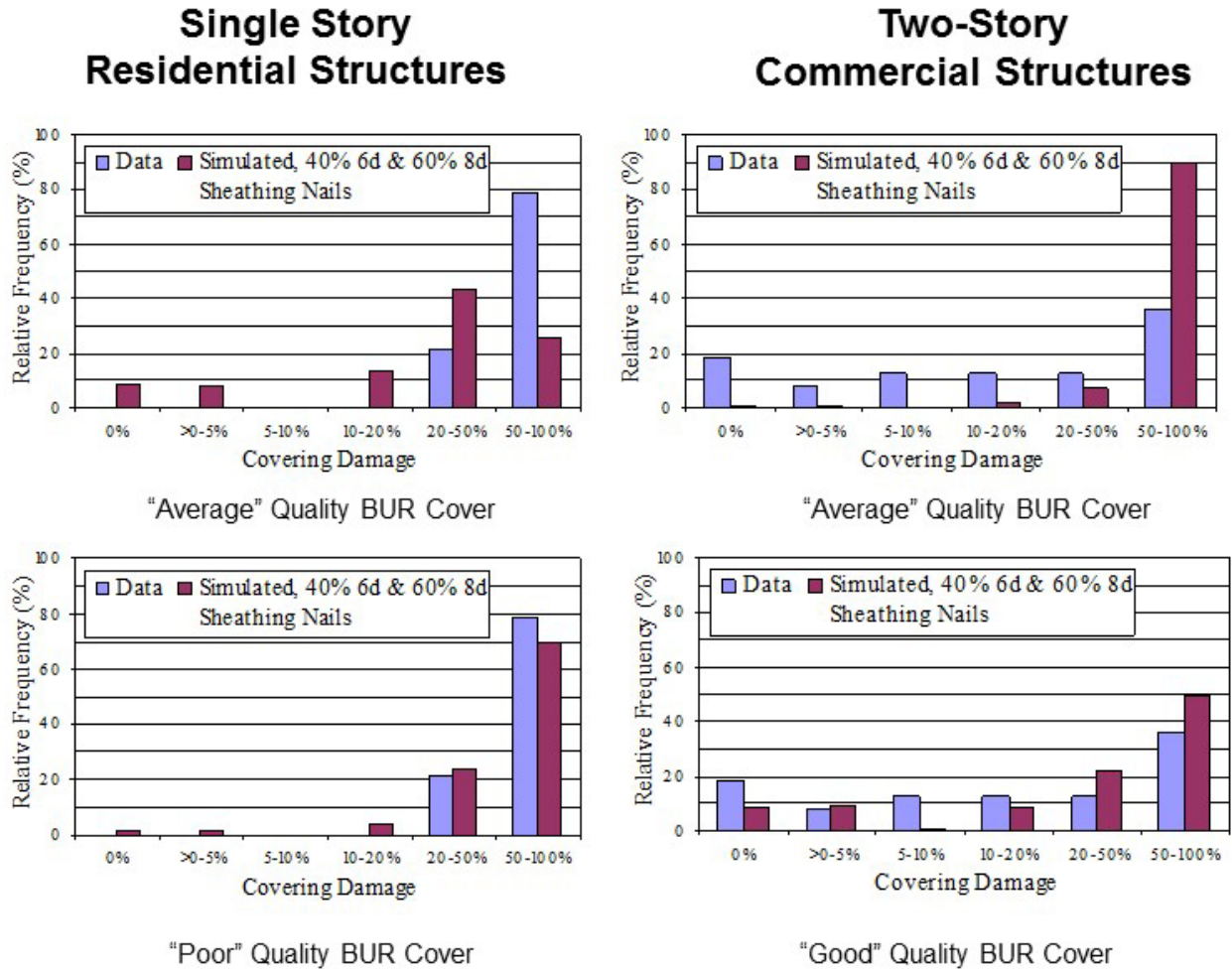


Figure 5-126 BUR Cover Damage for Hurricane Andrew - Dixie Highway

5.5.3.2 Hurricane Andrew (1992) – Aerial Photograph 3

The second validation study for Hurricane Andrew (1992) uses damage statistics observed from Aerial Photograph 3 (see description in Section 5.5.1). This photograph showed 15 one-story units with square plan dimensions and 15 one-story units with rectangular plan dimensions (the aspect ratios range from approximately 3 to 5). The residential buildings were built with 4'x8' plywood roof sheathing and BUR covers. The simulated BUR cover damage statistics are derived from 5,000 simulations using both a one-story square structure and a one-story rectangular structure (aspect ratio equal to four). The simulations are performed considering a 40%/60% mixture of buildings with 6d and 8d sheathing nails, respectively.

The comparisons given in Figure 5-127 show that the model under-predicts the BUR cover damage observed in the aerial photograph using the "average" quality BUR cover model and performs reasonably well using the "poor" quality model.

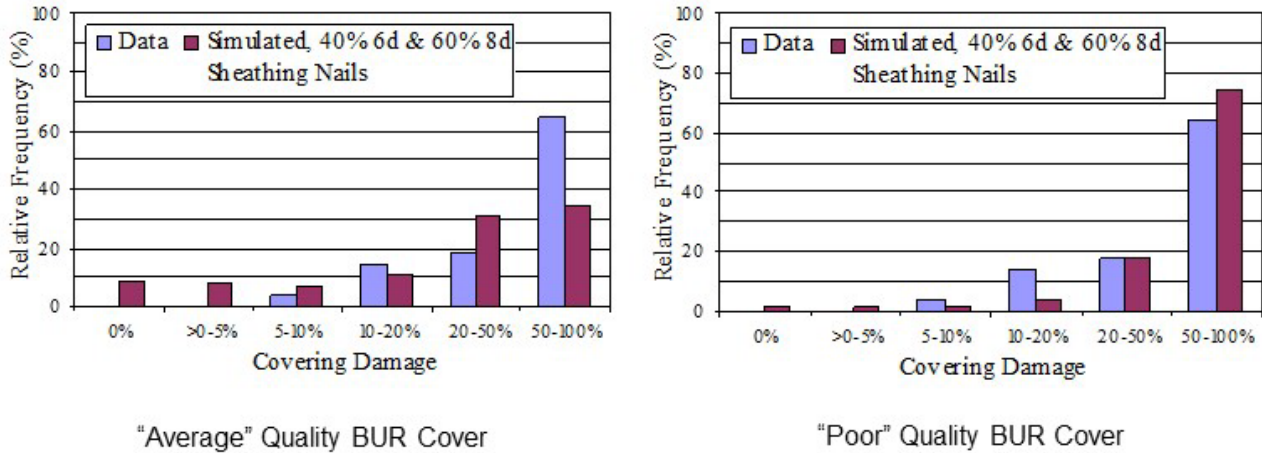


Figure 5-127 BUR Cover Damage for Hurricane Andrew - Aerial Photograph 3

5.6 Damage Model Results

5.6.1 Residential Buildings

Following an approach similar to that used by Vann and McDonald (1978) for defining damage states to manufactured homes, the damage state descriptions used for residential buildings are given in Table 5-44. The damage states are primarily governed by the performance of the building envelope, and are divided into five states, varying between 0 (no damage) and 4 (destruction). In Table 5-44, a building is considered to be in the higher damage state if any of the shaded damage indicators in the corresponding row occurs. For example, for a building to be considered to have sustained minor damage, the building must not have sustained structural failure or sheathing failure, and either one fenestration (window, door, garage door) failed or more than 2% but less than 15% of the roof cover failed. Photographs of buildings in each of Damage States 0 through 4 are given in Figure 5-128, Figure 5-129, Figure 5-131, Figure 5-132, and Figure 5-133.

Table 5-44 Damage States for Residential Construction Classes

Damage State	Qualitative Damage Description	Roof Cover Failure	Window Door Failures	Roof Deck	Missile Impacts on Walls	Roof Structure Failure	Wall Structure Failure
0	<u>No Damage or Very Minor Damage</u> Little or no visible damage from the outside. No broken windows, or failed roof deck. Minimal loss of roof over, with no or very limited water penetration.	≤2%	No	No	No	No	No

Damage State	Qualitative Damage Description	Roof Cover Failure	Window Door Failures	Roof Deck	Missile Impacts on Walls	Roof Structure Failure	Wall Structure Failure
1	<u>Minor Damage</u> Maximum of one broken window, door or garage door. Moderate roof cover loss that can be covered to prevent additional water entering the building. Marks or dents on walls requiring painting or patching for repair.	>2% and ≤15%*	One window, door, or garage door failure*	No	<5 impacts	No	No
2	<u>Moderate Damage</u> Major roof cover damage, moderate window breakage. Minor roof sheathing failure. Some resulting damage to interior of building from water	>15% and ≤50%*	> one and ≤ the larger of 20% & 33%*	1 to 3 panels*	Typically 5 to 10 impacts	No	No
3	<u>Severe Damage</u> Major window damage or roof sheathing loss. Major roof cover loss. Extensive damage to interior from water.	>50%*	> the larger of 20% & 33% and ≤50%*	>3 and ≤25%*	Typically 10 to 20 impacts	No	No
4	<u>Destruction</u> Complete roof failure and/or, failure of wall frame. Loss of more than 50% of roof sheathing.	Typically >50%	>50%*	>25%*	Typically >20 impacts	Yes*	Yes*

* Shaded cells with an asterisk are buildings considered to be in the higher damage state.

Eight different geometric representations (four basic shapes with both a gable roof and hip roof) of “typical” residential buildings were developed for the damage assessment. The model buildings are shown pictorially in Figure 5-135 and represent the basic building geometries used to develop the residential building classification scheme and the development of estimated damage states for each building as a function of wind speed. All buildings have been modeled as having asphalt shingle roofs. All windows are treated as being comprised of single pane annealed glass, and all sliding glass doors are considered to be comprised of tempered glass. In the case of a gable roof home, the connections between the roof and the wall are assumed to exist at the base of every truss with no connections along the gable end. In the case of the hip roof, connections between the roof and the wall are assumed to exist along the entire perimeter of the wall. During the simulation, the walls are modeled as being connected to the foundation and the roof, until the roof fails, after which time the wall connection at the roof level is released. The model homes reflect the fact that homes with attached garages are typically bigger than those without garages. The parameters varied in the building description are as follows:

- *Building Size:* Four Samples as in Figure 5-135 (gable roof only shown)
- *Roof Shape:* Hip or Gable
- *Wall Construction:* Wood, Unreinforced Masonry, Reinforced Masonry
- *Roof Sheathing Attachment:* 6d or 8d
- *Roof-Wall Connections:* Strapped or Toe-Nailed
- *Garage:* None, Strong, Weak
- *Number of Stories:* One or Two

Damage simulations for each of the 144 different building types have been performed for the buildings located in terrains described with $z_0 = 0.03$ meters (open terrain), $z_0 = 0.35$ meters (typical suburban terrain), and $z_0 = 0.7$ meters (suburban terrain with some trees or densely spaced homes), $z_0 = 1.0$ meters (treed suburban terrain).

The assumed component resistances used in the simulations are given in Table 5-45. In the case of the roof-wall connections a resistance factor of 0.8 was applied. A resistance factor of 0.9 was applied to the roof sheathing uplift capacity. The resistance parameters given in Table 5-45 are the unfactored values.

Statistics on damage states have been developed through the use of a 20,000-year simulation of hurricanes (derived using the South Florida Hurricane climate) by performing 30 damage simulations for each storm. Prior to the start of each of the 30 simulations, the resistances of the individual building components are re-sampled, and the building orientation is also re-sampled. The building damage indicators including roof cover loss (as a percentage), number of failed roof sheathing panels, number of failed windows, doors, sliding glass doors, and garage doors, number of failed wall sections, and the failure of the entire roof are recorded. This individual component failure information is then used to define the final damage state of the building as defined in Table 5-44.

For more information on the probabilities of achieving each building damage state and each individual component damage state as a function of wind speed, please contact the Hazus Help Desk (see Section 1.4) for the *Hazus Hurricane Model Technical Manual Appendices* (FEMA, 2021). The component damage states are the thresholds that move the building damage state from one definition to another in Table 5-44. For example, in the case of roof cover, Damage State 1 corresponds to roof cover loss of more than 2% but less than 15%. Only three damage states are given for roof cover, since only three roof cover damage states are used to define the total building damage state. The component damage states are presented to assist in determining which component drives the overall building damage state and to check how reasonably the damage model performs.



A) <2% Roof Cover



B) <2% Roof Cover

Figure 5-128 Damage State 0



A) 2% to 15% Roof Cover Loss, One Broken Window



B) 2% to 15% Roof Cover Loss

Figure 5-129 Damage State 1



C) 2% to 15% Roof Cover Loss



D) One Broken Window

Figure 5-130 Damage State 1 (concluded)



A) More than One Window but less than the Greater of 3 or 20% of the Windows



B) At least One Failed Sheathing but Less than Three Failed Pieces of Roof Sheathing

Figure 5-131 Damage State 2



More than Three Pieces of Failed Roof Sheathing but Less than 15% of the Panels Missing

Figure 5-132 Damage State 3



A) Complete Roof Failure



B) Complete Roof Failure, Greater than 25% Sheathing

Figure 5-133 Damage State 4



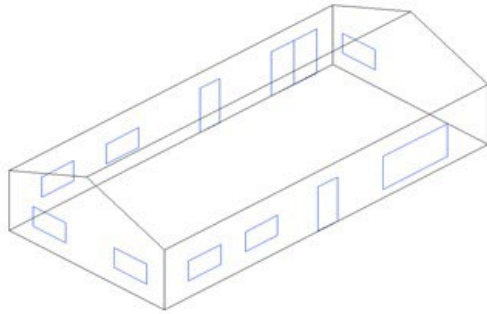
C) Wall Failure



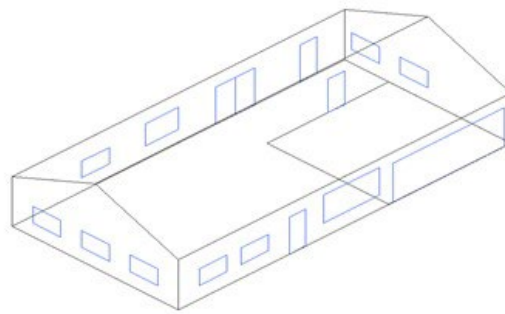
D) Whole Roof Failure, Wall Failure

Figure 5-134 Damage State (concluded)

One-Story Houses

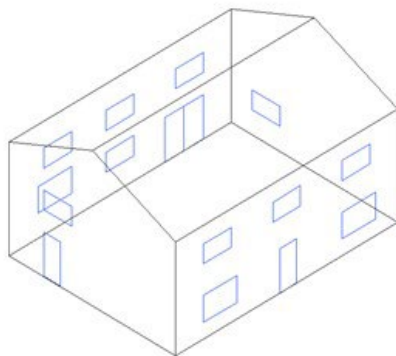


No Garage – 50' by 24' Plan, 9' Eave Height

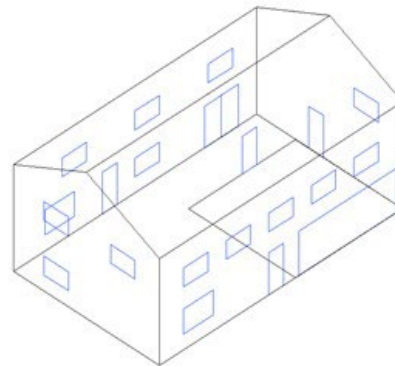


With Garage – 60' by 30' Plan, 9' Eave Height

Two-Story Houses



No Garage – 40' by 30' Plan, 17' Eave Height



With Garage – 60' by 30' Plan, 17' Eave Height

Figure 5-135 Model House Geometries Used in Damage Simulation Study

The relative performance of the different building types and the impact of terrain are shown in Table 5-46 through the use of the average per storm damage state. This average per storm damage state effectively collapses all the information obtained from the simulations into a single number, allowing a rapid evaluation of the importance of individual building parameters in assessing the damage potential of a particular building type. Note that this per storm damage state includes the effect of the hurricane climate since the modeled hurricanes are drawn directly from the 20,000-year simulation, which, of course, produces many more storms having low intensity winds than high intensity winds. In other words, the average building damage states given in Table 5-46 would be much lower if the storm simulation had been performed for a location in New England rather than South Florida.

The results shown in Table 5-46 can be used to ascertain the importance that the various building parameters and terrains have on the performance of residential buildings. The maximum and minimum changes in the per storm average damage state caused by changing a single parameter are summarized in Table 5-47. Note that the effect of any one parameter on the average damage state varies with other building parameters and with terrain.

The results clearly indicate that terrain is very important, where the average damage states are seen to increase by factors of between about 2 to 3 when moving from treed to open terrain. The impact of the number of stories on the average damage is a 35% to 75% increase in damage when the number of stories is increased from one to two.

The effect of roof shape (i.e., gable versus hip) on the damage state varies between about 11% and 33%, with the gable roof buildings experiencing more damage. The impact of changing from hip to gable is larger when the roof/wall is connected with toe-nails versus straps and is also larger when the roof sheathing is fastened with 6d nails versus 8d nails.

Table 5-45 Component Resistance Values Used to Model Residential Buildings

Component	Distribution	Distribution Parameters
Sheathing Panel (6d)	LogNormal	Mean = 54.6, COV = 0.11
Sheathing Panel (8d)	LogNormal	Mean = 103, COV = 0.11
Annealed Glass Impact	Deterministic	50 foot-pounds
Tempered Glass Impact	Deterministic	100 foot-pounds
Window/Sliding Glass Door Pressure	Normal	Mean = 40 psf, COV = 0.2
Window Glass (All Windows on One-Story)	Weibull	C = 54.9 psf, k = 4.7
Window Glass (Two Large Windows on Two Stories)	Weibull	C = 38.7 psf, k = 4.8
Sliding Glass Door Glass	Weibull	C = 101.5 psf, k = 4.5
Interior Garage Door Pressure	Normal	Mean = 30 psf, COV = 0.2
Entry Door Pressure	Normal	Mean = 50 psf, COV = 0.2
Double Garage Door Pressure (weak)	Normal	Mean = 10 psf, COV = 0.2
Double Garage Door Pressure (strong)	Normal	Mean = 20 psf, COV = 0.2
Strap Up-Lift Resistance	Normal	Mean = 1,200 lb., COV = 0.3
Toe-Nail Uplift Resistance	Normal	Mean = 415 lb., COV = 0.25

Table 5-46 Average Building Damage States

Building Characteristics					Hip roof				Gable roof			
Wall Const.	No. of Stories	Roof/ Wall Conn.	Sheath Nails	Garage door	Terrain Surface Roughness (m)				Terrain Surface Roughness (m)			
					0.03	0.35	0.70	1.0	0.03	0.35	0.70	1.0
Wood Frame	One	Straps	6d	None	0.510	0.306	0.230	0.198	0.617	0.378	0.295	0.256
				Strong	0.513	0.312	0.232	0.198	0.605	0.367	0.283	0.246
				Weak	0.557	0.322	0.240	0.204	0.661	0.382	0.292	0.253
			8d	None	0.489	0.291	0.219	0.189	0.563	0.336	0.258	0.226
				Strong	0.494	0.303	0.226	0.192	0.565	0.340	0.258	0.223
				Weak	0.526	0.311	0.229	0.196	0.592	0.347	0.263	0.227
		Toe-nails	6d	None	0.536	0.331	0.246	0.210	0.646	0.422	0.318	0.275
				Strong	0.544	0.327	0.244	0.206	0.648	0.400	0.302	0.263
				Weak	0.619	0.349	0.258	0.218	0.778	0.433	0.323	0.275
			8d	None	0.531	0.327	0.243	0.206	0.619	0.403	0.304	0.262
				Strong	0.540	0.324	0.241	0.203	0.623	0.387	0.291	0.249
				Weak	0.617	0.346	0.255	0.213	0.766	0.421	0.313	0.265
	Two	Straps	6d	None	0.725	0.470	0.380	0.337	0.862	0.576	0.475	0.429
				Strong	0.717	0.465	0.374	0.332	0.837	0.554	0.455	0.408
				Weak	0.777	0.486	0.391	0.347	0.903	0.580	0.472	0.422
			8d	None	0.706	0.456	0.369	0.327	0.810	0.533	0.438	0.389
				Strong	0.693	0.449	0.361	0.319	0.793	0.522	0.425	0.381
				Weak	0.749	0.466	0.372	0.329	0.830	0.531	0.432	0.385
		Toe-nails	6d	None	0.768	0.506	0.404	0.357	0.901	0.626	0.510	0.456
				Strong	0.761	0.492	0.393	0.346	0.885	0.583	0.476	0.423
				Weak	0.848	0.519	0.413	0.364	1.058	0.651	0.524	0.459
			8d	None	0.764	0.503	0.402	0.356	0.870	0.600	0.487	0.432
				Strong	0.757	0.486	0.388	0.341	0.864	0.565	0.459	0.408
				Weak	0.841	0.514	0.408	0.360	1.035	0.633	0.507	0.448
Unreinfor. Masonry	One	Straps	6d	None	0.507	0.306	0.232	0.198	0.618	0.377	0.293	0.257
				Strong	0.513	0.312	0.233	0.198	0.607	0.367	0.282	0.245
				Weak	0.561	0.324	0.239	0.204	0.659	0.384	0.292	0.254
			8d	None	0.494	0.292	0.220	0.189	0.566	0.335	0.258	0.225
				Strong	0.498	0.304	0.225	0.191	0.563	0.341	0.257	0.224
				Weak	0.528	0.309	0.230	0.196	0.592	0.347	0.263	0.225
		Toe-nails	6d	None	0.540	0.332	0.246	0.207	0.648	0.421	0.321	0.275
				Strong	0.544	0.328	0.242	0.207	0.647	0.398	0.304	0.264
				Weak	0.623	0.348	0.257	0.218	0.780	0.433	0.325	0.279
			8d	None	0.531	0.329	0.245	0.206	0.618	0.404	0.307	0.261
				Strong	0.540	0.324	0.241	0.203	0.624	0.386	0.292	0.249
				Weak	0.616	0.347	0.254	0.212	0.759	0.420	0.314	0.267

Building Characteristics					Hip roof				Gable roof				
Wall Const.	No. of Stories	Roof/ Wall Conn.	Sheath Nails	Garage door	Terrain Surface Roughness (m)				Terrain Surface Roughness (m)				
					0.03	0.35	0.70	1.0	0.03	0.35	0.70	1.0	
	Two	Straps	6d	None	0.507	0.306	0.232	0.198	0.618	0.377	0.293	0.257	
				Strong	0.513	0.312	0.233	0.198	0.607	0.367	0.282	0.245	
				Weak	0.561	0.324	0.239	0.204	0.659	0.384	0.292	0.254	
			8d	None	0.494	0.292	0.220	0.189	0.566	0.335	0.258	0.225	
				Strong	0.498	0.304	0.225	0.191	0.563	0.341	0.257	0.224	
				Weak	0.528	0.309	0.230	0.196	0.592	0.347	0.263	0.225	
		Toe-nails	6d	None	0.540	0.332	0.246	0.207	0.648	0.421	0.321	0.275	
				Strong	0.544	0.328	0.242	0.207	0.647	0.398	0.304	0.264	
				Weak	0.623	0.348	0.257	0.218	0.780	0.433	0.325	0.279	
			8d	None	0.531	0.329	0.245	0.206	0.618	0.404	0.307	0.261	
				Strong	0.540	0.324	0.241	0.203	0.624	0.386	0.292	0.249	
				Weak	0.616	0.347	0.254	0.212	0.759	0.420	0.314	0.267	
	Reinforced Masonry	One	Straps	6d	None	0.510	0.306	0.232	0.198	0.616	0.377	0.292	0.257
					Strong	0.514	0.311	0.233	0.197	0.608	0.366	0.283	0.245
					Weak	0.560	0.323	0.239	0.204	0.662	0.382	0.293	0.253
				8d	None	0.493	0.292	0.220	0.189	0.566	0.335	0.257	0.224
					Strong	0.497	0.304	0.225	0.191	0.565	0.340	0.258	0.222
					Weak	0.527	0.309	0.231	0.195	0.592	0.346	0.264	0.225
Toe-nails			6d	None	0.536	0.330	0.246	0.208	0.644	0.421	0.319	0.275	
				Strong	0.546	0.327	0.243	0.206	0.646	0.400	0.303	0.260	
				Weak	0.623	0.350	0.257	0.219	0.779	0.432	0.323	0.277	
			8d	None	0.530	0.328	0.244	0.206	0.618	0.404	0.305	0.262	
				Strong	0.538	0.325	0.238	0.203	0.625	0.385	0.292	0.249	
				Weak	0.616	0.344	0.255	0.215	0.766	0.421	0.313	0.265	
Two		Straps	6d	None	0.724	0.470	0.378	0.336	0.860	0.575	0.476	0.429	
				Strong	0.720	0.465	0.376	0.331	0.839	0.556	0.457	0.410	
				Weak	0.775	0.486	0.389	0.345	0.903	0.579	0.472	0.423	
			8d	None	0.710	0.459	0.369	0.327	0.811	0.538	0.438	0.392	
				Strong	0.692	0.451	0.361	0.317	0.794	0.522	0.426	0.382	
				Weak	0.748	0.468	0.374	0.328	0.832	0.536	0.431	0.385	
Toe-nails	6d	None	0.765	0.507	0.405	0.355	0.904	0.624	0.509	0.455			
		Strong	0.757	0.488	0.393	0.345	0.885	0.583	0.478	0.423			
		Weak	0.849	0.520	0.413	0.364	1.053	0.652	0.524	0.461			
	8d	None	0.765	0.503	0.403	0.356	0.871	0.603	0.485	0.430			
		Strong	0.756	0.485	0.387	0.341	0.861	0.567	0.460	0.409			
		Weak	0.848	0.513	0.411	0.359	1.036	0.639	0.507	0.446			

* Values in table represent the damage state probabilities (%). Damage state descriptions are described in Table 5-44.

Table 5-47 Percent Increases in the Per Storm Average Building Damage State Due to Changes in Building Parameters (Minimum/Average/Maximum) - Residential Buildings

Parameter	Increase in Per Storm Average Damage State		
	Min	Avg	Max
Treed to Open Terrain	98%	138%	190%
One-Story to Two Stories	35%	55%	75%
8d to 6d Roof Sheathing Nails	0%	4%	15%
Strapped to Toe-nailed Roof/Wall Connections	3%	10%	29%
Hip to Gable Roof	11%	21%	33%
No Garage to Strong Garage Door	-7%	-2%	4%
No Garage to Weak Garage Door	-2%	5%	24%
Reinforced Masonry to Unreinforced Masonry Walls	-1%	0%	1%
Unreinforced Masonry to Wood Frame Walls	-1%	0%	1%

In the case of gable roof homes, the use of 6d sheathing nails versus 8d sheathing nails increases the per storm average damage state by up to 15%, with the larger increases taking place on the homes with strapped roof-wall connections. In the case of hip roof homes, the use of 6d sheathing nails increases the mean damage state by up to 6%, also with the larger increases taking place on the homes with strapped roof-wall connections.

The effect of straps on the average damage state also depends on roof shape, with the reduction in damage associated with the addition of straps being larger in the case of gable roofs. The results also indicate that the effect of roof straps in reducing damage is greater for the case where the roof sheathing is attached with 8d nails versus 6d nails. Overall, the increase in the average damage state associated with the use of toe-nail connections versus straps is in the range of 3% to 29%.

The effect of adding a garage with a strong garage door was found to be negligible in comparison to the effects of other variables. Note that the homes modeled with garages are larger than those without garages, and as a result, the average damage state values also reflect the effects of changes in building size. The effect of adding a garage with a weak garage door is seen to produce an average increase in damage ranging from 2% to 24%. The increase in damage was most pronounced for the open terrain case and for buildings with toe-nailed roof/wall connections versus strapped roof/wall connections.

The difference between wood frame walls and unreinforced masonry walls is negligible, with the differences in the average damage states being no more than 1%. The effect of reinforced masonry on resulting damage state versus unreinforced masonry is also found to be negligible. The effect of walls on the average damage state is small since other types of damage (roof sheathing, whole roof failures, etc.) are already significant by the time the walls begin to fail. Note that none of the modeled reinforced masonry walls failed in the simulations.

5.6.1.1 Effect of Mitigation on Residential Building Damage

Damage simulations were performed with various mitigation strategies for each of the residential buildings described in the previous section. The three mitigation strategies considered are as follows:

1. Install Dade County approved shutters
2. Upgrade roof to new Dade County (SFBC) roof sheathing nail pattern, install more wind-resistant shingles and apply secondary water resistance
3. Install Dade County approved shutters, upgrade roof to new Dade County (SFBC) roof sheathing nail pattern, install more wind-resistant shingles and apply secondary water resistance

The upgraded roof cover (shingles) are modeled as having a capacity of 120% of the base case shingles. In the case of the shutters, a shutter is considered to have failed if it is impacted by debris having an energy equal to or greater than 350 foot-pounds (i.e., a 9 pounds. wood 2 by 4 impacting the shutter at a speed of 50 fps as required by the SFBC). The wind loads acting on the window behind the shutter are assumed to be reduced by 50%; however, the true amount of the reduction in the wind load is clearly dependent on the amount of leakage around the perimeter of the shutter. It is also assumed that the shutters do not fail due to pressure loading alone. In cases where shutters are added to a house and the house has a garage, the garage capacity is upgraded to meet the impact and pressure requirements of the Dade County building code. The effect of secondary water proofing is treated in the economic loss portion of the model and not in the damage portion of the model.

In the case of upgrading the roof nails, it is assumed that during re-roofing, the nail pattern on the existing roof sheathing panels is increased by nailing 8d nails in the field of the panel to achieve a 6" on center nailing over the entire panel. In the case of a roof having 8d nails prior to re-nailing, the resulting uplift capacity is equal to that which would be provided through the use of the Dade County SFBC on a new building (i.e., 8d nails at 6" on center in the field and along the edges).

For more information on example plots showing the probabilities of achieving each building damage state and each individual component damage state as a function of wind speed for the three sets of mitigated homes, please contact the Hazus Help Desk (see Section 1.5) for the *Hazus Hurricane Model Technical Manual Appendices* (FEMA, 2021). The average per storm building damage states for the three sets of buildings are given in Table 5-48, Table 5-49, and Table 5-50. Note in Table 5-48, Table 5-49, and Table 5-50, only one garage door case is given, since, when either a weak or a strong garage door is upgraded, they are upgraded to the same pressure resistance. By comparing the average damage states in Table 5-48, Table 5-49, and Table 5-50 with the average damage states given in Table 5-46, one can see the effect of the various mitigation techniques in reducing damage. The statistics of the reductions in the average per storm damage states as a result of mitigation are summarized in Table 5-51.

The effect of adding shutters (and upgrading the garage door, if applicable) is a reduction in the average damage ranging between 6% and 23% with a mean reduction in the average damage of 15%. The effect of upgrading the roof (sheathing attachments and roof cover) yields a reduction in the average damage ranging between 18% and 44%, with an average of 27%.

Table 5-48 Average Building Damage States - Install Shutters

Building Characteristics					Hip roof*				Gable roof*			
Wall Const.	No. of Stories	Roof/ Wall Conn.	Sheath Nails	Garage door	Terrain Surface Roughness (m)				Terrain Surface Roughness (m)			
					0.03	0.35	0.70	1.0	0.03	0.35	0.70	1.0
Wood Frame	One	Straps	6d	None	0.439	0.258	0.203	0.178	0.554	0.335	0.268	0.239
				Strong	0.424	0.252	0.197	0.173	0.524	0.314	0.255	0.224
			8d	None	0.414	0.242	0.190	0.170	0.480	0.288	0.230	0.205
				Strong	0.403	0.235	0.184	0.165	0.460	0.274	0.220	0.194
		Toe-nails	6d	None	0.446	0.266	0.209	0.182	0.561	0.344	0.273	0.241
				Strong	0.436	0.259	0.202	0.179	0.533	0.327	0.262	0.231
			8d	None	0.434	0.261	0.203	0.176	0.514	0.316	0.249	0.221
				Strong	0.424	0.255	0.196	0.173	0.491	0.304	0.238	0.213
	Two	Straps	6d	None	0.605	0.410	0.343	0.310	0.747	0.518	0.437	0.398
				Strong	0.595	0.402	0.334	0.302	0.704	0.489	0.413	0.375
			8d	None	0.586	0.391	0.328	0.299	0.650	0.448	0.376	0.345
				Strong	0.567	0.378	0.316	0.286	0.629	0.430	0.361	0.328
		Toe-nails	6d	None	0.610	0.420	0.349	0.313	0.757	0.529	0.445	0.404
				Strong	0.597	0.408	0.338	0.309	0.721	0.497	0.422	0.384
			8d	None	0.603	0.414	0.344	0.307	0.695	0.483	0.404	0.369
				Strong	0.588	0.399	0.333	0.300	0.671	0.462	0.391	0.354
Unreinforced Masonry	One	Straps	6d	None	0.440	0.258	0.203	0.176	0.556	0.334	0.269	0.240
				Strong	0.424	0.250	0.198	0.173	0.522	0.318	0.253	0.226
			8d	None	0.415	0.239	0.190	0.168	0.479	0.289	0.229	0.206
				Strong	0.400	0.234	0.184	0.165	0.456	0.272	0.221	0.196
		Toe-nails	6d	None	0.444	0.267	0.208	0.181	0.561	0.345	0.271	0.241
				Strong	0.437	0.259	0.202	0.178	0.529	0.329	0.261	0.231
			8d	None	0.433	0.262	0.202	0.176	0.514	0.318	0.248	0.220
				Strong	0.422	0.251	0.198	0.173	0.490	0.302	0.240	0.213
	Two	Straps	6d	None	0.605	0.411	0.343	0.311	0.743	0.516	0.438	0.398
				Strong	0.593	0.401	0.334	0.303	0.706	0.487	0.412	0.375
			8d	None	0.583	0.389	0.328	0.296	0.646	0.448	0.376	0.342
				Strong	0.568	0.377	0.317	0.285	0.626	0.428	0.361	0.328
		Toe-nails	6d	None	0.616	0.421	0.348	0.314	0.755	0.527	0.448	0.404
				Strong	0.600	0.409	0.340	0.308	0.721	0.498	0.422	0.382
			8d	None	0.604	0.414	0.343	0.307	0.691	0.482	0.405	0.368
				Strong	0.585	0.399	0.331	0.301	0.667	0.461	0.391	0.355
Reinforced Masonry	One	Straps	6d	None	0.439	0.258	0.202	0.176	0.554	0.335	0.268	0.238
				Strong	0.426	0.251	0.197	0.173	0.523	0.316	0.253	0.227

Building Characteristics					Hip roof*				Gable roof*				
Wall Const.	No. of Stories	Roof/ Wall Conn.	Sheath Nails	Garage door	Terrain Surface Roughness (m)				Terrain Surface Roughness (m)				
					0.03	0.35	0.70	1.0	0.03	0.35	0.70	1.0	
		Straps	8d	None	0.415	0.239	0.189	0.168	0.480	0.289	0.230	0.207	
				Strong	0.399	0.234	0.184	0.165	0.457	0.273	0.218	0.196	
		Toe-nails	6d	None	0.444	0.266	0.207	0.182	0.560	0.344	0.273	0.241	
				Strong	0.434	0.258	0.202	0.177	0.531	0.329	0.260	0.231	
		8d	None	0.432	0.262	0.202	0.176	0.512	0.317	0.250	0.220		
			Strong	0.421	0.252	0.195	0.171	0.491	0.304	0.240	0.212		
		Two	Straps	6d	None	0.606	0.412	0.343	0.310	0.744	0.518	0.438	0.399
					Strong	0.596	0.402	0.337	0.304	0.708	0.488	0.403	0.367
	8d			None	0.582	0.390	0.327	0.298	0.649	0.450	0.378	0.343	
				Strong	0.567	0.378	0.317	0.285	0.627	0.429	0.362	0.327	
	Toe-nails		6d	Name	0.612	0.421	0.349	0.314	0.753	0.526	0.445	0.402	
				Strong	0.599	0.409	0.340	0.306	0.708	0.499	0.421	0.377	
			8d	None	0.603	0.413	0.345	0.309	0.693	0.481	0.407	0.370	
				Strong	0.585	0.399	0.333	0.299	0.669	0.460	0.390	0.351	

*Values in table represent the damage state probabilities (%). Damage state descriptions are described in Table 5-44.

The combined effect of upgrading the roof and adding window protection is a reduction in the average building damage state ranging between 45% and 59% with a mean reduction of 52%. Note that the reduction in losses associated with the application of both window protection and roof strength enhancements results in a reduction in damage (52%), which is greater than the sum of the reduction in losses of the two mitigation methods applied separately (15% + 27% = 42%). This synergistic effect is expected since the full benefits of the individual techniques cannot be realized unless other failure modes of roughly equal probability are also addressed. Simply put, the building performance is governed by the performance of the weakest link in the chain. If there are two links of roughly equal weakness, both must be strengthened.

Table 5-49 Average Building Damage States - Upgrade Roof

Building Characteristics					Hip roof*				Gable roof*			
Wall Const.	No. of Stories	Roof/ Wall Conn.	Sheath Nails	Garage door	Terrain Surface Roughness (m)				Terrain Surface Roughness (m)			
					0.03	0.35	0.70	1.0	0.03	0.35	0.70	1.0
Wood Frame	One	Straps	6d	None	0.357	0.217	0.151	0.123	0.415	0.246	0.174	0.143
				Strong	0.380	0.238	0.164	0.132	0.429	0.258	0.181	0.150
			8d	None	0.358	0.218	0.151	0.122	0.410	0.243	0.173	0.143
				Strong	0.377	0.238	0.165	0.131	0.427	0.258	0.181	0.149
		Toe-nails	6d	None	0.401	0.258	0.179	0.142	0.469	0.320	0.227	0.186
				Strong	0.425	0.263	0.182	0.146	0.495	0.310	0.220	0.178

Building Characteristics					Hip roof*				Gable roof*						
Wall Const.	No. of Stories	Roof/ Wall Conn.	Sheath Nails	Garage door	Terrain Surface Roughness (m)				Terrain Surface Roughness (m)						
					0.03	0.35	0.70	1.0	0.03	0.35	0.70	1.0			
	Two	Straps	8d	None	0.402	0.258	0.179	0.142	0.471	0.319	0.225	0.186			
				Strong	0.425	0.263	0.182	0.146	0.494	0.310	0.220	0.180			
			6d	None	0.550	0.338	0.256	0.219	0.648	0.405	0.316	0.275			
				Strong	0.544	0.335	0.251	0.213	0.636	0.402	0.311	0.271			
			8d	None	0.549	0.338	0.257	0.218	0.649	0.406	0.316	0.274			
				Strong	0.546	0.337	0.252	0.213	0.638	0.401	0.311	0.269			
		Toe-nails	6d	None	0.613	0.391	0.292	0.247	0.707	0.482	0.371	0.318			
				Strong	0.604	0.375	0.279	0.238	0.708	0.447	0.346	0.302			
			8d	None	0.613	0.391	0.292	0.248	0.708	0.479	0.373	0.318			
				Strong	0.604	0.374	0.279	0.240	0.708	0.447	0.346	0.301			
			Unreinf. Masonry	One	Straps	6d	None	0.360	0.218	0.150	0.121	0.412	0.243	0.174	0.143
							Strong	0.379	0.238	0.165	0.132	0.429	0.258	0.181	0.148
8d	None	0.359				0.217	0.150	0.123	0.414	0.245	0.174	0.144			
	Strong	0.380				0.239	0.163	0.131	0.429	0.259	0.183	0.149			
Toe-nails	6d	None				0.401	0.258	0.178	0.141	0.470	0.320	0.227	0.186		
		Strong				0.424	0.263	0.181	0.147	0.495	0.308	0.219	0.181		
	8d	None			0.401	0.258	0.177	0.140	0.471	0.317	0.226	0.186			
		Strong			0.424	0.263	0.183	0.147	0.495	0.309	0.217	0.180			
Two	Straps	6d			None	0.550	0.340	0.258	0.219	0.650	0.407	0.317	0.275		
					Strong	0.547	0.338	0.251	0.214	0.635	0.399	0.314	0.270		
		8d			None	0.549	0.337	0.256	0.219	0.646	0.408	0.317	0.275		
					Strong	0.545	0.338	0.253	0.213	0.635	0.401	0.310	0.270		
		Toe-nails	6d	None	0.608	0.389	0.292	0.249	0.709	0.479	0.373	0.320			
				Strong	0.610	0.375	0.282	0.237	0.709	0.448	0.346	0.300			
	8d		None	0.608	0.389	0.291	0.249	0.705	0.480	0.369	0.320				
			Strong	0.610	0.374	0.282	0.240	0.708	0.446	0.346	0.299				
	Reinfor. Masonry	One	Straps	6d	None	0.361	0.218	0.152	0.122	0.414	0.245	0.174	0.143		
					Strong	0.380	0.236	0.165	0.134	0.430	0.258	0.181	0.149		
				8d	None	0.362	0.217	0.150	0.123	0.413	0.244	0.173	0.144		
					Strong	0.378	0.237	0.163	0.132	0.428	0.257	0.182	0.150		
Toe-nails				6d	None	0.402	0.258	0.178	0.141	0.471	0.317	0.226	0.185		
					Strong	0.428	0.262	0.180	0.146	0.494	0.309	0.220	0.180		
			8d	None	0.402	0.258	0.178	0.141	0.473	0.319	0.227	0.185			
				Strong	0.427	0.263	0.181	0.145	0.496	0.309	0.220	0.180			
Two			Straps	6d	None	0.553	0.339	0.256	0.220	0.649	0.406	0.316	0.275		
					Strong	0.543	0.337	0.251	0.214	0.637	0.400	0.310	0.268		
				8d	None	0.548	0.338	0.257	0.218	0.646	0.407	0.317	0.274		
					Strong	0.543	0.337	0.251	0.214	0.637	0.400	0.310	0.268		

Building Characteristics					Hip roof*				Gable roof*			
Wall Const.	No. of Stories	Roof/ Wall Conn.	Sheath Nails	Garage door	Terrain Surface Roughness (m)				Terrain Surface Roughness (m)			
					0.03	0.35	0.70	1.0	0.03	0.35	0.70	1.0
				Strong	0.545	0.334	0.253	0.214	0.635	0.400	0.312	0.267
		Toe-nails	6d	Name	0.609	0.388	0.293	0.248	0.707	0.480	0.371	0.319
				Strong	0.611	0.374	0.281	0.238	0.707	0.445	0.346	0.301
		8d		None	0.609	0.389	0.294	0.248	0.707	0.478	0.368	0.319
				Strong	0.611	0.377	0.281	0.239	0.708	0.444	0.344	0.300

*Values in table represent the damage state probabilities (%). Damage state descriptions are described in Table 5-44.

Table 5-50 Average Building Damage States - Install Shutters and Upgrade Roof

Building Characteristics					Hip roof*				Gable roof*			
Wall Const.	No. of Stories	Roof /Wall Conn.	Sheath Nails	Garage door	Terrain Surface Roughness (m)				Terrain Surface Roughness (m)			
					0.03	0.35	0.70	1.0	0.03	0.35	0.70	1.0
Wood Frame	One	Straps	6d	None	0.243	0.132	0.098	0.085	0.288	0.162	0.123	0.107
				Strong	0.237	0.133	0.096	0.083	0.275	0.156	0.119	0.102
			8d	None	0.243	0.131	0.097	0.084	0.289	0.163	0.123	0.107
				Strong	0.239	0.132	0.096	0.082	0.276	0.157	0.119	0.101
		Toe-nails	6d	None	0.266	0.158	0.114	0.095	0.333	0.200	0.148	0.125
				Strong	0.266	0.155	0.112	0.094	0.322	0.194	0.145	0.124
			8d	None	0.266	0.158	0.112	0.096	0.332	0.199	0.147	0.127
				Strong	0.265	0.156	0.111	0.094	0.321	0.193	0.144	0.125
	Two	Straps	6d	None	0.364	0.229	0.183	0.161	0.414	0.274	0.221	0.195
				Strong	0.351	0.221	0.176	0.156	0.400	0.260	0.209	0.187
			8d	None	0.363	0.228	0.184	0.164	0.412	0.272	0.218	0.196
				Strong	0.353	0.223	0.177	0.155	0.399	0.260	0.210	0.186
		Toe-nails	6d	None	0.387	0.258	0.204	0.178	0.472	0.318	0.259	0.231
				Strong	0.378	0.247	0.196	0.171	0.459	0.305	0.249	0.220
			8d	None	0.385	0.256	0.204	0.179	0.472	0.318	0.258	0.230
				Strong	0.377	0.247	0.195	0.171	0.457	0.306	0.247	0.221
Unreinf. Masonry	One	Straps	6d	None	0.241	0.133	0.097	0.085	0.288	0.163	0.123	0.107
				Strong	0.235	0.131	0.095	0.082	0.274	0.156	0.119	0.102
			8d	None	0.239	0.132	0.097	0.084	0.286	0.163	0.121	0.107
				Strong	0.235	0.132	0.096	0.082	0.273	0.156	0.118	0.102
		Toe-nails	6d	None	0.263	0.160	0.113	0.096	0.329	0.202	0.148	0.127
				Strong	0.265	0.157	0.112	0.095	0.322	0.193	0.146	0.124
			8d	None	0.263	0.159	0.113	0.095	0.330	0.197	0.147	0.126
				Strong	0.266	0.156	0.112	0.096	0.322	0.195	0.145	0.125
	Two	Straps	6d	None	0.359	0.229	0.184	0.162	0.413	0.274	0.222	0.195
				Strong	0.350	0.221	0.176	0.156	0.397	0.261	0.210	0.187
			8d	None	0.359	0.232	0.183	0.161	0.409	0.273	0.220	0.198
				Strong	0.350	0.222	0.176	0.156	0.397	0.261	0.208	0.184
		Toe-nails	6d	None	0.385	0.258	0.202	0.178	0.471	0.319	0.259	0.231
				Strong	0.377	0.248	0.194	0.173	0.454	0.303	0.247	0.223
			8d	None	0.384	0.257	0.203	0.179	0.468	0.319	0.257	0.233
				Strong	0.377	0.249	0.196	0.173	0.456	0.305	0.250	0.222
Reinfor. Masonry	One	Straps	6d	None	0.241	0.133	0.098	0.085	0.288	0.163	0.123	0.107
				Strong	0.236	0.131	0.097	0.082	0.274	0.157	0.118	0.102
			8d	None	0.240	0.131	0.098	0.084	0.286	0.163	0.122	0.108
				Strong	0.236	0.131	0.096	0.082	0.275	0.156	0.119	0.101

Building Characteristics					Hip roof*				Gable roof*			
Wall Const.	No. of Stories	Roof /Wall Conn.	Sheath Nails	Garage door	Terrain Surface Roughness (m)				Terrain Surface Roughness (m)			
					0.03	0.35	0.70	1.0	0.03	0.35	0.70	1.0
	Two	Toe-nails	6d	None	0.263	0.159	0.113	0.096	0.331	0.200	0.148	0.127
				Strong	0.266	0.156	0.112	0.095	0.320	0.193	0.146	0.124
			8d	None	0.263	0.157	0.113	0.096	0.328	0.198	0.148	0.126
				Strong	0.265	0.156	0.112	0.095	0.321	0.194	0.146	0.124
		Straps	6d	None	0.360	0.228	0.182	0.161	0.412	0.274	0.222	0.197
				Strong	0.351	0.221	0.176	0.156	0.396	0.259	0.209	0.187
			8d	None	0.359	0.229	0.184	0.163	0.412	0.274	0.221	0.195
				Strong	0.351	0.222	0.177	0.154	0.394	0.261	0.210	0.185
		Toe-nails	6d	None	0.384	0.255	0.201	0.178	0.468	0.318	0.258	0.231
				Strong	0.376	0.247	0.198	0.172	0.454	0.304	0.246	0.221
			8d	None	0.385	0.256	0.203	0.178	0.472	0.318	0.258	0.231
				Strong	0.376	0.248	0.198	0.173	0.458	0.307	0.248	0.221

*Values in table represent the damage state probabilities (%). Damage state descriptions are described in Table 5-44.

Table 5-51 Percent Decreases in the Per Storm Average Building Damage State Due to Mitigation (Minimum/Average/Maximum) - Residential Buildings

Mitigation Strategy	Decrease in Per Storm Average Damage State		
	Min	Avg	Max
Install Shutters	6%	15%	23%
Upgrade to Dade Roof	18%	27%	44%
Install Shutters and Upgrade to Dade Roof	45%	52%	59%

5.6.2 Manufactured Homes

Using the damage model described earlier combined with the wind speed and direction traces produced for a 20,000-year simulation of hurricanes for storms in the South Florida area, estimates of manufactured home damage states as a function of peak storm wind speed are produced for manufactured homes situated in four different terrains. In the development of the damage functions, for each simulated hurricane, 90 damage simulations are performed. At the start of each of the 90 damage simulations, the manufactured home is randomly oriented, and the component resistances are sampled. Upon completion of the damage simulation, all failure modes that occurred during the passage of the storm are recorded along with the peak gust wind speed produced by the storm. Following all the damage simulations for each simulated storm, the resulting damage experienced by each modeled manufactured home is categorized into one of the five damage states as defined in lower portion of Table 5-52. The fraction of manufactured homes experiencing a given damage state for a given peak gust wind speed at a height of 10 meters in open terrain is then computed and tabulated. The modeled damage states are given in wind speed increments of 5 mph, such that the fraction of homes experiencing a given damage state centered on a particular wind speed are used to compute the damage statistics for that wind speed.

Table 5-52 Damage Classes Described by Vann and McDonald

Damage Class	Description of Damage (Vann and McDonald, 1978)
0	<i>No Damage or Very Minor Damage</i> - Little or no visible damage from the outside. Slight shifting on the blocks that would suggest re-leveling, but not off the blocks. Some cracked windows, but no resulting water damage.
1	<i>Minor Damage</i> - Shifting off the blocks or so that blocks press up to the floor; re-leveling required. Walls, doors, etc., buckled slightly, but able to be corrected by re-leveling. Minor eave and upper wall damage, with slight water damage but roof not pulled all the way back. Minor pulling away of siding with slight water damage. Minor missile and/or tree damage. Slight window breakage and attendant water damage.
2	<i>Moderate Damage (Still Livable)</i> - Severe shifting off the blocks with some attendant floor and superstructure damage (punching, racking, etc.). Roof removed over a portion or all of the home but the joists remain intact, walls not collapsed. Missile and/or tree damage to a section of the wall or roof, including deep dents or punctures. Serious water damage from holes in roof, walls, windows, doors or floors.
3	<i>Severe Damage (Not Livable, but Repairable)</i> - Unit rolled onto side but frame intact. Extreme shifting causing severe racking and separations in the superstructure. Roof off, joists damaged or removed, walls damaged from lack of lateral support at top. Severe tree damage, including crushing of one wall or roof section. Superstructure partially separated from under frame.
4	<i>Destruction (Not Livable)</i> - Unit rolled onto top or rolled several times. Unit tossed or vaulted through the air. Superstructure separated from the underframe or collapsed to side of the underframe. Roof off, joists removed, and walls collapsed. Destruction of a major section by a falling tree.

Table 5-53 The Corresponding Damage States from the Damage Simulation Model

Damage Class	Modeled Damage States*					
	Roof Cover Damage	Siding Damage	Window and Door Failures	Roof Sheathing Failures	Roof to Wall and/or Wall to Foundation Connection Failures	Foundation to Ground Anchor Failures
0	≤10%	≤1 Panel	None	None	None	None
1	>10% to ≤25%*	>1 to ≤25%*	1 or 2*	None	None	Minor Sliding*
2	>25%*	>25%*	>2 to ≤50%*	>0% to ≤25%*	Minor*	Typically Minor Sliding
3	Typically >25%	Typically >25%	>50%*	>25%*	Typically Minor	Major Sliding*
4	Typically >25%	Typically >25%	Typically >50%	Typically >25%	Major*	Overturning *or Uplift

**If any one of the conditions in the shaded cells with an asterisk (*) of a given row is true, the mobile home is placed in that damage state)*

The resistance properties of the manufactured homes used in the development of the damage state curves are summarized in Table 5-54. The resistance values for the HUD and Pre-HUD buildings have been previously discussed. Note that the windows of the modeled manufactured homes are situated so that no windows are located in the high suction end zones along the walls and thus the siding capacity, which is at least partially located in an end zone, exceeds the window capacity for the HUD Wind Zone II and Wind Zone III cases.

Table 5-54 Resistance Parameters Used to Model Manufactured Homes

Building Component	Pre-HUD	HUD	1994 HUD Wind Zone I	1994 HUD Wind Zone II	1994 HUD Wind Zone III
Roof Cover Model	Residential Shingle Model	Residential Shingle Model	Residential Shingle Model	1.2 Times Residential Shingle Model	1.2 Times Residential Shingle Model
Roof Sheathing Capacity (psf)	Mean = 45 COV = 12%	Mean = 45 COV = 12%	Mean = 45 COV = 12%	Mean = 90 COV = 12%	Mean = 90 COV = 12%
Siding Resistance	Mean = 25 COV = 15%	Mean = 25 COV = 15%	Mean = 25 COV = 15%	Mean = 72 COV = 15%	Mean = 88 COV = 15%
Window Resistance	Mean = 32 COV = 18%	Mean = 32 COV = 18%	Mean = 32 COV = 18%	Mean = 57 COV = 18%	Mean = 72 COV = 18%
Design Uplift Load (psf)	15	15	9	27	32
Design Drag Load (psf)	25	25	15	39	47

Building Component	Pre-HUD	HUD	1994 HUD	1994 HUD	1994 HUD
			Wind Zone I	Wind Zone II	Wind Zone III
Roof-Wall Connection Safety Factor	Mean = 1.5 COV = 25%	Mean = 1.2 COV = 25%	Mean = 1.5 COV = 25%	Mean = 1.5 COV = 25%	Mean = 1.5 COV = 25%
Floor-Wall Connection Safety Factor	Mean = 1.6 COV = 24%	Mean = 1.6 COV = 24%	Mean = 1.6 COV = 24%	Mean = 1.6 COV = 24%	Mean = 1.6 COV = 24%
Anchor Pull Out Capacity (lb.)	Mean = 1,500 COV = 35%	Mean = 1,500 COV = 35%	Mean = 1,500 COV = 35%	Mean = 1,500 COV = 35%	Mean = 1,500 COV = 35%

For more information on computed damage state curves for all terrains, where HUD Code and tie-down combinations examined, please contact the Hazus Help Desk (see Section 1.5) for the *Hazus Hurricane Model Technical Manual Appendices* (FEMA, 2021). Table 5-55 lists the per storm average damage states.

Table 5-55 Per Storm Average Damage States

Mobile Home Construction	Terrain Surface Roughness (m)				
	z ₀ = 0.03	z ₀ = 0.15	z ₀ = 0.35	z ₀ = 0.7	z ₀ = 1.0
Pre-HUD, Not Tied Down	0.641	0.480	0.354	0.264	0.226
Pre-HUD, Tied Down	0.623	0.466	0.339	0.249	0.211
HUD, Not Tied Down	0.618	0.449	0.330	0.247	0.211
HUD, Tied Down	0.594	0.428	0.309	0.226	0.190
1994 HUD – Wind Zone I, Tied Down	0.697	0.537	0.402	0.306	0.262
1994 HUD – Wind Zone II, Tied Down	0.269	0.234	0.162	0.111	0.091
1994 HUD – Wind Zone III, Tied Down	0.249	0.214	0.151	0.106	0.087

*Values in table represent the damage state probabilities (%). Damage state descriptions are described in Table 5-52.

The manufactured home damage model has been validated through comparisons of damage states predicted from the above model to the damage states predicted from the models of Vann and McDonald (1978) and Vasquez (1994), as well as through comparisons of observed damage from Hurricane Bertha (1996) along the North Carolina coast, Hurricane Andrew (1992) in Dade County Florida and Hurricane Elena (1986) along the Central Gulf Coast.

5.6.3 Marginally- or Non-Engineered Hotel/Motel and Multi-Family Residential Buildings

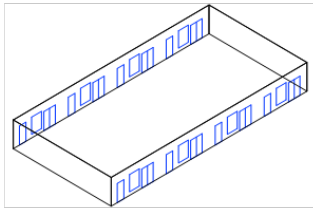
Nine different geometric representations of marginally engineered or non-engineered hotels/motels and multi-family residential buildings were developed, as shown pictorially in Figure 5-136. Using the wind loading models and the resistance models described earlier, damage states for each building as a function of wind speed have been estimated. All buildings with sloped roofs have been modeled as having asphalt shingle roofs, and the flat roof buildings are modeled as having either a built-up roof (BUR) or a single ply Ethylene Propylene Diene Monomer (EPDM) roof. The BUR and EPDM roofs are each modeled as being of “poor” quality and “average” quality. All windows are treated as being comprised of

single pane annealed glass, and all sliding glass doors are modeled with tempered glass. In the case of gable and flat roof structures, the connections between the roof and the wall are assumed to exist at the base of every truss with no connections along the short end wall. In the case of the hip roof structures, connections between the roof and the wall are assumed to exist along the entire perimeter of the wall. Whole roof failure is modeled in such a way that it fails as an entire unit. Each building has eight independent occupancy units on each floor (four at the front and four at the back). If a window or door breach occurs in any unit, the internal pressures are constrained to that unit. Each wall is modeled as having a horizontal span of 20' and a vertical span of 8' and is unsupported within the spans.

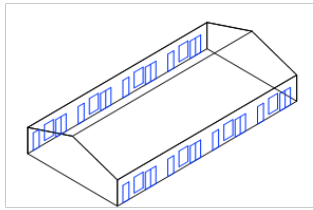
The parameters varied in the buildings are as follows:

- *Roof Shape:* Hip, Gable, and Flat
- *Roof Cover:* Asphalt Shingles (Hip and Gable Roofs) and BUR/EPDM (Flat Roofs, Examined for “Average” and “Poor” Quality)
- *Wall Construction:* Wood Frame (All Buildings) and Unreinforced/ Reinforced Masonry (One, Two, and Three-Story Buildings)
- *Roof Deck Attachment.:* 6d and 8d Nails
- *Roof/Wall Connection:* Strapped and Toe-Nailed
- *Number of Stories:* One, Two, Three, and Four

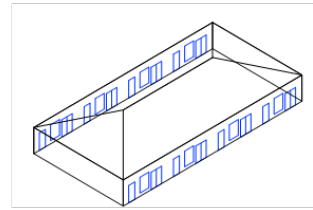
One-Story Buildings – 80’x40’ Plan, 10’ Eave Height



Flat Roof

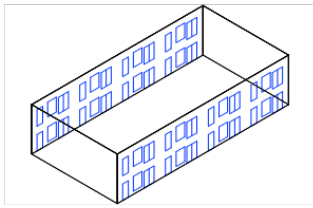


Gable Roof

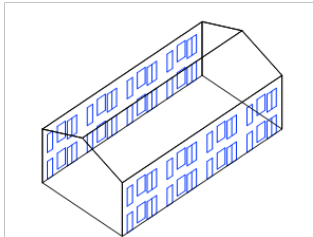


Hip Roof

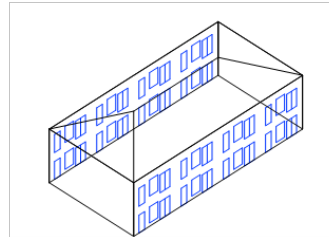
Two-Story Buildings – 80’x40’ Plan, 20’ Eave Height



Flat Roof

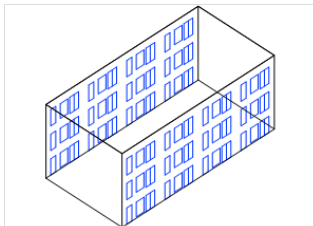


Gable Roof

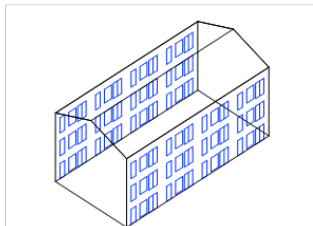


Hip Roof

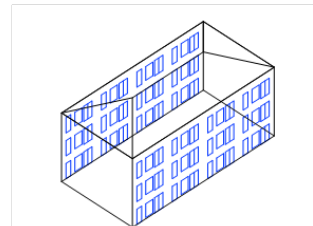
Three-Story Buildings – 80’x40’ Plan, 30’ Eave Height



Flat Roof

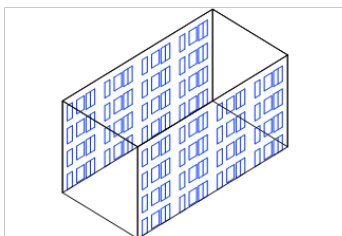


Gable Roof

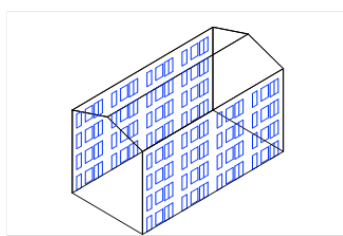


Hip Roof

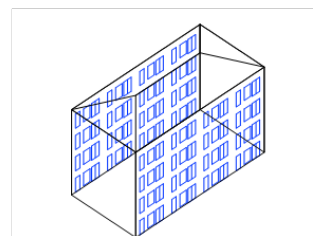
Four-Story Buildings – 80’x40’ Plan, 40’ Eave Height



Flat Roof



Gable Roof



Hip Roof

Figure 5-136 Model Building Geometries Used in Building Simulation Study

The assumed component resistances used in the simulations are given in Table 5-56. Damage simulations for each basic building type were performed for terrains described with $z_0 = 0.03$ meters (open terrain), $z_0 = 0.35$ meters (typical suburban terrain), $z_0 = 0.7$ meters (suburban terrain with some

trees), and $z_0 = 1.0$ meters (treed suburban terrain). All buildings are assumed to be exposed to a residential missile environment.

Table 5-56 Component Resistance Values Used to Model Marginally-Engineered or Non-Engineered Hotel/Motel and Multi-Family Residential Buildings

Component	Distribution	Distribution Parameters
Sheathing Panel (6d)	LogNormal	Mean = 54.6 psf, COV = 0.11
Sheathing Panel (8d)	LogNormal	Mean = 103 psf, COV = 0.11
Annealed Glass Impact	Deterministic	50 foot-pounds
Tempered Glass Impact	Deterministic	100 foot-pounds
Window/SG Door Pressure	Normal	Mean = 40 psf, COV = 0.2
Entry Door Pressure	Normal	Mean = 50 psf, COV = 0.2
Strap Up-Lift Resistance	Normal	Mean = 1,200 lb., COV = 0.30
Toe-Nail Uplift Resistance	Normal	Mean = 415 lb., COV = 0.25

The damage state definitions for marginally engineered or non-engineered hotels/motels and multi-family residential buildings are the same as those for the single-family residential buildings, which have been outlined in Table 5-44. Except, to make the damage state definitions with respect to roof damage (i.e., roof cover and roof deck) consistent between buildings with different numbers of stories, the threshold damage levels defining the roof damage states are modified by a factor which is a function of the number of stories. The concept is that 5% roof deck damage, for example, will have a greater effect in terms of economic losses on a one-story building compared to a two-story building. That is, in the case of the two-story building, only the top floor will experience similar damage due to the water infiltration associated with 5% roof deck loss to that experienced by the single-story building. The assumption made here for the purpose of the roof damage state definitions is that the intensity of damage on the bottom floor of the two, to the interior of the single-story building is arbitrarily set to 1, then the damage intensity to the two-story building will be $(1+0.5)/2 = 0.75$ (i.e., 1 represents the damage intensity story building will be half as much as that on the top floor. Thus, if the damage intensity of the top floor is represented by 1, and the damage intensity of the bottom floor is represented by 0.5 Therefore, to achieve a similar damage intensity to that associated with 5% roof deck damage on a single-story building, an otherwise similar two-story building would require 6.7% roof deck damage (i.e., $5\%/0.75$). The thresholds used to define the roof damage states listed in Table 5-44 were modified in the same manner as described above for the two-, three- and four-story buildings. The multiplicative factors are 1.33, 1.71, and 2.13, respectively. It can be seen, for example, that the four-story building cannot achieve a building Damage State 3 (i.e., severe damage) based on roof cover loss since the 50% threshold increases to more than 100% (i.e., $2.13*50\% > 100\%$). Also note that the two- and three-story buildings will be placed in Damage State 3 when the roof cover loss exceeds 67% and 86%, respectively.

Damage state versus wind speed plots have been developed using the same approach used for the single-family residential buildings by running 30 damage simulations per storm for 20,000 years of modeled storms. For more information on example building and component damage state plots, please contact the Hazus Help Desk (see Section 1.5) for the *Hazus Hurricane Model Technical Manual Appendices* (FEMA, 2021). The average per storm damage states are given in Table 5-57, Table 5-58,

and Table 5-59 and the impacts of the various building features on the average per storm damage are summarized in Table 5-60.

The results summarized in Table 5-60 indicate that the two parameters having the greatest impact on the average damage state for these buildings are the number of stories and, in the case of a flat roof, the change from modeling the roof cover as “average” quality versus “poor” quality. In the case of the poor-quality roof, the change from a built-up roof cover to a single ply membrane has a significant impact on the building damage state. Recall, however, that both the poor-quality roof cover model and the average quality roof cover model used in modeling both the BUR and the EPDM have been derived empirically using limited information obtained from post-storm damage data. The performance of either a built-up roof or a single ply roof in high wind events is subject to significant uncertainty and is heavily influenced by the quality of the installation. In the case of a poor-quality flat roof cover, the results given here indicate that the performance of the single ply membrane roof cover model governs the final damage state of the building.

The change from gable to flat (flat with a built-up roof) has an effect that is dependent on the number of stories and the assumed quality of the flat roof cover. A direct comparison of the performance of the flat roof building to that of the gable or hip buildings is made difficult because of the different roof covers; however, in general (for buildings other than single-story) the flat roof buildings tend to perform worse than the gable or hip roof buildings.

Table 5-57 Average Building Damage States – Marginally- or Non-Engineered Hotel/Motel and Multi-Family Residential Buildings – Gable/Hip Roof with Shingles

Building Characteristics				Strapped Roof-Wall Connections				Toe-Nailed Roof-Wall Connections			
				Terrain Surface Roughness (m)*				Terrain Surface Roughness (m)*			
No. of stories	Wall Const.	Roof Shape	Roof Deck Nails	0.03	0.35	0.70	1.0	0.03	0.35	0.70	1.0
One	Wood Frame	Gable	6d	0.565	0.356	0.284	0.250	0.593	0.375	0.298	0.260
			8d	0.494	0.316	0.244	0.216	0.542	0.349	0.272	0.237
		Hip	6d	0.455	0.284	0.217	0.187	0.476	0.301	0.228	0.197
			8d	0.428	0.271	0.206	0.178	0.459	0.291	0.221	0.190
	Unreinforced Masonry	Gable	6d	0.566	0.358	0.282	0.248	0.594	0.376	0.298	0.260
			8d	0.488	0.314	0.245	0.216	0.542	0.350	0.273	0.236
		Hip	6d	0.453	0.282	0.217	0.186	0.472	0.300	0.228	0.194
			8d	0.417	0.267	0.206	0.178	0.456	0.292	0.222	0.189
	Reinforced Masonry	Gable	6d	0.563	0.357	0.282	0.248	0.592	0.376	0.297	0.260
			8d	0.488	0.314	0.245	0.216	0.541	0.348	0.270	0.235
		Hip	6d	0.453	0.282	0.218	0.186	0.473	0.298	0.229	0.196
			8d	0.416	0.267	0.206	0.178	0.456	0.291	0.219	0.189
Two	Wood Frame	Gable	6d	0.755	0.522	0.436	0.393	0.788	0.548	0.454	0.410
			8d	0.674	0.459	0.376	0.337	0.718	0.497	0.407	0.365

Building Characteristics				Strapped Roof-Wall Connections				Toe-Nailed Roof-Wall Connections				
				Terrain Surface Roughness (m)*				Terrain Surface Roughness (m)*				
No. of stories	Wall Const.	Roof Shape	Roof Deck Nails	0.03	0.35	0.70	1.0	0.03	0.35	0.70	1.0	
Two	Wood Frame	Hip	6d	0.658	0.447	0.366	0.326	0.682	0.471	0.385	0.343	
			8d	0.627	0.422	0.345	0.306	0.662	0.456	0.373	0.330	
	Unreinforced Masonry	Gable	6d	0.743	0.515	0.431	0.389	0.780	0.545	0.453	0.409	
			8d	0.656	0.450	0.371	0.331	0.711	0.498	0.408	0.366	
		Hip	6d	0.641	0.441	0.362	0.323	0.677	0.468	0.381	0.342	
			8d	0.606	0.414	0.336	0.300	0.658	0.458	0.373	0.328	
	Reinforced Masonry	Gable	6d	0.741	0.515	0.429	0.390	0.781	0.544	0.454	0.409	
			8d	0.657	0.452	0.368	0.330	0.713	0.496	0.409	0.366	
		Hip	6d	0.643	0.440	0.362	0.323	0.678	0.469	0.385	0.343	
			8d	0.606	0.413	0.336	0.300	0.658	0.458	0.370	0.328	
	Three	Wood Frame	Gable	6d	0.876	0.630	0.543	0.497	0.904	0.655	0.564	0.517
				8d	0.783	0.553	0.462	0.421	0.831	0.593	0.500	0.455
Hip			6d	0.810	0.572	0.487	0.442	0.828	0.595	0.503	0.456	
			8d	0.772	0.545	0.460	0.417	0.804	0.575	0.486	0.441	
Unreinforced Masonry		Gable	6d	0.847	0.617	0.530	0.487	0.894	0.653	0.560	0.516	
			8d	0.748	0.533	0.449	0.406	0.813	0.587	0.497	0.451	
		Hip	6d	0.779	0.558	0.475	0.433	0.817	0.586	0.498	0.456	
			8d	0.728	0.519	0.439	0.401	0.788	0.571	0.479	0.440	
Reinforced Masonry		Gable	6d	0.848	0.616	0.531	0.488	0.895	0.651	0.558	0.515	
			8d	0.749	0.533	0.447	0.406	0.814	0.587	0.497	0.450	
		Hip	6d	0.778	0.558	0.473	0.433	0.819	0.589	0.501	0.456	
			8d	0.729	0.517	0.439	0.398	0.789	0.568	0.481	0.436	
Four	Wood Frame	Gable	6d	0.980	0.727	0.636	0.590	1.005	0.754	0.658	0.611	
			8d	0.884	0.636	0.543	0.498	0.927	0.675	0.581	0.535	
		Hip	6d	0.881	0.639	0.549	0.506	0.910	0.657	0.567	0.520	
			8d	0.853	0.609	0.518	0.472	0.881	0.636	0.546	0.502	

*Values in table represent the damage state probabilities (%). Damage state descriptions are described in Table 5-44.

Table 5-58 Average Building Damage States – Marginally- or Non-Engineered Hotel/Motel and Multi-Family Residential Buildings – Flat Roofs with BUR

Building Characteristics				Strapped Roof-Wall Connections*				Toe-Nailed Roof-Wall Connections*			
				Terrain Surface Roughness (m)				Terrain Surface Roughness (m)			
No. of stories	Wall Const.	Roof Quality	Roof Deck Nails	0.03	0.35	0.70	1.0	0.03	0.35	0.70	1.0
One	Wood Frame	Average	6d	0.387	0.242	0.176	0.150	0.397	0.248	0.181	0.153
			8d	0.342	0.221	0.164	0.137	0.364	0.238	0.169	0.144
		Poor	6d	0.596	0.371	0.290	0.257	0.607	0.377	0.294	0.263
			8d	0.580	0.362	0.288	0.255	0.602	0.372	0.292	0.261
	Unreinforced Masonry	Average	6d	0.383	0.240	0.178	0.148	0.393	0.249	0.182	0.155
			8d	0.338	0.221	0.163	0.137	0.365	0.237	0.171	0.141
		Poor	6d	0.594	0.366	0.290	0.258	0.606	0.377	0.299	0.265
			8d	0.575	0.360	0.286	0.254	0.602	0.373	0.292	0.258
	Reinforced Masonry	Average	6d	0.384	0.240	0.178	0.148	0.396	0.249	0.182	0.155
			8d	0.336	0.223	0.163	0.137	0.362	0.237	0.171	0.143
		Poor	6d	0.595	0.368	0.290	0.258	0.604	0.377	0.296	0.265
			8d	0.574	0.360	0.286	0.254	0.601	0.370	0.292	0.258
Two	Wood Frame	Average	6d	0.654	0.444	0.359	0.315	0.675	0.463	0.376	0.335
			8d	0.616	0.418	0.334	0.296	0.650	0.451	0.360	0.319
		Poor	6d	0.982	0.698	0.594	0.544	1.008	0.723	0.616	0.561
			8d	0.976	0.691	0.591	0.539	1.005	0.717	0.612	0.559
	Unreinforced Masonry	Average	6d	0.642	0.435	0.353	0.312	0.670	0.464	0.373	0.334
			8d	0.601	0.409	0.330	0.292	0.640	0.446	0.360	0.320
		Poor	6d	0.972	0.691	0.589	0.539	1.004	0.718	0.613	0.560
			8d	0.962	0.684	0.584	0.535	1.001	0.716	0.612	0.558
	Reinforced Masonry	Average	6d	0.644	0.437	0.352	0.315	0.668	0.463	0.376	0.332
			8d	0.600	0.410	0.332	0.293	0.642	0.446	0.361	0.318
		Poor	6d	0.974	0.691	0.588	0.541	1.005	0.719	0.610	0.560
			8d	0.965	0.684	0.583	0.532	0.999	0.715	0.611	0.557
Three	Wood Frame	Average	6d	0.874	0.631	0.539	0.493	0.909	0.661	0.562	0.516
			8d	0.841	0.603	0.514	0.472	0.881	0.642	0.546	0.496
		Poor	6d	1.311	1.000	0.886	0.827	1.343	1.032	0.913	0.853
			8d	1.305	0.994	0.884	0.828	1.341	1.032	0.911	0.850
	Unreinforced Masonry	Average	6d	0.852	0.619	0.532	0.484	0.898	0.659	0.562	0.514
			8d	0.816	0.592	0.506	0.460	0.872	0.636	0.542	0.497
		Poor	6d	1.288	0.991	0.876	0.819	1.337	1.025	0.910	0.852
			8d	1.282	0.985	0.877	0.816	1.333	1.025	0.912	0.850
	Reinforced Masonry	Average	6d	0.851	0.620	0.530	0.478	0.898	0.656	0.563	0.513
			8d	0.814	0.593	0.502	0.461	0.871	0.637	0.540	0.496

Building Characteristics				Strapped Roof-Wall Connections*				Toe-Nailed Roof-Wall Connections*			
				Terrain Surface Roughness (m)				Terrain Surface Roughness (m)			
No. of stories	Wall Const.	Roof Quality	Roof Deck Nails	0.03	0.35	0.70	1.0	0.03	0.35	0.70	1.0
Four	Wood Frame	Poor	6d	1.289	0.988	0.883	0.819	1.333	1.025	0.911	0.850
			8d	1.282	0.983	0.876	0.822	1.333	1.029	0.911	0.852
		Average	6d	0.955	0.706	0.609	0.563	1.001	0.745	0.654	0.602
			8d	0.897	0.650	0.561	0.513	0.968	0.719	0.625	0.579
		Poor	6d	1.291	1.003	0.900	0.847	1.334	1.048	0.939	0.884
			8d	1.255	0.974	0.864	0.809	1.326	1.038	0.933	0.874

*Values in table represent the damage state probabilities (%). Damage state descriptions are described in Table 5-44.

Table 5-59 Average Building Damage States – Marginally- or Non-Engineered Hotel/Motel and Multi-Family Residential Buildings – Flat Roofs with EPDM

Building Characteristics				Strapped Roof-Wall Connections*				Toe-Nailed Roof-Wall Connections*			
				Terrain Surface Roughness (m)				Terrain Surface Roughness (m)			
No. of stories	Wall Const.	Roof Quality	Roof Deck Nails	0.03	0.35	0.70	1.0	0.03	0.35	0.70	1.0
One	Wood Frame	Average	6d	0.430	0.264	0.198	0.170	0.442	0.273	0.201	0.174
			8d	0.405	0.252	0.188	0.164	0.425	0.266	0.198	0.168
		Poor	6d	0.968	0.623	0.515	0.471	0.984	0.632	0.518	0.475
			8d	0.962	0.623	0.511	0.465	0.983	0.631	0.519	0.472
	Unreinforced Masonry	Average	6d	0.424	0.264	0.199	0.169	0.437	0.270	0.203	0.174
			8d	0.395	0.253	0.189	0.163	0.421	0.265	0.196	0.170
		Poor	6d	0.974	0.625	0.517	0.468	0.982	0.630	0.519	0.476
			8d	0.952	0.616	0.516	0.468	0.980	0.632	0.519	0.472
	Reinforced Masonry	Average	6d	0.427	0.265	0.199	0.169	0.437	0.270	0.203	0.174
			8d	0.395	0.251	0.189	0.163	0.420	0.263	0.196	0.170
		Poor	6d	0.971	0.625	0.517	0.468	0.979	0.630	0.520	0.476
			8d	0.954	0.616	0.516	0.468	0.979	0.633	0.519	0.472
Two	Wood Frame	Average	6d	0.732	0.500	0.412	0.370	0.757	0.525	0.433	0.383
			8d	0.714	0.489	0.403	0.363	0.747	0.519	0.427	0.384
		Poor	6d	1.419	1.054	0.922	0.853	1.443	1.080	0.940	0.878
			8d	1.421	1.049	0.923	0.854	1.438	1.078	0.940	0.874
	Unreinforced Masonry	Average	6d	0.722	0.498	0.408	0.366	0.752	0.526	0.433	0.387
			8d	0.703	0.482	0.402	0.359	0.745	0.515	0.426	0.380
		Poor	6d	1.419	1.049	0.922	0.853	1.444	1.080	0.942	0.873

Building Characteristics				Strapped Roof-Wall Connections*				Toe-Nailed Roof-Wall Connections*			
				Terrain Surface Roughness (m)				Terrain Surface Roughness (m)			
No. of stories	Wall Const.	Roof Quality	Roof Deck Nails	0.03	0.35	0.70	1.0	0.03	0.35	0.70	1.0
Two	Reinforced Masonry	Poor	8d	1.409	1.049	0.919	0.851	1.440	1.078	0.941	0.871
		Average	6d	0.727	0.497	0.409	0.366	0.754	0.527	0.431	0.387
			8d	0.702	0.483	0.402	0.360	0.742	0.517	0.425	0.382
		Poor	6d	1.411	1.052	0.922	0.855	1.441	1.076	0.941	0.867
8d	1.409		1.055	0.915	0.849	1.443	1.073	0.943	0.874		
Three	Wood Frame	Average	6d	1.024	0.753	0.654	0.602	1.051	0.782	0.675	0.627
			8d	1.011	0.749	0.649	0.593	1.043	0.775	0.673	0.621
		Poor	6d	1.767	1.418	1.282	1.211	1.805	1.446	1.312	1.233
			8d	1.769	1.417	1.281	1.204	1.801	1.445	1.307	1.232
	Unreinforced Masonry	Average	6d	1.000	0.743	0.646	0.594	1.046	0.779	0.676	0.623
			8d	0.985	0.734	0.635	0.585	1.044	0.771	0.672	0.622
		Poor	6d	1.754	1.406	1.270	1.202	1.795	1.439	1.305	1.231
			8d	1.746	1.405	1.272	1.199	1.797	1.445	1.306	1.231
	Reinforced Masonry	Average	6d	0.997	0.741	0.647	0.592	1.045	0.780	0.665	0.613
			8d	0.989	0.730	0.638	0.584	1.035	0.776	0.672	0.624
		Poor	6d	1.748	1.405	1.272	1.200	1.795	1.446	1.309	1.233
			8d	1.745	1.408	1.269	1.196	1.798	1.444	1.309	1.235
Four	Wood Frame	Average	6d	1.046	0.782	0.685	0.638	1.089	0.824	0.727	0.675
			8d	1.005	0.747	0.650	0.603	1.076	0.814	0.716	0.664
		Poor	6d	1.591	1.294	1.181	1.119	1.631	1.335	1.216	1.154
			8d	1.543	1.260	1.149	1.088	1.620	1.328	1.213	1.148

*Values in table represent the damage state probabilities (%). Damage state descriptions are described in Table 5-44.

Table 5-60 Percent Increases in the Per Storm Average Building Damage State Due to Changes in Building Parameters (Minimum/Average/Maximum) - Marginally- or Non-Engineered Hotel/Motel and Multi-Family Residential Buildings

Roof Type	Parameter	Number of Stories														
		All			One			Two			Three			Four		
		Min	Avg	Max	Min	Avg	Max	Min	Avg	Max	Min	Avg	Max	Min	Avg	Max
Gable and Hip Roof With Singles	Unreinforced Masonry to Wood Frame Walls	-1%	1%	6%	-1%	0%	3%	0%	1%	3%	0%	2%	6%	N/A		
	Reinforced Masonry to Unreinforced Masonry Walls	-1%	0%	1%	-1%	0%	1%	-1%	0%	1%	-1%	0%	1%			
	Hip to Gable Roof Shape	0%	14%	34%	16%	24%	34%	7%	13%	21%	0%	7%	13%	4%	10%	17%
	8d to 6d Roof Deck Nails	2%	9%	20%	2%	8%	16%	2%	9%	18%	3%	10%	20%	3%	9%	19%
	Strapped to Toe-Nailed Roof/Wall Connections	2%	7%	11%	4%	7%	11%	4%	7%	11%	2%	7%	11%	3%	4%	7%
	One to Two Stories	31%	53%	76%	N/A											
	Two to Three Stories	14%	24%	36%												
	Three to Four Stories	9%	14%	19%												
Flat Roofs With BUR	Unreinforced Masonry to Wood Frame Walls	-1%	1%	3%	-1%	0%	2%	0%	1%	3%	0%	1%	3%	N/A		
	Reinforced Masonry to Unreinforced Masonry Walls	-1%	0%	1%	-1%	0%	1%	-1%	0%	1%	-1%	0%	1%			
	Hip to Gable Roof Shape	33%	62%	86%	51%	66%	86%	49%	64%	83%	48%	63%	78%	33%	45%	58%
	8d to 6d Roof Deck Nails	0%	3%	14%	1%	5%	14%	0%	3%	7%	0%	2%	6%	1%	4%	10%
	Strapped to Toe-Nailed Roof/Wall Connections	1%	5%	13%	1%	3%	8%	3%	5%	9%	2%	5%	8%	3%	7%	13%
	One to Two Stories	64%	94%	127%	N/A											
	Two to Three Stories	32%	45%	60%												
	Three to Four Stories	-4%	6%	17%												

Roof Type	Parameter	Number of Stories															
		All			One			Two			Three			Four			
		Min	Avg	Max	Min	Avg	Max	Min	Avg	Max	Min	Avg	Max	Min	Avg	Max	
Flat Roofs With EPDM	Unreinforced Masonry to Wood Frame Walls	-1%	0%	3%	-1%	0%	3%	-1%	0%	2%	0%	1%	3%	N/A			
	Reinforced Masonry to Unreinforced Masonry Walls	-1%	0%	2%	-1%	0%	1%	-1%	0%	1%	-1%	0%	2%				
	Average to Poor Quality Cover	50%	114%	188%	123%	153%	188%	91%	115%	137%	72%	90%	105%	50%	66%	80%	
	8d to 6d Roof Deck Nails	-2%	1%	8%	-1%	2%	8%	-1%	1%	4%	-2%	0%	2%	0%	2%	6%	
	One to Two Stories	45%	85%	128%	N/A												
	Two to Three Stories	24%	43%	64%													
	Three to Four Stories	-2%	-13%	8%													

5.6.4 Low-Rise Masonry Strip Mall Buildings

Small office and retail buildings are often constructed with units separated by fire walls, each having separate roof structures but a common roof cover. These low-rise buildings typically have flat roofs and are one-story high. They are usually built with a masonry or concrete wall system. The roof structures are typically constructed using wood trusses and a plywood deck, open web steel joists, and a metal deck, or a cast-in-place concrete deck. Because the units are separated by firewalls and have separate roof systems, window breaches in one unit do not impact either the internal pressure or the water infiltration of the adjacent unit(s). This building class is treated here as a separate building class from those constructed as a single unit, but of comparable size and usage. The damage state definitions for low-rise masonry strip mall buildings type are described in Table 5-61.

Table 5-61 Damage States for Low-Rise Masonry Strip Mall Construction

Damage State	Qualitative Damage Description	Roof Cover Failure	Window and Door Failures	Roof Deck Failure	Whole Roof Failure	Joist Failure	Wall Failure
					6 Units	6 Units	
					1 Unit	1 Unit	
0	<u>No Damage or Very Minor Damage</u> Little or no visible damage from the outside. No broken windows, or failed roof deck. Minimal loss of roof cover, with no or very limited water penetration.	≤2%	No	No	No	No	No
					No	No	
1	<u>Minor Damage</u> Maximum of one broken window or door. Moderate roof cover loss that can be covered to prevent additional water entering the building. Marks or dents on walls requiring painting or patching for repair.	>2% to ≤15%*	1 window or door failure*	No	No	No	No
					No	No	
2	<u>Moderate Damage</u> Major roof cover damage, moderate window breakage. Minor roof sheathing failure. Some resulting damage to interior of building from water.	>15% to ≤50%*	2 to ≤ the greater of 20% and 3*	1 to 3 panels*	No	No	No
					No	No	
3	<u>Severe Damage</u> Major window damage or roof sheathing loss. Major roof cover loss. Extensive damage to interior from water. Limited, local joist failures. Failure of one wall.	>50%*	> the greater of 20% and 3 to ≤50%*	>3 to ≤25%*	1 unit*	1 Unit to 1/3 of the units with joist failures*	1 wall*
					No	>0% to >25% joist failures*	
4	<u>Destruction</u> Complete roof failure on 1/3 or more of the units and/or failure of more than one wall. Loss of more than 25% of roof sheathing.	Typically >50%	>50%*	>25%*	2 or more units*	>1/3 of the units with joist failures*	2 or more walls
					Yes*	>25% joist failures*	

If any one of the conditions in the shaded cells with an asterisk () of a given row is true, the building is placed in that damage state)

The representative low-rise building used for small offices and retail is modeled here with masonry walls (either reinforced or unreinforced) and with either a lightweight open web steel joist (OWSJ) roof system or a wood roof system. The model buildings have a length of 184', a width of 40' and a roof height of either 12' or 20'. The overall building geometry, along with the placement and relative size of the windows and doors is shown in Figure 5-137 for the building with a 12' roof height. The building with the 20' roof height is otherwise the same as that shown in Figure 5-137. The different building configurations (with respect to building height, number of units, and roof system) modeled in this section are shown in Table 5-62.

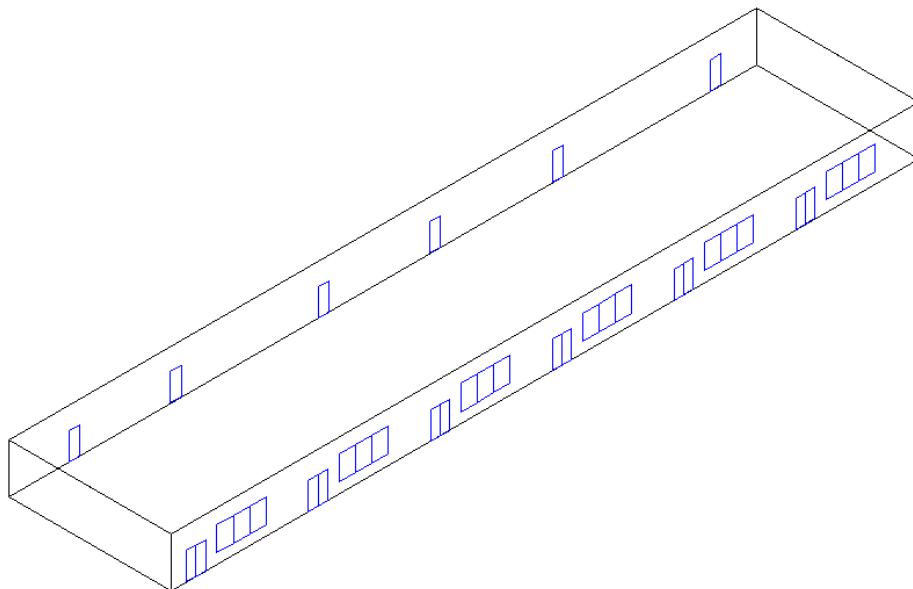


Figure 5-137 Model Building for One-Story Low-Rise Masonry Strip Mall Building with Roof Height = 12'

Table 5-62 Description of Low-Rise Masonry Strip Mall Buildings

Building Designation	Roof Height (ft)	No. of Units	Roof System(s)
A	12	6	Steel Deck on Steel Roof Joists; Joist Spacing = 4'; Joist Span = 30' (5 Units) and 34' (1 Unit); Joists Parallel to Long Building Edge
			Wood Deck on Wood Roof Trusses
B	20	6	Steel Deck on Steel Roof Joists; Joist Spacing = 4' Joist Span = 30' (5 Units) and 34' (1 Unit); Joists Parallel to Long Building Edge
			Wood Deck on Wood Roof Trusses
C	20	6	Steel Deck on Steel Roof Joists; Joist Spacing = 6' Joist Span = 30' (5 Units) and 34' (1 Unit); Joists Parallel to Long Building Edge
D	20	1	Steel Deck on Steel Roof Joists; Joist Spacing = 6' Joist Span = 40'; Joists Parallel to Short Building Edge

The multi-unit buildings have five units with a width of 30' and one end-unit with a width of 34'. Each of these units has three 6'x4' tempered glass windows and one tempered double glass entry door. The rear entry doors are modeled as standard residential type metal doors. The entire building has a total of 30 fenestrations, 24 of which have glazing and therefore, can be broken by missile impact. The roof cover is modeled as BUR or EPDM single-ply membrane ("average" quality in both cases).

For the buildings with wood roof structures, the wood roof trusses are spaced at 2' on center, and the roof-wall connections are modeled using either toe-nailed connections or strapped connections. The plywood roof sheathing is modeled as being attached to the roof trusses using either 6d or 8d nails with a standard 6"/12" spacing.

The OWSJs are designed to resist the uplift forces and moments computed using both ASCE 7-88 and the 1988 Version of SBC, as described in Section 5.4.10, for a design wind speed of 100 mph. In the case of the ASCE 7 loads, the building is assumed to be designed for open terrain (Exposure C) conditions. The metal deck is modeled as being connected to the joists using either screws or welds. The weld and screw designs are assumed to meet the loading requirements as given in ASCE 7 and SBC and are designed using the methods outlined in Section 5.4.11.

The assumed component resistances are given in Table 5-63. The very high uplift capacities associated with the steel deck are brought about by the minimum requirements for connection fastening, and the short (4') distance between joists. These uplift values are for the as-installed roof, but a sensitivity study was performed where the uplift capacities of the screwed and welded connections were reduced by 50% to allow for the effect of age and fatigue. This 50% reduction is comparable to the reduction in the pullout capacity of fasteners in metal decks, as reported by Baskaran and Dutt (1995).

Four different missile environments are considered in the analysis. The missile environments include combinations of residential-type missiles (i.e., roof shingles, roof tiles, and roof sheathing) and commercial-type missiles (i.e., roof gravel). Details on the windborne debris models are given in Section 5.2.2. In the case of the high-density commercial missile environment, the buildings from which the roof gravel originate are modeled as having a mean roof height of about 15' and mean building spacing of about 200'. The different missile environments are examined to determine the impact of the missile modeling on the building damage states. Table 5-64 gives descriptions of the four missile environments considered in the analysis.

For more information on example building and component damage state plots, please contact the Hazus Help Desk (see Section 1.5) for the *Hazus Hurricane Model Technical Manual Appendices* (FEMA, 2021). The storm average damage states are given in Table 5-65 and Table 5-66 for buildings with a wood roof system and Table 5-67, Table 5-68, and Table 5-69 for buildings with a steel roof system. They are developed using 20,000 years of simulated storms and performing 30 damage simulations for each storm.

The effects of the various building parameters on the storm-average damage states for the buildings with a wood roof system are summarized in

Table 5-69. It is evident that the missile environment has a large impact on the overall building damage state, increasing the mean per storm damage by 23% to 106% for the 12' high building and by 9% to 46% for the 20' high building when the missile environment changes from no windborne debris (Missile Environment D) to a mixed residential/commercial type environment (Missile Environment A). The effect of using toe-nails for the roof wall connections (versus straps) ranges from a 4% to 29% increase in the average damage state. Using 6d roof sheathing nails in place of 8d nails increases the storm average damage state by up to 15%. The relatively small effect of roof nails in these examples is associated with the fact that other severe damage states, which drive the overall building damage state, have already occurred before a significant amount of roof sheathing is lost. The effect of EPDM roof cover versus BUR roof cover ranges from a 4% to 32% increase in the average damage state. This increase in damage is attributed to the fact that the modeling of the EPDM roof allows the entire roof membrane to fail more readily than the BUR roof, once the initial local failure has occurred.

The building parameter sensitivity results for buildings with steel roof systems are shown in Table 5-70. The results show that when the uplift capacity of the steel roof deck is reduced by 50% to account for age and fatigue, the storm average damage state increases by as much as 31% when the joist spacing is 6' (Buildings C and D) and has a negligible effect when the joist spacing is 4' (Buildings A and B). The effect of using welds versus screws to fasten the steel roof deck to the joists ranges from a 2% decrease to a 9% increase in the average damage for the buildings having a 6' joist spacing. The effect of the roof deck fastener is negligible when the joist spacing is 4'. Similarly, the result of using the SBCCI versus the ACSE metal roof design criteria (both with a 100 mph design speed) ranges from a 1% decrease to a 23% increase in the average damage state for the buildings having a 6' joist spacing. The effect of the metal deck design criteria is negligible when the joist spacing is 4'. The impact of metal deck quality, installation, and design criteria on the storm average damage states, as discussed above, is more significant when the joist spacing is larger because the larger spacing reduces the uplift capacity of the roof panels (see Table 5-71). Therefore, the metal deck damage has a larger weight in the overall damage state.

Table 5-63 Component Resistance Values Used for Strip-Mall Type Building

Fenestrations		
Component	Distribution	Distribution Parameters
Tempered Glass Small Missile Impact	Deterministic	0.01 slug-ft/sec (Momentum)
Tempered Glass Large Missile Impact	Deterministic	100 foot-pounds (Energy)
Window/SG Door System Pressure	Normal	Mean = 40 psf, COV = 0.2
Entry Door System Pressure	Normal	Mean = 50 psf, COV = 0.2
Tempered Glass Pressure (Windows)	Weibull	C = 168 psf, k = 4.8
Tempered Glass Pressure (SG Doors)	Weibull	C = 175 psf, k = 6.1

Wood Deck on Wooden Roof Trusses		
Component	Distribution	Distribution Parameters
Sheathing Panel (6d)	LogNormal	Mean = 54.6 psf, COV = 0.11
Sheathing Panel (8d)	LogNormal	Mean = 103 psf, COV = 0.11
Strap Uplift Resistance	Normal	Mean = 1,200 lb., COV = 0.3
Toe-Nail Uplift Resistance	Normal	Mean = 415 lb., COV = 0.25
Steel Deck on Steel Roof Joists – Building Height = 12’, Joist Spacing = 4’		
Component	Distribution	Distribution Parameters (Field, Edge, Corner)
Screwed Steel Deck – SBCCI 100mph	LogNormal	Mean = 187, 187, 187 psf, COV = 0.13, 0.13, 0.13
Screwed Steel Deck – ASCE 100mph	LogNormal	Mean = 187, 187, 212 psf, COV = 0.13, 0.13, 0.11
Welded Steel Deck – SBCCI 100mph	LogNormal	Mean = 169, 169, 169 psf, COV = 0.13, 0.13, 0.13
Welded Steel Deck – ASCE 100mph	LogNormal	Mean = 169, 169, 222 psf, COV = 0.13, 0.13, 0.18
Steel Deck on Steel Roof Joists – Building Height = 20’, Joist Spacing = 4’		
Component	Distribution	Distribution Parameters (Field, Edge, Corner)
Screwed Steel Deck – SBCCI 100mph	LogNormal	Mean = 187, 187, 187 psf, COV = 0.13, 0.13, 0.13
Screwed Steel Deck – ASCE 100mph	LogNormal	Mean = 187, 187, 212 psf, COV = 0.13, 0.13, 0.11
Welded Steel Deck – SBCCI 100mph	LogNormal	Mean = 169, 169, 169 psf, COV = 0.13, 0.13, 0.13
Welded Steel Deck – ASCE 100mph	LogNormal	Mean = 169, 169, 222 psf, COV = 0.13, 0.13, 0.18
Steel Deck on Steel Roof Joists – Building Height = 20’, Joist Spacing = 6’		
Component	Distribution	Distribution Parameters (Field, Edge, Corner)
Screwed Steel Deck – SBCCI 100mph	LogNormal	Mean = 109, 109, 109 psf, COV = 0.21, 0.21, 0.21
Screwed Steel Deck – ASCE 100mph	LogNormal	Mean = 109, 127, 165 psf, COV = 0.21, 0.21, 0.21
Welded Steel Deck – SBCCI 100mph	LogNormal	Mean = 91, 91, 97 psf, COV = 0.19, 0.19, 0.19
Welded Steel Deck – ASCE 100mph	LogNormal	Mean = 91, 123, 155 psf, COV = 0.19, 0.19, 0.19

Table 5-64 Description of Missile Environments

Missile Environment Designation	Missile Source Environment, C = Commercial Type Missiles, R = Residential Type Missiles, M = Equal Mix of Commercial and Residential Type Missiles, N = No Missiles							
	Center of 45° Directional Sector							
	N	NE	E	SE	S	SW	W	NW
A	M	M	M	M	M	M	M	M
B	R	C	R	R	C	R	R	R
C	R	R	R	R	R	R	R	R
D	N	N	N	N	N	N	N	N

The use of EPDM roof cover versus BUR roof cover increases the overall storm average damage states by a range of 5% to 34%. The effect of the roof cover type is similar for each of the four buildings examined. Walls constructed with unreinforced masonry versus reinforced masonry yield mean damage states which are up to 15% larger for the buildings with a roof height of 20' (Buildings B, C and D) and has a much less significant effect (2% decrease to 4% increase) when the roof height is 12' (Building A). Again, the different missile environments have a large impact on the storm average damage states as seen from the last three rows of Table 5-72. The largest effect is found when changing from no windborne missiles (Missile Environment D) to a mixed residential/commercial type environment (Missile Environment A) where the storm average damage states increased from a range of 24% to 115% for the 12' high building cases and a range of 8% to 39% for the 20' high building cases. The elimination of glass breakage associated with windborne debris (i.e., as produced when changing the modeled Missile Environment from A to D) has a smaller impact on the overall damage state for the 20' high building cases compared to the 12' high building cases since the overall damage state is more influenced by roof damage compared to fenestration damage for the taller buildings.

Table 5-73 summarizes the influence of building height, joist spacing, and number of units on the storm average damage state. The building height is shown to have the most significant effect, increasing the damage states from a range of 25% to 126% when the building height increases from 12' to 20'. Increasing the joist spacing from 4' to 6' increases the mean damage state by up to 31%. It is also shown in Table 5-73 that by going from the multi-unit buildings to the single unit buildings, the mean per storm damage state increases by no more than 4%.

Table 5-65 Average Damage States for Building A - Twelve Foot High Strip Mall Building with Six Units and Wood Deck with Two Foot Truss Spacing

Building Characteristics				Toe-Nailed Roof-Wall Connection*				Strapped Roof-Wall Connection*			
				Terrain Surface Roughness (m)				Terrain Surface Roughness (m)			
Wall Type	Missile Environ	Wood Deck Nail Size	Roof Cover	0.03	0.35	0.70	1.0	0.03	0.35	0.70	1.0
Unreinforced Masonry	A	6d	EPDM	0.694	0.459	0.340	0.285	0.571	0.425	0.314	0.267
			BUR	0.660	0.440	0.319	0.267	0.531	0.405	0.296	0.248

Building Characteristics				Toe-Nailed Roof-Wall Connection*				Strapped Roof-Wall Connection*				
				Terrain Surface Roughness (m)				Terrain Surface Roughness (m)				
Wall Type	Missile Environ	Wood Deck Nail Size	Roof Cover	0.03	0.35	0.70	1.0	0.03	0.35	0.70	1.0	
		8d	EPDM	0.688	0.454	0.338	0.282	0.555	0.414	0.310	0.260	
			BUR	0.641	0.431	0.314	0.263	0.506	0.392	0.288	0.239	
	B	6d	EPDM	0.600	0.391	0.291	0.249	0.525	0.361	0.267	0.230	
			BUR	0.560	0.369	0.271	0.226	0.478	0.332	0.245	0.206	
		8d	EPDM	0.594	0.386	0.291	0.246	0.508	0.353	0.264	0.222	
			BUR	0.545	0.359	0.263	0.221	0.449	0.318	0.233	0.193	
	C	6d	EPDM	0.518	0.331	0.249	0.214	0.475	0.288	0.221	0.190	
			BUR	0.468	0.301	0.225	0.186	0.423	0.254	0.190	0.163	
		8d	EPDM	0.508	0.324	0.247	0.209	0.459	0.275	0.211	0.182	
			BUR	0.452	0.291	0.211	0.180	0.390	0.232	0.173	0.148	
	D	6d	EPDM	0.483	0.267	0.211	0.188	0.459	0.253	0.198	0.177	
			BUR	0.428	0.227	0.177	0.155	0.408	0.215	0.164	0.146	
		8d	EPDM	0.478	0.261	0.206	0.180	0.450	0.246	0.190	0.167	
			BUR	0.408	0.213	0.164	0.142	0.372	0.192	0.147	0.129	
	Reinforced Masonry	A	6d	EPDM	0.683	0.458	0.340	0.284	0.565	0.429	0.315	0.268
				BUR	0.655	0.432	0.320	0.269	0.530	0.404	0.298	0.247
8d			EPDM	0.686	0.453	0.333	0.279	0.548	0.417	0.311	0.259	
			BUR	0.644	0.429	0.316	0.261	0.499	0.391	0.287	0.239	
B		6d	EPDM	0.595	0.388	0.290	0.246	0.519	0.355	0.270	0.229	
			BUR	0.553	0.363	0.266	0.226	0.474	0.330	0.244	0.205	
		8d	EPDM	0.589	0.387	0.288	0.244	0.499	0.344	0.262	0.222	
			BUR	0.539	0.358	0.260	0.217	0.444	0.315	0.232	0.193	
C		6d	EPDM	0.510	0.327	0.248	0.213	0.470	0.284	0.219	0.191	
			BUR	0.463	0.302	0.219	0.187	0.417	0.254	0.190	0.163	
		8d	EPDM	0.505	0.324	0.245	0.208	0.451	0.271	0.210	0.182	
			BUR	0.442	0.288	0.214	0.179	0.381	0.230	0.171	0.147	
D		6d	EPDM	0.475	0.263	0.209	0.186	0.457	0.253	0.199	0.179	
			BUR	0.419	0.223	0.176	0.153	0.402	0.213	0.164	0.145	
		8d	EPDM	0.468	0.258	0.204	0.180	0.443	0.242	0.190	0.166	
			BUR	0.396	0.209	0.162	0.142	0.367	0.189	0.147	0.126	

*Values in table represent the damage state probabilities (%). Damage state descriptions are described in Table 5-61.

Table 5-66 Average Damage States for Building B - Twenty Foot High Strip Mall Building with Six Units and Wood Deck with Two Foot Truss Spacing

Building Characteristics				Toe-Nailed Roof-Wall Connection*				Strapped Roof-Wall Connection*			
				Terrain Surface Roughness (m)				Terrain Surface Roughness (m)			
Wall Type	Missile Environ	Wood Deck Nail Size	Roof Cover	0.03	0.35	0.70	1.0	0.03	0.35	0.70	1.0
Unreinforced Masonry	A	6d	EPDM	0.933	0.666	0.531	0.463	0.835	0.585	0.466	0.414
			BUR	0.863	0.620	0.485	0.422	0.757	0.533	0.419	0.365
		8d	EPDM	0.928	0.665	0.532	0.460	0.822	0.579	0.465	0.409
			BUR	0.852	0.613	0.477	0.415	0.733	0.523	0.407	0.350
	B	6d	EPDM	0.861	0.596	0.486	0.430	0.792	0.546	0.443	0.392
			BUR	0.795	0.546	0.433	0.380	0.715	0.486	0.390	0.341
		8d	EPDM	0.859	0.601	0.483	0.428	0.785	0.539	0.438	0.387
			BUR	0.775	0.537	0.421	0.373	0.692	0.468	0.372	0.326
	C	6d	EPDM	0.800	0.548	0.448	0.400	0.763	0.503	0.415	0.374
			BUR	0.719	0.484	0.393	0.346	0.673	0.435	0.355	0.316
		8d	EPDM	0.798	0.543	0.444	0.401	0.757	0.496	0.412	0.369
			BUR	0.703	0.470	0.378	0.337	0.651	0.418	0.335	0.301
	D	6d	EPDM	0.789	0.510	0.428	0.390	0.758	0.490	0.409	0.368
			BUR	0.705	0.441	0.365	0.330	0.667	0.416	0.343	0.307
		8d	EPDM	0.785	0.506	0.427	0.386	0.753	0.484	0.404	0.364
			BUR	0.681	0.425	0.353	0.316	0.649	0.396	0.326	0.290
Reinforced Masonry	A	6d	EPDM	0.903	0.659	0.524	0.460	0.789	0.567	0.458	0.401
			BUR	0.838	0.609	0.479	0.412	0.708	0.516	0.406	0.352
		8d	EPDM	0.897	0.653	0.523	0.457	0.769	0.560	0.448	0.396
			BUR	0.821	0.598	0.472	0.404	0.674	0.493	0.382	0.337
	B	6d	EPDM	0.832	0.590	0.480	0.426	0.751	0.526	0.431	0.381
			BUR	0.764	0.534	0.425	0.372	0.667	0.466	0.372	0.325
		8d	EPDM	0.829	0.585	0.475	0.424	0.735	0.514	0.418	0.374
			BUR	0.746	0.521	0.415	0.365	0.630	0.441	0.352	0.308
	C	6d	EPDM	0.761	0.533	0.440	0.397	0.719	0.484	0.403	0.361
			BUR	0.684	0.470	0.382	0.340	0.631	0.417	0.342	0.303
		8d	EPDM	0.763	0.531	0.436	0.392	0.708	0.471	0.394	0.355
			BUR	0.666	0.459	0.370	0.332	0.596	0.383	0.314	0.282
D	6d	EPDM	0.755	0.497	0.417	0.382	0.718	0.468	0.395	0.359	

Building Characteristics				Toe-Nailed Roof-Wall Connection*				Strapped Roof-Wall Connection*			
				Terrain Surface Roughness (m)				Terrain Surface Roughness (m)			
Wall Type	Missile Environ	Wood Deck Nail Size	Roof Cover	0.03	0.35	0.70	1.0	0.03	0.35	0.70	1.0
			BUR	0.661	0.423	0.358	0.324	0.626	0.393	0.327	0.295
		8d	EPDM	0.745	0.492	0.413	0.378	0.706	0.458	0.383	0.349
			BUR	0.641	0.411	0.344	0.309	0.590	0.367	0.303	0.273

*Values in table represent the damage state probabilities (%). Damage state descriptions are described in Table 5-61.

Table 5-67 Average Damage States for Building A - Twelve Foot High Strip Mall Building with Six Units and Metal Deck with Four Foot Joist Spacing

Building Characteristics					No Reduction in Metal Deck Capacity*				50% Reduction in Metal Deck Capacity*			
					Terrain Surface Roughness (m)				Terrain Surface Roughness (m)			
Wall Type	Missile Environ.	Design Code	Wood Deck Nail Size	Roof Cover	0.03	0.35	0.70	1.0	0.03	0.35	0.70	1.0
Unreinfor. Masonry	A	SBCCI	Screws	EPDM	0.540	0.421	0.312	0.259	0.537	0.418	0.310	0.261
				BUR	0.490	0.391	0.287	0.237	0.489	0.392	0.284	0.235
			Welds	EPDM	0.538	0.419	0.312	0.260	0.540	0.419	0.312	0.261
				BUR	0.487	0.393	0.286	0.240	0.487	0.392	0.286	0.237
		ABSCE	Screws	EPDM	0.540	0.419	0.313	0.262	0.539	0.418	0.309	0.258
				BUR	0.490	0.394	0.287	0.236	0.487	0.394	0.288	0.236
			Welds	EPDM	0.536	0.420	0.310	0.260	0.537	0.416	0.312	0.261
				BUR	0.488	0.394	0.286	0.237	0.488	0.394	0.289	0.236
	B	SBCCI	Screws	EPDM	0.494	0.349	0.262	0.223	0.489	0.348	0.261	0.223
				BUR	0.433	0.310	0.229	0.194	0.432	0.314	0.231	0.196
			Welds	EPDM	0.489	0.346	0.261	0.222	0.491	0.346	0.262	0.222
				BUR	0.431	0.315	0.230	0.194	0.433	0.314	0.231	0.191
		ABSCE	Screws	EPDM	0.489	0.350	0.260	0.221	0.489	0.346	0.260	0.220
				BUR	0.429	0.314	0.231	0.195	0.428	0.315	0.231	0.194
			Welds	EPDM	0.491	0.348	0.262	0.223	0.489	0.348	0.261	0.223
				BUR	0.431	0.315	0.231	0.194	0.431	0.313	0.230	0.195
	C	SBCCI	Screws	EPDM	0.441	0.269	0.208	0.181	0.441	0.270	0.207	0.180
				BUR	0.372	0.230	0.172	0.145	0.369	0.228	0.170	0.146
			Welds	EPDM	0.441	0.271	0.208	0.181	0.442	0.271	0.207	0.180
				BUR	0.370	0.227	0.168	0.144	0.373	0.226	0.171	0.145
		ABSCE	Screws	EPDM	0.441	0.268	0.209	0.180	0.439	0.270	0.209	0.183
				BUR	0.369	0.227	0.169	0.145	0.369	0.227	0.171	0.144
			Welds	EPDM	0.439	0.269	0.209	0.179	0.439	0.270	0.207	0.180
				BUR	0.368	0.226	0.170	0.145	0.369	0.228	0.171	0.146
	D	SBCCI	Screws	EPDM	0.430	0.240	0.191	0.170	0.431	0.242	0.190	0.169
				BUR	0.359	0.188	0.145	0.128	0.359	0.188	0.147	0.129
			Welds	EPDM	0.431	0.241	0.191	0.170	0.431	0.239	0.191	0.168
				BUR	0.356	0.187	0.146	0.128	0.358	0.189	0.147	0.129
ABSCE		Screws	EPDM	0.431	0.240	0.191	0.170	0.433	0.239	0.189	0.169	
			BUR	0.354	0.187	0.145	0.128	0.353	0.187	0.146	0.128	
		Welds	EPDM	0.432	0.239	0.191	0.170	0.432	0.240	0.190	0.169	
			BUR	0.354	0.187	0.145	0.128	0.354	0.187	0.146	0.129	
A	A	SBCCI	Screws	EPDM	0.532	0.418	0.313	0.260	0.531	0.416	0.310	0.260

Building Characteristics					No Reduction in Metal Deck Capacity*				50% Reduction in Metal Deck Capacity*				
					Terrain Surface Roughness (m)				Terrain Surface Roughness (m)				
Wall Type	Missile Environ.	Design Code	Wood Deck Nail Size	Roof Cover	0.03	0.35	0.70	1.0	0.03	0.35	0.70	1.0	
Reinforced Masonry				BUR	0.481	0.391	0.289	0.237	0.483	0.390	0.287	0.240	
				Welds	EPDM	0.534	0.419	0.310	0.262	0.534	0.420	0.311	0.259
				BUR	0.479	0.390	0.286	0.236	0.484	0.391	0.283	0.236	
				Welds	EPDM	0.533	0.417	0.308	0.258	0.535	0.420	0.310	0.261
			ABSCE	BUR	0.478	0.391	0.287	0.237	0.482	0.390	0.286	0.236	
				Welds	EPDM	0.533	0.418	0.313	0.258	0.533	0.418	0.311	0.258
			BUR	0.482	0.390	0.284	0.237	0.483	0.392	0.283	0.237		
			Welds	EPDM	0.485	0.347	0.262	0.217	0.483	0.346	0.263	0.221	
		B	SBCCI	Screws	EPDM	0.485	0.347	0.262	0.217	0.483	0.346	0.263	0.221
					BUR	0.423	0.312	0.230	0.191	0.424	0.314	0.231	0.193
			Welds		EPDM	0.484	0.347	0.260	0.221	0.483	0.343	0.260	0.220
					BUR	0.424	0.311	0.227	0.191	0.425	0.313	0.229	0.195
		ABSCE	Screws	EPDM	0.481	0.346	0.261	0.222	0.483	0.346	0.261	0.220	
				BUR	0.425	0.313	0.228	0.190	0.423	0.313	0.228	0.192	
		Welds		EPDM	0.485	0.346	0.261	0.219	0.487	0.345	0.260	0.222	
				BUR	0.423	0.311	0.229	0.192	0.426	0.311	0.228	0.191	
	C		SBCCI	Screws	EPDM	0.433	0.266	0.207	0.179	0.432	0.268	0.207	0.180
					BUR	0.360	0.226	0.167	0.144	0.361	0.224	0.169	0.144
				Welds	EPDM	0.429	0.267	0.205	0.179	0.431	0.267	0.205	0.180
				BUR	0.360	0.226	0.169	0.144	0.363	0.226	0.168	0.145	
				ABSCE	Screws	EPDM	0.433	0.269	0.207	0.180	0.433	0.268	0.208
			BUR			0.360	0.226	0.169	0.144	0.361	0.226	0.168	0.144
			Welds		EPDM	0.432	0.268	0.206	0.179	0.433	0.269	0.208	0.178
					BUR	0.361	0.225	0.168	0.144	0.363	0.224	0.171	0.144
		D	SBCCI	Screws	EPDM	0.423	0.239	0.189	0.167	0.422	0.237	0.188	0.168
					BUR	0.345	0.184	0.144	0.126	0.348	0.183	0.144	0.126
				Welds	EPDM	0.425	0.239	0.189	0.167	0.427	0.236	0.188	0.167
				Welds		BUR	0.346	0.185	0.143	0.125	0.350	0.182	0.144
ABSCE	Screws					EPDM	0.425	0.237	0.189	0.167	0.424	0.237	0.187
			BUR	0.347	0.184	0.143	0.126	0.346	0.184	0.143	0.127		
	Welds		EPDM	0.421	0.237	0.189	0.167	0.421	0.237	0.191	0.168		
			BUR	0.344	0.183	0.143	0.126	0.349	0.184	0.143	0.127		

*Values in table represent the damage state probabilities (%). Damage state descriptions are described in Table 5-61.

Table 5-68 Average Damage States for Building B - Twenty Foot High Strip Mall Building with Six Units and Metal Deck with Four Foot Joist Spacing

Building Characteristics					No Reduction in Metal Deck Capacity*				50% Reduction in Metal Deck Capacity*				
					Terrain Surface Roughness (m)				Terrain Surface Roughness (m)				
Wall Type	Missile Environ.	Design Code	Metal Deck Attach	Roof Cover	0.03	0.35	0.70	1.0	0.03	0.35	0.70	1.0	
Unreinfor. Masonry	A	SBCCI	Screws	EPDM	0.813	0.574	0.463	0.406	0.813	0.575	0.464	0.406	
				BUR	0.724	0.519	0.406	0.352	0.724	0.515	0.404	0.352	
			Welds	EPDM	0.815	0.574	0.457	0.407	0.809	0.576	0.464	0.406	
				BUR	0.726	0.517	0.402	0.350	0.725	0.519	0.404	0.350	
		ABSCE	Screws	EPDM	0.814	0.577	0.461	0.407	0.814	0.579	0.465	0.409	
				BUR	0.725	0.517	0.405	0.351	0.726	0.517	0.404	0.348	
			Welds	EPDM	0.814	0.578	0.463	0.408	0.812	0.581	0.462	0.410	
				BUR	0.725	0.517	0.408	0.350	0.723	0.518	0.404	0.352	
		B	SBCCI	Screws	EPDM	0.781	0.532	0.435	0.385	0.773	0.534	0.434	0.387
					BUR	0.680	0.465	0.366	0.325	0.677	0.464	0.368	0.323
				Welds	EPDM	0.776	0.534	0.433	0.387	0.772	0.537	0.431	0.384
					BUR	0.682	0.466	0.366	0.324	0.684	0.466	0.368	0.322
	ABSCE		Screws	EPDM	0.775	0.535	0.433	0.383	0.775	0.534	0.434	0.386	
				BUR	0.680	0.464	0.367	0.322	0.680	0.465	0.369	0.323	
			Welds	EPDM	0.772	0.536	0.434	0.385	0.775	0.535	0.433	0.387	
				BUR	0.681	0.467	0.367	0.321	0.683	0.461	0.369	0.322	
	C		SBCCI	Screws	EPDM	0.745	0.491	0.408	0.363	0.746	0.492	0.406	0.364
					BUR	0.641	0.408	0.334	0.296	0.641	0.408	0.333	0.295
				Welds	EPDM	0.742	0.492	0.409	0.365	0.743	0.493	0.406	0.364
					BUR	0.640	0.408	0.333	0.296	0.640	0.408	0.335	0.298
		ABSCE	Screws	EPDM	0.742	0.491	0.409	0.366	0.744	0.493	0.406	0.367	
				BUR	0.637	0.411	0.332	0.297	0.641	0.410	0.333	0.297	
			Welds	EPDM	0.744	0.489	0.407	0.364	0.742	0.491	0.403	0.365	
				BUR	0.643	0.412	0.336	0.298	0.640	0.410	0.335	0.294	
D		SBCCI	Screws	EPDM	0.747	0.480	0.400	0.362	0.740	0.478	0.399	0.365	
				BUR	0.633	0.392	0.323	0.289	0.636	0.391	0.323	0.290	
			Welds	EPDM	0.744	0.477	0.399	0.362	0.743	0.479	0.401	0.358	
				BUR	0.635	0.391	0.322	0.286	0.637	0.391	0.323	0.289	
	ABSCE	Screws	EPDM	0.749	0.478	0.397	0.363	0.744	0.479	0.400	0.359		
			BUR	0.635	0.392	0.322	0.286	0.632	0.391	0.319	0.287		

Building Characteristics					No Reduction in Metal Deck Capacity*				50% Reduction in Metal Deck Capacity*				
					Terrain Surface Roughness (m)				Terrain Surface Roughness (m)				
Wall Type	Missile Environ.	Design Code	Metal Deck Attach	Roof Cover	0.03	0.35	0.70	1.0	0.03	0.35	0.70	1.0	
Reinfor. Masonry			Welds	EPDM	0.743	0.478	0.398	0.361	0.742	0.479	0.399	0.360	
				BUR	0.637	0.392	0.322	0.286	0.637	0.392	0.321	0.287	
	A	SBCCI	Screws	EPDM	0.739	0.555	0.443	0.394	0.739	0.555	0.445	0.393	
				BUR	0.634	0.489	0.384	0.330	0.638	0.491	0.382	0.332	
			Welds	EPDM	0.739	0.556	0.443	0.392	0.738	0.556	0.444	0.389	
				BUR	0.638	0.492	0.384	0.331	0.640	0.492	0.383	0.334	
			ABSCE	Screws	EPDM	0.739	0.554	0.443	0.392	0.736	0.554	0.444	0.395
					BUR	0.640	0.490	0.386	0.332	0.640	0.494	0.385	0.332
		Welds	EPDM	0.735	0.554	0.445	0.392	0.740	0.555	0.443	0.393		
			BUR	0.640	0.491	0.383	0.332	0.640	0.492	0.384	0.332		
		B	SBCCI	Screws	EPDM	0.707	0.506	0.415	0.369	0.706	0.507	0.417	0.371
					BUR	0.601	0.438	0.344	0.301	0.599	0.438	0.345	0.304
				Welds	EPDM	0.708	0.509	0.414	0.371	0.708	0.508	0.415	0.369
					BUR	0.602	0.433	0.345	0.302	0.602	0.435	0.345	0.303
	ABSCE		Screws	EPDM	0.704	0.508	0.413	0.368	0.707	0.506	0.415	0.369	
				BUR	0.601	0.434	0.346	0.305	0.602	0.434	0.346	0.303	
	Welds	EPDM	0.711	0.508	0.416	0.369	0.710	0.506	0.414	0.369			
		BUR	0.601	0.435	0.347	0.302	0.603	0.432	0.344	0.300			
	C	SBCCI	Screws	EPDM	0.677	0.457	0.384	0.345	0.677	0.460	0.384	0.345	
				BUR	0.561	0.370	0.303	0.273	0.562	0.372	0.304	0.273	
			Welds	EPDM	0.679	0.457	0.382	0.346	0.680	0.457	0.382	0.348	
				BUR	0.562	0.374	0.306	0.274	0.565	0.375	0.305	0.273	
		ABSCE	Screws	EPDM	0.679	0.458	0.380	0.347	0.677	0.461	0.380	0.345	
				BUR	0.562	0.371	0.304	0.273	0.562	0.373	0.306	0.274	
Welds			EPDM	0.677	0.456	0.383	0.344	0.679	0.459	0.381	0.346		
			BUR	0.562	0.371	0.305	0.272	0.565	0.371	0.303	0.272		
D	SBCCI	Screws	EPDM	0.676	0.446	0.378	0.347	0.674	0.452	0.378	0.345		
			BUR	0.555	0.356	0.297	0.267	0.557	0.356	0.295	0.266		
		Welds	EPDM	0.679	0.448	0.378	0.345	0.676	0.447	0.376	0.344		
			BUR	0.558	0.355	0.296	0.268	0.561	0.357	0.296	0.267		
	ABSCE	Screws	EPDM	0.677	0.446	0.379	0.346	0.677	0.447	0.375	0.344		
			BUR	0.557	0.357	0.294	0.268	0.558	0.355	0.296	0.267		

Building Characteristics					No Reduction in Metal Deck Capacity*				50% Reduction in Metal Deck Capacity*			
					Terrain Surface Roughness (m)				Terrain Surface Roughness (m)			
Wall Type	Missile Environ.	Design Code	Metal Deck Attach	Roof Cover	0.03	0.35	0.70	1.0	0.03	0.35	0.70	1.0
			Welds	EPDM	0.680	0.446	0.378	0.346	0.678	0.446	0.377	0.343
				BUR	0.559	0.355	0.295	0.268	0.559	0.355	0.296	0.267

*Values in table represent the damage state probabilities (%). Damage state descriptions are described in Table 5-61.

Table 5-69 Average Damage States for Building C - Twenty Foot High Strip Mall Building with Six Units and Metal Deck with Six Foot Joist Spacing

Building Characteristics					No Reduction in Metal Deck Capacity				50% Reduction in Metal Deck Capacity				
					Terrain Surface Roughness (m)*				Terrain Surface Roughness (m)*				
Wall Type	Missile Environ	Design Code	Metal Deck Attach.	Roof Cover	0.03	0.35	0.70	1.0	0.03	0.35	0.70	1.0	
Unreinfor. Masonry	A	SBCCI	Screws	EPDM	0.816	0.57	0.46	0.40	0.85	0.60	0.48	0.430	
				BUR	0.729	0.52	0.40	0.35	0.79	0.55	0.44	0.389	
			Welds	EPDM	0.816	0.57	0.46	0.40	0.88	0.62	0.50	0.445	
				BUR	0.729	0.52	0.40	0.34	0.82	0.58	0.46	0.412	
		ABSCE	Screws	EPDM	0.810	0.57	0.46	0.40	0.82	0.58	0.47	0.416	
				BUR	0.725	0.52	0.40	0.35	0.74	0.52	0.41	0.364	
	B	SBCCI	Screws	EPDM	0.778	0.53	0.43	0.38	0.81	0.56	0.46	0.409	
				BUR	0.682	0.46	0.36	0.32	0.74	0.51	0.41	0.365	
			Welds	EPDM	0.775	0.53	0.43	0.38	0.83	0.57	0.47	0.424	
				BUR	0.679	0.46	0.36	0.32	0.78	0.54	0.43	0.387	
		ABSCE	Screws	EPDM	0.772	0.53	0.43	0.38	0.79	0.54	0.44	0.395	
				BUR	0.677	0.46	0.36	0.32	0.70	0.48	0.38	0.336	
	C	SBCCI	Screws	EPDM	0.747	0.49	0.40	0.36	0.78	0.52	0.43	0.393	
				BUR	0.643	0.41	0.33	0.29	0.71	0.46	0.38	0.343	
			Welds	EPDM	0.746	0.49	0.40	0.36	0.80	0.54	0.44	0.404	
				BUR	0.641	0.41	0.33	0.29	0.74	0.49	0.40	0.366	
					EPDM	0.748	0.49	0.40	0.36	0.75	0.50	0.41	0.373

Building Characteristics					No Reduction in Metal Deck Capacity				50% Reduction in Metal Deck Capacity					
					Terrain Surface Roughness (m)*				Terrain Surface Roughness (m)*					
Wall Type	Missile Environ	Design Code	Metal Deck Attach.	Roof Cover	0.03	0.35	0.70	1.0	0.03	0.35	0.70	1.0		
	D	ABSCE	Screws	BUR	0.642	0.41	0.33	0.29	0.66	0.43	0.34	0.313		
			Welds	EPDM	0.747	0.49	0.40	0.36	0.75	0.49	0.41	0.371		
		SBCCI	Screws	EPDM	0.746	0.47	0.39	0.36	0.78	0.50	0.42	0.389		
				BUR	0.635	0.39	0.32	0.28	0.70	0.44	0.37	0.335		
			Welds	EPDM	0.744	0.47	0.39	0.35	0.79	0.52	0.44	0.401		
				BUR	0.636	0.39	0.32	0.28	0.74	0.47	0.39	0.359		
		ABSCE	Screws	EPDM	0.744	0.47	0.39	0.36	0.75	0.48	0.40	0.367		
				BUR	0.634	0.39	0.32	0.28	0.65	0.40	0.33	0.302		
			Welds	EPDM	0.740	0.47	0.39	0.36	0.74	0.48	0.40	0.369		
				BUR	0.637	0.39	0.32	0.28	0.65	0.40	0.33	0.295		
		Reinfor. Masonry	A	SBCCI	Screws	EPDM	0.738	0.55	0.44	0.39	0.81	0.58	0.47	0.418
						BUR	0.638	0.49	0.38	0.33	0.74	0.54	0.43	0.379
	Welds				EPDM	0.737	0.55	0.44	0.39	0.84	0.60	0.49	0.437	
					BUR	0.644	0.49	0.38	0.33	0.79	0.56	0.45	0.402	
	ABSCE			Screws	EPDM	0.740	0.55	0.44	0.39	0.77	0.56	0.45	0.404	
					BUR	0.640	0.49	0.38	0.33	0.69	0.51	0.40	0.350	
				Welds	EPDM	0.738	0.55	0.44	0.39	0.78	0.56	0.45	0.402	
					BUR	0.642	0.48	0.38	0.33	0.69	0.50	0.40	0.348	
B	SBCCI			Screws	EPDM	0.707	0.51	0.41	0.37	0.77	0.54	0.44	0.399	
					BUR	0.603	0.43	0.34	0.30	0.70	0.49	0.40	0.353	
				Welds	EPDM	0.706	0.50	0.41	0.37	0.80	0.56	0.46	0.413	
					BUR	0.602	0.43	0.34	0.30	0.75	0.52	0.42	0.379	
	ABSCE		Screws	EPDM	0.708	0.50	0.41	0.37	0.74	0.52	0.42	0.382		
				BUR	0.604	0.43	0.34	0.30	0.64	0.45	0.36	0.323		
C	SBCCI		Screws	EPDM	0.679	0.46	0.38	0.34	0.74	0.50	0.41	0.380		
				BUR	0.564	0.37	0.30	0.27	0.67	0.44	0.36	0.330		
			Welds	EPDM	0.678	0.46	0.38	0.34	0.77	0.52	0.43	0.398		
				BUR	0.560	0.37	0.30	0.27	0.71	0.48	0.39	0.358		
	ABSCE	Screws	EPDM	0.674	0.46	0.38	0.34	0.71	0.48	0.40	0.362			
			BUR	0.564	0.37	0.30	0.27	0.61	0.40	0.33	0.294			

Building Characteristics					No Reduction in Metal Deck Capacity				50% Reduction in Metal Deck Capacity			
					Terrain Surface Roughness (m)*				Terrain Surface Roughness (m)*			
Wall Type	Missile Environ	Design Code	Metal Deck Attach.	Roof Cover	0.03	0.35	0.70	1.0	0.03	0.35	0.70	1.0
	D	SBCCI	Welds	EPDM	0.675	0.45	0.38	0.34	0.71	0.48	0.40	0.361
				BUR	0.563	0.37	0.30	0.27	0.61	0.40	0.33	0.294
			Screws	EPDM	0.679	0.44	0.37	0.34	0.74	0.49	0.41	0.375
				BUR	0.559	0.35	0.29	0.26	0.66	0.42	0.35	0.325
			Welds	EPDM	0.676	0.44	0.37	0.34	0.76	0.51	0.43	0.390
				BUR	0.560	0.35	0.29	0.26	0.70	0.46	0.38	0.348
		ABSCE	Screws	EPDM	0.676	0.44	0.37	0.34	0.70	0.46	0.39	0.356
				BUR	0.562	0.35	0.29	0.26	0.60	0.38	0.31	0.289
			Welds	EPDM	0.678	0.44	0.37	0.34	0.70	0.46	0.39	0.358
				BUR	0.556	0.357	0.296	0.267	0.607	0.380	0.318	0.285

*Values in table represent the damage state probabilities (%). Damage state descriptions are described in Table 5-61.

Table 5-70 Average Damage States for Building D - Twenty Foot High Strip Mall Building with One Unit and Metal Deck with Six Foot Joist Spacing

° Building Characteristics					No Reduction in Metal Deck Capacity				50% Reduction in Metal Deck Capacity			
					Terrain Surface Roughness (m)				Terrain Surface Roughness (m)			
Wall Type	Missile Environ.	Design Code	Metal Deck Attach.	Roof Cover	0.03	0.35	0.70	1.0	0.03	0.35	0.70	1.0
Unreinfor. Masonry	A	SBCCI	Screws	EPDM	0.829	0.583	0.468	0.410	0.876	0.612	0.495	0.435
				BUR	0.744	0.521	0.411	0.354	0.813	0.569	0.450	0.395
			Welds	EPDM	0.832	0.583	0.467	0.409	0.896	0.628	0.508	0.453
				BUR	0.746	0.522	0.408	0.353	0.851	0.594	0.473	0.417
		ABSCE	Screws	EPDM	0.831	0.581	0.469	0.412	0.845	0.592	0.474	0.418
				BUR	0.746	0.524	0.408	0.355	0.771	0.540	0.421	0.368
			Welds	EPDM	0.828	0.583	0.466	0.409	0.844	0.587	0.472	0.416
				BUR	0.743	0.521	0.410	0.352	0.765	0.533	0.419	0.364
	B	SBCCI	Screws	EPDM	0.792	0.542	0.436	0.392	0.832	0.572	0.466	0.415
				BUR	0.700	0.472	0.375	0.327	0.766	0.525	0.420	0.372
			Welds	EPDM	0.791	0.542	0.437	0.391	0.856	0.588	0.482	0.428
				BUR	0.701	0.472	0.374	0.329	0.807	0.545	0.442	0.391
		ABSCE	Screws	EPDM	0.796	0.538	0.436	0.388	0.806	0.548	0.447	0.398

° Building Characteristics					No Reduction in Metal Deck Capacity				50% Reduction in Metal Deck Capacity							
					Terrain Surface Roughness (m)				Terrain Surface Roughness (m)							
Wall Type	Missile Environ.	Design Code	Metal Deck Attach.	Roof Cover	0.03	0.35	0.70	1.0	0.03	0.35	0.70	1.0				
				BUR	0.697	0.472	0.375	0.328	0.722	0.490	0.390	0.342				
				Welds	EPDM	0.788	0.542	0.438	0.387	0.807	0.546	0.445	0.397			
			C	SBCCI	Screws	EPDM	0.763	0.500	0.416	0.372	0.805	0.532	0.442	0.397		
						BUR	0.666	0.422	0.341	0.305	0.729	0.476	0.391	0.350		
					Welds	EPDM	0.764	0.501	0.411	0.370	0.817	0.554	0.455	0.414		
						BUR	0.662	0.422	0.345	0.299	0.765	0.506	0.413	0.374		
				ABSCE	Screws	EPDM	0.763	0.499	0.413	0.374	0.775	0.511	0.423	0.378		
						BUR	0.661	0.419	0.342	0.303	0.684	0.441	0.356	0.317		
					Welds	EPDM	0.762	0.498	0.415	0.370	0.771	0.507	0.422	0.379		
						BUR	0.661	0.420	0.340	0.303	0.681	0.434	0.355	0.318		
			D	SBCCI	Screws	EPDM	0.763	0.488	0.405	0.370	0.798	0.515	0.433	0.391		
						BUR	0.656	0.403	0.330	0.298	0.722	0.458	0.377	0.342		
					Welds	EPDM	0.760	0.487	0.408	0.370	0.818	0.532	0.446	0.401		
						BUR	0.655	0.400	0.329	0.298	0.755	0.482	0.403	0.363		
					ABSCE	Screws	EPDM	0.764	0.484	0.409	0.367	0.773	0.495	0.413	0.372	
							BUR	0.660	0.398	0.330	0.295	0.674	0.416	0.343	0.307	
				Welds		EPDM	0.762	0.486	0.407	0.369	0.766	0.491	0.411	0.372		
						BUR	0.655	0.399	0.329	0.296	0.670	0.414	0.341	0.303		
				Reinfor. Masonry	A	SBCCI	Screws	EPDM	0.757	0.563	0.452	0.399	0.827	0.598	0.480	0.426
								BUR	0.660	0.499	0.389	0.340	0.760	0.550	0.438	0.384
Welds	EPDM	0.752					0.560	0.452	0.394	0.865	0.615	0.499	0.442			
	BUR	0.660					0.499	0.388	0.337	0.812	0.580	0.464	0.405			
ABSCE	Screws	EPDM	0.752			0.562	0.448	0.397	0.788	0.572	0.460	0.404				
		BUR	0.658			0.499	0.386	0.336	0.707	0.518	0.406	0.355				
	Welds	EPDM	0.752			0.560	0.448	0.395	0.798	0.571	0.456	0.405				
		BUR	0.657			0.502	0.388	0.337	0.714	0.516	0.403	0.349				
B	SBCCI	Screws	EPDM			0.722	0.519	0.419	0.374	0.789	0.550	0.454	0.407			
			BUR			0.622	0.443	0.354	0.310	0.720	0.503	0.406	0.361			
		Welds	EPDM			0.726	0.515	0.421	0.375	0.824	0.573	0.470	0.422			
			BUR			0.622	0.443	0.352	0.307	0.768	0.532	0.432	0.382			
	ABSCE	Screws	EPDM		0.721	0.519	0.420	0.376	0.752	0.529	0.432	0.389				
			BUR		0.620	0.443	0.349	0.310	0.669	0.465	0.372	0.327				

° Building Characteristics					No Reduction in Metal Deck Capacity				50% Reduction in Metal Deck Capacity					
					Terrain Surface Roughness (m)				Terrain Surface Roughness (m)					
Wall Type	Missile Environ.	Design Code	Metal Deck Attach.	Roof Cover	0.03	0.35	0.70	1.0	0.03	0.35	0.70	1.0		
			Welds	EPDM	0.722	0.517	0.414	0.371	0.764	0.530	0.433	0.387		
				BUR	0.617	0.445	0.350	0.309	0.669	0.465	0.372	0.328		
			C	SBCCI	Screws	EPDM	0.694	0.468	0.392	0.350	0.758	0.512	0.428	0.384
						BUR	0.584	0.381	0.314	0.282	0.685	0.455	0.374	0.339
					Welds	EPDM	0.694	0.467	0.391	0.350	0.794	0.536	0.447	0.402
						BUR	0.583	0.386	0.314	0.280	0.729	0.488	0.406	0.364
			ABSCE		Screws	EPDM	0.694	0.467	0.388	0.353	0.730	0.489	0.405	0.366
						BUR	0.585	0.383	0.312	0.279	0.631	0.414	0.339	0.302
					Welds	EPDM	0.691	0.468	0.388	0.350	0.735	0.490	0.406	0.366
						BUR	0.579	0.384	0.313	0.279	0.632	0.416	0.340	0.302
			D	SBCCI	Screws	EPDM	0.696	0.457	0.385	0.349	0.754	0.497	0.415	0.378
						BUR	0.582	0.367	0.306	0.275	0.673	0.434	0.362	0.325
					Welds	EPDM	0.698	0.456	0.385	0.348	0.779	0.517	0.436	0.391
						BUR	0.585	0.367	0.306	0.273	0.716	0.469	0.394	0.355
				ABSCE	Screws	EPDM	0.691	0.458	0.384	0.348	0.722	0.474	0.399	0.360
						BUR	0.576	0.365	0.304	0.274	0.621	0.393	0.328	0.294
Welds	EPDM	0.691			0.455	0.382	0.349	0.727	0.474	0.398	0.359			
	BUR	0.574			0.365	0.305	0.274	0.621	0.390	0.324	0.290			

*Values in table represent the damage state probabilities (%). Damage state descriptions are described in Table 5-61.

Table 5-71 Percent Increases in the Per Storm Average Building Damage State due to Changes in Building Parameters (Minimum/Average/Maximum) - Strip Mall Building with Wood Roof System

Building Parameter	Building Designation					
	Building A			Building B		
	Min	Avg	Max	Min	Avg	Max
8d to 6d Roof Deck Nails	0%	4%	15%	-1%	3%	9%
Strap to Toe-Nail Roof/Wall Connections	4%	12%	29%	4%	12%	24%
Built-up to Single ply Membrane Roof Cover	4%	13%	32%	7%	15%	28%
Reinforced to Unreinforced Masonry Walls	-2%	1%	3%	1%	4%	10%
Missile Environment D to C	2%	16%	38%	0%	4%	12%
Missile Environment C to B	10%	22%	27%	4%	9%	15%
Missile Environment B to A	9%	18%	24%	5%	9%	15%

Table 5-72 Percent Increases in the Per Storm Average Building Damage State due to Changes in Building Parameters (Minimum/Average/Maximum) - Strip Mall Building with Steel Roof System

Building Parameter	Building Designation											
	Building A			Building B			Building C			Building D		
	Min	Avg	Max	Min	Avg	Max	Min	Avg	Max	Min	Avg	Max
0% to 50% Reduction in Metal Roof Deck Resistance	-2%	0%	2%	-1%	0%	1%	1%	9%	31%	1%	9%	30%
Screwed to Welded Metal Roof Deck	-2%	0%	2%	-2%	0%	1%	-2%	1%	9%	-2%	1%	9%
ASCE to SBCCI Metal Roof Deck Design Criteria	-2%	0%	2%	-2%	0%	2%	-1%	5%	22%	-1%	5%	23%
Built-up to Single ply Membrane Roof Cover	6%	18%	34%	11%	20%	30%	6%	17%	29%	5%	16%	27%
Reinforced to Unreinforced Masonry Walls	-2%	1%	4%	3%	8%	14%	1%	6%	15%	1%	6%	15%
Missile Environment D to C	1%	11%	24%	-1%	2%	5%	-1%	2%	6%	-1%	2%	7%
Missile Environment C to B	11%	27%	40%	4%	9%	18%	3%	8%	17%	3%	7%	16%

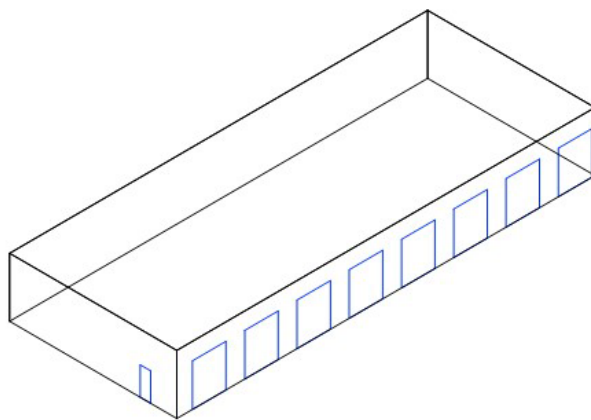
Building Parameter	Building Designation											
	Building A			Building B			Building C			Building D		
	Min	Avg	Max	Min	Avg	Max	Min	Avg	Max	Min	Avg	Max
Missile Environment B to A	9%	19%	26%	3%	8%	14%	4%	8%	14%	4%	7%	13%

Table 5-73 Percent Increases in the Per Storm Average Building Damage State Due to Changes in Building Configuration (Minimum/Average/Maximum)

Building Configuration	Increase in Average Annual Building Loss		
	Min	Avg	Max
Building A to B – Wood Roof System (12’ to 20’ Roof Height)	26%	67%	125%
Building A to B – Steel Roof System (12’ to 20’ Roof Height)	25%	69%	126%
Building B to C – Steel Roof System (4’ to 6’ Joist Spacing)	-1%	5%	31%
Building C to D – Steel Roof System (6 Units to 1 Unit)	-1%	2%	4%

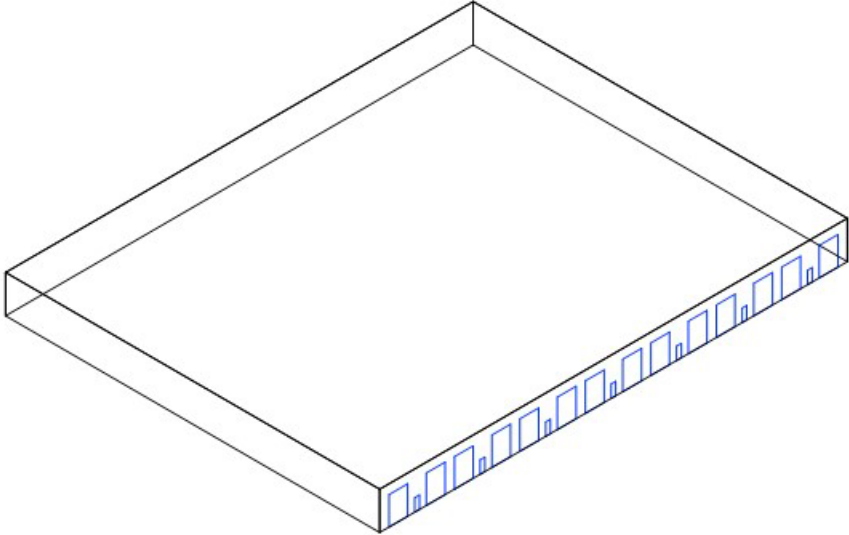
5.6.5 Pre-Engineered Metal Buildings

Three metal buildings were modeled as shown in Figure 5-138, Figure 5-139, and Figure 5-140. The building damage states associated with the metal buildings are defined in Table 5-74. Note that no frame failures are modeled, with the entire performance of the building governed by the performance of the cladding and the fenestrations. The degrees of roof sheathing damage required to move the building from one damage state to another are similar to those used for the residential buildings. The fenestration damage requirements are less stringent than those used in the case of residential buildings, where here, 75% of the fenestrations must fail to enter damage state four, versus only 50% in the residential building case. The resistance parameters are given for all components in Table 5-75.



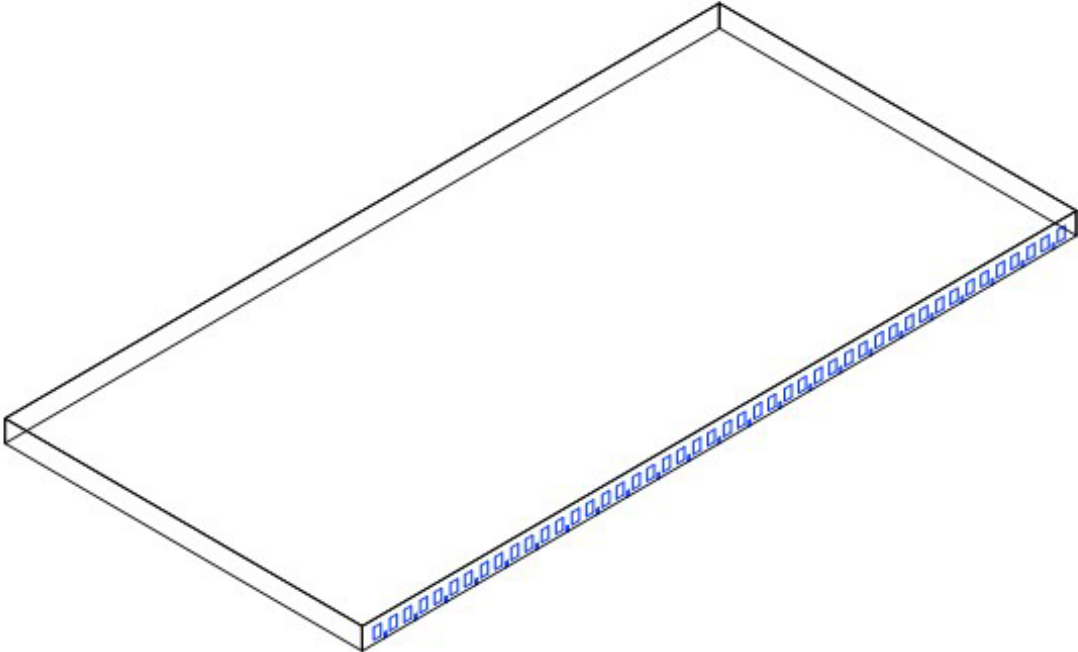
Small Metal Building, L = 100', W = 40', H = 14'

Figure 5-138 Geometries of Small Metal Buildings Used in Study



Medium Metal Building, L = 250', W = 200', H = 25'

Figure 5-139 Geometries of Medium Metal Buildings Used in Study



Large Metal Building, L = 1000', W = 500', H = 30'

Figure 5-140 Geometries of Large Metal Buildings Used in Study

Table 5-74 Damage States Metal Buildings

Damage State	Qualitative Damage Description	Entry/Over-head Door Failures	Metal Roof Deck Failures	Metal Wall Siding Failures	Missile Impacts on Walls
0	<u>No Damage or Very Minor Damage</u> Little or no visible damage from the outside. No broken windows, or failed roof deck. None or very limited water penetration.	No	No	No	No
1	<u>Minor Damage</u> Maximum of one broken window or, door or wall panel. Marks or dents on walls requiring painting or patching for repair.	One door*	No	One panel*	Typically <5 impacts
2	<u>Moderate Damage</u> Moderate fenestration failures. Minor roof panel failures, or wall panel failures. Some resulting damage to interior of building from water.	>One to ≤33%*	One to two panels*	>One to ≤15%*	Typically 5 to 10 impacts
3	<u>Severe Damage</u> Major window damage or roof sheathing loss. Extensive damage to the interior from water. Some frame damage likely.	>33% to ≤75%*	>2 to ≤10%*	>15% to ≤33%*	Typically 10 to 20 impacts
4	<u>Destruction</u> Significant failures of fenestrations, significant roof and wall panel failures. Significant frame damage likely.	>75%*	>10%*	>33%*	Typically >20 impacts

* If any one of the conditions in the shaded cells with an asterisk (*) of a given row is true, the building is placed in that damage state)

Table 5-75 Component Resistances for Pre-Engineered Metal Buildings

Component	Distribution	Distribution Parameters
Metal Roof Deck - 100mph Design Speed - Corner	Normal	Mean = 151 psf COV = 0.11
Metal Roof Deck - 100mph Design Speed - Edge	Normal	Mean = 89 psf COV = 0.11
Metal Roof Deck - 100mph Design Speed - Field	Normal	Mean = 89 psf COV = 0.11

Component	Distribution	Distribution Parameters
Metal Roof Deck - 90 mph Design Speed - Corner	Normal	Mean = 104 psf COV = 0.11
Metal Roof Deck - 90 mph Design Speed - Edge	Normal	Mean = 89 psf COV = 0.11
Metal Roof Deck - 90 mph Design Speed - Field	Normal	Mean = 89 psf COV = 0.11
Metal Wall Cladding	Normal	Mean = 84 psf COV = 0.09
Overhead Roll-Up Doors	Normal	Mean = 15 psf COV = 0.2
Entry Door Pressure	Normal	Mean = 50 psf COV = 0.2

Two analyses were performed for each building, one with the resistance of the metal cladding modeled as given in Table 5-75, and the second analysis with the resistance of the metal components reduced by 50%, to account for aging and fatigue.

For more information on example building and component damage state plots, please contact the Hazus Help Desk (see Section 1.5) for the *Hazus Hurricane Model Technical Manual Appendices* (FEMA, 2021). The results presented in the appendices indicate that the performance of the model buildings is governed by the performance of the fenestrations. This is particularly evident in the case of the large metal building, which has more doors than either the small or medium-sized building. The failure sequence of the doors is such that more than one door often fails during the storm, and there is consequently little distinction between Damage States 1, 2, and 3. In the examples presented herein, the weak overhead doors (modeled as having a mean failure capacity of 15 psf) represent the first mode of failure. The wall cladding failures are infrequent compared to field observations, suggesting the modeled wall capacity may be too high.

The average per storm damage states are summarized in Table 5-76. The impact of changing the various building parameters is summarized in Table 5-77. The results indicate that the size of the building has a significant impact on the average per storm damage state. On average, the per storm average damage states increased by 20% for the medium-sized building versus the small building and 57% for the large building versus the medium-sized building. Note that the size effect is coupled with the effect of the increased number of overhead doors associated with the larger buildings. Metal roof decks that have experienced age and fatigue (modeled with a 50% reduction in the uplift capacity) were found to have average per storm damage states 6% to 53% higher than new metal roof decks with all else being the same. Of the building parameters considered, the roof design code was found to have the smallest impact on building damage (see Table 5-77).

Table 5-76 Average Per Storm Damage States for Pre-Engineered Metal Buildings

Building Characteristics		No Reduction in Metal Panel Capacity*				50% Reduction in Metal Panel Capacity*			
		Terrain Surface Roughness (m)				Terrain Surface Roughness (m)			
Design Speed	Plan Size	0.03	0.35	0.70	1.0	0.03	0.35	0.70	1.0
90 mph	Small	0.765	0.382	0.287	0.245	0.843	0.450	0.350	0.305
	Med.	0.763	0.427	0.332	0.291	0.964	0.607	0.497	0.446
	Large	1.087	0.709	0.588	0.525	1.232	0.835	0.710	0.647
100 mph	Small	0.765	0.385	0.289	0.245	0.813	0.433	0.335	0.287
	Med.	0.761	0.424	0.332	0.289	0.890	0.534	0.433	0.386
	Large	1.086	0.704	0.588	0.526	1.225	0.827	0.698	0.638

* Values in table represent the damage state probabilities (%). Damage state descriptions are described in Table 5-74.

Table 5-77 Percent Increases in the Per Storm Average Building Damage State Due to Changes in Building Parameters (Minimum/Average/Maximum) - Pre-Engineered Metal Buildings

Parameter	Change in Average Per Storm Damage		
	Min	Avg	Max
Small to Medium-sized Building	-1%	20%	46%
Medium-sized to Large Building	28%	57%	82%
100 mph to 90 mph Roof Design Code	-1%	3%	16%
0% to 50% Reduction in Metal Deck Capacity (i.e., Age and Fatigue)	6%	23%	53%

5.6.6 Engineered Residential and Commercial Buildings

The fully engineered buildings being considered have a structural system comprised of either concrete or steel. In the case of the concrete buildings, it has been assumed that the roof slab is a poured concrete slab that cannot be penetrated by water if the roof cover fails. Thus, in the case of concrete buildings, the damage state of the building is driven entirely by the performance of the windows. The damage state definitions proposed for the steel buildings are given in Table 5-78.

The steel buildings are modeled as having an open web steel joist roof system with a metal deck welded to the joists. The uplift capacities of the metal roof panels are estimated based on the ASCE design code for a 100 mph fastest mile design speed (see Section 5.4.10). The roof cover is modeled as either a good quality single ply membrane or a good quality built-up roof. The prime variables being altered for the engineered buildings are the fraction of the walls covered by glass (nominally 20%, 33%, and 50%) and the number of stories (two, five, and eight). The building models are shown in Figure 5-141, Figure 5-142, and Figure 5-143. The environmental variables considered in the analysis are missile source environment and terrain exposure. The four missile environments used for the strip-mall study (see Table 5-64) are used again here for the engineered-building study. The four terrain environments considered are open (zo

= 0.03 meters), suburban ($z_0 = 0.35$ meters), lightly treed suburban ($z_0 = 0.7$ meters), and heavily treed suburban ($z_0 = 1.0$ meters).

Table 5-78 Damage State Definitions for Engineered Steel Buildings

Damage State	Qualitative Damage Description	Roof Cover Failure	Window / Door Failures	Roof Deck Failure	Missile Impacts on Walls	Joist Failures
0	<u>No Damage or Very Minor Damage</u> Little or no visible damage from the outside. No broken windows, or failed roof deck. Minimal loss of roof cover, with no or very limited water penetration.	≤2%	No	No	No	No
1	<u>Minor Damage</u> Maximum of one broken window or door. Moderate roof cover loss that can be covered to prevent additional water entering the building. Marks or dents on walls requiring painting or patching for repair.	>2% to ≤15%*	One window or door*	No	Typically <5 impacts	No
2	<u>Moderate Damage</u> Major roof cover damage, moderate window breakage. Minor roof deck failure. Some resulting damage to interior of building from water.	>15% to ≤50%*	>One to ≤2%*	One or two panels*	Typically 5 to 10 impacts	No
3	<u>Severe Damage</u> Major window damage or roof sheathing loss. Major roof cover loss. Extensive damage to interior from water. Limited, local joist failures.	>50%*	>2% to ≤25%*	>Two to ≤25%*	Typically 10 to 20 impacts	One Joist to ≤25%*
4	<u>Destruction</u> Essentially complete roof failure and/or of more than 25% of roof sheathing. Significant amount of the wall envelope opened through windows failure. Extensive damage to interior	Typically >50%	>25%*	>25%*	Typically >20 impacts	>25%*

* If any one of the conditions in the shaded cells with an asterisk (*) of a given row is true, the building is placed in that damage state)

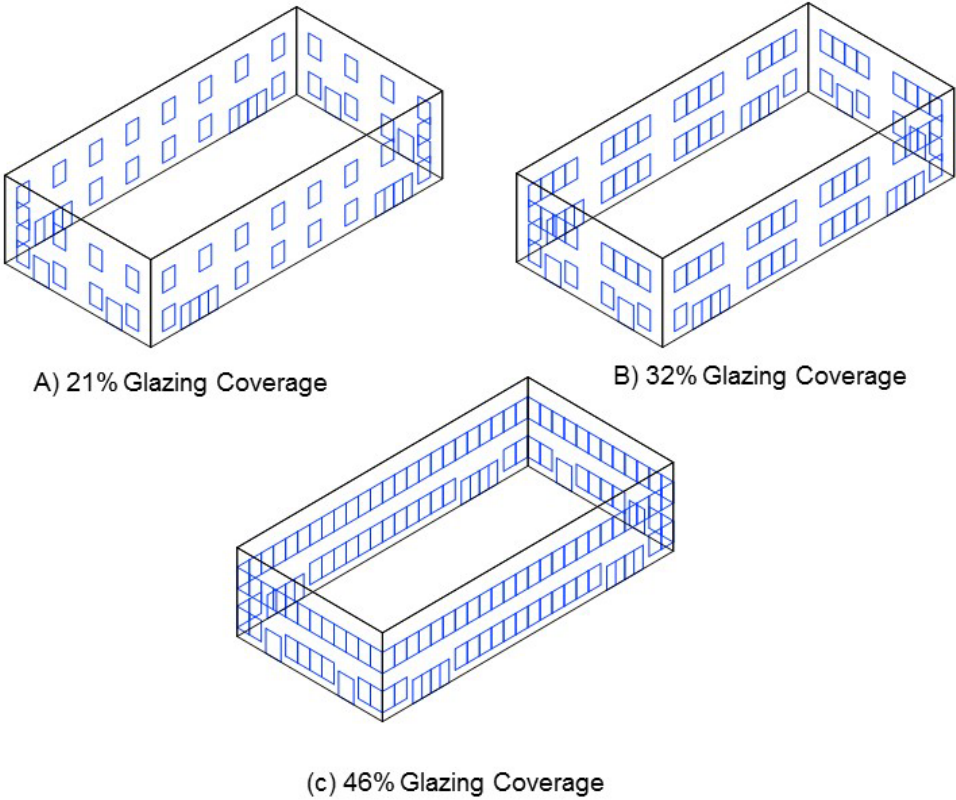


Figure 5-141 Modeled Two-Story Fully-Engineered Buildings

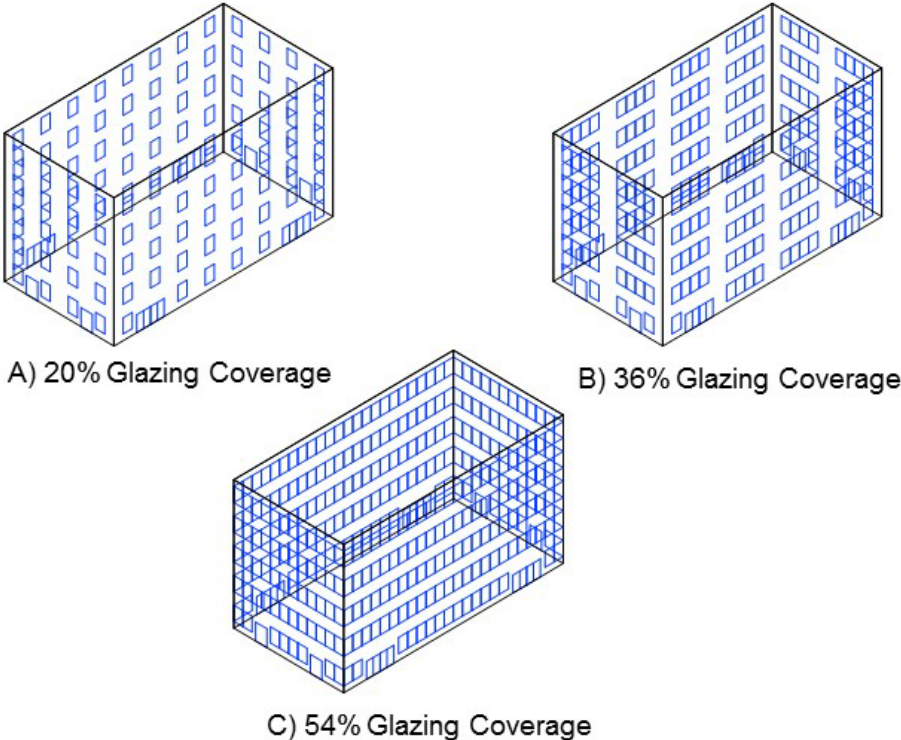


Figure 5-142 Modeled Five-Story Fully-Engineered Buildings.

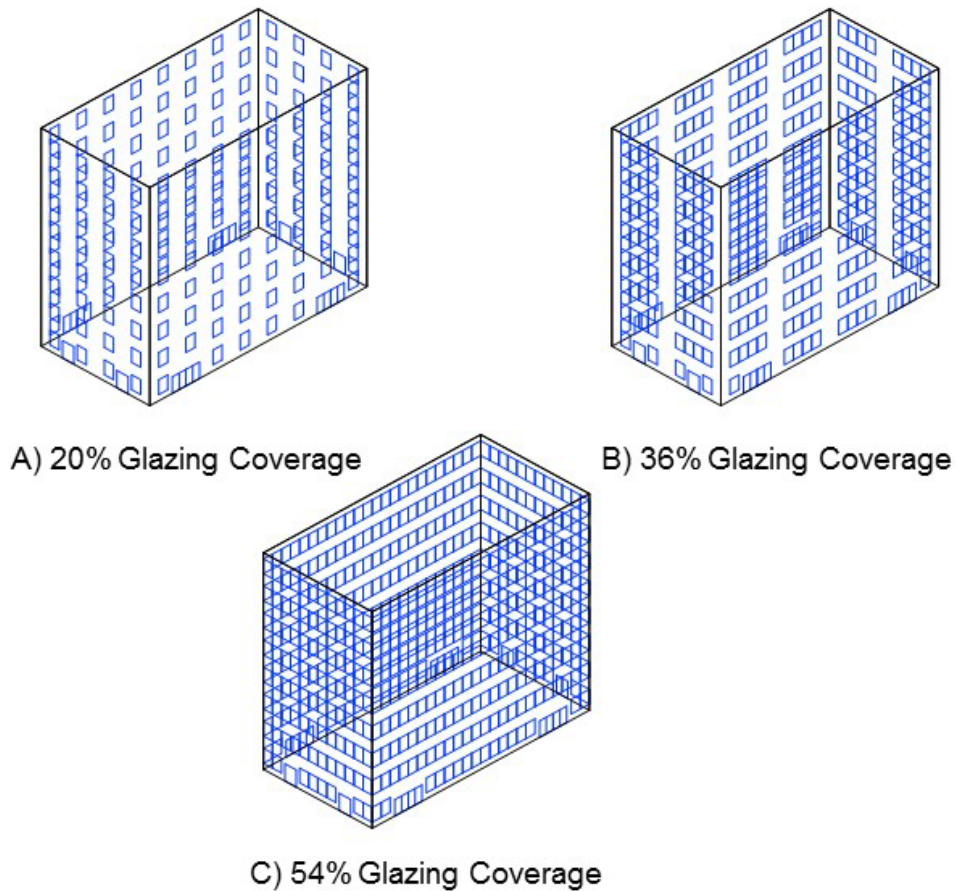


Figure 5-143 Modeled Eight-Story Fully-Engineered Buildings

The residential buildings have eight separate units per floor and the commercial buildings have a single unit per floor. The internal pressure associated with glass breakage is confined to the unit in which the window damage occurs. That is, it is assumed that no air leakage occurs between the adjacent units on the same floor and that no air leakage occurs between the adjacent units on different floors.

All glass is modeled as single pane (non-insulated) tempered glass. The window frame system is modeled with a mean failure pressure of 75 psf and a coefficient of variation of 20%. The metal deck failure pressures are modeled with normal distributions. The distribution parameters are listed in Table 5-79.

The damage simulation results show that building performance is strongly driven by the performance of the roof cover. Recalling that the single-ply membrane and the built-up roof cover models were developed using limited empirical data, it appears that the damage results given here overestimate the failure rates for these roof covers. To obtain a better understanding of the effect of the other parameters (window area, missile environment, number of units per floor, etc.) on the average per storm damage states, the effect of the roof cover damage was removed from the building damage state definitions, and the damage analysis was re-run. Damage state results have been presented, either including or excluding the roof cover effect on the overall damage state.

To make the damage state definitions with respect to roof damage (i.e., roof cover, roof deck, and roof joists) consistent between the buildings with a different number of stories, the threshold damage levels defining the damage states are modified by a factor which is a function of the number of stories. The concept is that 5% roof deck damage, for example, will have a greater effect in terms of economic losses on a one-story building compared to a two-story building. That is, in the case of the two-story building, only the top floor will experience similar damage due to the water infiltration associated with 5% roof deck loss to that experienced by the single-story building. The assumption made here for the purpose of the roof damage state definitions is that the intensity of damage on the bottom floor of the two-story building will be half as much as that on the top floor. Thus, if the damage intensity to the interior of the single-story building is arbitrarily set to one, then the damage intensity to the two-story building will be $(1+0.5)/2 = 0.75$ (i.e., One represents the damage intensity of the top floor and 0.5 represents the damage intensity of the bottom floor). Therefore, to achieve a similar damage intensity to that associated with 5% roof deck damage on a single-story building, an otherwise similar two-story building would require 6.7% roof deck damage (i.e., $5\%/0.75$). The thresholds used to define the roof damage states listed in Table 5-83 were modified in the same manner as described above for the two-, five-, and eight-story buildings. The multiplicative factors are 1.33, 2.58, and 4.02, respectively. It can be seen, for example, that the five- and eight story building cannot achieve a building Damage State 3 (i.e., severe damage) based on roof cover loss since the 50% threshold increases to more than 100% in both cases. Also note that the two-story building will be placed in Damage State 3 when the roof cover loss exceeds 67%.

For more information on example building and component damage state plot, please contact the Hazus Help Desk (see Section 1.5) for *Hazus Hurricane Model Technical Manual Appendices (FEMA, 2021)*. Table 5-80,

Table 5-81, and Table 5-82 list the average per storm damage states for the two, five, and eight-story buildings, respectively. A summary of the effects of the various parameters on the average per storm damage states is given in Table 5-82. The average per storm damage states presented in Table 5-80 and Table 5-81 were computed with the roof cover damage criteria included and excluded. As noted above, the roof cover was found to govern the overall building damage state in many of the cases and thus, to better examine the effects of the other variables, both sets of damage states have been given.

The average per storm damage states are found to increase by up to 33% when the roof cover is modeled with an EPDM single ply membrane versus a built-up roof cover. The effect of having a single unit per floor (commercial usage) compared to multi-units per floor (residential usage) is at most an 8% increase in the mean per storm damage state.

Table 5-79 Failure Pressure Models for Metal Deck on Steel Joists

Number of Stories	Mean Failure Pressure (Standard Deviation), psf			
	ACSE Design, 100 mph Wind Speed Zone, Welded Deck			
	Roof Zone 1	Roof Zone 2	Roof Zone 3	Roof Zone 4*
2	91 (17)	145 (27)	155 (29)	-
5	123 (23)	155 (29)	214 (41)	-
8	145 (27)	155 (29)	214 (41)	285 (45)

* Roof Zone 4 only applicable for buildings more than 60' high

The average per storm damage states increased by as much as 13% when the glazing coverage changed from 20% to 33% and by as much as 18% when the glazing coverage changed from 33% to 50%. The impact of the missile environment on building damage states is more pronounced on the two-story buildings than it is on either the five or eight-story buildings. This trend results from the fact that the modeled average heights of the buildings from which the commercial and residential type missiles originate are lower than the five and eight-story engineered buildings. Thus, the glazing on the upper floors of the five and eight-story buildings are less susceptible to missile damage than the glazing on the lower floors.

Table 5-80 Average Building Damage States – Two-Story Engineered Building

Building Characteristics				Residential Buildings (8 Units per Floor)*				Commercial Buildings (1 Unit per Floor)*			
				Terrain Surface Roughness (m)				Terrain Surface Roughness (m)			
Roof Cover Effect	Missile Environ.	Glazing Coverage	Roof Cover	0.03	0.35	0.70	1.0	0.03	0.35	0.70	1.0
Included	A	20%	EPDM	0.607	0.542	0.393	0.322	0.610	0.541	0.392	0.322
			BUR	0.629	0.548	0.403	0.335	0.629	0.547	0.401	0.334
		33%	EPDM	0.684	0.593	0.433	0.356	0.684	0.593	0.434	0.356
			BUR	0.699	0.598	0.439	0.365	0.695	0.598	0.439	0.364
		50%	EPDM	0.769	0.663	0.484	0.397	0.768	0.664	0.485	0.396
			BUR	0.776	0.667	0.488	0.403	0.774	0.669	0.489	0.405
	B	20%	EPDM	0.470	0.415	0.303	0.252	0.476	0.413	0.304	0.250
			BUR	0.512	0.433	0.322	0.272	0.516	0.435	0.325	0.272
		33%	EPDM	0.525	0.458	0.333	0.277	0.529	0.455	0.333	0.275
			BUR	0.557	0.472	0.351	0.291	0.560	0.468	0.351	0.293
		50%	EPDM	0.595	0.510	0.370	0.305	0.597	0.512	0.373	0.308
			BUR	0.620	0.520	0.387	0.323	0.624	0.521	0.387	0.323
C	20%	EPDM	0.364	0.312	0.231	0.194	0.373	0.312	0.232	0.192	
		BUR	0.422	0.339	0.260	0.223	0.430	0.339	0.260	0.222	
	33%	EPDM	0.400	0.346	0.254	0.213	0.409	0.349	0.255	0.211	
		BUR	0.448	0.371	0.281	0.237	0.457	0.368	0.279	0.239	

Building Characteristics				Residential Buildings (8 Units per Floor)*				Commercial Buildings (1 Unit per Floor)*				
				Terrain Surface Roughness (m)				Terrain Surface Roughness (m)				
Roof Cover Effect	Missile Environ.	Glazing Coverage	Roof Cover	0.03	0.35	0.70	1.0	0.03	0.35	0.70	1.0	
	D	50%	EPDM	0.450	0.386	0.284	0.233	0.456	0.388	0.282	0.235	
			BUR	0.487	0.403	0.304	0.256	0.492	0.405	0.303	0.258	
		20%	EPDM	0.279	0.181	0.152	0.137	0.284	0.182	0.153	0.138	
			BUR	0.356	0.238	0.202	0.182	0.360	0.238	0.201	0.184	
		33%	EPDM	0.279	0.182	0.153	0.138	0.286	0.185	0.153	0.139	
			BUR	0.359	0.237	0.202	0.183	0.362	0.242	0.203	0.185	
	50%	EPDM	0.291	0.187	0.158	0.143	0.305	0.196	0.161	0.147		
		BUR	0.363	0.243	0.204	0.184	0.376	0.249	0.208	0.189		
	Exclude	A	20%	N/A	0.580	0.530	0.378	0.305	0.584	0.529	0.377	0.304
			33%		0.665	0.583	0.419	0.340	0.666	0.583	0.420	0.341
			50%		0.755	0.654	0.473	0.384	0.754	0.655	0.474	0.383
		B	20%	N/A	0.409	0.390	0.272	0.217	0.419	0.387	0.275	0.217
33%			0.479		0.437	0.308	0.248	0.484	0.434	0.307	0.247	
50%			0.562		0.493	0.350	0.282	0.565	0.495	0.352	0.285	
C		20%	N/A	0.270	0.272	0.184	0.144	0.285	0.273	0.188	0.144	
		33%		0.326	0.315	0.217	0.171	0.339	0.317	0.217	0.171	
		50%		0.397	0.361	0.254	0.200	0.403	0.364	0.254	0.203	
D		20%	N/A	0.092	0.041	0.030	0.025	0.098	0.042	0.031	0.025	
		33%		0.096	0.041	0.030	0.025	0.104	0.043	0.032	0.026	
		50%		0.145	0.075	0.060	0.050	0.160	0.085	0.067	0.059	

* Values in table represent the damage state probabilities (%). Damage state descriptions are described in Table 5-74.

Table 5-81 Average Building Damage States – Five-Story Engineered Building

Building Characteristics				Residential Buildings (8 Units Per Floor)*				Commercial Buildings (1 Unit per Floor)*			
				Terrain Surface Roughness (m)				Terrain Surface Roughness (m)			
Roof Cover Effect	Missile Environ.	Glazing Coverage	Roof Cover	0.03	0.35	0.70	1.0	0.03	0.35	0.70	1.0
Included	A	20%	EPDM	0.628	0.562	0.428	0.367	0.643	0.566	0.433	0.372
			BUR	0.667	0.591	0.467	0.410	0.681	0.597	0.471	0.411
		33%	EPDM	0.711	0.618	0.469	0.399	0.724	0.624	0.472	0.399
			BUR	0.741	0.644	0.501	0.437	0.754	0.645	0.506	0.442
		50%	EPDM	0.795	0.677	0.512	0.436	0.805	0.681	0.518	0.440

Building Characteristics				Residential Buildings (8 Units Per Floor)*				Commercial Buildings (1 Unit per Floor)*				
				Terrain Surface Roughness (m)				Terrain Surface Roughness (m)				
Roof Cover Effect	Missile Environ.	Glazing Coverage	Roof Cover	0.03	0.35	0.70	1.0	0.03	0.35	0.70	1.0	
	B	20%	BUR	0.817	0.695	0.542	0.470	0.826	0.697	0.546	0.474	
			EPDM	0.542	0.477	0.372	0.324	0.557	0.482	0.376	0.331	
		33%	BUR	0.598	0.516	0.420	0.375	0.612	0.523	0.426	0.379	
			EPDM	0.604	0.524	0.407	0.351	0.623	0.528	0.409	0.355	
		50%	BUR	0.649	0.560	0.448	0.400	0.668	0.565	0.453	0.403	
			EPDM	0.682	0.576	0.446	0.384	0.700	0.580	0.452	0.392	
	C	20%	BUR	0.719	0.608	0.484	0.426	0.734	0.612	0.490	0.432	
			EPDM	0.481	0.416	0.334	0.297	0.502	0.425	0.341	0.302	
		33%	BUR	0.546	0.467	0.388	0.351	0.566	0.474	0.398	0.361	
			EPDM	0.534	0.459	0.364	0.318	0.554	0.466	0.369	0.324	
		50%	BUR	0.594	0.505	0.415	0.370	0.610	0.509	0.417	0.376	
			EPDM	0.599	0.506	0.399	0.349	0.616	0.508	0.404	0.355	
	D	20%	BUR	0.648	0.543	0.442	0.398	0.670	0.549	0.448	0.403	
			EPDM	0.400	0.302	0.268	0.250	0.417	0.304	0.273	0.254	
		33%	BUR	0.489	0.376	0.337	0.317	0.503	0.379	0.342	0.320	
			EPDM	0.407	0.305	0.269	0.254	0.425	0.311	0.275	0.256	
		50%	BUR	0.496	0.378	0.338	0.318	0.511	0.384	0.345	0.321	
			EPDM	0.447	0.342	0.303	0.285	0.479	0.368	0.324	0.303	
	Exclude	A	20%	N/A	0.572	0.522	0.373	0.301	0.589	0.527	0.378	0.307
			33%	N/A	0.669	0.586	0.423	0.343	0.682	0.591	0.425	0.345
50%			N/A	0.763	0.650	0.475	0.388	0.774	0.654	0.480	0.393	
B		20%	N/A	0.448	0.412	0.292	0.235	0.466	0.418	0.295	0.239	
		33%	N/A	0.529	0.472	0.338	0.272	0.551	0.476	0.340	0.277	
		50%	N/A	0.627	0.533	0.390	0.320	0.645	0.537	0.396	0.326	
C		20%	N/A	0.355	0.332	0.234	0.185	0.378	0.339	0.239	0.192	
		33%	N/A	0.433	0.392	0.280	0.223	0.456	0.398	0.283	0.230	
		50%	N/A	0.523	0.450	0.330	0.272	0.543	0.454	0.335	0.278	
D		20%	N/A	0.151	0.083	0.066	0.057	0.164	0.086	0.068	0.059	
		33%	N/A	0.160	0.088	0.069	0.059	0.179	0.094	0.073	0.063	
		50%	N/A	0.273	0.188	0.164	0.150	0.303	0.216	0.185	0.170	

* Values in table represent the damage state probabilities (%). Damage state descriptions are described in Table 5-74.

Table 5-82 Average Building Damage States – Eight-Story Engineered Building

Building Characteristics				Residential Buildings (8 Units per Floor)*				Commercial Buildings (1 Unit per floor)*			
				Terrain Surface Roughness (m)				Terrain Surface Roughness (m)			
Roof Cover Effect	Missile Environ	Glazing Coverage	Roof Cover	0.03	0.35	0.70	1.0	0.03	0.35	0.70	1.0
Included	A	20%	BUR	0.761	0.684	0.598	0.557	0.768	0.682	0.599	0.560
			EPDM	0.857	0.770	0.691	0.653	0.861	0.773	0.692	0.652
		33%	BUR	0.809	0.724	0.620	0.575	0.821	0.727	0.625	0.577
			EPDM	0.900	0.801	0.711	0.666	0.912	0.811	0.712	0.668
		50%	BUR	0.896	0.780	0.667	0.613	0.922	0.802	0.690	0.635
			EPDM	0.978	0.862	0.752	0.704	1.001	0.879	0.771	0.728
	B	20%	BUR	0.729	0.640	0.574	0.545	0.732	0.640	0.574	0.547
			EPDM	0.832	0.734	0.670	0.640	0.839	0.737	0.671	0.639
		33%	BUR	0.759	0.673	0.591	0.556	0.773	0.676	0.594	0.558
			EPDM	0.856	0.762	0.686	0.647	0.870	0.765	0.689	0.653
		50%	BUR	0.833	0.722	0.634	0.593	0.866	0.747	0.656	0.614
			EPDM	0.929	0.811	0.724	0.684	0.960	0.831	0.750	0.707
	C	20%	BUR	0.706	0.616	0.562	0.535	0.711	0.619	0.565	0.537
			EPDM	0.814	0.717	0.661	0.634	0.818	0.717	0.663	0.633
		33%	BUR	0.729	0.641	0.574	0.540	0.743	0.642	0.577	0.547
			EPDM	0.836	0.737	0.672	0.639	0.850	0.737	0.675	0.645
		50%	BUR	0.792	0.683	0.610	0.577	0.827	0.706	0.636	0.604
			EPDM	0.898	0.780	0.709	0.674	0.928	0.797	0.732	0.696
	D	20%	BUR	0.685	0.590	0.551	0.530	0.688	0.590	0.552	0.532
			EPDM	0.801	0.694	0.652	0.628	0.806	0.696	0.654	0.629
		33%	BUR	0.694	0.590	0.552	0.533	0.708	0.596	0.557	0.532
			EPDM	0.808	0.697	0.655	0.631	0.823	0.704	0.656	0.629
		50%	BUR	0.738	0.627	0.588	0.563	0.785	0.669	0.627	0.599
			EPDM	0.856	0.735	0.686	0.663	0.902	0.775	0.727	0.697
Exclude	A	20%		0.554	0.496	0.368	0.307	0.560	0.496	0.370	0.312
		33%	N/A	0.631	0.559	0.411	0.343	0.645	0.561	0.414	0.346
		50%		0.746	0.637	0.482	0.406	0.776	0.660	0.501	0.430
	B	20%		0.458	0.405	0.309	0.265	0.464	0.408	0.309	0.266
		33%	N/A	0.521	0.459	0.344	0.292	0.538	0.462	0.346	0.293
		50%		0.631	0.537	0.415	0.357	0.667	0.561	0.437	0.381
	C	20%		0.388	0.342	0.267	0.235	0.394	0.345	0.270	0.234
		33%	N/A	0.444	0.390	0.300	0.256	0.461	0.395	0.302	0.259
		50%		0.547	0.468	0.367	0.322	0.587	0.489	0.390	0.350
	D	20%		0.278	0.220	0.199	0.187	0.281	0.221	0.201	0.188
		33%	N/A	0.286	0.223	0.200	0.188	0.304	0.227	0.204	0.190

Building Characteristics				Residential Buildings (8 Units per Floor)*				Commercial Buildings (1 Unit per floor)*			
				Terrain Surface Roughness (m)				Terrain Surface Roughness (m)			
Roof Cover Effect	Missile Environ	Glazing Coverage	Roof Cover	0.03	0.35	0.70	1.0	0.03	0.35	0.70	1.0
		50%		0.382	0.306	0.277	0.263	0.433	0.347	0.320	0.301

* Values in table represent the damage state probabilities (%). Damage state descriptions are described in Table 5-74.

Table 5-83 Percent Increases in the Per Storm Average Building Damage State Due to Changes in Building Parameters (Minimum/Average/Maximum) - Engineered Residential and Commercial Buildings

Building Parameter	Roof Cover Effect Included			Roof Cover Effect Excluded		
	Min	Avg	Max	Min	Avg	Max
Two-Story Engineered Buildings						
Residential to Commercial Building Class	-1%	1%	5%	-1%	2%	16%
Built-up to Single Ply Membrane Roof Cover	1%	12%	33%	N/A		
20% to 33% Glazing Coverage	0%	7%	13%	-2%	11%	21%
33% to 50% Glazing Coverage	0%	9%	13%	12%	34%	128%
Missile Environment D to C	19%	49%	107%	152%	406%	664%
Missile Environment C to B	20%	28%	33%	36%	43%	52%
Missile Environment B to A	22%	27%	31%	32%	36%	42%
Five-Story Engineered Buildings						
Residential to Commercial Building Class	0%	2%	8%	0%	4%	15%
Built-up to Single Ply Membrane Roof Cover	2%	13%	26%	N/A		
20% to 33% Glazing Coverage	0%	7%	13%	3%	14%	23%
33% to 50% Glazing Coverage	6%	10%	18%	11%	43%	171%
Missile Environment D to C	11%	25%	51%	63%	195%	349%
Missile Environment C to B	5%	10%	15%	17%	21%	27%
Missile Environment B to A	9%	14%	18%	20%	24%	30%
Eight-Story Engineered Buildings						
Residential to Commercial Building Class	0%	2%	7%	-1%	3%	16%
Built-up to Single Ply Membrane Roof Cover	9%	15%	19%	N/A		
20% to 33% Glazing Coverage	0%	3%	7%	0%	10%	17%
33% to 50% Glazing Coverage	5%	8%	13%	14%	28%	58%
Missile Environment D to C	0%	3%	9%	15%	42%	75%

Building Parameter	Roof Cover Effect Included			Roof Cover Effect Excluded		
	Min	Avg	Max	Min	Avg	Max
Missile Environment C to B	1%	3%	6%	9%	15%	19%
Missile Environment B to A	2%	5%	8%	13%	19%	22%
All Engineered Buildings						
Two to Five Stories	2%	36%	105%	-2%	41%	198%
Five to Eight Stories	13%	54%	112%	-6%	35%	233%

5.6.7 Damage Model Results for Industrial Buildings

Large industrial buildings typically have flat roofs and are usually built with a masonry wall system. The roof structure is typically constructed using open web steel joists and a metal deck. The damage states for large industrial buildings are described in Table 5-84. The representative industrial building is modeled here with masonry walls (either reinforced or unreinforced) and with a lightweight open web steel joist (OWSJ) roof system. The model building has a length of 200', a width of 120' and a roof height of 20'.

Table 5-84 Damage States for Industrial Buildings

Damage State	Qualitative Damage Description	Roof Cover Failure	Door Failures	Roof Deck Failures	Missile Impacts on Walls	Joist Failures	Wall Failures
0	<u>No Damage or Very Minor Damage</u> Little or no visible damage from the outside. No failed doors or roof deck. Minimal loss of roof cover, with no or very limited water penetration.	≤2%	No	No	No	No	No
1	<u>Minor Damage</u> Maximum of one failed door. Moderate roof cover loss that can be covered to prevent additional water entering the building. Marks or dents on walls requiring painting or patching for repair.	>2% to ≤15%*	1 door*	No	Typically <5 impacts	No	No
2	<u>Moderate Damage</u> Major roof cover damage, moderate window breakage. Minor roof sheathing failure. Some resulting damage to interior of building from water.	>15% to ≤50%*	2 to £ the greater of 15% & 3*	1 or 2 panels*	Typically 5 to 10 impacts	No	No

Damage State	Qualitative Damage Description	Roof Cover Failure	Door Failures	Roof Deck Failures	Missile Impacts on Walls	Joist Failures	Wall Failures
3	<u>Severe Damage</u> Major window damage or roof sheathing loss. Major roof cover loss. Extensive damage to interior from water. Limited, local joist failures. Failure of one wall.	>50%*	> the greater of 15% & 3 to ≤50%*	3 to ≤25%*	Typically 10 to 20 impacts	1 joist to ≤25%*	1 wall*
4	<u>Destruction</u> Complete roof failure on 1/3 or more of the units and/or failure of more than one wall. Loss of more than 25% of roof sheathing.	Typically >50%	>50%*	>25%*	Typically >20 impacts	>25%*	2 or more*

* If any one of the conditions in the shaded cells with an asterisk (*) of a given row is true, the building is placed in that damage state)

The overall building geometry, along with the placement and relative size of the overhead rollup doors and entry doors is shown in Figure 5-144. The roof is divided into three sections each being 200' long and 40' wide. The joists span 40' with their ends supported by a perimeter wall or a main structural beam and are spaced at 6'. Note that the entry doors and overhead rollup doors are not glazed and thus no envelope breaches can be caused by missile impacts. The roof cover is modeled as an average quality EPDM single ply membrane.

The OWSJs are designed to resist the uplift forces and moments computed using ASCE 7-88, as described in Section 5.4.10, for a fastest-mile design wind speed of 100 mph. The building is assumed to be designed for open terrain (Exposure C) conditions.

The metal deck is modeled as being connected to the joists using welds. The weld design is assumed to meet the loading requirements as given in ASCE 7 and is designed using the methods outlined in Section 5.4.11.

The assumed component resistances are given in Table 5-85. The uplift values are for the as-installed roof, but a sensitivity study was performed where the uplift capacities of the welded connections were reduced by 50% to allow for the effect of age and fatigue. This 50% reduction is comparable to the reduction in the pullout capacity of fasteners in metal decks as reported by Baskaran and Dutt (1995).

For more information on example building and component damage state plots, please contact the Hazus Help Desk (see Section 1.5) for the *Hazus Hurricane Model Technical Manual Appendices* (FEMA, 2021). The average per storm damage states are given in Table 5-86. Reviewing the data in Table 5-86, it can be seen that per storm average building damage states vary by no more than 5% over the entire range of building parameters examined. As expected, there are negligible differences between the per storm average building damage states due to the different missile environments since the structure does not have any glazing. The different missile environments were included, however, since they will have an impact on the losses associated with refinishing the masonry wall surfaces and replacing damaged

overhead/entry doors due to damage by missile impacts. It is evident from the damage state plots shown in the appendices that building Damage State 1 is driven primarily by roof cover damage and that building Damage States 3 and 4 are driven primarily by entry/overhead door damage. The entry/overhead door damage states are primarily governed by the overhead garage doors, which are modeled as having a mean pressure resistance of 15 psf.

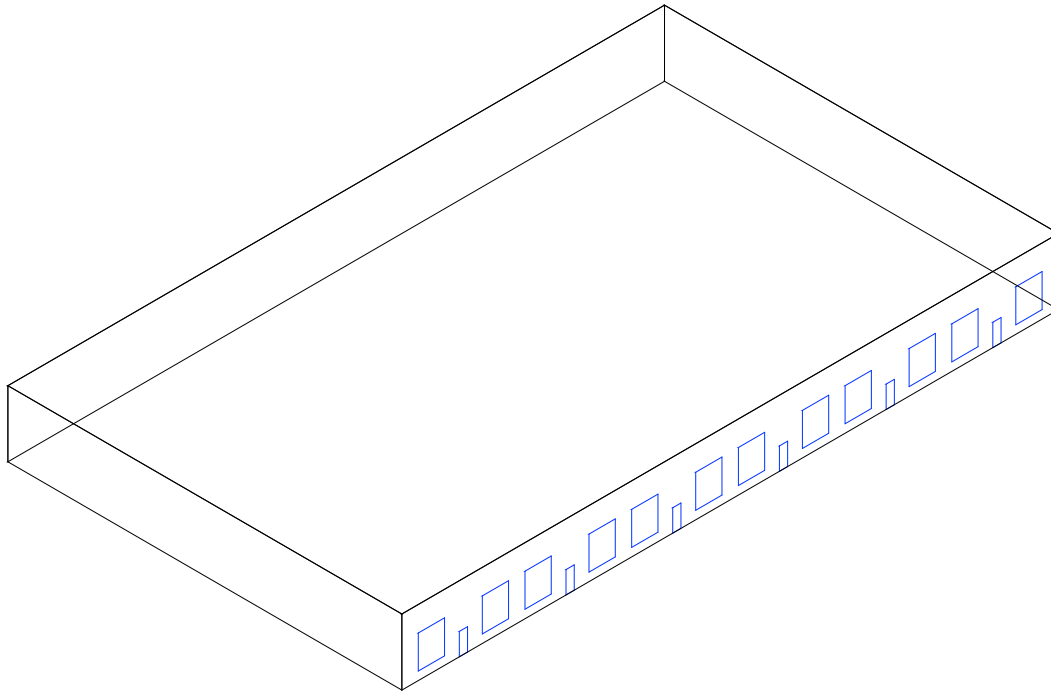


Figure 5-144 Model Building for Large Industrial Building – 200’x120’x20’ High

Table 5-85 Component Resistance Values Used for Strip-Mall Type Building

Fenestrations		
Component	Distribution	Distribution Parameters
Entry Door Pressure	Normal	Mean = 50 psf, COV = 0.2
Overhead Rollup Garage Door Pressure	LogNormal	Mean = 15 psf, COV = 0.2
Steel Deck on Steel Roof Joists – Building Height = 20’, Joist Spacing = 6’		
Component	Distribution	Distribution Parameters (Field, Edge, Corner)
Welded Steel Deck – ASCE 100mph	Normal	Mean = 91, 123, 155 psf, COV = 0.19, 0.19, 0.19

Table 5-86 Per Storm Average Building Damage States - Industrial Building

Building Characteristics		100% Roof Deck Capacity*				50% Roof Deck Capacity*			
		Terrain Surface Roughness (m)				Terrain Surface Roughness (m)			
Wall Construction	Missile Environment	0.03	0.35	0.70	1.0	0.03	0.35	0.70	1.0
Unreinforced Masonry	A	1.152	0.688	0.560	0.498	1.157	0.695	0.564	0.504
	B	1.155	0.691	0.559	0.496	1.157	0.696	0.564	0.501
	C	1.149	0.689	0.558	0.499	1.159	0.694	0.566	0.506
	D	1.151	0.690	0.561	0.497	1.159	0.695	0.565	0.505
Reinforced Masonry	A	1.105	0.678	0.554	0.493	1.115	0.680	0.560	0.498
	B	1.108	0.674	0.549	0.493	1.112	0.683	0.558	0.502
	C	1.103	0.678	0.553	0.492	1.112	0.682	0.555	0.502
	D	1.107	0.674	0.553	0.492	1.113	0.684	0.561	0.499

* Values in table represent the damage state probabilities (%). Damage state descriptions are described in Table 5-74.

5.6.8 Essential Facilities

Essential facilities consist of police stations, fire stations, schools, hospitals and emergency operation centers (EOC). Of these, fire stations, schools and hospitals have been explicitly modeled. Fire stations and schools are often low-rise structures and have been modeled as such, while hospitals can be low-rise or high-rise in nature. Police stations and EOCs were modeled as average government buildings.

For the purpose of this analysis, essential facility damage is limited to entry doors and windows, overhead doors (fire station only), and metal roof systems. All essential facilities were modeled assuming that whole wall failure and roof framing member failure would not occur. Other damage characteristics specific to each model is described below.

While damage data for essential facilities is scarce, Figure 5-145, Figure 5-146, Figure 5-147, and Figure 5-148 show examples of wind-induced damage to several fire stations in the Houston area as a result of Hurricane Ike (2008).

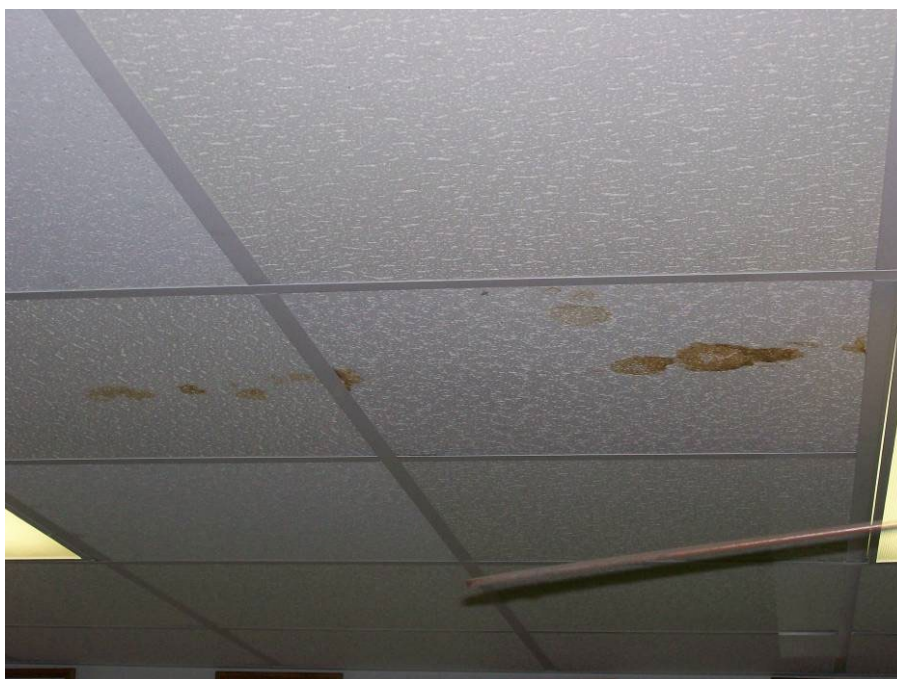


Figure 5-145 Water Damage to Interior Ceiling of a Fire Station in the Houston Area as a Result of Roof Damage (2008, Hurricane Ike)



Figure 5-145 Water Damage to Interior Ceiling of a Fire Station in the Houston Area as a Result of Roof Damage (2008, Hurricane Ike)



Figure 5-146 Bent Bay Door Rollers for a Fire Station in the Houston Area (2008, Hurricane Ike)



Figure 5-147 Torn Awning over Rear Entry Door for a Fire Station in the Houston Area (2008, Hurricane Ike)



Figure 5-148 Panel Damage to Bay Doors for a Fire Station in the Houston Area (2008, Hurricane Ike)

5.6.8.1 Fire Stations

Fire stations are often one-story structures with flat roofs that house both vehicles and personnel. The portion housing vehicles tends to have a separate roof but shares the same roof cover type as the rest of the building. Fire stations have been modeled with two compartments that share damages in the event of a window breach via internal doors that allow internal pressure and water infiltration to occur between the two. Two large overhead doors that measure 12' by 12' have also been modeled. The damage state definitions are the same as those as strip malls as described in Table 5-61.

The modeled fire station measures 75' wide and 85' long, with a 14' roof height for the portion housing vehicles and 10' roof height for the portion over personnel as shown in Figure 5-149. The fire station was sized as a representative case from RSMeans (~6,000 square feet). The windows measure 4'-6"x9' long, and together with the entry doors and overhead doors give a total of 15 fenestrations along the building envelope. The welded metal roof deck, roof cover, terrain exposure, fenestration resistances, and missile environment are as per the 12' strip mall with joist spacing of 4'. The storm average damage states are given in Table 5-87.

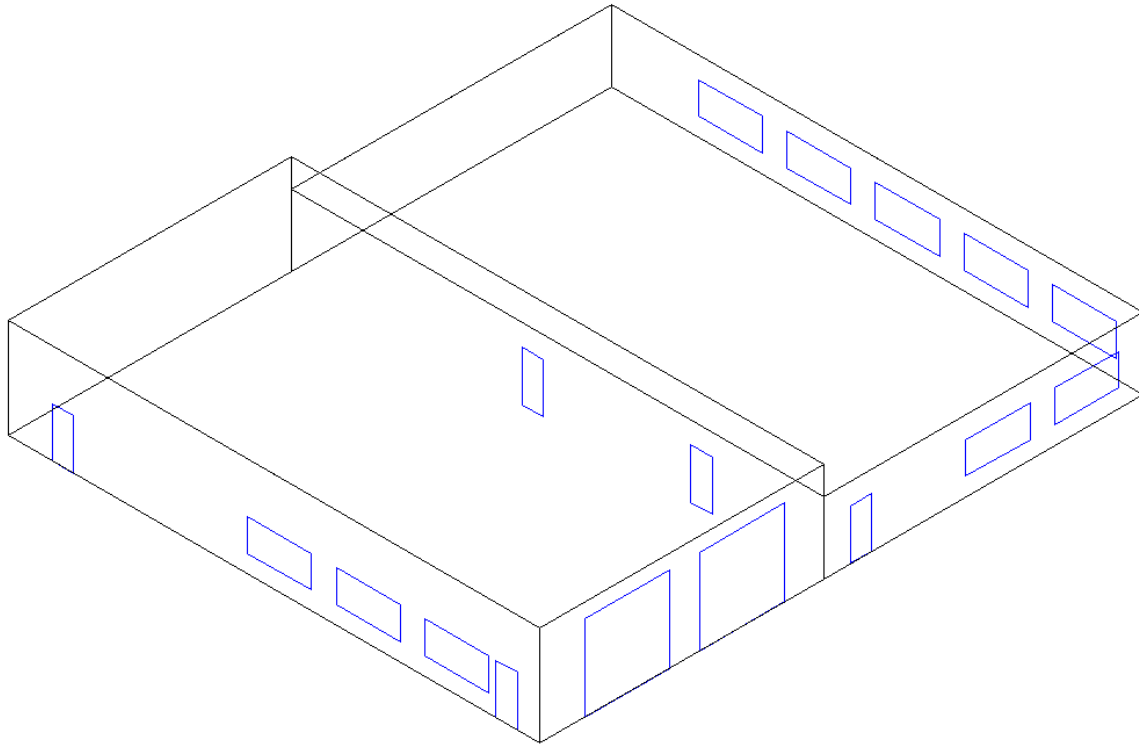


Figure 5-149 Fire Station Geometry Used in Study

Table 5-87 Average Damage States for the Fire Station Building

Deck Mitigation	Metal Panel Capacity	Shutters	Missile Environment	Roof Cover	Terrain Surface Roughness*				
					0.03	0.15	0.35	0.7	1
Mitigated	100%	No	A	BUR	0.429	0.558	0.404	0.284	0.226
				EPDM	0.433	0.561	0.406	0.286	0.229
			B	BUR	0.386	0.471	0.337	0.236	0.187
				EPDM	0.393	0.473	0.338	0.234	0.188
			C	BUR	0.277	0.287	0.197	0.129	0.101
				EPDM	0.286	0.288	0.200	0.135	0.105
			D	BUR	0.227	0.133	0.090	0.061	0.050
				EPDM	0.240	0.146	0.101	0.070	0.058
		Yes	A	BUR	0.144	0.115	0.080	0.055	0.045
				EPDM	0.166	0.129	0.091	0.065	0.053
			B	BUR	0.146	0.117	0.082	0.057	0.046
				EPDM	0.167	0.131	0.091	0.065	0.055
			C	BUR	0.152	0.132	0.090	0.061	0.050
				EPDM	0.173	0.145	0.100	0.070	0.058
			D	BUR	0.139	0.090	0.065	0.048	0.041
				EPDM	0.161	0.107	0.081	0.059	0.051

Deck Mitigation	Metal Panel Capacity	Shutters	Missile Environment	Roof Cover	Terrain Surface Roughness*				
					0.03	0.15	0.35	0.7	1
Unmitigated	100%	No	A	BUR	0.498	0.576	0.420	0.299	0.241
				EPDM	0.501	0.576	0.420	0.298	0.244
			B	BUR	0.462	0.499	0.362	0.258	0.212
				EPDM	0.467	0.499	0.364	0.258	0.213
			C	BUR	0.379	0.334	0.241	0.173	0.143
				EPDM	0.382	0.336	0.244	0.173	0.144
		D	BUR	0.343	0.227	0.167	0.128	0.111	
			EPDM	0.347	0.230	0.169	0.129	0.112	
		Yes	A	BUR	0.324	0.233	0.173	0.130	0.114
				EPDM	0.328	0.234	0.177	0.132	0.113
			B	BUR	0.326	0.231	0.174	0.130	0.112
				EPDM	0.328	0.237	0.174	0.134	0.114
	C		BUR	0.330	0.242	0.180	0.133	0.115	
			EPDM	0.332	0.242	0.182	0.137	0.117	
	D	BUR	0.321	0.218	0.163	0.125	0.109		
		EPDM	0.324	0.221	0.168	0.127	0.110		
	50%	No	A	BUR	0.536	0.587	0.431	0.398	0.252
				EPDM	0.538	0.590	0.435	0.311	0.254
			B	BUR	0.505	0.514	0.379	0.273	0.223
				EPDM	0.508	0.516	0.379	0.273	0.224
			C	BUR	0.427	0.361	0.269	0.195	0.164
				EPDM	0.428	0.365	0.268	0.196	0.165
			D	BUR	0.393	0.266	0.203	0.156	0.136
				EPDM	0.395	0.269	0.204	0.159	0.137
Yes			A	BUR	0.380	0.273	0.208	0.159	0.137
				EPDM	0.385	0.276	0.202	0.160	0.137
			B	BUR	0.380	0.274	0.206	0.159	0.138
				EPDM	0.384	0.276	0.208	0.160	0.139
	C	BUR	0.382	0.281	0.212	0.163	0.141		
		EPDM	0.388	0.285	0.213	0.162	0.140		
	D	BUR	0.376	0.259	0.199	0.154	0.135		
		EPDM	0.378	0.262	0.201	0.157	0.136		

* Values in table represent the damage state probabilities (%). Damage state descriptions are described in Table 5-74.

The building parameter sensitivity results for fire stations are shown in Table 5-88. It is evident that the missile environment has a large impact on the overall building damage state, increasing the mean per storm damage by 89% on average when the missile environment changes from no windborne debris (Missile Environment D) to a mixed residential/commercial type environment (Missile Environment A).

The use of EPDM roof cover versus BUR roof cover increases the overall storm average damage states by 4% on average, while a resistance reduction of 50% in the metal deck increases the damage state by 15%.

Mitigation techniques such as shutters have a great effect in reducing damage in this analysis since window breakage and metal deck failure are the primary drivers of damage. Damage increases by 95% when the shutter to no shutter case is considered and increases by 72% when the deck is no longer mitigated.

Table 5-88 Percent Increases in the Per Storm Average Building Damage State due to Changes in Building Parameters (Minimum/Average/Maximum) – Fire Station

Building Parameter	Min	Avg	Max
Built-up to Single ply Membrane Roof Cover	-3%	4%	24%
Missile environment D to C	2%	30%	119%
Missile Environment C to B	-3%	36%	85%
Missile Environment B to A	-3%	7%	22%
Mitigated Deck to Unmitigated Deck	3%	72%	166%
0% to 50% Reduction in Metal Roof Deck Resistance	2%	15%	24%
Shutters to No Shutters	1%	95%	417%

5.6.8.2 Elementary Schools

Elementary schools are often low-rise structures, with flat roofs being common. Gyms are typically taller than the rest of the building containing offices and classrooms but shares the same roof cover. Wide hallways connect classrooms, offices, and open gathering spaces such as the gym. In this one-story building, the gym has its own compartment with no glazed openings and can communicate with the rest of the building in the event of a window breach, allowing internal pressure and water infiltration to occur via internal doors. The damage state definitions are the same as strip malls, as described in Table 5-61.

The elementary school measures 140' wide by 330' long, with a 12' roof height for the portion over the classrooms and offices and 20' for the portion over the gym, as shown in Figure 5-150. The elementary school was sized as a representative case from RSMeans (~45,000 square feet). The windows measure 4'x6' long, and together with the entry doors give a total of 148 fenestrations along the building envelope. The welded metal roof deck, roof cover, terrain exposure, and missile environment are the same as the 12' strip mall with joist spacing of 4'. The storm average damage states are given in Table 5-89.

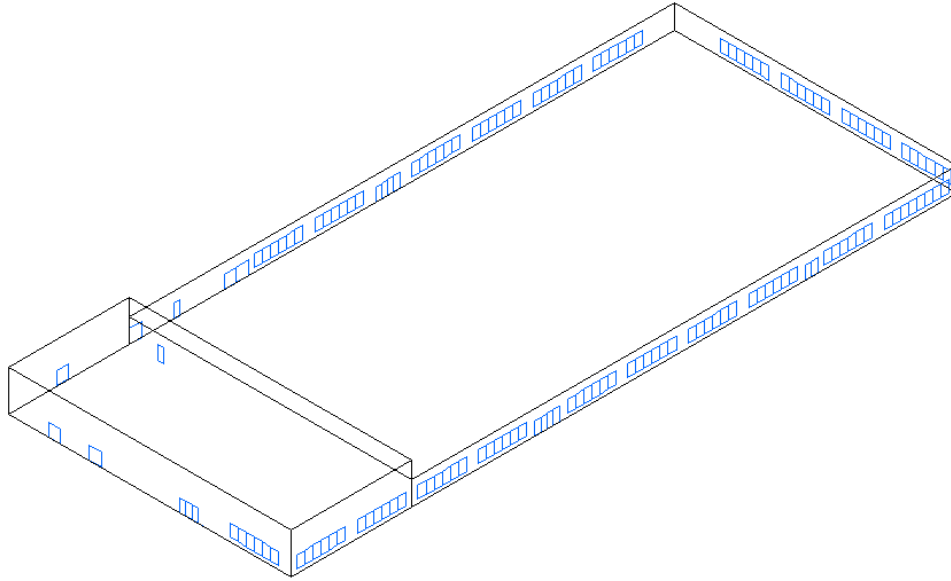


Figure 5-150 Elementary School Geometry Used in Study

Table 5-89 Average Damage States for the Elementary School Building

Deck Mitigation	Metal Panel Capacity	Shutters	Missile Environment	Roof Cover	Terrain Surface Roughness (m)*				
					0.03	0.15	0.35	0.7	1
Mitigated	100%	No	A	BUR	0.751	0.829	0.620	0.448	0.365
				EPDM	0.749	0.829	0.622	0.449	0.366
			B	BUR	0.618	0.646	0.474	0.340	0.273
				EPDM	0.622	0.646	0.476	0.339	0.274
			C	BUR	0.487	0.473	0.340	0.238	0.191
				EPDM	0.487	0.474	0.340	0.239	0.194
			D	BUR	0.374	0.230	0.163	0.116	0.100
				EPDM	0.378	0.230	0.164	0.119	0.101
		Yes	A	BUR	0.195	0.189	0.127	0.083	0.065
				EPDM	0.202	0.193	0.133	0.088	0.068
			B	BUR	0.207	0.199	0.136	0.090	0.070
				EPDM	0.214	0.204	0.140	0.093	0.073
			C	BUR	0.226	0.219	0.150	0.101	0.077
				EPDM	0.231	0.224	0.156	0.104	0.080
			D	BUR	0.132	0.082	0.056	0.040	0.035
				EPDM	0.146	0.089	0.064	0.046	0.040
Unmitigated	100%	No	A	BUR	0.789	0.836	0.626	0.457	0.374
				EPDM	0.792	0.839	0.627	0.457	0.374
				BUR	0.664	0.666	0.493	0.357	0.292

Deck Mitigation	Metal Panel Capacity	Shutters	Missile Environment	Roof Cover	Terrain Surface Roughness (m)*					
					0.03	0.15	0.35	0.7	1	
Unmitigated	100%	No	B	EPDM	0.666	0.665	0.493	0.358	0.294	
			C	BUR	0.541	0.507	0.371	0.268	0.219	
				EPDM	0.543	0.507	0.371	0.267	0.218	
			D	BUR	0.437	0.285	0.213	0.160	0.138	
				EPDM	0.441	0.285	0.214	0.161	0.138	
			Yes	A	BUR	0.351	0.295	0.220	0.164	0.139
		EPDM			0.354	0.295	0.223	0.165	0.141	
		B		BUR	0.360	0.304	0.226	0.167	0.142	
				EPDM	0.363	0.308	0.228	0.170	0.143	
		C		BUR	0.370	0.319	0.237	0.174	0.147	
				EPDM	0.375	0.322	0.237	0.176	0.148	
		D	BUR	0.318	0.227	0.176	0.139	0.123		
	EPDM		0.319	0.227	0.177	0.138	0.123			
	50%	No	A	BUR	0.824	0.847	0.639	0.467	0.382	
				EPDM	0.826	0.848	0.639	0.467	0.383	
			B	BUR	0.703	0.684	0.512	0.373	0.307	
				EPDM	0.704	0.683	0.514	0.373	0.307	
			C	BUR	0.579	0.534	0.394	0.287	0.240	
				EPDM	0.580	0.535	0.396	0.286	0.239	
			D	BUR	0.482	0.323	0.244	0.189	0.161	
				EPDM	0.484	0.325	0.248	0.189	0.163	
			Yes	A	BUR	0.411	0.338	0.255	0.195	0.168
					EPDM	0.411	0.342	0.261	0.196	0.169
				B	BUR	0.417	0.348	0.263	0.199	0.169
EPDM					0.417	0.353	0.264	0.200	0.171	
C	BUR	0.428		0.363	0.272	0.205	0.175			
	EPDM	0.430		0.364	0.276	0.208	0.176			
D	BUR	0.378	0.276	0.213	0.173	0.518				
	EPDM	0.376	0.276	0.216	0.174	0.152				

* Values in table represent the damage state probabilities (%). Damage state descriptions are described in Table 5-74.

Table 5-90 shows the building parameter sensitivity results for elementary schools. Missile environment has a large impact on the overall building damage state, in particular increasing the mean per storm damage by 103% on average when the missile environment changes from no windborne debris (Missile Environment D) to a residential type environment (Missile Environment A).

The use of EPDM roof cover versus BUR roof cover increases the overall storm average damage states by 1% on average, while a 50% reduction in metal deck resistance increases the damage state by 13%.

Mitigation techniques, such as shutters, have a great effect in reducing damage in this analysis since window breakage and metal deck failure are the primary drivers of damage. Damage increases by 128% on average when shutters are not part of the analysis and increases by 57% on average when the deck is not mitigated.

Table 5-90 Percent Increases in the Per Storm Average Building Damage State due to Changes in Building Parameters (Minimum/Average/Maximum) – Elementary School

Building Parameter	Min	Avg	Max
Built-up to Single ply Membrane Roof Cover	-1%	1%	15%
Missile Environment D to C	13%	62%	169%
Missile Environment C to B	-11%	13%	43%
Missile Environment B to A	-7%	11%	34%
Mitigated Deck to Unmitigated Deck	1%	57%	252%
0% to 50% Reduction in Metal Roof Deck Resistance	1%	13%	25%
Shutters to No Shutters	6%	128%	461%

5.6.8.3 High Schools

Like elementary schools, high schools are often low-rise structures with flat roofs. Gyms can be taller than the remaining portion of the building depending on the height, and typically share the same roof cover as the remainder of the building. Wide hallways connect classrooms, offices, and open gathering spaces such as the gym, while stairways connect floors. For this two- or three-story building, the gym has its own compartment, and can share damages from the rest of the first floor in the event of a window breach, allowing internal pressure and water infiltration to occur via internal doors. The remaining floors have been modeled as separate compartments, and the damage state definitions are the same as those as strip malls as described in Table 5-61.

The high school measures 135' wide and 330' long, with 12' stories and a gym height of 27 feet for the two-story case as shown in Figure 5-151 and is 36' for the three-story case as shown in Figure 5-152. The high school was sized as a representative case from RSMeans (~90,000 and ~135,000 square feet for the two- and three-story model respectively). The windows measure 4'x6' long, and together with the entry doors give a total of 165 fenestrations along the building envelope for the two-story case, and 243 for the three-story case. The welded metal roof deck, roof cover, fenestration resistances, terrain exposure, and missile environment are as per the two-story steel commercial building. The storm average damage states are given in Table 5-91 and Table 5-92.

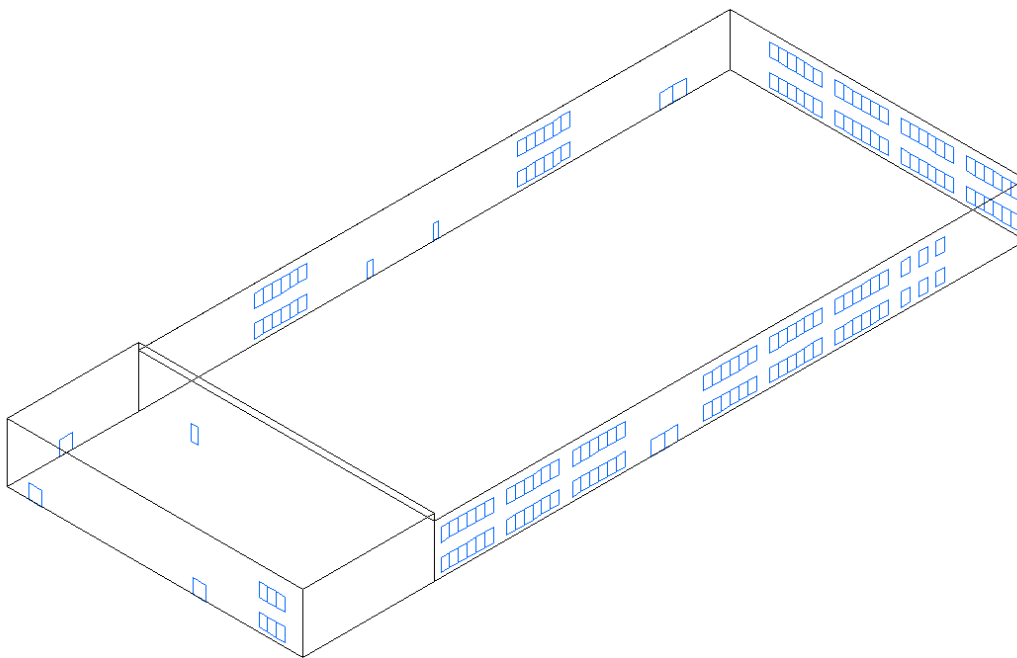


Figure 5-151 High School (Two-Story) Geometry Used in Study

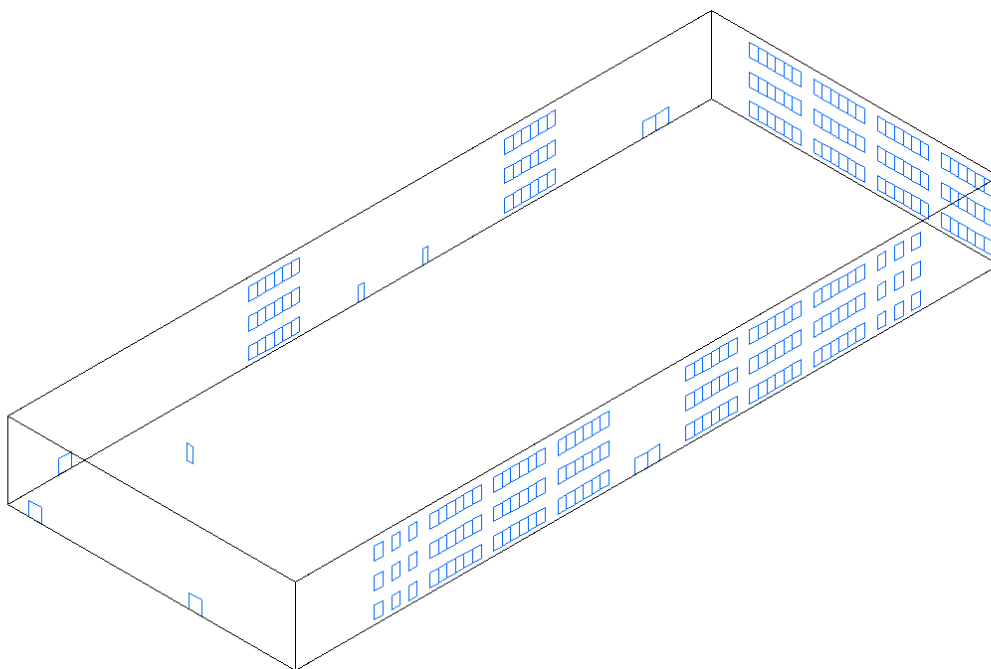


Figure 5-152 Large High School (Three-Story) Geometry Used in Study

Table 5-91 Average Damage States – Two-Story High School

Deck Mitigation	Shutters	Missile Environment	Roof Cover	Terrain Surface Roughness (m)*				
				0.03	0.15	0.35	0.7	1
Mitigated	No	A	BUR	0.672	0.802	0.602	0.436	0.356
			EPDM	0.682	0.804	0.604	0.444	0.365
		B	BUR	0.559	0.650	0.484	0.353	0.288
			EPDM	0.578	0.659	0.495	0.362	0.301
		C	BUR	0.420	0.467	0.346	0.252	0.207
			EPDM	0.452	0.481	0.361	0.269	0.225
		D	BUR	0.270	0.200	0.162	0.132	0.119
			EPDM	0.331	0.254	0.211	0.174	0.159
	Yes	A	BUR	0.264	0.245	0.189	0.148	0.129
			EPDM	0.324	0.285	0.228	0.184	0.163
		B	BUR	0.271	0.250	0.193	0.149	0.131
			EPDM	0.329	0.288	0.230	0.186	0.164
		C	BUR	0.282	0.269	0.205	0.157	0.135
			EPDM	0.338	0.304	0.240	0.190	0.167
		D	BUR	0.236	0.186	0.154	0.127	0.116
			EPDM	0.304	0.242	0.204	0.171	0.157
Unmitigated	No	A	BUR	0.897	0.905	0.700	0.538	0.462
			EPDM	0.900	0.906	0.705	0.542	0.463
		B	BUR	0.804	0.782	0.612	0.481	0.413
			EPDM	0.812	0.784	0.617	0.483	0.416
		C	BUR	0.702	0.656	0.521	0.415	0.364
			EPDM	0.712	0.659	0.524	0.420	0.369
		D	BUR	0.613	0.491	0.421	0.356	0.324
			EPDM	0.621	0.499	0.422	0.357	0.331
	Yes	A	BUR	0.611	0.517	0.432	0.365	0.326
			EPDM	0.617	0.526	0.439	0.371	0.334
		B	BUR	0.615	0.525	0.436	0.365	0.330
			EPDM	0.617	0.532	0.443	0.370	0.334
		C	BUR	0.625	0.533	0.444	0.369	0.332
			EPDM	0.635	0.540	0.448	0.374	0.331
		D	BUR	0.583	0.476	0.413	0.351	0.321
			EPDM	0.592	0.482	0.413	0.355	0.327

* Values in table represent the damage state probabilities (%). Damage state descriptions are described in Table 5-74.

Table 5-92 Average Damage States – Three-Story High School

Deck Mitigation	Shutters	Missile Environment	Roof Cover	Terrain Surface Roughness (m)*				
				0.03	0.15	0.35	0.7	1
Mitigated	No	A	BUR	0.708	0.799	0.608	0.456	0.377
			EPDM	0.733	0.811	0.624	0.475	0.402
		B	BUR	0.621	0.674	0.516	0.387	0.327
			EPDM	0.658	0.699	0.541	0.419	0.360
		C	BUR	0.511	0.534	0.411	0.315	0.270
			EPDM	0.564	0.565	0.446	0.354	0.312
		D	BUR	0.375	0.303	0.258	0.222	0.201
			EPDM	0.462	0.383	0.330	0.288	0.264
	Yes	A	BUR	0.364	0.332	0.273	0.228	0.207
			EPDM	0.450	0.396	0.339	0.289	0.265
		B	BUR	0.367	0.333	0.276	0.231	0.207
			EPDM	0.453	0.399	0.338	0.288	0.265
		C	BUR	0.379	0.353	0.287	0.235	0.212
			EPDM	0.458	0.409	0.345	0.294	0.268
		D	BUR	0.339	0.285	0.247	0.216	0.198
			EPDM	0.433	0.367	0.321	0.282	0.260
Unmitigated	No	A	BUR	1.057	1.025	0.833	0.681	0.604
			EPDM	1.068	1.029	0.840	0.686	0.611
		B	BUR	0.977	0.930	0.770	0.636	0.572
			EPDM	0.986	0.938	0.773	0.643	0.577
		C	BUR	0.901	0.842	0.702	0.596	0.543
			EPDM	0.915	0.847	0.713	0.604	0.549
		D	BUR	0.823	0.698	0.620	0.546	0.508
			EPDM	0.832	0.704	0.627	0.555	0.511
	Yes	A	BUR	0.819	0.720	0.629	0.553	0.512
			EPDM	0.823	0.726	0.636	0.556	0.518
		B	BUR	0.819	0.725	0.633	0.552	0.519
			EPDM	0.828	0.732	0.641	0.562	0.518
		C	BUR	0.823	0.734	0.638	0.563	0.511
			EPDM	0.834	0.746	0.645	0.563	0.518
		D	BUR	0.795	0.681	0.608	0.539	0.502
			EPDM	0.804	0.688	0.615	0.546	0.505

* Values in table represent the damage state probabilities (%). Damage state descriptions are described in Table 5-74.

The building parameter sensitivity results for high schools are shown in Table 5-93. Changing the missile environments between no windborne debris (Missile Environment D) to a mixed residential/commercial

type environment (Missile Environment A) increases observed damage 56% on average for the two-story case, 30% for the three-story case, and increases the observed damage 43% overall. This trend results from the fact that the modeled average heights of the buildings from which the commercial and residential type missiles originate are lower than the three-story buildings. Thus, the glazing on the upper floors of the three-story buildings are less susceptible to missile damage than the glazing on the lower floors.

The use of EPDM roof cover versus BUR roof cover increases the overall storm average damage states by 9%-10% on average for both the two- and three-story case.

Mitigation techniques such as shutters have a great effect in reducing damage in this analysis since window breakage and metal deck failure are the primary drivers of damage. Damage increases by 31% on average for the three-story case, 56% for the two-story case, and 44% overall when shutters are not in place.

The mitigated deck to unmitigated deck scenario increases damage by 88% and 91% for the two- and three-story case respectively, and 89% overall. The three-story case is more influenced by roof damage compared to fenestration damage.

Overall, increasing story height from two to three increases average damage by 38%.

Table 5-93 Percent Increases in the Per Storm Average Building Damage State due to Changes in Building Parameters (Minimum/Average/Maximum) – High School

Building Parameters	Number of Stories								
	All			Two			Three		
	Min	Avg	Max	Min	Avg	Max	Min	Avg	Max
Built-up to Single ply Membrane roof cover	0%	9%	35%	0%	9%	35%	0%	10%	31%
Missile Environment D to C	2%	24%	134%	3%	31%	134%	2%	16%	76%
Missile Environment C to B	-7%	9%	40%	-7%	12%	40%	-6%	6%	26%
Missile Environment B to A	-3%	7%	24%	-3%	8%	24%	-1%	6%	18%
Mitigated Deck to Unmitigated deck	13%	89%	176%	13%	88%	176%	27%	91%	153%
Shutters to No Shutters	1%	44%	227%	1%	56%	227%	1%	31%	140%
Two to Three Stories	0%	38%	70%	N/A					

5.6.8.4 Hospitals

Hospitals are often designed as both low-rise and high-rise structures. Wide hallways connect open spaces such as waiting rooms and cafeterias, as well as offices and laboratories. Elevators, in addition to stairwells, connect floors. The hospital buildings selected for modeling have one, four, and eight stories. Damage state definitions are the same as those as strip malls as described in Table 5-61.

The hospital measures 180' wide and 180' long, with 12' stories as shown in Figure 5-153, Figure 5-154, and Figure 5-155. Hospital dimensions were determined based on the number of beds it contains. The small hospital model (~41 beds) was sized assuming that each bed corresponded to 800 square feet of facility space, while larger hospitals (~93 and ~185 beds) corresponded to 1,400 square feet. The windows measure 4'x6' long, and together with the entry doors give a total of 61, 234, and 462 fenestrations along the building envelope for the one, four, and eight-story cases, respectively. The welded metal roof deck, roof cover, fenestration resistances, terrain exposure, and missile environment for the one, four, and eight-story modeled hospitals correspond to the two, five, and eight stories in the modeled steel commercial buildings, respectively.

Table 5-94, Table 5-95, and Table 5-96 list the average per storm damage states for the small, medium, and large hospitals.

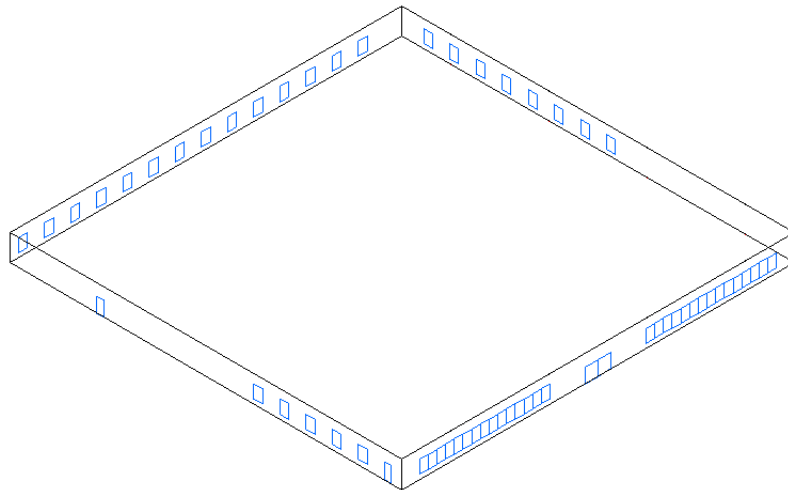


Figure 5-153 Small Hospital (<50 beds) Geometry Used in Study

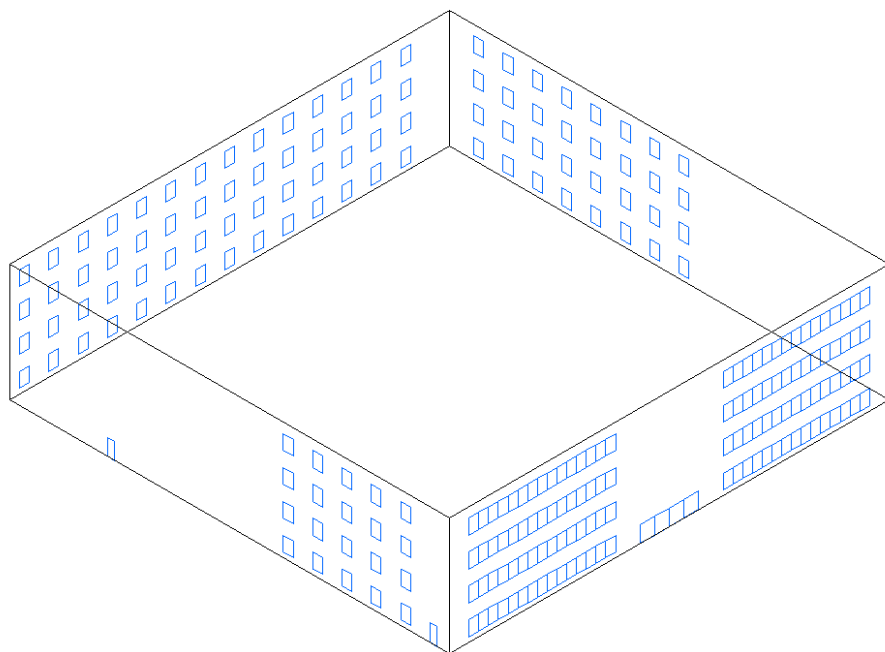


Figure 5-154 Medium Hospital (50-150 beds) Geometry Used in Study

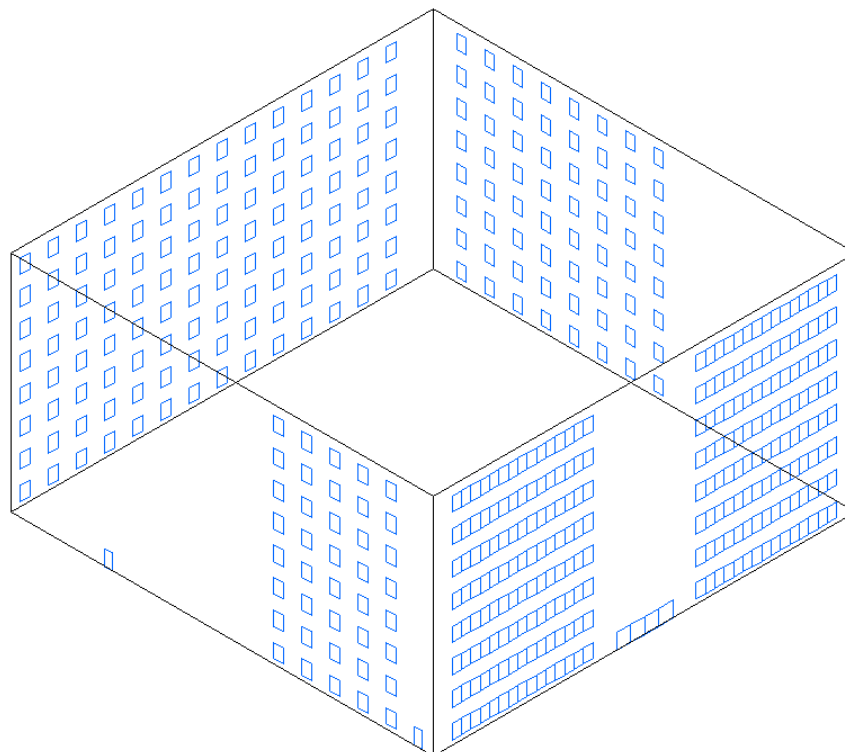


Figure 5-155 Large Hospital (>150 beds) Geometry Used in Study

Table 5-94 Average Damage States – Small Hospital

Deck Mitigation	Shutters	Missile Environment	Roof Cover	Terrain Surface Roughness (m)*				
				0.03	0.15	0.35	0.7	1
Mitigated	No	A	BUR	0.535	0.717	0.528	0.375	0.302
			EPDM	0.542	0.718	0.528	0.376	0.303
		B	BUR	0.397	0.528	0.382	0.269	0.214
			EPDM	0.409	0.531	0.384	0.273	0.217
		C	BUR	0.261	0.351	0.246	0.168	0.132
			EPDM	0.280	0.356	0.252	0.173	0.138
		D	BUR	0.128	0.080	0.058	0.043	0.038
			EPDM	0.165	0.109	0.081	0.061	0.055
	Yes	A	BUR	0.135	0.135	0.093	0.063	0.050
			EPDM	0.170	0.152	0.109	0.077	0.064
		B	BUR	0.144	0.149	0.102	0.069	0.054
			EPDM	0.178	0.166	0.117	0.082	0.067
		C	BUR	0.153	0.161	0.112	0.075	0.059
			EPDM	0.184	0.177	0.125	0.088	0.071
		D	BUR	0.114	0.077	0.057	0.042	0.038
			EPDM	0.155	0.108	0.080	0.060	0.054
Unmitigated	No	A	BUR	0.662	0.738	0.545	0.390	0.316
			EPDM	0.669	0.741	0.549	0.392	0.319
		B	BUR	0.546	0.577	0.422	0.300	0.244
			EPDM	0.552	0.581	0.425	0.304	0.249
		C	BUR	0.429	0.422	0.307	0.219	0.179
			EPDM	0.438	0.429	0.313	0.223	0.182
		D	BUR	0.295	0.203	0.157	0.124	0.107
			EPDM	0.304	0.213	0.164	0.129	0.112
	Yes	A	BUR	0.312	0.257	0.191	0.141	0.120
			EPDM	0.319	0.265	0.195	0.146	0.123
		B	BUR	0.323	0.270	0.198	0.144	0.122
			EPDM	0.329	0.278	0.202	0.149	0.127
		C	BUR	0.330	0.279	0.204	0.149	0.124
			EPDM	0.341	0.287	0.210	0.154	0.131
		D	BUR	0.386	0.200	0.156	0.124	0.107
			EPDM	0.295	0.211	0.164	0.129	0.112

* Values in table represent the damage state probabilities (%). Damage state descriptions are described in Table 5-74.

Table 5-95 Average Damage States – Medium Hospital

Deck Mitigation	Shutters	Missile Environment	Roof Cover	Terrain Surface Roughness (m)*				
				0.03	0.15	0.35	0.7	1
Mitigated	No	A	BUR	0.762	0.802	0.633	0.497	0.434
			EPDM	0.823	0.836	0.677	0.548	0.490
		B	BUR	0.694	0.706	0.565	0.451	0.401
			EPDM	0.764	0.753	0.618	0.515	0.461
		C	BUR	0.630	0.623	0.506	0.417	0.374
			EPDM	0.709	0.681	0.568	0.481	0.439
		D	BUR	0.539	0.457	0.405	0.359	0.336
			EPDM	0.642	0.552	0.493	0.440	0.413
	Yes	A	BUR	0.517	0.466	0.409	0.361	0.335
			EPDM	0.621	0.555	0.495	0.442	0.412
		B	BUR	0.523	0.474	0.412	0.362	0.337
			EPDM	0.628	0.560	0.498	0.445	0.412
		C	BUR	0.527	0.481	0.419	0.362	0.338
			EPDM	0.628	0.568	0.502	0.443	0.414
		D	BUR	0.506	0.435	0.392	0.351	0.331
			EPDM	0.615	0.533	0.482	0.432	0.410
Unmitigated	No	A	BUR	1.097	1.050	0.889	0.764	0.701
			EPDM	1.110	1.065	0.905	0.778	0.717
		B	BUR	1.063	1.005	0.862	0.749	0.692
			EPDM	1.083	1.022	0.878	0.767	0.711
		C	BUR	1.041	0.965	0.842	0.735	0.689
			EPDM	1.062	0.984	0.858	0.754	0.702
		D	BUR	0.977	0.854	0.773	0.697	0.658
			EPDM	0.988	0.870	0.788	0.714	0.673
	Yes	A	BUR	0.960	0.868	0.780	0.701	0.663
			EPDM	0.980	0.880	0.791	0.714	0.674
		B	BUR	0.962	0.869	0.781	0.703	0.659
			EPDM	0.987	0.889	0.798	0.717	0.674
		C	BUR	0.972	0.881	0.785	0.708	0.663
			EPDM	0.986	0.892	0.801	0.719	0.677
		D	BUR	0.958	0.844	0.767	0.693	0.655
			EPDM	0.968	0.860	0.781	0.710	0.670

*Values in table represent the damage state probabilities (%). Damage state descriptions are described in Table 5-74.

Table 5-96 Average Damage States – Large Hospital

Deck Mitigation	Shutters	Missile Environment	Roof Cover	Terrain Surface Roughness (m)*				
				0.03	0.15	0.35	0.7	1
Mitigated	No	A	BUR	1.477	1.398	1.312	1.231	1.187
			EPDM	1.700	1.612	1.529	1.451	1.407
		B	BUR	1.471	1.390	1.299	1.231	1.187
			EPDM	1.697	1.609	1.522	1.452	1.408
		C	BUR	1.462	1.374	1.294	1.227	1.188
			EPDM	1.692	1.600	1.519	1.448	1.407
		D	BUR	1.425	1.366	1.293	1.222	1.187
			EPDM	1.661	1.595	1.519	1.444	1.406
	Yes	A	BUR	1.424	1.341	1.277	1.212	1.175
			EPDM	1.661	1.570	1.504	1.434	1.394
		B	BUR	1.424	1.339	1.273	1.212	1.174
			EPDM	1.658	1.568	1.501	1.432	1.393
		C	BUR	1.424	1.570	1.272	1.210	1.173
			EPDM	1.657	1.339	1.500	1.435	1.391
		D	BUR	1.423	1.339	1.278	1.208	1.174
			EPDM	1.657	1.568	1.503	1.430	1.394
Unmitigated	No	A	BUR	2.615	2.524	2.446	2.368	2.314
			EPDM	2.630	2.534	2.458	2.382	2.327
		B	BUR	2.618	2.522	2.446	2.367	2.320
			EPDM	2.631	2.539	2.460	2.374	2.331
		C	BUR	2.621	2.521	2.445	2.365	2.316
			EPDM	2.628	2.534	2.456	2.379	2.329
		D	BUR	2.618	2.527	2.444	2.365	2.318
			EPDM	2.630	2.354	2.457	2.378	2.329
	Yes	A	BUR	2.613	2.517	2.440	2.367	2.316
			EPDM	2.627	2.535	2.452	2.375	2.328
		B	BUR	2.617	2.519	2.443	2.364	2.316
			EPDM	2.622	2.534	2.455	2.379	2.331
		C	BUR	2.612	2.518	2.444	2.365	2.318
			EPDM	2.623	2.534	2.460	2.379	2.329
		D	BUR	2.613	2.525	2.443	2.365	2.318
			EPDM	2.625	2.534	2.456	2.378	2.328

* Values in table represent the damage state probabilities (%). Damage state descriptions are described in Table 5-74.

Table 5-97 displays the building parameter sensitivity results for hospital buildings. Changing the missile environments from no windborne debris (Missile Environment D) to a mixed residential/commercial type environment (Missile Environment A) increases observed damage by 165%, 13%, and less than 1% on average for the one, four, and eight-story cases respectively, and 51% overall. These damage trends are a

result of the modeled average heights of the buildings. The original modeled building heights for commercial and residential type missiles are lower than the four and eight-story buildings. Thus, the glazing on the upper floors of the four and eight-story buildings are less susceptible to missile damage than the glazing on the lower floors.

The use of an EPDM roof cover versus a BUR roof cover increases the overall storm average damage states by 9%-10% on average for all cases.

Mitigation techniques, such as shutters, tend to have a significant effect in reducing damage, since window breakage and metal deck failure are the primary drivers of damage. Damage increases by 1% on average for the eight-story case, 15% for the two-story case, 129% for the one-story case, and 48% overall when shutters are not in place. The change from a mitigated deck to an unmitigated deck increases damage by 66% to 76% for all story height cases. The cases that include a higher number of stories are more disposed to roof damage compared to fenestration damage.

Overall, damage is most influenced by story height. Increasing story height from one to four stories increases average damage by 278% and increases damages by 193% when increasing the story height from four stories to eight stories.

Table 5-97 Percent Increases in the Per Storm Average Building Damage State due to Changes in Building Parameters (Minimum/Average/Maximum) – Hospital

Building Parameters	Number of Stories											
	All			One			Four			Eight		
	Min	Avg	Max	Min	Avg	Max	Min	Avg	Max	Min	Avg	Max
Built-up to Single ply Membrane Roof	0%	10%	44%	0%	10%	44%	1%	10%	24%	0%	9%	19%
Missile Environment D to C	0%	34%	338%	15%	94%	338%	1%	8%	36%	0%	0%	1%
Missile Environment C to B	-9%	7%	61%	-9%	20%	61%	-2%	2%	13%	0%	0%	1%
Missile Environment B to A	-9%	5%	41%	-9%	14%	41%	-2%	3%	14%	0%	0%	1%
Mitigated Deck to Unmitigated Deck	3%	73%	194%	3%	76%	194%	27%	66%	98%	55%	76%	98%
Shutters to No Shutters	0%	48%	503%	0%	129%	503%	0%	15%	72%	0%	1%	4%

Building Parameters	Number of Stories												
	All			One			Four			Eight			
	Min	Avg	Max	Min	Avg	Max	Min	Avg	Max	Min	Avg	Max	
One to Four Stories	12%	278%	778%	N/A									
Four to Eight Stories	74%	193%	255%										

Section 6. Induced Damage Methods – Building and Tree Debris

Debris generated by severe wind events can be categorized into five general types (Holmlin, 1993): medical (or bio-hazardous) wastes, hazardous or toxic wastes (HTWs), household garbage, burnable roadside debris, and construction and demolition debris. Burnable roadside debris, which is primarily trees and other yard wastes, is often the largest among those five types of debris. Only debris generated from damaged buildings (i.e., construction and demolition debris produced immediately after the event and during the rebuilding and repairing phases) and tree blowdown are calculated in the current version of the Hazus model.

Building debris consists of construction and demolition waste that is generally non-hazardous and not water soluble. Construction and demolition debris can be further categorized as wood (which is bio-degradable), masonry, metal (which is recyclable), and other (which includes gypsum board, carpet, asphalt roofing material, insulation, ceiling, pipe, etc.). Masonry and other debris are usually disposed of in authorized landfills. Debris removal is often one of the most costly and challenging operations following a natural disaster (Holmlin, 1993). Due to contamination with different types of waste materials, it is also difficult to recycle most of the structural waste (debris). Accurate and prompt estimation of the total debris generated, and its distribution is vital to ensure the success of a debris removal operation after a hurricane.

At the time the models described in this section were developed (1998-2001), a simple model for estimating the volume and type of debris had been developed by the U.S. Army Corps of Engineers (USACE) using historical data from Hurricanes Frederic, Hugo, and Andrew. The USACE model was used to estimate debris produced in Escambia County for hurricanes Erin and Opal. This simple model was intended to be used for estimating debris produced by single-family residential buildings only. The model yielded estimates of the expected volumes of burnable debris, landfill debris, soil debris, and metallic debris based on the category of hurricane winds occurring in a county, combined with factors related to business use, the number of households, vegetation density (light, medium, or heavy) and a storm wet/dry multiplier. The model error was typically within $\pm 30\%$ (Moorse, 2001). Enhancements to the USACE model enabled the analysis to be done at a Census tract level, resulting in higher accuracy. The major limitation of the model at the time was the inability to consider various construction and usage classes. For example, the model significantly overestimated the building debris produced by Typhoon Paka in Guam because the model could not consider the reduction in building losses associated with a large number of residential buildings having hardened concrete roofs.

To overcome the limitations of the USACE model, a new debris estimation model was developed for Hazus based on the damage states for structural and nonstructural components of several model buildings. For each damaged component, the debris generated in each category (wood, masonry, metal, and other) is calculated based on the component's damage state and weight statistics. Then, by adding up the debris produced by all the damaged components, the total debris weight for that model building can be estimated. The debris volume is estimated by dividing the debris weight by its density. The accuracy of the current model depends heavily on the accuracy of underlying databases (which includes unit weights of the building components, debris distribution matrix, and detailed building configuration).

Limited case studies were conducted to test and calibrate the current model, and the results are summarized at the end of this section. Section 6.1 describes the methodology Hazus uses to calculate building-related debris.

Hurricanes generate considerable amounts of debris from tree blowdown. In most cases, SLTT governments, with federal assistance, are responsible for collecting and disposing of this debris. Tree debris disposal from Hurricane Isabel in North Carolina totaled over 3.2 million cubic yards and cost communities in the state over \$31 million to collect and dispose of this debris. A description of the tree debris methodology can be found in Section 6.3.

6.1 Description of Building Debris Generation Methodology

Since the building component weights and debris distribution vectors are available from a number of sources, the only new input needed is to define the damage intensity functions. The debris module has to produce debris estimation based on the damage states provided by the load-resistance physical damage model, which includes the number of damaged fenestrations, roof cover damage, roof sheathing damage, wall damage, and water damage (amount of water entering the building). The building components can be divided into two categories: those modeled explicitly by the damage model (primarily damage to the building envelope) and those modeled implicitly by the damage model (i.e., their damage states have to be estimated based on envelope damage). For components that are modeled explicitly in the damage model, it was assumed that $f(d_i) = d_i$. For components that are not modeled explicitly (e.g., building interior), the damage intensity functions were assumed to be similar in format to those used in the economic loss model, however, with different parameters. For example, the interior damage due to water entering damaged fenestration was modeled as one-fourth of the rate defined by the damage intensity function in the economic loss module. Those parameters were developed using a combination of historical data and expert judgment.

The form of the debris model is:

Equation 6-1

$$D = \sum_{i=1}^n W_i f(d_i) D_i$$

Where:

- | | |
|------------|--|
| D | is the debris distribution vector for the model building, which consists of debris from wood, masonry, metal and other, respectively |
| W_i | is the total weight of building component i |
| $f(\cdot)$ | is the damage intensity function, $0 \leq f(\cdot) \leq 1$ |
| d_i | is the damage state of building component i, which is obtained from the physical damage model |

D_i is the debris distribution vector for building component i , which specifies the fractions of total component weight in wood, masonry, metal, and other building types

The interior damage intensity functions for roof cover, roof sheathing, and fenestration damages are defined as:

Equation 6-2

$$I_{cv} = f(d_{cv}) = \begin{cases} 0.5d_{cv} & \text{without secondary water resistance} \\ 0.05d_{cv} & \text{with secondary water resistance} \end{cases}$$

Equation 6-3

$$I_{sh} = f(d_{sh}) = 1.8d_{sh}$$

Equation 6-4

$$I_{fen} = f(d_{fen}) = 1.0d_{fen}$$

Where:

- I_{cv} is the interior damage level due to roof cover damage
- d_{cv} is the percentage of roof cover damage
- I_{sh} is the interior damage level due to roof sheathing damage
- d_{sh} is the percentage of roof sheathing damage
- I_{fen} is the interior damage level due to fenestration damage
- d_{fen} is the amount (in.) of wind driven rain in the interior due to fenestration damage

The final interior damage level (I) is calculated as the maximum of interior damage levels due to roof cover, roof sheathing, and fenestration damages, i.e., $I = \max(I_{cv}, I_{sh}, I_{fen})$. The damage levels for all interior assemblies, such as partition wall, ceiling, floor finish, wall finish, content, etc., given an interior damage level, are assumed to be the same. Therefore, the total interior debris is estimated by (assuming m interior components):

Equation 6-5

$$D_{int} = I \sum_{i=1}^m W_i D_i$$

Where:

- D_{int} is the interior debris distribution vector

- W_i is the total weight of building component i
- D_i is the debris distribution vector for building component i , which specifies the fractions of total component weight in wood, masonry, metal, and other building types

It is further assumed that, for engineered buildings, non-modeled load-bearing structural components (such as columns and beams, concrete or metal deck floors, and load-bearing partition walls) will not be damaged, and therefore, no debris could be produced from those components. However, finishes on those components can be damaged by water entering the building.

For buildings that reach the destruction damage state (see definitions in Section 5), the entire building will be torn down, and the debris produced by demolition will be equal to the total building weight. In the present debris model, global damage indicators (such as total roof cover damage ratio, total roof deck damage ratio, roof frame failure, wall frame failure, etc.) are monitored, and once the destruction state is reached, the total building weight will be used as the total debris weight. The total building weight is pre-calculated based on the specified construction for the model building (in the case when construction types for certain components are not given, default construction types are used in the analysis). Note that the weight of the foundation is not included in the total building weight calculation. The default construction characteristics for the Economy, Average, Custom, and Luxury residential buildings are defined in the residential economic loss module in Section 8.1. The default construction characteristics for commercial buildings will be discussed later in this section.

After the total debris weight in each category (wood, masonry, metal, and other) is determined, the total debris volume is estimated by dividing the total debris weight of each type by its density. However, since debris cannot be fully packed, the debris density will be much less than its material's density. In the debris model, the debris density for masonry is assumed to be two-thirds of concrete masonry density (125 per cubic foot (pcf)) and the debris densities for the remaining types of debris are assumed to be one-half of their material densities. Due to a mixture of different materials, the material density for "other" types of debris is not readily available. The "other" category is assumed to be 70 pcf in the present debris model (between the densities of wood and masonry).

6.1.1 Component Unit Weight

Building component (or assembly) weights are closely related to building dead loads, while content weights are closely related to sustained live loads. Therefore, it is natural to refer to the current building code for this information. Specifically, the ASCE 7-98 Commentary (1999) is used to obtain the building component weights and live load statistics in this study. For items that are not included in the ASCE Commentary, references are made to the manufacturer's manuals. RSMMeans (2001) is also used to obtain unit weights for a number of building assemblies. Table 6-1 lists the collected average building component weights. The COV for each item is assumed to be 20%. Table 6-2 lists the sustained live load statistics for residential buildings and several types of commercial buildings. For building usage types that are not listed in this table, a mean of 10 point spread function (psf) and a standard deviation of 5 psf are assumed. Note that sustained live load statistics are based on specified areas of observation (see Table 6-2 Sustained Load Statistics). The standard deviation of the average sustained load for an area greater than the observation area is:

Equation 6-6

$$\sigma_n = \sqrt{\frac{\sigma}{n}}$$

Where:

- σ_n is the standard deviation of the sustained load for an area n times of the observation area
- σ is the observed standard deviation of the sustained load

Table 6-1 Component Unit Weights Used in the Debris Model

Category	Component	Unit Weight (psf)
Roof Cover	Slate, 1/4"	10
	26 gauge metal shingle or metal panel	2
	Wood shingles	3
	Three-ply ready roofing	1
	Asbestos-cement shingles	4
	Slate, 3/16"	7
	Single-ply, sheet membranes	0.7
	Roman tile	12
	Ludowici tile	10
	Liquid applied membranes	1
	Five-ply felt and gravel	6
	Corrugated asbestos-cement roofing	4
	Copper or tin	1
	Cement tile	16
	Book tile, 3"	20
	Book tile, 2"	12
	Bituminous, smooth surface membranes	1.5
	Bituminous, gravel-covered membranes	5.5
	Asphalt shingles	2
	Four-ply felt and gravel	5.5
Spanish	19	
Roof Deck	Decking, 2" wood	5
	Wood sheathing (per in. thickness)	3
	Decking, 3" (Douglas fir)	8
	Deck, metal, 20 gauge	2.5
	Deck, metal, 18 gauge	3
	Plywood (per in. thickness)	3.2

Category	Component	Unit Weight (psf)
Roof Frame	16" deep @ 6' Bar Joist	17.5
	2x4 @24" slope 4/12	2.0
	2x6 @ 48" 2x3 batten@36"	1.2
	Metal truss	12
	Post and beam	8
Insulation	Rigid insulation, 1/2"	0.8
	Urethane foam with skin	0.5
	Polystyrene foam insulation	0.2
	Fibrous glass insulation (4" thick)	4.4
	Fiberboard insulation	1.5
	Cellular glass insulation (4" thick)	2.8
	Perlite insulation	0.8
Ceiling	Acoustical fiber board	1
	Gypsum Board (1/2" thickness)	2
	Mechanical duct allowance	4
	Plaster on tile or concrete	5
	Plaster on wood lath	8
	Suspended metal lath and cement plaster	15
	Suspended metal lath and gypsum plaster	10
	Suspended steel channel system	2
	Wood furring suspension system	2.5
Coverings, Roof, and Wall	Fiberboard, 1/2"	0.8
	Gypsum sheathing, 1/2"	2
Exterior Wall	8" medium weight hollow CMU, grout 40" O.C.	45
	6" normal weight solid CMU	64
	4" normal weight solid CMU	41
	6" light weight solid CMU	51
Exterior Wall	6" medium weight hollow CMU, full grout	59
	6" medium weight hollow CMU, grout 16" O.C.	44
	6" medium weight hollow CMU, grout 24" O.C.	39
	6" medium weight hollow CMU, grout 32" O.C.	36
	6" medium weight hollow CMU, grout 40" O.C.	34
	6". medium weight hollow CMU, grout 48" O.C.	33
	6". medium weight hollow CMU, no grout	28
	6" medium weight solid CMU	60
	4" medium weight solid CMU	38

Category	Component	Unit Weight (psf)
Exterior Wall	8" clay brick wythes	79
	8" light weight solid CMU	69
	8" medium weight hollow CMU, full grout	81
	8" medium weight hollow CMU, grout 16" O.C.	59
	4" medium weight hollow CMU, no grout	26
	8" medium weight hollow CMU, grout 32" O.C.	47
	2x6 @ 16", 5/8" gypsum, insulated, 3/8" siding	12
	8" medium weight hollow CMU, grout 48" O.C.	44
	8" medium weight hollow CMU, no grout	36
	8" medium weight solid CMU	81
	8" normal weight solid CMU	87
	Exterior stud walls with brick veneer	48
	8" medium weight hollow CMU, grout 24" O.C.	51
	10" normal weight solid CMU	110
	10" light weight solid CMU	87
	10" medium weight hollow CMU, full grout	102
	10" medium weight hollow CMU, grout 16" O.C.	73
	10" medium weight hollow CMU, grout 24" O.C.	63
	10" medium weight hollow CMU, grout 32" O.C.	58
	10" medium weight hollow CMU, grout 40" O.C.	56
	10" medium weight hollow CMU, grout 48" O.C.	54
	4-" light weight solid CMU	32
	10" medium weight solid CMU	102
	12" clay brick wythes	115
	12" light weight solid CMU	105
	12" medium weight hollow CMU, full grout	123
	2x4 @ 16", 5/8" gypsum, insulated, 3/8" siding	11
	12" medium weight hollow CMU, grout 24" O.C.	75
	12" medium weight hollow CMU, grout 32" O.C.	68
	4" clay brick wythes	39
	12" medium weight hollow CMU, grout 40" O.C.	65
	12" medium weight hollow CMU, grout 48" O.C.	62
	12" medium weight hollow CMU, no grout	50
	12" medium weight solid CMU	124
12" normal weight solid CMU	133	
16" clay brick wythes	155	

Category	Component	Unit Weight (psf)
Exterior Wall	12" medium weight hollow CMU, grout 16" O.C.	87
	10" medium weight hollow CMU, no grout	44
Floors and Floor Finishes	Asphalt block (2"), 1/2" mortar	30
	Cement finish (1") on stone-concrete fill	32
Floor and Floor Finishes	Ceramic or quarry tile (3/4") on 1/2" mortar bed	16
	Ceramic or quarry tile (3/4") on 1" mortar bed	23
	Hardwood flooring, 7/7"	4
	Linoleum or asphalt tile, 1/4"	1
	Terrazzo (1") on stone-concrete fill	32
	Concrete floor on steel beam (Commercial)	38
	Steel deck on steel beam (Commercial)	30
	Concrete fill finish (per inch thickness)	12
	Carpet	2
	Wood block (3") on 1/2" mortar base	16
	Terrazzo (1") on 2" stone-concrete	32
	Terrazzo (1-1/2") directly on slab	19
	Subflooring, 3/4"	3
	Solid flat tile on 1" mortar base	23
	Slate (per mm thickness)	15
	Marble and mortar on stone-concrete file	33
Wood block (3" 0 on mastic, no fill	10	
Floors, Wood-Joist	2x6 joists, 12" spacing double wood floor	6
	2x8 joists, 12" spacing double wood floor	6
	2x8 joists, 24" spacing double wood floor	5
	2x8 joists, 16" spacing double wood floor	8
	2x10 joists, 12" spacing double wood floor	7
	2x10 joists, 16" spacing double wood floor	6
	2x12 joists, 24" spacing double wood floor	6
	2x12 joists, 16" spacing double wood floor	7
	2x12 joists, 12" spacing double wood floor	8
	2x10 joists, 24" spacing double wood floor	6
	2x6 joists, 16" spacing double wood floor	5
	2x6 joists, 24" spacing double wood floor	5
Frame Partitions	Movable steel partitions	4
	Wood studs, 2x4, unplastered	4
	Wood studs, 2x4, plastered two sides	20

Category	Component	Unit Weight (psf)
Frame Partitions	Wood or steel studs, 1/2" gypsum board each side	8
	Wood studs, 2x4, plastered one side	12
	Gypsum board and sound deadening board on wood or steel stud	15
Doors	Interior and Exterior	10
Garage Doors	Regular garage doors	1.6
Skylight	Skylight, metal frame, 3/8" wire glass	8
Sliders	3/16" tempered sliding glass door	4
Windows	Windows, glass, frame and sash	8

Table 6-2 Sustained Load Statistics

Usage Type	Occupancy	Mean (psf)	Std (psf)	Area (ft ²)
Office Building	Offices	10.9	5.9	200
Residential	Renter	6	2.6	200
Residential	Owner	6	2.6	200
Residential	Attic	2	0.87	200
Commercial	Default	10	5	200
Hotel	Guest room	4.5	1.2	200
School	Classrooms	12	2.7	1,000

The debris distribution matrix defines how the debris is distributed among the four debris types (wood, masonry, metal, and other). As shown in Table 6-3, for each building component, four numbers are given which represent the portion of debris in each debris type. For example, for combined wood and masonry exterior wall, 45% of the debris is wood, 45% of the debris is masonry, 5% of the debris is metal, and the remaining 5% of the debris is other. Even though most of the time, the debris distribution is intuitive and readily determined (such as metal shingle, plywood deck, and fibrous glass insulation), there are still cases that require engineering judgment.

Table 6-3 Debris Distribution Matrix

Category	Type	Wood	Masonry	Metal	Other
Ceiling	Gypsum board (2 mm thickness)	0.00	0.00	0.00	1.00
	Gypsum board or plaster on wood furring	0.10	0.00	0.00	0.90
	Suspended metal lath and gypsum plaster	0.00	0.00	0.15	0.85
	Suspended steel channel system	0.00	0.00	1.00	0.00
Content	Commercial	0.30	0.00	0.20	0.50
	Residential	0.60	0.00	0.00	0.40
Exterior Wall	Combined wood and masonry	0.45	0.45	0.05	0.05

Category	Type	Wood	Masonry	Metal	Other
	Unreinforced and reinforced Masonry	0.00	0.90	0.05	0.05
	Wood	0.90	0.00	0.05	0.05
Exterior Wall Siding	Aluminum siding, metal panel	0.00	0.00	1.00	0.00
	Brick veneer, block	0.00	1.00	0.00	0.00
	Stone veneer, vinyl, stucco	0.00	0.00	0.00	1.00
	Wood	1.00	0.00	0.00	0.00
Floors	Commercial (concrete)	0.05	0.00	0.05	0.90
	Commercial (steel joist, flat form, concrete)	0.00	0.00	0.40	0.60
	Commercial (steel joist/truss)	0.00	0.00	0.80	0.20
	Residential	0.70	0.00	0.00	0.30
Garage Doors	All	0.00	0.00	1.00	0.00
Insulation	Fibrous glass, All other	0.00	0.00	0.00	1.00
Interior Partition	50% Concrete, 50% Wood Stud	0.10	0.00	0.00	0.90
	Concrete Block	0.00	0.00	0.00	1.00
	Movable Steel Partition	0.00	0.00	0.90	0.10
	Steel stud	0.00	0.00	0.20	0.80
	Wood stud	0.20	0.00	0.00	0.80
Regular Doors	All	0.90	0.00	0.00	0.10
Roof Cover	Asphalt shingle, asbestos shingle, flat tile, other tile, Slate, built-up roof, single-ply membrane, and Other	0.00	0.00	0.00	1.00
	Metal shingle, metal panel	0.00	0.00	1.00	0.00
	Wood shake	1.00	0.00	0.00	0.00
Roof Deck	Concrete	0.00	0.00	0.00	1.00
	Plywood, T&G, OSB, Dimensional lumber, Batten	1.00	0.00	0.00	0.00
Roof Frame	Metal truss	0.00	0.00	1.00	0.00
	Wood truss, wood joist, post and beam	1.00	0.00	0.00	0.00
Skylight	All	0.00	0.00	0.10	0.90
Sliders	All	0.00	0.00	0.10	0.90
Windows	All	0.20	0.00	0.10	0.70

6.1.2 Default Component Construction Types for Commercial Buildings

For components that are not specified in the model building, the default construction types are assumed to be the same as those specified in the RSMeans (2001). Table 6-4 lists the indices of the construction types for roof frame, insulation, partition construction, floor construction, floor finish, ceiling finish, and wall finish. The descriptions and weights for related indices are listed in Table 6-5, Table 6-6, Table 6-7, Table 6-8, Table 6-9, Table 6-10, and Table 6-11, respectively. The weights for floor finish and wall finish are calculated based on their finish composition.

Table 6-4 Default Building Component Construction Types

Building Type	Roof Frame (ID Number in Table 6-5)	Insul. (ID Number in Table 6-6)	Partit. Const. (ID Number in Table 6-7)	Floor Const. (ID Number in Table 6-9)	Floor Finish (ID Number in Table 6-8)	Ceiling Finish (ID Number in Table 6-11)	Wall Finish (ID Number in Table 6-10)
Apartment, One-Three Stories	6	5	5	7	9	11	13
Apartment, Four-Seven Stories	6	5	5	7	9	11	13
Apartment, 8-24 Stories	6	5	6	7	9	11	13
Auditorium	9	5	4	7	23	14	14
Bank	1	5	7	10	3	7	5
Bowling Alley	6	5	3	10	34	14	21
Bus Terminal	6	5	3	10	6	7	20
Car Wash	6	5	3	10	36	17	21
Church	5	7	10	10	33	17	21
Club, Country	11	10	7	10	1	5	2
Club, Social	6	5	3	10	10	7	10
College, Classroom, Two-Three Stories	6	5	3	7	22	7	19
College, Dorm, Two-Three Stories	2	5	6	2	24	1	19
College, Dorm, Four - Eight Stories	3	5	3	3	24	7	19
College, Laboratory	6	5	3	5	11	7	8
College, Student Union	2	5	7	2	5	14	5
Community Center	6	5	7	10	5	7	21
Courthouse, One-Story	1	5	10	10	12	4	12
Courthouse, Two-Tree Stories	3	5	10	3	12	4	12

Building Type	Roof Frame (ID Number in Table 6-5)	Insul. (ID Number in Table 6-6)	Partit. Const. (ID Number in Table 6-7)	Floor Const. (ID Number in Table 6-9)	Floor Finish (ID Number in Table 6-8)	Ceiling Finish (ID Number in Table 6-11)	Wall Finish (ID Number in Table 6-10)
Factory, One-Story	6	5	4	10	34	2	21
Factory, Three-Story	2	5	7	2	31	2	21
Fire Station, One-Story	6	5	4	10	8	2	21
Fire Station, Two-Story	6	5	4	7	8	2	21
Fraternity/Sorority House	10	3	7	6	16	3	21
Funeral Home	11	6	5	10	18	2	7
Garage, Auto Sales	6	5	7	10	8	2	21
Garage, Parking	12	10	3	10	36	17	21
Garage, Underground Parking	1	10	3	1	36	17	21
Garage, Repair	6	5	4	10	31	3	21
Garage, Service Station	11	5	4	10	34	10	21
Gymnasium	5	6	4	10	30	7	4
Hangar, Aircraft	6	2	4	10	36	17	21
Hospital, Two-Three Stories	1	5	6	1	13	15	1
Hospital, Four-Eight Stories	6	5	5	3	13	15	1
Hotel, Four-Seven Stories	6	5	5	3	24	7	17
Hotel, 8-24 Stories	6	5	5	7	24	11	17
Jail	3	5	3	3	20	7	21
Laundromat	6	5	7	10	34	2	21

Building Type	Roof Frame (ID Number in Table 6-5)	Insul. (ID Number in Table 6-6)	Partit. Const. (ID Number in Table 6-7)	Floor Const. (ID Number in Table 6-9)	Floor Finish (ID Number in Table 6-8)	Ceiling Finish (ID Number in Table 6-11)	Wall Finish (ID Number in Table 6-10)
Library	4	5	7	4	4	7	21
Medical Office, One-Story	11	3	5	10	5	7	5
Medical Office, Two-Story	6	5	5	7	5	7	6
Motel, One-Story	11	3	5	10	27	10	18
Motel, Two-Three Stories	7	5	3	28	8	18	8
Movie Theatre	6	5	4	4	7	21	7
Nursing Home	8	5	7	32	9	6	9
Office, Two-Four Stories	6	5	7	9	7	9	7
Office, 5-10 Stories	6	5	7	9	3	9	7
Office, 11-20 Stories	6	5	7	9	3	9	7
Police Station	6	5	4	20	7	18	7
Post Office	6	5	4	8	10	21	7
Racquetball Court	6	5	6	25	7	21	7
Religious Education	6	5	4	5	10	21	7
Restaurant	11	3	7	14	10	16	7
Restaurant, Fast Food	6	5	7	35	10	21	7
Rink, Hockey/Indo or Soccer	6	5	3	26	10	21	7
School, Elementary	6	5	4	15	10	15	7
School, High, Two-Three Stories	2	5	4	21	2	15	7

Building Type	Roof Frame (ID Number in Table 6-5)	Insul. (ID Number in Table 6-6)	Partit. Const. (ID Number in Table 6-7)	Floor Const. (ID Number in Table 6-9)	Floor Finish (ID Number in Table 6-8)	Ceiling Finish (ID Number in Table 6-11)	Wall Finish (ID Number in Table 6-10)
School, Jr. High, Two-Three Stories	6	5	4	7	7	3	7
School, Vocational	6	5	4	21	7	3	7
Store, Convenience	11	3	7	34	10	21	7
Store, Department, One-Story	7	5	7	4	10	21	7
Store, Department, Three-Story	6	5	7	2	3	11	7
Store, Retail	6	5	7	34	10	21	7
Supermarket	6	5	2	34	10	21	7
Swimming Pool, Enclosed	11	5	4	19	10	20	7
Telephone Exchange	6	5	7	29	10	21	2
Town hall, One-Story	6	5	7	17	10	18	7
Town Hall, Two-Three Stories	6	5	7	17	7	18	7
Warehouse	6	5	3	31	7	21	7
Warehouse, Mini	6	5	6	36	10	21	17

Table 6-5 Roof Frame Construction Types and Unit Weights

ID	Construction Type	Weight (psf)
1	Cast-in-place concrete slab	48.0
2	Concrete flat plate (8")	96.0
3	Concrete slab on metal deck and beam	34.0
4	Concrete waffle slab (10")	120.0
5	Laminated wood arches	3.0
6	Open web steel joist	17.5
7	Pre-cast concrete beam and plank	80.0
8	Pre-cast double tees	42.0

ID	Construction Type	Weight (psf)
9	Steel Truss	3.0
10	Wood Rafter	1.2
11	Wood Truss	2.0

Table 6-6 Insulation Types and Unit Weights

ID	Construction Type	Weight (psf)
1	Cellular glass insulation (4" thick)	2.8
2	Fiberboard	1.5
3	Fiberglass sheets	1.5
4	Fibrous glass insulation (4" thick)	4.4
5	Perlite/EPS composite	0.8
6	Polyisocyanurate sheets	0.4
7	Polystyrene (2" thick)	0.4
8	Rigid insulation, 1/2"	0.8
9	Urethane foam with skin	0.5

Table 6-7 Partition Construction Types and Unit Weights

ID	Construction Type	Weight (psf)
1	2x4 unplastered wood or metal studs	4
2	50% concrete block, 50% gypsum board on metal studs	22
3	Concrete block	36
4	Concrete block and toilet partitions	26
5	Gypsum board and sound deadening board on wood or metal studs	15
6	Gypsum board on concrete block and metal studs	32
7	Gypsum board on wood or metal studs	8
8	Lightweight concrete block	24
9	Movable steel partitions	4
10	One side plaster on wood or metal studs	12
11	Two sides plaster on wood or metal studs	20

Table 6-8 Floor Finish Types and Unit Weights

ID	Finish Type	Weight (psf)
1	50% carpet, 30% hardwood, 20% ceramic tile	6.8
2	50% carpet, 40% marble tile, 10% terrazzo	17.4

ID	Finish Type	Weight (psf)
3	50% carpet, 40% vinyl composition tile, 10% quarry tile	3.7
4	50% carpet, 50% ceramic tile	12.5
5	50% carpet, 50% vinyl composition tile	1.5
6	50% quarry tile, 50% vinyl composition tile	12.0
7	50% vinyl composition tile, 30% carpet, 20% terrazzo	7.5
8	50% vinyl composition tile, 50% paint	0.5
9	60% carpet, 30% vinyl composition tile, 10% ceramic tile	3.8
10	60% carpet, 35% hardwood, 5% ceramic tile	3.8
11	60% epoxy, 20% carpet, 20% vinyl composition tile	5.0
12	60% hardwood, 20% carpet, 20% terrazzo	9.2
13	60% vinyl composition tile, 20% ceramic tile, 20% terrazzo	11.6
14	65% carpet, 35% quarry tile	9.4
15	65% vinyl composition tile, 25% carpet, 10% terrazzo	4.4
16	70% carpet, 10% hardwood, 20% ceramic tile	6.4
17	70% carpet, 15% terrazzo, 15% vinyl composition tile	6.4
18	70% carpet, 30% ceramic tile	8.3
19	70% terrazzo, 30% ceramic tile	29.3
20	70% vinyl composition tile, 20% carpet, 10% ceramic tile	3.4
21	70% vinyl composition tile, 20% carpet, 10% terrazzo	4.3
22	70% vinyl composition tile, 25% carpet, 5% ceramic tile	2.4
23	70% vinyl composition tile, 30% carpet	1.3
24	80% carpet, 10% vinyl composition tile, 10% ceramic tile	4.0
25	80% carpet, 20% ceramic tile	6.2
26	80% rubber mat, 20% paint	1.6
27	85% carpet, 15% ceramic tile	5.2
28	85% carpet, 5% vinyl composition tile, 10% ceramic tile	4.1
29	90% carpet, 10% terrazzo	5.0
30	90% hardwood, 10% ceramic tile	5.9
31	90% metallic hardener, 10% vinyl composition tile	1.9
32	95% vinyl tile, 5% ceramic tile	2.1
33	Carpet	2.0
34	Vinyl composition tile	1.0
35	Quarry tile	23.0

Table 6-9 Floor Construction Types and Unit Weights

ID	Construction Type	Weight (psf)
1	Cast-in-place concrete beam and slab	120.0
2	Concrete flat plate	120.0
3	Concrete slab with metal deck and beams	38.0
4	Concrete waffle slab	120.0
5	Metal deck on open web steel joist	17.5
6	Wood joist	6.0
7	Open web steel joists, slab form, concrete	30.0
8	Pre-cast concrete beam and plank	80.0
9	Pre-cast double tees with concrete topping	58.0

Table 6-10 Wall Finish Types and Unit Weights

ID	Construction Type	Weight (psf)
1	40% vinyl wall covering, 35% ceramic tile, 25% epoxy coating	8.5
2	40% vinyl wall covering, 40% paint, 20% ceramic tile	5.0
3	50% paint, 40% glazed coating, 10% ceramic tile	2.3
4	50% paint, 50% ceramic tile	11.5
5	50% paint, 50% vinyl wall covering	0.5
6	50% vinyl wall covering, 45% paint, 5% ceramic tile	1.7
7	50% wallpaper, 25% wood paneling, 25% paint	1.1
8	60% paint, 40% epoxy coating	0.0
9	60% vinyl wall covering, 40% paint	0.6
10	65% paint, 25% vinyl wall covering, 10% ceramic tile	2.6
11	70% paint, 20% vinyl wall covering, 10% ceramic tile	2.5
12	70% paint, 20% wood paneling, 10% vinyl wall covering	0.9
13	70% paint, 25% vinyl wall covering, 5% ceramic tile	1.4
14	70% paint, 30% epoxy coating	0.0
15	75% paint, 15% glazed coating, 10% ceramic tile	2.3
16	75% paint, 25% ceramic tile	5.8
17	75% vinyl covering, 20% paint, 5% ceramic tile	1.9
18	90% paint, 10% ceramic tile	2.3
19	95% paint, 5% ceramic tile	1.2
20	Glazed coating	0.0
21	Paint	0.0

Table 6-11 Ceiling Finish Types and Unit Weights

ID	Finish Type	Weight (psf)
1	90% paint, 10% suspended fiberglass board	0.2
2	Fiberglass board on exposed grid system	3.0
3	Gypsum board on wood furring	4.5
4	Gypsum plaster on suspended metal lath	10.0
5	Gypsum plaster on wood furring	10.0
6	Mechanical duct allowance	4.0
7	Mineral fiber tile on concealed zee bars	2.0
8	Textured finish	0.2
9	Painted gypsum board	2.0
10	Painted gypsum board on furring	3.0
11	Painted gypsum board on resilient channels	2.0
12	Plaster on tile or concrete	5.0
13	Plaster on wood lath	8.0
14	Suspended fiberglass board	1.5
15	Suspended metal lath and cement plaster	15.0
16	Suspended steel channel system	2.0

6.2 Building Debris Validation Studies

USACE is often the principal organization assigned by FEMA to be responsible for debris clean-up and removal. Other SLTT agencies may also coordinate the debris clean-up efforts. USACE after action reports are the most readily available sources for model validation and testing. These reports contain information on the total amount (either by volume or by weight) of debris produced by hurricanes. However, since the after action reports do not differentiate burnable roadside debris from construction and demolition debris, assumptions have to be made to the ratio of these two types of debris (recall that only construction and demolition debris is estimated by the present debris model), which is not ideal for a validation study. Therefore, references were made to a number of published papers on debris removal (Dowd, 1990; Tansel, 1993, Dewberry and Davis, 1993) to identify appropriate cases for model validation.

After Hurricane Andrew, Tansel (1993) carried out a detailed debris analysis for five zones with significant structural damage in Dade County, Florida. Table 6-12 lists the zone location, number of buildings, exterior wall construction distribution, average exterior damage ratio, and total structural debris for each of the five zones investigated. The amount of structural debris was estimated based on an average type of residence and structural damage states. The damage statistics in each zone were calculated using the data collected by the Metro-Dade County Building and Zoning Department. Structures with more than 50% damage were judged uninhabitable and assumed to be demolished. The debris simulation is performed using model buildings with different combinations of the number of stories (One-story or Two-story), roof shape (hip or gable), wall construction (wood frame or masonry), nail size (6d or 8d), and roof cover type (shingle or tile). The total debris produced by each model

building under the simulated wind speed in each zone is calculated and then aggregated within the zone to obtain the average amount of debris per building (weighted by the assumed building stock). The total amount of structural debris in each zone is calculated by multiplying the average amount of debris per building with the total number of buildings in that zone. For Dade County, the building stock is modeled, assuming 80% of the homes are single-story. 75% of the homes are assumed to have gable roofs, and 25% of the homes are assumed to have hip roofs. The number of homes having shingle roof cover is assumed to be the same as that having tile roof cover. 40% of the homes are assumed to use 6d nails on the roof deck, and the remaining homes are assumed to use 8d nails. All the homes are assumed to have straps for roof-to-wall connection. The distribution of exterior wall construction types in each zone is assumed to be the same as that listed in Table 6-12. The exterior wall construction distribution for Zone 4, which is not given in the paper by Tansel (1993), is assumed to be the same as that of Zone 5 (in the same zip code). Table 6-12 also shows the simulated average debris weight per building, average debris volume per building, total structural debris weight in each zone, and the ratio between simulated and actual debris in each zone. The mean of the model-to-actual ratios is 1.05, and the standard deviation is 0.58. The result is very promising, given that the debris model relies heavily on engineering judgment.

Table 6-12 shows debris comparisons for hurricanes Hugo and Andrew at a regional level. Dowd (1990) reported the debris removal and channel shoaling of USACE for hurricane Hugo. Political subdivisions made 359 requests to FEMA, and an estimated 15,500,000 cubic yards of debris were removed by or for these subdivisions. USACE assisted and administrated the debris removal mission in seven counties in South Carolina (Berkeley, Charleston, Darlington, Dorchester, Lancaster, Orangeburg, and Sumter), with a total of 4,589,559 cubic yards of debris removed. Tansel (1993) estimated that Hurricane Andrew generated 2.9 million tons of construction and demolition debris. The USACE after action report (USACE, 1993) gives an estimate of 40 million cubic yards of debris in Dade County.

The process for debris simulation is performed at a zip code level. Similar to the first validation study, the average debris weight and volume per building in each zip code are simulated first (using the assumed building stock). The total debris weight or volume in each zip code is then calculated by multiplying the total number of houses in each zip code with the average debris weight or volume per building. The total amount of debris in the Study Region is estimated by adding up the total debris in each zip code. The default building stock in Dade County is assumed to be the same as that in the first validation study and the default building stock for South Carolina is assumed to be: 70% one-story and 30% two-story; 75% gable and 25% hip; 30% using 6d nails and 70% using 8d nails; 10% using straps and 90% using toe-nails for roof-to-wall connection. The total number of houses in each zip code is estimated using 1990 Census data. As shown in Table 6-13, the debris model underestimated the debris volume in South Carolina and overestimated debris volume in the regions administrated by USACE (seven counties).

Table 6-12 Structural Debris Comparison for Hurricane Andrew

Zone (zip code)	Actual Data				Simulation Results			Model to Actual Ratio
	Number of Buildings	Exterior Wall Construction Distribution	Average Exterior Damage Ratio	Structural Debris (tons)	Average Debris Weight per Building (lb.)	Average Debris Volume per Building (yard ³)	Total Structural Debris (tons)	
Zone 1 (33186)	14,000	85% wood frame	63%	182,650	27,252	145	173,215	0.95
Zone 2 (33156)	18,000	75% concrete	24%	456,365	25,864	127	211,364	0.46
Zone 3 (33156)	604	50% wood frame; 50% concrete	53%	11,376	24,665	125	6,764	0.59
Zone 4 (33031)	2,500	-	48%	42,900	53,232	264	60,418	1.41
Zone 5 (33031)	1,100	85% wood frame	47%	14,390	53,232	264	26,584	1.85

Table 6-13 Debris Comparison for Hurricanes Hugo and Andrew

Storm	Region	Actual Weight (tons)	Actual Volume (yard ³)	Modeled Weight (tons)	Modeled Volume (yard ³)	Model/ Actual (weight)	Model/ Actual (volume)
Hugo	South Carolina	-	15,500,000	951,009	9,130,843	-	0.59
Hugo	USACE Admin. Region	-	4,589,559	782,480	7,366,394	-	1.61
Andrew	Dade County	2,900,000	40,000,000	3,396,991	35,323,080	1.17	0.88

For Hurricane Andrew, both the modeled debris weight and debris volume are reasonably close to the actual values. It is not clear in the paper by Dowd (1990) whether all the political subdivisions that made requests to FEMA for debris removal assistance are within South Carolina. Therefore, the actual Study Region may cover a larger area than the state of South Carolina, which may help to explain the underestimation of debris volume by the model. The overestimation of the debris volume in the USACE administrated region may likely be the opposite. The Study Region may only include portions (most likely just municipalities) of the seven counties that were mentioned in the paper.

6.3 Description of Tree Debris Methodology

6.3.1 Total Weight and Volume of Downed Trees

The tree debris module combines the tree coverage database and the tree blowdown module to produce estimates of tree debris weight by Census tract (or Census block in combined wind/flood Study Regions). The tree debris weight reported by Hazus is the expected green weight of trees greater than

30 feet tall that are expected to fail at a given wind speed for a given density of trees. The entire weight is reported as debris, even though tree debris in unpopulated areas may not be collected.

Hazus computes the total weight of tree debris based on the modeled wind speed and the density of trees for the Census tract (or block). The tree blowdown functions presented in Section 5.3 are converted to debris functions by relating the C_dLAI values (where C_d is a drag coefficient and LAI is the Leaf Area Index) to the number of trees per acre and multiplying the probability of blowdown values by the total expected weight of trees per acre, for the given type, height, and density of trees. Figure 6-1 shows the tree debris functions implemented in Hazus.

Research into appropriate bulking factors to be used to convert the weight of tree debris to volume has revealed a wide range of factors used by various sources. Table 6-14 shows bulking factors developed from several sources as part of the development of the tree debris model created for the software.

Table 6-14 Tree Debris Related Bulking Factors from Various Sources

Source	Description	Bulking Factor (CY/ton*)
FEMA 9580.1	Woody Debris	4
SC Dept of Health and Environmental Control	Wood Chips	4
MS Dept of Environmental Quality	Uncompacted Limbs and Leaves	12
CA Integrated Waste Management Board	Large Limbs and Stumps	1.85
	Mixed Yard Trimmings	18.5
	Wood Chips	4
	Prunings, Dry	54
	Prunings, Wet	43
	Prunings, Shredded	3.8
	Leaves, Dry	5.8
	Leaves	24
Solid Waste Authority of Palm Beach County, FL	Vegetative Debris	5.5
Alachua County, FL Public Works Department	Hurricane Debris from Frances and Jeanne	10.5
City of Honolulu, HI Refuse Department	Uncompacted Yard Waste	8
	Compacted Yard Waste	4.6
	Wood Chips	4
	Loose Brush	10

*CY/ton = cubic yard per ton

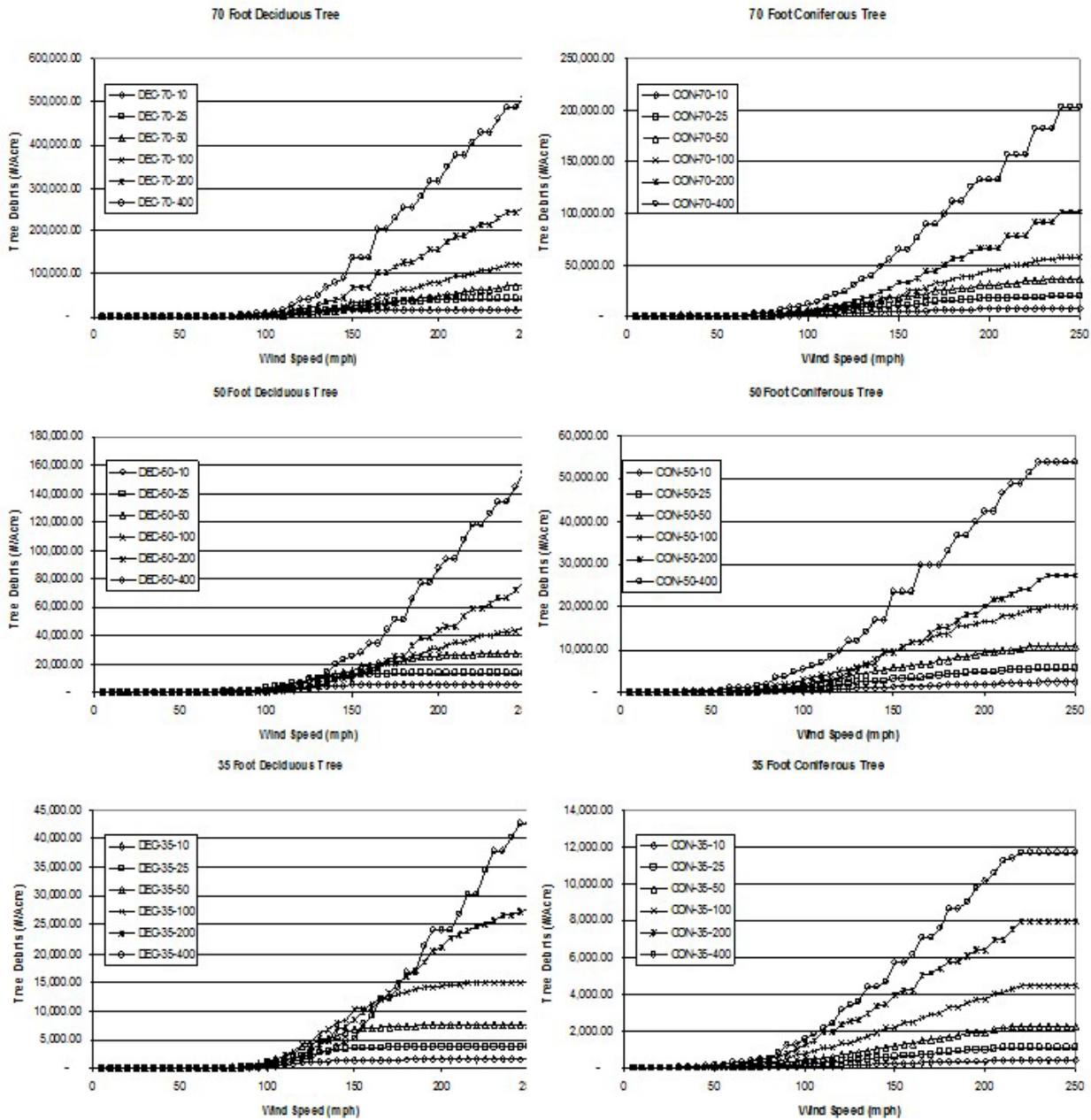


Figure 6-1 Tree Debris Functions in Pounds per Acre

Based on the data presented in Table 6-14, it appears that the actual bulking factor should be based on a number of different types of debris – from leaves and loose brush to large limbs and stumps. It is also likely that the appropriate bulking factor will be a function of the strength of the hurricane. The majority of tree debris from weaker storms will be the result of failed limbs within the crown and will not include very many entire trees or stumps. In contrast, stronger storms will cause more complete tree uprooting and devastating crown damage and result in denser tree debris.

A bulking factor of four is more appropriate for chipped or compacted tree debris, while a factor of 10 represents bulkier, uncompacted, unclipped debris. For the base estimation of tree debris volume, the

bulking factor in Hazus is now taken as 10 cubic yards per ton to represent uncompacted and unchipped debris. Users performing an advanced analysis are encouraged to develop their own local bulking factors based on the relationship between tree debris volume and weight from earlier or current hurricanes affecting their areas, and/or modifying the bulking factor to reflect their local debris chipping/compacting procedures.

6.3.2 Tree Debris Collection Model

The methodology for estimating tree debris collection quantities is based on building density, length of roads, and Census block shapes. This empirical method is based on the concept that trees downed in close proximity to streets, highways, or buildings make up the great majority of trees brought to the curb for collection and disposal. As such, an area reduction factor was developed based on a predetermined collection area around each of the streets and buildings within a Study Region.

The model applies a reduction factor to the overall estimate of downed trees currently produced, as described in Section 6.3.1. The tree debris collection model is expressed in Equation 6-7.

Equation 6-7

$$D_c = \sum_{i=1}^n D_i * \frac{A_{ci}}{A_{Ti}}$$

Where:

- D_c is the tree debris collected
- D_i is the total tree debris predicted by Hazus for Census block i
- A_{ci} is the collection area calculated for Census block i
- A_{Ti} is the total area of Census block i
- n is the number of Census blocks in the Study Region

The model was developed by running Hazus at the Census block level. The Census block level was chosen because the boundaries of Census blocks are most often represented by highways, streets, and roads with relatively few streets contained inside. A method for aggregating Census block factors to the Census tract level for Study Regions defined at the Census tract level is discussed in Section 4.4.5.

The collection area (A_{ci}) for each Census block is first calculated based on the density of buildings within the Census block (buildings per acre). As a baseline, it is assumed that downed trees will be picked up for an area of one acre per building in the Census block, with a maximum collection area set to the area of the Census block. The result is that all tree debris is assumed to be collected in Census blocks when the building density is equal to or greater than one building per acre.

For Census blocks with building densities lower than one building per acre, the model also determines an alternative collection area along the Census block perimeter and any roads within the Census block.

The depth of this perimeter collection area varies based on the building density of the Census block because areas with little or no development will only have enough trees cleared to keep the roads safe for travel. The depth of the perimeter collection area varies from 25 to 200 feet linearly as building density varies from 0 to 1 building per acre.

Twenty-five feet was chosen as the minimum depth for the perimeter collection area to account for trees that fall into roadways and rights of way in undeveloped areas. Two hundred feet was chosen as the upper bound, to be consistent with the building-based collection area described above, because a 200 foot by 200-foot square is approximately one acre in area.

The perimeter collection area is calculated in the following manner:

- The perimeter and area of each Census block are calculated.
- The ratio of the square root of the area to the perimeter is then used to approximate the aspect ratio of each Census block. This ratio is 0.25 for square blocks and approaches 0.0 for long slender blocks.
- From the aspect ratio and total area of each block, the width and length of an equivalent rectangle are determined.
- Perimeter collection areas are calculated for each block using the approximate length and width with the perimeter collection area depth, as shown in Figure 6-2.
- For Census blocks that contain roads within their boundaries, an interior road collection area is calculated using the length of the interior roads and the depth of the perimeter collection area determined above. This area is added to the perimeter collection area.
- The perimeter collection area is then compared to the building-based collection area (number of buildings times one acre). The larger of the two areas is retained as the total collection area (A_{Ci}), provided that the area is less than the overall Census block area.

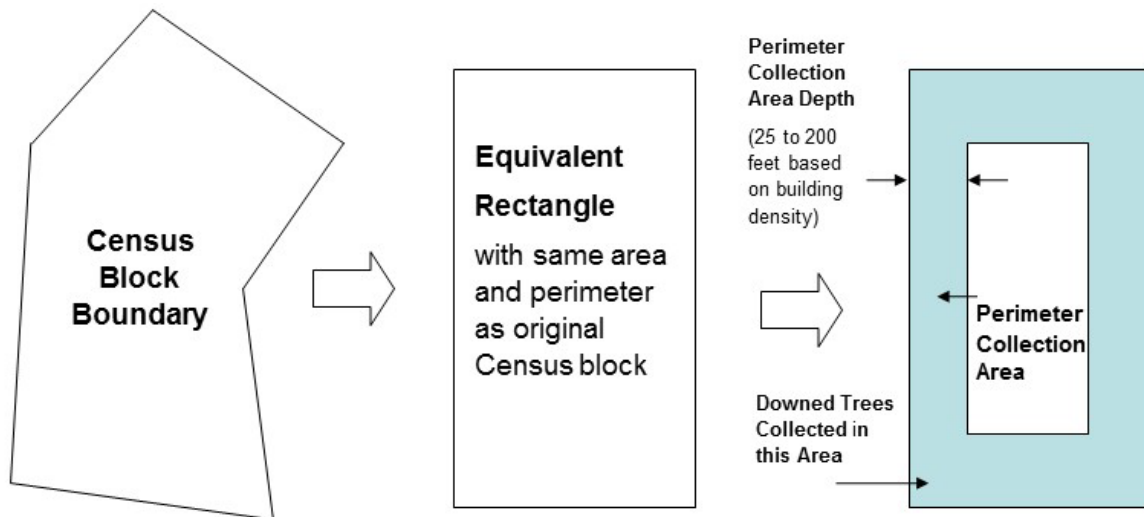


Figure 6-2 Calculation of Perimeter Collection Area

The presence and length of interior roads present inside each Census block were determined by overlaying Esri Streetmap USA data on the Hazus Census blocks.

Figure 6-2 shows the relationship between equivalent Census block width and building density for each Census block analyzed in the Hampton Roads region of Virginia. The equivalent Census block width is defined as the smaller dimension of the equivalent rectangular area calculated for each Census block. The different series in the graph represent different ranges of the calculated tree debris collection factors (A_{Ci}/A_{Ti}). The collection factors are:

- Less than 0.5 for Census blocks that are substantially wider than four times the perimeter collection area depth and/or that have less than 0.5 buildings per acre
- Equal to 1.0 for Census blocks with widths less than or equal to twice the perimeter collection area depth and/or with more than one building per acre
- Between 0.5 and 1.0 for Census blocks that have widths between two and four times the perimeter collection area depth and/or building densities between 0.5 and 1.0 buildings per acre

Thus, Figure 6-3 shows that only wide Census blocks with low building densities are assigned collection factors less than 0.5.

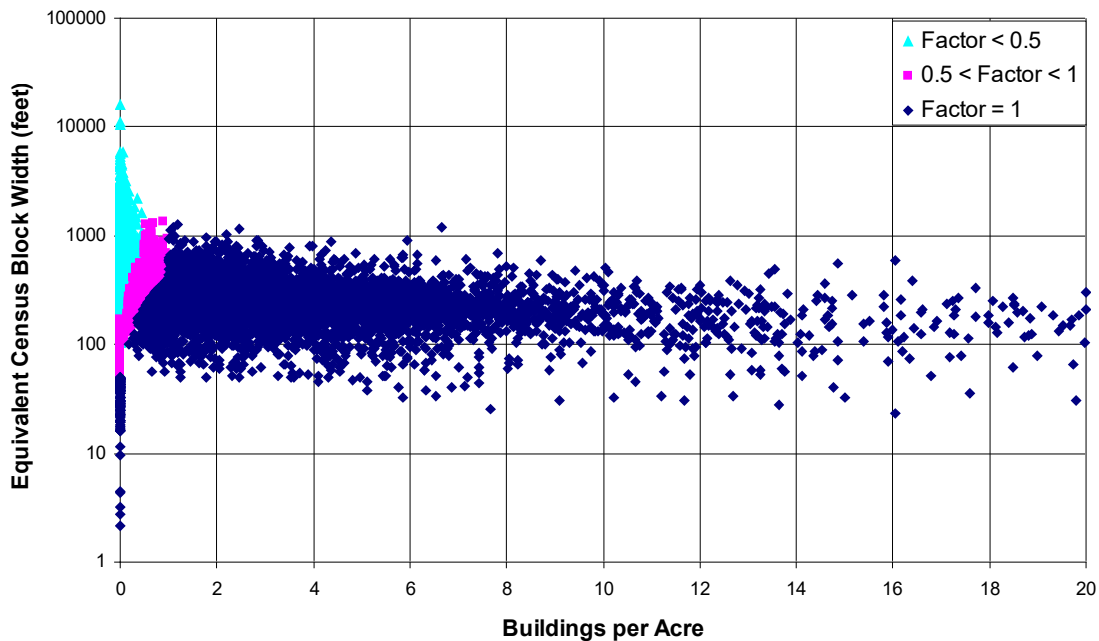


Figure 6-3 Equivalent Census Block Width versus Buildings per Acre for Hampton Roads Region of Virginia

The resulting factors are then applied to the Hazus results for tree debris quantities for each Census block.

6.3.3 Implementing into Hazus

Factors for all Census blocks are pre-calculated for inclusion in Hazus. These reduction values are stored in the “Tree Parameters” table in the “Tree Debris Collection Factor” column, as shown in Figure 6-4. Like the other tree parameter data, this field could also be modified by the user if more detailed information is available for individual areas at the local level.

Hazus multiplies both the weight and volume of tree debris estimates in the debris analysis results table by the collection factors and then presents two columns of output, as indicated in Figure 6-5.

Requiring that this analysis be completed at the Census block level greatly increases the time it takes to run Hazus. In order to accommodate analyses, run at the Census tract level, the factors developed for individual Census blocks are aggregated to the Census tract level using the following equation:

Equation 6-8

$$F_{CT} = \sum_{i=1}^n \left[\frac{(A_{CBi} * F_{CBi})}{\sum_{i=1}^n A_{CBi}} \right]$$

Where:

- F_{CT} is the tree debris collection factor for a given Census tract
- A_{CBi} is the area of Census block i
- F_{CBi} is the tree debris collection factor for Census block i (A_{Ci}/A_{Ti})
- A_{CT} is the area of corresponding Census tract
- n is the number of Census blocks in the current Census tract

If Hazus is run using uniform tree characteristics within each Census tract (as is the case with the baseline data provided in Hazus), identical estimates of tree debris generation and collection will be produced regardless of whether the analysis is run at the Census tract or Census block level. However, if the tree parameter data is changed such that the data vary by Census block within a Census tract, then results will differ and Hazus must be run at the Census block level for the desired results.

	Census Tract	Predominate Tree Type	Stems per Acre	Tree Height Less 40 ft	Tree Height 40 ft To 60 ft	Tree Height Greater than 60 ft	Tree Collection Factor
1	37183050100	Mixed	20	36	38	26	0.57
2	37183050300	Deciduous	45	36	38	26	0.82
3	37183050400	Deciduous	49	36	38	26	0.69
4	37183050500	Mixed	89	36	38	26	0.73
5	37183050600	Mixed	59	36	38	26	0.75
6	37183050700	Mixed	99	36	38	26	0.77
7	37183050800	Mixed	99	36	38	26	0.44
8	37183050900	Deciduous	46	36	38	26	0.70
9	37183051000	Deciduous	38	36	38	26	0.80
10	37183051100	Mixed	51	36	38	26	0.19
11	37183051200	Deciduous	59	36	38	26	0.82
12	37183051400	Mixed	91	36	38	26	0.96
13	37183051501	Mixed	130	36	38	26	0.87
14	37183051502	Mixed	113	36	38	26	0.91
15	37183051600	Mixed	111	36	38	26	0.97
16	37183051700	Mixed	122	36	38	26	0.77
17	37183051800	Mixed	67	36	38	26	0.78
18	37183051900	Mixed	114	36	38	26	0.82
19	37183052001	Mixed	97	36	38	26	0.43
20	37183052002	Mixed	104	36	38	26	0.93
21	37183052101	Mixed	125	36	38	26	0.64
22	37183052102	Mixed	150	36	38	26	0.26

Figure 6-4 Addition of Tree Collection Factor to Tree Parameter Table in Hazus

	Census Tract	Brick/Wood (1 tons)	Concrete/Steel (1 tons)	Eligible Tree Weight (tons)	Eligible Tree Volume (cu. yards)	Trees (1 tons)	Tree Volume (1 cu. yards)
1	37183050100	178.00	0.00	90.06	324.54	158.00	569.36
2	37183050300	127.00	0.00	40.18	144.45	49.00	176.16
3	37183050400	64.00	0.00	45.54	164.26	66.00	238.06
4	37183050500	119.00	0.00	186.15	669.01	255.00	916.46
5	37183050600	90.00	0.00	92.25	331.59	123.00	442.12
6	37183050700	74.00	0.00	111.65	401.89	145.00	521.93
7	37183050800	72.00	0.00	72.16	259.99	164.00	590.89
8	37183050900	75.00	0.00	51.80	187.51	74.00	267.88
9	37183051000	101.00	0.00	50.40	180.72	63.00	225.89
10	37183051100	11.00	0.00	30.40	109.29	160.00	575.23
11	37183051200	110.00	0.00	58.22	210.32	71.00	256.48
12	37183051400	139.00	0.00	165.12	593.60	172.00	618.33
13	37183051501	91.00	0.00	249.69	900.02	287.00	1,034.51
14	37183051502	72.00	0.00	190.19	683.06	209.00	750.61
15	37183051600	122.00	0.00	288.09	1,036.23	297.00	1,068.28
16	37183051700	100.00	0.00	284.13	1,023.68	369.00	1,329.45
17	37183051800	173.00	0.00	218.40	785.35	280.00	1,006.86
18	37183051900	125.00	0.00	262.40	944.07	320.00	1,151.30
19	37183052001	113.00	0.00	109.22	393.29	254.00	914.62
20	37183052002	112.00	0.00	257.61	926.87	277.00	996.63
21	37183052101	107.00	0.00	339.20	1,222.12	530.00	1,909.56
22	37183052102	57.00	0.00	176.76	636.68	491.00	1,768.57
23	37183052201	49.00	0.00	42.33	152.85	83.00	299.70
24	37183052202	127.00	0.00	315.02	1,134.23	829.00	2,984.80
25	37183052301	102.00	0.00	164.68	592.08	358.00	1,287.14
26	37183052302	141.00	0.00	268.92	968.45	747.00	2,690.14
27	37183052401	71.00	0.00	125.60	452.17	785.00	2,826.03
28	37183052402	223.00	0.00	336.24	1,209.89	467.00	1,680.40
29	37183052404	84.00	0.00	218.96	785.99	238.00	855.47

Figure 6-5 Hazus Debris Results Table

While the collection factors can be aggregated to the Census tract level as discussed, the tree debris generation and collection results are sensitive to whether tree parameters are tabulated at the block or the tract level.

Prior to Hazus 2.0, the tree parameter data were assumed to be the same for every Census block within a given Census tract. This situation can introduce substantial biases in the tree debris generation and collection estimates for rural counties where Census tracts are very large geographically, and there may be only one or two Census tracts for an entire county. One such area is Camden County, NC.

Tree fall frequencies surveyed in Camden County following Hurricane Isabel in 2003 demonstrated that tree coverage was scattered throughout the county with large areas of open land and smaller areas of clustered trees. Since Camden County has only one Census tract, Hazus considered the county to have uniform tree coverage prior to the release of Hazus 2.0.

In order to further investigate the MRLC (Multi-Resolution Land Characteristics) land use, land cover data was revisited for a rural, four-county Study Region in North Carolina. Tree density statistics were recalculated at the Census block level for Camden, Chowan, Gates, and Perquimans counties. The revised tree parameters were input into Hazus, and the Hurricane Isabel scenario was rerun. Table 6-15 summarizes the results of this reanalysis for these four counties.

The large reductions in debris generated and collected indicate that the tree debris estimation is sensitive to the tree parameter data that is input to the tree blowdown and debris collection models. This indicates that when running an advanced analysis with refined local data, it is desirable to reclassify the land use, land cover data by Census block when using Hazus to predict tree debris generation and collection quantities. This is especially true for rural counties with large Census tracts.

Table 6-15 Comparison of Modeled Tree Debris Generation and Collection Weight with Tree Parameters Compiled at the Census Tract and Census Block Levels

County Name	Tree Debris Generated (tons)			Tree Debris Collected (tons)		
	Standard Tree Parameters	Revised Tree Parameters	Percent Reduction	Standard Tree Parameters	Revised Tree Parameters	Percent Reduction
Camden	338,711	199,911	41.0%	9,453	6,199	34.4%
Chowan	311,757	264,208	15.3%	17,539	11,276	35.7%
Gates	1,130,284	889,938	21.3%	36,609	27,493	24.9%
Perquimans	540,251	314,369	41.8%	23,386	12,631	46.0%

6.3.4 Comparison of Modeled and Reported Tree Debris

This section describes the methodology and presents a comparison of a prototype implementation of the methodology with tree debris statistics received from the North Carolina and Virginia (Roarty, 2004) Departments of Emergency Management following Hurricane Isabel in 2003 (Roarty, 2004).

6.3.4.1 Example Tree Collection Data – Hurricane Isabel, North Carolina

Tree debris collection data were obtained from the North Carolina Department of Emergency Management to assess how the methodology performs on an actual storm. Data were available for all counties in North Carolina that filed for federal assistance for debris cleanup. The data for the counties analyzed in this study are presented in Table 6-16.

These data were compiled by the North Carolina Department of Emergency Management using tree debris quantities from project worksheets completed by local governments following Hurricane Isabel. The numbers represent a combination of actual and estimated tree debris quantities by county, based on their availability on the project worksheets. It is also important to note that there is a separate line noted for “State Agencies.” The debris quantity reported for this entry is likely to result from additional

debris collected from several of the affected counties studied. Because of this, the tree debris volumes reported by the county are likely to be slightly lower than actual. However, this volume is less than 2% of the total tree debris volume reported.

Hazus was run using a Hurricane Isabel scenario for the 20 North Carolina counties listed in Table 6-16. Figure 6-6 compares modeled tree debris weight (total and collected) to the actual weight of tree debris reported collected by the county in North Carolina for Hurricane Isabel (reported weights calculated from reported cubic yards with an assumed bulking factor of 10 cubic yards per ton). The series labeled “All Downed Trees” represents the total tree debris estimated by Hazus before applying the collection factors.

Table 6-16 North Carolina Tree Debris Collection Data for Hurricane Isabel (2003)

County	Tree Debris Volume (Cubic Yard)	Collection/Disposal Cost (\$)	Unit Cost (\$/Cubic Yard)
Beaufort	436,323	10,781,089	24.71
Bertie	82,222	932,359	11.34
Camden	706	28,765	40.74
Carteret	135,434	802,920	5.93
Chowan	476,768	3,704,690	7.77
Craven	52,729	453,677	8.60
Currituck	60,400	402,098	6.66
Dare	220,113	1,973,850	8.97
Gates	4,094*	45,688	11.16
Hertford	58,194	400,399	6.88
Hyde	48,503	384,263	7.92
Jones	3,414	44,924	13.16
Martin	69,951	283,732	4.06
Northampton	37,747	228,001	6.04
Onslow	8,881	260,441	29.33
Pamlico	4,697	159,095	33.87
Pasquotank	773,216	3,039,044	3.93
Perquimans	33,600	239,320	7.12
Tyrrell	3,700	43,424	11.74
Washington	152,404	361,538	2.37
State Agencies	53,121	974,307	18.34
Region Total	2,716,217	25,543,624	9.40

* Volume estimated from cost of removal

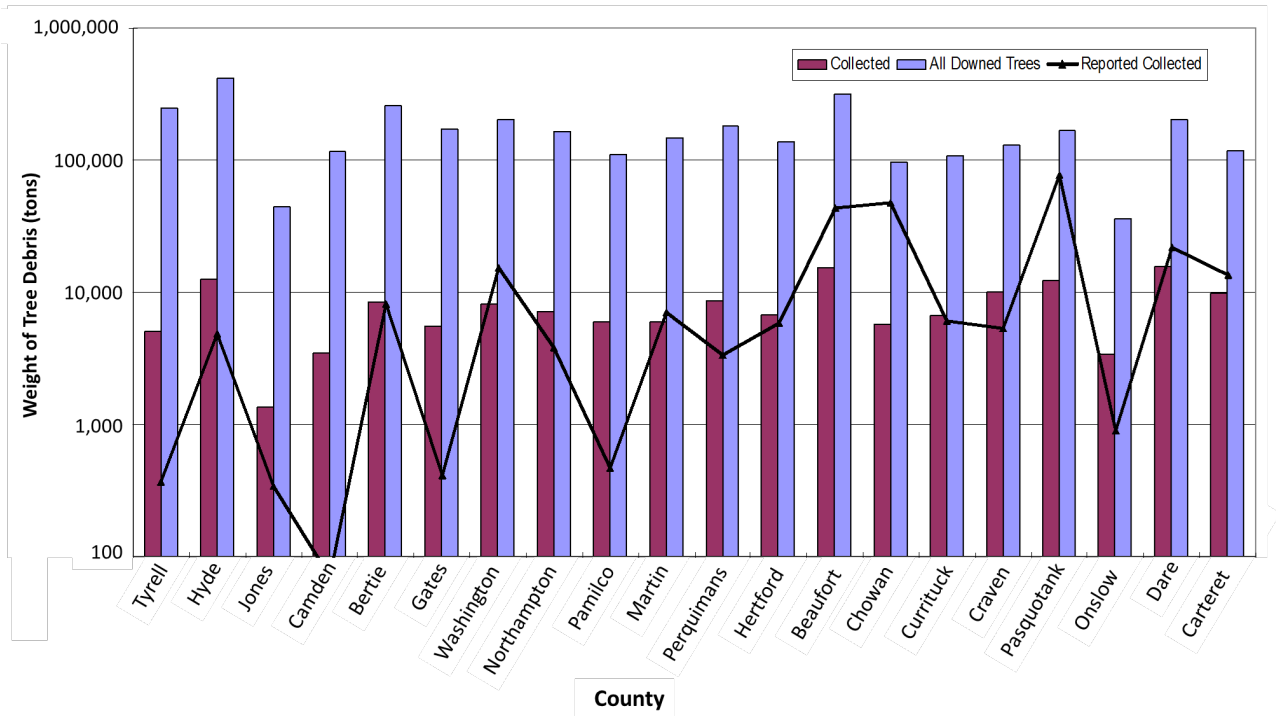


Figure 6-6 Comparison of Modeled Total and Collected Tree Debris Weight with Collection Totals Reported by NC Department of Emergency Management by County in North Carolina for Hurricane Isabel

In Figure 6-6, the county names along the x-axis are ordered by increasing average Census block building density. In other words, most rural counties appear on the left, and the least rural (most urban/suburban) appear on the right. There appears to be a trend of greater over prediction of tree debris for the more rural counties. It is not possible to determine whether this trend is due to an overestimate of the number of trees blown down, an overestimate of the collection factors in rural areas, an underreporting of tree debris collection in some rural counties, or some combination of the three.

The overall estimate of tree debris collected for the 20 North Carolina counties considered is about 41% lower than the actual totals collected by the Department of Emergency Management.

6.3.4.2 Example Tree Collection Data – Hurricane Isabel, Virginia

Data from the Virginia Department of Emergency Management were available for the 16 counties and communities that make up the Hampton Roads area. These data were compiled by the Hampton Roads Planning District for the Virginia Department of Emergency Management. The debris data for Virginia are shown in Table 6-17.

The debris data received from the Virginia Department of Emergency Management included the following caveats:

- Debris quantities from military facilities in the region are not included.

- The data shown above is for all debris, not just trees/vegetative debris. However, conversations with the Virginia Department of Emergency Management (DEM) and the Hampton Roads Planning District confirmed that over 95% of the debris reported was from vegetative sources.
- Approximately 25% of the debris was reported by the Hampton Roads District of the Virginia Department of Transportation (VDOT). This debris was collected from the study area, but the proportion belonging to each county or community is unknown and is not included in the analysis.
- VDOT is responsible for the collection of vegetative debris from federal highways in the entire Hampton Roads region, as well as for the collection of debris along state roads in the counties not labeled “(city).” Debris collection from state roads in counties labeled “(city)” is the responsibility of the city government.

The modeled tree debris weight was compared directly to the data provided by the Virginia DEM without modifications for the caveats listed above, assuming a bulking factor of 10 cubic yards per ton. The counties appear in order of increasing average Census block building density.

Figure 6-7 shows that for 12 of the 16 counties, the total weight of tree debris generated by all downed trees is less than that reported by the Virginia Department of Emergency Management, indicating either that the default tree densities and/or the calculated tree blowdown rates are too low in these counties or that there are other sources of debris that are not being modeled in Hazus.

Table 6-17 Virginia Debris Collection Data for Hurricane Isabel (2003)

County	Debris Volume (CY)
Chesapeake (city)	915,101
Franklin (city)	119,000
Gloucester	190,000
Hampton (city)	749,503
Isle of Wight	152,953
James City	411,848
Newport News (city)	577,045
Norfolk (city)	1,014,000
Poquoson (city)	175,795
Portsmouth (city)	430,000
Southampton	185,200
Suffolk (city)	400,000
Surry	59,514
Virginia Beach (city)	922,000
Williamsburg (city)	79,000
York	602,830
VDOT HR District	2,365,860
Total Debris:	9,349,649

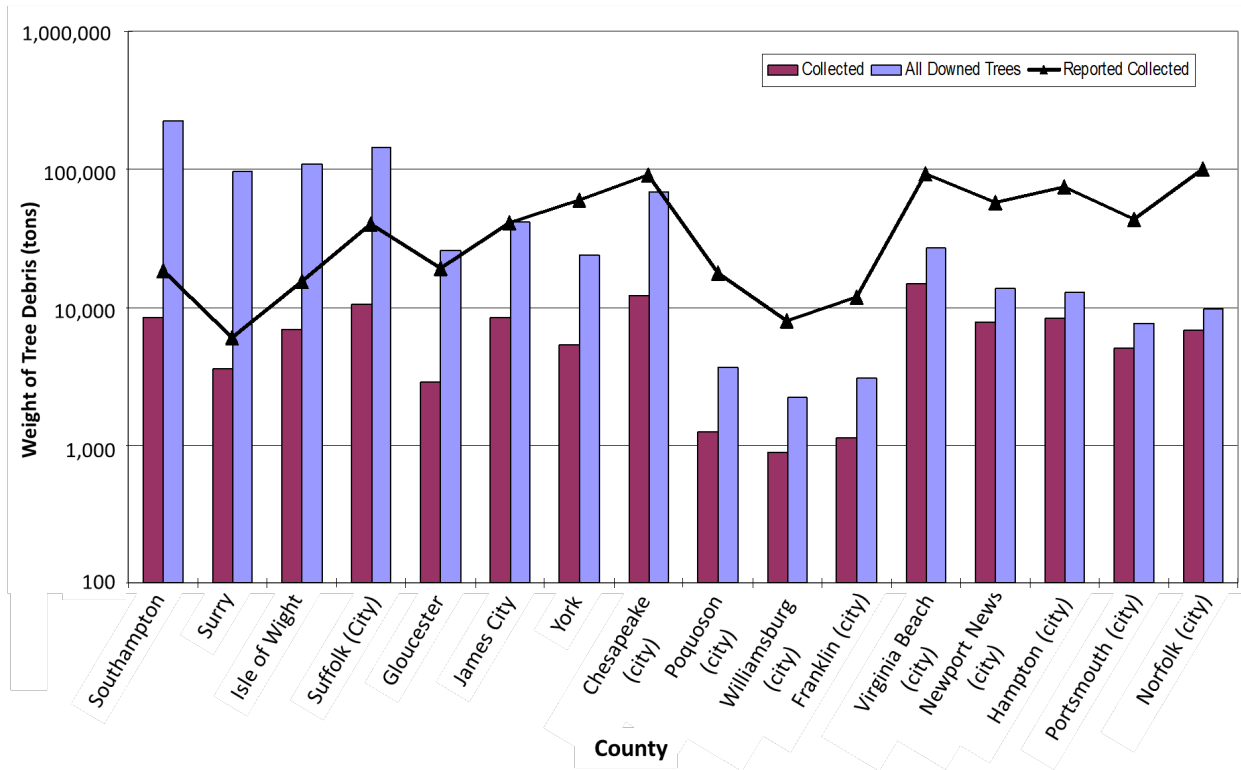


Figure 6-7 Ratio of Modeled Tree Debris to Actual Debris Collected by County in Virginia for Hurricane Isabel

After aggregating the data over all 16 Hampton Roads communities, the results show that the debris collection model underestimates the total debris collected (excluding the VDOT contribution) by about 90%. However, given that the tree blowdown model is apparently underpredicting the quantity of downed trees and the various limitations of the raw data set discussed above, it is difficult to conclude that the Virginia example indicates any serious flaws in the model. The model appears to capture the proper trends and produce reasonable estimates of tree debris collection rates in rural, suburban, and urban areas. Additional validation and refinement of the model is recommended as similar data sets become available for future hurricanes of varying intensities and geographic locations.

It is important to note that, in general, the Virginia Counties considered to have substantially higher building densities (areas are more urban/suburban) than the counties analyzed in North Carolina. Table 6-18 lists the building densities for each of the 36 counties investigated with the average modeled tree debris collection rates. Building densities are calculated as the total number of buildings in the Hazus General Building Stock (GBS) model divided by the land area of the county or region. Likewise, average modeled tree debris collection rates are determined by dividing the total collected tree debris volume by the total blown down tree volume modeled by Hazus for the county and region levels.

Table 6-18 Building Density and Average Tree Debris Collection Rate by County for North Carolina and Virginia

North Carolina			Virginia		
County	Buildings per Acre	Average Tree Collection Rate (%)	County	Buildings per Acre	Average Tree Collection Rate (%)
Beaufort	0.039	4.93	Chesapeake (city)	0.308	17.88
Bertie	0.019	3.24	Franklin (city)	0.502	37.11
Camden	0.019	3.00	Gloucester	0.099	10.91
Carteret	0.113	8.33	Hampton (city)	1.325	64.92
Chowan	0.053	5.95	Isle of Wight	0.058	6.45
Craven	0.076	7.80	James City	0.220	19.99
Currituck	0.067	6.18	Newport News (city)	1.132	57.63
Dare	0.106	7.77	Norfolk (city)	1.717	69.96
Gates	0.020	3.23	Poquoson (city)	0.446	33.96
Hertford	0.039	4.92	Portsmouth (city)	1.451	66.52
Hyde	0.008	3.00	Southampton	0.017	3.79
Jones	0.015	3.00	Suffolk (city)	0.085	7.43
Martin	0.034	4.01	Surry	0.017	3.74
Northampton	0.028	4.32	Virginia Beach (city)	0.865	54.10
Onslow	0.103	9.52	Williamsburg (city)	0.496	39.54
Pamlico	0.031	5.41	York	0.306	22.12
Pasquotank	0.084	7.17			
Perquimans	0.034	4.79			
Tyrrell	0.008	2.00			
Washington	0.025	3.98			
20 NC Counties	0.047	4.68	16 VA Counties	0.231	12.87

For the Virginia counties considered, the tree debris collection model estimates 12.9% of the total tree debris being collected versus only about 4.7% for the more rural counties of North Carolina. Note that although the average building density exceeds 1.0 buildings per acre for several Virginia counties, the average tree collection ratios are still less than 100% because some of the Census blocks in those counties have building densities lower than 1.0 buildings per acre.

The trend of decreased over-prediction of tree debris as building density increases may also be due in part to different disposal means used in rural versus urban areas. In rural areas, it is common to see residents and farmers burning tree debris from their property immediately following the storm or chopping and storing the wood for use to heat their homes for the winter. This behavior reduces the amount of debris that will actually be brought to the curb for collection by local and state governments.

By contrast, residents of urban and suburban areas tend to not only bring the tree debris that falls to the curb but create additional debris by removing any part of the broken trees that remained standing. These residents may also take advantage of the opportunity to dispose of other vegetative debris stored on their property. This behavior may lead to increased tree debris generated and collected in urban and suburban areas.

A potential example of this trend was discovered in the data received from the North Carolina Department of Emergency Management. One largely urban and suburban county reported over 65,000 cubic yards of vegetative debris at a removal cost of over \$1.5M, while Hazus did not predict any downed trees for this county because the wind speeds in Hurricane Isabel did not exceed 50 mph (3-second gust).

Another observation that may lead to underestimating tree blowdown in urban/suburban areas is that the tree database and tree blowdown model only consider trees greater than 30 feet tall. The percentage of tree weight or volume coming from trees less than 30 feet tall is likely to be larger in urban/suburban areas than for rural areas.

6.3.4.3 Comparison to Other Collection Data

In addition to the county data compared for Hurricane Isabel in NC and VA, tree debris estimates were also available from the storms listed in Table 6-19, which presents a list of areas for which estimates of tree debris collected are available for the corresponding storms.

Table 6-19 Locations of Collected Tree Debris Estimates by Hurricane Name and Year

Storm – Year	Locations with Data
Rita – 2005	State of Texas
Wilma – 2005	Palm Beach, Broward, & Miami-Dade Counties, FL
Charley + Frances + Jeanne + Ivan – 2004	State of Florida, Alachua & Orange Counties, FL
Isabel – 2003	States of North Carolina & Virginia
Erin + Opal – 1995	Escambia County, FL

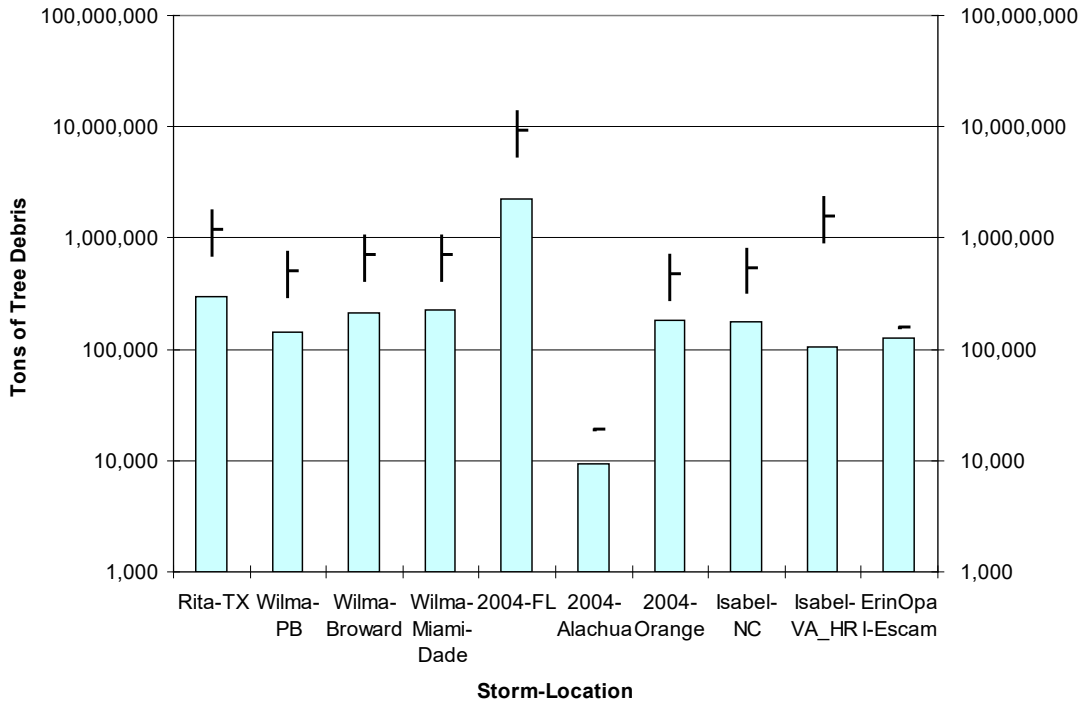


Figure 6-8 Comparison of Modeled Tree Debris Collected to Reported Amounts for Various Locations and Various Hurricanes

Figure 6-8 presents a comparison of modeled tree debris collected to actual quantities reported for the hurricanes and locations mentioned above. This comparison considers the weight of tree debris in tons. However, most hurricane tree debris reports are based on volume (cubic yards). The vertical line for each storm-location combination represents a range of weights based on bulking factors ranging from 4 to 10 cubic yards per ton. The small horizontal line represents either the actual tonnage reported (if no vertical line is present) or the tonnage estimated, assuming a bulking factor of 6 cubic yards per ton.

Section 7. Direct Social Losses – Displaced Households and Short-Term Shelter Needs

Hurricanes can cause loss of function or habitability of buildings that contain housing units, displacing the households that reside there. Displaced households may need short-term shelter provided by public agencies or relief organizations such as the Red Cross, Salvation Army, and others, or alternative shelter, provided by family, friends, or by renting apartments or houses. For housing units where repair takes longer than a few weeks, long-term alternative housing can be accommodated by importing mobile homes, occupancy of vacant units, net emigration from the impacted area, and, eventually, by the repair or reconstruction of new public and private housing. While the number of people seeking short-term public shelter is of great concern to emergency response organizations, the longer-term impacts on the housing stock, which are not currently modeled, are also of concern to local governments, such as cities and counties.

7.1 Scope

The model for estimating the number of displaced households and short-term shelter needs follows that used for the Hazus Earthquake Model. The concept and formulation are described in Section 13 of the *Hazus Earthquake Technical Manual* (FEMA, 2022). The only modification for the Hurricane Model is the building loss ratios, instead of building damage states, are used to estimate the proportion of uninhabitable housing units.

The shelter model provides two estimates for each Census tract (or Census block for combined wind/flood Study Regions):

- The number of displaced households due to loss of habitability.
- The number of people requiring only short-term public shelter based on loss of habitability and demographics.

Loss of habitability is calculated from modeled damage to residential buildings, whose severity is expressed in terms of loss ratios due to physical damage. The methodology provides for the capability to incorporate estimated loss of water or power supply to residential buildings or units; however, the Hazus Hurricane Model does not currently support this capability.

7.2 Displaced Household

The total number of uninhabitable dwelling units for each Census tract (or Census block for combined wind/flood Study Regions) of the Study Region is the output of this portion of the module. In addition, by applying an occupancy rate (households versus dwelling units), the module converts the habitability data to the number of displaced households. The number of displaced households will be used in Section 7.3 to estimate the short-term shelter needs.

7.2.1 Input Requirements

The following inputs at the Census tract level (or Census block for combined wind/flood Study Regions) are required to compute the number of uninhabitable dwelling units and the number of displaced households. The total number of dwelling units or households is provided in the baseline inventory data (refer to the *Hazus Inventory Technical Manual* (FEMA, 2022) for additional information). The user can update these demographic data if improved or updated information is available.

- Demographic data
 - Total Number of Single-Family Dwelling Units (S), including mobile homes
 - Total Number of Multi-Family Dwelling Units (M)
 - Total Number of Households (H)
- Census tract (or block) level results from the General Building Stock Economic Loss Module (see Section 8)
 - Loss ratio in the single-family residential occupancy classes (X_s)
 - Loss ratio in the multi-family residential occupancy classes (X_m)

7.2.2 Description of Methodology

The estimated number of uninhabitable dwelling units is calculated by applying an occupancy rate (households versus dwelling units) and identifying a set of probability density functions and uninhabitability functions of loss ratio x for single- and multi-family buildings. Examples of the modeled probability density function $f_s(x)$, for the case of single-family buildings for the building stock in North Florida, are shown in Figure 7-1, Figure 7-2, and Figure 7-3 in the form of probability mass functions. As wind speed increases, the mass of the probability moves toward unity, indicating that all buildings experience a complete loss. Building stock data used for the loss ratio computations for Florida are presented in Figure 7-4

Modeled Probability Mass Functions of Loss Ratio, Conditional on Peak Gust Speed

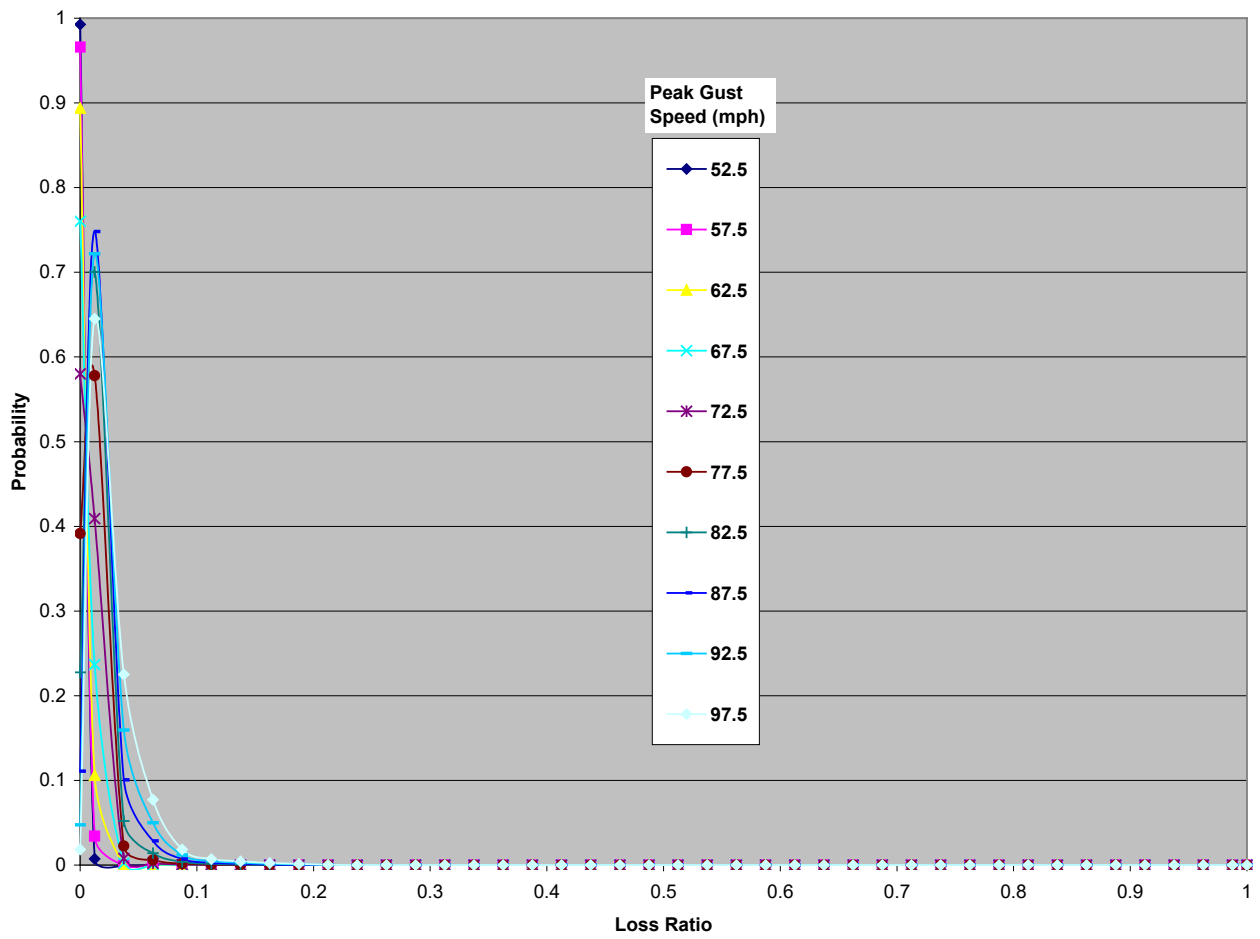


Figure 7-1 Modeled Probability Mass Function of Loss Ratios for Lower Peak Gust Wind Speeds (between 50 mph and 100 mph)

Modeled Probability Mass Functions of Loss Ratio, Conditional on Peak Gust Speed

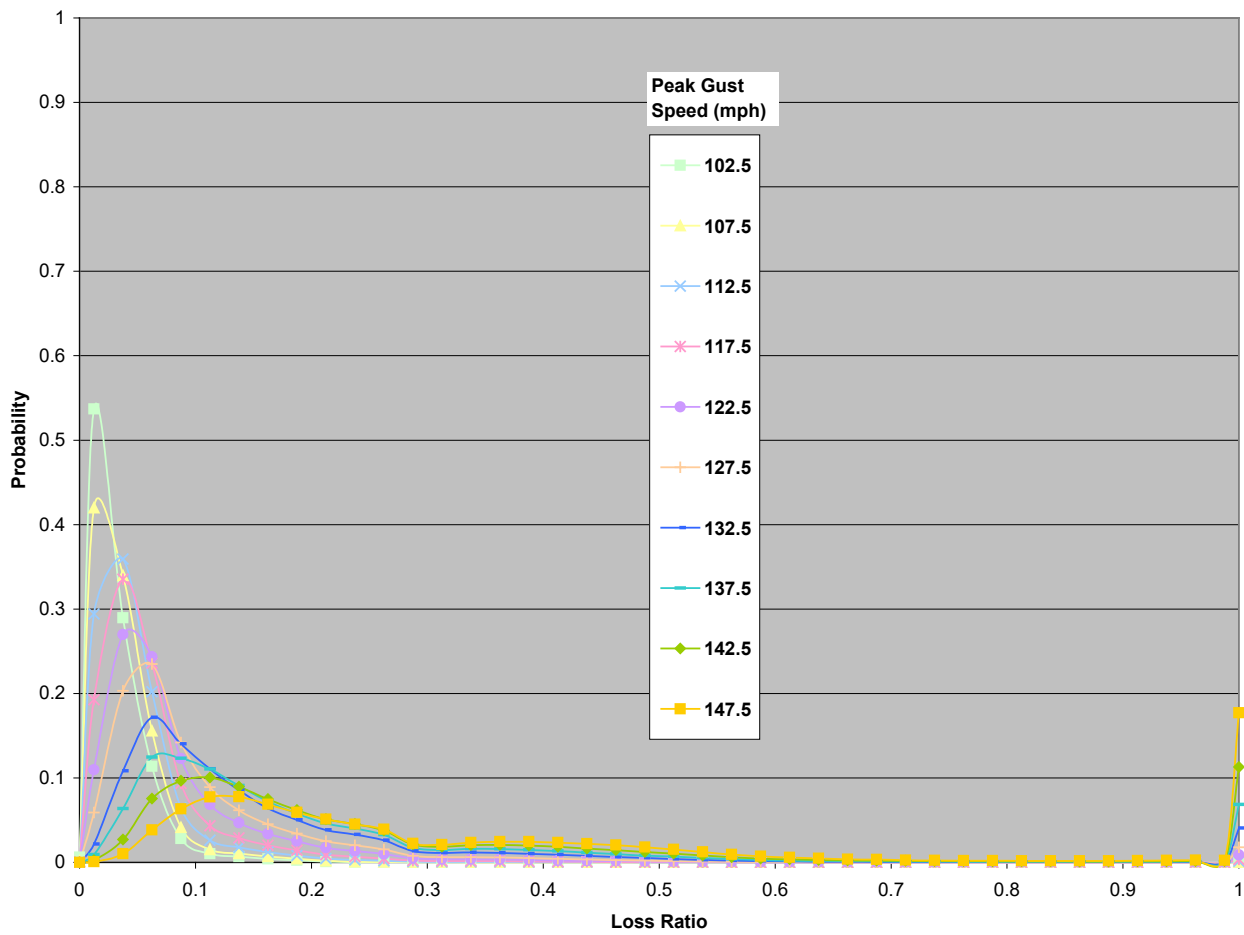


Figure 7-2 Modeled Probability Mass Function of Loss Ratios for Medium Peak Gust Wind Speeds (between 100 mph and 150 mph)

Modeled Probability Mass Functions of Loss Ratio, Conditional on Peak Gust Speed

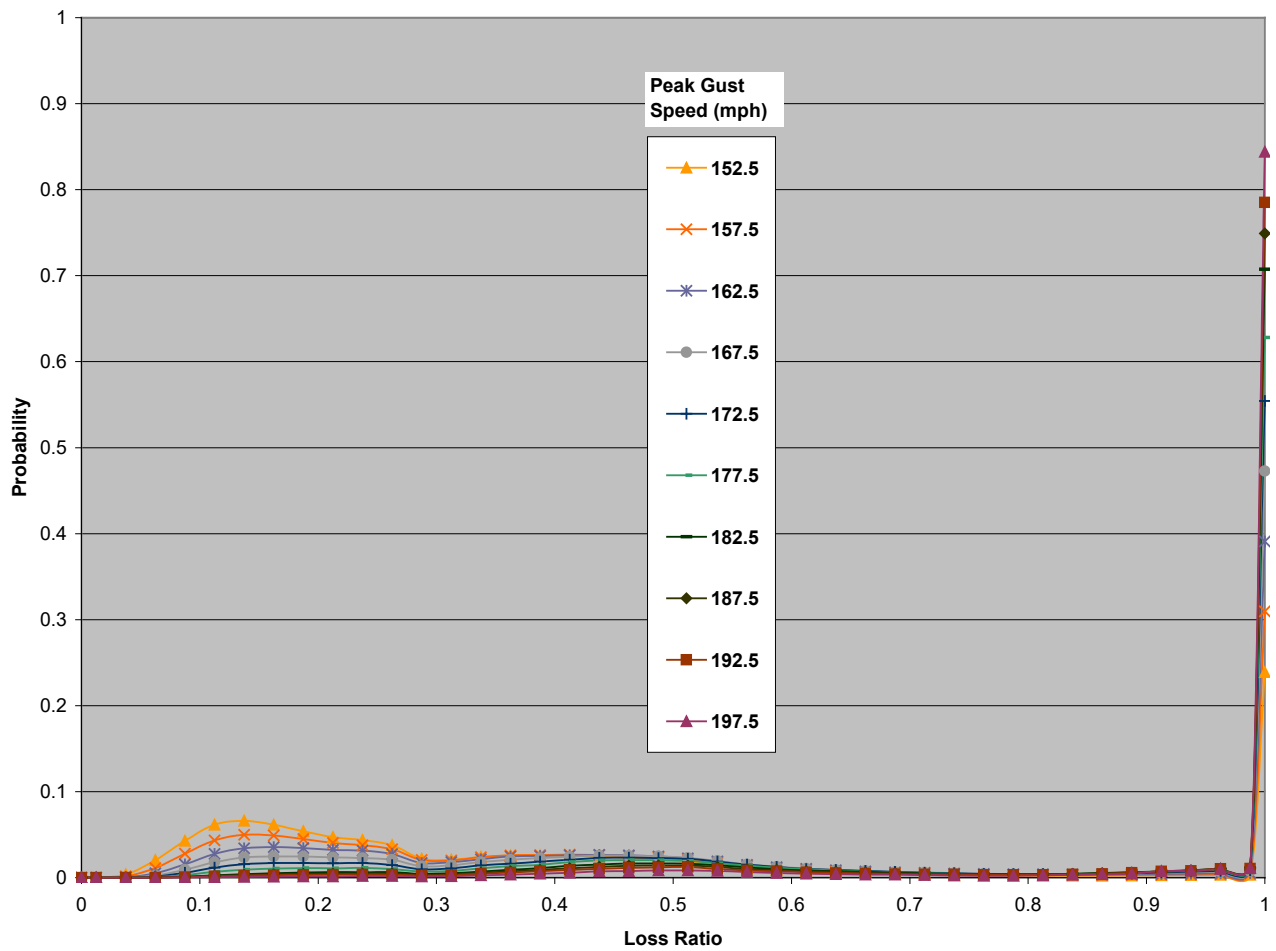


Figure 7-3 Modeled Probability Mass Function of Loss Ratios for High Peak Gust Wind Speeds (between 150 mph and 200 mph)

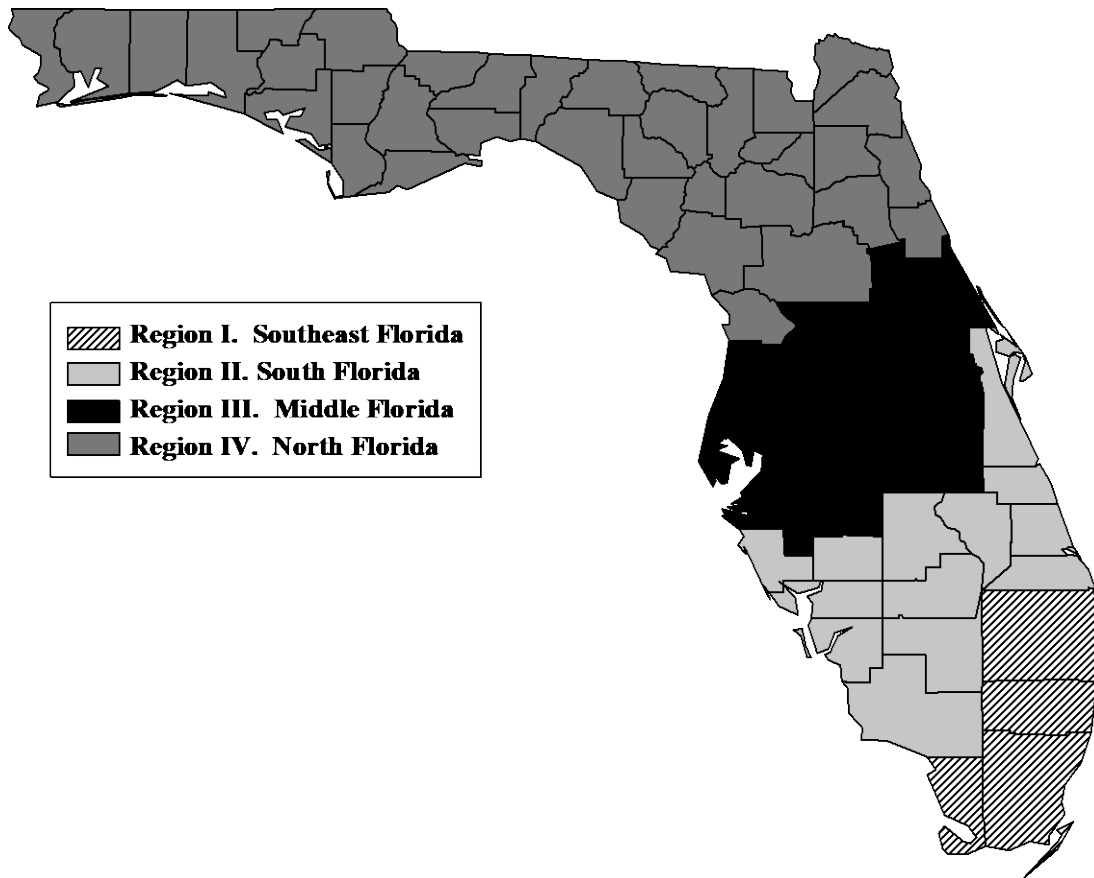


Figure 7-4 Building Stock Regions Used for the Loss Ratio Computation

Figure 7-5 shows an empirical uninhabitability function for single-family buildings in terms of loss ratio x , where a building sustaining a loss ratio below 20% is considered still habitable, above 50% is assumed to be completely uninhabitable, and buildings with a loss ratio between these two values use a linear proportion to determine uninhabitable. For multi-family buildings, as shown in Figure 7-6, the linear range is defined between 10% and 50% empirically, since some of the units in a building with relatively mild overall damage and loss may already have become uninhabitable.

Examples of computed percentage of households being displaced are shown in Figure 7-7.

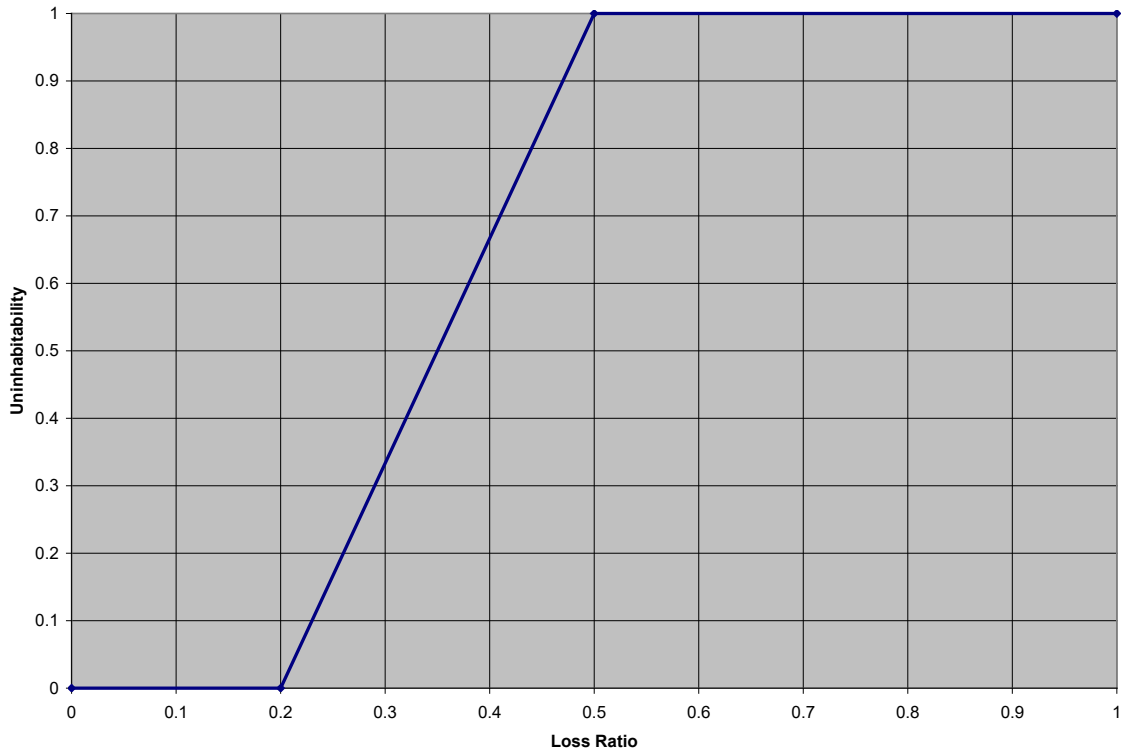


Figure 7-5 Empirical Uninhabitability Function for Single-Family Buildings

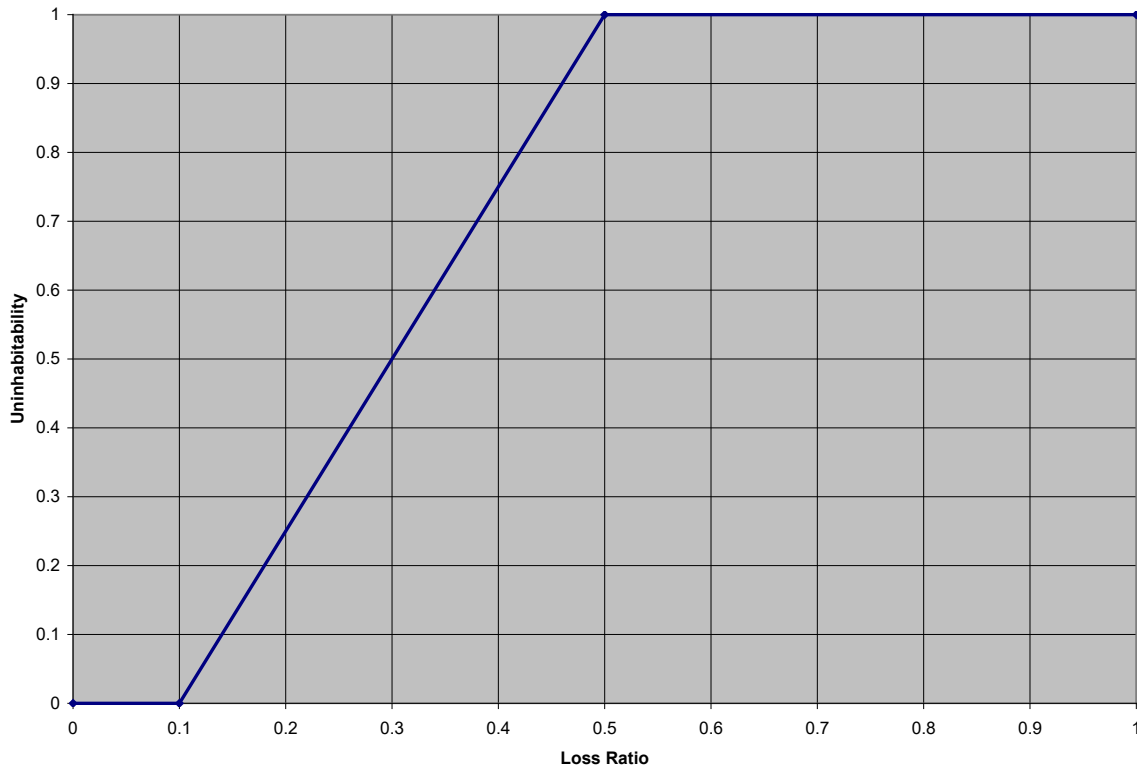


Figure 7-6 Empirical Uninhabitability Function for Multi-Family Buildings

Percentage of Household Being Displaced vs Peak Gust Speed at Site
 Example for Florida

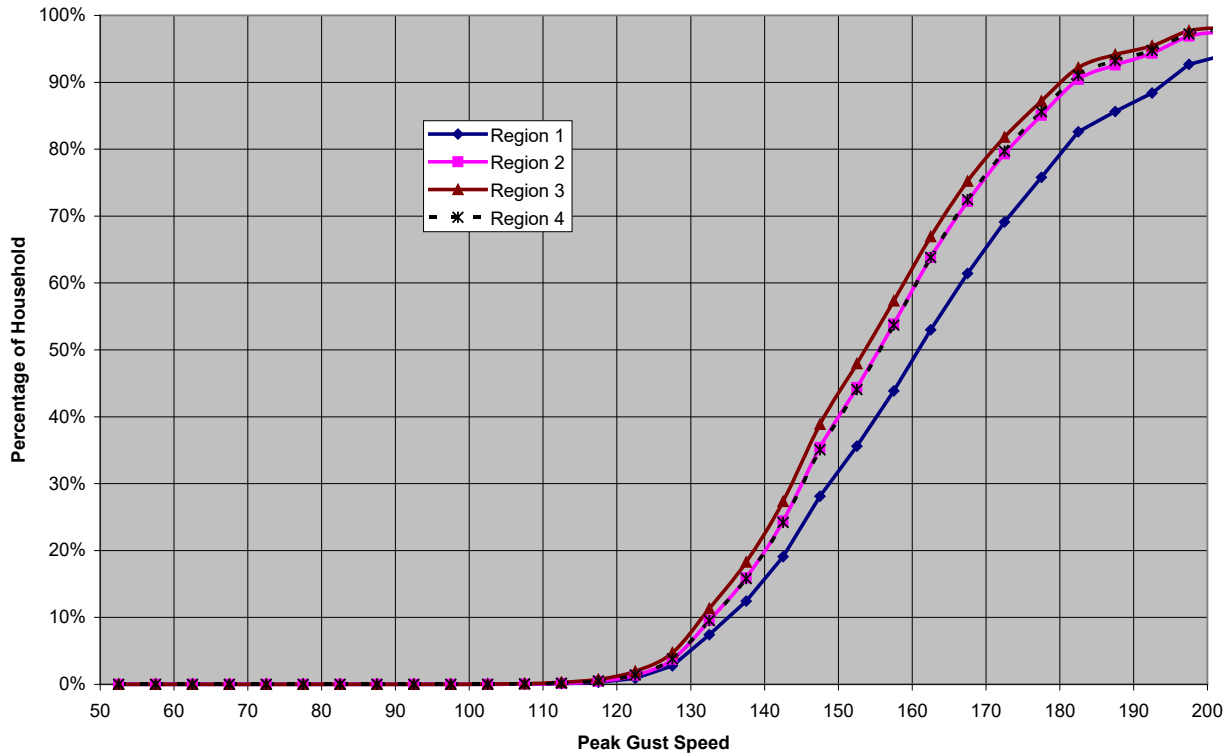


Figure 7-7 Example of Computed Percentage of Household Being Displaced as a Function of Peak Gust Wind Speed at Site

The number of displaced households is calculated using the following equations.

Equation 7-1

$$D = (U) \frac{H}{S + M}$$

Where:

D is the number of displaced households

U is the number of uninhabitable units due to damage (Equation 7-2)

H is the total number of households

S is the total number of single-family dwelling units

M is the total number of dwelling units in multi-family buildings

$\frac{H}{S + M}$ represents the occupancy rate averaged over the single-family and multi-family categories.

U is estimated as follows:

Equation 7-2

$$U = S \cdot \int_0^1 f_s(x) * w_s(x) dx + M \cdot \int_0^1 f_m(x) * w_m(x) dx$$

Where:

- $f_s(x)$ is the probability density function of loss ratio x for single-family buildings
- $f_m(x)$ is the probability density function of loss ratio x for multi-family buildings
- $w_s(x)$ is the uninhabitability function in terms of loss ratio x, single-family buildings
- $w_m(x)$ is the uninhabitability function in terms of loss ratio x, multi-family buildings

The methodology represented by Equation 7-2 requires the full probability density function of building loss as a function of peak gust wind speed. In an effort to reduce the data storage requirements and computational requirements imposed by Equation 7-2, a simplification has been developed to estimate the integrated uninhabitability ratio using mean building losses instead of the probability density functions of building loss. Mean building loss is readily available within Hazus.

A study was carried out to examine the relations between the integrated uninhabitability ratios, which are evaluated by the integrals in Equation 7-2, and the mean building loss ratios. The results are shown in Figure 7-8 and Figure 7-9 for single-family and multi-family buildings, respectively. It is found that the scatter is very insignificant; that is, the mean building loss is a good predictor of the uninhabitability. Fitted mean functions are also shown in Equation 7-4 and Equation 7-5. These functions are used in Hazus in place of Equation 7-2 as follows:

Equation 7-3

$$U = S * F_S(X_S) + M * F_M(X_M)$$

Where:

Equation 7-4

$$F_S(X_S) = \frac{2X_S^{1.6}}{1 + X_S^{2.6}}$$

Equation 7-5

$$F_M(X_M) = \frac{2X_M^{1.3}}{1 + X_M^{2.2}}$$

X_s and X_M denote the mean building loss ratios for single-family and multi-family buildings, respectively. Equation 7-4 and Equation 7-5 are plotted in Figure 7-8 and Figure 7-9, respectively.

Because of the small amount of scatter in Figure 7-8 and Figure 7-9, results computed using Equation 7-3 instead of Equation 7-2 are nearly identical to those shown in Figure 7-5 and Figure 7-6. Therefore, the simplified approach is used in the fast-running implementation of the Hazus software to compute displaced households.

7.3 Short-term Shelter Needs

All households living in uninhabitable dwellings are expected to seek alternative shelter. Many displaced individuals will stay with friends, relatives, or in the family car. Some will stay in public shelters provided by the Red Cross or others or rent a motel or an apartment. This methodology estimates the number of displaced persons seeking public shelter. In addition, observations from past disasters show that approximately 80% of the pre-disaster homeless will also seek public shelter. The user could increase the number of displaced persons to account for the loss of water and power.

7.3.1 Input Requirements

The inputs required to estimate short-term shelter needs are obtained from the displaced household calculations described in Section 5.3 and from the baseline demographic data (refer to the *Hazus Inventory Technical Manual* (FEMA, 2022) for additional information). As with the entire methodology, these demographic data can be modified with improved or updated user information. The inputs listed below are the required demographic data input for the short-term shelter estimates:

- Number of people in Census tract (or block for combined wind/flood Study Regions) (P)
- Number of Households (H)
- Percentage of households whose income is under \$10,000 (I₁)
- Percentage of households whose income is \$10,001 to \$20,000 (I₂)
- Percentage of households whose income is \$20,001 to \$30,000 (I₃)
- Percentage of households whose income is \$30,001 to \$40,000 (I₄)
- Percentage of households whose income is over \$40,000 (I₅)
- Percentage of white households (E₁)
- Percentage of black households (E₂)
- Percentage of Hispanic households (E₃)
- Percentage of Native American households (E₄)
- Percentage of Asian households (E₅)
- Percentage of households owned by householder (O₁)

- Percentage of households rented by householder (O₂)
- Percentage of population under 16 years old (A₁)
- Percentage of population between 16 and 65 years old (A₂)
- Percentage of population over 65 years old (A₃)

7.3.2 Description of Methodology

Those seeking public shelter can be estimated from data on past disasters, including both hurricanes and earthquakes. Those seeking shelter typically have very low incomes, for these families have fewer options. In addition, they tend to be over the age of 65 or have young children. Finally, even given similar incomes, populations from Central America and Mexico tend to be more concerned about reoccupying damaged buildings than other ethnic groups. This tendency appears to be because of the fear of collapsed buildings instilled from past disastrous Latin American earthquakes. For each Census tract (or block for combined wind/flood Study Regions), the number of people who will utilize public short-term shelter can be calculated using the following relationship.

Equation 7-6

$$N = \frac{D * P}{H} \sum_{i=1}^5 \sum_{j=1}^5 \sum_{k=1}^2 \sum_{l=1}^3 (\alpha_{ijkl} * I_i E_j O_k A_l)$$

Where:

- N is the number of people likely seeking public shelter
- D is the number of displaced households
- P is the population
- H is the total number of households
- I_i is the percentage of population in the ith income class
- E_j is the percentage of population in the jth ethnic class
- O_k is the percentage of population in the kth ownership class
- A_l is the percentage of population in the lth age class
- α_{ijkl} is a fractional coefficient, which is a weighted average of empirical fractions of displaced households from various demographic classes who seek public shelter

The value of the constant α_{ijkl} (i.e., the percentage of each category that will seek shelter) can be calculated as shown in Equation 7-7 using a combination of shelter category "weights" (Table 7-1),

which sum to 1.00, and assigning a relative modification factor (Table 7-2) for each subcategory. In the methodology, default values are found in Table 7-1 and Table 7-2.

The weighting factors for ownership (OW) and age (AW) are zero.

Equation 7-7

$$\alpha_{ijkl} = w_I(F_I)_i + w_E(F_E)_j + w_O(F_O)_k + w_A(F_A)_l$$

The weights and fractions are defined in Table 7-1 and Table 7-2, respectively, which include their default values.

Table 7-1 Default Weights for Demographic Variables

Symbol	Description	Default Value
W _I	Income Factor Weighting	0.73
W _E	Ethnic Factor Weighting	0.27
W _O	Ownership Factor Weighting	0.00
W _A	Age Factor Weighting	0.00
(W _I + W _E + W _O + W _A)	Total	1.00

Table 7-2 Default Fractions of Displaced Households Seeking Public Shelter

Variable	Category	Symbol	Default Value
Income	Household Income < \$10,000	(F _I) ₁	0.62
	\$10,000 < Household Income < \$20,000	(F _I) ₂	0.42
	\$20,000 < Household Income < \$30,000	(F _I) ₃	0.29
	\$30,000 < Household Income < \$40,000	(F _I) ₄	0.22
	\$40,000 < Household Income	(F _I) ₅	0.13
Ethnicity	White	(F _E) ₁	0.24
	Black	(F _E) ₂	0.48
	Hispanic	(F _E) ₃	0.47
	Asian	(F _E) ₄	0.26
	Native American	(F _E) ₅	0.26
Ownership	Own Dwelling Unit	(F _O) ₁	0.40
	Rent Dwelling Unit	(F _O) ₂	0.40
Age	Population Under 16 Years Old	(F _A) ₁	0.40
	Population Between 16 and 65 Years	(F _A) ₂	0.40

Variable	Category	Symbol	Default Value
	Population Over 65 Years Old	$(F_A)_3$	0.40

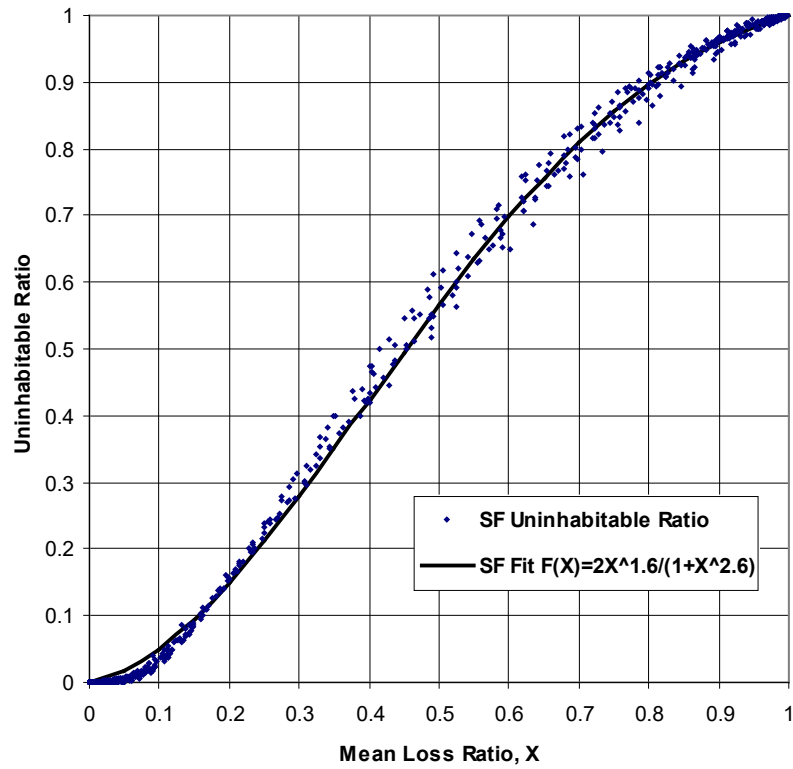


Figure 7-8 Uninhabitability as a Function of Mean Building Loss for Single-Family Buildings

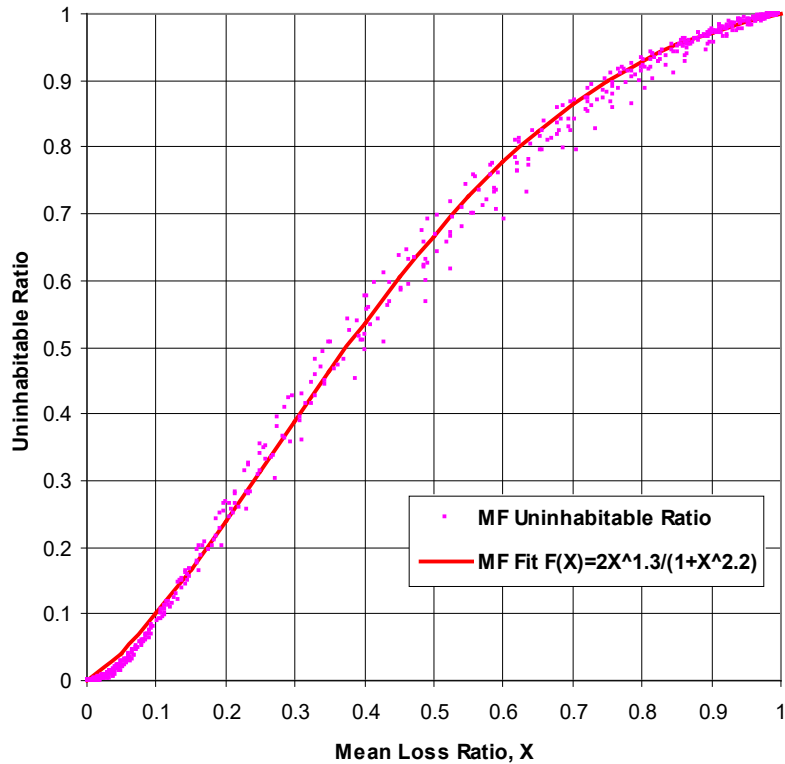


Figure 7-9 Uninhabitability as a Function of Mean Building Loss for Multi-Family Buildings

7.4 Guidance for Estimates Using Advanced Data and Models

7.4.1 Changes to Shelter Weighting and Modification Factors

In the methodology, weights can be added which account for age, ethnicity, income, and ownership. As noted in Section 7.3.2, the required population distribution data are available, and the weights must sum to 1.0. In some disasters, young families tended to seek shelter in a larger proportion than other age groups, in part because of their lower per capita income. In hurricanes, elderly populations were also more likely to seek public shelter. There should be special care taken when adding ownership weights to ensure that they are not double counted, because the multi-family versus single-family issue has already been considered when estimating habitability (i.e., moderately damaged multi-family units are considered uninhabitable while moderately damaged single-family units are considered habitable).

Most recent hurricanes have occurred in warm weather areas. Informal shelter locations utilized included the family car and tents in the family's backyard. Should a hurricane occur during extreme temperatures, more people would likely find these alternate shelters unacceptable. In the Hazus Methodology, the factors specifying the percentage of those displaced that seek public shelter) are able to be adjusted. When planning for hurricanes, a user can change the shelter model's modification factors to look at a variety of scenarios, including unfavorable weather conditions.

7.4.2 Guidance for Estimating Long-Term Housing Recovery

Although long-term housing requirements are not calculated by the methodology, the damage to residential units (calculated in the general building stock) can be combined with relationships between

damage and restoration times to estimate the need for longer-term replacement housing. Longer-term needs are accommodated by importing mobile homes, reductions in the vacancy rates, net emigration from an area, and eventual repair or reconstruction of the housing units. Because replacement of permanent housing is subject to normal market and financial forces, low-income housing is generally the last type of housing to be replaced.

Housing recovery times can span a wide range and are longer than most commercial, industrial, and institutional recovery. Housing recovery tends to be dependent on the settlement of insurance claims, federal disaster relief, the effectiveness of the generally smaller contractors who are occupied with a high volume of residential projects, the financial viability of the home or apartment owner, actions taken by state and local governments to expedite the process, and public support of reconstruction (such as the potential desire for historic preservation). The median recovery time figures for residential occupancies reflect these issues, but there may be significant variation in actual recovery times for individual buildings. Recovery times for non-wood frame multi-family housing, especially low-income single room occupancy buildings, should be measured in years.

Section 8. Direct Economic Losses

The loss model is a physically-based, damage-to-loss model that computes direct economic losses using a combination of explicit and implicit costing techniques. The loss model subdivides buildings into costing subassemblies. This approach provides significant costing flexibility and the capability to process a wide range of building types. The loss model is designed to process detailed building envelope damage states, and it provides the added capability of estimating building interior and content dollar losses by directly considering the volume of water penetrating through failed fenestrations (windows, doors, garage doors, etc.). The modeling approach is also well-suited for estimating the loss of use and repair time.

8.1 Methodology

8.1.1 Residential Input Parameters

A schematic representation of the residential loss model is given in Figure 8-1. Cost data are obtained from RSMMeans Residential Cost Data (2001). These data are based on national averages and require certain adjustments that consider the specific geographical location of the loss, the level of work difficulty associated with repair and remodeling work, and the contractor's overhead and profit. Cost adjustment indices are not applied to content or loss of use dollars. Default subassembly cost ratios are modified by the building characterization inputs and reflect actual building materials and construction types.

Loss model input parameters are grouped into two basic categories: building characterization parameters and building envelope damage parameters. Building characterization parameters include building material, building construction, fenestration, basic geometry, and building/content value information. Building envelope damage parameters include roof cover, roof deck, window damage, building missile hits, etc. Table 8-1 lists model input parameters as a function of input category. Implicit and explicit costing will be further explained in Sections 8.1.3 and 8.1.4.

The roof type input parameter is used to categorize the overall roof geometry and modifies the base square foot costs of installed roofing materials. The roof type parameter considers the decrease in labor output as the level of work difficulty increases. Roof type cost adjustment factors are listed in Table 8-3. The roof slope parameter modifies the base cost of installed roofing materials and reflects the increase in work difficulty.

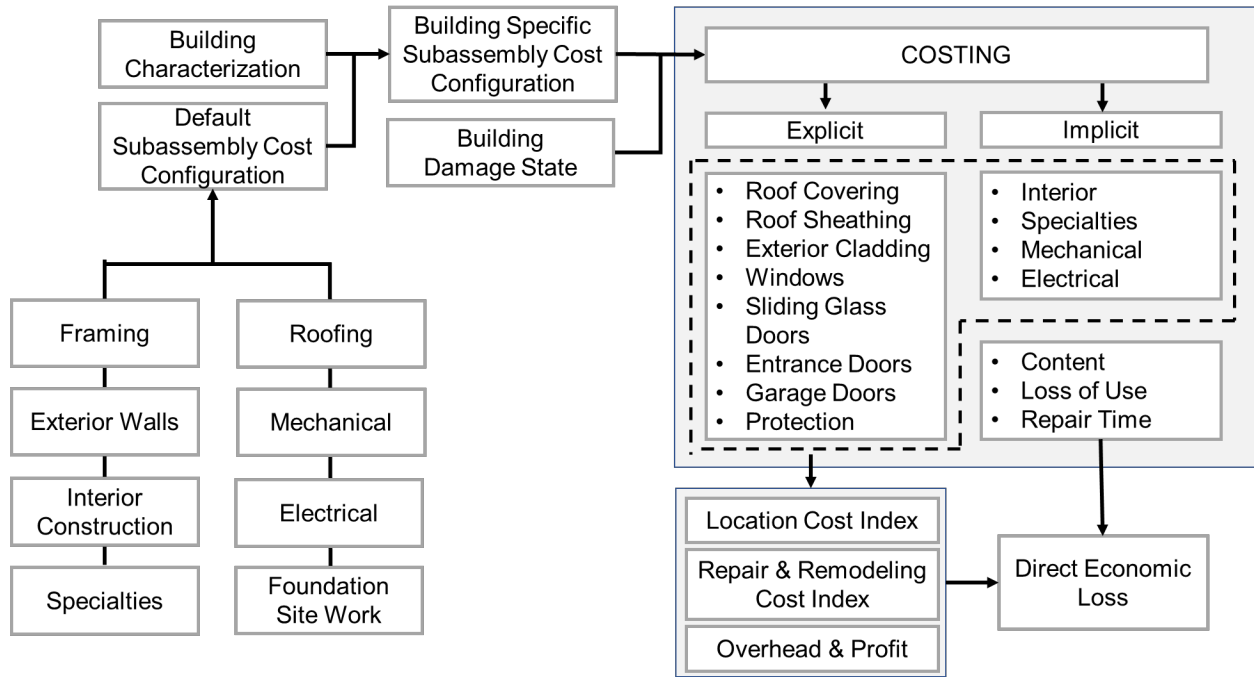


Figure 8-1 Schematic Representation of the Residential Damage-to-Loss Model

Table 8-1 Model Parameters - Building Characteristics

Building Characterization
ZIP Code
Value Group
Number of Floors
Plan Area
Wall Area
Roof Type
Roof Slope
Roof Area
Roof Cover Material
Exterior Construction
Exterior Cladding
Entrance Door
Window
Sliding Glass Door
Skylight
Garage Door
Protection (e.g., Shutters)

Table 8-2 Model Parameters - Damage State

Damage State
Percent Roof Covering Damaged
Percent Roof Sheathing Damaged
Missile Hits to Exterior Cladding
Volume of Water Penetrating Envelope
Door
Window
Sliding Glass Door
Skylight
Garage Door
Protection

Table 8-3 Roof Installed Materials Cost Modification Factors

Roof Type	Difficulty Index
Shed	0.90
Gable	1.00
Gambrel	1.14
Hip	1.26
Mansard	1.49
Complex	1.49

8.1.2 Residential Subassembly Costs

Residential structures are grouped into four classes according to the income ratio of the Census block: Economy, Average, Custom, and Luxury. Table 8-4 shows how the square footage for each of the four classes change with the income ratio. The square foot value grouping of residential structures is primarily used to reflect the quality of construction, uniqueness of design, overall living area, and cost. The loss model can estimate the cost of residential structures falling into any of the above value groups. This is possible since the majority of all residential structures, regardless of square foot value classification, consist of nine basic subassemblies: site work, foundation, framing, exterior walls, roofing, interiors, specialties, mechanical, and electrical. These nine basic subassemblies are used throughout the industry for both the costing of installed materials and the scheduling of labor and tasks.

Table 8-4 Residential Classification Based on Income Ratio

Income Ratio (IR)	Luxury	Custom	Average	Economy
IR < 0.5	0	0	0	100%
0.5 <= IR < 0.85	0	0	25%	75%
0.85 <= IR < 1.25	0	25%	75%	0
1.25 <= IR < 2.0	0	100%	0	0
IR >= 2.0	100%	0	0	0

The loss model is designed to take advantage of the construction subassembly concept by assigning a cost ratio to each of the subassemblies within the default building. The cost ratio of a subassembly is defined as the ratio of the cost to complete the subassembly to the total cost of the entire residential building.

8.1.2.1 Default Residence

The default Economy house is a masonry single-story building having a living area of approximately 1,200 square feet and an overall value in 2020 dollars of \$117,132, or \$97.61 per square foot of living space. The Economy residence is mass-produced from stock plans, the materials and workmanship are sufficient only to satisfy minimum building codes, and the design is seldom anything other than square or rectangular.

- Site work consists of preparation for a poured slab and excavation of a 4' deep trench for a foundation wall. The foundation is typically a continuous concrete footing 8" deep by 18" wide. The foundation wall is built with 8" thick concrete blocks and is 4' deep. A 4" trowel finished concrete slab is poured onto a 4" crushed stone base.
- Roof framing costs are based on a 4:12 pitch roof using 2x4 wood trusses spaced 24" on center with 3/8" plywood sheathing. Exterior walls are constructed of 8" concrete block sealed and painted on the exterior with furring on the interior for drywall. The residence will typically have two flush solid core wood exterior doors and aluminum or wood awning windows.
- Roof covering consists of 14 squares of asphalt shingles with 15 lb. roofing paper, aluminum flashing, and attic insulation.
- The interiors are constructed with 1/2" drywall taped and finished and painted with primer and one finish coat. Softwood baseboard and trim are used and painted with primer and one finish coat. Floor finishes consist of rubber backed carpeting over 80% of the floor area and tile over the remainder. There are typically 15 to 20 hollow core wood interior doors.
- Specialties include 6 linear feet of the kitchen wall and base cabinets with a laminated plastic countertop.
- Mechanical considerations consist of one wall hung lavatory, one water closet, one porcelain enamel steel bathtub, one stainless steel kitchen sink, a 30-gallon gas fired water heater, and gas fired forced air heat.

- The electrical subassembly consists of a 100-ampere service with Romex wiring, incandescent lighting fixtures, switches, and receptacles.

8.1.2.2 Subassembly Cost Ratios

Default residential subassembly cost ratios are given as a function of the number of stories in Table 8-5. For residential structures falling outside of the default building definition, cost ratios are easily modified to accommodate departures from the default material and construction configurations. A comparison between subassembly cost ratios for homes having tile versus asphalt shingle roof covering is provided in Table 8-6. For one-story homes with tile roofing, the cost ratio increases significantly for the roofing subassembly and the ratios for other subassemblies decrease. The impact of this roofing material change is less for two- and three-story residences.

Table 8-5 Default Residential Subassembly Cost Ratios

Subassembly	One-Story	Two-Story	Three-Story
Site Work	1%	1%	1%
Foundation	13%	8%	5%
Framing	13%	11%	14%
Exterior Wall	22%	25%	26%
Roofing	3%	2%	1%
Interiors	32%	38%	39%
Specialties	4%	4%	4%
Mechanical	9%	8%	7%
Electrical	3%	3%	3%
Total	100%	100%	100%

Table 8-6 Subassembly Cost Ratios - Tiles versus Shingle

Assembly	One-Story		Two-Story		Three-Story	
	Shingle	Tile	Shingle	Tile	Shingle	Tile
Site Work	1%	1%	1%	1%	1%	1%
Foundation	13%	11%	8%	7%	5%	5%
Framing	13%	13%	11%	11%	14%	11%
Exterior Wall	22%	17%	25%	23%	26%	26%
Roofing	3%	13%	2%	7%	1%	5%
Interiors	32%	30%	38%	36%	39%	38%
Specialties	4%	4%	4%	4%	4%	4%
Mechanical	9%	8%	8%	8%	7%	7%
Electrical	3%	3%	3%	3%	3%	3%
Total	100%	100%	100%	100%	100%	100%

Table 8-7 shows a comparison between cost ratios for the default single-story home and a modified single-story home (brick veneer and tile roof). Using preprocessed cost data, the square foot cost of

exterior wall and roofing subassemblies are adjusted to consider the increase in cost of using brick and tile. Modified cost ratios are then easily computed as shown in Equation 8-1.

Table 8-7 Cost Ratio Comparison for Brick and Tile Modification

Subassembly	Default One-Story	Modified Brick/Tile	Default One-Story	Modified Brick/Tile
Site Work	\$0.60	\$0.60	1%	1%
Foundation	\$7.19	\$7.19	13%	10%
Framing	\$7.83	\$7.83	13%	11%
Exterior Wall	\$12.10	\$18.60	22%	28%
Roofing	\$1.79	\$7.17	3%	10%
Interiors	\$18.42	\$18.42	32%	27%
Specialties	\$2.52	\$2.52	4%	4%
Mechanical	\$4.92	\$4.92	9%	7%
Electrical	\$1.65	\$1.65	3%	2%
Subtotal	\$57.02	\$68.90	100%	100%
Profit & Overhead	\$2.86	\$3.46		
Total	\$59.88	\$72.36	100%	100%

If the modified building of Table 8-7 has a value of \$65,000 and was to suffer damage to 50% of its interior subassembly, the base cost to repair the interior subassembly only (excluding city cost index, repair and remodeling adjustments, and overhead and profit) is approximately $0.5 * 0.27 * \$65,000$ or \$8,775.

Using the above approach, all residential structures can easily be sub-divided into their subassemblies and their respective cost ratios computed. For buildings falling outside the scope of the default building definition, modified cost ratios are easily computed as shown in Table 8-7. This approach provides the loss model with an extraordinary degree of flexibility for costing. Once the cost ratios are computed, the building value is used to assign dollar values to the various subassemblies. Given a damage state to a particular subassembly, the cost to repair is easily computed as follows:

Equation 8-1

$$C = D * C_R * V$$

Where:

- C is the base cost to repair
- D is a fraction of the subassembly to be replaced or repaired
- C_R is the cost ratio for the subassembly

V is the building value

The base cost, C, is then adjusted to consider city cost index, repair and remodeling adjustments, and overhead and profit.

8.1.3 Explicit Costing of Residential Losses

The explicit costing method directly calculates the repair and replacement costs for damaged building envelope components using a combination of RSMeans unit, linear foot, and square foot costs. Explicit costing is used within the model for several building envelope components, such as roof covering, roof sheathing, windows, entrance doors, garage doors, fenestration protection, etc. Dollar losses associated with these components are directly calculated using actual building damage states and damage replacement thresholds. Damage replacement thresholds are the minimum damage levels at which building components are completely replaced. Replacement thresholds are an important model parameter and can significantly impact final losses. This is especially true of tile roof coverings. Replacement thresholds will typically vary between building component type; however, in the present loss model, damage replacement thresholds are currently set at a 0.5% damage state for both asphalt roof covering and tile roof covering. A 5% threshold for roof sheathing is used. In addition to replacement thresholds, the loss model also considers building component replacement based on serviceability considerations. For those building envelope components (windows, entrance doors, garage doors, and fenestration protection) that do not fail under applied load, they may still require replacement after undergoing thousands of load cycles as they become prone to permanent set. This is especially true when load cycles approach the ultimate capacity of the component. The loss model takes serviceability considerations into account by replacing those components that sustain loads exceeding 85% of their ultimate capacity.

The cost data used in the explicit costing portion of the loss model is derived from the RSMeans Residential Cost Data and is based on national averages for new construction materials and installation. Continuous deterministic functions are used to cost windows, doors, protection (coverings, sheathing, shutters, etc.), garage doors, skylights, etc., as a function of type, material, and size. For example, for double hung wood windows, the following functions are used to estimate the replacement cost:

- *Standard glass*: Replacement Cost = $10.00 * (\text{AREA} - 12.00) + 225.00$
- *Insulating glass*: Replacement Cost = $14.40 * (\text{AREA} - 12.00) + 270.00$

Where:

AREA is the overall area of the window unit

All building envelope fenestration (windows, entrance doors, garage doors, and protection) have conceptually similar functions. Roof covering costs are calculated as:

Equation 8-2

$$RC = R_A * (C_C + C_0)$$

Where

- RC is the base roof cost
- R_A is the roof area to replace
- C_c is the covering cost
- C_o are other roofing costs

Roof sheathing costs are determined similarly.

The loss model cost data are obtained from RSMeans Residential Cost Data (2001). These data are based on national averages and require certain adjustments, which consider the specific geographical location of the loss, the level of work difficulty, and the contractor’s overhead and profit. Consequently, the model uses a city cost index to modify losses as a function of the ZIP Code. A partial listing of city cost indices is provided in Table 8-8. Furthermore, loss model cost data are based on new construction costs and it is essential to adjust the computed base costs to consider the repair and remodeling nature of the work. Costs are typically increased due to the decrease in labor output typically associated with repair and remodeling work. Additional costs also arise when protecting existing work. To account for these increases in cost, base costs are adjusted using a repair and remodeling cost adjustment factor of 1.25. This factor was determined using expert judgment, field observation, and literature review (RSMeans).

Table 8-8 Location Index Factor – Florida

ZIP Code	City	Index
320, 322	Jacksonville	0.81
321	Daytona Beach	0.82
323	Tallahassee	0.80
324	Panama City	0.81
325	Pensacola	0.84
326	Gainesville	0.80
327, 328, 347	Orlando	0.81
329	Melbourne	0.82
330, 331, 332, 340	Miami	0.79
333	Fort Lauderdale	0.80
334, 349	West Palm Beach	0.80
335, 336, 346	Tampa	0.82
337	St. Petersburg	0.81
338	Lakeland	0.79
339	Fort Myers	0.79
342	Sarasota	0.83

8.1.4 Modeling of Residential Interior and Content Losses and Loss of Use

Unlike the case of building exterior, where the cost associated with the predicted or modeled damage can be explicitly estimated, the interior damage and, hence, resulting loss is estimated using an implicit model. In this model, the economic loss is estimated using simple functions developed primarily based on experience and judgment. The economic damage to the interior of the building is a function of the damage to the roof cover, roof sheathing, roof structure, and the windows and doors. The basic premise used in the development of these simple models is that once the envelope is breached, most of the damage to the interior of the building is a function of the amount of water that enters the building.

8.1.4.1 Economic Damage to Building Interior

The economic damage to the interior of the building is taken as the maximum of the economic damage estimated to be a result of roof cover damage, roof sheathing damage, and window damage. The interior economic damage associated with loss of roof cover, L_{RC} , is given as:

Equation 8-3

$$L_{RC} = f_1(R_{RC})(1 - f_2(A_{RC}))f_3(R_{RC})V_1$$

Where:

- R_{RC} is the fraction of failed roof cover
- A_{RC} is the area of failed roof cover (square feet)
- V_1 is the value of the interior of the building

The functions, f_1 , f_2 , and f_3 are described below.

Equation 8-4

$$f_1(R_{RC}) = 1.11R_{RC}, \text{ for } R_{RC} \leq 0.9$$

$$f_1(R_{RC}) = 1.0, \text{ for } R_{RC} > 0.9$$

Where:

- R_{RC} is the fraction of failed or missing roof cover

The function f_1 represents the fractional amount of the interior area affected by the loss of a fraction of the roof cover.

Equation 8-5

$$f_2(A_{RC}) = 1 - 0.005A_{RC}, \text{ for } A_{RC} \leq 200 \text{ ft}^2$$

$$f_2(A_{RC}) = 0, \text{ for } A_{RC} > 200 \text{ ft}^2$$

Where:

A_{RC} is the area of failed roof cover

The function f_2 represents a term that accounts for when the amount of roof cover damage is relatively small, which means water is not able to enter the building because the underlayment remains intact or no gaps in the roof sheathing are exposed.

Equation 8-6

$$f_3(R_{RC}) = 0.1, \quad \text{for } R_{RC} \leq 0.05$$

$$f_3(R_{RC}) = 2.0R_{RC}, \quad \text{for } 0.05 < R_{RC} \leq 0.5$$

$$f_3(R_{RC}) = 1.0, \quad \text{for } R_{RC} > 0.5$$

The function f_3 represents a term that accounts for the fact that the resulting interior economic damage becomes more severe as the area of interior damage becomes larger. Examples of severe damage include ceiling sheet rock collapsing and damaging flooring, cabinets, etc., or water migrating behind walls and damaging the electrical systems, etc. The three functions noted above are shown in graphical form in Figure 8-2.

The implicit economic damage caused by failure of the roof sheathing is modeled in the form:

Equation 8-7

$$L_S = (3.6R_S + 0.1)V_I + R_S V_{RF}, \quad \text{for } 0 < R_S < 0.25$$

Where:

- L_S is the economic damage associated with loss of roof sheathing
- R_S is the fraction of missing roof sheathing
- V_{RF} is the value of the roof framing (V_{RF} typically represents only 4%-5% of the total value of a house)

This equation, derived primarily from experience, in addition to the damage and loss data for individual buildings given in Bhinderwala (1995), yields an interior loss of approximately 10-15% (depending on the size of the house and the size of the sheathing) following failure of the first piece of sheathing. The interior of the house is assumed to require replacement when 25% of the roof sheathing has failed. These two points (the first sheathing failure and the 25% loss of sheathing) were used to bound the linear model for the prediction of interior loss given sheathing failure.

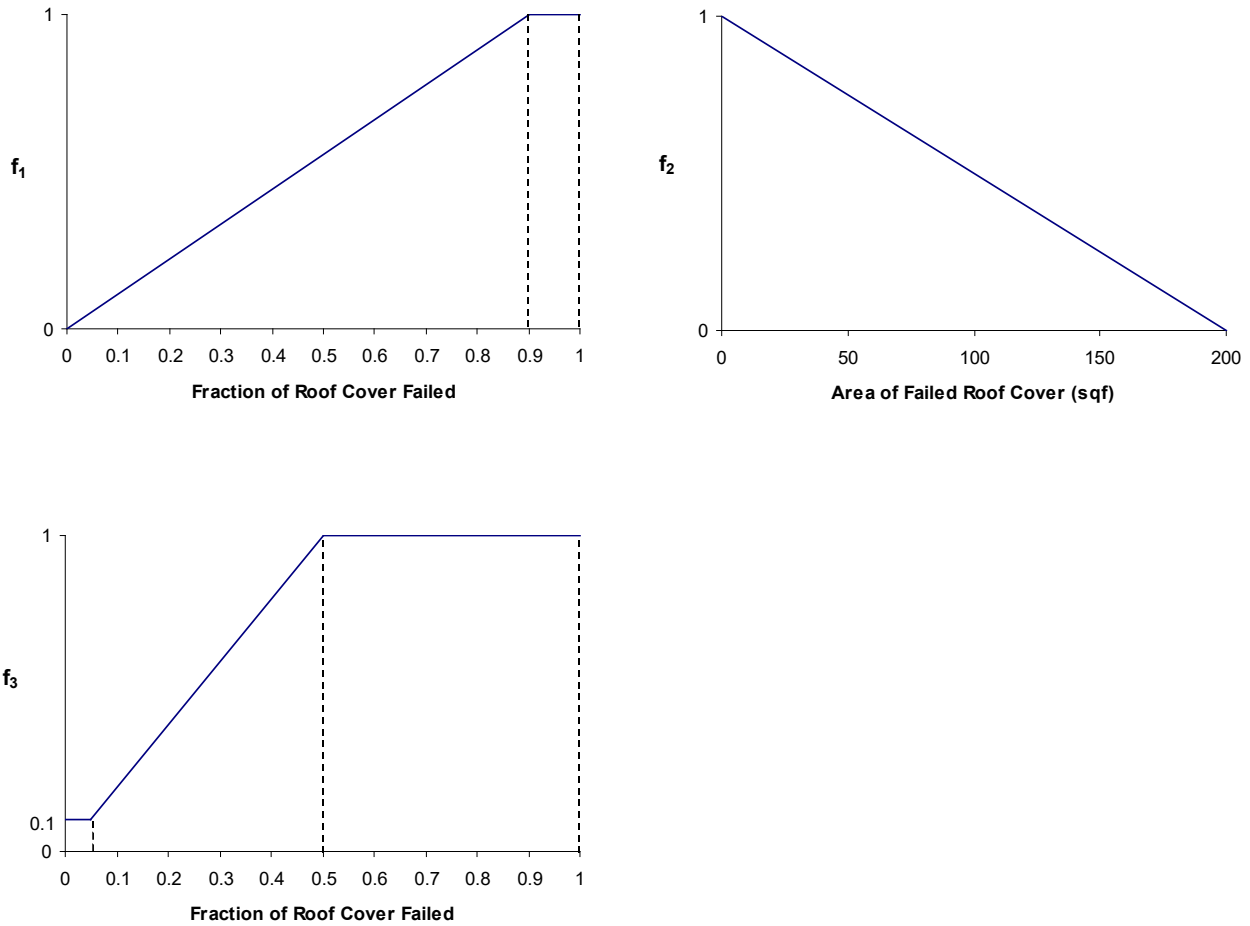


Figure 8-2 Implicit Loss Functions Associated with Damage to the Roof Cover

The economic damage produced by the failure of windows and doors is modeled as:

Equation 8-8

$$L_F = (4D_W)V_I, \quad \text{for } 0 \leq D_W \leq 0.25$$

Where:

L_F is the economic damage associated with failure of windows and doors

D_w is the depth of water, in inches, averaged over the floor area of the building

The simple loss model associated with water entering through failed fenestration was developed with the assumption that the losses increase linearly with an increasing amount of water entering the building, and that 0.25" of water (distributed uniformly over the floor area of the house) is sufficient to produce a 100% loss to the interior of the building.

The estimates of losses produced to the interior of the building are adjusted to consider the additional costs associated with repair and replacement, and to include an allowance for overhead and profit. The

total economic loss of the building, including both the exterior losses and the interior losses, is constrained not to exceed the assumed value of the building.

8.1.4.2 Economic Damage to Contents

Content losses are modeled using the assumption that the damage to contents is highly correlated with damage to the interior of the building. This assumption posits that damage to contents only begins to occur after at least some damage has been done to the interior of the building. The model assumes that losses are associated with water entering the building. Figure 8-3 and Figure 8-4 show examples of content damage produced by roof and window failures. Note that in the roof failure example (Figure 8-3), the damage to the contents is ultimately caused by a failure of the interior (i.e., ceiling) of the building.



Figure 8-3 Content and Interior Losses Associated with Roof Sheathing Failure



Figure 8-4 Content Losses Due to Fenestration Breach

Content losses associated with roof cover loss are accrued at one half the rate associated with losses to the interior of the building, except that in the case of roof cover loss, no contents are damaged until a threshold of 20% roof cover loss has occurred. This jump at 20% is based on the premise that there must be water collected above the ceiling to cause the ceiling to fail, and initiate content damage. The content loss associated with fenestration failure is accrued at the same rate as the economic loss associated with the interior of the building. The content loss associated with sheathing loss is given as:

Equation 8-9

$$L_C = 4R_S, \quad \text{for } R_S < 0.25$$

$$L_C = 1.0, \quad \text{for } R_S > 0.25$$

Where:

L_C is the economic damage associated with content loss

The economic loss associated with damage to the contents of the building is taken to be the maximum among the losses produced by roof cover damage, roof sheathing damage, or fenestration damage.

8.1.4.3 Loss of Use for Residential Buildings

Loss of use estimates for residential buildings are based on the approach used in the Hazus Earthquake Model for estimating recovery (reconstruction) time as a function of the building damage state (FEMA, 1999). Five damage states (None, Slight, Moderate, Extensive, and Complete) are employed in the earthquake model. For the purposes of estimating the loss of use due to hurricanes, these five damage states are assumed to correspond to mean building loss ratios of 0%, 2%, 10%, 50%, and 100%, respectively. These damage state thresholds were identified by using the description of the damage to key building components associated with the specific damage state and using expert judgment.

For single-family dwellings, the expected recovery times for the five key damage states in the Earthquake Model are 0, 5, 120, 360, and 720 days, respectively. These five recovery times are used to define the recovery time curve in the Hurricane Model, with the expected building loss ratio used as the input instead of the damage state. Linear interpolation is used to obtain the recovery times for buildings with expected loss ratios from 0-2%, 2-5%, 5-10%, 10-50%, or 50-100%.

The economic losses associated with building recovery time consider the amount of time persons in a damaged home will require temporary lodging. A loss of use multiplier is applied to the expected recovery time to consider the fact that homeowners may be able to remain in their homes when buildings have slight to moderate damage. The loss of use multipliers for None, Slight, Moderate, Extensive, and Complete Damage States are 0, 0, 0.5, 1, and 1, respectively, in the earthquake model (FEMA, 1999). These same factors are used in the hurricane model at building loss ratios of 0%, 2%, 10%, 50%, and 100%, respectively. As with the recovery times, linear interpolation is used to obtain the loss of use multipliers for buildings with expected loss ratios between these five key values.

8.1.5 Residential Loss Model Validation Examples

The residential damage-to-loss model has been validated using a set of residential claim folders that document wind-induced economic losses following Hurricanes Erin, Opal, Bertha, and Fran. The houses analyzed are screened from over 140 individual claim folders. Individual claim folders were considered only a minimal degree of uncertainty exists with respect to the characterization of the building and the associated loss, that is, insured value, roof type, roof area, plan area, etc., building damage state, and dollar loss. Files containing information, which suggests flooding may have occurred are rejected, as are those files having insufficient data to explicitly rule out the possibility of flooding. The initial selection criteria were constrained to include only those claim folders having a damage state limited to roof covering and roof sheathing.

Model losses were obtained by running the model with observed damage states and building-specific information such as insured value, roof type, roof area, plan area, etc. These data are gathered by carrying out a careful study of the claim folder documentation. The documentation typically includes loss estimates, claim folder damage pictures, a written description of the damage state, and sketches showing a plan view of the building and the damage locations on the roof. A rigorous investigation of the claim pictures provides an estimate of the building envelope damage and characterization of the building in general. The insurance policy provides the building insured value while the estimates are used to obtain the actual dollar loss information Table 8-9 summarizes the compiled data and associated losses reported as a ratio of building value. The average prediction error ratio (defined as

the actual loss divided by the predicted loss) is 0.83. This suggests a reasonable agreement between the predicted and actual losses. Figure 8-5 compares predicted losses and actual loss data. In some cases, the actual loss dollars are adjusted to eliminate the contribution of loss dollars from components that are not explicitly modeled. For example, costs associated with outside deck repairs are omitted since the residential damage and loss models do not model these components. Hence, if the total loss for a given building was \$10,000, but \$3,500 of the loss originated from deck and sprinkler system damage, the overall dollar loss would be adjusted by subtracting from the total loss those loss dollars associated with non-modeled components (i.e., deck and sprinkler).

Table 8-9 Predicted and Actual Losses

Case Number	Building Characteristics				Building Losses			Content Losses		
	Value (\$)	Roof Area (ft ²)	Roof Cover*	Damage (%)	Actual	Model	Ratio	Actual	Model	Ratio
1	281,000	3,125	AS	2.5	0.037	0.023	1.59	0.00	0.00	0.00
2	57,600	770	BUR	50.0	0.502	0.493	1.02	0.00	0.14	0.00
3	199,000	3,300	AS	1.0	0.017	0.029	0.60	0.00	0.00	0.00
4	230,000	3,200	AS	2.5	0.029	0.022	1.31	0.00	0.00	0.00
5	191,000	2,100	AS	2.5	0.025	0.020	1.25	0.00	0.00	0.00
6	452,200	3,500	AS	2.5	0.016	0.016	0.98	0.00	0.00	0.00
7	375,000	3,500	AS	7.5	0.041	0.027	1.53	0.00	0.00	0.00
8	226,000	2,150	AS	0.5	0.019	0.018	1.03	0.00	0.00	0.00
9	212,000	4,800	AS	4.0	0.039	0.038	1.03	0.00	0.00	0.00
10	506,000	3,100	AS	0.5	0.009	0.011	0.82	0.00	0.00	0.00
11	302,200	3,600	AS	2.0	0.012	0.019	0.61	?	0.00	0.00
12	152,000	2,750	AS	2.5	0.027	0.028	0.94	0.00	0.00	0.00
13	74,737	1,205	AS	2.5	0.013	0.025	0.52	0.00	0.00	0.00
14	245,000	2,640	TILE	2.5	0.048	0.068	0.70	0.00	0.00	0.00
15	137,000	1,650	AS	2.5	0.004	0.019	0.24	0.00	0.00	0.00
16	68,000	1,800	AS	10.0	0.066	0.057	1.14	0.00	0.00	0.00
17	153,400	1,900	AS	10.0	0.030	0.037	0.81	0.00	0.00	0.00
18	81,000	1,900	AS	5.0	0.054	0.038	1.42	?	0.00	0.00
19	253,000	4,000	AS	3.0	0.057	0.026	2.20	0.00	0.00	0.00
20	537,000	7,000	WS	3.0	0.058	0.050	1.15	0.00	0.00	0.00
21	508,000	2,000	AS	0.5	0.006	0.006	1.05	0.00	0.00	0.00
22	178,000	2,000	BUR	5.0	0.077	0.024	3.19	0.00	0.00	0.00
23	120,000	2,000	BUR	60.0	0.154	0.592	0.26	?	0.17	0.00
24	119,000	1,100	BUR	20.0	0.095	0.093	1.03	0.06	0.06	1.00
25	156,000	2,300	AS	1.0	0.059	0.023	2.59	0.00	0.00	0.00
Average					0.060	0.072	0.83	0.003	0.014	0.21

*AS = Asphalt Shingle, BUR = Built-Up Roof, Tile = Tile Roof

The table entries denoted by the question mark symbol (?), correspond to cases where the content loss was ambiguous.

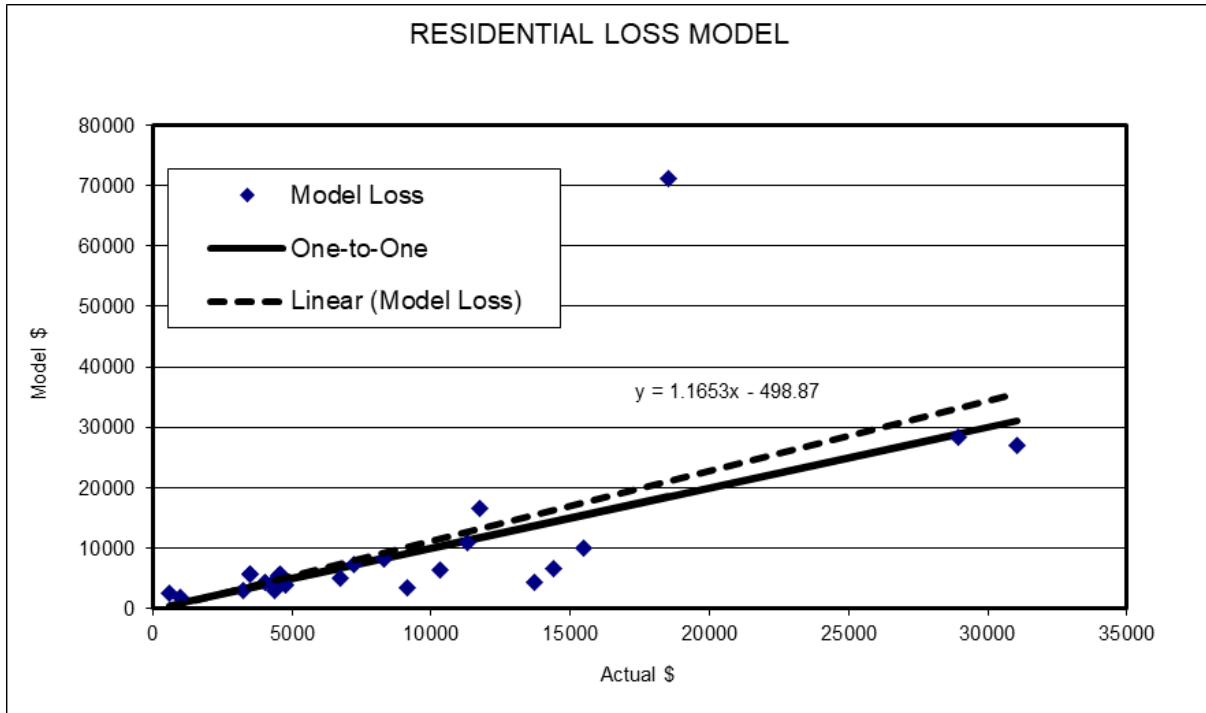


Figure 8-5 Predicted and Actual Losses

For the 25 validation cases considered, Table 8-9 lists the actual and predicted loss ratios for both building and content losses. The case-by-case variability is not unexpected given that most cases are at the low end of the loss curve. In such circumstances, the governing damage state is usually roof cover damage and is generally limited to less than 10%. The variability seen in Table 8-9 is primarily linked to the total replacement threshold. If the computed cost is less than the default minimum repair cost of \$250, the default minimum is registered. Roof cover damage states which do not exceed 0.5% will typically correspond to roof cover tab damage in the case of shingles, or in the case of tile roofs, scattered individual tiles, typically located at the ridges. These types of damage can usually be repaired with minimal effort. However, if the roof cover damage exceeds 0.5%, claim folder data has suggested that the repair costs are often based on a complete or partial re-roofing of the entire roof surface. For example, a gable receiving minimal damage to one side may have the entire cover replaced. The decision to replace the entire roof cover or a portion of the roof cover is at the discretion of the claim adjuster. Factors that are considered when making this decision are the age of the roof, color compatibility issues, discontinuation of or availability of the existing roofing materials, etc. As a result, the adjuster may or may not sanction a total or partial replacement of roofing materials depending on the overall circumstances. The loss model replaces the total roof surface given a damage state exceeding 0.5%.

Table 8-9 also list comparisons of actual and predicted content losses. The model accurately predicted zero content losses for the majority of cases. For case 23, a 17% building value content loss was predicted. The claim folder did not report the actual content dollar loss since the content losses were below the 15% deductible. However, it was reported that there was extensive content damage that approached the 15% deductible, suggesting the predicted 17% content loss is reasonable.

8.1.6 Manufactured Home Loss Module

The manufactured home (MH) loss module is a physically-based damage-to-loss model that computes building economic losses using a combination of explicit and implicit costing techniques. The loss module uses the same modeling approach as the residential loss module (i.e., subdividing the structure into costing subassemblies). Eight basic subassemblies are used: foundation, framing, exterior walls, roofing, interiors, specialties, mechanical, and electrical. The prototypical MH is defined as having an average cost of \$48.86 per square foot (2020 dollars).

8.1.6.1 Losses Associated with Exterior Damage

Losses associated with damage to the building exterior are computed using an explicit costing technique. The explicit costing method directly calculates the repair and replacement costs for damaged MH envelope components using a combination of RSMMeans unit, linear foot, and square foot costs. Explicit costing within the model is carried out for several envelope components such as roof covering, roof decking, windows, entrance doors, fenestration protection, exterior siding, etc. Dollar losses associated with these components are directly calculated using actual damage states and damage replacement thresholds. Damage replacement thresholds are the minimum damage levels at which a building component is completely replaced. Damage replacement thresholds are currently set at a 2.5% damage state for the roof covering (rather than 0.5% for site-built homes) and 5% for roof sheathing, which are determined from field observations and judgment. In addition to replacement thresholds, the loss model also considers building component replacement based on serviceability considerations. For those MH envelope components (windows, entrance doors, garage doors, and fenestration protection) that do not fail under applied load, they may still require replacement after undergoing thousands of load cycles as they become prone to permanent set. The loss model takes serviceability considerations into account by replacing those components that sustain loads exceeding 85% of their ultimate capacity.

As in the residential case, the cost data used in the explicit costing portion of the loss model are derived from the RSMMeans Residential Cost Data and are based on national averages for new construction materials and installation. These data are adjusted to consider the specific geographical location of the loss, the level of work difficulty, and the contractor’s overhead and profit.

8.1.6.2 Losses Associated with Frame Damage or Foundation Failure

Loss ratios associated with the failure of roof-wall connections, wall failure following partial or whole roof failure, floor-wall connection failure, and foundation failure through sliding or overturning are summarized in Table 8-10. The values listed in Table 8-10 are percentages of the MH replacement cost value or the content cost value. Hence, a MH sustaining minor sliding will have a building loss of 10% and a content loss of 0%. The values used in Table 8-10 are compiled from field observations and engineering judgment.

Table 8-10 Building and Content Losses Associated with Manufactured Home Frame Damage or Foundation Failure

Modeled Structure Damage State	Structure Loss (% of Building Value)	Building/Content Loss (% of Content Value)
Minor Roof-Wall Connection Failure	20	0

Modeled Structure Damage State	Structure Loss (% of Building Value)	Building/Content Loss (% of Content Value)
Major Roof-Wall Connection Failure	100	100
Wall Failure Following Roof Failure	100	100
Minor Floor-Wall Connection Failure	30	0
Major Floor-Wall Connection Failure	100	100
Minor Sliding Failure	10	0
Major Sliding Failure	100	100
Overturning	100	100

8.1.6.3 Interior and Content Losses

The implicit costing method calculates losses to the interior and framing of the building as a function of water volume penetrating the building envelope. The functions which relate the volume of water to building losses are based on engineering judgment and field observations and are identical to the residential case.

8.1.7 Economic Loss Module for Commercial Buildings and Essential Facilities

Similar to the residential and manufactured home (MH) loss modules, the commercial and essential facilities loss module is also developed using explicit and implicit costing techniques. The commercial and essential facilities loss model differs from the residential and MH loss models in how the total cost of the building is distributed amongst the subassemblies. Due to the scope of the current commercial model, detailed unit costs are not used to derive the explicit loss for failed components. Rather, subassemblies are cost directly from their damage ratios calculated from the damage model. Changes in cost distribution among subassemblies associated with differences in exterior wall types and common additives are ignored. It is also noted that the commercial model described herein uses different influence functions or cost functions from those used in the residential loss model. Unless noted otherwise, details regarding essential facilities are like those used for commercial buildings.

Due to the scarcity of high-quality loss data, limited calibration has been done with the commercial and essential facilities loss module, which has been developed primarily on the basis of experience and judgment.

8.1.7.1 Subassembly Cost Ratios

The subassembly cost ratios for the model buildings are based on square foot estimates from the RSMeans construction cost data. Seventy commercial/industrial building types are listed in RSMeans, including apartments, banks, churches, factories, hotels, motels, department stores, etc. The Hazus model buildings, which are selected to represent certain building classes, are mapped to one of those 70 building types with possible adjustments to the RSMeans cost ratios according to the number of stories, percentage of exterior door area to the total exterior wall area, and percentage of windows and glazed wall area to the total exterior wall area of the model building.

8.1.7.1.1 Cost Ratio Adjustment – Number of Stories

As indicated in RSMeans, for similar building types, the cost ratios for foundations, substructure, exterior closure, roofing, and mechanical decrease with the increase in the number of stories.

Alternatively, the cost ratios for interior construction and conveying increase with the increase in the number of stories. The changes in superstructure and electrical are not monotonic. Since these changes can be significant, adjustments must be made to the cost ratios if the number of stories for the selected model building is different from that for the model building listed in RSMMeans. Based on the data from RSMMeans, the functions shown in Equation 8-10, Equation 8-11, Equation 8-12, Equation 8-13, and Equation 8-14 are developed to adjust the cost ratio according to the story number of the selected model building.

1. Foundation, substructure, and roofing:

Equation 8-10

$$R'_C = R_C \left(1 - 2.20 \left(\frac{N_m}{N} - 1 \right) \right), \quad \text{for } N_m < N$$

$$R'_C = R_C \left(1 - 0.4 \left(\frac{N_m}{N} - 1 \right) \right), \quad \text{for } N_m > N$$

2. Superstructure:

Equation 8-11

$$R'_C = R_C \left(1 + 0.6 \left(\frac{N_m}{N} - 1 \right) \right), \quad \text{for } N_m < N$$

$$R'_C = R_C \left(1 - 0.8 \left(\frac{N_m}{N} - 1 \right) \right), \quad \text{for } N_m > N$$

3. Exterior closure and mechanical:

Equation 8-12

$$R'_C = R_C \left(1 - 0.2 \left(\frac{N_m}{N} - 1 \right) \right), \quad \text{for } N_m < N$$

$$R'_C = R_C, \quad \text{for } N_m > N$$

4. Interior construction:

Equation 8-13

$$R'_C = R_C \left(1 + 0.2 \left(\frac{N_m}{N} - 1 \right) \right), \quad \text{for } N_m < N$$

$$R'_C = R_C \left(1 + 0.133 \left(\frac{N_m}{N} - 1 \right) \right), \quad \text{for } N_m > N$$

5. Conveying:

Equation 8-14

$$R'_C = R_C \left(1 + 0.6 \left(\frac{N_m}{N} - 1 \right) \right), \quad \text{for } N_m < N$$

$$R'_C = R_C \left(1 + 0.133 \left(\frac{N_m}{N} - 1 \right) \right), \quad \text{for } N_m > N$$

Where:

- N_m is the number of stories for selected model building
- N is the number of stories for the building listed in RSMeans
- R_c is the unadjusted cost ratio
- R'_c is the adjusted cost ratio

No adjustments are made for site work, specialities, or electrical subassemblies.

8.1.7.1.2 Cost Ratio Adjustment – Door, Window, and Glazed Wall Areas

Since exterior closure plays an important role in determining losses, adjustments are made to the cost distributions among all the subassemblies based on the difference in exterior closure between the Hazus model building and the RSMeans model building. Specifically, the costs per square foot for walls, doors, windows and glazed walls are adjusted based on the percentage of the wall area of each subassembly. For example, if the RSMeans model building has 14% of the wall area with windows and glazed walls (cost per square foot=\$1.37) and a Hazus model building has 20% of the wall area with windows, and glazed walls, the adjusted cost per square foot will be \$1.37/0.14*0.20=\$1.96. Note

that since changing cost per square foot for one subassembly will affect the cost ratio for all other subassemblies (because the subtotal changes), the cost ratios for all other subassemblies must be updated accordingly.

Even though other parameters, such as square footage of floor area, perimeter length, exterior wall type, and frame type can also change the cost ratio distribution, it is assumed that their influences can be neglected. Table 8-11 lists the comparison between the cost ratios from RSMMeans (motel, two-three stories) and adjusted cost ratios for the selected model building (a four-story motel). For some subassemblies, the changes in cost ratio can be substantial (e.g., roofing).

Table 8-11 Cost Ratio – RSMMeans Model Building and Hazus Model Building

Damage Variables	RSMMeans Model Building (Three-Story Motel)		Hazus Model Building (Four-Story Motel)	
Foundations				
Footings & Foundations	2.0%	2.5%	1.7%	2.2%
Piles & Caissons	0.0%		0.0%	
Excavation & Backfill	0.5%		0.5%	
Substructures				
Slab on Grade	1.7%	1.7%	1.5%	1.5%
Special Substructures	0.0%		0.0%	
Superstructure				
Columns and Beams	0.0%	13.8%	0.0%	13.6%
Structural Walls	2.6%		2.5%	
Elevated Floors/Diaphragms	6.6%		6.5%	
Roof Decking/Framing	3.2%		3.2%	
Stairs	1.4%		1.4%	
Exterior Closure				
Walls	4.7%	10.3%	4.3%	8.8%
Exterior Wall Finishes	0.0%		0.0%	
Doors	3.9%		3.9%	
Windows & Glazed Walls	1.8%		0.6%	
Roofing				
Roof Covering	1.1%	2.1%	1.0%	1.8%
Insulation	0.7%		0.6%	
Openings & Specialties	0.3%		0.2%	
Interior Construction				
Partitions	8.9%	35.6%	9.4%	37.6%
Interior Doors	7.9%		8.3%	
Wall Finishes	3.7%		3.9%	

Damage Variables	RSMean Model Building (Three-Story Motel)		Hazus Model Building (Four-Story Motel)	
Floor Finishes	9.3%		9.8%	
Ceiling Finishes	4.6%		4.9%	
Interior Surface of Exterior Walls	1.2%		1.3%	
Conveying				
Elevators	2.7%	2.7%	2.8%	2.8%
Special Conveyors	0.0%		0.0%	
Mechanical				
Plumbing	15.9%	22.9%	16.1%	23.2%
Fire Protection	1.8%		1.8%	
Heating	0.0%		0.0%	
Cooling	5.2%		5.3%	
Special Systems	0.0%		0.0%	
Electrical				
Service & Distribution	0.5%	8.4%	0.5%	8.5%
Lighting & Power	7.4%		7.5%	
Special Electrical	0.5%		0.5%	
Special Construction				
Specialties (& Additives)	0.0%	0.0%	0.0%	0.0%
Total	100%	100%	100%	100%

8.1.7.2 Building Loss Model

The damage state parameters required for the commercial loss model include damage to windows, doors, roof covering, roof decking, and roof framing, damaged wall surface area, water from fenestration damage, water from roof cover damage, and water from roof sheathing damage. It is assumed that the explicit losses are caused primarily by the damage to windows, doors, roofs, and walls, while water entering the building is the major cause of losses to the interior, mechanical, electrical, and conveying systems (i.e., implicit losses). To reflect the different damage-to-loss propagation mechanisms for different components, a set of costing functions are developed based on experience and judgment. Table 8-12 and Table 8-13 show the influence matrixes for explicit loss and implicit loss, respectively. Each row in Table 8-12 and Table 8-13 indicate a subassembly and each column indicates an input damage state. The value in each cell of Table 8-12 or Table 8-13 is a cost function index, which indicates the function type used to map damage to loss for a given damage parameter. For example, damage to the roof cover, roof deck, and roof frame all can result in insulation losses. However, the insulation loss ratios due to the same damage ratios from roof cover, roof deck, and roof frame are different. The cost functions for explicit insulation losses due to roof cover, roof deck, and roof frame are determined to be type 1, type 4, and type 4, respectively (see Table 8-12). The cost function indices, as well as their associated formulas, are shown in Table 8-14. Figure 8-6 shows

the plots of these influence functions. In determining the loss ratios associated with roof cover damage, the influence functions for mechanical, electrical, and special construction are multiplied by 0.1, 0.2, and 0.3, respectively, to account for the reduced damage severity than by the interior construction (based on limited calibration studies).

Several repair and replacement thresholds are used in the current commercial model to reflect the fact that when a certain percentage of damage to a subassembly is achieved, the entire subassembly will be replaced. These thresholds are 5%, 10%, and 30% for roof cover, roof deck, and wall cladding, respectively.

For the subassemblies with more than one damage variable involved, the possibility of overlapping is considered using their joint probability. Hence, the resulted loss ratio (R) for a subassembly with two contributing variables is approximated by $R=R_1+R_2-R_1R_2$, with R_1 =loss ratio resulted from the first variable only and R_2 =loss ratio resulted from the second variable only. After the loss ratio for each subassembly has been calculated, the total building loss ratio is obtained by simply adding up the loss ratios for the subassemblies. The building loss ratio is then multiplied by a repair and replacement factor of 1.25 and an overhead and profit factor of 1.20 to account for the additional costs associated with the repair and remodeling. The total economic loss of the building is also constrained not to exceed the total replacement cost.

Figure 8-7 shows a scatter plot of the calculated losses due to building envelope breaches) are seen to contribute most to the total building loss. The explicit losses caused by damage to roofs, walls, and fenestration account for less building loss ratio as a function of open terrain peak gust wind speed based on 20,000-year simulation for a four-story motel in the Miami area. The contribution to the total building loss ratio from each damage state considered is also shown in this figure. Implicit losses (interior, mechanical, and electrical than 20% of the total building loss.

Table 8-12 Influence Matrix for Explicit Building Loss

Damage Variables	Windows	Doors	Roof Covering	Roof Decking	Roof Framing	Wall Surf. by Missile	Wall Surf. by Pressure	Wall Structure
Superstructure								
Columns and Beams	0	0	0	0	0	0	0	5
Structural Walls	0	0	0	0	0	0	0	1
Elevated Floors/ Diaphragms	0	0	0	0	0	0	0	5
Roof Decking/ Framing	0	0	0	2	1	0	0	0
Stairs	0	0	0	0	0	0	0	0
Exterior Closure								
Walls	0	0	0	0	0	9	1	1

Damage Variables	Windows	Doors	Roof Covering	Roof Decking	Roof Framing	Wall Surf. by Missile	Wall Surf. by Pressure	Wall Structure
Exterior Wall Finishes	0	0	0	0	0	9	1	1
Doors	0	1	0	0	0	0	0	1
Windows & Glazed Walls	1	0	0	0	0	0	0	1
Roofing								
Roof Covering	0	0	3	0	0	0	0	0
Insulation	0	0	1	4	4	0	0	0
Openings & Specialties	0	0	1	1	4	0	0	0

Table 8-13 Influence Matrix for Implicit Building Loss

Damage Variables	Water Depth by Fen.	Water Depth by Cover	Water Depth by Sheath	Wet Area by Cover	Wet Area by Sheath
Interior Construction					
Partitions	6	0	0	7	8
Interior Doors	6	0	0	7	8
Wall Finishes	6	0	0	7	8
Floor Finishes	6	0	0	7	8
Ceiling Finishes	6	0	0	7	8
Interior Surface of Exterior Walls	6	0	0	7	8
Conveying					
Elevators	0	0	0	0	0
Special Conveyors	0	0	0	0	0
Mechanical					
Plumbing	6	0	0	7	8
Fire Protection	6	0	0	7	8
Heating	6	0	0	7	8
Cooling	6	0	0	7	8
Special Systems	6	0	0	7	8
Electrical					
Service & Distribution	6	0	0	7	8
Lighting & Power	6	0	0	7	8
Special Electrical	6	0	0	7	8
Special Construction					

Damage Variables	Water Depth by Fen.	Water Depth by Cover	Water Depth by Sheath	Wet Area by Cover	Wet Area by Sheath
Specialties (& Additives)	6	0	0	7	8

Table 8-14 Influence Functions

Function Index	Formula*
1	$y = x$
2	$y = \frac{2}{\pi} \tan^{-1}(e^{0.8x} - 1)$
3	$y = \frac{2}{\pi} \tan^{-1}(e^{50.0x^{1.5}} - 1)$
4	$y = \frac{2}{\pi} \tan^{-1}(e^{5.0x} - 1)$
5	$y = \frac{2}{\pi} \tan^{-1}(e^{0.4x} - 1)$
6	$y = \frac{2}{\pi} \tan^{-1}(e^{10.0x} - 1)$
7	$y = \frac{2}{\pi} \tan^{-1}(e^{3.1x^{2.0}} - 1)$
8	$y = \frac{2}{\pi} \tan^{-1}(e^{8.0x} - 1)$
9	$y = \frac{2}{\pi} \tan^{-1}(e^{1.4x} - 1)$

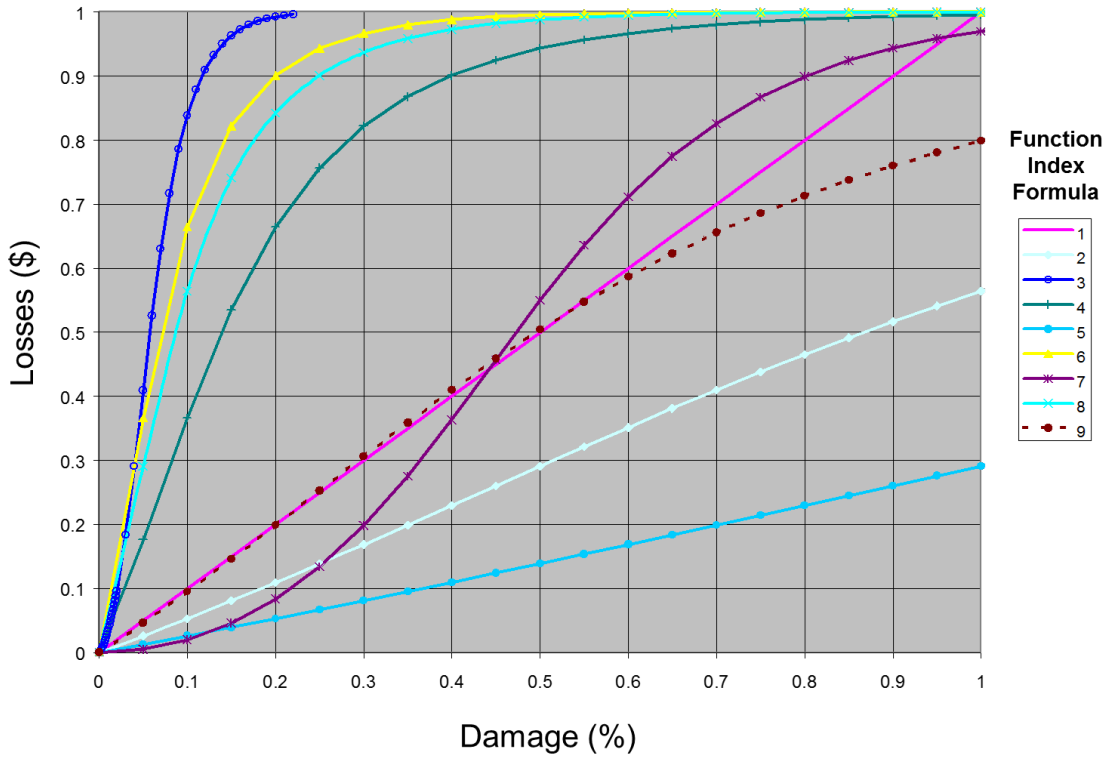


Figure 8-6 Plots of Influence Functions

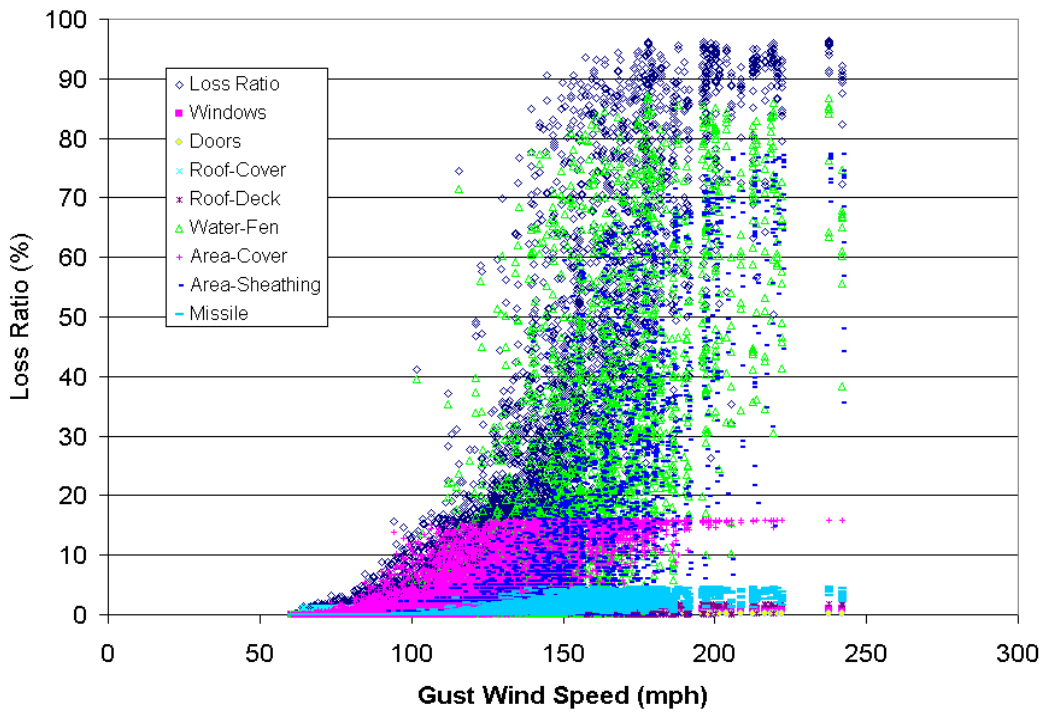


Figure 8-7 Relationship between Open Terrain Gust Wind Speed and Building Loss Ratio for a Four-Story Motel

8.1.7.3 Content Loss Model

The content loss model for commercial buildings is almost identical to the content loss model for residential buildings developed previously. Content losses are assumed to be highly correlated with the damage to the interior of the building, but only begin after at least some damage has been done to the interior of the building. Water entering the building is also believed to be the major cause of content loss. Three modeled damage variables (water depth due to fenestration damage, wetted interior area due to roof cover damage, and wetted interior area due to roof sheathing damage) are used to model the content loss. Note that each of these three variables are related to the water entering a building after the breach of the building envelope.

Content losses due to fenestration damage are modeled as:

Equation 8-15

$$L_{c1} = 4.0D_{fen}, \quad \text{for } D_{fen} < 0.25''$$

$$L_{c1} = 1.0, \quad \text{for } D_{fen} \geq 0.25$$

Where:

L_{c1} is content loss ratio due to fenestration damage

D_{fen} is the accumulated water depth due to fenestration damage

Content losses due to roof cover damage are assumed to be accrued at one half the rate associated with losses to the interior building. It is also assumed that no contents are damaged until a threshold of 20% of roof cover damage has occurred. A linear approximation is made to the costing function of the interior damage due to roof cover damage to derive the costing function for content loss:

Equation 8-16

$$L_{c2} = 0.0, \quad \text{for } R_{cover} < 0.2$$

$$L_{c2} = 1.67(R_{cover} - 0.2)(0.5), \quad \text{for } R_{cover} \geq 0.2$$

Where:

L_{c2} is content loss ratio due to roof cover damage

R_{cover} is the wetted interior ratio due to roof cover damage

The content loss associated with roof sheathing damage is modeled as:

Equation 8-17

$$L_{c3} = 4.0R_{sheath}, \quad \text{for } R_{sheath} < 0.25$$

$$L_{c3} = 1.0, \quad \text{for } R_{sheath} \geq 0.25$$

Where:

L_{c3} is the content loss ratio due to roof sheathing damage

R_{sheath} is the wetted interior ratio due to roof sheathing damage

The final content loss is taken to be the maximum among the losses produced by fenestration damage, roof cover damage or roof sheathing damage, i.e., $\max(L_{c1}, L_{c2}, L_{c3})$. Figure 8-8 shows the relationship between building loss ratio and content loss ratio for a four-story motel located in the Miami area using a 20,000-year simulation.

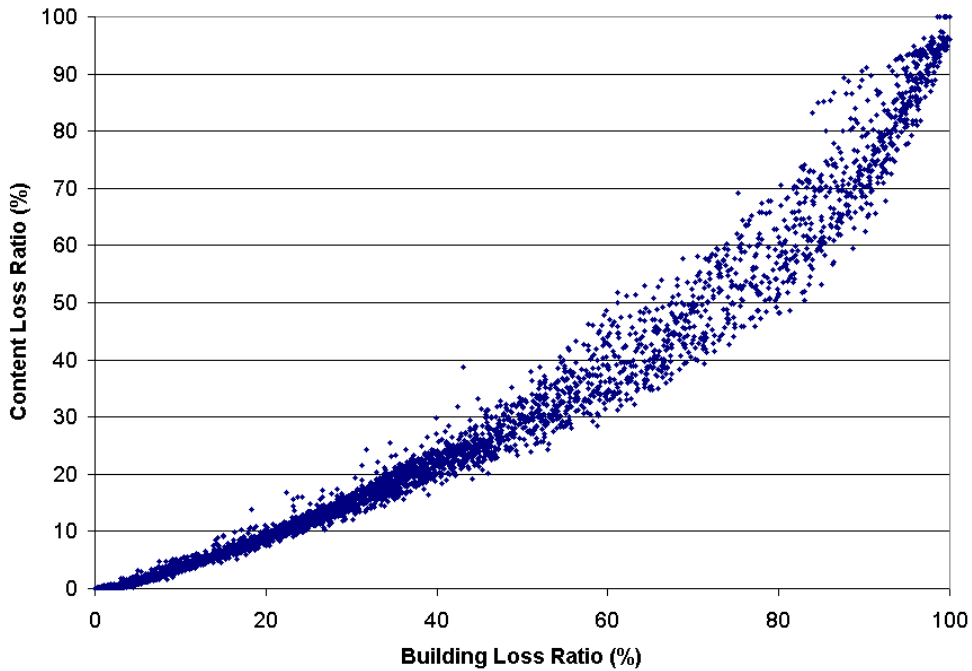


Figure 8-8 Relationship between Building Loss Ratio and Content Loss Ratio for a Four-Story Motel

8.1.8 Business Interruption Model

The business interruption model for commercial buildings follows the business interruption model developed for earthquakes in Hazus-99 (FEMA, 1999). The model applies a multiplier to expected loss of use to estimate the duration of business interruption. The model for expected loss of use follows the approach presented in Section 8.1.4.3 for single-family buildings. The default multipliers for estimating business interruption are provided in Table 8-15. As explained in the *Hazus Earthquake Model Technical Manual* (FEMA, 2022), the business interruption multiplier reflects the fact that business interruption is not directly related to loss of use for certain types of business (since they can rent alternative space or use spare industrial/commercial capacity elsewhere). The output from the business interruption model is the expected number of days for a business to be fully recovered. The relationship between the business interruption, N (days), and building loss ratio can be expressed as:

Equation 8-18

$$N = N_{lou} (R_{building}) * Mod(R_{building})$$

Where:

$N_{lou}()$ is the building loss of use (days) considering delays in decision-making, financing, inspection, etc.

$Mod()$ is the business interruption multiplier from Table 8-15

Both loss of use and business interruption multiplier are modeled as functions of building loss ratio ($R_{building}$). Figure 8-9 illustrates the relationship between loss of use, business interruption, and building loss for a motel (RES4).

Table 8-15 Business Interruption Timetable

Specific Occupancy Type	Occupancy Class	Loss of Use Multiplier				
		Building Loss Ratio				
		0%	2%	10%	50%	100%
RES3	Multi-Family Dwelling	0	0	0.5	1	1
RES4	Temporary Lodging	0	0	0.5	1	1
RES5	Institutional Dormitory	0	0	0.5	1	1
RES6	Nursing Home	0	0	0.5	1	1
COM1	Retail Trade	0.5	0.1	0.1	0.3	0.4
COM2	Wholesale Trade	0.5	0.1	0.2	0.3	0.4
COM3	Personal and Repair Service	0.5	0.1	0.2	0.3	0.4
COM4	Professional/Technical/Business Services	0.5	0.1	0.1	0.2	0.3
COM5	Banks/Financial Institutions	0.5	0.1	0.05	0.03	0.03
COM6	Hospital	0.5	0.1	0.5	0.5	0.5
COM7	Medical Office/Clinic	0.5	0.1	0.5	0.5	0.5
COM8	Entertainment & Recreation	0.5	0.1	1	1	1
COM9	Theaters	0.5	0.1	1	1	1
COM10	Parking	0.1	0.1	1	1	1
IND1	Heavy Industrial Factory	0.5	0.5	1	1	1
IND2	Light Industrial Factory	0.5	0.1	0.2	0.3	0.4
IND3	Food/Drug/Chemicals Factory	0.5	0.2	0.2	0.3	0.4
IND4	Metals/Minerals Processing Factory	0.5	0.2	0.2	0.3	0.4
IND5	High Technology Factory	0.5	0.2	0.2	0.3	0.4
IND6	Construction	0.5	0.1	0.2	0.3	0.4
AGR	Agriculture	0	0	0.05	0.1	0.2
REL	Church/Membership Organization	1	0.2	0.05	0.03	0.03

Specific Occupancy Type	Occupancy Class	Loss of Use Multiplier				
		Building Loss Ratio				
		0%	2%	10%	50%	100%
GOV1	General Service	0.5	0.1	0.02	0.03	0.03
GOV2	Emergency Response	0.5	0.1	0.02	0.03	0.03
ED1	Schools/Libraries	0.5	0.1	0.02	0.05	0.05
ED2	College/University	0.5	0.1	0.02	0.03	0.03

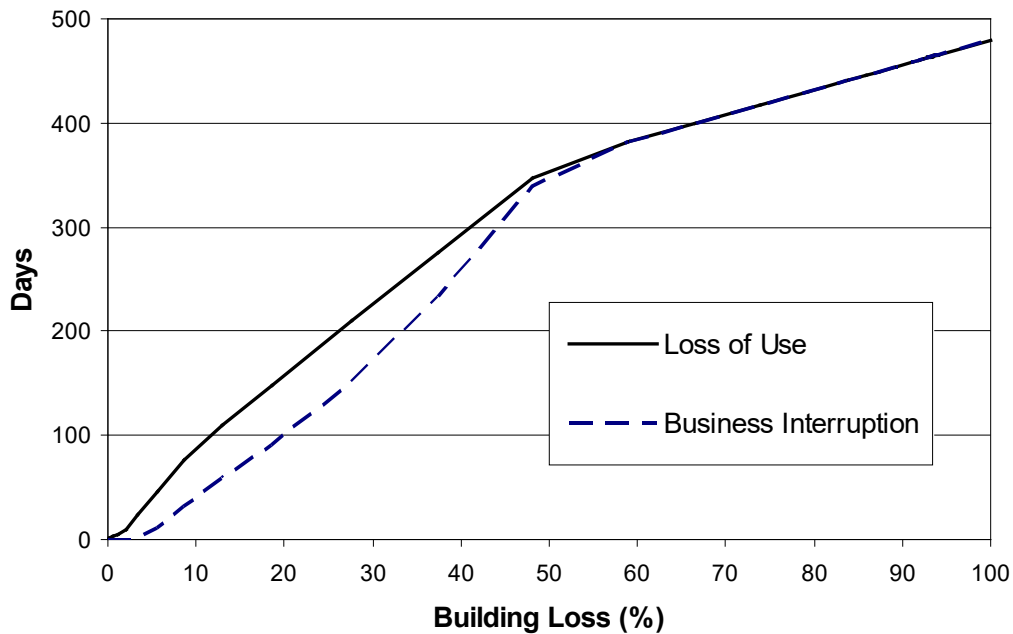


Figure 8-9 Relationship between Building Loss, Loss of Use, and Business Interruption for a Motel

8.1.8.1 Loss of Function for Essential Facilities

Loss of function is the amount of time (days) that a facility is unable to provide the public with general services from a specific facility. This would represent the amount of time a school is closed to students, and the number of days a specific fire station cannot provide emergency fire and rescue services to its designated coverage area.

Most of the validation data obtained in developing loss of function models comes from a phone survey of individual facilities conducted in the Houston area regarding Hurricane Ike (2008) and in Escambia County in Florida after Hurricane Ivan (2004) in 2011. Data from the FEMA HMTAP 440 report was also used.

8.1.8.2 Loss of Function for Fire Stations

The model for fire station loss of function represents the average amount of time (days) fire stations in a given area will not be able to provide service to the public from that facility. While an individual fire station may suffer a disruption in its ability to provide emergency services, the public, as a whole, may

not be affected at all since the equipment and resources of these disrupted facilities can be moved to other neighboring stations. Fire station loss of function is intended to alert the decision maker that facilities in a given Study Region may not be able to provide service after an event and aid the decision maker in equipment and personnel re-assignment.

A phone survey of fire stations in the Houston area that were affected by Hurricane Ike (2008) showed that while fire stations can experience wind-induced damage, they typically do not close due to minor damage and power loss. For one facility, building loss was estimated to be greater than 10% when wind lifted roof panels, and allowed water to enter the facility. Despite this, the fire station did not close. Only one fire station was found to have suffered enough damage to close for 60 days due to wind damage among the 50+ fire stations contacted. Building loss was unknown for this case and is assumed to be an isolated case in Figure 8-9. With respect to power loss, fire stations typically have back-up generators in place or are brought to the site.

The modeled curve in Figure 8-10 represents a fire station of moderate strength in light suburban terrain, in an area that could produce a mix of residential and commercial wind-borne debris. It has been assumed that loss of function around one day starts to occur when the building experiences roughly 6% building loss (the replacement value of the roof cover).

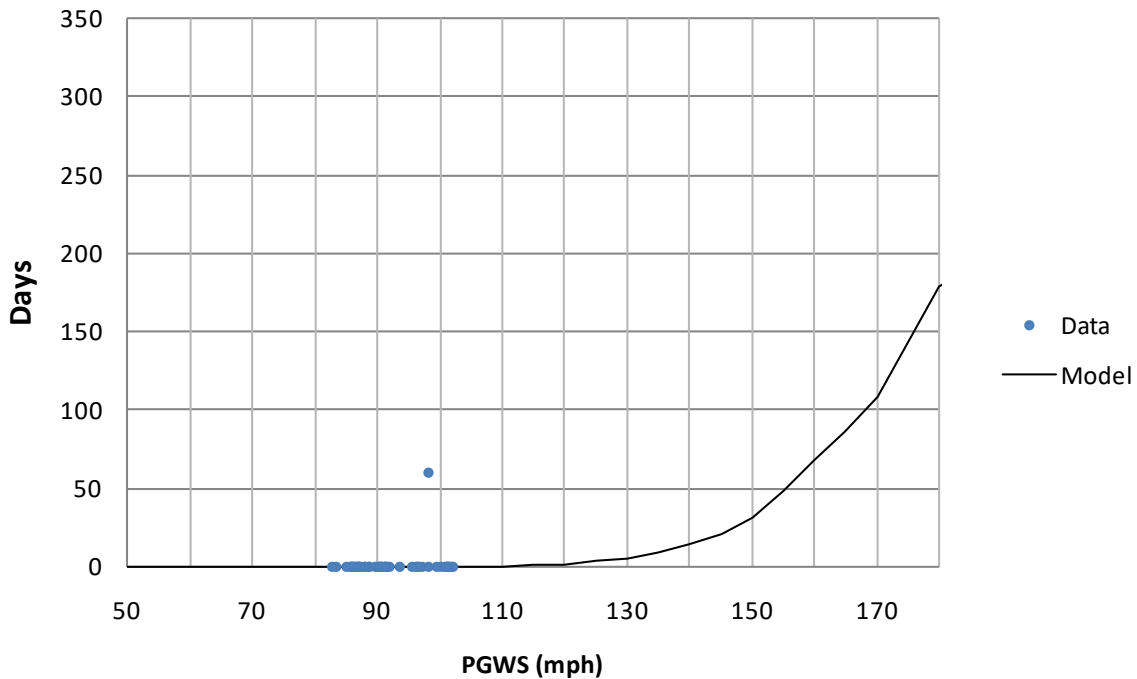


Figure 8-10 Relationship Between Modeled loss of Function and Actual Loss of Function for a Given Fire Station

8.1.8.3 Loss of Function for Schools

The model for school loss of function represents the average amount of time (days) a school will be closed to students, while essential personnel may still report to the school during this period. The data displayed in Figure 8-11 are for independent school districts (ISDs) from the Houston area (Hurricane Ike, 2008) and Escambia County (Hurricane Ivan, 2004). The loss of function model for schools was

calibrated against ISD data as a whole, rather than individual schools, since decisions about school closings are typically made at the district level, rather than at the facility level. From the phone survey conducted, ISDs typically closed due to lack of electricity.

A school in suburban terrain, susceptible to residential wind-borne debris of moderate strength, was assumed when calibrating the loss of function model. Loss of function for schools is not defined by a specific building value or building feature, as is the case with fire stations, but has more to do with a loss of power as a function of wind speed. At higher wind speeds, it is assumed that building damage will drive the loss of function rather than power restoration. Building loss data accompanying loss of function data obtained from the phone survey for individual schools was typically less than 1% of the estimated building value.

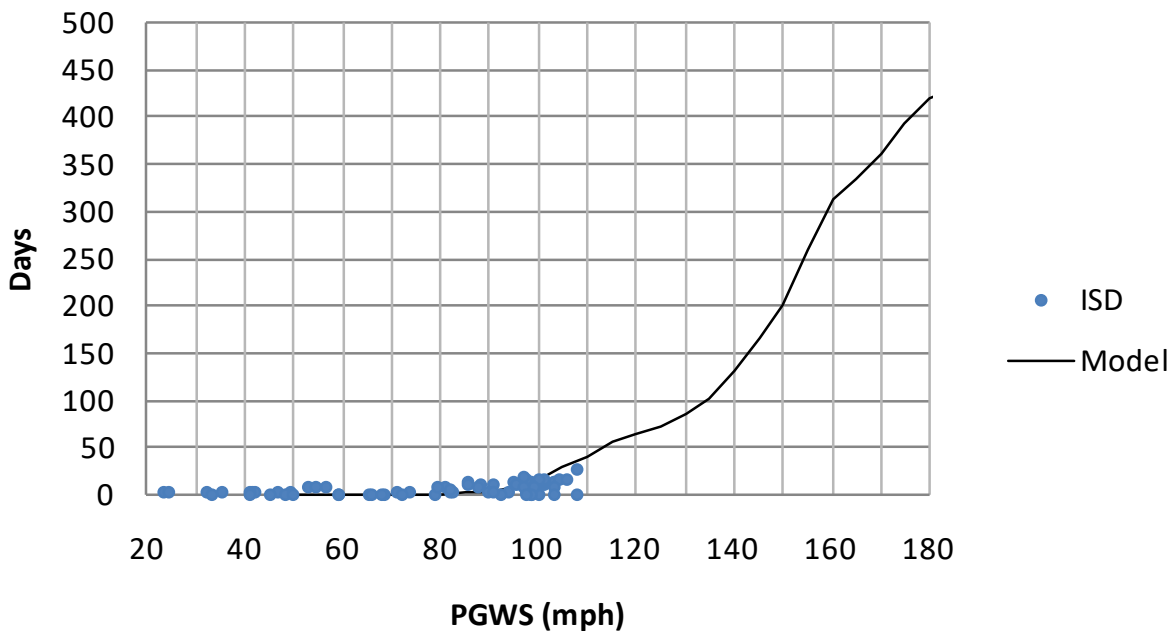


Figure 8-11 Relationship Between Modeled Loss of Function and Actual Loss of Function for an Elementary School of Moderate Strength located in a Residential Area

8.1.8.4 Loss of Function for Hospitals

The model for hospital loss of function represents the average amount of time (days) that all beds in a hospital will be unavailable to patients. While a hospital may technically be “closed” to the general public during a hurricane, if all beds are still available to patients (patients were not moved from the facility), then the loss of function recorded was zero days.

Several hospitals contacted in the Houston area who were affected by Hurricane Ike (2008) were noted to have closed due to lack of power, but most had emergency back-up power in place, aiding in their ability to stay open. While several hospitals did experience damage, specific building loss and building value were unavailable.

Modeled loss of function of a day is assumed to occur close to 1% of the building’s value (roof cover cost). Figure 8-12, Figure 8-13, and Figure 8-14 plot modeled loss of function and phone survey data, along with FEMA HMTAP 440 data due to Hurricane Charley (2004), Ike (2008), and Ivan (2004) for averagely constructed small, medium, and large hospitals respectively.

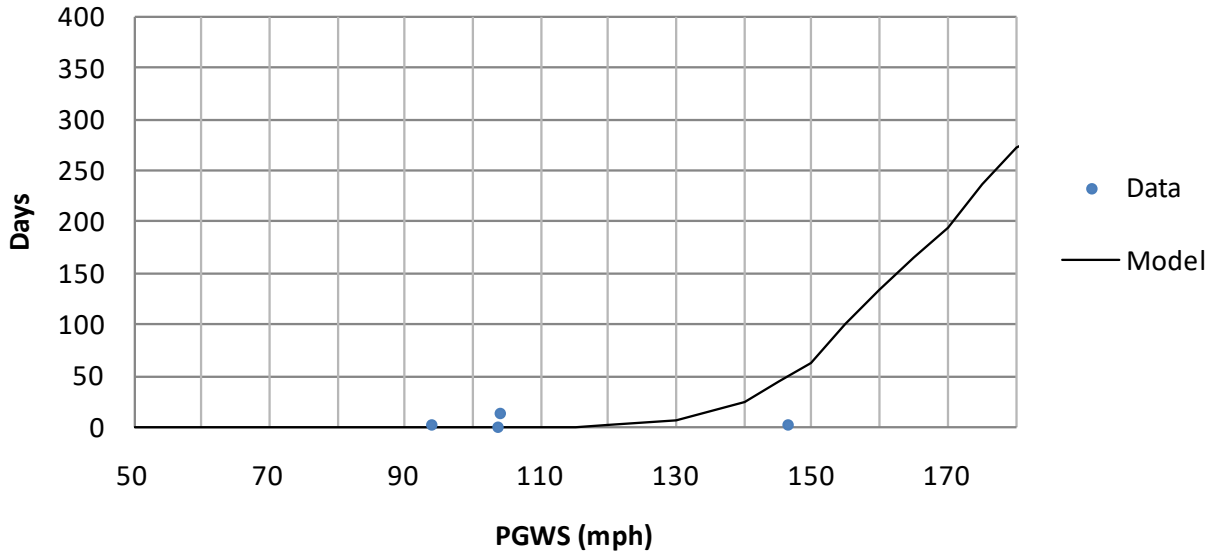


Figure 8-12 Relationship Between Modeled Loss of Function and Actual Loss of Function for a Small Hospital

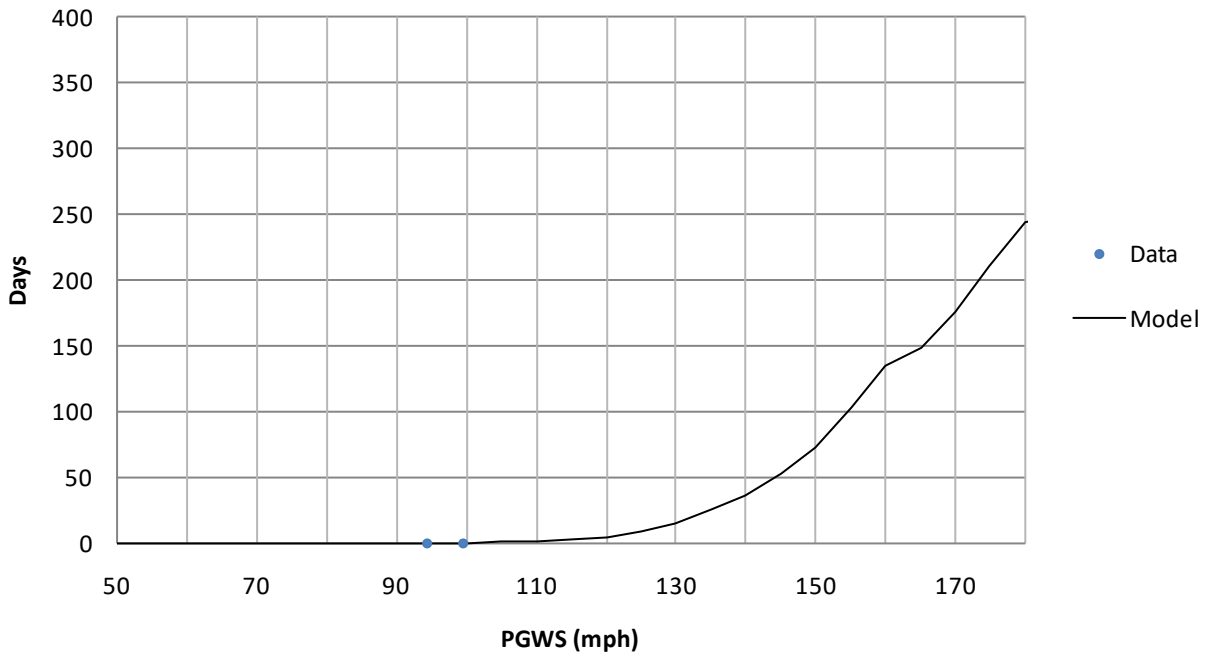


Figure 8-13 Relationship Between Modeled Loss of Function and Actual Loss of Function for a Medium Hospital

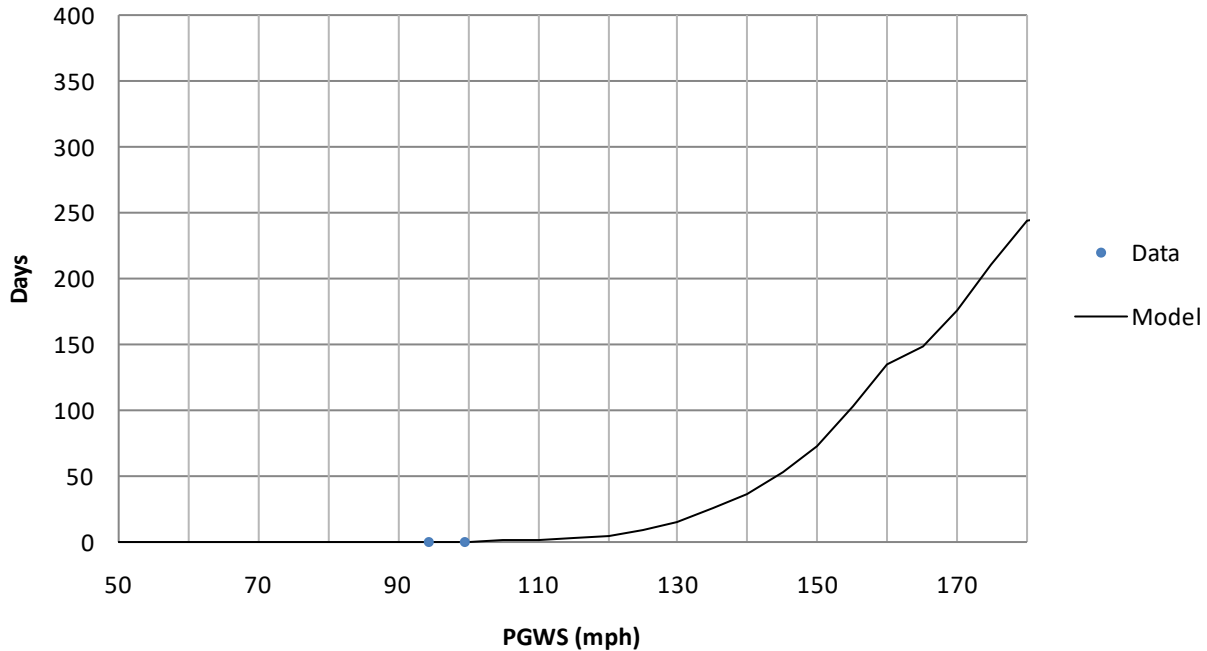


Figure 8-14 Relationship Between Model Loss of Function and Actual Loss of Function for a Large Hospital

8.2 Average Annual Losses

The hurricane average annual loss considers all future losses for a hurricane hazard resulting from possible hazard events with different magnitudes and return periods averaged on a “per year” basis. It can be used to help examine the benefits of mitigation and compare the economic risks of different hazards in one location.

Hazus can be used to generate the average annual loss by summing all the losses produced during the 20,000-year simulation of hurricanes and dividing by 20,000 years.

8.2.1 Residential Buildings

Using the same hurricane wind speed and direction data used in the development of the damage curves for residential buildings, per storm losses were estimated using the building and content loss models described earlier. Loss functions have been produced for the basic, unmitigated buildings (one-story or two-story, hip or gable, 6d or 8d sheathing nails, straps or toe-nails, wood frame, reinforced masonry or unreinforced masonry, no garage, 20 psf garage door or 10 psf garage door) for the four basic terrain categories: open, suburban, lightly treed suburban, and heavily treed suburban.

For more information on example plots of building loss versus wind speed, where the building loss is expressed as a fraction of the total value of the building and thus ranges between zero and one, please contact the Hazus Help Desk (see Section 1.5) for the *Hazus Hurricane Model Technical Manual Appendices* (FEMA, 2021). The appendices also included loss functions associated with contents loss expressed as a fraction of the assumed content value (taken as 50% of the value of the building).

Also in the Appendices, are the average annual building loss, content loss, and total loss by building construction, for all of the 144 residential building configurations (e.g., single-story, hip roof, 6d sheathing nails, toe-nailed roof-wall connection, wood frame, no garage residence) provided in Hazus can also be found in the appendices. Note that the losses are normalized by the building value in all cases and that the total loss represents the sum of building, contents, and alternate living expenses. Again, the values given in the tables reflect the average annual losses for structures located in the South Florida area (South Florida wind building characteristics distribution). Although 2003 replacement costs were used for the analysis, the 2003 annual losses were normalized by the 2003 replacement costs making the analysis still relevant today.

8.2.1.1 Mitigation

In order to examine the effect of mitigation on residential building losses, five different mitigation cases were examined as indicated below:

1. Installation of shutters.
2. Upgrade roof (roof sheathing and roof cover).
3. Upgrade roof and apply secondary water resistance.
4. Install shutters and upgrade roof.
5. Install shutters, upgrade roof, and apply secondary water resistance.

The upgraded roof is modeled assuming that the existing roof (nailed with either 6d nails or 8d nails with a 6"/12" spacing), is upgraded by adding 8d nails so the deck is connected to the roof trusses with a 6"/6" pattern. At the same time, it is assumed that more wind resistant roof shingles are installed. These upgraded shingles are modeled by increasing the resistance of the basic shingles by 20%.

Secondary water resistance is provided by applying a waterproof seal, or cover, over the spaces between the roof sheathing panels that prevents water from entering the building through the roof if the roof cover fails in a storm.

Methods for applying secondary water resistance include hot-mopping the entire roof deck with tar prior to the application of the roof cover or covering the spaces between sheathing panels with bituminous strips, usually manufactured for use as ice guards.

There are several products on the market now that are used in roofing of commercial and residential buildings to stop the formation of ice dams. This class of products are correctly referred to as "Self-Adhering Modified Bitumen" products but are generically referred to as Ice & Water shields. These products are an asphalt product with a polymer modifier added to give it a rubber gasket texture. The backing has an adhesive with a paper covering that is removed upon application. The top of the sheet is often a sand roughened surface or plastic film that keeps the product from sticking to itself during shipping and provides a skid resistant surface to work on after application.

This product is installed after the old roofing material is removed down to the deck and before the new roofing material is installed. It should be installed along all edges of the roof and along *all* joints between the plywood sheets. This will prevent water from penetrating through the joints after the loss of the roof covering occurs. The product is manufactured in various widths. An economical use of the product for plywood joint sealing is the 6" width rather than the 3' width typical of many of the products. An example of the application of this type of secondary water protection is shown in Figure 8-15.

In order to model the effect of secondary water resistance, it is assumed that this mitigation approach is 95% effective, thus when the roof cover fails, the ensuing losses associated with roof cover failure (described in Section 8.1.4) are reduced to 5% of the baseline (no secondary water resistance) estimates.



Figure 8-15 Example of Self-Adhering Waterproof Underlayment Used to Tape Plywood Joints, Ridges and Eaves; Photo Depicts Use Around Fenestrations

The loss analysis performed for the unmitigated buildings is repeated for the mitigated buildings to produce loss versus wind speed curves as well as average annual losses. For more information on example loss function plots, please contact the Hazus Help Desk (see Section 1.5) for the *Hazus Hurricane Model Technical Manual Appendices (FEMA, 2021)*. Also in the Appendices, are the average annual losses (building, contents, and total) for the five mitigation strategies listed above. Table 8-16 summarizes the effect of the various building parameters on the average annual building loss and Table 8-17 gives ranges of the reductions in total loss associated with the five mitigation strategies.

Table 8-16 Percent Increases in the Average Annual Total Loss Due to Changes in Building Parameters – Residential Buildings

Parameter	Increase in Average Annual Building Loss		
	Min	Avg	Max
Treed to Open Terrain	141%	230%	320%
One-Story to Two-Story	38%	73%	129%
8d to 6d Roof Sheathing Nails	-1%	5%	31%
Strapped to Toe-Nailed Roof/Wall Connections	10%	31%	82%
Hip to Gable Roof	2%	22%	41%
No Garage to Strong Garage Door	-14%	-5%	5%
No Garage to Weak Garage Door	-8%	6%	43%
Reinforced Masonry to Unreinforced Masonry Walls	-2%	0%	2%
Unreinforced Masonry to Wood Frame Walls	-2%	0%	2%

Table 8-17 Percent Decreases in the Average Annual Total Loss Due to Mitigation Parameters– Residential Buildings

Mitigation Strategy	Decrease in Average Annual Building Loss		
	Min	Avg	Max
Install Shutters	17%	33%	46%
Upgrade Roof	3%	16%	49%
Add Secondary Water Resistance	3%	12%	35%
Install Shutters and Upgrade Roof	46%	59%	71%
Install Shutters, Upgrade Roof, and Add Secondary Water Resistance	51%	68%	85%
Upgrade Roof and Add Secondary Water Resistance	4%	19%	57%

8.2.2 Manufactured Homes

Using the hurricane wind speed and direction data used to develop the damage function curves for manufactured homes, the storm losses were estimated through the combination of the loss model described above and the storm-by-storm damage estimates, to produce estimates of economic loss as a function of peak gust wind speed in open terrain. The resulting loss functions, computed separately for the economic losses to the building and to the contents, are given in the Appendices. For more information on the resulting loss functions, please contact the Hazus Help Desk (see Section 1.5) for the *Hazus Hurricane Model Technical Manual Appendices* (FEMA, 2021). Table 8-18 and Table 8-19 lists the average annual loss data for each of the manufactured homes analyzed.

Table 8-18 Annual Average Building Loss Ratios – Manufactured Homes

Average Annual Building Loss Normalized by Building Value					
Mobile Home Construction	Terrain Surface Roughness (m)				
	$z_0 = 0.03$	$z_0 = 0.15$	$z_0 = 0.35$	$z_0 = 0.7$	$z_0 = 1.0$
Pre-HUD, Not Tied Down	0.0303	0.0225	0.0167	0.0126	0.0110
Pre-HUD, Tied Down	0.0277	0.0203	0.0147	0.0106	0.0090
HUD, Not Tied Down	0.0294	0.0211	0.0157	0.0119	0.0104
HUD, Tied Down	0.0262	0.0183	0.0131	0.0094	0.0079
1994 HUD – Wind Zone I, Tied Down	0.0314	0.0240	0.0179	0.0136	0.0117
1994 HUD – Wind Zone II, Tied Down	0.0129	0.0099	0.0069	0.0048	0.0040
1994 HUD – Wind Zone III, Tied Down	0.0121	0.0091	0.0064	0.0046	0.0038

Table 8-19 Annual Average Content Losses – Manufactured Homes

Average Annual Content Loss Normalized by Building Value					
Mobile Home Construction	Terrain Surface Roughness (m)				
	$z_0 = 0.03$	$z_0 = 0.15$	$z_0 = 0.35$	$z_0 = 0.7$	$z_0 = 1.0$
Pre-HUD, Not Tied Down	0.0139	0.0102	0.0075	0.0055	0.0047
Pre-HUD, Tied Down	0.0121	0.0088	0.0061	0.0041	0.0034
HUD, Not Tied Down	0.0134	0.0095	0.0070	0.0052	0.0044
HUD, Tied Down	0.0113	0.0077	0.0052	0.0034	0.0027
1994 HUD – Wind Zone I, Tied Down	0.0139	0.0107	0.0077	0.0057	0.0047
1994 HUD – Wind Zone II, Tied Down	0.0049	0.0039	0.0025	0.0016	0.0013
1994 HUD – Wind Zone III, Tied Down	0.0044	0.0034	0.0023	0.0015	0.0012

8.2.3 Marginally Engineered or Non-Engineered Hotel/Motel and Multi-Family Residential Buildings

The commercial loss model described in Section 8.1.7 has been coupled with the damage results for the multi-family residential buildings to produce estimates of losses as a function of wind speed. The same 20,000-year storm simulation used to produce the loss plots for the single-family residential buildings was used for the multi-family buildings. The assumed subassembly cost distributions are listed in Table 8-20, Table 8-21, and Table 8-22 for one-story motels, two to three-story motels, and four to seven-story hotels, respectively.

For more information on example building and content loss functions, please contact the Hazus Help Desk (see Section 1.5) for the *Hazus Hurricane Model Technical Manual Appendices* (FEMA, 2021). The appendices also present the average annual building loss (expressed as a fraction of the total building value) for gable/hip roofs with shingles, flat roofs with built-up roof cover and flat roofs with single ply

membrane roof covers, and the average annual content loss (also expressed as a fraction of the building value) for the same three building classes, respectively.

Table 8-23 presents a summary of the effects of various building parameters on average annual building loss.

Table 8-20 Subassembly Cost Distributions for One-Story Motels

Subassemblies	Cost Ratios	
Foundations		
Footings & Foundations	8.1%	9.8%
Piles & Caissons	0.0%	
Excavation & Backfill	1.6%	
Substructures		
Slab on Grade	4.7%	4.7%
Special Substructures	0.0%	
Superstructure		
Columns and Beams	0.0%	6.6%
Structural Walls	0.0%	
Elevated Floors/Diaphragms	0.0%	
Roof Decking/Framing	6.6%	
Stairs	0.0%	
Exterior Closure		
Walls	10.1%	18.4%
Exterior Wall Finishes	0.0%	
Doors	4.0%	
Windows & Glazed Walls	4.2%	
Roofing		
Roof Covering	1.6%	3.6%
Insulation	1.3%	
Openings & Specialties	0.7%	
Interior Construction		
Partitions	6.5%	25.8%
Interior Doors	1.7%	
Wall Finishes	2.7%	
Floor Finishes	8.8%	
Ceiling Finishes	4.4%	
Interior Surface of Exterior Walls	1.7%	
Conveying		
Elevators	0.0%	0.0%

Subassemblies	Cost Ratios	
Special Conveyors	0.0%	
Mechanical		
Plumbing	15.8%	23.5%
Fire Protection	3.1%	
Heating	0.0%	
Cooling	4.7%	
Special Systems	0.0%	
Electrical		
Service & Distribution	0.8%	7.6%
Lighting & Power	6.4%	
Special Electrical	0.4%	
Special Construction		
Specialties (& Additives)	0.0%	0.0%
Total	100%	100%

Table 8-21 Subassembly Cost Distributions for Two and Three-Story Motels

Subassemblies	Cost Ratios	
Foundations		
Footings & Foundations	2.0%	2.5%
Piles & Caissons	0.0%	
Excavation & Backfill	0.5%	
Substructures		
Slab on Grade	1.7%	1.7%
Special Substructures	0.0%	
Superstructure		
Columns and Beams	0.0%	13.8%
Structural Walls	2.6%	
Elevated Floors/Diaphragms	6.6%	
Roof Decking/Framing	3.2%	
Stairs	1.4%	
Exterior Closure		
Walls	4.7%	10.3%
Exterior Wall Finishes	0.0%	
Doors	3.9%	
Windows & Glazed Walls	1.8%	
Roofing		

Subassemblies	Cost Ratios	
Roof Covering	1.1%	2.1%
Insulation	0.7%	
Openings & Specialties	0.3%	
Interior Construction		
Partitions	8.9%	35.6%
Interior Doors	7.9%	
Wall Finishes	3.7%	
Floor Finishes	9.3%	
Ceiling Finishes	4.6%	
Interior Surface of Exterior Walls	1.2%	
Conveying		
Elevators	2.7%	2.7%
Special Conveyors	0.0%	
Mechanical		
Plumbing	15.9%	22.9%
Fire Protection	1.8%	
Heating	0.0%	
Cooling	5.2%	
Special Systems	0.0%	
Electrical		
Service & Distribution	0.5%	8.4%
Lighting & Power	7.4%	
Special Electrical	0.5%	
Special Construction		
Specialties (& Additives)	0.0%	0.0%
Total	100%	100%

Table 8-22 Subassembly Cost Distributions for Four to Seven-Story Hotels

Subassemblies	Cost Ratios	
Foundations		
Footings & Foundations	1.6%	1.8%
Piles & Caissons	0.0%	
Excavation & Backfill	0.2%	
Substructures		
Slab on Grade	0.7%	0.7%
Special Substructures	0.0%	

Subassemblies		Cost Ratios
Superstructure		
Columns and Beams	0.0%	13.7%
Structural Walls	0.0%	
Elevated Floors/Diaphragms	12.1%	
Roof Decking/Framing	1.1%	
Stairs	0.5%	
Exterior Closure		
Walls	7.0%	10.1%
Exterior Wall Finishes	0.0%	
Doors	0.2%	
Windows & Glazed Walls	2.9%	
Roofing		
Roof Covering	0.5%	0.9%
Insulation	0.3%	
Openings & Specialties	0.1%	
Interior Construction		
Partitions	6.0%	25.8%
Interior Doors	8.3%	
Wall Finishes	2.8%	
Floor Finishes	5.9%	
Ceiling Finishes	1.8%	
Interior Surface of Exterior Walls	1.0%	
Conveying		
Elevators	5.1%	5.1%
Special Conveyors	0.0%	
Mechanical		
Plumbing	14.5%	31.2%
Fire Protection	1.9%	
Heating	3.7%	
Cooling	10.9%	
Special Systems	0.0%	
Electrical		
Service & Distribution	1.1%	10.7%
Lighting & Power	7.2%	
Special Electrical	2.5%	
Special Construction		

Subassemblies	Cost Ratios	
Specialties (& Additives)	0.0%	0.0%
Total	100%	100%

Table 8-23 Percent Increases in the Average Annual Total Loss Due to Changes in Building Parameters – Marginally- or Non-Engineered Hotel/Motel and Multi-Family Residential Buildings

Parameter	Number of Stories														
	All			One			Two			Three			Four		
	Min	Avg	Max	Min	Avg	Max	Min	Avg	Max	Min	Avg	Max	Min	Avg	Max
Gable and Hip Roofs with Singles															
Unreinforced Masonry to Wood Frame Walls	0%	5%	18%	0%	4%	18%	1%	4%	7%	3%	6%	10%	N/A		
Reinforced Masonry to Unreinforced Masonry Walls	-2%	0%	3%	-1%	0%	3%	-2%	0%	2%	-1%	1%	2%			
Hip to Gable Roof Shape	9%	23%	59%	22%	37%	59%	13%	21%	30%	9%	13%	17%	9%	16%	22%
8d to 6d Roof Deck Nails	2%	21%	71%	2%	28%	71%	2%	19%	46%	2%	18%	42%	3%	14%	34%
Strapped to Toe-Nailed Roof/ Wall Connections	21%	48%	103%	27%	61%	103%	21%	45%	79%	22%	42%	72%	24%	42%	69%
One to Two Stories	48%	91%	135%	N/A											
Two to Three Stories	17%	28%	49%												
Three to Four Stories	3%	9%	14%												
Flat Roofs with BUR															
Unreinforced Masonry to Wood Frame Walls	0%	4%	15%	0%	3%	15%	1%	3%	6%	2%	4%	7%	N/A		
Reinforced Masonry to Unreinforced Masonry Walls	-1%	0%	2%	-1%	0%	2%	-1%	0%	1%	-1%	0%	1%			
Average to Poor Quality Cover	13%	40%	98%	24%	53%	98%	24%	40%	69%	21%	35%	56%	13%	21%	35%
8d to 6d Roof Deck Nails	1%	15%	50%	6%	24%	50%	3%	11%	29%	3%	11%	28%	1%	10%	25%

Parameter	Number of Stories														
	All			One			Two			Three			Four		
	Min	Avg	Max	Min	Avg	Max	Min	Avg	Max	Min	Avg	Max	Min	Avg	Max
Strapped to Toe-Nailed Roof/Wall Connections	12%	31%	68%	12%	33%	68%	14%	29%	56%	14%	28%	52%	21%	37%	65%
One to Two Stories	97%	167%	261%	N/A											
Two to Three Stories	31%	49%	70%												
Three to Four Stories	-4%	5%	20%												
Flat Roofs with EPDM															
Unreinforced Masonry to Wood Frame Walls	-1%	3%	14%	-1%	2%	14%	0%	2%	5%	2%	3%	7%	N/A		
Reinforced Masonry to Unreinforced Masonry Walls	-1%	0%	2%	0%	0%	1%	-1%	0%	1%	-1%	0%	2%			
Average to Poor Quality Cover	20%	87%	246%	77%	146%	246%	50%	80%	124%	33%	51%	77%	20%	32%	48%
8d to 6d Roof Deck Nails	1%	11%	37%	4%	16%	37%	2%	8%	22%	2%	9%	23%	1%	8%	20%
Strapped to Toe-Nailed Roof/Wall Connections	5%	23%	54%	5%	21%	52%	9%	21%	44%	12%	22%	42%	18%	32%	54%
One to Two Stories	69%	136%	247%	N/A											
Two to Three Stories	16%	40%	67%												
Three to Four Stories	-12%	-1%	12%												

8.2.4 Low-Rise Masonry Strip Mall Buildings

Loss functions have been developed for low-rise masonry strip mall buildings using the same hurricane wind speed and direction data (20,000 years of storm simulation) used in the development of the damage curves. The model buildings were assumed to be used as department stores. The assumed subassembly cost distributions are listed in Table 8-24.

Table 8-24 Subassembly Cost Distributions for Low-Rise Masonry Strip Mall

Subassemblies	Cost Ratios	
Foundations		
Footings & Foundations	2.2%	4.2%
Piles & Caissons	0.0%	
Excavation & Backfill	2.0%	
Substructures		
Slab on Grade	6.4%	6.4%
Special Substructures	0.0%	
Superstructure		
Columns and Beams	1.1%	29.2%
Structural Walls	0.0%	
Elevated Floors/Diaphragms	0.0%	
Roof Decking/Framing	28.1%	
Stairs	0.0%	
Exterior Closure		
Walls	6.2%	8.1%
Exterior Wall Finishes	0.0%	
Doors	0.5%	
Windows & Glazed Walls	1.4%	
Roofing		
Roof Covering	3.6%	6.4%
Insulation	2.6%	
Openings & Specialties	0.2%	
Interior Construction		
Partitions	1.3%	15.7%
Interior Doors	1.8%	
Wall Finishes	0.4%	
Floor Finishes	8.6%	
Ceiling Finishes	2.6%	
Interior Surface of Exterior Walls	0.9%	
Conveying		
Elevators	0.0%	0.0%
Special Conveyors	0.0%	
Mechanical		
Plumbing	1.3%	18.2%
Fire Protection	2.8%	

Subassemblies	Cost Ratios	
Heating	0.0%	
Cooling	13.6%	
Special Systems	0.0%	
Electrical		
Service & Distribution	1.1%	12.3%
Lighting & Power	10.6%	
Special Electrical	0.6%	
Special Construction		
Specialties (& Additives)	0.0%	0.0%
Total	100%	100%

For more information on example building and content loss functions, please contact the Hazus Help Desk (see Section 1.5) for the *Hazus Hurricane Model Technical Manual Appendices* (FEMA, 2021). The average annual building and content losses (both normalized by the total building value) for all the buildings examined are presented in the appendices. The average annual loss is obtained by summing all losses produced during the 20,000-year hurricane simulation period and dividing it by 20,000 years.

Table 8-25 through Table 8-27 present a summary of the effects of various building parameters on the average annual total loss. The configuration of model buildings (and consequently, the roof height and the joist spacing) plays a significant role in determining the average annual losses.

Table 8-25 Percent Increases in the Average Annual Total Loss Due to Changes in Building Parameters –Strip Mall Building with Wood Roof System

Building Parameter	Increase in Average Annual Building Loss					
	Building A			Building B		
	Min	Avg	Max	Min	Avg	Max
8d to 6d Roof Deck Nails	-1%	17%	64%	-1%	9%	37%
Strap to Toe-Nail Roof/Wall Connections	15%	92%	239%	17%	57%	141%
Built-up to Single ply Membrane Roof Cover	1%	11%	39%	3%	10%	26%
Reinforced to Unreinforced Masonry Walls	-1%	4%	9%	3%	12%	27%
Missile Environment D to C	4%	42%	92%	2%	13%	26%
Missile Environment C to B	2%	13%	29%	2%	11%	21%
Missile Environment B to A	2%	15%	28%	4%	12%	21%

Table 8-26 Percent Increases in the Average Annual Total Loss Due to Changes in Building Parameters – Strip Mall Building with Steel Roof System

Building Parameter	Increase in Average Annual Building Loss											
	Building A			Building B			Building C			Building D		
	Min	Avg	Max	Min	Avg	Max	Min	Avg	Max	Min	Avg	Max
0% to 50% Reduction in Metal Roof Deck Resistance	-1%	6%	22%	-1%	7%	23%	11%	46%	115%	9%	42%	109%
Screwed to Welded Metal Roof Deck	-3%	2%	7%	-2%	1%	7%	-2%	6%	22%	-2%	6%	23%
ASCE to SBCCI Metal Roof Deck Design Criteria	-3%	1%	6%	-2%	1%	4%	0%	9%	34%	-2%	9%	33%
Built-up to Single ply Membrane Roof Cover	9%	22%	44%	9%	20%	35%	6%	16%	34%	5%	14%	31%
Reinforced to Unreinforced Masonry Walls	2%	14%	41%	19%	39%	68%	4%	24%	55%	3%	27%	60%
Missile Environment D to C	2%	18%	33%	1%	8%	13%	1%	9%	19%	1%	9%	20%
Missile Environment C to B	2%	10%	18%	1%	5%	9%	2%	5%	8%	2%	5%	11%
Missile Environment B to A	2%	7%	14%	1%	5%	10%	1%	6%	12%	1%	4%	7%

Table 8-27 Percent Increases in the Average Annual Total Loss Due to Changes in Building Configuration

Building Configuration	Increase in Average Annual Building Loss		
	Min	Avg	Max
Building A to B – Wood Roof System (12’ to 20’ Roof Height)	30%	116%	277%
Building A to B – Steel Roof System (12’ to 20’ Roof Height)	65%	145%	266%
Building B to C – Steel Roof System (4’ to 6’ Joist Spacing)	1%	25%	109%
Building C to D – Steel Roof System (6 Units to 1 Unit)	-1%	8%	17%

8.2.5 Pre-Engineered Metal Buildings

Using the same hurricane wind speed and direction data (20,000 years of storm simulation) used in the development of the damage curves for the pre-engineered metal buildings, average annual losses were estimated using the commercial loss model described in Section 8.1.7. The metal buildings are assumed to be used as warehouses. The assumed subassembly cost distributions are listed in Table 8-28. Even though other occupancy types are applicable, and slightly different results may be obtained,

a warehouse is believed to be an appropriate usage type for the model buildings used in the present simulation.

For more information on example building and content loss functions, please contact the Hazus Help Desk (see Section 1.5) for the *Hazus Hurricane Model Technical Manual Appendices* (FEMA, 2021). The average annual building and content losses (both normalized by the total building value) for all metal buildings examined are presented in Table 8-29 and Table 8-30, respectively. The average annual loss is obtained by summing all losses produced during the 20,000-year hurricane simulation period and dividing it by 20,000 years. The values given in Table 8-29 and Table 8-30 reflect the average annual losses for metal buildings located in the South Florida area. Table 8-31 presents a summary of the effects of the various building parameters on average annual building loss. The configuration of model buildings (and consequently the size of the building and the percentage of wall area covered by fenestrations) plays a significant role in determining the average annual loss. For example, the decreases in average annual total loss between small metal buildings and medium-sized metal buildings (with all other parameters being equal) range from 39% to 56%. Changing from the medium-sized metal building to the large metal buildings results in a 4% to 43% increase in average annual loss. The reduction in the metal roof panel resistance (to account for aging and fatigue) also has substantial effects on the simulated losses, where an increase of up to 55% was observed. However, the differences in total loss using different design wind speeds (90 mph versus 100 mph) are minimal. The $\pm 2\%$ difference in simulated loss can be taken as randomness involved in the modeling process.

Table 8-28 Subassembly Cost Distributions for Pre-Engineered Metal Buildings

Subassemblies	Cost Ratios	
Foundations		
Footings & Foundations	6.0%	8.6%
Piles & Caissons	0.0%	
Excavation & Backfill	2.6%	
Substructures		
Slab on Grade	16.6%	16.6%
Special Substructures	0.0%	
Superstructure		
Columns and Beams	0.0%	13.1%
Structural Walls	0.0%	
Elevated Floors/Diaphragms	3.0%	
Roof Decking/Framing	9.2%	
Stairs	0.9%	
Exterior Closure		
Walls	10.8%	12.4%
Exterior Wall Finishes	0.0%	
Doors	1.5%	
Windows & Glazed Walls	0.0%	

Subassemblies	Cost Ratios	
Roofing		
Roof Covering	5.1%	9.2%
Insulation	3.3%	
Openings & Specialties	0.8%	
Interior Construction		
Partitions	1.1%	8.3%
Interior Doors	0.3%	
Wall Finishes	0.4%	
Floor Finishes	2.9%	
Ceiling Finishes	0.8%	
Interior Surface of Exterior Walls	2.8%	
Conveying		
Elevators	0.0%	0.0%
Special Conveyors	0.0%	
Mechanical		
Plumbing	3.7%	18.2%
Fire Protection	4.7%	
Heating	7.9%	
Cooling	1.9%	
Special Systems	0.0%	
Electrical		
Service & Distribution	0.8%	9.4%
Lighting & Power	7.9%	
Special Electrical	0.7%	
Special Construction		
Specialties (& Additives)	4.3%	4.3%
Total	100%	100%

Table 8-29 Average Annual Building Loss Normalized by Building Value for Pre-Engineered Metal Buildings (Annual Loss Ratio)

Building Characteristics		No Reduction in Metal Panel Capacity				50% Reduction in Metal Panel Capacity			
		Terrain Surface Roughness (m)				Terrain Surface Roughness (m)			
Design Speed (mph)	Plan Size	0.03	0.35	0.70	1.0	0.03	0.35	0.70	1.0
90	Small	0.0402	0.0201	0.0147	0.0125	0.0412	0.0209	0.0155	0.0130
	Medium	0.0187	0.0103	0.0072	0.0056	0.0222	0.0127	0.0093	0.0076
	Large	0.0200	0.0117	0.0088	0.0071	0.0254	0.0155	0.0125	0.0109
100	Small	0.0402	0.0203	0.0149	0.0125	0.0406	0.0205	0.0155	0.0128
	Medium	0.0187	0.0103	0.0071	0.0056	0.0220	0.0126	0.0092	0.0076
	Large	0.0200	0.0117	0.0088	0.0072	0.0254	0.0158	0.0124	0.0108

Table 8-30 Average Annual Content Loss Normalized by Building Value for Pre-Engineered Metal Buildings (Annual Loss Ratio)

Building Characteristics		No Reduction in Metal Panel Capacity				50% Reduction in Metal Panel Capacity			
		Terrain Surface Roughness (m)				Terrain Surface Roughness (m)			
Design Speed (mph)	Plan Size	0.03	0.35	0.70	1.0	0.03	0.35	0.70	1.0
90	Small	0.0162	0.0080	0.0059	0.0050	0.0166	0.0084	0.0062	0.0052
	Medium	0.0080	0.0041	0.0028	0.0022	0.0091	0.0050	0.0037	0.0030
	Large	0.0080	0.0045	0.0034	0.0027	0.0102	0.0062	0.0050	0.0044
100	Small	0.0162	0.0081	0.0059	0.0050	0.0164	0.0082	0.0062	0.0051
	Medium	0.0080	0.0041	0.0028	0.0022	0.0091	0.0050	0.0036	0.0030
	Large	0.0080	0.0045	0.0034	0.0028	0.0103	0.0063	0.0050	0.0044

Table 8-31 Percent Increases in the Average Annual Total Loss due to Changes in Building Parameters – Pre-Engineered Metal Buildings

Parameter	Change in Average Building Loss Ratio		
	Min	Avg	Max
Small Building to Medium Building	-56%	-47%	-39%
Medium Building to Large Building	4%	23%	43%
100 mph to 90 mph Roof Design Speed	-2%	0%	2%
0% to 50% Reduction in Roof Deck Resistance	1%	24%	55%

8.2.6 Engineered Residential and Commercial Buildings

Similar to the other model building classes, loss functions for engineered residential and commercial buildings have been developed using 20,000 years of hurricane simulations in the South Florida area. Model buildings with eight units per floor are assumed to be used as apartments, while model buildings with one unit per floor are assumed to be used as office buildings. Table 8-32 through Table 8-37 show the assumed subassembly cost distributions for two, five, and eight-story apartments and office buildings, respectively. The subassembly cost ratios listed in Table 8-32 through Table 8-37 have already been adjusted for the number of stories and glazing areas according to the commercial loss model described in Section 8.1.7. The values included in Table 8-32 through Table 8-37 correspond to the model buildings with 32% glazing coverage for two-story buildings and 36% glazing coverage for five and eight-story buildings. Slightly different subassembly cost ratios can be expected for modeled buildings with higher or lower glazing coverage.

Table 8-32 Subassembly Cost Distributions for Two-Story Apartments

Subassemblies	Cost Ratios	
Foundations		
Footings & Foundations	5.1%	5.9%
Piles & Caissons	0.0%	
Excavation & Backfill	0.8%	
Substructures		
Slab on Grade	2.4%	2.4%
Special Substructures	0.0%	
Superstructure		
Columns and Beams	0.9%	11.0%
Structural Walls	0.0%	
Elevated Floors/Diaphragms	7.1%	
Roof Decking/Framing	1.7%	
Stairs	1.3%	
Exterior Closure		
Walls	8.3%	12.4%
Exterior Wall Finishes	0.0%	
Doors	0.3%	
Windows & Glazed Walls	3.9%	
Roofing		
Roof Covering	2.0%	3.0%
Insulation	1.0%	
Openings & Specialties	0.0%	
Interior Construction		
Partitions	3.7%	22.2%

Subassemblies	Cost Ratios	
Interior Doors	5.7%	
Wall Finishes	2.2%	
Floor Finishes	5.3%	
Ceiling Finishes	3.6%	
Interior Surface of Exterior Walls	1.6%	
Conveying		
Elevators	3.0%	3.0%
Special Conveyors	0.0%	
Mechanical		
Plumbing	12.9%	30.4%
Fire Protection	2.4%	
Heating	6.6%	
Cooling	8.5%	
Special Systems	0.0%	
Electrical		
Service & Distribution	1.1%	7.9%
Lighting & Power	5.9%	
Special Electrical	0.9%	
Special Construction		
Specialties (& Additives)	1.7%	1.7%
Total	100%	100%

Table 8-33 Subassembly Cost Distributions for Five-Story Apartments

Subassemblies	Cost Ratios	
Foundations		
Footings & Foundations	2.1%	2.4%
Piles & Caissons	0.0%	
Excavation & Backfill	0.3%	
Substructures		
Slab on Grade	1.0%	1.0%
Special Substructures	0.0%	
Superstructure		
Columns and Beams	1.9%	16.6%
Structural Walls	0.0%	
Elevated Floors/Diaphragms	12.1%	
Roof Decking/Framing	1.0%	

Subassemblies	Cost Ratios	
Stairs	1.4%	
Exterior Closure		
Walls	7.0%	11.8%
Exterior Wall Finishes	0.0%	
Doors	0.2%	
Windows & Glazed Walls	4.6%	
Roofing		
Roof Covering	0.8%	1.2%
Insulation	0.4%	
Openings & Specialties	0.0%	
Interior Construction		
Partitions	4.9%	25.6%
Interior Doors	7.1%	
Wall Finishes	2.8%	
Floor Finishes	5.5%	
Ceiling Finishes	3.7%	
Interior Surface of Exterior Walls	1.6%	
Conveying		
Elevators	5.2%	5.2%
Special Conveyors	0.0%	
Mechanical		
Plumbing	11.3%	26.7%
Fire Protection	2.3%	
Heating	5.6%	
Cooling	7.5%	
Special Systems	0.0%	
Electrical		
Service & Distribution	1.2%	7.6%
Lighting & Power	5.9%	
Special Electrical	0.5%	
Special Construction		
Specialties (& Additives)	2.0%	2.0%
Total	100%	100%

Table 8-34 Subassembly Cost Distributions for Eight-Story Apartments

Subassemblies	Cost Ratios	
Foundations		
Footings & Foundations	1.9%	2.1%
Piles & Caissons	0.0%	
Excavation & Backfill	0.2%	
Substructures		
Slab on Grade	0.5%	0.5%
Special Substructures	0.0%	
Superstructure		
Columns and Beams	2.5%	12.2%
Structural Walls	0.0%	
Elevated Floors/Diaphragms	8.3%	
Roof Decking/Framing	0.2%	
Stairs	1.1%	
Exterior Closure		
Walls	6.9%	12.8%
Exterior Wall Finishes	0.0%	
Doors	1.6%	
Windows & Glazed Walls	4.3%	
Roofing		
Roof Covering	0.4%	0.7%
Insulation	0.2%	
Openings & Specialties	0.0%	
Interior Construction		
Partitions	10.2%	28.6%
Interior Doors	6.4%	
Wall Finishes	2.5%	
Floor Finishes	4.9%	
Ceiling Finishes	3.3%	
Interior Surface of Exterior Walls	1.3%	
Conveying		
Elevators	5.2%	5.2%
Special Conveyors	0.0%	
Mechanical		
Plumbing	11.8%	27.8%
Fire Protection	2.8%	

Subassemblies	Cost Ratios	
Heating	5.7%	
Cooling	7.6%	
Special Systems	0.0%	
Electrical		
Service & Distribution	0.6%	8.5%
Lighting & Power	6.1%	
Special Electrical	1.8%	
Special Construction		
Specialties (& Additives)	1.8%	1.8%
Total	100%	100%

Table 8-35 Subassembly Cost Distributions for Two-Story Office Buildings

Subassemblies	Cost Ratios	
Foundations		
Footings & Foundations	3.3%	4.3%
Piles & Caissons	0.0%	
Excavation & Backfill	1.0%	
Substructures		
Slab on Grade	3.1%	3.1%
Special Substructures	0.0%	
Superstructure		
Columns and Beams	0.9%	10.7%
Structural Walls	0.0%	
Elevated Floors/Diaphragms	7.3%	
Roof Decking/Framing	1.7%	
Stairs	0.9%	
Exterior Closure		
Walls	8.8%	12.6%
Exterior Wall Finishes	0.0%	
Doors	0.4%	
Windows & Glazed Walls	3.4%	
Roofing		
Roof Covering	2.1%	3.3%
Insulation	1.3%	
Openings & Specialties	0.0%	

Subassemblies		Cost Ratios	
Interior Construction			
Partitions	2.5%	23.0%	
Interior Doors	4.5%		
Wall Finishes	1.3%		
Floor Finishes	8.1%		
Ceiling Finishes	5.3%		
Interior Surface of Exterior Walls	1.4%		
Conveying			
Elevators	3.1%	3.1%	
Special Conveyors	0.0%		
Mechanical			
Plumbing	2.9%	25.4%	
Fire Protection	0.4%		
Heating	0.0%		
Cooling	22.1%		
Special Systems	0.0%		
Electrical			
Service & Distribution	1.6%	14.6%	
Lighting & Power	12.6%		
Special Electrical	0.3%		
Special Construction			
Specialties (& Additives)	0.0%	0.0%	
Total	100%	100%	

Table 8-36 Subassembly Cost Distributions for Five-Story Office Buildings

Subassemblies		Cost Ratios	
Foundations			
Footings & Foundations	2.9%	3.3%	
Piles & Caissons	0.0%		
Excavation & Backfill	0.4%		
Substructures			
Slab on Grade	1.1%	1.1%	
Special Substructures	0.0%		
Superstructure			
Columns and Beams	2.5%	15.5%	

Subassemblies	Cost Ratios	
Structural Walls	0.0%	
Elevated Floors/Diaphragms	11.2%	
Roof Decking/Framing	0.6%	
Stairs	1.1%	
Exterior Closure		
Walls	8.4%	14.8%
Exterior Wall Finishes	0.0%	
Doors	0.2%	
Windows & Glazed Walls	6.2%	
Roofing		
Roof Covering	0.8%	1.3%
Insulation	0.5%	
Openings & Specialties	0.0%	
Interior Construction		
Partitions	2.2%	19.2%
Interior Doors	2.1%	
Wall Finishes	1.0%	
Floor Finishes	7.5%	
Ceiling Finishes	4.9%	
Interior Surface of Exterior Walls	1.6%	
Conveying		
Elevators	7.6%	7.6%
Special Conveyors	0.0%	
Mechanical		
Plumbing	2.0%	23.0%
Fire Protection	0.2%	
Heating	0.0%	
Cooling	20.8%	
Special Systems	0.0%	
Electrical		
Service & Distribution	1.3%	14.2%
Lighting & Power	11.8%	
Special Electrical	1.2%	
Special Construction		
Specialties (& Additives)	0.0%	0.0%
Total	100%	100%

Table 8-37 Subassembly Cost Distributions for Eight-Story Office Buildings

Subassemblies	Cost Ratios	
Foundations		
Footings & Foundations	1.6%	1.8%
Piles & Caissons	0.0%	
Excavation & Backfill	0.2%	
Substructures		
Slab on Grade	0.6%	0.6%
Special Substructures	0.0%	
Superstructure		
Columns and Beams	3.1%	19.3%
Structural Walls	0.0%	
Elevated Floors/Diaphragms	14.0%	
Roof Decking/Framing	0.8%	
Stairs	1.4%	
Exterior Closure		
Walls	7.6%	13.5%
Exterior Wall Finishes	0.0%	
Doors	0.2%	
Windows & Glazed Walls	5.8%	
Roofing		
Roof Covering	0.5%	0.7%
Insulation	0.3%	
Openings & Specialties	0.0%	
Interior Construction		
Partitions	2.3%	20.1%
Interior Doors	2.2%	
Wall Finishes	1.1%	
Floor Finishes	7.8%	
Ceiling Finishes	5.1%	
Interior Surface of Exterior Walls	1.6%	
Conveying		
Elevators	9.4%	9.4%
Special Conveyors	0.0%	
Mechanical		
Plumbing	1.8%	20.7%

Subassemblies	Cost Ratios	
Fire Protection	0.2%	
Heating	0.0%	
Cooling	18.7%	
Special Systems	0.0%	
Electrical		
Service & Distribution	1.3%	13.8%
Lighting & Power	11.4%	
Special Electrical	1.1%	
Special Construction		
Specialties (& Additives)	0.0%	0.0%
Total	100%	100%

As explained in Section 5.2, wind-driven missiles are the primary cause of damage to engineered residential/commercial buildings. In open terrain, virtually no missiles can be produced from the surrounding area of a building. Contrarily, once the wind speed reaches a certain threshold in a suburban terrain, significant amounts of wind-driven missiles can be produced as a result of damage sustained by surrounding buildings. Therefore, higher damages, and accordingly losses, can be expected for a building located in a suburban terrain compared to the same building situated in an open terrain (even though the local wind speed is higher in open terrain than in suburban terrain).

The average annual building losses (normalized by the total building value) for the two-, five- and eight-story engineered residential and commercial buildings are presented in the appendices. The average annual loss is obtained by summing all losses produced during the 20,000-year hurricane simulation period and then dividing the sum by 20,000. For more information on example building and content loss functions and the average annual building losses, please contact the Hazus Help Desk (see Section 1.5) for the *Hazus Hurricane Model Technical Manual Appendices* (FEMA, 2021). Note that the loss functions cross over between open terrain ($z_0=0.03$ meters) and suburban terrain ($z_0=0.35$ meters) for a number of cases.

Table 8-38 presents a summary of the effects of the various building parameters on the average annual total loss. Considering the buildings constructed with a metal roof deck on steel joists, the average annual losses are found to increase by up to 46% when the roof cover is modeled with EPDM single-ply membrane versus a built-up roof cover. The corresponding increase to the total loss for buildings constructed with a concrete roof deck is found to be about half this value (i.e., 25%) since, in the case of the concrete deck, there is no deck failure contributing to the roof cover failure, and no water can permeate the concrete deck (even when the cover has failed) to damage the interior of the building. The effect of using a metal roof deck versus an impervious concrete roof deck results in an increase of up to 458% in the average annual loss.

The following analysis pertains to the engineered buildings constructed with metal roof deck on steel joists. The effect of having a single unit per floor (commercial usage) compared to multi-units per floor (residential usage) is at most a 45% increase in the average annual total loss. The average annual total

loss increased by as much as 28% when the glazing coverage changed from 20% to 33% and by as much as 145% when the glazing coverage changed from 33% to 50%. Also, as evidenced in Table 8-38, the surrounding missile environment has its largest impact on average annual losses for the two-story engineered buildings. This trend results from the fact that the modeled average heights of the buildings from which the commercial and residential type missiles originate are lower than the five and eight-story engineered buildings. Thus, the glazing on the upper floors of the five- and eight-story buildings are less susceptible to missile damage than the glazing on the lower floors.

In terms of the average annual loss, the effects of glazing coverage, building usage, and missile environment are found to be more pronounced on the buildings constructed with concrete roof decks than on the buildings constructed with metal roof decks. This relates to the fact that roof deck damage is eliminated, roof cover damage is reduced (since deck failures will not contribute to roof cover failure). Interior damage is reduced (since no water infiltration through the roof system can occur) for concrete roof decks. Therefore, losses are primarily driven by glazing damage, which is influenced by both usages, since internal pressure is confined to smaller internal areas when there are multiple units, and missile environment.

The number of stories also has a significant impact on the normalized average annual total losses (see the last two rows of Table 8-38). For example, with all else being the same, the predicted average annual losses for the five-story engineered buildings are up to 242% higher than those for the two-story engineered buildings.

Table 8-38 Percent Increases in the Average Annual Total Loss due to Changes in Building Parameters – Engineered Residential and Commercial Buildings

Building Parameter	Metal Roof Deck			Concrete Roof Deck		
	Min	Avg	Max	Min	Avg	Max
Two-Story Engineered Buildings						
Residential to Commercial Building Class	0%	24%	42%	23%	46%	87%
Built-up to Single Ply Membrane Roof Cover	2%	14%	46%	-1%	4%	25%
20% to 33% Glazing Coverage	0%	16%	28%	5%	28%	44%
33% to 50% Glazing Coverage	17%	32%	99%	18%	90%	435%
Missile Environment D to C	37%	103%	253%	66%	368%	808%
Missile Environment C to B	18%	29%	42%	25%	44%	72%
Missile Environment B to A	18%	28%	44%	28%	37%	58%
Concrete to Metal Roof Deck	Min		Avg		Max	
	1%		66%		458%	
Five-Story Engineered Buildings						
Residential to Commercial Building Class	-6%	25%	45%	30%	65%	98%
Built-up to Single Ply Membrane Roof Cover	4%	12%	29%	-1%	2%	13%
20% to 33% Glazing Coverage	3%	14%	21%	21%	32%	40%
33% to 50% Glazing Coverage	21%	43%	145%	28%	92%	321%

Building Parameter	Metal Roof Deck			Concrete Roof Deck		
	Min	Avg	Max	Min	Avg	Max
Missile Environment D to C	14%	56%	130%	18%	142%	294%
Missile Environment C to B	0%	3%	7%	-2%	4%	9%
Missile Environment B to A	2%	8%	15%	4%	10%	21%
Concrete to Metal Roof Deck	Min		Avg		Max	
	6%		58%		395%	
Eight-Story Engineered Buildings						
Residential to Commercial Building Class	-7%	12%	26%	47%	61%	76%
Built-up to Single Ply Membrane Roof Cover	4%	9%	16%	-3%	1%	6%
20% to 33% Glazing Coverage	5%	10%	15%	19%	27%	37%
33% to 50% Glazing Coverage	29%	48%	100%	51%	109%	221%
Missile Environment D to C	2%	13%	35%	2%	29%	61%
Missile Environment C to B	1%	3%	6%	1%	5%	10%
Missile Environment B to A	3%	5%	10%	3%	9%	14%
Concrete to Metal Roof Deck	Min		Avg		Max	
	12%		82%		334%	
All Engineered Buildings						
Two to Five Stories	-23%	25%	130%	-40%	32%	242%
Five to Eight Stories	-4%	33%	105%	-25%	18%	122%

8.2.7 Industrial Buildings

Loss functions for industrial buildings have been developed following the same procedure as the other model building classes (based on 20,000 years of hurricane simulation). The model buildings are assumed to be used as factories. The assumed subassembly cost distributions are listed in Table 8-39.

For more information on example building and content loss functions, please contact the Hazus Help Desk (see Section 1.5) for the *Hazus Hurricane Model Technical Manual Appendices* (FEMA, 2021). The average annual building and content losses (both normalized by the total building value) for all industrial buildings examined are presented in Table 8-40 and Table 8-41, respectively. The average annual loss is obtained by summing all losses produced during the 20,000-year hurricane simulation period and then dividing by 20,000 years. The values given in Table 8-40 and Table 8-41 reflect the average annual losses for industrial buildings located in the South Florida area.

Table 8-42 presents a summary of the effects of the various building parameters on a normalized average annual total loss. The wall construction has the largest impact on average annual loss with an increase of 34% on average for unreinforced masonry walls versus reinforced masonry walls. This is due to the weaker resistance of the joist/wall connections for unreinforced masonry versus reinforced masonry walls since unreinforced masonry walls do not contain bond beams or tie beams with reinforcement to which the anchorage can be welded to or wrapped around (NRC, 1991). Average annual total losses are shown to increase by 16% on average when the metal roof deck has aged and

fatigued, which has been modeled with a 50% reduction in the base uplift resistance. The effect of the surrounding missile environment on building losses is small since the modeled industrial building does not comprise glazing. However, small increases were observed (up to 3%) when the missile environment changed from the no-missile environment (D) to the environment associated with a mixture of commercial and residential type missiles (A) since costs are associated with re-finishing wall surfaces and replacing entry and/or overhead doors that have been impacted by windborne debris.

Table 8-39 Subassembly Cost Distributions for Industrial Buildings

Subassemblies	Cost Ratios	
Foundations		
Footings & Foundations	4.8%	7.0%
Piles & Caissons	0.0%	
Excavation & Backfill	2.2%	
Substructures		
Slab on Grade	6.8%	6.8%
Special Substructures	0.0%	
Superstructure		
Columns and Beams	0.0%	10.5%
Structural Walls	0.0%	
Elevated Floors/Diaphragms	0.0%	
Roof Decking/Framing	10.5%	
Stairs	0.0%	
Exterior Closure		
Walls	4.7%	6.1%
Exterior Wall Finishes	0.0%	
Doors	1.4%	
Windows & Glazed Walls	0.0%	
Roofing		
Roof Covering	4.5%	7.9%
Insulation	2.7%	
Openings & Specialties	0.7%	
Interior Construction		
Partitions	4.0%	9.8%
Interior Doors	1.9%	
Wall Finishes	1.0%	
Floor Finishes	0.6%	
Ceiling Finishes	0.7%	
Interior Surface of Exterior Walls	1.6%	

Subassemblies		Cost Ratios	
Conveying			
Elevators	0.0%	0.0%	
Special Conveyors	0.0%		
Mechanical			
Plumbing	6.2%	37.2%	
Fire Protection	4.4%		
Heating	11.8%		
Cooling	14.8%		
Special Systems	0.0%		
Electrical			
Service & Distribution	1.7%	14.8%	
Lighting & Power	12.5%		
Special Electrical	0.6%		
Special Construction			
Specialties (& Additives)	0.0%	0.0%	0.0%
Total		100%	100%

Table 8-40 Average Annual Building Loss Normalized by Building Value – Industrial Building

Building Characteristics		100% Roof Deck Capacity				50% Roof Deck Capacity			
		Terrain Surface Roughness (m)				Terrain Surface Roughness (m)			
Wall Construction	Missile Environment	0.03	0.35	0.70	1.0	0.03	0.35	0.70	1.0
Unreinforced Masonry (Annual Loss Ratio)	A	0.0286	0.0147	0.0107	0.0088	0.0297	0.0155	0.0115	0.0096
	B	0.0286	0.0147	0.0107	0.0088	0.0296	0.0155	0.0116	0.0097
	C	0.0286	0.0148	0.0107	0.0089	0.0297	0.0157	0.0117	0.0098
	D	0.0285	0.0145	0.0106	0.0087	0.0295	0.0153	0.0114	0.0096
Reinforced Masonry (Annual Loss Ratio)	A	0.0200	0.0108	0.0081	0.0067	0.0231	0.0130	0.0100	0.0084
	B	0.0201	0.0109	0.0081	0.0068	0.0231	0.0131	0.0099	0.0085
	C	0.0201	0.0110	0.0081	0.0068	0.0231	0.0132	0.0100	0.0086
	D	0.0200	0.0106	0.0079	0.0066	0.0230	0.0128	0.0098	0.0084

Table 8-41 Average Annual Content Loss Normalized by Building Value – Industrial Building

Building Characteristics		100% Roof Deck Capacity				50% Roof Deck Capacity			
		Terrain Surface Roughness (m)				Terrain Surface Roughness (m)			
Wall Construction	Missile Environment	0.03	0.35	0.70	1.0	0.03	0.35	0.70	1.0
Unreinforced Masonry (Annual Loss Ratio)	A	0.0126	0.0057	0.0038	0.0029	0.0128	0.0059	0.0041	0.0032
	B	0.0126	0.0057	0.0038	0.0029	0.0128	0.0059	0.0041	0.0033
	C	0.0126	0.0057	0.0038	0.0030	0.0128	0.0060	0.0041	0.0033
	D	0.0126	0.0057	0.0038	0.0029	0.0128	0.0059	0.0041	0.0033
Reinforced Masonry (Annualized Loss Ratio)	A	0.0069	0.0031	0.0021	0.0016	0.0085	0.0044	0.0032	0.0026
	B	0.0069	0.0031	0.0021	0.0016	0.0086	0.0044	0.0031	0.0026
	C	0.0069	0.0031	0.0021	0.0016	0.0086	0.0044	0.0032	0.0027
	D	0.0069	0.0031	0.0021	0.0016	0.0086	0.0044	0.0032	0.0027

Table 8-42 Percent Increase in Average Annual Total Loss Due to Changes in Building Parameters – Industrial Buildings

Parameter	Increase in Building Loss		
	Min	Avg	Max
Reinforced Masonry to Unreinforced Masonry Walls	16%	34%	53%
Missile Environment D to A	0%	1%	3%
0% to 50% Reduction in Roof Deck Resistance	3%	16%	34%

8.2.8 Essential Facilities

Loss functions for essential facilities have been developed following the same procedure as other model building classes (based on 20,000 years of hurricane simulation). Assumed subassembly cost distributions for fire stations, elementary schools, high schools, and hospitals are listed in Table 8-43 through Table 8-47. Police stations and EOCs are modeled as average government buildings.

Table 8-43 Subassembly Cost Distributions for Fire Stations

Subassemblies	Cost Ratios	
Foundations		
Footings & Foundations	6.4%	8.2%
Piles & Caissons	0.0%	
Excavation & Backfill	1.7%	
Substructures		
Slab on Grade	5.3%	5.3%
Special Substructures	0.0%	

Subassemblies	Cost Ratios	
Superstructure		
Columns and Beams	0.0%	3.8%
Structural Walls	0.0%	
Elevated Floors/Diaphragms	0.0%	
Roof Decking/Framing	3.8%	
Stairs	0.0%	
Exterior Closure		
Walls	15.7%	21.0%
Exterior Wall Finishes	0.0%	
Doors	3.4%	
Windows & Glazed Walls	2.0%	
Roofing		
Roof Covering	3.7%	6.6%
Insulation	1.8%	
Openings & Specialties	1.1%	
Interior Construction		
Partitions	5.1%	14.5%
Interior Doors	1.5%	
Wall Finishes	1.9%	
Floor Finishes	2.8%	
Ceiling Finishes	2.3%	
Interior Surface of Exterior Walls	0.9%	
Conveying		
Elevators	0.0%	0.0%
Special Conveyors	0.0%	
Mechanical		
Plumbing	9.4%	33.1%
Fire Protection	2.9%	
Heating	0.0%	
Cooling	20.8%	
Special Systems	0.0%	
Electrical		
Service & Distribution	1.3%	7.5%
Lighting & Power	5.8%	
Special Electrical	0.4%	
Special Construction		
Specialties (& Additives)	0.0%	0.0%

Subassemblies	Cost Ratios	
Total	100%	100%

Table 8-44 Subassembly Cost Distributions for Small Hospitals

Subassemblies	Cost Ratios	
Foundations		
Footings & Foundations	1.6%	1.9%
Piles & Caissons	0.0%	
Excavation & Backfill	0.3%	
Substructures		
Slab on Grade	1.0%	1.0%
Special Substructures	0.0%	
Superstructure		
Columns and Beams	1.3%	14.1%
Structural Walls	0.0%	
Elevated Floors/Diaphragms	8.0%	
Roof Decking/Framing	3.8%	
Stairs	0.9%	
Exterior Closure		
Walls	8.2%	9.5%
Exterior Wall Finishes	0.0%	
Doors	0.2%	
Windows & Glazed Walls	1.1%	
Roofing		
Roof Covering	0.7%	1.2%
Insulation	0.4%	
Openings & Specialties	0.1%	
Interior Construction		
Partitions	4.0%	25.1%
Interior Doors	5.9%	
Wall Finishes	5.5%	
Floor Finishes	6.2%	
Ceiling Finishes	3.1%	
Interior Surface of Exterior Walls	0.3%	
Conveying		
Elevators	2.5%	2.5%
Special Conveyors	0.0%	

Subassemblies	Cost Ratios	
Mechanical		
Plumbing	15.6%	28.1%
Fire Protection	1.4%	
Heating	2.7%	
Cooling	8.5%	
Special Systems	0.0%	
Electrical		
Service & Distribution	1.0%	10.7%
Lighting & Power	7.3%	
Special Electrical	2.4%	
Special Construction		
Specialties (& Additives)	5.9%	5.9%
Total	100%	100%

Table 8-45 Subassembly Cost Distributions for Medium and Large Hospitals

Subassemblies	Cost Ratios	
Foundations		
Footings & Foundations	6.4%	8.2%
Piles & Caissons	0.0%	
Excavation & Backfill	1.7%	
Substructures		
Slab on Grade	5.3%	5.3%
Special Substructures	0.0%	
Superstructure		
Columns and Beams	0.0%	3.8%
Structural Walls	0.0%	
Elevated Floors/Diaphragms	0.0%	
Roof Decking/Framing	3.8%	
Stairs	0.0%	
Exterior Closure		
Walls	15.7%	21.0%
Exterior Wall Finishes	0.0%	
Doors	3.4%	
Windows & Glazed Walls	2.0%	
Roofing		

Subassemblies	Cost Ratios	
Roof Covering	3.7%	6.6%
Insulation	1.8%	
Openings & Specialties	1.1%	
Interior Construction		
Partitions	5.1%	14.5%
Interior Doors	1.5%	
Wall Finishes	1.9%	
Floor Finishes	2.8%	
Ceiling Finishes	2.3%	
Interior Surface of Exterior Walls	0.9%	
Conveying		
Elevators	0.0%	0.0%
Special Conveyors	0.0%	
Mechanical		
Plumbing	9.4%	33.1%
Fire Protection	2.9%	
Heating	0.0%	
Cooling	20.8%	
Special Systems	0.0%	
Electrical		
Service & Distribution	1.3%	7.5%
Lighting & Power	5.8%	
Special Electrical	0.4%	
Special Construction		
Specialties (& Additives)	0.0%	0.0%
Total	100%	100%

Table 8-46 Subassembly Cost Distributions for Elementary Schools

Subassemblies	Cost Ratios	
Foundations		
Footings & Foundations	6.4%	8.2%
Piles & Caissons	0.0%	
Excavation & Backfill	1.7%	
Substructures		
Slab on Grade	5.3%	5.3%

Subassemblies	Cost Ratios	
Special Substructures	0.0%	
Superstructure		
Columns and Beams	0.0%	3.8%
Structural Walls	0.0%	
Elevated Floors/Diaphragms	0.0%	
Roof Decking/Framing	3.8%	
Stairs	0.0%	
Exterior Closure		
Walls	15.7%	21.0%
Exterior Wall Finishes	0.0%	
Doors	3.4%	
Windows & Glazed Walls	2.0%	
Roofing		
Roof Covering	3.7%	6.6%
Insulation	1.8%	
Openings & Specialties	1.1%	
Interior Construction		
Partitions	5.1%	14.5%
Interior Doors	1.5%	
Wall Finishes	1.9%	
Floor Finishes	2.8%	
Ceiling Finishes	2.3%	
Interior Surface of Exterior Walls	0.9%	
Conveying		
Elevators	0.0%	0.0%
Special Conveyors	0.0%	
Mechanical		
Plumbing	9.4%	33.1%
Fire Protection	2.9%	
Heating	0.0%	
Cooling	20.8%	
Special Systems	0.0%	
Electrical		
Service & Distribution	1.3%	7.5%
Lighting & Power	5.8%	
Special Electrical	0.4%	

Subassemblies	Cost Ratios	
Special Construction		
Specialties (& Additives)	0.0%	0.0%
Total	100%	100%

Table 8-47 Subassembly Cost Distributions for High Schools

Subassemblies	Cost Ratios	
Foundations		
Footings & Foundations	6.4%	8.2%
Piles & Caissons	0.0%	
Excavation & Backfill	1.7%	
Substructures		
Slab on Grade	5.3%	5.3%
Special Substructures	0.0%	
Superstructure		
Columns and Beams	0.0%	3.8%
Structural Walls	0.0%	
Elevated Floors/Diaphragms	0.0%	
Roof Decking/Framing	3.8%	
Stairs	0.0%	
Exterior Closure		
Walls	15.7%	21.0%
Exterior Wall Finishes	0.0%	
Doors	3.4%	
Windows & Glazed Walls	2.0%	
Roofing		
Roof Covering	3.7%	6.6%
Insulation	1.8%	
Openings & Specialties	1.1%	
Interior Construction		
Partitions	5.1%	14.5%
Interior Doors	1.5%	
Wall Finishes	1.9%	
Floor Finishes	2.8%	
Ceiling Finishes	2.3%	
Interior Surface of Exterior Walls	0.9%	

Subassemblies	Cost Ratios	
Conveying		
Elevators	0.0%	0.0%
Special Conveyors	0.0%	
Mechanical		
Plumbing	9.4%	33.1%
Fire Protection	2.9%	
Heating	0.0%	
Cooling	20.8%	
Special Systems	0.0%	
Electrical		
Service & Distribution	1.3%	7.5%
Lighting & Power	5.8%	
Special Electrical	0.4%	
Special Construction		
Specialties (& Additives)	0.0%	0.0%
Total	100%	100%

8.2.8.1 Loss Model Results for Fire Stations

The average annual building and content losses (both normalized by the total building value) for all fire stations examined are presented in the appendices. The average annual loss is obtained by summing all losses produced during the 20,000-year hurricane simulation period and then dividing by 20,000 years. For more information on the average annual building and content losses, contact the Hazus Help Desk (see Section 1.5) for the *Hazus Hurricane Model Technical Manual Appendices* (FEMA, 2021).

The building parameter sensitivity results are shown in Table 8-48. It is evident that the missile environment has a large impact on overall loss, increasing the mean per storm loss by 121% on average when the missile environment changes from no windborne debris (Missile Environment D) to a mixed residential/commercial type environment (Missile Environment A).

The use of EPDM roof cover versus BUR roof cover increases the overall storm average loss by 6% on average, while a reduction in metal deck resistance of 50% increases losses by 46%.

Mitigation techniques such as shutters have a great effect in reducing damage in this analysis since window breakage and metal deck failure are the primary drivers of damage. Losses increase by 161% when shutters are not used and increase by 46% when the deck is no longer mitigated.

Table 8-48 Percent Increases in the Average Annual Total Loss due to Changes in Building Parameters – Fire Station

Building Parameter	Min	Avg	Max
Built-up to Single ply Membrane Roof Cover	0%	6%	42%

Building Parameter	Min	Avg	Max
Missile Environment D to C	6%	79%	235%
Missile Environment C to B	-9%	13%	32%
Missile Environment B to A	-6%	9%	35%
Mitigated Deck to Unmitigated Deck	5%	46%	148%
0% to 50% Reduction in Metal Roof Deck Resistance	3%	14%	31%
Shutters versus. No Shutters	37%	161%	512%

8.2.8.2 Loss Model Results for Elementary Schools

The average annual building and content losses (both normalized by the total building value) for all elementary schools examined are presented in the appendices. The average annual loss is obtained by summing all losses produced during the 20,000-year hurricane simulation period and then dividing by 20,000 years. The contents limit for elementary schools has been assumed to be 15% of the building value based on expert opinion. For more information on the average annual losses for elementary schools located in the South Florida area, please contact the Hazus Help Desk (see Section 1.5) for the *Hazus Hurricane Model Technical Manual Appendices* (FEMA, 2021).

Table 8-49 shows the building parameter sensitivity results. Missile environment has a large impact on the overall loss, increasing the mean per storm loss by 107% on average when the missile environment changes from no windborne debris (Missile Environment D) to a residential type environment (Missile Environment C).

The use of EPDM roof cover versus BUR roof cover increases the overall storm average loss by 6% on average, while a reduction in metal deck resistance of 50% increases losses by 46%.

Mitigation techniques such as shutters have a great effect in reducing damage in this analysis since window breakage and metal deck failure are the primary drivers of damage. Losses increase by 161% on average when shutters are not considered and increase by 46% when the deck is no longer mitigated.

Table 8-49 Percent Increases in the Average Annual Total Loss due to Changes in Building Parameters – Elementary School

Building Parameter	Min	Avg	Max
Built-up to Single ply Membrane Roof Cover	0%	6%	42%
Missile Environment D to C	6%	79%	235%
Missile Environment C to B	-14%	6%	32%
Missile Environment B to A	-6%	9%	35%
Mitigated Deck to Unmitigated Deck	5%	46%	148%
0% to 50% Reduction in Metal Roof Deck Resistance	3%	14%	31%
Shutters versus No Shutters	37%	161%	512%

8.2.8.3 Loss Model Results for High Schools

The average annual building and content losses (both normalized by the total building value) for all high schools examined are presented in the appendices. The average annual loss is obtained by summing all losses produced during the 20,000-year hurricane simulation period and then dividing by 20,000 years. The contents limit for high schools has been assumed to be 15% of the building value. For more information on the average annual losses for high schools located in the South Florida area, contact the Hazus Help Desk (see Section 1.5) for the *Hazus Hurricane Model Technical Manual Appendices* (FEMA, 2021)

The building parameter sensitivity results for high schools are shown in Table 8-50. Changing the missile environments between no windborne debris (Missile Environment D) to a mixed residential/commercial type environment (Missile Environment A) increases losses 85% on average for the two-story case, increases losses 43% for the three-story case, and increases losses 64% overall. This trend results from the fact that the modeled average heights of the buildings from which the commercial and residential type missiles originate are lower than the three-story buildings. Thus, the glazing on the upper floors of the three-story buildings are less susceptible to missile damage than the glazing on the lower floors.

The use of EPDM roof cover versus BUR roof cover increases losses by 15%-16% on average for both the two- and three-story case.

Mitigation techniques such as shutters have a great impact on reducing damage in this analysis since window breakage and metal deck failure are the primary drivers of damage. Losses increase by 72% on average for the two-story case, 46% for the three-story case, and 59% overall when shutters are not in place. The mitigated deck to unmitigated deck increases losses by 103% and 115% for the two- and three-story case, respectively, and 109% overall. The three-story case is more influenced by roof damage compared to fenestration damage.

Overall, increasing story height from two to three increases average loss by 51% on average.

Table 8-50 Percent Increases in the Average Annual Total Loss due to Changes in Building Parameters – High Schools

Building Parameter	Number of Stories								
	All			Two			Three		
	Min	Avg	Max	Min	Avg	Max	Min	Avg	Max
Built-up to Single ply Membrane Roof Cover	0%	16%	35%	0%	16%	35%	1%	15%	24%
Missile Environment D to C	1%	50%	134%	3%	65%	134%	1%	35%	36%
Missile Environment C to B	-7%	3%	40%	-7%	5%	40%	-2%	2%	13%
Missile Environment B to A	-3%	6%	24%	-3%	7%	24%	-2%	4%	14%
Mitigated Deck to Unmitigated Deck	13%	109%	176%	13%	103%	176%	27%	115%	98%

Building Parameter	Number of Stories								
	All			Two			Three		
	Min	Avg	Max	Min	Avg	Max	Min	Avg	Max
0% to 50% Reduction in Metal Roof Deck Resistance	0%	59%	227%	1%	72%	227%	0%	46%	72%
Shutters versus. No Shutters	-2%	51%	102%	N/A					

8.2.8.4 Loss Model Results for Hospitals

The average annual building and content losses (both normalized by the total building value) for all hospitals examined are presented in the appendices. The average annual loss is obtained by summing all losses produced during the 20,000-year hurricane simulation period and then dividing by 20,000 years. The contents limit for hospitals has been assumed to be 50% of the building value. For more information on the average annual losses for hospitals located in the South Florida area, contact the Hazus Help Desk (see Section 1.5) for the *Hazus Hurricane Model Technical Manual Appendices* (FEMA, 2021)

Table 8-51 displays the building parameter sensitivity results for hospital buildings. Changing the missile environments between no windborne debris (Missile Environment D) to a mixed residential/commercial type environment (Missile Environment A) increases losses by 205%, 31%, and 3% on average for the one-, four-, and eight-story cases respectively, and 80% overall. This trend results from the fact that the modeled average heights of the buildings from which the commercial and residential type missiles originate are lower than the four and eight-story buildings. Thus, the glazing on the upper floors of the four and eight-story buildings are less susceptible to missile damage than the glazing on the lower floors.

The use of EPDM roof cover versus BUR roof cover increases the overall losses between 9%, 11%, and 24% for the one-, four-, and eight-story buildings, respectively, and 15% on average for all cases.

Mitigation techniques such as adding shutters have a strong impact on reducing damage in this analysis since window breakage and metal deck failure are the primary drivers of damage. Losses increase by 27% on average for the eight-story case, 45% for the two-story case, 99% for the one-story case, and 57% overall when shutters are not in place. The mitigated to unmitigated deck scenario increases losses between 114% and 202%, and 149% overall. The cases with more stories are more influenced by roof damage compared to fenestration damage.

Overall, losses are most impacted by story height. Increasing story height from one to four increases losses by 369%, and an increase of 81% is seen when story height is changed from four to eight.

Table 8-51 Percent Increases in the Average Annual Total Loss Due to Changes in Building Parameters – Hospitals

Building Parameter	Number of Stories											
	All			One			Four			Eight		
	Min	Avg	Max	Min	Avg	Max	Min	Avg	Max	Min	Avg	Max
Built-up to Single ply Membrane Roof Cover	3%	15%	115%	3%	24%	115%	4%	11%	32%	3%	9%	18%
Missile Environment D to C	0%	71%	443%	37%	176%	443%	10%	32%	93%	0%	3%	12%
Missile Environment C to B	-20%	2%	45%	-20%	6%	45%	-7%	-1%	6%	-2%	0%	1%
Missile Environment B to A	-17%	3%	52%	-17%	10%	52%	-6%	0%	10%	-2%	0%	3%
Mitigated Deck to Unmitigated Deck	43%	149%	410%	43%	202%	410%	66%	132%	258%	67%	114%	171%
Shutters versus No Shutters	2%	57%	458%	2%	99%	458%	10%	45%	116%	8%	27%	61%
One to Four Stories	55%	369%	1,794%	N/A								
Four to Eight Stories	28%	81%	199%									

8.3 Additional Losses to Single-Family Homes Due to Tree Blowdown

As described in Section 5.3, the severity of tree damage and subsequent loss to buildings is dependent on the tree impact energy and the structure’s impact resistance. The Wind Load Test conducted at Clemson University and previously described in Section 5.3 used tree drop tests on modeled partial house structures. To simulate the tree trunk, the Clemson tests used two steel pipes of different weights, namely 450 pounds and 950 pounds, both at a length of 20 feet. The pipes were released from standing position on a rig about 18 feet from the modeled structure and free-fell to the modeled house structure. The lighter pipe hits the eave with an impact energy of 3,600 foot-pounds, and the larger pipe hits with an impact energy of 7,600 foot-pounds. Based on the limited number of tree drop damage states recorded by Clemson University and additional engineering inferences, an extended number of damage states were defined for the subsequent estimation of direct economic losses, in relation to impact energy.

8.3.1 Cost Estimation Assumptions and Data

For the tree blowdown methodology, the cost estimates for tree blowdown losses were prepared with data from RSMMeans 2002 Repair and Remodeling Cost Data, and the Means CostWorks 2002 software. The cost estimates have prices adjusted locally for Miami, which is consistent with the costing data of the original loss curves. Although the values are from 2002, they were used to determine the component values as a percentage of the overall structure value and are therefore still relevant with present day replacement values.

In preparing these cost estimates, the following assumptions about the construction were made:

- Roof covering is shingles
- One-half inch plywood roof deck
- Wood truss roof structure
- The average room size is 200 square feet
- There are seven rooms on average in a one-story building, and 14 rooms in a two-story building
- There is one bathroom in a one-story building, and two in a two-story building
- Contents value per square foot are 50% of the building value
- Value of the building is 80 dollars per square foot

The general approach consisted of estimating the size of the opening that was created for each of the damage states, then estimating the extent of damage to various components of the building such as roof covering, roof structure, walls, flooring, contents, and electrical, etc. The extent of the area damaged accounted for the replacement of “units” of a component – for example, an even number of 4’x8’ sheets of plywood on the roof, etc. Table 8-52 and Table 8-53 list the assumed damage areas used in the one-story and two-story cost estimates, respectively. Content damage is estimated using the areas in Table 8-52 and Table 8-53 and a simple cost per square foot valued at 50% of the assumed building value (i.e., \$40 per square foot). The damage states are defined in Section 5.3.

Table 8-52 Assumed Damage Areas Used in One-Story Cost Estimates

Building Components	Damage State # (Defined in Table 5-15)			
	1	3	4	5
	Surface Damage	Roof Only	Roof and 1/4 Wall	Roof and Wall
Component				
Window (Square Feet)	0	0	1.75 or 0	7
Roof Structure (Square Feet)	0	200	200	200
Roof Covering (Square Fee)	100	210	210	210
Walls (Square Feet)	32	32	32 or 10	64
Electrical (Linear Feet)	0	0	10	50
Flooring (Square Feet)	0	75	200	200
Floor Structure (Square Feet)	0	0	0	0
Contents (Square Feet)	0	100	150	150
Partitions (Square Feet wall)	0	200	320	400
Plumbing (% damage)	0	0.07	0.11	0.14

Building Components	Damage State # (Defined in Table 5-15)			
	1	3	4	5
	Surface Damage	Roof Only	Roof and 1/4 Wall	Roof and Wall
Heating (Square Feet area)	0	100	160	200
Kitchen and Appliances (% damage)	0	0.07	0.12	0.14
Assumed Opening Size				
Roof (Square Feet)	0	16	40	48
Wall (Square Feet)	0	0	12	48

Table 8-53 Assumed Damage Areas Used in Two-Story Cost Estimates

Building Components	Damage State # (Defined in Table 5-15)			
	1	3	4	5
	Surface Damage	Roof Only	Roof and 1/4 Wall	Roof and Wall
Component				
Window (Square Feet)	0	0	3 or 0	14
Roof Structure (Square Feet)	0	200	200	200
Roof Covering Square Feet	100	210	210	210
Walls(Square Feet)	64	64	32 or 10	128
Electrical (Linear Feet)	0	0	30	100
Flooring(Square Feet)	0	300	300	400
Floor Structure(Square Feet)	0	0	0	64
Contents(Square Feet)	0	150	200	300
Partitions(Square Feet wall)	0	210	420	600
Plumbing(% damage)	0	0.05	0.1	0.28
Heating(Square Feet area)	0	105	210	300
Kitchen and Appliances(% damage)	0	0.025	0.05	0.14
Assumed Opening Size				
Roof (Square Feet)	0	16	40	48
Wall (Square Feet)	0	0	12	96

8.3.2 Additional Assumptions for One-Story

The cost estimates for Damage State 5 (roof and wall) include 50% of a 3'x5' typical window, assuming that there is a 50% chance that a window will be involved in the damaged area. The assumption is that the amount of glazing on a home is approximately 20% of the wall area, which translates to about a 50% chance that any vertical slice will involve a window. For Damage State 4, (roof and 1/4 wall) the area of the window was reduced further still to reflect the likelihood that the damage is only to the wall above the window, and repair to the window may be less likely. For masonry homes, it was assumed that the windows would not be affected by this damage state.

One-seventh of the cost of a set of kitchen appliances and cabinets was included to reflect the fact that one in seven rooms is a kitchen, which is likely involved in the damaged area. Similarly, for plumbing, one-seventh of a package of plumbing cost is included (which is dominated by bathroom fixtures), based on the assumption that one in seven rooms is a bathroom.

The extent of required wall repair in Damage State 4 for masonry walls is assumed to be less than for wood frame walls, because the CMU units are smaller, and therefore the area to be repaired can be more localized.

8.3.3 Additional Assumptions for Two-Story

Damage State 8 includes one full window in the cost estimate. In the same manner as the one-story building, it is assumed that there is a 50% chance that a window will be damaged on each story, or the equivalent of one full window.

For kitchens and plumbing (bathrooms), the likelihood of impacting one of seven rooms on any floor was accounted for in the estimate by costing in one-seventh of the cost of a complete set of kitchen appliances/cabinets or plumbing fixtures.

The area of flooring affected in each damage state accounts for the dripping of water from one story to another.

The completed cost estimates are presented in Table 8-54. The estimates are also illustrated in Figure 8-16, Figure 8-17, and Figure 8-18 for building, contents, and combined costs as functions of impact energy. For damage states whose costs were not estimated item-by-item, overall costs were estimated based on incremental costs by comparing to the costs estimated item-by-item. Maximum potential losses resulting from one tree hit are also estimated to be approximately \$10,000 of structure and \$8,000 of contents for one-story, and \$17,000 and \$13,000 for two-story, all assumed to be reached at an impact energy of 100,000 foot-pounds.

Table 8-54 Estimated Building Repair Costs to Wood Buildings by Damage State

Damage State (Defined in Table 5-15)		1 Surface damage	2 Roof deck crack	3 Top- plates rupture	4 One-Fourth Cut into upper wall	5 Cut through upper wall	6 Floor- plates rupture	7 One-Fourth Cut into lower wall	8 Cut through lower wall
12-Story Wood	Impact Energy (foot- pound) ¹	250	2,000	5,600	6,400	8,800			
	Building Cost (\$)	125	800	3,789	5,752	6,212			
	Contents Cost (\$)	0	200	4,000	6,000	7,000			
	Combined Cost (\$)	125	1,000	7,789	11,752	13,212			
Two- Story Wood	Impact Energy (foot- pound)	250	2,000	5,600	6,400	8,800	14,400	15,200	17,600
	Building Cost (\$)	162	1,000	3,937	5,923	7,000	7,800	9,600	10,283
	Contents Cost (\$)	0	200	5,500	8,000	9,000	10,200	11,400	12,000
	Combined Cost (\$)	162	1,200	9,437	13,923	16,000	18,000	21,000	22,283

Table 8-55 Estimated Building Repair Costs to Masonry Buildings by Damage State

Damage State (Defined in Table 5-15)		1 Surface damage	2 Roof deck crack	3 Bond- beam rupture	4 One-Fourth Cut into upper wall	5 Cut through upper wall	6 Floor- plates rupture	7 One-Fourth Cut into lower wall	8 Cut through lower wall
12-Story Masonry	Impact Energy (foot- pound)	250	2,000	11,000	13,000	19,000			
	Building Cost (\$)	101	600	3,765	5,539	6,692			
	Contents Cost (\$)	0	200	4,000	6,000	7,000			

Damage State (Defined in Table 5-15)	1 Surface damage	2 Roof deck crack	3 Bond-beam rupture	4 One-Fourth Cut into upper wall	5 Cut through upper wall	6 Floor-plates rupture	7 One-Fourth Cut into lower wall	8 Cut through lower wall
Combined Cost (\$)	101	800	7,765	11,539	13,692			
Two-Story Masonry								
Impact Energy (foot-pound)	250	2,000	11,000	13,000	19,000	30,000	32,000	38,000
Building Cost (\$)	114	700	3,888	5,708	7,000	7,800	9,600	11,243
Contents Cost (\$)	0	200	5,500	8,000	9,000	10,200	11,400	12,000
Combined Cost (\$)	114	900	9,388	13,708	16,000	18,000	21,000	23,243

Building Loss due to One Tree Hit

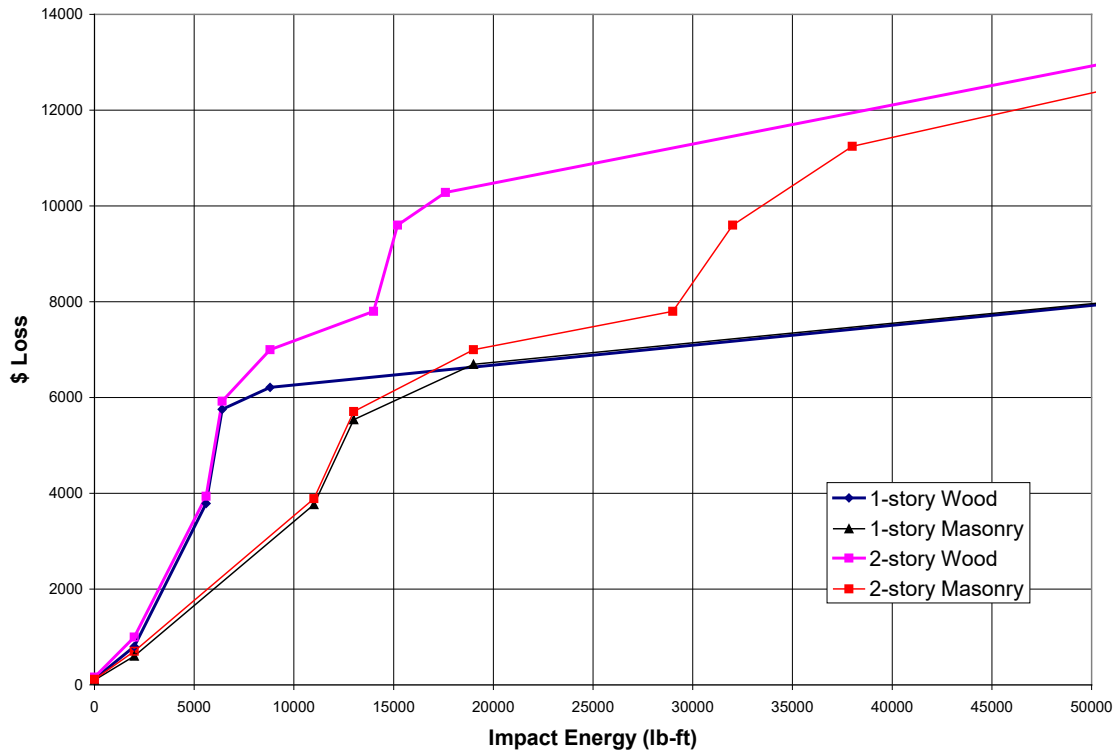


Figure 8-16 Building Repair Cost Estimates as Functions of Impact Energy

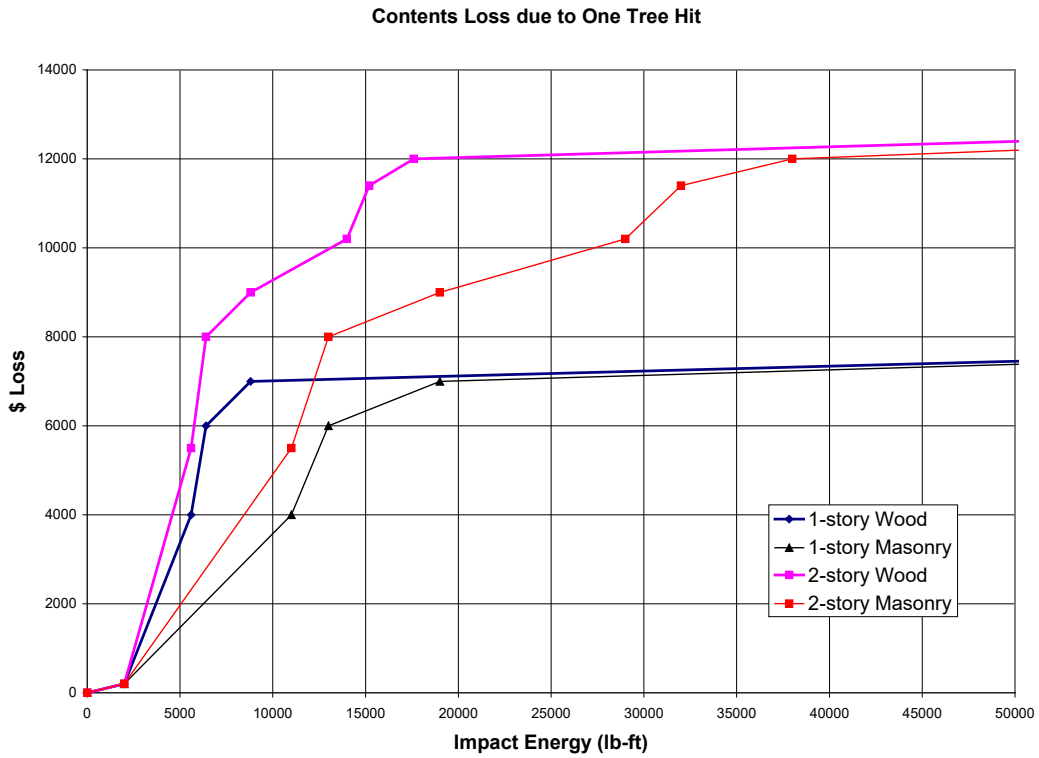


Figure 8-17 Contents Repair Cost Estimates as Functions of Impact Energy

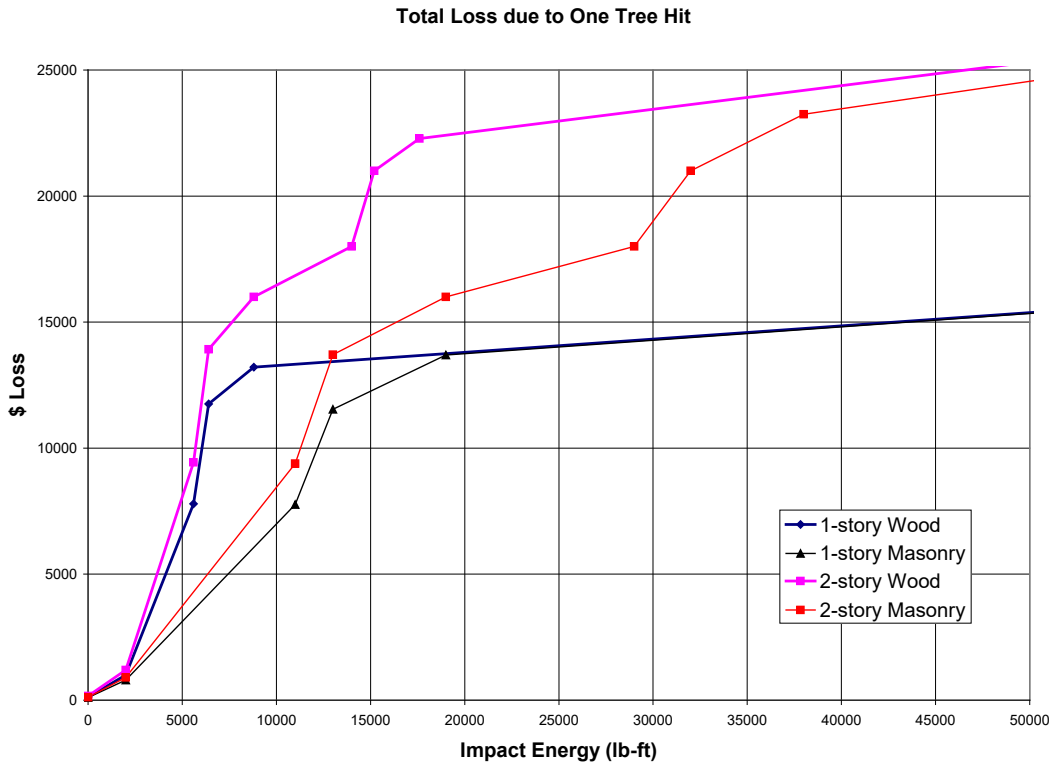


Figure 8-18 Total Repair Cost Estimates as Functions of Impact Energy

8.3.4 Losses Due to Tree Blowdown

Using the methodology illustrated in Section 8.3 and the assumptions and results discussed in the previous sections, mean building and contents losses are derived as functions of peak gust speed based on 10,000 simulations for each of the 288 cases summarized in Table 8-56. In the simulations, trees are assumed to be distributed evenly over areas not occupied by the building, with a 10 feet clearance from the building perimeter. The fall azimuth is also assumed to be uniformly random.

Table 8-56 Parameter Matrix for the 288 Cases Studied

Parameter	Wall Type	Dimension (Value \$)	Tree Type	Tree Height	Tree Density
Values	Wood	50x24x 9 (96k)	Evergreen	312-40 feet	10
	Masonry	60x30x 9 (144k)	Deciduous	412-60 feet	25
		40x30x17 (192k)	Deciduous	≥60 feet	50
		50x30x17 (240k)	Deciduous	≥60 feet	100
		50x30x17 (240k)	Deciduous	≥60 feet	200
		(all hip roofs)	Deciduous	≥60 feet	400

For multiple impacts, each impact is assumed to damage a previously undamaged portion of the structure.

Examples of building and contents loss functions are presented in Figure 8-19, Figure 8-20, Figure 8-21, Figure 8-22, and Figure 8-23, each of which demonstrates the dependence of loss functions on one of the parameters listed in Table 8-56. Figure 8-24 compares the building and content losses for one specific combination of input parameters. For additional information on combination figures, please contact the Hazus Help Desk (see Section 1.5) for the *Hazus Hurricane Model Technical Manual Appendices* (FEMA, 2021).

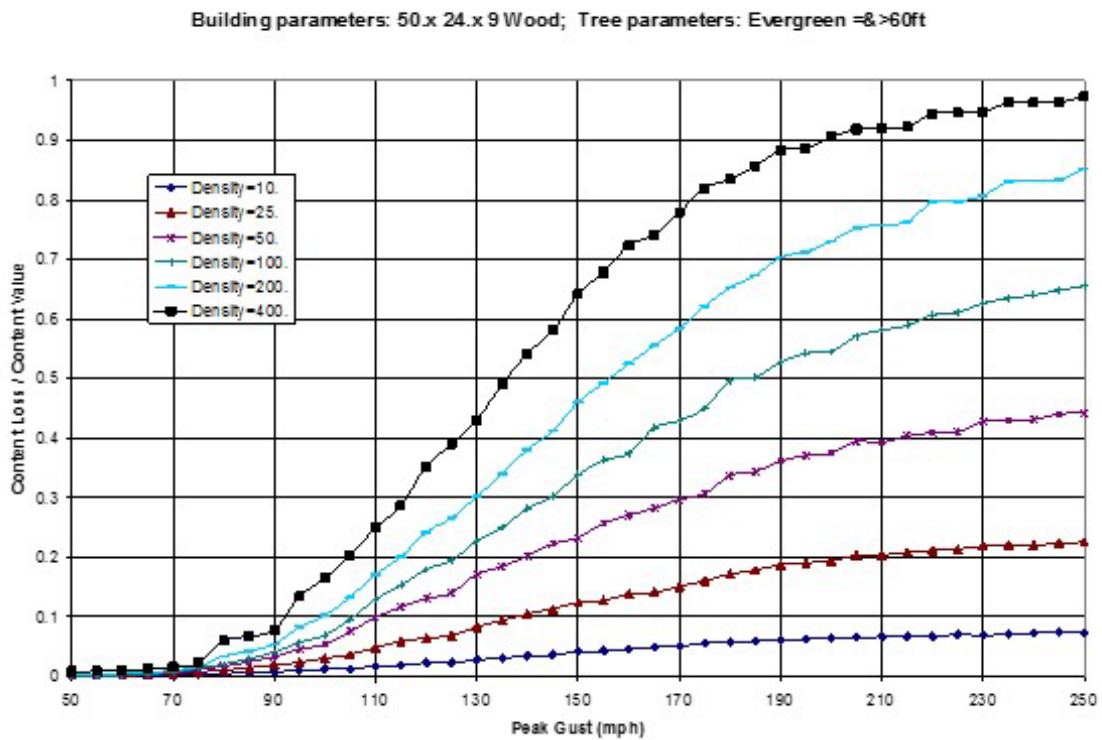
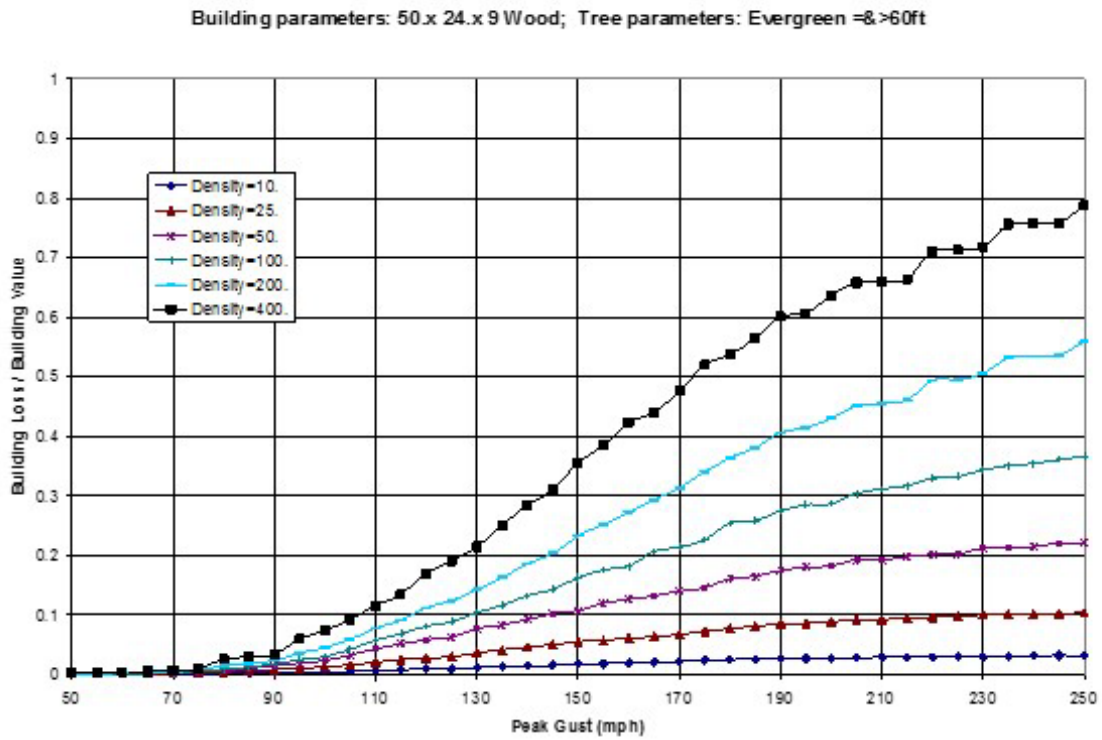
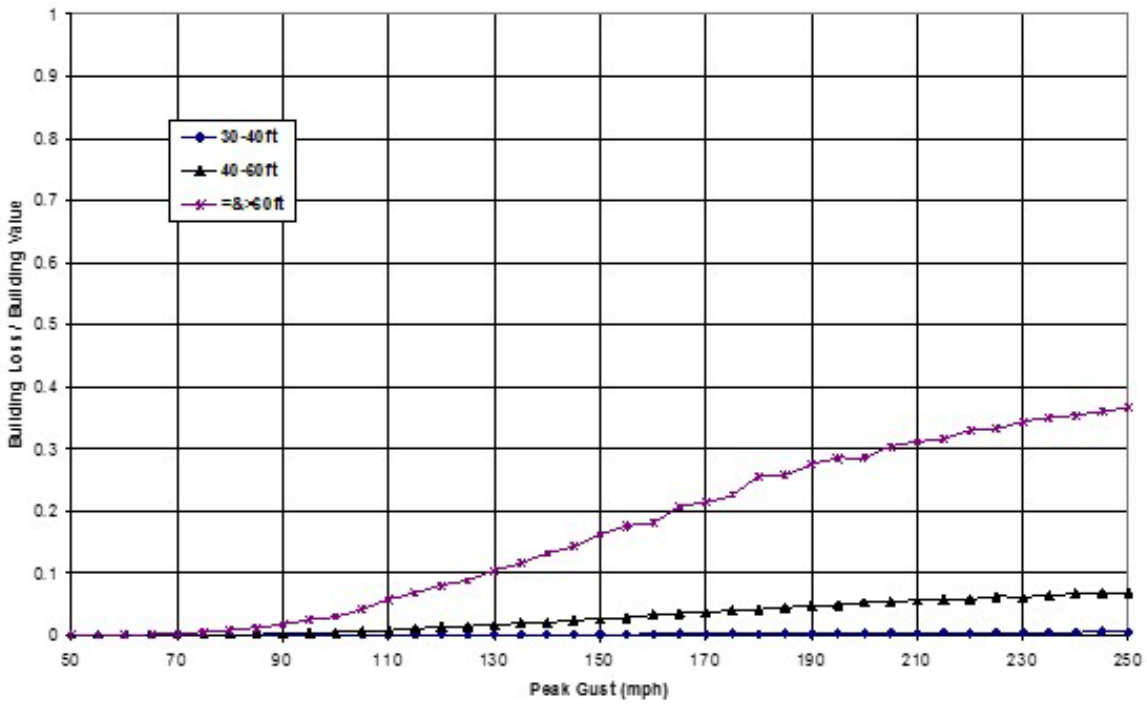


Figure 8-19 Dependence on Tree Density of Building (Upper) and Contents (Lower) Loss Functions

Building parameters: 50.x 24.x 9 Wood; Tree parameters: Evergreen Density=100.



Building parameters: 50.x 24.x 9 Wood; Tree parameters: Evergreen Density=100.

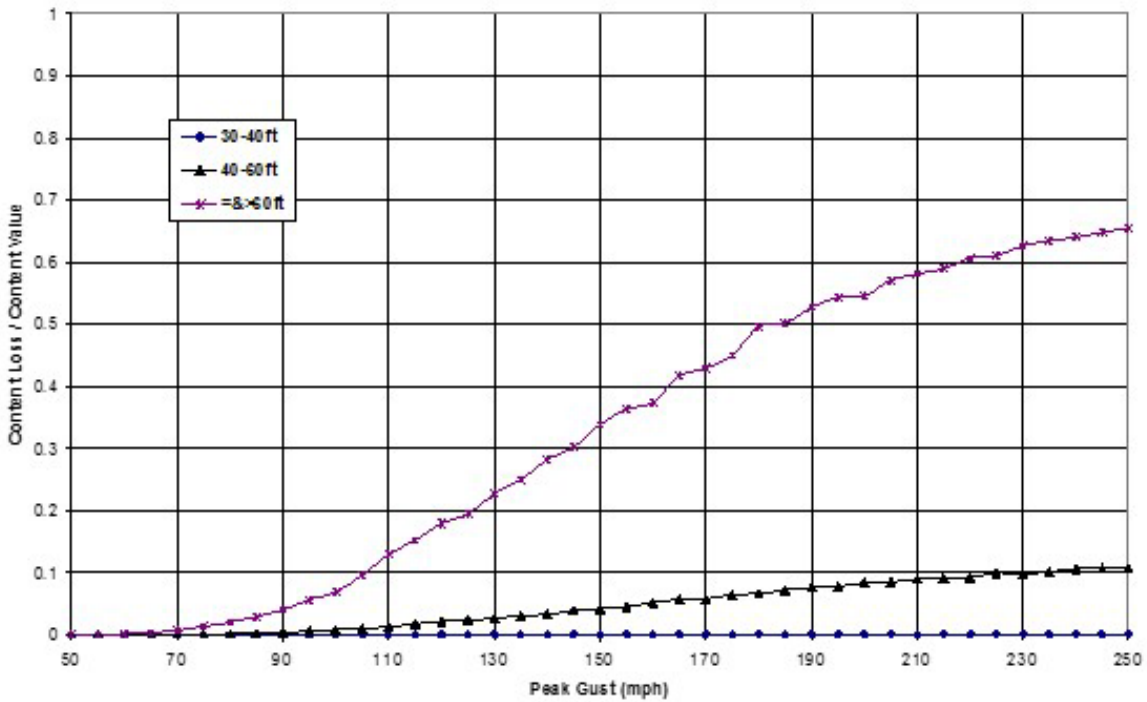
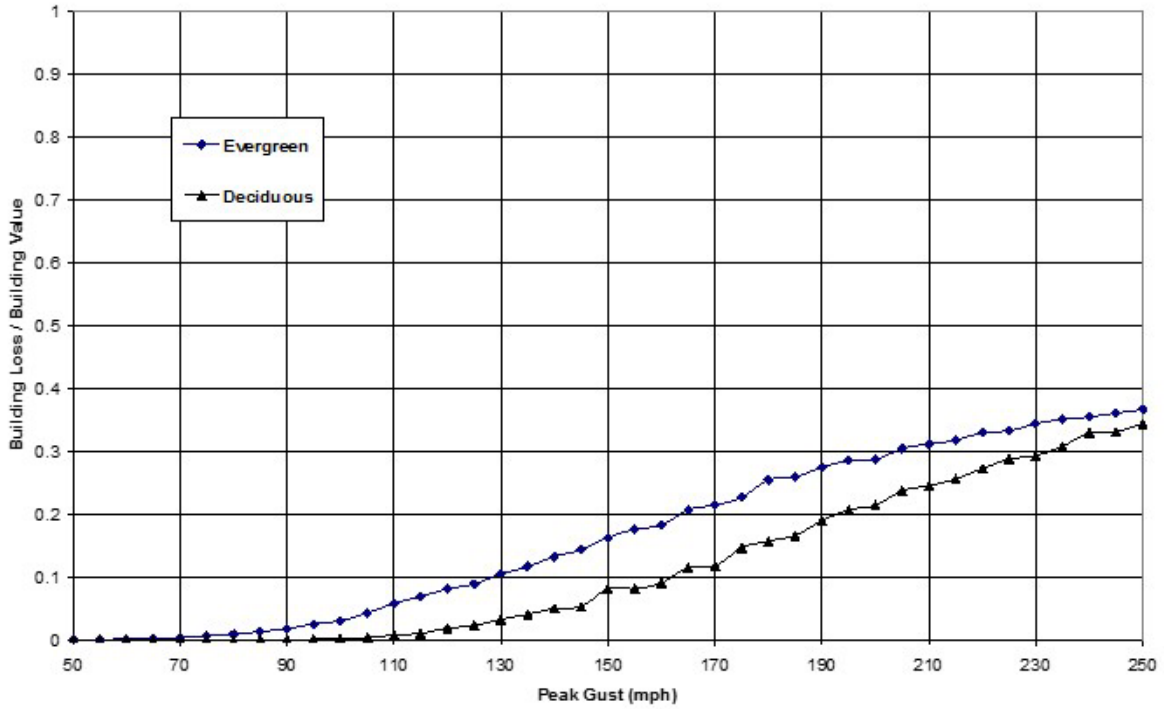


Figure 8-20 Dependence on Tree Height of Building (Upper) and Contents (Lower) Loss Functions

Building parameters: 50.x 24.x 9 Wood; Tree parameters: =8>60ft Density=100.



Building parameters: 50.x 24.x 9 Wood; Tree parameters: =8>60ft Density=100.

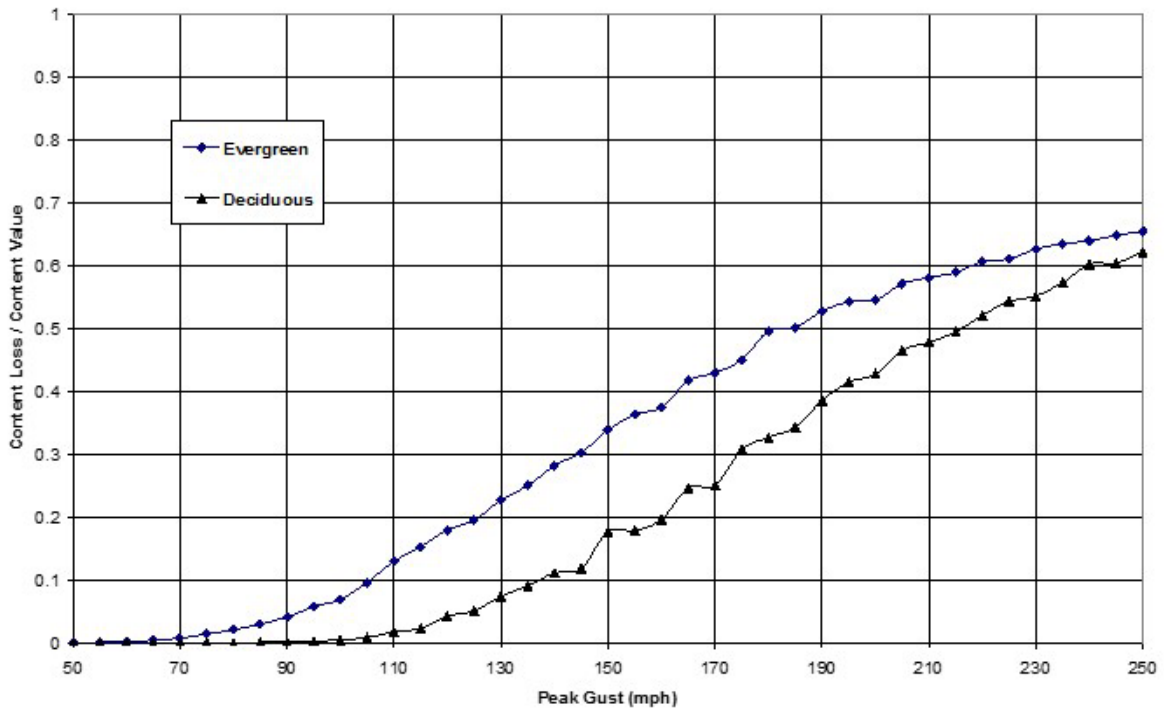
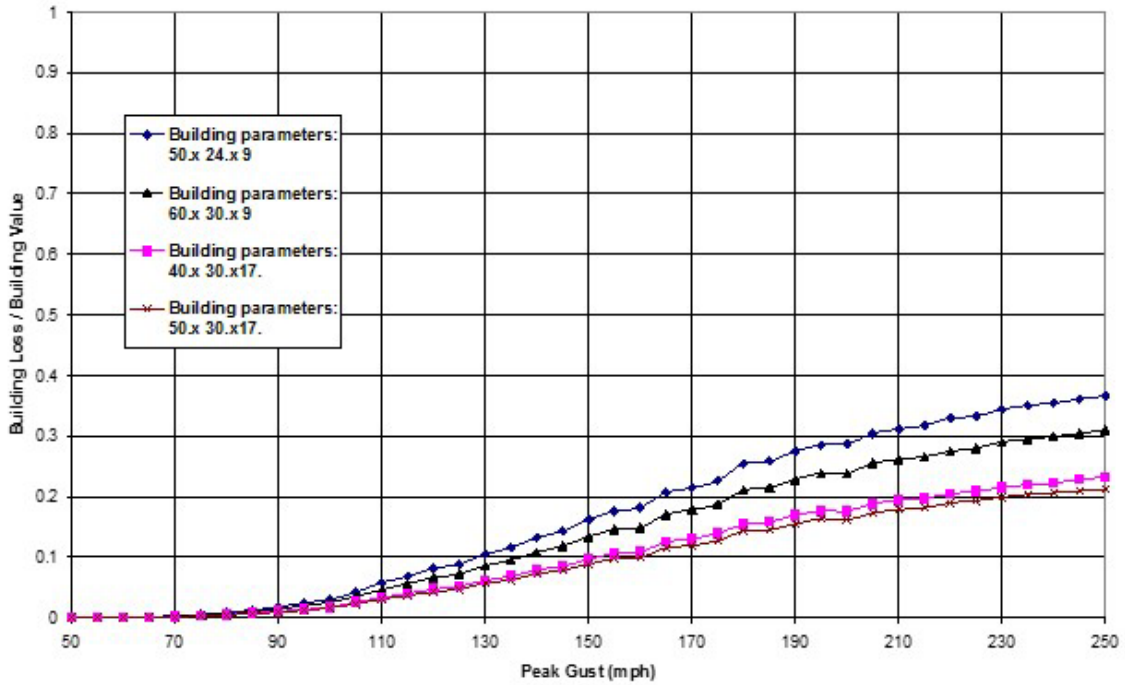


Figure 8-21 Dependence on Tree Type of Building (Upper) and Contents (Lower) Loss Functions

Woodframe Building; Tree parameters: Evergreen =>60ft Density= 100.



Woodframe Building; Tree parameters: Evergreen =>60ft Density= 100.

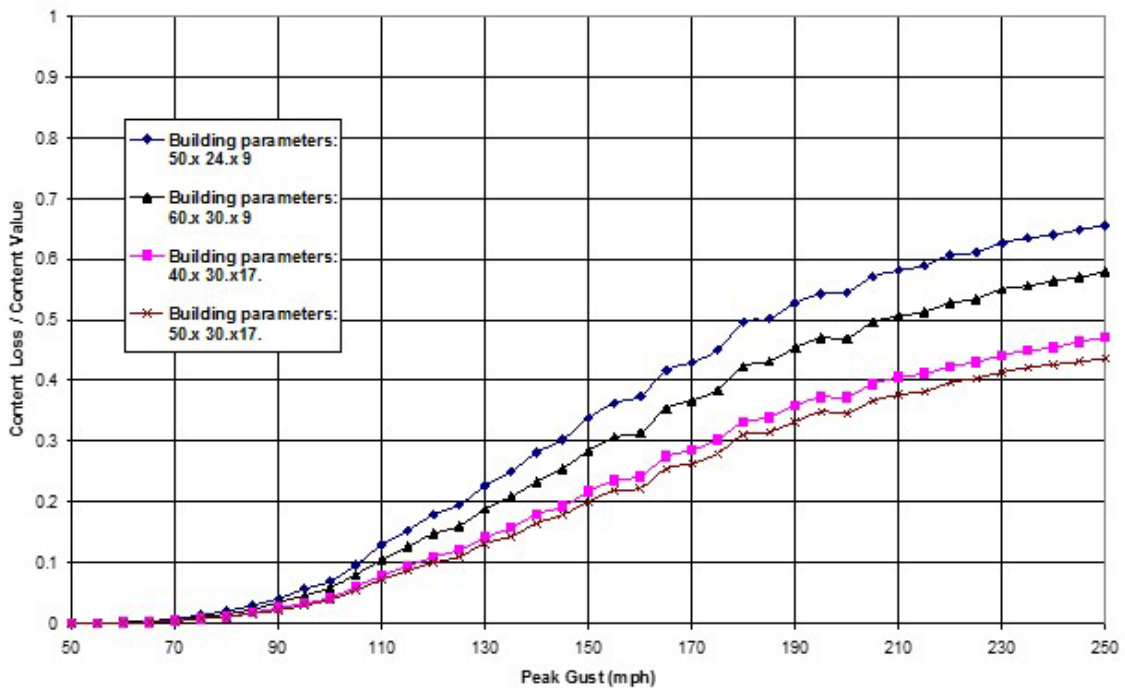
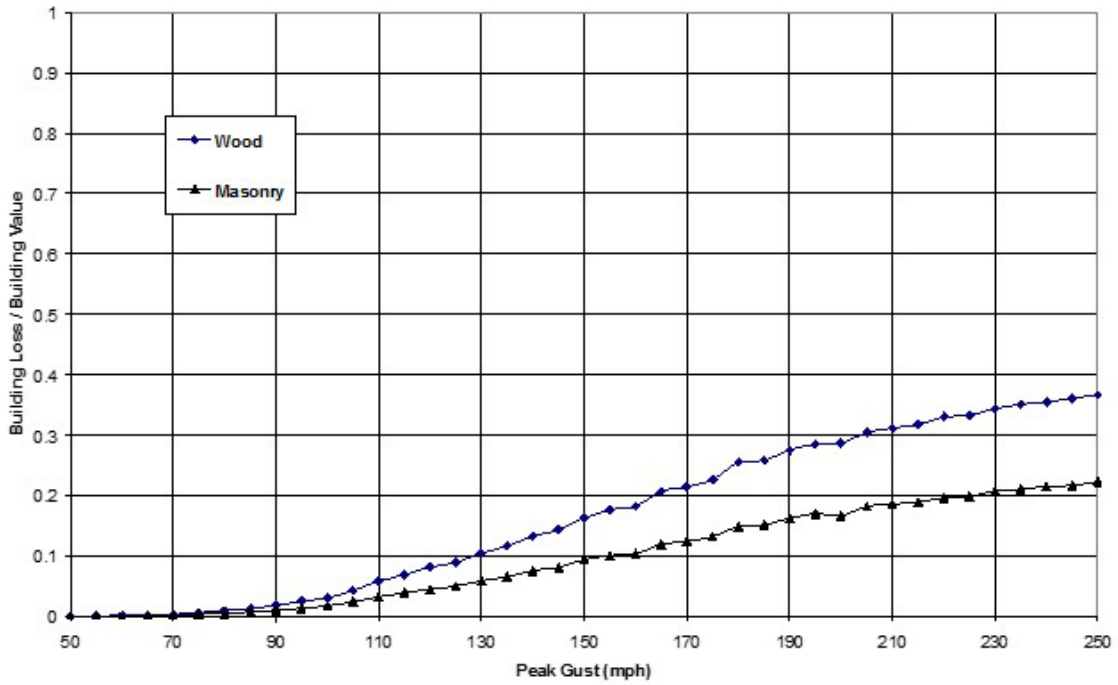


Figure 8-22 Dependence on Building Dimensions (ft) of Building (Upper) and Contents (Lower) Loss Functions

Building parameters: 50.x 24.x 9; Tree parameters: E vergreen =>60ft D density=100.



Building parameters: 50.x 24.x 9; Tree parameters: E vergreen =>60ft D density=100.

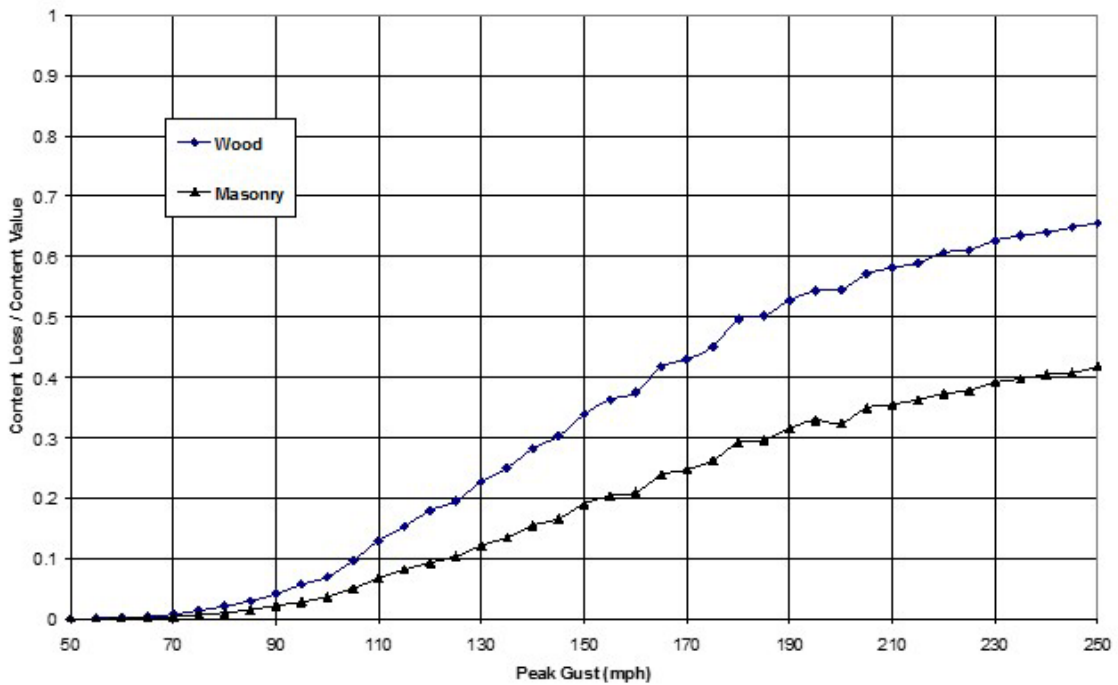


Figure 8-23 Dependence on Wall Type of Building (Upper) and Contents (Lower) Loss Functions

Building parameters: 50.x 24.x 9 Wood; Tree parameters: Evergreen =>60ft Density=100.

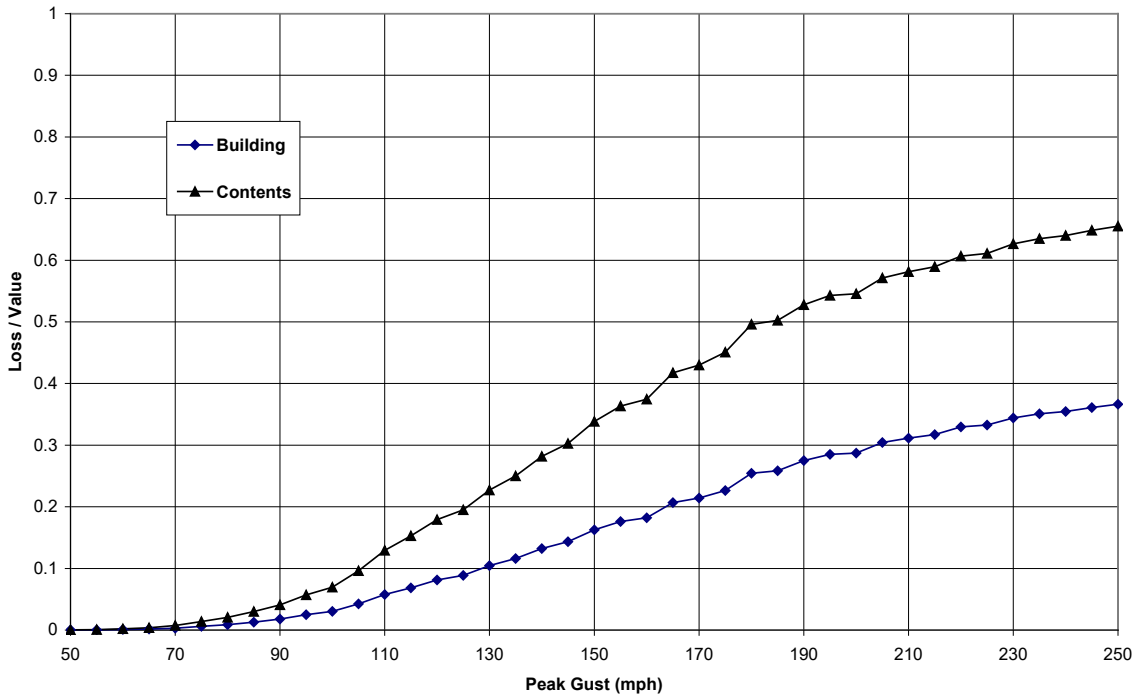


Figure 8-24 Building and Contents Loss Comparison

8.3.5 Loss Function for a Specific Building Type in Given Census Tract

The basic normalized loss functions and the tree inventory data are used in Hazus as follows to derive a normalized loss function for a specific building type in a specific Census tract (or block):

- *Input:* Census tract (or block) tree inventory data: dominant tree type, tree density, and tree height distribution
- *For Evergreen:* Census tract (or block) loss function = height group proportion weighted average of loss functions for the three height groups, for the Census tract (or block) tree type and density, and for the specific building mapped
- *For Deciduous:* Census tract (or block) loss function = height group proportion weighted average of loss functions for the three height groups, for the Census tract (or block) tree type and density, and for the specific building mapped
- *For Mixed:* Census tract (or block) loss function = sum of height group proportion weighted averages of loss functions for the three height groups for the two base tree types divided by 2, for the Census tract (or block) tree density, and for the specific building mapped

The following simplified method is used to combine the tree blowdown normalized loss with the basic fast-running loss functions described in Section 8.2.1 for single-family residential building and content losses:

Equation 8-19

$$\text{Total Loss} = \text{Basic Loss Ratio} + \text{Tree Damage Loss Ratio} - (\text{Basic Loss Ratio} * \text{Tree Damage Loss Ratio})$$

This equation assumes that the probabilities of wind damage and tree damage can be approximated as being mutually independent.

8.4 Combined Wind and Flood Losses for Coastal Storm Surge

This section describes the methodology for combining wind and flood losses to buildings in Hazus due to hurricane storm surge and waves. The objective of the combined loss methodology is to estimate the total losses sustained by the General Building Stock (GBS) within a region due to the winds and coastal storm surge generated by a single, hurricane scenario.

The combined wind and flood loss methodology builds upon the existing Hazus Wind Loss and Coastal Flooding Loss Methodologies to model a combined loss by analyzing different building components separately and combining the individual results into a combined loss while still providing wind and flood only losses.

The primary motivation for the combined wind and flood loss methodology is to avoid “double counting” of damage. At a minimum, the combined wind and flood loss must be at least the larger of the wind-only or the flood-only loss. At a maximum, the combined loss must be no larger than the lesser of the sum of the wind-only and flood-only losses, or 100% of the building (or contents or inventory) replacement value. These constraints can be written as:

Equation 8-20

$$\max(W, F) \leq C \leq \min(W+F, 1.00)$$

Where:

- W is the modeled wind-only building (or contents or inventory) loss ratio expressed as a fraction of the building (or contents or inventory) replacement value
- F is the modeled flood-only building (or contents or inventory) loss ratio
- C is the combined wind and flood loss ratio

As an example, consider a scenario in which the wind-only loss estimate for a single-family wood frame house is 70% of the building replacement cost and the flood-only loss estimate is 50%. In this situation, the lower and upper bounds of the combined wind and flood would be 70% and 100%, respectively, of the building replacement value. loss

For a special case, where the wind-induced damage and flood-induced damage are spread uniformly and randomly over a building, the two damage mechanisms can be treated as independent and the expected combined loss ratio is expressed as the simplified equation:

Equation 8-21

$$C = W + F - W * F$$

An idealized combined wind and flood loss matrix based on Equation 8-21 is shown in Table 8-57. This simplified approach is currently used in Hazus for content and inventory losses, instead of the full sub-assembly approach. Users should check their results in case any adjustments are required. Note that the combined wind and flood loss estimate in each cell of the table is always less than or equal to the sum of the wind-only loss and flood-only loss shown in its column and row headings, respectively.

Table 8-57 Combined Wind and Flood Loss Matrix for the Idealized Case of Wind and Flood Losses

Flood-Only Building Loss	Wind-Only Building Loss										
	0%	10%	20%	30%	40%	50%	60%	70%	80%	90%	100%
0%	0%	10%	20%	30%	40%	50%	60%	70%	80%	90%	100%
10%	10%	19.0%	28.0%	37.0%	46.0%	55.0%	64.0%	73.0%	82.0%	91.0%	100%
20%	20%	28.5%	36.0%	44.0%	52.0%	60.0%	68.0%	76.0%	84.0%	92.0%	100%
30%	30%	37.0%	44.0%	51.0%	58.0%	65.0%	72.0%	79.0%	86.0%	93.0%	100%
40%	40%	46.0%	52.0%	58.0%	64.0%	70.0%	76.0%	82.0%	88.0%	94.0%	100%
50%	50%	55.0%	60.0%	65.0%	70.0%	75.0%	80.0%	85.0%	90.0%	95.0%	100%
60%	60%	64.0%	68.0%	72.0%	76.0%	80.6%	84.0%	88.0%	92.0%	96.0%	100%
70%	70%	73.0%	76.0%	79.0%	82.0%	85.0%	88.0%	91.0%	94.0%	97.0%	100%
80%	80%	82.0%	84.0%	86.0%	88.0%	90.0%	92.0%	94.0%	96.0%	98.0%	100%
90%	90%	91.0%	92.0%	93.0%	94.0%	95.0%	96.0%	97.0%	98.0%	99.0%	100%
100%	100%	100%	100%	100%	100%	100%	100%	100%	100%	100%	100%

While the idealized combined wind and flood building loss matrix shown in Table 8-57 satisfies the constraints specified in Equation 8-20, it is nonetheless clear that neither wind nor storm surge damages are uniformly and randomly distributed throughout a structure. Wind damage is most frequently initiated at the roof and fenestrations (i.e., windows, doors, or other openings in the building envelope), whereas flood damage is most frequently initiated at the lowest elevations of the structure (e.g., basement or first finished floor) and progresses upward through the structure as the depth of flooding increases.

The approach for incorporating the non-uniformity of wind and flood damage into the combined loss methodology is based on allocating wind and flood losses to building subassemblies as a function of the building type and the overall wind-only and flood-only loss estimate. The concept of building subassemblies is widely used in construction cost estimation and is used in the Hazus wind-only loss methodology (see Section 4.6). A study from the USACE New Orleans District (GEC 2006) also provides guidance for allocating flood losses to building subassemblies. It is important to note that no attempt is made in the methodology to allocate or apportion the combined loss into wind and flood loss components. While the apportioning of losses may be of great interest in situations where the financial

stakeholders and/or indemnification terms for wind and flood losses differ, such situations require careful consideration of building construction details, hurricane hazard details (e.g., the magnitudes, timing, duration, and directionality of wind, surge, and waves), and site details (e.g., aerodynamic roughness and hydrodynamic roughness) that are clearly beyond the scope of a regional loss estimation and hazard mitigation tool such as Hazus.

8.4.1 Building Subassembly Approach

The existing Hazus Wind Loss Estimation Methodology is a physically-based, damage-to-loss methodology that computes direct economic losses to buildings using a combination of explicit and implicit costing techniques. Detailed simulations of building envelope damage are used to explicitly estimate expected repair and replacement costs for the wind-damaged components of the building envelope, such as roof covering, roof sheathing, windows, doors, and wall covering. It also estimates expected losses to the building interior and contents through a combination of the roofing damage fraction and the volume of rainwater penetrating through failed fenestrations (windows, doors, garage doors, etc.). This methodology is described in detail in Section 8.1.4.

A study for the New Orleans District of the USACE (GEC 2006) provides estimates of overall building and contents losses due to flooding as a function of building type (e.g., one-story house on slab foundation), type of flooding (e.g., short or long duration, freshwater or saltwater), and depth of flooding (i.e., flood level relative to first floor). The GEC study is similar to the Hazus Wind Loss Methodology in that it builds up the overall flood loss by summing the losses to building components, such as the structural frame, doors/trim, plumbing, cabinets, etc. For single-family homes on slab foundations, the building flood loss estimates are built-up by estimating damage to a total of 20 different building components. The component loss estimates are based on interviews with homeowners and business operators and the collective judgment of nine experts in the fields of construction, repair and restoration, and insurance claims adjustment.

By grouping the wind loss components and flood loss components into a consistent set of building subassemblies, Equation 8-21 can more accurately apply to each subassembly instead of applying it to the entire building. For this purpose, seven major building subassemblies are defined:

1. *Foundation*: Includes site work, footings, and walls, slabs, piers or piles
2. *Below First Floor*: Items other than the foundation that are located below the first floor of the structure, such as mechanical equipment, stairways, parking pads, break away flood walls, etc.
3. *Structure Framing*: Includes all of the main load carrying structural members of the building below the roof framing and above the foundation
4. *Roof Covering*: Includes the roof membrane material and flashing
5. *Roof Framing*: Includes trusses, rafters, and sheathing (For a one-story, wood frame house on a slab foundation, the total framing cost is assumed to be distributed as 39% exterior wall framing, 26% interior wall framing, and 35% roof framing.)
6. *Exterior Walls*: Includes wall covering, windows, exterior doors, and insulation
7. *Interiors*: Includes interior wall and floor framing, drywall, paint, interior trim, floor coverings, cabinets, counters, mechanical, and electrical

These groupings allow, for example, roof covering loss to contribute more, on average, to the overall wind-only loss than it would to the same overall level of flood-only loss.

To illustrate the approach, the methodology considers a one-story, wood frame house on a slab foundation exposed to Coastal Zone A flooding. The default Hazus Flood Model depth-damage curve for this specific occupancy in the Coastal Zone A is plotted in Figure 8-25. Using Table 11 from the GEC (2006) report, the flood losses are allocated into five subassemblies. In this example, the methodology chooses to neglect the Below First Floor subassembly and merge the Structure Framing subassembly into the Exterior Walls subassembly for simplicity. The results are shown in Table 8-58.

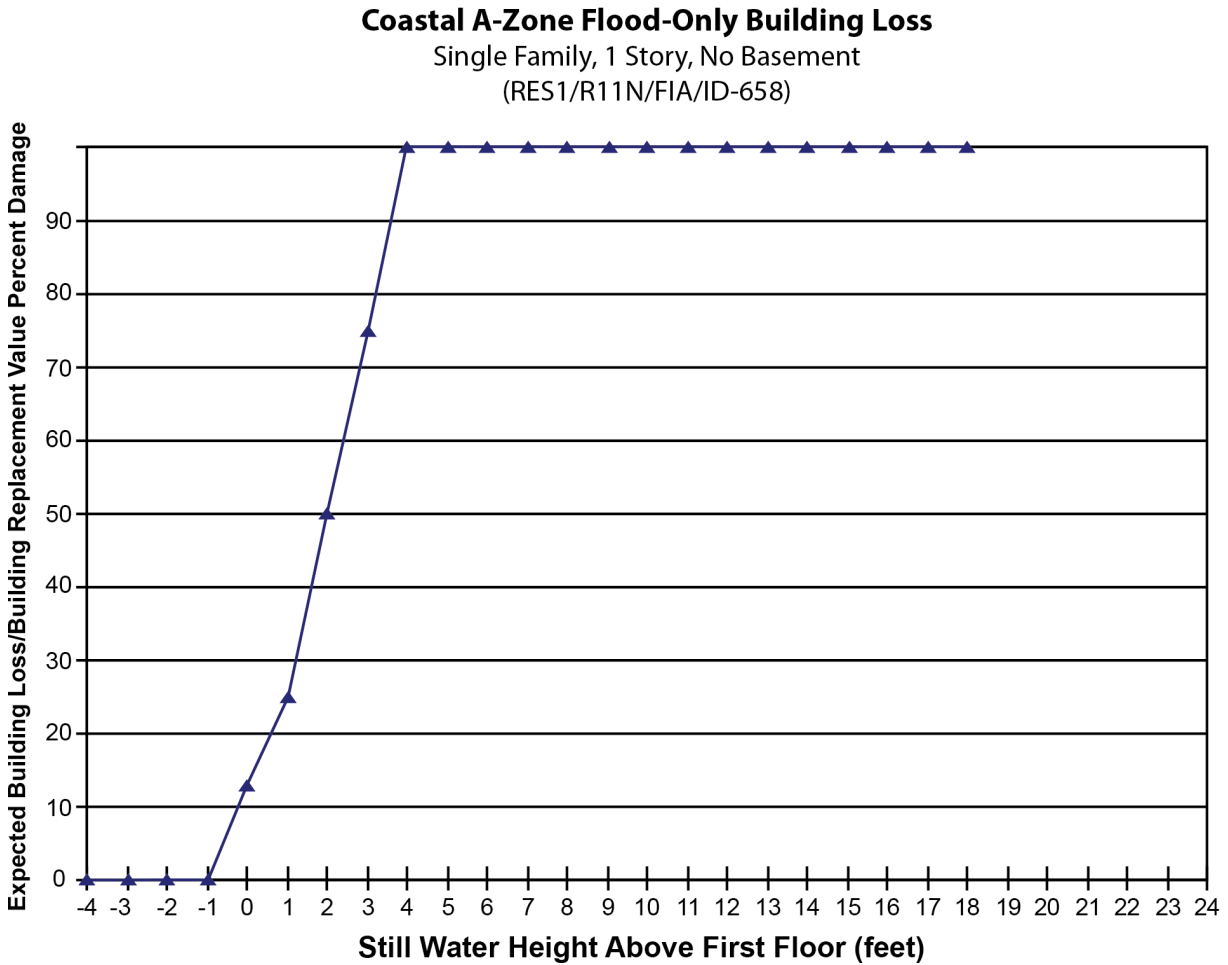


Figure 8-25 Depth-Damage Curve in Hazus for One-Story, Single-Family Houses on Slab Foundations in the Coastal Zone A

Table 8-58 Distribution of Flood Losses to Building Subassemblies as a Function of Still Water Height Above First Floor

Subassembly	0.0	1.0	2.0	3.0	4.0	5.0	6.0	7.0
Foundation	0.0%	0.0%	0.0%	0.0%	0.0%	0.0%	0.0%	0.0%
Roof Covering	0.0%	0.0%	0.0%	0.0%	0.0%	0.0%	0.0%	0.0%
Roof Framing	0.0%	0.0%	0.0%	0.0%	0.0%	0.0%	0.0%	0.0%
Exterior Wall	10.0%	15.2%	18.9%	20.4%	22.5%	23.7%	24.0%	23.8%
Interiors	90.0%	84.8%	81.1%	79.6%	77.5%	76.3%	76.0%	76.2%
Total	100%	100%	100%	100%	100%	100%	100%	100%

Table 8-59 Distribution of Flood Losses to Building Subassemblies as a Function of Depth of Flooding (Concluded)

Subassembly	8.0	9.0	10.0	11.0	12.0	13.0	14.0	15.0
Foundation	0.0%	0.0%	0.0%	0.0%	0.0%	0.0%	0.0%	0.0%
Roof Covering	0.0%	0.5%	1.4%	1.6%	1.6%	2.4%	2.4%	2.4%
Roof Framing	0.0%	0.4%	0.4%	0.4%	0.4%	0.4%	0.4%	0.4%
Exterior Wall	23.6%	22.6%	22.6%	22.5%	22.5%	22.4%	22.4%	22.4%
Interiors	76.4%	76.6%	75.6%	75.5%	75.5%	74.9%	74.9%	74.9%
Total	100%	100%	100%	100%	100%	100%	100%	100%

Note: Distribution of Flood Losses to Building Subassemblies as a Function of Depth of Flooding for a One-Story, Single-Family House (RES1) on Slab Foundation in a Coastal Zone A Exposed to Short Duration Saltwater Flooding.

Using the depths associated with flood-only losses of 10%, 20%, ..., 90% from Figure 8-25 and interpolating from Table 8-58, the flood-only building loss can be apportioned to the five retained subassemblies. The results for the example house are shown in Table 8-60.

Table 8-60 Distribution of Flood Losses to Building Subassemblies as a Function of Flood-Only Building Loss

Building Loss	Foundation	Below First Floor	Structure Frame	Roof Cover	Roof Frame	Exterior Wall	Interiors	Total
10.0%	0.0%	1.5%	0.0%	0.0%	0.0%	0.5%	8.0%	10.0%
20.0%	0.0%	3.0%	0.2%	0.1%	0.1%	3.5%	12.9%	19.7%
30.0%	0.0%	3.0%	1.0%	0.4%	0.4%	5.5%	19.6%	29.9%
40.0%	0.0%	3.0%	1.3%	0.5%	0.5%	7.5%	27.0%	39.8%
50.0%	0.0%	3.0%	1.6%	0.6%	0.6%	10.5%	33.7%	50.1%
60.0%	0.1%	3.0%	2.1%	0.8%	0.8%	12.8%	40.4%	60.0%
70.0%	0.4%	3.0%	2.6%	1.0%	1.0%	15.5%	46.6%	70.0%
80.0%	0.6%	3.0%	3.3%	1.3%	1.3%	17.5%	52.7%	79.5%
90.0%	1.0%	3.0%	3.9%	1.5%	1.5%	19.5%	60.0%	90.4%
100.0%	1.5%	3.0%	5.5%	2.1%	2.1%	25.0%	61.0%	100.3%

Note: Distribution of Flood Losses to Building Subassemblies as a Function of Flood-Only Building Loss for a One-Story, Single-Family House (RES1) on Slab Foundation in a Coastal Zone A Exposed to Short Duration Saltwater Flooding

The wind-only loss simulation results for the example house can likewise be distributed to the same five major subassemblies. The Below First Floor subassembly is neglected and the Structure Framing subassembly is merged into the Exterior Walls subassembly for simplicity. The hurricane wind losses from each of 107,910 building damage simulations described at the beginning of this section are grouped by overall wind-only building loss with the average contributions from each of the five major subassemblies. The results for the example house are shown in Table 8-61.

Table 8-61 Distribution of Wind Losses to Subassemblies Relative to Building Value as a Function of Wind-Only Building Loss

Building Loss	Foundation	Roof Covering	Roof Framing	Exterior Walls	Interiors
10%	0.0%	4.3%	0.0%	0.8%	4.9%
20%	0.0%	4.7%	0.0%	1.5%	13.8%
30%	0.0%	4.7%	0.0%	2.3%	23.0%
40%	0.0%	4.8%	0.0%	2.9%	32.4%
50%	0.0%	4.8%	0.0%	3.0%	42.2%
60%	0.0%	4.9%	0.0%	3.8%	51.3%
70%	0.0%	4.9%	0.1%	4.9%	60.1%
80%	0.0%	5.2%	0.3%	14.3%	60.2%
90%	0.0%	5.2%	0.8%	23.8%	60.2%

**The results shown in Table 8-61 are for a one-story, wood frame house located in suburban terrain with a gable roof, no garage, roof-to-wall straps, no opening protection, 8d roof deck nails at 6/12 spacing, and no secondary water resistance*

The numbers shown in Table 8-62 result from applying Equation 8-21 and Equation 8-22 to each subassembly loss ratio; then multiplying those results by the total repair and replacement cost of each subassembly (shown in the Foundation, Roof Covering, Roof Framing, Exterior Walls, and Interiors columns); and finally summing all the individual subassembly loss percentages together (shown in the Building Loss column).

Table 8-62 Combined Wind and Flood Loss Matrix Assuming Wind and Flood Losses are each Uniformly Distributed within each of Five Building Subassemblies

Flood-Only Building Loss	Wind-Only Building Loss										
	0%	10%	20%	30%	40%	50%	60%	70%	80%	90%	100%
0%	0%	10%	20%	30%	40%	50%	60%	70%	80%	90%	100%
10%	10%	19.5%	28.7%	37.9%	47.1%	56.2%	65.3%	74.5%	84.4%	94.3%	100%
20%	20%	29.1%	37.5%	45.9%	54.3%	62.5%	70.9%	79.4%	89.1%	98.9%	100%
30%	30%	38.8%	46.7%	54.5%	61.3%	70.0%	77.8%	85.7%	95.0%	100.0%	100%
40%	40%	48.4%	55.7%	62.8%	69.9%	76.9%	84.0%	91.2%	100.0%	100.0%	100%
50%	50%	58.0%	64.6%	71.1%	77.5%	83.8%	90.3%	96.9%	100.0%	100.0%	100%
60%	60%	67.6%	73.5%	79.3%	85.0%	90.6%	96.4%	100.0%	100.0%	100.0%	100%
70%	70%	77.2%	82.4%	87.5%	92.5%	97.3%	100.0%	100.0%	100.0%	100.0%	100%
80%	80%	86.8%	91.4%	95.7%	100.0%	100.0%	100.0%	100.0%	100.0%	100.0%	100%
90%	90%	96.4%	100.0%	100.0%	100.0%	100.0%	100.0%	100.0%	100.0%	100.0%	100%
100%	100%	100%	100%	100%	100%	100%	100%	100%	100%	100%	100%

The results show that the combined loss estimates in Table 8-62 are indeed larger than the corresponding loss estimates in Table 8-57, and that the 100% cap is reached in approximately one-third of the interior cells. Additionally, the results show that the combined loss estimates in Table 8-62 are slightly asymmetric. For example, using Equation 8-21, when W=50% and F=20%, C=62.5%. Alternatively, when W=20% and F=50%, C=64.6%.

8.4.2 Development of Subassembly Replacement Cost Tables

To implement the combined loss methodology, subassembly replacement cost and subassembly loss tables are needed for each of the 33 SOCC and five GBT classes. A description of these specific occupancies and general building types can be found in the *Hazus Inventory Technical Manual (2022)*.

The subassembly replacement costs (as a percentage of total building replacement cost) were developed using RSMMeans (2009) data for typical model buildings representing each SOCC. The GBT subassembly replacement costs were then estimated using a Hazus SOCC-GBT mapping scheme for the southeastern United States, which best represented the building stock typically exposed to Hazus-supported hurricanes (east coast and gulf states only). Replacement costs are summarized in Table 8-63 and Table 8-64 for two cases: Pre-FIRM construction and Post-FIRM construction, respectively. As a rough rule, the foundation subassembly costs were typically assumed to increase by 5% when going from Pre-FIRM to Post-FIRM construction. To compensate for the increase in foundation cost, the interiors were typically assumed to decrease by 3% and the structure frame and exterior walls subassemblies were each typically assumed to decrease by 1%.

Table 8-63 Subassembly Replacement Cost by Specific Occupancy or General Building Type as a Percentage of Total Building Replacement Cost (Pre-FIRM)

Specific Occupancy or General Building Type		Pre-FIRM							
		Foundation	Below First Floor	Structure Frame	Roof Covering	Roof Framing	Exterior Wall	Interiors	Total
RES1	Single	6%	2%	13%	5%	5%	20%	49%	100%
RES2	MH	6%	2%	10%	3%	5%	20%	54%	100%
RES3A	Duplex	6%	2%	13%	5%	5%	20%	49%	100%
RES3B	3-4 Units	6%	2%	13%	5%	5%	20%	49%	100%
RES3C	5-9 units	5%	1%	10%	2%	3%	10%	69%	100%
RES3D	10-19 units	5%	1%	10%	2%	3%	10%	69%	100%
RES3E	20-19 units	5%	1%	13%	1%	3%	10%	67%	100%
RES3F	50+ units	3%	0%	13%	1%	1%	13%	69%	100%
RES4	Temp. Lodging	3%	1%	9%	1%	2%	10%	74%	100%
RES5	Institutional Dormitory	4%	0%	14%	1%	3%	14%	64%	100%
RES6	Nursing Home	5%	0%	10%	3%	2%	13%	67%	100%
COM1	Retail	6%	1%	10%	5%	5%	10%	63%	100%
COM2	Wholesale	20%	1%	7%	9%	7%	11%	45%	100%
COM3	Personal & Repair Services	10%	1%	8%	7%	3%	10%	61%	100%
COM4	Professional/Business	4%	1%	11%	1%	3%	17%	63%	100%
COM5	Banks	6%	0%	10%	4%	9%	8%	63%	100%
COM6	Hospitals	2%	0%	7%	1%	4%	7%	79%	100%
COM7	Medical Office	5%	1%	5%	3%	2%	12%	72%	100%
COM8	Entertainment	9%	1%	10%	4%	3%	8%	65%	100%
COM9	Theaters	6%	1%	10%	5%	6%	10%	62%	100%
COM10	Parking	12%	0%	40%	0%	10%	9%	29%	100%
IND1	Heavy	14%	1%	3%	7%	3%	10%	62%	100%
IND2	Light	15%	1%	4%	9%	7%	11%	53%	100%
IND3	Food/Chemicals	11%	1%	4%	8%	6%	11%	59%	100%
IND4	Metals/Minerals Processing	7%	0%	25%	2%	6%	8%	52%	100%
IND5	High Technology	11%	0%	5%	4%	4%	4%	72%	100%
IND6	Construction	20%	1%	7%	9%	7%	11%	45%	100%
AGR1	Agriculture	26%	0%	8%	9%	9%	12%	36%	100%
REL1	Church	10%	1%	12%	4%	17%	10%	46%	100%
GOV1	General Services	10%	1%	12%	6%	4%	8%	59%	100%
GOV2	Emergency Response	6%	0%	15%	2%	2%	12%	63%	100%

Specific Occupancy or General Building Type		Pre-FIRM							
		Foundation	Below First Floor	Structure Frame	Roof Covering	Roof Framing	Exterior Wall	Interiors	Total
EDU1	School	4%	1%	12%	3%	6%	10%	64%	100%
EDU2	College	4%	1%	10%	2%	3%	8%	72%	100%
Wood		6%	1%	13%	4%	4%	16%	56%	100%
Steel		4%	0%	12%	1%	2%	15%	66%	100%
Masonry		7%	1%	14%	3%	3%	18%	54%	100%
Concrete		4%	0%	12%	1%	2%	15%	66%	100%
MH		6%	2%	10%	3%	5%	20%	54%	100%

Table 8-64 Subassembly Replacement Costs by Specific Occupancy or General Building Type as a Percentage of Total Building Replacement Cost (Post-FIRM)

Specific Occupancy or General Building Type		Post-FIRM							
		Foundation	Below First Floor	Structure Frame	Roof Covering	Roof Framing	Exterior Wall	Interiors	Total
RES1	Single	11%	3%	10%	5%	5%	19%	47%	100%
RES2	MH	8%	2%	10%	3%	5%	20%	52%	100%
RES3A	Duplex	11%	3%	10%	5%	5%	19%	47%	100%
RES3B	3-4 Units	11%	3%	10%	5%	5%	19%	47%	100%
RES3C	5-9 units	10%	1%	9%	2%	3%	9%	66%	100%
RES3D	10-19 units	10%	1%	9%	2%	3%	9%	66%	100%
RES3E	20-19 units	10%	1%	12%	1%	3%	10%	63%	100%
RES3F	50+ units	8%	0%	12%	1%	1%	12%	66%	100%
RES4	Temp. Lodging	8%	1%	8%	1%	2%	9%	71%	100%
RES5	Institutional Dormitory	9%	0%	13%	1%	3%	13%	61%	100%
RES6	Nursing Home	10%	1%	9%	3%	2%	12%	63%	100%
COM1	Retail	11%	1%	9%	5%	5%	9%	60%	100%
COM2	Wholesale	25%	1%	6%	9%	7%	10%	42%	100%
COM3	Personal & Repair Services	15%	1%	7%	7%	3%	9%	58%	100%
COM4	Professional/Business	9%	1%	10%	1%	3%	16%	60%	100%
COM5	Banks	11%	0%	9%	4%	9%	7%	60%	100%
COM6	Hospitals	7%	0%	6%	1%	4%	6%	76%	100%
COM7	Medical Office	10%	1%	4%	3%	2%	11%	69%	100%
COM8	Entertainment	14%	1%	9%	4%	3%	7%	62%	100%
COM9	Theaters	11%	1%	9%	5%	6%	9%	59%	100%
COM10	Parking	17%	0%	39%	0%	10%	8%	26%	100%

Specific Occupancy or General Building Type		Post-FIRM							
		Foundation	Below First Floor	Structure Frame	Roof Covering	Roof Framing	Exterior Wall	Interiors	Total
IND1	Heavy	19%	1%	2%	7%	3%	9%	59%	100%
IND2	Light	20%	1%	3%	9%	7%	10%	50%	100%
IND3	Food/Chemicals	16%	1%	3%	8%	6%	10%	56%	100%
IND4	Metals/Minerals Processing	12%	0%	24%	2%	6%	7%	49%	100%
IND5	High Technology	16%	0%	4%	4%	4%	3%	69%	100%
IND6	Construction	25%	1%	6%	9%	7%	10%	42%	100%
AGR1	Agriculture	31%	0%	7%	9%	9%	11%	33%	100%
REL1	Church	15%	1%	11%	4%	17%	9%	43%	100%
GOV1	General Services	15%	1%	11%	6%	4%	7%	56%	100%
GOV2	Emergency Response	11%	0%	14%	2%	2%	11%	60%	100%
EDU1	School	9%	1%	11%	3%	6%	9%	61%	100%
EDU2	College	9%	1%	9%	2%	3%	7%	69%	100%
Wood		11%	1%	12%	4%	4%	15%	53%	100%
Steel		9%	0%	11%	1%	2%	14%	63%	100%
Masonry		12%	1%	13%	3%	3%	17%	51%	100%
Concrete		11%	0%	11%	3%	2%	11%	62%	100%
MH		8%	2%	10%	3%	5%	20%	52%	100%

8.4.2.1 Development of Subassembly Loss Tables for Wind Losses

To implement the combined loss methodology, wind-induced subassembly losses as a function of overall building loss are required at increments of 10% overall wind loss for the five Hazus General Building Types (wood, concrete, masonry, steel, and manufactured housing) and the 33 Hazus Specific Occupancies (RES1, RES2, ...). In the Hazus Hurricane Model, the five GBTs and 33 SOCCs are each represented by a weighted combination of the 39 Specific Building Types (SBTs) described in the *Hazus Inventory Technical Manual* (2022). Although the SBT weights vary by region in Hazus, it was found that the resulting wind subassembly loss tables were relatively insensitive to these regional variations. It was also found that the wind sub-assembly loss tables were relatively insensitive to variations in terrain. The primary sensitivity of the wind subassembly loss tables is to the wind resistive features of the SBT, such as opening protection, roof shape, roof cover strength, roof deck strength, and roof-to-wall connection strength.

Since there are typically dozens or hundreds of building variations within each Hazus Hurricane SBT category, a limited number of specific building configurations were chosen to represent the range of building strengths present within each SBT. To select the specific configurations, each possible building configuration was first classified as being weak, medium, or strong. To do this, the building configurations within a given SBT were ranked from lowest to highest in terms of expected average annual loss (AAL) at one suburban location in Florida. Within each SBT, a specific building configuration was considered to be weak if it had an AAL that was greater than the 80th percentile AAL for that SBT, and it was considered to be strong if it had an AAL that was less than the 20th percentile AAL for that SBT. All other buildings were considered to be medium strength. Finally, the building configuration that

had an AAL closest to the 10th percentile was used to represent the strong buildings, the building configuration closest to the 90th was used to represent the weak buildings, and the one closest to the 50th percentile was used to represent a medium strength building.

Subassembly losses were computed for the weak, medium, and strong building configurations selected for each SBT. For each simulated event, the overall loss relative to the building value and the subassembly losses were recorded and binned into a 10% interval. For example, if a record in a given loss file had an overall loss of 5.9%, it would be assigned to the 10% overall loss bin. The average of all records at each 10% increment was calculated. Since subassembly losses do not necessarily sum up to the overall loss of their corresponding bin, subassembly losses were adjusted by the ratio of their loss bin and subassembly value sum. Loss bins that had no data were filled by interpolation. The subassembly wind loss table for a given SBT is then generated by weighting the full set of building configurations within the SBT using the representative weak, medium, or strong subassembly loss distributions.

Of the seven subassemblies, foundation and below first floor subassemblies are assumed to be undamaged by wind. Consistent with the original methodology used to develop the Hazus Hurricane Model loss functions, each subassembly loss was capped to 125% of their subassembly replacement cost. The additional 25% approximates the added costs associated with repair and reconstruction compared to new construction costs. The overall loss calculated by adding all the subassembly components together is still capped at 100% of the structure value, however.

To correct any minor reversals due to insufficient simulations at certain loss levels, the subassembly losses were “forced” to increase with increasing overall loss. Since the sum of the subassembly losses at a given loss interval may now no longer sum to the loss interval, all the subassemblies at this loss interval were uniformly scaled to sum the target overall loss level (e.g., 70%). Since this adjustment could again induce minor non-monotonic behaviors, the process of forcing and adjusting was repeated until the following equation was satisfied:

Equation 8-22

$$\left| r - \sum_{c=1}^7 B_c(r) \right| \leq 0.05\%$$

Where:

- r is the target loss result as a percentage of the replacement cost
- B_c(r) is the loss result (as a percentage of the replacement) for each of the seven building components

Component losses are never allowed to go beyond 125% of the component’s value. Thus far, the foundation and below first floor subassembly losses have been null. However, it might not be possible to satisfy Equation 8-7 at higher levels of loss (e.g., 90% or 100%) because the remaining five components may already have achieved maximum loss. In this case, the foundation subassembly loss increased from zero until Equation 8-22 was satisfied. For example, if the sum of the sub-assembly

losses at the 90% loss interval comes to 88%, the foundation subassembly will be assumed to experience a 2% loss. This scenario did not occur at the SBT level except at 100% overall loss. Table 8-65 shows an example of the final subassembly loss table for a case in which the foundation subassembly loss had to be increased from 0% when the overall building loss reached 100%. Note that the sum of the subassembly caps at 125%.

Table 8-65 Sample Subassembly Losses Relative to Total Building Replacement Cost

Overall Loss	Foundation	Structure Below First Floor	Structure Frame	Roof Cover	Roof Frame	Exterior Wall	Interior
10%	0.00%	0.00%	0.00%	0.48%	0.29%	1.36%	7.87%
20%	0.00%	0.00%	0.00%	0.48%	0.29%	2.16%	17.07%
30%	0.00%	0.00%	0.00%	0.48%	0.29%	3.08%	26.16%
40%	0.00%	0.00%	0.00%	0.51%	0.29%	4.66%	34.54%
50%	0.00%	0.00%	0.00%	0.52%	0.29%	4.94%	44.26%
60%	0.00%	0.00%	0.00%	0.53%	0.29%	5.05%	54.13%
70%	0.00%	0.00%	0.00%	0.54%	0.30%	7.29%	61.87%
80%	0.00%	0.00%	0.00%	0.57%	0.34%	8.33%	70.75%
90%	0.00%	0.00%	0.00%	0.57%	0.39%	9.38%	79.66%
100%	0.13%	0.00%	1.02%	0.57%	1.26%	17.19%	79.82%
Cap	3.03%	1.3%	23.14%	0.57%	1.26%	17.19%	79.82%

8.4.2.1.1 Computing Subassembly Wind Losses at the Specific Occupancy Level

Developing subassembly losses at the specific occupancy (SOCC) level is very similar to the SBT level, except that SBT subassembly loss tables are used as inputs instead of the weak, medium, and strong subassembly loss tables.

Since there are differences between the SOCC subassembly values from the original wind model development effort and those provided in Table 8-63 for Pre-FIRM and Table 8-64 for Post-FIRM construction, an additional step was needed. The subassembly losses were multiplied by the subassembly ratios provided in Table 8-63 and Table 8-64 (building component as a percentage of total replacement cost) and again to those developed through aggregation at the SOCC level from the original subassembly values. The resulting subassembly losses were then forced and adjusted using Equation 8-22 in a similar fashion to SBT subassembly values.

However, unlike the SBT subassembly losses, it is possible to have foundation subassembly losses prior to 90% overall loss. This is a result of a wide variety of building strengths contributing to a SOC. For example, Table 8-66 shows sub-assembly losses for specific occupancy COM1 with pre-FIRM sub-assembly values. COM1 is composed of several SBTs, one of which is SPMBs (Steel, Pre-Engineer Metal Building, Small). According to Table 8-66, at an overall loss of 40%, the foundation subassembly starts to accumulate losses, which are due to the contribution of SPMBs. Specifically, the wind speed that induces a 40% loss in COM1 is 151 mph. At this wind speed, the loss induced in SPMBs turns out to be

95%. When applying Equation 8-9, and examining the foundation subassembly losses for this SBT (Table 8-67), it is apparent that a non-zero foundation sub-assembly loss value will result when interpolating between 90% and 100% (highlighted in Table 8-67). Closer examination of Table 8-67 shows that all of the subassembly losses other than the foundation and below first floor have reached their limits at the 90% overall wind loss level. Foundation loss is not totally unexpected, given that a large portion of the building value for this SBT is in the foundation.

Table 8-66 Sample Subassembly Losses Relative to Building Value for COM1

Overall Loss	Foundation	Structure Below First Floor	Structure Frame	Roof Cover	Roof Frame	Exterior Wall	Interior
10%	0.0%	0.0%	0.0%	2.2%	0.2%	0.8%	6.8%
20%	0.0%	0.0%	0.0%	3.6%	0.8%	1.6%	14.0%
30%	0.0%	0.0%	0.2%	4.6%	1.3%	2.5%	21.4%
40%	0.1%	0.0%	0.4%	5.2%	1.8%	3.2%	29.3%
50%	0.2%	0.0%	0.5%	5.4%	2.0%	4.0%	38.0%
60%	0.3%	0.0%	0.7%	5.6%	2.2%	4.6%	46.6%
70%	0.3%	0.0%	0.9%	5.8%	2.5%	5.5%	55.1%
80%	0.3%	0.0%	1.1%	6.0%	2.8%	7.0%	62.8%
90%	0.3%	0.0%	3.2%	6.0%	4.2%	7.9%	68.4%
100%	0.3%	0.0%	3.6%	6.3%	4.7%	8.8%	76.4%
Cap	7.5%	1.3%	12.5%	6.3%	6.3%	12.5%	78.8%

Table 8-67 Subassembly Losses Relative to Building Value for SBT SPMBs

Overall Loss	Foundation	Structure Below First Floor	Structure Frame	Roof Cover	Roof Frame	Exterior Wall	Interior
10%	0.0%	0.0%	0.0%	0.1%	0.1%	4.3%	5.5%
20%	0.0%	0.0%	0.0%	0.2%	0.1%	4.5%	15.2%
30%	0.0%	0.0%	0.0%	0.6%	0.3%	4.8%	24.3%
40%	0.0%	0.0%	0.0%	1.1%	0.4%	5.7%	32.7%
50%	0.0%	0.0%	0.0%	1.6%	2.3%	6.5%	39.6%
60%	0.0%	0.0%	0.0%	2.9%	5.7%	9.7%	41.8%
70%	0.0%	0.0%	0.5%	4.0%	8.5%	11.5%	45.4%
80%	0.0%	0.0%	1.3%	5.1%	10.8%	14.7%	48.1%
90%	0.0%	0.0%	3.3%	6.6%	14.0%	17.1%	49.0%
100%	5.9%	0.0%	4.8%	7.2%	15.3%	17.9%	49.0%
Cap	30.9%	0.0%	4.8%	7.2%	15.3%	17.9%	49.0%

Note: Highlighted rows with italics represent zero foundation subassembly loss values result from interpolating between 90% and 100%

8.4.2.1.2 Computing Subassembly losses at GBT Level

The development of the subassembly losses at the general building type level is very similar to the SOCC level, except that SOCC subassembly loss tables are used as inputs rather than SBT subassembly loss tables, and ratios of SOCC exposure to the total exposure were used.

The resulting table is similar to Table 8-66, except that it describes subassembly losses at the GBT level. These values were then forced and adjusted in a similar fashion to the way SBT and SOC subassembly values were forced to be monotonic and adjusted to match the overall building loss.

8.4.2.1.3 Final Wind Subassembly Loss Tables

An example of the final wind subassembly loss tables is provided in Table 8-68. The values represent the subassembly losses as a percentage of the subassembly replacement cost.

Table 8-68 Sample Final Wind Subassembly Loss Relative to Subassembly Replacement Cost for RES1 (%) , Pre-FIRM Construction

Occupancy	Building Loss	Foundation	Below First Floor	Structure Frame	Roof Cover	Roof Framing	Exterior Wall	Interiors
RES1	10%	0.0%	0.0%	0.0%	42.1%	0.3%	2.4%	11.0%
RES1	20%	0.0%	0.0%	0.0%	66.9%	0.5%	4.5%	23.9%
RES1	30%	0.0%	0.0%	0.1%	70.9%	1.1%	5.9%	39.2%
RES1	40%	0.0%	0.0%	0.3%	75.2%	1.8%	7.8%	54.2%
RES1	50%	0.0%	0.0%	0.6%	77.8%	3.0%	11.1%	68.7%

Occupancy	Building Loss	Foundation	Below First Floor	Structure Frame	Roof Cover	Roof Framing	Exterior Wall	Interiors
RES1	60%	0.0%	0.0%	1.3%	89.0%	8.2%	17.0%	80.8%
RES1	70%	0.0%	0.0%	7.0%	96.6%	16.6%	28.9%	89.1%
RES1	80%	0.0%	0.0%	15.3%	100.0%	26.2%	40.4%	97.2%
RES1	90%	0.0%	0.0%	24.7%	100.0%	50.2%	61.4%	100.0%
RES1	100%	0.0%	0.0%	44.3%	100.0%	100.0%	76.2%	100.0%

For more information on the final subassembly loss tables for wind loss by SOCC and GBT for Pre-FIRM and Post-FIRM construction, please contact the Hazus Help Desk for the *Hazus Hurricane Model Technical Manual Appendices* (FEMA, 2021).

8.4.2.2 Development of Subassembly Loss Tables for Flood Losses

Because flood losses by building component or building subassembly are only available for a handful of building types and occupancies from the GEC (2006) study, an entire set of flood subassembly loss tables were developed for Hazus based on engineering analysis. The guidelines given in Table 8-69 were used to facilitate the process and achieve consistency across specific occupancies and general building types.

Table 8-69 Guidelines for Development of Flood Subassembly Loss Tables

Subassembly	Pre-Firm Foundation Zone A Conditions	Pre-FIRM Foundation Zone CA/ V Conditions	Post-FIRM Foundation Zone A Conditions	Post-FIRM Zone CA / V Conditions
Foundation	Start damaging foundation at 80% (first non-zero value is 90%) damage and max damage at 50% Pre-FIRM value (e.g., 3% if foundation represents 6% of structure value).	Start damaging foundation at 50% first non-zero value is 60%) damage and max damage at 80% Pre-FIRM value (e.g., 5% if foundation represents 6% of structure value).	Start damaging foundation at 80% (first non-zero value is 90%) damage and max damage at 50% Pre-FIRM value (e.g., 3% if foundation represents 6% of structure value).	Start damaging foundation at 80% (first non-zero value is 90%) damage and max damage at 50% Pre-FIRM value (e.g., 3% if foundation represents 6% of structure value).
Below First Floor	Start damaging below first floor at 0% damage (first non-zero value is 10%) and achieve 100% Pre-FIRM value by 40% building damage.	Start damaging below first floor at 0% damage (first non-zero value is 10%) and achieve 100% Pre-FIRM value at 20% building damage.	Start damaging below first floor at 0% damage (first non-zero value is 10%) and achieve 100% Pre-FIRM value by 40% building damage.	Start damaging below first floor at 0% damage (first non-zero value is 10%) and achieve 100% Pre-FIRM value at 20% building damage

Subassembly	Pre-Firm Foundation Zone A Conditions	Pre-FIRM Foundation Zone CA/ V Conditions	Post-FIRM Foundation Zone A Conditions	Post-FIRM Zone CA / V Conditions
Structure Frame	Start damaging structure frame at 70% damage (first non-zero value is 80%) and achieve 100% Pre-FIRM value at 100% building damage.	Start damaging structure frame at 10% damage (first non-zero value is 20%) and achieve 100% Pre-FIRM value at 90% building damage.	Start damaging structure frame at 70% damage (first non-zero value is 80%) and achieve 100% Pre-FIRM value at 100% building damage.	Start damaging structure frame at 10% damage (first non-zero value is 20%) and achieve 100% Pre-FIRM value at 90% building damage
Roof Cover	Same as Structure	Same as Structure	Same as Structure	Same as Structure
Roof Frame	Same as Structure	Same as Structure	Same as Structure	Same as Structure
Exterior Walls	Start damaging exterior walls at 0% damage (first non-zero value at 10%) and reach maximum Pre-FIRM value (100%) at 100% building damage.	Start damaging exterior walls at 10% damage (first non-zero value at 10%) and reach maximum Pre-FIRM value (100%) at 90% building damage.	Start damaging exterior walls at 0% damage (first non-zero value at 10%) and reach maximum Pre-FIRM value (100%) at 100% building damage.	Start damaging exterior walls at 10% damage (first non-zero value at 10%) and reach maximum Pre-FIRM value (100%) at 90% building damage.
Interiors	Start damaging interior at 0% damage (first non-zero value at 10%) and reach maximum Pre-FIRM value (100%) at 80% building damage.	Start damaging interior at 0% (first non-zero value at 10%) and reach maximum Pre-FIRM value (100%) at 80% building damage.	Start damaging interior at 0% damage (first non-zero value at 10%) and reach maximum Pre-FIRM value (100%) at 80% building damage.	Start damaging interior at 0% (first non-zero value at 10%) and reach maximum Pre-FIRM value (100%) at 80% building damage.

As indicated in Table 8-69, separate subassembly loss tables were developed for Pre- and Post-FIRM construction subjected to either Zone A conditions (i.e., controlling wave heights less than 1.5 feet) or Zone CA/V conditions (i.e., controlling wave heights greater than or equal to 1.5 feet). This results in twice as many subassembly flood loss tables as subassembly wind loss tables since the wind loss tables are independent of wave conditions.

Figure 8-26 illustrates the sub-assembly losses for single-family occupancies. Separate plots are shown for each combination of construction type (Pre- or Post-FIRM) and wave conditions (Zone A or CA/V). In each plot, the horizontal axis is the overall building loss as a percentage of building replacement cost and the vertical axis is the subassembly loss as a percentage of its own replacement cost. Note that losses to the interior’s subassembly play a relatively larger role under Zone A wave conditions, whereas losses to the below first floor and foundation subassemblies play larger roles under Zone CA or V wave conditions. The differences between Pre-FIRM and Post-FIRM subassembly loss contributions are generally less pronounced for this occupancy class than the differences between Zone A and Zone CA/V.

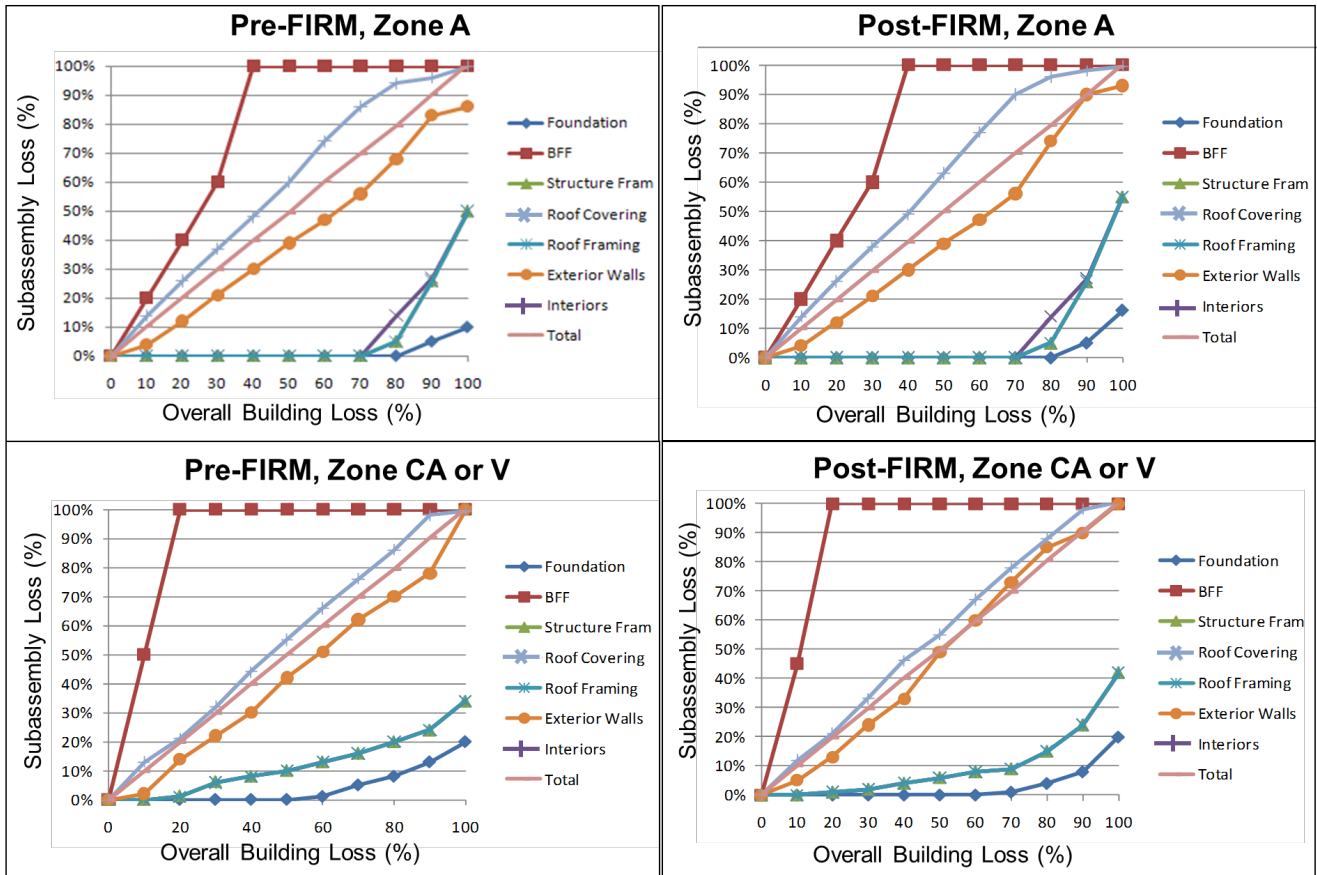


Figure 8-26 RES1 (Single-Family) Subassembly Losses for Flood as a Percentage of Subassembly Replacement Cost

An example of the final flood subassembly loss tables is provided in Table 8-70. The values represent the subassembly losses as a percentage of the subassembly replacement cost.

Table 8-70 Sample Final Flood Subassembly Loss Relative to Subassembly Replacement Cost for RES1, Pre-FIRM, Zone A Construction

Occupancy	Building Loss	Foundation	Below First Floor	Structure Frame	Roof Cover	Roof Framing	Exterior Wall	Interiors
RES1	10%	0.0%	20.0%	0.0%	0.0%	0.0%	4.0%	14.0%
RES1	20%	0.0%	40.0%	0.0%	0.0%	0.0%	12.0%	26.0%
RES1	30%	0.0%	60.0%	0.0%	0.0%	0.0%	21.0%	37.0%
RES1	40%	0.0%	100.0%	0.0%	0.0%	0.0%	30.0%	48.0%
RES1	50%	0.0%	100.0%	0.0%	0.0%	0.0%	39.0%	60.0%
RES1	60%	0.0%	100.0%	0.0%	0.0%	0.0%	47.0%	74.0%
RES1	70%	0.0%	100.0%	0.0%	0.0%	0.0%	56.0%	86.0%
RES1	80%	0.0%	100.0%	5.0%	14.0%	5.0%	68.0%	94.0%
RES1	90%	5.0%	100.0%	26.0%	27.0%	26.0%	83.0%	96.0%
RES1	100%	10.0%	100.0%	50.0%	50.0%	50.0%	86.0%	100.0%

For more information on the final subassembly loss tables for flood loss by SOCC and GBT for Pre-FIRM and Post-FIRM construction and Zone A and Zone CA / V conditions, please contact the Hazus Help Desk (see Section 1.5) for the *Hazus Hurricane Model Technical Manual Appendices* (FEMA, 2021).

8.4.3 Combined Building Contents and Inventory Approach

To determine the combined losses to the building contents and inventory, Equation 8-20 and Equation 8-21 are used with the GBS content and inventory loss results at the Census block level. The amount of loss for each specific occupancy and pre- or post-FIRM construction in each Census block is calculated for wind and flood and these values are used with Equation 8-21 to determine the combined loss by occupancy and pre-/post-FIRM categories. Then Equation 8-20 is used to ensure that the minimum and maximum limits are not exceeded.

Section 9. References

- AFPA/AWC (1996). Wood Frame Construction Manual for One- and Two-Family Dwellings, 1995 SBC High Wind Edition, *American Forest and Paper Association/American Wood Council*, p. 71.
- AFPA/AWC (1997). National Design Specification for Wood Construction, *American Forest and Paper Association/American Wood Council*, August 7.
- AISC (1995). Load Resistance Factor Design, Manual of Steel Construction 2nd Edition, *American Institute of Steel Construction*, Chicago, IL, Volumes I and II, pp. 6-73 – 6-79 and pp. 8-98 – 8-130.
- AISI (1996) Specification for the Design of Cold-Formed Steel Structural Members, *American Iron and Steel Institute* Washington, DC.
- Alliss, R. (1992). The Utilization of SSM/I Data in Analysis of Tropical and Extra-Tropical Cyclones, M.S. Thesis, *Department of Marine, Earth, Atmospheric Sciences, North Carolina State University*, Raleigh, NC.
- Alliss, R., G.D. Sandlin, S.W. Chang, and S. Raman (1993). Applications of SSM/I Data in the Analysis of Hurricane Florence, *Journal of Applied Meteorology*, Volume 32, pp. 1581-1591
- Alliss, R.J., S. Raman, and S.W. Chang (1992). Special Sensor Microwave/Imager (SSM/I) Observations of Hurricane Hugo (1989), *Monthly Weather Review*, Volume 120, pp. 2723-2737.
- Amiro, B.D. (1990a). Comparison of Turbulence Statistics Within Three Boreal Forest Canopies, *Boundary-Layer Meteorology*, Volume 51, pp. 99-121.
- Amiro, B.D. (1990b). Drag Coefficients and Turbulence Spectra Within Three Boreal Forest Canopies, *Boundary-Layer Meteorology*, Volume 52, pp. 227-246.
- Amiro, B.D., and P.A. Davis (1988). Statistics of Atmospheric Turbulence Within a Natural Black Spruce Forest Canopy, *Boundary-Layer Meteorology*, Volume 44, pp. 267-283.
- Anderson, J.R., E.E. Hardy, J.T. Roach, and R.E. Witmer, (1976). A land use and land cover classification system for use with remote sensor data, Geological Survey Professional Paper 964, U.S. *Dept. of the Interior*.
- Applied Research Associates, Inc. (2001). Hazard Mitigation Study for the Hawaii Hurricane Relief Fund.
- Arya, S.P.S. (1988). Introduction to Micrometeorology, *Academic Press*.
- ASCE (1990). Minimum Design Loads for Buildings and Other Structures ASCE 7-88, *American Society of Civil Engineers*, New York, NY.
- ASCE (1999). Minimum Design Loads for Buildings and Other Structures ASCE 7-98, *American Society of Civil Engineers*, New York, NY.

- Baik, Jong-Jin (1989). Tropical Cyclone Simulations with the Betts Convective Adjustment Scheme, Ph. D. Thesis, *Department of Marine, Earth, Atmospheric Sciences, North Carolina State University*, Raleigh, NC, pp.159.
- Baker, C.J., and H.J. Bell (1991). The Aerodynamics of Urban Trees, Preprints, *6th International Conference on Wind Engineering*, London, Ontario, Canada, July.
- Baldocchi, D.D., and T.P. Meyers (1988). A Spectral and Lag-Correlation Analysis of Turbulence in a Deciduous Forest Canopy, *Boundary-Layer Meteorology*, Volume 45, pp. 31-38.
- Baskaran, B.A., and O. M. Dutt (1995). Evaluation of Roof Fasteners under Dynamics Wind Loading, *Proceedings: 9th International Conference on Wind Engineering*, New Delhi, India, pp. 1207-1218.
- Batts, M.E., M.R. Cordes, C.R. Russell, J.R. Shaver, and E. Simiu (1980). Hurricane Windspeeds in The United States, National Bureau of Standards Report Number BSS-124, U.S. *Dept. of Commerce*, Washington, DC.
- Beason, W.L., G.E. Meyers, and R.W. James (1984).Hurricane Related Window Glass Damage in Houston, *ASCE Journal of the Structural Division*, Volume 110, Number 12, pp. 2843-2857, December.
- Behr, R.A., and J.E. Minor (1994). A Survey of Glazing System Behavior in Multi-Story Buildings During Hurricane Andrew, *The Structural Design of Tall Buildings*, Volume 3, pp.143-161.
- Behr, R.A., J.E. Minor, and H.S. Norville (1993). Structural Behavior of Architectural Laminated Glass, *Journal of Structural Engineering*, Volume 119, Number 1.
- Behre, C.E. (1927). Form-Class Taper Curves and Vol. Tables and Their Application, *Journal of Agricultural Research*, Volume 35, Number 8, Washington, DC., October.
- Bergstrom, H., and U. Hogstrom, (1989). Turbulent Exchange Above a Pine Forest, II. Organized Structures, *Boundary-Layer Meteorology*, Volume 49, pp. 231-263.
- Bhinderwala, S. (1995). Insurance Loss Analysis of Single Family Dwellings Damaged in Hurricane Andrew, M.S. Thesis, Clemson University, Clemson, SC.
- Blackburn, P., and J.A. Petty (1988). Theoretical Calculations of the Influence of Spacing on Stand Stability, *Forestry*, Volume 61, p. 3.
- Boissonnade, A., and W-M. Dong (1993). Hurricane Loss Estimation and Forecasting: Applications to Risk Management, *Proceedings 7th US National Conference on Wind Engineering*, Los Angeles, CA, pp. 115-124.
- Bowen, A.J., R.G.J. Flay, and H.A. Panofsky (1983). Vertical Coherence and Phase Delay Between Wind Components in Strong Winds Below 20 m, *Boundary Layer Meteorology*, Volume 26, pp. 313-324.

- Brook, R.R. (1972). Measurements of Turbulence in a City Environment, *Journal of Applied Meteorology*, Volume 11, pp. 443-450.
- Canfield, L.R., S.H. Niu, and H. Liu (1991). Uplift Resistance of Various Rafter-Wall Connections, *Forest Products Journal*, Volume 41, Number 7/8, July/August.
- Case, P.C. (1996). Wind Loads on Low Buildings with 4:12 Gable Roofs, M.S. Thesis, University of Western Ontario, London, Ontario, Canada, May.
- Chen, S.S., J.A. Knaff, and F.D. Marks Jr., 2006: Effects of vertical wind shear and storm motion on 692 tropical cyclone rainfall asymmetries. *Mon. Wea. Rev.*, 134, 3190– 693 3208, <https://doi.org/10.1175/MWR3245.1>.
- Cherry, N.J. (1991). Fixing Studies for MRTI Normal Weight Tiles SBCCI Submission, Redland Technology Limited, New Technology & Product Development Centre, Horsham, West Sussex, England, December.
- Cionco, R.M. (1965). A Mathematical Model for Airflow in a Vegetative Canopy, *Journal of Applied Meteorology*, Volume 4, pp. 517-522.
- Cionco, R.M. (1972). A Wind-Profile Index for Canopy Flow. *Boundary-Layer Meteorology*, Volume 3, pp. 255-263.
- Clark, K.M. (1987). A Formal Approach to Catastrophe Risk Assessment and Management, *Proceedings November 9-11, 1986*, Volume LXXIII, Number 140, pp. 69-91.
- CMHC (1989). Canadian Wood-Frame House Construction, Canada Mortgage and Housing Corporation, p. 48.
- Conner, H.W., D.S. Gromala, and D.W. Burgess (1997). "Roof Connections in Houses: Key to Wind Resistance," *Journal of Structural Engineering*, Volume 113, Number 12, pp. 2459-2474, December.
- Cook, R.A. (1990). Hurricane Hugo vs. Critical Lifelines – Lessons Learned and Implications for the Future," *Proceedings of Hurricane Hugo One Year Later*, 13-15 September.
- Cooper (1988). Chapter 2, pg. 48
- Crandell, J.H., M. Nowak, E.M. Laatsch, A. van Overeem, C.E. Barbour, R. Dewey, H. Reigel, and H. Angleton (1993). Assessment of Damage to Single-Family Homes Caused by Hurricanes Andrew and Iniki, Contract HC-5911, NAHB Research Center, Upper Marlboro, MD, for U.S. Department of Housing and Urban Development Office of Policy Development and Research, September.
- Cunningham, T.P. (1993). Roof Sheathing Fastening Schedules for Wind Uplift, APA Report T92-28, American Plywood Association, Tacoma, WA, March.

Daneshvaran, S., and R.E. Morden (1998). Fast Hurricane Wind Analysis Using the Orthogonal Decomposition Method, *Journal of Wind Engineering and Industrial Aerodynamics*, Volumes 77/78 Complete, pp. 703-714.

Darling, R.W.R. (1991). Estimating Probabilities of Hurricane Wind Speeds Using a Large-Scale Empirical Model, *Journal of Climate*, Volume 4, Number 10, pp. 1035-1046.

Davenport, A.G. (1961). The Application of Statistical Concepts to the Wind Loading of Structures, *Proceedings Institute of Civil Engineers*, Volume 19, pp. 449-472.

Dawe, J.L., and G.G. Aridru (1993). Prestressed Concrete Masonry Walls Subjected to Uniform Out-of-Plane Loading, *Canadian Journal of Civil Engineering*, Volume 20, pp. 969-979.

Deaves, D. M. (1981). Terrain-dependence of longitudinal R.M.S. velocities in the neutral atmosphere. *J. Wind Engrg. and Industrial Aerodynamics*, Amsterdam, The Netherlands, 8, 259–274.

Delft University of Technology. (2020). USER MANUAL SWAN Cycle III version 41.31A. *Delft University of Technology*. Faculty of Civil Engineering and Geosciences. Environmental Fluid Mechanics Section. http://swanmodel.sourceforge.net/online_doc/swanuse/swanuse.html

Dewberry and Davis (1993) – Chapter 10, pg. 551

Djakovich (1985) – chapter 4, pg. 170

Dowd (1990) – Chapter 10, pg. 551

Drury, S., and Evans, J. (1998) Modeling of tropical cyclone intensification as a result of interaction with mid-latitude troughs. Preprints, Symp. on Tropical Cyclone Intensity Change, Phoenix, AZ, *Amer. Meteor. Soc.*, 65–72. Drysdale, R.G., and A.S. Essawy (1988). Out-of Plane Bending of Concrete Block Walls, *ASCE Journal of Structural Engineering*, Volume 114, Number 1, pp. 121-133, January.

Duchêne-Marullaz, P. (1979). Effect of High Roughness on the Characteristics of Turbulence in Cases of Strong Winds, *Proceedings 5th International Conference on Wind Engineering*, Fort Collins, CO, p. 15.

East, J.W., Turco, M.J., and Mason, R.R., Jr. (2008). Monitoring inland storm surge and flooding from Hurricane Ike in Texas and Louisiana, September 2008: *U.S. Geological Survey Open-File Report 2008–1365* [<http://pubs.usgs.gov/of/2008/1365/>].

Ellifritt, D.S., and R. Burnette (1990). Pull-Over Strength of Screws in Simulated Building Tests, *Proceedings: 10th International Specialty Conference on Cold-Formed Steel Structures*, University of Missouri-Rolla, MO, pp. 589-603.

Elsberry, R.L, L.E Carr III, and M.A. Boothe (1998). Progress Toward a Generalized Description of the Environment Structure Contribution to Tropical Cyclone Track Types, *Meteorological Atmospheric Physics*, Volume 67, pp. 93-115.

- ESDU (1975). Characteristics of Atmospheric Turbulence Near the Ground, Part II: Single Point Data for Strong Winds (Neutral Atmosphere), *Engineering Science Data Unit*, Data Item # 86010, London, England.
- ESDU (1982). Strong Winds in the Atmospheric Boundary Layer, Part 1: Mean Hourly Wind Speed, *Engineering Science Data Unit*, Data Item Number 82026, London, England.
- ESDU (1983). Strong Winds in the Atmospheric Boundary Layer, Part 2: Discrete Gust Speeds, *Engineering Science Data Unit*, Data Item Number 83045, London, England.
- Fattal, S.G., and L.E. Cattaneo (1977). Evaluation of Structural Properties of Masonry in Existing Buildings, *U.S. Department of Commerce, National Bureau of Standards*, p.13.
- FEMA (1992). Building Performance: Hurricane Andrew in Florida, *Federal Emergency Management Agency, Federal Insurance Administration, FIA-22 (2/93)*. December 21.
- FEMA (2001). HAZUS® 99 Estimated Annualized Earthquake Losses for the United States, *Federal Emergency Management Agency, Mitigation Directorate, FEMA 366*, February.
- FEMA (2009a). HAZUS-MH MR4 Hurricane Model Technical Manual, *Federal Emergency Management Agency, Mitigation Division*, Washington, D.C., 2009.
- FEMA (2009b). HAZUS-MH MR4 Flood Model Technical Manual, *Federal Emergency Management Agency, Mitigation Division*, Washington, D.C., 2009.
- FEMA (2015). Guidance for Flood Risk Analysis and Mapping: Overland Wave Propagation. *Federal Emergency Management Agency, Mitigation Division*, Washington, D.C., November 2015
- FEMA (2020a). Hazus Hurricane Model Technical Manual, *Federal Emergency Management Agency, Mitigation Division*, Washington, D.C., 2020.
- FEMA (2022). Hazus Flood Model Technical Manual, *Federal Emergency Management Agency, Mitigation Division*, Washington, D.C., 2022.
- FEMA (2021). Hazus Hurricane Wind for Puerto Rico and the U.S. Virgin Islands, *Federal Emergency Management Agency, Mitigation Division*, Washington, D.C., 2021.
- Ferguson and Cardwell (1992). Hurricane Andrew , Monday, August 24, 1992, South Florida – Dade County. Report Prepared for Manufactured Housing Institute, Compliance Systems Publications, Inc. Atlanta, GA. October 24.
- Ferraro, R. (1996). An Eight-Year (1987-1994) Time Series of Rainfall, Clouds, Water Vapor, Snow Cover, and Sea Ice Derived from SSM/I Measurements, *Bulletin of the American Meteorological Society*, Volume 77, pp. 891- 906.
- Forest Products Laboratory (1987). Wood Handbook: Wood as an Engineering Material, *U.S. Department of Agriculture*, Washington, DC.

Frank, R.A., C.E. Murphy, L.A. Twisdale, and T.A. Reinhold (1987). Data Collection and Analysis for Full-Scale Drag Tests: MISTY PINE Experiment, DAAL03-86-D-0001, *Ballistic Research Laboratory*, Aberdeen Proving Ground, MD, January.

Frank, R.A., M.D. Smith, L.A. Twisdale, and R.G. Pearson (1989). Mechanical Property Tests on Selected Trees from MISTY PICTURE, DAAA15-87-D-0008, Tasks 4 and 6, *Ballistic Research Laboratory*, Aberdeen Proving Ground, MD, 30 December.

Frank, R.A., M.D. Smith, P.J. Vickery, L.A. Twisdale, and M.B. Hardy (1991). Blast Effects on Forests: MISERS GOLD Data Report (Exp. 1200), DAAA15-89-D-0008, Task 2, *US Army Armament Research and Development Command*, Ballistic Research Laboratory, Aberdeen Proving Ground, MD, 7 June.

Franklin, J.L., M.L. Black, and K. Valde, (2003). GPS dropwindsonde wind profiles in hurricanes and their operational implications. *Wea. Forecasting*, 18, 32–44.

Friedman, D.G. (1987). US Hurricanes & Windstorms, *DYP Insurance & Reinsurance Group Ltd*.

Galinski, W. (1989). A Windthrow Risk Estimation for Coniferous Trees, *Forestry*, Volume 62, Number 2.

Gardiner, B.A. (1994). Wind and Wind Forces in a Plantation Spruce Forest, *Boundary-Layer Meteorology*, Volume 67, pp. 161-186.

García, J.M. (1994). The Wind Loading of Fasteners, Corrugated Materials and Roofing of Low-Rise Buildings, *MS Thesis, Department of Civil Engineering*, The University of Western Ontario, London, Ontario, Canada.

GEC (2006). Depth-Damage Relationships for Structures, Contents, and Vehicles and Content-to-Structure Value Ratios (CSVR) in Support of the Donaldsonville to the Gulf, Louisiana, *Feasibility Study, Gulf Engineers & Consultants, Contract No. DACW29-00-D-0001, Delivery Order No. 0038, G.E.C. Project No. 22316638, prepared for U.S. Army Corps of Engineers New Orleans District, New Orleans, Louisiana, March 2006*

Georgiou, P.N. (1985). Design Windspeeds in Tropical Cyclone-Prone Regions, Ph.D. Thesis, *Faculty of Engineering Science, University of Western Ontario*, London, Ontario, Canada.

Georgiou, P.N., A.G. Davenport, and B.J. Vickery (1983). Design Wind Speeds in Regions Dominated by Tropical Cyclones, *Journal of Wind Engineering and Industrial Aerodynamics*, Volume 13, Numbers 1-3, pp. 139-152.

Ghali, A., and A.M. Neville (Eds.) (1989). *Structural Analysis – A Unified Classical and Matrix Approach*, 3rd Edition, Chapman and Hall.

Gilhousen, D.B. (2006). A complete explanation of why moored buoy winds are less than ship winds, *Mariners Weather Log*, Vol. 50, No. 1, National Weather Service, 4–7.

Grimm, C.T. (1999). Walls May Be Half as Strong as They Say!, *Southern Building*, p. 19, January/February.

Gross, J.G., R.D. Dijkers, and J.C. Grogan (1969). Recommended Practice for Engineered Brick Masonry, *Brick Industry Association*, Reston, VA.

Haseltine, 1975 – chapter 6, pg. 225

Hebert, P.J., J.D. Jarrell, and B.M. Mayfield (1996). The Deadliest, Costliest, and Most Intense United States Hurricanes of This Century (and Other Frequently Requested Hurricane Facts), NOAA Technical Memorandum NWS-NHC-31, p. 41.

Hendry and Kheir (1976) - chapter 6, pg. 225

Ho, F.P., et al. (1987). Hurricane Climatology for the Atlantic and Gulf Coasts of the United States, NOAA Technical Report NWS38, *Federal Emergency Management Agency*.

Ho, T.C.E. (1992). Variability of Low Building Wind Loads, Ph.D. Thesis, *Faculty of Engineering Science*, University of Western Ontario, London, Ontario, Canada.

Hock and Franklin (1999) – chapter 2 pg. Hogan, M., and K. Karwoski (1990). Masonry Performance in the Coastal Zone, in Proceedings Hurricane Hugo One Year Later, B. L. Sill and P. R. Sparks (Eds.), Charleston, SC, September.

Holland, G.J. (1980). An Analytic Model of the Wind and Pressure Profiles in Hurricanes, *Monthly Weather Review*, Volume 108, Number 8, pp. 1212-1218.

Holmes (1994) – Chapter 4, pg. 157

Holmlin (1993) – Chapter 10, pg. 539

Hong, X., S.W. Chang, S. Raman, L.K. Shay, and R. Hodur (1998). The Interaction Between Hurricane Opal (1995) and a Warm Core Eddy in the Gulf of Mexico, Submitted to *Monthly Weather Review*.

Houston, S.H., and M.D. Powell (1993). Surface Wind Fields During Hurricane Bob's (1991) Landfall in New England, *Proceedings 20th Conference on Hurricanes and Tropical Meteorology*, American Meteorological Society, San Antonio, TX, May 10-14.

Houston, S.H., M.D. Powell, and P.P. Dodge (1997). Surface Wind Fields in 1996 Hurricanes Bertha and Fran at Landfall, *Proceedings 22nd Conference on Hurricanes and Tropical Meteorology*, American Meteorological Society, Fort Collins, CO, May 19-23.

HUD (1980). Economic Benefit-Cost and Risk Analysis of Mobile Home Safety Research: Wind Safety Analysis, *Office of Policy Development and Research, Department of Housing and Urban Development*.

HUD (1993). Assessment of Damage to Single-Family Homes Caused by Hurricanes Andrew and Iniki, *U.S. Department of Housing and Urban Development, Office of Policy Development and Research*, March.

HUD (1994). Final Rule – Manufactured Home Construction and Safety Standards on Wind Standards, Office of the Assistant Secretary for Housing, Department of Housing and Urban Development, *Federal Register*, Volume 59, Number 10, pp. 2456-2475.

Jelesnianski, C.P., Chen, J., and Shaffer, W.A. (1992). *SLOSH: Sea, Lake, and Overland Surges from Hurricanes*, NOAA Technical Report NWS 48, National Weather Service, Silver Spring, MD.

Jensen, M. (1958). The Model-Law for Phenomena in Natural Wind, *Ingeniøren*, Volume 2, pp. 121-128.

Johnson, R.C., Jr., G.D. Ramey, and D.S. O'Hagan (1982). Wind-Induced Forces on Trees, *Journal of Fluids Engineering*, Volume 104, March.

Jones, R. (1987). A Simulation of Hurricane Land Fall with a Numerical Model Featuring Latent Heating by the Resolvable Scales, *Monthly Weather Review*, Volume 115, pp. 2279-2297.

Kareem, A., and J.G. Stevens (1985). Window Glass Performance and Analysis in Hurricane Alicia, *ASCE Proceedings Specialty Conference: "Hurricane Alicia: One Year Later, Galveston, TX (August 1984)*, A. Kareem (Ed.), pp.178-186.

Karlsson, S. (1986). The Applicability of Wind Profile Formulas to an Urban-Rural Interface Site, *Boundary Layer Meteorology*, Volume 34, pp. 333-355.

Kepert, J. D. (2001). The dynamics of boundary layer jets within the tropical cyclone core. Part I: Linear theory. *J. Atmos. Sci.*, 58, 2469–2484.

Kepert, J. D. and Y. Wang (2001). The dynamics of boundary layer jets within the tropical cyclone core. Part II: Non-linear enhancements. *J. Atmos. Sci.*, 58, 2485–2501.

Kind, R.J., and R.L. Wardlaw (1984). Behavior in Wind of Loose-Laid Roof Insulation Systems, Part I: Stone Scour and Blow-Off, *Proceedings 4th Canadian Workshop on Wind Engineering*, Toronto, Canada, pp. 141-149.

Kovacs, W.W., and F.Y. Yokel (1979), Soil and Rock Anchors for Mobile Homes – A State of the Art Report, U.S. Department of Commerce, NBS Building Sciences Series 107, National Bureau of Standards, Washington, DC.

LaBoube, R.A. and W.W. Yu (1993). Behavior of Arc Spot Weld Connections in Tension," *ASCE Journal of Structural Engineering*, Volume 119, Number 7, pp. 2187-2198.

Lai, W. (1955). Aerodynamic Crown Drag of Several Broadleaf Tree Species, AFSWP-863, *US Forest Service*, Division of Fire Research, Washington, DC.

Leland, K.B. (1988). The Strength of Roof Anchorage in Unreinforced Concrete Masonry, Masters Thesis, *Clemson University*, Clemson, SC, August.

- Lettau, H.H. (1969). Note on Aerodynamic Roughness-Parameter Estimation on the Basis of Roughness-Element Description, *Journal of Applied Meteorology*, Volume 8, pp. 828-832.
- Li, Z.J., D.R. Miller, and J.D. Lin (1985). A First-Order Closure Scheme to Describe Counter-Gradient Momentum Transport in Plant Canopies, *Boundary-Layer Meteorology*, Volume 33, pp. 77-83.
- Li, Z.J., J.D. Lin, and D.R. Miller (1990). Air Flow Over and Through a Forest Edge: A Steady-State Numerical Simulation, *Boundary-Layer Meteorology*, Volume 51, pp. 179-197.
- Lin, J.X., and D. Surry (1997). Simultaneous Time Series of Pressures on the Envelope of Two Large Low-Rise Buildings, Boundary Layer Wind Tunnel Laboratory Report, BLWTL-SS7-1997, *University of Western Ontario, London, Ontario, Canada*, for Dr. E. Simiu, National Institute of Standards and Technology, March.
- Lohmander, P., and F. Helles (1987). Windthrow Probability as a Function of Stand Characteristics and Shelter, *Scan. Journal of Forest Research*, Volume 2, pp. 227-238.
- Macha, J., J. Sevier, and J. Bertin (1983). Comparison of Wind Pressures on a Mobile Home in Model and Full Scale, *Journal of Wind Engineering and Industrial Aerodynamics*, Volume 12, pp. 109-124.
- Mahendran, M. (1994). "Behaviour and Design of Crest-Fixed Profiled Steel Roof Claddings under Wind Uplift, *Engineering Structures*, Volume 16, Number 5, pp. 368-376.
- Mahendran, M. (1997). Review of Current Test Methods for Screwed Connections, *ASCE Journal of Structural Engineering*, Volume 123, Number 3, pp. 321-325.
- Mahendran, M., and R. B. Tang (1998). Pull-Out Strength of Steel Roof and Wall Cladding Systems, *ASCE Journal of Structural Engineering*, Volume 124, Number 10, pp. 1192-1201.
- Mark, F. (1985). Evolution and Structure of Precipitation in Hurricane Allen (1980), *Monthly Weather Review*, Volume 113, pp. 909-930.
- Marshall, R. (1977). The Measurement of Wind Loads on a Full Scale Mobile Home, NBSIR 77-1289, National Bureau of Standards, Washington, DC, p. 120.
- Marshall, R.D. (1993). Wind Load Provisions of Manufactured Home Construction and Safety Standards – A Review and Recommendation for Improvement, NISTIR 5189, *Building and Fire Research Laboratory, Gaithersburg, MD*, for Department of Housing and Urban Development, Washington, DC, May.
- Marshall, R.D. (1994). Manufactured Homes – Probability of Failure and the Need for Better Windstorm Protection Through Improved Anchoring Systems, NISTIR 5370, *Building and Fire Research Laboratory, Gaithersburg, MD*, for Department of Housing and Urban Development, Washington, DC, November.

- Marshall, R.D., and F.Y. Yokel (1995). Recommended Performance-Based Criteria for the Design of Manufactured Home Foundation Systems to Resist Wind and Seismic Loads, NISTIR 5664, *Building and Fire Research Laboratory, Gaithersburg, MD*, for Department of Housing and Urban Development, Washington, DC, August.
- Massman, W. (1987). A Comparative Study of Some Mathematical Models of the Mean Wind Structure and Aerodynamic Drag of Plant Canopies, *Boundary-Layer Meteorology*, Volume 40, pp. 179-197.
- Mayhead, G.J., J.B.H. Gardiner, and D.W. Durant (1975). "A Report on the Physical Properties of Conifers in Relation to Plantation Stability, Forest Commission Report, Silviculture Section, Northern Research Station, Edinburgh, Scotland, June.
- MBMA (1996). *Low Rise Building Systems Manual*, Metal Building Manufacturers Association, Cleveland, OH.
- McDonald, J.R., and W.V. Pennington (1986). Hurricane Damage to Manufactured Homes, *Presented at American Society of Civil Engineers Structures Congress '86*, New Orleans, LA, September.
- McDonald, J.R., H. Jiang, and J. Yin (1997). Full-Scale Measurements of Wind Loads on Metal Edge Flashings and Copings, *Final Report, Institute for Disaster Research*, Texas Tech University, Lubbock, TX, for Roofing Industry Consortium, February.
- Meecham, D. (1988). Wind Action on Hip and Gable Roofs, *M.S. Thesis, University of Western Ontario*, London, Ontario, Canada, August.
- Mehta, K. (1984). Wind Load Provisions Ansi #A58.1-1982. *Journal of Structural Engineering*. Vol. 110, Issue 4 (April 1984)
- Melbourne, (1992) – Chapter 2, pg. 36
- Meyers, T., and K.T. Paw (1986). Testing of a Higher-Order Closure Model for Modeling Airflow Within and Above Plant Canopies, *Boundary-Layer Meteorology*, Volume 37, pp. 297-311.
- MHCSS (1992). Manufactured Home Construction and Safety Standards, 24 CFR Chapter XX, Part 3280.
- Miller, D.R., J.D. Lin, and Z.N. Lu (1991). Air Flow Across an Alpine Forest Clearing: A Model and Field Measurements, *Agriculture and Forest Meteorology*, Volume 56, pp. 209-225.
- Milne, R., and T.A. Browne (1990). Tree Stability and Form, Final Report CEC/NERC Contract MA-0061-UK (BA), August.
- Milne (1993) – Chapter 12, pg. 577
- Minor, J.E. (1985). Window Glass Performance and Hurricane Effects, *ASCE Proceedings Specialty Conference: "Hurricane Alicia: One Year Later," Galveston, TX (August 1984)*, A. Kareem (Ed.), pp.151-167

Minor, J.E. (1994). Wind-Borne Debris and the Building Envelope, *Journal of Wind Engineering and Industrial Aerodynamics*, Volume 53, pp. 207-227.

Minor, J.E., and R.A. Behr (1993a). Architectural Glazing Systems in Hurricanes: Performance, Design Criteria and Designs, *Proceedings 7th U.S. National Conference on Wind Engineering*, Los Angeles, CA, Volume II, pp. 453-461.

Minor, J.E., and R.A. Behr (1993b). Improving the Performance of Architectural Glazing in Hurricanes, *Hurricanes of 1992*, R.A. Cook and M. Soltani (Eds.), ASCE, pp. 476-485.

Minor, J.E., W.L. Beason, and P.L. Harris (1978). Designing for Wind-Borne Missiles in Urban Areas, *ASCE Journal of the Structural Division*, Volume 104, Number ST11, pp. 1749-1760.

Mizzel, 1994- chapter 6, pg. 220

Monroe, J.S. (1996). Wind Tunnel Modeling of Low Rise Structures in a Validated Open Country Simulation, M.S. Thesis, Clemson University, Clemson, S, August.

Moorse, 2001 – Chapter 10, pg. 539

National Roofing Contractors Association (1996). *NRCA Roofing and Waterproofing Manual*, Fourth Edition.

NCS BCS (1988). Manufactured Home Installations, NCS BCS A225.1/ANSI A225.1-1987, National Conference of States on Building Codes and Standards, Inc., Herndon, VA, p. 49.

NCS BCS (1994). Manufactured Home Installations, NCS BCS/ANSI A225.1-1994, National Conference of States on Building Codes and Standards, Inc., Herndon, VA, p. 29.

Neumann, C.J. (1991). The National Hurricane Center Risk Analysis Program (HURISK), NOAA Technical Memorandum NWS NHC 38, *National Oceanic and Atmospheric Administration, Washington, DC*.

Newman, A. (1997). *Metal Building Systems*, McGraw-Hill, New York, NY.

NFPA (1973). Standard for Mobile Homes, NFPA Number 501B-1973/ANSI A119.1, p. 33.

NRC (1991). Hurricane Elena, Gulf Coast August 29 – September 2, 1985, Natural Disasters Studies, Volume Two, HA 286, *Committee on Natural Disasters, National Research Council, Washington, DC* pp. 51-58.

Oliver, H.R., and G.J. Mayhead (1974). Wind Measurements in a Pine Forest During a Destructive Gale, *Forestry*, Volume 47 , p. 2, 1974.

Parris, S. (1996). Design of Wind Uplift Capacities and Retro-Fitted Adhesives, 490 and 491 Project Presentation, Clemson University, Clemson, SC, August.

- Peterka, J.A., Hosoya, N., Cermak, J. E., Cochran, L. S., Cochran, B. C., Derickson, R. G., Harper, C., Jones, J., and B., Metz. (1997). "Wind Uplift Model for Asphalt Shingles." *Journal of Architectural Engineering*, 3(4), Pgs. 147-155.
- Pekoz, T. (1990). Design of Cold-Formed Steel Screw Connections, *Proceedings 10th International Specialty Conference on Cold-Formed Steel Structures*, University of Missouri-Rolla, Rolla, MO, pp. 575-587.
- Powell, M.D. (1987). Changes in the Low-Level Kinematic and Thermodynamic Structure of Hurricane Alicia (1983) of Landfall, *Monthly Weather Review*, Volume 115, pp. 75-99.
- Powell, M.D., and S.H. Houston (1996). Hurricane Andrew's Landfall in South Florida – Part II: Surface Wind Fields and Potential Real-Time Applications, *Weather and Forecasting*, Volume 11, Number 3, pp. 329-349.
- Powell, M.D., and S.H. Houston (1998). Surface Wind Fields of 1995 Hurricanes Erin, Opal, Luis, Marilyn, and Roxanne at Landfall to appear in *Monthly Weather Review*.
- Powell, M.D., P.P. Dodge, and L.B. Black (1991). The Landfall of Hurricane Hugo in the Carolinas: Surface Wind Distribution, *Weather and Forecasting*, Volume 6, pp. 379-399.
- Powell, M.D., P.J. Vickery, and T.A. Reinhold (2003). Reduced drag coefficient for high wind speeds in tropical cyclones, *Nature*, 422, 279-283.
- Raman, S., and N. Reddy (1996). Numerical Simulation of a Mesolow Over a Gulf Stream Filament, *Pure and Applied Geophysics*, Volume 147, pp. 789-819.
- Reddy, N., and S. Raman (1997). Influence of Soil Moisture Parameterization on the Simulation of a Mesoscale Coastal Front, *Pure and Applied Geophysics*, under revision.
- Reed, T.D., D.V. Rosowsky, and S.D. Schiff (1996). Roof Rafter to Top-Plate Connection in Coastal Residential Construction, *Proceedings International Wood Engineering Conference*, pp. 4-458 – 4-465.
- Reed, T.D., D.V. Rosowsky, and S.D. Schiff (1997). Uplift Capacity of Light-Frame Rafter to Top Plate Connections, *Journal of Architectural Engineering*, pp. 157-163, December.
- Roarty (2004) – Chapter 12, pg. 602
- Rodgers, E., S. Chang, and H. Pierce (1994). A Satellite Observational and Numerical Study of Precipitation Characteristics in Western North Atlantic Cyclones, *Journal Applied Meteorology*, Volume 33, pp. 129-139.
- Rosowsky, D.V., and T.A. Reinhold (1999). Rate-of-Load and Duration-of-Load Effects for Wood Fasteners, *ASCE Journal of Structural Engineering*, Volume 125, Number 7, pp.719-724, July.
- Rosowsky and Schiff, (1997) – chapter 6, pg. 220

Roy, R. (1983). Wind Tunnel Measurements of Total Loads on a Mobile Home, *Journal of Wind Engineering and Industrial Aerodynamics*, Volume 13, pp. 327-338.

RSMeans (2001). *Residential Cost Data: 20th Annual Edition*, RSMeans, Kingston, MA, 2001.

RSMeans (2009). *Square Foot Costs: 30th Annual Edition*, RSMeans, Kingston, MA, 2009.

Russell, L.R. (1968). Probability Distributions for Texas Gulf Hurricane Effects of Engineering Interest, Ph.D. Thesis, Stanford University, Stanford, CA.

Russell, L.R. (1971). Probability Distributions for Hurricane Effects, *Journal of Waterways, Harbors, and Coastal Engineering Division*, Number 1, pp. 139-154.

Russell, L.R., and G.F. Schueller (1974). Probabilistic Models for Texas Gulf Coast Hurricane Occurrences, *Journal Petroleum Technology*, pp. 279-288.

Sauer, F.M., W.L. Fons, and K. Arnold (1951). Experimental Investigation of Aerodynamic Drag in Tree Crowns Exposed to Steady Wind—Conifers (U), *US Department of Agriculture.*, Forest Service, Division of Fire Research, Washington, DC, Phase Report, 20 December 1951.

SBCCI (1977) – Standard Building Code 1977 Edition, *Southern Building Code Congress International*, Birmingham, AL

SBCCI (1988). Standard Building Code 1988 Edition, *Southern Building Code Congress International*, Birmingham, AL.

SBCCI (1991). Standard Building Code: Appendix H, Manufactured Home Tie Down Standards, *Southern Building Code Congress International, Inc.*, Birmingham, AL, pp. 601-606.

Schneider, D. (1998). Structural and Intensity Changes of Hurricane Opal (1995) and Hurricane Fran (1996). M.S. Thesis, *Department of Marine, Earth, Atmospheric Sciences*, North Carolina State University, pp. 80.

Schwerdt, R.W., F.P. Ho, and R.R. Watkins (1979). Meteorological criteria for standard project hurricane and probable maximum hurricane wind fields, *Gulf and East Coasts of the United States*. NOAA Tech. Rep. NWS 23, 317 pp.

Seginer, I., P.J. Mulhearn, E.F. Bradley, and J.J. Finnigan (1976). Turbulent Flow in a Model Plant Canopy, *Boundary-Layer Meteorology*, Volume 10, pp. 423-453, 1976.

Shane, 1996 – chapter 6, pg. 220

Shapiro, L.J. (1983). The Asymmetric Boundary Layer Flow Under a Translating Hurricane, *Journal of Atmospheric Science*, Volume 40, Number 8, pp. 1984-1998.

Shaw, R.H., and A.R. Pereira (1982). Aerodynamic Roughness of a Plant Canopy: A Numerical Experiment,” *Agricultural Meteorology*, Volume 26, pp. 51-65.

- Shi, J., S. Chang, and S. Raman (1998). Interaction Between Hurricane Florence (1988) and an Upper-Tropospheric Westerly Trough as Revealed by the Numerical Experiments, *Journal of Atmospheric Science*, Volume 54, pp. 1231-1240.
- Shiotani, M. (1962). The Relationship between Wind Profiles and Stabilities of the Air Layer in the Outskirts of a City, *Journal of Meteorological Society, Japan*, Volume 40, pp. 315-329.
- Simiu, E., and R.H. Scanlan (1996). *Wind Effects on Structures: Fundamental and Applications to Design*, 3rd Edition, John Wiley & Sons, New York, NY.
- Slodicak, M. (1993). Thinning Regime in Stands of Norway Spruce Subjected to Snow and Wind Damage, *Wind-Related Damage to Trees*. IUFRO Conference, Edinburgh, Scotland, June.
- Smith, T. L. (1995). "Insights on Metal Roof Performance in High-Wind Regions, Professional Roofing, pp. 12-16.
- Smith, T.L. (1999). Records of Survey on Building Damages Caused by Hurricane Andrew, Personal Communications, TLSmith Consulting.
- Somerville, F. (1993). Wind Damage to New Zealand State Plantation Forests, *Wind-Related Damage to Trees*, IUFRO Conference, Edinburgh, Scotland, June.
- Sparks, P.R., S.D. Schiff and T.A. Reinhold (1994). Wind Damage to Envelopes of Houses and Consequent Insurance Losses, *Journal of Wind Engineering and Industrial Aerodynamics*, Volume 53, pp. 145-155.
- Stacey, G.R., et al. (1994) Wind Flows and Forces in a Model Spruce Forest, *Boundary-Layer Meteorology*.
- Stathopoulos, T. (1979). Turbulent Wind Action on Low Rise Buildings, Ph.D. Thesis, University of Western Ontario, London, Ontario, Canada, February.
- Steel Deck Institute (1992a). *SDI Manual of Construction with Steel Deck*.
- Steel Deck Institute (1992b). *Standard Practice Details for Composite Floor Deck, Non-Composite Form Deck, and Steel Roof Deck*.
- Steel Joint Institute (1994). Catalogue of Standard Specifications, Load Tables, and Weight Tables for Steel Joists and Joist Girders, Steel Joist Institute, Myrtle Beach, SC.
- Steel Joint Institute (1998). Structural Design of Steel Joist Roofs to Resist Uplift Loads, *Technical Digest*, Number 6, Steel Joist Institute, Myrtle Beach, SC.
- Steyn, D.G. (1982). Turbulence in an Unstable Surface Layer over Suburban Terrain, *Boundary Layer Meteorology*, Volume 22, pp. 183-191.

Storey, T.G., and W.L. Fons (1956). Natural Period Characteristics of Selected Tree Species, AFSWP-864, DASIAC 06224, US Forest Service, Washington, DC, October.

Storey, Fons, and Sauer, 1955 Crown characteristics of several coniferous tree species: relations between weight of crown, branchwood and foliage and stem diameter. Interim Technical Report AFSWP - 416, Division of Fire Research, Forest Service, U.S. Department of Agriculture.

Storey, T.G., and W.Y. Pong (1957). Crown Characteristics of Several Hardwood Tree Species, AFSWP-968, US Forest Service, Division of Fire Research, Washington, DC, May.

Strehmeyer, E.H. (1990). An Overview of Hurricane Damage to Military Facilities and the Storm Recovery Role Played by the Southern Div. Naval Facilities Engineering Command, *Proceedings of Hurricane Hugo One Year Later*, 13-15 September.

Surry, Davenport, and Mikituk (1993) - Chapter 4, pg. 148

Tansel (1993) - Chapter 10, pg. 551

Thompson, N. (1979). Turbulence Measurements Above a Pine Forest, *Boundary-Layer Meteorology*, Volume 16, pp. 293-310.

Thompson, E.F., and Cardone, V.J. (1996). 'Practical modeling of hurricane surface wind fields.' *J. Wtrwy., Port, Coast., and Oc. Engrg.*, ASCE, 122(4), 195-205.

Tom, A., G. Sedlacek, and K. Weynand (1993). Connections in Cold-Formed Steel, *Thin-Walled Structures*, Volume 16, pp. 219-237.

Tryggvason, B.V., D. Surry, and A.G. Davenport (1976). Predicting Wind-Induced Response in Hurricane Zones, *Journal of Structural Division*, Volume 102, Number 12, pp. 2333-2350.

Twisdale, L.A., and W.L. Dunn (1983). Extreme Wind Risk Analysis of the Indian Point Nuclear Generation Station, Final Rep. 44T-2491, Addendum to Rep. 44T-2171, Research Triangle Institute, Research Triangle Park, NC.

Twisdale, L.A., R.A. Frank, and C.E. Murphy (1986). *Data Collection and Analysis for Mechanical Property Tests on Selected Trees*, DAAG29-81-D-0100, Ballistic Research Laboratory, Aberdeen Proving Ground, MD, January.

Twisdale, L.A., R.A. Frank, and P.J. Vickery (1989). Update and Application of the BLOWTRAN Methodology to Forest and Damage Prediction (Version 2.3), DAAA15-87-D-0008, Task 1, *Ballistic Research Laboratory*, Aberdeen Proving Ground, MD, December.

Twisdale, L.A., R.A. Frank, C.E. Murphy, and M.B. Hardy (1984). Forest Blowdown and Debris Transport Methodology, DAAK11 -84-C-0089, *Ballistic Research Laboratory*, Aberdeen Proving Ground, MD, May.

- Twisdale, L.A., P.J. Vickery, and A.C. Steckley (1996). Analysis of Hurricane Windborne Debris Impact Risk for Residential Structures, *Applied Research Associates*, Raleigh, NC, March.
- Twisdale, L.A., P.J. Vickery, J.X. Lin, and A.C. Steckley (2000a). Analysis of Hurricane Windborne Debris Impact Risk for Residential Structures: Part I, to be submitted to the *ASCE Journal of Structural Engineering*.
- Twisdale, L.A., P.J. Vickery, J.X. Lin, and A.C. Steckley (2000b). Analysis of Hurricane Windborne Debris Impact Risk for Residential Structures: Part II, to be submitted to the *ASCE Journal of Structural Engineering*.
- Uematsu, Y., and N. Isyumov (1998). Peak Gust Pressures Acting on the Roof and Wall Edges of a Low-Rise Building, *Journal of Wind Engineering and Industrial Aerodynamics*, Volumes 77 and 78, pp. 217-231.
- US Congress, (1981) – Chapter 6, pg. 281
- United States Department of Agriculture, (1974). USDA Wood Handbook: Wood as an Engineering Material, *Forest Products Laboratory*, Forest Service, Agriculture Handbook No. 72, Revised August.
- United Steel Deck, Inc. (1997). USD Catalog #303-14.
- United Steel Deck, Inc. (1998). Wall and Roof Systems, USD Siding Manual.
- Vann, P.W., and J.R. McDonald (1978), An Engineering Analysis: Mobile Homes in Windstorms, Report prepared for Disaster Preparedness Staff, *National Weather Service*, NOAA, Silver Spring, MD, Institute for Disaster Research, Lubbock, TX.
- Vasquez, J.L. (1994). Development of a Windspeed-Damage Correlation Model for Manufactured Housing Subjected to Extreme Winds, M.S. Thesis, *Louisiana State University and Agricultural and Mechanical College*, December.
- Vickery, P.J., R.A. Frank, M.D. Smith, and L.A. Twisdale (1991). Blast Effects on Forests: Hardwood Breakage Tests and Mechanical Property Tests, DAAA15-89-D-0008, *Ballistic Research Laboratory*, Aberdeen Proving Ground, MD, 31 December.
- Vickery, P.J., R.A. Frank, and L.A. Twisdale (1993). Blast Effects on Forests: Forest Classification, Sensitivity Studies, and Model Evaluation, DAAA15-89-D-0008, Task Order 5, *Ballistic Research Laboratory*, Aberdeen Proving Ground, MD, 6 May.
- Vickery, P.J., and L.A. Twisdale (1995a). Wind-Field and Filling Models for Hurricane Wind-Speed Predictions, *Journal of Structural Engineering*, Volume 121, Number 11, pp. 1700-1709.
- Vickery, P.J., and L.A. Twisdale (1995b). Prediction of Hurricane Wind Speeds in The United States, *Journal of Structural Engineering*, Volume 121, Number 11, pp. 1691-1699.

- Vickery, P.J., P.F. Skerj, and L.A. Twisdale (2000a). Simulation of Hurricane Risk in the United States Using Empirical Track Model, *Journal of Structural Engineering*, Volume 126, Number 10, pp. 1222-1237.
- Vickery, P.J., P.F. Skerj, A.C. Steckley, and L.A. Twisdale (2000b). Hurricane Wind Field Model for Use in Hurricane Simulations, *Journal of Structural Engineering*, Volume 126, Number 10, pp. 1203-1221.
- Vickery, P. J. (2005). Simple empirical models for estimating the increase in the central pressure of tropical cyclones after landfall along the coastline of the United States, *J. Appl. Meteor*, 44, 1807-1826.
- Vickery, P. J. and P.F. Skerlj (2005). Hurricane gust factors revisited, *J. Struct. Eng.*, 131, 825-832.
- Vickery, P. J., J. X. Lin, P. F. Skerlj and L. A. Twisdale, Jr. (2006). The HAZUS-MH hurricane model methodology part I: hurricane hazard, terrain and wind load modeling, *Nat. Hazards Rev.*, 7, 82-93.
- Vickery, P. J., P F. Skerlj, J. X. Lin, L. A. Twisdale, Jr., M.A. Young and F.M. Lavelle (2006). The HAZUS-MH hurricane model methodology part II: damage and loss estimation, *Nat. Hazards Rev.*, 7, 94-103.
- Vickery, P. J. and D. Wadhwa (2008). Statistical models of the Holland pressure profile parameter and radius to maximum winds of hurricanes from flight level pressure and H*Wind data, *J. Appl. Meteor.*, 47, 2497-2517.
- Vickery, P.J., Wadhwa, D., Powell, M.D., and Chen, Y. (2009a). A Hurricane Boundary Layer and Wind Field Model for Use in Engineering Applications, *Journal of Applied Meteorology and Climatology*, 48, pp. 381-405.
- Vickery, P. J., D. Wadhwa, L. A. Twisdale, Jr. and F. M. Lavelle (2009b). United States hurricane wind speed risk and uncertainty, *J. Struct. Eng.*, 135, 301-320.
- Wang, C-K, and C.G. Salmon (1997). *Reinforced Concrete Design*, Fifth Edition.
- West et al. (1973a) – chapter 6, pg. 225
- West et al. (1973b) – chapter 6, pg. 225
- Wieringa, J. (1992). Updating the Davenport Roughness Classification, *Journal of Wind Engineering and Industrial Aerodynamics*, Volume 41-44, pp. 357-368.
- Wieringa, J. (1993). Representative Roughness Parameters for Homogeneous Terrain, *Boundary Layer Meteorology*, Volume 63, pp. 323-363.
- Willoughby. H.E., R.W.R. Darling, and M.E. Rahn (2006). Parametric representation of the primary hurricane vortex. Part II: A new family of sectional continuous profiles, *Mon. Wea. Rev.*, 134, 1102–1120.

- Yersel, M., and R. Goble (1986). Roughness Effects on Urban Turbulence Parameters, *Boundary Layer Meteorology*, Volume 37, pp. 271-284.
- Yokel, F.Y., R.M. Chung, F.A. Rankin, and C.W.C. Yancey (1982), Load-Displacement Characteristics of Shallow Soil Anchors U.S. Department of Commerce, *NBS Building Sciences Series 142, National Bureau of Standards*, Washington, DC.
- Young, M.A., and B.J. Vickery (1994). A Study of Roof Uplift Forces on Three Schools of Windsor Roman Catholic Separate School Board, *Final Report BLWT-SS29-1994, The Boundary Layer Wind Tunnel Laboratory*, The University of Western Ontario, Ontario, Canada.
- Zaitz, M.D. (1994). Roof Sheathing Racking Effect on Fastener Withdrawal Capacities, M.S. Thesis, *Clemson University, Clemson, SC*, pp.4-5, August.
- Zollo, R.F. (1993). Hurricane Andrew: August 24, 1992, Structural Performance of Buildings in Dade County, Florida, *Technical Report No. CEN 93-1, University of Miami*, Miami, FL, March.